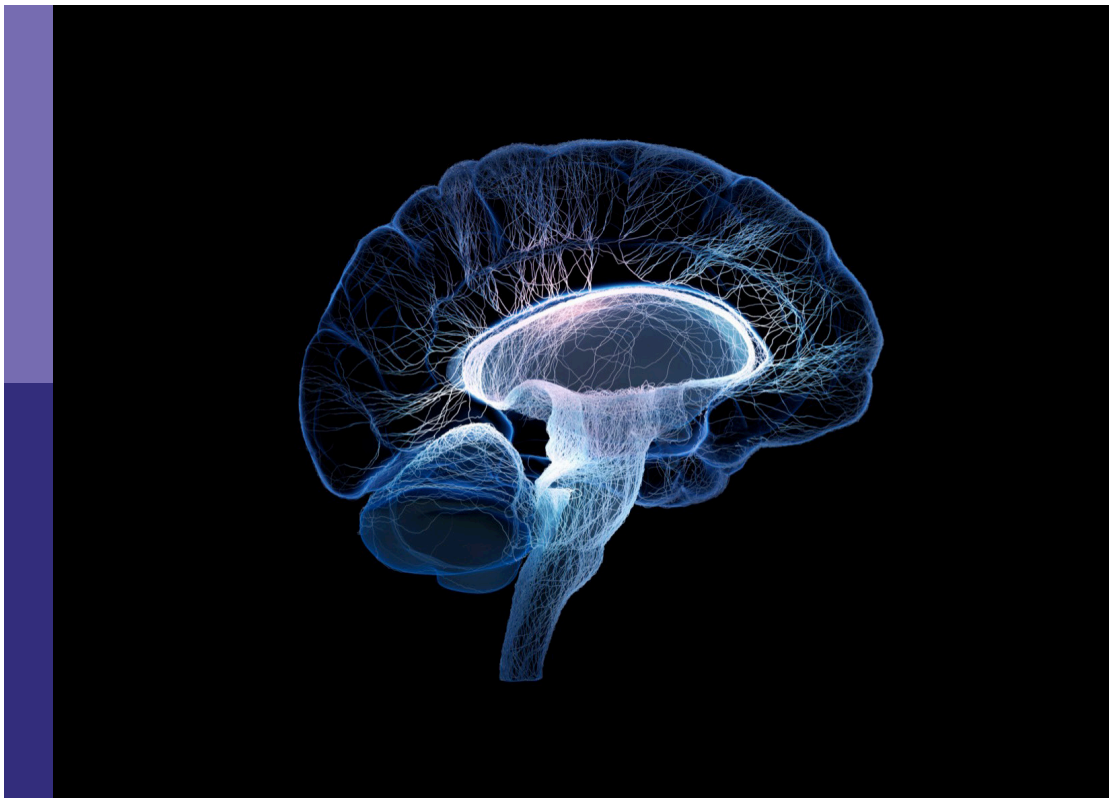
frontiers | Research Topics

Perspectives and recent advances in fetal alcohol spectrum disorders research

Edited by
Hermes H. Yeh, Lisa Akison, Carlos Fernando Valenzuela,
Paola A. Haeger and Kirsten A. Donald

Published in
Frontiers in Neuroscience
Frontiers in Public Health
Frontiers in Pediatrics



FRONTIERS EBOOK COPYRIGHT STATEMENT

The copyright in the text of individual articles in this ebook is the property of their respective authors or their respective institutions or funders. The copyright in graphics and images within each article may be subject to copyright of other parties. In both cases this is subject to a license granted to Frontiers.

The compilation of articles constituting this ebook is the property of Frontiers.

Each article within this ebook, and the ebook itself, are published under the most recent version of the Creative Commons CC-BY licence. The version current at the date of publication of this ebook is CC-BY 4.0. If the CC-BY licence is updated, the licence granted by Frontiers is automatically updated to the new version.

When exercising any right under the CC-BY licence, Frontiers must be attributed as the original publisher of the article or ebook, as applicable.

Authors have the responsibility of ensuring that any graphics or other materials which are the property of others may be included in the CC-BY licence, but this should be checked before relying on the CC-BY licence to reproduce those materials. Any copyright notices relating to those materials must be complied with.

Copyright and source acknowledgement notices may not be removed and must be displayed in any copy, derivative work or partial copy which includes the elements in question.

All copyright, and all rights therein, are protected by national and international copyright laws. The above represents a summary only. For further information please read Frontiers' Conditions for Website Use and Copyright Statement, and the applicable CC-BY licence.

ISSN 1664-8714
ISBN 978-2-8325-4223-1
DOI 10.3389/978-2-8325-4223-1

About Frontiers

Frontiers is more than just an open access publisher of scholarly articles: it is a pioneering approach to the world of academia, radically improving the way scholarly research is managed. The grand vision of Frontiers is a world where all people have an equal opportunity to seek, share and generate knowledge. Frontiers provides immediate and permanent online open access to all its publications, but this alone is not enough to realize our grand goals.

Frontiers journal series

The Frontiers journal series is a multi-tier and interdisciplinary set of open-access, online journals, promising a paradigm shift from the current review, selection and dissemination processes in academic publishing. All Frontiers journals are driven by researchers for researchers; therefore, they constitute a service to the scholarly community. At the same time, the *Frontiers journal series* operates on a revolutionary invention, the tiered publishing system, initially addressing specific communities of scholars, and gradually climbing up to broader public understanding, thus serving the interests of the lay society, too.

Dedication to quality

Each Frontiers article is a landmark of the highest quality, thanks to genuinely collaborative interactions between authors and review editors, who include some of the world's best academicians. Research must be certified by peers before entering a stream of knowledge that may eventually reach the public - and shape society; therefore, Frontiers only applies the most rigorous and unbiased reviews. Frontiers revolutionizes research publishing by freely delivering the most outstanding research, evaluated with no bias from both the academic and social point of view. By applying the most advanced information technologies, Frontiers is catapulting scholarly publishing into a new generation.

What are Frontiers Research Topics?

Frontiers Research Topics are very popular trademarks of the *Frontiers journals series*: they are collections of at least ten articles, all centered on a particular subject. With their unique mix of varied contributions from Original Research to Review Articles, Frontiers Research Topics unify the most influential researchers, the latest key findings and historical advances in a hot research area.

Find out more on how to host your own Frontiers Research Topic or contribute to one as an author by contacting the Frontiers editorial office: frontiersin.org/about/contact

Perspectives and recent advances in fetal alcohol spectrum disorders research

Topic editors

Hermes H. Yeh — Dartmouth College, United States
Lisa Akison — The University of Queensland, Australia
Carlos Fernando Valenzuela — University of New Mexico, United States
Paola A. Haeger — Universidad Católica del Norte, Chile
Kirsten A. Donald — University of Cape Town, South Africa

Citation

Yeh, H. H., Akison, L., Valenzuela, C. F., Haeger, P. A., Donald, K. A., eds. (2024). *Perspectives and recent advances in fetal alcohol spectrum disorders research*. Lausanne: Frontiers Media SA. doi: 10.3389/978-2-8325-4223-1

Table of contents

06 Editorial: Perspectives and recent advances in Fetal Alcohol Spectrum Disorders research
Lisa K. Akison, Kirsten A. Donald, Paola A. Haeger, C. Fernando Valenzuela and Hermes H. Yeh

11 Prenatal alcohol exposure results in brain region- and sex-specific changes in *circHomer1* expression in adult mouse brain
Grigorios Papageorgiou, Stephen K. Amoah, Caroline Pierotti, Madison Otero, Sophie Eckel, Kacie Coffey, Andrea M. Allan, Kevin K. Caldwell and Nikolaos Mellios

21 Ethanol-induced cerebellar transcriptomic changes in a postnatal model of fetal alcohol spectrum disorders: Focus on disease onset
Kalee N. Holloway, James C. Douglas, Tonya M. Rafferty, Ania K. Majewska, Cynthia J. M. Kane and Paul D. Drew

38 Somatostatin neuron contributions to cortical slow wave dysfunction in adult mice exposed to developmental ethanol
Donald A. Wilson, G. Fleming, C. R. O. Williams, C. M. Teixeira, J. F. Smiley and Mariko Saito

49 Prenatal ethanol exposure leads to persistent anxiety-like behavior during adulthood indicated by reduced horizontal and vertical exploratory behaviors
An-Li Wang, Veronika B. Micov, Francis Kwarteng, Ruixiang Wang, Kathryn A. Hausknecht, Saida Oubraim, Samir Haj-Dahmane and Roh-Yu Shen

60 Atypical developmental trajectories of white matter microstructure in prenatal alcohol exposure: Preliminary evidence from neurite orientation dispersion and density imaging
Blake A. Gimbel, Donovan J. Roediger, Abigail M. Ernst, Mary E. Anthony, Erik de Water, Madeline N. Rockhold, Bryon A. Mueller, Sarah N. Mattson, Kenneth L. Jones, Edward P. Riley, Kelvin O. Lim, CIFASD and Jeffrey R. Wozniak

76 Reinforcer value moderates the effects of prenatal alcohol exposure on learning and reversal
Jayapriya Chandrasekaran, Belkis Jacquez, Jennifer Wilson and Jonathan L. Brigman

89 Estimates of total neuron number show that neonatal ethanol causes immediate and lasting neuron loss in cortical and subcortical areas
John F. Smiley, Cynthia Bleiwas, Brandon M. Marino, Prerana Vaddi, Stefanie Canals-Baker, Donald A. Wilson and Mariko Saito

97 Effects of retinoic acid receptor α modulators on developmental ethanol-induced neurodegeneration and neuroinflammation
Mariko Saito, Shivakumar Subbanna, Xiuli Zhang, Stefanie Canals-Baker, John F. Smiley, Donald A. Wilson and Bhaskar C. Das

110 Developmental ethanol exposure has minimal impact on cerebellar microglial dynamics, morphology, and interactions with Purkinje cells during adolescence
MaKenna Y. Cealie, James C. Douglas, Linh H. D. Le, Erik D. Vonkaenel, Matthew N. McCall, Paul D. Drew and Ania K. Majewska

125 Postnatal ethanol exposure impairs social behavior and operant extinction in the adult female mouse offspring
Sebastiano Bariselli, Noa Reuveni, Nina Westcott, Yolanda Mateo and David M. Lovinger

138 Arcuate fasciculus and pre-reading language development in children with prenatal alcohol exposure
Curtis Ostertag, Jess E. Reynolds, Preeti Kar, Deborah Dewey, W. Ben Gibbard, Christina Tortorelli and Catherine Lebel

149 A systematic review: facial, dental and orthodontic findings and orofacial diagnostics in patients with FASD
Moritz Blanck-Lubarsch, Dieter Dirksen, Reinhold Feldmann and Ariane Hohoff

177 Mapping corpus callosum surface reduction in fetal alcohol spectrum disorders with sulci and connectivity-based parcellation
Justine Fraize, Gabrielle Convert, Yann Leprince, Florent Sylvestre-Marconville, Eliot Kerdreux, Guillaume Auzias, Julien Lefèvre, Richard Delorme, Monique Elmaleh-Bergès, Lucie Hertz-Pannier and David Germanaud

191 Prenatal alcohol exposure dysregulates spinal and circulating immune cell circular RNA expression in adult female rats with chronic sciatic neuropathy
Shahani Noor, Ariana N. Pritha, Andrea A. Pasmay, Jacob E. Sanchez, Joshua J. Sanchez, Annette K. Fernandez-Oropeza, Melody S. Sun, Michela Dell'Orco, Suzy Davies, Daniel D. Savage, Nikolaos Mellios and Erin D. Milligan

210 Loss of *Nicotinamide nucleotide transhydrogenase* sensitizes embryos to ethanol-induced neural crest and neural apoptosis via generation of reactive oxygen species
Rayna Mazumdar and Johann K. Eberhart

223 Prenatal alcohol and tetrahydrocannabinol exposure: Effects on spatial and working memory
Annie Lei, Kristen R. Breit and Jennifer D. Thomas

239 Microbiota and nutrition as risk and resiliency factors following prenatal alcohol exposure
Deepa Upreti, Siara K. Rouzer, Abigail Bowring, Emma Labbe, Rosaline Kumar, Rajesh C. Miranda and Amanda H. Mahnke

260 Ethanol-induced transcriptional and translational changes in Aldh1l1-Egfp/Rpl10a cortical astrocyte cultures
Joel G. Hashimoto, Xiaolu Zhang and Marina Guizzetti

274 A tornado in the family: fetal alcohol spectrum disorder and aggression during childhood and adolescence: a scoping review
Maude Champagne, Jeffrey McCrossin, Jacqueline Pei and James N. Reynolds

284 Prenatal alcohol exposure alters mRNA expression for stress peptides, glucocorticoid receptor function and immune factors in acutely stressed neonatal brain
Chaselyn D. Ruffaner-Hanson, Annette K. Fernandez-Oropeza, Melody S. Sun, Kevin K. Caldwell, Andrea M. Allan, Daniel D. Savage, C. Fernando Valenzuela, Shahani Noor and Erin D. Milligan

303 Effect of moderate prenatal ethanol exposure on the differential expression of two histamine H3 receptor isoforms in different brain regions of adult rat offspring
Suzy Davies, Kiana S. Lujan, Ella J. Rappaport, Carlos F. Valenzuela and Daniel D. Savage

319 Behavioral changes in *FPR2/ALX* and *Chemr23* receptor knockout mice are exacerbated by prenatal alcohol exposure
Sandra M. Mooney, Elanaria Billings, Madison McNew, Carolyn A. Munson, Saame R. Shaikh and Susan M. Smith

331 Impact of the COVID-19 pandemic on adults with Fetal Alcohol Spectrum Disorder: linking immune function to mental health status
Tamara S. Bodnar, Amanda Chao, Parker J. Holman, Linda Ellis, Charlis Raineki and Joanne Weinberg

341 An evaluation of a multi-site fetal alcohol spectrum disorder models of care project
Kirsten R. Panton, James P. Fitzpatrick and Carmela F. Pestell

349 Effects of genetics and sex on adolescent behaviors following neonatal ethanol exposure in BXD recombinant inbred strains
Jessica A. Baker, Megan K. Mulligan and Kristin M. Hamre

364 *In utero* ethanol exposure induces mitochondrial DNA damage and inhibits mtDNA repair in developing brain
Nune Darbinian, Armine Darbinyan, Nana Merabova, Myrna Kassem, Gabriel Tatevosian, Shohreh Amini, Laura Goetzl and Michael E. Selzer

379 Brain structural differences in children with fetal alcohol spectrum disorder and its subtypes
Theresah Boateng, Kathryn Beauchamp, Faerl Torres, Chaselyn D. Ruffaner-Hanson, John F. L. Pinner, Kishore Vakamudi, Cassandra Cerros, Dina E. Hill and Julia M. Stephen

391 The ameliorative effects of choline on ethanol-induced cell death in the neural tube of susceptible BXD strains of mice
Fannia Xu, Jennifer D. Thomas, Dan Goldowitz and Kristin M. Hamre

frontiers | Frontiers in Neuroscience

TYPE Editorial
PUBLISHED 15 December 2023
DOI 10.3389/fnins.2023.1341186

Check for updates

OPEN ACCESS

EDITED AND REVIEWED BY
Brian R. Christie,
University of Victoria, Canada

*CORRESPONDENCE
Lisa K. Akison
✉ l.akison@uq.edu.au
Kirsten A. Donald
✉ kirsty.donald@uct.ac.za
Paola A. Haeger
✉ phaeger@ucn.cl
C. Fernando Valenzuela
✉ FValenzuela@salud.unm.edu
Hermes H. Yeh
✉ Hermes.Hsiao-mei.Yeh@dartmouth.edu

RECEIVED 20 November 2023
ACCEPTED 04 December 2023
PUBLISHED 15 December 2023

CITATION
Akison LK, Donald KA, Haeger PA, Valenzuela CF and Yeh HH (2023) Editorial: Perspectives and recent advances in Fetal Alcohol Spectrum Disorders research. *Front. Neurosci.* 17:1341186. doi: 10.3389/fnins.2023.1341186

COPYRIGHT
© 2023 Akison, Donald, Haeger, Valenzuela and Yeh. This is an open-access article distributed under the terms of the Creative Commons Attribution License (CC BY). The use, distribution or reproduction in other forums is permitted, provided the original author(s) and the copyright owner(s) are credited and that the original publication in this journal is cited, in accordance with accepted academic practice. No use, distribution or reproduction is permitted which does not comply with these terms.

Editorial: Perspectives and recent advances in Fetal Alcohol Spectrum Disorders research

Lisa K. Akison[1]*, Kirsten A. Donald[2]*, Paola A. Haeger[3]*, C. Fernando Valenzuela[4]* and Hermes H. Yeh[5]*

[1]School of Biomedical Sciences, Faculty of Medicine, The University of Queensland, Brisbane, QLD, Australia, [2]Department of Paediatrics and Child Health, Faculty of Health Sciences, University of Cape Town, Cape Town, South Africa, [3]Departamento de Ciencias Biomédicas, Facultad de Medicina, Universidad Católica del Norte, Coquimbo, Chile, [4]Department of Neurosciences, School of Medicine, University of New Mexico Health Sciences Center, Albuquerque, NM, United States, [5]Department of Molecular and Systems Biology, Geisel School of Medicine at Dartmouth, Hanover, NH, United States

KEYWORDS

fetal, alcohol, mechanisms, behavior, pathology, FASD, neurodevelopment, neuroanatomy

Editorial on the Research Topic
Perspectives and recent advances in Fetal Alcohol Spectrum Disorders research

This *Frontiers in Neuroscience* Research Topic entitled *"Perspectives and recent advances in Fetal Alcohol Spectrum Disorders research"* was launched shortly after the 45th Annual Research Society on Alcohol Scientific Meeting held in Orlando, Florida from June 25–29, 2022. The basic concept was to provide a forum for scientific communication and cross-fertilization to advance our understanding of the short- and long-term effects and consequences of prenatal alcohol exposure (PAE) and Fetal Alcohol Spectrum Disorder (FASD). Our goal was to integrate the latest original research, reviews, methods and perspectives on foundational, translational and clinical topics in the field. In this context, we cast a wide net, inviting both preclinical and clinical articles covering diverse areas of FASD research for peer review.

FASD is the most common cause of environmentally-induced intellectual disability, and a serious public health problem. Unfortunately, our understanding of this predominantly neurodevelopmental disorder across the lifespan, as well as its etiology and mechanistic underpinnings, is incomplete. The team of Co-Editors have identified three themes that embody the twenty-eight peer reviewed articles constituting this Research Topic:

1. Effects of prenatal ethanol exposure on behavior and brain function.
2. Molecular and cellular mechanisms of ethanol-induced damage.
3. Neuroanatomical and brain structure changes due to prenatal ethanol exposure.

Collectively, the included articles highlight that FASD is a highly complex neurodevelopmental disorder with life-long consequences that calls for concerted efforts of investigation on all fronts, at all levels, and across lifespan, to advance and improve treatment and management of FASD. Although research in this field has indeed come a long way, knowledge gaps remain and must be addressed, potentially utilizing some of the advances described in this Research Topic.

1 Effects of prenatal ethanol exposure on behavior and brain function

The long-term impact of PAE is a subject of critical research aimed at understanding the adverse effects on brain function during adolescence and adulthood. Extensive information is available on how prenatal alcohol exposure affects various behaviors, but there is still much to discover. In this context, Chandrasekaran et al. presented new evidence regarding the influence of different types of rewards on the learning and adaptability of mice exposed to prenatal alcohol. Their study revealed that the effects of PAE vary depending on the type of reward, with liquid rewards proving to be more effective in motivating task learning in prenatally alcohol-exposed animals. Additionally, it is important to note that individuals with FASD are more likely to experience mental health issues and coping difficulties. Bodnar et al. found that while the COVID-19 pandemic did not significantly impact mental health differently between individuals with FASD and controls, it revealed distinct associations between inflammation and mood in those with FASD. This study highlights the importance of recognizing the unique challenges and heightened vulnerability of individuals with FASD during public health crises.

PAE leads to persistent neuroinflammation, suggesting this could be a potential target for future therapies. Mooney et al. demonstrated that specialized pro-resolving lipid mediator (SPM) receptors, specifically FPR2 and ChemR23 receptors involved in anti-inflammatory processes, play a significant role in anxiety and memory formation. Knockout mice with alterations in these receptors exhibit impairments, exacerbated when they are exposed to ethanol in utero. Since dietary-derived forms of omega-3 polyunsaturated fatty acids (PUFA) are ligands of these receptors, this study offers new insights into potential molecular mechanisms for dietary prevention or treatment of FASD, as well as the role of SPM receptors in mitigating cognitive impairments resulting from PAE.

Four studies highlight the influence of genetics, age, sex, and poly-drug consumption on the behavioral consequences of PAE. Baker et al. found that the effects of PAE varied significantly among mouse strains, with some strains showing minimal effects and others displaying substantial changes in hippocampal-dependent behavior. They also noted strain-sex interactions underscoring the complex interplay that determines behavioral outcomes. However, sexual dimorphism was dependent on the type of behavior analyzed. Furthermore, Bariselli et al. observed in a mouse model of moderate postnatal ethanol exposure (third-trimester equivalent) that female, but not male, mice exhibited mild social impairments and altered extinction of operant responding. However, Wang et al. discovered that heavy PAE mimicking second-trimester exposure in humans resulted in persistent anxiety-like behavior in both male and female rats. This suggests that the timing and dose of exposure is important. Interestingly, acute stress was found to mask the effects of PAE in males but not females. Additionally, Lei et al. investigated the combined effects of PAE and Δ-9-tetrahydrocannabinol on cognitive and emotional development, revealing substance- and sex-specific patterns of impairment and highlighting the need for public health policies addressing the use of alcohol and cannabis during pregnancy. The findings of these studies underscore the enduring impact of PAE on mental health and emphasize the significance of considering sex and co-exposures in understanding the risk for development of FASD.

FASD prevalence is often underestimated due to limited diagnostic tools and the absence of self-reporting of alcohol consumption. In this context, Panton et al. evaluated a multi-site project to improve FASD diagnosis and awareness in Australia. The project's success in refining FASD diagnosis and enhancing community education illustrates the importance of coordinated efforts to address the challenges of FASD diagnosis and management.

A final article in this theme sheds light on a critical but understudied aspect of FASD—the aggression displayed by affected children and youth toward their family members. The review by Champagne et al. emphasizes the lack of interventions targeting this specific behavior and underscores the urgent need for research in this area.

Taken together, these clinical and preclinical studies highlight the complex factors underlying the risk for the development of behaviors characteristic of FASD, as well as the challenges in diagnosis and management of this condition.

2 Molecular and cellular mechanisms of ethanol-induced damage

Several studies in this theme contribute significant insights into the effects of ethanol on transcription and translation in the developing brain. Holloway et al. focused on early transcriptomic changes in the cerebellum in a mouse model of FASD, identifying key pathways and cellular functions altered by PAE, including immune function, cytokine signaling, and cell cycle regulation. Notably, there was an increase in transcripts associated with neurodegenerative microglia and reactive astrocyte phenotypes. Hashimoto et al. characterized the impact of ethanol exposure on astrocytes using translating ribosome affinity purification (TRAP). They found significant overlap between ethanol-affected genes in the total RNA pool and the translating RNA pool. Moreover, the overlap between ethanol-regulated genes in this study and other *in vivo* exposure models supports the generalizability of these findings to various PAE scenarios. Ruffaner-Hanson et al. studied the impact of PAE on stress-responsive brain regions in mice, emphasizing sex-dependent responses. PAE resulted in dysregulated neuroendocrine and neuroimmune activation, primarily in females. The findings highlight the importance of considering sex-specific effects and the role of Toll-like receptor 4 (TLR4) signaling in the context of PAE. The study by Papageorgiou et al. is the first to highlight the emerging role of circular RNAs (circRNAs) in the context of PAE, demonstrating sex- and brain region-specific alterations in circRNAs as well as in long non-coding RNA (lncRNA) expression. Notably, CircHomer1, a circRNA abundant in the postnatal brain, is significantly reduced in the frontal cortex and hippocampus of male mice exposed to moderate PAE. Meanwhile, there was an increase in the expression of the embryonic brain-enriched lncRNA H19 in the frontal cortex of these male PAE mice. In a related study by Noor et al., PAE led to alterations in the levels of circRNAs associated with immune function and suggested a

potential link between PAE-induced neuroimmune actions and adult-onset pain dysregulation. Lastly, Davies et al. examined the effects of PAE on gene expression of two histamine H3 receptor isoforms (rH_{3A} and rH_{3C}) in different brain regions in the rat. Interestingly, changes were detected in brain regions where the investigators had previously observed PAE-induced changes in H3R-effector coupling.

Two studies specifically examined the role of mitochondria and oxidative stress in the mechanism of action of PAE. Mazumdar and Eberhart addressed the genetic factors influencing susceptibility to ethanol-induced birth defects, focusing on the role of nicotinamide nucleotide transhydrogenase (Nnt) in mitigating oxidative stress. This study, conducted in zebrafish embryos, demonstrated that ethanol exposure leads to increased apoptosis and craniofacial malformations in Nnt mutants due to elevated reactive oxygen species. Importantly, antioxidant treatment rescued these defects. To further explore the mechanisms underlying PAE-induced oxidative stress, Darbinian et al. examined mitochondrial DNA (mtDNA) in fetal brain tissues from PAE-exposed rats and humans, as well as fetal brain-derived exosomes (FB-Es) obtained from maternal blood. Human tissues of this type with complementary records of maternal alcohol exposure are rarely available. PAE resulted in mtDNA damage in both the rat and human fetal brain tissue, as well as FB-Es from maternal blood. mtDNA damage in FB-Es also correlated with reduced fetal eye size. This suggests that FB-Es may be useful clinically as a surrogate marker for mtDNA damage in the fetal brain and thus predict risk for FASD. *In vitro* treatment of neuronal cells with ethanol also showed mtDNA damage leading to oxidative stress and apoptosis while insulin-like growth factor 1 (IGF1) was shown to rescue mtDNA from this damage.

Two studies delved into potential factors that may modulate the effect of PAE. Upreti et al. introduced the gut microbiota as a potential factor in FASD pathophysiology. The link between gut microbiota and neurodevelopmental disorders was explored, suggesting that microbiota dysbiosis may play a role in the development of FASD. This area of research is in its early stages but holds promise in understanding the long-term health effects of PAE. Choline has been identified as a potential supplement to ameliorate behavioral, neurological, and cognitive deficits from PAE (see Akison et al., 2018 for a review of preclinical and Ernst et al., 2022 for a review of clinical studies). Xu et al. investigated the potential therapeutic benefits of choline in mitigating ethanol-induced cell death in the developing neural tube using BXD strains of mice, known to vary in their sensitivity to ethanol's teratogenic effects (Downing et al., 2012). Choline administration effectively reduced cell death in all strains, without causing harm in un-exposed mice. However, there were some dose-dependent differences across strains and brain regions, indicating that there is genetic variability in the response to choline treatment as well as ethanol sensitivity.

A final study in this theme investigated the role of somatostatin (SST) GABAergic neurons in sleep circuitry and their sensitivity to developmental ethanol exposure (Wilson et al.). Optical activation of prefrontal cortex SST neurons induced slow-wave potentials and delayed single-unit excitation in mice treated with saline but not in those exposed to ethanol during the brain growth spurt (third-trimester equivalent). When these neurons were activated in a closed-loop manner during spontaneous slow waves, it enhanced cortical delta oscillations, an effect that was more pronounced in saline-treated mice compared to ethanol-exposed mice. These findings indicate that SST cortical neurons may play a role in the impaired slow-wave activity observed after PAE.

These studies collectively show the multifaceted molecular and cellular mechanisms underlying PAE-induced damage in the brain. These include early transcriptomic changes, genetic factors, mitochondrial dysfunction, stress responses, gut microbiota dysbiosis, and the role of specific molecular players like circRNAs, lncRNAs, somatostatin neurons, and histamine receptors. Moreover, these investigations highlight the significance of considering sex-specific effects and genetic variability in response to interventions.

3 Neuroanatomical and brain structure changes due to prenatal ethanol exposure

While FASD has recently been recognized as a 'whole body diagnosis' (Himmelreich et al., 2020), undoubtedly the major focus of research is on the impacts of the teratogenic effects of ethanol on the developing brain. However, the available diagnostic criteria for FASD do not include specific neuroanatomical or structural brain changes. There are well-documented reductions in brain size, but there is less consistency in reports of specific anatomical markers that may provide a reliable phenotype for prenatal alcohol-induced damage. Studies investigating the complex relationship between PAE, structural brain changes, and cognitive and behavioral outcomes, highlight the need for prevention strategies as well as tailored interventions in children with prenatal exposure to alcohol.

Four clinical studies used innovative methods and approaches to explore morphological changes in the brain induced by PAE that may be potentially responsible for FASD-related cognitive and behavioral deficits. Boateng et al. used structural magnetic resonance imaging (MRI) to measure overall brain volume, as well as volume and surface area of specific brain regions, in children diagnosed with FASD and PAE compared to typically developing controls. While confirming previous reports of smaller brain volume in children with FASD/PAE (e.g., Treit et al., 2016), only specific FASD subtypes (pFAS/FAS) showed reduced volume in specific regions of the brain, notably the cerebellum, caudate, and pallidum. Also, for those tested, there was a significant correlation between volume and IQ.

Although focal abnormalities in the corpus callosum (CC) have been frequently reported clinically at various ages (see Moore and Xia, 2022 for review), Fraize et al. used an innovative method combining sulci-based cortical segmentation and connectivity-based parcellation of the CC to explore this further. They found that various CC parcels and corresponding cortical regions were smaller in individuals with FASD compared to controls. For example, even when adjusting for confounding factors such as age, sex and brain

size, the postcentral callosal parcel and its corresponding cortical region appeared to be persistently affected. Given the importance of the CC in interhemispheric communication in the brain, it is perhaps not surprising that the reduced size of these CC parcels may provide a clinically relevant neuroanatomical marker for FASD diagnosis and at least a partial explanation for the cognitive and motor deficits in individuals with FASD (Biffen et al., 2022). Additionally, Gimbel et al. used a combination of MRI tractography with a novel diffusion-weighted Neurite Orientation Dispersion and Density Imaging (NODDI) model to characterize the impact of PAE on longitudinal trajectories of developmental white matter microstructure. PAE resulted in atypical developmental trajectories from childhood (~9 years) through adolescence (~17 years). There were also sex-specific differences detected, particularly in the neurite density index, with males with PAE more severely affected than females.

Finally, Ostertag et al. used diffusion tensor imaging (DTI) to examine the arcuate fasciculus (AF), a white matter tract primarily in the left hemisphere of the brain that is important for language processing. Children with FASD are reported to have deficits in articulation, grammatical ability and both expressive and receptive language (Mattson et al., 2019) and therefore developmental impairment of the AF may help to explain these deficits. The results indicated that children with PAE show altered developmental trajectories of the AF, which were associated with lower pre-reading language ability, including phonological processing and speeded naming, well described as being affected in this group.

Three preclinical studies delved deeper into the cellular level effects of ethanol exposure during brain development, and investigated a potential therapeutic. Cealie et al. used a mouse-model of human third-trimester exposure to specifically focus on microglia dynamics, morphology and interactions with Purkinje cells within the cerebellum during offspring adolescence. Microglia are considered the 'immune cells of the brain' (Eyo and Wu, 2019) and have been shown to be susceptible to ethanol-induced cell death and altered phenotype in surviving cells (Kane et al., 2011). Perhaps surprisingly, PAE at this time-point produced minimal long-term effects on cerebellar microglia and their interactions with neurons, suggesting that at least in this region of the brain, these cells are relatively resilient when exposed to alcohol during this phase of development. However, a mouse study estimating neuron numbers in cortical and sub-cortical regions following PAE at a similar time-point (third trimester equivalent) paints a different picture. Smiley et al. used stereological cell counting to compare immediate (8h post) and long-term (post-natal day 70) neuron loss and showed both an immediate and lasting reduction in neuron numbers in various brain regions. This highlights the profound and persistent impact of neonatal ethanol exposure on neuron numbers in the developing brain. The study by Saito et al. explores the potential therapeutic effects of retinoic acid receptor α (RARα) modulators on ethanol-induced neurodegeneration and neuroinflammation in neonatal mice. The findings suggest that RARα antagonist partially blocks acute neurodegeneration and phagocytic cell elevation. On the other hand, an RARα agonist ameliorates long-lasting astrocyte activation and GABAergic cell deficits. These results indicate that modulating RARα signaling may have potential therapeutic benefits in mitigating the neurological consequences of developmental ethanol exposure. The study highlights the complex interplay between retinoic acid signaling, neurodegeneration, and neuroinflammation in FASD, offering insights into potential avenues for treatment.

Although not specifically focused on brain structural changes, Blanck-Lubarsch et al. provided a comprehensive systematic review of orofacial structural abnormalities in patients with FAS specifically, as well as across the FASD diagnostic spectrum. Dysmorphology in several orofacial features are typically part of the diagnostic criteria for FAS, but they are not used consistently across the various guidelines currently available. Additionally, there are other dysmorphologies which may prove to be potential diagnostic criterion across the spectrum. The review included 61 clinical studies evaluating various facial, oral, dental, and orthodontic features in patients with FASD. The most common orofacial features measured included palpebral fissure length, interpupillary distance, philtrum, upper lip, midfacial hypoplasia, and head circumference. The review emphasized the need for standardized and objective diagnostic criteria for orofacial features in FASD. Such criteria would enhance diagnostic accuracy and consistency, facilitating early identification and intervention for affected individuals.

Overall, while the preclinical studies advance our understanding of neurobiological mechanisms underpinning the developmental effects of PAE, the multimodal range of neuroimaging in clinical populations improves our understanding of potential neuro-physical features of FASD. Taken together, these studies provide an exploration of trajectories across the important early adolescent developmental window and potential targets for diagnosis and therapeutic interventions.

Author contributions

LA: Writing—original draft, Writing—review & editing. PH: Writing—original draft, Writing—review & editing. KD: Writing—original draft, Writing—review & editing. CV: Conceptualization, Writing—original draft, Writing—review & editing. HY: Conceptualization, Writing—original draft, Writing—review & editing.

Funding

The author(s) declare that no financial support was received for the research, authorship, and/or publication of this article.

Conflict of interest

The authors declare that the research was conducted in the absence of any commercial or financial relationships that could be construed as a potential conflict of interest.

The author(s) declared that they were an editorial board member of Frontiers, at the time of submission. This had no impact on the peer review process and the final decision.

Publisher's note

All claims expressed in this article are solely those of the authors and do not necessarily represent those of their affiliated organizations, or those of the publisher, the editors and the reviewers. Any product that may be evaluated in this article, or claim that may be made by its manufacturer, is not guaranteed or endorsed by the publisher.

References

Akison, L., Kuo, J., Reid, N., Boyd R. N., and Moritz, K. M. (2018). Effect of choline supplementation on neurological, cognitive, and behavioral outcomes in offspring arising from alcohol exposure during development: a quantitative systematic review of clinical and preclinical studies. *Alcohol. Clin. Exp. Res.* 42, 1591–1611. doi: 10.1111/acer.13817

Biffen, S. C., Dodge, N. C., Warton, C. M., Molteno, C. D., Jacobson, J. L., Meintjes, E. M., et al. (2022). Compromised interhemispheric transfer of information partially mediates cognitive function deficits in adolescents with fetal alcohol syndrome. *Alcoholism Clin. Exp. Res.* 46, 517–529. doi: 10.1111/acer.14795

Downing, C., Balderrama-Durbin, C., Kimball, A., Biers, J., Wright, H., Gilliam, D., and Johnson, T. E. (2012). Quantitative trait locus mapping for ethanol teratogenesis in BXD recombinant inbred mice. *Alcoholism Clin. Exp. Res.* 36, 1340–1354. doi: 10.1111/j.1530-0277.2012.01754.x

Ernst, A. M., Gimbel, B. A., de Water, M. K., Eckerle, E., Radke, J. K., Georgieff, J. P., et al. (2022). Prenatal and postnatal choline supplementation in fetal alcohol spectrum disorder. *Nutrients* 14, 688. doi: 10.3390/nu14030688

Eyo, U. B., and Wu, L. J. (2019). Microglia: Lifelong patrolling immune cells of the brain. *Prog. Neurobiol.* 179, 101614. doi: 10.1016/j.pneurobio.2019.04.003

Himmelreich, M., Lutke, C. J., and Hargrove, E. T. (2020). *Fetal Alcohol Spectrum Disorder (FASD) as a Whole-Body Diagnosis. The Routledge Handbook of Social Work and Addictive Behaviors*. London: Routledge.

Kane, C. J., Phelan, K. D., Han, L., Smith, R. R., Xie, J., Douglas, J. C., et al. (2011). Protection of neurons and microglia against ethanol in a mouse model of fetal alcohol spectrum disorders by peroxisome proliferator-activated receptor-γ agonists. *Brain Behav. Immun.* 25, S137–S145. doi: 10.1016/j.bbi.2011.02.016

Mattson, S. N., Bernes, G. A., and Doyle, L. R. (2019). Fetal alcohol spectrum disorders: a review of the neurobehavioral deficits associated with prenatal alcohol exposure. *Alcoholism Clin. Exp. Res.* 43, 1046–1062. doi: 10.1111/acer.14040

Moore, E. M., and Xia, Y. (2022). Neurodevelopmental trajectories following prenatal alcohol exposure. *Front. Hum. Neurosci.* 15, 695855. doi: 10.3389/fnhum.2021.695855

Treit, S., Zhou, D., Chudley, A. E., Andrew, G., Rasmussen, C., Nikkel, S. M., et al. (2016). Relationships between head circumference, brain volume and cognition in children with prenatal alcohol exposure. *PloS ONE* 11, e0150370. doi: 10.1371/journal.pone.0150370

frontiers | Frontiers in Neuroscience

TYPE Original Research
PUBLISHED 17 February 2023
DOI 10.3389/fnins.2023.1087950

Check for updates

OPEN ACCESS

EDITED BY
Hermes H. Yeh,
Dartmouth College, United States

REVIEWED BY
Sandra Mooney,
University of North Carolina at Chapel Hill, United States
Kristin Hamre,
The University of Tennessee Health Science Center (UTHSC), United States
Michael F. Miles,
Virginia Commonwealth University, United States

*CORRESPONDENCE
Nikolaos Mellios
✉ nmellios@salud.unm.edu

†PRESENT ADDRESS
Stephen K. Amoah,
Department of Anatomy and Cell Biology, School of Medical Sciences, College of Health and Allied Sciences, University of Cape Coast, Cape Coast, Ghana

SPECIALTY SECTION
This article was submitted to Neurodevelopment, a section of the journal Frontiers in Neuroscience

RECEIVED 02 November 2022
ACCEPTED 16 January 2023
PUBLISHED 17 February 2023

CITATION
Papageorgiou G, Amoah SK, Pierotti C, Otero M, Eckel S, Coffey K, Allan AM, Caldwell KK and Mellios N (2023) Prenatal alcohol exposure results in brain region- and sex-specific changes in *circHomer1* expression in adult mouse brain. *Front. Neurosci.* 17:1087950. doi: 10.3389/fnins.2023.1087950

COPYRIGHT
© 2023 Papageorgiou, Amoah, Pierotti, Otero, Eckel, Coffey, Allan, Caldwell and Mellios. This is an open-access article distributed under the terms of the Creative Commons Attribution License (CC BY). The use, distribution or reproduction in other forums is permitted, provided the original author(s) and the copyright owner(s) are credited and that the original publication in this journal is cited, in accordance with accepted academic practice. No use, distribution or reproduction is permitted which does not comply with these terms.

Prenatal alcohol exposure results in brain region- and sex-specific changes in *circHomer1* expression in adult mouse brain

Grigorios Papageorgiou[1], Stephen K. Amoah[1†], Caroline Pierotti[1], Madison Otero[1], Sophie Eckel[1], Kacie Coffey[1], Andrea M. Allan[1], Kevin K. Caldwell[1] and Nikolaos Mellios[1,2*]

[1]Department of Neurosciences, University of New Mexico School of Medicine, Albuquerque, NM, United States, [2]Autophagy, Inflammation, and Metabolism (AIM) Center, Albuquerque, NM, United States

Circular RNAs (circRNAs) are a novel category of covalently-closed non-coding RNAs mainly derived from the back-splicing of exons or introns of protein-coding genes. In addition to their inherent high overall stability, circRNAs, have been shown to have strong functional effects on gene expression *via* a multitude of transcriptional and post-transcriptional mechanisms. Furthermore, circRNAs, appear to be particularly enriched in the brain and able to influence both prenatal development and postnatal brain function. However, little is known about the potential involvement of circRNAs in the long term influence of prenatal alcohol exposure (PAE) in the brain and their relevance for Fetal Alcohol Spectrum Disorders (FASD). Using circRNA-specific quantification, we have found that *circHomer1*, an activity-dependent circRNA derived from Homer protein homolog 1 (*Homer1*) and enriched in postnatal brain, is significantly down-regulated in the male frontal cortex and hippocampus of mice subjected to modest PAE. Our data further suggest that the expression of *H19*, an imprinted embryonic brain-enriched long non-coding RNA (lncRNA), is significantly up-regulated in the frontal cortex of male PAE mice. Furthermore, we show opposing changes in the developmental- and brain region specific- expression of *circHomer1* and *H19*. Lastly, we show that knockdown of *H19* results in robust increases in *circHomer1* but not linear *HOMER1* mRNA expression in human glioblastoma cell lines. Taken together, our work uncovers notable sex- and brain region-specific alterations in circRNA and lncRNA expression following PAE and introduces novel mechanistic insights with potential relevance to FASD.

KEYWORDS

circRNA, lncRNA, *H19*, *circHomer1*, prenatal alcohol (ethanol) exposure, adult brain

Introduction

Fetal alcohol spectrum disorders (FASD) are an umbrella of alcohol-related neurodevelopmental disorders characterized by both growth, neurocognitive, and neurobehavioral deficits (Carter et al., 2016; Marquardt et al., 2020). FASD is characterized by various neurodevelopmental abnormalities that could lead to long-lasting neuropsychiatric impairments and are suggested to be dependent on the dose, timing, and duration of prenatal alcohol exposure (PAE) (Chudley et al., 2005; Valenzuela et al., 2012). Noteworthy in the USA almost $5.4 billion per year is spent on treating FASDs (Popova et al., 2011), which

impose a serious socioeconomic burden to patients and their families. It has been proposed that PAE could affect the regulation of gene expression by either impacting DNA methylation and histone modifications or by altering the expression of non-coding RNAs and especially microRNAs (Kaminen-Ahola, 2020). Previous studies have portrayed the miRNA dysregulation following ethanol exposure in CNS (Sathyan et al., 2007; Pappalardo-Carter et al., 2013; Mahnke et al., 2019), primarily focusing on miRNAs that are significant in the regulation of neurodevelopmental processes and inflammatory gene expression (Ibáñez et al., 2020). Such studies build up the potential importance of ncRNAs in the adverse effects PAE on brain development and suggest that they could be targets for novel therapeutics (Mahnke et al., 2018).

CircRNAs are a novel category of non-coding RNAs that are characterized by their unique circular secondary structure. CircRNAs are created by the back-splicing of a single-stranded linear transcript whose ends are covalently bound and are known to be much more stable than mRNAs, with a half-life time of days to a week (Jeck et al., 2013; Memczak et al., 2013; You et al., 2015; Enuka et al., 2016). Recent studies have shown that circRNAs are partially conserved between species with most highly-expressed and evolutionary-conserved circRNAs derived from exonic sequences (Lukiw, 2013; You et al., 2015; Gokool et al., 2020; Mehta et al., 2020). CircRNAs can be preferentially derived from genes that code for synaptic proteins and tend to be particularly responsive during both important stages of prenatal and postnatal brain development (Szabo et al., 2015; Dang et al., 2016), suggesting that circRNAs might serve as critical regulators of brain development and function (Rybak-Wolf et al., 2015; You et al., 2015). Recent studies have shown altered profile of expression of circRNAs in various psychiatric (Zimmerman et al., 2020) and neurodevelopmental disorders, as well as cocaine addiction (Bu et al., 2019) and Alzheimer's disease (Dube et al., 2019). Lastly, despite the fact that previous studies have highlighted the crucial role of circRNAs in embryonic and fetal development (Venø et al., 2015; Suenkel et al., 2020), not much is known about their implications in neurodevelopmental disorders such as FASD.

Using circRNA profiling and RNA seq we previously uncovered sex-specific changes in whole brain circRNA but not mRNA expression as a result of PAE and we showed that differentially expressed by PAE circRNAs were preferentially derived from genes with important roles in brain development and function (Paudel et al., 2020). However, little is known about the potential involvement of circRNAs in the long term influence of prenatal alcohol exposure (PAE) in the brain and their relevance for Fetal Alcohol Spectrum Disorders (FASD). We have previously demonstrated that *circHomer1* is an adult brain-enriched circRNA known to be dysregulated in psychiatric disorders and able to influence synaptic gene expression and cognitive function (You et al., 2015; Zimmerman et al., 2020; Hafez et al., 2022). Focusing on factors that can control *circHomer1* biogenesis, we have reported that the RNA-binding protein (RBP) eukaryotic initiation factor 4A-III (EIF4A3), a member of the exon junction complex important for brain development and synaptic function (Giorgi et al., 2007; Mao et al., 2016), is able to positively regulate *circHomer1* expression. A previous study suggested that EIF4A3 activity can be inhibited *via* its binding to *H19* (Han et al., 2016), an imprinted embryonic brain-enriched lncRNA previously shown to be epigenetically altered following PAE and linked to FASD-associated changes in head circumference (Marjonen et al., 2017, 2018; Zhong et al., 2021; Bestry et al., 2022).

Here, we provide strong evidence that *circHomer1*, is significantly down-regulated in the male frontal cortex and hippocampus of mice subjected to modest PAE. Our data further suggest that the expression of *H19* is significantly up-regulated in the frontal cortex of male PAE mice with opposing changes in the developmental- and brain region specific- expression to that of *circHomer1*. Importantly, knockdown of *H19* in human glioblastoma cell lines resulted in a robust up-regulation of *circHomer1* but not linear *HOMER1* mRNA. Taken together, our work uncovers notable sex- and brain region-specific alterations in circRNA and lncRNA expression following PAE and introduces novel mechanistic insights with potential relevance to FASD.

Materials and methods

Moderate prenatal alcohol exposure (PAE)

WT C57BL/6J mice derived from Jackson Laboratory were maintained on a reverse 12 h dark/light schedule (lights on at 8:00 p.m.) in single-housed cages. We utilized a well-validated moderate PAE paradigm (Brady et al., 2012; Paudel et al., 2020) that involves giving adult female mice access to either to a solution of either 10% (w/v) ethanol and 0.066% (w/v) saccharin or 0.066% (w/v) saccharin (control) for 4 h per day. After ensuring consistent drinking, mice were given access to these solutions during mating and for the whole duration of their pregnancy. Some dams were euthanized at the end of their pregnancy and whole brain samples were extracted from embryonic day 18 (E18) male and female pups and stored in a −80°C freezer (at least 4 SAC and 4 PAE litter groups were used). For adult tissue harvesting, male and female pups were left to grow till adulthood (P80-90) without any intervention and no access to ethanol, then were euthanized, and various brain regions (frontal cortex, hippocampus, occipital cortex, cerebellum) were extracted *via* micro dissection (at least 4 SAC and 4 PAE litter groups were used). For E18 brain extractions dams was euthanized by decapitation and the body was laid on ice. The uterine horn was rapidly removed and placed on a piece of glass on top of the ice. Each embryo was removed, decapitated and the brain isolated. All adult males were euthanized by CO2 asphyxiation. All procedures were approved by the University of New Mexico Health Sciences Center Institutional Animal Care and Use Committee.

RNA extraction and mRNA/circRNA quantification

RNA was isolated using the miRNeasy RNA isolation kit (Qiagen, Hilden, Germany) following the manufacturer's supplied protocol. RNA quality as well as concentration of isolated total RNA was assayed through Nanodrop 2000 spectrophotometer and Qubit 3 (Thermo Fisher Scientific, Waltham, Massachusetts, USA), with all samples passing the quality control measurements (A260/230 and A260/280). Reverse transcription of total RNA (100–500 nanograms depending on the Nanodrop concentration values) was carried out using the SuperScript IV First-Strand Synthesis System (Thermo

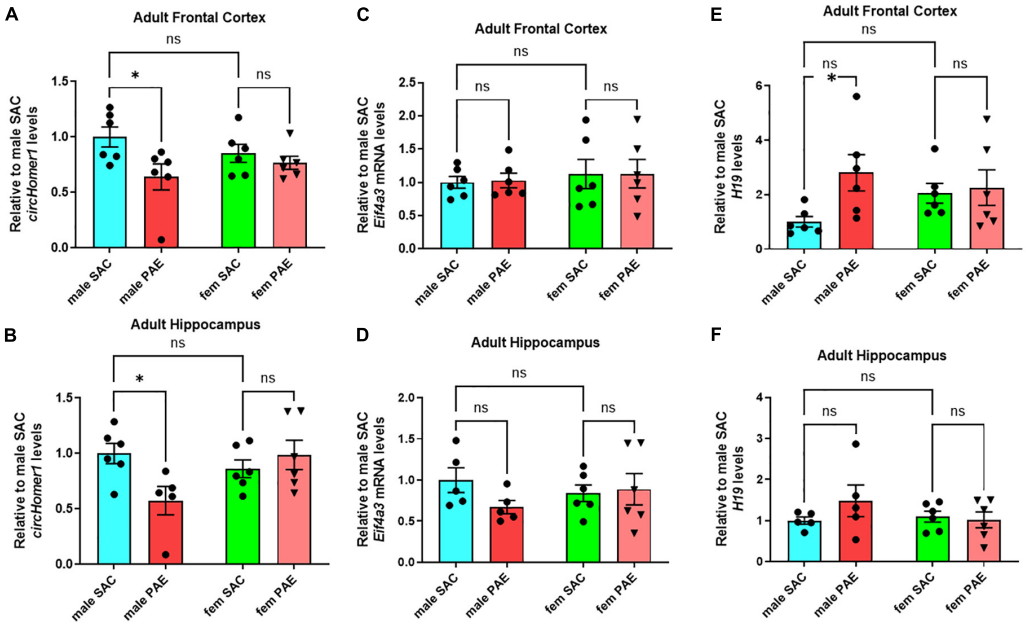


FIGURE 1
Expression of *circhomer1*, *Eif4a3*, and *H19* in the male and female adult frontal cortex and hippocampus. **(A,B)** Mean ± SEM *circHomer1* levels (normalized to *18S rRNA* and further normalized to the mean of Control male SAC *circHomer1* levels) in adult male and female (fem) PAE and SAC adult frontal cortex **(A)** and hippocampus **(B)**. For **(A)**: $p = 0.0242$, $t = 2.838$, df = 20 for male PAE vs. male SAC and $p = 0.7539$, $t = 0.6807$, df = 20 for female PAE vs. female SAC. For **(B)**: $p = 0.0160$, $t = 2.962$, df = 19 for male PAE vs. male SAC and $p = 0.7461$, $t = 0.6940$, df = 19 for female PAE vs. female SAC. **(C,D)** Mean ± SEM relative to male SAC *Eif4a3* mRNA levels (normalized to *18S rRNA*) in adult male and female (fem) PAE and SAC frontal cortex **(C)** and hippocampus **(D)**. For (C): $p = 0.9909$, $t = 0.1213$, df = 20 for male PAE vs. male SAC and $p = 0.995$, $t = 0.02928$, df = 20 for female PAE vs. female SAC. For **(D)**: $p = 0.2506$, $t = 1.568$, df = 18 for male PAE vs. male SAC and $p = 0.9575$, $t = 0.2647$, df = 20 for female PAE vs. female SAC. **(E,F)** Mean ± SEM relative to male SAC *H19* levels (normalized to *18S rRNA*) in adult male and female (fem) PAE and SAC frontal cortex **(E)** and hippocampus **(F)**. For **(E)**: $p = 0.0250$, $t = 2.741$, df = 20 for male PAE vs. male SAC and $p = 0.9504$, $t = 0.2868$, df = 20 for female PAE vs. female SAC. For **(F)**: $p = 0.2930$, $t = 1.469$, df = 18 for male PAE vs. male SAC and $p = 0.9569$, $t = 0.2670$, df = 18 for female PAE vs. female SAC. In **(A–F)**: $^*p < 0.05$ based on two-way ANOVA corrected with Šídák's multiple comparisons test. Individual biological replicates are shown in each graph.

Fisher Scientific, Waltham, MA, USA) with oligo-dT for linear mRNAs and random hexamers for circRNA detection. Quantitative RT-PCR was done using either PowerUp SYBR Green Master Mix (Thermo Fisher Scientific) along with custom designed, validated, and sequence-verified circRNA and mRNA primers or TaqMan Gene Expression Assays (Thermo Fisher Scientific) for mRNA detection. All circRNA qRT-PCR products were run on an agarose gel and sequence validated. At the end of each qPCR amplifications plots and melt curves (ΔRn vs. cycle per well) were automatically calculated by Quant Studio 7 Flex. *18S rRNA* was used as a normalizer for mRNA and circRNA expression levels. For mRNA qRT-PCR quantification the following formula was used: Relative value = $A^{\wedge}Ct^{18SrRNA}/A^{\wedge}Ct^{mRNA}$, where A = 10^ (−1/primer slope). For circRNA qRT-PCR quantification the following formula was used: Relative value = $A^{\wedge}Ct^{18SrRNA}/A^{\wedge}Ct^{circRNA}$, where A = 10^ (−1/primer slope) (Zimmerman et al., 2020; Hafez et al., 2022). All primers used in this study are shown in **Supplementary Table 1**.

SH-SY5y Human neuroblastoma cell *and H19* shRNA mediated KD

SH-SY5Y epithelial human neuroblastoma cell line was purchased from ATCC CRL-2266™. SY-5 can differentiate under certain circumstances. To that end, cells were fed for 5 days using Neurobasal Plus, 1XB27 Plus, 5% Pen/Strep ~ ThermoFisher Scientific. The neuronal-like morphology was observed under the microscope and by measuring the levels of beta-3 tubulin (ab18207; Abcam, Cambridge, United Kingdom), a neuronal marker *via* immunohistochemistry as done before (Zimmerman et al., 2020). After differentiation, SY-5 cells were plated in a 24 well plate at passage #7 at a concentration of 100,000 cells per well. 48 h later they were transfected with the shRNA clone for the gene of interest, *H19*, and a non-target shRNA clone. Transfections were performed using Lipofectamine™ 3000/P3000 reagent (500 ng DNA, 1 μl Lipofectamine and 1 μl P3000 reagent per well). 48 h following the transfection, the differentiated SH-SY5Y cells were subjected to RNA extraction and then qRT-PCR to assay overall changes in *circHomer1* expression. For the *H19* KD experiments, clones were purchased from OriGene Technologies, Inc. The product datasheet used for knocking down *H19* levels was the TL318197 *H19* Human shRNA Plasmid Kit (Locus ID 283120) including *H19*–Human, 4 unique 29mer shRNA constructs and a non-effective 29-mer scrambled shRNA cassette in pGFP-C-shLenti Vector, TR30021 (Non-effective control sequence: 5′ GCACTACCAGAGCTAACTCAGATAGTACT 3′). Regarding the TL318197 *H19* Human shRNA Plasmid Kit (Locus ID 283120) the clones that were able to KD the *H19* levels were the ones with the tube ID: TL318197C and TL318197D.

Statistical analysis

Normalized values were divided to the mean of each Control group and the relative to control ratios were plotted as

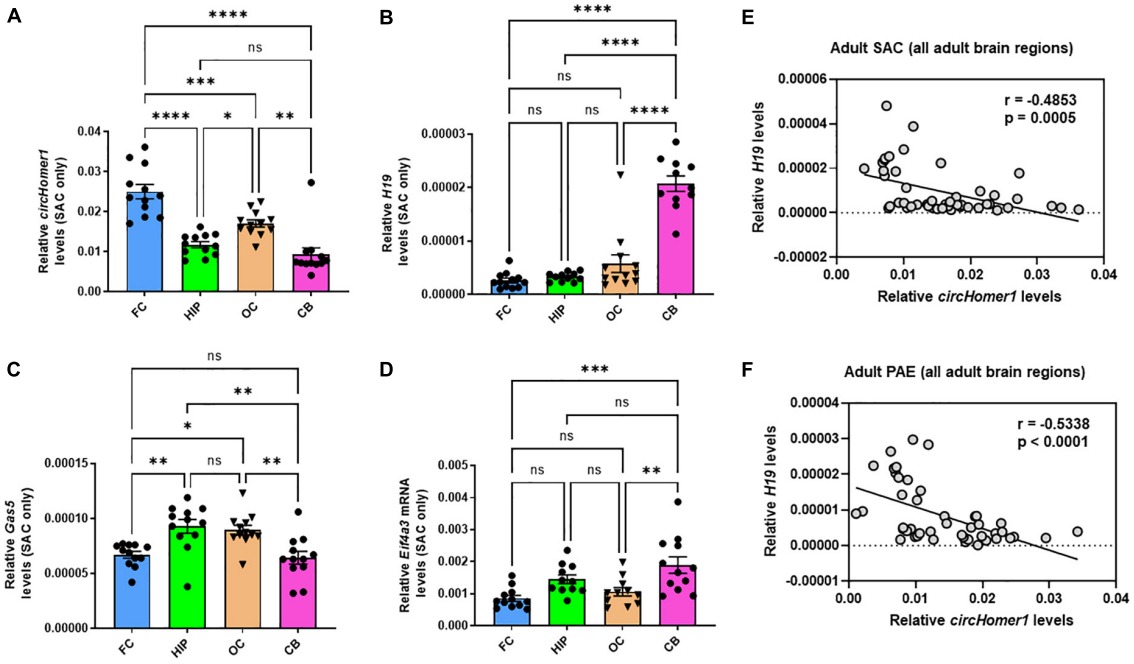


FIGURE 2
Brain region-specificity of *circhomer1*, *H19*, *Gas5,* and *Eif4a3* mRNA in four different adult brain regions. **(A–D)** Mean ± SEM relative *circHomer1* **(A)**, *H19* **(B)**, and Gas5 **(C)**, and *Eif4a3* mRNA **(D)** levels (normalized to 18S rRNA) in adult SAC frontal cortex (FC), hippocampus (HIP), occipital (OC), and cerebellum (CB). For *circHomer1* **(A)**: FC vs. HIP, $p < 0.0001$, q = 9.691, df = 44. For FC vs. OC, $p = 0.001$, q = 5.804, df = 44. For FC vs. CB, $p < 0.0001$, q = 11.49, df = 44. For HIP vs. OC, $p = 0.0414$, q = 3.888, df = 44. For HIP vs. CB, $p = 0.5840$, q = 1.802, df = 44. For OC vs. CB, $p = 0.0012$, q = 5.689, df = 44. For *H19* **(B)**: FC vs. HIP, $p < 0.0001$, q = 9.691, df = 44. For FC vs. OC, $p = 0.001$, q = 5.804, df = 44. For FC vs. CB, $p < 0.0001$, q = 11.49, df = 44. For HIP vs. OC, $p = 0.0414$, q = 3.888, df = 44. For HIP vs. CB, $p = 0.5840$, q = 1.802, df = 44. For OC vs. CB, $p = 0.0012$, q = 5.689, df = 44. For *H19* **(B)**: For FC vs. HIP, $p = 0.9743$, q = 0.5976, df = 42. For FC vs. OC, $p = 0.2030$, q = 2.833, df = 42. For FC vs. CB, $p < 0.0001$, q = 15.95, df = 42. For HIP vs. OC, $p = 0.4252$, q = 2.173, df = 42. For HIP vs. CB, $p < 0.0001$, q = 15.03, df = 42. For OC vs. CB, $p < 0.0001$, q = 13.18, df = 42. For *Gas5* **(C)**: For FC vs. HIP, $p = 0.0037$, q = 5.162, df = 44. For FC vs. OC, $p = 0.0143$, q = 4.479, df = 44. For FC vs. CB, $p = 0.9780$, q = 0.5662, df = 44. For HIP vs. OC, $p = 0.9625$, q = 0.6827, df = 44. For HIP vs. CB, $p = 0.0011$, q = 5.728, df = 44. For OC vs. CB, $p = 0.0047$, q = 5.046, df = 44. For *Eif4a3* **(D)**: For FC vs. HIP, $p = 0.0722$, q = 3.556, df = 42. For FC vs. OC, $p = 0.8258$, q = 1.215, df = 42. For FC vs. CB, $p = 0.0003$, q = 6.355, df = 42. For HIP vs. OC, $p = 0.3784$, q = 2.292, df = 42. For HIP vs. CB, $p = 0.2518$, q = 2.659, df = 42. For OC vs. CB, $p = 0.0054$, q = 5.000, df = 42. For **(A–D)** $^{*}p < 0.05$, $^{**}p < 0.01$, $^{***}p < 0.001$, $^{****}p < 0.0001$, based on one way ANOVA with *post-hoc* Tukey's multiple comparisons test. **(E,F)** Correlation between relative *circHomer1* and *H19* in all four brain regions of adult SAC **(E)** and PAE **(F)** mice. Spearman coefficient and two-tailed *p*-value is shown in the graph. Individual biological replicates are shown in each graph.

means ± S.E.M. using GraphPad Prism and after removing up to 2 outliers using Roots test (Graphpad Software, La Jolla, CA, USA). For the normality and log normality of the data sets, the following tests were conducted: Anderson-Darling, D'Agostino and Pearson and Shapiro–Wilk test. Due to the fact that the vast majority of datasets passed the tests for normal Gaussian distribution, one sample *t*-test was conducted for comparing two groups, while in the few cases where data showed a non-parametric distribution the Wilcoxon Signed Rank test was used instead. For comparisons involving more than two groups, a one-way Analysis of Variance (ANOVA) with Tukey's (comparison between all groups) or Dunnett's (comparisons vs. a single control group) for multiple comparisons for samples with normal distribution of data and Kruskal–Wallis test with Dunn's *post-hoc* correction for multiple comparisons was used for samples that did not display normal distribution. For comparisons comparing the effects of both treatment and sex, a two-way ANOVA with Šídák's multiple comparisons test was used. Outliers were identified based on Rout's test with Q = 1%. Spearman correlation coefficients and two-tailed *p*-values were calculated. Even though datasets were sampled from a Gaussian distribution, Spearman correlation was used due to the monotonic relationship of the variables and due to the more robust nature of this test for any outliers of the data set.

Results

Reductions in *circHomer1* in a mouse model of fetal alcohol spectrum disorder are sex- and brain-region specific

Using a well-established mouse model of moderate FASD (Brady et al., 2012; Paudel et al., 2020) in which adult female mice were given either a solution of 10% (w/v) ethanol and 0.066% (w/v) saccharin or just 0.066% (w/v) saccharin (SAC; control mice) for a total period of 4 h per day during mating and during the whole duration of their pregnancy, we had previously shown that prenatal ethanol exposure (PAE) can disturb the expression of circRNAs in a sex-specific manner in fetal brain (Paudel et al., 2020). In order to determine the long-term effects of PAE on postnatal brain circRNA expression, we used the same model of moderate PAE, but allowed SAC and PAE offspring to grow without any treatment into adulthood (P80-P90) and euthanized them to extract various brain regions of interest (frontal cortex, hippocampus, occipital cortex, cerebellum). We decided to focus on *circHomer1*, a brain-enriched circRNA previously shown to be associated with psychiatric and neurological disease, and known to regulate synaptic

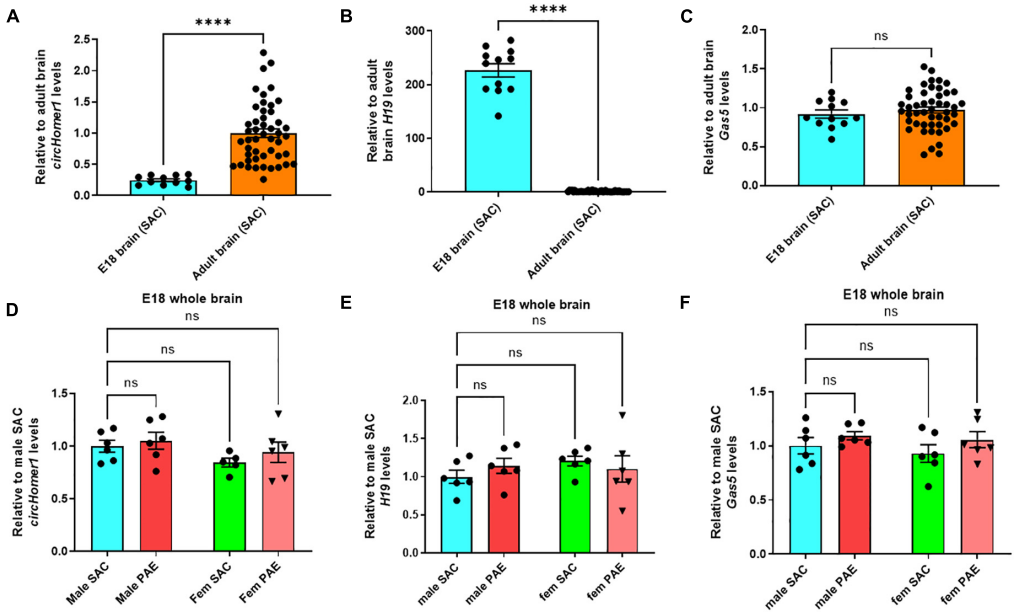


FIGURE 3
Developmental-specificity of *circhomer1*, *H19*, *Gas5* in control brain. **(A–C)** Mean ± SEM relative to adult brain *circHomer1* **(A)**, *H19* **(B)**, and *Gas5* **(C)** levels (normalized to 18S rRNA) in E18 whole brain and adult SAC brain (data from all four brain regions are included). For *circHomer1* **(A)**: $p < 0.0001$, $t = 33.77$, df = 10. For *H19* **(B)**: $p < 0.0001$, $t = 18.36$, df = 11. For *Gas5* **(C)**: $p = 0.15020$, $t = 1.547$, df = 11. For **(A–C)**: ****$p < 0.0001$ based on two-tailed one-sample *t*-test. Number of biological replicates shown in the graph. **(D–F)** Mean ± SEM relative to male SAC *circHomer1* **(D)**, *H19* **(E)**, and *Gas5* **(F)** levels (normalized to 18S rRNA) in E18 male and female (fem) PAE and SAC whole brain. For *circHomer1* **(D)**: $p = 0.8558$, $t = 0.5038$, df = 19 for male PAE vs. male SAC, and $p = 0.6115$, $t = 0.9052$, df = 19 for female PAE vs. female SAC. For *H19* **(E)**: $p = 0.6151$, $t = 0.8985$, df = 20 for male PAE vs. male SAC and $p = 0.7705$, $t = 0.6535$, df = 20 for female PAE vs. female SAC. For *Gas5* **(F)**: $p = 0.5839$, $t = 0.9471$, df = 20 for male PAE vs. male SAC and $p = 0.3797$, $t = 1.288$, df = 20 for female PAE vs. female SAC. For **(D–F)**, a two-way ANOVA corrected with Šídák's multiple comparisons test. Individual biological replicates are shown in each graph.

gene expression and cognitive function (Zimmerman et al., 2020; Hafez et al., 2022). In addition to the fact that *circHomer1* is a well-studied circRNA with important implications for neuronal function and behavior (Zimmerman et al., 2020; Hafez et al., 2022), we have previously demonstrated that down-regulation of *circHomer1* can impact the synaptic localization of numerous synaptic plasticity genes, including genes known to be implicated in FASD (Zimmerman et al., 2020; Hafez et al., 2022). Focusing on the changes in *circHomer1* levels in adult brain as a result of prenatal exposure to alcohol, we found that *circHomer1* was specifically reduced in male but not female adult frontal cortex and hippocampus (**Figures 1A, B**; two-way ANOVA with *post-hoc* Šídák's multiple comparisons test). However, no changes in *circHomer1* levels were observed in adult occipital cortex and cerebellum due to PAE (**Supplementary Figures 1A, B**). These data suggest that *circHomer1* is down-regulated in a brain region- and sex-specific manner in adult mouse brain as a result of prenatal exposure to alcohol.

Increased *H19* expression in male frontal cortex of mice prenatally-exposed to alcohol

We have previously shown that Eukaryotic initiation factor 4A-III (EIF4A3), an RNA-Binding protein (RBP) and component of the exon-junction complex known to be associated with circRNA biogenesis, can promote the expression of *circHomer1* (Hafez et al., 2022). Quantification of *Eif4a3* mRNA showed no significant changes in *Eif4a3* mRNA levels in response to PAE in male frontal cortex and hippocampus or the rest of the examined brain regions (**Figures 1C, D** and **Supplementary Figures 1C, D**; a 30% decrease in *Eif4a3* mRNA levels was found in male PAE hippocampus, but it did not reach statistical significance with ANOVA and *post-hoc* Šídák's multiple comparisons test). Thus, it is not likely, that changes in *Eif4a3* mRNA could be behind the significant down-regulation of *circHomer1* in adult male frontal cortex.

In order to identify additional genes that could modulate EIF4A3-mediated *circHomer1* biogenesis, we focused on the imprinted lncRNA *H19,* which has been previously shown to bind to EIF4A3 and obstruct its recruitment to downstream RNA targets (Han et al., 2016). Given that *H19* could potentially inhibit EIF4A3-mediated *circHomer1* biogenesis, we hypothesized that PAE-induced changes into *H19* expression might be opposite to what was observed for *circHomer1*. Focusing on changes in adult brain as a result of PAE, we found a more than 2.8-fold up-regulation in *H19* expression in male PAE adult frontal cortex (**Figure 1E**; based on ANOVA with *post-hoc* Šídák's multiple comparisons test). However, changes in *H19* expression in other adult brain regions in response to PAE were unremarkable (**Figure 1F** and **Supplementary Figures 1E, F**; a 48% non-significant increase in *H19* levels was seen in male PAE hippocampus). Of note, the expression of *Gas5* lncRNA, another lncRNA with potential relevance to PAE, also showed a modest up-regulation only in male PAE frontal cortex (**Supplementary Figures 2A–D**). We conclude that reduced *circHomer1* levels in adult male frontal cortex as a result of developmental exposure to alcohol are accompanied by significant increases in *H19* lncRNA expression.

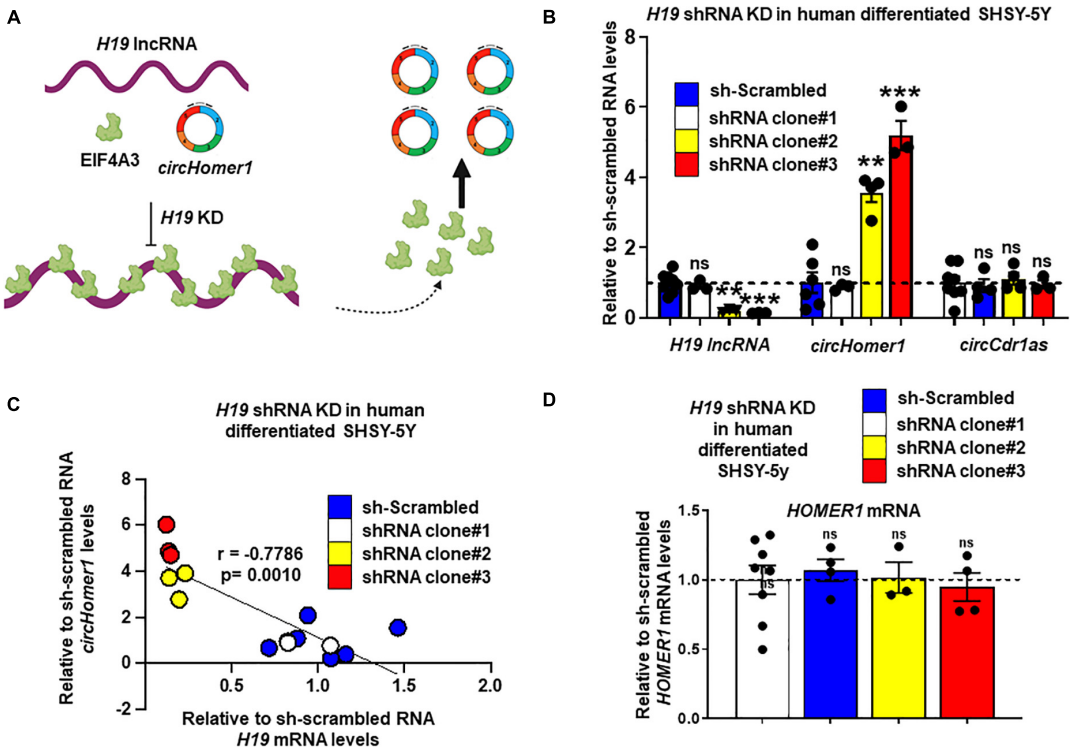


FIGURE 4
H19 knockdown increases *circHomer1* expression. **(A)** Proposed diagram depicting the hypothesized mechanism for *H19*/EIF4A3 regulation of *circHomer1* biogenesis. *H19* can bind and sequester EIF4A3, thus inhibiting EIF4A3-mediated *circHomer1* biogenesis. **(B)** Relative *H19*, *circHomer1*, and *circCDR1as* levels (based on qRT-PCR and normalized to *18s rRNA*) 48 h after shRNA-mediated knockdown of *H19* in human differentiated SH-SY5Y cells. Mean ± SEM. $^{**}p < 0.01$, $^{***}p < 0.001$, two-tailed one sample *t*-test relative to shRNA scrambled. For *H19* for clone 2: $p = 0.0011$, $t = 30.26$, df = 2. For *H19* for clone 3: $p < 0.0001$, $t = 116.7$, df = 2. For *circHomer1* for clone 2: $p = 0.0024$, $t = 9.612$, df = 3. For *circHomer1* for clone 3: $p = 0.0008$, $t = 14.09$, df = 3. **(C)** Correlation between relative sh-scrambled H19 and *circHomer1* levels following *H19* shRNA Knockdown in human differentiated SHSY-5Y. Spearman coefficient and two-tailed *p*-value is shown in the graph. **(D)** Relative to sh-scrambled *HOMER1* mRNA levels (based on qRT-PCR and normalized to 18s rRNA) 48 h after shRNA-mediated knockdown of *H19* in human differentiated SH-SY5Y cells. Mean ± SEM. For clone 2: $p = 0.8968$, $t = 0.1467$, df = 2. For clone 3: $p = 0.6432$, $t = 0.5132$, df = 3. Individual biological replicates are shown in each graph.

Opposing brain region- and developmental-specific changes in *H19* and *circHomer1* expression in mouse brain

Given the opposing changes in *circHomer1* and *H19* expression in the frontal cortex of adult male PAE mice, we decided to investigate whether the expression of *circHomer1* and *H19* could be displaying differential developmental- or brain region- specific changes in control mouse brains. Looking at the overall expression of *circHomer1* in frontal cortex, hippocampus, occipital cortex, and cerebellum of control SAC mice, we noticed that it was significantly enriched in adult frontal cortex (Figure 2A), a result which is consistent with previous findings in untreated mouse brain (Zimmerman et al., 2020). Expression of *circHomer1* was intermediate in adult occipital cortex and hippocampus, with the lowest levels detected in adult SAC cerebellum (Figure 2A). Previous studies have shown *H19* is a prenatal stage-enriched lncRNA important for embryogenesis (Poirier et al., 1991; Gabory et al., 2009; Li et al., 2019) and previously implicated in FASD (Marjonen et al., 2017, 2018; Bestry et al., 2022). However, its expression was still detectable in the adult brain in our control SAC brain samples, with higher levels in the cerebellum and lower expression in the adult frontal cortex (Figure 2B), which is the opposite of what was observed for *circHomer1*. On the other hand, Gas5 was expressed in comparable levels in frontal cortex and cerebellum, with a modest enrichment in hippocampus and occipital cortex (Figure 2C). Lastly, measuring the expression of *Eif4a3* mRNA, we found that it did not exhibit notable brain region-specific changes in control SAC adult brain, with an exception of a slightly higher expression in the cerebellum (Figure 2D). Comparing the brain region-specific expression of *circHomer1* to *H19* (Figure 2E) and *Gas5*, we found a significant inverse correlation between *circHomer1* and *H19* (Figure 2E), but not *circHomer1* and *Gas5* ($r = -0.1218$, $p = 0.4097$) in adult SAC brains. Of note, a negative correlation was also observed between *circHomer1* and *Eif4a3* across SAC brain regions ($r = -0.4260$, $p = 0.0032$). Interestingly, the negative correlation between *H19* and *circHomer1* between adult brain regions was also observed in PAE animals (Figure 2F).

We then compared their expression of *circHomer1* and *H19* and *Gas5* in adult frontal cortex, hippocampus, occipital cortex, and cerebellum of control SAC mice vs. E18 prenatal whole brain from SAC mice, in order to determine their developmental-specific expression in control animals. We found that *circHomer1* levels in control SAC mice were very low in the E18 brain, but robustly increased in the adult brain, with the highest expression in adult frontal cortex (Figure 3A), which is in accordance with previous findings in WT untreated mice (Zimmerman et al., 2020). Given that *H19* can inhibit EIF4A3-mediated *circHomer1* biogenesis, we hypothesized that developmental and PAE-induced changes into

H19 expression could potentially explain the observed changes in *circHomer1* expression during brain development. Our results showed that *H19* is significantly enriched in the prenatal brain of SAC control mice in comparison to adult brain (**Figure 3B**; close to 200-fold more *H19* found in prenatal brain), which is in accordance to previous literature suggesting that *H19* is a prenatal stage-enriched lncRNA important for embryogenesis (Poirier et al., 1991; Gabory et al., 2009; Li et al., 2019; Zhong et al., 2021). However, no changes were observed in Gas5 expression between E18 whole brain and adult brain (**Figure 3C**). Of note, looking at the PAE-induced changes in prenatal E18 whole brain, we found no significant effects on *circHomer1*, *H19, or Gas5* expression (**Figures 3D–F**). We conclude that changes in *circHomer1* expression during normal brain development and within different brain regions in the adult brain are inversely associated with *H19* expression and that PAE does not significantly impact their expression in E18 prenatal brain.

H19 can inhibit *circHomer1* biogenesis

Based on *in silico* analysis of RBP binding sites (Li et al., 2014), *H19* is predicted to have 17 different binding sites for EIF4A3. We hypothesized that direct binding of multiple EIF4A3 proteins on *H19*, would reduce the availability of EIF4A3 to promote *circHomer1* biogenesis (**Figure 4A**). In order to test this hypothesis, we utilized shRNA-mediated KD of *H19* in human differentiated SHSY-5Y cells. We used three different shRNAs against *H19* and extracted RNA for *circHomer1* and *H19* measurements *via* qRT-PCR after 2 days of shRNA treatment. Our results suggested that shRNA clones 2 and 3 resulted in a robust reduction in *H19*, whereas shRNA clone 1 was not efficient in knocking down *H19* (**Figure 4B**). Remarkably, *circHomer1* levels were unchanged following treatment with shRNA clone 1 but were robustly up-regulated after *H19* knockdown with shRNA clones 2 and 3 (**Figure 4B**). This effect was specific to *circHomer1* since no changes were seen in *circCDR1as* following *H19* knockdown (**Figure 4B**). Interestingly, relative *circHomer1* expression was found to be significantly inversely associated with *H19* levels (**Figure 4C**), further suggesting that the level of *H19* knockdown was inversely proportional to the up-regulation observed in *circHomer1* expression. However, no changes were seen in overall *HOMER1* mRNA levels in this experiment (**Figure 4D**).

Conclusion

Numerous studies have suggested the importance of circRNAs for brain development and function and their relevance for neurodevelopmental and psychiatric disorders (Lukiw, 2013; Mehta et al., 2020; Zimmerman et al., 2020; Li M. L. et al., 2021; Hafez et al., 2022). Our previous work uncovered circRNAs associated with neurogenesis and neuronal development that are altered in prenatal brain in a sex-specific manner as a result of PAE (Paudel et al., 2020). Moreover, additional research has suggested that circRNAs could be associated with the biological mechanisms underlying alcohol addiction or could serve as biomarkers of alcohol dependence (Liu et al., 2021; Vornholt et al., 2021). However, the role of circRNAs in the long-term effects of PAE and the mechanisms that could underlie PAE-associated changes in circRNA expression have not being adequately explored. Here we show evidence that *circHomer1*, an abundantly expressed circRNA in adult brain that has been previously linked to cognitive function and psychiatric disorders (Zimmerman et al., 2020; Hafez et al., 2022), is significantly down-regulated in the frontal cortex and hippocampus of adult male but not female mice prenatally exposed to alcohol. Moreover, we demonstrate that *H19*, an imprinted lncRNA known to inhibit the function of an RBP capable of promoting *circHomer1* biogenesis, is significantly up-regulated in male adult frontal cortex and displays a developmental- and brain region-specific expression that is opposite to what is observed for *circHomer1*. Lastly, we show that knockdown of H19 results in a significant up-regulation of *circHomer1* in human glioblastoma cell lines. Taken together our results, uncover a novel antagonistic interaction between a circRNA and a lncRNA with potential relevance to brain development and FASD.

Previous work from our lab and others have suggested that *circHomer1* is an activity-dependent, postnatal brain-enriched circRNA, that can significantly affect synaptic gene expression, *Homer1* mRNA isoform synaptic localization, neuronal activity, and frontal cortex-mediated cognitive flexibility (Giorgi et al., 2007; Venø et al., 2015; Zimmerman et al., 2022). Moreover, changes in *circHomer1* expression have been reported in numerous psychiatric and neurological disorders (Dube et al., 2019; Zimmerman et al., 2020; Hafez et al., 2022). We recently showed that EIF4A3, an RBP associated with the exon junction complex, binds to *circHomer1* and is a potent positive regulator for its biogenesis (Hafez et al., 2022). We also demonstrated that both *circHomer1* and *Eif4a3* are experience-dependent in the frontal cortex and appear to be positively correlated in mouse and human frontal cortex (Hafez et al., 2022). However, in this current study we found that PAE induces a significant down-regulation in the expression of *circHomer1* in adult male frontal cortex without any changes in *Eif4a3* mRNA expression; thus making it unlikely that such changes in *circHomer1* levels are a result of a transcriptional increase in *Eif4a3* expression. Looking at potential regulators of EIF4A3 activity, however, we were able to find a robust up-regulation in male PAE frontal cortex in the expression of *H19*, a lncRNA that we also found to have a strong inhibitory effect in *circHomer1* expression. Given the previous report that *H19* can bind to EIF4A3 protein and sequester it from binding to its RNA targets, it is tempting to hypothesize, that an up-regulation in *H19* levels could result in reduced EIF4A3-mediated *circHomer1* synthesis. The fact that the developmental and brain region-specific expression of *circHomer1* and *H19* appeared to be inversely associated further supports the potential of an inhibitory interaction between these important ncRNAs. Furthermore, given the robust developmental down-regulation of *H19* in the postnatal brain, it is tempting to hypothesize that PAE could delay or reduce this normal developmental decrease in *H19* expression *via* potential epigenetic mechanisms such as DNA methylation. This in turn could result in relatively higher levels of *H19*, which can in turn down-regulate *circHomer1* expression in adult animals following PAE. However, additional research will be needed to further explore such a potential mechanism, especially given the many reported mechanisms of action for H19 (Bestry et al., 2022). Moreover, the modest increases in *H19* and reductions in *Eif4a3* mRNA observed in adult male hippocampus as a result of PAE were not significant, thus allowing for other potential mechanisms to explain the observed changes in *circHomer1* in this brain region.

One important limitation of our work is that our data were limited to E18 and adult stages of development, so that we were not able to properly access the exact developmental trajectories

in gene expression that could have resulted from prenatal alcohol exposure. Moreover, our experiment using knockdown of *H19* was conducted in human neuroblastoma cell lines and was not replicated in mouse neuronal cultures or *in vivo*. On a similar note, our measurements of *H19* levels in adult mouse brains displayed high overall variability due to the low expression of this lncRNA in adult stages of development. It is worth mentioning that cessation of alcohol exposure in our mouse model of FASD was after birth, since dams were exposed to alcohol during breeding and gestation. As a result, do not believe that our observed effects in gene expression in adult mouse brains are likely to be a result of withdrawal given the prolonged time from cessation of alcohol exposure. Furthermore, our previous work identified numerous genes involved in synaptic plasticity with potential relevance to FASD to be up-regulated within synaptosomes following *in vivo* knockdown of *circHomer1* in the frontal cortex (Zimmerman et al., 2020). Among these genes, were Glutamate [NMDA] receptor subunit epsilon-2 (*Glun2*), Fragile X Messenger Ribonucleoprotein 1 (*Fmr1*), Sodium channel protein type 1 subunit alpha (*Scn1a*), Neurexin 1 (*Nrxn1*), and cAMP response element-binding protein (*Creb*) (Zimmerman et al., 2020). Therefore, future work is needed to identify whether PAE-mediated changes in *circHomer1* in adult brain could be involved in the dysregulation of synaptic gene expression.

Previous work has uncovered sex-specific effect of PAE in brain and other tissues (Weinberg et al., 2008; Terasaki et al., 2016; Loke et al., 2018; Bake et al., 2021). On a similar note, our previous study revealed that circRNAs are altered in a sex-specific manner in E18 prenatal brain following PAE (Paudel et al., 2020). Interestingly, *H19* has been reported to have sex-specific expression and to be differentially affected by estrogen and androgen treatment (Sun et al., 2015; Basak et al., 2018; Ozgur and Gezer, 2020; Li T. et al., 2021). Moreover, *H19* has been previously linked with changes in head circumference in FASD and reported to be epigenetically altered in various tissues (Marjonen et al., 2017, 2018; Bestry et al., 2022). Taken together, this allows us to hypothesize that PAE could induce epigenetic changes in the *H19* locus in a sex-specific manner, which could result in opposing changes in *circHomer1* expression. However, new research is needed to potentially account for the brain region-specific effects observed in *H19 and circHomer1* expression as a result of PAE.

Regardless of the exact mechanism underlying the inhibitory effect of *H19* on *circHomer1*, it is also worth mentioning that our findings are the first to uncover such an antagonist effect between a lncRNA and a circRNA in the brain. Based on our data this inhibitory effect of *H19* on *circHomer1* expression, could potentially be important for normal brain development and maturation, as well as the control of brain region-specific expression for *circHomer1*. Given the link of *circHomer1* with additional neuropsychiatric disorders (Zimmerman et al., 2020; Hafez et al., 2022), and the increased prevalence of neuropsychiatric disturbances in patients with FASD, it would be interesting to further dissect the interaction between *H19* and *circHomer1*, and mechanistically study its relevance to brain development, function, disease.

Data availability statement

The original contributions presented in the study are included in the article/**Supplementary material**, further inquiries can be directed to the corresponding author/s.

Ethics statement

The animal study was reviewed and approved by University of New Mexico Health Sciences Center Institutional Animal Care and Use Committee.

Author contributions

NM and GP conceived the hypothesis, designed and conducted the experiments, analyzed the data, and wrote the manuscript. AA and KC designed and conducted the experiments. All authors conducted the experiments and analyzed the data and helped with manuscript preparation.

Funding

This work was supported by a NIAAA P50 Grant (2P50AA022534-06 to AA, KKC, and NM), and a mentored PI grant as part of a P20 Grant from the NIGMS (1P20GM121176-01 to NM and SA). This work was also supported in part by Dedicated Health Research Funds from the University of New Mexico School of Medicine (NM).

Acknowledgments

We would like to thank Dr. Fernando Valenzuela for useful advice and feedback.

Conflict of interest

NM has a financial interest in Circular Genomics Inc., a company focused on the use of circRNAs as biomarkers for psychiatric disorders.

The remaining authors declare that the research was conducted in the absence of any commercial or financial relationships that could be construed as a potential conflict of interest.

Publisher's note

All claims expressed in this article are solely those of the authors and do not necessarily represent those of their affiliated organizations, or those of the publisher, the editors and the reviewers. Any product that may be evaluated in this article, or claim that may be made by its manufacturer, is not guaranteed or endorsed by the publisher.

Supplementary material

The Supplementary Material for this article can be found online at: https://www.frontiersin.org/articles/10.3389/fnins.2023.1087950/full#supplementary-material

References

Bake, S., Pinson, M. R., Pandey, S., Chambers, J. P., Mota, R., Fairchild, A. E., et al. (2021). Prenatal alcohol-induced sex differences in immune, metabolic and neurobehavioral outcomes in adult rats. *Brain. Behav. Immun.* 98, 86–100. doi: 10.1016/j.bbi.2021.08.207

Basak, P., Chatterjee, S., Bhat, V., Su, A., Jin, H., Lee-Wing, V., et al. (2018). Long non-coding RNA H19 acts as an estrogen receptor modulator that is required for endocrine therapy resistance in ER+ breast cancer cells. *Cell. Physiol. Biochem. Int. J. Exp. Cell. Physiol. Biochem. Pharmacol.* 51, 1518–1532. doi: 10.1159/000495643

Bestry, M., Symons, M., Larcombe, A., Muggli, E., Craig, J. M., Hutchinson, D., et al. (2022). Association of prenatal alcohol exposure with offspring DNA methylation in mammals: A systematic review of the evidence. *Clin. Epigenetics* 14:12. doi: 10.1186/s13148-022-01231-9

Brady, M. L., Allan, A. M., and Caldwell, K. K. (2012). A limited access mouse model of prenatal alcohol exposure that produces long-lasting deficits in hippocampal-dependent learning and memory. *Alcohol. Clin. Exp. Res.* 36, 457–466. doi: 10.1111/j.1530-0277.2011.01644.x

Bu, Q., Long, H., Shao, X., Gu, H., Kong, J., Luo, L., et al. (2019). Cocaine induces differential circular RNA expression in striatum. *Transl. Psychiatry* 9:199. doi: 10.1038/s41398-019-0527-1

Carter, R. C., Jacobson, J. L., Molteno, C. D., Dodge, N. C., Meintjes, E. M., and Jacobson, S. W. (2016). Fetal alcohol growth restriction and cognitive impairment. *Pediatrics* 138:e20160775. doi: 10.1542/peds.2016-0775

Chudley, A. E., Conry, J., Cook, J. L., Loock, C., Rosales, T., LeBlanc, N., et al. (2005). Fetal alcohol spectrum disorder: Canadian guidelines for diagnosis. *CMAJ Can. Med. Assoc. J.* 172, S1–S21. doi: 10.1503/cmaj.1040302

Dang, Y., Yan, L., Hu, B., Fan, X., Ren, Y., Li, R., et al. (2016). Tracing the expression of circular RNAs in human pre-implantation embryos. *Genome Biol.* 17:130. doi: 10.1186/s13059-016-0991-3

Dube, U., Del-Aguila, J. L., Li, Z., Budde, J. P., Jiang, S., Hsu, S., et al. (2019). An atlas of cortical circular RNA expression in Alzheimer disease brains demonstrates clinical and pathological associations. *Nat. Neurosci.* 22, 1903–1912. doi: 10.1038/s41593-019-0501-5

Enuka, Y., Lauriola, M., Feldman, M. E., Sas-Chen, A., Ulitsky, I., and Yarden, Y. (2016). Circular RNAs are long-lived and display only minimal early alterations in response to a growth factor. *Nucleic Acids Res.* 44, 1370–1383. doi: 10.1093/nar/gkv1367

Gabory, A., Ripoche, M., Digarcher, A. L., Watrin, F., Ziyyat, A., Forné, T., et al. (2009). H19 acts as a trans regulator of the imprinted gene network controlling growth in mice. *Dev. Camb. Engl.* 136, 3413–3421. doi: 10.1242/dev.036061

Giorgi, C., Yeo, G. W., Stone, M. E., Katz, D. B., Burge, C., Turrigiano, G., et al. (2007). The EJC factor eIF4AIII modulates synaptic strength and neuronal protein expression. *Cell* 130, 179–191. doi: 10.1016/j.cell.2007.05.028

Gokool, A., Anwar, F., and Voineagu, I. (2020). The landscape of circular RNA expression in the human brain. *Biol. Psychiatry* 87, 294–304. doi: 10.1016/j.biopsych.2019.07.029

Hafez, A. K., Zimmerman, A. J., Papageorgiou, G., Chandrasekaran, J., Amoah, S. K., Lin, R., et al. (2022). A bidirectional competitive interaction between circHomer1 and Homer1b within the orbitofrontal cortex regulates reversal learning. *Cell Rep.* 38:110282. doi: 10.1016/j.celrep.2021.110282

Han, D., Gao, X., Wang, M., Qiao, Y., Xu, Y., Yang, J., et al. (2016). Long noncoding RNA H19 indicates a poor prognosis of colorectal cancer and promotes tumor growth by recruiting and binding to eIF4A3. *Oncotarget* 7, 22159–22173. doi: 10.18632/oncotarget.8063

Ibáñez, F., Ureña-Peralta, J. R., Costa-Alba, P., Torres, J., Laso, F., Marcos, M., et al. (2020). Circulating MicroRNAs in extracellular vesicles as potential biomarkers of alcohol-induced neuroinflammation in adolescence: Gender differences. *Int. J. Mol. Sci.* 21:6730. doi: 10.3390/ijms21186730

Jeck, W. R., Sorrentino, J. A., Wang, K., Slevin, M. K., Burd, C. E., Liu, J., et al. (2013). Circular RNAs are abundant, conserved, and associated with ALU repeats. *RNA N. Y.* 19, 141–157. doi: 10.1261/rna.035667.112

Kaminen-Ahola, N. (2020). Fetal alcohol spectrum disorders: Genetic and epigenetic mechanisms. *Prenat. Diagn.* 40, 1185–1192. doi: 10.1002/pd.5731

Li, J.-H., Liu, S., Zhou, H., Qu, L.-H., and Yang, J.-H. (2014). starBase v2.0: Decoding miRNA-ceRNA, miRNA-ncRNA and protein-RNA interaction networks from large-scale CLIP-Seq data. *Nucleic Acids Res.* 42, D92–D97. doi: 10.1093/nar/gkt1248

Li, L., Zhuang, Y., Zhao, X., and Li, X. (2019). Long non-coding RNA in neuronal development and neurological disorders. *Front. Genet.* 9:744. doi: 10.3389/fgene.2018.00744

Li, M. L., Wang, W., and Jin, Z.-B. (2021). Circular RNAs in the central nervous system. *Front. Mol. Biosci.* 8:629593. doi: 10.3389/fmolb.2021.629593

Li, T., Jiang, H., Li, Y., Zhao, X., and Ding, H. (2021). Estrogen promotes lncRNA H19 expression to regulate osteogenic differentiation of BMSCs and reduce osteoporosis via miR-532-3p/SIRT1 axis. *Mol. Cell. Endocrinol.* 527:111171. doi: 10.1016/j.mce.2021.111171

Liu, Y., Li, J., Bu, H., Wang, H., Zhang, Y., Shen, Q., et al. (2021). Circular RNA expression alteration identifies a novel circulating biomarker in serum exosomal for detection of alcohol dependence. *Addict. Biol.* 26:e13031. doi: 10.1111/adb.13031

Loke, Y. J., Muggli, E., Nguyen, L., Ryan, J., Saffery, R., Elliott, E. J., et al. (2018). Time- and sex-dependent associations between prenatal alcohol exposure and placental global DNA methylation. *Epigenomics* 10, 981–991. doi: 10.2217/epi-2017-0147

Lukiw, W. J. (2013). Circular RNA (circRNA) in Alzheimer's disease (AD). *Front. Genet.* 4:307. doi: 10.3389/fgene.2013.00307

Mahnke, A. H., Adams, A. M., Wang, A. Z., and Miranda, R. C. (2019). Toxicant and teratogenic effects of prenatal alcohol. *Curr. Opin. Toxicol.* 14, 29–34. doi: 10.1016/j.cotox.2019.08.002

Mahnke, A. H., Salem, N. A., Tseng, A. M., Chung, D. D., and Miranda, R. C. (2018). Nonprotein-coding RNAs in Fetal Alcohol Spectrum Disorders. *Prog. Mol. Biol. Transl. Sci.* 157, 299–342. doi: 10.1016/bs.pmbts.2017.11.024

Mao, H., McMahon, J. J., Tsai, Y. H., Wang, Z., and Silver, D. L. (2016). Haploinsufficiency for core exon junction complex components disrupts embryonic neurogenesis and causes p53-mediated microcephaly. *PLoS Genet.* 12:e1006282. doi: 10.1371/journal.pgen.1006282

Marjonen, H., Kahila, H., and Kaminen-Ahola, N. (2017). rs10732516 polymorphism at the IGF2/H19 locus associates with a genotype-specific trend in placental DNA methylation and head circumference of prenatally alcohol-exposed newborns. *Hum. Reprod. Open* 2017:hox014. doi: 10.1093/hropen/hox014

Marjonen, H., Toivonen, M., Lahti, L., and Kaminen-Ahola, N. (2018). Early prenatal alcohol exposure alters imprinted gene expression in placenta and embryo in a mouse model. *PLoS One* 13:e0197461. doi: 10.1371/journal.pone.0197461

Marquardt, K., Cavanagh, J. F., and Brigman, J. L. (2020). Alcohol exposure in utero disrupts cortico-striatal coordination required for behavioral flexibility. *Neuropharmacology* 162:107832. doi: 10.1016/j.neuropharm.2019.107832

Mehta, S. L., Dempsey, R. J., and Vemuganti, R. (2020). Role of circular RNAs in brain development and CNS diseases. *Prog. Neurobiol.* 186:101746. doi: 10.1016/j.pneurobio.2020.101746

Memczak, S., Jens, M., Elefsinioti, A., Torti, F., Krueger, J., Rybak, A., et al. (2013). Circular RNAs are a large class of animal RNAs with regulatory potency. *Nature* 495, 333–338. doi: 10.1038/nature11928

Ozgur, E., and Gezer, U. (2020). Investigation of lncRNA H19 in prostate cancer cells and secreted exosomes upon androgen stimulation or androgen receptor blockage. *Bratisl. Lek. Listy* 121, 362–365. doi: 10.4149/BLL_2020_058

Pappalardo-Carter, D. L., Balaraman, S., Sathyan, P., Carter, E. S., Chen, W. A., and Miranda, R. C. (2013). Suppression and epigenetic regulation of miR-9 contributes to ethanol teratology: Evidence from zebrafish and murine fetal neural stem cell models. *Alcohol. Clin. Exp. Res.* 37, 1657–1667. doi: 10.1111/acer.12139

Paudel, P., Pierotti, C., Lozano, E., Amoah, S. K., Gardiner, A. S., Caldwell, K. K., et al. (2020). Prenatal alcohol exposure results in sex-specific alterations in circular rna expression in the developing mouse brain. *Front. Neurosci.* 14:1165. doi: 10.3389/fnins.2020.581895

Poirier, F., Chan, C. T., Timmons, P. M., Robertson, E. J., Evans, M. J., and Rigby, P. W. (1991). The murine H19 gene is activated during embryonic stem cell differentiation in vitro and at the time of implantation in the developing embryo. *Dev. Camb. Engl.* 113, 1105–1114. doi: 10.1242/dev.113.4.1105

Popova, S., Lange, S., Bekmuradov, D., Mihic, A., and Rehm, J. (2011). Fetal alcohol spectrum disorder prevalence estimates in correctional systems: A systematic literature review. *Can. J. Public Health Rev. Can. Santé Publique* 102, 336–340. doi: 10.1007/BF03404172

Rybak-Wolf, A., Stottmeister, C., Glažar, P., Jens, M., Pino, N., Giusti, S., et al. (2015). Circular RNAs in the mammalian brain are highly abundant, conserved, and dynamically expressed. *Mol. Cell* 58, 870–885. doi: 10.1016/j.molcel.2015.03.027

Sathyan, P., Golden, H. B., and Miranda, R. C. (2007). Competing interactions between Micro-RNAs determine neural progenitor survival and proliferation after ethanol exposure: Evidence from an Ex vivo model of the fetal cerebral cortical neuroepithelium. *J. Neurosci.* 27, 8546–8557. doi: 10.1523/JNEUROSCI.1269-07.2007

Suenkel, C., Cavalli, D., Massalini, S., Calegari, F., and Rajewsky, N. (2020). A highly conserved circular RNA Is required to keep neural cells in a progenitor state in the mammalian brain. *Cell Rep.* 30, 2170–2179.e5. doi: 10.1016/j.celrep.2020.01.083

Sun, H., Wang, G., Peng, Y., Zeng, Y., Zhu, Q., Li, T., et al. (2015). H19 lncRNA mediates 17β-estradiol-induced cell proliferation in MCF-7 breast cancer cells. *Oncol. Rep.* 33, 3045–3052. doi: 10.3892/or.2015.3899

Szabo, L., Morey, R., Palpant, N. J., Wang, P. L., Afari, N., Jiang, C., et al. (2015). Statistically based splicing detection reveals neural enrichment and tissue-specific induction of circular RNA during human fetal development. *Genome Biol.* 16:126. doi: 10.1186/s13059-015-0690-5

Terasaki, L. S., Gomez, J., and Schwarz, J. M. (2016). An examination of sex differences in the effects of early-life opiate and alcohol exposure. *Philos. Trans. R. Soc. Lond. B. Biol. Sci.* 371:20150123. doi: 10.1098/rstb.2015.0123

Valenzuela, C. F., Morton, R. A., Diaz, M. R., and Topper, L. (2012). Does moderate drinking harm the fetal brain? Insights from animal models. *Trends Neurosci.* 35, 284–292. doi: 10.1016/j.tins.2012.01.006

Venø, M. T., Hansen, T. B., Venø, S. T., Clausen, B. H., Grebing, M., Finsen, B., et al. (2015). Spatio-temporal regulation of circular RNA expression during porcine embryonic brain development. *Genome Biol.* 16:245. doi: 10.1186/s13059-015-0801-3

Vornholt, E., Drake, J., Mamdani, M., McMichael, G., Taylor, Z. N., Bacanu, S., et al. (2021). Identifying a novel biological mechanism for alcohol addiction associated with circRNA networks acting as potential miRNA sponges. *Addict. Biol.* 26:e13071. doi: 10.1111/adb.13071

Weinberg, J., Sliwowska, J. H., Lan, N., and Hellemans, K. G. C. (2008). Prenatal alcohol exposure: Foetal programming, the hypothalamic-pituitary-adrenal axis and sex differences in outcome. *J. Neuroendocrinol.* 20, 470–488.

You, X., Vlatkovic, I., Babic, A., Will, T., Epstein, I., Tushev, G., et al. (2015). Neural circular RNAs are derived from synaptic genes and regulated by development and plasticity. *Nat. Neurosci.* 18, 603–610. doi: 10.1038/nn.3975

Zhong, L., Liu, P., Fan, J., and Luo, Y. (2021). Long non-coding RNA H19: Physiological functions and involvements in central nervous system disorders. *Neurochem. Int.* 148:105072. doi: 10.1007/978-1-0716-1697-0

Zimmerman, A. J., Hafez, A. K., Amoah, S. K., Rodriguez, B. A., Dell'Orco, M., Lozano, E., et al. (2020). A psychiatric disease-related circular RNA controls synaptic gene expression and cognition. *Mol. Psychiatry* 25, 2712–2727. doi: 10.1038/s41380-020-0653-4

Zimmerman, A., Weick, J., Papageorgiou, G., Mellios, N., and Brigman, J. (2022). Knockdown of circHomer1 in the orbitofrontal cortex results in differential encoding of salient stimuli. *Res. Sq.* [Preprint]. doi: 10.21203/rs.3.rs-1862282/v2

frontiers | Frontiers in Neuroscience

TYPE Original Research
PUBLISHED 16 March 2023
DOI 10.3389/fnins.2023.1154637

Check for updates

OPEN ACCESS

EDITED BY
Carlos Fernando Valenzuela,
The University of New Mexico, United States

REVIEWED BY
Tou Yia Vue,
The University of New Mexico Health Sciences Center, United States
J. N. Reynolds,
Queen's University, Canada

*CORRESPONDENCE
Paul D. Drew
✉ drewpauld@uams.edu

SPECIALTY SECTION
This article was submitted to Neurodevelopment, a section of the journal Frontiers in Neuroscience

RECEIVED 30 January 2023
ACCEPTED 27 February 2023
PUBLISHED 16 March 2023

CITATION
Holloway KN, Douglas JC, Rafferty TM, Majewska AK, Kane CJM and Drew PD (2023) Ethanol-induced cerebellar transcriptomic changes in a postnatal model of fetal alcohol spectrum disorders: Focus on disease onset. *Front. Neurosci.* 17:1154637. doi: 10.3389/fnins.2023.1154637

COPYRIGHT
© 2023 Holloway, Douglas, Rafferty, Majewska, Kane and Drew. This is an open-access article distributed under the terms of the Creative Commons Attribution License (CC BY). The use, distribution or reproduction in other forums is permitted, provided the original author(s) and the copyright owner(s) are credited and that the original publication in this journal is cited, in accordance with accepted academic practice. No use, distribution or reproduction is permitted which does not comply with these terms.

Ethanol-induced cerebellar transcriptomic changes in a postnatal model of fetal alcohol spectrum disorders: Focus on disease onset

Kalee N. Holloway[1], James C. Douglas[1], Tonya M. Rafferty[1], Ania K. Majewska[2], Cynthia J. M. Kane[1] and Paul D. Drew[1,3]*

[1]Department of Neurobiology and Developmental Sciences, University of Arkansas for Medical Sciences, Little Rock, AR, United States, [2]Department of Neuroscience, University of Rochester Medical Center, Rochester, NY, United States, [3]Department of Neurology, University of Arkansas for Medical Sciences, Little Rock, AR, United States

Fetal alcohol spectrum disorders (FASD) are a group of neurodevelopmental disorders caused by ethanol exposure *in utero*, which can result in neurocognitive and behavioral impairments, growth defects, and craniofacial anomalies. FASD affects up to 1-5% of school-aged children in the United States, and there is currently no cure. The underlying mechanisms involved in ethanol teratogenesis remain elusive and need greater understanding to develop and implement effective therapies. Using a third trimester human equivalent postnatal mouse model of FASD, we evaluate the transcriptomic changes induced by ethanol exposure in the cerebellum on P5 and P6, after only 1 or 2 days of ethanol exposure, with the goal of shedding light on the transcriptomic changes induced early during the onset and development of FASD. We have highlighted key pathways and cellular functions altered by ethanol exposure, which include pathways related to immune function and cytokine signaling as well as the cell cycle. Additionally, we found that ethanol exposure resulted in an increase in transcripts associated with a neurodegenerative microglia phenotype, and acute- and pan-injury reactive astrocyte phenotypes. Mixed effects on oligodendrocyte lineage cell associated transcripts and cell cycle associated transcripts were observed. These studies help to elucidate the underlying mechanisms that may be involved with the onset of FASD and provide further insights that may aid in identifying novel targets for interventions and therapeutics.

KEYWORDS

FASD, microglia, astrocytes, oligodendrocytes, transcriptomics

Introduction

Fetal Alcohol Spectrum Disorders (FASD) are a leading cause of preventable developmental abnormalities around the world, and result in a range of clinical outcomes that can include craniofacial anomalies, neurological malformations, cognitive and behavioral impairment, and growth defects (Hoyme et al., 2016). FASD are not only

devastating to affected individuals, but also have significant economic impact globally (Greenmyer et al., 2018; Sokol, 2018). The global prevalence of FASD varies by region, with a mean of 0.8 percent (Lange et al., 2017). The prevalence has been estimated to be as high as 1-5 percent of school age children in the United States (May et al., 2018). There is no cure for FASD, and elucidation of the underlying mechanisms which regulate development of these disorders is needed to generate effective therapies.

Fetal ethanol exposure can induce neuropathology in multiple brain regions, including the cerebellum. Human studies have demonstrated cerebellar susceptibility to ethanol exposure during development, including diminished cerebellar volume and white matter abnormalities, which likely contribute to impaired motor coordination, and learning and memory deficits often found in individuals with FASD (Riley and McGee, 2005; Lebel et al., 2008; Norman et al., 2009).

Rodent models of FASD have been valuable in studying fetal ethanol exposure. In mice for instance, the first two postnatal weeks coincide with the third trimester of human gestation (Clancy et al., 2001), a critical period for cerebellar development. During this time the cerebellum undergoes a period of secondary neurogenesis, cell migration, and synaptogenesis. This period also exhibits oligodendrocyte maturation and myelination (Rice and Barone, 2000; Camarillo and Miranda, 2007; Wilhelm and Guizzetti, 2016). Rodent studies using third trimester equivalent ethanol exposure paradigms have shown ethanol-induced cerebellar alterations associated with activation of both astrocytes and microglia. The activation states of these cells can affect their overall function, including changes in expression of pro-inflammatory molecules, suggesting ethanol-induced cerebellar neuroinflammation could be associated with FASD (Kane et al., 2011; Drew et al., 2015; Topper et al., 2015).

In recent years, RNA sequencing (RNAseq) has become more readily accessible and cost efficient making it a highly effective tool to assess ethanol-induced transcriptomic changes in the CNS (Farris and Mayfield, 2014; Berres et al., 2017; Erickson et al., 2019; Pinson et al., 2021). Using our neonatal model of FASD, in which mice were treated with ethanol on postnatal days (P) 4-9 and tissues harvested on P10, we recently reported that ethanol stimulated transcriptomic changes associated with cell cycle and microglia regulation, and oligodendrocyte lineages in the cerebellum (Pinson et al., 2021). In the current studies, we evaluated ethanol-induced transcriptomic changes in the cerebellum on postnatal days 5 and 6 in this FASD model. These findings may provide further insight into the underlying mechanisms associated with the early onset of FASD as well as identifying potential targets for clinical interventions and therapeutics.

Materials and methods

Animals

C57BL/6J mice were purchased from The Jackson Laboratory (Bar Harbor, ME; stock #000664) and housed in the federally approved Division of Laboratory Animal Medicine facility at the University of Arkansas for Medical Sciences (UAMS) where an in-house breeding colony was established to produce experimental animals. All animal use protocols were reviewed and approved by the UAMS Institutional Animal Care and Use Committee. Individually housed pregnant dams were kept on a 10:14 hour light:dark cycle in static cages on an open-air rack and were checked twice daily for birth of pups, with postnatal day 0 (P0) being designated as the day of birth. Cages were changed weekly or as needed. Dams were allowed unlimited access to food and water for the duration of the experiments. Experimental litters contained 4-8 neonates that were distributed among treatment groups, Ethanol (E) or vehicle Control (C) and were separated according to sex as evenly as possible for each individual litter. Handled-only, untreated Control animals were not included in this study, based on no difference for analogous endpoints from previous studies (Kane et al., 2011; Drew et al., 2015). On P4-5, Ethanol treated animals were administered 4 g/kg/day of ethanol in 20% intralipid (Fresenius Kabi, Uppsala, Sweden) while Control animals received 20% intralipid in which ethanol was substituted with an equal volume of water. Ethanol and water were administered via intragastric gavage. On P5 or P6, 24 hours after the last ethanol treatment on P4 or P5, respectively, animals were anesthetized using isoflurane vapor and transcardially perfused with phosphate-buffered saline containing 5 U/mL heparin. The brain was removed, the cerebellum was microdissected, flash-frozen in liquid nitrogen, and stored at −80°C until used for RNA isolation and subsequent sequencing. 1 male and 1 female Control, and 1 male and 1 female Ethanol were randomly selected from each of 3 litters for sequencing on P5 and P6 (N = 6 total litters, 3 male/3 female per treatment group, per timepoint). To determine mean Blood Ethanol Concentration (BEC), 3 separate litters were treated with ethanol as described above and blood was collected from half of each litter on either P4 or P5, 90 minutes after ethanol administration. Briefly, animals were anesthetized using isoflurane vapor and trunk blood was collected in heparinized capillary tubes following decapitation. Blood was centrifuged at 4000 RPM for 5 minutes and serum was removed for BEC determination using an Analox AM1 alcohol analyzer (Analox Technologies USA, Atlanta, GA) and companion Alcohol Reagent Kit (Analox #GMRD-113) according to manufacturer specifications. P4 mean BEC was 324.6 mg/dL ± 7.2 mg/dL SEM, ($n = 7$ male, 4 female) and P5 mean BEC was 333.7 mg/dL ± 12.6 mg/dL SEM, ($n = 7$ male, 5 female).

Isolation of RNA, RNA-seq library preparation, and sequencing

Frozen cerebellar tissues were rapidly thawed and homogenized in Qiazol with 0.5 mm glass beads (Qiagen #13116-50) in a PowerLyzer 24 homogenizer (Qiagen #13155) for 30s at 3500 rpm. Total RNA was isolated using an miRNeasy Mini kit (Qiagen #217084) and DNA was removed with on-column DNase1 digestion (Qiagen #79254) following manufacturer protocol (Qiagen, Valencia, CA). RNA quantity was evaluated using the Qubit 3.0 fluorometer with the Qubit Broad-Range RNA Assay kit (Thermo Fisher Scientific, Waltham, MA). RNA quality was assessed using the Agilent Fragment Analyzer with the Standard Sensitivity RNA Gel Kit (Agilent Technologies, Santa Clara, CA). RNA-seq libraries were prepared using the Illumina TruSeq mRNA

Library Prep Kit with TruSeq unique dual-indexed adapters (Illumina, San Diego, CA). Libraries were quantified with the Qubit 1X dsDNA High-Sensitivity NGS Gel Kit (Thermo Fisher), and additionally characterized for functionality with the KAPA Library Quantification Kit (Roche, Basel, Switzerland) and for fragment size using the Agilent Fragment Analyzer with the High-Sensitivity NGS Gel Kit (Agilent). According to manufacturer's specification for clustering, library molarities were calculated followed by dilution and denaturation. Control and Ethanol-exposed animals were clustered on a high-output NextSeq 500 flow cell and paired-end sequenced with 150-cycle SBS kit for 2 × 75 reads (Illumina).

Bioinformatic analysis

Raw RNA-sequence data [NCBI gene expression omnibus (GEO) series succession number GSE226532 (Edgar et al., 2002)] was analyzed to identify significant differences in mRNA gene expression and global biological pathways associated with alterations of cerebellar genes between Control and Ethanol treatment groups. Using the Nextflow RNAseq pipeline, nf-core/rnaseq (version 3.4) available at DOI: 10.5281/zenodo.1400710, RNAseq reads were quality-checked, trimmed, and aligned, with the resulting gene counts transformed to Log_2 counts per million (CPM) and lowly expressed genes were filtered out (Liao et al., 2014). Libraries were normalized by trimmed mean of M-values (Robinson and Oshlack, 2010). To calculate differential gene expression, the Limma R package was used (Ritchie et al., 2015). Genes with an adjusted p-value (adj. $p < 0.05$) were considered statistically significant and Log_2 fold change values were calculated for Ethanol compared to Control.

Heatmaps, principal component analysis (PCA), and volcano plots were generated in R from the processed differential gene expression data. Specifically, the *EnhancedVolcano* package was used to generate the volcano plots (Blighe et al., 2022). Utilizing the "Core Expression Analysis" in the QIAGEN Ingenuity Pathway Analysis (IPA) software (QIAGEN Inc.)[1], pathway and network analysis were conducted. In IPA, the analysis parameter setting for "species" was set to "mouse" and the "tissues and cell lines" parameter was set to "brain". The gene cut off criteria was set to an adj. $p < 0.05$. Once all analysis parameters were set, the analysis was run.

Publicly available single-cell RNA seq (scRNA-seq) resources were used to investigate the specific cell types and cellular processes that may be altered by ethanol exposure in the cerebellum in our dataset. We and others have used this analysis technique to deduce cell composition of bulk RNAseq tissue previously (Jew et al., 2020; Pinson et al., 2021). Subsequently, we compiled a list of 822 microglia associated genes (**Supplementary Table 1A**), 309 astrocyte associated genes (**Supplementary Table 2**), and 799 oligodendrocyte lineage associated genes (**Supplementary Table 3**) utilizing this approach (Zeisel et al., 2015; Artegiani et al., 2017; Sousa et al., 2018; Jurga et al., 2020; Ochocka and Kaminska, 2021).

Cell type specific gene lists were further characterized by transcripts associated with specific phenotypes for each of the glial cell populations. Microglia associated genes, for example, were subcategorized into transcripts related to homeostasis or neurodegenerative diseases (Keren-Shaul et al., 2017; Krasemann et al., 2017; Butovsky and Weiner, 2018; Tatsuyuki Matsudaira, 2022) (**Supplementary Table 1B**). Astrocyte associated genes were subcategorized into transcripts related to acute injury, chronic injury, or pan-injury, with pan-injury including genes associated with both acute and chronic reactive astrogliosis (Das et al., 2020) (**Supplementary Table 2**). Oligodendrocyte lineage cell associated genes were subcategorized into transcripts related to oligodendrocyte precursor cells (OPCs), committed oligodendrocyte precursor cells (COPs), newly-formed oligodendrocytes (NFOL), myelin forming oligodendrocytes (MFOL), and mature oligodendrocytes (MOL) (Zeisel et al., 2015, 2018; Artegiani et al., 2017) (**Supplementary Table 3**).

Each of these phenotype specific lists was cross-referenced to the transcripts significantly dysregulated by Ethanol (adj. $p < 0.05$) when compared to Control in our data set for both P5 and P6 and was tested for statistical significance. To accomplish this, R statistical software was utilized to generate individual z-scores for each transcript of interest and each experimental animal within a given phenotype list. These z-scores were then averaged across transcripts for each individual animal. Control versus Ethanol groups were then tested for statistically significant variance in R by two-tailed, student's t-test, and graphical results were generated.

Our previous studies demonstrated that ethanol altered the expression of molecules associated with various stages of the cell cycle in our FASD model in which animals were treated with ethanol from P4-P9 and cerebellar RNA isolated on P10 (Pinson et al., 2021). In the current study, we performed similar analysis to determine if ethanol altered cell cycle progression during the onset of FASD in this model. Thus, from the Mouse Genome Database Gene Ontology Browser (Bult et al., 2019), we extracted gene lists associated with positive and negative regulation of both G1-S phase transition and G2-M phase transition. Average z-score analysis was conducted in a manner consistent with the glial cell types above.

Results

Cerebellar differential gene expression following the onset of ethanol exposure in the third trimester

We evaluated gene expression profiles at P5 and P6, 24 and 48 hours, respectively, after ethanol exposure began. First, a principal component analysis (PCA) was performed on male and female Control and Ethanol treated animals to evaluate distinct differences between the two datasets at P5 and P6 (**Figures 1A, B**). The first and second principal components encapsulate gene expression patterns that differentiate Control versus Ethanol treated animals. The PCA analysis suggested there were minimum sex differences in the ethanol regulation of gene expression, thus we combined sexes for the remainder of the analysis. Secondly, hierarchical clustering analysis using Pearson correlation was conducted on those genes that were identified as significantly dysregulated by ethanol (adj. $p < 0.05$) at P5 and P6 (**Figures 1C, D**). Volcano plot analysis identified 2,440 genes that were significantly dysregulated (adj. $p < 0.05$ and $log_2FC \pm 0.5$)

1 https://digitalinsights.qiagen.com/IPA

at P5 and 1,348 genes at P6. Of the 2,440 genes at P5, 1,419 were upregulated and 1,021 were downregulated (Figure 1E). Of the 1,348 genes at P6, 840 were upregulated and 508 were downregulated (Figure 1F).

Pathway and cellular function analysis of genes dysregulated by ethanol at P5 and P6

IPA was utilized to determine specific pathways and cellular functions associated with genes significantly (adj. $p < 0.05$) dysregulated by ethanol. Results of the top canonical pathway categories altered by ethanol exposure common to P5 and P6, included neurotransmitters and other nervous system signaling, cytokine signaling, cellular immune response, intracellular and second messenger signaling, degradation/utilization/assimilation, humoral immune response, nuclear receptor signaling, ingenuity toxicity list pathways, organismal growth and development, cellular stress and injury, cell cycle regulation, disease-specific pathways, cellular growth and development, and cancer (Figures 2A, B). The top altered diseases and biological function categories of genes dysregulated by ethanol conserved between P5 and P6 included cell death and survival, neurological disease, organismal injury and abnormalities, cell-to-cell signaling and interaction, nervous system development and function, cellular growth and proliferation, tissue development, cellular assembly and organization, cellular movement, immune cell trafficking, cellular compromise, cellular function and maintenance, free radical scavenging, psychological disorders, organismal development, lipid metabolism, metabolic disease, molecular transport, small molecule biochemistry, cell morphology, developmental disorder, embryonic development, inflammatory response, and organ morphology (Tables 1 and 2). The tabular descriptions of the diseases and functions categories, including annotations, p-value, and associated transcripts that correlate with these diseases and biological function categories are listed in Supplementary Tables 4A for P5 and 4B for P6.

Ethanol induced alterations in microglia phenotypic states at P5 and P6

In the current study, we compared the list of 822 microglia associated genes (described in the *Bioinformatic Analysis* subsection of the Materials and Methods) to the list of genes dysregulated by ethanol (adj. $p < 0.05$) at P5 and P6. We identified 175 microglia associated genes at P5 (Supplementary Table 5A)

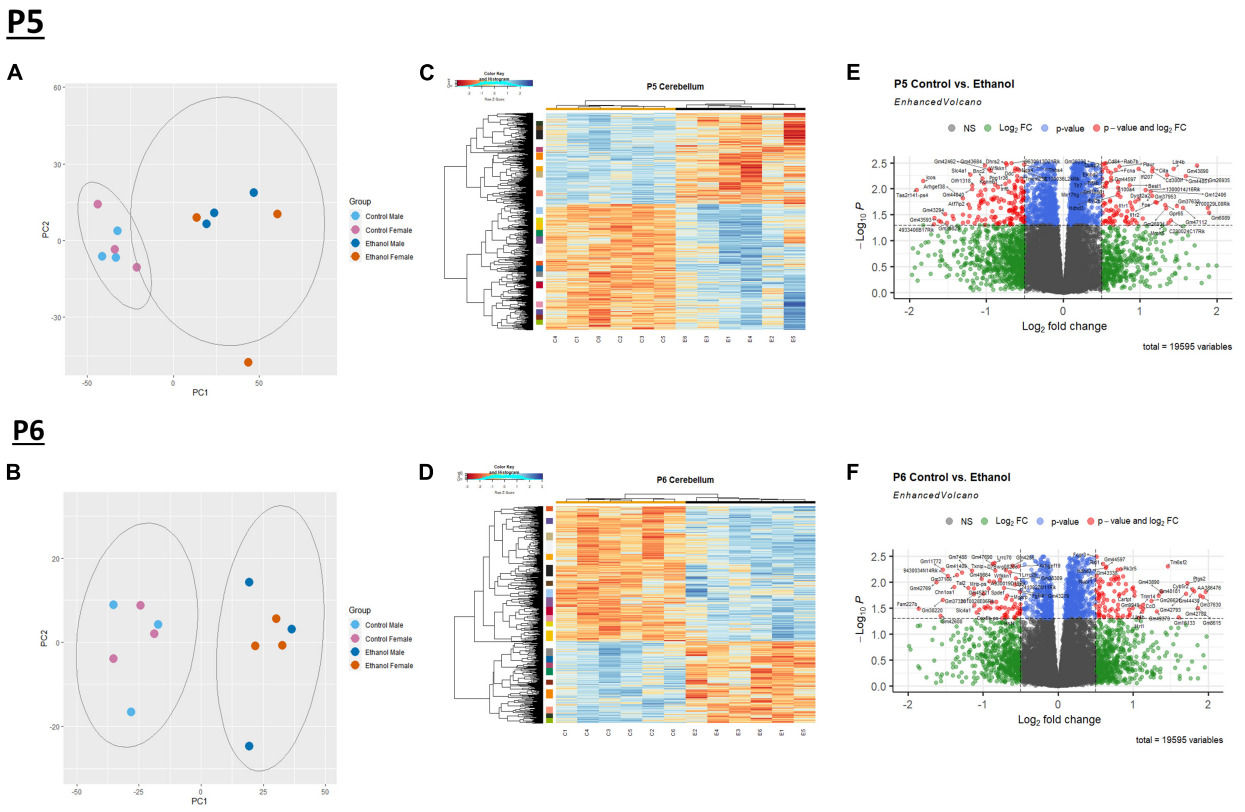


FIGURE 1
Ethanol-induced differential gene expression in the cerebellum. Principle component analysis (PCA) of the variance of genes in the cerebellum between ethanol (E) and control (C) at P5 **(A)** and P6 **(B)**. A heatmap and hierarchical clustering dendrogram of the of relative gene expression across samples for the significantly (adj. $p < 0.05$) altered genes for P5 **(C)** and P6 **(D)**. A volcano plot displaying fold change versus adjusted *p*-value of all detected genes in the cerebellum at P5 and P6. 2,440 of 19,595 total identified transcripts at P5 **(E)** and 1,348 of 19,595 total identified transcripts at P6 **(F)** displayed an adjusted $p < 0.05$ and Log_2 fold change ≥ 0.5 or ≤ -0.5, shown in red. PCA, heatmaps, and volcano plots (*Enhanced Volcano* package) were generated using R statistical software. $n = 3$ males and 3 females per treatment group E or C.

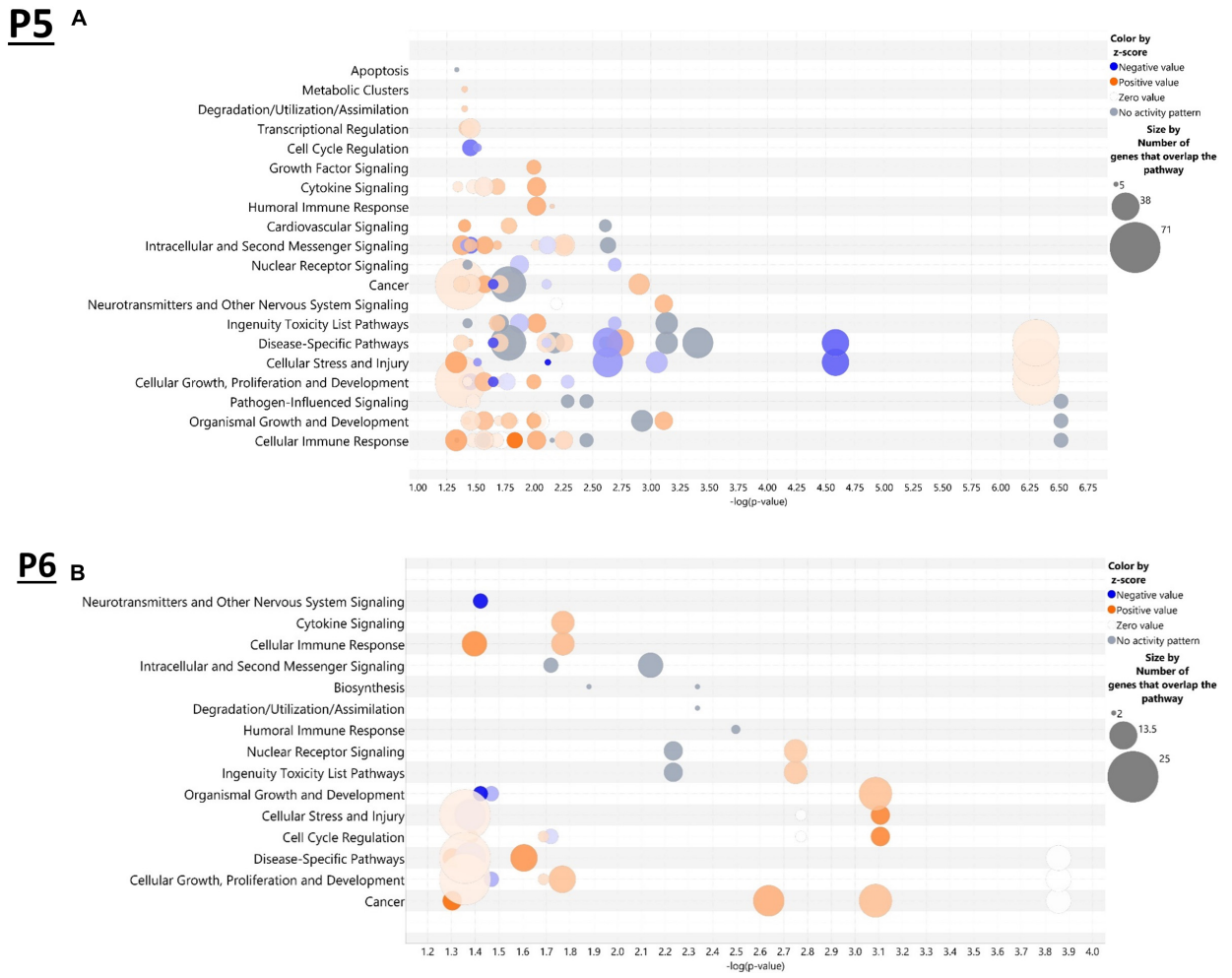


FIGURE 2
Top canonical pathways altered in the brain by ethanol exposure at P5 and P6. Qiagen Ingenuity Pathway Analysis (IPA) software was employed to assess the top canonical pathways altered by ethanol at P5 **(A)** and P6 **(B)**. All analyses were restricted to genes with an adj. $p < 0.05$ and analysis settings were set to "brain" in IPA. $n = 3$ males and 3 females per treatment group E or C.

and 105 microglia associated genes at P6 (Supplementary Table 5B) that were significantly dysregulated by ethanol. We further categorized these 175 and 105 dysregulated microglia associated genes as being either typical of a homeostatic or a neurodegenerative phenotype (Supplementary Tables 5C, D), as previously defined (Supplementary Table 1B; Keren-Shaul et al., 2017; Krasemann et al., 2017; Butovsky and Weiner, 2018; Sousa et al., 2018; Tatsuyuki Matsudaira, 2022). Heatmaps illustrating relative gene expression across transcripts for significantly altered ($p < 0.05$) homeostatic and neurodegenerative disease microglial associated genes are depicted in Figures 3A, C for P5 and 3B and 3D for P6. A student's t-test comparing the average z-scores across all relevant genes indicated that ethanol exposure did not significantly alter expression of homeostatic transcripts at P5, $p = 0.7464$ (Figure 4A) or P6, $p = 0.0817$ (Figure 4B), though P6 appears to approach significance. Examination of the average z-scores across all neurodegenerative disease associated microglia genes by student's t-test showed ethanol induced a significant upregulation of these genes at both P5, $p = 2.967e\text{-}06$ (Figure 4C) and P6, $p = 3.069e\text{-}05$ (Figure 4D).

Ethanol induced astrocyte phenotypic switch following neonatal ethanol exposure

When comparing the list of 309 astrocyte associated genes (described in the *Bioinformatic Analysis* subsection of the Materials and Methods) to our list of genes dysregulated by ethanol (adj. $p < 0.05$) at P5 and P6, we identified 58 astrocyte associated genes at P5 and 33 genes at P6. We further characterized these genes as belonging to an acute injury, chronic neurodegenerative diseases, or pan-injury phenotype (Supplementary Tables 6A, B; Das et al., 2020). Heatmaps illustrating relative gene expression across transcripts for significantly altered ($p < 0.05$) acute injury, pan-injury, and chronic neurodegenerative diseases associated genes are depicted in Figures 5A, C, E for P5 and Figures 5B, D, F for P6. A student's *t*-test comparing the average z-scores of all relevant astrocyte associated genes indicated that ethanol induced a significant increase in astrocyte associated acute injury transcripts at both P5, $p = 2.3e\text{-}05$ (Figure 6A) and P6, $p = 0.0376$ (Figure 6B), and pan-injury transcripts at both P5, $p = 1.465e\text{-}07$ (Figure 6C)

TABLE 1 P5-Top diseases and biological functions altered by ethanol exposure.

Category	*P*-value range
Cellular development	5.63E-05–4.91E-02
Nervous system development and function	5.63E-05–4.91E-02
Tissue development	5.63E-05–4.91E-02
Tissue morphology	7.94E-05–3.92E-02
Cellular growth and proliferation	7.32E-04–4.91E-02
Neurological disease	7.36E-04–4.87E-02
Organismal injury and abnormalities	7.36E-04–4.87E-02
Psychological disorders	7.36E-04–2.81E-02
Cell morphology	1.01E-03–3.85E-02
Cellular assembly and organization	1.01E-03–4.63E-02
Cellular function and maintenance	1.01E-03–4.63E-02
Organismal development	1.01E-03–4.86E-02
Cell death and survival	1.64E-03–3.34E-02
Embryonic development	1.64E-03–3.88E-02
Organ morphology	2.67E-03–3.81E-02
Behavior	4.39E-03–4.86E-02
Cancer	5.09E-03–4.87E-02
Free radical scavenging	7.05E-03–7.05E-03
Cardiovascular disease	7.5E-03–1.93E-02
Cell–mediated immune response	9.11E-03–1.93E-02
Cellular movement	9.11E-03–3.44E-02
Hematological system development and function	9.11E-03–3.88E-02
Immune cell trafficking	9.11E-03–2.23E-02
Lipid metabolism	9.11E-03–4.87E-02
Molecular transport	9.11E-03–4.87E-02
Small molecule biochemistry	9.11E-03–4.87E-02
Endocrine system disorders	9.57E-03–9.57E-03
Gastrointestinal disease	9.57E-03–9.57E-03
Metabolic disease	9.57E-03–3.17E-02
Organ development	1.62E-02–3.88E-02
Cardiovascular system development and function	1.93E-02–4.86E-02
Cell–to–cell signaling and interaction	1.93E-02–3.85E-02
Developmental disorder	1.93E-02–1.93E-02
Hereditary disorder	1.93E-02–1.93E-02
Inflammatory response	1.93E-02–1.93E-02
Organismal functions	1.93E-02–1.93E-02
Endocrine system development and function	2.15E-02–2.97E-02
Cellular compromise	2.23E-02–2.23E-02
Amino acid metabolism	3.85E-02–3.85E-02

All analyses were restricted to genes with an adj. $p < 0.05$ and analysis settings were set to "brain" in IPA. $n = 3$ males and 3 females per treatment group E or C.

and P6, $p = 0.0006$ (Figure 6D). Astrocyte associated chronic neurodegenerative diseases transcripts showed no significant difference between Control and Ethanol groups for P5, $p = 0.4234$

TABLE 2 P6-Top diseases and biological functions altered by ethanol exposure.

Category	*P*-value range
Cell death and survival	4.7E-04–4.46E-02
Neurological disease	4.7E-04–4.93E-02
Organismal injury and abnormalities	4.7E-04–4.93E-02
Cardiovascular disease	1.18E-03–4.02E-02
Cell–to–cell signaling and interaction	1.18E-03–4.02E-02
Nervous system development and function	1.18E-03–4.97E-02
Cellular growth and proliferation	2.81E-03–4.97E-02
Tissue development	2.81E-03–4.97E-02
Cellular assembly and organization	4.61E-03–4.97E-02
Cardiovascular system development and function	4.73E-03–4.17E-02
Cellular movement	4.73E-03–2.61E-02
Hematological system development and function	4.73E-03–2.61E-02
Immune cell trafficking	4.73E-03–2.61E-02
Organ development	4.73E-03–4.73E-03
Tissue morphology	9.76E-03–4.97E-02
Cellular compromise	1.35E-02–2.52E-02
Cellular function and maintenance	1.35E-02–4.97E-02
Free radical scavenging	1.35E-02–1.35E-02
Psychological disorders	1.35E-02–4.93E-02
Organismal development	1.39E-02–4.97E-02
Carbohydrate metabolism	1.92E-02–1.92E-02
Lipid metabolism	1.92E-02–2.61E-02
Metabolic disease	1.92E-02–1.92E-02
Molecular transport	1.92E-02–2.61E-02
Small molecule biochemistry	1.92E-02–2.61E-02
Cell morphology	2.52E-02–4.97E-02
Cellular development	2.52E-02–4.97E-02
Developmental disorder	2.52E-02–2.52E-02
Embryonic development	2.52E-02–4.97E-02
Inflammatory response	2.52E-02–2.52E-02
Organ morphology	3.42E-02–4.02E-02

All analyses were restricted to genes with an adj. $p < 0.05$ and analysis settings were set to "brain" in IPA. $n = 3$ males and 3 females per treatment group E or C.

(Figure 6E), but ethanol significantly increased expression of these transcripts at P6, $p = 0.0073$ (Figure 6F).

Oligodendrocyte lineage cells have mixed effects under ethanol exposure at P5 and P6

Comparing our list of genes dysregulated by ethanol (adj. $p < 0.05$) to the extracted list of oligodendrocyte lineage genes, at P5 we identified 65 OPCs, 14 COPs, 0 NFOL, 45 MFOL, and 1 MOL associated genes (Supplementary Table 7A), and at P6 we identified 32 OPCs, 3 COPs, 0 NFOLs, 24 MFOLs, and 0 MOL

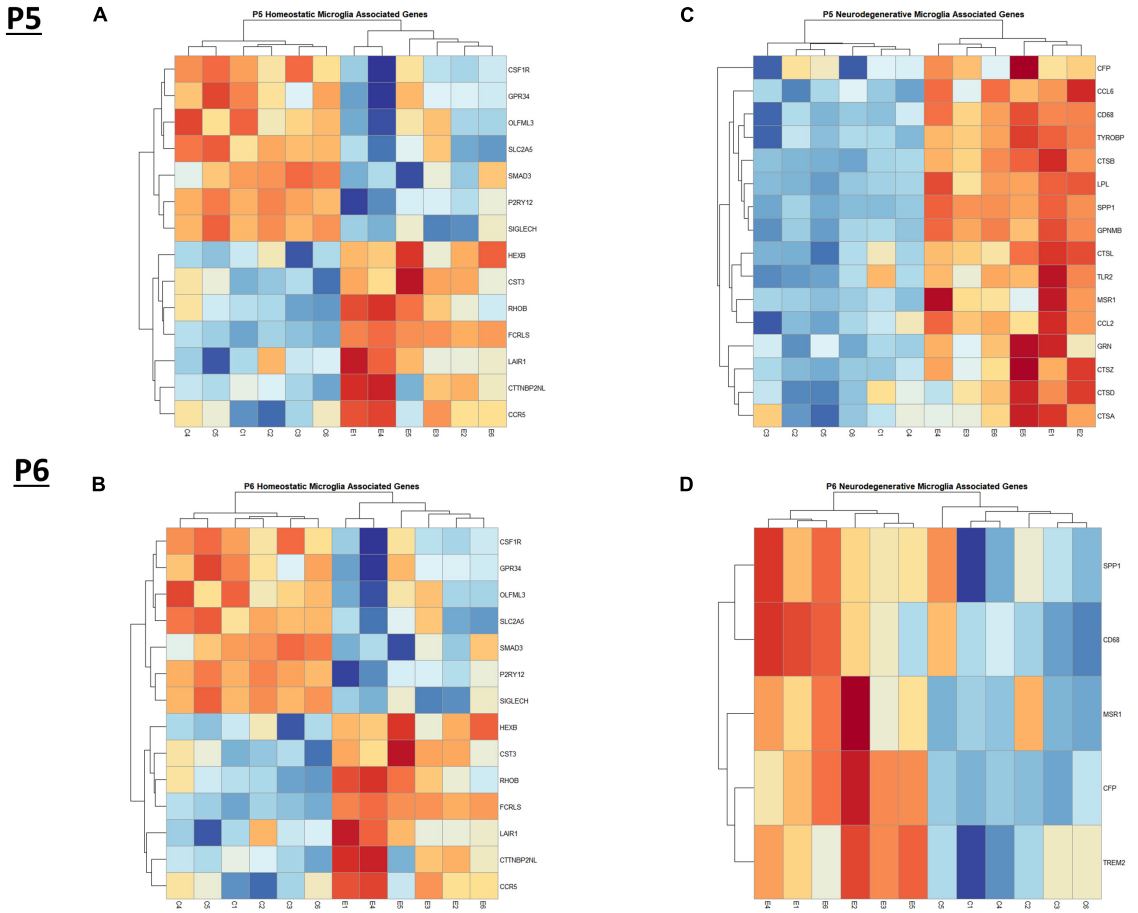


FIGURE 3
Heatmap and hierarchical clustering of microglia associated genes at P5 and P6. R statistical software was utilized to construct heatmaps and hierarchical clustering dendrogram of relative gene expression across samples for significantly altered (adj. $p < 0.05$) and categorized microglia associated genes as detailed in Methods. Microglia homeostatic associated gene expression is depicted in panel **(A)** for P5 and panel **(B)** for P6. Microglia neurodegenerative associated gene expression is depicted in panel **(C)** for P5 and panel **(D)** for P6.

associated genes (Supplementary Table 7B). Heatmaps illustrating relative gene expression across transcripts for significantly altered ($p < 0.05$) OPC, COP, and MFOL associated genes are depicted in Figures 7A, C, E for P5 and Figures 7B, D, F for P6. Student's *t*-test comparing the average z-scores across relevant genes showed that ethanol induced a significant upregulation of OPC associated transcripts at P5, $p = 0.0219$ (Figure 8A), with no significant effect on OPC associated transcripts at P6, $p = 0.1887$ (Figure 8B). In terms of COP associated genes, ethanol induced a significant upregulation at P5, $p = 0.0219$ (Figure 8C) but no effect at P6, $p = 0.2924$ (Figure 8D). Lastly, ethanol induced a significant upregulation of MFOL associated genes at P5, $p = 0.0009$ (Figure 8E), but a significant downregulation of MFOL associated genes at P6, $p = 0.0340$ (Figure 8F). NFOL and MOL were not analyzed.

Alteration of cell cycle progression following ethanol exposure

We previously determined, using a third trimester human equivalent mouse model of FASD in which animals were treated with ethanol from P4-9 and cerebellar RNA isolated at P10 followed by RNASeq analysis, that ethanol increased the expression of molecules associated with the S and G2M phases of the cell cycle. In addition, our current IPA analysis (Figures 2A, B) suggests that cell cycle associated pathways may be altered by ethanol. Thus, we sought to determine if ethanol altered the expression of transcripts involved in cell cycle progression as early as P5 and P6. Using the Mouse Genome Database Gene Ontology Browser (Bult et al., 2019), genes associated with G1-S phase transition and G2-M phase transition cell cycle phases were extracted. Heatmaps illustrating relative gene expression across transcripts for significantly altered ($p < 0.05$) positive and negative regulation of G1-S transition associated genes and positive and negative regulation of G2-M transition associated genes are depicted in Figures 9A, C, E, G for P5 and Figures 9B, D, F, H for P6. For the positive regulation of G1-S phase transition, there was no significant difference between Control and Ethanol treated groups at P5, $p = 0.6024$ (Figure 10A); however, ethanol did induce a significant increase in those genes associated with this phase at P6, $p = 0.0027$ (Figure 10B). Ethanol induced a significant increase in those genes associated with the negative regulation of G1-S phase transition at both P5, $p = 3.004e\text{-}05$ (Figure 10C), and P6, $p = 0.0006$

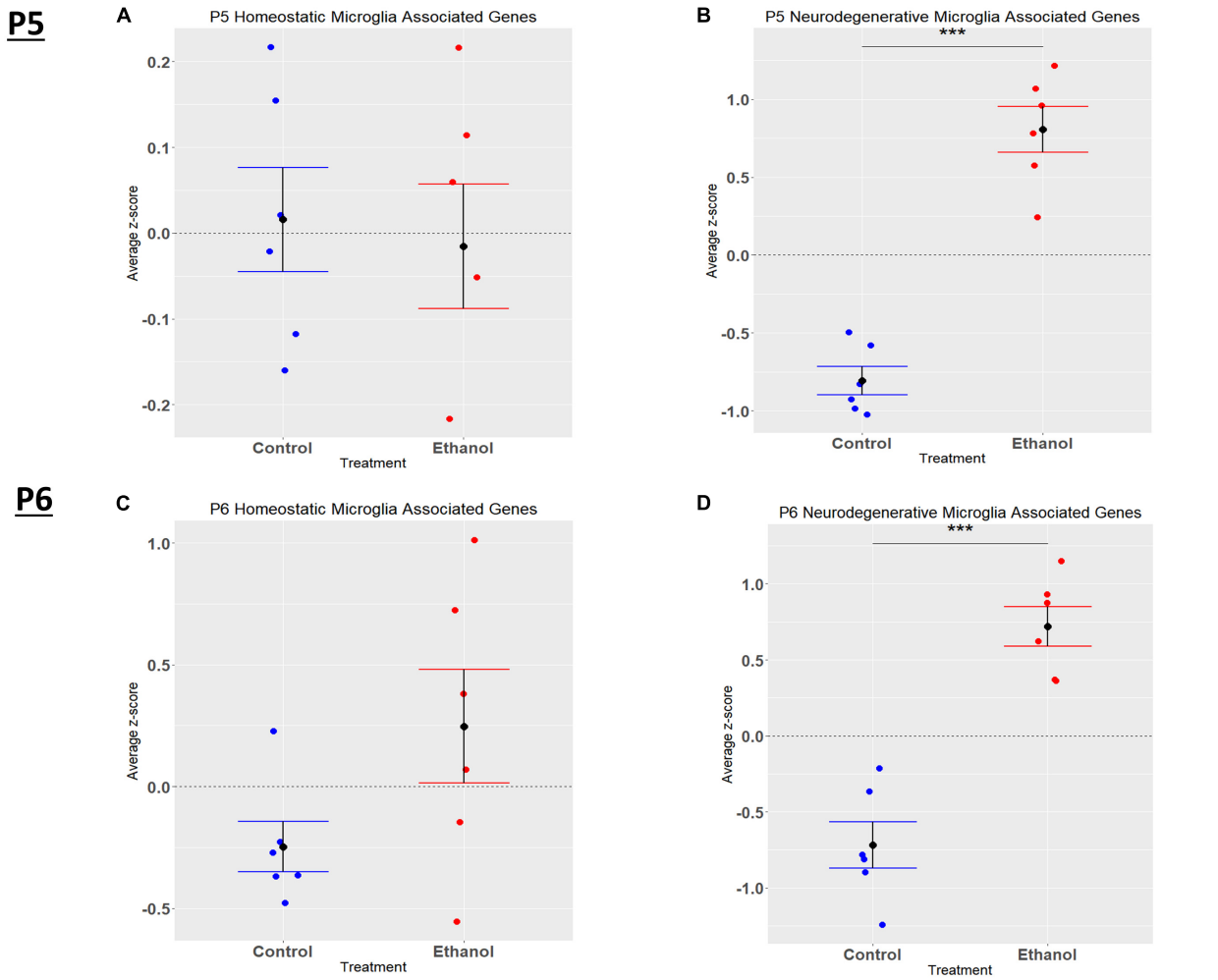


FIGURE 4
Microglia associated genes altered by ethanol exposure at P5 and P6 in the cerebellum. Microglia associated genes were extracted as detailed in Methods. R statistical software was utilized to generate individual z-scores for each transcript of interest and each experimental animal. These *z*-scores were then averaged across transcripts for each individual animal. Control versus Ethanol groups were then tested for statistically significant variance in R by two-tailed, student's *t*-test, and graphical results were generated. Quantification by average *z*-score of homeostatic microglia associated genes at P5 **(A)** and P6 **(B)** and neurodegenerative microglia associated genes at P5 **(C)** and P6 **(D)**. $n = 3$ males and 3 females per treatment group E or C; ***$p < 0.001$.

(Figure 10D). Looking at the positive regulation of G2-M phase transition, ethanol induced a significant downregulation of genes associated with this phase at P5, $p = 0.0021$ (Figure 10E), with no significant changes between our Control and Ethanol groups at P6, $p = 0.9278$ (Figure 10F). Lastly, looking at the negative regulation of G2-M phase transition, ethanol induced a significant increase in those genes associated with this phase at both P5, $p = 0.0002$ (Figure 10G), and P6, $p = 3.042e\text{-}05$ (Figure 10H).

Discussion

The current study was designed to evaluate the effects of ethanol on transcriptomic profiles in the cerebellum of early postnatal mice, which approximates the third trimester of gestation in humans. This is a period of secondary neurogenesis, and ethanol exposure at this time can result in FASD. The proposed studies were also designed to evaluate the effects of ethanol at early times following exposure to begin to assess transcriptomic changes that may contribute to initial development of FASD. Pathway analysis suggested that ethanol may alter immune related pathways at P5 and P6 soon after initial ethanol exposure. We previously demonstrated that ethanol induced microglial activation, production of pro-inflammatory cytokines and chemokines, as well as neuron cell loss in animals treated with ethanol from P4-P9 and tissue harvested at P10 (Kane et al., 2011, 2021; Drew et al., 2015; Pinson et al., 2021). Others have used similar FASD models and have also observed ethanol induced neuroinflammation (Topper et al., 2015; Zhang et al., 2018). Thus, the current studies suggest that ethanol-induced neuroinflammation occurs rapidly following ethanol exposure and may contribute to the initial neuropathology associated with FASD. In an attempt to define possible mechanisms by which ethanol induces early immune activation in the current studies, we identified immune related transcripts whose expression was strongly altered by ethanol in our transcriptomic data. At P5 and

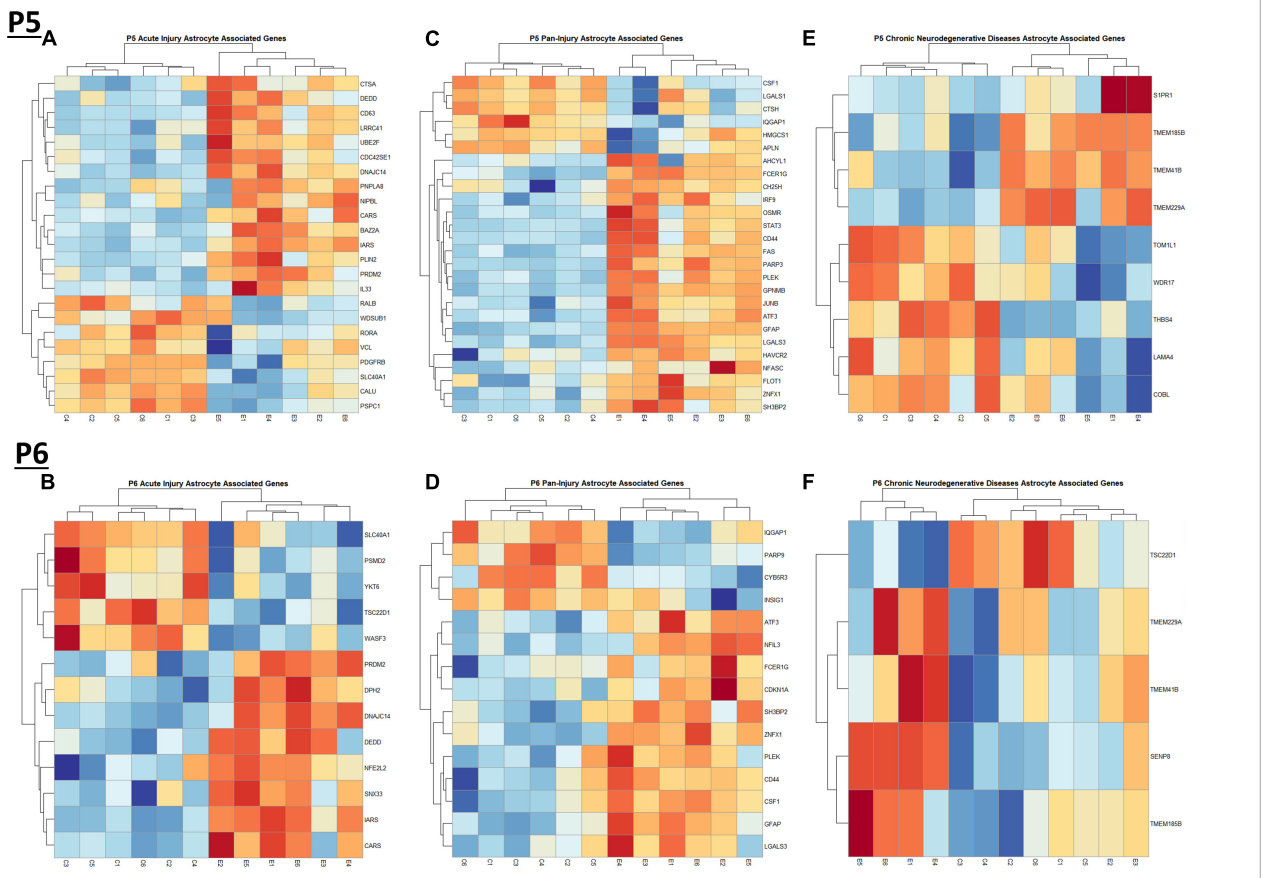


FIGURE 5
Heatmap and hierarchical clustering of astrocyte associated genes at P5 and P6. R statistical software was utilized to construct heatmaps and hierarchical clustering dendrogram of relative gene expression across samples for significantly altered (adj. $p < 0.05$) and categorized astrocyte associated genes as detailed in Methods. Astrocyte acute injury astrocyte associated gene expression is depicted in panel **(A)** for P5 and panel **(B)** for P6. Astrocyte pan-injury astrocyte associated gene expression is depicted in panel **(C)** for P5 and panel **(D)** for P6. Astrocyte chronic neurodegenerative diseases astrocyte gene expression is depicted in panel **(E)** for P5 and **(F)** for P6.

P6, top upregulated transcripts (**Supplementary Tables 5A, B**) included SPP1, CCL3, C5AR1, C3AR1, MSR1, and CD14. At P5, but not P6, CCL2 transcript levels were highly increased by ethanol. SPP1, which is also termed osteopontin, is a secretory molecule expressed by a variety of immune cells which has functions including immunomodulation, chemotaxis, and cell adhesion (Lin et al., 2022). SPP1 plays a role in alcohol liver disease (Apte et al., 2005; Seth et al., 2006; Lebel et al., 2008; Das et al., 2022). In the presence of ethanol, SPP1 binds to integrins and CD44 and activates transcription factors AP-1 and NF-κB (Das et al., 2005; Bellahcène et al., 2008). These transcription factors regulate the expression of pro-inflammatory cytokines that amplify the immune response and are also linked to addictive behaviors (Crews et al., 2017). AP1 consists as a dimer of Fos and Jun proteins, and it is interesting the ethanol increased the expression of Fos and Jun transcripts at P5 (**Supplementary Table 5A**). Furthermore, CCL2 and CCL3, target genes of NF-κB, are induced by ethanol and are key mediators of CNS inflammation and alcohol drinking behavior (Blednov et al., 2005; He and Crews, 2008). We previously demonstrated that ethanol induced the expression of CCL2 in animal models of FASD (Drew et al., 2015) as well as adult models of alcohol use disorder (Kane et al., 2014). Complement receptor C3AR1 expression is induced by ethanol resulting in altered phagocytosis by microglia (Kalinin et al., 2018). Previous studies also indicated that C5AR1 is involved in alcohol-induced inflammation (Blednov et al., 2005; He and Crews, 2008). Collectively, these results suggest potential mechanisms by which ethanol-induced neuroinflammation may contribute to the early onset of neuropathology associated with FASD.

Microglia play a role in several developmental homeostatic functions, including synapse development, plasticity, and maintaining the health of neurons, which are altered in FASD (Drew and Kane, 2014). Microglia are the primary resident immune cell in the CNS and become activated in response to a variety of stimuli (Lynch et al., 2010). Ethanol exposure has previously been demonstrated to result in microglial activation and production of pro-inflammatory cytokines and chemokines that may contribute to the neuropathology associated with FASD (Kane et al., 2011; Drew et al., 2015). Activated microglia are responsible for aiding in immune functions including phagocytosis, antigen presentation, and generation of inflammatory cytokines and chemokines (Ransohoff and Perry, 2009; Saijo and Glass, 2011; Ransohoff and Brown, 2012). Our IPA analysis indicated that exposure to ethanol resulted in microgliosis of the brain at both P5 and P6. Microgliosis occurs during pathogenic insults to the CNS (Li and Zhang, 2016). Traditionally, microglia

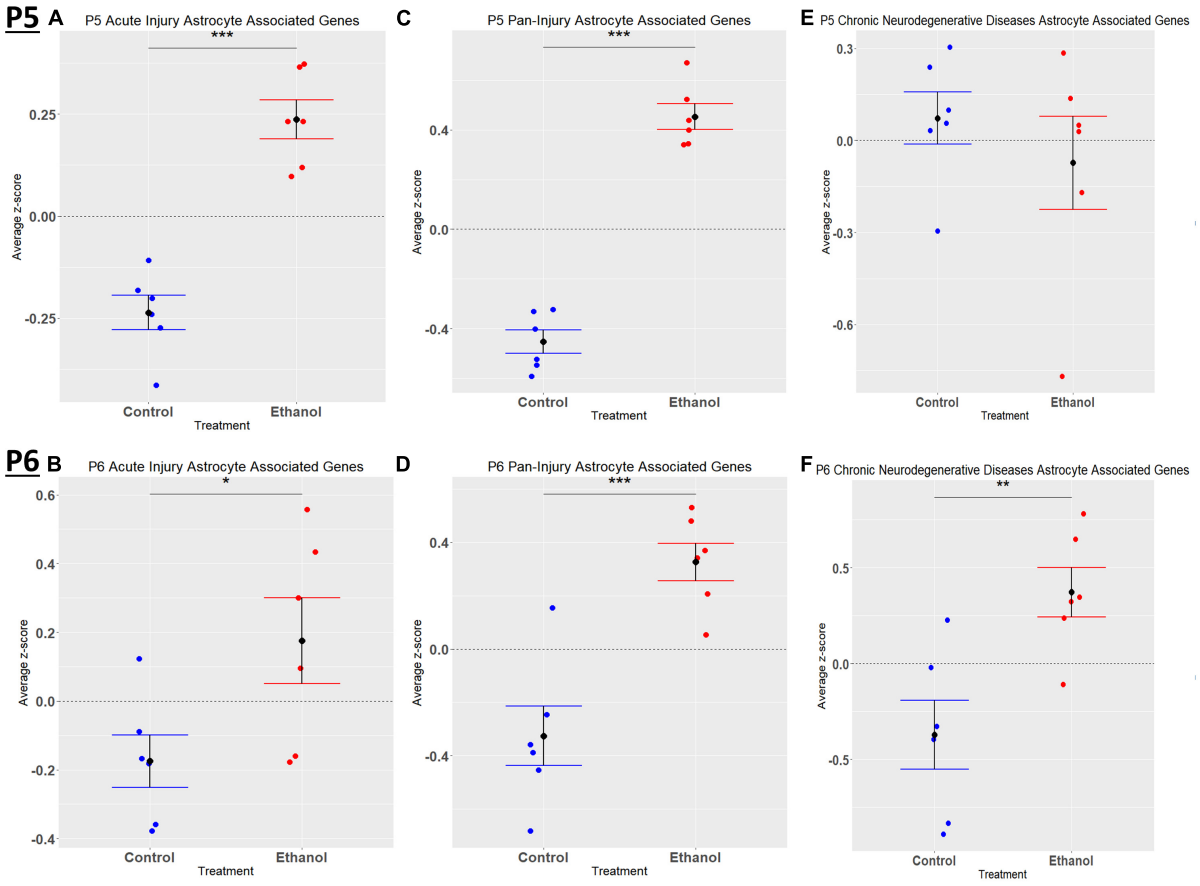


FIGURE 6
Astrocyte associated genes altered by ethanol exposure at P5 and P6 in the cerebellum. Astrocyte associated genes were extracted as detailed in Methods. R statistical software was utilized to generate individual *z*-scores for each transcript of interest and each experimental animal. These *z*-scores were then averaged across transcripts for each individual animal. Quantification by average *z*-score of acute injury astrocyte associated genes at P5 **(A)** and P6 **(B)**, pan-injury astrocyte associated genes at P5 **(C)** and P6 **(D)**, and chronic neurodegenerative diseases associated genes at P5 **(E)** and P6 **(F)**. $n = 3$ males and 3 females per treatment group E or C; $^{*}p < 0.05$, $^{**}p < 0.01$, $^{***}p < 0.001$.

activation has been separated into either an M1 pro-inflammatory phenotype or an M2 anti-inflammatory phenotype (Franco and Fernández-Suárez, 2015; Tang and Le, 2016). However, recent literature suggests that microglia phenotypes do not fit into this simple binary system (Franco and Fernández-Suárez, 2015). Because microglia phenotypes are complex, several microglial phenotypes corresponding to different diseases and physiological states have been described. However, two microglial gene expression profiles appear across multiple studies - homeostatic and neurodegenerative disease associated. Homeostatic microglia are believed to aid in synaptic plasticity and synaptogenesis, neurogenesis, and immune cell recruitment (Butovsky and Weiner, 2018). The neurodegenerative disease related microglia phenotype results from insult to the CNS, and microglia lose their homeostatic signature and gain a chronic inflammatory signature (Holtman et al., 2015; Moore et al., 2015; Paolicelli et al., 2022). Although there are a variety of neurodegenerative diseases, assessment of microglia phenotype during these disease states have identified a common neurodegenerative disease related microglia phenotype (Naj et al., 2014; Moore et al., 2015; Keren-Shaul et al., 2017; Butovsky and Weiner, 2018). When examining microglia phenotypic states in the current study, ethanol induced a phenotypic switch at both P5 and P6 in the cerebellum, resulting in upregulation of neurodegenerative disease associated transcripts. The expression of homeostatic associated genes was not altered at P5 or P6 in the current studies. However, three of the top four most strongly ethanol-downregulated microglial associated molecules at P5 are considered homeostatic molecules (**Supplementary Tables 1B, 5A**). Additionally, microglia homeostatic associated molecules at P6 trended toward significance. This might suggest ethanol decreases the expression of at least a subset of homeostatic microglial associated transcripts in the current study which could in turn change the phenotype of microglia and alter specific developmental functions.

Astrocytes, like microglia, play a role in immune responses in the CNS and produce cytokines and chemokines, nitric oxide, and reactive oxygen species (Ransohoff and Brown, 2012). Astrocytes also play roles in maintaining the blood brain barrier and neurotransmitter levels, along with regulating energy balance and modulating synaptic plasticity (Santello et al., 2019). They also have a significant immune function, mediating both pro-inflammatory and anti-inflammatory activities in response to CNS insult (Dong and Benveniste, 2001). Astrocyte production of immune mediators is suspected to contribute to neuropathology

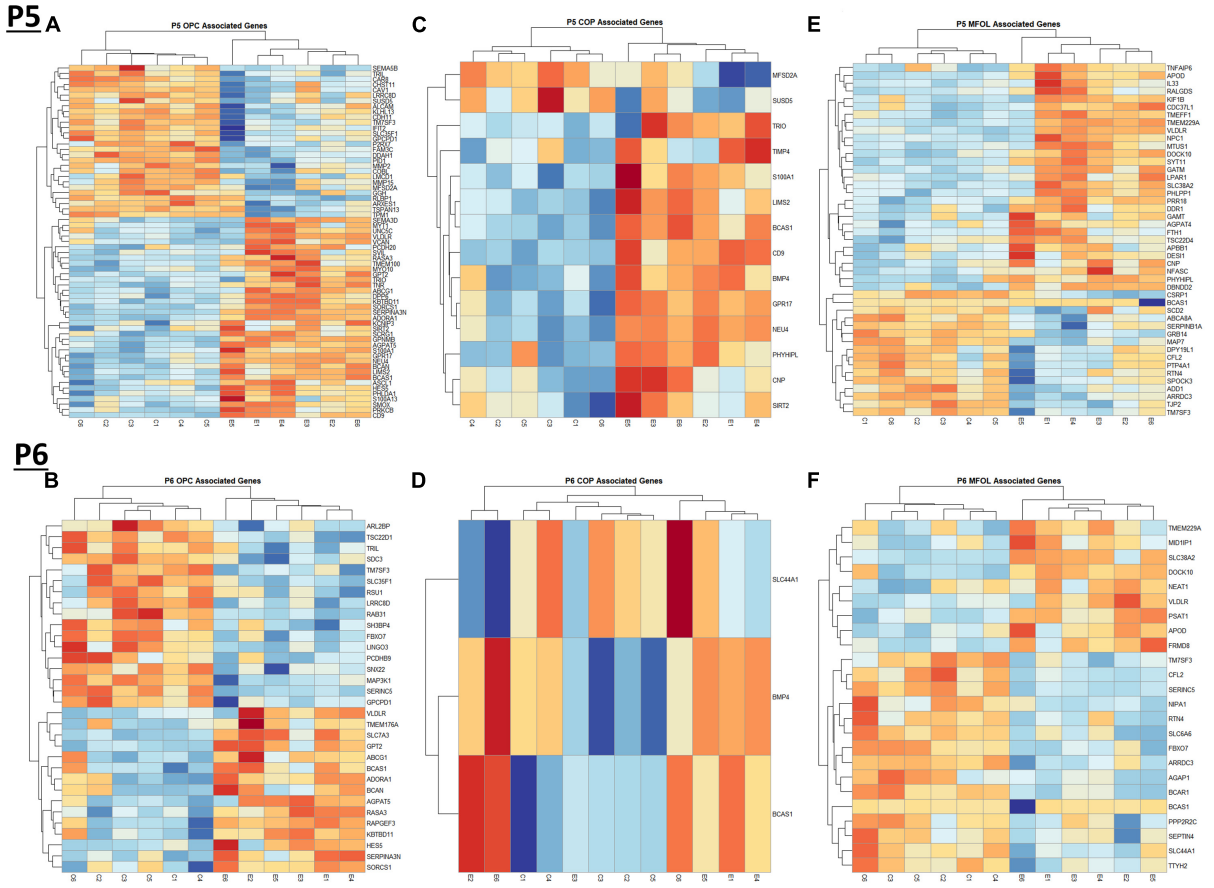


FIGURE 7
Heatmap and hierarchical clustering of oligodendrocyte lineage associated genes at P5 and P6. R statistical software was utilized to construct heatmaps and hierarchical clustering dendrogram of relative gene expression across samples for significantly altered (adj. $p < 0.05$) and categorized oligodendrocyte lineage associated genes as detailed in Methods. OPC associated gene expression is depicted in panel **(A)** for P5 and panel **(B)** for P6. COP associated gene expression is depicted in panel **(C)** for P5 and panel **(D)** for P6. MFOL associated gene expression is depicted in panel **(E)** for P5 and panel **(F)** for P6.

associated with FASD (Guizzetti et al., 2014; Wilhelm and Guizzetti, 2016). Astrocytes may become reactive in response to various stimuli, resulting in astrogliosis/astrocytosis. During astrogliosis/astrocytosis, astrocytes undergo a phenotypic change which has historically been referred to result in an A1 reactive phenotype characterized as being neurotoxic or an A2 reactive phenotype described as being neuroprotective (Zamanian et al., 2012; Liddelow et al., 2017). However, classifying reactive astrocytes into these two categories does not appear to be adequate. A recent meta-analysis of mouse transcriptomic studies aimed to better categorize astrocyte reactive states (Das et al., 2020). The nomenclature used in this study classified reactive astrocytes as having three different phenotypes; acute injury, chronic neurodegenerative diseases, or pan-injury which has characteristics of both acute injury and chronic neurodegenerative diseases phenotypes (Das et al., 2020). In the current study, at P5, our IPA analysis indicated that ethanol treatment resulted in alterations related to the development of astrocytes, formation of astrocyte precursor cells, and quantity of astrocytes, and at P6, our IPA analysis revealed that ethanol treatment stimulated astrocytosis and gliosis of astrocytes in the cerebellum. These results suggest that 24 h following initial ethanol exposure, astrocyte development and quantity is altered, and after 48 h of ethanol exposure, those astrocytes that are present are becoming reactive. We also revealed that at both P5 and P6, ethanol stimulated an acute injury and pan-injury reactive astrocyte phenotype, with a chronic neurodegenerative diseases phenotype also being seen at P6, but not P5. LPS is known to induce an immune response in the CNS, and was demonstrated to trigger an acute injury astrocyte phenotype (Das et al., 2020). Like LPS, ethanol is believed to trigger immune responses, at least in part, through activation of TLR4 signaling pathways (Blanco et al., 2005; Floreani et al., 2010; Alfonso-Loeches et al., 2014). Therefore, in this model of FASD, it is possible that ethanol stimulates an acute or pan-injury reactive phenotypic state at both P5 and P6, possibly through activation of TLR4. It will be important in the future to define the mechanisms by which ethanol alters astrocyte phenotype and immune responses and how this may contribute to ethanol-induced neuropathology associated with FASD.

Oligodendrocytes generate the myelin sheath which wraps axons to promote the conduction of electrical impulses (Baumann and Pham-Dinh, 2001). Prior to myelination, oligodendrocytes undergo a series of differentiation steps, beginning as OPCs and terminating as mature myelinating oligodendrocytes

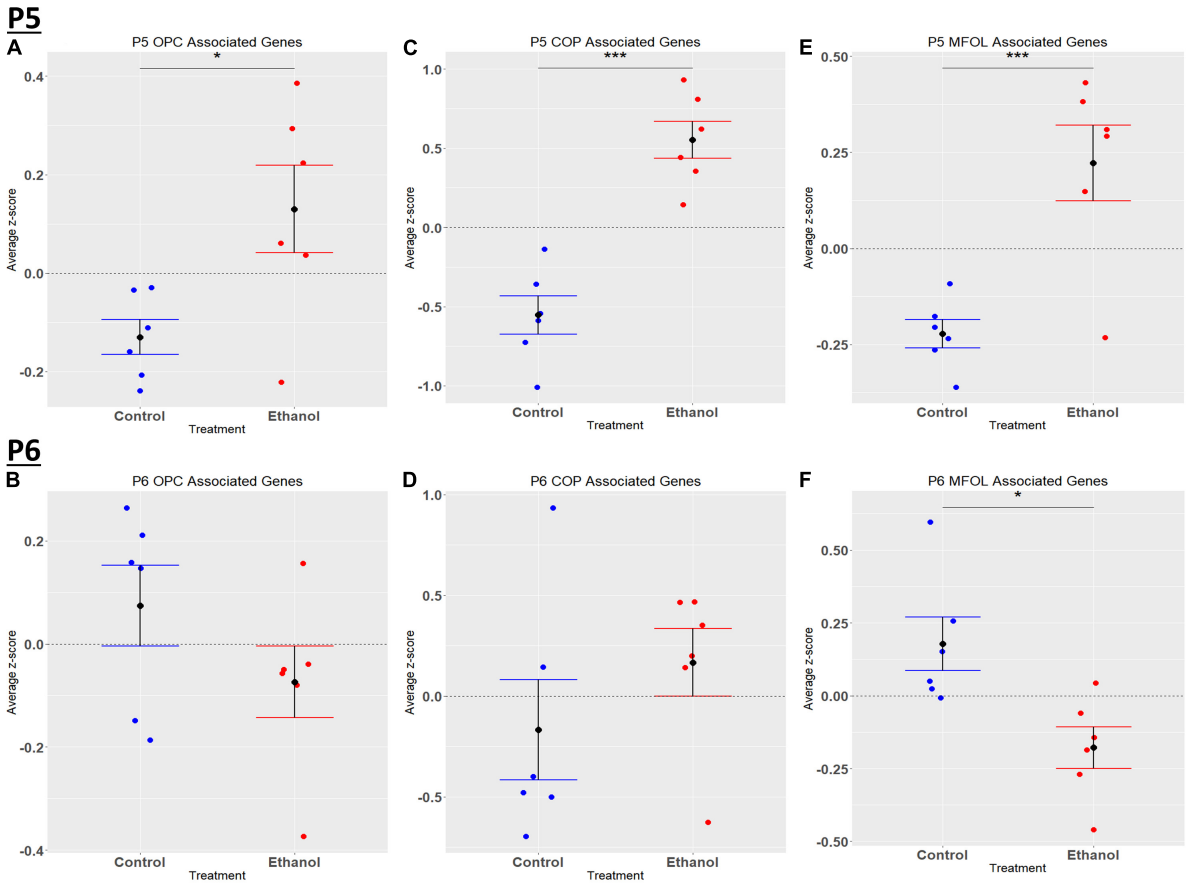


FIGURE 8
Oligodendrocyte lineage associated altered genes by ethanol exposure at P5 and P6 in the cerebellum. Oligodendrocyte lineage associated genes were extracted as detailed in Methods. R statistical software was utilized to generate individual *z*-scores for each transcript of interest and each experimental animal. These *z*-scores were then averaged across transcripts for each individual animal. Quantification by average z-score of OPC associated genes at P5 **(A)** and P6 **(B)**, COP associated genes at P5 **(C)** and P6 **(D)**, and MFOL associated genes at P5 **(E)** and P6 **(F)**. $n = 3$ males and 3 females per treatment group E or C; $*p < 0.05$, $***p < 0.001$.

(Bradl and Lassmann, 2010; El Waly et al., 2014). Studies of children and adolescents with FASD have demonstrated white matter abnormalities, suggesting that ethanol has a long-lasting impact on myelination (Wilhelm and Guizzetti, 2016). During development, OPCs migrate from their origin to their functional site where they differentiate into mature myelinating oligodendrocytes. In rodents, myelin formation occurs abundantly during the first two postnatal weeks; however, OPC differentiation into mature myelinating oligodendrocytes can occur throughout life (El Waly et al., 2014). Ethanol effects on myelination in animal models of FASD have begun to be investigated. Studies have demonstrated that postnatal ethanol exposure in rats resulted in myelin deficits and aberrant eye-blink conditioning, which is a cerebellum-dependent learning task (Rufer et al., 2012). Using a similar postnatal model of FASD, ethanol was demonstrated to decrease both proliferating OPCs and mature oligodendrocytes in the corpus callosum. Interestingly, the effects of ethanol on OPCs depended on the ontogenetic origin of these cells. Furthermore, although OPC and oligodendrocyte numbers recovered by adulthood, the myelin microstructure remained aberrant as determined by diffusion tensor imaging (Newville et al., 2017). Myelin was also aberrant in third trimester models of FASD in sheep (Dalitz et al., 2008) and oligodendrocyte apoptosis was abundant in a third trimester FASD model in macaques (Creeley et al., 2013). We have recently demonstrated that ethanol dysregulated transcripts associated with OPCs, pre-myelinating oligodendrocytes, and mature oligodendrocytes in a postnatal mouse model of FASD in which animals were treated with ethanol from P4-9 and cerebellum isolated at P10 (Niedzwiedz-Massey et al., 2021a). Using the same model, we demonstrated that ethanol decreased the expression of transcripts associated with OPCs and mature oligodendrocytes in the hippocampus (Niedzwiedz-Massey et al., 2021b). In the current study, we evaluated the effects of ethanol on immature oligodendrocyte lineage cells and mature myelinating oligodendrocytes at P5 and P6. Interestingly, at P5, ethanol induced a significant increase in transcripts associated with both immature oligodendrocyte lineage cells and myelinating oligodendrocytes. This increase in the expression of oligodendrocyte related transcripts, particularly those associated with OPCs may result from an initial compensatory response to the toxic effects of ethanol. OPCs are highly proliferative during this stage of development and continue to proliferate until a balanced number of OPCs is reached (Hughes et al., 2013). If this balance is disrupted, perhaps as a response to ethanol, OPCs are triggered

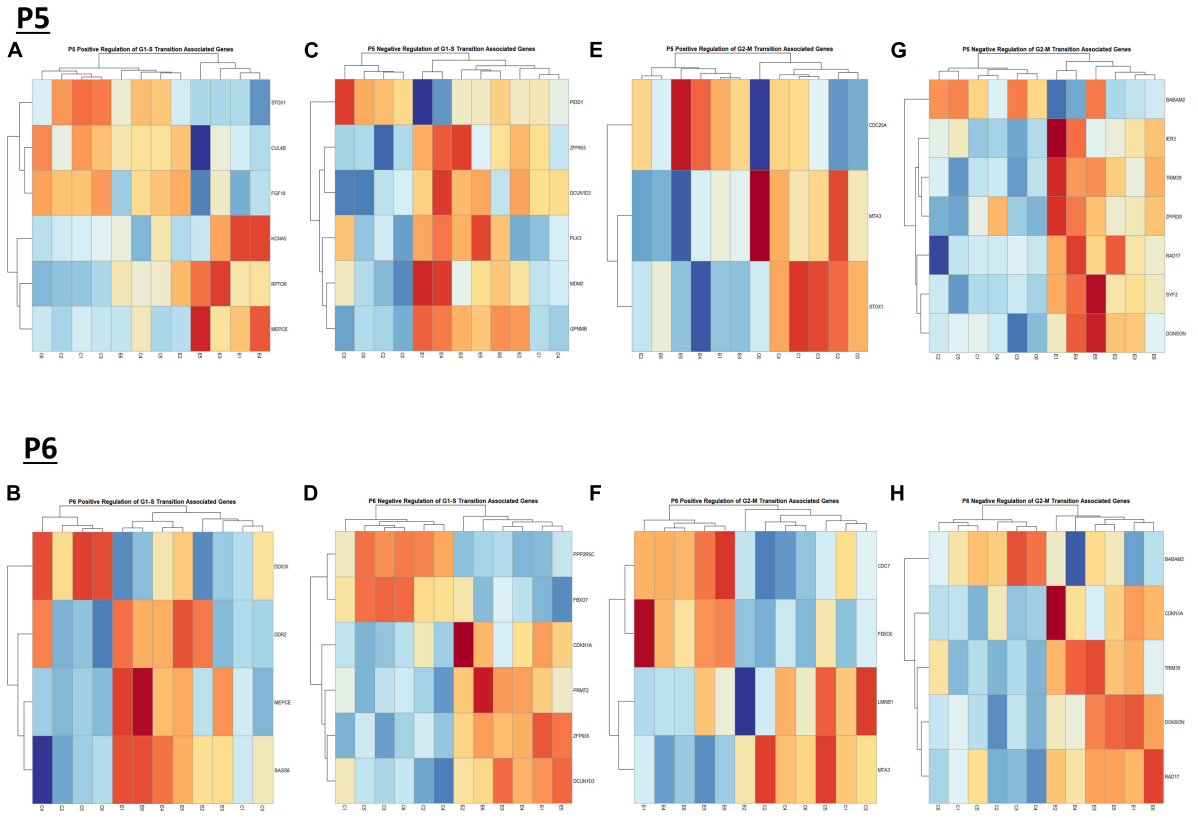


FIGURE 9
Heatmap and hierarchical clustering of cell cyle associated genes at P5 and P6. R statistical software was utilized to construct heatmaps and hierarchical clustering dendrogram of relative gene expression across samples for significantly altered (adj. $p < 0.05$) and categorized cell cycle associated genes as detailed in Methods. Positive regulation of G1-S transition associated gene expression is depicted in panel **(A)** for P5 and panel **(B)** for P6. Negative regulation of G1-S transition associated gene expression is depicted in panel **(C)** for P5 and **(D)** for P6. Positive regulation of G2-M transition associated gene expression is depicted in panel **(E)** for P5 and **(F)** for P6. Negative regulation of G2-M transition associated genes is depicted in panel **(G)** for P5 and panel **(H)** for P6.

to continue proliferation in order to maintain a consistent pool (Hughes et al., 2013). At P6, ethanol did not alter the expression of transcripts associated with early-stage oligodendrocytes but decreased the expression of transcripts associated with mature oligodendrocytes. The decrease in myelin forming oligodendrocyte transcripts seen at P6 could result in decreased myelination observed in FASD. These results suggest that after two days of consecutive ethanol exposure one begins to see a depletion in myelinating oligodendrocytes.

Developmental alcohol exposure is known to affect cell cycle regulation and apoptosis related events (Anthony et al., 2008). At P5, we saw no significant effect of ethanol on transcripts associated with the positive regulation of G1-S transition, and an increase in transcripts involved in negative regulation of this cell cycle phase. Ethanol also decreased the expression of positive regulators and increased the expression of negative regulators of the G2-M phase at P5. Collectively, these data suggest that ethanol negatively impacts G1-S and G2-M transitions at P5. At P6, ethanol increased the expression of transcripts involved in both positive and negative regulation of the G1-S transition. Ethanol did not alter the expression of positive regulators but increased the expression of negative regulators of the G2-M transition at P6. Collectively, these data show no clear effect of ethanol on G1-S transition and a decrease in G2-M transition at P6. During early postnatal development in rodents, cells in the external germinal layer of the cerebellum undergo vast proliferation to generate a substantial pool of cerebellar granule progenitors, which eventually form cerebellar neurons (Miale and Sidman, 1961; Altman, 1997; Li et al., 2002). Additionally, cerebellar interneurons are born and migrate to their final destination to form synaptic connections with Purkinje cells (Schilling et al., 2008; Leto and Rossi, 2012). Our data suggest that early third trimester equivalent ethanol exposure halts cell cycle progression in both the synthesis and mitosis phases, preventing cells from replicating. The accumulation of cells in these phases could result in a potential decrease in the pool of cerebellar granule cells that will eventually form mature neurons while also limiting the generation of interneurons. Having deficits in both granule cells and interneurons of the cerebellum could contribute to the reduced cerebellar volume and aberrant motor function and cognitive deficits seen in individuals with FASD. However, further studies are needed to evaluate this possibility.

The current study demonstrated that ethanol altered the transcriptomic profile in the cerebellum in a postnatal model of FASD. However, there are several limitations in the experimental design which should be considered when interpreting these data. For example, it should be acknowledged that alterations in transcript expression in the current RNASeq analysis will need to be confirmed by RT-PCR analysis. Furthermore, these transcript

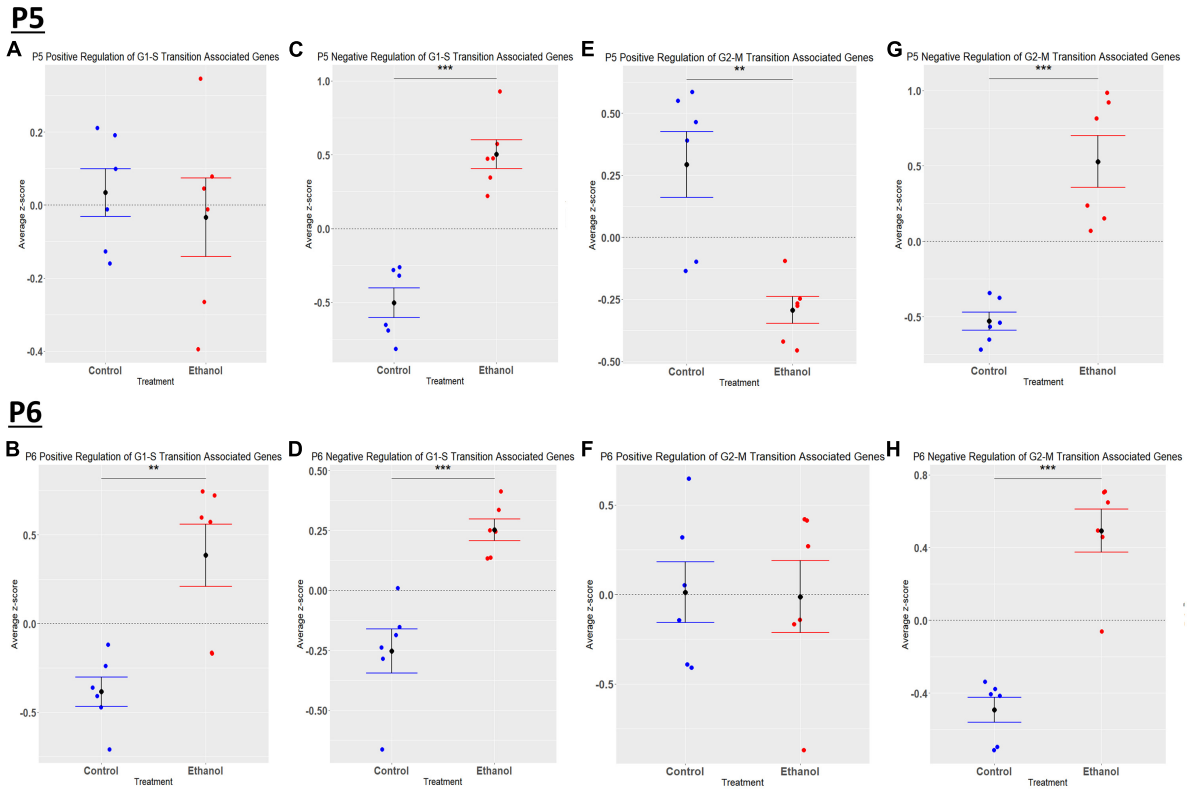


FIGURE 10
Ethanol-induced alterations in cell cycle regulation at P5 and P6 in the cerebellum. Gene list associated with positive and negative regulation of G1-S transition and positive and negative regulation of G2-M transition were extracted from the Mouse Genome Database. Genes associated with each cell cycle stage in our dataset at P5 and P6 were extracted as detailed in Methods. R statistical software was utilized to generate individual z-scores for each transcript of interest and each experimental animal. These z-scores were then averaged across transcripts for each individual animal. Quantification by average z-score of positive regulation of G1-S transition associated genes at P5 **(A)** and P6 **(B)**, negative regulation of G1-S transition associated genes at P5 **(C)** and P6 **(D)**, positive regulation of G2-M transition associated genes at P5 **(E)** and P6 **(F)**, and negative regulation of G2-M transition associated genes at P5 **(G)** and P6 **(H)**. $n = 3$ males and 3 females per treatment group E or C; $^{**}p < 0.01$, $^{***}p < 0.001$.

changes need to be evaluated at the level of protein expression. Increasing the sample size would also add confidence that the observed results will be experimentally reproducible. The levels of alcohol used in the current studies are also relatively high. Future studies are needed to determine transcriptomic changes in mice treated with more moderate levels of ethanol. It also should be acknowledged that some of the transcriptomic changes observed may not result solely or specifically due to ethanol but could result from a more general acute stress response to high doses of ethanol. Future studies are also needed to determine which transcripts and pathways altered by ethanol in these studies may contribute to the pathogenesis of FASD and thus represent potential targets for FASD therapy. We also note that the expression of more transcripts was observed at P5 after a single dose of ethanol than at P6 after two doses of ethanol. Additional studies are needed to determine the potential relevance of these temporal changes in transcriptomic profiles to FASD.

In conclusion, the current studies demonstrate that ethanol has profound effects on the transcriptomic profile in the developing cerebellum, early following initial ethanol exposure which may be critical in the development of FASD. IPA analysis indicated that ethanol likely alters pathways involved in immune signaling and cell cycle. With regard to glia, ethanol induced an increase in transcripts related to a neurodegenerative microglia phenotype along with an increase in transcripts associated with acute and pan-injury reactive astrocyte phenotypes at both P5 and P6 and additionally a chronic neurodegenerative disease astrocyte phenotype at P6 but not P5. Lastly, ethanol induced differing effects in the expression of genes associated with immature oligodendrocyte lineage cells and myelinating oligodendrocytes. These studies may begin to unravel the effects of ethanol during the onset of FASD.

Data availability statement

The data discussed in this publication have been deposited in NCBI's Gene Expression Omnibus and are accessible through GEO Series accession number: GSE226532 (https://www.ncbi.nlm.nih.gov/geo/query/acc.cgi?acc=GSE226532).

Ethics statement

This animal study was reviewed and approved by University of Arkansas for Medical Sciences, Institutional Animal Care and Use Committee (IACUC).

Author contributions

PD, CK, and AM: conceptualization. KH, JD, and PD: writing—original draft. KH, JD, TR, AM, CK, and PD: writing—review and editing. KH, JD, and TR: investigation and visualization. KH and JD: formal analysis. PD and AM: supervision. All authors had access to the data for the study, made substantial contributions to the manuscript, approved the submitted version of the manuscript, and take responsibility for the accuracy and integrity of the data.

Funding

This work was supported by grants from the National Institutes of Health, National Institute on Alcohol Abuse and Alcoholism, RO1 AA024695, RO1 AA026665, and RO1 AA027111.

Acknowledgments

RNA sequencing was performed by the UAMS Genomics Core which is supported by the Winthrop P. Rockefeller Cancer Institute, University of Arkansas for Medical Sciences.

Conflict of interest

The authors declare that the research was conducted in the absence of any commercial or financial relationships that could be construed as a potential conflict of interest.

Publisher's note

All claims expressed in this article are solely those of the authors and do not necessarily represent those of their affiliated organizations, or those of the publisher, the editors and the reviewers. Any product that may be evaluated in this article, or claim that may be made by its manufacturer, is not guaranteed or endorsed by the publisher.

Supplementary material

The Supplementary Material for this article can be found online at: https://www.frontiersin.org/articles/10.3389/fnins.2023.1154637/full#supplementary-material

References

Alfonso-Loeches, S., Ureña-Peralta, J. R., Morillo-Bargues, M. J., Oliver-De La Cruz, J., and Guerri, C. (2014). Role of mitochondria ROS generation in ethanol-induced NLRP3 inflammasome activation and cell death in astroglial cells. *Front. Cell Neurosci.* 8:216. doi: 10.3389/fncel.2014.00216

Altman, J. (1997). *Development of the cerebellar system in relation to its evolution, structure, and functions*. New York, NY: CRC Press.

Anthony, B., Zhou, F. C., Ogawa, T., Goodlett, C. R., and Ruiz, J. (2008). Alcohol exposure alters cell cycle and apoptotic events during early neurulation. *Alcohol Alcohol.* 43, 261–273. doi: 10.1093/alcalc/agm166

Apte, U. M., Banerjee, A., McRee, R., Wellberg, E., and Ramaiah, S. K. (2005). Role of osteopontin in hepatic neutrophil infiltration during alcoholic steatohepatitis. *Toxicol. Appl. Pharmacol.* 207, 25–38. doi: 10.1016/j.taap.2004.12.018

Artegiani, B., Lyubimova, A., Muraro, M., van Es, J. H., van Oudenaarden, A., and Clevers, H. (2017). A single-cell RNA sequencing study reveals cellular and molecular dynamics of the hippocampal neurogenic niche. *Cell Rep.* 21, 3271–3284. doi: 10.1016/j.celrep.2017.11.050

Baumann, N., and Pham-Dinh, D. (2001). Biology of oligodendrocyte and myelin in the mammalian central nervous system. *Physiol. Rev.* 81, 871–927. doi: 10.1152/physrev.2001.81.2.871

Bellahcène, A., Castronovo, V., Ogbureke, K. U., Fisher, L. W., and Fedarko, N. S. (2008). Small integrin-binding ligand N-linked glycoproteins (SIBLINGs): Multifunctional proteins in cancer. *Nat. Rev. Cancer* 8, 212–226. doi: 10.1038/nrc2345

Berres, M. E., Garic, A., Flentke, G. R., and Smith, S. M. (2017). Transcriptome profiling identifies ribosome biogenesis as a target of alcohol teratogenicity and vulnerability during early embryogenesis. *PLoS One* 12:e0169351. doi: 10.1371/journal.pone.0169351

Blanco, A. M., Vallés, S. L., Pascual, M., and Guerri, C. (2005). Involvement of TLR4/type I IL-1 receptor signaling in the induction of inflammatory mediators and cell death induced by ethanol in cultured astrocytes. *J. Immunol.* 175, 6893–6899. doi: 10.4049/jimmunol.175.10.6893

Blednov, Y. A., Bergeson, S. E., Walker, D., Ferreira, V. M., Kuziel, W. A., and Harris, R. A. (2005). Perturbation of chemokine networks by gene deletion alters the reinforcing actions of ethanol. *Behav. Brain Res.* 165, 110–125. doi: 10.1016/j.bbr.2005.06.026

Blighe, K., Rana, S., and Lewis, M. (2022). *EnhancedVolcano: Publication-ready volcano plots with enhanced colouring and labeling*. R package version 1.16.0. Available online at: https://github.com/kevinblighe/EnhancedVolcano

Bradl, M., and Lassmann, H. (2010). Oligodendrocytes: Biology and pathology. *Acta Neuropathol.* 119, 37–53. doi: 10.1007/s00401-009-0601-5

Bult, C. J., Blake, J. A., Smith, C. L., Kadin, J. A., and Richardson, J. E. (2019). Mouse genome database (MGD) 2019. *Nucleic Acids Res.* 47, D801–D806. doi: 10.1093/nar/gky1056

Butovsky, O., and Weiner, H. L. (2018). Microglial signatures and their role in health and disease. *Nat. Rev. Neurosci.* 19, 622–635. doi: 10.1038/s41583-018-0057-5

Camarillo, C., and Miranda, R. C. (2007). Ethanol exposure during neurogenesis induces persistent effects on neural maturation: Evidence from an ex vivo model of fetal cerebral cortical neuroepithelial progenitor maturation. *Gene Expr.* 14, 159–171.

Clancy, B., Darlington, R. B., and Finlay, B. L. (2001). Translating developmental time across mammalian species. *Neurosci. Lett.* 105, 7–17.

Creeley, C. E., Dikranian, K. T., Johnson, S. A., Farber, N. B., and Olney, J. W. (2013). Alcohol-induced apoptosis of oligodendrocytes in the fetal macaque brain. *Acta Neuropathol. Commun.* 1:23. doi: 10.1186/2051-5960-1-23

Crews, F. T., Lawrimore, C. J., Walter, T. J., and Coleman, L. G. Jr. (2017). The role of neuroimmune signaling in alcoholism. *Neuropharmacology* 122, 56–73. doi: 10.1016/j.neuropharm.2017.01.031

Dalitz, P., Cock, M., Harding, R., and Rees, S. (2008). Injurious effects of acute ethanol exposure during late gestation on developing white matter in fetal sheep. *Int. J. Dev. Neurosci.* 26, 391–399. doi: 10.1016/j.ijdevneu.2008.03.008

Das, R., Philip, S., Mahabeleshwar, G. H., Bulbule, A., and Kundu, G. C. (2005). Osteopontin: It's role in regulation of cell motility and nuclear factor kappa B-mediated urokinase type plasminogen activator expression. *IUBMB Life* 57, 441–447. doi: 10.1080/15216540500159424

Das, S., Li, Z., Noori, A., Hyman, B. T., and Serrano-Pozo, A. (2020). Meta-analysis of mouse transcriptomic studies supports a context-dependent astrocyte reaction in acute CNS injury versus neurodegeneration. *J. Neuroinflammation* 17:227. doi: 10.1186/s12974-020-01898-y

Das, S., Song, Z., Han, H., Ge, X., Desert, R., Athavale, D., et al. (2022). Intestinal osteopontin protects from alcohol-induced liver injury by preserving the gut microbiome and the intestinal barrier function. *Cell Mol. Gastroenterol. Hepatol.* 14, 813–839. doi: 10.1016/j.jcmgh.2022.06.012

Dong, Y., and Benveniste, E. N. (2001). Immune function of astrocytes. *Glia* 36, 180–190. doi: 10.1002/glia.1107

Drew, P. D., and Kane, C. J. (2014). Fetal alcohol spectrum disorders and neuroimmune changes. *Int. Rev. Neurobiol.* 118, 41–80. doi: 10.1016/B978-0-12-801284-0.00003-8

Drew, P. D., Johnson, J. W., Douglas, J. C., Phelan, K. D., and Kane, C. J. M. (2015). Pioglitazone blocks ethanol induction of microglial activation and immune responses in the hippocampus, cerebellum, and cerebral cortex in a mouse model of fetal alcohol spectrum disorders. *Alcohol. Clin. Exp. Res.* 39, 445–454. doi: 10.1111/acer.12639

Edgar, R., Domrachev, M., and Lash, A. E. (2002). Gene expression omnibus: NCBI gene expression and hybridization array data repository. *Nucleic Acids Res.* 30, 207–210. doi: 10.1093/nar/30.1.207

El Waly, B., Macchi, M., Cayre, M., and Durbec, P. (2014). Oligodendrogenesis in the normal and pathological central nervous system. *Front. Neurosci.* 8:145. doi: 10.3389/fnins.2014.00145

Erickson, E. K., Blednov, Y. A., Harris, R. A., and Mayfield, R. D. (2019). Glial gene networks associated with alcohol dependence. *Sci. Rep.* 9:10949. doi: 10.1038/s41598-019-47454-4

Farris, S. P., and Mayfield, R. D. (2014). RNA–Seq reveals novel transcriptional reorganization in human alcoholic brain. *Int. Rev. Neurobiol.* 116, 275–300. doi: 10.1016/B978-0-12-801105-8.00011-4

Floreani, N. A., Rump, T. J., Abdul Muneer, P. M., Alikunju, S., Morsey, B. M., Brodie, M. R., et al. (2010). Alcohol-induced interactive phosphorylation of Src and toll-like receptor regulates the secretion of inflammatory mediators by human astrocytes. *J. Neuroimmune Pharmacol.* 5, 533–545. doi: 10.1007/s11481-010-9213-z

Franco, R., and Fernández-Suárez, D. (2015). Alternatively activated microglia and macrophages in the central nervous system. *Prog. Neurobiol.* 131, 65–86. doi: 10.1016/j.pneurobio.2015.05.003

Greenmyer, J. R., Klug, M. G., Kambeitz, C., Popova, S., and Burd, L. (2018). A Multicountry updated assessment of the economic impact of fetal alcohol spectrum disorder: Costs for children and adults. *J. Addict. Med.* 12, 466–473. doi: 10.1097/ADM.0000000000000438

Guizzetti, M., Zhang, X., Goeke, C., and Gavin, D. P. (2014). Glia and neurodevelopment: Focus on fetal alcohol spectrum disorders. *Front. Pediatr.* 2:123. doi: 10.3389/fped.2014.00123

He, J., and Crews, F. T. (2008). Increased MCP-1 and microglia in various regions of the human alcoholic brain. *Exp. Neurol.* 210, 349–358.

Holtman, I. R., Raj, D. D., Miller, J. A., Schaafsma, W., Yin, Z., Brouwer, N., et al. (2015). Induction of a common microglia gene expression signature by aging and neurodegenerative conditions: A co-expression meta-analysis. *Acta Neuropathol. Commun.* 3:31. doi: 10.1186/s40478-015-0203-5

Hoyme, H. E., Kalberg, W. O., Elliott, A. J., Blankenship, J., Buckley, D., Marais, A.-S., et al. (2016). Updated clinical guidelines for diagnosing fetal alcohol spectrum disorders. *Pediatrics* 138:e20154256.

Hughes, E. G., Kang, S. H., Fukaya, M., and Bergles, D. E. (2013). Oligodendrocyte progenitors balance growth with self-repulsion to achieve homeostasis in the adult brain. *Nat. Neurosci.* 16, 668–676. doi: 10.1038/nn.3390

Jew, B., Alvarez, M., Rahmani, E., Miao, Z., Ko, A., Garske, K. M., et al. (2020). Accurate estimation of cell composition in bulk expression through robust integration of single-cell information. *Nat. Commun.* 11:1971.

Jurga, A. M., Paleczna, M., and Kuter, K. Z. (2020). Overview of general and discriminating markers of differential microglia phenotypes. *Front. Cell Neurosci.* 14:198. doi: 10.3389/fncel.2020.00198

Kalinin, S., González-Prieto, M., Scheiblich, H., Lisi, L., Kusumo, H., Heneka, M. T., et al. (2018). Transcriptome analysis of alcohol-treated microglia reveals downregulation of beta amyloid phagocytosis. *J. Neuroinflammation* 15:141. doi: 10.1186/s12974-018-1184-7

Kane, C. J. M., Douglas, J. C., Rafferty, T., Johnson, J. W., Niedzwiedz-Massey, V. M., Phelan, K. D., et al. (2021). Ethanol modulation of cerebellar neuroinflammation in a postnatal mouse model of fetal alcohol spectrum disorders. *J. Neurosci. Res.* 99, 1986–2007. doi: 10.1002/jnr.24797

Kane, C. J., Phelan, K. D., Douglas, J. C., Wagoner, G., Johnson, J. W., Xu, J., et al. (2014). Effects of ethanol on immune response in the brain: Region-specific changes in adolescent versus adult mice. *Alcohol. Clin. Exp. Res.* 38, 384–391. doi: 10.1111/acer.12244

Kane, C. J., Phelan, K. D., Han, L., Smith, R. R., Xie, J., Douglas, J. C., et al. (2011). Protection of neurons and microglia against ethanol in a mouse model of fetal alcohol spectrum disorders by peroxisome proliferator-activated receptor-γ agonists. *Brain Behav. Immun.* 25, S137–S145. doi: 10.1016/j.bbi.2011.02.016

Keren-Shaul, H., Spinrad, A., Weiner, A., Matcovitch-Natan, O., Dvir-Szternfeld, R., Ulland, T. K., et al. (2017). A unique microglia type associated with restricting development of Alzheimer's disease. *Cell* 169, 1276–1290.e17. doi: 10.1016/j.cell.2017.05.018

Krasemann, S., Madore, C., Cialic, R., Baufeld, C., Calcagno, N., El Fatimy, R., et al. (2017). The TREM2-APOE pathway drives the transcriptional phenotype of dysfunctional microglia in neurodegenerative diseases. *Immunity* 47, 566–581.e9. doi: 10.1016/j.immuni.2017.08.008

Lange, S., Probst, C., Gmel, G., Rehm, J., Burd, L., and Popova, S. (2017). Global prevalence of fetal alcohol spectrum disorder among children and youth: A systematic review and meta-analysis. *JAMA Pediatr.* 171, 948–956.

Lebel, C., Walker, L., Leemans, A., Phillips, L., and Beaulieu, C. (2008). Microstructural maturation of the human brain from childhood to adulthood. *Neuroimage* 40, 1044–1055.

Leto, K., and Rossi, F. (2012). Specification and differentiation of cerebellar GABAergic neurons. *Cerebellum* 11, 434–435.

Li, T., and Zhang, S. (2016). Microgliosis in the injured brain: Infiltrating cells and reactive microglia both play a role. *Neuroscientist* 22, 165–170. doi: 10.1177/1073858415572079

Li, Z., Miller, M. W., and Luo, J. (2002). Effects of prenatal exposure to ethanol on the cyclin-dependent kinase system in the developing rat cerebellum. *Brain Res. Dev. Brain Res.* 139, 237–245. doi: 10.1016/s0165-3806(02)00573-4

Liao, Y., Smyth, G. K., and Shi, W. (2014). featureCounts: An efficient general purpose program for assigning sequence reads to genomic features. *Bioinformatics* 30, 923–930. doi: 10.1093/bioinformatics/btt656

Liddelow, S. A., Guttenplan, K. A., Clarke, L. E., Bennett, F. C., Bohlen, C. J., Schirmer, L., et al. (2017). Neurotoxic reactive astrocytes are induced by activated microglia. *Nature* 541, 481–487.

Lin, E. Y., Xi, W., Aggarwal, N., and Shinohara, M. L. (2022). Osteopontin (OPN)/SPP1: From its biochemistry to biological functions in the innate immune system and the central nervous system (CNS). *Int. Immunol.* dxac060. doi: 10.1093/intimm/dxac060 [Epub ahead of print].

Lynch, A. M., Murphy, K. J., Deighan, B. F., O'Reilly, J. A., Gun'ko, Y. K., Cowley, T. R., et al. (2010). The impact of glial activation in the aging brain. *Aging Dis.* 1, 262–278.

May, P. A., Chambers, C. D., Kalberg, W. O., Zellner, J., Feldman, H., Buckley, D., et al. (2018). Prevalence of fetal alcohol spectrum disorders in 4 US communities. *JAMA* 319, 474–482.

Miale, I. L., and Sidman, R. L. (1961). An autoradiographic analysis of histogenesis in the mouse cerebellum. *Exp. Neurol.* 4, 277–296.

Moore, C. S., Ase, A. R., Kinsara, A., Rao, V. T., Michell-Robinson, M., Leong, S. Y., et al. (2015). P2Y12 expression and function in alternatively activated human microglia. *Neurol. Neuroimmunol. Neuroinflamm.* 2:e80.

Naj, A. C., Jun, G., Reitz, C., Kunkle, B. W., Perry, W., Park, Y. S., et al. (2014). Effects of multiple genetic loci on age at onset in late-onset Alzheimer disease: A genome-wide association study. *JAMA Neurol.* 71, 1394–1404. doi: 10.1001/jamaneurol.2014.1491

Newville, J., Valenzuela, C. F., Li, L., Jantzie, L. L., and Cunningham, L. A. (2017). Acute oligodendrocyte loss with persistent white matter injury in a third trimester equivalent mouse model of fetal alcohol spectrum disorder. *Glia* 65, 1317–1332. doi: 10.1002/glia.23164

Niedzwiedz-Massey, V. M., Douglas, J. C., Rafferty, T., Kane, C. J. M., and Drew, P. D. (2021a). Ethanol effects on cerebellar myelination in a postnatal mouse model of fetal alcohol spectrum disorders. *Alcohol* 96, 43–53. doi: 10.1016/j.alcohol.2021.07.003

Niedzwiedz-Massey, V. M., Douglas, J. C., Rafferty, T., Wight, P. A., Kane, C. J. M., and Drew, P. D. (2021b). Ethanol modulation of hippocampal neuroinflammation, myelination, and neurodevelopment in a postnatal mouse model of fetal alcohol spectrum disorders. *Neurotoxicol. Teratol.* 87:107015. doi: 10.1016/j.ntt.2021.107015

Norman, A. L., Crocker, N., Mattson, S. N., and Riley, E. P. (2009). Neuroimaging and fetal alcohol spectrum disorders. *Dev. Disabil. Res. Rev.* 15, 209–217.

Ochocka, N., and Kaminska, B. (2021). Microglia diversity in healthy and diseased brain: Insights from single-cell omics. *Int. J. Mol. Sci.* 22:3027. doi: 10.3390/ijms22063027

Paolicelli, R. C., Sierra, A., Stevens, B., Tremblay, M. E., Aguzzi, A., Ajami, B., et al. (2022). Microglia states and nomenclature: A field at its crossroads. *Neuron* 110, 3458–3483. doi: 10.1016/j.neuron.2022.10.020

Pinson, M. R., Holloway, K. N., Douglas, J. C., Kane, C. J. M., Miranda, R. C., and Drew, P. D. (2021). Divergent and overlapping hippocampal and cerebellar transcriptome responses following developmental ethanol exposure during the secondary neurogenic period. *Alcohol. Clin. Exp. Res.* 45, 1408–1423. doi: 10.1111/acer.14633

Ransohoff, R. M., and Brown, M. A. (2012). Innate immunity in the central nervous system. *J. Clin. Invest.* 122, 1164–1171. doi: 10.1172/JCI58644

Ransohoff, R. M., and Perry, V. H. (2009). Microglial physiology: Unique stimuli, specialized responses. *Annu. Rev. Immunol.* 27, 119–145. doi: 10.1146/annurev.immunol.021908.132528

Rice, D., and Barone, S. Jr. (2000). Critical periods of vulnerability for the developing nervous system: Evidence from humans and animal models. *Environ. Health Perspect.* 108(Suppl. 3), 511–533.

Riley, E. P., and McGee, C. L. (2005). Fetal alcohol spectrum disorders: An overview with emphasis on changes in brain and behavior. *Exp. Biol. Med.* 230, 357–365. doi: 10.1177/15353702-0323006-03

Ritchie, M. E., Phipson, B., Wu, D., Hu, Y., Law, C. W., Shi, W., et al. (2015). Limma powers differential expression analyses for RNA-sequencing and microarray studies. *Nucleic Acids Res.* 43:e47. doi: 10.1093/nar/gkv007

Robinson, M. D., and Oshlack, A. (2010). A scaling normalization method for differential expression analysis of RNA-seq data. *Genome Biol.* 11:R25. doi: 10.1186/gb-2010-11-3-r25

Rufer, E. S., Tran, T. D., Attridge, M. M., Andrzejewski, M. E., Flentke, G. R., and Smith, S. M. (2012). Adequacy of maternal iron status protects against behavioral, neuroanatomical, and growth deficits in fetal alcohol spectrum disorders. *PLoS One* 7:e47499. doi: 10.1371/journal.pone.0047499

Saijo, K., and Glass, C. K. (2011). Microglial cell origin and phenotypes in health and disease. *Nat. Rev. Immunol.* 11, 775–787. doi: 10.1038/nri3086

Santello, M., Toni, N., and Volterra, A. (2019). Astrocyte function from information processing to cognition and cognitive impairment. *Nat. Neurosci.* 22, 154–166.

Schilling, K., Oberdick, J., Rossi, F., and Baader, S. L. (2008). Besides Purkinje cells and granule neurons: An appraisal of the cell biology of the interneurons of the cerebellar cortex. *Histochem. Cell Biol.* 130, 601–615. doi: 10.1007/s00418-008-0483-y

Seth, D., Gorrell, M. D., Cordoba, S., McCaughan, G. W., and Haber, P. S. (2006). Intrahepatic gene expression in human alcoholic hepatitis. *J. Hepatol.* 45, 306–320. doi: 10.1016/j.jhep.2006.04.013

Sokol, R. J. (2018). A Current evaluation of the economic costs for fetal alcohol spectrum disorder (FASD): A comment on the systematic review by Greenmeyer et al. *J. Addict. Med.* 12, 426–427. doi: 10.1097/ADM.0000000000000439

Sousa, C., Golebiewska, A., Poovathingal, S. K., Kaoma, T., Pires-Afonso, Y., Martina, S., et al. (2018). Single-cell transcriptomics reveals distinct inflammation-induced microglia signatures. *EMBO Rep.* 19:e46171. doi: 10.15252/embr.201846171

Tang, Y., and Le, W. (2016). Differential roles of M1 and M2 microglia in neurodegenerative diseases. *Mol. Neurobiol.* 53, 1181–1194. doi: 10.1007/s12035-014-9070-5

Tatsuyuki Matsudaira, M. P. (2022). Life and death of microglia: Mechanisms governing microglial states and fates. *Immunol. Lett.* 245, 51–60. doi: 10.1016/j.imlet.2022.04.001

Topper, L. A., Baculis, B. C., and Valenzuela, C. F. (2015). Exposure of neonatal rats to alcohol has differential effects on neuroinflammation and neuronal survival in the cerebellum and hippocampus. *J. Neuroinflammation* 12, 1–22. doi: 10.1186/s12974-015-0382-9

Wilhelm, C. J., and Guizzetti, M. (2016). Fetal alcohol spectrum disorders: An overview from the glia perspective. *Front. Integr. Neurosci.* 9:65. doi: 10.3389/fnint.2015.00065

Zamanian, J. L., Xu, L., Foo, L. C., Nouri, N., Zhou, L., Giffard, R. G., et al. (2012). Genomic analysis of reactive astrogliosis. *J. Neurosci.* 32, 6391–6410. doi: 10.1523/JNEUROSCI.6221-11.2012

Zeisel, A., Hochgerner, H., Lönnerberg, P., Johnsson, A., Memic, F., van der Zwan, J., et al. (2018). Molecular architecture of the mouse nervous system. *Cell* 174, 999–1014.e22. doi: 10.1016/j.cell.2018.06.021

Zeisel, A., Muñoz-Manchado, A. B., Codeluppi, S., Lönnerberg, P., La Manno, G., Juréus, A., et al. (2015). Brain structure. Cell types in the mouse cortex and hippocampus revealed by single-cell RNA-seq. *Science* 347, 1138–1142. doi: 10.1126/science.aaa1934

Zhang, K., Wang, H., Xu, M., Frank, J. A., and Luo, J. (2018). Role of MCP-1 and CCR2 in ethanol-induced neuroinflammation and neurodegeneration in the developing brain. *J. Neuroinflammation* 15:197. doi: 10.1186/s12974-018-1241-2

frontiers | Frontiers in Neuroscience

TYPE Original Research
PUBLISHED 20 March 2023
DOI 10.3389/fnins.2023.1127711

Check for updates

OPEN ACCESS

EDITED BY
Hermes H. Yeh,
Dartmouth College, United States

REVIEWED BY
Srdjan Joksimovic,
University of Pennsylvania, United States
Emi Hasegawa,
Kyoto University, Japan

*CORRESPONDENCE
Donald A. Wilson
✉ dwilson@nki.rfmh.org

SPECIALTY SECTION
This article was submitted to Neurodevelopment, a section of the journal Frontiers in Neuroscience

RECEIVED 19 December 2022
ACCEPTED 06 March 2023
PUBLISHED 20 March 2023

CITATION
Wilson DA, Fleming G, Williams CRO, Teixeira CM, Smiley JF and Saito M (2023) Somatostatin neuron contributions to cortical slow wave dysfunction in adult mice exposed to developmental ethanol.
Front. Neurosci. 17:1127711.
doi: 10.3389/fnins.2023.1127711

COPYRIGHT
© 2023 Wilson, Fleming, Williams, Teixeira, Smiley and Saito. This is an open-access article distributed under the terms of the Creative Commons Attribution License (CC BY). The use, distribution or reproduction in other forums is permitted, provided the original author(s) and the copyright owner(s) are credited and that the original publication in this journal is cited, in accordance with accepted academic practice. No use, distribution or reproduction is permitted which does not comply with these terms.

Somatostatin neuron contributions to cortical slow wave dysfunction in adult mice exposed to developmental ethanol

Donald A. Wilson[1,2,3]*, G. Fleming[1], C. R. O. Williams[1], C. M. Teixeira[1,2], J. F. Smiley[1,4] and Mariko Saito[1,4]

[1]Nathan S. Kline Institute for Psychiatric Research, Orangeburg, NY, United States, [2]Department of Child and Adolescent Psychiatry, New York University School of Medicine, New York, NY, United States, [3]Department of Neuroscience and Physiology, New York University School of Medicine, New York, NY, United States, [4]Department of Psychiatry, New York University School of Medicine, New York, NY, United States

Introduction: Transitions between sleep and waking and sleep-dependent cortical oscillations are heavily dependent on GABAergic neurons. Importantly, GABAergic neurons are especially sensitive to developmental ethanol exposure, suggesting a potential unique vulnerability of sleep circuits to early ethanol. In fact, developmental ethanol exposure can produce long-lasting impairments in sleep, including increased sleep fragmentation and decreased delta wave amplitude. Here, we assessed the efficacy of optogenetic manipulations of somatostatin (SST) GABAergic neurons in the neocortex of adult mice exposed to saline or ethanol on P7, to modulate cortical slow-wave physiology.

Methods: SST-cre × Ai32 mice, which selectively express channel rhodopsin in SST neurons, were exposed to ethanol or saline on P7. This line expressed similar developmental ethanol induced loss of SST cortical neurons and sleep impairments as C57BL/6By mice. As adults, optical fibers were implanted targeting the prefrontal cortex (PFC) and telemetry electrodes were implanted in the neocortex to monitor slow-wave activity and sleep-wake states.

Results: Optical stimulation of PFC SST neurons evoked slow-wave potentials and long-latency single-unit excitation in saline treated mice but not in ethanol mice. Closed-loop optogenetic stimulation of PFC SST neuron activation on spontaneous slow-waves enhanced cortical delta oscillations, and this manipulation was more effective in saline mice than P7 ethanol mice.

Discussion: Together, these results suggest that SST cortical neurons may contribute to slow-wave impairment after developmental ethanol.

KEYWORDS

fetal alcohol spectrum disorder (FASD), somatostatin, slow wave sleep (SWS), prefrontal cortex, GABA, cortical interneurons, closed loop optogenetics

1. Introduction

Developmental ethanol exposure disrupts subsequent normal sleep structure in animal models (Stone et al., 1996; Criado et al., 2008; Volgin and Kubin, 2012; Wilson et al., 2016; Ipsiroglu et al., 2019) and humans (Pesonen et al., 2009; Jan et al., 2010; Wengel et al., 2011; Chen et al., 2012; Inkelis and Thomas, 2018). Given the critical role of sleep for synaptic homeostasis (Tononi and Cirelli, 2014), emotional regulation (Goldstein and Walker, 2014; Ben Simon et al., 2020), memory consolidation (Born et al., 2006; Stickgold and Walker, 2007; Diekelmann and Born, 2010), and many other basic neurocognitive functions, this developmental ethanol-induced sleep impairment could contribute to a variety of behavioral outcomes associated with fetal alcohol spectrum disorder (FASD). The sleep impairment can include reduced time in slow wave sleep, increased sleep fragmentation, reduced cortical slow wave (delta) amplitude, reduced sleep spindle density, and impaired sleep homeostasis following sleep deprivation (Stone et al., 1996; Criado et al., 2008; Troese et al., 2008; Wengel et al., 2011; Chen et al., 2012; Volgin and Kubin, 2012; Wilson et al., 2016; Inkelis and Thomas, 2018; Lewin et al., 2018; Ipsiroglu et al., 2019). These diverse aspects of sleep/wake physiology are under the control of diverse brain regions and diverse neuromodulatory systems. However, GABAergic inhibitory interneurons, across multiple brain regions also play an important role in many aspects of sleep physiology (Pace-Schott and Hobson, 2002; Saper et al., 2010; Adamantidis et al., 2019). For example, sleep-wake state changes and state maintenance are stabilized by hypothalamic and basal forebrain circuits wherein inhibitory interneurons suppress activity of the ascending reticular activating system while the subject is asleep and a different population of GABAergic neurons suppress sleep circuits while the subject is awake (Saper et al., 2010; Xu et al., 2015). In addition, inhibitory interneurons in the neocortex are involved in entraining delta band slow-wave oscillations that occur during non-REM, slow-wave sleep (Steriade et al., 1993b; Pace-Schott and Hobson, 2002; Funk et al., 2017). Large amplitude slow-wave oscillations are critical for memory consolidation, synaptic homeostasis, and metabolic waste clearance that occur during sleep (Knyazev, 2012; Harmony, 2013; Xie et al., 2013).

During slow wave sleep, slow (<1 Hz) cortical oscillations (Steriade et al., 1993b) are spontaneously initiated primarily in prefrontal cortex and travel as an anterior-posterior wave across the cortex (Massimini et al., 2004; Niethard et al., 2018; Timofeev et al., 2020). These slow waves help organize and synchronize other slow wave sleep events such as the large amplitude delta frequency band (1–5 Hz) oscillations characteristic of slow wave sleep and sleep spindles (Molle and Born, 2011; Staresina et al., 2015). Slow wave oscillation amplitude during sleep can be enhanced by applying reinforcing stimulation (Bellesi et al., 2014). For example, in humans, transcranial stimulation oscillating at <1 Hz using a variety of technical approaches can enhance slow wave and delta band power as well as the time spent in slow wave sleep (Marshall et al., 2006; Massimini et al., 2007; Ketz et al., 2018). Auditory stimulation applied in closed loop feedback with spontaneous slow waves (<1 Hz) can similarly enhance slow wave amplitude as well as sleep spindle power (Ngo et al., 2013). Importantly enhancing slow wave sleep with either technique enhances hippocampal-dependent memory (Marshall et al., 2006; Ngo et al., 2013; Henin et al., 2019). Similar stimulation-induced slow waves (Vyazovskiy et al., 2009) and closed loop modulation of slow wave oscillations and memory have been observed in rodents (Moreira et al., 2021).

One class of GABAergic cells involved in cortical sleep-related oscillations is somatostatin expressing (SST) neurons (Kuki et al., 2015; Xu et al., 2015; Yavorska and Wehr, 2016; Funk et al., 2017; Espinosa et al., 2019; Bugnon et al., 2022). In rodents, SST neurons in the neocortex help promote slow wave neural oscillations by inducing 100–200 ms of inhibition (i.e., a cortical down-state) following the excitation induced by thalamic and cortical excitation of pyramidal cells as shown both *in vivo* (Funk et al., 2017) and in computational modeling (Bugnon et al., 2022). Cortical SST neuron activity is phase locked to cortical slow wave oscillations (Funk et al., 2017). This cycling between excitation and inhibition is observed as slow-wave oscillations in slow-wave sleep EEG. Chemogenetic or optogenetic activation of neocortical SST neurons enhance cortical slow wave amplitude and slow wave sleep duration and the extensive anterior-posterior extent of cortical SST+ axons could promote slow-wave propagation across the cortex (Funk et al., 2017). Overall SST activity is reduced during slow-wave sleep, which has been suggested to result in disinhibition of parvalbumin-expressing interneurons to promote cortical sleep spindles (Niethard et al., 2018).

Developmental ethanol exposure has profound effects on GABAergic neurons in several brain regions (Skorput et al., 2015; Smiley et al., 2015), and we have previously reported that postnatal day 7 (P7) ethanol exposure significantly reduces SST neuron number in neocortex through adulthood (Smiley et al., 2019). Furthermore, P7 ethanol can reduce time spent in slow-wave sleep (Wilson et al., 2016; Lewin et al., 2018), enhances sleep fragmentation (increased state transitions) (Wilson et al., 2016; Lewin et al., 2018), and reduces delta band oscillation amplitude in neocortex (Apuzzo et al., 2020). Here we began to explore whether the loss of SST GABAergic neurons in the neocortex could contribute to the changes in adult mice slow-wave activity known to be induced by developmental ethanol exposure. As a starting point, we focused on a single important variable out of the myriad factors involved in sleep physiology and sleep function. We used optogenetic activation of spared SST neurons in ethanol exposed and saline control mice to manipulate cortical slow-wave activity (Funk et al., 2017; Bugnon et al., 2022). Identifying mechanisms of developmental ethanol-induced sleep impairments is a first step toward cell-targeted treatment.

2. Materials and methods

2.1. Subjects

Male and female SST-Cre (Jackson stock 013044) × Ai32 (Jackson stock 024109) mice were used. These mice express channelrhodopsin-2/EYFP in all SST neurons (Madisen et al., 2012). At postnatal-day seven (P7) mice were injected

Abbreviations: FASD, fetal alcohol spectrum disorder; GABA, gamma amino butyric acid; LFP, local field potential; PFC, prefrontal cortex; PV, parvalbumin; SST, somatostatin.

subcutaneously in the back with ethanol (2.5 g/kg), while littermate controls were injected with the same volume of saline solution as previously described (Olney et al., 2002; Saito et al., 2007). All mice in a litter were randomly assigned to either ethanol or saline treatment. Pups were injected twice, 2 h apart and immediately returned to the home cage after each injection. This P7 ethanol treatment protocol induces a peak truncal blood alcohol level of 0.5 g/dL (i.e., highest level observed within 6 h of the second injection) as analyzed with an Alcohol Reagent Set (Pointe Scientific, Canton, MI, USA) (Saito et al., 2007). This is a commonly used model of late term binge ethanol exposure that allows ethanol exposure at a precise developmental point, allows littermate controls, and does not impact the maternal physiology (Olney et al., 2002; Saito et al., 2007; Wilson et al., 2016). Pups were weaned at P28 and then housed (cage width × length × height:18 × 28 × 12 cm) with same sex littermates until testing at P90 ± 10 days. Food and water were available ad lib and a 12:12 light dark cycle was used. All animal protocols were performed with approval of the Nathan S. Kline Institute for Psychiatric Research Institutional Animal Care and Use Committee's and were in accord with National Institutes of Health guidelines. Animal use followed the recommendations of the ARRIVE guidelines (Kilkenny et al., 2010).

2.2. Local field potential (LFP) recording and optical fiber implants

When the animals neared P90 they were implanted with either a single channel LFP telemetry device (model ETA-F10, DSI) with a 1 mm long bare electrode inserted in the frontal cortex (2.5 mm anterior to bregma, 2 mm lateral) to monitor sleep and wake bouts, or with a dual channel transmitter (model HD-X02, DSI) with a surface electrode in the frontal cortex and another in the ipsilateral visual cortex (4.0 mm posterior to Bregma, 3 mm lateral). Both spontaneous, and stimulus-evoked LFP data were digitized at 1,000 Hz and analyzed with Spike2 software. All animals also had bilateral optical fibers (Doric Lenses, MFC 200/250-0.66 ZF1.25(G) FLT) implanted in the frontal cortex at the coordinates of the LFP electrode.

2.3. Slow-wave sleep analyses

As previously described (Wilson et al., 2016), mice used for slow-wave sleep analyses were allowed to recover alone in their home cage for 3–5 days before 24-h recordings of basal sleep/wake cycling were begun. Data used for analysis began at 7 days post-surgery. Telemetry recordings do not require handling of the animals and continuous recordings post-surgery demonstrate normal sleep-wake cycles within 3 days. The transmitters used did not allow EMG measures, thus REM sleep was not monitored. All recordings were made from animals housed individually in sound attenuating chambers with developmentally ethanol-exposed and saline-exposed mice recorded simultaneously. Cortical LFP's were acquired and digitized at 1,000 Hz and analyzed using Spike2 software (CED, Inc.). Slow-wave activity was identified by band-pass filtering for delta frequency (0.1–5 Hz) and root mean square (r.m.s.) delta amplitude extracted. Delta amplitude was determined in 14 s epochs and periods of high delta were identified as being at least 1 standard deviation above the mean r.m.s. amplitude over a given 24 h period. Artifacts were removed before mean and standard deviation calculations. The analyses of slow-wave bouts included the mean percent time in slow-wave over 24 h, mean slow-wave bout duration, and the mean number of slow-wave bout transitions/h of slow-wave activity. The accuracy of slow-wave sleep scoring was also confirmed in a small set of animals with simultaneous visual scoring over 1–2 h periods ($n = 4$) to ensure scored sleep epochs corresponded to behavioral sleep periods (Lewin et al., 2019).

2.4. Frontal cortex optical stimulation

Following 7 days of recovery, recordings and optogenetic manipulations were begun. Animals were placed in a chamber (14 cm wide × 30 cm long × 20 cm high) situated over the telemetry receiver for LFP recording and were connected to a 473 nm laser (Shanghai Laser and Optics Century Co.; model BL473T3H-100FC) *via* optical cables (Doric; SBP(2)200/230/900-0.57 2 m FCM-2xZF1.25) and an optical swivel (Doric; FRJ FC:FC) to allow free movement. Power output at the optical fiber tip was 8–10 mW. For assessment of SST-induced traveling cortical slow-waves, unilateral single pulse flashes (50 ms duration) were delivered at 20 s ISI with the animal freely moving (>200 repeats) and evoked responses recorded from both the site of the stimulus (frontal cortex) and simultaneously 6 mm posterior in the visual cortex. For closed loop stimulation triggered on spontaneous cortical slow-waves, the mice received bilateral 50 ms flash triggered on the frontal cortex LFP negative wave during slow-wave sleep at either 0 or 50 ms delay from the slow-wave trough nadir. Closed loop stimulation was controlled by a custom script in Spike2. The effect of this closed loop stimulation on on-going frontal cortex delta band oscillation amplitude was assessed with Fast-Fourier Transform [FFT] using 2 Hz bins during slow-wave bouts (>100 s periods) with and without optical stimulation. The temporal order of stimulation and no stimulation periods was counterbalanced across animals.

In addition to local field potential recordings in freely moving mice, SST-Cre × Ai32 mice ($n = 4$ saline and 4 ethanol exposed) were anesthetized with urethane (1 g/kg) and prepared for single-unit recording with an optotrode targeting the frontal cortex. Unit activity was recorded with a tungsten microelectrode (5 MOhms) attached to an optical fiber (200 μ). Single-unit activity was extracted with template matching (Spike2). Spontaneous activity and light-evoked activity (50 ms flash, 20 s ISI) were quantified with peristimulus time histograms, with attention paid to the early period of induced inhibition and the later excitation as previously described (Funk et al., 2017).

2.5. Histology

Following data collection, animals were perfused (PBS and 4% paraformaldehyde) and brains sectioned to identify electrode and optical fiber placements.

A separate set of mice were used to confirm P7 ethanol exposure effects on adult (>P90) SSTcre × Ai32 mice. Stereological counts of SST neuron number in neocortex compared 5 mice treated with P7 ethanol with 5 saline injected mice, using methods previously described (Smiley et al., 2015, 2019). At P90–110 mice were anesthetized by intraperitoneal injection of 200 mg/kg ketamine and 10 mg/kg xylazine, and transcardially perfused with heparinized 4% paraformaldehyde in phosphate buffer, pH 7.2. Brains were embedded in agar blocks for simultaneous sectioning and processing. The agar-embedded brains were cryoprotected by sinking in 20% buffered glycerol, prior to freezing and sectioning in coronal orientation at 50 μm thickness on a sliding microtome. A series of sections containing every 12th consecutive section through the cerebral cortex was process for double immunofluorescent labeling using chicken anti-GFP (1:500 dilution, Abcam, ab13970) that was visualized with Alexa Fluor 488 (Abcam, cat # 150173), and rabbit anti-somatostatin (1:1,000, Origen cat# AP33464SU-N) that was visualized by consecutive incubations in biotinylated goat anti-rabbit (Vectastain Cat# BA-1000) and streptavidin 594 (Invitrogen Cat# S11227).

Estimates of cell number used the Nv x Vref method (Gundersen et al., 1988). Labeled cells were sampled with a Basler acA5472 camera mounted on a motorized Nikon E600 microscope controlled with ImageJ software. Sections were systematically sampled at a grid of sites covering the left neocortex in each section. At each sampling site identically focused Z-stacks were obtained for the GFP- and somatostatin-immunolabels. Each Z-stack contained 6 images, with 3 μm spacing between images. Cell counting was done on optical disector counting boxes that were drawn on each Z-stack so that both labels could be simultaneously viewed, and counting boxes were 9 μm deep (3 Z-slices) with upper and lower guard zones of 3 and 6 μm, respectively. Each brain was sampled with 213 +/– 19 (mean +/– S.D.) sampling sites, and the coefficient of error for cell number (Dorph-Petersen et al., 2009) was 0.07 +/– 0.01. Average on-slide section thickness was 56 +/– 2 μm.

2.6. Data analyses

Data were analyzed using ANOVA and or *t*-tests, with repeated measures ANOVA's used as appropriate. *Post hoc* comparisons were made with Fisher LSD tests. Significance was set at $p < 0.05$ for all tests.

3. Results

We first confirmed (n = 8/treatment group) that P7 ethanol induces similar effects on sleep in adult SST-Cre × Ai32 mice as previously reported in C57BL/6By mice (Wilson et al., 2016; Lewin et al., 2018; Apuzzo et al., 2020). As shown in **Figure 1**, SWS bout duration was significantly reduced [$t(14) = 2.96$, $p = 0.01$] and SWS transitions/hour of SWS were increased [$t(14) = 3.15$, $p = 0.007$] in P7 EtOH mice compared to saline controls. Cortical delta oscillation amplitude was also modified by P7 ethanol in a manner similar to that in C57BL/6By mice (Apuzzo et al., 2020) with a narrowing of the frequency distribution of delta amplitudes in ethanol mice (**Figure 1D**), including significantly reduced large amplitude oscillations [P7 exposure group × delta amplitude ANOVA, main effect of amplitude bin $F(32,448) = 7.52$, $p < 0.0001$] and exposure × bin interaction [$F(32,448) = 1.49$, $p = 0.044$]. Regions of significant *post hoc* differences are shown in **Figure 1D**. Large amplitude delta oscillations occur during slow-wave sleep thus the decrease in ethanol treated animals suggests an additional impact on sleep quality (Apuzzo et al., 2020).

In addition, we confirmed that SST neuron number was reduced in this mouse line by P7 ethanol. Stereological cell counts evaluated the reduction of somatostatin cells in whole neocortex caused by P7 ethanol treatment. Double labeling immunofluorescence identified somatostatin cells by GFP immunolabeling that was concentrated on the cell membrane, and somatostatin immunolabeling that was typically concentrated in cytoplasm of the cell soma (**Figure 1E**). Comparison of the two labels showed that about 85% of GFP cells had clearly distinguishable somatostatin-immunolabeling. Conversely, we did not find SST-immunolabeled cells that lacked SST-Cre. Comparison of ethanol and saline treated mice (n = 5 per treatment group) showed 16% reduction of GFP cells caused by ethanol treatment [**Figure 1F**, $t(8) = 3.23$, $p = 0.01$], and 15% reduction of SST-immunolabeled cells [**Figure 1G**, $t(8) = 2.71$, $p = 0.027$]. Separation of stereological cell counts by anterior-posterior section number (**Figures 1H, I**) indicated that the decrease of SST cell density was similar across cortex, as previously shown for parvalbumin and calretinin GABA cells after P7 ethanol treatment (Smiley et al., 2015).

To examine the function of spared SST neurons in cortical circuit activity *in vivo* optogenetic stimulation protocols were used. Optical stimulation of PFC SST neurons (**Figure 2A**) evoked a response in the local field potential recorded in both the prefrontal cortex and the visual cortex (**Figures 2B, C**). The evoked potential in the visual cortex evoked by PFC activation is consistent with a rostral-caudal traveling slow-wave (Massimini et al., 2004; Niethard et al., 2018). In adults exposed to saline at P7 (n = 5), the evoked potential consisted of a short latency positive wave, followed by a lower amplitude, long-lasting (200–400 ms) positive wave in both the prefrontal and visual cortices. These potentials may reflect a synaptic inhibition and excitation sequence occurring in response to GABAergic inhibition evoked by the simultaneous activation of SST neurons (Funk et al., 2017). In contrast, in adults exposed to ethanol at P7 (n = 9), the long latency, prolonged positive evoked potential was absent in both the prefrontal and visual cortices (**Figure 2D**). Mean evoked potentials were significantly different between saline and ethanol treated animals in both the prefrontal cortex [ANOVA, time post-stimulus × P7 treatment interaction, $F(300,2099) = 1.203$, $p = 0.0145$] and the visual cortex [time × P7 treatment interaction, $F(300,1798) = 4.877$, $p < 0.0001$]. *Post hoc* Fisher comparisons revealed the differences were most pronounced during the period of the late positive wave. This suggests an impairment in SST neuron activation to induce slow-wave cortical oscillations in developmental ethanol exposed mice compared to saline exposed mice shown here, and as compared to previous reports (Funk et al., 2017).

As an initial assessment of the neural activity underlying these evoked potentials, single-unit activity in response to SST optical stimulation was examined in the PFC of urethane-anesthetized mice (n = 8 mice; 4 saline mice, n = 47 units; 4 EtOH mice, n = 46 units). As shown in **Figures 3A, B**, a subset of the units

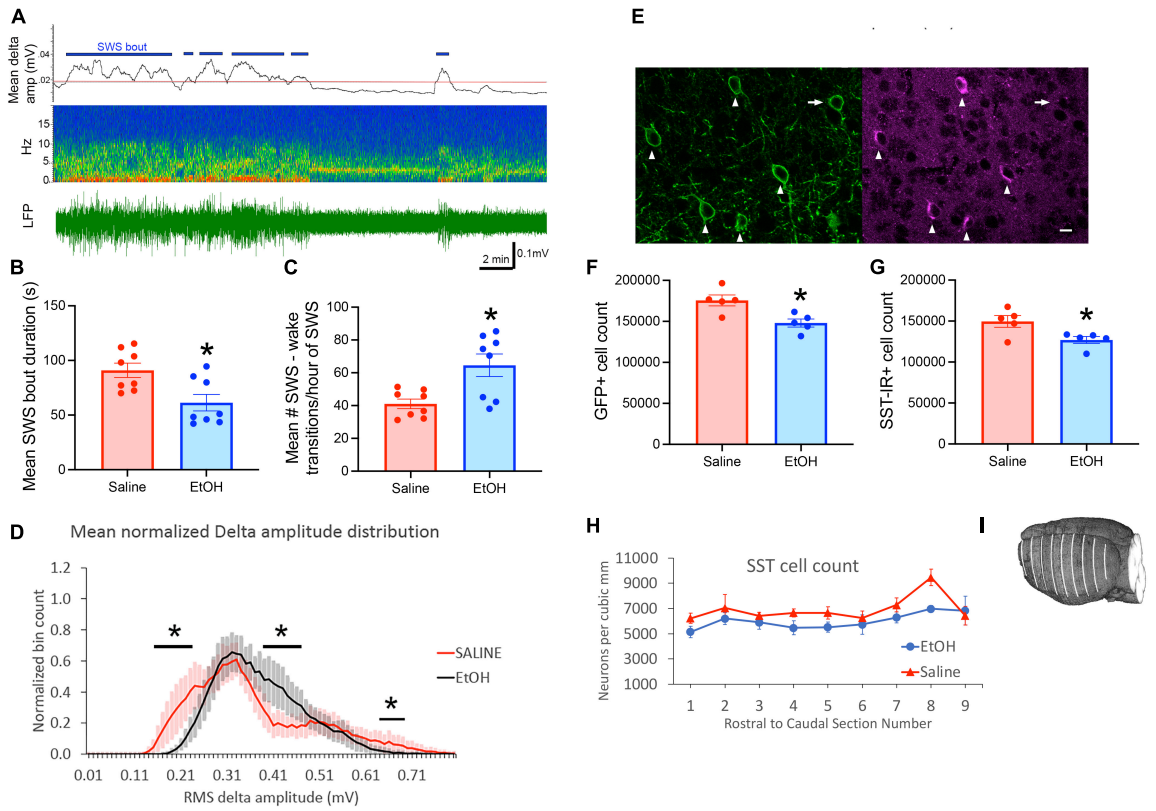


FIGURE 1
Slow-wave sleep in adult SST cre × Ai32 mice exposed to ethanol at P7 was impaired compared to saline controls. **(A)** Representative cortical LFP recording with raw LFP shown in bottom trace and time-frequency pseudocolor spectrograph shown in center. Top trace shows r.m.s. delta amplitude and 1 standard deviation above mean delta amplitude (red line) extracted from a 24 h recording. Periods of delta amplitude above the red line were classified as slow-wave sleep (horizontal blue markers) and coincided with behavioral inactivity as previously described (Wilson et al., 2016; Lewin et al., 2018). Slow-wave changes in ethanol mice compared to saline (n = 8/group) included **(B)** shorter SWS bout durations and **(C)** increased sleep-wake transitions, which together constitute sleep fragmentation. **(D)** In addition, delta amplitude oscillations were modified to display significantly fewer high amplitude waves. Horizontal lines highlight regions of significant *post hoc* comparisons between treatment groups ($p < 0.05$). **(E)** Stereological cell counts were used to evaluate the number of somatostatin cells in neocortex, in sections double labeled with ant-GFP and anti-somatostatin antibodies (n = 5 mice/group). In 85% of the SST-Cre cells, SST-immunolabeling (arrowheads) was found, but it was not confirmed in the remaining cells (arrow). We did not find SST-immunolabeled cells that lacked SST-Cre. Scale bar = 10 um. **(F,G)** P7 Ethanol exposure significantly reduced SST cell count as assessed in both GFP cells and SST immunolabeled cells. **(H)** Separation of stereological cell counts by anterior-posterior location indicated that the ethanol-induced reduction of SST cells is similar throughout the neocortex. Measured neuron densities were separated by their rostral-caudal section number. In brains that had more than 9 sections, the final small end sections were combined. This line graph provides a qualitative overview of local differences, as the stereological strategy was designed to sample the whole cortex, and data from each section includes an average of only 24 sampling sites from each brain. **(I)** The location of the neocortex (white lines) that was sampled for stereological estimates of SST neuron number and density is shown on a reconstruction of one brain made from block-face images taken during sectioning. Every 12th 50 uM thick coronal section through the neocortex was sampled. Asterisks signify significant difference between ethanol and saline conditions in all panels.

showed strong excitation during light stimulation, consistent with them being putative SST neurons. Immediately after light offset, about a third of all cells showed suppression which lasted < 200 ms, consistent with previous reports (Funk et al., 2017). In saline treated animals, a similar proportion also showed a late onset, rebound excitation which temporally coincides with the late positive wave recorded in the evoked potential. However, while units in P7 ethanol-exposed mice displayed a similar probability of initial suppression to the stimulus, significantly fewer cells showed the late onset excitation [$t(6) = 2.187$, $p = 0.036$], similar to the loss of the late evoked potential in ethanol-treated mice (**Figure 3E**). Similar analyses limited to putative SST neurons as determined by short latency excitation during light exposure (n = 20 saline, 13 EtOH) revealed similar effects of P7 ethanol [$t(5) = 4.38$, $p = 0.004$; **Figure 3F**]. There was no detectable difference in spontaneous activity between SST units recorded saline and ethanol-treated mice [saline mean = 1.48 ± 0.33 Hz, ethanol mean = 1.01 ± 0.25 Hz; t-test, $t(29) = 1.06$, $p = 0.29$]. These results suggest that the developmental ethanol-induced modification of cortical LFP slow wave oscillations is associated with an underlying impairment in SST single-unit activation.

Closed-loop stimulation triggered on cortical slow-waves can enhance cortical delta oscillations in humans and rodents (Ngo et al., 2013; Moreira et al., 2021). Similarly, direct modulation of cortical SST neuron activity can modify cortical slow-waves (Funk et al., 2017). Here, we used a closed loop optical stimulation paradigm to determine whether enhancing SST activity in-phase with spontaneous slow-waves could enhance delta oscillations and whether any such effect was impaired in mice with reduced numbers of SST neurons caused by P7 ethanol exposure (**Figure 1**;

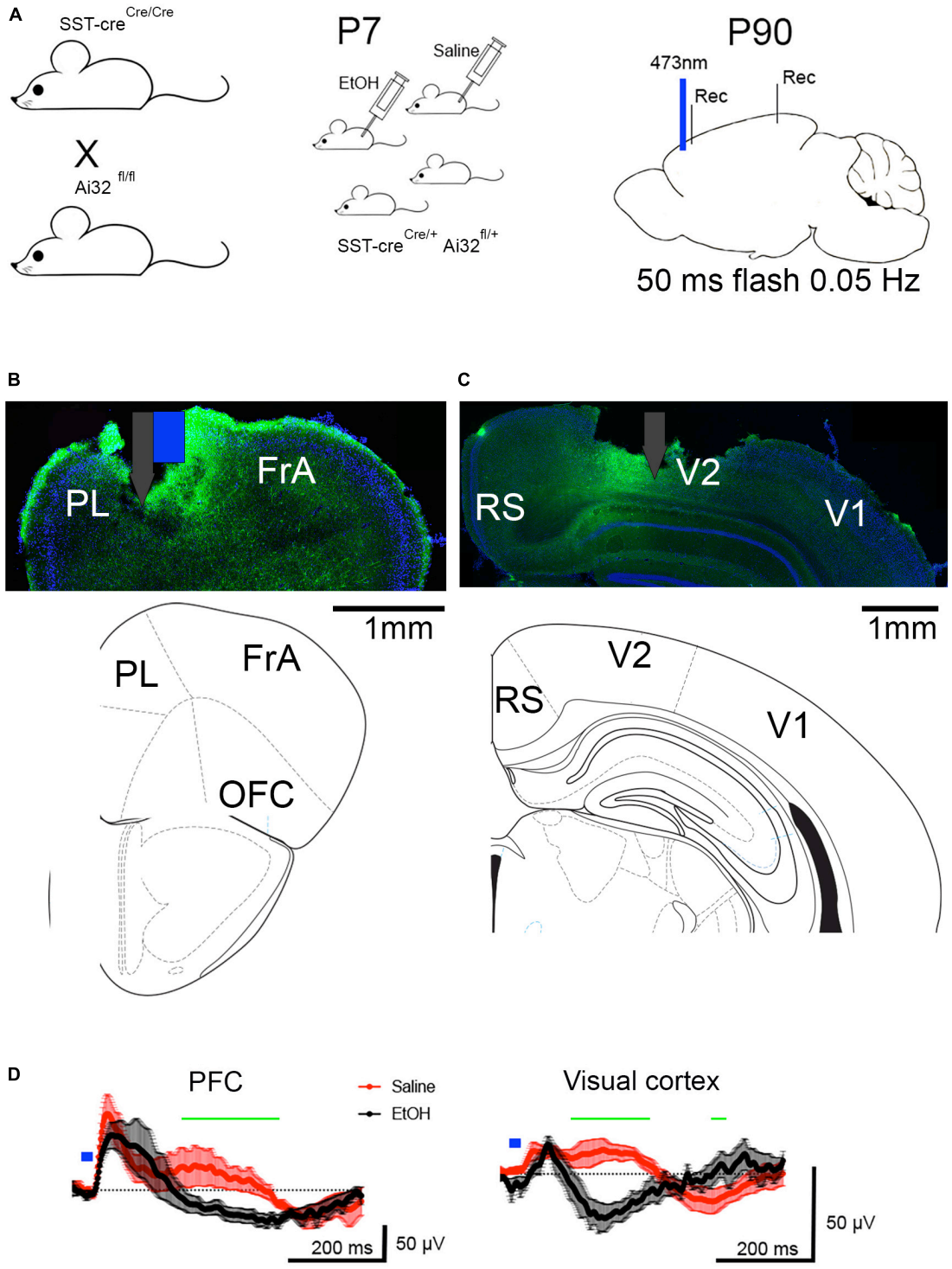


FIGURE 2
(A) Adult SSTcreXAi32 mice exposed to EtOH (n = 9) or saline (n = 5) at P7, received optical stimulation of SST neurons in prefrontal cortex. **(B)** Histological section showing typical prefrontal cortex optotrode location (including surface damage during histology). Associated atlas image below. White and Blue markers denote electrode (gray) attached to optical fiber (blue). PrL, prelimbic cortex; FrA, frontal association cortex, OFC, orbitofrontal cortex. Blue shows DAPI staining and green shows SST-GFP expression. **(C)** Histological and atlas section showing visual cortex electrode location (including surface damage during histology). RS, retrosplenial cortex, V1, primary visual cortex, V2, secondary visual cortex. **(D)** Prefrontal cortex optical stimulation evoked a robust, positive wave lasting 200–400 ms, which corresponds to a 2–5 Hz oscillation (delta frequency band) in P7 saline-treated adult mice and which traveled the anterior-posterior extent of the neocortex, producing a similar, though smaller wave in the visual cortex. The same stimulation in P7 ethanol-treated adult mice evoked an early field potential without the later evoked slow-wave. No evoked slow-wave was observed in the visual cortex of P7 ethanol-treated mice. Shown are means (solid line, $n > 5$ mice) and SEM. Blue mark indicates 473 nm, 50 ms flash in prefrontal cortex. Repeated measures ANOVA detects a significant difference between evoked waveforms in saline and ethanol treated mice at time points marked by green horizontal line. In PFC, the difference between saline and ethanol responses was primarily >200 ms post flash.

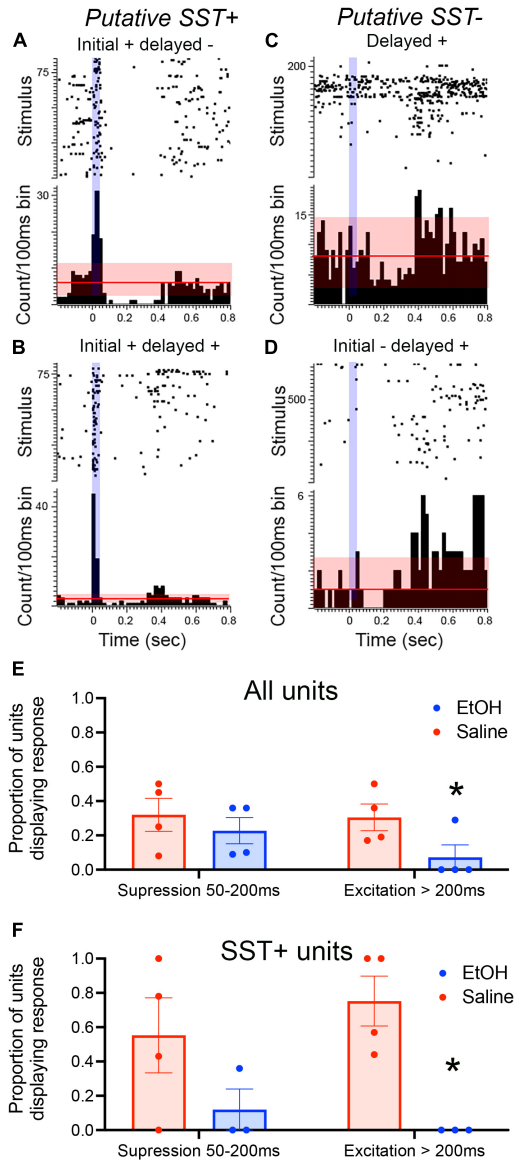


FIGURE 3
PFC unit recordings from adult SSTcreXAi32 mice exposed to P7 saline or ethanol (n = 4 saline mice, n = 47 units; 4 EtOH mice, n = 46 units). **(A–D)** Rasterplots and peri-stimulus time histogram examples of diverse unit responses to 50 ms, 473 nm light (vertical blue mark) in PFC of saline-treated mice. **(A)** A putative SST neuron in an ethanol exposed mouse excited during the light followed by suppression (relative to pre-stimulus activity). Horizontal line represents mean spontaneous activity with red shading representing ± 2 S.D. **(B)** A putative SST neuron in a saline-exposed mouse excited during the light and showing an excitatory rebound 300–400 ms later. **(C)** An ethanol-exposed non-SST neuron (i.e., no excitation to light) showing a delayed excitatory response 400–500 ms post flash. **(D)** A saline-exposed non-SST neuron displaying suppression 100–200 ms post-flash and an excitatory rebound at >400 ms. **(E)** Proportion of all units showing early (<200 ms) suppression and late (>200 ms) excitation in adults exposed to P7 saline or ethanol. There was a significant decrease in the probability of showing a late excitation response in the ethanol-treated mice (asterisk, p < 0.05). **(F)** Proportion of optogenetically identified putative SST neurons showing early (<200 ms) suppression and late (>200 ms) excitation in adults exposed to P7 saline or ethanol. There was a significant decrease in the probability of showing a late excitation response in the ethanol-treated mice (asterisk, p < 0.05) compared to saline controls.

Smiley et al., 2019). Prefrontal cortex local field potentials were recorded near the implanted optical fiber in freely moving mice. Slow-waves were detected using voltage threshold to identify slow-wave troughs. Three different stimulation conditions were presented in a randomized order, block design wherein trough detection evoked a 50 ms flash either immediately or at a 50 ms delay, or no flash was evoked (Figure 4). The stimulation latencies were chosen based on preliminary data that showed a 50 ms delay evoked the strongest reinforcement of ongoing slow-wave activity in the evoked potential (Figure 4C).

In P7 saline exposed adult mice (n = 6), bilateral, prolonged (30–60 min), closed loop stimulation enhanced delta band oscillation power during the stimulation period compared to no stimulation periods before or after. As shown in Figure 4D, closed loop SST neuron stimulation at a 50 ms delay from the negative peak of spontaneous slow-waves significantly enhanced delta band power normalized to no stimulation [one-sample t-test, Saline normalized delta power was significantly greater than 1, $t(5) = 5.218$, $p = 0.0034$] and compared to stimulation at 0 ms delay [Saline 50 ms vs. 0 ms delta power, frequency × delay ANOVA, main effect of delay $F(1,8) = 5.61$, $p = 0.045$, frequency × delay interaction $F(5,40) = 3.217$, $p = 0.015$; *post-hoc* tests revealed significant difference in delta power enhancement between 0 and 50 ms delay]. However, the same SST stimulation protocol was ineffective in P7 ethanol-exposed adults [n = 6; Figure 4E; one-sample t-test, Ethanol normalized delta power was not significantly different from 1, $t(5) = 1.309$, $p = 0.2474$]. Neither stimulation latency produced a significant enhancement in delta power compared to no stimulation [Ethanol, 50 ms vs. 0 ms delta power, frequency × delay ANOVA, main effect of delay, $F(1,15) = 0.099$, $p = 0.756$; frequency × delay interaction, $F(5,75) = 2.055$, $p = 0.081$]. A direct comparison between the saline and ethanol P7 treatments (Figures 4F, G) revealed a significant difference between the exposure groups in the 50 ms delay protocol [frequency × treatment ANOVA, main effect of frequency, $F(2.816,28.16) = 8.045$, $p = 0.0006$; main effect of P7 treatment, $F(1,10) = 5.101$, $p = 0.047$; frequency × treatment interaction, $F(5,50) = 1.99$, $p = 0.097$]. There were no significant differences between saline and ethanol treatments with the 0 ms latency protocol. Importantly the effect of closed loop SST stimulation was selective for cortical delta power in these same animals. Analysis of mean normalized theta power (7–15 Hz) during slow-wave triggered optical stimulation detected no difference in theta power between saline (mean normalized change from no stimulation = 1.07 ± 0.07) and ethanol (mean = 1.02 ± 0.07) exposed mice [t-test, $t(10) = 0.62$, $p = 0.55$], nor any significant increase in normalized theta power compared to no stimulation control [saline, $t(10) = 1.49$, $p = 0.17$; ethanol, $t(12) = 0.33$, $p = 0.74$] (data not shown).

Together these results suggest a P7 ethanol exposure-induced impairment in neocortical SST neurons that may contribute to the known reduction in cortical delta oscillation amplitude and impaired sleep quality in these mice (Apuzzo et al., 2020).

4. Discussion

GABAergic neurons, including SST cells, are reduced in many structures by P7 ethanol exposure (Figure 1)

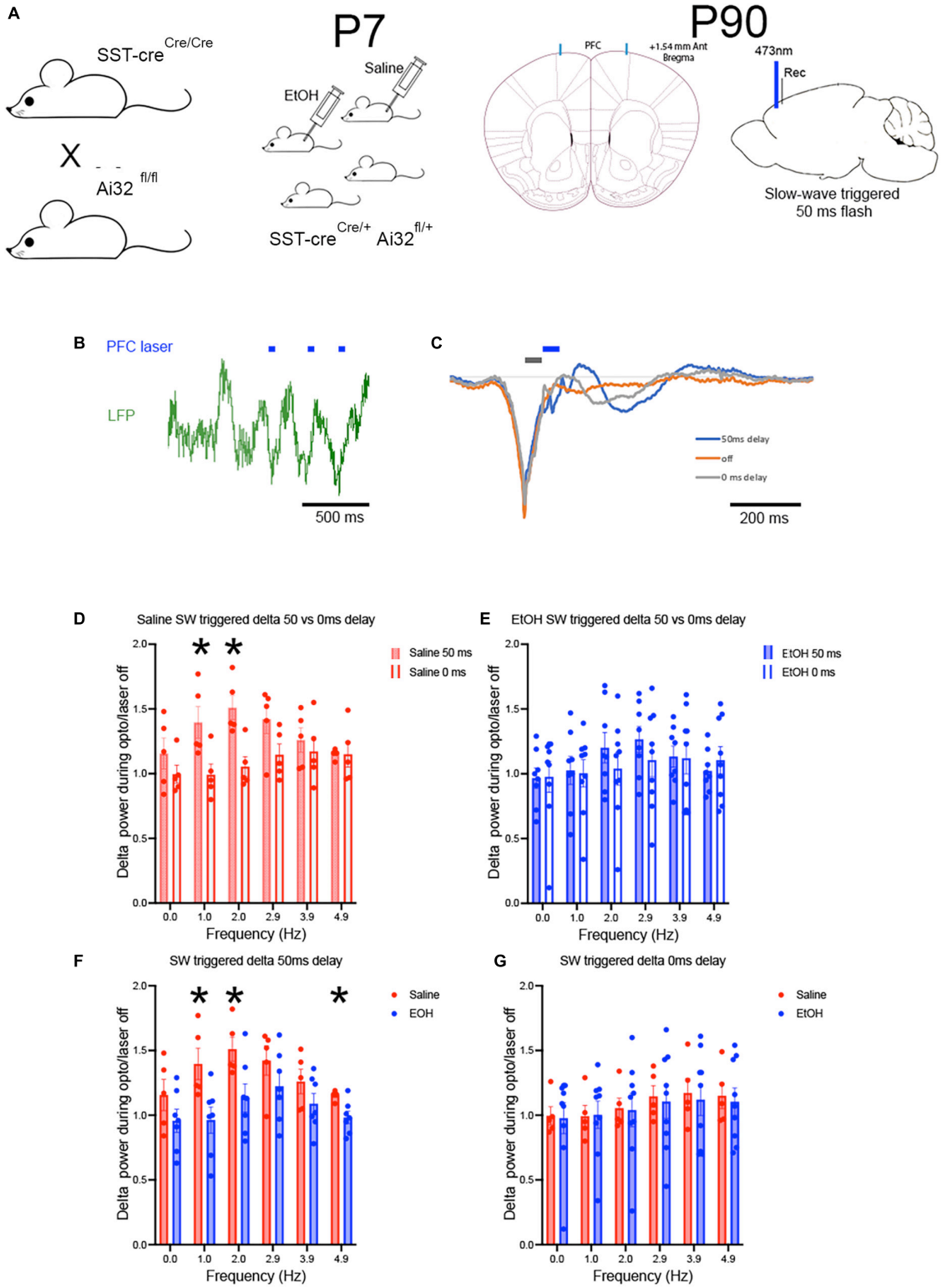


FIGURE 4
Using adult SSTcreXAi32 mice exposed to EtOH (n = 6) or saline at P7 (n = 6) **(A)**, closed loop optical stimulation of cortical SST GABAergic neurons in frontal cortex **(B)** with 50 ms flashes triggered on spontaneously occurring slow-waves, induced sustained slow wave activity in saline but not EtOH mice. Blue marks signify timing of light flashes. **(C)** A 50 ms delay in light activation reinforced slow-wave activity compared to no light, while a 0 ms delay was much less effective. Gray and blue marks signify timing of light flashes starting either 0 or 50 ms, respectively, post slow-wave sleep peak. **(D)** Over a prolonged period (30–60 min) of such stimulation, delta band oscillation amplitude was significantly enhanced in saline controls stimulated at the 50 ms delay but not at the 0 ms delay. Asterisks = sig. diff between delays. **(E)** In P7 EtOH treated adult mice, neither stimulation protocol was effective at enhancing delta oscillation amplitude. **(F,G)** Replotting the data shows the robust enhancement of delta amplitude in saline treated mice, but not in P7 EtOH treated mice, suggesting that stimulation of spared SST cortical neurons cannot compensate to improve sleep-related slow-wave amplitude. Asterisks = significant *post-hoc* test differences between groups.

(Smiley et al., 2015, 2019). These neurons play important roles in sleep physiology, which is also disrupted by P7 ethanol exposure (**Figure 1**) (Wilson et al., 2016; Lewin et al., 2018; Apuzzo et al., 2020). Through cell type-specific, optogenetic targeting of SST neurons in neocortex of saline control mice, we could evoke cortical slow-waves across the anterior-posterior axis of the cortex (**Figure 2**) and enhance delta band oscillation amplitude (**Figure 4**) during sleep as has previously been reported (Funk et al., 2017; Bugnon et al., 2022). However, in P7 ethanol exposed mice, the efficacy of this optogenetic manipulation was severely impaired, suggesting an SST neuron contribution to ethanol effects on slow-wave sleep cortical activity (Wilson et al., 2016; Apuzzo et al., 2020). More specifically, in saline control mice, selective stimulation of SST neurons in the PFC evoked a prolonged evoked potential and temporally coincident inhibition/excitation single-unit activity sequence (**Figure 3**) with time courses similar to a delta oscillation. This slow-wave evoked in the PFC propagated caudally to the visual cortex. Furthermore, closed-loop stimulation of PFC SST neurons in phase with spontaneous slow-waves enhanced delta band oscillation power during the stimulation. These results support the hypothesized role of SST neurons in cortical slow-wave oscillations that occur during non-REM sleep (Kuki et al., 2015; Funk et al., 2017; Niethard et al., 2018; Adamantidis et al., 2019; Bugnon et al., 2022), though do not exclude contributions of other cell types.

Postnatal-day seven ethanol exposure impaired SST neuron stimulation-induced evoked potentials, evoked potential propagation, single-unit late onset excitation, as well as the efficacy of closed loop SST stimulation to enhance cortical delta oscillations compared to saline controls. Together, these results support a significant contribution of developmental ethanol-induced SST neuron loss/dysfunction to at least one aspect of disrupted sleep physiology–abnormal cortical delta oscillations. It is not clear whether the impairments are due solely to SST cell loss, or whether SST cell function and connectivity are also modified. For example, while there was a 15% loss of cortical SST neurons following early ethanol, the large majority were spared. It is not clear however, whether the spared cells maintain normal network connectivity, excitability and/or pre- and post-synaptic strength. Cortical interneurons are capable of a variety of forms of plasticity (McFarlan et al., 2022). Specifically, the majority of cortical SST neurons are Martinotti cells (Funk et al., 2017; Bugnon et al., 2022) which have extensive axonal outputs targeting multiple layers but especially layer I where they could influence a relatively large population of pyramidal neurons (Wang et al., 2004; Funk et al., 2017). A decrease in the number or efficacy of these cells could decrease slow-wave amplitude by reducing the down-state magnitude and or synchrony. Slow-waves are propagated through cortico-cortical excitatory connections (Steriade et al., 1993a) although a subset of cortical SST also have long range projections (Tomioka et al., 2005; Funk et al., 2017). Again, a decrease in the number or efficacy SST cells in regions targeted by these connections could contribute to the reduced spread of slow waves as observed here in P7 ethanol treated adults. An examination of the effects of developmental ethanol exposure on cortical SST neuron axonal and dendritic elaboration and synaptic density, as well as cell excitability is warranted. Given the diverse contributions of cortical SST neurons in sleep, reduced or impaired SST neuron function may also contribute to other aspects of impaired sleep following early ethanol exposure, such as the observed decrease in sleep spindle density (Apuzzo et al., 2020).

That SST cells may contribute to modified delta oscillations in ethanol exposed mice suggests the possibility of artificially increasing the activity of spared SST neurons to improve cortical slow-wave amplitude. However, the impairment in closed-loop SST stimulation enhancement in delta oscillation amplitude observed here suggests that this type of manipulation may not be an effective treatment. Similar approaches in humans have revealed mixed results when using closed loop stimulation to enhance delta oscillations in elderly humans. For example, closed loop transcranial stimulation and auditory closed loop stimulation during slow wave sleep have both been shown to enhance slow-wave activity and memory consolidation in older adults (Ladenbauer et al., 2017; Papalambros et al., 2017). However, auditory closed loop stimulation was much less effective in older adults with mild cognitive impairment (Papalambros et al., 2019). Examination of more diverse closed-loop protocols (e.g., temporal patterns, intensity) in these different target populations may revealed maintained treatment efficacy in these populations.

Similar to SST neurons, parvalbumin (PV) expressing GABAergic neurons are also reduced (i.e., loss of neurons and/or protein expression) by early developmental ethanol exposure (Coleman et al., 2012; Smiley et al., 2015; Saito et al., 2019), however, post-exposure environment can reverse those effects (Apuzzo et al., 2020). Environmental enrichment can also reverse SST cell loss in cortex and hippocampus induced by developmental MK-801 (Murueta-Goyena et al., 2020), though the effects of this treatment on SST neurons after early ethanol exposure have not yet been tested. Given that postnatal environment can modulate many effects of developmental ethanol (Hannigan and Berman, 2000; Hamilton et al., 2014; Raineki et al., 2018) including reversing sleep impairment (Apuzzo et al., 2020), analysis of the effects of post-exposure environment on SST neurons and their sleep-related physiology is warranted.

Together, these findings implicate SST neuron loss as underlying at least one aspect of adult sleep dysfunction following developmental ethanol. Further identification of how different classes of SST (Yavorska and Wehr, 2016) and other GABAergic neurons mediate specific sleep related functions, and how these diverse cell types are affected by developmental ethanol may provide insight into possible targets for treatment of sleep impairment, and the resulting cascade of cognitive and emotional consequences following developmental EtOH.

Data availability statement

The raw data supporting the conclusions of this article will be made available by the authors, without undue reservation.

Ethics statement

This animal study was reviewed and approved by the Nathan S. Kline Institute for Psychiatric Research Institutional Animal Care and Use Committee.

Author contributions

DW conceived of the project, designed the project, collected the data, analyzed the data, wrote manuscript draft and edited, and obtained the funding. GF and CW collected the data. CT provided the transgenic animal lines. JS analyzed the SST histology, discussed the project, edited the manuscript, and obtained the funding. MS discussed the project, edited the manuscript, and obtained the funding. All authors contributed to the article and approved the submitted version.

Funding

This work was supported by the NIAAA R01AA023181 to DW, JS, and MS.

Conflict of interest

The authors declare that the research was conducted in the absence of any commercial or financial relationships that could be construed as a potential conflict of interest.

Publisher's note

All claims expressed in this article are solely those of the authors and do not necessarily represent those of their affiliated organizations, or those of the publisher, the editors and the reviewers. Any product that may be evaluated in this article, or claim that may be made by its manufacturer, is not guaranteed or endorsed by the publisher.

References

Adamantidis, A. R., Gutierrez Herrera, C., and Gent, T. C. (2019). Oscillating circuitries in the sleeping brain. *Nat. Rev. Neurosci.* 20, 746–762.

Apuzzo, J., Saito, M., and Wilson, D. A. (2020). Post-exposure environment modulates long-term developmental ethanol effects on behavior, neuroanatomy, and cortical oscillations. *Brain Res* 1748:147128. doi: 10.1016/j.brainres.2020.147128

Bellesi, M., Riedner, B. A., Garcia-Molina, G. N., Cirelli, C., and Tononi, G. (2014). Enhancement of sleep slow waves: Underlying mechanisms and practical consequences. *Front. Syst. Neurosci.* 8:208. doi: 10.3389/fnsys.2014.00208

Ben Simon, E., Vallat, R., Barnes, C. M., and Walker, M. P. (2020). Sleep loss and the socio-emotional brain. *Trends Cogn. Sci.* 24, 435–450.

Born, J., Rasch, B., and Gais, S. (2006). Sleep to remember. *Neuroscientist* 12, 410–424. doi: 10.3389/fpsyg.2019.01766

Bugnon, T., Mayner, W. G. P., Cirelli, C., and Tononi, G. (2022). Sleep and wake in a model of the thalamocortical system with Martinotti cells. *Eur. J. Neurosci.* doi: 10.1111/ejn.15836 [Epub ahead of print].

Chen, M. L., Olson, H. C., Picciano, J. F., Starr, J. R., and Owens, J. (2012). Sleep problems in children with fetal alcohol spectrum disorders. *J. Clin. Sleep Med.* 8, 421–429.

Coleman, L. G. Jr., Oguz, I., Lee, J., Styner, M., and Crews, F. T. (2012). Postnatal day 7 ethanol treatment causes persistent reductions in adult mouse brain volume and cortical neurons with sex specific effects on neurogenesis. *Alcohol* 46, 603–612. doi: 10.1016/j.alcohol.2012.01.003

Criado, J. R., Wills, D. N., Walker, B. M., and Ehlers, C. L. (2008). Effects of adolescent ethanol exposure on sleep in adult rats. *Alcohol* 42, 631–639.

Diekelmann, S., and Born, J. (2010). The memory function of sleep. *Nat. Rev. Neurosci.* 11, 114–126.

Dorph-Petersen, K. A., Delevich, K. M., Marcsisin, M. J., Zhang, W., Sampson, A. R., Gundersen, H. J., et al. (2009). Pyramidal neuron number in layer 3 of primary auditory cortex of subjects with schizophrenia. *Brain Res.* 1285:42–57.

Espinosa, N., Alonso, A., Morales, C., Espinosa, P., Chavez, A. E., and Fuentealba, P. (2019). Basal forebrain gating by somatostatin neurons drives prefrontal cortical activity. *Cereb. Cortex* 29, 42–53. doi: 10.1093/cercor/bhx302

Funk, C. M., Peelman, K., Bellesi, M., Marshall, W., Cirelli, C., and Tononi, G. (2017). Role of somatostatin-positive cortical interneurons in the generation of sleep slow waves. *J. Neurosci.* 37, 9132–9148.

Goldstein, A. N., and Walker, M. P. (2014). The role of sleep in emotional brain function. *Annu. Rev. Clin. Psychol.* 10, 679–708.

Gundersen, H. J., Bagger, P., Bendtsen, T. F., Evans, S. M., Korbo, L., Marcussen, N., et al. (1988). The new stereological tools: Disector, fractionator, nucleator and point sampled intercepts and their use in pathological research and diagnosis. *APMIS* 96, 857–881. doi: 10.1111/j.1699-0463.1988.tb00954.x

Hamilton, G. F., Jablonski, S. A., Schiffino, F. L., St Cyr, S. A., Stanton, M. E., and Klintsova, A. Y. (2014). Exercise and environment as an intervention for neonatal alcohol effects on hippocampal adult neurogenesis and learning. *Neuroscience* 265, 274–290.

Hannigan, J. H., and Berman, R. F. (2000). Amelioration of fetal alcohol-related neurodevelopmental disorders in rats: Exploring pharmacological and environmental treatments. *Neurotoxicol. Teratol.* 22, 103–111. doi: 10.1016/s0892-0362(99)00050-1

Harmony, T. (2013). The functional significance of delta oscillations in cognitive processing. *Front. Integr. Neurosci.* 7:83. doi: 10.3389/fnint.2013.00083

Henin, S., Borges, H., Shankar, A., Sarac, C., Melloni, L., Friedman, D., et al. (2019). Closed-loop acoustic stimulation enhances sleep oscillations but not memory performance. *eNeuro* 6. 6:ENEURO.0306-19.

Inkelis, S. M., and Thomas, J. D. (2018). Sleep in infants and children with prenatal alcohol exposure. *Alcohol Clin. Exp. Res.* doi: 10.1111/acer.13803 [Epub ahead of print].

Ipsiroglu, O. S., Wind, K., Hung, Y. A., Berger, M., Chan, F., Yu, W., et al. (2019). Prenatal alcohol exposure and sleep-wake behaviors: Exploratory and naturalistic observations in the clinical setting and in an animal model. *Sleep Med.* 54, 101–112. doi: 10.1016/j.sleep.2018.10.006

Jan, J. E., Asante, K. O., Conry, J. L., Fast, D. K., Bax, M. C., Ipsiroglu, O. S., et al. (2010). Sleep health issues for children with FASD: Clinical considerations. *Int. J. Pediatr.* 2010:639048. doi: 10.1155/2010/639048

Ketz, N., Jones, A. P., Bryant, N. B., Clark, V. P., and Pilly, P. K. (2018). Closed-loop slow-wave tACS improves sleep-dependent long-term memory generalization by modulating endogenous oscillations. *J. Neurosci.* 38, 7314–7326. doi: 10.1523/JNEUROSCI.0273-18.2018

Kilkenny, C., Browne, W. J. I, Cuthill, C., Emerson, M., and Altman, D. G. (2010). Improving bioscience research reporting: The ARRIVE guidelines for reporting animal research. *PLoS Biol.* 8:e1000412. doi: 10.1371/journal.pbio.1000412

Knyazev, G. G. (2012). EEG delta oscillations as a correlate of basic homeostatic and motivational processes. *Neurosci. Biobehav. Rev.* 36, 677–695. doi: 10.1016/j.neubiorev.2011.10.002

Kuki, T., Fujihara, K., Miwa, H., Tamamaki, N., Yanagawa, Y., and Mushiake, H. (2015). Contribution of parvalbumin and somatostatin-expressing GABAergic neurons to slow oscillations and the balance in beta-gamma oscillations across cortical layers. *Front. Neural Circuits* 9:6. doi: 10.3389/fncir.2015.00006

Ladenbauer, J., Ladenbauer, J., Kulzow, N., de Boor, R., Avramova, E., Grittner, U., et al. (2017). Promoting sleep oscillations and their functional coupling by transcranial stimulation enhances memory consolidation in mild cognitive impairment. *J. Neurosci.* 37, 7111–7124. doi: 10.1523/JNEUROSCI.0260-17.2017

Lewin, M., Ilina, M., Betz, J., Masiello, K., Hui, M., Wilson, D. A., et al. (2018). Developmental ethanol-induced sleep fragmentation, behavioral hyperactivity, cognitive impairment and parvalbumin cell loss are prevented by lithium co-treatment. *Neuroscience* 369, 269–277. doi: 10.1016/j.neuroscience.2017.11.033

Lewin, M., Lopachin, J., Delorme, J., Opendak, M., Sullivan, R. M., and Wilson, D. A. (2019). Early life trauma has lifelong consequences for sleep and behavior. *Sci. Rep.* 9:16701.

Madisen, L., Mao, T., Koch, H., Zhuo, J. M., Berenyi, A., Fujisawa, S., et al. (2012). A toolbox of Cre-dependent optogenetic transgenic mice for light-induced activation and silencing. *Nat. Neurosci.* 15, 793–802. doi: 10.1038/nn.3078

Marshall, L., Helgadottir, H., Molle, M., and Born, J. (2006). Boosting slow oscillations during sleep potentiates memory. *Nature* 444, 610–613.

Massimini, M., Ferrarelli, F., Esser, S. K., Riedner, B. A., Huber, R., Murphy, M., et al. (2007). Triggering sleep slow waves by transcranial magnetic stimulation. *Proc. Natl. Acad. Sci. U.S.A.* 104, 8496–8501.

Massimini, M., Huber, R., Ferrarelli, F., Hill, S., and Tononi, G. (2004). The sleep slow oscillation as a traveling wave. *J. Neurosci.* 24, 6862–6870.

McFarlan, A. R., Chou, C. Y. C., Watanabe, A., Cherepacha, N., Haddad, M., Owens, H., et al. (2022). The plasticitome of cortical interneurons. *Nat. Rev. Neurosci.* 24, 80–97. doi: 10.1038/s41583-022-00663-9

Molle, M., and Born, J. (2011). Slow oscillations orchestrating fast oscillations and memory consolidation. *Prog. Brain Res.* 193, 93–110.

Moreira, C. G., Baumann, C. R., Scandella, M., Nemirovsky, S. I., Leach, S., Huber, R., et al. (2021). Closed-loop auditory stimulation method to modulate sleep slow waves and motor learning performance in rats. *Elife* 10:e68043. doi: 10.7554/eLife.68043

Murueta-Goyena, A., Ortuzar, N., Lafuente, J. V., and Bengoetxea, H. (2020). Enriched environment reverts somatostatin interneuron loss in MK-801 model of schizophrenia. *Mol. Neurobiol.* 57, 125–134. doi: 10.1007/s12035-019-01762-y

Ngo, H. V., Martinetz, T., Born, J., and Molle, M. (2013). Auditory closed-loop stimulation of the sleep slow oscillation enhances memory. *Neuron* 78, 545–553.

Niethard, N., Ngo, H. V., Ehrlich, I., and Born, J. (2018). Cortical circuit activity underlying sleep slow oscillations and spindles. *Proc. Natl. Acad. Sci. U.S.A.* 115, E9220–E9229.

Olney, J. W., Tenkova, T., Dikranian, K., Qin, Y. Q., Labruyere, J., and Ikonomidou, C. (2002). Ethanol-induced apoptotic neurodegeneration in the developing C57BL/6 mouse brain. *Brain Res. Dev. Brain Res.* 133, 115–126.

Pace-Schott, E. F., and Hobson, J. A. (2002). The neurobiology of sleep: Genetics, cellular physiology and subcortical networks. *Nat. Rev. Neurosci.* 3, 591–605. doi: 10.1038/nrn895

Papalambros, N. A., Santostasi, G., Malkani, R. G., Braun, R., Weintraub, S., Paller, K. A., et al. (2017). Acoustic enhancement of sleep slow oscillations and concomitant memory improvement in older adults. *Front. Hum. Neurosci.* 11:109. doi: 10.3389/fnhum.2017.00109

Papalambros, N. A., Weintraub, S., Chen, T., Grimaldi, D., Santostasi, G., Paller, K. A., et al. (2019). Acoustic enhancement of sleep slow oscillations in mild cognitive impairment. *Ann. Clin. Transl. Neurol.* 6, 1191–1201.

Pesonen, A. K., Raikkonen, K., Matthews, K., Heinonen, K., Paavonen, J. E., Lahti, J., et al. (2009). Prenatal origins of poor sleep in children. *Sleep* 32, 1086–1092. doi: 10.1093/sleep/32.8.1086

Raineki, C., Ellis, L., and Weinberg, J. (2018). Impact of adolescent stress on the expression of stress-related receptors in the hippocampus of animals exposed to alcohol prenatally. *Hippocampus* 28, 201–216. doi: 10.1002/hipo.22823

Saito, M., Mao, R. F., Wang, R., Vadasz, C., and Saito, M. (2007). Effects of gangliosides on ethanol-induced neurodegeneration in the developing mouse brain. *Alcohol. Clin. Exp. Res.* 31, 665–674.

Saito, M., Smiley, J. F., Hui, M., Masiello, K., Betz, J., Ilina, M., et al. (2019). Neonatal ethanol disturbs the normal maturation of parvalbumin interneurons surrounded by subsets of perineuronal nets in the cerebral cortex: Partial reversal by lithium. *Cereb. Cortex* 29, 1383–1397. doi: 10.1093/cercor/bhy034

Saper, C. B., Fuller, P. M., Pedersen, N. P., Lu, J., and Scammell, T. E. (2010). Sleep state switching. *Neuron* 68, 1023–1042.

Skorput, A. G., Gupta, V. P., Yeh, P. W., and Yeh, H. H. (2015). Persistent interneuronopathy in the prefrontal cortex of young adult offspring exposed to ethanol in utero. *J. Neurosci.* 35, 10977–10988. doi: 10.1523/JNEUROSCI.1462-15.2015

Smiley, J. F., Bleiwas, C., Masiello, K., Petkova, E., Betz, J., Hui, M., et al. (2019). Effects of neonatal ethanol on cerebral cortex development through adolescence. *Brain Struct. Funct.* 224, 1871–1884.

Smiley, J. F., Saito, M., Bleiwas, C., Masiello, K., Ardekani, B., Guilfoyle, D. N., et al. (2015). Selective reduction of cerebral cortex GABA neurons in a late gestation model of fetal alcohol spectrum disorder. *Alcohol* 49, 571–580. doi: 10.1016/j.alcohol.2015.04.008

Staresina, B. P., Bergmann, T. O., Bonnefond, M., van der Meij, R., Jensen, O., Deuker, L., et al. (2015). Hierarchical nesting of slow oscillations, spindles and ripples in the human hippocampus during sleep. *Nat. Neurosci.* 18, 1679–1686. doi: 10.1038/nn.4119

Steriade, M., Contreras, D., Curro Dossi, R., and Nunez, A. (1993a). The slow (< 1 Hz) oscillation in reticular thalamic and thalamocortical neurons: Scenario of sleep rhythm generation in interacting thalamic and neocortical networks. *J. Neurosci.* 13, 3284–3299. doi: 10.1523/JNEUROSCI.13-08-03284.1993

Steriade, M., Nunez, A., and Amzica, F. (1993b). A novel slow (< 1 Hz) oscillation of neocortical neurons in vivo: Depolarizing and hyperpolarizing components. *J. Neurosci.* 13, 3252–3265. doi: 10.1523/JNEUROSCI.13-08-03252.1993

Stickgold, R., and Walker, M. P. (2007). Sleep-dependent memory consolidation and reconsolidation. *Sleep Med.* 8, 331–343.

Stone, W. S., Altman, H. J., Hall, J., Arankowsky-Sandoval, G., Parekh, P., and Gold, P. E. (1996). Prenatal exposure to alcohol in adult rats: Relationships between sleep and memory deficits, and effects of glucose administration on memory. *Brain Res.* 742, 98–106. doi: 10.1016/s0006-8993(96)00976-6

Timofeev, I., Schoch, S. F., LeBourgeois, M. K., Huber, R., Riedner, B. A., and Kurth, S. (2020). Spatio-temporal properties of sleep slow waves and implications for development. *Curr. Opin. Physiol.* 15, 172–182. doi: 10.1016/j.cophys.2020.01.007

Tomioka, R., Okamoto, K., Furuta, T., Fujiyama, F., Iwasato, T., Yanagawa, Y., et al. (2005). Demonstration of long-range GABAergic connections distributed throughout the mouse neocortex. *Eur. J. Neurosci.* 21, 1587–1600. doi: 10.1111/j.1460-9568.2005.03989.x

Tononi, G., and Cirelli, C. (2014). Sleep and the price of plasticity: From synaptic and cellular homeostasis to memory consolidation and integration. *Neuron* 81, 12–34. doi: 10.1016/j.neuron.2013.12.025

Troese, M., Fukumizu, M., Sallinen, B. J., Gilles, A. A., Wellman, J. D., Paul, J. A., et al. (2008). Sleep fragmentation and evidence for sleep debt in alcohol-exposed infants. *Early Hum. Dev.* 84, 577–585. doi: 10.1016/j.earlhumdev.2008.02.001

Volgin, D. V., and Kubin, L. (2012). Reduced sleep and impaired sleep initiation in adult male rats exposed to alcohol during early postnatal period. *Behav. Brain Res.* 234, 38–42. doi: 10.1016/j.bbr.2012.06.002

Vyazovskiy, V. V., Faraguna, U., Cirelli, C., and Tononi, G. (2009). Triggering slow waves during NREM sleep in the rat by intracortical electrical stimulation: Effects of sleep/wake history and background activity. *J. Neurophysiol.* 101, 1921–1931. doi: 10.1152/jn.91157.2008

Wang, Y., Toledo-Rodriguez, M., Gupta, A., Wu, C., Silberberg, G., Luo, J., et al. (2004). Anatomical, physiological and molecular properties of Martinotti cells in the somatosensory cortex of the juvenile rat. *J. Physiol.* 561, 65–90. doi: 10.1113/jphysiol.2004.073353

Wengel, T., Hanlon-Dearman, A. C., and Fjeldsted, B. (2011). Sleep and sensory characteristics in young children with fetal alcohol spectrum disorder. *J. Dev. Behav. Pediatr.* 32, 384–392. doi: 10.1097/DBP.0b013e3182199694

Wilson, D. A., Masiello, K., Lewin, M. P., Hui, M., Smiley, J. F., and Saito, M. (2016). Developmental ethanol exposure-induced sleep fragmentation predicts adult cognitive impairment. *Neuroscience* 322, 18–27. doi: 10.1016/j.neuroscience.2016.02.020

Xie, L., Kang, H., Xu, Q., Chen, M. J., Liao, Y., Thiyagarajan, M., et al. (2013). Sleep drives metabolite clearance from the adult brain. *Science* 342, 373–377.

Xu, M., Chung, S., Zhang, S., Zhong, P., Ma, C., Chang, W. C., et al. (2015). Basal forebrain circuit for sleep-wake control. *Nat. Neurosci.* 18, 1641–1647.

Yavorska, I., and Wehr, M. (2016). Somatostatin-expressing inhibitory interneurons in cortical circuits. *Front. Neural Circuits* 10:76. doi: 10.3389/fncir.2016.00076

frontiers | Frontiers in Neuroscience

TYPE Original Research
PUBLISHED 06 April 2023
DOI 10.3389/fnins.2023.1163575

Check for updates

OPEN ACCESS

EDITED BY
Carlos Fernando Valenzuela,
University of New Mexico,
United States

REVIEWED BY
Kristen Breit,
West Chester University,
United States
Benjamin J. Clark,
University of New Mexico,
United States

*CORRESPONDENCE
Roh-Yu Shen
✉ rshen@buffalo.edu

†These authors have contributed equally to this work and share first authorship

SPECIALTY SECTION
This article was submitted to Neurodevelopment, a section of the journal Frontiers in Neuroscience

RECEIVED 10 February 2023
ACCEPTED 15 March 2023
PUBLISHED 06 April 2023

CITATION
Wang A-L, Micov VB, Kwarteng F, Wang R, Hausknecht KA, Oubraim S, Haj-Dahmane S and Shen R-Y (2023) Prenatal ethanol exposure leads to persistent anxiety-like behavior during adulthood indicated by reduced horizontal and vertical exploratory behaviors.
Front. Neurosci. 17:1163575.
10.3389/fnins.2023.1163575

COPYRIGHT
© 2023 Wang, Micov, Kwarteng, Wang, Hausknecht, Oubraim, Haj-Dahmane and Shen. This is an open-access article distributed under the terms of the Creative Commons Attribution License (CC BY). The use, distribution or reproduction in other forums is permitted, provided the original author(s) and the copyright owner(s) are credited and that the original publication in this journal is cited, in accordance with accepted academic practice. No use, distribution or reproduction is permitted which does not comply with these terms.

Prenatal ethanol exposure leads to persistent anxiety-like behavior during adulthood indicated by reduced horizontal and vertical exploratory behaviors

An-Li Wang†, Veronika B. Micov†, Francis Kwarteng, Ruixiang Wang, Kathryn A. Hausknecht, Saida Oubraim, Samir Haj-Dahmane and Roh-Yu Shen*

Department of Pharmacology and Toxicology, Jacob School of Medicine and Biomedical Sciences, University at Buffalo, Buffalo, NY, United States

Background: Fetal alcohol spectrum disorders (FASD) caused by prenatal ethanol exposure (PE) consist of many cognitive/behavioral deficits. Studies have reported that PE leads to impairments of learning and memory, attention, executive function, and anxiety. Open field (OF) is a common behavioral model which offers comprehensive ethological information. Here, we analyzed multiple parameters of OF to examine anxiety behavior and habituation after PE.

Material and Methods: Pregnant Sprague Dawley rats were gavaged twice/day with 0 or 3g/kg/treatment ethanol (15% w/v) during gestational day (GD) 8–20, mimicking second-trimester heavy PE in humans. The control and PE adult offspring were subjected to OF task in different ambient light levels with or without acute stress.

Results: Prenatal ethanol exposure did not influence the overall locomotor activities or habituation in the OF. In lower ambient light, no PE effects could be detected. In higher ambient light, female PE rats showed less activities in the center zone, indicative of increased anxiety. Males show lower activities in the center zone only after acute stress. Rats spent <2% of the time in the center zone compared to >75% of the time in the corner zone where they engaged in frequent rearing activities (vertical exploration; exploratory rearing). Prenatal ethanol exposure led to lower rearing activities in the corner in both males and females. Acute stress masks the PE effects in males but not in females.

Discussion: The results support that heavy PE leads to persistent anxiety-like behavior during adulthood in both sexes. This conclusion is supported by using multiple parameters of exploratory behavior in the OF, including the rearing activities in the corner to reach reliable quantification of anxiety-like behavior.

KEYWORDS

fetal alcohol spectrum disorders, anxiety-like behavior, open field, acute restraint stress, exploratory rearing

Introduction

Prenatal ethanol exposure (PE) leads to structural and functional abnormalities (Tang et al., 2019) in the brain, which can cause lifelong cognitive/behavioral deficits and mood disorders (Pyman et al., 2021). The term fetal alcohol spectrum disorders (FASD) is used to represent multiple cognitive/behavioral/emotional deficits caused by PE. The global

prevalence of FASD in children and youth population was estimated to be 7.7 per 1,000 population (Lange et al., 2017). The prevalence rate of FASD is persistently high (2–5%) in the general population of the US (May et al., 2009, 2014). Currently, understanding of FASD pathology and treatment strategies is limited. With such high prevalence and accompanying huge economic costs (Greenmyer et al., 2018), it is crucial to understand the mechanisms caused by PE in order to develop effective intervention strategies.

The cognitive/behavioral deficits in FASD include poor executive function (Kingdon et al., 2016), learning and memory deficits (Mattson et al., 2011), hyperactivity (Mattson et al., 2011) and attention deficits (Pyman et al., 2021). In addition, individuals with FASD also show mood disorders such as anxiety and depression (Famy et al., 1998; Fryer et al., 2007; Hellemans et al., 2010a) and vulnerability to stress (Hellemans et al., 2010a; Keiver et al., 2015). The above deficits can be observed in rodent models of PE including the attention deficit (Wang et al., 2020, 2021), sensory processing deficit, and habituation deficit (Wang et al., 2022). Prenatal ethanol exposure in rodents also leads to depressive-like and anxiety-like behaviors (Hellemans et al., 2010b). The anxiety-like behavior is shown using various behavioral tasks including elevated plus-maze task (Osborn et al., 1998; Dursun et al., 2006; Hwang and Hashimoto-Torii, 2022; Oubraim et al., 2022) and elevated zero maze task (Oubraim et al., 2022), novelty-induced hypophagia, light–dark box, and open field (OF) (Rouzer et al., 2017). In addition, PE reduces social behaviors in the social interaction task (Diaz et al., 2016, 2020). These studies show inconsistent results possibly due to PE paradigms (route, timing, and duration), rodent species/strains, sexes and behavioral tasks used. The elevated plus-maze is one of the most popular ethological models to measure anxiety levels, which has numerous advantages (e.g., does not require training, or water/food deprivation, and simplicity of design) (Carobrez and Bertoglio, 2005). However, the elevated plus-maze task and other similar tasks (e.g., light–dark box) cannot offer comprehensive information related to exploratory behaviors which is important for inferring anxiety.

Open field task, on the other hand, allows us to fully examine exploratory behavior. In the OF task, animals are allowed to explore the entire arena freely. They usually locomote around the walls and avoid the center open area. The behavioral pattern is termed thigmotaxis. Reduced center zone activities represent lower horizontal exploratory activities and higher anxiety levels. In addition to the center zone activities as an index of anxiety, some evidence shows that vertical exploratory behavior (rearing; high-leaning behavior) could also infer anxiety levels in rodents (Kuniishi et al., 2017; Sturman et al., 2018). However, most investigators only use center zone exploratory activities in the OF, ignoring the vertical exploratory behavior (rearing) which takes place much more frequently than center zone activities. So far, there are no studies investigating chronic heavy PE on anxiety-like behavior in both sexes using the OF with detailed analysis of exploratory behavior. In the present study, we investigate the effects of heavy PE during the second-trimester equivalent using detailed analyses of both horizontal and vertical exploratory behaviors. Additionally, we analyzed the anxiety-like behavior after 2 h acute restraint stress (ARS) since animals were more vulnerable to stress after exposure to ethanol prenatally (Hellemans et al., 2010b; Wieczorek et al., 2015).

Materials and methods

Animals

Rats were bred in house to prevent potential stress from transportation and to strictly control the prenatal environment. The procedure of breeding, ethanol exposure, and cross-fostering were described in previous reports (Wang et al., 2020, 2021). Briefly, male and virgin female Sprague–Dawley rats (Envigo, Indianapolis, IN, United States) were housed in the breeding cages with food and water *ad lib.* Gestational day 0 is designated when copulatory vaginal plugs were found. The holding room was maintained a 12 h/12 h regular light–dark cycle (lights on 7:00 a.m.) with temperature and humidity well-controlled.

Pregnant dams were randomly assigned to vehicle control (22.5% w/v sucrose water, isocaloric to ethanol) or ethanol (3 g/kg; 15% w/v) group. Our previous study reported that the blood alcohol concentration of this PE paradigm was 116.8 ± 10.5 mg/dl 1 h after the second ethanol treatment on GD 15 (Shen et al., 1999; Wang et al., 2019). This ethanol dosage in rats is comparable to heavy prenatal alcohol exposure in humans (Wang et al., 2020). From GD 8 to GD 20, both groups were administered twice (0 or 3 g/kg ethanol; 5–6 h apart) *via* intragastric gavage every weekday. On weekends, a single treatment with 0 or 4 g/kg ethanol solution was given daily. Control dams were pair-fed with ethanol treated dams on GDs 8–20 to equate nutrient intake from rat chow across groups. Food was *ad lib* after GD 20. Both control and ethanol groups were injected thiamine-containing vitamin B-complex (containing 8 mg/kg; i.m.; twice/week during GDs 8–20; Super B Complex, Vedco, Saint Joseph, MO) to compensate for potential thiamine deficiency caused by ethanol treatment or the pair-feeding condition (Ba et al., 1996).

Each litter was culled to 10 pups with equal number of pups in each sex (5 males and 5 females), when possible, on postnatal day 1. The pups of PE dams were fostered by extra dams without any treatment and gave birth 1–2 day(s) earlier. The cross-fostering procedure was to prevent the potential maternal negligence or undernutrition from alcohol withdrawal of PE dams. The pups of each control dam were switched. However, cross-fostering might lead to other physiological changes and might not be translational to clinical studies (Giberson and Weinberg, 1997; Bartolomucci et al., 2004). Twenty-five male rats (control: 12 from 8 litters; PE: 13 from 8 litters) and 26 female rats (control: 14 from 8 litters; PE: 12 from 8 litters) were utilized in the current study. Before the behavioral experiment start, animals were handled for 3 consecutive days (5 min/rat/day). Animals entered behavioral experiments at 8–9 weeks old. All procedures were followed by the guidelines of the National Institutes of Health regarding laboratory animal care and use, and approved by the Institutional Animal Care and Use Committee of University at Buffalo.

Apparatus

Open field

Four identical OF apparatuses were used for testing. Each OF apparatus consisted of a square arena (100 × 100 cm) with black rubber floor and 46 cm high walls. The lights offered 2 levels of even illumination: the lower light level (~14 lux at center, ~9 lux

at corners of the OF) and the higher light level (~60 lux at center, ~40 lux at corners). White noise was provided in the testing room. One camera was placed 2.4 m above each OF apparatus. All tests were recorded and analyzed automatically with ANY-maze version 6 software (Stoelting Co., Illinois, United States). Each OF was virtually divided into the following zones on the floor (Figure 1): (A) center (at the center area with a diameter of 43 cm), (B) peripheral zone (the area between center and edge zones), (C) edge zone (10 cm distance from each wall), (D) corner zone. The position of the animal in zones A–D was measured with a center point on the torso area. The following variables were collected from zones A–D: distance moved (m), duration (s), frequency (number of entries), and latency(s) of the first-time entry. Area under the curve (AUC) of total distance was calculated to reflect the habituation of the locomotor activities in the OF. Lower AUC represents faster habituation (Wang et al., 2018a). The rearing behavior was measured when animal's nose position was tracked and went over the virtual line on the wall which was 13 cm above the floor in the corner area (zone E, Figure 1). During rearing, the distance of head movement and head turn angle which are features of exploratory behavior (Lever et al., 2006) were also recorded. For example, rats moved their heads 15 degrees to the left and then moved their heads 45 degrees to the right in a rearing event, the head turn angle would be 60 degrees. In addition, duration (s), frequency (number of entries), head distance moved (m), and latency (s) of the first-time entry of rearing behavior were also recorded.

Acute restraint stress

The ARS procedure was applied to enhance psychological stress and without causing physical injury (Briski and Gillen, 2001). Transparent cylinders with ventilation holes were used for ARS. The cylinders were 23 cm long, 6.3 cm in diameter (Model 81, IITC Life Science Inc., United States).

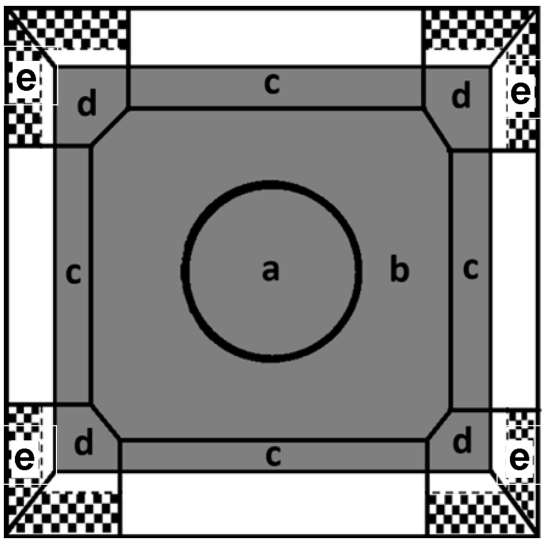


FIGURE 1
The illustration of each zone in the OF task. (a) Center zone, (b) peripheral zone, (c) edge zone, and (d) corner zone. An additional rearing zone was defined on the upper wall in the corner (e).

Behavioral testing

Under the lower ambient light condition, animals were habituated in the OF testing room for 15 min before the OF tests. Each animal was placed in the center of the OF at the start of the test. Each animal was allowed to explore the entire OF freely for 18 min. Four weeks later when animals were 12–13 weeks old, they were habituated in the testing room for 15 min prior to the OF tests under the higher ambient light for 18 min (Baseline). Three weeks later when animals were 15–16 weeks old, an acute restraint stress (ARS) was performed right before the OF test. Under bright light, animals were restrained in the rodent restrainers for 2 h. After the ARS, animals were returned to their home cages and immediately brought to the testing room for 15 min habituation, where animals were allowed to move freely to avoid non-specific motor effects due to movement restriction during restraint. Then the animals were placed in the OF apparatuses for the 18 min test (after ARS).

Statistics

A two- or three-way repeated measures ANOVA with litter as a nested factor was used in statistical analysis when appropriate. We use statistical approach to control for possible litter effects and increase the rigor of the current study. "Litters" were nested under prenatal treatment conditions and used as a nested factor. Significant litter effects were also reported in statistical analysis. This approach was used successfully for controlling litter effects in our previous studies (Wang et al., 2018b; Aghaie et al., 2020). Lazic and Essioux (2013) argue that the nested design can avoid statistical bias when the whole litter is subject to the same experimental procedure *in utero*. Planned comparison was used after ANOVA for pairwise comparison. Independent *t*-test was applied for the data under lower ambient light condition. Values represented Mean ± SEM. The significant levels were set as $p \leq 0.05$. All calculations were performed with STATISTICA 7 (Stat Soft. Inc., Oklahoma, United States).

Results

Prenatal ethanol exposure slightly lowered litter size and pup weight on postnatal day 1

Eight control and 8 PE dams gave birth to a total 174 pups: 89 males and 85 females, respectively (Table 1). Prenatal treatment decreased the litter size (independent *t*-test: df = 14, $t = 3.1$, $p < 0.01$). Prenatal treatment also slightly decreased the pup weight on postnatal day 1 (two-way repeated measures ANOVA with litter as a nested factor: prenatal treatment, sex: main effect of prenatal treatment, $F(1, 142) = 20.08$, $p < 0.001$, main effect of sex, $F(1, 142) = 18.21$, $p < 0.001$; litter effect, $F(28, 142) = 4.92$, $p < 0.001$). Planned comparison after ANOVA showed prenatal treatment led to slightly lower weight in both male and female pups. These results are

consistent with our previous report (Wang et al., 2020), which suggested that the current PE condition did not cause major teratogenic effects.

Prenatal ethanol exposure did not result in differences in overall locomotor activities in male and female rats under lower ambient light

We analyzed the total distance of locomotor activities in the entire OF under lower ambient light. Prenatal ethanol exposure did not impact the total distance in males or females (two-way repeated measures ANOVA with litter as a nested factor: prenatal treatment, 2-min epoch; Figure 2A). In addition, PE did not affect duration in the center zone in either male or female rats (independent *t*-test). The results did not show PE effects in males and females (Figure 2B). When we compare the total distance of locomotor activities under the lower and higher ambient light level under the baseline condition, we did not observe PE effects.

TABLE 1 Birth outcome.

	Control: 8L	PE: 8L	Value of *p*
	(Mean±SEM)	(Mean±SEM)	
Litter size	12.50 ± 0.78	9.37 ± 0.65	<0.01
Pup weight on postnatal day 1			
Male pups' weight (g)	6.33 ± 0.13	5.97 ± 0.12	<0.01
Female pups' weight (g)	6.02 ± 0.10	5.53 ± 0.13	<0.01

Data are represented as Mean ± SEM. PE, prenatal ethanol exposure.

Prenatal ethanol exposure did not result in differences in overall locomotor activities or habituation in male and female rats under higher ambient light condition

We compared the total distance travelled in the OF under lower and higher ambient light levels and found rats travelled greater distance under lower light condition. In addition, female rats travelled greater distance (three-way repeated measures ANOVA with litter as a nested factor: prenatal treatment, sex, light level: main effect of sex, $F(1, 23) = 9.06$, $p < 0.01$; main effect of light level, $F(1, 23) = 39.71$, $p < 0.001$).

Next, we compare the duration rats spent in the center zone in the OF under lower and higher ambient light levels. We find rats spent significantly less time (<10%) in the center zone under higher ambient light in both sexes (two-way repeated measures ANOVA with litter as a nested factor: sex, light level: interaction effect of sex and light level, $F(1, 23) = 14.19$, $p < 0.01$, planned comparison, male: lower vs. higher light, $p < 0.001$, female: lower vs. higher light, $p < 0.001$).

In males, we observed ARS reduced distance travelled without any PE effects (three-way repeated measures ANOVA: prenatal treatment, ARS, 2-min epoch with litter as a nested factor: interaction effect of ARS and epoch, $F(8, 184) = 4.23$, $p < 0.001$; Figure 3B). Planned comparison showed ARS effect ($p < 0.001$; Figure 3A). In females, we did not observe any PE or ARS effects (three-way repeated measures ANOVA: prenatal treatment, ARS, 2-min epoch with litter as a nested factor: main effect of epoch, $F(8, 192) = 102.18$,

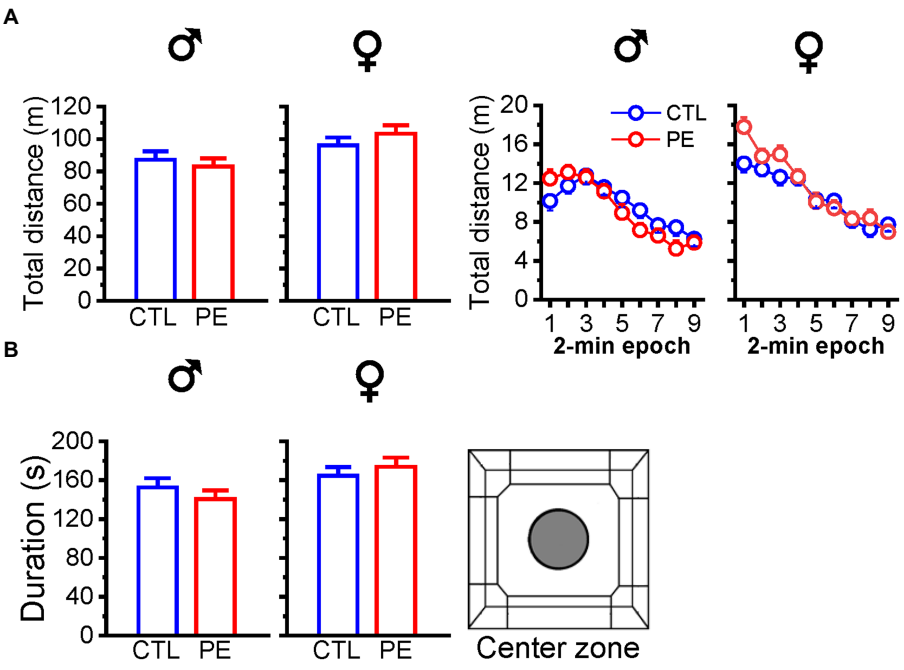


FIGURE 2
Effects of prenatal ethanol exposure (PE) on total distance in the OF and duration in the center zone in male and female rats under lower ambient light (14 lux). Prenatal ethanol exposure did not alter total distance travelled in the OF **(A)** or duration spent in the center zone **(B)**.

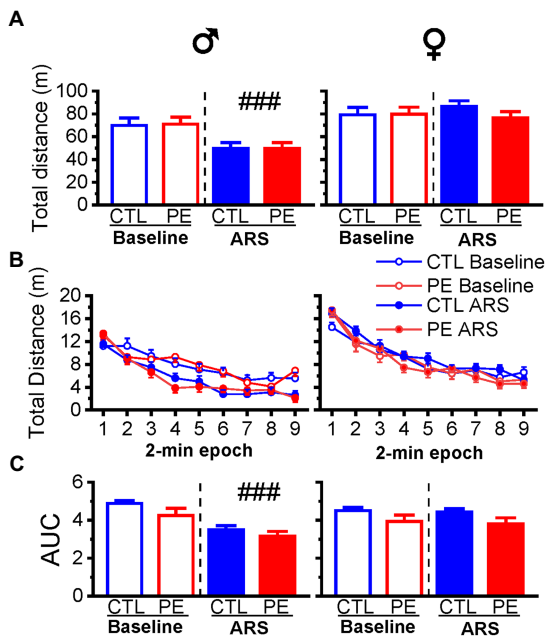


FIGURE 3
Effects of prenatal ethanol exposure (PE) on locomotor activity and its habituation under higher ambient light (60 lux). Prenatal ethanol exposure did not impact total distance travelled under the basal condition **(A,B)**. In males, acute restraint stress (ARS) decreased total distance travelled in the OF. Prenatal ethanol exposure did not alter habituation of the locomotor activity in the OF in either sex **(C)**. Acute restraint stress facilitated the habituation of locomotor activity shown as reduced value of area under the curve (AUC). Data are represented as Mean±SEM. ###p<0.001, baseline condition vs. ARS. CTL, control.

$p<0.001$).Lastly, we analyzed the AUC to examine habituation of locomotor activities under baseline condition and after ARS. In males, we did not observe an effect of PE. Only ARS effect was observed (two-way repeated measures ANOVA: prenatal treatment, ARS with litter as a nested factor: main effect of ARS, $F(1, 10) = 27.05$, $p<0.001$; Figure 3C). We did not observe any PE or ARS effects in females.

Prenatal ethanol exposure reduced the locomotor activities in the center zone under baseline condition in females, indicating increased anxiety-like behavior: Such an effect was observed in males only after ARS

In males, prenatal treatment showed a decrease in duration in the center zone only after ARS, indicating increased anxiety-like behavior. Two-way repeated measures ANOVA with litter as a nested factor (prenatal treatment, ARS) showed a main effect of ARS in the latency of the first-time entry ($F(1, 23) = 19.76$, $p<0.001$; Figure 4A). Planned comparisons after ANOVA showed a significant difference between control and PE males in duration after ARS ($p=0.05$; Figure 4C). Prenatal ethanol exposure did not impact other center zone activities.

In females, PE led to reduced activities in the center zone under baseline condition but not after ARS (two-way repeated measures ANOVA with litter as a nested factor: prenatal treatment, ARS; latency of the first-time entry: main effect of prenatal treatment, $F(1, 13) = 7.91$, $p<0.05$; Figure 4A; frequency: main effect of ARS, $F(1, 13) = 12.18$, $p<0.01$; Figure 4B; duration: main effect of ARS, $F(1, 13) = 10.92$, $p<0.01$; Figure 4C; distance: main effect of prenatal treatment, $F(1, 13) = 6.73$, $p<0.05$, main effect of ARS, $F(1, 13) = 10.31$, $p<0.01$; Figure 4D). Planned comparison after ANOVA showed differences between control and PE females under baseline condition (frequency, $p<0.05$; duration, $p=0.05$; distance, $p<0.01$). Overall, center zone activities were relatively low over 18 min (Figures 4B–D).

Many OF studies use shorter duration of center zone activities in the OF task (e.g., 5 min) (Prut and Belzung, 2003) to infer anxiety-like behavior. We also analyzed the center zone activities in the first 6 min and did not find any PE or ARS effects in males. Prenatal ethanol exposure decreased the center zone distance but not other center zone measurements in females. Only ARS effect on center zone duration was observed (three-way repeated measures ANOVA with litter as a nested factor: prenatal treatment, ARS, 2-min epoch; duration: interaction effect of ARS and epoch, $F(2, 48) = 5.82$, $p<0.01$; frequency: interaction effect of prenatal treatment and ARS, $F(2, 48) = 3.41$, $p<0.05$; distance: interaction effect of ARS and epoch, $F(2, 48) = 9.68$, $p<0.001$, main effect of prenatal treatment, $F(1, 24) = 9.00$, $p<0.01$). Planned comparison showed ARS effect on duration ($p<0.05$) and prenatal treatment effects on distance under basal condition ($p<0.01$). Analyzing only 6 min of center zone activities is not sufficient to show group differences possibly due to very low level of activities.

Prenatal ethanol exposure did not impact the durations in the edge, peripheral and corner zones

We analyzed duration animal spent in the edge zone, the peripheral zone, and the corner zone in each sex using two-way repeated measures ANOVA with litter as a nested factor (prenatal treatment, ARS). We did not observe any PE effects. Nevertheless, ARS effects were observed in males and females, respectively. In males, main effects of ARS were found in the edge zone ($F(1, 23) = 9.33$, $p<0.01$; Figure 5A), peripheral zone ($F(1, 23) = 16.94$, $p<0.001$; Figure 5B) and corner zone ($F(1, 23) = 19.66$, $p<0.001$; Figure 5C). In females, main effects of ARS were found in the edge zone ($F(1, 24) = 8.36$, $p<0.01$) and peripheral zone ($F(1, 24) = 11.49$, $p<0.01$).

Prenatal ethanol exposure reduced rearing (vertical exploration) in the corner in both sexes: This effect was also observed in females after ARS

When we examined the duration spent in each zone (Figure 6), it was obvious that animals spent most of time in the corner zone (>75%) in contrast to the center zone (<2%). The major behavior animals engaged in the corner is rearing, which represents vertical exploratory activity. Increased rearing indicates lower anxiety (Zimcikova et al., 2017). We analyzed the latency of the first-time entry, frequency, duration, head distance, and head turn angle of rearing behavior (Figure 7). Movements such as head distance and

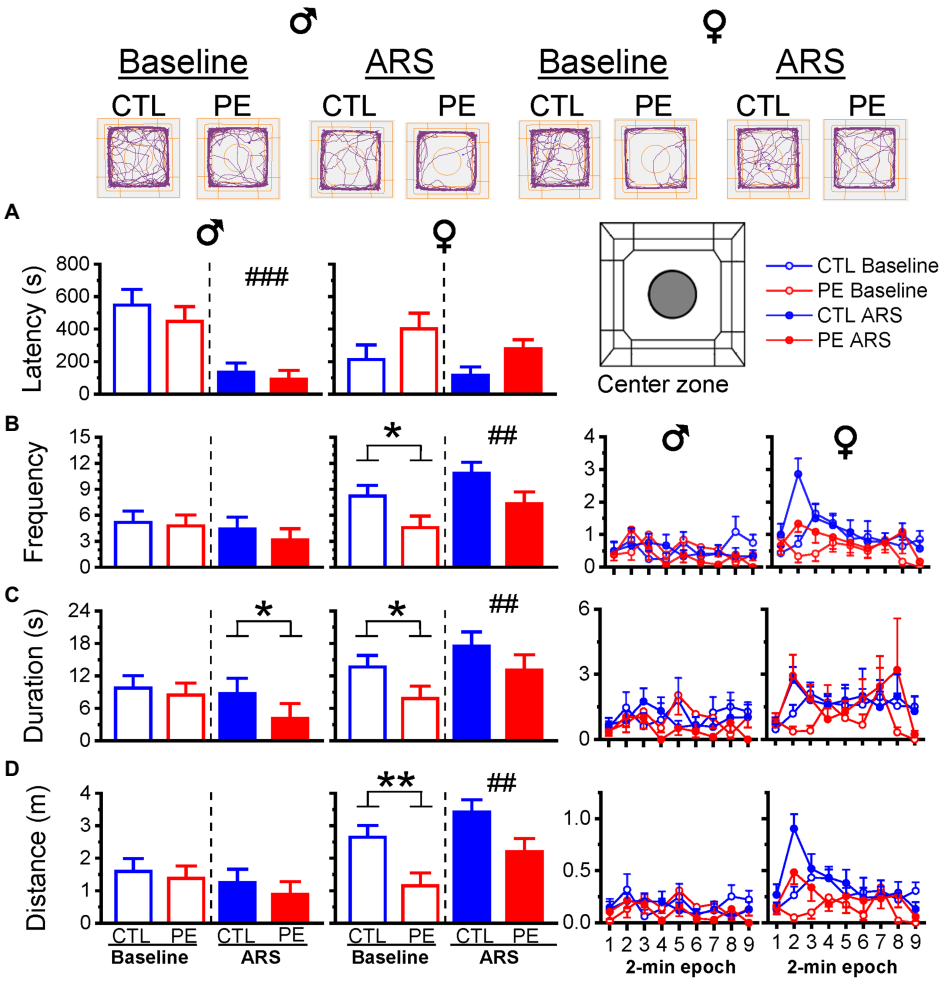


FIGURE 4
Prenatal ethanol exposure (PE) and acute restraint stress (ARS) effects on activities in the center zone. Upper panel reveals the representative tracking plots in the OF task. Prenatal ethanol exposure decreased the duration in the center zone after ARS in male rats **(C)**. Whereas, PE reduced the frequency, duration, and distance travelled under the baseline condition in female rats **(B–D)**. Prenatal ethanol did not impact the latency in males and females **(A)**. The right panels display the frequency, duration and distance of activities in the center zone in 2-min epoch. Data are represented as Mean±SEM. *$p \leq 0.05$, **$p < 0.01$, control vs. PE. ##$p < 0.01$, ###$p < 0.001$, baseline vs. ARS. CTL, control.

head turn angle during rearing are important ethological indicators of exploratory behavior (Haddad et al., 2021).

We examined the first 6 min of rearing behavior because rats engaged in maximal rearing behavior in the beginning of the test. In males, PE decreased the duration, head distance, and head turn angle during rearing behavior in the corner indicating increased anxiety-like behavior (three-way repeated measures ANOVA with litter as a nested factor: prenatal treatment, ARS, 2-min epoch; duration: main effect of prenatal treatment, $F(1, 23) = 6.15$, $p < 0.05$; Figure 7C; head distance: main effect of prenatal treatment, $F(1, 23) = 4.76$, $p < 0.05$; Figure 7D; head turn angle: an interaction of prenatal treatment, ARS and epoch, $F(2, 46) = 3.96$, $p < 0.05$; Figure 7E). Planned comparisons after ANOVA confirmed that under basal condition, PE reduced rearing duration ($p < 0.01$), head distance ($p < 0.05$), and head turn angle ($p < 0.05$). The PE effects were not observed after ARS.

As for females, PE decreased rearing behavior in the frequency, duration, head distance, and head turn angle (three-way repeated measures ANOVA with litter as a nested factor: prenatal treatment, ARS, 2-min epoch; frequency: main effect of prenatal treatment, $F(1, 24) = 12.96$, $p < 0.01$, main effect of ARS, $F(1, 24) = 22.42$, $p < 0.001$; Figure 7B; duration: main effect of prenatal treatment, $F(1, 24) = 10.00$, $p < 0.01$, main effect of ARS, $F(1, 24) = 18.05$, $p < 0.001$; Figure 7C; head distance: an interaction of ARS and epoch, $F(2, 48) = 3.21$, $p < 0.05$; Figure 7D; head turn angle: main effect of prenatal treatment, $F(1, 24) = 8.98$, $p < 0.01$, main effect of ARS, $F(1, 24) = 36.45$, $p < 0.001$; Figure 7E). Planned comparisons showed that PE reduced rearing behaviors under baseline condition (frequency: $p < 0.01$; duration: $p < 0.001$; head distance: $p < 0.05$; head turn angle: $p < 0.01$) and after ARS (frequency: $p < 0.01$; duration: $p < 0.01$; head distance: $p < 0.01$; head turn angle: $p < 0.05$).

Discussion

The current study reveals that heavy PE leads to increased anxiety-like behavior during adulthood in both sexes. The expression of anxiety-like behavior depends on ambient light levels. Group differences cannot be observed when ambient light is low (14 lux). At

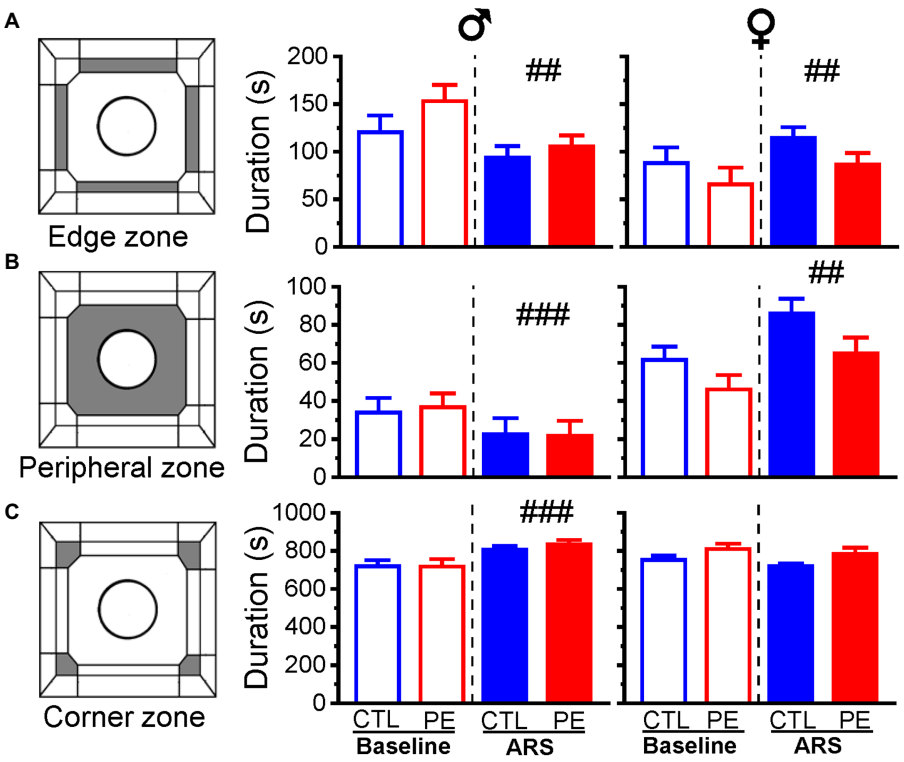


FIGURE 5
Effects of prenatal ethanol exposure (PE) and acute restraint stress (ARS) on duration spent in different zones in the OF: edge zone **(A)**, peripheral zone **(B)**, and corner zone **(C)** in the baseline and after ARS in both male and female rats. Prenatal ethanol exposure did not change the duration in any of the zones. Acute restraint stress exerted sex dimorphic effects on duration in each zone. Data are represented as Mean±SEM. CTL, ##p<0.01, ###p<0.001, baseline condition vs. ARS.

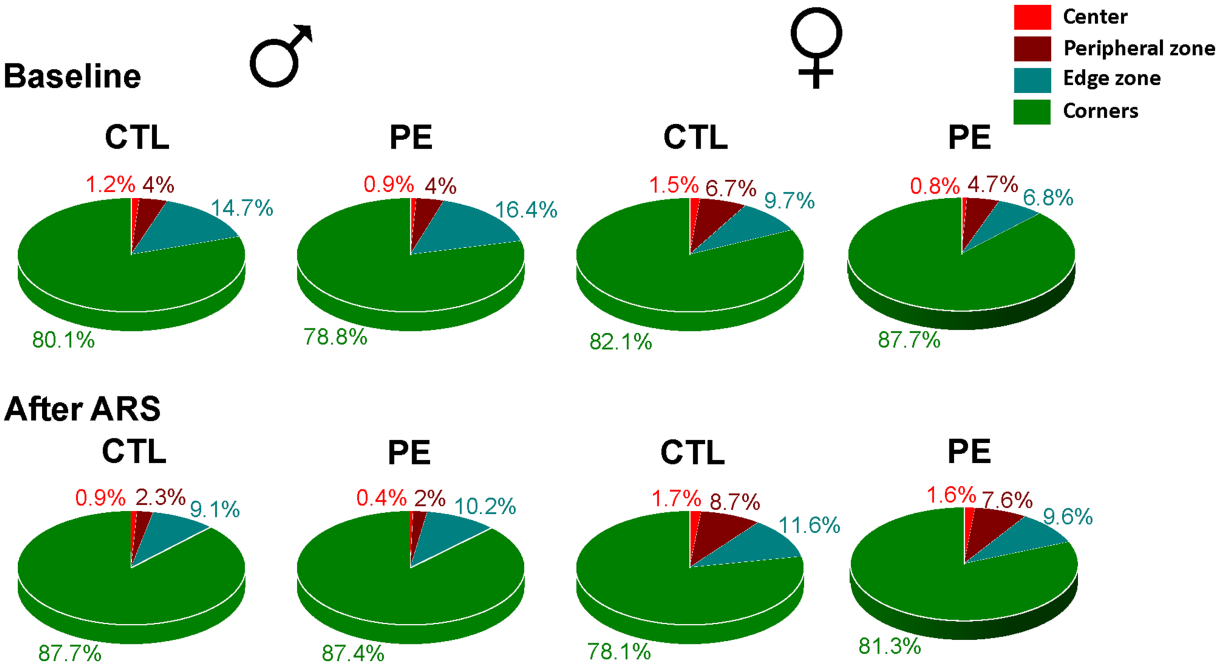


FIGURE 6
Percentages of time spent in the center, peripheral, edge, and corner zone in the OF task. Rats in all group spent >75% of time in the corner zone but <2% in the center zone.

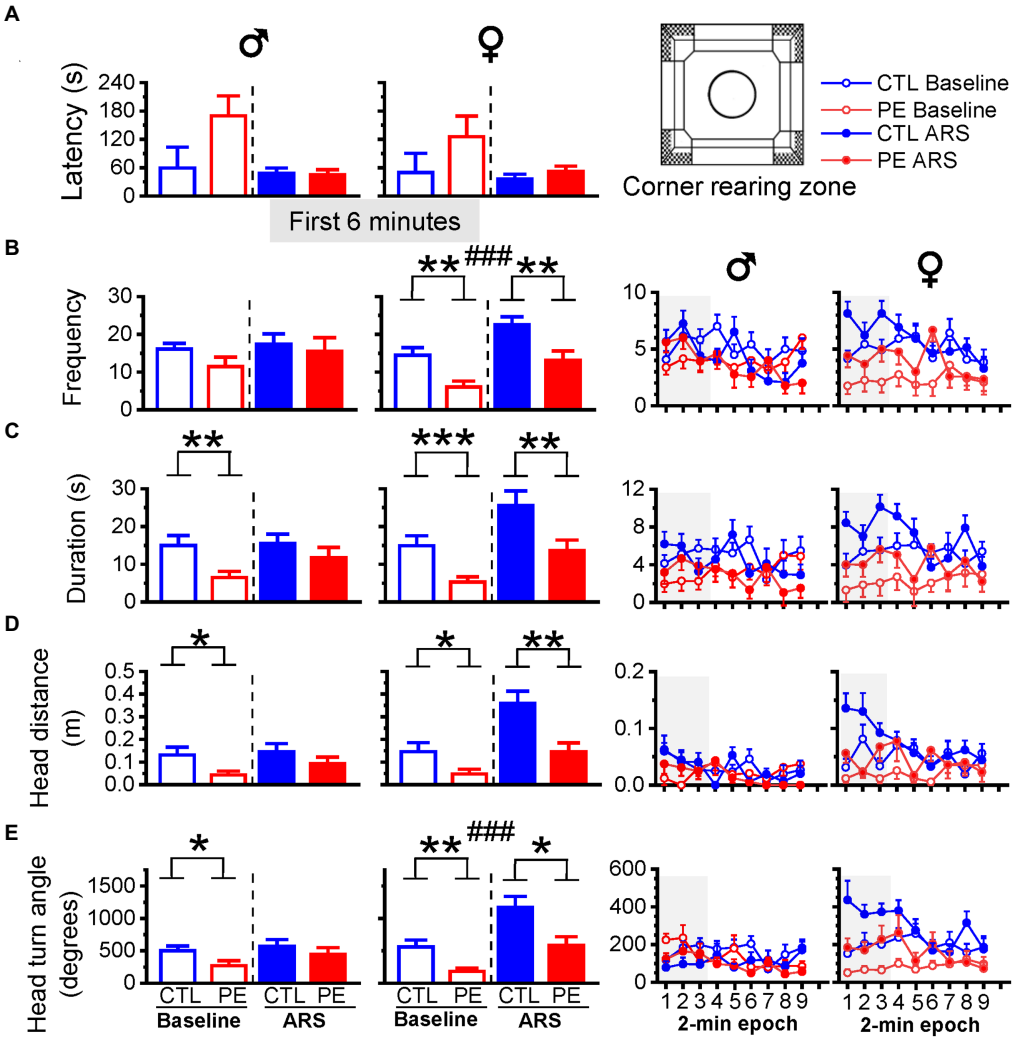


FIGURE 7
Effects of prenatal ethanol exposure (PE) and acute restraint stress (ARS) on rearing behaviors in the corner in the first 6min of the OF task. In male rats, PE reduced the duration, head distance, head turn angle, indicating increased anxiety-like behavior **(C–E)**. In female rats, PE reduced the frequency, duration, head distance and the head turn angle under baseline condition and after ARS **(B–E)**. Prenatal ethanol did not impact the latency in males and females **(A)**. The right panels display the frequency, duration, head movement, and head turn angle of rearing in 2-min epoch. Data are represented as Mean±SEM. *$p \leq 0.05$, **$p<0.01$, ***$p<0.001$, control vs. PE. ###$p<0.001$, baseline condition vs. ARS.

higher ambient light level, the anxiety-like behavior is observed only in PE females using the traditional index of reduced activities in the center zone of the OF. On the other hand, reduced activities in the center zone could be observed after acute stress in males. Importantly, we have observed that PE reduces vertical exploratory behavior (rearing) in the corner of the OF in both sexes under basal condition. Overall, PE does not impact locomotor activities or its habituation indicating the expression of anxiety-like behavior is not confounded by altered movement.

Animals tend to locomote and explore along the vertical surface in an unfamiliar, novel environment (Lever et al., 2006) instead of venturing into the center zone to avoid dangers (e.g., the threat from predators). Decreased activity level and duration in the center zone of the OF is commonly used to infer anxiety (Prut and Belzung, 2003). In this study, we first demonstrate that locomotor activity in the center zone is affected by ambient light level (Kuniishi et al., 2017). In lower ambient light setting (14 lux), animals show increased activities in the center zone compared to that in higher light setting (60 lux) and no PE effects are observed in either sex. In the higher light setting, we are able to observe that female PE rats show reduced locomotor activities in the center zone compared to controls, supporting PE leads to increased anxiety in females. The observations are consistent with those obtained from previous studies of early life stress showing the optimal light level for studying group differences in anxiety tasks is between 10–75 lux (Kuniishi et al., 2017). Ambient light level also impacts other anxiety tasks in a similar way such as the elevated-plus maze (Garcia et al., 2005). Taken together, sufficient ambient light is critical for the expression of anxiety-like behavior. Additional observation is that female rats have higher locomotor activities in general, which is also consistent with a previous study (Hellemans et al., 2010b). Prenatal ethanol exposure induced decreases in center zone activities is not observed in males. A clear decrease in center zone activity can be observed in male PE rats only when acute stress (ARS) was applied immediately before the OF test. The results indicate

that PE effects on anxiety-like behavior interact with sex and acute stress.

We have observed that rats of both sexes spend very little time (<2%) in the center zone but more than 75% of the time in the corner zone of the OF. Therefore, we carefully examine the behavior in the corner zone and observe that animals often engage in rearing behavior, especially in the beginning of the OF test. Although rats also display rearing in the edge zone, its frequency is relatively low because rats spend limited time in this zone. When rats rear in the corner, they stand on the hind legs, extend their body upward, put their front paws on the wall, and engage in side-to-side head movement. Rearing is considered spontaneous vertical exploratory behavior to novelty in rodents which is similar to horizontal exploration. The rearing behavior observed is similar to that described for exploratory behavior in rodents for information gathering, food forage, or escape described in a previous publication (Lever et al., 2006). Rearing behavior had a negative correlation with anxiety level through confirmatory factor analysis (Brenes Saenz et al., 2006). The results from the present study show that duration of rearing and parameters of head movement during rearing are all decreased significantly in PE animals in both sexes. These observations support PE reduces exploratory behavior and increases anxiety. Overall, the PE-induced effect on rearing is not dependent on duration spent in the corner which are similar between control and PE rats. However, compared to males, females engage in more rearing behavior and in a more sustained pattern, consistent with greater locomotor activities in females. Taken together, we show that rearing behavior in the corner of the OF can be quantified in detail using a camera-based data acquisition system. Reduced rearing in the corner could be used as a reliable index of anxiety-like behavior in addition to activity/duration in the center zone in the OF task.

The current PE paradigm does not impact the overall locomotor activities of both sexes under higher ambient light. We use the traditional center zone activity as well a new measurement of corner rearing behavior to infer anxiety. Prenatal ethanol treatment does not cause the differences in center activities in male rats under basal condition. On the contrary, PE reduces the frequency, duration and distance of female rats in the center zone, indicating PE leads to increased anxiety-like behavior in female rats. On the other hand, PE reduces activities in the center zone (increases anxiety-like behavior) after acute stress in male but not female rats. Animals spend most of the time in the corner. When using reduced corner rearing behavior for increased anxiety, we observe increased anxiety in both male and female rats under the basal condition including reduced rearing duration, head distance and head turn angle. Increased anxiety-like behavior is only observed in females after acute stress. The above results show PE reduces activities in the center zone and rearing behavior. The results raise a possibility that these effects could be caused by impaired motor function in PE rats. However, observations from our present and previous studies do not support this notion. In the present study, there are no differences in overall locomotor activity in control and PE rats in either sex. In addition, when locomotor activity was evaluated in a confined space ($42.5 \times 22.5 \times 19.25$ cm) using the same PE paradigm in male rats in a previous study, we actually observed increased overall locomotor activity (Wang et al., 2019). In the same study, no group differences were found in rearing frequency in 60 min between control and PE rats (control: 163.08 ± 14.68 vs. PE: 182.58 ± 15.19; unpublished data). Anxiety behavior is also affected by acute stress (Sturman et al., 2018). Strong evidence shows that PE leads to augmented stress reactivity indicated by increased cortisol level (Hellemans et al., 2010a,b). In the present study, we use 2 h restraint right before the OF test to examine effects of acute stress on anxiety behavior. The results show acute stress increases anxiety-like behavior indicated by decreased activities in center zone in males which is not observed under basal conditions. Acute stress does not further augment anxiety-like behavior in females. These observations are consistent with previous studies showing ARS increases stress reactivity (Sturman et al., 2018). When corner rearing behavior is evaluated, we have not observed acute stress further increases anxiety-like behavior in either males or females. However, we observe an overall increase in rearing activities in females after acute stress. Taken together, PE effects on rearing behavior are not altered by acute stress.

It has been found that PE impacts anxiety-like behavior. However, the PE effects on anxiety-like behavior are inconsistent due to different behavioral tasks, ethanol exposure paradigms, sex and age. Acute ethanol exposure on GD 12 *via* intraperitoneal injection reduces social preference (a measurement of social anxiety-like behavior) in female adult rats but not in males (Diaz et al., 2020). Ethanol vapor exposure for 6 h on GD 12 enhances anxiety-like behavior in male adolescent rats in the novelty-induced hypophagia task, light–dark box, and OF, but not in female adolescent offspring (Rouzer et al., 2017). Ethanol exposure (4 g/kg) on GD 16 and 17 *via* intraperitoneal injection increases anxiety in adolescent male and female mice (Hwang and Hashimoto-Torii, 2022) in the elevated plus-maze task. Chronic ethanol exposure with liquid diet during GDs 10–21 leads to reduced anxiety-like behavior in adult male rats in the elevated plus-maze task (Ohta et al., 2010). Conversely, chronic ethanol exposure from GDs 7–20 using intragastric intubation leads to increased anxiety-like behavior in male offspring (Dursun et al., 2006). Another study shows no impact of chronic ethanol exposure using ethanol vapor during GDs 5–20 in rats of both sexes using an OF task (Breit et al., 2022). Using the current chronic heavy PE paradigm, we observed increased anxiety-like behavior using elevated plus-maze and zero maze tasks in adult male rats (Oubraim et al., 2022), which is consistent with the current study. The inconsistent observations of anxiety-like behavior after chronic PE could be due to PE paradigms as well as different behavioral tasks used. Some researchers resort to more than one behavioral tasks to measure anxiety-like behavior (Cullen et al., 2013; Wieczorek et al., 2015; Rouzer et al., 2017) in order to reach a clear conclusion. Results from the present study indicate rearing behavior in the corner of the OF task is a reliable measurement for anxiety-like behavior in both sexes. Rearing behavior in the corner zone is also multifaceted and complex. Behavioral parameters such as head movement and head turn angle, which are specific features of vertical exploratory behavior, can provide additional ethological information. Combined analyses of horizontal and vertical exploratory behavior in the OF task could provide a reasonable and simple approach to investigate anxiety-like behavior.

The mechanism of anxiety is complex and often interacts with depression-like behaviors (Hellemans et al., 2010b). In clinic studies, Niclasen et al. (2014) observed prenatal exposure to binge drinking in pregnancy was associated positively with impaired behavioral and emotional development in preadolescent boys. In adults with FASD, females show much higher propensity for depression and anxiety than males (Famy et al., 1998). Together, strong evidence showed that PE increases anxiety-like behavior. Therefore, it is crucial to understand

the underlying neuronal mechanisms caused by PE in order to develop effective intervention strategies.

The neural circuitries underlying rearing are not fully understood. However, it has been proposed that the hippocampus is involved (Sturman et al., 2018). When animals rear, better view is obtained for enhanced space exploration (Lever et al., 2006). The hippocampus is involved in space navigation and interconnected with stress centers including hypothalamus, amygdala, and other limbic structures (Bannerman et al., 2014). Specifically, the ventral hippocampus interconnection with the hypothalamus plays an important role in regulating stress responses (Tannenholz et al., 2014). Prenatal alcohol exposure is known to affect hippocampal functions (Sanchez et al., 2019; Dodge et al., 2020) and alter the sensitivity of HPA axis (Hellemans et al., 2010b; Wieczorek et al., 2015) which could mediate increased anxiety-like behavior. Other neural circuitries and neurotransmitter systems could also mediate PE-induced reduction in rearing/increased anxiety. Studies have reported that PE persistently alters several neurotransmitter systems involved in regulating emotional behavior, including the serotonin (5-HT) system. Prenatal ethanol exposure causes lower density of 5-HT neurons (Druse et al., 1991; Ohta et al., 2010), fewer 5-HT fibers, impaired 5-HT projections (Zhou et al., 2001), which suggest PE leads to expression of the anxiety-like behavior in animals. A recent study has discovered that PE induced persistent activation of 5-HT neurons and its glutamate synapses by increasing nitrergic function and degrading endocannabinoids signaling in the dorsal raphe 5-HT neurons (Oubraim et al., 2022). This activation exertes the anxiogenic effect, thereby PE animals express anxiety-like behavior. Through the morphological studies, prenatal ethanol exposure, regardless of the consumption volume, results in neuronal morphological alterations in the amygdala (Cullen et al., 2013) and striatum (Ma, 2019). These changes could mediate increased anxiety-like behavior.

Conclusion

The results from the present study show chronic heavy PE causes a persistent increase in anxiety-like behavior in adulthood in both sexes. This conclusion is based on improvement of traditional OF task. Specifically, the vertical exploratory behavior (rearing) in the corner zone is analyzed in detail, which has not been emphasized before. This approach can be a reliable indicator for anxiety-like behavior in general.

Data availability statement

The raw data supporting the conclusions of this article will be made available by the authors, without undue reservation.

Ethics statement

The animal study was reviewed and approved by University at Buffalo, Institutional Animal Care and Use Committee.

Author contributions

VM and FK performed behavioral tests. A-LW, VM, RW, KH, and R-YS completed data analyses. KH, SO, and R-YS conducted breeding and prenatal ethanol treatments. R-YS, VM, KH, RW, and SH-D participated in the experimental design. R-YS and SH-D directed the project. A-LW and R-YS wrote the manuscript. All authors contributed to the article and approved the submitted version.

Funding

This study was support by grant AA026421 and AA026601 from the National Institutes of Health awarded to R-YS and SH-D.

Conflict of interest

The authors declare that the research was conducted in the absence of any commercial or financial relationships that could be construed as a potential conflict of interest.

Publisher's note

All claims expressed in this article are solely those of the authors and do not necessarily represent those of their affiliated organizations, or those of the publisher, the editors and the reviewers. Any product that may be evaluated in this article, or claim that may be made by its manufacturer, is not guaranteed or endorsed by the publisher.

References

Aghaie, C. I., Hausknecht, K. A., Wang, R., Dezfuli, P. H., Haj-Dahmane, S., Kane, C. J. M., et al. (2020). Prenatal ethanol exposure and postnatal environmental intervention Alter dopaminergic neuron and microglia morphology in the ventral tegmental area during adulthood. *Alcohol. Clin. Exp. Res.* 44, 435–444. doi: 10.1111/acer.14275

Ba, A., Seri, B. V., and Han, S. H. (1996). Thiamine administration during chronic alcohol intake in pregnant and lactating rats: effects on the offspring neurobehavioural development. *Alcohol Alcohol.* 31, 27–40. doi: 10.1093/oxfordjournals.alcalc.a008113

Bannerman, D. M., Sprengel, R., Sanderson, D. J., McHugh, S. B., Rawlins, J. N., Monyer, H., et al. (2014). Hippocampal synaptic plasticity, spatial memory and anxiety. *Nat. Rev. Neurosci.* 15, 181–192. doi: 10.1038/nrn3677

Bartolomucci, A., Gioiosa, L., Chirieleison, A., Ceresini, G., Parmigiani, S., and Palanza, P. (2004). Cross fostering in mice: behavioral and physiological carry-over effects in adulthood. *Genes Brain Behav.* 3, 115–122. doi: 10.1111/j.1601-183x.2003.00059.x

Breit, K. R., Rodriguez, C. G., Lei, A., Hussain, S., and Thomas, J. D. (2022). Effects of prenatal alcohol and delta-9-tetrahydrocannabinol exposure via electronic cigarettes on motor development. *Alcohol. Clin. Exp. Res.* 46, 1408–1422. doi: 10.1111/acer.14892

Brenes Saenz, J. C., Villagra, O. R., and Fornaguera Trias, J. (2006). Factor analysis of forced swimming test, sucrose preference test and open field test on enriched, social and isolated reared rats. *Behav. Brain Res.* 169, 57–65. doi: 10.1016/j.bbr.2005.12.001

Briski, K., and Gillen, E. (2001). Differential distribution of Fos expression within the male rat preoptic area and hypothalamus in response to physical vs. psychological stress. *Brain Res. Bull.* 55, 401–408. doi: 10.1016/s0361-9230(01)00532-9

Carobrez, A. P., and Bertoglio, L. J. (2005). Ethological and temporal analyses of anxiety-like behavior: the elevated plus-maze model 20 years on. *Neurosci. Biobehav. Rev.* 29, 1193–1205. doi: 10.1016/j.neubiorev.2005.04.017

Cullen, C. L., Burne, T. H., Lavidis, N. A., and Moritz, K. M. (2013). Low dose prenatal ethanol exposure induces anxiety-like behaviour and alters dendritic morphology in the

basolateral amygdala of rat offspring. *PLoS One* 8:e54924. doi: 10.1371/journal.pone.0054924

Diaz, M. R., Johnson, J. M., and Varlinskaya, E. I. (2020). Increased ethanol intake is associated with social anxiety in offspring exposed to ethanol on gestational day 12. *Behav. Brain Res.* 393:112766. doi: 10.1016/j.bbr.2020.112766

Diaz, M. R., Mooney, S. M., and Varlinskaya, E. I. (2016). Acute prenatal exposure to ethanol on gestational day 12 elicits opposing deficits in social behaviors and anxiety-like behaviors in Sprague Dawley rats. *Behav. Brain Res.* 310, 11–19. doi: 10.1016/j.bbr.2016.05.003

Dodge, N. C., Thomas, K. G. F., Meintjes, E. M., Molteno, C. D., Jacobson, J. L., and Jacobson, S. W. (2020). Reduced hippocampal volumes partially mediate effects of prenatal alcohol exposure on spatial navigation on a virtual water maze task in children. *Alcohol. Clin. Exp. Res.* 44, 844–855. doi: 10.1111/acer.14310

Druse, M. J., Kuo, A., and Tajuddin, N. (1991). Effects of in utero ethanol exposure on the developing serotonergic system. *Alcohol. Clin. Exp. Res.* 15, 678–684. doi: 10.1111/j.1530-0277.1991.tb00578.x

Dursun, I., Jakubowska-Dogru, E., and Uzbay, T. (2006). Effects of prenatal exposure to alcohol on activity, anxiety, motor coordination, and memory in young adult Wistar rats. *Pharmacol. Biochem. Behav.* 85, 345–355. doi: 10.1016/j.pbb.2006.09.001

Famy, C., Streissguth, A. P., and Unis, A. S. (1998). Mental illness in adults with fetal alcohol syndrome or fetal alcohol effects. *Am. J. Psychiatry* 155, 552–554. doi: 10.1176/ajp.155.4.552

Fryer, S. L., McGee, C. L., Matt, G. E., Riley, E. P., and Mattson, S. N. (2007). Evaluation of psychopathological conditions in children with heavy prenatal alcohol exposure. *Pediatrics* 119, e733–e741. doi: 10.1542/peds.2006-1606

Garcia, A. M., Cardenas, F. P., and Morato, S. (2005). Effect of different illumination levels on rat behavior in the elevated plus-maze. *Physiol. Behav.* 85, 265–270. doi: 10.1016/j.physbeh.2005.04.007

Giberson, P. K., and Weinberg, J. (1997). Effect of surrogate fostering on splenic lymphocytes in fetal ethanol exposed rats. *Alcohol. Clin. Exp. Res.* 21, 44–55. doi: 10.1111/j.1530-0277.1997.tb03727.x

Greenmyer, J. R., Klug, M. G., Kambeitz, C., Popova, S., and Burd, L. (2018). A multicountry updated assessment of the economic impact of fetal alcohol Spectrum disorder: costs for children and adults. *J. Addict. Med.* 12, 466–473. doi: 10.1097/ADM.0000000000000438

Haddad, F. L., Ghahremani, M., de Oliveira, C., Doornaert, E. E., Johnston, K. D., Everling, S., et al. (2021). A novel three-choice touchscreen task to examine spatial attention and orienting responses in rodents. *eNeuro* 8, ENEURO.0032–ENEU20.2021. doi: 10.1523/ENEURO.0032-20.2021

Hellemans, K. G., Sliwowska, J. H., Verma, P., and Weinberg, J. (2010a). Prenatal alcohol exposure: fetal programming and later life vulnerability to stress, depression and anxiety disorders. *Neurosci. Biobehav. Rev.* 34, 791–807. doi: 10.1016/j.neubiorev.2009.06.004

Hellemans, K. G., Verma, P., Yoon, E., Yu, W. K., Young, A. H., and Weinberg, J. (2010b). Prenatal alcohol exposure and chronic mild stress differentially alter depressive- and anxiety-like behaviors in male and female offspring. *Alcohol. Clin. Exp. Res.* 34, 633–645. doi: 10.1111/j.1530-0277.2009.01132.x

Hwang, H. M., and Hashimoto-Torii, K. (2022). Activation of the anterior cingulate cortex ameliorates anxiety in a preclinical model of fetal alcohol spectrum disorders. *Transl. Psychiatry* 12:24. doi: 10.1038/s41398-022-01789-1

Keiver, K., Bertram, C. P., Orr, A. P., and Clarren, S. (2015). Salivary cortisol levels are elevated in the afternoon and at bedtime in children with prenatal alcohol exposure. *Alcohol* 49, 79–87. doi: 10.1016/j.alcohol.2014.11.004

Kingdon, D., Cardoso, C., and McGrath, J. J. (2016). Research review: executive function deficits in fetal alcohol spectrum disorders and attention-deficit/hyperactivity disorder – a meta-analysis. *J. Child Psychol. Psychiatry* 57, 116–131. doi: 10.1111/jcpp.12451

Kuniishi, H., Ichisaka, S., Yamamoto, M., Ikubo, N., Matsuda, S., Futora, E., et al. (2017). Early deprivation increases high-leaning behavior, a novel anxiety-like behavior, in the open field test in rats. *Neurosci. Res.* 123, 27–35. doi: 10.1016/j.neures.2017.04.012

Lange, S., Probst, C., Gmel, G., Rehm, J., Burd, L., and Popova, S. (2017). Global prevalence of fetal alcohol Spectrum disorder among children and youth: a systematic review and meta-analysis. *JAMA Pediatr.* 171, 948–956. doi: 10.1001/jamapediatrics.2017.1919

Lazic, S. E., and Essioux, L. (2013). Improving basic and translational science by accounting for litter-to-litter variation in animal models. *BMC Neurosci.* 14:37. doi: 10.1186/1471-2202-14-37

Lever, C., Burton, S., and O'Keefe, J. (2006). Rearing on hind legs, environmental novelty, and the hippocampal formation. *Rev. Neurosci.* 17, 111–133. doi: 10.1515/revneuro.2006.17.1-2.111

Ma, Y. Y. (2019). Striatal morphological and functional alterations induced by prenatal alcohol exposure. *Pharmacol. Res.* 142, 262–266. doi: 10.1016/j.phrs.2019.02.022

Mattson, S. N., Crocker, N., and Nguyen, T. T. (2011). Fetal alcohol spectrum disorders: neuropsychological and behavioral features. *Neuropsychol. Rev.* 21, 81–101. doi: 10.1007/s11065-011-9167-9

May, P. A., Baete, A., Russo, J., Elliott, A. J., Blankenship, J., Kalberg, W. O., et al. (2014). Prevalence and characteristics of fetal alcohol spectrum disorders. *Pediatrics* 134, 855–866. doi: 10.1542/peds.2013-3319

May, P. A., Gossage, J. P., Kalberg, W. O., Robinson, L. K., Buckley, D., Manning, M., et al. (2009). Prevalence and epidemiologic characteristics of FASD from various research methods with an emphasis on recent in-school studies. *Dev. Disabil. Res. Rev.* 15, 176–192. doi: 10.1002/ddrr.68

Niclasen, J., Nybo Andersen, A. M., Teasdale, T. W., and Strandberg-Larsen, K. (2014). Prenatal exposure to alcohol, and gender differences on child mental health at age seven years. *J. Epidemiol. Community Health* 68, 224–232. doi: 10.1136/jech-2013-202956

Ohta, K., Sakata-Haga, H., and Fukui, Y. (2010). Alteration in anxiety-related behaviors and reduction of serotonergic neurons in raphe nuclei in adult rats prenatally exposed to ethanol. *Congenit Anom (Kyoto)* 50, 105–114. doi: 10.1111/j.1741-4520.2010.00269.x

Osborn, J. A., Kim, C. K., Steiger, J., and Weinberg, J. (1998). Prenatal ethanol exposure differentially alters behavior in males and females on the elevated plus maze. *Alcohol. Clin. Exp. Res.* 22, 685–696. doi: 10.1111/j.1530-0277.1998.tb04312.x

Oubraim, S., Wang, R., Hausknecht, K., Kaczocha, M., Shen, R. Y., and Haj-Dahmane, S. (2022). Prenatal ethanol exposure causes anxiety-like phenotype and alters synaptic nitric oxide and endocannabinoid signaling in dorsal raphe nucleus of adult male rats. *Transl. Psychiatry* 12:440. doi: 10.1038/s41398-022-02210-7

Prut, L., and Belzung, C. (2003). The open field as a paradigm to measure the effects of drugs on anxiety-like behaviors: a review. *Eur. J. Pharmacol.* 463, 3–33. doi: 10.1016/s0014-2999(03)01272-x

Pyman, P., Collins, S. E., Muggli, E., Testa, R., and Anderson, P. J. (2021). Cognitive and behavioural attention in children with low-moderate and heavy doses of prenatal alcohol exposure: a systematic review and meta-analysis. *Neuropsychol. Rev.* 31, 610–627. doi: 10.1007/s11065-021-09490-8

Rouzer, S. K., Cole, J. M., Johnson, J. M., Varlinskaya, E. I., and Diaz, M. R. (2017). Moderate maternal alcohol exposure on gestational day 12 impacts anxiety-like behavior in offspring. *Front. Behav. Neurosci.* 11:183. doi: 10.3389/fnbeh.2017.00183

Sanchez, L. M., Goss, J., Wagner, J., Davies, S., Savage, D. D., Hamilton, D. A., et al. (2019). Moderate prenatal alcohol exposure impairs performance by adult male rats in an object-place paired-associate task. *Behav. Brain Res.* 360, 228–234. doi: 10.1016/j.bbr.2018.12.014

Shen, R. Y., Hannigan, J. H., and Kapatos, G. (1999). Prenatal ethanol reduces the activity of adult midbrain dopamine neurons. *Alcohol. Clin. Exp. Res.* 23, 1801–1807. doi: 10.1111/j.1530-0277.1999.tb04076.x

Sturman, O., Germain, P. L., and Bohacek, J. (2018). Exploratory rearing: a context- and stress-sensitive behavior recorded in the open-field test. *Stress* 21, 443–452. doi: 10.1080/10253890.2018.1438405

Tang, S., Xu, S., Waddell, J., Zhu, W., Gullapalli, R. P., and Mooney, S. M. (2019). Functional connectivity and metabolic alterations in medial prefrontal cortex in a rat model of fetal alcohol Spectrum disorder: a resting-state functional magnetic resonance imaging and in vivo proton magnetic resonance spectroscopy study. *Dev. Neurosci.* 41, 67–78. doi: 10.1159/000499183

Tannenholz, L., Jimenez, J. C., and Kheirbek, M. A. (2014). Local and regional heterogeneity underlying hippocampal modulation of cognition and mood. *Front. Behav. Neurosci.* 8:147. doi: 10.3389/fnbeh.2014.00147

Wang, R., Hausknecht, K. A., Haj-Dahmane, S., Shen, R. Y., and Richards, J. B. (2018a). Decreased environmental complexity during development impairs habituation of reinforcer effectiveness of sensory stimuli. *Behav. Brain Res.* 337, 53–60. doi: 10.1016/j.bbr.2017.09.032

Wang, R., Hausknecht, K. A., Shen, Y. L., Haj-Dahmane, S., Vezina, P., and Shen, R. Y. (2018b). Environmental enrichment reverses increased addiction risk caused by prenatal ethanol exposure. *Drug Alcohol Depend.* 191, 343–347. doi: 10.1016/j.drugalcdep.2018.07.013

Wang, R., Martin, C. D., Lei, A. L., Hausknecht, K. A., Ishiwari, K., Oubraim, S., et al. (2021). Moderate prenatal ethanol exposure leads to attention deficits in both male and female rats. *Alcohol. Clin. Exp. Res.* 45, 1122–1135. doi: 10.1111/acer.14599

Wang, R., Martin, C. D., Lei, A. L., Hausknecht, K. A., Ishiwari, K., Richards, J. B., et al. (2020). Prenatal ethanol exposure leads to attention deficits in both male and female rats. *Front. Neurosci.* 14:12. doi: 10.3389/fnins.2020.00012

Wang, R., Martin, C. D., Lei, A. L., Hausknecht, K. A., Turk, M., Micov, V., et al. (2022). Prenatal ethanol exposure impairs sensory processing and habituation to visual stimuli, effects normalized by enrichment of postnatal environmental. *Alcohol. Clin. Exp. Res.* 46, 891–906. doi: 10.1111/acer.14818

Wang, R., Shen, Y. L., Hausknecht, K. A., Chang, L., Haj-Dahmane, S., Vezina, P., et al. (2019). Prenatal ethanol exposure increases risk of psychostimulant addiction. *Behav. Brain Res.* 356, 51–61. doi: 10.1016/j.bbr.2018.07.030

Wieczorek, L., Fish, E. W., O'Leary-Moore, S. K., Parnell, S. E., and Sulik, K. K. (2015). Hypothalamic-pituitary-adrenal axis and behavioral dysfunction following early binge-like prenatal alcohol exposure in mice. *Alcohol* 49, 207–217. doi: 10.1016/j.alcohol.2015.01.005

Zhou, F. C., Sari, Y., Zhang, J. K., Goodlett, C. R., and Li, T. (2001). Prenatal alcohol exposure retards the migration and development of serotonin neurons in fetal C57BL mice. *Brain Res. Dev. Brain Res.* 126, 147–155. doi: 10.1016/s0165-3806(00)00144-9

Zimcikova, E., Simko, J., Karesova, I., Kremlacek, J., and Malakova, J. (2017). Behavioral effects of antiepileptic drugs in rats: are the effects on mood and behavior detectable in open-field test? *Seizure* 52, 35–40. doi: 10.1016/j.seizure.2017.09.015

frontiers | Frontiers in Neuroscience

TYPE Original Research
PUBLISHED 24 April 2023
DOI 10.3389/fnins.2023.1172010

Check for updates

OPEN ACCESS

EDITED BY
Paola A. Haeger,
Catholic University of the North, Coquimbo, Chile

REVIEWED BY
Donald A. Wilson,
Grossman School of Medicine, New York University, United States
Renata B. Cupertino,
University of Vermont, United States

*CORRESPONDENCE
Jeffrey R. Wozniak
✉ jwozniak@umn.edu

SPECIALTY SECTION
This article was submitted to Neurodevelopment, a section of the journal Frontiers in Neuroscience

RECEIVED 22 February 2023
ACCEPTED 30 March 2023
PUBLISHED 24 April 2023

CITATION
Gimbel BA, Roediger DJ, Ernst AM, Anthony ME, de Water E, Rockhold MN, Mueller BA, Mattson SN, Jones KL, Riley EP, Lim KO, CIFASD and Wozniak JR (2023) Atypical developmental trajectories of white matter microstructure in prenatal alcohol exposure: Preliminary evidence from neurite orientation dispersion and density imaging. *Front. Neurosci.* 17:1172010. doi: 10.3389/fnins.2023.1172010

COPYRIGHT
© 2023 Gimbel, Roediger, Ernst, Anthony, de Water, Rockhold, Mueller, Mattson, Jones, Riley, Lim, CIFASD and Wozniak. This is an open-access article distributed under the terms of the Creative Commons Attribution License (CC BY). The use, distribution or reproduction in other forums is permitted, provided the original author(s) and the copyright owner(s) are credited and that the original publication in this journal is cited, in accordance with accepted academic practice. No use, distribution or reproduction is permitted which does not comply with these terms.

Atypical developmental trajectories of white matter microstructure in prenatal alcohol exposure: Preliminary evidence from neurite orientation dispersion and density imaging

Blake A. Gimbel[1], Donovan J. Roediger[1], Abigail M. Ernst[1], Mary E. Anthony[1], Erik de Water[2], Madeline N. Rockhold[3], Bryon A. Mueller[1], Sarah N. Mattson[4], Kenneth L. Jones[5], Edward P. Riley[4], Kelvin O. Lim[1], CIFASD and Jeffrey R. Wozniak[1]*

[1]Department of Psychiatry and Behavioral Sciences, University of Minnesota Twin Cities, Minneapolis, MN, United States, [2]Great Lakes Neurobehavioral Center, Edina, MN, United States, [3]Department of Psychology, University of Rochester, Rochester, NY, United States, [4]Department of Psychology, San Diego State University, San Diego, CA, United States, [5]Department of Pediatrics, University of California, San Diego, San Diego, CA, United States

Introduction: Fetal alcohol spectrum disorder (FASD), a life-long condition resulting from prenatal alcohol exposure (PAE), is associated with structural brain anomalies and neurobehavioral differences. Evidence from longitudinal neuroimaging suggest trajectories of white matter microstructure maturation are atypical in PAE. We aimed to further characterize longitudinal trajectories of developmental white matter microstructure change in children and adolescents with PAE compared to typically-developing Controls using diffusion-weighted Neurite Orientation Dispersion and Density Imaging (NODDI).

Materials and methods: Participants: Youth with PAE (n=34) and typically-developing Controls (n=31) ages 8–17years at enrollment. Participants underwent formal evaluation of growth and facial dysmorphology. Participants also completed two study visits (17months apart on average), both of which involved cognitive testing and an MRI scan (data collected on a Siemens Prisma 3T scanner). Age-related changes in the orientation dispersion index (ODI) and the neurite density index (NDI) were examined across five corpus callosum (CC) regions defined by tractography.

Results: While linear trajectories suggested similar overall microstructural integrity in PAE and Controls, analyses of symmetrized percent change (SPC) indicated group differences in the timing and magnitude of age-related increases in ODI (indexing the bending and fanning of axons) in the central region of the CC, with PAE participants demonstrating atypically steep increases in dispersion with age compared to Controls. Participants with PAE also demonstrated greater increases in ODI in the mid posterior CC (trend-level group difference). In addition, SPC in ODI and NDI was differentially correlated with executive function performance for PAE participants and Controls, suggesting an atypical relationship between white matter microstructure maturation and cognitive function in PAE.

Discussion: Preliminary findings suggest subtle atypicality in the timing and magnitude of age-related white matter microstructure maturation in PAE

compared to typically-developing Controls. These findings add to the existing literature on neurodevelopmental trajectories in PAE and suggest that advanced biophysical diffusion modeling (NODDI) may be sensitive to biologically-meaningful microstructural changes in the CC that are disrupted by PAE. Findings of atypical brain maturation-behavior relationships in PAE highlight the need for further study. Further longitudinal research aimed at characterizing white matter neurodevelopmental trajectories in PAE will be important.

KEYWORDS

FASD, neurodevelopment, longitudinal, corpus callosum, NODDI

1. Introduction

Prenatal alcohol exposure (PAE) impacts the developing brain widely (Jones and Smith, 1973; Mattson et al., 2010b; Riley et al., 2011), resulting in cognitive, behavioral, and adaptive functioning difficulties. The term fetal alcohol spectrum disorder (FASD) describes a group of neurodevelopmental disorders that result from PAE. Subtypes of FASD are defined based on the presence of alcohol exposure, growth deficits, cognitive impairment, and facial dysmorphology. There are numerous diagnostic systems of FASD (Astley and Clarren, 2000; Bertrand et al., 2005; Chudley et al., 2005) including the one used here which parses FASD into fetal alcohol syndrome (FAS), partial fetal alcohol syndrome (PFAS), and alcohol-related neurodevelopmental disorder (ARND) (Hoyme et al., 2016; Wozniak et al., 2019). FASDs are highly prevalent (Lange et al., 2018; May et al., 2018) and yet often unrecognized and misdiagnosed (Chasnoff et al., 2015; McLennan, 2015).

White matter diffusion abnormalities are often seen in individuals with PAE, including lower fractional anisotropy (FA), higher mean diffusivity (MD), and higher radial diffusivity (RD) across a majority of white matter pathways, and the corpus callosum (CC) has been particularly implicated in PAE (Sherbaf et al., 2019). Several studies have also reported shape abnormalities and volume reductions in the splenium, genu, and isthmus of the CC even after controlling for total brain size (Riley et al., 1995; Lebel et al., 2008; Sherbaf et al., 2019). These abnormalities in CC volume, shape, and diffusion have been associated with poorer performance on tasks of eyeblink conditioning (Fan et al., 2015), working memory (Wozniak et al., 2009), mathematics (Lebel et al., 2010), language and reading skill (Treit et al., 2013), and interhemispheric information transfer (Biffen et al., 2022), as well as other features of FASD such as the presence of the characteristic facial features (Astley et al., 2009; Fryer et al., 2009; Li et al., 2009). Results of cross-sectional investigations suggest steeper age-related increases in FA in controls compared to participants with PAE (Treit et al., 2017) and sex-specific trajectory abnormalities potentially related to neuroendocrine factors (Uban et al., 2017). Emerging data from longitudinal studies suggest atypical brain development trajectories in PAE (Moore and Xia, 2021), highlighting the need for further study. Longitudinal findings from DTI have suggested atypical rate and timing of age-related microstructural changes across several white matter tracts in PAE (Treit et al., 2013; Kar et al., 2022). To date, studies have relied primarily on traditional diffusion tensor imaging (e.g., FA and MD) to examine white matter abnormalities in PAE. These techniques provide insight into general white matter integrity without identifying more detailed underlying mechanisms of reduced microstructural integrity (e.g., differences in density or bending and fanning of axons). In addition, DTI is unable to handle complex microstructure architectures, such as crossing fibers. Using novel diffusion modeling approaches may identify potential white matter microstructural abnormalities with greater specificity (Sherbaf et al., 2019; Figley et al., 2021).

In this study, we aimed to further explore potential atypicality in age-related corpus callosum white matter diffusion trajectories in youth with PAE using Neurite Orientation Dispersion and Density Imaging (NODDI) (Zhang et al., 2012), a diffusion MRI method that models multiple biophysically-relevant "compartments" of tissue water: intra-neurite, extra-neurite, and free water. We also aimed to explore potential sex-based differences in corpus callosum white matter diffusion trajectories given previous findings of sex-based differences in white matter diffusion trajectories in both typically-developing (Wang et al., 2012; Simmonds et al., 2014; Genc et al., 2018) youth and those with a history of PAE (Uban et al., 2017).

NODDI metrics of interest included the neurite density index (NDI), which characterizes the density of axons and dendrites, and the orientation dispersion index (ODI), which characterizes the alignment (dispersion) of tissue fibers (Mah et al., 2017; Kamiya et al., 2020). Given the close correspondence between NODDI metrics and underlying white matter integrity, this novel approach is well-suited for exploring potentially atypical white matter microstructure trajectories in youth with neurodevelopmental conditions (Young et al., 2019; Kamiya et al., 2020), such as FASD. NODDI metrics have been shown to have high scan-rescan reliability comparable to traditional diffusion metrics (Huber et al., 2019; Andica et al., 2020) and are known to correlate well with histology (Parvathaneni et al., 2018; Andica et al., 2020; Lucignani et al., 2021) – in some cases more strongly than traditional DTI metrics such as FA (Schilling et al., 2018). To our knowledge, age-related changes in white matter microstructure using NODDI have not yet been studied in PAE. We hypothesized that youth with PAE would demonstrate atypical linear trajectories of age-related change in white matter microstructure, as well as atypicality in the developmental timing and magnitude of change in microstructure, compared to unexposed, typically-developing controls (Riley et al., 1995; Lebel et al., 2008; Sherbaf et al., 2019). We also hypothesized that PAE and Control participants would show differences in correlations between age-related change in NODDI metrics and cognitive performance, consistent with prior findings (Wozniak et al., 2009; Lebel et al., 2010; Fan et al., 2015).

2. Materials and methods

2.1. Participants

All participants enrolled in this study were part of the Collaborative Initiative on Fetal Alcohol Spectrum Disorders (CIFASD) study[1] (Mattson et al., 2010a). Participants included children with PAE ($n = 46$) and non-exposed Controls ($n = 49$). Participants were enrolled between 2017 and 2019, with the last follow-up visit occurring in 2021. Staff recruited participants with PAE from the University of Minnesota Fetal Alcohol Spectrum Disorder Clinic and other local clinics *via* brochures, letters, and self-referral. Control participants were recruited from study brochures, letters, advertisements, local community events, and mailings to Control participants from previous studies. All participants were screened by telephone. Trained staff administered IRB-approved consent and assent procedures to the participants and their guardian or parent at enrollment. Participants were compensated for study participation.

Research staff conducted phone screens and reviewed records (i.e., retrospective maternal report, social service, legal, and/or medical records) to determine PAE history of participants. Inclusion criteria for the PAE group included evidence of heavy PAE, defined as 13 or more drinks per week or 4 or more drinks per occasion at least once per week during pregnancy. Some individuals who had "suspected" but unconfirmed exposure were included if they met diagnostic criteria for pFAS or FAS based on dysmorphology and growth characteristics. Individuals who had minimal to no PAE based on available records and did not meet diagnostic criteria were excluded from the PAE group.

An expert dysmorphologist (KLJ) who had not previously met participants and who was blinded to the child's status (PAE or Control) completed a standardized physical evaluation. Twelve participants were not able to be evaluated by KLJ due to COVID-19 pandemic restrictions. These participants were instead evaluated by the principal investigator (JRW), who has been trained by KLJ over several years and was also blinded to the child's status. Afterward, photographs and physical measurements of each of these 12 cases were reviewed together by JRW and KLJ to reach a final consensus. For all participants, the physical assessment included the following components: ratings of the vermillion border of the upper lip and the philtrum; measurement of the palpebral fissure length (PFL), occipital-frontal circumference (OFC), height, and weight. Normative data from the University of Washington's 4-Digit Diagnostic System was used for the vermillion and philtrum (Astley, 2004), Stromland data for PFL (Stromland et al., 1999), Nellhaus data for head circumference percentiles (Nellhaus, 1968), and the Centers for Disease Control and Prevention (CDC) growth chart data for height and weight (Kuczmarski et al., 2000). The Modified Institute of Medicine criteria were used for FASD diagnostic classification (Hoyme et al., 2016). Standardized neuropsychological assessments and parent-rated measures were administered to characterize neurobehavioral functioning, including global intellectual ability, behavioral and self-regulation abilities, other cognitive functions (memory, executive functioning, and visual spatial processing), and adaptive functioning. Consistent with Hoyme criteria (Hoyme et al., 2016), participants were considered "impaired" in a neurobehavioral domain if the standardized score was less than or equal to 1.5 standard deviations (SD) below the normative mean. Participants in the PAE group had either an intellectual impairment (IQ 1.5 standard deviations or more below the normative mean) or impairment in two or more domains of functioning (scores more than 1.5 standard deviations below the normative mean). The requirement of two impaired domains is slightly more conservative than the Hoyme criteria, which requires impairment in only one domain.

For both groups, exclusion criteria included the following: presence of a neurological or developmental disorder (e.g., epilepsy or autism spectrum disorder), severe psychiatric disabilities that would prevent participation (e.g., psychosis or mania), drug or alcohol use by the participant, very low birthweight (<1,500 grams), and contraindications to MRI scanning (e.g., non-MR-safe medical devices, braces, or claustrophobia). Prenatal exposure to substances other than alcohol (e.g., methamphetamine, marijuana, cocaine, tobacco, etc.) was not exclusionary for the PAE group because it is the most common presenting pattern. Prenatal alcohol and drug exposure (excluding tobacco and caffeine) was an exclusion criterion for the Control group.

A total of 95 participants were enrolled between the ages of 8 and 17 years at their first visit. Over the course of the longitudinal study, 25 participants failed to contribute either a baseline scan or a second scan. Loss to follow-up (which was exacerbated by the COVID-19 pandemic) was due to: inability to contact (7 PAE, 6 Control), MRI contraindications (e.g., braces; 4 PAE, 4 Control), concern about time commitment (2 Control) and no reason provided (1 PAE, 1 Control). Four participants were excluded from subsequent analysis due to image quality concerns: one due to susceptibility artifact from a dental appliance (control), one due to operator error during image acquisition (control), and two due to excessive head motion and/or aberrant FreeSurfer processing (PAE). 65 participants (PAE = 34; Control = 31) who contributed at least one scan were included in the primary analyses. Table 1 contains demographic information for the participants.

Subset analyses examining symmetrized percent change (SPC) were conducted with participants for whom full MRI datasets including diffusion data from both time points were available. A total of 59 participants who completed follow-up diffusion MRI scanning (PAE = 30; Control = 29) were included in the subset analyses of SPC in NODDI diffusion metrics.

2.2. Evaluations

Participants were asked to complete two visits (with a target inter-scan interval of 15 months; actual interval: mean = 17.76; SD = 3.09) at the University of Minnesota. At the first visit, trained staff administered the full Wechsler Intelligence Scale for Children, 5th Edition [WISC-V; (Wechsler, 2014)]; the Trail Making, Verbal Fluency, and Color-Word Interference subtests from the Delis-Kaplan Executive Functioning System [D-KEFS; (Delis et al., 2001)]; and the Dimensional Change Card Sort and Flanker tests from NIH toolbox (Weintraub et al., 2013). At the follow-up visit, participants completed only the Digit Span, Coding, and Symbol Search subtests of the

1 www.cifasd.org

TABLE 1 Demographic characteristics of participants included in primary analyses.

	PAE (n=34)	Control (n=31)	Statistical Test
Age [M (SD)]*	12.32 (2.41)	12.45 (2.69)	$t(60) = 0.20$, $p = 0.841$
Intelligence Quotient [M (SD)]†	94.79 (15.93)	117.27 (13.90)	$t(61) = 6.03$, $p < 0.001$
Months between scans [M (SD)]‡	18.55 (3.20)	16.89 (2.38)	$t(60) = -2.39$, $p = 0.020$
Sex [n (%Female)]	17 (50%)	15 (48%)	$\chi^2 = 0.02$, $p = 0.897$
Ethnicity [n (%Hispanic)]	0	2 (6%)	$\chi^2 = 2.26$, $p = 0.133$
Race§			
[n (%American Indian/Alaska Native)]	3 (8%)	0	$\chi^2 = 5.33$, $p = 0.021$
[n (%Asian)]	1 (3%)	0	$\chi^2 = 1.92$, $p = 0.166$
[n (%Black or African American)]	11 (32%)	0	$\chi^2 = 15.80$, $p < 0.001$
[n (%White)]	15 (44%)	30 (97%)	$\chi^2 = 21.12$, $p < 0.001$
[n (%Multiracial)]	4 (12%)	1 (3%)	$\chi^2 = 4.16$, $p = 0.041$
Handedness [n (%Right)]‖	26 (76%)	26 (84%)	$\chi^2 = 1.14$, $p = 0.565$
Physical characteristics			
[a]Growth Deficiency	3 (9%)	2 (6%)	$\chi^2 = 0.13$, $p = 0.720$
[b]Microcephaly	3 (9%)	0	$\chi^2 = 2.67$, $p = 0.101$
[c]Dysmorphic Face	7 (21%)	2 (6%)	$\chi^2 = 2.40$, $p = 0.122$

Demographics are from the 65 participants included in the primary analyses. Age range at baseline evaluation ranged from 8 to 17 years. PAE, Prenatal Alcohol Exposure group. *Age at baseline evaluation. †Intelligence Quotient as measured during the baseline evaluation. ‡For the calculation of group means for duration between scans in months, the mean value was substituted for cases with missing data (i.e., cases for whom only one diffusion scan was available). §Chi square tests reflect comparisons of each racial group to the proportion of participants who identified as White (e.g., proportion of participants who identified as Multiracial to proportion of those who identified as White). ‖Handedness information was not available for 5 participants (4 PAE, 1 Control). [a]Height or weight ≤ 10%ile. [b]Head circumference ≤ 10%ile. [c]At least two of the following: Palpebral Fissure Length ≤ 10%ile, thin vermillion border, smooth philtrum (4 or 5 on lipometer scale). The two Control participants who had "dysmorphic faces" had scores of 4 on the philtrum and 4 on the vermillion border; neither had any other facial features nor abnormal growth parameters.

TABLE 2 MRI acquisition parameters.

Sequence	Imaging parameters
T1-weighted	Multi-echo MP-RAGE sequence with TR = 2,500 ms, TE = 1.8/3.6/5.4/7.2 ms, TI = 1,000 ms, voxel size = 0.8 mm isotropic, flip angle = 8 degrees
T2-weighted	SPACE sequence with TR = 3,200 ms, TE = 564 ms, voxel size = 0.8 mm isotropic, variable flip angle
Diffusion-weighted	Multi-band EPI sequence with TR = 3,230 ms, TE = 89.2 ms, voxel size = 1.5 mm isotropic, MB = 4. Four consecutive runs of about 5:31 each were acquired as 2 pairs with opposite phase encoding (A to P, P to A). Each scan had 2 shells (b = 1,500 and 3,000 s/mm^2) and 46 directions each and 7 volumes with b = 0 s/mm^2.

TR, repetition time; TE, echo time; MB, multiband; ms, milliseconds.

WISC-V or the Wechsler Adult Intelligence Scale 4th Edition (WAIS-IV) (Wechsler, 2008) if they were 17 years old, the Trail Making and Verbal Fluency subtests from the D-KEFS, and the NIH toolbox tasks. These cognitive assessments measure working memory, visual-motor processing speed and visual attention, number and letter sequencing, inhibitory control, and cognitive flexibility.

2.3. MRI acquisition and processing

Participants completed MRI scans at the University of Minnesota's Center for Magnetic Resonance Research on a Siemens 3 T Prisma scanner (Siemens, Erlangen, Germany) equipped with a standard 32-channel head coil. The MRI acquisition matched the structural portion of the Lifespan Human Connectome Project Development (HCP-D) project (Harms et al., 2018). The T1-weighted and T2-weighted scans were acquired at each visit (baseline and follow-up) using custom pulse sequences that included automatic real-time motion detection and k-space line rejection and replacement software (Tisdall et al., 2012). The diffusion weighted scans were acquired using multiband pulse sequence, gradient tables and acquisition strategy used by HCP-D. Key scan parameters used in the MRI scans are shown in Table 2.

The HCP Minimal Preprocessing Pipelines (v4.0.1) were used to preprocess the imaging data (Glasser et al., 2013). For structural images, this processing included alignment between the T1-weighted and T2-weighted volumes, bias field and gradient distortion corrections, and registration of the data to MNI space followed by volume segmentation and surface parcellation using FreeSurfer (v6.0.0). Subsequently, we utilized FreeSurfer's longitudinal processing stream wherein an unbiased within-subject template space and image are created (Reuter et al., 2010; Reuter and Fischl, 2011) and several steps of the FreeSurfer processing are reinitialized with common information from the within-subject template. This approach results in improved reliability over standard cross-sectional processing (Reuter et al., 2012). For diffusion-weighted images, HCP

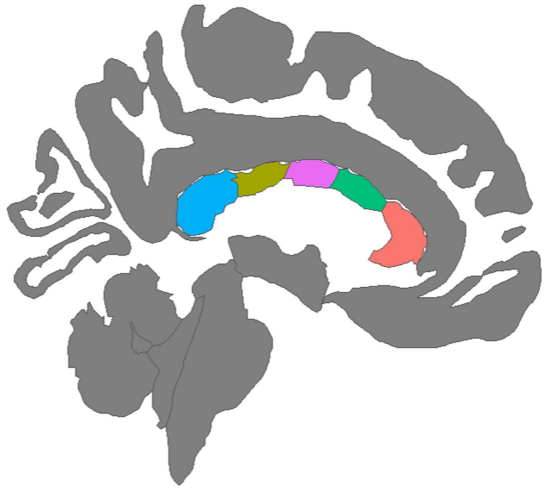


FIGURE 1
Mid-sagittal view of five corpus callosum tracts generated by tractography: (left to right) Blue=Posterior, Olive=Mid Posterior, Purple=Central, Green=Mid Anterior, Orange=Anterior.

preprocessing included rigid AC-PC alignment to the structural images, correction for susceptibility related distortions using FSL's "topup" (Andersson et al., 2003; Smith et al., 2004), and eddy current and movement-induced distortion correction using FSL's "eddy" tool (v6.0.1) (Andersson and Sotiropoulos, 2016). For improved performance, eddy was run with the optional slice outlier replacement, slice-to-volume motion correction and susceptibility-by motion correction routines (Andersson et al., 2016, 2017, 2018).

To assess white matter microstructure, the Neurite Orientation Dispersion and Density Imaging model (NODDI) (Zhang et al., 2012) was applied to the diffusion signal. Voxel-wise NODDI metrics were estimated using the Accelerated Microstructure Imaging *via* Convex Optimization (AMICO) toolkit (Daducci et al., 2015). Mean NODDI parameters were calculated within each of the five corpus callosum segments identified by the FreeSurfer longitudinal stream by registering the white matter segmentations to the AC-PC aligned diffusion images then extracting regional averages for each scalar metric using FreeSurfer's mri_segstats function. A graphical depiction of the five CC regions was created with the ggseg package in the R library (Figure 1; Mowinckel and Vidal-Piñeiro, 2020). An experienced rater (DJR) visually inspected all structural images and NODDI scalar maps, checked for aberrant FreeSurfer processing using ENIGMA quality control protocols (Thompson et al., 2020), and ensured that movement-induced artifacts in diffusion images were adequately resolved during preprocessing.

Longitudinal changes in both the orientation dispersion index (ODI) and the neurite density index (NDI) were evaluated. NDI models the intracellular fraction of the tissue, reflecting the density of white matter axonal fibers and possibly dendritic projections (Zhang et al., 2012). Well-established relationships between dendritic arbor complexity and cognitive function suggest that neurite density is functionally relevant (Kaufmann and Moser, 2000). Higher NDI values in white matter are thought to reflect axonal growth, greater axonal density, and/or myelination (Mah et al., 2017). In contrast, ODI models the extracellular fraction of tissue (between axons) and, thus, reflects the degree of bending and fanning of axons in white matter as represented by the angular variation of diffusion orientation (Zhang et al., 2012).

2.4. Statistical analyses

Using the "stats" package in RStudio version 4.1.1 (R Core Team, 2021), chi-square and independent samples *t*-tests were used to test group differences in demographic characteristics. Longitudinal changes in NODDI diffusion metrics (i.e., ODI and NDI) for each of the five corpus callosum regions were evaluated with two separate approaches. First, linear mixed effects models were evaluated using the "lme4" (Bates et al., 2015) and "lmerTest" (Kuznetsova et al., 2017) packages in RStudio. As linear mixed effects models are robust to missing data, we used this approach so that participants with missing diffusion data at one time point could be included (thus boosting statistical power). Linear (y = age + sex + age × diagnostic group + sex × diagnostic group [1 | subject]) terms were modeled. Age, sex, diagnostic group, and interactions were modeled as fixed factors with random subject-specific intercepts. Restricted maximum likelihood (REML) estimation was set to true. Interaction terms that were not significant or at the trend-level were removed and the model was run without them. False discovery rate (FDR) was used to correct for 10 multiple comparisons for analyses of NDI and ODI (5 CC regions and 2 diffusion metrics). FDR was also used to correct for 10 multiple comparisons for analyses of NDI and ODI using general linear models as described below (5 CC regions and 2 diffusion metrics). FDR correction was performed for the entire family of analyses together (i.e., linear mixed effects models and general linear models). Significance for these analyses was set at $q < 0.05$. *Post hoc* analyses (i.e., to further examine main effects for group and sex) were performed using analyses of covariance (with inter-scan interval as a covariate) and Tukey's Test for multiple comparisons with the "stats" package. Importantly, although white matter microstructure maturation is known to be non-linear across larger developmental timescales (Lebel et al., 2019), given the relatively narrow duration between scans (17 months on average) in this study, the modest sample size (PAE = 34; Control = 31), and the novel, exploratory nature of our investigation of NODDI with this population, linear models of microstructure diffusion trajectories were believed to be appropriate.

In alternate analyses of a subset of participants with two scans, we examined symmetrized percent change (SPC), a dimensionless measure of change (Berry and Ayers, 2006; Reuter et al., 2012) across two time points for the 59 participants for whom both baseline and follow-up diffusion MRI scans were available (PAE = 30; Control = 29). SPC was calculated as:

$$SPC = \frac{(Scan2 - Scan1)}{(Scan2 + Scan1)} \times 100$$

where Scan1 represents diffusion values at baseline scan, and Scan2 represents diffusion values at follow-up scan. This approach was used in order to further characterize potential group differences in the rate and timing of age-related changes in white matter microstructure. For these analyses, we used the "stats" package in RStudio version 4.1.1 (R Core Team, 2021). SPC values across five regions of the corpus callosum were computed for each participant from the two time points. General linear models were performed with SPC in ODI/NDI as the dependent variable and age, sex, diagnostic group (PAE vs. Control), age-by-group, and sex-by-group interactions as predictors. Interaction terms that were not significant or at the trend-level were

removed and the model was run without them. Mean age (i.e., the midpoint between the two scans) was used in general linear models to be consistent with the fact that SPC represents two time points. Although mean age was investigated as both a linear and quadratic (i.e., age ^2) variable in SPC analyses, no meaningful difference between variables with linear versus quadratic age was observed. Therefore, the more parsimonious models using linear age were used.

Exploratory analyses were performed with Pearson correlations to investigate the relationship between SPC in corpus callosum diffusion metrics across all five regions and executive function test performance at follow-up testing. Separate analyses were completed independently for each diagnostic group (PAE vs. Control). False discovery rate (FDR) was used to correct for 150 multiple comparisons for PAE participants (15 executive function tasks and SPC in two diffusion metrics [NDI and ODI] across five CC regions), and 150 multiple comparisons for Control participants (15 executive function tasks and SPC in two diffusion metrics [NDI and ODI] across five CC regions). Significance for these analyses was set at $q < 0.05$. Correlations between all executive function measures and SPC across the five regions of the CC were visualized with the "corrplot" package (Wei and Simko, 2017).

Lastly, exploratory analyses were performed with independent sample t-tests to examine the relationship of symmetrized percent change in corpus callosum microstructure to facial dysmorphology across the entire sample. Specifically, facial features (i.e., palpebral fissure length, upper lip vermillion border, and philtrum) rated at the baseline evaluation were categorized into dichotomous variables (i.e., dysmorphic vs. non-dysmorphic). Comparisons were examined between participants with and without dysmorphic faces (i.e., two of the following: palpebral fissure length ≤ 10%ile; scores of 4 or 5 on ratings of the upper lip vermillion border and philtrum), as well as comparisons between participants with and without dysmorphology in each facial feature (i.e., palpebral fissure length, upper lip, philtrum). Given the exploratory nature of these analyses, results were not corrected for multiple comparisons.

3. Results

3.1. Participant characteristics

As shown in Table 1, the PAE and Control groups did not differ significantly with respect to demographic variables including age, sex, ethnicity, and handedness, although there were differences in race with more individuals identifying as non-white in the PAE group. As expected, the PAE group had lower mean IQ scores ($M = 94.79$; average range) compared to the Control group ($M = 117.27$; high average range–a mean score difference of approximately 22 points). Estimates of head motion during diffusion scans (FSL Eddy-derived metric) were not significantly different between diagnostic groups at baseline ($t[61] = 0.96$, $p = 0.339$) or follow-up scan ($t[45] = -0.82$, $p = 0.418$). Despite efforts to complete follow-up MRIs within 15-months of the baseline scan for all participants, the PAE group demonstrated a slightly longer mean inter-scan interval than Controls (approximately two months longer on average). There were no outliers in terms of inter-scan interval. Inter-scan interval (months) was not significantly correlated with symmetrized percent change in NDI in any CC region and was only correlated significantly with ODI in one of five CC regions (mid posterior) (r [57] = 0.28, $p = 0.029$). Duration between scans was not significantly correlated with executive function performance at follow-up testing. Therefore, we did not consider the inter-scan interval to be a confounding variable. However, for significant or trend-level findings in SPC in ODI in the mid posterior region of the CC, we conservatively performed additional analyses with the inclusion of inter-scan interval as a covariate. We also conservatively included the inter-scan interval as a covariate in *post hoc* analyses to further characterize the group and sex differences in absolute NDI and ODI values at baseline and follow-up scan.

TABLE 3 Linear mixed effects model results for NDI.

Neurite Density Index (NDI)	PE (SE)	*t*	*p*
Anterior CC			
Intercept	0.67 (0.02)	28.49	<0.001
Age	0.00 (0.00)	2.66	**0.009***
Sex	0.01 (0.01)	1.12	0.265
Group	−0.00 (0.01)	−0.88	0.383
Mid Anterior CC			
Intercept	0.59 (0.02)	24.49	<0.001
Age	0.01 (0.00)	3.31	**0.001***
Sex	−0.00 (0.01)	−0.16	0.871
Group	−0.00 (0.01)	−0.13	0.899
Central CC			
Intercept	0.56 (0.02)	25.45	<0.001
Age	0.01 (0.00)	4.48	**<0.001***
Sex	0.00 (0.01)	0.49	0.629
Group	0.01 (0.01)	1.40	0.165
Sex-by-group	−0.01 (0.01)	−1.79	0.078
Mid Posterior CC			
Intercept	0.59 (0.02)	31.27	<0.001
Age	0.01 (0.00)	3.95	**<0.001***
Sex	0.00 (0.00)	0.12	0.907
Group	0.00 (0.00)	0.98	0.330
Posterior CC			
Intercept	0.70 (0.02)	35.44	<0.001
Age	0.01 (0.00)	3.49	**<0.001***
Sex	0.00 (0.00)	0.42	0.677
Group	−0.00 (0.01)	−0.03	0.979

Results are displayed for linear mixed effects models examining group differences (PAE vs. Control) in age-related linear trajectories of corpus callosum white matter microstructure. Significant main effects for age and sex that survived FDR correction are indicated with bold text and with *. Interactions that were not significant or trend-level were removed from the model. Abbreviations: PE, parameter estimate; SE, standard error; CC, corpus callosum.

3.2. Neurite density index

A main effect for age was observed for NDI across all five CC regions, where NDI increased linearly with age across diagnostic groups (Table 3). There were no significant main effects for group

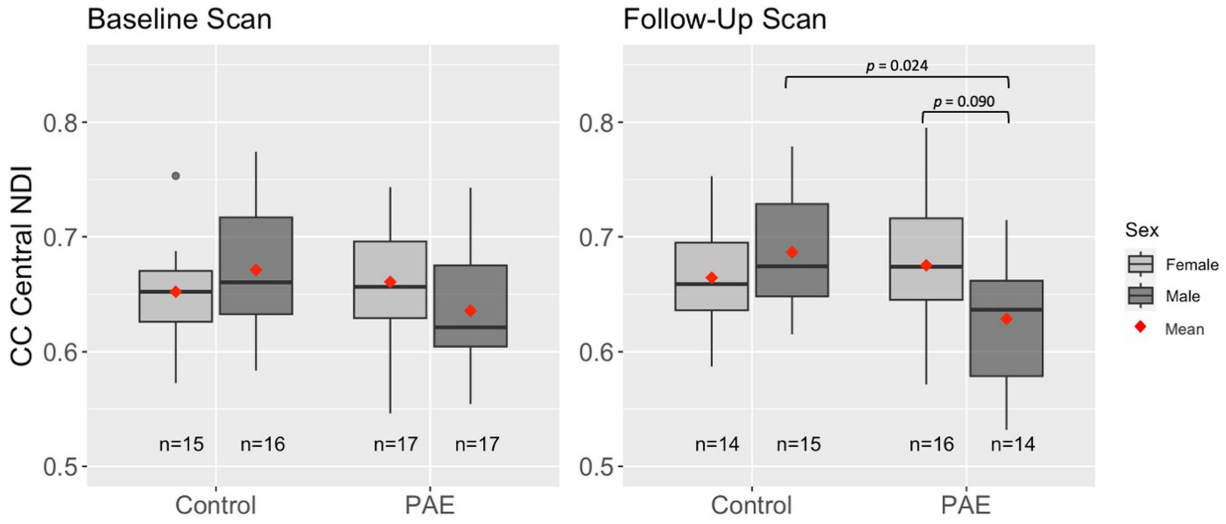


FIGURE 2
Differences in mean NDI in the central CC at baseline and follow-up scan by group and sex. Results are displayed for linear mixed effects models examining group differences (PAE vs. Control) in age-related trajectories of corpus callosum white matter microstructure. Interactions that were not significant or trend-level were removed from the model.

(PAE vs. Control) or sex (male vs. female). However, there was a trend-level sex-by-group interaction ($p = 0.078$) for NDI in the central CC. *Post hoc* analyses revealed that male participants in the PAE group ($M = 0.64$) demonstrated marginally lower mean NDI in the central CC at baseline scan compared to female PAE participants ($M = 0.66$) and both male ($M = 0.67$) and female ($M = 0.65$) Control participants. At follow-up scan, male PAE participants ($M = 0.63$) had lower mean NDI in the central CC compared to female PAE participants ($M = 0.68$), measured at the trend level ($p = 0.090$), and significantly lower mean NDI compared to male Controls ($M = 0.69$; $p = 0.024$) (Figure 2). No significant age-by-group interactions were observed for NDI across CC regions.

3.3. Orientation dispersion index

A main effect for age was observed for ODI across the central, mid posterior, and posterior CC regions, where ODI increased linearly with age across diagnostic groups (Table 4). Similarly, a trend-level main effect for age was observed in the anterior CC. There was not a significant effect for group (PAE vs. Control) across any CC regions. However, there was a main effect for sex ($p = 0.001$; $q = 0.004$) in the central CC and the mid posterior CC ($p = 0.044$; $q = 0.117$). *Post hoc* analyses revealed that, collapsing across PAE and Control groups, male participants demonstrated significantly higher mean ODI in the central CC at baseline scan ($M = 0.049$) compared to female participants ($M = 0.047$), $F(1, 62) = 7.49$, $p = 0.008$. Similarly, at the follow-up scan, male participants ($M = 0.050$) had significantly higher mean central CC ODI compared to female participants ($M = 0.047$), $F(1, 56) = 9.18$, $p = 0.004$. Of note, group mean differences are here reported at the third decimal place for clarity. No significant age-by-group or sex-by-group interactions were observed for ODI across CC regions.

3.4. Symmetrized percent change in NDI

No significant main effect for age, group (PAE vs. Control), or interaction effects (mean age-by-group and sex-by-group) were found for SPC in NDI across the 5 regions of the corpus callosum (Table 5). However, a significant main effect for sex ($p = 0.014$; $q = 0.042$) was observed in the anterior CC, such that females demonstrated greater percent increases in NDI compared to males when collapsing across diagnostic groups (PAE vs. Control).

3.5. Symmetrized percent change in ODI

No significant main effects for age or group were observed for SPC across the five CC regions (Table 6). A significant main effect of sex was observed for SPC in the anterior CC, such that females demonstrated greater percent increases in ODI compared to males when collapsing across diagnostic groups (PAE vs. Control). For four out of five regions of the CC, no interaction effects (mean age-by-group and sex-by-group) were found for SPC in ODI. However, for the fifth region (central CC), a significant mean age-by-group interaction effect was observed (Figure 3), such that PAE participants demonstrated minimal changes in ODI at younger ages, and increases in ODI at older ages compared to Controls, who showed minimal changes in ODI with age ($p = 0.023$; $q = 0.064$). In addition, a trend-level sex-by-group interaction was observed for ODI in the central CC ($p = 0.062$). That is, female participants in the Control group demonstrated reductions in central CC ODI, while male Control participants and both female and male PAE participants demonstrated increases in ODI. Lastly, a main effect for group was observed for SPC in ODI in the mid posterior CC, with PAE participants demonstrating significantly greater percent increases in ODI than Controls ($p = 0.021$; $q = 0.061$) (Figure 3). This uncorrected finding was reduced to the

TABLE 4 Linear mixed effects model results for ODI.

Orientation Dispersion Index (ODI)	PE (SE)	*t*	*p*
Anterior CC			
Intercept	0.04 (0.00)	27.94	<0.001
Age	0.00 (0.00)	1.79	0.077
Sex	−0.00 (0.00)	−0.60	0.553
Group	−0.00 (0.00)	−0.07	0.941
Mid Anterior CC			
Intercept	0.05 (0.00)	23.67	<0.001
Age	0.00 (0.00)	1.44	0.151
Sex	−0.00 (0.00)	−1.11	0.269
Group	−0.00 (0.00)	−0.40	0.694
Central CC			
Intercept	0.04 (0.00)	26.70	<0.001
Age	0.00 (0.00)	2.74	**0.007***
Sex	−0.00 (0.00)	−3.32	**0.001***
Group	−0.00 (0.00)	−0.31	0.755
Mid Posterior CC			
Intercept	0.04 (0.00)	37.53	<0.001
Age	0.00 (0.00)	3.00	**0.003***
Sex	−0.00 (0.00)	−2.06	*0.044*
Group	0.00 (0.00)	0.96	0.343
Posterior CC			
Intercept	0.04 (0.00)	28.32	<0.001
Age	0.00 (0.00)	3.44	**<0.001***
Sex	0.00 (0.00)	0.98	0.333
Group	−0.0 (0.00)	−0.01	0.992

Results are displayed for linear mixed effects models examining group differences (PAE vs. Control) in age-related linear trajectories of corpus callosum white matter microstructure. Significant main effects for age and sex that survived FDR correction are indicated with bold text and with *. Significant main effects that did not survive FDR correction are marked in italics. Interactions that were not significant or trend-level were removed from the model. PE, parameter estimate; SE, standard error; CC, corpus callosum.

TABLE 5 General linear model results for SPC in NDI.

Neurite Density Index (NDI)	PE (SE)	*t*	*p*
Anterior CC			
Intercept	2.01 (1.74)	1.16	0.252
Age	−0.04 (0.12)	−0.34	0.733
Sex	−1.62 (0.64)	−2.55	**0.014***
Group	−0.29 (0.64)	−0.46	0.646
Mid Anterior CC			
Intercept	0.37 (1.59)	0.23	0.816
Age	0.04 (0.11)	0.38	0.704
Sex	−0.67 (0.58)	−1.15	0.257
Group	0.29 (0.58)	0.50	0.618
Central CC			
Intercept	1.79 (1.61)	1.11	0.270
Age	−0.04 (0.11)	−0.32	0.748
Sex	−0.59 (0.59)	−1.00	0.321
Group	−0.46 (0.59)	−0.78	0.442
Mid Posterior CC			
Intercept	2.81 (1.78)	1.58	0.121
Age	−0.17 (0.13)	−1.32	0.193
Sex	0.00 (0.66)	0.00	0.999
Group	−0.47 (0.66)	−0.72	0.473
Posterior CC			
Intercept	−0.25 (1.22)	−0.20	0.841
Age	0.04 (0.09)	0.49	0.624
Sex	−0.19 (0.45)	−0.44	0.666
Group	0.27 (0.45)	0.61	0.545

Results are displayed for general linear models examining group differences (PAE vs. Control) in symmetrized percent change of corpus callosum white matter microstructure. Significant main effects for sex that survived FDR correction are indicated with bold text and with *. Interactions that were not significant or trend-level were removed from the model. PE, parameter estimate; SE, standard error; CC, corpus callosum.

trend-level ($p = 0.072$) with the inclusion of inter-scan interval as a covariate.

3.6. Exploratory correlations between change in white matter microstructure and executive function performance

Exploratory analyses performed separately for each group (PAE and Control) revealed divergent patterns of associations between change in corpus callosum microstructure and executive function performance at follow-up evaluation. Correlation matrices generated separately for each group (PAE and Control) suggested Controls demonstrated a greater number of negative correlations between percent change in NDI and executive function performance compared to PAE participants, indicating that greater negative percent change in NDI (i.e., reductions in the density of white matter fibers) was associated with better performance (Figure 4). In contrast, PAE participants demonstrated a number of significant positive correlations between percent change in NDI and executive function performance. Similarly, results suggest a greater number of negative correlations between percent change in ODI and executive function performance for Controls compared to PAE participants. That is, greater negative percent change in ODI (i.e., reductions in the bending and fanning of axons) was associated with better task performance (Figure 5). No significant correlations survived FDR correction for multiple comparisons.

3.7. Exploratory analyses examining the relationship between white matter microstructure and facial dysmorphology

Results of independent samples *t*-tests indicated that, collapsing across diagnostic groups, there were no differences between

TABLE 6 General linear model results for SPC in ODI.

Orientation Dispersion Index (ODI)	PE (SE)	*t*	*p*
Anterior CC			
Intercept	−1.81 (1.41)	−0.84	0.408
Age	0.15 (0.10)	1.48	0.144
Sex	−1.51 (0.52)	−2.90	**0.005***
Group	0.24 (0.52)	0.46	0.647
Mid Anterior CC			
Intercept	−1.48 (2.03)	−0.73	0.470
Age	0.17 (0.14)	1.17	0.249
Sex	−1.00 (0.75)	−1.33	0.188
Group	0.23 (0.75)	0.31	0.759
Central CC			
Intercept	0.67 (2.06)	0.32	0.747
Age	−0.08 (0.15)	−0.53	0.601
Sex	1.50 (0.83)	1.81	0.076
Group	−5.05 (3.09)	−1.64	0.108
Age-by-Group	0.53 (0.23)	2.34	*0.023*
Sex-by-Group	−2.21 (1.16)	−1.90	0.062
Mid Posterior CC			
Intercept	−1.01 (1.26)	−0.80	0.427
Age	0.07 (0.09)	0.79	0.431
Sex	0.43 (0.46)	0.93	0.357
Group	1.10 (0.46)	2.38	*0.021*
Posterior CC			
Intercept	−0.00 (1.31)	−0.00	0.997
Age	0.04 (0.09)	0.46	0.649
Sex	−0.04 (0.48)	−0.09	0.929
Group	0.59 (0.48)	1.23	0.225

Results are displayed for general linear models examining group differences (PAE vs. Control) in symmetrized percent change of corpus callosum white matter microstructure. Significant main effects for sex that survived FDR correction are indicated with bold text and with *. Significant main effects for group that did not survive multiple comparison correction are indicated with italics. Interactions that were not significant or trend-level were removed from the model. PE, parameter estimate; SE, standard error; CC, corpus callosum.

dysmorphology groups (i.e., two of the following: palpebral fissure length ≤ 10%ile, thin upper lip vermillion border, smooth philtrum) in SPC in ODI and NDI across the five regions of the CC. However, participants with abnormal philtrum measurements (i.e., a score of 4 or 5) had greater SPC increases in ODI in the posterior CC than those with a normal philtrum, measured at the trend level, $t(14) = -1.80$, $p = 0.094$. Participants with abnormal upper lip measurements (i.e., a score of 4 or 5) had significantly greater SPC increases in ODI in the posterior CC than those with a normal upper lip, $t(15) = -3.29$, $p = 0.005$.

4. Discussion

The data described here show significant age effects for NDI and ODI, demonstrating that these NODDI metrics are sensitive to typical developmental changes in the central white matter during childhood and adolescence. Age was positively associated with diffusion metrics that reflect increased axonal density (NDI) and axonal organization (ODI). These data are consistent with findings of relatively steep increases in NDI with age from early childhood to adulthood and more modest (but significant) age-related increases in ODI when examining callosal white matter as well as association fibers and projection fibers (Chang et al., 2015). The authors of this study interpreted their findings in the context of prior diffusion tensor imaging studies suggesting that increases in axonal diameter and myelination may be the prominent underlying developmental processes responsible for these observed patterns. A similar study found an exponential increase in NDI during infancy and childhood but a plateauing in NDI during adolescence (Lynch et al., 2020), and relatively less change in ODI over the same developmental time frame. Consistent with these findings, Mah et al. (2017) demonstrated increases in NDI with age across the brain in typically developing children and adolescents (ages 8–13 years). However, they found no age-related increases in ODI, which they interpreted as suggesting that age-related changes in white matter microstructure are primarily driven by changes in axon density and myelination, rather than increasing axon coherence/organization. Lastly, in a large study of white matter change across the lifespan, Slater et al. (2019) also documented rapid changes in NODDI metrics during childhood and adolescence. Together, the literature and our findings demonstrate that NODDI is sensitive to typical maturational change in white matter microstructure in children and adolescents and may, therefore, be sensitive to altered developmental trajectories like those seen following PAE in other brain metrics such as cortical thickness, gyrification, and gray and white matter volumes (Moore and Xia, 2021).

Thus far, although NODDI has proven to be sensitive to frank neuropathological processes especially in white matter, such as demyelination in multiple sclerosis (Collorone et al., 2020), Wallerian degeneration in stroke (Mastropietro et al., 2019), and corticospinal lesions underlying cerebral palsy (Nemanich et al., 2019), it has not yet been applied widely to neurodevelopmental disorders (Kamiya et al., 2020). Some of the few NODDI studies to examine neurodevelopment show that preterm infants have lower cortical NDI compared to term infants (Batalle et al., 2017; Dimitrova et al., 2021) and higher ODI in white matter (suggesting organizational anomalies) compared to term infants (Blesa et al., 2020). In children born prematurely, lower NDI appears to be associated with lower IQ (Kelly et al., 2016). White matter alterations in neurofibromatosis type 1 have been also detected using NODDI (Billiet et al., 2014), and the diffusion abnormalities have been attributed to intra-myelin edema. Similarly, neonates with congenital heart disease demonstrate higher ODI in the corpus callosum and lower NDI in the corpus callosum, uncinate fasciculus, and superior fronto-occipital fasciculus compared to typically developing controls (Karmacharya et al., 2018). Another study demonstrated associations between maternal depression/anxiety and NODDI metrics in infants during the first month of life (Dean et al., 2018). Together, these studies suggest that, in addition to characterizing frank neuropathology, NODDI metrics are also sensitive to more subtle types of white matter disturbances in a range of neurodevelopmental conditions.

In the current study, we did not find overall differences in white matter microstructural integrity of the corpus callosum for participants with PAE compared to controls, but we did observe

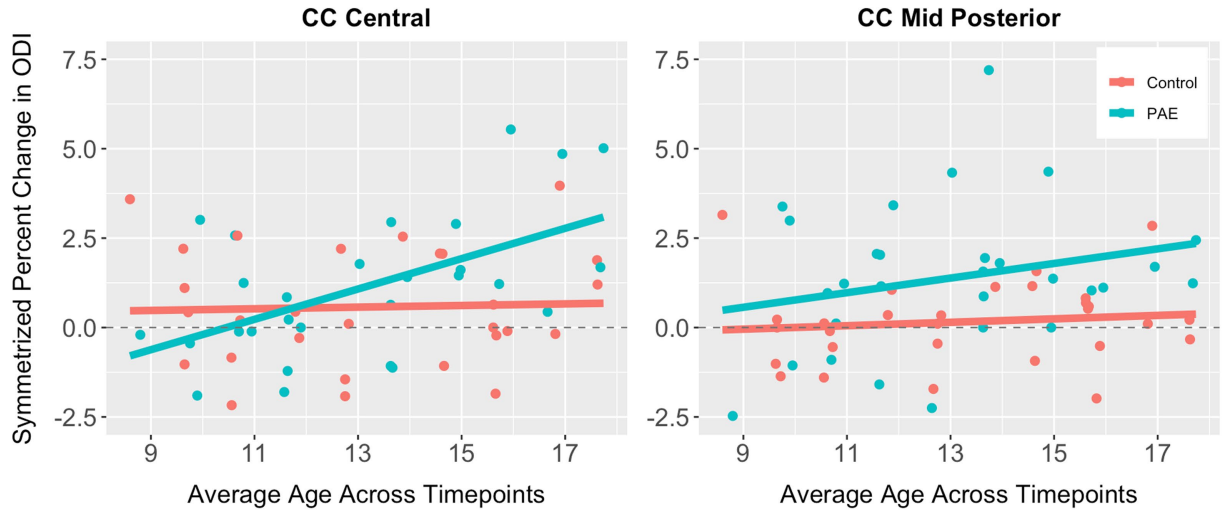


FIGURE 3
Scatterplots illustrating group differences in symmetrized percent change in ODI in the central and mid posterior corpus callosum. Results are displayed for general linear models examining group differences (PAE vs. Control) in developmental timing and degree of change in corpus callosum white matter microstructure.

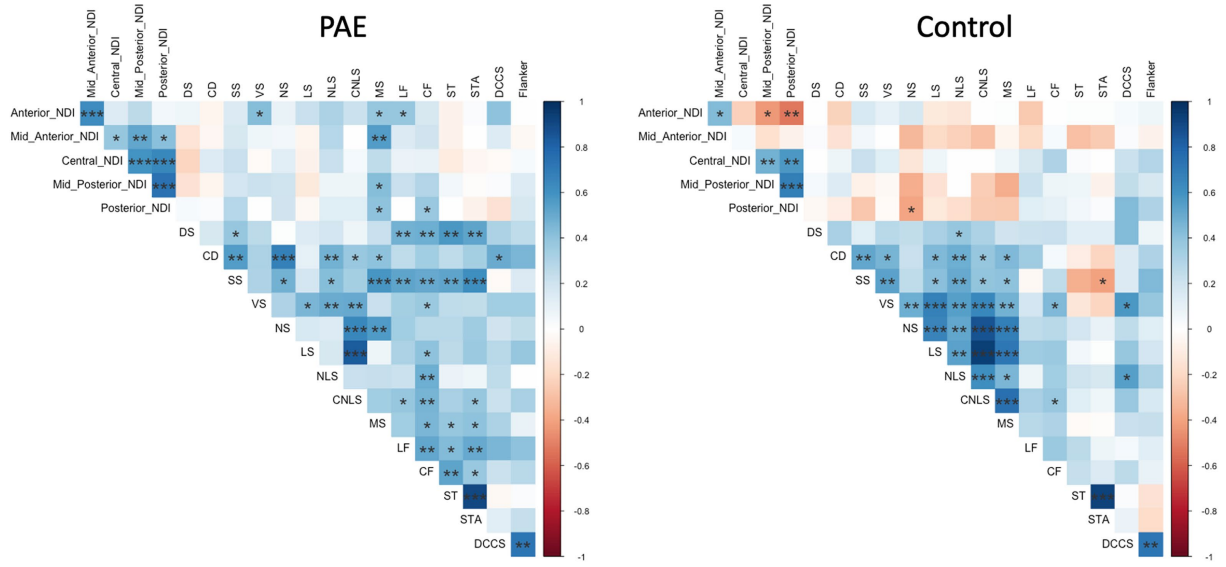


FIGURE 4
Correlation between SPC in corpus callosum NDI and executive function performance. DS, Digit Span; CD, Coding; SS, Symbol Search; *VS*, Visual Scanning; NS, Number Sequencing; LS, Letter Sequencing; NLS, Number-Letter Sequencing; CNLS, Combined Number-Letter Sequencing; MS, Motor Speed; LF, Letter Fluency; CF, Category Fluency; ST, Switching Total; STA, Switching Total Accuracy; DCCS, Dimensional Change Card Sort; blue shaded cells indicate positive correlations; red shaded cells indicate negative correlations. *p<0.05, **p<0.01, ***p<0.001.

marginally lower NDI for PAE males in one region (central CC) at baseline and a significant abnormality in NDI for PAE males in the same region at follow-up. We expected to see larger, more widespread effects, given that a large number of cross-sectional studies have shown that children and adolescents with PAE display atypical white matter microstructure, particularly in the CC (Riley et al., 1995; Lebel et al., 2008; Sherbaf et al., 2019). Using DTI, we have previously shown white matter alterations in PAE in the central and posterior CC (Wozniak et al., 2006, 2009) and demonstrated associations with disrupted functional connectivity between cortical regions served by those CC regions (Wozniak et al., 2011). Importantly, to date, studies of white matter microstructure in PAE have utilized traditional diffusion metrics such as FA and MD. While these findings have shed light on important white matter anomalies associated with PAE, interpretation of metrics such as FA and MD is impacted by several limitations, including the non-specificity of water diffusion restriction, as diffusion of water in white matter fibers may be restricted by fiber diameter and density, membrane permeability, myelination, and directional organization (Figley et al., 2021). Similarly, an estimated 60 to 90 percent of white matter voxels in a given brain contain

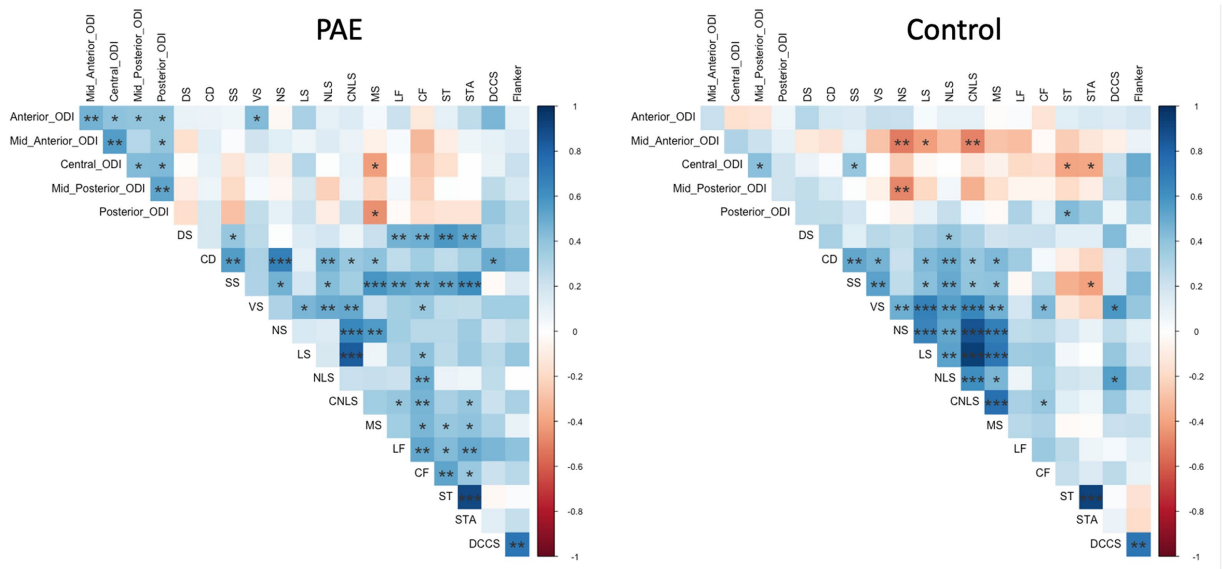


FIGURE 5
Correlation between SPC in corpus callosum ODI and executive function performance. DS, Digit Span; CD, Coding; SS, Symbol Search; *VS*, Visual Scanning; NS, Number Sequencing; LS, Letter Sequencing; NLS, Number-Letter Sequencing; CNLS, Combined Number-Letter Sequencing; MS, Motor Speed; LF, Letter Fluency; *CF*, Category Fluency; ST, Switching Total; STA, Switching Total Accuracy; DCCS, Dimensional Change Card Sort; blue shaded cells indicate positive correlations; red shaded cells indicate negative correlations. *$p<0.05$, **$p<0.01$, ***$p<0.001$.

multiple fiber bundles with different orientations (Jeurissen et al., 2013). Together, these factors limit the specificity with which biologically-meaningful interpretations of traditional diffusion metrics (e.g., FA) can be made, as developmental anomalies in these metrics may be due to a wide array of biological mechanisms. The use of NODDI in this study represents a novel application of this diffusion modeling approach to investigate white matter microstructure development in PAE. As NODDI has been shown to demonstrate a closer relationship with histology (Grussu et al., 2017; Schilling et al., 2018), this approach may be particularly well-suited to characterizing atypical WM microstructure trajectories in youth with neurodevelopmental conditions such as FASD (Young et al., 2019; Kamiya et al., 2020). Findings presented here suggest that NODDI modeling may provide additional insights into atypical white matter microstructural development in PAE. Specifically, findings of the current study suggest that corpus callosum microstructural anomalies in PAE documented in previous studies may be driven primarily by disruptions in axonal coherence/organization and geometry rather than myelination and density. An important consideration for interpretation of our results include recent findings of variation of axonal tortuosity and diameter along the longitudinal axis (de Kouchkovsky et al., 2016; Abdollahzadeh et al., 2019), which may reflect age-related microstructural changes (e.g., myelination). These factors may partially explain our observations of age-related changes in ODI in this study. Future research will benefit from further characterizing the nature and developmental timing of corpus callosum microstructural anomalies associated with PAE.

While data presented here suggest linear trajectories in corpus callosum neurite density and organization are similar in participants with PAE compared to Controls, we did find that the amount and timing of changes in fiber organization differed significantly by group for the central region of the CC, and this group difference appeared to widen during adolescence. Participants with PAE demonstrated minimal changes in ODI (indexing the bending and fanning of axons) at younger ages and an atypical degree of increased ODI at older ages. In contrast, Controls demonstrated minimal changes in ODI with age. This atypically steep change in bending and fanning of axons in corpus callosum fibers during adolescence in the PAE group may suggest a "catch-up" period to compensate for delayed maturation earlier in childhood, consistent with findings from previous studies. Treit et al. (2013) evaluated DTI in a small sample of children ages 5 to 15 years who completed two or three MRI scans across approximately two to four years. Results indicated age-by-group interactions for several white matter tracts (i.e., superior longitudinal fasciculus, superior and inferior fronto-occipital fasciculus), suggesting greater reductions in mean diffusivity in the FASD group and a delayed pattern of microstructural maturation compared to unexposed controls. Using a similar longitudinal methodology, Kar et al. (2021) compared white matter microstructural trajectories in a younger sample of children with PAE and controls ages 2 to 8 years. Results indicated a flatter trajectory of change (decreases) in mean diffusivity across time in the PAE group compared to controls. Specific tracts in which age-by-group differences were observed included the genu of the corpus callosum, uncinate fasciculus, inferior longitudinal fasciculus, and inferior fronto-occipital fasciculus. The authors speculated that this delay in white matter development associated with PAE could reflect reduced brain plasticity, potentially explaining discrepancies between cross-sectional findings of lower MD in young children (e.g., Kar et al., 2021) and higher MD in older children and adolescents (e.g., Fan et al., 2016). Together, data presented here are broadly consistent with these two longitudinal studies (the only published longitudinal studies of white matter microstructure maturation in PAE conducted to date) of atypical developmental timing of white matter microstructural maturation associated with

PAE. Future studies will benefit from larger sample sizes (thus increasing statistical power to detect developmental differences) and the inclusion of multiple diffusion modeling approaches in order to better characterize white matter microstructural maturation across development in PAE.

In the current study, we observed several notable differences in white matter microstructure maturation by sex, as well as several sex-by-group interactions. Specifically, linear trajectories in orientation dispersion in the central CC varied by sex at the whole-group level, suggesting that males in both groups demonstrated higher mean ODI. Analyses of symmetrized percent change also revealed sex differences in the magnitude of change in neurite density and orientation dispersion in the anterior CC, with females showing greater increases than males. These findings align with previous work suggesting sex differences in white matter development in typically-developing individuals, including relative delays in microstructural development (e.g., as measured by DTI) in males compared to females (Wang et al., 2012; Simmonds et al., 2014; Genc et al., 2018), which may reflect developmental differences by sex in the timing of puberty onset (also delayed in males) and the role gonadal hormones in white matter development (Sisk and Foster, 2004; Chavarria et al., 2014; Ho et al., 2020). In contrast, two studies examining white matter microstructure development in typically-developing samples using NODDI found no sex differences in ODI and NDI (Mah et al., 2017; Lynch et al., 2020), and a third study did not examine sex differences in maturational trajectories (Chang et al., 2015). As such, further research exploring potential sex differences in NODDI metrics is needed.

In addition to effects for sex at the whole-group level, we observed a trend-level sex-by-group interaction for linear trajectories of neurite density in the central CC. Further analyses showed that males with PAE demonstrated lower mean neurite density at both scans compared to females with PAE and both male and female Controls. A similar sex-by-group interaction was observed for symmetrized percent change in ODI in the central CC, with female Control participants showing greater reductions in ODI in the central CC compared to male Controls and both female and male PAE participants. A range of sex differences have been documented in animal models of PAE including differences in behavioral functioning and in hypothalamic–pituitary–adrenal axis and neurotransmitter function (Sliwowska et al., 2008; Weinberg et al., 2008; Uban et al., 2013; Roselli et al., 2020). In a recent human study of youth ages 9 to 16 years, Uban et al. (2017) found that girls with PAE demonstrated lower FA across several white matter tracts, whereas males with PAE showed higher FA (including in the body of the corpus callosum) compared to non-exposed controls, with important group differences by sex in relationships between white matter microstructure and gonadal hormones such as testosterone and progesterone. Similarly, expected positive correlations between age and white matter FA were not observed for males with PAE, suggesting a greater degree of atypicality in white matter microstructure development compared to females. In addition, correlations of DTI metrics with gonadal hormone levels were atypical in PAE, with notable sex differences. Together, data presented here may suggest that white matter microstructure maturation is more atypical in males compared to females with PAE, which may reflect differences in neuroendocrine function, and further research will be important.

Exploratory correlations between change in NDI and ODI and executive function performance may suggest atypical relationships between corpus callosum microstructural maturation and cognitive functioning in youth with PAE. Across regions of the CC, reduction in the bending and fanning of axons (ODI) was associated with better task performance for Control participants but not those with PAE. Similarly, correlation matrices suggested that for Controls, greater negative percent change in NDI (i.e., reductions in the density of white matter fibers) was associated with better task performance. Corpus callosum microstructural integrity has been linked to cognitive performance in children and adolescents with PAE in previous studies, including visual–spatial processing skills (Wozniak et al., 2009), working memory and verbal memory (Gautam et al., 2014), and processing speed and eyeblink conditioning (Fan et al., 2016). Emerging longitudinal research suggests atypical brain maturation-behavior relationships in individuals with PAE as measured by a variety of brain metrics (e.g., cortical thickness, cortical volume, white matter volume, FA/MD) (Moore and Xia, 2021). Our preliminary findings may reflect typical corpus callosum white matter microstructure development in Controls and abnormal experience-dependent development in the PAE group, warranting further exploration in future studies.

Results of exploratory analyses suggest that atypicality in the developmental timing and degree of age-related change in CC microstructure in participants with PAE is associated with dysmorphic facial features. Specifically, dysmorphic features (i.e., philtrum and upper lip) were associated with greater percent change increases in ODI in the posterior CC. Our findings align with several prior studies suggesting a relationship between facial dysmorphology and CC microstructure (Astley et al., 2009; Fryer et al., 2009; Li et al., 2009). However, it is important to note that several other studies found no such relationship (Ma et al., 2005; Wozniak et al., 2006, 2009, 2011). Despite these inconsistencies, a relationship between white matter microstructure and facial dysmorphology is biologically plausible given that midline facial tissues (e.g., eyes, lips, mouth) and midline brain structures (i.e., CC) share the same progenitor cells, which are known to be susceptible to the teratogenic effects of PAE (Sulik, 2005; O'Leary-Moore et al., 2011; Sherbaf et al., 2019). Similarly, prior research has suggested a dose-dependent relationship between the amount of PAE and microstructural abnormalities in the splenium and isthmus of the CC (Fan et al., 2016), and a higher degree of facial dysmorphology has been associated with greater amounts of PAE (Roussotte et al., 2012). As such, our preliminary findings may reflect biologically-meaningful relationships between CC microstructure development and dysmorphic facial features, warranting further study with advanced biophysical modeling of diffusion data (e.g., with NODDI) that may be sensitive to subtle developmental disruptions in white matter microstructure in individuals with PAE. Indeed, preliminary data from our recent study examining long-term outcomes following early choline supplementation in young children with PAE suggested a significant correlation between splenium ODI and the degree of facial dysmorphology (Gimbel et al., 2022), highlighting the need for further investigation.

This study has several important limitations. Due to the modest sample size, subtle (yet potentially meaningful) interaction effects (e.g., sex-by-group, age-by-group) with small

to medium effect sizes may have been missed. Given limitations in the sample size, we did not include potential covariates in correlations between change in NODDI metrics and executive function performance. We aim to further explore these relationships in a future study. While the inter-scan interval was significantly longer in the PAE group than in the Control group, the direction of our findings did not change after controlling for the inter-scan interval in analyses. Our sample was also limited in terms of racial and ethnic diversity, resulting in group differences in racial identities for participants in the PAE and Control groups. While FASD is known to affect individuals of all racial and ethnic backgrounds (Olson et al., 2007), group differences in this study may limit the generalizability of our findings. In this study, prenatal exposure to substances other than alcohol was not exclusionary for the PAE group, as this pattern is common. Although brain-based differences resulting from other prenatal exposure to other substances has the potential to add additional noise to the data in studies of PAE, prenatal exposure to alcohol alone has well-documented direct effects on neurodevelopment (Wozniak et al., 2019). Future studies will benefit from further exploration of potential additive or synergistic effects of prenatal polysubstance exposure on white matter longitudinal trajectories. Additionally, in this study we used linear models of microstructure diffusion trajectories to explore white matter microstructure maturation in PAE as we believed linear models to be appropriate given the duration between scans (17 months on average) and the modest sample size. However, white matter development is known to be non-linear, particularly across larger timescales (Lebel et al., 2019), and future studies may benefit from further exploration of potentially atypical non-linear trajectories of white matter change associated with PAE. In addition, the modest sample size examined in this study may have contributed to our finding of trend-level (after FDR correction) diagnostic group differences in ODI symmetrized percent change in the central CC. Future research will benefit from larger sample sizes providing improved statistical power in order to better characterize white matter microstructure maturation in PAE.

5. Conclusion

To conclude, data presented here suggest an atypical amount and timing of age-related changes in white matter microstructure (i.e., axon bending and fanning) in the CC in children and adolescents with PAE compared to typically-developing Controls. These findings add to the existing literature on neurodevelopmental trajectories in PAE and suggest that advanced biophysical diffusion modeling (NODDI) may be sensitive to biologically-meaningful microstructural changes in the CC that are disrupted by PAE. Findings of atypical brain maturation-behavior relationships in PAE highlight the need for further study.

Data availability statement

The raw data supporting the conclusions of this article will be made available by the authors, without undue reservation.

Ethics statement

The studies involving human participants were reviewed and approved by Institutional Review Board of the University of Minnesota. Written informed consent to participate in this study was provided by the participants' legal guardian/next of kin.

Author contributions

BAG participated in the analysis of the study as well as the writing of the manuscript. DJR and BAM participated in the design and conduct of the study including neuroimaging data acquisition, neuroimaging data inspection and analysis, and the writing of the manuscript. AME and MNR participated in the data collection, analysis, and the writing of the manuscript. MEA participated in the analysis and the writing of the manuscript. EW participated in the writing of the manuscript. SNM, KLJ, EPR, and KOL participated in the design and conduct of the study and the writing of the manuscript. JRW participated in the design and execution of the study, analysis, and the writing of the manuscript. All authors read and approved the final manuscript.

Funding

This study was supported by National Institute on Alcohol Abuse and Alcoholism: U01AA026102, U24AA014815, U01AA014834, and U24AA014811; the Biotechnology Research Center: P41EB015894, the National Institute of Neurological Disorders and Stroke Institutional Center Core Grants to Support Neuroscience Research: P30 NS076408; and the High Performance Connectome Upgrade for Human 3T MR Scanner: 1S10OD017974.

Acknowledgments

All or part of this work was done in conjunction with the Collaborative Initiative on Fetal Alcohol Spectrum Disorders (CIFASD), which is funded by grants from the National Institute on Alcohol Abuse and Alcoholism (NIAAA). Additional information about CIFASD can be found at www.cifasd.org.

Conflict of interest

The authors declare that the research was conducted in the absence of any commercial or financial relationships that could be construed as a potential conflict of interest.

Publisher's note

All claims expressed in this article are solely those of the authors and do not necessarily represent those of their affiliated organizations, or those of the publisher, the editors and the reviewers. Any product that may be evaluated in this article, or claim that may be made by its manufacturer, is not guaranteed or endorsed by the publisher.

References

Abdollahzadeh, A., Belevich, I., Jokitalo, E., Tohka, J., and Sierra, A. (2019). Automated 3D axonal morphometry of white matter. *Sci. Rep.* 9:6084. doi: 10.1038/s41598-019-42648-2

Andersson, J. L. R., Graham, M. S., Drobnjak, I., Zhang, H., and Campbell, J. (2018). Susceptibility-induced distortion that varies due to motion: correction in diffusion MR without acquiring additional data. *NeuroImage* 171, 277–295. doi: 10.1016/j.neuroimage.2017.12.040

Andersson, J. L. R., Graham, M. S., Drobnjak, I., Zhang, H., Filippini, N., and Bastiani, M. (2017). Towards a comprehensive framework for movement and distortion correction of diffusion MR images: within volume movement. *NeuroImage* 152, 450–466. doi: 10.1016/j.neuroimage.2017.02.085

Andersson, J. L. R., Graham, M. S., Zsoldos, E., and Sotiropoulos, S. N. (2016). Incorporating outlier detection and replacement into a non-parametric framework for movement and distortion correction of diffusion MR images. *NeuroImage* 141, 556–572. doi: 10.1016/j.neuroimage.2016.06.058

Andersson, J. L. R., Skare, S., and Ashburner, J. (2003). How to correct susceptibility distortions in spin-echo echo-planar images: application to diffusion tensor imaging. *NeuroImage* 20, 870–888. doi: 10.1016/S1053-8119(03)00336-7

Andersson, J. L. R., and Sotiropoulos, S. N. (2016). An integrated approach to correction for off-resonance effects and subject movement in diffusion MR imaging. *NeuroImage* 125, 1063–1078. doi: 10.1016/j.neuroimage.2015.10.019

Andica, C., Kamagata, K., Hayashi, T., Hagiwara, A., Uchida, W., Saito, Y., et al. (2020). Scan-rescan and inter-vendor reproducibility of neurite orientation dispersion and density imaging metrics. *Neuroradiology* 62, 483–494. doi: 10.1007/s00234-019-02350-6

Astley, S. J. (2004). *Diagnostic Guide for Fetal Alcohol Spectrum Disorders: The 4-Digit Diagnostic Code. 3rd Edn*. Seattle, WA: University of Washington.

Astley, S. J., Aylward, E. H., Olson, H. C., Kerns, K., Brooks, A., Coggins, T. E., et al. (2009). Magnetic resonance imaging outcomes from a comprehensive magnetic resonance study of children with fetal alcohol spectrum disorders. *Alcohol. Clin. Exp. Res.* 33, 1671–1689. doi: 10.1111/j.1530-0277.2009.01004.x

Astley, S. J., and Clarren, S. K. (2000). Diagnosing the full spectrum of fetal alcohol-exposed individuals: introducing the 4-digit diagnostic code. *Alcohol Alcohol.* 35, 400–410. doi: 10.1093/alcalc/35.4.400

Batalle, D., Hughes, E. J., Zhang, H., Tournier, J.-D., Tusor, N., Aljabar, P., et al. (2017). Early development of structural networks and the impact of prematurity on brain connectivity. *NeuroImage* 149, 379–392. doi: 10.1016/j.neuroimage.2017.01.065

Bates, D., Mächler, M., Bolker, B., and Walker, S. (2015). Fitting linear mixed-effects models using lme4. arXiv [stat.CO]. Available at: http://arxiv.org/abs/1406.5823 (Accessed February 22, 2023).

Berry, D. A., and Ayers, G. D. (2006). Symmetrized percent change for treatment comparisons. *Am. Stat.* 60, 27–31. doi: 10.1198/000313006X90684

Bertrand, J., Floyd, L. L., and Weber, M. K.Fetal Alcohol Syndrome Prevention Team, Division of Birth Defects and Developmental Disabilities, National Center on Birth Defects and Developmental Disabilities, Centers for Disease Control and Prevention (CDC) (2005). Guidelines for identifying and referring persons with fetal alcohol syndrome. *MMWR Recomm. Rep.* 54, 1–14.

Biffen, S. C., Dodge, N. C., Warton, C. M. R., Molteno, C. D., Jacobson, J. L., Meintjes, E. M., et al. (2022). Compromised interhemispheric transfer of information partially mediates cognitive function deficits in adolescents with fetal alcohol syndrome. *Alcohol. Clin. Exp. Res.* 46, 517–529. doi: 10.1111/acer.14795

Billiet, T., Mädler, B., D'Arco, F., Peeters, R., Deprez, S., Plasschaert, E., et al. (2014). Characterizing the microstructural basis of "unidentified bright objects" in neurofibromatosis type 1: a combined in vivo multicomponent T2 relaxation and multi-shell diffusion MRI analysis. *NeuroImage Clin.* 4, 649–658. doi: 10.1016/j.nicl.2014.04.005

Blesa, M., Galdi, P., Sullivan, G., Wheater, E. N., Stoye, D. Q., Lamb, G. J., et al. (2020). Peak width of skeletonized Water diffusion MRI in the neonatal brain. *Front. Neurol.* 11:235. doi: 10.3389/fneur.2020.00235

Chang, Y. S., Owen, J. P., Pojman, N. J., Thieu, T., Bukshpun, P., Wakahiro, M. L. J., et al. (2015). White matter changes of neurite density and fiber orientation dispersion during human brain maturation. *PLoS One* 10:e0123656. doi: 10.1371/journal.pone.0123656

Chasnoff, I. J., Wells, A. M., and King, L. (2015). Misdiagnosis and missed diagnoses in foster and adopted children with prenatal alcohol exposure. *Pediatrics* 135, 264–270. doi: 10.1542/peds.2014-2171

Chavarria, M. C., Sánchez, F. J., Chou, Y.-Y., Thompson, P. M., and Luders, E. (2014). Puberty in the corpus callosum. *Neuroscience* 265, 1–8. doi: 10.1016/j.neuroscience.2014.01.030

Chudley, A. E., Conry, J., Cook, J. L., Loock, C., Rosales, T., LeBlanc, N., et al. (2005). Fetal alcohol spectrum disorder: Canadian guidelines for diagnosis. *CMAJ* 172, S1–S21. doi: 10.1503/cmaj.1040302

Collorone, S., Cawley, N., Grussu, F., Prados, F., Tona, F., Calvi, A., et al. (2020). Reduced neurite density in the brain and cervical spinal cord in relapsing–remitting multiple sclerosis: a NODDI study. *Mult. Scler.* 26, 1647–1657. doi: 10.1177/1352458519885107

Daducci, A., Canales-Rodríguez, E. J., Zhang, H., Dyrby, T. B., Alexander, D. C., and Thiran, J.-P. (2015). Accelerated microstructure imaging via convex optimization (AMICO) from diffusion MRI data. *NeuroImage* 105, 32–44. doi: 10.1016/j.neuroimage.2014.10.026

de Kouchkovsky, I., Fieremans, E., Fleysher, L., Herbert, J., Grossman, R. I., and Inglese, M. (2016). Quantification of normal-appearing white matter tract integrity in multiple sclerosis: a diffusion kurtosis imaging study. *J. Neurol.* 263, 1146–1155. doi: 10.1007/s00415-016-8118-z

Dean, D. C. 3rd, Planalp, E. M., Wooten, W., Kecskemeti, S. R., Adluru, N., Schmidt, C. K., et al. (2018). Association of Prenatal Maternal Depression and Anxiety Symptoms with Infant White Matter Microstructure. *JAMA Pediatr.* 172, 973–981. doi: 10.1001/jamapediatrics.2018.2132

Delis, D. C., Kaplan, E., and Kramer, J. H. (2001). *Delis-Kaplan Executive Function System (D-KEFS)*. San Antonio: Harcourt Assessment, Inc.

Dimitrova, R., Pietsch, M., Ciarrusta, J., Fitzgibbon, S. P., Williams, L. Z. J., Christiaens, D., et al. (2021). Preterm birth alters the development of cortical microstructure and morphology at term-equivalent age. *NeuroImage* 243:118488. doi: 10.1016/j.neuroimage.2021.118488

Fan, J., Jacobson, S. W., Taylor, P. A., Molteno, C. D., Dodge, N. C., Stanton, M. E., et al. (2016). White matter deficits mediate effects of prenatal alcohol exposure on cognitive development in childhood. *Hum. Brain Mapp.* 37, 2943–2958. doi: 10.1002/hbm.23218

Fan, J., Meintjes, E. M., Molteno, C. D., Spottiswoode, B. S., Dodge, N. C., Alhamud, A. A., et al. (2015). White matter integrity of the cerebellar peduncles as a mediator of effects of prenatal alcohol exposure on eyeblink conditioning. *Hum. Brain Mapp.* 36, 2470–2482. doi: 10.1002/hbm.22785

Figley, C. R., Uddin, M. N., Wong, K., Kornelsen, J., Puig, J., and Figley, T. D. (2021). Potential pitfalls of using fractional anisotropy, axial diffusivity, and radial diffusivity as biomarkers of cerebral white matter microstructure. *Front. Neurosci.* 15:799576. doi: 10.3389/fnins.2021.799576

Fryer, S. L., Schweinsburg, B. C., Bjorkquist, O. A., Frank, L. R., Mattson, S. N., Spadoni, A. D., et al. (2009). Characterization of white matter microstructure in fetal alcohol spectrum disorders. *Alcohol. Clin. Exp. Res.* 33, 514–521. doi: 10.1111/j.1530-0277.2008.00864.x

Gautam, P., Nuñez, S. C., Narr, K. L., Kan, E. C., and Sowell, E. R. (2014). Effects of prenatal alcohol exposure on the development of white matter volume and change in executive function. *Neuroimage Clin* 5, 19–27. doi: 10.1016/j.nicl.2014.05.010

Genc, S., Malpas, C. B., Ball, G., Silk, T. J., and Seal, M. L. (2018). Age, sex, and puberty related development of the corpus callosum: a multi-technique diffusion MRI study. *Brain Struct. Funct.* 223, 2753–2765. doi: 10.1007/s00429-018-1658-5

Gimbel, B. A., Anthony, M. E., Ernst, A. M., Roediger, D. J., de Water, E., Eckerle, J. K., et al. (2022). Long-term follow-up of a randomized controlled trial of choline for neurodevelopment in fetal alcohol spectrum disorder: corpus callosum white matter microstructure and neurocognitive outcomes. *J. Neurodev. Disord.* 14:59. doi: 10.1186/s11689-022-09470-w

Glasser, M. F., Sotiropoulos, S. N., Wilson, J. A., Coalson, T. S., Fischl, B., Andersson, J. L., et al. (2013). The minimal preprocessing pipelines for the human connectome project. *NeuroImage* 80, 105–124. doi: 10.1016/j.neuroimage.2013.04.127

Grussu, F., Schneider, T., Tur, C., Yates, R. L., Tachrount, M., Ianuş, A., et al. (2017). Neurite dispersion: a new marker of multiple sclerosis spinal cord pathology? *Ann. Clin. Transl. Neurol.* 4, 663–679. doi: 10.1002/acn3.445

Harms, M. P., Somerville, L. H., Ances, B. M., Andersson, J., Barch, D. M., Bastiani, M., et al. (2018). Extending the human connectome project across ages: imaging protocols for the lifespan development and aging projects. *NeuroImage* 183, 972–984. doi: 10.1016/j.neuroimage.2018.09.060

Ho, T. C., Colich, N. L., Sisk, L. M., Oskirko, K., Jo, B., and Gotlib, I. H. (2020). Sex differences in the effects of gonadal hormones on white matter microstructure development in adolescence. *Dev. Cogn. Neurosci.* 42:100773. doi: 10.1016/j.dcn.2020.100773

Hoyme, H. E., Kalberg, W. O., Elliott, A. J., Blankenship, J., Buckley, D., Marais, A.-S., et al. (2016). Updated clinical guidelines for diagnosing fetal alcohol Spectrum disorders. *Pediatrics* 138:4256. doi: 10.1542/peds.2015-4256

Huber, E., Henriques, R. N., Owen, J. P., Rokem, A., and Yeatman, J. D. (2019). Applying microstructural models to understand the role of white matter in cognitive development. *Dev. Cogn. Neurosci.* 36:100624. doi: 10.1016/j.dcn.2019.100624

Jeurissen, B., Leemans, A., Tournier, J.-D., Jones, D. K., and Sijbers, J. (2013). Investigating the prevalence of complex fiber configurations in white matter tissue with diffusion magnetic resonance imaging. *Hum. Brain Mapp.* 34, 2747–2766. doi: 10.1002/hbm.22099

Jones, K. L., and Smith, D. W. (1973). Recognition of the fetal alcohol syndrome in early infancy. *Lancet* 302, 999–1001. doi: 10.1016/S0140-6736(73)91092-1

Kamiya, K., Hori, M., and Aoki, S. (2020). NODDI in clinical research. *J. Neurosci. Methods* 346:108908. doi: 10.1016/j.jneumeth.2020.108908

Kar, P., Reynolds, J. E., Gibbard, W. B., McMorris, C., Tortorelli, C., and Lebel, C. (2022). Trajectories of brain white matter development in young children with prenatal alcohol exposure. *Hum. Brain Mapp.* 43, 4145–4157. doi: 10.1002/hbm.25944

Kar, P., Reynolds, J. E., Grohs, M. N., Gibbard, W. B., McMorris, C., Tortorelli, C., et al. (2021). White matter alterations in young children with prenatal alcohol exposure. *Dev. Neurobiol.* 81, 400–410. doi: 10.1002/dneu.22821

Karmacharya, S., Gagoski, B., Ning, L., Vyas, R., Cheng, H. H., Soul, J., et al. (2018). Advanced diffusion imaging for assessing normal white matter development in neonates and characterizing aberrant development in congenital heart disease. *Neuroimage Clin.* 19, 360–373. doi: 10.1016/j.nicl.2018.04.032

Kaufmann, W. E., and Moser, H. W. (2000). Dendritic anomalies in disorders associated with mental retardation. *Cereb. Cortex* 10, 981–991. doi: 10.1093/cercor/10.10.981

Kelly, C. E., Thompson, D. K., Chen, J., Leemans, A., Adamson, C. L., Inder, T. E., et al. (2016). Axon density and axon orientation dispersion in children born preterm. *Hum. Brain Mapp.* 37, 3080–3102. doi: 10.1002/hbm.23227

Kuczmarski, R. J., Ogden, C. L., Grummer-Strawn, L. M., Flegal, K. M., Guo, S. S., Wei, R., et al. (2000). CDC growth charts: United States. *Adv. Data*, 1–27.

Kuznetsova, A., Brockhoff, P. B., and Christensen, R. H. B. (2017). lmerTest package: tests in linear mixed effects models. *J. Stat. Softw.* 82, 1–26. doi: 10.18637/jss.v082.i13

Lange, S., Probst, C., Gmel, G., Rehm, J., Burd, L., and Popova, S. (2018). Global prevalence of fetal alcohol Spectrum disorder among children and youth: a systematic review and meta-analysis. *Obstet. Gynecol. Surv.* 73, 189–191. doi: 10.1097/01.ogx.0000532194.88210.00

Lebel, C., Rasmussen, C., Wyper, K., Andrew, G., and Beaulieu, C. (2010). Brain microstructure is related to math ability in children with fetal alcohol spectrum disorder. *Alcohol. Clin. Exp. Res.* 34, 354–363. doi: 10.1111/j.1530-0277.2009.01097.x

Lebel, C., Rasmussen, C., Wyper, K., Walker, L., Andrew, G., Yager, J., et al. (2008). Brain diffusion abnormalities in children with fetal alcohol spectrum disorder. *Alcohol. Clin. Exp. Res.* 32, 1732–1740. doi: 10.1111/j.1530-0277.2008.00750.x

Lebel, C., Treit, S., and Beaulieu, C. (2019). A review of diffusion MRI of typical white matter development from early childhood to young adulthood. *NMR Biomed.* 32:e3778. doi: 10.1002/nbm.3778

Li, L., Coles, C., Lynch, M., and Hu, X. (2009). Voxelwise and skeleton-based region of interest analysis of fetal alcohol syndrome and fetal alcohol Spectrum disorders in Young adults. *NeuroImage* 47:S47. doi: 10.1016/s1053-8119(09)70073-4

Lucignani, M., Breschi, L., Espagnet, M. C. R., Longo, D., Talamanca, L. F., Placidi, E., et al. (2021). Reliability on multiband diffusion NODDI models: a test retest study on children and adults. *NeuroImage* 238:118234. doi: 10.1016/j.neuroimage.2021.118234

Lynch, K. M., Cabeen, R. P., Toga, A. W., and Clark, K. A. (2020). Magnitude and timing of major white matter tract maturation from infancy through adolescence with NODDI. *NeuroImage* 212:116672. doi: 10.1016/j.neuroimage.2020.116672

Ma, X., Coles, C. D., Lynch, M. E., LaConte, S. M., Zurkiya, O., Wang, D., et al. (2005). Evaluation of corpus callosum anisotropy in young adults with fetal alcohol syndrome according to diffusion tensor imaging. *Alcohol. Clin. Exp. Res.* 29, 1214–1222. doi: 10.1097/01.ALC.0000171934.22755.6D

Mah, A., Geeraert, B., and Lebel, C. (2017). Detailing neuroanatomical development in late childhood and early adolescence using NODDI. *PLoS One* 12:e0182340. doi: 10.1371/journal.pone.0182340

Mastropietro, A., Rizzo, G., Fontana, L., Figini, M., Bernardini, B., Straffi, L., et al. (2019). Microstructural characterization of corticospinal tract in subacute and chronic stroke patients with distal lesions by means of advanced diffusion MRI. *Neuroradiology* 61, 1033–1045. doi: 10.1007/s00234-019-02249-2

Mattson, S. N., Foroud, T., Sowell, E. R., Jones, K. L., Coles, C. D., Fagerlund, A., et al. (2010a). Collaborative initiative on fetal alcohol spectrum disorders: methodology of clinical projects. *Alcohol* 44, 635–641. doi: 10.1016/j.alcohol.2009.08.005

Mattson, S. N., Roesch, S. C., Fagerlund, A., Autti-Rämö, I., Jones, K. L., May, P. A., et al. (2010b). Toward a neurobehavioral profile of fetal alcohol spectrum disorders. *Alcohol. Clin. Exp. Res.* 34, 1640–1650. doi: 10.1111/j.1530-0277.2010.01250.x

May, P. A., Chambers, C. D., Kalberg, W. O., Zellner, J., Feldman, H., Buckley, D., et al. (2018). Prevalence of fetal alcohol Spectrum disorders in 4 US communities. *JAMA* 319, 474–482. doi: 10.1001/jama.2017.21896

McLennan, J. D. (2015). Misattributions and potential consequences: the case of child mental health problems and fetal alcohol Spectrum disorders. *Can. J. Psychiatr.* 60, 587–590. doi: 10.1177/070674371506001210

Moore, E. M., and Xia, Y. (2021). Neurodevelopmental trajectories following prenatal alcohol exposure. *Front. Hum. Neurosci.* 15:695855. doi: 10.3389/fnhum.2021.695855

Mowinckel, A. M., and Vidal-Piñeiro, D. (2020). Visualization of brain statistics with R packages ggseg and ggseg3d. *Adv. Methods Pract. Psychol. Sci.* 3, 466–483. doi: 10.1177/2515245920928009

Nellhaus, G. (1968). Head circumference from birth to eighteen years. Practical composite international and interracial graphs. *Pediatrics* 41, 106–114. doi: 10.1542/peds.41.1.106

Nemanich, S. T., Mueller, B. A., and Gillick, B. T. (2019). Neurite orientation dispersion and density imaging quantifies corticospinal tract microstructural organization in children with unilateral cerebral palsy. *Hum. Brain Mapp.* 40, 4888–4900. doi: 10.1002/hbm.24744

O'Leary-Moore, S. K., Parnell, S. E., Lipinski, R. J., and Sulik, K. K. (2011). Magnetic resonance-based imaging in animal models of fetal alcohol spectrum disorder. *Neuropsychol. Rev.* 21, 167–185. doi: 10.1007/s11065-011-9164-z

Olson, H. C., Jirikowic, T., Kartin, D., and Astley, S. (2007). Responding to the challenge of early intervention for fetal alcohol Spectrum disorders. *Infants Young Child.* 20, 172–189. doi: 10.1097/01.IYC.0000264484.73688.4a

Parvathaneni, P., Nath, V., Blaber, J. A., Schilling, K. G., Hainline, A. E., Mojahed, E., et al. (2018). Empirical reproducibility, sensitivity, and optimization of acquisition protocol, for neurite orientation dispersion and density imaging using AMICO. *Magn. Reson. Imaging* 50, 96–109. doi: 10.1016/j.mri.2018.03.004

R Core Team (2021). R: A language and environment for statistical computing. Available at: URL https://www.R-project.org/ (Accessed February 22, 2023).

Reuter, M., and Fischl, B. (2011). Avoiding asymmetry-induced bias in longitudinal image processing. *NeuroImage* 57, 19–21. doi: 10.1016/j.neuroimage.2011.02.076

Reuter, M., Rosas, H. D., and Fischl, B. (2010). Highly accurate inverse consistent registration: a robust approach. *NeuroImage* 53, 1181–1196. doi: 10.1016/j.neuroimage.2010.07.020

Reuter, M., Schmansky, N. J., Rosas, H. D., and Fischl, B. (2012). Within-subject template estimation for unbiased longitudinal image analysis. *NeuroImage* 61, 1402–1418. doi: 10.1016/j.neuroimage.2012.02.084

Riley, E. P., Infante, M. A., and Warren, K. R. (2011). Fetal alcohol spectrum disorders: an overview. *Neuropsychol. Rev.* 21, 73–80. doi: 10.1007/s11065-011-9166-x

Riley, E. P., Mattson, S. N., Sowell, E. R., Jernigan, T. L., Sobel, D. F., and Jones, K. L. (1995). Abnormalities of the corpus callosum in children prenatally exposed to alcohol. *Alcohol. Clin. Exp. Res.* 19, 1198–1202. doi: 10.1111/j.1530-0277.1995.tb01600.x

Roselli, V., Guo, C., Huang, D., Wen, D., Zona, D., Liang, T., et al. (2020). Prenatal alcohol exposure reduces posterior dorsomedial striatum excitability and motivation in a sex- and age-dependent fashion. *Neuropharmacology* 180:108310. doi: 10.1016/j.neuropharm.2020.108310

Roussotte, F. F., Sulik, K. K., Mattson, S. N., Riley, E. P., Jones, K. L., Adnams, C. M., et al. (2012). Regional brain volume reductions relate to facial dysmorphology and neurocognitive function in fetal alcohol spectrum disorders. *Hum. Brain Mapp.* 33, 920–937. doi: 10.1002/hbm.21260

Schilling, K. G., Janve, V., Gao, Y., Stepniewska, I., Landman, B. A., and Anderson, A. W. (2018). Histological validation of diffusion MRI fiber orientation distributions and dispersion. *NeuroImage* 165, 200–221. doi: 10.1016/j.neuroimage.2017.10.046

Sherbaf, F. G., Aarabi, M. H., Yazdi, M. H., and Haghshomar, M. (2019). White matter microstructure in fetal alcohol spectrum disorders: a systematic review of diffusion tensor imaging studies. *Hum. Brain Mapp.* 40, 1017–1036. doi: 10.1002/hbm.24409

Simmonds, D. J., Hallquist, M. N., Asato, M., and Luna, B. (2014). Developmental stages and sex differences of white matter and behavioral development through adolescence: a longitudinal diffusion tensor imaging (DTI) study. *NeuroImage* 92, 356–368. doi: 10.1016/j.neuroimage.2013.12.044

Sisk, C. L., and Foster, D. L. (2004). The neural basis of puberty and adolescence. *Nat. Neurosci.* 7, 1040–1047. doi: 10.1038/nn1326

Slater, D. A., Melie-Garcia, L., Preisig, M., Kherif, F., Lutti, A., and Draganski, B. (2019). Evolution of white matter tract microstructure across the life span. *Hum. Brain Mapp.* 40, 2252–2268. doi: 10.1002/hbm.24522

Sliwowska, J. H., Lan, N., Yamashita, F., Halpert, A. G., Viau, V., and Weinberg, J. (2008). Effects of prenatal ethanol exposure on regulation of basal hypothalamic–pituitary–adrenal activity and hippocampal 5-HT1A receptor mRNA levels in female rats across the estrous cycle. *Psychoneuroendocrinology* 33, 1111–1123. doi: 10.1016/j.psyneuen.2008.05.001

Smith, S. M., Jenkinson, M., Woolrich, M. W., Beckmann, C. F., Behrens, T. E. J., Johansen-Berg, H., et al. (2004). Advances in functional and structural MR image analysis and implementation as FSL. *NeuroImage* 23, S208–S219. doi: 10.1016/j.neuroimage.2004.07.051

Stromland, K., Chen, Y., Norberg, T., Wennerstrom, K., and Michael, G. (1999). Reference values of facial features in Scandinavian children measured with a range-camera technique. *Scand. J. Plast. Reconstr. Surg. Hand Surg.* 33, 59–65. doi: 10.1080/02844319950159631

Sulik, K. K. (2005). Genesis of alcohol-induced craniofacial dysmorphism. *Exp. Biol. Med.* 230, 366–375. doi: 10.1177/15353702-0323006-04

Thompson, P. M., Jahanshad, N., Ching, C. R. K., Salminen, L. E., Thomopoulos, S. I., Bright, J., et al. (2020). ENIGMA and global neuroscience: a decade of large-scale studies of the brain in health and disease across more than 40 countries. *Transl. Psychiatry* 10:100. doi: 10.1038/s41398-020-0705-1

Tisdall, M. D., Hess, A. T., Reuter, M., Meintjes, E. M., Fischl, B., and van der Kouwe, A. J. W. (2012). Volumetric navigators for prospective motion correction and selective reacquisition in neuroanatomical MRI. *Magn. Reson. Med.* 68, 389–399. doi: 10.1002/mrm.23228

Treit, S., Chen, Z., Zhou, D., Baugh, L., Rasmussen, C., Andrew, G., et al. (2017). Sexual dimorphism of volume reduction but not cognitive deficit in fetal alcohol spectrum disorders: a combined diffusion tensor imaging, cortical thickness and brain volume study. *NeuroImage Clin.* 15, 284–297. doi: 10.1016/j.nicl.2017.05.006

Treit, S., Lebel, C., Baugh, L., Rasmussen, C., Andrew, G., and Beaulieu, C. (2013). Longitudinal MRI reveals altered trajectory of brain development during childhood and adolescence in fetal alcohol spectrum disorders. *J. Neurosci.* 33, 10098–10109. doi: 10.1523/JNEUROSCI.5004-12.2013

Uban, K. A., Comeau, W. L., Ellis, L. A., Galea, L. A. M., and Weinberg, J. (2013). Basal regulation of HPA and dopamine systems is altered differentially in males and females by prenatal alcohol exposure and chronic variable stress. *Psychoneuroendocrinology* 38, 1953–1966. doi: 10.1016/j.psyneuen.2013.02.017

Uban, K. A., Herting, M. M., Wozniak, J. R., and Sowell, E. R.CIFASD (2017). Sex differences in associations between white matter microstructure and gonadal hormones in children and adolescents with prenatal alcohol exposure. *Psychoneuroendocrinology* 83, 111–121. doi: 10.1016/j.psyneuen.2017.05.019

Wang, Y., Adamson, C., Yuan, W., Altaye, M., Rajagopal, A., Byars, A. W., et al. (2012). Sex differences in white matter development during adolescence: a DTI study. *Brain Res.* 1478, 1–15. doi: 10.1016/j.brainres.2012.08.038

Wechsler, D. (2008). *WAIS-IV: Wechsler Adult Intelligence Scale. 4th Edn*. San Antonio, TX: Pearson Assessment.

Wechsler, D. (2014). *Wechsler Intelligence Scale for Children-(WISC-V)*. London: Pearson Education.

Wei, T., and Simko, V. (2017). *R Package "corrplot": Visualization of a Correlation Matrix (Version 0.84)*.

Weinberg, J., Sliwowska, J. H., Lan, N., and Hellemans, K. G. C. (2008). Prenatal alcohol exposure: Foetal programming, the hypothalamic-pituitary-adrenal Axis and sex differences in outcome. *J. Neuroendocrinol.* 20, 470–488. doi: 10.1111/j.1365-2826.2008.01669.x

Weintraub, S., Dikmen, S. S., Heaton, R. K., Tulsky, D. S., Zelazo, P. D., Bauer, P. J., et al. (2013). Cognition assessment using the NIH toolbox. *Neurology* 80, S54–S64. doi: 10.1212/WNL.0b013e3182872ded

Wozniak, J. R., Mueller, B. A., Chang, P. N., Muetzel, R. L., Caros, L., and Lim, K. O. (2006). Diffusion tensor imaging in children with fetal alcohol spectrum disorders. *Alcohol. Clin. Exp. Res.* 30, 1799–1806. doi: 10.1111/j.1530-0277.2006.00213.x

Wozniak, J. R., Mueller, B. A., Muetzel, R. L., Bell, C. J., Hoecker, H. L., Nelson, M. L., et al. (2011). Inter-hemispheric functional connectivity disruption in children with prenatal alcohol exposure. *Alcohol. Clin. Exp. Res.* 35, 849–861. doi: 10.1111/j.1530-0277.2010.01415.x

Wozniak, J. R., Muetzel, R. L., Mueller, B. A., McGee, C. L., Freerks, M. A., Ward, E. E., et al. (2009). Microstructural corpus callosum anomalies in children with prenatal alcohol exposure: an extension of previous diffusion tensor imaging findings. *Alcohol. Clin. Exp. Res.* 33, 1825–1835. doi: 10.1111/j.1530-0277.2009.01021.x

Wozniak, J. R., Riley, E. P., and Charness, M. E. (2019). Clinical presentation, diagnosis, and management of fetal alcohol spectrum disorder. *Lancet Neurol.* 18, 760–770. doi: 10.1016/S1474-4422(19)30150-4

Young, J. M., Vandewouw, M. M., Mossad, S. I., Morgan, B. R., Lee, W., Smith, M. L., et al. (2019). White matter microstructural differences identified using multi-shell diffusion imaging in six-year-old children born very preterm. *Neuroimage Clin.* 23:101855. doi: 10.1016/j.nicl.2019.101855

Zhang, H., Schneider, T., Wheeler-Kingshott, C. A., and Alexander, D. C. (2012). NODDI: practical in vivo neurite orientation dispersion and density imaging of the human brain. *NeuroImage* 61, 1000–1016. doi: 10.1016/j.neuroimage.2012.03.072

frontiers | Frontiers in Neuroscience

TYPE Original Research
PUBLISHED 25 April 2023
DOI 10.3389/fnins.2023.1147536

Check for updates

OPEN ACCESS

EDITED BY
Hermes H. Yeh,
Dartmouth College, United States

REVIEWED BY
Anushree N. Karkhanis,
Binghamton University, United States
Donald A. Wilson,
Grossman School of Medicine,
New York University, United States

*CORRESPONDENCE
Jonathan L. Brigman
✉ jbrigman@salud.unm.edu

SPECIALTY SECTION
This article was submitted to Neurodevelopment, a section of the journal Frontiers in Neuroscience

RECEIVED 18 January 2023
ACCEPTED 14 March 2023
PUBLISHED 25 April 2023

CITATION
Chandrasekaran J, Jacquez B, Wilson J and Brigman JL (2023) Reinforcer value moderates the effects of prenatal alcohol exposure on learning and reversal.
Front. Neurosci. 17:1147536.
doi: 10.3389/fnins.2023.1147536

COPYRIGHT
© 2023 Chandrasekaran, Jacquez, Wilson and Brigman. This is an open-access article distributed under the terms of the Creative Commons Attribution License (CC BY). The use, distribution or reproduction in other forums is permitted, provided the original author(s) and the copyright owner(s) are credited and that the original publication in this journal is cited, in accordance with accepted academic practice. No use, distribution or reproduction is permitted which does not comply with these terms.

Reinforcer value moderates the effects of prenatal alcohol exposure on learning and reversal

Jayapriya Chandrasekaran[1], Belkis Jacquez[1,2], Jennifer Wilson[1] and Jonathan L. Brigman[1,2]*

[1]Department of Neurosciences, University of New Mexico School of Medicine, Albuquerque, NM, United States, [2]New Mexico Alcohol Research Center, UNM Health Sciences Center, Albuquerque, NM, United States

Introduction: Fetal Alcohol Spectrum Disorders (FASD) are the leading cause of preventable developmental disability and are commonly characterized by alterations in executive function. Reversal learning tasks are reliable, cross-species methods for testing a frequently impaired aspect of executive control, behavioral flexibility. Pre-clinical studies commonly require the use of reinforcers to motivate animals to learn and perform the task. While there are several reinforcers available, the most commonly employed are solid (food pellets) and liquid (sweetened milk) rewards. Previous studies have examined the effects of different solid rewards or liquid dietary content on learning in instrumental responding and found that rodents on liquid reward with higher caloric content performed better with increased response and task acquisition rate. The influence of reinforcer type on reversal learning and how this interacts with developmental insults such as prenatal alcohol exposure (PAE) has not been explored.

Methods: We tested whether reinforcer type during learning or reversal would impact an established deficit in PAE mice.

Results: We found that all male and female mice on liquid reward, regardless of prenatal exposure were better motivated to learn task behaviors during pre-training. Consistent with previous findings, both male and female PAE mice and Saccharine control mice were able to learn the initial stimulus reward associations irrespective of the reinforcer type. During the initial reversal phase, male PAE mice that received pellet rewards exhibited maladaptive perseverative responding whereas male mice that received liquid rewards performed comparable to their control counterparts. Female PAE mice that received either reinforcer types did not exhibit any deficits on behavioral flexibility. Female saccharine control mice that received liquid, but not pellet, rewards showed increased perseverative responding during the early reversal phase.

Discussion: These data suggest that reinforcer type can have a major impact on motivation, and therefore performance, during reversal learning. Highly motivating rewards may mask behavioral deficits seen with more moderately sought rewards and gestational exposure to the non-caloric sweetener, saccharine, can impact behavior motivated by those reinforcers in a sex-dependent manner.

KEYWORDS

reward value, touchscreen, development, FASD, non-nutrient sweetener

Introduction

Fetal alcohol spectrum disorders (FASDs) are the leading cause of preventable developmental disability (Popova et al., 2017, 2018) and are characterized by deficits in executive function

(Chudasama, 2011). Findings in children with FASD suggest that difficulties in planning, cognitive flexibility, and inhibition are better predictors of behavioral problems than intelligence-based measures (Mattson et al., 1999; Kodituwakku et al., 2001). Behavioral flexibility, one of the core dimensions of executive functioning, is crucial for an individual to adapt to the ever-changing environment. Impairment in behavioral flexibility is a common feature across neuropsychiatric and neurodevelopmental disorders, including FASD, and has also been documented in prenatal alcohol exposure (PAE) rodent models (Elliott, 2003; Holmes and Wellman, 2009; Chudasama, 2011). Reversal learning paradigms, which are widely used for assessing behavioral flexibility across species, have been shown to be consistently impaired by PAE across numerous routes of alcohol administration, doses, and assessment modalities including spatial, operant, tactile, and olfactory (Wainwright et al., 1990; Thomas et al., 2004; Marquardt et al., 2014; Atalar et al., 2016; Marquardt and Brigman, 2016; Waddell and Mooney, 2017).

Over the past ~20 years, numerous studies have demonstrated that the formation of a stimulus-outcome association during discrimination learning is mediated by the dorsal striatum (DS), whereas the reversal of these associations is mediated by cortical areas including the orbital frontal cortex (OFC) (Brigman et al., 2010c; Graybeal et al., 2011). For example, *in vivo* electrophysiology studies have shown that the DS mediates associative learning *via* the integration of state-action-outcome associations (Yin et al., 2009; Corbit et al., 2012; Brigman et al., 2013; Bergstrom et al., 2018), while the OFC encodes response outcomes and tracks changes in choice value (Schoenbaum et al., 2003; Bissonette et al., 2008; Moorman and Aston-Jones, 2014; Marquardt et al., 2017). Regardless of modality (e.g., spatial or operant), a common feature of most reversal tasks is the need to reinforce choice decisions (Bussey et al., 2008; Horner et al., 2013), while there are several reinforcers available, most operant tasks employ reinforcers either solid (e.g., dustless pellets) or increasingly, liquid sweetened reward (e.g., strawberry milkshake).

It has been increasingly recognized that reward type can have a major influence on incentive motivation to both learn an initial association and reverse previously learned associations. There is a broad range of reinforcers available from solid to liquid reinforcers (Horner et al., 2013), and several reports confirm that both the type and amount of the reinforcer affect the performance of rodents on various tasks used to assess cognition (Skjoldager et al., 1993; Eagle et al., 1999; Youn et al., 2012; Hutsell and Newland, 2013). The ability of three different inbred mice strains (BALB/c, C57BL/6, DBA/2) to respond on a fixed reinforcement schedule using qualitatively different reinforcers such as flavored pellets or milk was examined. Interestingly, mice reinforced with milk had higher response rates when compared to mice reinforced with pellets on moderate ratios (Hutsell and Newland, 2013).

Strawberry milkshake has been more commonly used as a reinforcer in touchscreen-based tasks (Phillips et al., 2017) following informal observations about it being a powerful reinforcer when testing cognition and behavior (Horner et al., 2013; Mar et al., 2013). Using touchscreen-based pairwise discrimination and reversal tasks, the reinforcer strength of strawberry milk was compared to that of super saccharine (1.5% or 2% (w/v) saccharin solution). Mice on strawberry milk acquired the task faster and performed fewer errors when compared to the mice on super saccharine, thus reaffirming the superior strength of strawberry milk and confirming the differential role of the type of reinforcement of the performance of behavioral assessment (Phillips et al., 2017). Furthermore, there exists diversity in the type of strawberry milk used based on its caloric content and the sweeteners it contains (Kim et al., 2017). It was observed that the caloric content of the liquid reinforcer determined the incentive value rather than the fat content, sugar content, or flavor of the reinforcer (Kim et al., 2017). Youn et al. (2012) reported a difference in performance on spatial memory tasks between two genetically different mouse strains and determined that it was due to differential reinforcer impact rather than genetic differences.

Previously, we have examined the effects of PAE on behavioral flexibility utilizing a touchscreen reversal task motivated *via* flavorless dustless 14 mg pellets. We showed that male and female PAE mice exhibit behavioral inflexibility, as measured by increased perseverative responses during the early stages of a reversal task (Marquardt et al., 2014, 2020). Given the increasing awareness that reinforcer type can alter performance on various behavioral tasks, we examined whether a more motivating reinforcer, such as strawberry milk, would change the performance of the PAE mice on the touchscreen-based discrimination and reversal task.

Materials and methods

Prenatal alcohol exposure model

Male and female C57BL/6J mice were used for all behavioral experiments (Figure 1). The moderate PAE model used here has been previously described (Brady et al., 2012, 2013). Briefly, following habituation, female C57BL/6J mice (Jackson Laboratory, Bar Harbor, ME) were gradually acclimated to drinking 10% (w/v) ethanol (EtOH) solution in a stepwise manner. Mice were first allowed to drink either 0.066% (w/v) saccharin or 5% (w/v) EtOH solution sweetened with 0.066% (w/v) saccharine for 4 h every day (from 10:00 to 14:00 h) for 4 days. Next, the concentration of EtOH solution was increased to 10% w/v sweetened with 0.066% (w/v) saccharin. This protocol has previously been shown to produce blood ethanol concentration (BEC) of 80–90 mg/dl (Brady et al., 2012, 2013) when tested at the end of the 4-h alcohol access period. After 7 days of drinking 10% EtOH or saccharin, female mice were placed in a cage along with a singly housed male for 2 h to enable mating immediately following drinking. The mating period lasted for 5 days during which female mice continued to have access to either 10% EtOH solution or saccharin control solution. Dams were weighed every 3–4 days to monitor weight gain, which indicates pregnancy. Following parturition, the access to EtOH solution or saccharin was weaned off using a step-down procedure over a 6-day period. Offspring produced from saccharin (SAC) and PAE dams were weaned at 21–23 days of age. The pups were then housed in same-sex pairs in cages in a temperature- and humidity-controlled environment under a reverse 12 h light/dark cycle (lights off at 8:00 h, on at 20:00 h). All the behavioral experiments were conducted during the dark phase in both male and female PAE and SAC control offspring (no more than 2/litter, $n = 8$ to 9 per sex/treatment; ~8–9 weeks at the onset of pretraining). All experimental procedures were performed in accordance with the National Institutes of Health Guide for Care and Use of Laboratory Animals and were approved by the University of New Mexico

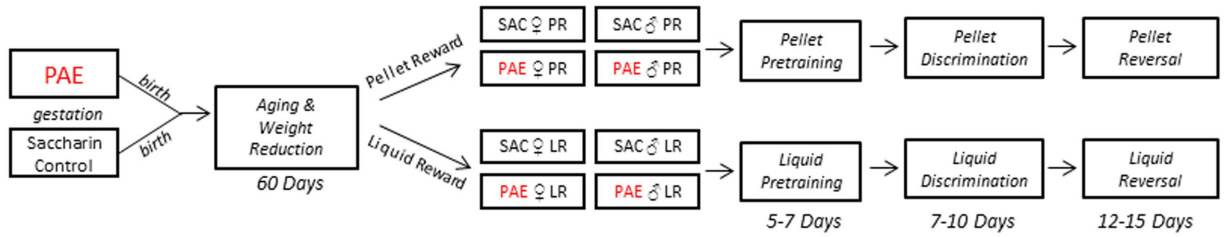


FIGURE 1
Experimental timeline of exposure and operant testing. Following weaning, mice were allowed to age to 8weeks prior to weight reduction and assignment to experimental reward groups. Mice then underwent pretraining to initiate and respond to visual stimuli. Following the acquisition of task behaviors, all mice underwent testing on pairwise discrimination followed by reversal learning. LR, liquid reward; PR, pellet reward.

Health Sciences Center Institutional Animal Care and Use Committee.

Operant apparatus

Behavioral flexibility was tested using a touchscreen-based discrimination and reversal learning paradigm, as described previously (Marquardt et al., 2014, 2020). Briefly, a sound- and light-attenuating box housed the operant chamber measuring 21.6 cm × 17.8 cm × 12.7 cm (model # ENV-307 W; Med Associates, St. Albans, VT). The floor of the chamber was a solid acrylic plate resting on the standard grid floor to facilitate ambulation. All chambers were equipped with both pellet dispensers (#F05684; Bio-Serv, Frenchtown, NJ) and peristaltic pumps (Lafayette Instruments, Lafayette, IN) to enable solid or liquid reward delivery into the magazine located at one end of the chamber. Beside the magazine is an ultra-sensitive lever. This end of the chamber is also equipped with a house light and a magazine light within the magazine. At the opposite end of the chamber is a touch-sensitive screen (Conclusive Solutions, Sawbridgeworth, United Kingdom) covered by a black acrylic aperture plate which allows two areas sensitive to touch (7.5 cm × 7.5 cm) which are separated by 1 cm and located at a height of 0.8 cm from the floor of the chamber. Stimulus presentation in the response windows and touches was controlled and recorded by the Limbic Software package (Conclusive Solutions).

Pretraining

Male and female mice were gradually weight-reduced over a 10–14 day period and then maintained at 85% of their free-feeding body weight. Mice were then acclimated to the behavioral testing room and to the chosen reward over a 3–4-day period. Male and female PAE and SAC mice were randomly assigned to either the liquid or pellet reward groups. During pretraining and testing, mice received either precision food pellet reward (PR: 14 mg dustless pellets, Bio-Serv) or sweetened strawberry milk (LR: 30 µl, Nesquik. S.A., Vevey, Switzerland, non-fat milk). The reward was placed in a weigh boat in the home cage, and the total amount consumed was recorded daily. Mice were then habituated to the operant chamber to retrieve the reward out of the magazine in 30 min. Mice retrieving 10 rewards within 30 min were then moved to pretraining. First, mice were trained to obtain a reward by pressing a lever within the chamber. Mice pressing the lever and collecting 30 rewards in under 30 min were moved to the next stage, touch training, where the lever press led to the presentation of a stimulus (variously shaped and equi-luminescent) in either one of the response windows (spatially pseudorandomized). The touches in the window with no image had no response and the stimulus remained on the screen until nose poke on the window with the image elicited a response. Mice initiating, touching, and retrieving 30 rewards within 30 minutes were moved to the final stage of pretraining: punished training. This stage is similar to the touch training except the responses at a blank window during stimulus presentation were now considered errors and resulted in turning on the house light for a 15 s time-out period to discourage indiscriminate screen responding. While the correct responses resulted in moving on to the next trial, errors were followed by correction trials where the same stimulus was presented in the same left/right position until a correct response was made. Mice getting ≥75% correct responses (excluding correction trials) in under 30 min were moved on to the testing stage, the discrimination stage.

Reward-based discrimination and reversal testing

All mice were tested on a pairwise discrimination-reversal paradigm where the mice learned to discriminate between two equi-luminescent stimuli followed by the reversal learning stage. The sessions lasted for a period of 60 min or until 30-first presentation trials were completed based on which criterion was reached first. During discrimination learning, two novel approximately equi-luminescent (Fan, Marbles) appeared on the touchscreen in a spatially pseudorandomized manner over 30-first presentation trials with a 5 s intertrial interval. The stimuli stayed on the screen until a response was made. Responses at one stimulus resulted in the reward (signaled by 1 s tone and magazine light turning on), while responses at the other stimulus resulted in a punishment time-out of 15 s (signaled by the house light turning on). Both the assignment of the initial stimulus and the reward type were randomized across treatment and both sexes. While the correct responses resulted in the reward followed by moving on to the next first presentation trial, errors on the first presentation trials were followed by correction trials where the same stimulus appeared on the same window until a correct response was made. Once the mice learned the stimulus reward association, where they were performing at ≥85% correct (excluding correction trials) over two consecutive days, they were considered to have reached the criterion and were moved onto the reversal stage. During the reversal

stage, in order to test the ability to behave flexibly, the stimulus-reward contingencies were simply switched. Previously correct choice resulting in the reward is now the incorrect choice resulting in punishment time-out and vice versa. Mice were tested on 30-trial 1-h daily sessions similar to the discrimination stage. They are considered to have reached the criterion in this stage, once they have re-learned the new stimulus reward association and performed at ≥85% correct over 2 consecutive days (excluding the correction trials). The testing period ends once they reach the reversal criterion.

Statistical analysis

For pretraining stages, the number of sessions required to pass each stage was analyzed by treatment (SAC vs. PAE) and reward (PR vs. LR) group. The following dependent measures were taken during discrimination and reversal: correct responses made, errors (i.e., incorrect responses made), and correction errors (i.e., correction trials made) which are a putative measure of perseveration during reversal (Brigman et al., 2013), stimulus-response (i.e., time from trial initiation to touchscreen response), and reward response (i.e., time from touchscreen response to reward retrieval). As correct and incorrect response measures were consistent in all analyses, incorrect responses and correction trials are reported throughout. Discrimination performance was analyzed across all sessions required to reach the criterion. In order to examine distinct phases of reversal (early perseverative and late learning), we separately analyzed errors and correction errors for sessions where performance was below 50% and performance from 50% to criterion, as previously described (Brigman et al., 2010b, 2013). The main effects of sex, treatment (PAE vs. SAC), reward (liquid vs. pellet), and interaction were compared for all measures using analysis of variance (ANOVA) followed by Tukey's *post-hoc* test using Prism (GraphPad Prism 9.4.1, San Diego, CA).

Results

PAE intake

We found that the limited access paradigm yielded ethanol consumption levels in dams similar to those producing BACs of approximately 80–90 mg/dl (Brady et al., 2012, 2013). Offspring tested were taken from litters born to dams with an average consumption of 4.66 ± 0.09 g of EtOH/kg of body weight/day and 1% SAC. No significant differences were seen in alcohol consumption for PAE mice tested on PR vs. LR or by sex (Table 1). However, the total saccharin intake was significantly higher for SAC animals regardless of sex or reward ($F1,64 = 69.19$, $p < 0.001$; Table 1).

Operant training

An analysis of the three-stage pretraining revealed a significant main effect of both sex ($F1,64 = 16.17$, $p < 0.001$) and reinforcer ($F1,64 = 12.92$, $p < 0.001$) during lever-press training. A *post-hoc* analysis showed male LR mice taking significantly fewer sessions than female PR mice. Following bar-press training, there were no significant differences by sex, reinforcer or treatment, or interactions in the touch training or punishment training stages (Table 1).

Discrimination learning

Consistent with previous reports, an analysis of pairwise discrimination learning revealed that female mice made significantly more errors ($F1,64 = 7.27$, $p < 0.001$; Figure 2A) and correction errors ($F1,64 = 7.17$, $p < 0.001$; Figures 2A,B) to attain criterion versus male mice. In addition, there was a significant sex × reinforcer × treatment interaction for errors ($F1,64 = 4.10$, $p = 0.04$) and correction errors ($F1,64 = 3.95$, $p = 0.05$). Male PAE mice made fewer errors and correction errors regardless of reinforcer group. In contrast, female PR-PAE mice made significantly more errors and correction errors than SAC controls, while female LR-PAE mice made significantly fewer errors and correction errors than the control (Figures 2A,B). Tukey's *post-hoc* tests additionally revealed that the female PR-PAE mice had significantly more correction errors than male LR-SAC ($p = 0.0458$), male LR-SAC ($p = 0.0094$), and male PR-PAE ($p = 0.0186$) mice. Interestingly, an analysis of secondary measures found a significant main effect of treatment on reaction time ($F1,64 = 5.00$, $p = 0.03$; Figure 2C) with PAE mice having faster response times with no main effect of sex, reinforcer, or interactions. In contrast, an analysis of latency to retrieve rewards revealed a significant main effect of the reinforcer ($F1,64 = 17.81$, $p < 0.0001$; Figure 2D) with LR mice retrieving reward faster with no main effect of sex or treatment and no significant interactions.

Reversal learning

An analysis of errors made across the entire reversal problem revealed a significant reinforcer × treatment interaction ($F1,64 = 7.28$, $p < 0.001$) and a significant sex × treatment ($F1,64 = 4.03$, $p = 0.04$) effect for errors (Figure 3A). Both male and female PR-PAE mice performed more poorly than LR-SAC mice, with male LR-PAE mice performing significantly worse. In contrast, female LR-SAC mice performed significantly worse than female LR-PAE mice, while male LR mice did not significantly differ (Figure 3A). An analysis of correction trials found a significant main effect of sex ($F1,64 = 6.64$, $p = 0.01$) and a sex × reinforcer

TABLE 1 Performance on training sessions (average sessions to criterion ± SEM).

Training stages	Liquid reward				Pellet reward			
	SAC		PAE		SAC		PAE	
	Male	Female	Male	Female	Male	Female	Male	Female
Lever press	2.10 ± 0.3	3.25 ± 1.0	2.27 ± 0.1	3.14 ± 0.8	3.25 ± 0.4	4.90 ± 0.9	2.75 ± 0.3	6.5 ± 0.7
Touch	4.3 ± 0.8	3.13 ± 0.5	3.18 ± 0.5	3.14 ± 0.3	3.25 ± 0.4	3.20 ± 0.5	2.63 ± 0.6	4.10 ± 0.4
punish	1.00 ± 0.0	1.00 ± 0.0	1.00 ± 0.0	1.00 ± 0.0	1.00 ± 0.0	1.10 ± 0.1	1.00 ± 0.0	1.20 ± 0.2

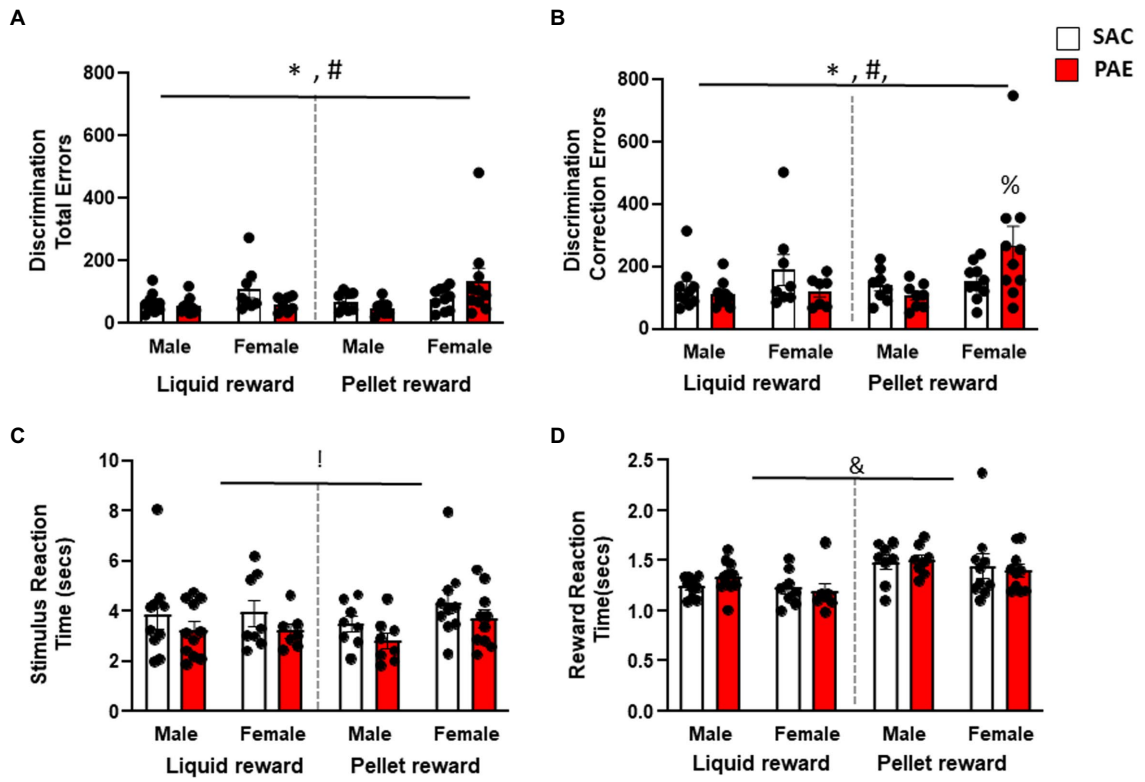


FIGURE 2
Sugar-sweetened liquid reinforcer (LR) is significantly more motivating than unsweetened pellet reinforcer (PR) during the initial phase of discrimination learning. **(A)** Female mice performed significantly more errors than male mice during the initial discrimination phase with female PAE PR mice making the most errors. **(B)** Female mice made significantly increased perseverative errors than the male mice during initial discrimination learning again driven by PAE PR female mice. **(C)** PAE mice had significantly reduced stimulus reaction times regardless of sex or reinforcer. **(D)** Liquid-reinforced mice had significantly shorter reward retrieval latencies when compared to pellet-reinforced mice. *=p<0.05 main effect of sex, !=p<0.05 main effect of treatment, &=p<0.05 main effect of reinforcer, †=p<0.05 sex × reinforcer interaction, ‡=p<0.05 sex × treatment reinforcer, ∑=p<0.05 reinforcer×treatment, #=p<0.05 sex×treatment×reinforcer; %=significant Tukey's *post-hoc* test. Data are group mean±SEM.

(F1,64 = 5.51, p = 0.02), sex × treatment (F1,64 = 15.56, p < 0.001), and reinforcer × treatment (F1,64 = 18.19, p < 0.001). Similar to total errors, male and female PR-PAE mice made more correction errors than LR-SAC mice, with male LR-PAE mice making significantly more perseverative errors. As in the error analysis, female LR-SAC mice made significantly more correction errors than femaleLR-PAE mice, while male LR mice did not significantly differ by treatment (Figure 3B). Furthermore, Tukey's *post-hoc* test revealed that the female LR-SAC mice had significantly greater correction errors than all the other groups except male PR-PAE such as female LR-PAE (p = 0.0003), female PR-SAC (p = 0.0023), female PR-PAE (p = 0.0037), male LR-SAC (p = 0.0001), male LR-PAE (p < 0.0001), and male PR-SAC (p < 0.001) mice. An analysis of secondary measures found no significant difference in stimulus reaction time, while an analysis of latency to retrieve rewards again revealed a significant main effect of the reinforcer (F1,64 = 5.45, p < 0.002; Figures 3C,D) with LR mice retrieving rewards faster with no main effect of sex or treatment and no significant interactions (Figure 3D).

Reversal stage analysis

To examine the pattern of learning across the reversal problem, errors and correction errors were analyzed separately for early perseverative (<50% correct) and later learning (≥50%) sessions. An analysis of total errors during early perseverative sessions (Figure 4A) revealed a significant main effect of sex (F1,64 = 4.46, p = 0.0387), a reinforcer × treatment interaction (F1,64 = 9.35, p = 0.0033), and a sex × reinforcer × treatment interaction (F1,64 = 5.41, p = 0.0232; Figure 4A). Similarly, an analysis of correction errors during the early perseverative phase (Figure 4B) found a main effect of sex (F1,64 = 9.524, p = 0.003), a significant sex × reinforcer (F1,64 = 4.312, p = 0.04), sex × treatment (F1,64 = 16.53, p = 0.0001), and reinforcement × treatment (F1,64 = 13.18, p = 0.0006) effect for profound perseverative impairment in PAE mice. Furthermore, Tukey's *post-hoc* test revealed that female LR-PAE mice had significantly more correction errors than all other groups except male PR-PAE such as female LR-PAE (p = 0.0013), female PR-SAC (p = 0.0127), female PR-PAE (p = 0.037), male LR-SAC (p < 0.0001), male LR-PAE (p = 0.004), and male PR-SAC (p < 0.0001) mice. An analysis of the later learning stage of reversal (Figure 4B) found no significant differences for total errors and a significant reinforcer × treatment effect for correction errors (F1,64 = 4.86, p = 0.031), whereby male LR-PAE mice made significantly more correction errors on learning, while female PR-SAC again made significantly more errors of this type. Reversal performance *via* correction errors once animals had attained chance found no main effect of sex, treatment, or reinforcer and no significant interactions (Figure 4B). Similar to discrimination performance, analysis of latency

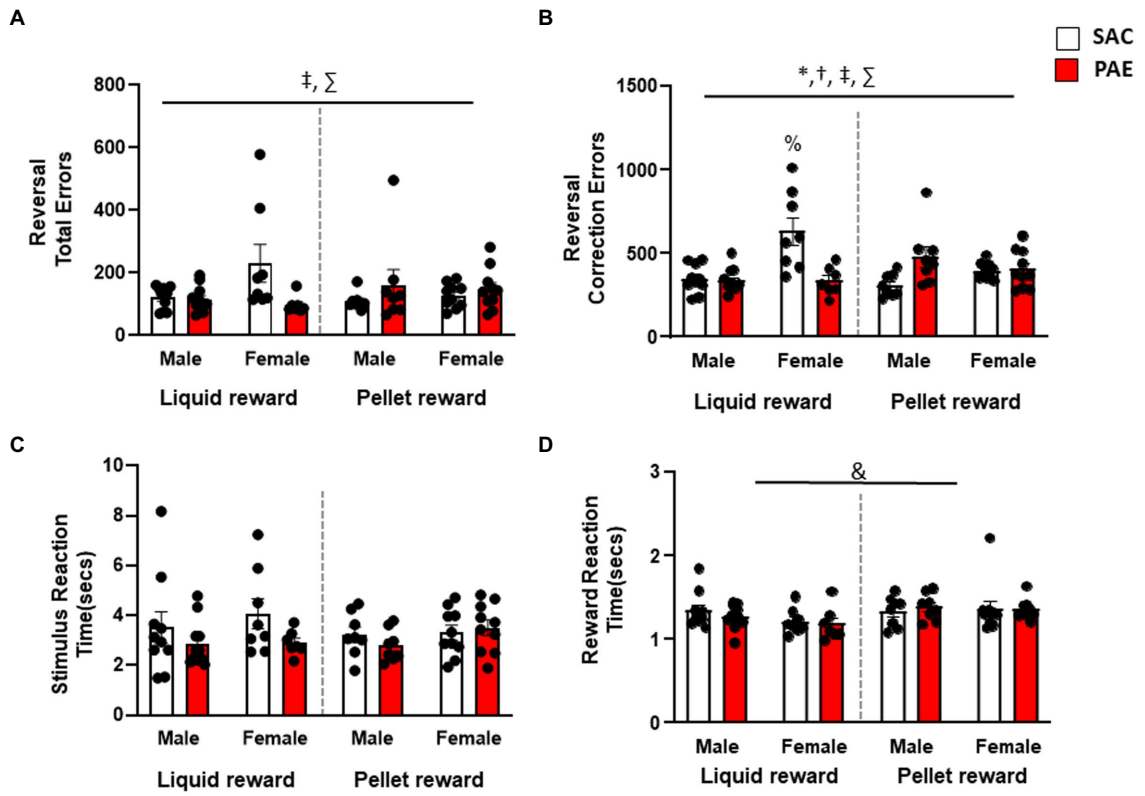


FIGURE 3
Reversal performance differed by sex and treatment depending on reward type. **(A)** Analysis of total errors during the reversal session showed that male PR-PAE mice were significantly worse than SAC controls, while female LR-SAC mice made significantly more errors than PAE female mice. **(B)** Analysis of total perseverative errors during the reversal session showed a similar pattern in which male PR-PAE mice were significantly worse than SAC controls, while female LR-SAC mice made significantly more errors than PAE female mice. **(C)** No significant differences were seen in stimulus reaction time across the reversal problem. **(D)** LR mice were significantly more motivated than the pellet-reinforced mice in both treatment groups and both sexes as measured by reward reaction time. *=p<0.05 main effect of sex, !=p<0.05 main effect of treatment, &=p<0.05 main effect of reinforcer, †=p<0.05 sex×reinforcer interaction, ‡=p<0.05 sex×tretatment reinforcer, ∑=p<0.05 reinforcer×treatment, #=p<0.05 sex × treatment × reinforcer; %=significant Tukey's *post-hoc* test. Data are group mean±SEM.

to retrieve reward revealed a significant main effect of reinforcer on sessions where performance was below 50% correct ($F1,64 = 6.69$, $p = 0.04$; Figure 4D) with no main effect of sex or treatment and no interactions. Interestingly, there was a significant main effect of treatment ($F1,64 = 5.59$, $p = 0.04$) on stimulus reaction time with PAE mice making significantly faster choices when performing above, but not below, 50% accuracy (Figure 4C).

Trial-type analysis

In order to characterize changes in behavioral patterns across the different trial types, data were analyzed as pairs of consecutive responses to determine the total number of correct responses followed by another correct response (win→stay), error responses followed by a correct response (lose→shift), correct responses followed by an error (regressive), and error responses followed by another error (lose→stay). The total number of each pair type was analyzed separately for reward type during early perseverative (<50% correct) sessions and later learning (≥50%) sessions. Analysis of the total number of trial types performed during the early perseverative phase in the LR group (Figure 5A) revealed the main effect of sex ($F1,128 = 16.98$, $p < 0.0001$), treatment ($F1,128 = 16.86$, $p < 0.0001$), trial types ($F3,128 = 110.2$, $p < 0.0001$), trial type × treatment ($F3,128 = 4.35$, $p = 0.0059$), and sex × treatment ($F1,128 = 21.98$, $p < 0.0001$) effects, whereby female mice performed more number of all trial types driven by female LR-SAC mice with more lose→stay responses (Figure 5A). An analysis during the later learning stage (Figure 5B) revealed the main effect of sex ($F1,128 = 12.49$, $p = 0.006$), treatment ($F1,128 = 6.129$, $p = 0.0146$), and trial types ($F3,128 = 19.52$, $p < 0.0001$). While lose→stay trials predominated during the early perseverative phase, as the mice re-learned the changed stimulus reward associations during the late learning stage, there was a change in the trial types being performed with an increase in win→stay trial type (Figures 5A,B). Female LR-SAC mice had an overall increase in the number of total trials being performed, specifically increased lose→stay trials during the early perseverative phase. A similar analysis performed in the PR group during the early perseverative phase (Figure 5C) revealed the main effect of sex ($F1,128 = 4.014$, $p = 0.0449$), treatment ($F1,128 = 4.309$, $p = 0.0399$), and trial types ($F3,128 = 92.37$, $p < 0.0001$) with increased lose→stay trial type predominating among both treatment groups in male and female mice, female mice performing more number of total trials when compared to male mice similar to the LR group. Male PR-PAE mice

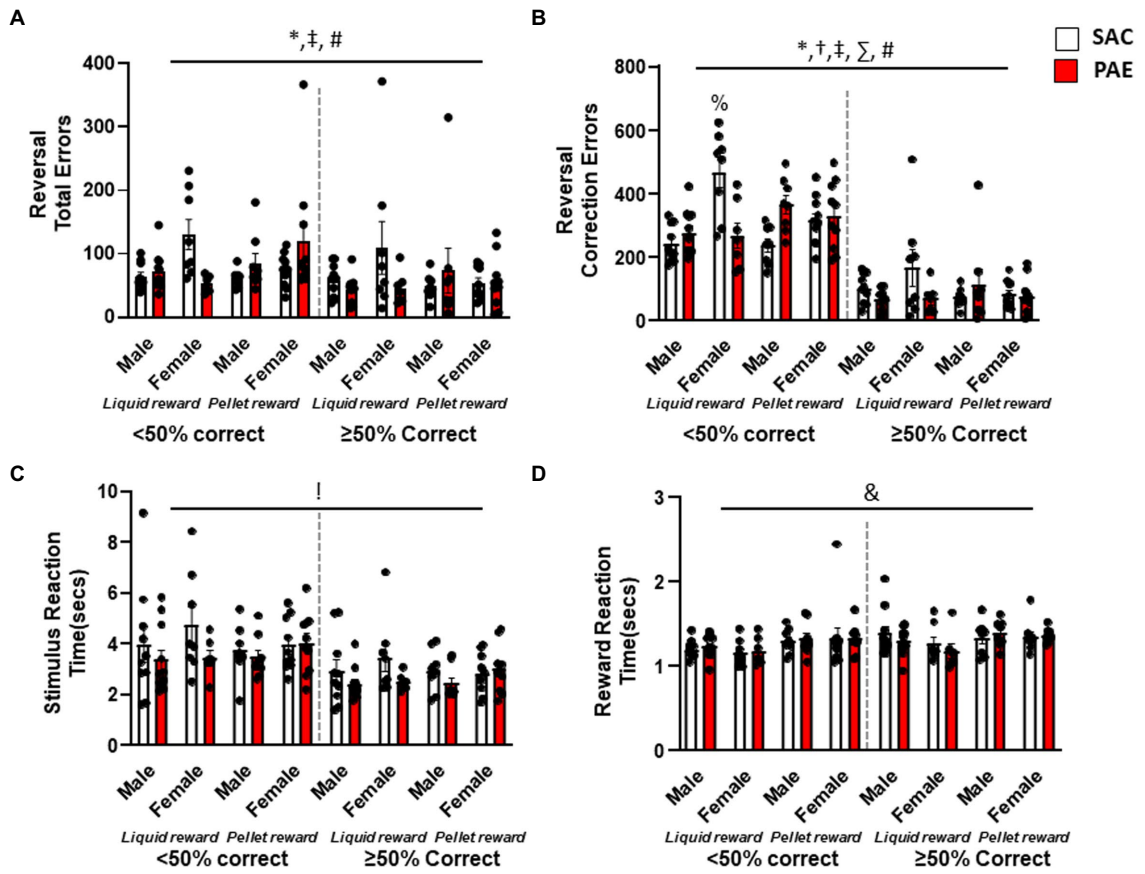


FIGURE 4
Sugar-sweetened liquid reinforcement changes the effects of moderate prenatal alcohol exposure. **(A)** Analysis of total errors during the early perseverative phase (when mice performed <50% correct) showed that female mice had significantly more errors when compared to male mice, with female LR-SAC mice making significantly more errors, while PR-PAE male and female? mice were significantly worse than the controls. **(B)** Similarly, male PR-PAE mice showed increased perseverative responding when compared to saccharine control mice but not on liquid reinforcement. No deficit following prenatal alcohol exposure was seen in female mice in either of the reinforcement groups, while female saccharine control mice on liquid reinforcer showed increased perseverative responding when compared to PAE mice. **(C)** No difference in motor behaviors was seen during the early perseverative phase, but PAE mice had faster stimulus reaction time when compared to saccharine control mice during the late reversal phase. **(D)** Liquid-reinforced mice were significantly faster to retrieve the reward during the early perseverative phase. *=p<0.05 main effect of sex, !=p<0.05 main effect of treatment, &=p<0.05 main effect of reinforcer, †=p<0.05 sex × reinforcer interaction, ‡=p<0.05 sex × tretatment reinforcer, ∑=p<0.05 reinforcer × treatment, #=p<0.05 sex × treatment × reinforcer; %=significant Tukey's *post-hoc* test. Data are group mean±SEM.

had a non-significant increase in the perseverative trial type, lose→stay when compared to the male PR-SAC mice (Figure 5C). Interestingly, in the PR group, PAE mice performed more trials when compared to the SAC mice but in the LR group with female LR-SAC mice performing an excessive number of all trial types, SAC mice had more total trial types than the PAE mice (Figures 4A,C). Furthermore, an analysis during the later learning stage (Figure 5D) showed the main effect of trial type ($F3,128 = 24.20$, $p < 0.0001$) with win→stay trial type predominating in both treatment groups in male and female mice.

Correlational analysis with saccharine intake

To further investigate the unexpectedly increased perseverative behavior among the female LR-SAC mice, we performed the correlational analysis with the amount of maternal saccharine intake to the trial types. Female mice showed a positive correlation of saccharine intake to the number of correction errors ($r^2 = 0.2621$, $p = 0.0255$; Figure 6A) and the total number of lose→stay trial types ($r^2 = 0.2401$, $p = 0.0319$; Figure 6B), indicating that the maladaptive perseverative behavior might be related to the saccharine intake.

Discussion

We have previously shown that moderate PAE during the first- and second-trimester equivalent is sufficient to impair reversal by increasing perseverative responding during the early stages of a pellet-rewarded reversal learning task (Marquardt et al., 2014, 2020). In the current study, we compared the efficacy of two reward types, high-sugar LR and low-calorie compressed food PR used previously. We found that liquid reinforcement drove faster initial training as LR mice were able to acquire the initial lever training at a significantly faster rate when compared to mice on PR in both sexes. We also show that LR mice were more reward focused, as measured by latency to retrieve rewards, through the entire course of the behavioral paradigm.

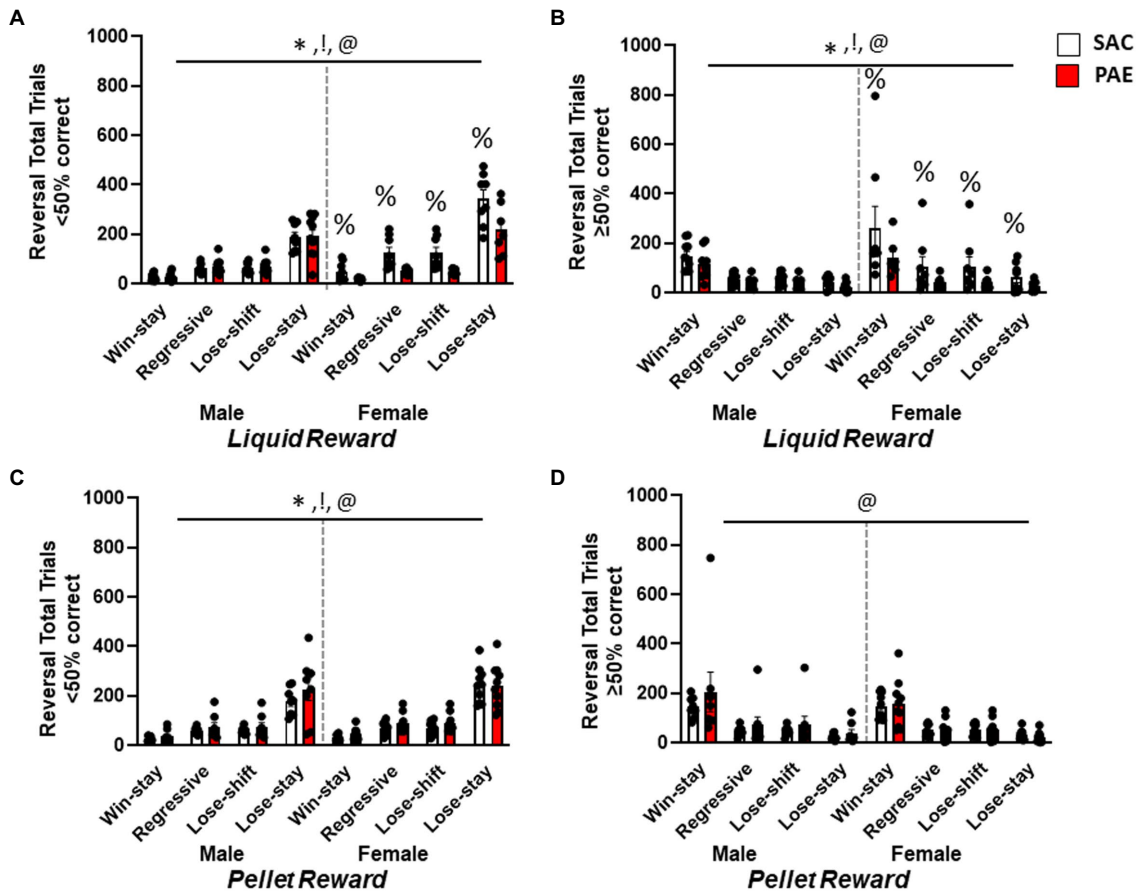


FIGURE 5
Female saccharine control mice had an increased number of all trial types during reversal learning. **(A)** Analysis of trial types for liquid-reinforced mice revealed a significant main effect of sex and treatment trial type whereby all mice made significantly more Lose→Stay trials than any other type. Female LR-SAC mice made a significantly increased number of Lose→Stay trial types when compared to liquid-reinforced female PAE mice. **(B)** In the liquid-reinforced group, during the learning phase (when mice were performing ≥50% correct), there was a significant main effect of sex, treatment, and trial type as the Win→Stay trial type predominated when compared to all other trial types. Female SAC LR mice had an increased number of total trials when compared to liquid-reinforced female PAE mice. **(C)** Analysis of trial types for pellet-reinforced mice showed a main effect of sex, treatment, and trial type whereby all mice made significantly more lose-stay trials, female mice made more of all trial types and PAE mice made significantly more of all trials. **(D)** When trial types were analyzed for learning sessions (when mice were performing ≥50% correct), there was a main effect of trial type whereby all mice made significantly more win-stay trials. *=p<0.0005 main effects of sex, !=p<0.0005 main effect of treatment, @=p<0.0001 main effect of trial type; %=significant Tukey's *post-hoc* test vs. SAC. Data are group mean±SEM.

Interestingly, male PAE mice rewarded with pellets (PR-PAE) again demonstrated impaired behavioral flexibility during early reversal learning (Marquardt et al., 2014, 2020). However, this effect was not seen in male LR-PAE mice. In contrast, female LR-SAC mice showed significantly *increased* perseveration during reversal. Together, our data underscore the importance of the motivational value of the reinforcers and suggest a critical need to examine how the reward content can alter performance and interact in unexpected ways with alcohol exposure and even saccharine during development.

Increasingly, the behavioral neuroscience community has focused on the standardization of behavioral paradigms to improve the reliability, reproducibility, and accuracy of translational neuroscience research (Steckler, 2015; Kim et al., 2017). The use of touchscreen-based operant testing with automated systems and computerized data collection has helped increase the standardization of testing protocols (Bussey et al., 2008; Brigman et al., 2010a; Horner et al., 2013; Dumont et al., 2021). However, the use of reinforcers, an essential motivational component of behavioral testing, has not been standardized (Kim et al., 2017; Phillips et al., 2017). Various types of liquid vs. solid reinforcers with different caloric values, fat and sugar content, and taste have been used in various studies. It has been repeatedly demonstrated that liquid rewards, particularly high-sugar strawberry milkshakes, are powerful reinforcers that enhance the performance of animals in operant touchscreen-based behavioral paradigms (Hutsell and Newland, 2013; Heath et al., 2015; Phillips et al., 2017). Although flavored pellets and sugar pellets have been used as reinforcers, to our knowledge, no study has directly compared their motivational value to highly potent liquid reinforcers. An added benefit of liquid rewards is that they avoid potential difficulties with solid food reinforcers such as dry mouth, difficulty in chewing, and satiety which can be particularly acute among inbred strains (Horner et al., 2013; Kim et al., 2017). Among liquid reinforcers, milk-based reinforcers such as high-sugar strawberry milkshakes are preferred over non-milk-based saccharine solutions (Phillips et al., 2017). In addition, liquid rewards with higher caloric content have been shown to speed operant training acquisition rates and reduce the duration of testing (Kim et al., 2017)

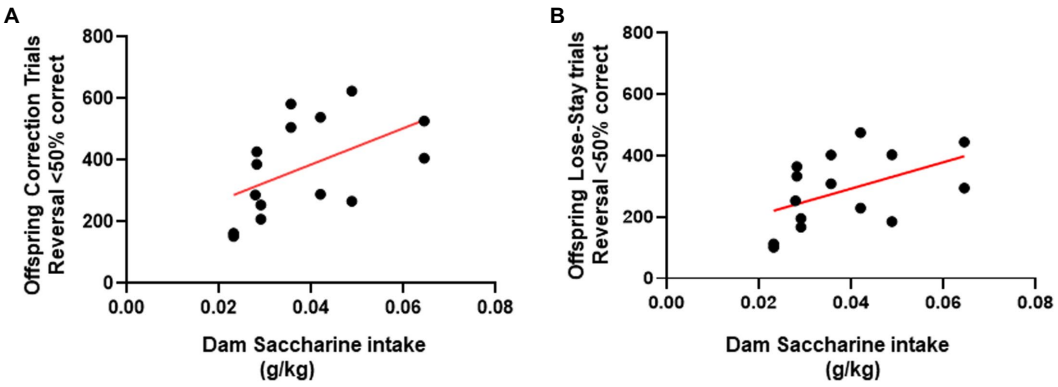


FIGURE 6
Female saccharine intake positively correlated with the perseverative trial types during the early perseverative reversal phase. **(A)** Saccharine intake in female mice positively correlated with the total number of correction errors performed during the early perseverative reversal phase. **(B)** Saccharine intake in female mice positively correlated with the total number of lose-stay errors performed during the early perseverative reversal phase. *=$p<0.05$, r^2 =0.2621, #=$p<0.05$, r^2 =0.2401.

which has led to them being widely adopted. As touchscreen-based approaches have become commonly used to test a host of behavioral domains, animal models of various disorders, and now cross-species translation approaches (Nithianantharajah et al., 2015; MacQueen et al., 2018; Cavanagh et al., 2021), the role that reinforcer types play in training and task performance becomes increasingly important.

Our current results show that mice on LR were significantly faster to pass the initial lever-press training with both PAE and SAC male and female LR mice having faster initial stage training versus PR mice. This observation is directly in line with several studies showing that liquid reinforcers, especially rewards with higher caloric value, had a faster operant training acquisition rate (Hutsell and Newland, 2013; Kim et al., 2017; Phillips et al., 2017). It is a commonly employed practice to reduce the rodents to 85% of their free-feeding weight to motivate them to perform the task (Marquardt et al., 2014) and internal states such as satiety and preference for the type of food reward can directly alter brain reward circuits (de Araujo et al., 2008). It is hypothesized that this difference in the level of motivation in turn affects the performance of the rodents on the operant tasks (Kim et al., 2017).

Consistent with our previous findings, our current data show that neither male nor female PAE mice differed from SAC mice on initial discrimination learning, although the analysis of secondary measures suggests reward type did alter motivation. LR mice had significantly shorter reward response times, suggesting that they were more motivated to perform the task when compared to PR mice. In addition, we also found sex-specific differences such as female mice taking longer to learn the initial discrimination association and making more errors than male mice, which is directly in line with our previous observation (Marquardt et al., 2014).

We have previously shown that both male and female PR-PAE mice exhibited behavioral inflexibility during the early reversal phase by performing an increased number of perseverative responses when compared to the saccharine control mice (Marquardt et al., 2014). Furthermore, single unit recording studies revealed that PAE decreased OFC while increasing DS firing rate during reversal learning. PAE also resulted in decreased oscillatory field activity between OFC and DS, thereby resulting in decreased coordinated activity between the two regions which is essential for efficient flexible behavior (Marquardt et al., 2020). Here, we found that male PR-PAE mice exhibited behavioral inflexibility as shown by an increase in correction trials during the early phase of reversal. However, male LR-PAE mice performed at levels comparable to controls, although both groups had similar average alcohol exposure *in utero*. Similar to discrimination performance, male LR mice had significantly shorter reward latencies compared to PR mice, suggesting a stronger motivation to retrieve reward during reversal. Together, the lack of perseverative responding and shortened reward latencies suggest that the highly motivational quality of the liquid reward was sufficient to overcome the effects of moderate PAE. Interestingly, enhancing motivational state has been shown to improve cognitive performance in rodents (Avlar et al., 2015) and humans (Nieto-Márquez et al., 2021) and has provided a framework for using intrinsic motivation states to improve cognitive abilities in neurodegenerative (Braver et al., 2014; Manera et al., 2017; Ruiz-González et al., 2021), neurodevelopmental (Prins et al., 2011; Demurie et al., 2012), and neuropsychiatric disorders (Choi and Medalia, 2010). The current data suggest that the motivational state may be a target for enhancing therapeutic efficacy in FASD.

Female PR-PAE mice showed a non-significant increase in errors and correction errors, while female LR-PAE mice showed no behavioral deficit during the early perseverative stage of reversal. Several factors may be contributing to the lack of significant impairment in female mice including the total exposure level in the current cohorts. Dams in the current study drank an average of 4.66 ± 0.09 g of EtOH/kg of body weight/day whereas our previous studies (Marquardt et al., 2014) utilized dams with an average drinking of 6.31 ± 0.34 g of EtOH/kg of body weight/day, suggesting that the critical exposure amount before deficits are seen may differ depending on the sex of the offspring. Perhaps most strikingly, we found that female LR-SAC mice showed the highest levels of perseveration, as measured by correction trials during the early phase of reversal. These levels were well outside what is typically seen in either male or female control animals when utilizing PR and were wholly unexpected because no study has reported any behavioral deficits in the control mice exposed to saccharine alone during the gestational period to our knowledge. We investigated if the level of saccharine intake by the dams could influence the performance of the pups and found that both male and female control mice had significantly increased

amounts of saccharine intake when compared to the PAE mice (Table 2). This was because of the overall increase in fluid consumption by the control mice. The lack of bitter taste which was present in the saccharine-sweetened alcohol solution given to PAE mice and the improved taste of the drinking water by the addition of saccharine is thought to be the cause of increased fluid intake in the control mice and thus resulting in increased saccharine intake.

Saccharine intake in female LR-SAC mice showed a positive correlation with the number of perseverative errors and the lose-stay trial type, suggesting that the increase in maternal saccharine intake during pregnancy affected the cognitive ability of the pups, especially when engaging in goal-directed or stimulus-driven tasks rewarded with sweetened strawberry milk with high reward value. Pre-clinical studies examining the effects of prenatal exposure to sugar have shown that increased sugar consumption during pregnancy can alter the reward circuitry in the newborn. Specifically, dams given high fat, high-sugar diet 4 weeks prior and during the entire period of gestation had offspring that later exhibited an increased preference for palatable, high-caloric food driven by the permanent changes in the mesolimbic reward system such as increased expression of mu-opioid receptor mRNA and decreased expression of dopamine transporter DAT (Ong and Muhlhausler, 2011). Increased maternal sugar consumption has also been found to increase apoptosis and alter apoptotic signaling factors in the hippocampus of rats exposed to prenatal high-sugar diets concomitant with deficits in spatial acquisition tasks (Kuang et al., 2014). Data from human studies have shown similar findings. Project Viva, a prospective observational cohort study in humans conducted to understand the effects of both increased maternal and child sugar consumption on the child's cognition, found that increased maternal sugar consumption particularly from sugar-sweetened beverages during pregnancy negatively impacted children's learning and memory (Cohen et al., 2018). Together, these data suggest that prenatal exposure consumption of high sugar can negatively impact cognitive abilities. In contrast, little is known about how PAE alters hedonic value for rewards during adolescence and adulthood. While it has been shown that prenatal exposure in humans can lead to increased appetitive responses to alcohol-associated cues later in life, less is known about responses to non-alcohol rewards (Faas et al., 2015). In one rodent study, male mice exposed to alcohol *via* an *ad libitum* liquid diet during gestation and then given chronic unpredictable stress were shown to have significantly decreased intake of high-content sucrose during preference testing, but how PAE alone affects preference for sweetened rewards has not been examined in detail (Hellemans et al., 2010).

In our current study, dams were exposed to saccharine which is a non-nutritive sweetener (NNS), which has comparable hedonic value as sugar while being calorie deficient. Nutrient intake is regulated by both the hedonic value and nutrient value of the food, which are encoded by different neuronal circuitry and the dorsal and ventral striatum, respectively. NNS, having no nutritive value, may have differential effects on the satiety center and post-ingestion neuroendocrine signaling that could later influence preferences for sweetened rewards *via* alterations in glycemic control and altered gut microbiome. This is supported by a randomized cross over trial which found that sucralose, a NNS, altered both appetite and reward processing using fMRI (Yunker et al., 2021). Female participants with obesity on NNS consuming more calories and showing greater neuronal responses to food cue in the medial frontal cortex and orbito-frontal cortex. NNS consumption may also affect offspring during development and infancy, as studies have confirmed that NNS can be transferred to the fetus through the placenta and to the infant *via* breast milk (Palatnik et al., 2020). Prenatal and postnatal exposure to NNS has been shown to significantly alter the microbiome and metabolic alterations in rodents and in humans (Englund-Ögge et al., 2012; Olivier-Van Stichelen et al., 2019). Specifically, maternal consumption of NNS during pregnancy and lactation enhances sweet preference and lowers the preference thresholds (Zhang et al., 2011; Chen et al., 2013) and metabolic dysregulation in the offspring (Araújo et al., 2014; Olivier-Van Stichelen et al., 2019).

Overall, our findings of intact reversal learning for low-sugar food pellets and impaired reversal for high-sugar liquid reinforcers in female mice exposed to NNS during development suggest an important role for motivated cognition in reversal learning. Cognition and motivation are not separate subsystems but rather integrated processes (Yarrow and Messer, 1983; Hughes and Zaki, 2015; Madan, 2017) involved in goal-directed behavior across species (Chiew and Braver, 2011; Braver et al., 2014; Botvinick and Braver, 2015; Bergstrom et al., 2018). Corticostriatal networks involved in behavioral flexibility (Brigman et al., 2013; Marquardt et al., 2017), working memory (Gilbert and Fiez, 2004), inhibitory control (Gilbert and Fiez, 2004; Diamond, 2013), and temporal cognition (Avlar et al., 2015) have been shown to process information regarding motivational states. Human imaging studies have shown that the lateral prefrontal cortex acts as a confluence zone where the information regarding cognition and motivation is integrated (Braver et al., 2014; Botvinick and Braver, 2015), and motivational state is thought to drive cognitive processing in the prefrontal cortex by affecting the preparatory processing such as selective attention, perception, and action selection (Hughes and Zaki, 2015). Furthermore, the neuromodulatory effects of dopamine both at cellular and circuit levels in the cortex and striatum have been strongly implicated as a candidate for mediating the cognition–motivation interaction (Braver et al., 2014). To date, it is not well understood how differences in the motivational state might affect behavioral flexibility in rodents, but there is evidence to suggest that motivation for reward plays a large part in determining the performance in behavioral tasks such as reversal learning. Our findings, that SAC Female mice have discrimination rates similar to control regardless of reinforcer and significantly impaired reversal

TABLE 2 Average intake (g/kg±SEM).

Intake g/kg	Liquid reward				Pellet reward			
	SAC		PAE		SAC		PAE	
	Male	Female	Male	Female	Male	Female	Male	Female
Saccharine	0.047 ± 0.002	0.048 ± 0.004	0.027 ± 0.001	0.027 ± 0.001	0.052 ± 0.004	0.049 ± 0.003	0.027 ± 0.001	0.028 ± 0.001
EtOH	N/A	N/A	4.286 ± 0.164	4.481 ± 0.175	N/A	N/A	4.561 ± 0.169	4.624 ± 0.143

only to high-sugar rewards, suggest that gestational exposure to NSS that improves motivated learning may conversely impair flexible choices when motivation is high. In addition, the hedonic value of the rewards used may have profound effects on results with models of neurodevelopmental insults including PAE by altering brain reward circuitry (de Araujo et al., 2008).

In conclusion, we found that moderate PAE results in maladaptive perseveration, and this behavioral response is dependent on the motivating factors present such as the reinforcer type. Sugar-sweetened liquid reinforcers are more powerful and have better motivational value when compared to unsweetened solid reinforcers with lesser hedonic value. These results suggest that prenatal saccharine exposure alters the response to high-sugar rewards during adulthood and underlines the importance of understanding the influence of hedonic systems in driving the motivational state of rodents being trained on operant tasks. While there are no current standards set for NNS intake during pregnancy, our current results also underline the need to carefully examine the effects of NNS, and NNS plus alcohol intake on later behavior in offspring.

Data availability statement

The raw data supporting the conclusions of this article will be made available by the authors, without undue reservation.

Ethics statement

The animal study was reviewed and approved by University of New Mexico Health Sciences Center Institutional Animal Care and Use Committee.

Author contributions

JC designed and conducted experiments, analyzed data, and wrote the manuscript. BJ and JW conducted experiments and analyzed data. JB conceived the research, analyzed data, and wrote the manuscript. All authors contributed to the article and approved the submitted version.

Funding

This manuscript was supported by the National Institute on Alcohol Abuse and Alcoholism grants P50AA022534 and R01-AA025652. Data are available upon request from the authors.

Conflict of interest

The authors declare that the research was conducted in the absence of any commercial or financial relationships that could be construed as a potential conflict of interest.

Publisher's note

All claims expressed in this article are solely those of the authors and do not necessarily represent those of their affiliated organizations, or those of the publisher, the editors and the reviewers. Any product that may be evaluated in this article, or claim that may be made by its manufacturer, is not guaranteed or endorsed by the publisher.

References

Araújo, J. R., Martel, F., and Keating, E. (2014). Exposure to non-nutritive sweeteners during pregnancy and lactation: impact in programming of metabolic diseases in the progeny later in life. *Reprod. Toxicol.* 49, 196–201. doi: 10.1016/j.reprotox.2014.09.007

Atalar, E. G., Uzbay, T., and Karakas, S. (2016). Modeling symptoms of attention-deficit hyperactivity disorder in a rat model of fetal alcohol syndrome. *Alcohol Alcohol.* 51, 684–690. doi: 10.1093/alcalc/agw019

Avlar, B., Kahn, J. B., Jensen, G., Kandel, E. R., Simpson, E. H., and Balsam, P. D. (2015). Improving temporal cognition by enhancing motivation. *Behav. Neurosci.* 129, 576–588. doi: 10.1037/bne0000083

Bergstrom, H. C., Lipkin, A. M., Lieberman, A. G., Pinard, C. R., Gunduz-Cinar, O., Brockway, E. T., et al. (2018). Dorsolateral striatum engagement interferes with early discrimination learning. *Cell Rep.* 23, 2264–2272. doi: 10.1016/j.celrep.2018.04.081

Bissonette, G. B., Martins, G. J., Franz, T. M., Harper, E. S., Schoenbaum, G., and Powell, E. M. (2008). Double dissociation of the effects of medial and orbital prefrontal cortical lesions on attentional and affective shifts in mice. *J. Neurosci.* 28, 11124–11130. doi: 10.1523/JNEUROSCI.2820-08.2008

Botvinick, M., and Braver, T. (2015). Motivation and cognitive control: from behavior to neural mechanism. *Annu. Rev. Psychol.* 66, 83–113. doi: 10.1146/annurev-psych-010814-015044

Braver, T. S., Krug, M. K., Chiew, K. S., Kool, W., Westbrook, J. A., Clement, N. J., et al. (2014). Mechanisms of motivation-cognition interaction: challenges and opportunities. *Cogn. Affect. Behav. Neurosci.* 14, 443–472. doi: 10.3758/s13415-014-0300-0

Brady, M. L., Allan, A. M., and Caldwell, K. K. (2012). A limited access mouse model of prenatal alcohol exposure that produces long-lasting deficits in hippocampal-dependent learning and memory. *Alcohol Clin Exp Res* 36:457–466. doi: 10.1111/j.1530-0277.2011.01644.x

Brady, M. L., Diaz, M. R., Iuso, A., Everett, J. C., Valenzuela, C. F., and Caldwell, K. K. (2013). Moderate prenatal alcohol exposure reduces plasticity and alters NMDA receptor subunit composition in the dentate gyrus. *J Neurosci*, 33:1062–1067. doi: 10.1523/JNEUROSCI.1217-12.2013

Brigman, J. L., Daut, R. A., Wright, T., Gunduz-Cinar, O., Graybeal, C., Davis, M. I., et al. (2013). GluN2B in corticostriatal circuits governs choice learning and choice shifting. *Nat. Neurosci.* 16, 1101–1110. doi: 10.1038/nn.3457

Brigman, J. L., Graybeal, C., and Holmes, A. (2010a). Predictably irrational: assaying cognitive inflexibility in mouse models of schizophrenia. *Front. Neurosci.* 4:13. doi: 10.3389/neuro.01.013.2010

Brigman, J. L., Mathur, P., Harvey-White, J., Izquierdo, A., Saksida, L. M., Bussey, T. J., et al. (2010b). Pharmacological or genetic inactivation of the serotonin transporter improves reversal learning in mice. *Cereb. Cortex* 20, 1955–1963. doi: 10.1093/cercor/bhp266

Brigman, J. L., Wright, T., Talani, G., Prasad-Mulcare, S., Jinde, S., Seabold, G. K., et al. (2010c). Loss of GluN2B-containing NMDA receptors in CA1 hippocampus and cortex impairs long-term depression, reduces dendritic spine density, and disrupts learning. *J. Neurosci.* 30, 4590–4600. doi: 10.1523/JNEUROSCI.0640-10.2010

Bussey, T. J., Padain, T. L., Skillings, E. A., Winters, B. D., Morton, A. J., and Saksida, L. M. (2008). The touchscreen cognitive testing method for rodents: how to get the best out of your rat. *Learn. Mem.* 15, 516–523. doi: 10.1101/lm.987808

Cavanagh, J. F., Gregg, D., Light, G. A., Olguin, S. L., Sharp, R. F., Bismark, A. W., et al. (2021). Electrophysiological biomarkers of behavioral dimensions from cross-species paradigms. *Transl. Psychiatry* 11:482. doi: 10.1038/s41398-021-01562-w

Chen, M.-L., Liu, S.-S., Zhang, G.-H., Quan, Y., Zhan, Y.-H., Gu, T.-Y., et al. (2013). Effects of early intraoral acesulfame-K stimulation to mice on the adult's sweet preference and the expression of α-gustducin in fungiform papilla. *Chem. Senses* 38, 447–455. doi: 10.1093/chemse/bjt001

Chiew, K., and Braver, T. (2011). Positive affect versus reward: emotional and motivational influences on cognitive control. *Front. Psychol.* 2:279. doi: 10.3389/fpsyg.2011.00279

Choi, J., and Medalia, A. (2010). Intrinsic motivation and learning in a schizophrenia spectrum sample. *Schizophr. Res.* 118, 12–19. doi: 10.1016/j.schres.2009.08.001

Chudasama, Y. (2011). Animal models of prefrontal-executive function. *Behav. Neurosci.* 125, 327–343. doi: 10.1037/a0023766

Cohen, J. F. W., Rifas-Shiman, S. L., Young, J., and Oken, E. (2018). Associations of prenatal and child sugar intake with child cognition. *Am. J. Prev. Med.* 54, 727–735. doi: 10.1016/j.amepre.2018.02.020

Corbit, L. H., Nie, H., and Janak, P. H. (2012). Habitual alcohol seeking: time course and the contribution of subregions of the dorsal striatum. *Biol. Psychiatry* 72, 389–395. doi: 10.1016/j.biopsych.2012.02.024

de Araujo, I. E., Oliveira-Maia, A. J., Sotnikova, T. D., Gainetdinov, R. R., Caron, M. G., Nicolelis, M. A. L., et al. (2008). Food reward in the absence of taste receptor signaling. *Neuron* 57, 930–941. doi: 10.1016/j.neuron.2008.01.032

Demurie, E., Roeyers, H., Baeyens, D., and Sonuga-Barke, E. (2012). Temporal discounting of monetary rewards in children and adolescents with ADHD and autism spectrum disorders. *Dev. Sci.* 15, 791–800. doi: 10.1111/j.1467-7687.2012.01178.x

Diamond, A. (2013). Executive functions. *Annu. Rev. Psychol.* 64, 135–168. doi: 10.1146/annurev-psych-113011-143750

Dumont, J. R., Salewski, R., and Beraldo, F. (2021). Critical mass: the rise of a touchscreen technology community for rodent cognitive testing. *Genes Brain Behav.* 20:e12650. doi: 10.1111/gbb.12650

Eagle, D. M., Humby, T., Howman, M., Reid-Henry, A., Dunnett, S. B., and Robbins, T. W. (1999). Differential effects of ventral and regional dorsal striatal lesions on sucrose drinking and positive and negative contrast in rats. *Psychobiology* 27, 267–276. doi: 10.3758/BF03332120

Elliott, R. (2003). Executive functions and their disorders. *Br. Med. Bull.* 65, 49–59. doi: 10.1093/bmb/65.1.49

Englund-Ögge, L., Brantsæter, A. L., Haugen, M., Sengpiel, V., Khatibi, A., Myhre, R., et al. (2012). Association between intake of artificially sweetened and sugar-sweetened beverages and preterm delivery: a large prospective cohort study. *Am. J. Clin. Nutr.* 96, 552–559. doi: 10.3945/ajcn.111.031567

Faas, A. E., March, S. M., Moya, P. R., and Molina, J. C. (2015). Alcohol odor elicits appetitive facial expressions in human neonates prenatally exposed to the drug. *Physiol. Behav.* 148, 78–86. doi: 10.1016/j.physbeh.2015.02.031

Gilbert, A. M., and Fiez, J. A. (2004). Integrating rewards and cognition in the frontal cortex. *Cogn. Affect. Behav. Neurosci.* 4, 540–552. doi: 10.3758/CABN.4.4.540

Graybeal, C., Feyder, M., Schulman, E., Saksida, L. M., Bussey, T. J., Brigman, J. L., et al. (2011). Paradoxical reversal learning enhancement by stress or prefrontal cortical damage: rescue with BDNF. *Nat. Neurosci.* 14, 1507–1509. doi: 10.1038/nn.2954

Heath, C. J., Bussey, T. J., and Saksida, L. M. (2015). Motivational assessment of mice using the touchscreen operant testing system: effects of dopaminergic drugs. *Psychopharmacology* 232, 4043–4057. doi: 10.1007/s00213-015-4009-8

Hellemans, K. G., Verma, P., Yoon, E., Yu, W. K., Young, A. H., and Weinberg, J. (2010). Prenatal alcohol exposure and chronic mild stress differentially alter depressive- and anxiety-like behaviors in male and female offspring. *Alcohol. Clin. Exp. Res.* 34, 633–645. doi: 10.1111/j.1530-0277.2009.01132.x

Holmes, A., and Wellman, C. L. (2009). Stress-induced prefrontal reorganization and executive dysfunction in rodents. *Neurosci. Biobehav. Rev.* 33, 773–783. doi: 10.1016/j.neubiorev.2008.11.005

Horner, A. E., Heath, C. J., Hvoslef-Eide, M., Kent, B. A., Kim, C. H., Nilsson, S. R., et al. (2013). The touchscreen operant platform for testing learning and memory in rats and mice. *Nat. Protoc.* 8, 1961–1984. doi: 10.1038/nprot.2013.122

Hughes, B. L., and Zaki, J. (2015). The neuroscience of motivated cognition. *Trends Cogn. Sci.* 19, 62–64. doi: 10.1016/j.tics.2014.12.006

Hutsell, B. A., and Newland, M. C. (2013). A quantitative analysis of the effects of qualitatively different reinforcers on fixed ratio responding in inbred strains of mice. *Neurobiol. Learn. Mem.* 101, 85–93. doi: 10.1016/j.nlm.2013.01.005

Kim, E. W., Phillips, B. U., Heath, C. J., Cho, S. Y., Kim, H., Sreedharan, J., et al. (2017). Optimizing reproducibility of operant testing through reinforcer standardization: identification of key nutritional constituents determining reward strength in touchscreens. *Mol. Brain* 10:31. doi: 10.1186/s13041-017-0312-0

Kodituwakku, P. W., Kalberg, W., and May, P. A. (2001). The effects of prenatal alcohol exposure on executive functioning. *Alcohol Res. Health* 25, 192–198. http://www.ncbi.nlm.nih.gov/pubmed/11810957.

Kuang, H., Sun, M., Lv, J., Li, J., Wu, C., Chen, N., et al. (2014). Hippocampal apoptosis involved in learning deficits in the offspring exposed to maternal high sucrose diets. *J. Nutr. Biochem.* 25, 985–990. doi: 10.1016/j.jnutbio.2014.04.012

MacQueen, D. A., Minassian, A., Henry, B. L., Geyer, M. A., Young, J. W., and Perry, W. (2018). Amphetamine modestly improves Conners' continuous performance test performance in healthy adults. *J. Int. Neuropsychol. Soc.* 24, 283–293. doi: 10.1017/s135561771700090x

Madan, C. R. (2017). Motivated cognition: effects of reward, emotion, and other motivational factors across a variety of cognitive domains. *Collabra Psychol.* 3:24. doi: 10.1525/collabra.111

Manera, V., Ben-Sadoun, G., Aalbers, T., Agopyan, H., Askenazy, F., Benoit, M., et al. (2017). Recommendations for the use of serious games in neurodegenerative disorders: 2016 Delphi panel. *Front. Psychol.* 8:1243. doi: 10.3389/fpsyg.2017.01243

Mar, A. C., Horner, A. E., Nilsson, S. R., Alsiö, J., Kent, B. A., Kim, C. H., et al. (2013). The touchscreen operant platform for assessing executive function in rats and mice. *Nat. Protoc.* 8, 1985–2005. doi: 10.1038/nprot.2013.123

Marquardt, K., and Brigman, J. L. (2016). The impact of prenatal alcohol exposure on social, cognitive and affective behavioral domains: insights from rodent models. *Alcohol* 51, 1–15. doi: 10.1016/j.alcohol.2015.12.002

Marquardt, K., Cavanagh, J. F., and Brigman, J. L. (2020). Alcohol exposure in utero disrupts cortico-striatal coordination required for behavioral flexibility. *Neuropharmacology* 162:107832. doi: 10.1016/j.neuropharm.2019.107832

Marquardt, K., Sigdel, R., and Brigman, J. L. (2017). Touch-screen visual reversal learning is mediated by value encoding and signal propagation in the orbitofrontal cortex. *Neurobiol. Learn. Mem.* 139, 179–188. doi: 10.1016/j.nlm.2017.01.006

Marquardt, K., Sigdel, R., Caldwell, K., and Brigman, J. L. (2014). Prenatal ethanol exposure impairs executive function in mice into adulthood. *Alcohol. Clin. Exp. Res.* 38, 2962–2968. doi: 10.1111/acer.12577

Mattson, S. N., Goodman, A. M., Caine, C., Delis, D. C., and Riley, E. P. (1999). Executive functioning in children with heavy prenatal alcohol exposure. *Alcohol. Clin. Exp. Res.* 23, 1808–1815. doi: 10.1111/j.1530-0277.1999.tb04077.x

Moorman, D. E., and Aston-Jones, G. (2014). Orbitofrontal cortical neurons encode expectation-driven initiation of reward-seeking. *J. Neurosci.* 34, 10234–10246. doi: 10.1523/JNEUROSCI.3216-13.2014

Nieto-Márquez, N. L., Garcia-Sinausia, S., and Pérez Nieto, M. Á. (2021). Relaciones de la motivación con la metacognición y el desempeño en el rendimiento cognitivo en estudiantes de educación primaria. *An. Psicol.* 37, 51–60. doi: 10.6018/analesps.383941

Nithianantharajah, J., McKechanie, A. G., Stewart, T. J., Johnstone, M., Blackwood, D. H., St Clair, D., et al. (2015). Bridging the translational divide: identical cognitive touchscreen testing in mice and humans carrying mutations in a disease-relevant homologous gene. *Sci. Rep.* 5:14613. doi: 10.1038/srep14613

Olivier-Van Stichelen, S., Rother, K. I., and Hanover, J. A. (2019). Maternal exposure to non-nutritive sweeteners impacts progeny's metabolism and microbiome. *Front. Microbiol.* 10:1360. doi: 10.3389/fmicb.2019.01360

Ong, Z. Y., and Muhlhausler, B. S. (2011). Maternal "junk-food" feeding of rat dams alters food choices and development of the mesolimbic reward pathway in the offspring. *FASEB J.* 25, 2167–2179. doi: 10.1096/fj.10-178392

Palatnik, A., Moosreiner, A., and Olivier-Van Stichelen, S. (2020). Consumption of non-nutritive sweeteners during pregnancy. *Am. J. Obstet. Gynecol.* 223, 211–218. doi: 10.1016/j.ajog.2020.03.034

Phillips, B. U., Heath, C. J., Ossowska, Z., Bussey, T. J., and Saksida, L. M. (2017). Optimisation of cognitive performance in rodent operant (touchscreen) testing: evaluation and effects of reinforcer strength. *Learn. Behav.* 45, 252–262. doi: 10.3758/s13420-017-0260-7

Popova, S., Lange, S., Probst, C., Gmel, G., and Rehm, J. (2017). Estimation of national, regional, and global prevalence of alcohol use during pregnancy and fetal alcohol syndrome: a systematic review and meta-analysis. *Lancet Glob. Health* 5, e290–e299. doi: 10.1016/S2214-109X(17)30021-9

Popova, S., Lange, S., Probst, C., Gmel, G., and Rehm, J. (2018). Global prevalence of alcohol use and binge drinking during pregnancy, and fetal alcohol spectrum disorder. *Biochem. Cell Biol.* 96, 237–240. doi: 10.1139/bcb-2017-0077

Prins, P. J., Dovis, S., Ponsioen, A., ten Brink, E., and van der Oord, S. (2011). Does computerized working memory training with game elements enhance motivation and training efficacy in children with ADHD? *Cyberpsychol. Behav. Soc. Netw.* 14, 115–122. doi: 10.1089/cyber.2009.0206

Ruiz-González, D., Hernández-Martínez, A., Valenzuela, P. L., Morales, J. S., and Soriano-Maldonado, A. (2021). Effects of physical exercise on plasma brain-derived neurotrophic factor in neurodegenerative disorders: a systematic review and meta-analysis of randomized controlled trials. *Neurosci. Biobehav. Rev.* 128, 394–405. doi: 10.1016/j.neubiorev.2021.05.025

Schoenbaum, G., Setlow, B., Nugent, S. L., Saddoris, M. P., and Gallagher, M. (2003). Lesions of orbitofrontal cortex and basolateral amygdala complex disrupt acquisition of odor-guided discriminations and reversals. *Learn. Mem.* 10, 129–140. doi: 10.1101/lm.55203

Skjoldager, P., Pierre, P. J., and Mittleman, G. (1993). Reinforcer magnitude and progressive ratio responding in the rat: effects of increased effort, prefeeding, and extinction. *Learn. Motiv.* 24, 303–343. doi: 10.1006/lmot.1993.1019

Steckler, T. (2015). Preclinical data reproducibility for R&D—the challenge for neuroscience. *Psychopharmacology* 232, 317–320. doi: 10.1007/s00213-014-3836-3

Thomas, J. D., Garrison, M., and O'Neill, T. M. (2004). Perinatal choline supplementation attenuates behavioral alterations associated with neonatal alcohol exposure in rats. *Neurotoxicol. Teratol.* 26, 35–45. doi: 10.1016/j.ntt.2003.10.002

Waddell, J., and Mooney, S. M. (2017). Choline and working memory training improve cognitive deficits caused by prenatal exposure to ethanol. *Nutrients* 9:1080. doi: 10.3390/nu9101080

Wainwright, P. E., Ward, G. R., Winfield, D., Huang, Y. S., Mills, D. E., Ward, R. P., et al. (1990). Effects of prenatal ethanol and long-chain n-3 fatty acid supplementation on development in mice. 1. Body and brain growth, sensorimotor development, and water T-maze reversal learning. *Alcohol. Clin. Exp. Res.* 14, 405–412. doi: 10.1111/j.1530-0277.1990.tb00495.x

Yarrow, L. J., and Messer, D. J. (1983). "Motivation and cognition in infancy" in *Origins of Intelligence: Infancy and Early Childhood*. ed. M. Lewis (Springer US.), 451–477.

Yin, H. H., Mulcare, S. P., Hilario, M. R., Clouse, E., Holloway, T., Davis, M. I., et al. (2009). Dynamic reorganization of striatal circuits during the acquisition and consolidation of a skill. *Nat. Neurosci.* 12, 333–341. doi: 10.1038/nn.2261

Youn, J., Ellenbroek, B. A., van Eck, I., Roubos, S., Verhage, M., and Stiedl, O. (2012). Finding the right motivation: genotype-dependent differences in effective reinforcements for spatial learning. *Behav. Brain Res.* 226, 397–403. doi: 10.1016/j.bbr.2011.09.034

Yunker, A. G., Alves, J. M., Luo, S., Angelo, B., DeFendis, A., Pickering, T. A., et al. (2021). Obesity and sex-related associations with differential effects of sucralose vs sucrose on appetite and reward processing: a randomized crossover trial. *JAMA Netw. Open* 4:e2126313. doi: 10.1001/jamanetworkopen.2021.26313

Zhang, G.-H., Chen, M.-L., Liu, S.-S., Zhan, Y.-H., Quan, Y., Qin, Y.-M., et al. (2011). Effects of mother's dietary exposure to acesulfame-K in pregnancy or lactation on the adult offspring's sweet preference. *Chem. Senses* 36, 763–770. doi: 10.1093/chemse/bjr050

frontiers | Frontiers in Neuroscience

TYPE Original Research
PUBLISHED 02 May 2023
DOI 10.3389/fnins.2023.1186529

Check for updates

OPEN ACCESS

EDITED BY
Carlos Fernando Valenzuela,
University of New Mexico, United States

REVIEWED BY
Jia Luo,
The University of Iowa, United States
Lee Cunningham,
University of New Mexico, United States

*CORRESPONDENCE
John F. Smiley
✉ smiley@nki.rfmh.org

RECEIVED 14 March 2023
ACCEPTED 13 April 2023
PUBLISHED 02 May 2023

CITATION
Smiley JF, Bleiwas C, Marino BM, Vaddi P, Canals-Baker S, Wilson DA and Saito M (2023) Estimates of total neuron number show that neonatal ethanol causes immediate and lasting neuron loss in cortical and subcortical areas. *Front. Neurosci.* 17:1186529. doi: 10.3389/fnins.2023.1186529

COPYRIGHT
© 2023 Smiley, Bleiwas, Marino, Vaddi, Canals-Baker, Wilson and Saito. This is an open-access article distributed under the terms of the Creative Commons Attribution License (CC BY). The use, distribution or reproduction in other forums is permitted, provided the original author(s) and the copyright owner(s) are credited and that the original publication in this journal is cited, in accordance with accepted academic practice. No use, distribution or reproduction is permitted which does not comply with these terms.

Estimates of total neuron number show that neonatal ethanol causes immediate and lasting neuron loss in cortical and subcortical areas

John F. Smiley[1,2]*, Cynthia Bleiwas[1], Brandon M. Marino[1], Prerana Vaddi[1], Stefanie Canals-Baker[1], Donald A. Wilson[1,3,4] and Mariko Saito[1,2]

[1]Nathan Kline Institute for Psychiatric Research, Orangeburg, NY, United States, [2]Department of Psychiatry, School of Medicine, New York University, New York, NY, United States, [3]Department of Child and Adolescent Psychiatry, School of Medicine, New York University, New York, NY, United States, [4]Department of Neuroscience and Physiology, School of Medicine, New York University, New York, NY, United States

In neonatal brain development there is a period of normal apoptotic cell death that regulates adult neuron number. At approximately the same period, ethanol exposure can cause a dramatic spike in apoptotic cell death. While ethanol-induced apoptosis has been shown to reduce adult neuron number, questions remain about the regional selectivity of the ethanol effect, and whether the brain might have some capacity to overcome the initial neuron loss. The present study used stereological cell counting to compare cumulative neuron loss 8h after postnatal day 7 (P7) ethanol treatment to that of animals left to mature to adulthood (P70). Across several brain regions we found that the reduction of total neuron number after 8h was as large as that of adult animals. Comparison between regions revealed that some areas are more vulnerable, with neuron loss in the anterior thalamic nuclei > the medial septum/vertical diagonal band, dorsal subiculum, and dorsal lateral geniculate nucleus > the mammillary bodies and cingulate cortex > whole neocortex. In contrast to estimates of total neuron number, estimates of apoptotic cell number in Nissl-stained sections at 8h after ethanol treatment provided a less reliable predictor of adult neuron loss. The findings show that ethanol-induced neonatal apoptosis often causes immediate neuron deficits that persist in adulthood, and furthermore suggests that the brain may have limited capacity to compensate for ethanol-induced neuron loss.

KEYWORDS

fetal alcohol (FAS FASD), apoptosis, thalamus, cerebral cortex, subiculum, medial septum and diagonal band of broca, mammillary body, cingulate cortex

Introduction

In neonatal brain development there is a period of apoptotic neuron loss, or "normal programmed cell death" that eliminates a large fraction of neurons. This pruning of excess neurons is thought to be key developmental mechanism that determines adult neuron number. In mice, the peak episode of this apoptotic event occurs mainly between embryonic day 17 and postnatal day 7 (PD7), depending on the brain region (Forger et al., 2004; Ahern et al., 2013;

Mosley et al., 2017). At approximately the same developmental period, ethanol exposure can cause a dramatic spike of apoptosis in some brain areas. Like normal programmed cell death, the brain areas affected by ethanol vary depending on the developmental age. Exposure around birth preferentially affects ventral hypothalamic and ventral thalamic regions whereas exposure from P0-P7 affects dorsal thalamic, hippocampal, and striatal regions, and the cerebral cortex is most affected at around P7 (Ikonomidou et al., 2000). Like normal programmed cell death, ethanol-induced apoptosis reduces adult neuron number, as shown by estimates of total neuron number in several brain regions of adult animals that were treated with neonatal ethanol (Bonthius and West, 1991; Napper and West, 1995a; Goodlett and Eilers, 1997; Livy et al., 2003; Tran and Kelly, 2003; Dursun et al., 2013; Gursky et al., 2019; Smiley et al., 2021).

There is interest in developing treatments to prevent or reverse the effects of neonatal ethanol, and thus it is of interest to know specifically which brain regions and cell types are most vulnerable. However, our current understanding of this issue is patchy. Estimates of neuron loss in adult animals have been done in a limited number of regions, and differences in dose and timing of ethanol treatment make it difficult to compare studies. A more common approach has been to estimate the number of apoptotic cells, using histological sampling within hours or days after ethanol treatment. However, interpretation is complicated by the short duration of the apoptotic response, and differential timing of the response between regions. As a result, substantial apoptotic events that occur a few hours before or after the time of sampling may be overlooked (Olney et al., 2002a; Tenkova et al., 2003). Additionally, it has been suggested that the brain may have some capacity to overcome apoptosis after neonatal lesions, perhaps by downregulating ongoing normal programmed cell death or replacing neurons by neurogenesis or neuronal migration (Mooney and Napper, 2005; Fagel et al., 2006; Smiley et al., 2019). However, it is notable that there is little direct evidence that these compensatory mechanisms occur in significant magnitude to overcome large neuron deficits (Salmaso et al., 2014; Shin et al., 2020).

As an alternative method to evaluate ethanol-induced apoptosis in the neonatal brain, the current study used stereological methods to estimate the cumulative neuron loss that occurred by 8 h after P7 ethanol, or by early adulthood (P70). These results were then compared with a more traditional approach that estimated apoptotic cell number at 8 h after ethanol treatment. Neuron number estimates were taken from several brain regions to obtain an initial evaluation of the regional selectivity of the ethanol effect. Regions were selected because they were previously shown to have robust apoptotic response to P7 ethanol and/or they are representative of distinct forebrain circuitries.

Materials and methods

A total of 40 C57BL/6J mice were used for this study. Mice originated from 6 different mouse litters with 5–8 animals per litter. Each litter was divided into ethanol and saline treatment groups matched as closely as possible for sex and body weight. At P7, pups were subcutaneously injected with saline or 2.5 g/kg ethanol per injections, with 2 injections separated by 2 h, as previously described (Ikonomidou et al., 2000; Saito et al., 2007). Three of the litters ($N = 8$ saline and 9 ethanol mice) were transcardially perfused 8 h after the first injection, with 4% buffered paraformaldehyde containing 4% sucrose. The remaining litters ($N = 11$ saline and 12 ethanol mice) were weaned at P25-30 and perfused at P70 with 4% buffered paraformaldehyde. The P70 mice used in this study are a subset of the 5 litters used in a previous study (Smiley et al., 2021). The 3 litters at P70 were selected so that average body weight (3.6 +/−0.4 g) was matched as closely as possible to that of the P7 litters (3.3 +/− 0.1 g). All brains were postfixed for 2–4 days and embedded in agar blocks so that matched ethanol and saline treated brains from each litter were simultaneously sectioned and processed (Nagamoto-Combs et al., 2016; Smiley et al., 2019). Blocks were coronally sectioned at 50uM thickness, and a series of every 2nd or 3rd (P7) or 3rd or 4th (P70) consecutive section was dried on chrom-alum subbed slides before staining with thionin and coverslipping with permount. For cleaved caspase-3 (CC3) immunolabeling, free-floating sections were exposed to 1:400 dilution of primary antibody (Cell signaling catalog #9664) that was visualized using the streptavidin-biotin-peroxidase method with diaminobenzidine as the reaction product, and then mounted and dried on subbed slides before coverslipping with permount. All procedures were approved by the Nathan Kline Institute IACUC and were in accordance with NIH guidelines for the proper treatment of animals.

Stereological estimates of total Nissl-stained neuron numbers used the Nv x Vref method (Gundersen et al., 1988). Cell sampling was done using ImageJ software to control a motorized Nikon E-600 microscope equipped with Ludl X, Y, and Z motors, a Heidenhain z-axis microcator, and a Basler acA5472-17 camera. The full rostral-caudal extent of each area was sampled in evenly spaced sections through each structure, using an average of 7.1 +/− 2.4 sections per neuron number estimate (mean +/− S.D., $N = 353$ estimates of total neuron number). In each section, the outlined area of interest was sampled with an evenly spaced grid of sites. At each site a z-stack of six images with 1- or 1.5-micron z-spacing was saved to a computer, and an optical disector counting box was then drawn on each z-stack using the first slice as an upper guard zone, the next 3 slices as a counting box, and the remaining slices as a bottom guard zone. All z-stacks were taken using a 1.3 N.A. 100x objective. Neurons were distinguished from glia by morphological features including their well stained cytoplasm and prominent nucleolus. Separate counts of apoptotic nuclei used the same z-stacks as for total cell number but with a larger counting box. Apoptotic nuclei were easily identified by darkly stained balls of dense chromatin, consistent with previous descriptions (Olney et al., 2002a).

Across all estimates of total neuron number, the average number of disectors (157 +/49) and number of cells counted (190 +/−84) was adjusted to obtain adequate precision, and in most cases the coefficient of error (CE) (Dorph-Petersen et al., 2009) was <0.1. Exceptions were the anterior dorsal thalamic nucleus in ethanol treated animals (average CE = 0.12), that had severely reduced cell numbers in some brains, and the anterior medial thalamic nucleus (average CE = 0.12 in both saline and control animals) that had inhomogeneous cell density across its rostral-caudal extent that resulted in high CE's. Additionally, CE's for estimates of pyknotic cell numbers in ethanol treated animals had CE's ranging from 0.11 to 0.16, due to low number of apoptotic cells in some brains. In saline-treated animals, pyknotic cell numbers were much lower, and are presented here only to confirm that ethanol-induced apoptosis is much higher than background. On-slide section thickness, that was measured to calculate z-axis tissue shrinkage, did not differ significantly between saline-and ethanol-treated animals in any experiment, but there was a difference between ages. Comparing the

average thickness from each of 5 areas that were counted at both ages, the thickness at P7 (10.0 +/− 1.1 microns) was less than that at P70 (11.6 +/−0.3 microns, $t(8) = -3.0$, $p < 0.02$, independent samples t-test).

Brain structures were identified as in the Allen Institute Brain Atlas (AIBA, 2011) unless otherwise stated. The anterior dorsal, anterior ventral, anterior medial, and dorsal lateral geniculate (dLGN) thalamic nuclei usually had unambiguous borders. However, the boundary separating the anterior ventral from anterior medial nucleus was less clear in P7 brains, and for this reason these nuclei were only measured in P70 brains. The mammillary body was easily identified, and cell counts included both the medial and lateral mammillary nuclei. The mammillary bodies were excluded from analysis of P7 brains due to tight cell packing in some brains that hindered cell counting. The borders of the medial septum/vertical diagonal band nuclei were identified as in our previous publication (Smiley et al., 2021), and to be consistent with that study we refer to this region as the Ch1/Ch2 nucleus, indicating that it is coextensive with the distribution of cholinergic neurons in this region (Mesulam et al., 1983). Briefly, this region is defined by the large Nissl-stained neurons in the medial septal area and vertical limb of the diagonal band, extending caudally to rostral tip of the third cerebral ventricle at the ventral surface of the brain, where there is often a separation between the vertical diagonal band and the horizontal diagonal band. The boundaries of whole neocortex were defined as in our previous studies (Smiley et al., 2015, 2019). Briefly this region includes most of the medial and lateral cortical surface, but excludes the lateral dysgranular limbic areas (i.e., pyriform, insular, and entorhinal cortex) and excludes retrosplenial cortex in sections caudal to the corpus callosum. Separate analyses of cingulate cortex used boundaries that corresponded approximately to areas 24a/24b of Vogt and Paxinos (2014). However, for simplicity we defined the rostral boundary at the rostral tip of the corpus collosum, and the caudal boundary at the rostral tip of the dorsal hippocampus. Dorsally, the border with motor cortex was identified by the comparatively high cell density in layer II of cingulate cortex (Figure 1B). The dorsal subiculum was identified as in the Allen Institute Mouse Brain Atlas (AIBA, 2011) thus including the subiculum in all sections where its lateral border abutted the hippocampal CA1 region, but excluding sections where its lateral border merged with the ventral subiculum. Thus, this boundary is defined by the shape of the subiculum as it wraps around the hippocampus CA1 region. While its volume was reasonably consistent in P70 brains, it was less reliable in P7 brains where the curvature of the hippocampus was still immature, and for this reason the dorsal subiculum was only measured in P70 brains.

Statistical analysis

Mice were taken from 3 litters at each age (P7 and P70). Within each litter, animals were selected so that ethanol and saline treated animals had approximately equal distributions of sex and body weight. Estimates of cell number were analyzed using two-way analysis of variance (ANOVA) models with treatment group, age, and sex included as independent variables, and litter as a blocking factor. Main effects of sex or interactions with sex were not encountered in any analyses. Statistical analysis was conducted using IBM SPSS version 24 software. We used mean ± S.D. and percent differences [i.e., (1-ethanol/saline)*100%] to describe the sample and quantify associations.

Results

Identification of apoptotic neurons by either CC3-immunolabeling or Nissl staining confirmed that P7 ethanol injections caused an obvious apoptotic response at 8 h after the initiation of treatment (Figure 1). Qualitatively, the distribution of apoptotic cells was similar in Nissl-stained sections and CC3-immunolabeled sections. As previously described, the response to P7 ethanol was dense in the anterior thalamic nuclei, and in several regions closely associated with these nuclei including the dorsal subiculum, mammillary bodies, and the cingulate, prefrontal and retrosplenial regions of midline cerebral cortex. Additionally, a comparatively dense apoptotic response was present in regions that do not have strong direct connections with the anterior thalamus, including the dLGN, Ch1/Ch2 region of the basal forebrain, and most of the dorsal lateral surface of the cerebral cortex.

Ethanol-induced neuron deficits are comparable at P7 and P70

Stereological estimates of total neuron number in Nissl-stained sections were used to compare neuron loss already present at 8 h after ethanol treatment with neuron loss in P70 animals. Several brain regions were selected based on their robust apoptotic response, and because they were representative of distinctly different functional systems in the forebrain. As described below, each of these regions had significant neuron loss at P7 that was not significantly different from the neuron loss at P70 (Figure 2).

In the anterior dorsal thalamic nucleus, ANOVA showed a main effect of ethanol treatment [$F(1,31.6) = 125$, $p < 0.001$] and a main effect of age [$F(1,4.0) = 42.4$, $p < 0.001$], but there was not a significant interaction of treatment and age [$F(1,30) = 1.9$, $p < 0.18$]. The main effect of age was due to a normal developmental neuron loss that caused nearly 50% reduction of neuron number from P7 to P70. Notably, this age-dependent neuron loss was also present in ethanol-treated animals, even after a large ethanol-induced neuron deficit at P7. The main effect of ethanol treatment was due to an average reduction of total cell number that was similar at P7 (average decrease of 6,686 neurons) or P70 (5,507 neurons). Because of the age-related decrease in total neuron number, these changes correspond to 35% of total neurons at P7, or 54% at P70. Estimates of total neuron number in additional untreated control animals confirmed that total neuron number consistently decreases after P7 in this nucleus (data not shown).

In the Ch1/Ch2 nuclei of the basal forebrain, only 5 saline-control and 6 ethanol-treated animals were available at P7 because this region was damaged during processing in one litter. In this region there was a main effect of ethanol treatment [$F(1,24.6) = 52.3$, $p < 0.001$]. There was not a main effect of age [$F(1,3.2) = 1.3$, $p = 0.36$], nor was there a significant interaction of treatment and age [$F(1,30) = 1.9$, $p < 0.18$]. Thus, the average 24% reduction of total neurons at P7 was not significantly different from the 29% reduction at P70.

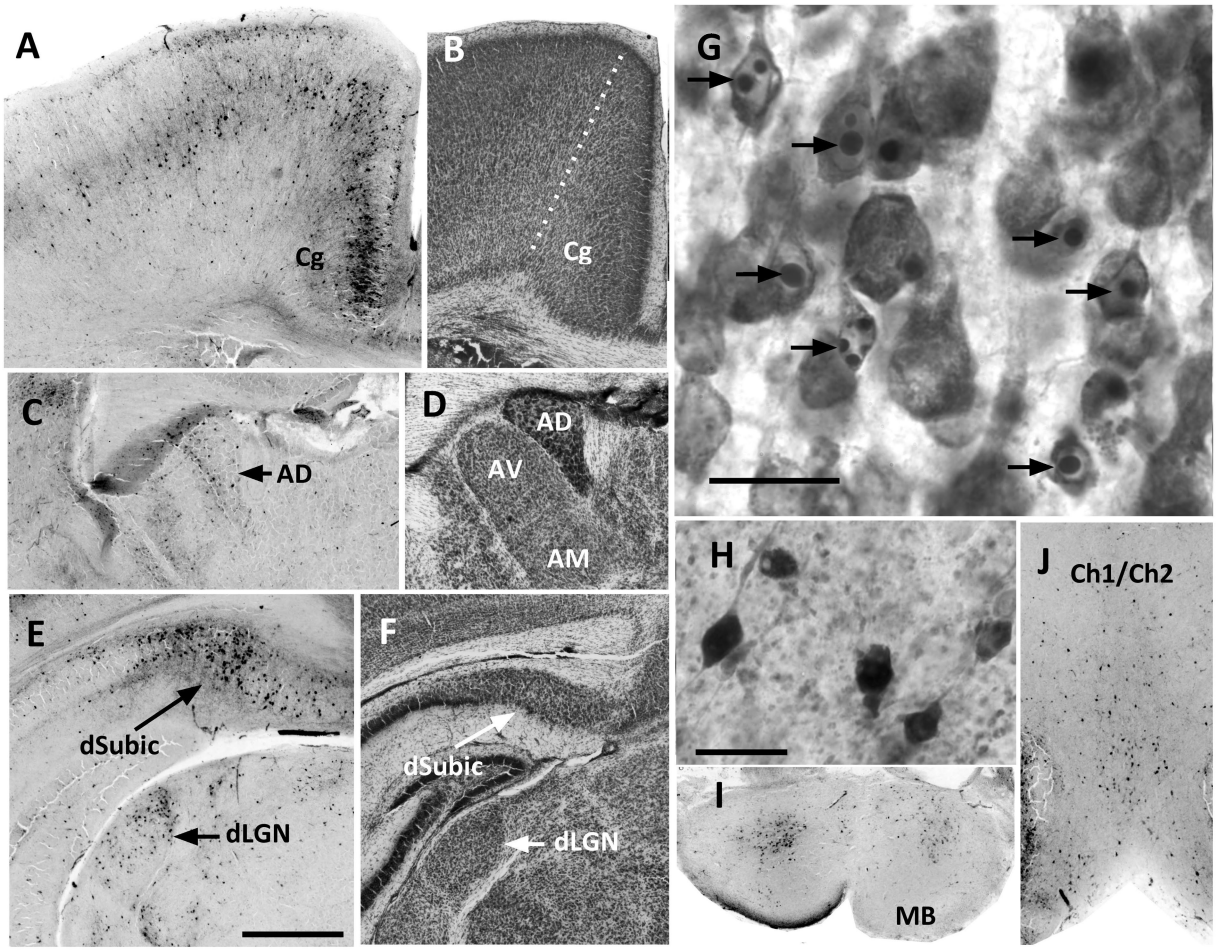


FIGURE 1
In P7 brains, identification of apoptotic neurons by either CC3-immunolabeling or Nissl staining confirmed an obvious apoptotic response at 8h after the initiation of treatment. **(A)** CC3-immunolabeling showed a high density of apoptotic cells in the cingulate cortex (Cg), that was present in all cortical layers but were especially dense in layer II and III/IV. **(B)** A Nissl-stained section shows the border (dotted line) of cingulate cortex with motor cortex laterally. Cingulate cortex was distinguished by the dense cell packing in layer II. **(C)** CC3 cell density was consistently high in the anterior dorsal nucleus of the thalamus (AD). **(D)** In Nissl-stained sections the AD nucleus has a characteristic dense appearance. The anterior ventral (AV) and anterior medial (AM) nuclei are also easily identified, although at P7 the border separating the two was somewhat indistinct. **(E)** The dorsal subiculum (dSubic) and dorsal lateral geniculate nucleus (dLGN) had a high density of CC3 cells after P7 ethanol. **(F)** In Nissl-stained sections the dSubic and dLGN were easily identified. **(G)** Higher magnification image of Nissl-stained cortex shows the typical appearance of apoptotic cells, which were easily identified by characteristic darkly stained ovals of condensed chromatin within the nucleus. **(H)** Higher magnification shows the appearance of CC3-immunolabeled cells, most of which had the appearance of neurons. **(I,J)** CC3-immunolabeling was prominent in the cell scattered throughout the mammillary bodies (MB) and the region of the medial septal nucleus/vertical diagonal band (Ch1/Ch2). Scale bar in *E*=0.5mm, and applies to all images except **(G,H)**. Scale bars in **(G,H)**=20μM.

In the dLGN there was a main effect of ethanol treatment [$F(1,31.7) = 43.5$, $p < 0.001$]. There was not a main effect of age [$F(1,4.0) = 0.48$, $p = 0.54$], nor was there a significant interaction of treatment and age [$F(1,30) = 0.24$, $p < 0.63$]. Thus, the average 25% reduction of total neurons at P7 was not significantly different from the 24% reduction at P70.

In the cingulate cortex, there was a main effect of ethanol treatment [$F(1,30.7) = 10.2$, $p < 0.01$]. There was not a main effect of age [$F(1,4.0) = 3.8$, $p = 0.12$] nor was there an interaction of treatment and age [$F(1,30) = 0.07$, $p < 0.78$]. In this region ethanol caused reductions of about 19% at P7 and 18% at P70.

In total neocortex, there was a main effect of ethanol treatment [$F(1,30.7) = 7.9$, $p < 0.01$]. There was not a main effect of age [$F(1,4.0) = 1.0$, $p = 0.37$] nor was there a significant interaction of treatment and age [$F(1,30) = 0.71$, $p < 0.41$]. In this region ethanol caused reductions of about 10% at P7 and 7% at P70.

In addition to the above age comparisons, we estimated neuron number only at P70 in other nuclei functionally associated with the anterior dorsal thalamic nuclei, including the anterior ventral and medial thalamic nuclei, the dorsal subiculum, and the mammillary bodies. As expected from the distribution of apoptotic neurons at P7, there was robust neuron loss in the anterior ventral 36% [$F(1,17) = 28.3$, $p < 0.001$] anterior medial 36% [$F(1,17) = 64.8$, $p < 0.001$] and dorsal subiculum 31% [$F(1,17) = 20.8$, $p < 0.001$]. Neuron loss was less pronounced in the mammillary bodies 15% [$F(1,17) = 7.9$, $p < 0.05$].

The above estimates show that some regions are more affected by P7 ethanol. To provide context for these findings, Figure 3 displays the number of surviving neurons as a fraction of control in different regions from the present study, and also in several immunolabeled neuron populations that were evaluated in our previous studies, using the same ethanol treatment paradigm and cell counting methods (Smiley et al., 2019, 2021). Currently, it remains unclear whether reduction of

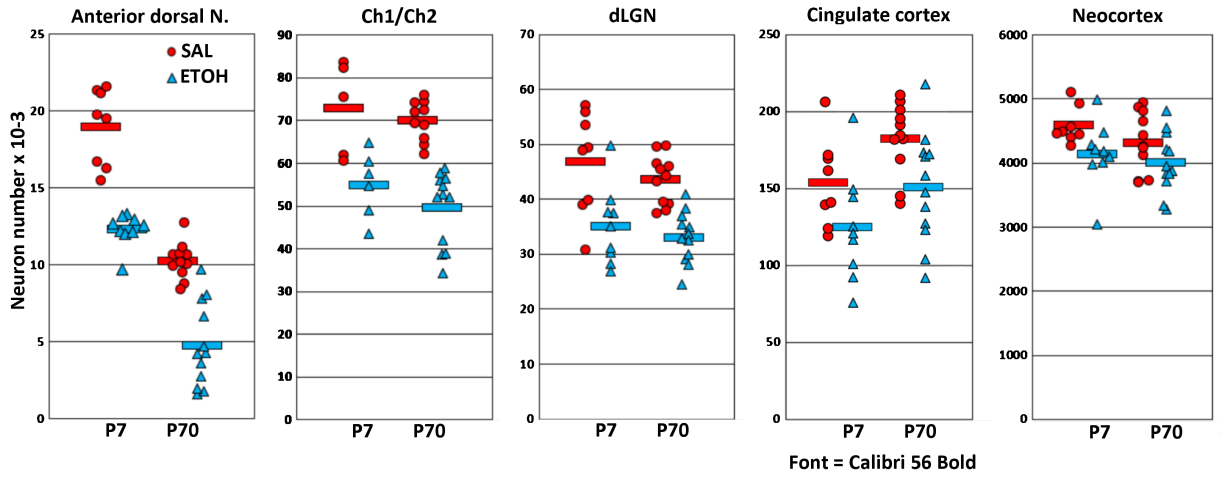


FIGURE 2
Graphs compare estimates of neuron number at P7 and P70 in 5 different areas, in saline (SAL) and ethanol (ETOH) treated mice. The graphs are ordered from left to right by severity of the ethanol effect. In all regions, the reduction of neuron number was not significantly different at P7 compared to P70. Ethanol caused the largest reduction in the anterior dorsal nucleus, and this nucleus also had a striking age effect, such that neuron number was higher at P7 than P70 in both the saline and ethanol treatment groups.

immunolabeled cells corresponds completely to neuron loss or might be partially caused by decreased immunolabeling. Nevertheless, these comparisons suggest that especially large reductions such as those in the anterior thalamus and in immunolabeled cholinergic and GABAergic neurons provide useful biomarkers for the effects of neonatal ethanol.

Estimates of the number of apoptotic nuclei are poor predictors of total neuron loss

Besides estimating total neuron loss, we additionally estimated the number of Nissl-stained apoptotic nuclei in P7 animals, using, using the same image stacks that were collected to estimate total cell number. While many apoptotic cells had the appearance of neurons, this estimate likely also includes some fraction of non-neuronal cells. In saline controls, the number of apoptotic cells, expressed as a percent of the total neuron number, did not exceed 0.8% in any region. In ethanol-treated animals, the average number of apoptotic cells was 4.2% of the total neuron number in neocortex, and between 6.7 and 7.6% in the other regions examined (Figure 4). Thus, in all regions the number of visible apoptotic cells was only a fraction of the cumulative neuron loss at 8 h after ethanol treatment (ranging from 20% in the anterior dorsal nucleus to 43% in neocortex). Additionally, there was not a significant correlation between the number of apoptotic neurons and the total neuron loss across the five regions examined at P7 [$r(8) = -0.66$, $p = 0.23$]. Thus, the number of apoptotic nuclei sampled at 8 h after treatment is a poor predictor of total neuron loss.

Discussion

Fetal alcohol can have distinct effects on brain development depending on the timing and dosage of ethanol exposure. In the present study we employed a specific exposure paradigm that is optimized to cause a spike of cellular apoptosis across several regions of the forebrain. While this apoptotic response has been extensively described, it is less well known whether the apoptotic response consistently causes permanent neuron loss. It has been suggested that the brain might have some capacity to compensate for the initial apoptotic loss of neurons by altering the course of still ongoing normal programmed cell death, or enhancing neurogenesis, and that some neuron populations may persist with altered or down-regulated phenotypes (e.g., Smiley et al., 2019). The results of the present study do not exclude that these compensatory processes occur to some extent in some neuron populations. However, they show in several brain regions that the magnitude of ethanol-induced neuron reduction at 8 h after ethanol exposure is comparable to the reduction found when animals are allowed to grow to adulthood. Thus, a common result of ethanol-induced apoptosis at the neonatal age is an immediate and lasting reduction of neuron number.

Previous studies of the P7 ethanol treatment used in the present study concluded that the mechanism of cell death is mainly or completely apoptotic, without obvious excitotoxic cell death (Olney et al., 2002b). Most studies that characterized the severity of this response have quantified the number or density of apoptotic cells, visualized with by methods including Nissl staining, CC3 immunolabeling, fluorojade labeling, TUNEL labeling, or deOlmos silver staining. A limitation of these methods is that the sampling is limited to the time of death and may overlook apoptosis that occurs earlier or later (Olney et al., 2002a; Young and Olney, 2006). Direct comparisons noted that CC3 immunolabeling peaks comparatively early (at approximately 2–10 h depending on the region) whereas Nissl-stained pyknotic nuclei are prominent somewhat later than CC3, and deOlmos silver staining reaches its maximum at about 12–20 h (Ikonomidou et al., 2000; Olney et al., 2002a,b; Tenkova et al., 2003). Olney and colleagues concluded that deOlmos staining after 12 h gives a more complete picture of the full extent of neuron loss. Using the deOlmos method, and the same ethanol-treatment paradigm as the present study but in rats, they estimated that

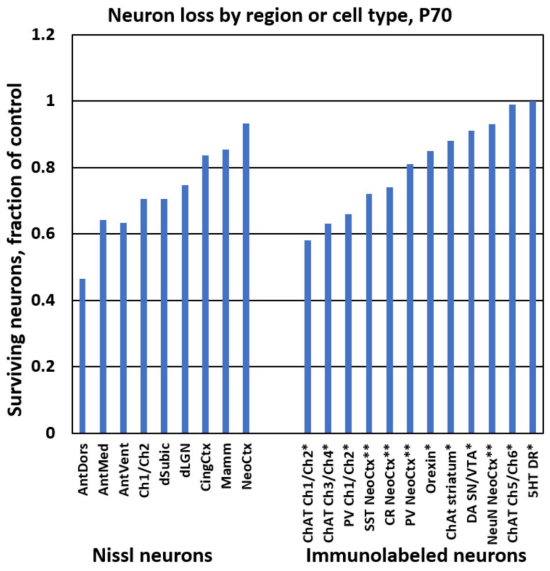


FIGURE 3
Bar graphs show the ethanol-induced neuron loss at P70 from different brain regions in the present study ("Nissl neurons," at left). For comparison, at right are stereological estimates of immunolabeled neuron populations from previous studies using the same treatment paradigm. * Results are from Smiley et al. (2021). ** Results are from Smiley et al. (2019). Abbreviations: 5HT DR, serotonin neurons of dorsal raphe; AntDors, anterior dorsal thalamic nucleus; AntMed, anterior medial thalamic nucleus; AntVent, anterior ventral thalamic nucleus; ChAT, choline acetyl transferase immunolabeled cells; Ch1/Ch2, medial septum and vertical diagonal band region; Ch3/Ch4, horizontal diagonal band and nucleus basalis region; Ch5/Ch6, pedunculopontine and lateral dorsal tegmental nuclei; CingCtx, cingulate cortex; CR, calretinin immunolabeled cells; DA SN/VTA, dopamine cells of substantia nigra and ventral tegmental area; dLGN, dorsal lateral geniculate nucleus; dSubic, dorsal subiculum; Mamm, mamillary bodies; NeoCtx, neocortex; NeuN, neuronal nuclear antibody immunolabeled cells; Orexin, orexin cells of the hypothalamus; PV, parvalbumin immunolabeled cells; SST, somatostatin immunolabeled cells.

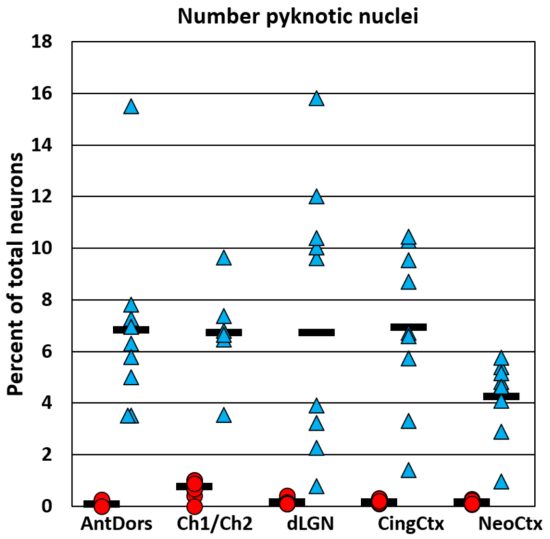


FIGURE 4
Graphs show the number of Nissl-stained apoptotic cells in each region, expressed as a percent of the total neuron number. The number of apoptotic cells was estimated in P7 brains at 8h after the onset of ethanol treatment. In each region ethanol treatment caused a robust increase in the number of apoptotic cells compared to saline controls. However, the percent of total cells identified as apoptotic was only a fraction of the total cumulative neuron loss (see Figure 2), indicating that most neurons that died in response to ethanol have already been cleared and are no longer detectable by this method.

approximately 20% of neurons were apoptotic in cingulate cortex, subiculum, and lateral dorsal thalamic nucleus (Ikonomidou et al., 2000). In the present study of mouse brains, we used an alternative approach that quantifies total neuron number, and thus provides an estimate of cumulative neuron loss that has occurred up to the time of sampling. Using regions comparable to the ones used by Ikonomidou et al. (2000), this method showed neuron losses in the range of 15–30%, thus approximately consistent with estimates derived from deOlmos silver staining. Based on these comparisons, we suggest that stereological quantification Nissl-stained neuron number provides a practical method to quantify regional differences and the developmental timing of ethanol-induced or normal developmental neuron loss.

We additionally quantified the number of apoptotic nuclei at 8h after P7 ethanol and found that their total number was only a fraction of the cumulative neuron loss. This indicates that many apoptotic nuclei are already fully cleared after 8h, consistent with previous estimates that CC3 immunolabeling in apoptotic cells is only present for 2–3h (Olney et al., 2002a). Thus, while these markers of apoptotic cells are useful to confirm the presence of apoptotic response, they are less reliable predictors of regional differences or total neuron loss.

Recently, we found that the Ch1/Ch2 nuclei of the basal forebrain have substantial neuron loss after P7 ethanol (Smiley et al., 2021) and a goal of the present study was to compare the loss in Ch1/Ch2 with that of other brain regions that have pronounced apoptotic response to P7 ethanol. Comparisons across areas showed that the anterior dorsal nucleus has especially severe neuron loss of about 50%, as expected from a previous report of volume loss in this nucleus (Wozniak et al., 2004). Somewhat less severe neuron reductions were found in brain regions that have strong synaptic and/or functional relationship with the anterior dorsal nucleus, including the anterior ventral and anterior medial nuclei, the mammillary bodies, the dorsal subiculum, as well as midline cingulate cortex that receives major thalamic inputs from the anterior thalamic nuclei. These regions are components of the hippocampal-anterior thalamic circuitry that is strongly involved in spatial memory and navigation (Aggleton et al., 2010; Jankowski et al., 2013), and these functions are notably disrupted by P7 ethanol treatment (Marquardt and Brigman, 2016). In the Ch1/Ch2 nuclei the magnitude of neuron loss was comparable to or slightly less than that in the anterior thalamic nuclei. Ch1/Ch2 has only minor connections with anterior thalamic region (Agostinelli et al., 2019), but it does project to hippocampal regions including the subiculum and CA1 region that are likely to also have significant cell loss (Ikonomidou et al., 2000). At present, it is not clear why certain brain areas are especially vulnerable to P7 ethanol. It is possible that they have a synchronous schedule of neuron development, and/or they share a common pharmacological profile.

The present study focused on several brain regions known to have a strong apoptotic response to P7 ethanol and provides only a partial

listing of brain areas that are likely to have substantial neuron loss. Other areas with high densities of apoptotic neurons after P7 ethanol include the thalamic reticular nucleus, thalamic lateral dorsal nucleus, superior colliculus, CA1 region of hippocampus, as well as other cortical areas in the mid-sagital sulcus (Ikonomidou et al., 2000; Tenkova et al., 2003) and prominent cell loss was shown in the thalamic nucleus reuniens (Ikonomidou et al., 2001; Gursky et al., 2019). Extensive neuron loss was also shown in cerebellar cortex and associated inferior olivary and deep cerebellar nuclei (Napper and West, 1995b; Pierce et al., 1999; Green et al., 2002; Nirgudkar et al., 2016). In cerebellar cortex, Purkinje cells were reduced by as much as 25–50% depending on the dose and timing of ethanol exposure, and the region of cortex. Although the peak vulnerability in the cerebellum was described as occurring around P4-5 in rats, there was still substantial cell loss at P6-7 (Hamre and West, 1993). While neuron deficits are likely in the above-mentioned areas, it is important to note that some neuron populations are comparatively unaffected by P7 ethanol. Using the same treatment as the current study, we previously found only minor changes in several brainstem nuclei (Figure 4), and in the present study we replicated our previous finding that whole neocortex has comparatively small deficits in total neuron number (Smiley et al., 2015, 2019).

In the present study we found in control brains that total neuron number in the anterior dorsal nucleus is not reduced to adult levels until after P7. To our knowledge, the timing of normal programmed cell death in the anterior thalamic nuclei has not been systematically studied. In most other forebrain regions, the main episode of neonatal programmed cell death is thought to be mainly completed by around P7 (Ahern et al., 2013; Mosley et al., 2017). However, there is precedence for later normal programmed cell death in some regions. For example, the substantia nigra has an early peak of apoptosis around P3 and a later peak around P14 (Oo and Burke, 1997). In the dLGN, total neuron number was shown to continue decreasing after P10, but those estimates were done in albino mice (Heumann and Rabinowicz, 1980), whereas a study of the dLGN in rats concluded that the peak of normal developmental apoptosis occurs around P1 and is complete by P7 (Zacharaki et al., 2010).

In summary, our findings show that estimation of total neuron number within hours of P7 ethanol provides a reliable method to assess regional differences in neuron loss caused by neonatal ethanol. Results obtained with this approach showed that a common outcome of ethanol-induced apoptosis is immediate and lasting neuron loss. Comparison between regions showed that neuron loss was most pronounced in the anterior dorsal thalamic nucleus, but other neuron populations in the anterior thalamus, subiculum and Ch1/Ch2 were also strongly affected, whereas comparatively modest neuron loss was detected in neocortex.

Data availability statement

The raw data supporting the conclusions of this article will be made available by the authors, without undue reservation.

Ethics statement

The animal study was reviewed and approved by Nathan Kline Institute IACUC.

Author contributions

JS involved in the study design and conception, data acquisition and analysis, and writing the manuscript. CB, BM, PV, and SC-B engaged in data acquisition and analyses and commenting and editing the drafts. MS and DW engaged in the study design and conception and commenting and editing the drafts. All authors contributed to the article and approved the submitted version.

Funding

This work was supported by R01AA023181 to MS, DW, and JS.

Conflict of interest

The authors declare that the research was conducted in the absence of any commercial or financial relationships that could be construed as a potential conflict of interest.

Publisher's note

All claims expressed in this article are solely those of the authors and do not necessarily represent those of their affiliated organizations, or those of the publisher, the editors and the reviewers. Any product that may be evaluated in this article, or claim that may be made by its manufacturer, is not guaranteed or endorsed by the publisher.

References

Aggleton, J. P., Omara, S. M., Vann, S. D., Wright, N. F., Tsanov, M., and Erichsen, J. T. (2010). Hippocampal-anterior thalamic pathways for memory: uncovering a network of direct and indirect actions. *Eur. J. Neurosci.* 31, 2292–2307. doi: 10.1111/j.1460-9568.2010.07251.x

Agostinelli, L. J., Geerling, J. C., and Scammell, T. E. (2019). Basal forebrain subcortical projections. *Brain Struct. Funct.* 224, 1097–1117. doi: 10.1007/s00429-018-01820-6

Ahern, T. H., Krug, S., Carr, A. V., Murray, E. K., Fitzpatrick, E., Bengston, L., et al. (2013). Cell death atlas of the postnatal mouse ventral forebrain and hypothalamus: effects of age and sex. *J. Comp. Neurol.* 521, 2551–2569. doi: 10.1002/cne.23298

AIBA (2011). Allen Mouse Brain. Available at: atlas.brain-map.org

Bonthius, D. J., and West, J. R. (1991). Permanent neuronal deficits in rats exposed to alcohol during the brain growth spurt. *Teratology* 44, 147–163. doi: 10.1002/tera.1420440203

Dorph-Petersen, K. A., Delevich, K. M., Marcsisin, M. J., Zhang, W., Sampson, A. R., Gundersen, H. J., et al. (2009). Pyramidal neuron number in layer 3 of primary auditory cortex of subjects with schizophrenia. *Brain Res.* 1285, 42–57. doi: 10.1016/j.brainres.2009.06.019

Dursun, I., Jakubowska-Dogru, E., Elibol-Can, B., Van Der List, D., Chapman, B., Qi, L., et al. (2013). Effects of early postnatal alcohol exposure on the developing retinogeniculate projections in C57BL/6 mice. *Alcohol* 47, 173–179. doi: 10.1016/j.alcohol.2012.12.013

Fagel, D. M., Ganat, Y., Silbereis, J., Ebbitt, T., Stewart, W., Zhang, H., et al. (2006). Cortical neurogenesis enhanced by chronic perinatal hypoxia. *Exp. Neurol.* 199, 77–91. doi: 10.1016/j.expneurol.2005.04.006

Forger, N. G., Rosen, G. J., Waters, E. M., Jacob, D., Simerly, R. B., and De Vries, G. J. (2004). Deletion of Bax eliminates sex differences in the mouse forebrain. *Proc. Natl. Acad. Sci. U. S. A.* 101, 13666–13671. doi: 10.1073/pnas.0404644101

Goodlett, C. R., and Eilers, A. T. (1997). Alcohol-induced Purkinje cell loss with a single binge exposure in neonatal rats: a stereological study of temporal windows of vulnerability. *Alcohol. Clin. Exp. Res.* 21, 738–744.

Green, J. T., Tran, T., Steinmetz, J. E., and Goodlett, C. R. (2002). Neonatal ethanol produces cerebellar deep nuclear cell loss and correlated disruption of eyeblink conditioning in adult rats. *Brain Res.* 956, 302–311. doi: 10.1016/S0006-8993(02)03561-8

Gundersen, H. J. G., Bagger, P., Bendtsen, T. F., Evans, S. M., Korbo, L., Marcussen, N., et al. (1988). The new stereological tools: dissector, fractionator, nucleator and point sampled intercepts and their use in pathological research and diagnosis. *Acta Pathol. Microbiol. Immunol. Scand.* 96, 857–881. doi: 10.1111/j.1699-0463.1988.tb00954.x

Gursky, Z. H., Savage, L. M., and Klintsova, A. Y. (2019). Nucleus reuniens of the midline thalamus of a rat is specifically damaged after early postnatal alcohol exposure. *Neuroreport* 30, 748–752. doi: 10.1097/WNR.0000000000001270

Hamre, K. M., and West, J. R. (1993). The effects of the timing of ethanol exposure during the brain growth spurt on the number of cerebellar Purkinje and granule cell nuclear profiles. *Alcohol. Clin. Exp. Res.* 17, 610–622. doi: 10.1111/j.1530-0277.1993.tb00808.x

Heumann, D., and Rabinowicz, T. (1980). Postnatal development of the dorsal lateral geniculate nucleus in the normal and enucleated albino mouse. *Exp. Brain Res.* 38, 75–85.

Ikonomidou, C., Bittigau, P., Ishimaru, M. J., Wozniak, D. F., Koch, C., Genz, K., et al. (2000). Ethanol-induced apoptotic neurodegeneration and fetal alcohol syndrome. *Science* 287, 1056–1060. doi: 10.1126/science.287.5455.1056

Ikonomidou, C., Bittigau, P., Koch, C., Genz, K., Hoerster, F., Felderhoff-Mueser, U., et al. (2001). Neurotransmitters and apoptosis in the developing brain. *Biochem. Pharmacol.* 62, 401–405. doi: 10.1016/S0006-2952(01)00696-7

Jankowski, M. M., Ronnqvist, K. C., Tsanov, M., Vann, S. D., Wright, N. F., Erichsen, J. T., et al. (2013). The anterior thalamus provides a subcortical circuit supporting memory and spatial navigation. *Front. Syst. Neurosci.* 7:45. doi: 10.3389/fnsys.2013.00045

Livy, D. J., Miller, E. K., Maier, S. E., and West, J. R. (2003). Fetal alcohol exposure and temporal vulnerability: effects of binge-like alcohol exposure on the developing rat hippocampus. *Neurotoxicol. Teratol.* 25, 447–458. doi: 10.1016/S0892-0362(03)00030-8

Marquardt, K., and Brigman, J. L. (2016). The impact of prenatal alcohol exposure on social, cognitive and affective behavioral domains: insights from rodent models. *Alcohol* 51, 1–15. doi: 10.1016/j.alcohol.2015.12.002

Mesulam, M. M., Mufson, E. J., Wainer, B. H., and Levey, A. I. (1983). Central cholinergic pathways in the rat: an overview based on an alternative nomenclature (Ch1-Ch6). *Neuroscience* 10, 1185–1201. doi: 10.1016/0306-4522(83)90108-2

Mooney, S. M., and Napper, R. M. (2005). Early postnatal exposure to alcohol reduces the number of neurons in the occipital but not the parietal cortex of the rat. *Alcohol. Clin. Exp. Res.* 29, 683–691. doi: 10.1097/01.ALC.0000158936.40150.5A

Mosley, M., Shah, C., Morse, K. A., Miloro, S. A., Holmes, M. M., Ahern, T. H., et al. (2017). Patterns of cell death in the perinatal mouse forebrain. *J. Comp. Neurol.* 525, 47–64. doi: 10.1002/cne.24041

Nagamoto-Combs, K., Manocha, G. D., Puig, K., and Combs, C. K. (2016). An improved approach to align and embed multiple brain samples in a gelatin-based matrix for simultaneous histological processing. *J. Neurosci. Methods* 261, 155–160. doi: 10.1016/j.jneumeth.2015.12.008

Napper, R. M., and West, J. R. (1995a). Permanent neuronal cell loss in the cerebellum of rats exposed to continuous low blood alcohol levels during the brain growth spurt: a stereological investigation. *J. Comp. Neurol.* 362, 283–292. doi: 10.1002/cne.903620210

Napper, R. M., and West, J. R. (1995b). Permanent neuronal cell loss in the inferior olive of adult rats exposed to alcohol during the brain growth spurt: a stereological investigation. *Alcohol. Clin. Exp. Res.* 19, 1321–1326. doi: 10.1111/j.1530-0277.1995.tb01619.x

Nirgudkar, P., Taylor, D. H., Yanagawa, Y., and Valenzuela, C. F. (2016). Ethanol exposure during development reduces GABAergic/glycinergic neuron numbers and lobule volumes in the mouse cerebellar vermis. *Neurosci. Lett.* 632, 86–91. doi: 10.1016/j.neulet.2016.08.039

Olney, J. W., Tenkova, T., Dikranian, K., Muglia, L. J., Jermakowicz, W. J., D'sa, C., et al. (2002a). Ethanol-induced caspase-3 activation in the in vivo developing mouse brain. *Neurobiol. Dis.* 9, 205–219. doi: 10.1006/nbdi.2001.0475

Olney, J. W., Tenkova, T., Dikranian, K., Qin, Y. Q., Labruyere, J., and Ikonomidou, C. (2002b). Ethanol-induced apoptotic neurodegeneration in the developing C57BL/6 mouse brain. *Brain Res. Dev. Brain Res.* 133, 115–126. doi: 10.1016/S0165-3806(02)00279-1

Oo, T. F., and Burke, R. E. (1997). The time course of developmental cell death in phenotypically defined dopaminergic neurons of the substantia nigra. *Brain Res. Dev. Brain Res.* 98, 191–196. doi: 10.1016/S0165-3806(96)00173-3

Pierce, D. R., Williams, D. K., and Light, K. E. (1999). Purkinje cell vulnerability to developmental ethanol exposure in the rat cerebellum. *Alcohol. Clin. Exp. Res.* 23, 1650–1659. doi: 10.1111/j.1530-0277.1999.tb04057.x

Saito, M., Mao, R. F., Wang, R., Vadasz, C., and Saito, M. (2007). Effects of gangliosides on ethanol-induced neurodegeneration in the developing mouse brain. *Alcohol. Clin. Exp. Res.* 31, 665–674. doi: 10.1111/j.1530-0277.2007.00351.x

Salmaso, N., Jablonska, B., Scafidi, J., Vaccarino, F. M., and Gallo, V. (2014). Neurobiology of premature brain injury. *Nat. Neurosci.* 17, 341–346. doi: 10.1038/nn.3604

Shin, J. E., Lee, H., Jung, K., Kim, M., Hwang, K., Han, J., et al. (2020). Cellular response of ventricular-subventricular neural progenitor/stem cells to neonatal hypoxic-ischemic brain injury and their enhanced neurogenesis. *Yonsei Med. J.* 61, 492–505. doi: 10.3349/ymj.2020.61.6.492

Smiley, J. F., Bleiwas, C., Canals-Baker, S., Williams, S. Z., Sears, R., Teixeira, C. M., et al. (2021). Neonatal ethanol causes profound reduction of cholinergic cell number in the basal forebrain of adult animals. *Alcohol* 97, 1–11. doi: 10.1016/j.alcohol.2021.08.005

Smiley, J. F., Bleiwas, C., Masiello, K., Petkova, E., Betz, J., Hui, M., et al. (2019). Effects of neonatal ethanol on cerebral cortex development through adolescence. *Brain Struct. Funct.* 224, 1871–1884. doi: 10.1007/s00429-019-01881-1

Smiley, J. F., Saito, M., Bleiwas, C., Masiello, K., Ardekani, B., Guilfoyle, D. N., et al. (2015). Selective reduction of cerebral cortex GABA neurons in a late gestation model of fetal alcohol spectrum disorder. *Alcohol* 49, 571–580. doi: 10.1016/j.alcohol.2015.04.008

Tenkova, T., Young, C., Dikranian, K., Labruyere, J., and Olney, J. W. (2003). Ethanol-induced apoptosis in the developing visual system during synaptogenesis. *Invest. Ophthalmol. Vis. Sci.* 44, 2809–2817. doi: 10.1167/iovs.02-0982

Tran, T. D., and Kelly, S. J. (2003). Critical periods for ethanol-induced cell loss in the hippocampal formation. *Neurotoxicol. Teratol.* 25, 519–528. doi: 10.1016/S0892-0362(03)00074-6

Vogt, B. A., and Paxinos, G. (2014). Cytoarchitecture of mouse and rat cingulate cortex with human homologies. *Brain Struct. Funct.* 219, 185–192. doi: 10.1007/s00429-012-0493-3

Wozniak, D. F., Hartman, R. E., Boyle, M. P., Vogt, S. K., Brooks, A. R., Tenkova, T., et al. (2004). Apoptotic neurodegeneration induced by ethanol in neonatal mice is associated with profound learning/memory deficits in juveniles followed by progressive functional recovery in adults. *Neurobiol. Dis.* 17, 403–414. doi: 10.1016/j.nbd.2004.08.006

Young, C., and Olney, J. W. (2006). Neuroapoptosis in the infant mouse brain triggered by a transient small increase in blood alcohol concentration. *Neurobiol. Dis.* 22, 548–554. doi: 10.1016/j.nbd.2005.12.015

Zacharaki, T., Sophou, S., Giannakopoulou, A., Dinopoulos, A., Antonopoulos, J., Parnavelas, J. G., et al. (2010). Natural and lesion-induced apoptosis in the dorsal lateral geniculate nucleus during development. *Brain Res.* 1344, 62–76. doi: 10.1016/j.brainres.2010.05.021

frontiers | Frontiers in Neuroscience

TYPE Original Research
PUBLISHED 02 May 2023
DOI 10.3389/fnins.2023.1170259

Check for updates

OPEN ACCESS

EDITED BY
Hermes H. Yeh,
Dartmouth College, United States

REVIEWED BY
Erin Milligan,
University of New Mexico, United States
Paul Drew,
University of Arkansas for Medical Sciences, United States

*CORRESPONDENCE
Mariko Saito
✉ mariko.saito@nki.rfmh.org
Bhaskar C. Das
✉ Bhaskar.Das@liu.edu

RECEIVED 20 February 2023
ACCEPTED 07 April 2023
PUBLISHED 02 May 2023

CITATION
Saito M, Subbanna S, Zhang X, Canals-Baker S, Smiley JF, Wilson DA and Das BC (2023) Effects of retinoic acid receptor α modulators on developmental ethanol-induced neurodegeneration and neuroinflammation. *Front. Neurosci.* 17:1170259. doi: 10.3389/fnins.2023.1170259

COPYRIGHT
© 2023 Saito, Subbanna, Zhang, Canals-Baker, Smiley, Wilson and Das. This is an open-access article distributed under the terms of the Creative Commons Attribution License (CC BY). The use, distribution or reproduction in other forums is permitted, provided the original author(s) and the copyright owner(s) are credited and that the original publication in this journal is cited, in accordance with accepted academic practice. No use, distribution or reproduction is permitted which does not comply with these terms.

Effects of retinoic acid receptor α modulators on developmental ethanol-induced neurodegeneration and neuroinflammation

Mariko Saito[1,2]*, Shivakumar Subbanna[1], Xiuli Zhang[1], Stefanie Canals-Baker[1], John F. Smiley[1,2], Donald A. Wilson[3,4] and Bhaskar C. Das[5,6]*

[1]Division of Neurochemistry, Nathan Kline Institute for Psychiatric Research, Orangeburg, NY, United States, [2]Department of Psychiatry, New York University School of Medicine, New York, NY, United States, [3]Emotional Brain Institute, Nathan Kline Institute for Psychiatric Research, Orangeburg, NY, United States, [4]Department of Child and Adolescent Psychiatry, New York University Medical Center, New York, NY, United States, [5]Arnold and Marie Schwartz College of Pharmacy and Health Sciences, Long Island University, Brooklyn, NY, United States, [6]Department of Medicine, Icahn School of Medicine at Mount Sinai, New York, NY, United States

Ethanol exposure in neonatal mice induces acute neurodegeneration followed by long-lasting glial activation and GABAergic cell deficits along with behavioral abnormalities, providing a third trimester model of fetal alcohol spectrum disorders (FASD). Retinoic acid (RA), the active form of vitamin A, regulates transcription of RA-responsive genes and plays essential roles in the development of embryos and their CNS. Ethanol has been shown to disturb RA metabolism and signaling in the developing brain, which may be a cause of ethanol toxicity leading to FASD. Using an agonist and an antagonist specific to RA receptor α (RARα), we studied how RA/RARα signaling affects acute and long-lasting neurodegeneration and activation of phagocytic cells and astrocytes caused by ethanol administered to neonatal mice. We found that an RARα antagonist (BT382) administered 30min before ethanol injection into postnatal day 7 (P7) mice partially blocked acute neurodegeneration as well as elevation of CD68-positive phagocytic cells in the same brain area. While an RARα agonist (BT75) did not affect acute neurodegeneration, BT75 given either before or after ethanol administration ameliorated long-lasting astrocyte activation and GABAergic cell deficits in certain brain regions. Our studies using Nkx2.1-Cre;Ai9 mice, in which major GABAergic neurons and their progenitors in the cortex and the hippocampus are labeled with constitutively expressed tdTomato fluorescent protein, indicate that the long-lasting GABAergic cell deficits are mainly caused by P7 ethanol-induced initial neurodegeneration. However, the partial reduction of prolonged GABAergic cell deficits and glial activation by post-ethanol BT75 treatment suggests that, in addition to the initial cell death, there may be delayed cell death or disturbed development of GABAergic cells, which is partially rescued by BT75. Since RARα agonists including BT75 have been shown to exert anti-inflammatory effects, BT75 may rescue GABAergic cell deficits by reducing glial activation/neuroinflammation.

KEYWORDS

fetal alcohol spectrum disorders, astrocyte, GABAergic neuron, boron-containing small molecules, retinoic acid receptor α agonist, retinoic acid receptor α antagonist, neurodegeneration, neuroinflammation

Introduction

Prenatal alcohol exposure causes adverse effects on fetal development especially in the brain, leading to fetal alcohol spectrum disorders (FASDs) in offspring. FASD neuropathology includes volume reduction in the corpus callosum, cerebral cortex, cerebellum, and subcortical structures such as the hippocampus, basal ganglia, amygdala, and thalamus, which associate with cognitive and behavioral abnormalities (Riley and McGee, 2005; Astley et al., 2009; May et al., 2009; Norman et al., 2009; Riley et al., 2011; May et al., 2014). While many factors can be involved in pathogenesis of FASD, retinoic acid (RA) signaling has been considered an important factor, based on clinical studies as well as studies using animal models for FASD (Duester, 1991; Johnson et al., 2007; Sapin, 2008; Kane et al., 2010; Young et al., 2014; Fainsod et al., 2020). RA, the active form of vitamin A, regulates transcription of RA-responsive genes *via* nuclear RA receptor (RAR)-α,β,γ and retinoid X receptor (RXR)-α,β,γ activation along with less frequent non-genomic regulation and plays essential roles in development of embryos and their CNS as well as in adult tissue homeostasis (Mey and Mccaffery, 2004; Niederreither and Dollé, 2008; Crandall et al., 2011; Rhinn and Dollé, 2012; Shearer et al., 2012; Haushalter et al., 2017; Dowling, 2020). Temporal and spatial RA distribution within embryonic cell population seems to be precisely controlled by dynamic expression patterns of synthesizing/metabolizing enzymes (Niederreither and Dollé, 2008; Rhinn and Dollé, 2012), and insufficient or excess RA causes teratogenic and/or toxic effects, which mimic the ethanol effects on the developing brain (Wolf, 2010; Fainsod et al., 2020). It has been shown that ethanol reduces RA levels due to the competition between ethanol clearance and RA biosynthesis (Duester, 1991; Johnson et al., 2007; Fainsod et al., 2020). The reduction in RA induces multiple deficits similar to FASD in both patients and animal models, and addition of RA or RA synthesizing enzymes restores the deficits in adult or embryonic brains of several species (Yelin et al., 2005; Johnson et al., 2007; Marrs et al., 2010; Shabtai et al., 2018). On the other hand, several reports indicate that both acute and chronic alcohol elevate RA in adult and fetal brain (Kane et al., 2010) and in the developing or adult cerebellum (McCaffery et al., 2004), and an antagonist of RARβ suppresses RARβ expression and reverses chronic ethanol-induced cognitive impairment (Alfos et al., 2001). The discrepancy may be due to the differences in the age and alcohol administration conditions.

Ethanol exposure in neonatal rodents causes acute neurodegeneration as well as long-lasting neuroanatomical and behavioral deficits, providing a third trimester binge drinking model. Previous studies have demonstrated that ethanol exposure in the P7 mouse brain induces robust acute neurodegeneration within 24 h in many brain regions especially in the cingulate and retrosplenial cortex and the thalamus (Olney et al., 2002a; Saito et al., 2007). These brain regions belong to the extended hippocampus circuitry important for spatial learning and memory functions, which may explain profound learning and memory deficits observed in this mouse model of FASD (Wozniak et al., 2004). The acute neurodegeneration detected by cleaved caspase 3 expression, Fluoro-Jade (FJ) C, and Tunel assay is accompanied by activation of microglia, which phagocytose FJ positive degenerating neurons, the subsequent activation of astrocytes, and long-lasting GABAergic cell deficits (Coleman et al., 2012; Saito et al., 2015; Smiley et al., 2015, 2019; Bird et al., 2018, 2020; Saito et al., 2019). The GABAergic cell deficits observed mainly in parvalbumin (PV) positive (+) and somatostatin (SST) + cells are more prominent than the total neuron deficits and may cause neurobehavioral abnormalities (Sadrian et al., 2012, 2014; Wilson et al., 2016; Lewin et al., 2018). However, mechanisms of this relatively specific long-lasting GABAergic cell loss are unclear. GABAergic cells or their progenitors exposed to P7 ethanol may die more than other types of neurons during acute neurodegeneration, and/or may be specifically affected by delayed cell loss or perturbed PV/SST expression. Since disturbed RA signaling is involved in ethanol toxicity in the developing brain (Duester, 1991; Alfos et al., 2001; McCaffery et al., 2004; Yelin et al., 2005; Johnson et al., 2007; Sapin, 2008; Kane et al., 2010; Marrs et al., 2010; Young et al., 2014; Shabtai et al., 2018; Fainsod et al., 2020) and influences GABAergic cell maturation in early postnatal mouse prefrontal cortex (Larsen et al., 2019), we examined how RARα modulation affects the course of P7 ethanol-induced neurodegeneration and neuroinflammation using a specific RARα agonist BT75 and an antagonist BT382. BT75 was previously synthesized as a borate containing derivative of RARα agonist Am580 and has been shown to be less toxic compared to all-trans retinoic acid (ATRA) or Am580 (Zhong et al., 2011). BT382 is an RARα antagonists identified in our previous studies (Anguiano et al., 2013).

Our present studies indicated that while BT382 partially attenuated P7 ethanol-induced acute neurodegeneration, BT75 alleviated long-term astrocyte activation and GABAergic cell loss in the cortex and hippocampus. RA signaling activation by BT75 may attenuate chronic neuroinflammation and improve survival/maturation of GABAergic neurons in the adult brain. Thus, our studies suggest that RA signaling is a promising target for developing neuroprotective agents against FASD.

Materials and methods

Syntheses of BT382 and BT75

Synthesis of BT382 (Figure 1) was performed as follows: To a solution of 2-amino-5-chlorophenol (A) (0.001 mol) in dichloromethane (40 ml) aqueous potassium carbonate (20% w/v) and tetrabutylammonium hydrogen sulfate (0.0005 mol) was added and mixture was stirred for 2 h at room temperature. After 2 h, 2-Bromo-4-methylacetophenone (0.01 mol) in 20 ml dichloromethane was added drop-wise through a course of 15 min and the resultant mixture was refluxed till completion for 3 h. The organic layer was extracted with dichloromethane and dried over sodium sulfate evaporated in vacuum to give crude solid product. The solid was then recrystallized with hot ethanol to obtain pure BT382. The purity was verified using NMR (1H, 13C), HRMS, and HPLC. The result of BT382 [7-Chloro-3-(p-tolyl)-2H-benzo(b)(1,4)oxazine]: (Yield = 77%), 1H NMR (600 MHz, DMSO-d6) δ 7.89 (d, J = 8.0 Hz, 2H), 7.33–7.31 (m, 3H), 7.08–7.02 (m, 2H), 5.19 (s, 2H), 2.48 (s, 3H). HRMS (ESI) calcd for C15H13ClNO 258.0680 found 258.1377 [M + H] + .

Synthesis of BT75 [Figure 1; (E)-2-(4-(2-(6,8-dichloro-2-phenyl-2H-chromen-3-yl)vinyl)phenyl)-4,4,5,5-tetramethyl-1,3,2-dioxaborolane] was performed as follows: A clean oven dried three-neck round bottom flask (RBF) was charged with aldehyde 1 (Das et al., 2010) (1 equiv.) in DMF. Then addition of salt 2 (1.2 equiv.) Sodium tertbutoxide (STB) (3 equiv.) was added into the reaction mixture at 0°C. The reaction mixture was stirred at room temperature for 24 h.

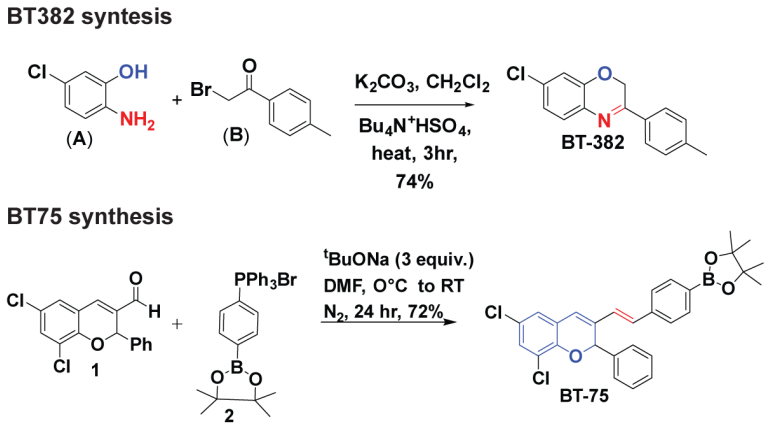


FIGURE 1
Synthesis of BT382 and BT75.

Progress of the reaction was monitored by TLC (100% Hexane). In TLC nonpolar spot was observed corresponding to aldehyde. After completion of the reaction, reaction mixture was neutralized by 2 N HCl. After neutralization, ethyl acetate was added in the reaction mixture; the combined organic layer was collected and dried with Na_2SO_4 and evaporated under reduced pressure. The crude material was purified by column chromatography (5% ethyl acetate: 95% hexane). After purification white solid was observed (BT75). The result of BT75 synthesis was: (Yield = 72%), ^{1}H NMR (600 MHz, DMSO-d_6) δ 7.61 (d, J = 7.8 Hz, 2H), 7.47 (d, J = 7.8 Hz, 2H), 7.42 (d, J = 7.2 Hz, 2H), 7.35–7.29 (m, 5H), 7.23 (d, J = 16.4 Hz, 1H), 7.01 (s, 1H), 6.71 (d, J = 16.5 Hz, 1H), 6.64 (s, 1H), 1.26 (s, 12H).

Animals

C57BL/6 J (#000664), C57BL/6 J-Tg(Nkx2-1-cre)2Sand/J (Nkx2.1-Cre, #008661), and B6.Cg-Gt(ROSA)26Sortm9(CAG-tdTomato)Hze/J (Ai9, #007909) mice were obtained from Jackson laboratories (Bar Harbor, ME) and bred at the Nathan Kline Institute animal facility under *ad lib* food and water at all times. All procedures were approved by the Nathan Kline Institute IACUC and were in accordance with NIH guidelines for the proper treatment of animals.

Treatments of C57BL/6J mice with ethanol, BT75, and BT382

P7 C57BL/6 J pups (both males and females) were injected subcutaneously (sc) with saline or ethanol (2.5 g/kg) twice at a 2 h interval as previously described (Olney et al., 2002a; Saito et al., 2007). Pups were returned to their home cage immediately following injections. Our previous studies showed that this P7 ethanol treatment induced a peak blood alcohol level (BAL) of 0.45 g/dl when truncal blood was collected at 0.5, 1, 3, and 6 h following the second ethanol injection and analyzed with an Alcohol Reagent Set (Pointe Scientific, Canton, MI, United States) (Saito et al., 2007). Pups were weaned at P28 into group cages of littermates. Same-sex mice were housed together in cages in numbers between two and four per cage. For BT75 and BT382 treatments, 2 µl (2.5 or 25 µg in 10% DMSO) of BT75, BT382, or 2 µl of the vehicle (10% DMSO) was administered by intracerebroventricular (icv) injection (Sadakata et al., 2007) 30 min before the first ethanol injection. At P8 (20 h after the first ethanol injection), P60, or P90, mice were perfusion-fixed for immunohistochemistry, or the cortex and hippocampus were dissected out and immediately frozen for Western blot analyzes. For the post-ethanol treatment of BT75, mice were injected intraperitoneally (ip) with BT75 (10 mg/kg, 20 µl/g in 10% DMSO) or vehicle (10% DMSO) once a day for 3 consecutive days starting 3 days after the first ethanol injection at P7. Mice were perfusion-fixed or the cortex and hippocampus were taken out at P30. Since significant sex differences in the effects of P7 ethanol have not been previously observed (Wilson et al., 2016; Saito et al., 2019), nor were any significant differences observed between sexes here, the data from males and females were combined.

Treatments of Nkx2.1-Cre;Ai9 mice with ethanol

Nkx2.1-Cre mice expressing Cre under the control of the Nkx2.1 promoter/enhancer regions were bred to Ai9 Cre-reporter mice, and the offspring (Nkx2.1-Cre;Ai9) were used for experiments. Since Nkx2.1 is a transcription factor, transiently (around embryonic day 10–14) expressed in the pallidal telencephalon and required for the specification of PV and SST cortical and hippocampal interneurons (Xu et al., 2008), PV and SST neurons and their progenitors in the postnatal cortex and the hippocampus can be identified by a constitutively expressed reporter florescent protein (tdTomato). These mice are useful for studying the fate of PV and SST neurons and their progenitors because of their tdTomato expression in these cells regardless of the presence of PV/SST. To examine the effects of P7 ethanol on acute and long-lasting GABAergic cell loss, Nkx2.1-Cre;Ai9 mice were treated with ethanol at P7 as described above for C57BL/6 J mice and perfusion-fixed at P8, P14, and P30 for histochemical analyzes of tdTomato+ cells. For comparison, immunohistochemical analyzes of PV+ and SST+ cells were also carried out using the same brain sections.

Fluoro-jade staining, immunohistochemistry and cell counting

In each experiment, 4 to 6 mice per each group derived from at least 3 different litters were used. Mice were perfused with a solution containing 4% paraformaldehyde and 4% sucrose in cacodylate buffer (pH 7.2), and the heads were removed and further fixed in the perfusion solution overnight. Then brains were removed, transferred to phosphate buffered saline (PBS) solution, and kept at 4°C for 2–5 days until cut with a vibratome into 50 μm thick coronal sections. For Fluoro-Jade C (FJ) (Sigma-Aldrich) staining, the free-floating sections rinsed in PBS were placed on slide glasses and processed as described in the manufacturer's instruction. For immunohistochemistry, the free-floating sections were rinsed in PBS, permeabilized in methanol for 10 min, and incubated for 30 min in blocking solution (PBS containing 5% BSA and 0.1% Triton X-100), followed by incubation overnight with antibodies against parvalbumin (PV) (PV25, Swant, Marly, Switzerland, used for detection of PV neurons), somatostatin (SST) (rabbit polyclonal antibody AP33464SU-N, OriGene, detection of SST neurons), GFAP (D1F4Q) (Rabbit mAb #12389, Cell Signaling, detection of astrocyte activation), GFAP (GA5) (Mouse mAb #3670, Cell Signaling), CD68 (Rat anti mouse monoclonal FA-11, BioRad, detection of phagocytic cell activation), phospho-NF-κB p65 (Ser536) (93H1) (Rabbit mAb #3033, Cell Signaling, detection of NF-κB activation), and NF-κB p65 (D14E12) (Rabbit mAb #8242, Cell Signaling) in PBS containing 3% BSA and 0.1% Triton X-100. Activation of NF-κB, a key nuclear transcription factor, is known to mediate inflammatory responses. Activated NF-κB translocates to the nucleus and is involved in the regulation of transcription of many inflammation-related genes. Furthermore, once activated, posttranslational modifications including phosphorylations allow the regulation of NF-κB transcriptional activity. Especially phosphorylation of p65 (a subfamily of NF-κB proteins) at serine 536 is important for P65 nuclear import (Mattioli et al., 2004). Here, antibodies against phospho (ser536)-NF-κB p65 and NF-κB p65 were used to examine the possibility of glial activation/inflammation through NF-κB activation. Brain sections incubated with one of these primary antibodies were then rinsed in 0.1% Triton X-100 in PBS three times and incubated with another primary antibody for 2 h at r.t., followed by incubation with Alexa Fluoro594 (or 488) goat anti-rabbit (mouse, rat) IgG (Life Technologies, Grand Island, NY) in 0.1% Triton X-100 in PBS containing 1% BSA for 1 h at r.t. Sections were finally rinsed in PBS three times, mounted, and coverslipped using ProLong Gold Antifade Reagent (Life Technologies). All photomicrographs were taken through a 4X, 10X, or 20X objective with a Nikon Eclipse TE2000 inverted microscope attached to a digital camera DXM1200F. Because our previous studies (Smiley et al., 2015) showed that both 2-dimensional and stereological 3-dimensional counting methods gave similar significant reduction in PV cell densities in the cortex by P7 ethanol treatment, the two-dimensional counting method was used in the present studies. The PV, SST, GFAP, and CD68 positive (+) cell number of each area of interest (AOI) and total dimensions of each AOI were measured using the Image-Pro software version 6.0 (Media Cybernetics, Silver Spring, MD). AOIs for cell counting were the cingulate cortex, retrosplenial cortex, dorsal hippocampal molecular layer of dentate gyrus, and dentate gyrus. These AOIs were defined according to the Atlas of mouse brain (Paxinos and Franklin, 2004) or Atlas of the Developing Mouse Brain at E17.5, P0, and P6 (Paxinos et al., 2007). The cell density of each AOI was calculated as the mean cell number per square millimeter from 4 to 6 mice (derived from 3 to 5 different litters) using 4 to 6 sections around bregma 0.98 to 0.14 mm for the cingulate cortex and 3 to 6 sections around bregma -1.22 to -1.94 mm for the retrosplenial cortex/dentate gyrus/molecular layer of dentate gyrus. However, this cell counting method does not provide total cell number in each brain region and is considered a semi-quantitative method, which is a limitation of our current study.

Brain tissue homogenate and Western blots

Brain tissues (cortex and hippocampus) were homogenized in 10:1 *v/w* tissue homogenization buffer (0.25 M sucrose, 20 mM Tris–HCl pH 7.4, 1 mM EDTA, 1 mM EGTA, all reagents from Sigma-Aldrich) supplemented with protease inhibitors (5 μg/ml leupeptin, 5 μg/ml antipain dihydrochloride, 5 μg/ml pepstatin A, 1 mM phenylmethanesulfonyl fluoride, 1 μM E64, all reagents from Sigma-Aldrich) and phosphatase inhibitors (PhosSTOP, Sigma) immediately before homogenization. The procedure was performed in ice-cold glass homogenizers with 20 complete strokes of Teflon pestles (Wheaton, DWK Life Sciences). The tissue homogenate analysis was performed on equal protein amounts (20 μg), as estimated by the BCA assay (Pierce, Thermo Scientific), and normalized to β-actin. The primary antibodies used are GFAP (D1F4Q) (Rabbit mAb #12389, Cell Signaling), phospho-NF-κB p65 (Ser536) (93H1) (Rabbit mAb #3033, Cell Signaling) and β-Actin (13E5) (Rabbit mAb #4970, Cell Signaling). The secondary antibodies (HRP-conjugated) were from Jackson ImmunoResearch (West Grove, PA, United States). The chemiluminescent substrate was either ECL or femto ECL (both from Pierce, Thermo Fisher Scientific) for either strong or weak signals, respectively. All protein bands were acquired with the iBright FL1500 imaging system (Thermo Fisher Scientific). For densitometry quantification of protein bands, the ImageJ software (National Institute of Health) was used. All histograms were plotted as mean ± standard error of the mean (SEM).

Statistics

Data were analyzed by Student's *t*-test for comparisons of two groups and one–or two-way ANOVA for comparisons of more than two groups/factors using SPSS statistics software (version 22). For *post hoc* analyzes, Tukey HSD or Fisher's LSD groups tests were used. For all analyzes, $p < 0.05$ was considered statistically significant. Values are expressed as mean ± SEM obtained from 4 to 6 animals.

Results

BT382, but not BT75, attenuated P7 ethanol-induced acute neurodegeneration

To examine the effects of BT382 (RARα antagonist) and BT75 (RARα agonist) on ethanol-induced acute neurodegeneration in neonatal mice, C57BL/6J mice were injected (icv) with BT382 (25 μg/2 μl), BT75 (25 μg/2 μl), or the vehicle (10% DMSO/2 μl) 30 min before the first saline/ethanol injection (sc) at P7. Then, the mice were perfusion-fixed 20 h after the first saline/ethanol injection, when robust neurodegeneration has been observed (Olney et al., 2002b),

and the brain sections were processed for detection of degenerating neurons by FJ staining. As reported previously (Sadrian et al., 2012), while FJ staining was very scarce in the saline controls, ethanol increased the density of FJ-positive (+) neurons in many brain regions including the cingulate cortex, retrosplenial cortex, and hippocampus. Figure 2A shows FJ+ cell densities in the cingulate cortex encompassed by white lines. Tukey HSD post-hoc test after one-way ANOVA indicated that the ethanol (EtOH) group is significantly different from the saline group, and also different from the EtOH+BT382 group, but not significantly different from EtOH+BT75 group, indicating significant reduction of neurodegeneration by BT382 but not by BT75.

Brain sections obtained for FJ staining were also fluorescence-labeled using anti-CD68 antibody, and CD68+ cell densities were counted in the cingulate cortex (Figure 2B). Similar to the results of FJ staining, Tukey HSD post-hoc test after one-way ANOVA indicated that the EtOH group was significantly different from the saline group and the EtOH+BT382 group, but not different from the EtOH+BT75 group, indicating significant reduction of CD68+ cells by BT382 but not by BT75. Our previous studies showed that after P7 ethanol treatment, Iba-1+ microglia found near dying neurons in the cortex became morphologically activated and subsequently phagocytosed FJ+ degenerated neurons, and these phagocytic microglia were co-localized with CD68+ cells (Saito et al., 2015). These studies suggest that CD68+ cells in the cingulate cortex in Figure 2B are activated phagocytic microglia, although some CD68+ phagocytic cells may be perivascular or invaded peripheral mononuclear macrophages. Thus, an RARα antagonist BT382 seems to attenuate P7 ethanol-induced acute neurodegeneration and the associated microglial activation and phagocytoses.

P7 ethanol induced long-lasting GABA neuron reduction, which was partially attenuated by BT75

Our previous studies indicated that P7 ethanol, which induced acute neurodegeneration, also caused long-lasting reduction in PV+ and SST+ neurons in the cortex and hippocampus, and the reduction was more prominent than that of total neuron numbers (Smiley et al., 2015, 2019; Saito et al., 2019). However, since PV or SST cell numbers were estimated by counting PV+ or SST+ cells, it is not clear if the long-lasting reduction of those cells is due to P7 ethanol-induced acute neurodegeneration (cell loss) or reduction of PV/SST expression by disturbed cell maturation/homeostasis of surviving neurons. To ask this question, Nkx2.1-Cre;Ai9 mice were injected with ethanol (2.5 g/kg, twice) at P7, and brains taken at P8, P14, and P30 were vibratome-sectioned to examine tdTomato+ cells. The brain sections were also fluorescence-labeled using anti-SST or anti-PV antibody to detect PV+ or SST+ cells. Numbers of these labeled cells were estimated in the cingulate cortex (Cg), retrosplenial cortex (RS), dorsal hippocampal dentate gyrus (DG), CA1, and CA2 + CA3 (CA2 + 3) regions. Figure 3A shows cell numbers of tdTomato+, SST+, or PV+ cells of P8 (20 h after ethanol treatment), P14, and P30 mice after treatment with saline/EtOH at P7. Since PV expression was barely detectable at P8, PV+ cells were only counted at P14 and P30. Two-way ANOVA indicated that there were significant main effects of treatment (saline/EtOH) in the number of tdTomato+ neurons in Cg, RS, DG, and CA1, but not in CA2 + 3. Also, there were main effects of time points in all these ROIs, and there were significant interactions between the two factors

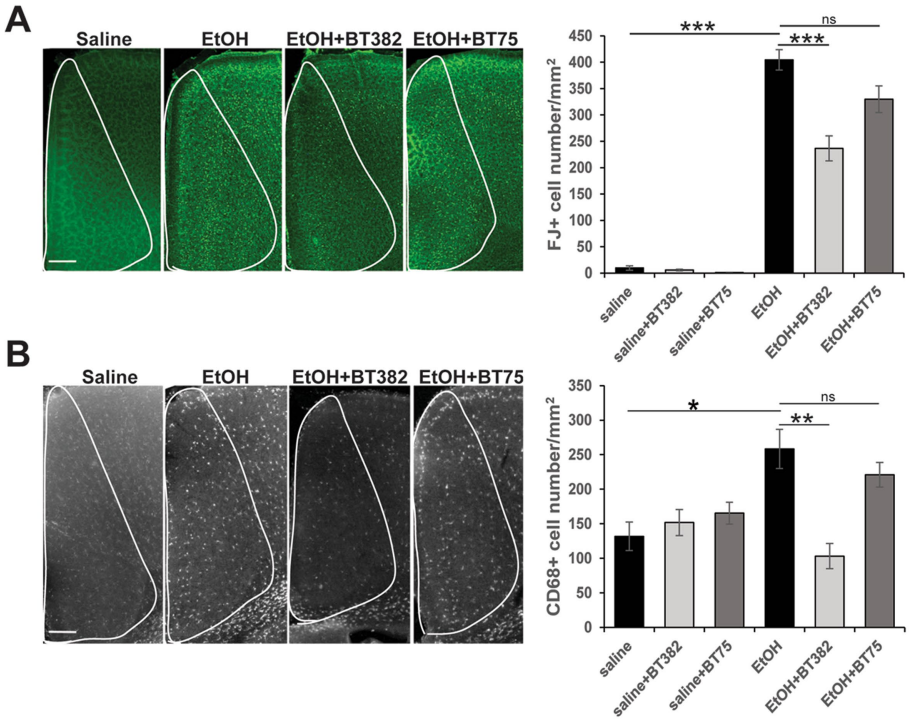


FIGURE 2
BT382 attenuated P7 ethanol-induced neurodegeneration. Mice were injected with saline/ethanol (EtOH) at P7, perfusion-fixed at P8 (20h after injections), and the brain sections were stained with FJ **(A)** or immunofluorescence-stained using anti-CD68 antibody **(B)**. Images are representative brain sections in the cingulate cortex area (scale bar=200μm), and the graphs show FJ+ cell densities **(A)** and CD68+ cell densities **(B)** in the cingulate cortex (encompassed by white lines). *p<0.05, **p<0.01, ***p<0.001 and ^{ns}not significant by a Tukey test after one-way ANOVA. n=4–5.

(treatment and time points) in the RS and DG. In SST+ and PV+ cells, there were significant main effects of treatment in all regions measured including CA2+3 region. Also, there were significant main effects of time points in all regions in SST+ cells, and in Cg and RS regions in PV+ cells. The results indicate that P7 ethanol acutely eliminates significant amounts of tdTomato+ cells in the cortex, especially in RS and the degree of reduction is similar to that found in SST-labeled cells. Figure 3B shows a representative image of tdTomato+ cells in RS 20 h after saline (Ctr) or EtOH treatment, indicating that P7 ethanol induced degeneration in some of the tdTomato+ cells. This agrees with previous studies describing apoptotic cell death detected by caspase 3 activation in GABAergic interneurons in RS, 2–8 h after P7 ethanol treatment (Bird et al., 2020). Since most of the SST+ or PV+ cells in the RS at P30 are tdTomato+ cells as shown in Figure 3C, and the majority of tdTomato+ cells in the cortex are SST+, PV+, or their progenitors (Xu et al., 2008), it is likely that the loss of tdTomato+ cells at P8 is due to the loss of SST+, PV+, and their progenitors, considering the number of lost cells of tdTomato+ (~223) and SST+ cells (~64) in RS. The control (saline-treated) neurons also decreased during the period (P8-P30), and the differences in neuron numbers between the control and ethanol groups shrank. However, the apparent decrease in the cell number during the time course (P8-P30) may be due to our 2-dimensional cell counting method. To obtain total cell number in each brain region, stereological 3-dimensional counting is necessary.

Thus, acute neurodegeneration triggered by P7 ethanol may primarily induce long-time GABAergic cell loss especially in the cortex. However, considering the greater reduction of SST+ and PV+ neuron numbers than tdTomato+ cell numbers by P7 ethanol found in the hippocampus CA2+3, it is possible that P7 ethanol not only induces acute neurodegeneration, but also decreases SST and PV expression of surviving neurons and contributes to long-lasting GABAergic cell deficits.

Since RARα agonists and RA have been shown to have neuroprotective effects (Lee et al., 2009; Cai et al., 2019; Tian et al., 2022; Kang et al., 2023), and BT75 did not induce significant protection against acute neurodegeneration induced by P7 ethanol, we next examined if BT75 can affect long-lasting GABAergic cell deficits observed in the adult brain. C57BL/6J mice were treated with BT75 and ethanol at P7,

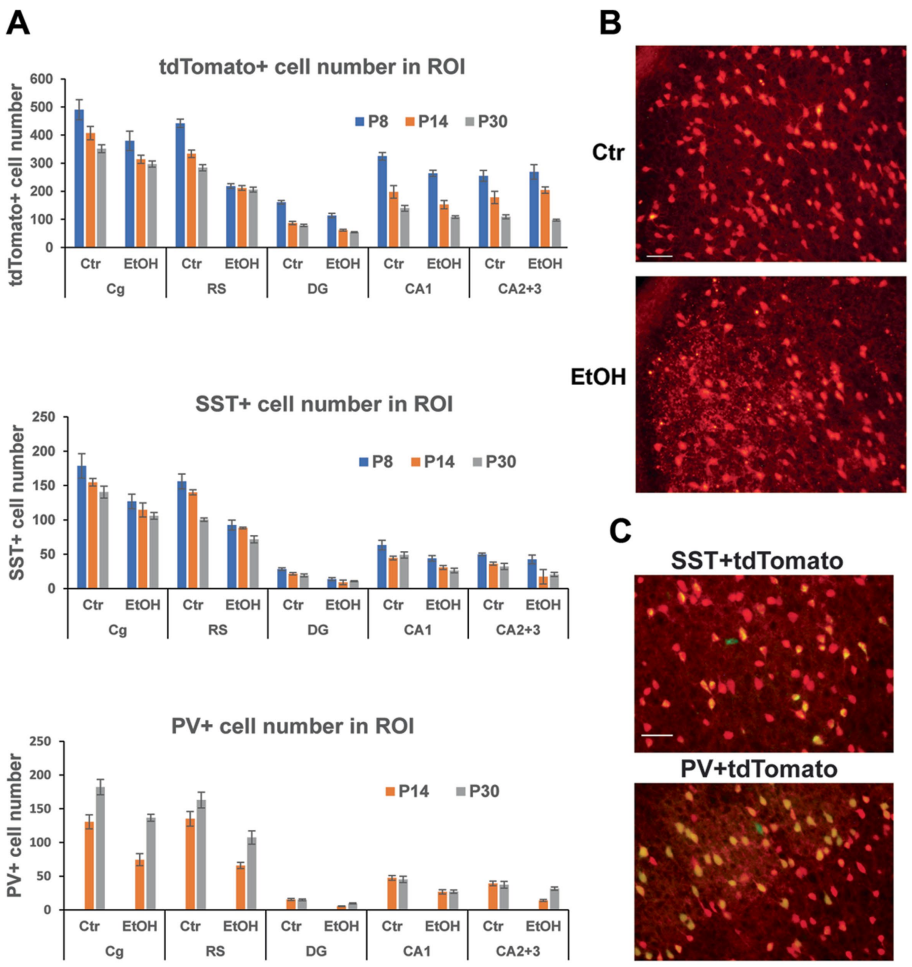


FIGURE 3
P7 ethanol induces long-lasting reduction in tdTomato+, SST+, and PV+ cells. **(A)** Nkx2.1-Cre;Ai9 mice were injected with saline (Ctr) or EtOH (2.5g/kg, twice) at P7, and brains were perfusion-fixed at P8, P14, and P30 and vibratome-sectioned to count tdTomato+, SST+, and PV+ cell number in the cingulate cortex (Cg), retrosplenial cortex (RS), dorsal hippocampal dentate gyrus (DG), CA1, and CA2+3 regions by 2-dimensional counting. PV, which is barely expressed at P8 was only counted at P14 and P30. Mean±SEM, n=4. **(B)** 20h after saline/EtOH treatment, Nkx2.1-Cre:Ai9 mice were perfusion-fixed, and brain sections were examined. EtOH treatment gave some cells neurodegenerative morphologies in RS. Scale bar=50μm. **(C)** PV+ cells (labeled green) and SST+ cells (green) were primarily co-localized with tdTomato+ cells (red) in the cortex at P30. Scale bar=50μm.

perfusion-fixed at P60, and the brain sections were used for PV immunohistochemistry. PV+ cell densities were counted in RS (Figures 4A,B) and DG (Figures 4C,D), where significant differences between saline and ethanol groups were detected in our previous studies (Lewin et al., 2018; Saito et al., 2019). In Figure 4A, Tukey HSD post-hoc test after one-way ANOVA indicated that the EtOH group was significantly different form the saline group and the EtOH+BT75 group. In Figure 4C, Fisher's LSD post-hoc test after one-way ANOVA indicated that the EtOH group was significantly different form the saline group and the EtOH+BT75 group. These results indicate that BT75 partially restored PV+ neurons in these brain regions. Figure 4A also showed that 2.5 and 25 μg BT75 gave the similar neuroprotective effects.

P7 ethanol induced long-lasting astrocyte activation, which was attenuated by BT75

P7 ethanol also induces long-lasting astrocyte activation. As previously reported (Saito et al., 2015), P7 ethanol-induced neurodegeneration is followed by microglial activation which peaks around 24 h, and then astrocyte activation which peaks around 36 h. While microglial morphology returns to the resting states by 48 h after ethanol treatment, the densities of GFAP+ astrocytes are still significantly higher even in the adult brain. Figure 5A shows images of brain sections from P90 mice treated with saline or ethanol at P7. The brain sections were labeled using anti-GFAP (green) or anti-phospho-NFκB P65 (p-NFκB) (red) antibody. Using these images, labeled cell densities of dorsal hippocampus CA3 were measured (Figure 5B). Both GFAP+ cell densities and p-NFκB+ cell densities were significantly higher in ethanol-treated mice (Student's *t*-test). Figure 5D indicates that p-NFκB+ cells were co-localized with GFAP+ cells. The area of Figure 5D is a part of dorsal hippocampal CA3 region, shown as a rectangle with white line in Figure 5C. Results of immunohistochemistry were confirmed by measuring the GFAP expression by Western blots using the hippocampus (HP) and neocortex (NC) of P60 mice treated with P7 saline/ethanol (Figure 5E). P7 ethanol also induced higher amounts of p-NFκB in the hippocampus but not in the cortex (Figure 5F).

To examine the effects of BT75 on the long-lasting elevation GFAP+ cells by P7 ethanol, C57BL/6 J mice were treated with BT75 or the vehicle 30 min before saline/ethanol injections at P7, perfusion-fixed at P60, and the brain sections were examined by immunohistochemistry. As shown in Figure 6, densities of GFAP+ cells in the cingulate cortex (Cg) (A) or in the molecular layer of dentate gyrus (MolDG) (B) in the EtOH group were significantly higher than those in the saline group or those in the EtOH+BT75 group by Tukey HSD post-hoc test after one-way ANOVA.

Post-ethanol administration of BT75 attenuated GABAergic cell deficits and astrocyte activation induced by P7 ethanol

Next, we examined if BT75 can attenuate P7 ethanol-induced GABAergic neuronal deficits or astrocyte activation, when BT75 is applied after ethanol administration. Three days after saline/ethanol

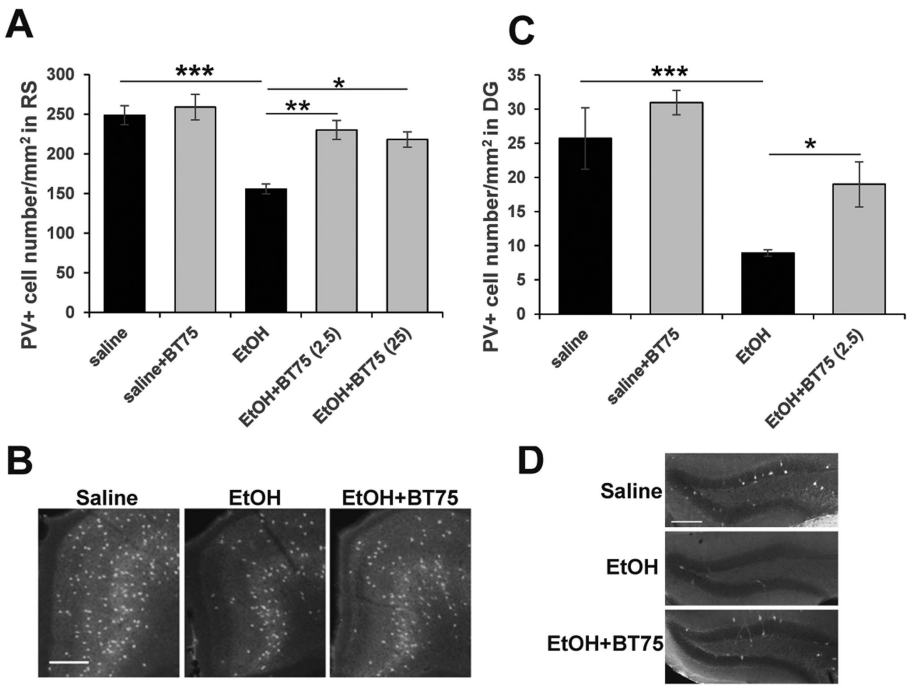


FIGURE 4
BT75 given before ethanol attenuates P7 ethanol-induced PV neuron deficits at P60. **(A)** 30min before saline/EtOH administration, P7 mice were injected (icv) with 10% DMSO or BT75 (2.5μg or 25μg) and were perfusion-fixed at P60. Then, PV+ cell densities were counted in RS. ***p<0.001, **p<0.01, and *p<0.05 by a Tukey post-hoc test after one-way ANOVA. n=4. **(B)** Representative images used in **A**. **(C)** PV+ cell densities were counted in DG. ***p<0.001 and *p<0.05 by a Fisher's LSD post-hoc test after one-way ANOVA. n=4. **(D)** Representative images used in **C**. In **B** and **D**, scale bar=200μm.

10.3389/fnins.2023.1170259

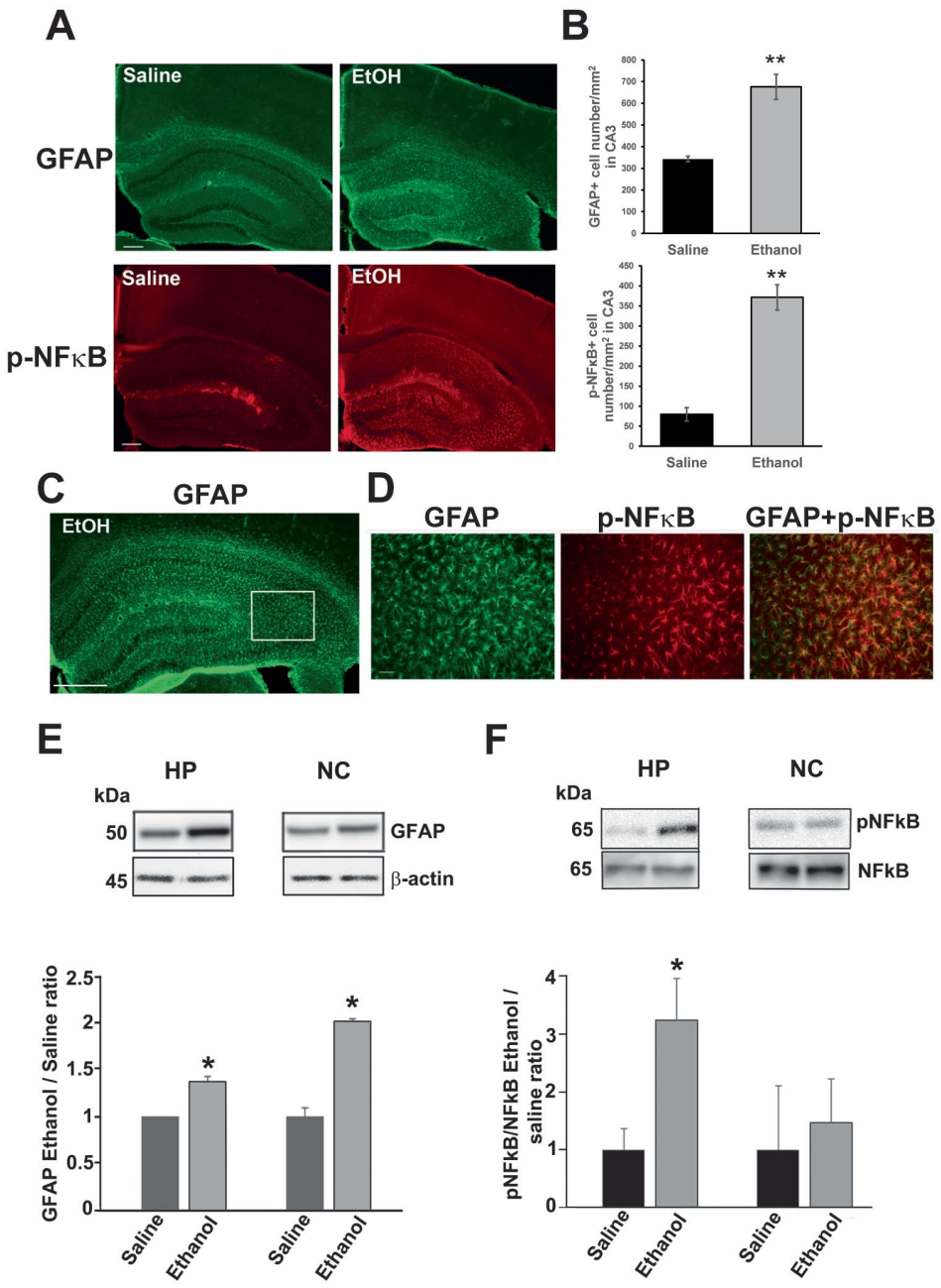


FIGURE 5
P7 ethanol increases GFAP and p-NFκB P65 levels at P90. **(A)** Mice injected with saline or ethanol at P7 were perfusion-fixed at P90, and the brain sections were immunostained by anti-GFAP antibody and anti-phospho-NFκB P65 (p-NFκB) antibody. Scale bar=200μm. **(B)** From the images, such as shown in **A**, GFAP+ and p-NFκB+ cell densities were measured in the dorsal hippocampal CA3 region. $^{**}p<0.01$ between saline and ethanol groups by Student's *t*-test. $n=4$. **(C,D)** Brain sections were dual-labeled with anti-GFAP antibody (green) and anti-p-NFκB antibody (red), and the images were overlaid. A rectangular region with white line (a part of the dorsal hippocampal CA3) in **C** was enlarged and shown in **D**. Scale bar=500μm in **C** and 50μm in **D**. **(E)** Mice injected with saline or ethanol at P7 were sacrificed at P60, and the hippocampus (HP) and neocortex (NC) samples were used for Western blot analyzes of amounts of GFAP. The amounts of GFAP were normalized to actin and the ratio of ethanol/saline was calculated. *Significantly different by Student's *t*-test. $n=4$. **(F)** Similarly, the effects of P7 ethanol on pNFκB expression were examined in hippocampus and cortex, The ratios of pNFκB and NFκB were compared as the ratios of ethanol/saline. $^{*}p<0.05$ by Student *t*-test. $n=4$.

injections at P7, BT75 were injected (ip) once a day for 3 days. At P30, the mice were perfusion-fixed, and PV+ or SST+ cell densities were counted in RS and DG. Figures 7A,B show that PV+ cell density in RS of EtOH group is significantly different from the saline group and EtOH+BT75 group by a Fisher's LSD post-hoc test after one-way ANOVA. However, as shown in Figure 7C, SST+ cell densities in RS of EtOH group, which is significantly different from saline group, is not different from EtOH+BT75 group by a LSD post-hoc test after one-way ANOVA. On the contrary, BT75 significantly (by Tukey HSD post-hoc test after one-way ANOVA) attenuated SST+ cell reduction in DG (Figures 7D,E), but did not attenuate PV+ cell reduction in DG by a Fisher's LSD post-hoc test) (Figure 7F). We also assessed if

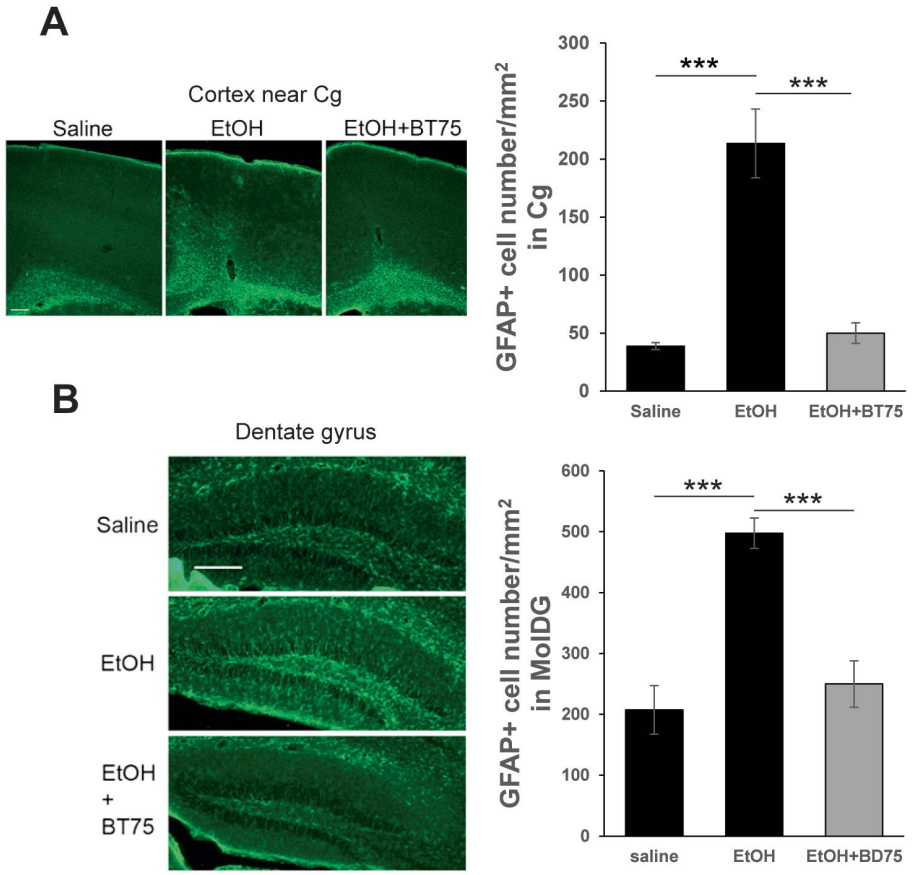


FIGURE 6
BT75 given before ethanol attenuates P7 ethanol-induced GFAP elevation at P60. **(A)** Mice were treated with BT75/vehicle and saline/EtOH at P7, and astrocyte activation was examined in the brain perfusion-fixed at P60. The brain sections were immunolabeled with anti-GFAP antibody. Scale bar=200μm. GFAP+ cell number was counted in the cingulate cortex (Cg). ***p<0.001 by Tukey test after one-way ANOVA. n=4. **(B)** GFAP+ cell number was counted in the molecular layers of dentate gyrus. ***p<0.001 by Tukey test after one-way ANOVA. n=4. Scale bar=200μm.

post-ethanol treatment by BT75 reduces elevation of GFAP expression. After mice were treated as described above, the hippocampus was dissected out at P30, and GFAP levels were analyzed by Western blots (Figure 8). The result shows that post-ethanol treatment by BT75 partially attenuated GFAP expression in the hippocampus, which was enhanced by P7 ethanol.

Thus, BT75 injected after ethanol treatment still attenuated P7 ethanol-induced GABAergic cell deficits and astrocyte activation in certain brain regions, which may emphasize the possibility that some of the GABAergic cell deficits induced by P7 ethanol are reversible.

Discussion

Previous studies have shown that ethanol induces robust neurodegeneration within 24 h in many brain regions of P7 mice (Olney et al., 2002a; Saito et al., 2007), and the reduction in number of GABAergic cells (mainly PV+ and SST+ neurons) in the cortex and hippocampus remains evident in the adult brain (Smiley et al., 2015, 2019; Saito et al., 2019), which may partially explain behavioral deficits observed in P7 ethanol-treated mice (Sadrian et al., 2012, 2014; Wilson et al., 2016; Lewin et al., 2018). Present studies indicated that an RARα specific antagonist BT382 and an agonist BT75 attenuated ethanol-induced cellular abnormalities in the developing brain in different manners. BT382 attenuated P7 ethanol-induced acute neurodegeneration detected by FJ staining 20 h after ethanol injection. Along with it, BT382 decreased the density of CD68+ cells. Our previous studies (Saito et al., 2015) have indicated that these CD68+ cells are co-localized with activated Iba-1+ cells which surround and phagocytose FJ+ degenerating neurons. These CD68 + Iba-1+ cells seem to be phagocytic microglia although some of these cells can be perivascular or invaded peripheral mononuclear macrophages. These results indicate that BT382 attenuated P7 ethanol-induced apoptotic neurodegeneration and the subsequent microglial activation, although we may need a time course study because BT382 may only shift the timing of neurodegeneration. Presently, mechanisms of neuroprotection by BT382 are unknown, but the toxic effects of excess RA may be reduced by the RARα antagonist because it has been reported that prenatal ethanol treatment increased ATRA in fetal hippocampus and cortex (Kane et al., 2010). Previous studies have also indicated that chaperon-mediated autophagy (CMA), which is inhibited by RARα, is activated by BT382 without inhibiting macroautophagy (Anguiano et al., 2013; Gomez-Sintes et al., 2022). CMA activation, which shows neuroprotection in neurodegenerative diseases and acute neurological insults (Cuervo and Wong, 2014; Kanno et al., 2022), may be related to the neuroprotective effects of BT382 against P7 ethanol

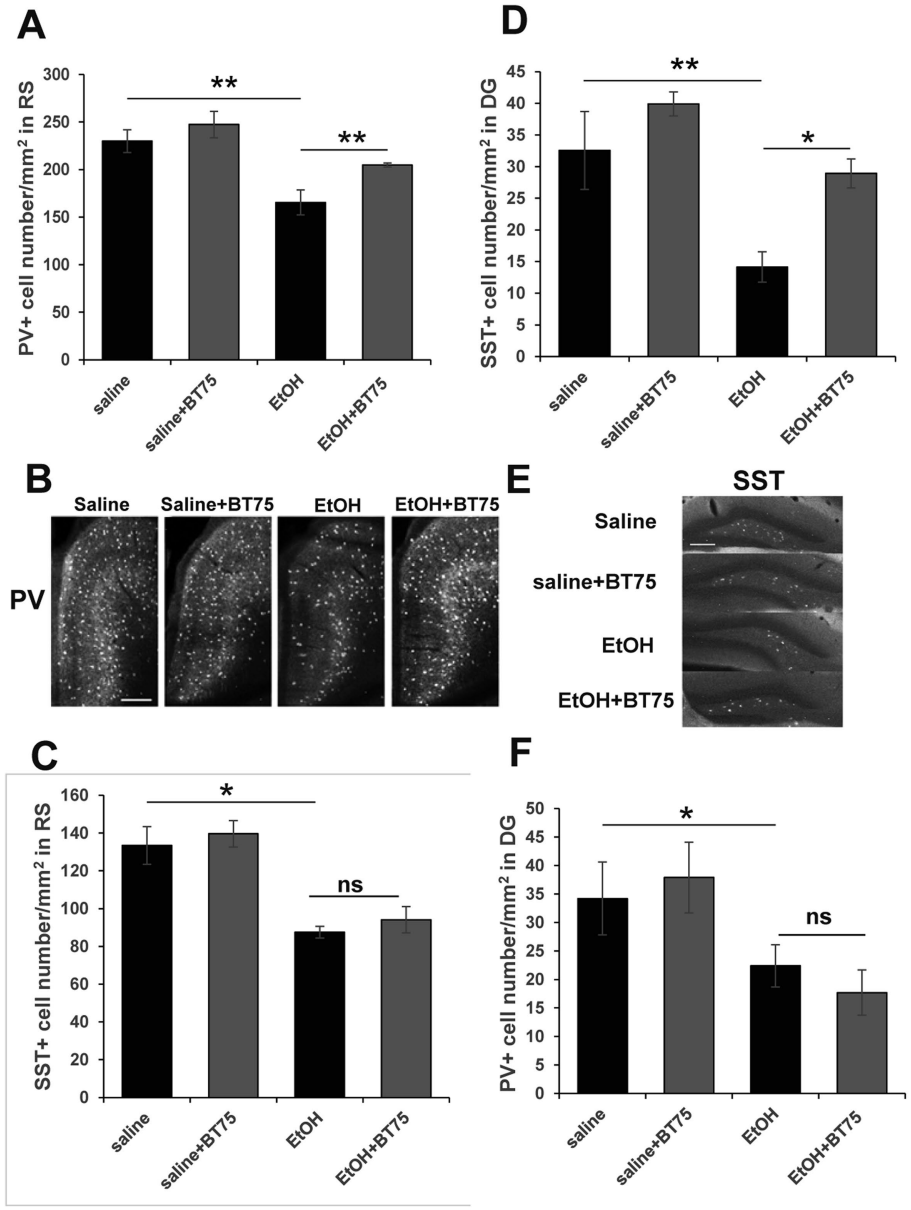


FIGURE 7
Post-ethanol treatment with BT75 attenuates P7 ethanol-induced GABA neuron deficits at P30. Three days after saline/ethanol injections at P7, mice were injected with BT75 (10mg/kg) or the vehicle (10% DMSO) by ip once a day for 3days. Then at P30, mice were perfusion-fixed and the brain sections were immunolabeled using anti-PV or anti-SST antibody. **(A)** PV+ cell density in RS. $^{**}p<0.01$ and $^{*}p<0.05$ by a Fisher's LSD post-hoc test after one-way ANOVA. $n=4$. **(B)** Representative images used for **A**. **(C)** SST+ cell densities in RS. $^{*}p<0.05$ and ^{ns}not significant by a Fisher's LSD post-hoc test after one-way ANOVA. $n=4$. **(D)** SST+ cell densities in DG. $^{**}p<0.01$ and $^{*}p<0.05$ by a Tukey post-hoc test after one-way ANOVA. $n=4$. **(E)** Representative images used for **D**. **(F)** PV+ cell densities in DG. $^{*}p<0.05$ and ^{ns}not significant by a Fisher's LSD post-hoc test after one-way ANOVA. $n=4$. In **B** and **E**, scale bar=200μm.

toxicity. Presently, we have not studied the long-term effects of BT382, partly because we expect that once initial apoptotic neurodegeneration is blocked, subsequent glial activation and GABAergic cell loss would be also blocked, as indicated in our previous studies using lithium (Sadrian et al., 2012; Lewin et al., 2018; Saito et al., 2019). However, studies on long-term effects of BT382, especially post-ethanol treatment by BT382 may be necessary to evaluate the efficacy of BT382 as a neuroprotective agent and to elucidate mechanisms of its action.

In contrast to the effects of BT382, RARα agonist BT75 did not affect the acute neurodegeneration but reduced long lasting GABAergic cell loss and chronic astrocyte activation induced by P7 ethanol. The long-term deficits of GABAergic neurons may be caused by acute apoptotic neurodegeneration at P7 and/or by delayed cell loss or disturbances in surviving neurons, which may lower expression of PV or SST. Studies using Nkx2.1-Cre;Ai9 mice (Figure 3A) showed that tdTomato+ cell numbers were reduced by ethanol in a similar manner as SST+ cells in the Cg and RS, indicating SST cell deficits observed in the adult cortex is mainly due to acute apoptotic neurodegeneration. The cell death that occurred in PV+ neurons at P7-P8 was not directly measured because of the lack of PV expression

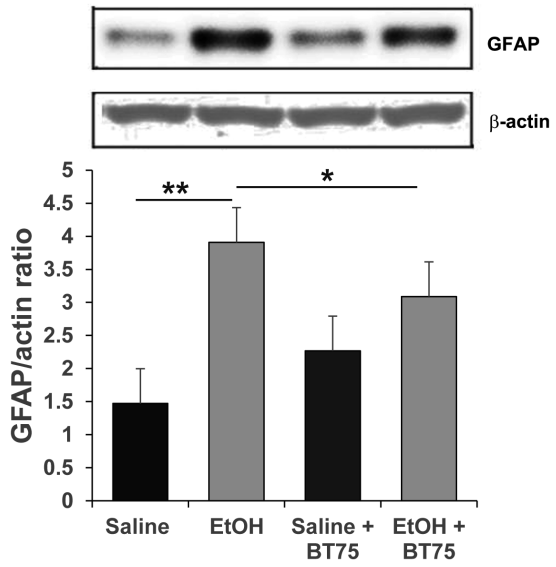


FIGURE 8
Post-ethanol treatment with BT75 attenuates P7 ethanol-induced GFAP elevation at P30. Mice were treated with BT75/vehicle (10mg/kg, once a day for 3days) starting 3days after saline/EtOH injections at P7, and the hippocampus was dissected at P30 and the ratio of GFAP/actin was measured by Western blot analyzes. BT75 significantly reduced astrocyte activation induced by EtOH. *p<0.05, **p<0.001, n=4.

at this time. However, the reduction in the number of tdTomato+ cells by ethanol in Cg or RS at P8 indicates that not only SST+ cells but also PV cell progenitors were decreased by acute neurodegeneration. However, in the hippocampus, effects of P7 ethanol are different between SST+ cells and tdTomato+ cells. Especially in CA2 and 3 regions, while tdTomato+ cell numbers were not significantly reduced by P7 ethanol at P30, SST+ or PV+ cell numbers were significantly reduced by ethanol. These results indicate that long-term reduction in SST+ or PV+ cells is due to acute neurodegeneration as well as impaired maturation or homeostasis of surviving neurons as suggested in our previous studies (Saito et al., 2019). Our results showing that BT75 increased PV+ or SST+ neurons in certain brain regions even though BT75 was given after P7 ethanol-induced neurodegeneration (Figure 7), also suggest that BT75 may restore the expression of PV or SST in some surviving neurons. Our previous experiments indicated that other neuroprotective treatments [lithium (Saito et al., 2019) and environmental enrichment/exercise (Apuzzo et al., 2020)] given after P7 ethanol treatment also partially restored the long-term PV+ neuron deficits induced by P7 ethanol. Interestingly, the decrease in PV+ neurons in the dentate gyrus by P7 ethanol was not rescued in all these post-ethanol treatments. Thus, these post-ethanol neuroprotective effects seem to be cell or brain region-specific. Mechanisms of such restoration of PV or SST neurons by BT75 is not clear. It may be related to previous studies indicating that RA signaling plays an important role in early postnatal development of prefrontal PV neurons (Larsen et al., 2019) and that RA regulates PV expression in the mouse model of ischemic stroke (Kang et al., 2023). Alternatively, the neuroprotective effects of BT75 may be related to its anti-inflammatory action. P7 ethanol induces chronic astrocyte activation detected by increases in GFAP+ cells in immunohistochemistry (Figure 6) or by increases in GFAP expression in Western blot (Figure 8). Such GFAP elevation was reduced by either pre–(Figure 6) or post-ethanol (Figure 8) BT75 administration. It has been also reported that RARα agonists show anti-inflammatory activity in both cultured cells and animal models (Tian et al., 2022). ATRA inhibits expression of TNFα and iNOS in primary rat microglia activated by LPS or Aβ (Dheen et al., 2005) and attenuates neuroinflammation induced by ethanol in adult rat brain by modulating SIRT1 and NF-κB (Priyanka et al., 2018). Our previous studies also indicate that BT75 is a potent anti-inflammatory agent in SIM-A9 microglial cell line activated with LPS (Zhang et al., 2023). Since excessive or chronic neuroinflammation has been implicated in ethanol-induced neurodegeneration (Chastain and Sarkar, 2014; Pascual et al., 2017; Zhang et al., 2018; Saito et al., 2019; Kane and Drew, 2021), anti-inflammatory action of BD75 may exert neuroprotection of PV and SST neurons.

Thus, our studies suggest the involvement of RA signaling in neonatal ethanol-induced neurodegeneration and neuroinflammation. RA/RARα signaling may serve as a target to improve developmental ethanol-induced brain abnormalities observed in FASD patients.

Data availability statement

The original contributions presented in the study are included in the article/supplementary material, further inquiries can be directed to the corresponding authors.

Ethics statement

The animal study was reviewed and approved by the Nathan Kline Institute Institutional Animal Care and Use Committee.

Author contributions

MS involved in the study design and conception, data acquisition and analysis, and writing the manuscript. SS, XZ, and SC-B engaged in data acquisition and analyzes and commenting and editing the drafts. JS and DW engaged in the study design and conception and commenting and editing the drafts. BD engaged in syntheses of BT75 and BT382, involved in the study design and conception and commenting and editing the drafts. All authors contributed to the article and approved the submitted version.

Funding

This work was supported by grants from National Institute on Alcohol Abuse and Alcoholism (R21AA027374 to BD and MS; R01AA023181 to MS, DW, and JS).

Conflict of interest

The authors declare that the research was conducted in the absence of any commercial or financial relationships that could be construed as a potential conflict of interest.

Publisher's note

All claims expressed in this article are solely those of the authors and do not necessarily represent those of their affiliated organizations, or those of the publisher, the editors and the reviewers. Any product that may be evaluated in this article, or claim that may be made by its manufacturer, is not guaranteed or endorsed by the publisher.

References

Alfos, S., Boucheron, C., Pallet, V., Higueret, D., Enderlin, V., Béracochéa, D., et al. (2001). A retinoic acid receptor antagonist suppresses brain retinoic acid receptor overexpression and reverses a working memory deficit induced by chronic ethanol consumption in mice. *Alcohol. Clin. Exp. Res.* 25, 1506–1514. doi: 10.1111/j.1530-0277.2001.tb02154.x

Anguiano, J., Garner, T. P., Mahalingam, M., Das, B. C., Gavathiotis, E., and Cuervo, A. M. (2013). Chemical modulation of chaperone-mediated autophagy by retinoic acid derivatives. *Nat. Chem. Biol.* 9, 374–382. doi: 10.1038/nchembio.1230

Apuzzo, J., Saito, M., and Wilson, D. A. (2020). Post-exposure environment modulates long-term developmental ethanol effects on behavior, neuroanatomy, and cortical oscillations. *Brain Res.* 1748:147128. doi: 10.1016/j.brainres.2020.147128

Astley, S. J., Aylward, E. H., Olson, H. C., Kerns, K., Brooks, A., Coggins, T. E., et al. (2009). Magnetic resonance imaging outcomes from a comprehensive magnetic resonance study of children with fetal alcohol spectrum disorders. *Alcohol. Clin. Exp. Res.* 33, 1671–1689. doi: 10.1111/j.1530-0277.2009.01004.x

Bird, C. W., Barber, M. J., Post, H. R., Jacquez, B., Chavez, G. J., Faturos, N. G., et al. (2020). Neonatal ethanol exposure triggers apoptosis in the murine retrosplenial cortex: role of inhibition of NMDA receptor-driven action potential firing. *Neuropharmacology* 162:107837. doi: 10.1016/j.neuropharm.2019.107837

Bird, C. W., Taylor, D. H., Pinkowski, N. J., Chavez, G. J., and Valenzuela, C. F. (2018). Long-term reductions in the population of GABAergic interneurons in the mouse hippocampus following developmental ethanol exposure. *Neuroscience* 383, 60–73. doi: 10.1016/j.neuroscience.2018.05.003

Cai, W., Wang, J., Hu, M., Chen, X., Lu, Z., Bellanti, J. A., et al. (2019). All trans-retinoic acid protects against acute ischemic stroke by modulating neutrophil functions through STAT1 signaling. *J. Neuro-Oncol.* 16:175. doi: 10.1186/s12974-019-1557-6

Chastain, L. G., and Sarkar, D. K. (2014). Role of microglia in regulation of ethanol neurotoxic action. *Int. Rev. Neurobiol.* 118, 81–103. doi: 10.1016/B978-0-12-801284-0.00004-X

Coleman, L. G., Oguz, I., Lee, J., Styner, M., and Crews, F. T. (2012). Postnatal day 7 ethanol treatment causes persistent reductions in adult mouse brain volume and cortical neurons with sex specific effects on neurogenesis. *Alcohol* 46, 603–612. doi: 10.1016/j.alcohol.2012.01.003

Crandall, J. E., Goodman, T., McCarthy, D. M., Duester, G., Bhide, P. G., Dräger, U. C., et al. (2011). Retinoic acid influences neuronal migration from the ganglionic eminence to the cerebral cortex. *J. Neurochem.* 119, 723–735. doi: 10.1111/j.1471-4159.2011.07471.x

Cuervo, A. M., and Wong, E. (2014). Chaperone-mediated autophagy: roles in disease and aging. *Cell Res.* 24, 92–104. doi: 10.1038/cr.2013.153

Das, B. C., Mohapatra, S., Campbell, P. D., Nayak, S., Mahalingam, S. M., and Evans, T. (2010). Synthesis of function-oriented 2-phenyl-2H-chromene derivatives using L-pipecolinic acid and substituted guanidine organocatalysts. *Tetrahedron Lett.* 51, 2567–2570. doi: 10.1016/j.tetlet.2010.02.143

Dheen, S. T., Jun, Y., Yan, Z., Tay, S. S., and Ling, E. A. (2005). Retinoic acid inhibits expression of TNF-alpha and iNOS in activated rat microglia. *Glia* 50, 21–31. doi: 10.1002/glia.20153

Dowling, J. E. (2020). Vitamin a: its many roles-from vision and synaptic plasticity to infant mortality. *J. Comp. Physiol. A Neuroethol. Sens Neural Behav. Physiol.* 206, 389–399. doi: 10.1007/s00359-020-01403-z

Duester, G. (1991). A hypothetical mechanism for fetal alcohol syndrome involving ethanol inhibition of retinoic acid synthesis at the alcohol dehydrogenase step. *Alcohol. Clin. Exp. Res.* 15, 568–572. doi: 10.1111/j.1530-0277.1991.tb00562.x

Fainsod, A., Bendelac-Kapon, L., and Shabtai, Y. (2020). Alcohol Spectrum disorder: embryogenesis under reduced retinoic acid signaling conditions. *Subcell. Biochem.* 95, 197–225. doi: 10.1007/978-3-030-42282-0_8

Gomez-Sintes, R., Xin, Q., Jimenez-Loygorri, J. I., McCabe, M., Diaz, A., Garner, T. P., et al. (2022). Targeting retinoic acid receptor alpha-corepressor interaction activates chaperone-mediated autophagy and protects against retinal degeneration. *Nat. Commun.* 13:4220. doi: 10.1038/s41467-022-31869-1

Haushalter, C., Asselin, L., Fraulob, V., Dollé, P., and Rhinn, M. (2017). Retinoic acid controls early neurogenesis in the developing mouse cerebral cortex. *Dev. Biol.* 430, 129–141. doi: 10.1016/j.ydbio.2017.08.006

Johnson, C. S., Zucker, R. M., Hunter, E. S. 3rd, and Sulik, K. K. (2007). Perturbation of retinoic acid (RA)-mediated limb development suggests a role for diminished RA signaling in the teratogenesis of ethanol. *Birth Defects Res. A Clin. Mol. Teratol.* 79, 631–641. doi: 10.1002/bdra.20385

Kane, C. J. M., and Drew, P. D. (2021). Neuroinflammatory contribution of microglia and astrocytes in fetal alcohol spectrum disorders. *J. Neurosci. Res.* 8, 1973–1985. doi: 10.1002/jnr.24735

Kane, M. A., Folias, A. E., Wang, C., and Napoli, J. L. (2010). Ethanol elevates physiological all-trans-retinoic acid levels in select loci through altering retinoid metabolism in multiple loci: a potential mechanism of ethanol toxicity. *FASEB J.* 24, 823–832. doi: 10.1096/fj.09-141572

Kang, J. B., Park, D. J., and Koh, P. O. (2023). Retinoic acid prevents the neuronal damage through the regulation of Parvalbumin in an ischemic stroke model. *Neurochem. Res.* 48, 487–501. doi: 10.1007/s11064-022-03769-9

Kanno, H., Handa, K., Murakami, T., Aizawa, T., and Ozawa, H. (2022). Chaperone-mediated autophagy in neurodegenerative diseases and acute neurological insults in the central nervous system. *Cells* 11:1205. doi: 10.3390/cells11071205

Larsen, R., Proue, A., Scott, E. P., Christiansen, M., and Nakagawa, Y. (2019). The thalamus regulates retinoic acid signaling and development of Parvalbumin interneurons in postnatal mouse prefrontal cortex. *eNeuro* 6:18. doi: 10.1523/ENEURO.0018-19.2019

Lee, H. P., Casadesus, G., Zhu, X., Lee, H. G., Perry, G., Smith, M. A., et al. (2009). All-trans retinoic acid as a novel therapeutic strategy for Alzheimer's disease. *Expert. Rev. Neurother.* 9, 1615–1621. doi: 10.1586/ern.09.86

Lewin, M., Ilina, M., Betz, J., Masiello, K., Hui, M., Wilson, D. A., et al. (2018). Developmental ethanol-induced sleep fragmentation, behavioral hyperactivity, cognitive impairment and Parvalbumin cell loss are prevented by lithium co-treatment. *Neuroscience* 369, 269–277. doi: 10.1016/j.neuroscience.2017.11.033

Marrs, J. A., Clendenon, S. G., Ratcliffe, D. R., Fielding, S. M., Liu, Q., and Bosron, W. F. (2010). Zebrafish fetal alcohol syndrome model: effects of ethanol are rescued by retinoic acid supplement. *Alcohol* 44, 707–715. doi: 10.1016/j.alcohol.2009.03.004

Mattioli, I., Sebald, A., Bucher, C., Charles, R. P., Nakano, H., Doi, T., et al. (2004). Transient and selective NF-kappa B p65 serine 536 phosphorylation induced by T cell costimulation is mediated by I kappa B kinase beta and controls the kinetics of p65 nuclear import. *J. Immunol.* 172:6336-44. doi: 10.4049/jimmunol.172.10.6336

May, P. A., Baete, A., Russo, J., Elliott, A. J., Blankenship, J., Kalberg, W. O., et al. (2014). Prevalence and characteristics of fetal alcohol spectrum disorders. *Pediatrics* 134, 855–866. doi: 10.1542/peds.2013-3319

May, P. A., Gossage, J. P., Kalberg, W. O., Robinson, L. K., Buckley, D., Manning, M., et al. (2009). Prevalence and epidemiologic characteristics of FASD from various research methods with an emphasis on recent in-school studies. *Dev. Disabil. Res. Rev.* 15, 176–192. doi: 10.1002/ddrr.68

McCaffery, P., Koul, O., Smith, D., Napoli, J. L., Chen, N., and Ullman, M. D. (2004). Ethanol increases retinoic acid production in cerebellar astrocytes and in cerebellum. *Brain Res. Dev. Brain Res.* 153, 233–241. doi: 10.1016/j.devbrainres.2004.09.003

Mey, J., and Mccaffery, P. (2004). Retinoic acid signaling in the nervous system of adult vertebrates. *Neuroscientist* 10, 409–421. doi: 10.1177/1073858404263520

Niederreither, K., and Dollé, P. (2008). Retinoic acid in development: towards an integrated view. *Nat. Rev. Genet.* 9, 541–553. doi: 10.1038/nrg2340

Norman, A. L., Crocker, N., Mattson, S. N., and Riley, E. P. (2009). Neuroimaging and fetal alcohol spectrum disorders. *Dev. Disabil. Res. Rev.* 15, 209–217. doi: 10.1002/ddrr.72

Olney, J. W., Tenkova, T., Dikranian, K., Muglia, L. J., Jermakowicz, W. J., D'Sa, C., et al. (2002b). Ethanol-induced caspase-3 activation in the in vivo developing mouse brain. *Neurobiol. Dis.* 9, 205–219. doi: 10.1006/nbdi.2001.0475

Olney, J. W., Tenkova, T., Dikranian, K., Qin, Y. Q., Labruyere, J., and Ikonomidou, C. (2002a). Ethanol-induced apoptotic neurodegeneration in the developing C57BL/6 mouse brain. *Brain Res. Dev. Brain Res.* 133, 115–126. doi: 10.1016/S0165-3806(02)00279-1

Pascual, M., Montesinos, J., Montagud-Romero, S., Forteza, J., Rodríguez-Arias, M., Miñarro, J., et al. (2017). TLR4 response mediates ethanol-induced neurodevelopment alterations in a model of fetal alcohol spectrum disorders. *J. Neuroinflammation* 14:145. doi: 10.1186/s12974-017-0918-2

Paxinos, G., and Franklin, K. B. J.. (2004). *The mouse brain in stereotaxic coordinates*. New York: Elsevier, Academic Press.

Paxinos, G., Halliday, G., Watson, C., Koutcherov, Y., and Wang, H.. (2007) *Atlas of the developing mouse brain at E17.5, P0, and P6*. New York: Elsevier, Academic Press.

Priyanka, S. H., Syam Das, S., Thushara, A. J., Rauf, A. A., and Indira, M. (2018). All trans retinoic acid attenuates markers of Neuroinflammation in rat brain by modulation of SIRT1 and NFκB. *Neurochem. Res.* 43, 1791–1801. doi: 10.1007/s11064-018-2595-7

Rhinn, M., and Dollé, P. (2012). Retinoic acid signalling during development. *Development* 139, 843–858. doi: 10.1242/dev.065938

Riley, E. P., Infante, M. A., and Warren, K. R. (2011). Fetal alcohol spectrum disorders: an overview. *Neuropsychol. Rev.* 21, 73–80. doi: 10.1007/s11065-011-9166-x

Riley, E. P., and McGee, C. L. (2005). Fetal alcohol spectrum disorders: an overview with emphasis on changes in brain and behavior. *Exp. Biol. Med. (Maywood)* 230, 357–365. doi: 10.1177/15353702-0323006-03

Sadakata, T., Washida, M., Iwayama, Y., Shoji, S., Sato, Y., Ohkura, T., et al. (2007). Autistic-like phenotypes in Cadps2-knockout mice and aberrant CADPS2 splicing in autistic patients. *J. Clin. Invest.* 117, 931–943. doi: 10.1172/JCI29031

Sadrian, B., Lopez-Guzman, M. L., Wilson, D. A., and Saito, M. (2014). Distinct neurobehavioral dysfunction based on the timing of developmental binge-like alcohol exposure. *Neuroscience* 280, 204–219. doi: 10.1016/j.neuroscience.2014.09.008

Sadrian, B., Subbanna, S., Wilson, D. A., Basavarajappa, B. S., and Saito, M. (2012). Lithium prevents long-term neural and behavioral pathology induced by early alcohol exposure. *Neuroscience* 206, 122–135. doi: 10.1016/j.neuroscience.2011.12.059

Saito, M., Mao, R. F., Wang, R., Vadasz, C., and Saito, M. (2007). Effects of gangliosides on ethanol-induced neurodegeneration in the developing mouse brain. *Alcohol. Clin. Exp. Res.* 31, 665–674. doi: 10.1111/j.1530-0277.2007.00351.x

Saito, M., Saito, M., and Das, B. C. (2019). Involvement of AMP-activated protein kinase in neuroinflammation and neurodegeneration in the adult and developing brain. *Int. J. Dev. Neurosci.* 77, 48–59. doi: 10.1016/j.ijdevneu.2019.01.007

Saito, M., Smiley, J. F., Hui, M., Masiello, K., Betz, J., Ilina, M., et al. (2019). Neonatal ethanol disturbs the Normal maturation of Parvalbumin interneurons surrounded by subsets of Perineuronal nets in the cerebral cortex: partial reversal by lithium. *Cereb. Cortex* 29, 1383–1397. doi: 10.1093/cercor/bhy034

Saito, M., Wu, G., Hui, M., Masiello, K., Dobrenis, K., Ledeen, R. W., et al. (2015). Ganglioside accumulation in activated glia in the developing brain: comparison between WT and GalNAc KO mice. *J. Lipid Res.* 56, 1434–1448. doi: 10.1194/jlr.M056580

Sapin, V. (2008). Alcohol and pregnancy: diagnostic aspects and abnormalities in the placental vitamin a pathway. *Ann. Biol. Clin. (Paris)* 66, 509–513. doi: 10.1684/abc.2008.0271

Shabtai, Y., Bendelac, L., Jubran, H., Hirschberg, J., and Fainsod, A. (2018). Acetaldehyde inhibits retinoic acid biosynthesis to mediate alcohol teratogenicity. *Sci. Rep.* 8:347. doi: 10.1038/s41598-017-18719-7

Shearer, K., Stoney, P. N., Morgan, P. J., and McCaffery, P. J. (2012). A vitamin for the brain. *Trends Neurosci.* 35, 733–741. doi: 10.1016/j.tins.2012.08.005

Smiley, J. F., Bleiwas, C., Masiello, K., Petkova, E., Betz, J., Hui, M., et al. (2019). Effects of neonatal ethanol on cerebral cortex development through adolescence. *Brain Struct. Funct.* 224, 1871–1884. doi: 10.1007/s00429-019-01881-1

Smiley, J. F., Saito, M., Bleiwas, C., Masiello, K., Ardekani, B., Guilfoyle, D. N., et al. (2015). Selective reduction of cerebral cortex GABA neurons in a late gestation model of fetal alcohol spectrum disorder. *Alcohol* 49, 571–580. doi: 10.1016/j.alcohol.2015.04.008

Tian, Y., Liu, B., Li, Y., Zhang, Y., Shao, J., Wu, P., et al. (2022). Activation of RARα receptor attenuates Neuroinflammation after SAH via promoting M1-to-M2 phenotypic polarization of microglia and regulating Mafb/Msr1/PI3K-Akt/NF-κB pathway. *Front. Immunol.* 13:839796. doi: 10.3389/fimmu.2022.839796

Wilson, D. A., Masiello, K., Lewin, M. P., Hui, M., Smiley, J. F., and Saito, M. (2016). Developmental ethanol exposure-induced sleep fragmentation predicts adult cognitive impairment. *Neuroscience* 322, 18–27. doi: 10.1016/j.neuroscience.2016.02.020

Wolf, G. (2010). Tissue-specific increases in endogenous all-trans retinoic acid: possible contributing factor in ethanol toxicity. *Nutr. Rev.* 68, 689–692. doi: 10.1111/j.1753-4887.2010.00323.x

Wozniak, D. F., Hartman, R. E., Boyle, M. P., Vogt, S. K., Brooks, A. R., Tenkova, T., et al. (2004). Apoptotic neurodegeneration induced by ethanol in neonatal mice is associated with profound learning/memory deficits in juveniles followed by progressive functional recovery in adults. *Neurobiol. Dis.* 17, 403–414. doi: 10.1016/j.nbd.2004.08.006

Xu, Q., Tam, M., and Anderson, S. A. (2008). Fate mapping Nkx2.1-lineage cells in the mouse telencephalon. *J. Comp. Neurol.* 506, 16–29. doi: 10.1002/cne.21529

Yelin, R., Schyr, R. B., Kot, H., Zins, S., Frumkin, A., Pillemer, G., et al. (2005). Ethanol exposure affects gene expression in the embryonic organizer and reduces retinoic acid levels. *Dev. Biol.* 279, 193–204. doi: 10.1016/j.ydbio.2004.12.014

Young, J. K., Giesbrecht, H. E., Eskin, M. N., Aliani, M., and Suh, M. (2014). Nutrition implications for fetal alcohol spectrum disorder. *Adv. Nutr.* 5, 675–692. doi: 10.3945/an.113.004846

Zhang, X., Subbanna, S., Williams, C. R. O., Canals-Baker, S., Smiley, J. F., Wilson, D. A., et al. (2023). Anti-inflammatory action of BT75, a novel RARα agonist, in cultured microglia and in an experimental mouse model of Alzheimer's disease. *Neurochem. Res.* 2023:3888. doi: 10.1007/s11064-023-03888-x

Zhang, K., Wang, H., Xu, M., Frank, J. A., and Luo, J. (2018). Role of MCP-1 and CCR2 in ethanol-induced neuroinflammation and neurodegeneration in the developing brain. *J. Neuroinflammation* 15:197. doi: 10.1186/s12974-018-1241-2

Zhong, Y., Wu, Y., Liu, R., Li, Z., Chen, Y., Evans, T., et al. (2011). Novel retinoic acid receptor alpha agonists for treatment of kidney disease. *PLoS One* 6:e27945. doi: 10.1371/journal.pone.0027945

frontiers | Frontiers in Neuroscience

TYPE Original Research
PUBLISHED 05 May 2023
DOI 10.3389/fnins.2023.1176581

Check for updates

OPEN ACCESS

EDITED BY
Carlos Fernando Valenzuela,
University of New Mexico, United States

REVIEWED BY
Shahani Noor,
University of New Mexico, United States
Marina Guizzetti,
Oregon Health and Science University,
United States

*CORRESPONDENCE
Ania K. Majewska
✉ ania_majewska@urmc.rochester.edu

RECEIVED 28 February 2023
ACCEPTED 17 April 2023
PUBLISHED 05 May 2023

CITATION
Cealie MY, Douglas JC, Le LHD, Vonkaenel ED, McCall MN, Drew PD and Majewska AK (2023) Developmental ethanol exposure has minimal impact on cerebellar microglial dynamics, morphology, and interactions with Purkinje cells during adolescence.
Front. Neurosci. 17:1176581.
doi: 10.3389/fnins.2023.1176581

COPYRIGHT
© 2023 Cealie, Douglas, Le, Vonkaenel, McCall, Drew and Majewska. This is an open-access article distributed under the terms of the Creative Commons Attribution License (CC BY). The use, distribution or reproduction in other forums is permitted, provided the original author(s) and the copyright owner(s) are credited and that the original publication in this journal is cited, in accordance with accepted academic practice. No use, distribution or reproduction is permitted which does not comply with these terms.

Developmental ethanol exposure has minimal impact on cerebellar microglial dynamics, morphology, and interactions with Purkinje cells during adolescence

MaKenna Y. Cealie[1], James C. Douglas[2], Linh H. D. Le[1], Erik D. Vonkaenel[3], Matthew N. McCall[3], Paul D. Drew[2] and Ania K. Majewska[1]*

[1]Majewska Laboratory, Department of Neuroscience, School of Medicine and Dentistry, University of Rochester, Rochester, NY, United States, [2]Drew Laboratory, Department of Neurobiology and Developmental Sciences, University of Arkansas for Medical Sciences, Little Rock, AR, United States, [3]McCall Laboratory, Department of Biostatistics and Computational Biology, School of Medicine and Dentistry, University of Rochester, Rochester, NY, United States

Introduction: Fetal alcohol spectrum disorders (FASD) are the most common cause of non-heritable, preventable mental disability, occurring in almost 5% of births in the United States. FASD lead to physical, behavioral, and cognitive impairments, including deficits related to the cerebellum. There is no known cure for FASD and their mechanisms remain poorly understood. To better understand these mechanisms, we examined the cerebellum on a cellular level by studying microglia, the principal immune cells of the central nervous system, and Purkinje cells, the sole output of the cerebellum. Both cell types have been shown to be affected in models of FASD, with increased cell death, immune activation of microglia, and altered firing in Purkinje cells. While ethanol administered in adulthood can acutely depress the dynamics of the microglial process arbor, it is unknown how developmental ethanol exposure impacts microglia dynamics and their interactions with Purkinje cells in the long term.

Methods: To address this question, we used a mouse model of human 3rd trimester exposure, whereby $L7^{cre}/Ai9^{+/-}/Cx3cr1^{G/+}$ mice (with fluorescently labeled microglia and Purkinje cells) of both sexes were subcutaneously treated with a binge-level dose of ethanol (5.0g/kg/day) or saline from postnatal days 4–9. Cranial windows were implanted in adolescent mice above the cerebellum to examine the long-term effects of developmental ethanol exposure on cerebellar microglia and Purkinje cell interactions using *in vivo* two-photon imaging.

Results: We found that cerebellar microglia dynamics and morphology were not affected after developmental ethanol exposure. Microglia dynamics were also largely unaltered with respect to how they interact with Purkinje cells, although subtle changes in these interactions were observed in females in the molecular layer of the cerebellum.

Discussion: This work suggests that there are limited *in vivo* long-term effects of ethanol exposure on microglia morphology, dynamics, and neuronal interactions, so other avenues of research may be important in elucidating the mechanisms of FASD.

KEYWORDS

microglia, cerebellum, Purkinje cell, immune system, ethanol, fetal alcohol spectrum disorders (FASD), prenatal alcohol exposure, neurodevelopment

1. Introduction

Fetal alcohol spectrum disorders (FASD) are the most common cause of non-heritable, preventable mental disability, occurring in almost 5% of births in the United States (May et al., 2014; Williams et al., 2015). There is no known cure for FASD, few therapies, and the mechanisms that underlie ethanol's effects in development remain unclear. Ethanol exposure during gestation can cause developmental and central nervous system abnormalities, which result in a wide range of cognitive, behavioral, and physical impairments (Wilhelm and Guizzetti, 2015; Saito et al., 2016), such as facial dysmorphia, decreased brain size, and abnormal brain structure (Hamre and West, 1993; Napper and West, 1995; Idrus and Napper, 2012). The cerebellum appears to be particularly vulnerable, displaying ethanol-induced anatomical changes which could underlie deficits in behaviors, such as impaired motor coordination and learning, that are associated with FASD (Servais et al., 2007; Topper et al., 2015). These changes are long lasting, with smaller cerebellar volumes and motor skill impairments reported in adolescents and young adults exposed to ethanol during gestation (Safe et al., 2018; Sullivan et al., 2020). Ethanol may have a strong effect on cerebellar structure and function due to the cerebellum's unique developmental timeline. Cerebellar development is protracted continuing into postnatal life, compared to areas like the cortex, where neurogenesis and migration are completed at birth in humans and mice (Stagni et al., 2015). The peak of cerebellar neurogenesis occurs postnatally in mice, around postnatal days (P) 4–9 (Stagni et al., 2015), which translates to a time of intense synaptogenesis in other brain regions, called the growth spurt period. This brain growth spurt period occurs in the third trimester in humans and may be a period of particular vulnerability to developmental ethanol exposure (Dobbing and Sands, 1979; Bayer et al., 1993; Wilhelm and Guizzetti, 2015; Saito et al., 2016).

One cerebellar cell type that develops during the early postnatal period in mice is the Purkinje cell, the sole output of the cerebellum. Around birth, Purkinje cells migrate and form the Purkinje Cell Layer (PCL) of the cerebellum (Altman and Bayer, 1978; Zhang and Goldman, 1996; Zhang et al., 2010). Initially the PCL is a multilayer but thins into a monolayer around P6 to P7 (Zhang et al., 2010). Postnatally, Purkinje cell dendrites grow and spread in the Molecular Layer (ML), with their distinct and elaborate dendritic fan shape growing by the third postnatal week (Berry and Bradley, 1976; Yamada et al., 2000). Other cerebellar cell types migrate, mature, and synapse with Purkinje cells throughout the first three postnatal weeks, making this a potential critical period for ethanol's effects on the cerebellar circuit as a whole (Zhang et al., 2010; Rahimi-Balaei et al., 2018). Indeed, it has been reported that Purkinje cells are impacted by ethanol. Reduced numbers of Purkinje cells have been reported when rodents were given ethanol postnatally, particularly from P4–5 (Goodlett et al., 1990; Hamre and West, 1993; Goodlett and Eilers, 1997; Topper et al., 2015). Additionally, effects on the surviving Purkinje cells have been described, such as increases in simple spike firing rate, decreased intrinsic excitability, and decreased strength of excitatory parallel fiber-Purkinje cell synapses (Servais et al., 2007; Zamudio-Bulcock et al., 2014), suggesting a multifactorial effect of ethanol on the cerebellar circuit.

Microglia, the immune cells of the central nervous system, are also affected by developmental ethanol exposure. Ethanol can induce cell death of microglia and alterations in the phenotype of surviving microglia (Kane et al., 2011). Ethanol-exposed microglia undergo morphological changes, displaying a phenotype associated with immune activation, and release inflammatory factors that could contribute to cerebellar neuronal cell death and changes in firing patterns (Drew et al., 2015; Topper et al., 2015; Kane et al., 2021; Lowery et al., 2021), suggesting a role for microglia in ethanol-induced Purkinje cell defects. Microglia and neuroinflammation have been an area of increasing interest in the study of FASD (Kane et al., 2021; Komada and Nishimura, 2022). In the healthy brain, microglia have a surveillance role and play an integral part in the development of neurons and connectivity through the phagocytosis of apoptotic neurons and the pruning and formation of synapses (Dean et al., 2012; Nakayama et al., 2018; Kana et al., 2019; Perez-Pouchoulen et al., 2019; Yamamoto et al., 2019). Microglia make physical contacts with neuronal dendrites, axons, and somas, influencing synaptic plasticity and neuronal firing (Cserép et al., 2021). Microglia can also release factors that influence cellular and circuit assembly (Marin-Teva et al., 2004; Wong et al., 2017). Disruption of these functions, particularly in development, may have long-lasting consequences and contribute to FASD pathology.

Microglia are highly dynamic cells, whose motile arbor can shape neuronal circuit development and connectivity in the cerebellum (Stoessel and Majewska, 2021). Microglia display regional heterogeneity, with cerebellar microglia displaying phenotypes that make them distinct from many other microglial populations. For instance, on a transcriptomic level, cerebellar and hippocampal microglia exhibit a more immune alert state and express more genes related to energy metabolism than cortical microglia (Grabert et al., 2016). Structurally, cerebellar microglia are less densely distributed and appear less ramified than those in the visual cortex (Stowell et al., 2018). Dynamically, cerebellar microglia survey less territory but display a unique somal motility *in vivo* (Stowell et al., 2018). In adulthood, microglia in the ML and PCL can contact and wrap Purkinje cell dendrites and somas (Stowell et al., 2018). If similar dynamic interactions between microglia and Purkinje cells occur during development, they could potentially influence processes that shape the development of cerebellar neurons and connectivity. In adulthood, acute ethanol administration resulted in microglia that were hyper-ramified and displayed decreased motility and surveillance in the PCL, whereas no effects were seen in the ML, suggesting a layer-specificity in microglial vulnerability (Stowell and Majewska, 2020). However, it is unknown if developmental ethanol exposure can affect microglia dynamics and their interactions with Purkinje cells later in life.

Here, we examine whether ethanol exposure in development can affect cerebellar microglia dynamics, morphology, and neuronal interactions in adolescence. While there is evidence that both microglia and Purkinje cells are altered by early ethanol exposure, there is currently no information on whether the interactions between these two cells also change. We attempt to fill this gap and examine if and how these interactions are altered by developmental ethanol using *in vivo* two-photon imaging. We use a mouse model of FASD, in which mice are exposed to binge-level amounts of ethanol from P4 through P9, the time period equivalent to the human third trimester. We found that *in vivo* microglia dynamics, motility and surveillance, as well as microglia morphology were relatively unchanged in adolescence after developmental ethanol exposure. Subtle differences in dynamic cell–cell interactions between Purkinje cells and microglia may have been triggered by ethanol specifically in females in the molecular layer. This work suggests that high levels of ethanol

exposure during the equivalent of the third trimester does not have profound effects on the structure and dynamics of cerebellar microglia or their interactions with Purkinje cells in early adolescence.

2. Materials and methods

2.1. Animals

All experimental protocols were carried out in strict accordance with the University of Rochester Committee on Animal Resources and National Institutes of Health Guidelines. All transgenic mice ($N = 24$) were bred on a C57BL/6J background (Jackson Labs strain 000664; RRID:IMSR_JAX:000664) in house, exposed to 12 h of light and 12 h of dark (6 AM lights on), with chow and water provided *ad libitum*. Cx3cr1-eGFP mice (Jung et al., 2000) (Jackson Labs strain 005582; RRID:IMSR_JAX:005582) were bred to a tdTomato (Ai9) (Jackson Labs strain 007909; RRID:IMSR_JAX:007909) mouse line. Cx3cr1, the fractalkine receptor, is expressed on microglia and monocytes and hetereozygocity of this line ($Cx3cr1^{G/+}$) allows the labeling of microglia with GFP with a haploinsufficiency for CX3CR1 (Jung et al., 2000). $Ai9^{+/+}/Cx3cr1^{G/G}$ mice were bred to a Purkinje cell specific cre line (L7-cre) (Jackson Labs strain 004146; RRID:IMSR_JAX:004146), which allows the fluorescent labeling of Purkinje cells. Together these allow the *in vivo* fluorescent imaging of microglia and Purkinje cells in the same $L7^{cre}/Ai9^{+/-}/Cx3cr1^{G/+}$ mouse. Both male and female mice were used in all the experiments and analyzed for sex-specific trends. Daily monitoring of breeding pairs occurred to check for the birth of pups, considered postnatal day (P) 0.

2.2. Ethanol dosing

On P4, pups were toe-clipped for identification. Male and female mice were weighed and subcutaneously injected from P4 to P9 with a 5.0 g/kg/day ethanol solution (20% v/v ethanol in saline) or saline (0.9% NaCl), broken into two doses, given 2 h apart. After injection, pups were returned to the breeding cages with the dams. This is an established model used previously in our laboratory (Wong et al., 2018, 2021). Injection of only the pups minimizes confounds of reduced maternal care due to intoxication and allows for littermate controls. Mixed litters were used with 1 male and 1 female taken for each cohort (Ethanol and Saline) for a total of 4 mice per litter, when possible. Distribution across treatment groups was as follows: Ethanol, $n = 12$, six males and six females; Saline, $n = 12$, six males and six females. Animals from 13 separate litters were used, as not all litters yielded males and females. Additionally, some animals did not survive cranial window surgery or did not have window quality sufficient to image and collect data. Animals were weaned on P21. All data analysis was performed blind to exposure group.

Separate cohorts of animals were generated for blood ethanol concentration (BEC) analysis. The 5.0 g/kg/day ethanol dosage produced BECs of ~450 mg/dl, considered a binge-level dose, in $L7^{cre}/Ai9^{+/-}/Cx3cr1^{G/+}$ mice on P4 and P9 (Figure 1B). A binge-level amount of ethanol is appropriate as mice metabolize ethanol more quickly than humans, so this mimics human exposure levels more accurately (Gohlke et al., 2008; Cederbaum, 2012). For the P4 timepoint, samples were derived from 5 male and 7 female ethanol treated pups, and from 1 male and 4 female saline treated pups spread across 5 litters. For the P9 timepoint, samples were derived from 4 male and 6 female ethanol treated pups, and from 2 male and 2 female saline treated pups spread across 4 litters. Whole trunk blood was collected 90 min after the second injection on either P4 or P9 *via* decapitation. Blood was centrifuged at 4,000 rpm for 5 min at 4°C (Jouan CR3i Multifunction Centrifuge), before being stored at −80°C until it was measured using an Analox Alcohol AM1 Analyzer (Analox Technologies, Atlanta, GA, United States) (Drew et al., 2015).

2.3. Cranial window surgeries

$L7^{cre}/Ai9^{+/-}/Cx3cr1^{G/+}$ mice given ethanol or saline from P4–9 had cranial windows implanted in adolescence (when the cerebellum is largely developed) to be used for subsequent visualization of microglia and Purkinje cells with *in vivo* two-photon imaging (Rahimi-Balaei et al., 2018). Adolescent mice between P25–31 (referred to hereafter as P28) were weighed and anesthetized with fentanyl cocktail (fentanyl 0.05 mg/kg; midazolam, 5.0 mg/kg; dexmetomidine, 0.05 mg/kg) delivered intraperitoneally (i.p.). Cranial windows were implanted over lobules IV/V of the cerebellum using methods described previously (Stowell et al., 2018; Wong et al., 2018, 2021; Stowell and Majewska, 2020). In brief, aseptic technique was adhered to during surgery. Animal body temperature was maintained at 37°C and the eyes were covered with lubricant ointment during all surgical procedures and later imaging. The scalp was partially removed and membranes over the cerebellum were cleared. A 3 mm circular craniotomy was made, and the skull replaced with a glass coverslip. A headpost was fitted to the scalp and the entire fixture secured with C&B Metabond dental cement (Parkell). Cement was allowed to dry for 1 h before imaging. Surgeries and imaging were performed throughout the animals' light phase at times dictated by equipment availability precluding controlling for circadian rhythm effects.

2.4. Two-photon *in vivo* imaging

Immediately after surgery and while still anesthetized, the $L7^{cre}/Ai9^{+/-}/Cx3cr1^{G/+}$ mice were affixed to an imaging stage. A custom two-photon laser-scanning microscope was used for *in vivo* imaging of microglia dynamics, morphology, and Purkinje cell interactions (Ti: Sapphire, Mai-Tai, Spectra Physics; modified Fluoview confocal scan head, 20X water-immersion objective, 0.95 numerical aperture, Olympus). Excitation was achieved with 100-fs laser pulses (80 MHz) at 920 nm with a power of ~30 mW measured at the sample. A 565 dichroic with 520/40 (GFP) and 598/30 (Ai9) filters was used to visualize microglia (GFP) and Purkinje cells (Ai9) in different channels simultaneously. Imaging of 101 μm z-stacks at a 1 μm z-step size with a 4x digital zoom with an 800 × 600 pixel frame size occurred with time-lapse imaging at 5-min intervals for 1 h per imaging session. All image analysis was run offline using Ilastik (Berg et al., 2019; RRID:SCR_015246), NIH ImageJ[1] (RRID:SCR_003070) or FIJI (see footnote 1; RRID:SCR_002285), and MATLAB (MathWorks, version

1 imagej.net

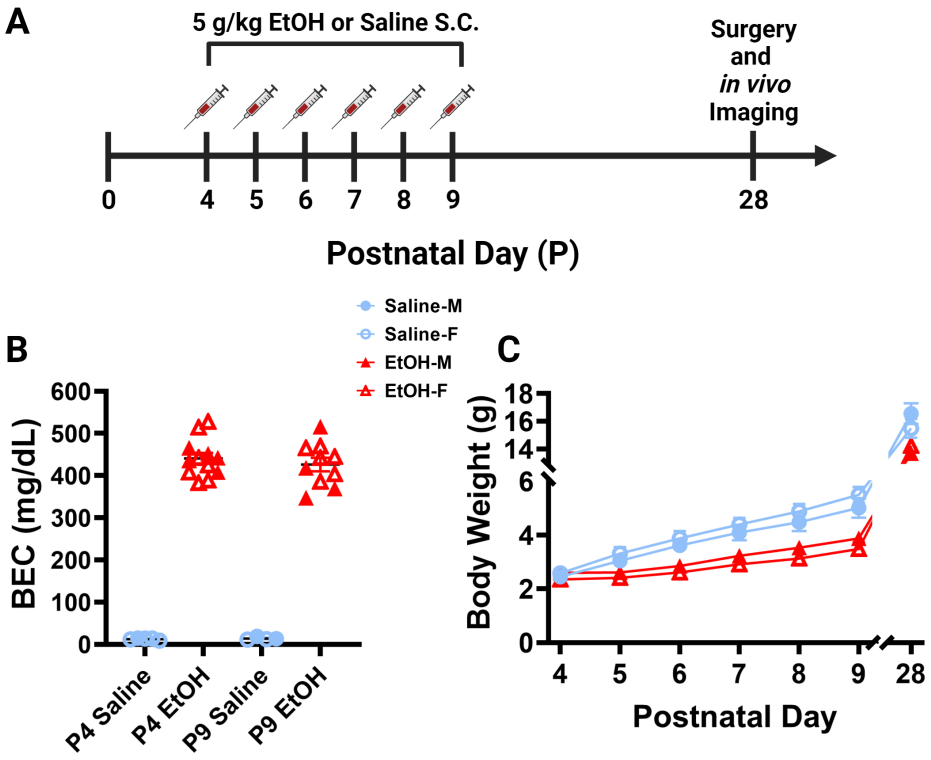


FIGURE 1
Mouse model of third trimester binge-level ethanol exposure. **(A)** Timeline of third trimester equivalent dosing paradigm. Mice were given subcutaneous injections of either 5.0g/kg/day of EtOH or Saline, given as 2 doses, separated by 2h each day from P4–9. Animals underwent cranial window surgery and *in vivo* two-photon imaging in adolescence around P28. **(B)** Blood EtOH Concentrations (BEC) were measured 90min after the second dose of ethanol on either P4 [5 males (M; closed shapes), 7 females (F; open shapes) or P9 (4M, 6F)]. Pups dosed with saline were measured 90min after the second dose as controls on P4 (1M, 4F) and P9 (2M, 2F). Individual points represent individual animals. Data are presented as the mean ± SEM. Animals dosed with EtOH displayed BECs of ~450mg/dl on P4 and P9. **(C)** Body weights of EtOH (6M, 6F) and Saline (6M, 6F) dosed mice. Weights were collected prior to the first dose of EtOH or saline from P4–9 and prior to surgery on P28. EtOH dosed mice weighed less than their control counterparts, but all animals gained weight consistently throughout the study. There was a significant interaction between age and treatment on weight when sexes were pooled [$F(6, 132)=7.249$, $p<0.0001$]. There was a main effect of age [$F(1.232, 27.11)=1,333$, $p<0.0001$] and a main effect of treatment on body weight over time [$F(1, 22)=30.15$, $p<0.0001$]. Saline animals gained weight every day ($p<0.01$) and EtOH animals gained weight every day ($p<0.05$) except for the first day between P4 and P5 ($p>0.99$). EtOH dosed animals had significantly lower weights than saline dosed animals every day except the first day when sexes were pooled ($p<0.05$). Saline and EtOH dosed males had no significant differences in weight at any age, while EtOH females weighed significantly less than saline females at P6 ($p=0.0277$), P7 ($p=0.0068$), P8 ($p=0.0054$), and P9 ($p=0.0030$). **(C)** Each datapoint represents a treatment group and sex. Data are presented as the mean ± SEM. Two-way ANOVA, repeated measures with Bonferroni *post hoc* comparisons.

R2020a; RRID:SCR_001622). Some bleed-through of the Ai9 Purkinje cell fluorescence into the background of the GFP microglia channel occurred due to spectral overlap and bleed-through correction was performed in ImageJ/FIJI as described below.

2.5. Image analysis

2.5.1. Image preprocessing

All images were blinded using a custom MATLAB script after collection and prior to analysis.

Bleed-through Correction: ImageJ/FIJI was used to subtract the Ai9 Purkinje cell channel from the GFP microglia channel using a modified protocol from (Wong et al., 2021). A custom FIJI/ImageJ macro was created to automate this process. In brief, the two-channel image was split into two separate Ai9 Purkinje cell and GFP microglia channels. For each channel, the image was further split into 12 separate time points. Each channel was corrected for background fluorescence, and then a brightness compensated Ai9 Purkinje cell channel was subtracted from the GFP microglia channel. The original, raw Ai9 channel images were used for microglia-Purkinje cell interaction analysis. The final background- and Ai9-subtracted GFP microglia images were used for all microglial analyses: dynamics, morphology, and interaction.

Denoising: Further preprocessing was done to denoise both microglia and Purkinje cells channels. To remove high frequency components responsible for image noise, Principal component analysis (PCA) was performed and images were reconstructed using a quantitatively-determined number of components with a custom MATLAB script.

Layer separation: Images were divided into the Molecular Layer (ML) and Purkinje Cell Layer (PCL) of the cerebellum. This was determined manually using the Ai9 Purkinje cell channel, through the identification of the Purkinje cells somas. When the somas could be identified, this was considered the start of the Purkinje Cell Layer and the end of the Molecular Layer. Number of z slices were kept uniform and the smallest number of z slices for each layer was chosen across all animals for consistency. Substacks were created in ImageJ/FIJI and all subsequent analysis was separated by layer.

2.5.2. Object classification

For automated detection of microglia and Purkinje cells, the image classification and segmentation software, Ilastik, was used. To train for pixel classification, microglia processes and somas were traced separately for both the ML and PCL, and Purkinje cell dendrites and branch points were traced separately in the ML while Purkinje cell somas were traced in the PCL. Appropriate thresholding and size exclusion criteria were applied for object classification. Microglia and Purkinje cell object output were binarized for further analysis. Microglia processes and somas, as well as Purkinje cell dendrites and branch points, were added together in ImageJ/FIJI to get whole microglia and whole Purkinje cell binary images.

2.5.3. Microglia dynamics

Microglia dynamics, quantified by microglia motility and surveillance, were analyzed for ML and PCL separately. As described above, 101 µm z-stacks were collected every 5 min for 1 h for a total of 12 time points, then subdivided into the ML and PCL. ImageJ/FIJI was used to drift-correct and create max projections of each time point for each layer, leading to 24 max z-projected images for each animal (12 time points for each of the 2 layers) (previously described in Sipe et al., 2016; Whitelaw et al., 2020). These max projected images were used in Ilastik for cell detection as described above. The Ilastik binarized output files were then compared across time points using a custom MATLAB script to record microglia motility and surveillance. The motility index (M.I.) of the microglial processes was calculated by dividing the sum of the thresholded extended and retracted pixels by stable pixels between consecutive timepoints to determine how microglia sample their environment. The surveillance index (S.I.) was calculated by dividing the number of binarized microglia pixels by all pixels in the maximum projection of all timepoints to determine how much of the parenchyma microglia survey over time.

2.5.4. Microglia morphology: Sholl

Microglial morphology in the first time point was assessed using Sholl analysis to quantify arbor complexity. In ImageJ/FIJI, 1–2 individual microglia were selected from the first time point of max projected images for each layer (projection creation described in microglia dynamics). The microglia processes were manually traced in ImageJ/FIJI. The ImageJ/FIJI Sholl analysis plug-in was run with concentric rings at 2 µm intervals out to 80 µm from the soma center. The number of intersections across each ring were used to create Sholl curves.

2.5.5. Microglia-Purkinje cell interactions

Microglia dynamic interactions with Purkinje cells were quantified over time in 3D. For each animal, the 12 z-stacks that were subdivided into the ML and PCL as described above were placed into Ilastik for cell identification and binarization (note these were not max projected as in microglia dynamics or morphology analysis). The binarized outputs were then entered into ImageJ/FIJI for further analysis. The number of pixels were measured for whole cells and their individual components. The binarized images were multiplied together to find the overlap between microglia and Purkinje cells. The number of pixels of the resultant images were also measured. These pixel numbers were compared across conditions and over time. Interactions were analyzed separately and normalized to the sum of the microglia and Purkinje cell pixels. All 12 timepoints were averaged for analysis of condition and sex differences. Additionally, the binarized resultant images displaying the overlap of microglia and Purkinje cells were processed with the microglia dynamics analysis described above. The resultant images were drift-corrected and max projected for each time point for each interaction type in ImageJ/FIJI. The max projected, binarized resultant images were then compared across time points using the custom MATLAB script to record interaction dynamics. The interaction coverage index (similar to the S.I. described above) was calculated by dividing the number of binarized interaction pixels by all pixels in the maximum projection of all timepoints to determine how much area microglia-Purkinje cell interactions cover over time.

2.6. Statistics

Statistical tests were run using GraphPad Prism IX statistical analysis software (La Jolla, CA; RRID:SCR_002798), which was also used for graphing. Student's unpaired *t*-tests were used to compared ethanol vs. saline treated animals when sexes were pooled. Two-Way ANOVAs were used to evaluate any sex differences in ethanol vs. saline treated animals with Bonferroni post-hoc comparisons used to evaluate significance where appropriate. Paired *t*-tests were used to assess layer specific changes in microglia. Detailed statistics are provided in the figure legends.

3. Results

3.1. Mouse model of third trimester binge-level ethanol exposure

To examine the later life effects of developmental ethanol exposure, we subcutaneously injected male and female $L7^{cre}/Ai9^{+/-}/Cx3cr1^{G/+}$ mouse pups with binge-level amounts of ethanol (EtOH) from postnatal day (P) 4–9 (Figure 1A). This time period is the equivalent of the human third trimester and a particularly vulnerable developmental window for Purkinje cells (Goodlett and Eilers, 1997). We injected 5.0 g/kg/day ethanol solution (20% v/v EtOH in saline), administered as two separate doses of 2.5 g/kg, given 2 h apart each day. Control littermates received equivalent volumes of saline (0.9% NaCl) injections. This is considered a high binge-level amount, producing blood ethanol concentrations (BEC) of ~450 mg/dl 19 min after the second injection on either P4 or P9 (Figure 1B). This level of ethanol exposure led to lower weights of ethanol-dosed animals compared to saline controls when sexes were pooled although all animals gained weight consistently throughout the study (Figure 1C). *Post hoc* testing showed no changes between control and EtOH-dosed males and only early changes in females that equalized after the dosing paradigm was complete, suggesting that EtOH's effect on weight gain was subtle. Subtle reductions in body weight after P4–9 ethanol exposure are consistent with previous studies (Wong et al., 2018, 2021). Pups were returned to the dams until weaning. In adolescence between P25–31, referred to as P28, mice were weighed again before undergoing cranial window surgeries (Figures 1A,C). While ethanol dosed animals weighed less than saline dosed animals at P28 when sexes were pooled, there was no significant effect of sex on body weight in either condition (Figure 1C). These surgeries allowed for immediate two-photon *in vivo* imaging of cerebellar microglia and Purkinje cells.

3.2. Adolescent cerebellar microglial dynamics are unaffected by binge-level developmental ethanol exposure

Using two-photon *in vivo* imaging, we examined cerebellar microglia dynamics. As highly motile cells, microglia play an important role in shaping neuronal development (Tremblay et al., 2010; Kana et al., 2019; Wong et al., 2021). Our L7^{cre}/Ai9$^{+/-}$/Cx3cr1$^{G/+}$ mice have fluorescent microglia, which allows for the visualization of microglia dynamics, such as motility and surveillance, after cranial window surgery. For each animal, we collected 101 µm *z*-stacks every 5 min for 1 h leading to a total of 12 time points for each animal. Within each *z*-stack, we captured both the Molecular Layer (ML) that houses the dendrites of the Purkinje cells, and the Purkinje Cell Layer (PCL) that houses the Purkinje cell somas.

Using these images, we examined microglia motility, which is a measure of the combined dynamics of extension and retraction in microglial processes. We calculated the motility index (M.I.) of the microglia by dividing the sum of the binarized extended and retracted pixels by the stable pixels between consecutive timepoints (Figure 2A). We found no differences between EtOH and saline dosed animals in the ML (Figure 2B) or PCL (Figure 2D) when sexes were pooled or analyzed individually (Figures 2C,E). Similar findings have been reported in the adolescent visual and somatosensory cortices (Wong et al., 2018, 2021), suggesting that developmental ethanol exposure has limited effects on microglia motility when measured in adolescence.

Using these same images, we also calculated the surveillance index (S.I.) by dividing the number of binarized microglia pixels by all pixels in the maximum projection of all timepoints to determine how much of the parenchyma microglia survey over time (Figure 3A). Similar to the M.I., the S.I. was unchanged in EtOH exposed animals compared to saline controls in both the ML (Figure 3B) or PCL (Figure 3D) when sexes were pooled or analyzed individually (Figures 3C,E).

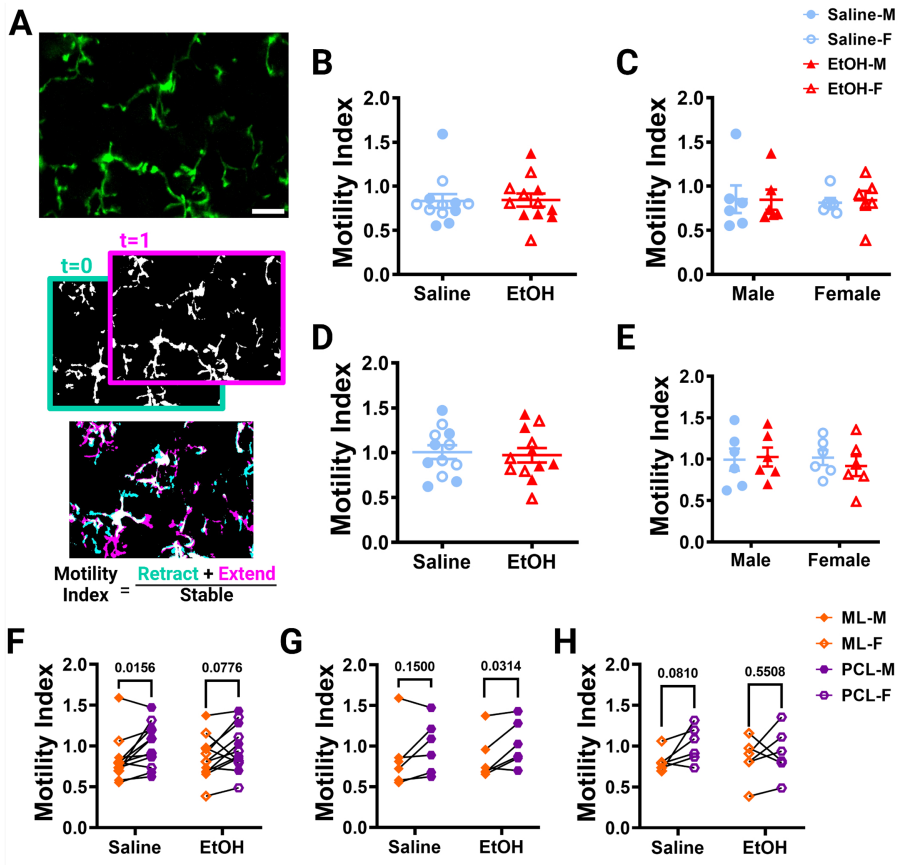


FIGURE 2
Microglia motility is unaffected by developmental ethanol exposure. **(A)** *In vivo* two-photon image of cerebellar microglia. Max z-projection of an individual timepoint (top). Binarized microglia from consecutive timepoints with time 0 in blue and time 1 in pink (middle). Overlay of the two timepoints with retracted (blue), extended (pink), and stable (white) pixels, used to create the motility index (bottom). Adolescent cerebellar microglia motility in the ML **(B,C)** and PCL **(D,E)** are unaffected by developmental ethanol exposure (triangles, 6M, 6F) compared to saline controls (circles, 6M, 6F) when sexes are pooled (**B**, ML: p=0.9216; **D**, PCL: p=0.7581) or examined individually **(C,E)**. There were no interactions between treatment or sex for ML [**C**, $F(1, 20)$=0.02137, p=0.8852] or PCL [**E**, $F(1, 20)$=0.3416, p=0.5654] motility. No main effects of treatment [**C**, ML: F (1, 20)=0.009031, p=0.9252; **E**, PCL: $F(1, 20)$=0.09055, p=0.7666] or sex [**C**, ML: $F(1, 20)$=0.04172, p=0.8402; **E**, PCL: $F(1, 20)$=0.1349, p=0.7173] were observed for either layer's motility. Individual points represent individual animals with closed shapes representing males and open shapes representing females. **(F–H)** When sexes were pooled, saline dosed animals displayed more microglia motility in the PCL than the ML (**F**, p=0.0156), but not when separated into males (**G**, p=0.1500) and females (**H**, p=0.0810). For EtOH dosed animals, PCL microglia were more motile than ML microglia only in males (**G**, p=0.0314), but not in females (**H**, p=0.5508) or when sexes were pooled (**F**, p=0.0776). **(B-H)** Each datapoint represents an individual animal. Data are presented as the mean ± SEM. **(B,D)** Unpaired *t*-tests; **(C,E)** two-way ANOVA; **(F,G)** paired *t*-tests. Scale=25µm.

Our lab previously reported layer specific differences in microglial dynamics in adult mice with PCL microglia displaying more motility than those of the ML (Stowell et al., 2018). Additionally, when mice were administered EtOH in adulthood, microglial dynamics were reduced in PCL microglia, but not ML microglia (Stowell and Majewska, 2020). We examined our mice to see if these differences were maintained in adolescent mice given EtOH postnatally. We found that PCL microglia displayed significantly more motility than those in the ML of saline-dosed animals when sexes were pooled (Figure 2F), but this significance was not maintained in either males (Figure 2G) or females (Figure 2H) individually. In EtOH-dosed animals, male mice had increased microglia motility in the PCL compared to the ML (Figure 2G), but not female (Figure 2H) or pooled (Figure 2F) mice. When we examined microglia surveillance, PCL microglia surveyed more of the parenchyma than ML microglia when sexes were pooled (Figure 3F), and when males (Figure 3G) and females (Figure 3H) were analyzed separately. This suggests that layer specific differences of microglia dynamics found in adulthood appear as early as adolescence. These differences appear to not be significantly affected by developmental EtOH exposure.

3.3. Adolescent cerebellar microglia morphology is unaffected by binge-level developmental ethanol exposure

Various studies have reported alterations in microglia morphology after developmental EtOH exposure, describing microglia as becoming more amoeboid and displaying hyperramification, consistent with an immune activated phenotype (Drew et al., 2015; Topper et al., 2015; Kane et al., 2021; Lowery et al., 2021). We examined *in vivo* microglia morphology in the ML and PCL of the cerebellum in these same mice (Figures 4A,B). Using the first of the 12 timepoints previously described, we traced the microglial arbors and performed Sholl analysis to examine

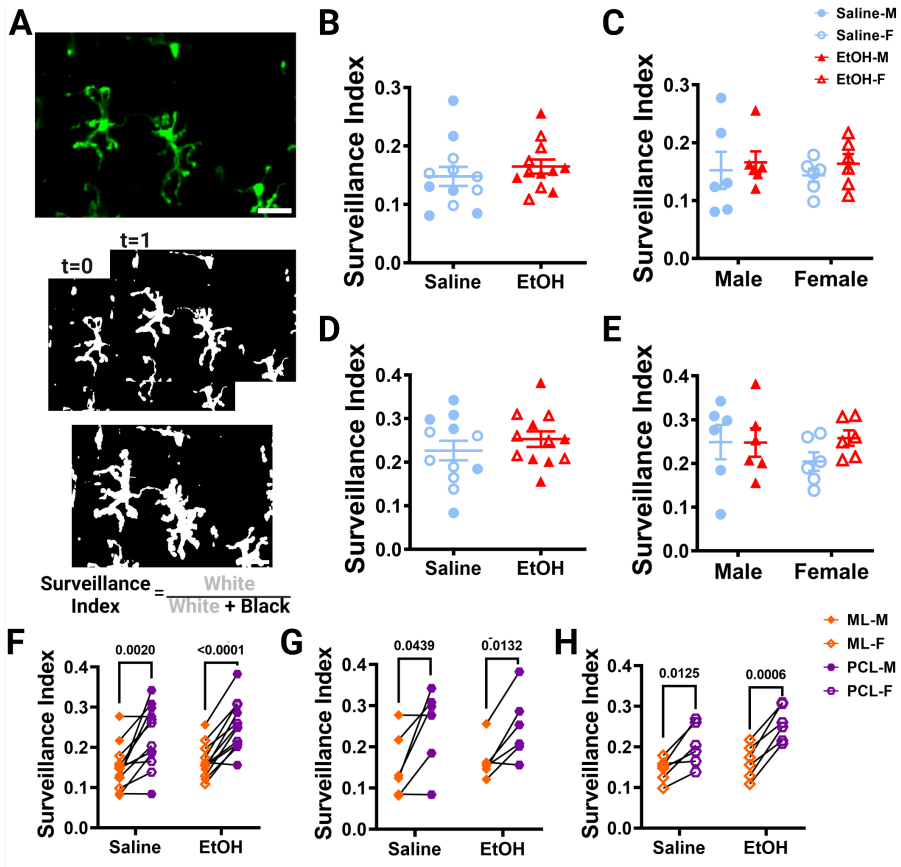


FIGURE 3
Microglia surveillance is unaffected by developmental ethanol exposure. **(A)** *In vivo* two-photon image of cerebellar microglia. Max z-projection of an individual timepoint (top). Binarized microglia from consecutive timepoints with time 0 and time 1 (middle). Overlay of all 12 timepoints with microglia (white) pixels and total (white+black) pixels, used to create the surveillance index (bottom). Adolescent cerebellar microglia surveillance in the ML **(B,C)** and PCL **(D,E)** are unaffected by developmental ethanol exposure (triangles, 6M, 6F) compared to saline controls (circles, 6M, 6F) when sexes are pooled (**B**, ML: p=0.4151; **D**, PCL: p=0. 0.3676) or examined individually **(C,E)**. There were no interactions between treatment or sex for ML [**C**, $F(1, 20)$=0.02197, p=0.8836] or PCL [**E**, $F(1, 20)$=0.8901, p=0.3567] surveillance. No main effects of treatment [**C**, ML: $F(1, 20)$=0.6302, p=0.4366; **E**, PCL: $F(1, 20)$=0.8167, p=0.3769] or sex [**C**, ML: $F(1, 20)$=0.06901, p=0.7955; **E**, PCL: $F(1, 20)$=0.3459, p=0.5630] were observed for either layer's surveillance. Individual points represent individual animals with closed shapes representing males and open shapes representing females. **(F–H)** Differences in microglia surveillance were discovered between the ML and PCL in both EtOH and saline dosed animals when sexes were pooled (**F**, saline: p=0.0020; EtOH: p<0.0001), and males (**G**, saline: p=0.0439; EtOH: p=0.0132) and females (**H**, saline: p=0.0125; EtOH: p=0.0006) were analyzed individually. **(B-H)** Each datapoint represents an individual animal. Data are presented as the mean ± SEM. **(B,D)** Unpaired t-tests; **(C,E)** two-way ANOVA; **(F,G)** paired t-tests. Scale=25μm.

10.3389/fnins.2023.1176581

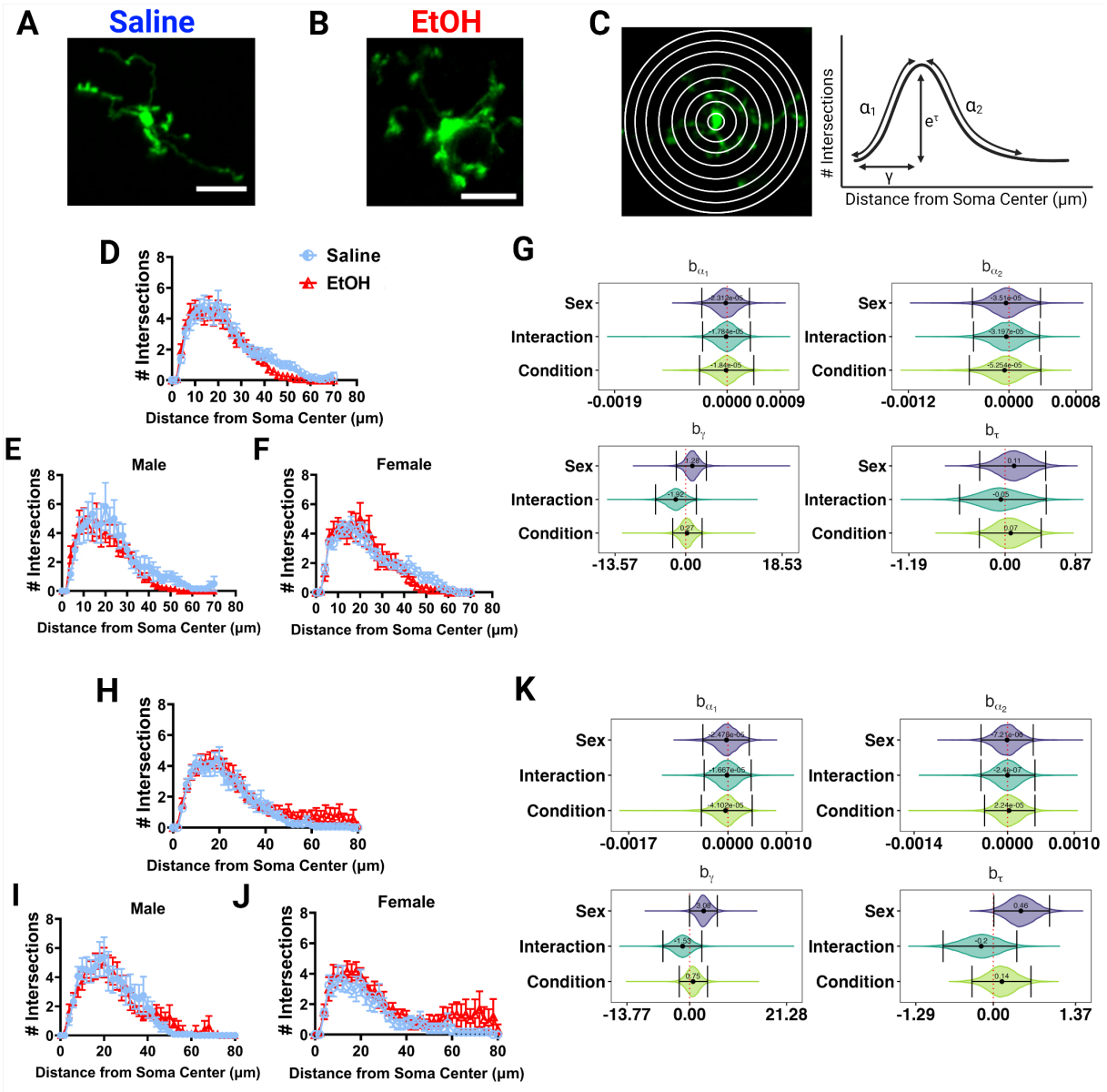


FIGURE 4
Microglia morphology is unaffected by developmental ethanol exposure. Two photon *in vivo* images of microglia in mice dosed with saline **(A)** or EtOH **(B)** from P4–9. **(C)** Two photon *in vivo* images of microglia with concentric circles drawn in increasing radii (left), which correspond to the x axis of the Sholl curves. Process intersections across these rings correspond to the y axis of the Sholl curves. Example curve (right) with labeled factors that provide information about the behavior of the Sholl curve: before the change-point (α_1); after the change-point (α_2); branch maximum (e^{τ}); change-point (γ) (modified from Vonkaenel et al., 2023). Sholl curves of microglia in the ML **(D–F)** and PCL **(H–J)** show no differences in ramification between EtOH and saline groups when sexes are pooled **(D,H)**, or separated into males **(E,I)** or females **(F,J)**. In the PCL, saline male **(I)** microglia were more ramified than saline female **(J)** microglia. **(D-F, H-J)** Each datapoint represents a treatment group and sex. Data are presented as the mean ± SEM. **(G,K)** Individual Sholl curves were fit using a hierarchical Bayesian approach to capture variation at each level of the experimental hierarchy. 95% credible intervals for effects on each parameter from **(C)** were calculated across treatments and sexes for the ML **(G)** and PCL **(K)**.

process ramification. This analysis generates Sholl curves that plot the number of intersections of microglia processes across concentric circles of increasing radii (Figure 4C).

EtOH and saline dosed mice had similar microglial morphologies in the ML or PCL when sexes were pooled or analyzed individually (Figures 4D–F, H–J). However in the PCL, microglia in male mice seemed to have increased ramification compared to female mice (Figures 4I,J). This was confirmed with further analysis using a novel fully parametric model-based approach (Figures 4G,K; Vonkaenel et al., 2023). Effect plots show that the branch maximum (e^{τ}) and change point (γ) were modulated with sex but not treatment in the PCL for saline, but not for EtOH dosed animals (Figure 4K). Limited effects of developmental ethanol exposure on microglia morphology have also been reported in the adolescent visual and somatosensory cortices (Wong et al., 2018, 2021). Ethanol administration in adulthood similarly did not affect ML microglia morphology (Stowell and Majewska, 2020). This suggests that developmental ethanol exposure does not have a large effect on cerebellar microglia morphology when assessed later in life.

3.4. Adolescent cerebellar microglia-Purkinje cell interactions may be affected by binge-level developmental ethanol exposure

While we found no differences in *in vivo* microglia dynamics or morphology, developmental ethanol exposure could affect how microglia interact with neurons. In the healthy brain, microglia play an important role in the development of neurons and connectivity by making physical contacts with neuronal somas, dendrites, and axons (Dean et al., 2012; Nakayama et al., 2018; Kana et al., 2019; Perez-Pouchoulen et al., 2019; Yamamoto et al., 2019; Cserép et al., 2021). Here, we characterized putative physical contacts between microglia and Purkinje cells in three dimensions over the 12 time points that encompass our imaging sessions in both the ML (Figure 5) and PCL (Figure 6).

Putative physical interactions were defined as areas that overlapped in signal between the microglia and Purkinje cell channels within each z plane (Figures 5A, 6A). To get further insight into the subcellular localization of interactions between microglia and Purkinje cells, we subdivided each cell into components (Supplementary Figure S1). For each layer, we further analyzed interactions with microglial somas or processes separately (as well as the whole microglia which included soma and processes). For the ML, Purkinje cell dendrites were divided into dendritic branch points (Stowell et al., 2018) or dendritic stretches outside of branch points, as well as the whole dendrite which included both types of structures. For the PCL, only the Purkinje cell somas were characterized. Various combinations of the above listed components were examined for interactions and no differences were observed (Supplementary Figure S2). The number of pixels occupied by microglia (Figure 5C, 6C) and Purkinje cells (Figures 5D, 6D) and their various sub-components (Supplementary Figure S1) were generally unchanged between sexes and conditions, except for the ML microglia soma, which had a main effect of treatment (Supplementary Figure S1), driven by increases in pixel numbers of EtOH females compared to saline females. While only one subcomponent was altered by EtOH, we normalized the value of these interactions to the sum of the microglia and Purkinje cell pixels to account for variations in microglia and Purkinje cell availability in each image (Figures 5E–J, 6E–H). In general, interactions were relatively stable over time for all conditions, sexes, and cells (components) in both the ML (Figure 5E) and PCL (Figure 6E), and averaged values across all 12 time points were used for comparisons (Figures 5F–J, 6F–H).

Developmental EtOH exposure may have mild effects on microglia-Purkinje cell interactions in the ML (Figure 5). Increased interactions in EtOH dosed mice compared to saline mice were observed for whole microglia interactions with whole Purkinje cells (Figure 5F), although these did not reach significance. Bonferroni post-hoc comparisons suggest this difference was driven by EtOH females having more interactions than saline females. We next wanted to see if these effects persisted in interactions between subcellular components. As microglial processes compose the majority of microglia, and in the ML, dendrites (without branch points) are the majority of Purkinje cells, we first examined these interactions as they would be the most likely drivers of the effect (Supplementary Figure S1). As expected, similar effects to the whole microglia and whole Purkinje cell were observed when limiting the analysis to just the microglial processes (excluding any contacts made with microglial somas) and non-branch areas of Purkinje cell dendrites (Figure 5G), with female EtOH mice having more interactions than female saline mice. Next, we examined the same non-branch areas of dendrites, but with microglia somas. Similar to their interactions with microglial processes, there was a trend to increased interactions when considering only microglial somas (no processes) and non-branch areas of Purkinje cell dendrites (Figure 5H), with female EtOH mice having more interactions than female saline mice. This suggests that EtOH may have similar effects on all microglial subcellular components when they interact with Purkinje cells' non-branch areas of dendrites.

We next examined branch points of Purkinje cells and their interactions with microglia components. While microglial processes' interactions with Purkinje cell dendrite branch points were unaffected by treatment (Figure 5I), there appeared to be a trend toward increased interactions in males compared to females (Figure 5I). Bonferroni post-hoc comparisons suggest this difference was driven by saline dosed animals. In the ML, microglia somas had no differences in interactions with branch areas of Purkinje dendrites in EtOH or saline mice (Figure 5J). This suggests that EtOH's effects may be limited to interactions with non-branch areas of Purkinje cell dendrites. This may be driven by the small size of branch areas of Purkinje cell dendrites, so there may be fewer opportunities for interactions with these subcellular components (Supplementary Figure S1). To determine the dynamics of microglia-Purkinje cell interactions, we performed a coverage analysis where we overlaid all areas of interaction across 12 time points in two dimensions for both the ML (Figure 5B) and PCL (Figure 6B). This allowed us to compare the cumulative interactions over the 1 h imaging period. We found that dynamic interactions between whole microglia and whole Purkinje cells covered a larger area in EtOH dosed animals (Figure 5K), an effect driven by increases in females. A similar effect was observed when coverage was computed for microglia process interactions with non-branch areas of Purkinje cells dendrites (Figure 5L), also driven by females.

No differences were noted between EtOH and saline dosed mice or between males and females in the PCL in whole microglia interactions with Purkinje cell somas (Figure 6F), microglia process interactions with Purkinje cell somas (Figure 6G), or microglia soma interactions with Purkinje cell somas (Figure 6H). Similarly, the dynamic coverage of microglia-Purkinje cell soma interactions was unaffected by EtOH for whole microglia and Purkinje cell soma interactions (Figure 6I), as well as microglia process and Purkinje cell soma interactions (Figure 6J). This suggests EtOH may affect microglia interactions with neurons later in life in a layer specific manner.

4. Discussion

While much work has been completed on microglia and Purkinje cells individually after developmental ethanol exposure, little is known about their interactions. Adolescent microglia dynamics in mice exposed to ethanol in development have been examined in the cortex but have thus far been unstudied in the cerebellum (Wong et al., 2018, 2021). As microglia display regional heterogeneity in the absence of

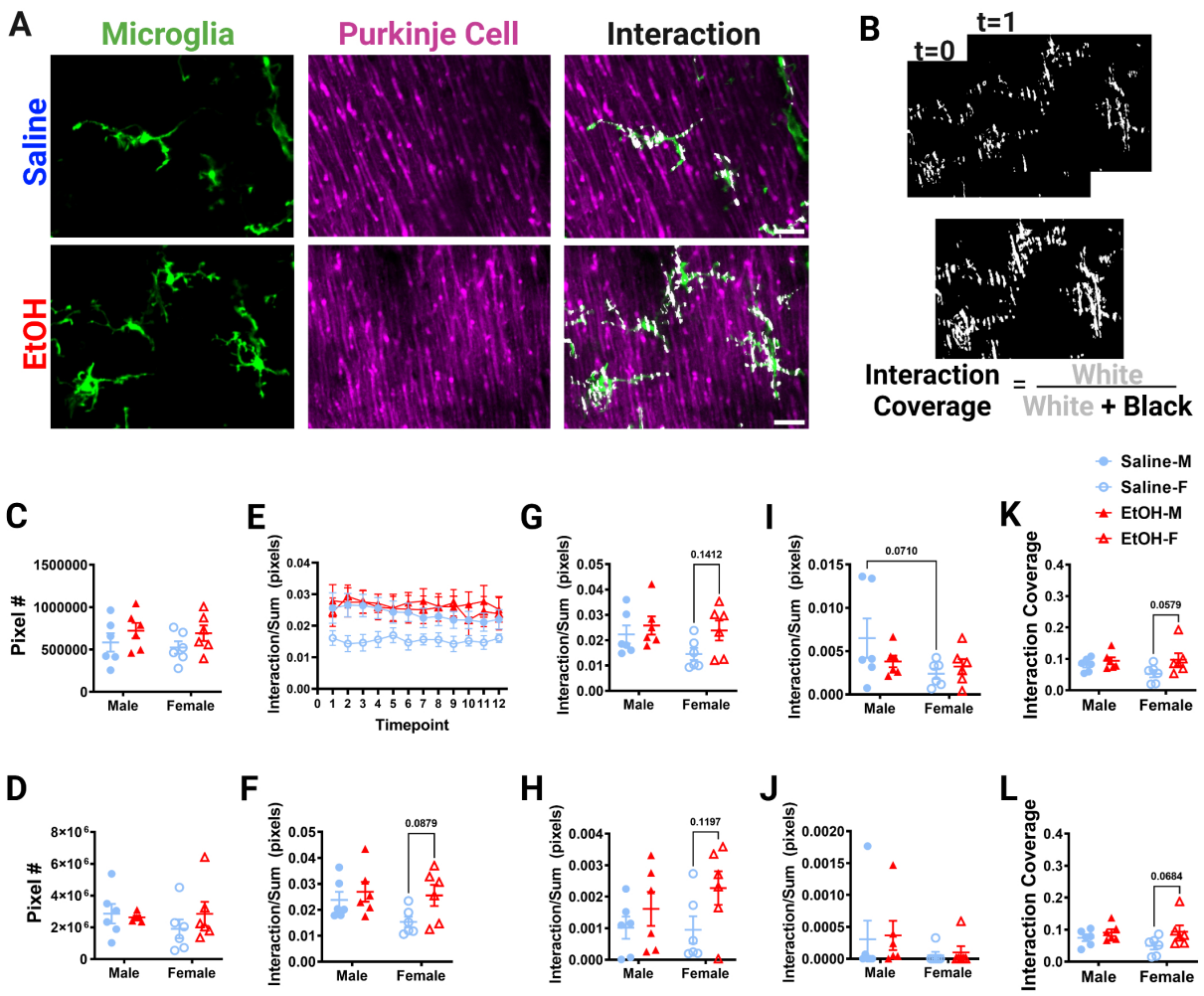


FIGURE 5
Molecular Layer cerebellar microglia-Purkinje cell interactions are relatively unaffected by ethanol. **(A)** Two-photon *in vivo* images of microglia (left), Purkinje cells (middle), and their interactions (right) when mice were given saline (top) or EtOH (bottom) from P4–9. The white overlay in the interaction images indicate the overlap between cells. **(B)** Binarized interactions from consecutive timepoints with time 0 and time 1 (top) from EtOH animal shown in **(A)**. Overlay of all 12 timepoints with interaction (white) pixels and total (white+black) pixels, used to create the interaction coverage (bottom). **(C)** Whole microglia (microglia somas and processes) pixel numbers were unaffected by treatment [$F(1, 20)=2.790$, $p=0.1104$]. **(D)** Whole Purkinje cell (branch points of dendrites and non-branch point areas of dendrites) pixel numbers were unaffected by treatment [$F(1, 20)=0.3868$, $p=0.5410$]. **(E)** Whole microglia-whole Purkinje cell interactions normalized to total pixels representing microglia (MG) and Purkinje cell (PC) pixels over the 12 timepoints. **(F–J)** Comparisons of microglia-Purkinje cell interactions normalized to the sum of MG and PC pixels when all timepoints are averaged together for the whole MG (processes+somas) and whole PC (dendrites+branchpoints) **(F)**; MG processes and PC dendrites **(G)**; MG somas and PC dendrites **(H)**; MG processes and PC branchpoints **(I)**; MG somas and PC branchpoints **(J)**. While none were statistically significant, some trends toward increased interactions in EtOH mice compared to saline mice were observed: **(F)** whole MG interactions with whole PC [$F(1, 20)=3.951$, $p=0.0607$], driven by EtOH females ($p=0.0879$); **(G)** MG processxPC dendrite [$F(1, 20)=3.477$, $p=0.0770$] driven by EtOH females ($p=0.1412$); **(H)** MG somaxPC dendrite [$F(1, 20)=4.186$, $p=0.0541$], driven by EtOH females ($p=0.1197$). Additionally sex differences were observed with a trend toward increased interactions in males compared to females in **(I)** MG processxPC branch [$F(1,20)=3.313$, $p=0.0838$], driven by saline males ($p=0.0710$), but interactions were unaffected by treatment [$F(1, 20)=0.5150$, $p=0.4813$]. **(J)** No differences were found in MG somaxPC branch interactions [$F(1, 20)=0.07120$, $p=0.7923$]. **(K,L)** Dynamic interactions in EtOH animals, particularly females, covered a significantly larger area than in saline animals for both the whole MG (processesxsomas) and whole PC (dendritesxbranchpoints) [**K**, $F(1, 20)=4.513$, $p=0.0463$, Bonferroni *post hoc* $p=0.0579$] and MG processes and PC dendrites [**L**, $F(1, 20)=4.882$, $p=0.0390$, Bonferroni *post hoc* 0.0684]. **(C,D, F–L)** Each datapoint represents an individual animal. Data are presented as the mean ± SEM. Two-way ANOVA with Bonferroni *post hoc* comparisons. **(E)** Each datapoint represents a treatment group and sex. Data are presented as the mean ± SEM. Scale=25μm.

perturbation (Grabert et al., 2016; Stowell et al., 2018) as well as after ethanol exposure (Drew et al., 2015), developmental ethanol exposure may have differing effects on cerebellar microglia dynamics compared with cortical microglia dynamics. A more immune alert state found in cerebellar microglia may translate to greater alterations in these cells after an insult or in disease compared to cortical microglia (Grabert et al., 2016). Additionally, while microglia-Purkinje cell interactions have been examined in the adult mouse, no work has examined these interactions in adolescence or after ethanol exposure (Stowell et al., 2018). Understanding the development of these interactions may be important for understanding FASD pathology and critical windows of development. At the time of our study, around four postnatal weeks of age, the cerebellum is mature (Rahimi-Balaei et al., 2018). Our P4–9 ethanol dosing model occurs during a critical period

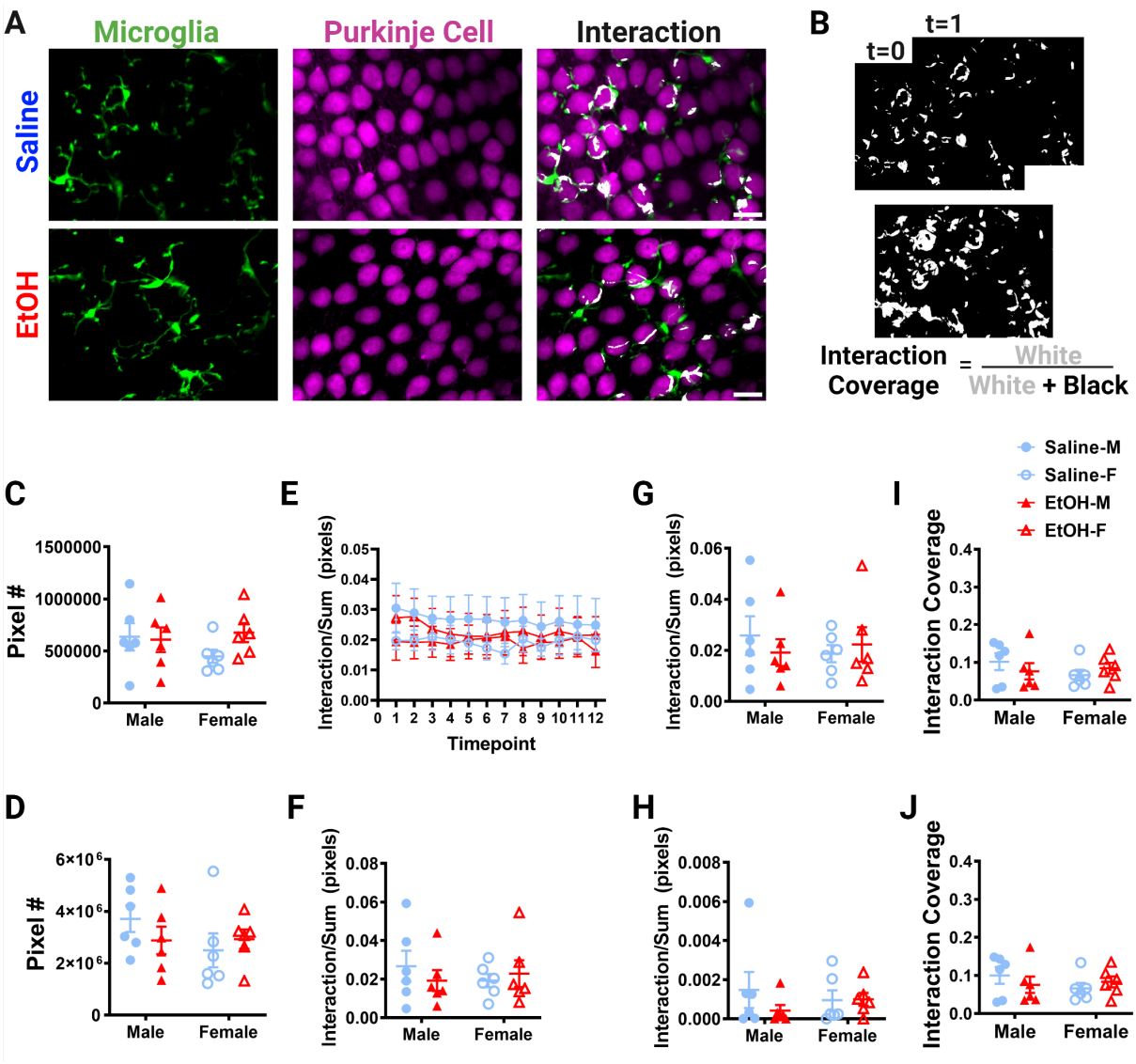


FIGURE 6
Purkinje cell layer cerebellar microglia-Purkinje cell interactions are unaffected by ethanol. **(A)** Two-photon *in vivo* images of microglia (left), Purkinje cells (middle), and their interactions (right) when mice were given saline (top) or EtOH (bottom) from P4–9. The white overlay in the interaction images indicate the overlap between cells. **(B)** Binarized interactions from consecutive timepoints with time 0 and time 1 (top) from saline animal shown in **(A)**. Overlay of all 12 timepoints with interaction (white) pixels and total (white+black) pixels, used to create the interaction coverage (bottom). **(C)** Whole microglia (microglia somas and processes) pixel numbers were unaffected by treatment [$F(1, 20)=0.9211$, $p=0.3487$]. **(D)** Purkinje cell soma pixel numbers were unaffected by treatment [$F(1, 20)=0.1463$, $p=0.7062$]. **(E)** Whole microglia-Purkinje cell soma interactions normalized to the sum of microglia (MG) and Purkinje cell (PC) pixels over the 12 timepoints for the whole MG (processes+somas) and PC somas. **(F–H)** Comparisons of microglia-Purkinje cell interactions normalized to the sum of MG and PC pixels when all timepoints are averaged together for the whole MG (processes+somas) and PC somas **(F)**; MG processes and PC somas **(G)**; MG somas and PC somas **(H)**. No differences were observed between mice given EtOH or saline in development in either male or female mice in whole MG x PC soma [**F**, $F(1, 20)=0.09261$, $p=0.7640$], MG processxPC soma [**G**, $F(1, 20)=0.06558$, $p=0.8005$], or MG soma x PC soma [**H**, $F(1, 20)=0.7771$, $p=0.3885$]. **(I,J)** Similarly, dynamic interaction coverage was unaffected by EtOH in the whole MG and PC soma [**I**, $F(1, 20)=0.03629$, $p=0.8508$] and MG process and PC soma [**J**, $F(1, 20)=0.03770$, $p=0.8480$]. **(C,D,F–J)** Each datapoint represents an individual animal. Data are presented as the mean ± SEM. Two-way ANOVA. **(E)** Each datapoint represents a treatment group and sex. Data are presented as the mean ± SEM. Scale=25μm.

of development for the cerebellum and Purkinje cells (Goodlett et al., 1990; Hamre and West, 1993; Goodlett and Eilers, 1997; Topper et al., 2015). Microglia-Purkinje cell interactions may be altered long-term by developmental EtOH exposure, and these alterations may contribute to FASD pathology.

In this work, we examine the effects of a binge-level exposure of ethanol on a mouse model in the human third trimester equivalent on cerebellar microglia and Purkinje cells. We sought to determine if microglia dynamics are affected later in life when mice are given ethanol in development. We found no changes in cerebellar microglia motility or surveillance in either the ML or PCL when mice were given ethanol compared to saline. However, PCL microglia were more motile and displayed more surveillance compared to ML microglia. While there were no differences in arbor complexity between EtOH and saline mice in the ML, male mice microglia were more ramified than female mice microglia in the PCL in saline dosed mice.

Additionally, while most of our data did not reach statistical significance, we found trends toward possible increases in microglia-Purkinje cell interactions in female mice in the ML, but not the PCL, after developmental EtOH exposure.

Our finding of unchanged microglia dynamics after developmental ethanol exposure is in line with other work that has reported no effect of developmental ethanol exposure in similarly aged mice on cortical microglia dynamics (Wong et al., 2018, 2021). While EtOH reduced microglia motility and surveillance in the cerebellum in adult mice, in that study EtOH was given acutely in adulthood immediately prior to imaging, instead of in development (Stowell and Majewska, 2020). EtOH may have similar effects on motility during an early exposure, but the weeks of time between the last EtOH exposure in our study and imaging may have been enough time for resolution of any ethanol induced effects and return to homeostasis. Examining the cerebellum immediately after the last ethanol exposure on P10 may be more likely to yield differences. Indeed, examination of the cerebellum and hippocampus at P10 after a similar developmental exposure uncovered increases in the proinflammatory factors, IL-1β, TNF-α, and CCL2 (Drew et al., 2015). Such effects of developmental ethanol exposure have been found to be transient in some cases. An acute, binge-level dose of EtOH in mice on P7 or P8 led to microglia displaying a more amoeboid phenotype and increases in pro-inflammatory cytokines, a phenotype that resolved within 24–48 h after exposure (Ahlers et al., 2015). Additionally, we examined microglial homeostatic functions, but not the immune function of these microglia, where an immune "second-hit" may be needed to uncover effects of developmental ethanol exposure later in life. In the cortex, adolescent microglia trended toward a faster response to a laser ablation injury when given ethanol in development compared to controls (Wong et al., 2018, 2021). A similar insult later in life could uncover long-lasting effects on cerebellar microglia that were not evident in this study, where we focused on microglial dynamics in the absence of additional insults. Future experiments to examine how developmentally exposed cerebellar microglia respond to immune challenge would be valuable to help us understand whether these cells' activity is altered by ethanol.

We also did not find ethanol-induced changes in microglial morphology. Developmental ethanol exposure has been known to increase amoeboid morphology and alter ramification (Ahlers et al., 2015; Topper et al., 2015), and a single binge-level exposure to ethanol can lead to subtle changes in glia when examined 24 h later (Lowery et al., 2021). While this could also be due to the time elapsed between exposure and our morphology assessment, another discrepancy may be that other studies examined microglia in fixed tissue, while we examined microglia *in vivo*. As we needed to image at sufficient magnification to capture microglia arbors, we were only able to visualize a few microglia in our field of view with two-photon imaging. During Sholl analysis, we only included microglia whose processes and somas fell within our image, so we were only able to include 1–2 microglia for each layer in each animal. The low number of microglia analyzed may mask any significant differences in EtOH versus saline mice. Additionally, a lack of morphological change does not necessarily mean that microglial function is unaltered, as microglia states are dynamic and structural changes cannot always be equated with functional ones (Paolicelli et al., 2022). This made it all the more important that we investigate other aspects of microglia function, such as their dynamic interactions with neurons that could inform on altered microglial function, as well as possible effects on neurons (Whitelaw et al., 2022).

Microglia are known to have dynamic interactions with neurons, both in the cortex and cerebellum (Wake et al., 2009; Tremblay et al., 2010, 2011; Stowell et al., 2018, 2019). In the cortex, microglia contact synapses and modulate dendritic spine formation and elimination in an activity and context-dependent manner (Tremblay et al., 2010; Sipe et al., 2016). In both the healthy brain and disease, microglia are known to phagocytose neurons and prune synapses (Marin-Teva et al., 2004; Schafer et al., 2012; Ayata et al., 2018), and both the complement system and fractalkine signaling have been implicated in microglia–neuron interactions and brain plasticity (Hoshiko et al., 2012; Schafer et al., 2012). While microglia motility may be unaltered by ethanol, changes in activity or the release of factors by either microglia or neurons may still affect their interactions, as microglia can release a number of soluble factors that modulate neuronal function but do not require physical proximity. Much of the work on microglia–neurons interactions has focused on the cortex, and the study of the effects of developmental ethanol exposure on microglia-Purkinje cell interactions is novel and has thus far not been characterized. While one study previously examined these interactions *in vivo*, this occurred in adult unperturbed mice (Stowell et al., 2018). Here, we develop new analyses to interrogate the interactions between microglial components and the components of Purkinje cells. Our work suggests EtOH may lead to layer specific alterations in microglia contact with neurons. Independently of the effects of ethanol, this work gives us new understanding of the interactions between microglia and Purkinje cells in adolescence and can open new pathways to understanding how microglia physically contact neurons. Our work here only characterized putative physical interactions, because light microscopy cannot resolve direct contact between membranes. In the future, electron microscopy should be used for higher resolution to differentiate between close proximity and contacts between the cells. Microglia are known to release factors after developmental ethanol exposure that lead to inflammation, which can also affect neurons (Drew et al., 2015; Kane et al., 2021). Additionally, signaling pathways may be disrupted, which could further impact microglia–neuron interactions, and such mechanisms remain to be investigated in the context of EtOH exposure (Hoshiko et al., 2012; Schafer et al., 2012).

While microglia dynamics, morphology, and interactions were minimally affected by developmental ethanol exposure, throughout this study, we found layer specific differences in microglia. The cerebellum's cytoarchitecture may underlie these layer specific differences. We examined the ML, which houses the dendrites of the Purkinje cells, and the PCL, which houses their somas. At the time of our imaging sessions, the PCL is a monolayer while the ML is densely packed with the Purkinje cells' unique, elaborate dendrite arbor. We found that microglial dynamics were generally increased in the PCL compared to the ML in both saline and EtOH dosed animals, consistent with previous findings (Stowell et al., 2018). Increased coverage of microglia, measured through surveillance, in the PCL may result from the fact that the PCL houses mainly Purkinje cell and

Bergmann glia somas, while the ML is filled with Purkinje cell dendrites, Bergmann glia fibers, parallel fibers of granule cells, basket and stellate cells. There may be more physical space for microglia to occupy in the PCL, which could provide more room for movement. The differences in number and type of cellular components between layers may also underlie the potential effects we observed for microglia-Purkinje cell interactions. Trends toward significant differences in microglia-Purkinje cell interactions were found between treatment and sex in the ML, but not the PCL. As the ML contains the Purkinje cell dendrites where most synapses occur, microglia may be interacting with synapses and potentially increasing pruning in EtOH dosed animals. This is consistent with the potential of increased interactions occurring in EtOH dosed animals compared to saline dosed animals in the ML, but not the PCL. It would be interesting to explore this further with future higher-resolution analysis to determine if these changes are occurring at synapses.

In addition to layer specific differences, we wanted to examine if any sex differences were observed. Current studies have not described many sex differences in the normally developing cerebellum. In one study, calbindin, a marker for Purkinje cells, was found to have higher levels of mRNA and protein in female mice than male mice around the third postnatal week (Abel et al., 2011). While we found no differences in pixel number of Purkinje cells' dendrites or somas in either the ML or PCL, differences in calbindin expression may not result from alterations in the number or complexity of Purkinje cells. While our measures of Purkinje cells were unchanged, we also examined microglia as sex differences in microglia density, morphology, and migration have been reported (Han et al., 2021). Indeed for morphology, sex differences were found in the PCL, but not in the ML, in saline but not the EtOH dosed animals, with male mice having more ramified microglia than female mice. In the ML, saline dosed male mice trended toward more microglia process interactions with Purkinje cell branch points than saline dosed female mice, which may reflect sex-differences in microglia–neuron interactions in the cerebellum. Despite this, effects of developmental EtOH on these interactions were driven by female mice. In the ML, increases in EtOH interactions between whole microglia and whole Purkinje cells, as well as Purkinje cell non-branch areas of dendrites with either microglia processes and somas, appeared to be driven by females. When microglia subcellular components were examined, microglia soma only pixel numbers in the ML were significantly increased in EtOH females compared to saline females. The lack of differences in males is interesting, as males are known to be at a higher risk for some neurodevelopmental disorders, such as Autism Spectrum Disorder (Roux et al., 2019). FASD diagnosis varies with age and sex, with higher FASD prevalence in males than females at young ages, but unaltered diagnosis rates in older ages (Terasaki et al., 2016). If this is due to deficits appearing later in life in females, this would be consistent with our results as we examined the effects of EtOH in adolescence.

While we found minimal effects of developmental ethanol exposure on cerebellar microglia and Purkinje cells, other avenues can be explored as well, such as molecular changes. Brain region-specific differences may be observed from similar levels of EtOH exposure, so examining other regions using the same dosage and administration method may show differential effects of ethanol on microglia–neuron interactions. We quantified one type of glia–neuron interaction, but it would be interesting to explore the *in vivo* effects of ethanol on Bergmann glia and their interactions with microglia or Purkinje cells. Microglia and astrocytes both release factors and influence neuronal development and circuitry (Stogsdill and Eroglu, 2017). In the cortex and hippocampus, microglia and astrocyte contacts have been characterized after developmental ethanol exposure (Lowery et al., 2021). Bergmann glia development also occurs during the early postnatal period and these cells sheath and regulate Purkinje cell synapses (Yamada et al., 2000; Lippman Bell et al., 2010). Reduced numbers of Bergmann glia and contacts between their fibers and Purkinje cell dendrites in the ML have been reported after ethanol (Shetty and Phillips, 1992; Shetty et al., 1994; González-Burgos and Alejandre-Gómez, 2005; Yang et al., 2014). If Bergmann glia development and regulation of synapses is affected by developmental ethanol exposure, altered excitability may occur in the cerebellum, leading to some of the cognitive and behavioral deficits found in FASD.

Overall, this work suggests that developmental EtOH exposure has minimal effects on microglia dynamics, morphology, or cell–cell physical interactions with Purkinje cells in adolescence. While the effect was not significant, we describe subtle differences in microglia-Purkinje cell interactions which may have an effect on synapses and the cerebellar circuit in adulthood contributing to EtOH-induced dysfunction. Additionally, our work suggests layer and sex specific differences which should be taken into account when studying the function and dysfunction of the cerebellum.

Data availability statement

The raw data supporting the conclusions of this article will be made available by the authors, without undue reservation.

Ethics statement

The animal study was reviewed and approved by University of Rochester Committee on Animal Resources.

Author contributions

MC, PD, and AM conceived the project and designed the experiments. MC and JD contributed to data collection. MC performed the experiments, imaging, and analysis for all figures. JD assisted with BEC analysis for Figure 1. LL developed some of the protocols and codes used in Figures 2–6. EV and MM assisted with the analysis and also helped interpret data presented in Figure 4. MC and AM wrote the first draft of the manuscript. All authors contributed to the final manuscript. All authors contributed to the article and approved the submitted version.

Funding

This study was supported by the NIH Fellowship F31AA030445 (MC), Grant from the NIAAA: RO1 AA027111 (AM and PD), T32

Training Grant T32NS115705 (MC), and University of Rochester Intellectual and Developmental Disabilities Research Center (UR-IDDRC HD103536).

Acknowledgments

Figures created with BioRender.com.

Conflict of interest

The authors declare that the research was conducted in the absence of any commercial or financial relationships that could be construed as a potential conflict of interest.

Publisher's note

All claims expressed in this article are solely those of the authors and do not necessarily represent those of their affiliated organizations, or those of the publisher, the editors and the reviewers. Any product that may be evaluated in this article, or claim that may be made by its manufacturer, is not guaranteed or endorsed by the publisher.

Supplementary material

The Supplementary material for this article can be found online at: https://www.frontiersin.org/articles/10.3389/fnins.2023.1176581/full#supplementary-material

References

Abel, J. M., Witt, D. M., and Rissman, E. F. (2011). Sex differences in the cerebellum and frontal cortex: roles of estrogen receptor alpha and sex chromosome genes. *Neuroendocrinology* 93, 230–240. doi: 10.1159/000324402

Ahlers, K. E., Karaçay, B., Fuller, L., Bonthius, D. J., and Dailey, M. E. (2015). Transient activation of microglia following acute alcohol exposure in developing mouse neocortex is primarily driven by BAX-dependent neurodegeneration. *Glia* 63, 1694–1713. doi: 10.1002/glia.22835

Altman, J., and Bayer, S. A. (1978). Prenatal development of the cerebellar system in the rat. I. Cytogenesis and histogenesis of the deep nuclei and the cortex of the cerebellum. *J. Comp. Neurol.* 179, 23–48. doi: 10.1002/cne.901790104

Ayata, P., Badimon, A., Strasburger, H. J., Duff, M. K., Montgomery, S. E., Loh, Y. E., et al. (2018). Epigenetic regulation of brain region-specific microglia clearance activity. *Nat. Neurosci.* 21, 1049–1060. doi: 10.1038/s41593-018-0192-3

Bayer, S. A., Altman, J., Russo, R. J., and Zhang, X. (1993). Timetables of neurogenesis in the human brain based on experimentally determined patterns in the rat. *Neurotoxicology* 14, 83–144.

Berg, S., Kutra, D., Kroeger, T., Straehle, C. N., Kausler, B. X., Haubold, C., et al. (2019). Ilastik: interactive machine learning for (bio)image analysis. *Nat. Methods* 16, 1226–1232. doi: 10.1038/s41592-019-0582-9

Berry, M., and Bradley, P. (1976). The growth of the dendritic trees of Purkinje cells in the cerebellum of the rat. *Brain Res.* 112, 1–35. doi: 10.1016/0006-8993(76)90331-0

Cederbaum, A. I. (2012). Alcohol metabolism. *Clin. Liver Dis.* 16, 667–685. doi: 10.1016/j.cld.2012.08.002

Cserép, C., Pósfai, B., and Dénes, Á. (2021). Shaping neuronal fate: functional heterogeneity of direct microglia-neuron interactions. *Neuron* 109, 222–240. doi: 10.1016/j.neuron.2020.11.007

Dean, S. L., Wright, C. L., Hoffman, J. F., Wang, M., Alger, B. E., and McCarthy, M. M. (2012). Prostaglandin E2 stimulates estradiol synthesis in the cerebellum postnatally with associated effects on Purkinje neuron dendritic arbor and electrophysiological properties. *Endocrinology* 153, 5415–5427. doi: 10.1210/en.2012-1350

Dobbing, J., and Sands, J. (1979). Comparative aspects of the brain growth spurt. *Early Hum. Dev.* 3, 79–83. doi: 10.1016/0378-3782(79)90022-7

Drew, P. D., Johnson, J. W., Douglas, J. C., Phelan, K. D., and Kane, C. J. (2015). Pioglitazone blocks ethanol induction of microglial activation and immune responses in the hippocampus, cerebellum, and cerebral cortex in a mouse model of fetal alcohol spectrum disorders. *Alcohol. Clin. Exp. Res.* 39, 445–454. doi: 10.1111/acer.12639

Gohlke, J. M., Griffith, W. C., and Faustman, E. M. (2008). Computational models of ethanol-induced neurodevelopmental toxicity across species: implications for risk assessment. *Birth Defects Res. B Dev. Reprod. Toxicol.* 83, 1–11. doi: 10.1002/bdrb.20137

González-Burgos, I., and Alejandre-Gómez, M. (2005). Cerebellar granule cell and Bergmann glial cell maturation in the rat is disrupted by pre- and post-natal exposure to moderate levels of ethanol. *Int. J. Dev. Neurosci.* 23, 383–388. doi: 10.1016/j.ijdevneu.2004.11.002

Goodlett, C., and Eilers, A. (1997). Alcohol-induced Purkinje cell loss with a single binge exposure in neonatal rats: a stereological study of temporal windows of vulnerability. *Alcohol. Clin. Exp. Res.* 21, 738–744. doi: 10.1111/j.1530-0277.1997.tb03831.x

Goodlett, C. R., Marcussen, B. L., and West, J. R. (1990). A single day of alcohol exposure during the brain growth spurt induces brain weight restriction and cerebellar Purkinje cell loss. *Alcohol (Fayetteville, NY)* 7, 107–114. doi: 10.1016/0741-8329(90)90070-s

Grabert, K., Michoel, T., Karavolos, M. H., Clohisey, S., Baillie, J. K., Stevens, M. P., et al. (2016). Microglial brain region-dependent diversity and selective regional sensitivities to aging. *Nat. Neurosci.* 19, 504–516. doi: 10.1038/nn.4222

Hamre, K., and West, J. (1993). The effects of the timing of ethanol exposure during the brain growth spurt on the number of cerebellar Purkinje and granule cell nuclear profiles. *Alcohol. Clin. Exp. Res.* 17, 610–622. doi: 10.1111/j.1530-0277.1993.tb00808.x

Han, J., Fan, Y., Zhou, K., Blomgren, K., and Harris, R. A. (2021). Uncovering sex differences of rodent microglia. *J. Neuroinflammation* 18:74. doi: 10.1186/s12974-021-02124-z

Hoshiko, M., Arnoux, I., Avignone, E., Yamamoto, N., and Audinat, E. (2012). Deficiency of the microglial receptor CX3CR1 impairs postnatal functional development of thalamocortical synapses in the barrel cortex. *J. Neurosci.* 32, 15106–15111. doi: 10.1523/JNEUROSCI.1167-12.2012

Idrus, N., and Napper, R. (2012). Acute and long-term Purkinje cell loss following a single ethanol binge during the early third trimester equivalent in the rat. *Alcohol. Clin. Exp. Res.* 36, 1365–1373. doi: 10.1111/j.1530-0277.2012.01743.x

Jung, S., Aliberti, J., Graemmel, P., Sunshine, M. J., Kreutzberg, G. W., Sher, A., et al. (2000). Analysis of fractalkine receptor CX3CR1 function by targeted deletion and green fluorescent protein reporter gene insertion. *Mol. Cell. Biol.* 20, 4106–4114. doi: 10.1128/mcb.20.11.4106-4114.2000

Kana, V., Desland, F. A., Casanova-Acebes, M., Ayata, P., Badimon, A., Nabel, E., et al. (2019). CSF-1 controls cerebellar microglia and is required for motor function and social interaction. *J. Exp. Med.* 216, 2265–2281. doi: 10.1084/jem.20182037

Kane, C. J. M., Douglas, J. C., Rafferty, T., Johnson, J. W., Niedzwiedz-Massey, V. M., Phelan, K. D., et al. (2021). Ethanol modulation of cerebellar neuroinflammation in a postnatal mouse model of fetal alcohol spectrum disorders. *J. Neurosci. Res.* 99, 1986–2007. doi: 10.1002/jnr.24797

Kane, C. J., Phelan, K. D., Han, L., Smith, R. R., Xie, J., Douglas, J. C., et al. (2011). Protection of neurons and microglia against ethanol in a mouse model of fetal alcohol spectrum disorders by peroxisome proliferator-activated receptor-γ agonists. *Brain Behav. Immun.* 25, S137–S145. doi: 10.1016/j.bbi.2011.02.016

Komada, M., and Nishimura, Y. (2022). Epigenetics and Neuroinflammation associated with neurodevelopmental disorders: a microglial perspective. *Front. Cell Develop. Biol.* 10:852752. doi: 10.3389/fcell.2022.852752

Lippman Bell, J. J., Lordkipanidze, T., Cobb, N., and Dunaevsky, A. (2010). Bergmann glial ensheathment of dendritic spines regulates synapse number without affecting spine motility. *Neuron Glia Biol.* 6, 193–200. doi: 10.1017/S1740925X10000165

Lowery, R., Cealie, M., Lamantia, C., Mendes, M., Drew, P., and Majewska, A. (2021). Microglia and astrocytes show limited, acute alterations in morphology and protein expression following a single developmental alcohol exposure. *J. Neurosci. Res.* 99, 2008–2025. doi: 10.1002/jnr.24808

Marin-Teva, J., Dusart, I., Colin, C., Gervais, A., Van Rooijen, N., and Mallat, M. (2004). Microglia promote the death of developing Purkinje cells. *Neuron* 41, 535–547. doi: 10.1016/s0896-6273(04)00069-8

May, P. A., Baete, A., Russo, J., Elliott, A. J., Blankenship, J., Kalberg, W. O., et al. (2014). Prevalence and characteristics of fetal alcohol spectrum disorders. *Pediatrics* 134, 855–866. doi: 10.1542/peds.2013-3319

Nakayama, H., Abe, M., Morimoto, C., Iida, T., Okabe, S., Sakimura, K., et al. (2018). Microglia permit climbing fiber elimination by promoting GABAergic inhibition in the developing cerebellum. *Nat. Commun.* 9:2830. doi: 10.1038/s41467-018-05100-z

Napper, R., and West, J. (1995). Permanent neuronal cell loss in the cerebellum of rats exposed to continuous low blood alcohol levels during the brain growth spurt: a stereological investigation. *J. Comp. Neurol.* 362, 283–292. doi: 10.1002/cne.903620210

Paolicelli, R. C., Sierra, A., Stevens, B., Tremblay, M. E., Aguzzi, A., Ajami, B., et al. (2022). Microglia states and nomenclature: a field at its crossroads. *Neuron* 110, 3458–3483. doi: 10.1016/j.neuron.2022.10.020

Perez-Pouchoulen, M., Yu, S. J., Roby, C. R., Bonsavage, N., and McCarthy, M. M. (2019). Regulatory control of microglial phagocytosis by estradiol and prostaglandin E2 in the developing rat cerebellum. *Cerebellum (London, England)* 18, 882–895. doi: 10.1007/s12311-019-01071-z

Rahimi-Balaei, M., Bergen, H., Kong, J., and Marzban, H. (2018). Neuronal migration during development of the cerebellum. *Front. Cell. Neurosci.* 12:484. doi: 10.3389/fncel.2018.00484

Roux, S., Bailly, Y., and Bossu, J. L. (2019). Regional and sex-dependent alterations in Purkinje cell density in the valproate mouse model of autism. *Neuroreport* 30, 82–88. doi: 10.1097/WNR.0000000000001164

Safe, B., Joosten, A., Bower, C., Condon, C., Watkins, R., Mutch, R., et al. (2018). A comparison of the motor skills of young people in a youth detention centre with diagnosed fetal alcohol spectrum disorder, prenatal alcohol exposure, and a reference population. *J. Fetal Alcohol Spectr. Disord.* 1, e17–e32. doi: 10.22374/jfasrp.v1i1.5

Saito, M., Chakraborty, G., Hui, M., Masiello, K., and Saito, M. (2016). Ethanol-induced neurodegeneration and glial activation in the developing brain. *Brain Sci.* 6:31. doi: 10.3390/brainsci6030031

Schafer, D. P., Lehrman, E. K., Kautzman, A. G., Koyama, R., Mardinly, A. R., Yamasaki, R., et al. (2012). Microglia sculpt postnatal neural circuits in an activity and complement-dependent manner. *Neuron* 74, 691–705. doi: 10.1016/j.neuron.2012.03.026

Servais, L., Hourez, R., Bearzatto, B., Gall, D., Schiffmann, S. N., and Cheron, G. (2007). Purkinje cell dysfunction and alteration of long-term synaptic plasticity in fetal alcohol syndrome. *Proc. Natl. Acad. Sci. U. S. A.* 104, 9858–9863. doi: 10.1073/pnas.0607037104

Shetty, A., Burrows, R., Wall, K., and Phillips, D. (1994). Combined pre- and postnatal ethanol exposure alters the development of Bergmann glia in rat cerebellum. *Int. J. Dev. Neurosci.* 12, 641–649. doi: 10.1016/0736-5748(94)90016-7

Shetty, A., and Phillips, D. (1992). Effects of prenatal ethanol exposure on the development of Bergmann glia and astrocytes in the rat cerebellum: an immunohistochemical study. *J. Comp. Neurol.* 321, 19–32. doi: 10.1002/cne.903210103

Sipe, G. O., Lowery, R. L., Tremblay, M. È., Kelly, E. A., Lamantia, C. E., and Majewska, A. K. (2016). Microglial P2Y12 is necessary for synaptic plasticity in mouse visual cortex. *Nat. Commun.* 7:10905. doi: 10.1038/ncomms10905

Stagni, F., Giacomini, A., Guidi, S., Ciani, E., and Bartesaghi, R. (2015). Timing of therapies for down syndrome: the sooner, the better. *Front. Behav. Neurosci.* 9:265. doi: 10.3389/fnbeh.2015.00265

Stoessel, M. B., and Majewska, A. K. (2021). Little cells of the little brain: microglia in cerebellar development and function. *Trends Neurosci.* 44, 564–578. doi: 10.1016/j.tins.2021.04.001

Stogsdill, J. A., and Eroglu, C. (2017). The interplay between neurons and glia in synapse development and plasticity. *Curr. Opin. Neurobiol.* 42, 1–8. doi: 10.1016/j.conb.2016.09.016

Stowell, R., and Majewska, A. (2020). Acute ethanol exposure rapidly alters cerebellar and cortical microglial physiology. *Eur. J. Neurosci.* 54, 5834–5843. doi: 10.1111/ejn.14706

Stowell, R. D., Sipe, G. O., Dawes, R. P., Batchelor, H. N., Lordy, K. A., Whitelaw, B. S., et al. (2019). Noradrenergic signaling in the wakeful state inhibits microglial surveillance and synaptic plasticity in the mouse visual cortex. *Nat. Neurosci.* 22, 1782–1792. doi: 10.1038/s41593-019-0514-0

Stowell, R. D., Wong, E. L., Batchelor, H. N., Mendes, M. S., Lamantia, C. E., Whitelaw, B. S., et al. (2018). Cerebellar microglia are dynamically unique and survey Purkinje neurons in vivo. *Dev. Neurobiol.* 78, 627–644. doi: 10.1002/dneu.22572

Sullivan, E. V., Moore, E. M., Lane, B., Pohl, K. M., Riley, E. P., and Pfefferbaum, A. (2020). Graded cerebellar lobular volume deficits in adolescents and young adults with fetal alcohol spectrum disorders (FASD). *Cerebral Cortex* 30, 4729–4746. doi: 10.1093/cercor/bhaa020

Terasaki, LS, Gomez, J, and Schwarz, JM. (2016). An examination of sex differences in the effects of early-life opiate and alcohol exposure. *Philos. Trans. R. Soc. Lond. Ser. B Biol. Sci.* 371:20150123. doi: 10.1098/rstb.2015.0123

Topper, L. A., Baculis, B. C., and Valenzuela, C. F. (2015). Exposure of neonatal rats to alcohol has differential effects on neuroinflammation and neuronal survival in the cerebellum and hippocampus. *J. Neuroinflammation* 12:160. doi: 10.1186/s12974-015-0382-9

Tremblay, M. È., Lowery, R. L., and Majewska, A. K. (2010). Microglial interactions with synapses are modulated by visual experience. *PLoS Biol.* 8:e1000527. doi: 10.1371/journal.pbio.1000527

Tremblay, M. È., Stevens, B., Sierra, A., Wake, H., Bessis, A., and Nimmerjahn, A. (2011). The role of microglia in the healthy brain. *J. Neurosci.* 31, 16064–16069. doi: 10.1523/JNEUROSCI.4158-11.2011

Vonkaenel, E., Feidler, A., Lowery, R., Andersh, K., Love, T., Majewska, A., et al. (2023). A model-based hierarchical Bayesian approach to Sholl analysis. *bioRxiv*. doi: 10.1101/2023.01.23.525256

Wake, H., Moorhouse, A. J., Jinno, S., Kohsaka, S., and Nabekura, J. (2009). Resting microglia directly monitor the functional state of synapses in vivo and determine the fate of ischemic terminals. *J. Neurosci.* 29, 3974–3980. doi: 10.1523/JNEUROSCI.4363-08.2009

Whitelaw, B. S., Matei, E. K., and Majewska, A. K. (2020). Phosphoinositide-3-kinase γ is not a predominant regulator of ATP-dependent directed microglial process motility or experience-dependent ocular dominance plasticity. *eNeuro* 7:ENEURO.0311-20.2020. doi: 10.1523/ENEURO.0311-20.2020

Whitelaw, B. S., Stoessel, M. B., and Majewska, A. K. (2022). Movers and shakers: microglial dynamics and modulation of neural networks. *Glia*. doi: 10.1002/glia.24323. [E-pub ahead of print].

Wilhelm, C. J., and Guizzetti, M. (2015). Fetal alcohol spectrum disorders: an overview from the glia perspective. *Front. Integr. Neurosci.* 9:65. doi: 10.3389/fnint.2015.00065

Williams, J. F., and Smith, V. C.Committee on Substance Abuse (2015). Fetal alcohol Spectrum disorders. *Pediatrics* 136, e1395–e1406. doi: 10.1542/peds.2015-3113

Wong, E. L., Lutz, N. M., Hogan, V. A., Lamantia, C. E., McMurray, H. R., Myers, J. R., et al. (2018). Developmental alcohol exposure impairs synaptic plasticity without overtly altering microglial function in mouse visual cortex. *Brain Behav. Immun.* 67, 257–278. doi: 10.1016/j.bbi.2017.09.003

Wong, E. L., Stowell, R. D., and Majewska, A. K. (2017). What the Spectrum of Microglial Functions Can Teach us About Fetal Alcohol Spectrum Disorder. *Front. Synaptic Neurosci.* 9:11. doi: 10.3389/fnsyn.2017.00011

Wong, E. L., Strohm, A., Atlas, J., Lamantia, C., and Majewska, A. K. (2021). Dynamics of microglia and dendritic spines in early adolescent cortex after developmental alcohol exposure. *Dev. Neurobiol.* 81, 786–804. doi: 10.1002/dneu.22843

Yamada, K., Fukaya, M., Shibata, T., Kurihara, H., Tanaka, K., Inoue, Y., et al. (2000). Dynamic transformation of Bergmann glial fibers proceeds in correlation with dendritic outgrowth and synapse formation of cerebellar Purkinje cells. *J. Comp. Neurol.* 418, 106–120. doi: 10.1002/(sici)1096-9861(20000228)418:1<106::aid-cne8>3.0.co;2-nnak

Yamamoto, M., Kim, M., Imai, H., Itakura, Y., and Ohtsuki, G. (2019). Microglia-triggered plasticity of intrinsic excitability modulates psychomotor behaviors in acute cerebellar inflammation. *Cell Rep.* 28, 2923–2938.e8. doi: 10.1016/j.celrep.2019.07.078

Yang, Y., Tang, Y., Xing, Y., Zhao, M., Bao, X., Sun, D., et al. (2014). Activation of liver X receptor is protective against ethanol-induced developmental impairment of Bergmann glia and Purkinje neurons in the mouse cerebellum. *Mol. Neurobiol.* 49, 176–186. doi: 10.1007/s12035-013-8510-y

Zamudio-Bulcock, P. A., Morton, R. A., and Valenzuela, C. F. (2014). Third trimester-equivalent ethanol exposure does not alter complex spikes and climbing fiber long-term depression in cerebellar Purkinje neurons from juvenile rats. *Alcohol. Clin. Exp. Res.* 38, 1293–1300. doi: 10.1111/acer.12362

Zhang, L., and Goldman, J. (1996). Generation of cerebellar interneurons from dividing progenitors in white matter. *Neuron* 16, 47–54. doi: 10.1016/s0896-6273(00)80022-7

Zhang, Y., Niu, B., Yu, D., Cheng, X., Liu, B., and Deng, J. (2010). Radial glial cells and the lamination of the cerebellar cortex. *Brain Struct. Funct.* 215, 115–122. doi: 10.1007/s00429-010-0278-5

frontiers | Frontiers in Neuroscience

TYPE Original Research
PUBLISHED 16 May 2023
DOI 10.3389/fnins.2023.1160185

Check for updates

OPEN ACCESS

EDITED BY
Hermes H. Yeh,
Dartmouth College, United States

REVIEWED BY
Balapal Basavarajappa,
New York University, United States
Kristen Breit,
West Chester University, United States

*CORRESPONDENCE
Sebastiano Bariselli
✉ sebastiano.bariselli@nih.gov

RECEIVED 06 February 2023
ACCEPTED 26 April 2023
PUBLISHED 16 May 2023

CITATION
Bariselli S, Reuveni N, Westcott N, Mateo Y and Lovinger DM (2023) Postnatal ethanol exposure impairs social behavior and operant extinction in the adult female mouse offspring.
Front. Neurosci. 17:1160185.
doi: 10.3389/fnins.2023.1160185

COPYRIGHT
© 2023 Bariselli, Reuveni, Westcott, Mateo and Lovinger. This is an open-access article distributed under the terms of the Creative Commons Attribution License (CC BY). The use, distribution or reproduction in other forums is permitted, provided the original author(s) and the copyright owner(s) are credited and that the original publication in this journal is cited, in accordance with accepted academic practice. No use, distribution or reproduction is permitted which does not comply with these terms.

Postnatal ethanol exposure impairs social behavior and operant extinction in the adult female mouse offspring

Sebastiano Bariselli*, Noa Reuveni, Nina Westcott, Yolanda Mateo and David M. Lovinger

Laboratory for Integrative Neuroscience (LIN), National Institute on Alcohol Abuse and Alcoholism, Bethesda, MD, United States

Fetal Alcohol Spectrum Disorder (FASD) comprises a group of neurodevelopmental deficits caused by alcohol exposure during pregnancy. Clinical studies suggest that while the male progeny experiences serious neurodevelopmental defects, female patients have more severe cognitive, social, and affective symptoms. Other than sex, dose, frequency, and timing of exposure determine the neurobehavioral outcomes in young and adult progeny. In this regard, human studies indicate that some individuals relapse during late-term gestational periods. In mice, this interval corresponds to the first 10 days after birth (postnatal, P0-P10). In our model of postnatal ethanol exposure (PEE$^{P0\text{-}P10}$), we tested whether adult female and male offspring show deficits in sociability, anxiety-like, reward consumption, and action-outcome associations. We report that female PEE$^{P0\text{-}P10}$ offspring have mild social impairments and altered extinction of operant responding in the absence of anxiety-like traits and reward consumption defects. None of these deficits were detected in the male PEE$^{P0\text{-}P10}$ offspring. Our data provide novel information on sex-specific neurobehavioral outcomes of postnatal ethanol exposure in female adult offspring.

KEYWORDS

late-term gestational ethanol exposure, social behavior, anhedonia, extinction, anxiety-like behaviors

Introduction

Fetal Alcohol Spectrum Disorder (FASD) is a class of heterogeneous neurobehavioral deficits caused by alcohol exposure during pregnancy, with current estimates indicating a prevalence of 71.4 out of 1,000 children (May et al., 2021; Glass et al., 2023) and high socio-economic costs (Ericson et al., 2017; Greenmyer et al., 2018). FASD clinical symptoms are heterogenous and include anatomical, motor, cognitive, and socioemotional abnormalities (Mattson et al., 2011, 2019; Riley et al., 2011; Hoyme et al., 2016). Although many clinical studies indicate that prenatal exposure to drugs, including alcohol, primarily affects male individuals (Traccis et al., 2020), the prevalence of FASD among sexes shows great variability across different patient cohorts. While some authors report a higher incidence of FASD among male individuals (May et al., 2000; Burd et al., 2003), others find a similar prevalence between sexes (Palmeter et al., 2021) or an even higher incidence of FASD diagnosis in the female subpopulation (Autti-Rämö et al., 2006). Moreover, male subjects have reduced survivability and heightened neurodevelopmental impairments when exposed to prenatal binge-like alcohol levels compared

to females (May et al., 2017; Flannigan et al., 2023). On the other hand, female FASD individuals display more severe cognitive, social, and affective symptoms (May et al., 2017; Flannigan et al., 2023). However, considering that most preclinical studies focused on the effects of fetal alcohol exposure on male progeny (Terasaki et al., 2016), whether female subjects show cognitive and socioemotional defects remains a fundamental research question. The answer will improve our understanding of whether biological sex interacts with alcohol to determine FASD severity and might ultimately help develop and tailor therapeutic strategies to specific subgroups of FASD individuals.

Besides the sex of the progeny, the dose and the frequency of maternal alcohol use influence the neurobehavioral outcomes of fetal alcohol exposure (Maier and West, 2001; May et al., 2014). Frequent maternal ingestion of large quantities of alcohol has been associated with higher severity of FASD symptoms (Maier and West, 2001; May and Gossage, 2011). For example, gestational binge-like levels of alcohol have been linked to more pronounced anatomical dysmorphology (Patra et al., 2011). During pregnancy, the fetus goes through various stages of organ formation and development; thus, the timing of alcohol exposure also largely influences the outcomes of FASD (May and Gossage, 2011). Considering that the human brain develops during pregnancy, the heterogeneity of FASD neurobehavioral symptoms might depend, at least partly, on the timing of alcohol exposure and the resulting developmental deficits in discrete brain regions (Guerri et al., 2009; Bariselli and Lovinger, 2021). Animal models of fetal alcohol exposure consider that the first ten embryonic days (E0-E10) corresponds to the first trimester of pregnancy, the second half of rodent pregnancy (E11-E20) to the second trimester, and the first 10–14 postnatal days (P0-P10/P14) to late-term gestational periods (Marquardt and Brigman, 2016). This reflects a different timing of neurodevelopmental milestones between rodents and humans. Events such as blood–brain barrier formation and increased axonal and dendritic density primarily occur within the uterus in humans and during early postnatal periods in rodents (Semple et al., 2013). Clinical evidence indicates that most women stop alcohol use once the pregnancy is ascertained, while 27% report alcohol use episodes throughout pregnancy (Muggli et al., 2016). In other studies, 40% of pregnant women reported alcohol drinking during the last trimester of gestation (Little et al., 1990), while about 30–50% of those who remained abstinent during pregnancy relapsed during the three-month post-parturition period (Jagodzinski and Fleming, 2007; Forray et al., 2015). These clinical data highlight the importance of investigating the behavioral outcomes of alcohol exposure during late-term gestational periods in adult progeny.

Individuals diagnosed with FASD (Kully-Martens et al., 2012) and animal models of fetal alcohol exposure display social deficits across their lifespan; prenatal and post-natal alcohol exposure impairs mother-pup interactions (Barron et al., 1991; Subramanian, 1992) and play behavior during adolescence in both sexes (Meyer and Riley, 1986). During adulthood, models of prenatal alcohol exposure display altered sexual maturation in male and female offspring (Creighton-Taylor and Rudeen, 1991; Mcgivern et al., 1992), with sexually dimorphic alterations in direct social interaction in the adult progeny (Kelly et al., 1994). Postnatal ethanol exposure (PEE) produces social interaction deficits in adolescent and adult male rats (Boschen et al., 2014) and social recognition deficits in adult male mice during dyadic conspecific interaction tests (Subbanna et al., 2018; Joshi et al., 2019; Shivakumar et al., 2021). In addition to dyadic social interaction, the social preference assay is widely used to characterize sociability and social preference in mouse models of neurodevelopmental disorders (Yang et al., 2011; Rein et al., 2020). However, whether male and female PEE mice display social preference and social approach deficits remains an open question.

In addition to social deficits, FASD is often associated with the appearance of psychiatric conditions, including anxiety and depression (Famy et al., 1998; Barr, 2006; Pei et al., 2011). Animal models of prenatal ethanol exposure show anxiety-like behavior in male and female progeny during elevated-plus or O-maze testing (Dursun et al., 2006; Cullen et al., 2013; Oubraim et al., 2022), with some experiments reporting anxiety-like traits in males only (Rouzer et al., 2017). PEE does not affect elevated plus-maze exploration (Gibula-Tarlowska et al., 2021) but impairs passive avoidance in adult male rats (Lopatynska-Mazurek et al., 2021b). Additionally, female PEE rats displayed a reduced time spent in the center of an open field compared to controls (Bianco et al., 2021). Prenatal ethanol exposure offspring also leads to heightened learned helplessness in the shuttle-box test and increased immobility time in the forced-swim task (Caldwell et al., 2008), originally developed to assess anti-depressive actions of pharmacological interventions (Porsolt et al., 1978). These deficits are associated with heightened sucrose responsivity in male mice (Hellemans et al., 2010) measured in the two-bottle choice test. Other studies found no difference (Sanchez Vega et al., 2013; Yu et al., 2020). Whether PEE induces anxiety-like and depressive-like states in the female and male adult mouse offspring remains under-investigated.

Laboratory animals used as models of FASD display deficits in associative learning and executive function (reviewed in Bariselli and Lovinger, 2021) throughout their lifespan. Prenatal exposure and PEE affect the acquisition and reversal of contextual associations during the T-, Y-Maze, Barnes Maze and Morris Water Maze tasks in male and female adolescent rats (O'Leary-Moore et al., 2006; Allan et al., 2014; Gibula-Tarlowska et al., 2021; Lopatynska-Mazurek et al., 2021a; Risbud et al., 2022), and impair contextual pre-exposure facilitation of fear learning (Heroux et al., 2019). During adulthood, PEE alters spatial associative learning in male and female mice (Subbanna et al., 2018; Joshi et al., 2019; Shivakumar et al., 2021). Instrumental learning tasks also revealed that prenatal exposure and PEE increase lever pressing under specific training schedules and interferes with habitual responding in the adult offspring (Cuzon Carlson et al., 2020). Changes in action strategy lead to behavioral maladaptations upon changes in cue-reward contingencies in both prenatally exposed and PEE male and female offspring (Marquardt et al., 2014; Gursky et al., 2021) and alter cue-mediated reinstatement in the progeny of both sexes (Olguin et al., 2019). However, whether PEE impairs the extinction of action-outcome associations in the adult offspring remains an open question.

Considering the impact of timing and sex in determining the neurobehavioral outcomes of fetal alcohol exposure, we aimed to characterize the neurobehavioral outcomes of binge-like PEE on the socio-emotional and cognitive behavioral domains during adulthood. In adult female offspring, we demonstrate that alcohol exposure during the equivalent of the third trimester induces mild impairments in social and cognitive function without causing major anxiety-like or reward-processing defects. These data help characterize the influence of the timing of developmental ethanol exposure on specific behavioral symptoms in a sex-specific subgroup of PEE subjects.

Methods

Experimental subjects

Pregnant C57Bl6/J WT female mice were purchased at embryonic day 7 (E7) from the Jackson Laboratory. The animals were acclimated to the procedure room for 3–4 days before pup delivery. Their progeny underwent air ($CE^{P0\text{-}P10}$) or postnatal ethanol exposure ($PEE^{P0\text{-}P10}$) between P0-P10 and were weaned at P21. The behavioral experiments described in this work were conducted on the adult male and female progeny of five PEE cohorts and their CE controls; cohorts #1 and #2 were used for operant training, while cohorts #3, #4, #5 were used for social preference, O-Maze, and sucrose preference assays. Animals were maintained on a 12-h dark/12-h light cycle for the whole duration of the experiments. Mice were treated in accordance with the *NIH Guide for the Care and Use of Laboratory Animals*. The data were collected through experimental procedures approved in the LIN-DL-1 protocol for animal authorization by the Animal Care and Use Committee of the NIAAA Division of Intramural Clinical and Biological Research.

Postnatal ethanol exposure protocol

At P0, the home cages with dams and pups were placed in air-tight plexiglass chambers. 190-proof EtOH was vaporized at a rate of 8–9 liter of air/min and adjusted to reach a concentration between 0.1–0.15 mg/dL of EtOH in the air. Pups and dams were exposed to EtOH (PEE) or air (CE) in a 16-h-ON/ 8-h-OFF cycle for 10 days, with a 3-day break. Ethanol and air exposures started between 5–6 p.m. and terminated at 9–10 a.m. Blood Alcohol Concentration (BAC) was measured from trunk blood collected after pup decapitation. Serum was obtained, diluted, and alcohol concentration was measured using a colorimetric assay (Pointe Alcohol Reagent Test).

Pup retrieval assay

Upon removing dams and pups from the vapor chambers, we conducted a pup retrieval assay to evaluate maternal behavior. $CE^{P0\text{-}P10}$ and $PEE^{P0\text{-}P10}$ dams were placed in a home cage-like arena with their litter and nest for at least 5 min for habituation. Afterward, we performed a pup retrieval assay by removing one pup at a time from their nest for 10 consecutive trials with no breaks in between trials. One trial began upon placing a pup on the opposite corner of the arena relative to the nest. The latency to pup retrieval was measured as the time between pup removal from the nest by the experimenter and nest placement by the dam. Each trial lasted a maximum of 120 s. This time limit was based on previous studies using pup retrieval assay (Marlin et al., 2015; Carcea et al., 2019).

Three-chamber sociability task

During adulthood (P70-P260), male and female mice from cohorts #3, #4, and #5 underwent a three-chamber assay in a black-walled plexiglass arena divided into three chambers. The social and object chambers (18 cm x 20 cm) contained an enclosure with or without a sex-matched (either male or female) younger conspecific (6–8 weeks of age). The two chambers were connected through a smaller corridor (20 cm x 10 cm). During the habituation phase, animals were placed in the arena for 10 min. During the sociability phase, animals were briefly confined in the corridor, and the object and the social stimuli (male or female) were inserted in the opposite sides of the arena. As reported in previous studies (Bariselli et al., 2016), during this phase animals were allowed to explore the arena for 10 min. Video recordings were obtained and analyzed using EthoVision software. The animal's exploratory behavior was automatically scored to avoid camera artifacts and experimenter biases. We delimited a 2–3 cm region around the enclosure (proximal zone), while the rest was considered the distal zone relative to the social stimulus. We automatically scored distance moved, time spent in either chamber and time spent in the proximal or distal zone of the social stimulus. We expressed these data as a percentage of total exploration time.

Elevated O-maze

One day after completing the three-chamber task, male and female $CE^{P0\text{-}P10}$ and $PEE^{P0\text{-}P10}$ mice (P70-P260) from cohorts #3, #4, and #5 underwent testing in the elevated O-maze. The circular maze (60 cm diameter) was elevated 50 cm from the ground, with portions enclosed by 16 cm high removable walls on either side. The O-maze area inside the walls was considered "closed," and the area with only the base and no surrounding walls was considered "open." After at least 30 min of habituation to the room, one mouse was placed inside a closed area to start and allowed to explore the arena, while recordings were performed with a camera placed above the maze using Bonzai software. Time spent in open areas and distance moved was automatically scored using Ethovision software for video recording analysis for a total of 5 min, as reported in previous studies (Braun et al., 2011). The first 30 s of each video were excluded from the analysis to avoid camera artifacts.

Sucrose preference test

In the 2 days following the completion of the O-maze, male and female $CE^{P0\text{-}P10,}$ and $PEE^{P0\text{-}P10}$ (P70-P260) mice from cohorts #3, #4, and #5 underwent a sucrose preference test in their home cage. Mice were separated and placed in cages with lids equipped to hold two sipper bottles. Both sipper tubes were filled with regular tap water for the habituation phase, and mice were allowed uninhibited drinking for 5 h. At the end of the day, sipper bottles were exchanged for one water bottle identical to the habituation bottle and one sipper bottle filled with 1% sucrose. All bottles were weighed beforehand, and cages were counterbalanced for which sipper bottle contained sucrose (left or right). Sixteen hours later, on the morning of the following day, bottles were removed and weighed. Mice received two new bottles with only tap water for 8 h. At the end of the day, the same protocol was carried out except with 8% sucrose, and the location of the sucrose bottles was switched from the previous day. The next morning, bottles were weighed, and mice were re-housed in their original groups. Our 16-h 1 and 8% sucrose preference test is based on previous reports of a duration of the test between 1 and 24-h (Bariselli et al., 2016;

Hoffman, 2016). Liquid consumption was normalized to each animal's body weight ($g_{consumed}/kg_{bodyweight}$). Preference for sucrose over the water was determined by dividing water consumed (g/kg) by sucrose consumed (g/kg).

Operant training

Male and female $CE^{P0\text{-}P10}$ and $PEE^{P0\text{-}P10}$ experimental subjects (P55-P80) from cohorts #1 and #2 were food restricted to 85–95% of their baseline body weight 3–5 days before the beginning of operant training and throughout the entire behavioral protocol. Subjects were handled for 3–5 min for 3–5 days before the start of the experiments. On day 0 (shaping), subjects were placed in the operant box (MedAssociates), and reward delivery (20% sucrose solution) occurred at random intervals every 60 s on average.

Acquisition

During the acquisition phase, from day 1 to day 4, subjects were trained to press a single lever (left or right) to obtain one reward (FR1) consisting of a drop of 20% sucrose delivered in a reward cup. Levers were counterbalanced across experimental subjects. A session ended upon delivery of 30 rewards or when 60 min elapsed (Cuzon Carlson et al., 2020). On day 5, an inactive lever (left or right, counterbalanced) was introduced. Subjects had to press the active lever at FR1 to obtain a maximum of 30 rewards or until 60 min elapsed for 3 consecutive sessions. On day 8, the reward schedule switched from FR1 to FR5 (in which five lever presses were required per reward), and operant conditioning continued for two additional days.

Reversal Learning

The day following the last FR5 session, the order of active and inactive levers was switched while maintaining the FR5 schedule of reinforcement. Reversal learning continued for five additional days.

Extinction and reinstatement of operant responding

After the last reversal learning session, subjects were tested on a Random Ratio (RR) schedule of reinforcement (Cuzon Carlson et al., 2020). Experimental subjects made an average of 10 (for 2 days), then 20 (for 2 days) active lever presses to obtain a reward, while the other lever remained inactive. The last RR20 session was followed by three extinction sessions, during which RR20 responding was never followed by reward delivery. After the last extinction session, reinstatement of responding was assessed by reintroducing sucrose delivery upon RR20 responding.

Subjects returned to their home cage upon completing each behavioral session. They were fed a grain-based rodent diet (BioServ, F0171) according to their food restriction regime.

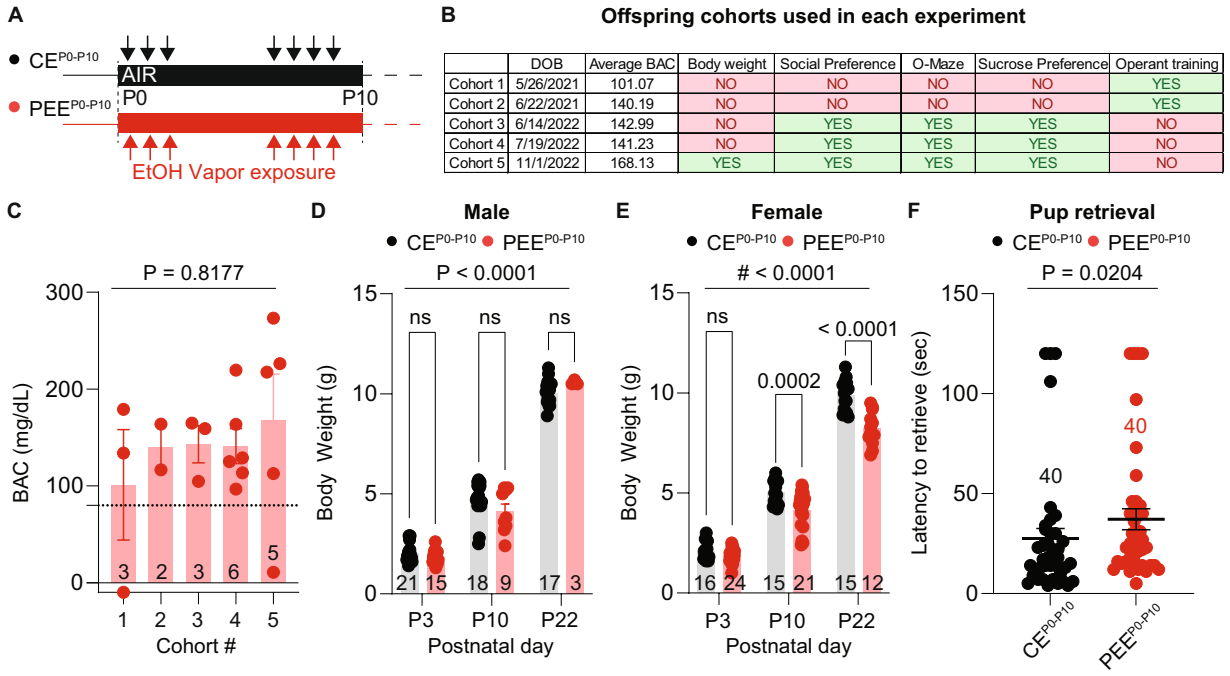
Statistical analysis

For the data reported in this work, each experimental group had a sample size similar to studies previously performed in the laboratory (Cuzon Carlson et al., 2020). Experimental subjects that spent less than 25% of their time in the social chamber (1 $CE^{P0\text{-}P10}$ female excluded) or did not acquire lever pressing behavior during operant training (2 $PEE^{P0\text{-}P10}$ females excluded, 1 $CE^{P0\text{-}P10}$ and 1 $PEE^{P0\text{-}P10}$ male excluded) were excluded from the analysis. Subsequently, statistical outliers were identified with the ROUT method (Q = 10%) on object, corridor, and social chamber exploration (none removed), on open arm exploration (1 $PEE^{P0\text{-}P10}$ male excluded), consumption of 1% sucrose (1 $PEE^{P0\text{-}P10}$ female and 1 $PEE^{P0\text{-}P10}$ male excluded), consumption of 8% sucrose (1 $PEE^{P0\text{-}P10}$ female excluded), and active lever press at extinction day 1 (2 $CE^{P0\text{-}P10}$ and 1 $PEE^{P0\text{-}P10}$ female excluded) and removed from the analysis. The normality of sample distribution was assessed with the Shapiro–Wilk test. Two-sample distributions were compared with a two-tailed parametric t-test or non-parametric Mann–Whitney test. Analysis of variance was conducted using repeated measures ANOVA (RM ANOVA), RM two-way ANOVA, or two-way ANOVA followed by *post hoc* tests as reported in each figure graph and legend. Nested analysis of latency to social approach and active lever pressing at extinction day 1 were conducted using a nested t-test that considers each pup a biological replicate of a litter (random factor), while treatment (CE vs. PEE) as a fixed factor. A value of $p < 0.05$ was set to determine the statistical significance of two-sample comparisons, main effects, and interactions. Graphs were created, and statistical analysis was conducted with GraphPad/Prism.

Results

Postnatal ethanol exposure alters maternal behavior and female offspring growth

Our study used a mouse model of postnatal ethanol exposure ($PEE^{P0\text{-}P10}$) by exposing dams and pups to ethanol vapor between days P0-P3 and P6-P10 in a 16-h-ON/8-h-OFF pattern (Figure 1A). We included a total of five cohorts of alcohol-exposed dams and pups (Figure 1B): cohorts 1 and 2, with 3 and 2 litters, respectively, were used for the operant training experiments; cohorts 3 and 4, with 3 and 6 litters, respectively, were used for the social preference, two-bottle sucrose preference test, and O-Maze, and cohort 5, with 5 litters, was used to monitor body weight during early development, and all behavioral assays except for operant training. Age-matched air-exposed offspring ($CE^{P0\text{-}P10}$) was used for all the behavioral experiments. Between P3 and P9, we sacrificed one pup per litter and measured Blood Alcohol Concentration (BAC) from trunk blood. On average, we detected a BAC above the intoxication threshold of 80 mg/dL, which did not differ across the 5 mouse cohorts (Figure 1C). In cohort 5, we monitored pup growth by measuring their body weights at three developmental time points (P3, P10, and P22). In male $PEE^{P0\text{-}P10}$, we did not observe any body weight difference compared to $CE^{P0\text{-}P10}$ (Figure 1D). However, $PEE^{P0\text{-}P10}$ female pups had a lower body weight at P10 and P22 than $CE^{P0\text{-}P10}$ female pups (Figure 1E). We then performed a pup-retrieval assay (Marlin et al., 2015) to investigate whether alcohol vapor exposure impairs maternal behavior. We observed that $PEE^{P0\text{-}P10}$ dams had a longer latency to pup retrieval than the $CE^{P0\text{-}P10}$ dams (Figure 1F). Altogether, these data indicate that alcohol vapor exposure during postnatal periods affects maternal behavior and female offspring growth in a sex-specific manner.



	DOB	Average BAC	Body weight	Social Preference	O-Maze	Sucrose Preference	Operant training
Cohort 1	5/26/2021	101.07	NO	NO	NO	NO	YES
Cohort 2	6/22/2021	140.19	NO	NO	NO	NO	YES
Cohort 3	6/14/2022	142.99	NO	YES	YES	YES	NO
Cohort 4	7/19/2022	141.23	NO	YES	YES	YES	NO
Cohort 5	11/1/2022	168.13	YES	YES	YES	YES	NO

FIGURE 1
PEE increases BAC and alters offspring growth. **(A)** Ethanol vapor exposure timeline. Pups and dams were exposed to ethanol or air for 16-h sessions during the first 10 postnatal days with a 3-day break. **(B)** Assignment of offspring cohorts used in each experiment and their average blood alcohol concentration (BAC). **(C)** The average BAC in PEE$^{P0\text{-}P10}$ pups for each cohort [one-way ANOVA; $F_{(4,14)}$=0.3822, p=0.8177]. Number of mice per cohort are indicated on the graph. **(D)** Body weights of CE$^{P0\text{-}P10}$ and PEE$^{P0\text{-}P10}$ male offspring at postnatal days 3, 10, and 22 [two-way ANOVA; treatment main effect: $F_{(1,77)}$=0.1801, p=0.6725; time main effect $F_{(2,77)}$=621.7, p<0.0001; treatment x time interaction $F_{(2,77)}$=2.633, p=0.0784 followed by Sidak *post hoc* multiple comparison test]. **(E)** Body weights of CE$^{P0\text{-}P10}$ and PEE$^{P0\text{-}P10}$ female offspring at postnatal days 3, 10, and 22 [two-way ANOVA; treatment main effect: $F_{(1,97)}$=47.33, p<0.0001; time main effect $F_{(2,97)}$=896.5, p<0.0001; treatment x time interaction $F_{(2,97)}$=10, p=0.0001 followed by Sidak *post hoc* multiple comparison test]. **(F)** Latency to pup retrieval in CE$^{P0\text{-}P10}$ and PEE$^{P0\text{-}P10}$ dams (Mann Whitney test U=560, p=0.0204). Data are expressed as mean±SEM. Number of mice or trials indicated on each graph.

Postnatal ethanol exposure induces mild social deficits in the adult female progeny

Previous studies showed that fetal alcohol exposure impairs adolescent and adult progeny sociability. Thus, we assessed whether adult PEE$^{P0\text{-}P10}$ offspring display social interaction deficits compared to control exposure (CE$^{P0\text{-}P10}$) when given a choice between an unfamiliar same-sex conspecific or an unfamiliar object. These experiments were conducted on the male and female offspring of cohorts #3, #4, and #5 between P70-P260. We used a modified version of the three-chamber sociability assay (Yang et al., 2011). We automatically scored the percentage of time each mouse spent in the corridor, social, and object chambers (Figure 2A). In this task, CE$^{P0\text{-}P10}$ and PEE$^{P0\text{-}P10}$ female offspring showed a longer time spent in the social compared to the object chamber (Figures 2B,C). Similarly, CE$^{P0\text{-}P10}$ (Figure 2D) and PEE$^{P0\text{-}P10}$ (Figure 2E) male progeny spent more time in the social, compared to the object, compartment. Distance moved during the social preference assay did not differ between sexes, CE$^{P0\text{-}P10}$ and PEE$^{P0\text{-}P10}$ offspring (Figure 2F). We then analyzed the exploratory behavior of the animals within the social chamber as time spent in areas proximal or distal to the same-sex unfamiliar social stimulus. We observed that both CE$^{P0\text{-}P10}$ and PEE$^{P0\text{-}P10}$ male progeny spent a longer time in the proximity of the social stimulus compared to more distal areas (Figure 2G). CE$^{P0\text{-}P10}$ female mice did not show differences in exploratory behavior between proximal and distal areas (Figure 2H). In contrast, PEE$^{P0\text{-}P10}$ female mice spent more time in the distal than the proximal location relative to the social stimulus (Figure 2H). We then tested whether this different exploratory behavior resulted in changes in social interaction by quantifying the latency to first approach the social stimulus in our experimental groups. While no difference was detected between CE$^{P0\text{-}P10}$ and PEE$^{P0\text{-}P10}$ male progeny (Figure 2I), we observed that PEE$^{P0\text{-}P10}$ female mice had longer delays in interacting with their conspecifics compared to the CE$^{P0\text{-}P10}$ group (Figure 2I). To exclude that social approach deficits result from multiple representations of sex and exposure due to the inclusion of more than one pup per litter, we performed a nested analysis that considers each pup a biological replicate of each litter. This per-litter analysis revealed that PEE$^{P0\text{-}P10}$ female offspring had a longer latency to approach the social stimulus than CE$^{P0\text{-}P10}$ mice (Figure 2J). Thus, while PEE$^{P0\text{-}P10}$ adult male and female mice do not have major sociability abnormalities, female PEE$^{P0\text{-}P10}$ progeny show a sex-specific deficit in exploratory behavior and longer delays in social approach.

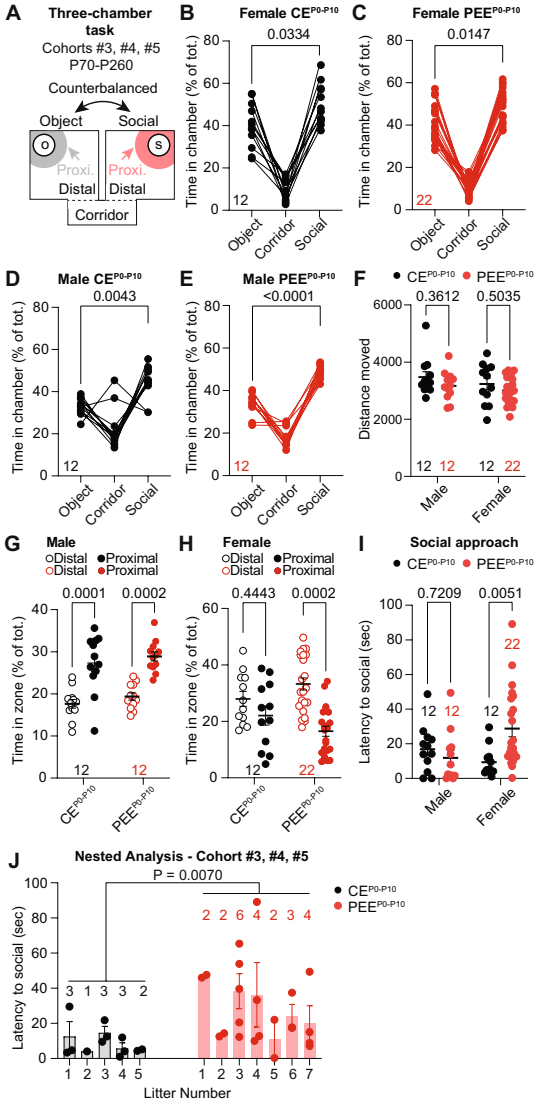


FIGURE 2
PEE induces mild social deficits in the adult female progeny. **(A)** Schematic diagram of the three-chamber apparatus used in the three-chamber task. **(B)** Percentage of time spent in the corridor, object, and social chamber in CE$^{P0\text{-}P10}$ adult female mice (RM ANOVA; $F_{(2,22)}$=45.93, p<0.0001 followed by Sidak *post hoc* multiple comparison test). **(C)** Percentage of time spent in the corridor, object, and social chamber in PEE$^{P0\text{-}P10}$ adult female mice (RM ANOVA; $F_{(1.212,\ 25.45)}$=125.1, p<0.0001 followed by Sidak multiple comparison test). **(D)** Percentage of time spent in the corridor, object, and social chamber in CE$^{P0\text{-}P10}$ adult male mice (RM ANOVA; $F_{(2,22)}$=19.04, p<0.0001 followed by Sidak *post hoc* multiple comparison test). **(E)** Percentage of time spent in the corridor, object, and social chamber in PEE$^{P0\text{-}P10}$ adult male mice (RM ANOVA; $F_{(1.716,\ 18.88)}$=96.11, p<0.0001 followed by Sidak multiple comparison test). **(F)** Distance moved during the sociability assay in male and female CE$^{P0\text{-}P10}$ and PEE$^{P0\text{-}P10}$ adult progeny (two-way ANOVA; treatment main effect: $F_{(1,54)}$=2.791, p=0.1006; sex main effect: $F_{(1,54)}$=1.591, p=0.2127; treatment × sex interaction: $F_{(1,54)}$=0.0757, p=0.7842). **(G)** Percentage of time spent in distal or proximal areas to social stimulus for CE$^{P0\text{-}P10}$ and PEE$^{P0\text{-}P10}$ adult male mice (RM two-way ANOVA; zone main effect: $F_{(1,22)}$=47.83, p<0.0001; treatment main effect: $F_{(1,22)}$=1.771, p=0.1969, zone × treatment interaction: $F_{(1,22)}$=0.0035, p=0.9535; followed by Sidak *post hoc* multiple comparison test). **(H)** Percentage of time spent in distal or proximal areas to social stimulus for CE$^{P0\text{-}P10}$ and PEE$^{P0\text{-}P10}$ adult female mice (RM two-way ANOVA; zone main effect: $F_{(1,32)}$=12.88, p=0.0011; treatment main effect: $F_{(1,32)}$=0.007, p=0.9340, zone × treatment interaction: $F_{(1,32)}$=2.967, p=0.0946; followed by Sidak *post hoc* multiple comparison test). **(I)** Latency to first social approach in CE$^{P0\text{-}P10}$ and PEE$^{P0\text{-}P10}$ adult female and male mice (two-way ANOVA; treatment main effect: $F_{(1,54)}$=2.392, p=0.1278; sex main effect: $F_{(1,54)}$=1.021, p=0.3168; treatment × sex interaction: $F_{(1,54)}$=6.946, p=0.0109). **(J)** Nested analysis of the latency to first social approach in CE$^{P0\text{-}P10}$ and PEE$^{P0\text{-}P10}$ female offspring (nested t-test, $t_{(32)}$=2.883, p=0.007). Data are expressed as mean±SEM. Number of mice are indicated on each graph.

Postnatal ethanol exposure fails to induce either anxiety-like or reward-processing deficits in the adult female offspring

Animals used to model prenatal and PEE display deficits in affective behaviors, mainly related to anxiety-like (Bianco et al., 2021; Lopatynska-Mazurek et al., 2021b; Rouzer and Diaz, 2022) and depressive-like traits (Caldwell et al., 2008; Lopatynska-Mazurek et al., 2021b). To evaluate whether post-natal alcohol exposure would lead to similar deficits, we tested the PEE$^{P0\text{-}P10}$ adult male and female progeny in the O-Maze test (Figure 3A), a high construct validity task to assess anxiety-like behavior in rodents (Walf and Frye, 2007; Braun et al., 2011). For these experiments, we used the adult offspring of cohorts #3, #4, and #5 at the age of P70-P260. First, we quantified the

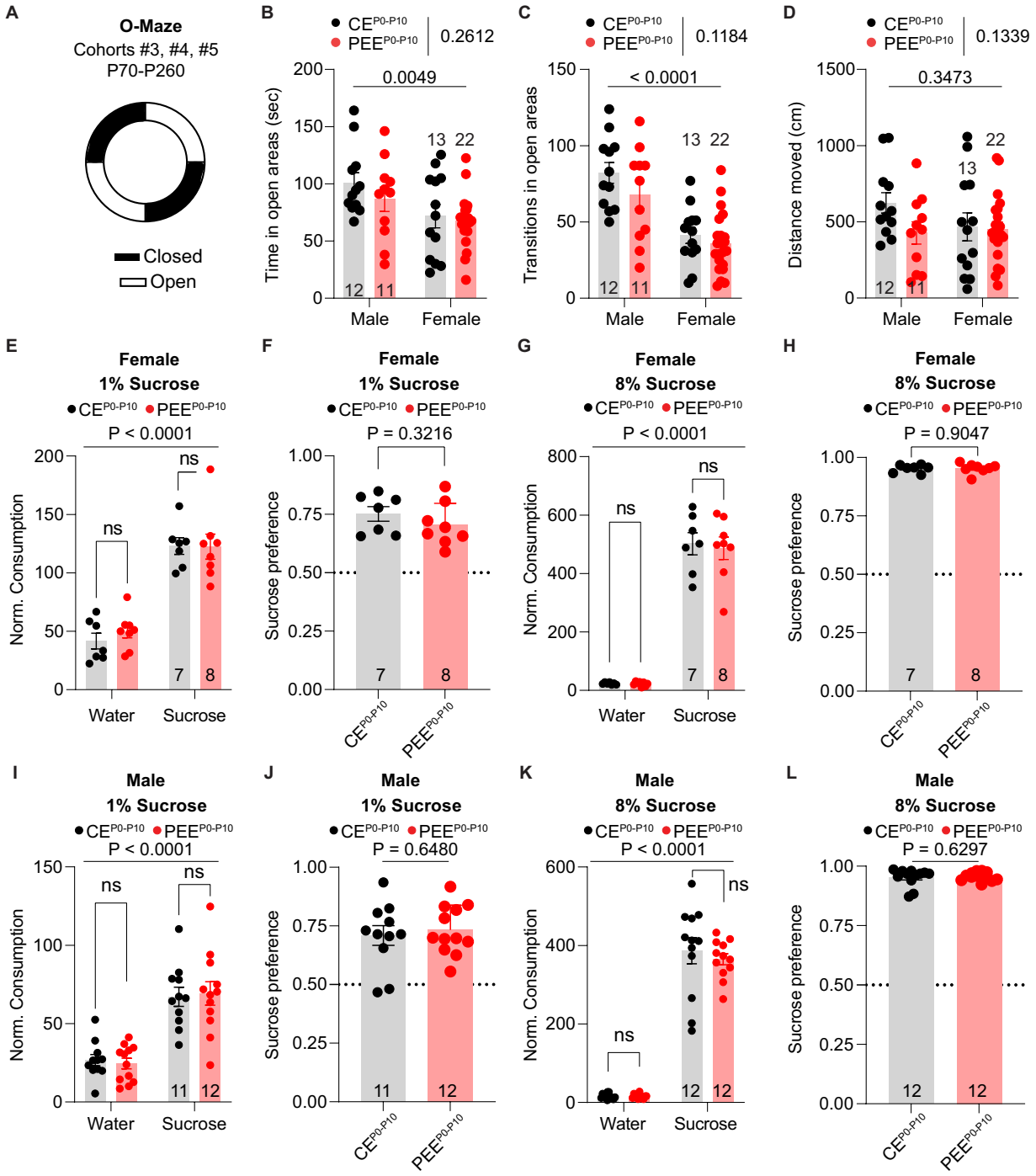


FIGURE 3
PEE fails to induce anxiety-like and reward consumption deficits in both sexes. **(A)** Schematic diagram of the O-Maze used to assess anxiety-like behavior. **(B)** Time spent in the open areas of the O-Maze in $CE^{P0\text{-}P10}$ and $PEE^{P0\text{-}P10}$ adult male and female mice (two-way ANOVA; treatment main effect: $F_{(1,54)}$=1.289, p=0.2612; sex main effect: $F_{(1,54)}$=8.617, p=0.0049; treatment × sex interaction: $F_{(1,54)}$=0.3904, p=0.5347). **(C)** Number of open arm transitions in $CE^{P0\text{-}P10}$ and $PEE^{P0\text{-}P10}$ adult male and female mice (two-way ANOVA; treatment main effect: $F_{(1,54)}$=2.518, p=0.1184; sex main effect: $F_{(1,54)}$=35.23, p<0.0001; treatment × sex interaction: $F_{(1,54)}$=0.5011, p=0.4821). **(D)** Distance moved for $CE^{P0\text{-}P10}$ and $PEE^{P0\text{-}P10}$ adult male and female mice (two-way ANOVA; treatment main effect: $F_{(1,54)}$=2.315, p=0.1339; sex main effect: $F_{(1,54)}$=0.8988, p=0.3473; treatment × sex interaction: $F_{(1,54)}$=1.757, p=0.1906). **(E)** Normalized consumption (g/Kg) of sucrose and water consumed during the 1% sucrose preference test in $CE^{P0\text{-}P10}$ and $PEE^{P0\text{-}P10}$ adult female mice (RM two-way ANOVA; sucrose main effect: $F_{(1,13)}$=71.25, p<0.0001; treatment main effect: $F_{(1,13)}$=0.3502, p=0.5641; sucrose × treatment interaction: $F_{(1,13)}$=0.2342, p=0.6365, followed by Sidak *post hoc* multiple comparison test). **(F)** Sucrose preference index in $CE^{P0\text{-}P10}$ and $PEE^{P0\text{-}P10}$ adult female mice during 1% sucrose preference test (unpaired *t*-test, $t_{(13)}$=1.03, p=0.3216). **(G)** Normalized consumption (g/Kg) of sucrose and water consumed during the 8% sucrose preference test in $CE^{P0\text{-}P10}$ and $PEE^{P0\text{-}P10}$ adult female mice (RM two-way ANOVA; sucrose main effect: $F_{(1,13)}$=295.4, p<0.0001; treatment main effect: $F_{(1,13)}$=0.0943, p=0.7637; sucrose × treatment interaction: $F_{(1,13)}$=0.0659, p=0.8014, followed by *post hoc* Sidak multiple comparison test). **(H)** Sucrose preference index in $CE^{P0\text{-}P10}$ and $PEE^{P0\text{-}P10}$ adult female mice during 8% sucrose preference test (unpaired *t*-test, $t_{(13)}$=0.1221, p=0.9047). **(I)** Normalized consumption (g/Kg) of sucrose and water consumed during the 1% sucrose preference test in $CE^{P0\text{-}P10}$ and

(Continued)

FIGURE 3 (Continued)
$PEE^{P0\text{-}P10}$ adult male mice (RM two-way ANOVA; sucrose main effect: $F_{(1,21)}$=53.91, p<0.0001; treatment main effect: $F_{(1,21)}$<0.0001, p=0.9948; sucrose × treatment interaction: $F_{(1,21)}$=0.1377, p=0.7143, followed by Sidak *post hoc* multiple comparison test). **(J)** Sucrose preference index in $CE^{P0\text{-}P10}$ and $PEE^{P0\text{-}P10}$ adult male mice during 1% sucrose preference test (unpaired *t*-test, $t_{(21)}$=0.4632, p=0.648). **(K)** Normalized consumption (g/Kg) of sucrose and water consumed during the 8% sucrose preference test in $CE^{P0\text{-}P10}$ and $PEE^{P0\text{-}P10}$ adult male mice (RM two-way ANOVA; sucrose main effect: $F_{(1,22)}$=373.9, p<0.0001; treatment main effect: $F_{(1,22)}$=0.3951, p=0.5361; sucrose × treatment interaction: $F_{(1,22)}$=0.3446, p=0.5632, followed by *post hoc* Sidak multiple comparison test). **(L)** Sucrose preference index in $CE^{P0\text{-}P10}$ and $PEE^{P0\text{-}P10}$ adult male mice during 8% sucrose preference test (Mann–Withney U=63, p=0.6297). Data are expressed as mean±SEM. Number of mice are indicated on each graph.

time spent in the open areas of the O-Maze and observed that, while males spent a longer time in the open areas compared to female mice, no difference was observed between $CE^{P0\text{-}P10}$ and $PEE^{P0\text{-}P10}$ progeny (Figure 3B). Second, we observed that while male subjects made more transitions in and out of open areas than females, $CE^{P0\text{-}P10}$ and $PEE^{P0\text{-}P10}$ adult offspring behaved similarly (Figure 3C). As in the three-chamber assay, no difference in distance moved was noted during the O-Maze task (Figure 3D). These data indicate that $PEE^{P0\text{-}P10}$ does not induce significant anxiety-like deficits in either male or female adult offspring. To assess whether $PEE^{P0\text{-}P10}$ impairs reward processing, we conducted a two-bottle sucrose preference test routinely used to evaluate anhedonia in rodents (Hoffman, 2016; Liu et al., 2018). Here, we tested the ability of the adult offspring to discriminate and consume a sucrose solution at two different concentrations during two consecutive 16-h periods. For these experiments, we used the adult offspring of cohorts #3, #4, and #5 in the age range P70-P260. In this test, $CE^{P0\text{-}P10}$ and $PEE^{P0\text{-}P10}$ female mice consumed more 1% sucrose solution than water (Figure 3E). There was a similar preference for the 1% sucrose solution in $CE^{P0\text{-}P10}$ and $PEE^{P0\text{-}P10}$ offspring (Figure 3F). We obtained similar results when the sucrose concentration was increased to 8%, with no differences in either sucrose consumption (Figure 3G) or preference (Figure 3H) between $CE^{P0\text{-}P10}$ and $PEE^{P0\text{-}P10}$ offspring. As in the female offspring, $PEE^{P0\text{-}P10}$ male mice did not show deficits in sucrose 1% consumption (Figure 3I), sucrose 1% preference (Figure 3J), sucrose 8% consumption (Figure 3K), and sucrose 8% preference (Figure 3L). These data indicate that PEE does not induce significant abnormalities in hedonic/consummatory behavior, at least for a highly palatable carbohydrate in either male or female offspring.

Postnatal ethanol exposure impairs the extinction of operant behavior in the adult female offspring

We then assessed the impact of $PEE^{P0\text{-}P10}$ on instrumental conditioning during adulthood. These experiments included the offspring of cohorts #1 and #2 and began when animals reached an age of P55-P80. We trained animals in a 4-day single-lever schedule to obtain one sucrose reward (FR1), followed by dual-lever training when an inactive lever was introduced and counterbalanced across mice. This phase consisted of 3 days of FR1 training followed by 3 days on an FR5 schedule. At the end of the acquisition period, animals underwent an FR5 reversal learning phase when active and inactive levers were switched. After six training sessions, animals were retrained on a random-ratio (RR) reinforcement schedule followed by extinction when lever pressing was no longer reinforced (Figure 4A). Neither $PEE^{P0\text{-}P10}$ female nor male mice show deficits in active lever press frequency during single lever training (Figure 4B) or in active (Figure 4C) and inactive lever press frequency (Figure 4D) during dual-lever training. Across reversal learning sessions, both $CE^{P0\text{-}P10}$ and $PEE^{P0\text{-}P10}$ male and female offspring increased their active lever press frequency to the same levels as the last acquisition day (Figure 4E) and decreased inactive lever press frequency (Figure 4F). During random ratio training, female $PEE^{P0\text{-}P10}$ mice showed no difference in active lever press frequency but heightened active lever press frequency during extinction day 1 (Figure 4G), with no statistically significant difference in reinstatement (Figure 4G). Active lever press frequency during random ratio, extinction, and reinstatement was similar between $CE^{P0\text{-}P10}$ and $PEE^{P0\text{-}P10}$ adult male offspring (Figure 4G). To exclude that extinction deficits derived from multiple representations of litter exposure due to including more than one pup per litter, we performed a nested analysis that considers each pup as a biological replicate of each litter. This per-litter analysis confirms that the $PEE^{P0\text{-}P10}$ female offspring have a higher lever press frequency on extinction day 1 than the $CE^{P0\text{-}P10}$ offspring (Figure 4H). These data reveal a sex-specific persistence of action-outcome associations in $PEE^{P0\text{-}P10}$ adult female, but not male, offspring.

Discussion

This study aimed to investigate the socioemotional and cognitive deficits in the progeny of a $PEE^{P0\text{-}P10}$ mouse model. $PEE^{P0\text{-}P10}$ adult female, but not male, offspring show altered social approach and impaired extinction of instrumental action-outcome associations. These sex-specific socioemotional and cognitive deficits were not due to significant abnormalities in locomotor activity, exploration of the open areas in the O-maze task, or sucrose preference in a two-bottle choice paradigm, which indicate the absence of major anxiety-like or anhedonic states. However, some considerations are warranted.

In the present study, we included five cohorts of mice postnatally exposed to alcohol, which reached an average BAC of 150 mg/dL. This concentration is well above the intoxication threshold of 80 mg/dL and induces severe behavioral symptoms in humans (Koob et al., 2014). The combination of cyclic exposures (P0-P3, P6-P10) and the high BAC relate to the binge-like patterns of gestational alcohol use observed in about 3% of the general pregnant population in European, African and American countries (Popova et al., 2018). This exposure pattern induced a sex-specific reduction in the body weight of female $PEE^{P0\text{-}P10}$ offspring, resembling anatomical dysmorphologies seen in humans exposed to high alcohol levels during development (Mattson and Riley, 1998). Whether changes in corticosterone, growth hormone, and testosterone (Gabriel et al., 1998) levels underlie these defects in the female $PEE^{P0\text{-}P10}$ offspring remains an open question.

Individuals with FASD (Kully-Martens et al., 2012) and the male progeny of animal models of PEE show dyadic social interaction and recognition deficits during adulthood (Boschen

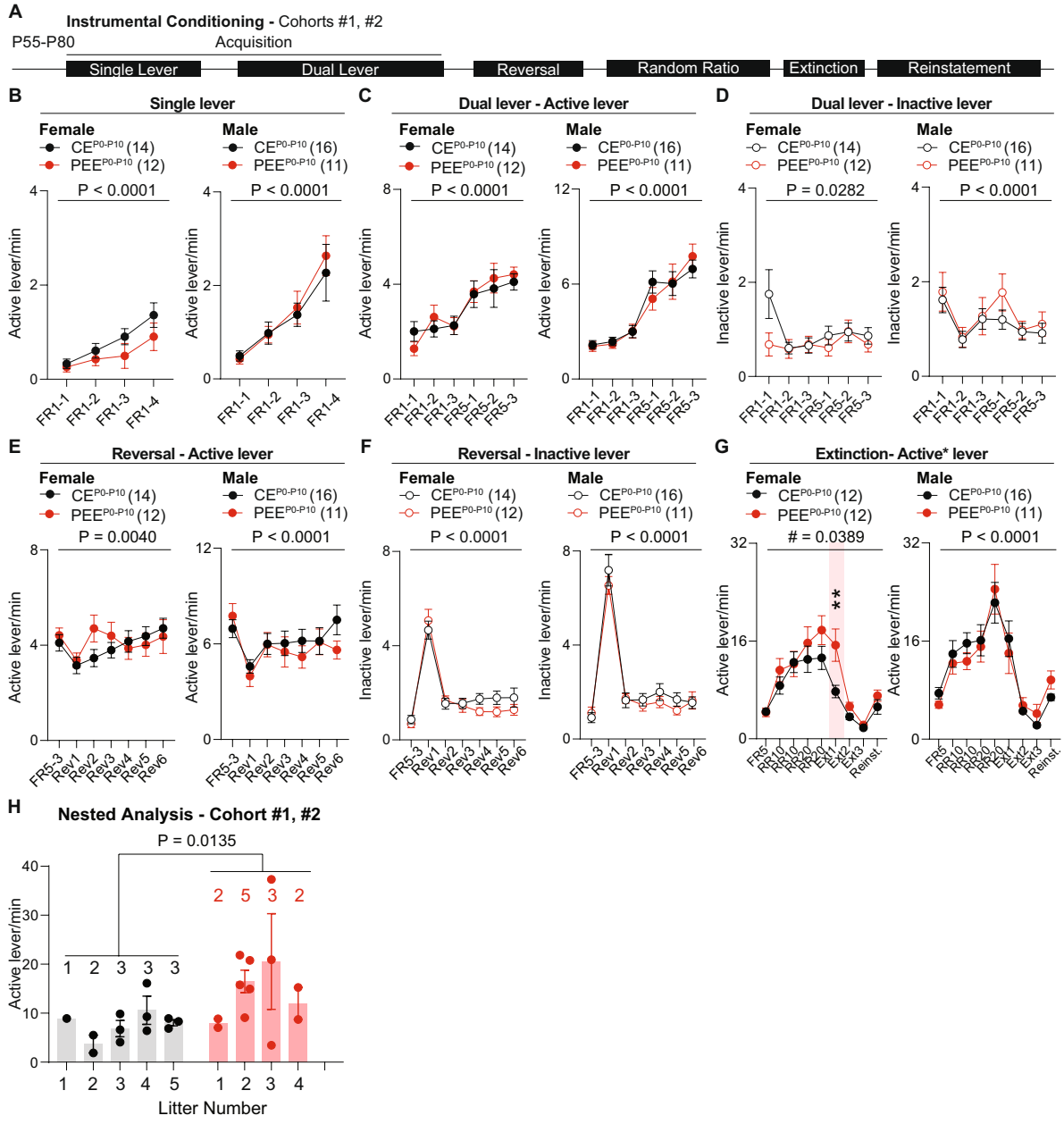


FIGURE 4
PEE impairs the extinction of operant behavior in the adult female offspring. **(A)** Timeline of behavioral experiments. **(B)** Active lever press frequency during single lever training in $CE^{P0\text{-}P10}$ and $PEE^{P0\text{-}P10}$ female and male mice (Female mice: RM two-way ANOVA; treatment main effect: $F_{(1,24)}$=1.613, p=0.2162; session main effect $F_{(3,72)}$=12.84, p<0.0001; treatment × session interaction: $F_{(3,72)}$=0.87, p=0.4608; Male mice: RM two-way ANOVA; treatment main effect: $F_{(1,25)}$=0.0994, p=0.7552; session main effect $F_{(3,75)}$=16.74, p<0.0001; treatment × session interaction: $F_{(3,75)}$=0.2246, p=0.879). **(C)** Active lever press frequency during dual lever training in $CE^{P0\text{-}P10}$ and $PEE^{P0\text{-}P10}$ female and male offspring (Female mice: RM two-way ANOVA; treatment main effect: $F_{(1,24)}$=0.0435, p=0.8365; session main effect $F_{(5,120)}$=17.34, p<0.0001; treatment × session interaction: $F_{(5,120)}$=0.7638, p=0.5777; Male mice: RM two-way ANOVA; treatment main effect: $F_{(1,25)}$=0.0132, p=0.9094; session main effect $F_{(5,125)}$=38.69, p<0.0001; treatment × session interaction: $F_{(5,125)}$=0.7055, p=0.6203). **(D)** Inactive lever press frequency during dual lever training in $CE^{P0\text{-}P10}$ and $PEE^{P0\text{-}P10}$ female and male mice (Female mice: RM two-way ANOVA; treatment main effect: $F_{(1,24)}$=1.233, p=0.2778; session main effect $F_{(5,120)}$=2.608, p=0.0282; treatment × session interaction: $F_{(5,120)}$=2.234, p=0.0552; Male mice: RM two-way ANOVA; treatment main effect: $F_{(1,25)}$=0.4609, p=0.5034; session main effect $F_{(5,125)}$=6.081, p<0.0001; treatment × session interaction: $F_{(5,125)}$=0.5391, p=0.7463). **(E)** Active lever press frequency during reversal of action-outcome associations in $CE^{P0\text{-}P10}$ and $PEE^{P0\text{-}P10}$ female and male offspring (Female mice: RM two-way ANOVA; treatment main effect: $F_{(1,24)}$=0.1697, p=0.684; session main effect $F_{(6,144)}$=3.36, p=0.004; treatment × session interaction: $F_{(6,144)}$=1.914, p=0.0823; Male mice: RM two-way ANOVA; treatment main effect: $F_{(1,25)}$=0.3561, p=0.556; session main effect $F_{(6,150)}$=6.051, p<0.0001; treatment × session interaction: $F_{(6,150)}$=1.236, p=0.2908). **(F)** Inactive lever press frequency during reversal training in $CE^{P0\text{-}P10}$ and $PEE^{P0\text{-}P10}$ female and male offspring (Female mice: RM two-way ANOVA; treatment main effect: $F_{(1,24)}$=0.6529, p=0.427; session main effect $F_{(6,144)}$=64.74, p<0.0001; treatment × session interaction: $F_{(6,144)}$=1.305, p=0.2584; Male mice: RM two-way ANOVA; treatment main effect: $F_{(1,25)}$=0.3105, p=0.5823; session main effect $F_{(6,150)}$=119.7, p<0.0001; treatment × session interaction: $F_{(6,150)}$=0.7679, p=0.5963). **(G)** Active lever press frequency during random ratio training, extinction, and reinstatement of action-outcome associations in $CE^{P0\text{-}P10}$ and $PEE^{P0\text{-}P10}$ female and male offspring (Female mice: RM two-way ANOVA; treatment main effect: $F_{(1,22)}$=2.255, p=0.1474; session main effect $F_{(8,176)}$=31.71, p<0.0001; treatment × session interaction: $F_{(8,176)}$=2.092, p=0.0389; between-group Sidak *post hoc* test, **=0.0077; Male mice: RM two-way ANOVA; treatment main effect:

(Continued)

FIGURE 4 (Continued)
$F_{(1,25)}$=0.0137, p=0.9079; session main effect $F_{(8,200)}$=24.76, p<0.0001; treatment × session interaction: $F_{(8,200)}$=0.7263, p=0.6682). **(H)** Nested analysis of active lever press frequency in $CE^{P0\text{-}P10}$ and $PEE^{P0\text{-}P10}$ female offspring on the first day of extinction (nested t-test, $t_{(22)}$=2.685, p=0.0135). Data are expressed as mean±SEM. Number of mice are indicated on each graph.

et al., 2014; Subbanna et al., 2018; Joshi et al., 2019; Shivakumar et al., 2021). We observed that $PEE^{P0\text{-}P10}$ male and female offspring have intact sociability, expressed as longer time spent in the unfamiliar social vs. object chamber (Yang et al., 2011) and similar locomotor activity during the three-chamber sociability test. However, our automated analysis of exploratory behavior revealed a clear preference for the distal vs. proximal location relative to the same-sex conspecific in $PEE^{P0\text{-}P10}$ females, which was not observed in $CE^{P0\text{-}P10}$ adult females. These impairments might be interpreted as a mild social avoidance phenotype. Previous studies defined strain-specific social avoidance in female mice as a relative reduction in exploratory behavior in the presence vs. absence of a social stimulus (Brodkin et al., 2004). In mice, social avoidance can also be quantified as the relative reduction in the time spent in proximal vs. distal areas to a social stimulus after a chronic social defeat paradigm (Harris et al., 2018). Thus, one hypothesis might be that the unfamiliar conspecific might represent an aversive stimulus for the adult $PEE^{P0\text{-}P10}$ female progeny, which would acquire an even stronger negative valence upon chronic social stress paradigms.

During the three-chamber sociability test, we also observed a longer latency to first approach the novel social stimulus in the $PEE^{P0\text{-}P10}$ compared to the $CE^{P0\text{-}P10}$ progeny, which might indicate novelty-induced avoidance. Notably, previous models of prenatal (Rouzer et al., 2017) and adolescent alcohol exposure followed by acute restrain stress (Kasten et al., 2020) reported novelty-induced hypophagia in male and female subjects, respectively. These data highlight the possibility that the adult offspring of $PEE^{P0\text{-}P10}$ might also display negative affective states exacerbated by novel stimuli of different nature.

Depending on the exposure paradigm, PEE causes anxiety-like behavior in male and female rats (Bianco et al., 2021; Lopatynska-Mazurek et al., 2021b), reminiscent of co-morbid anxiety symptoms observed in FASD patients (Famy et al., 1998; Barr, 2006; Pei et al., 2011). We did not observe significant anxiety-like behavior during the elevated O-maze test in the adult $PEE^{P0\text{-}P10}$ mouse offspring. However, it is crucial to recognize that previous authors reported anxiety-like behavior in prenatal and PEE progeny (Rouzer et al., 2017; Bianco et al., 2021; Lopatynska-Mazurek et al., 2021b; Rouzer and Diaz, 2022) using different behavioral paradigms, including the open field test (Bianco et al., 2021), elevated plus maze (Dursun et al., 2006; Cullen et al., 2013), light–dark box test (Cullen et al., 2013), and novelty-induced hypophagia (Rouzer et al., 2017; Bianco et al., 2021). Thus, additional behavioral experiments might reveal anxiety-like traits in the adult $PEE^{P0\text{-}P10}$ male and female offspring. As discussed earlier, the increased time spent in distal areas to a novel social stimulus and the increased latency to social approach might indicate anxiety-like traits related to social interaction. Whether social avoidance phenotypes are due to the novel and anxiogenic nature of the stimulus or can be exacerbated by post-natal stressors (Hellemans et al., 2008) will be addressed in future studies.

Similar to anxiety, depression is a comorbidity often observed in individuals who received an FASD diagnosis (Pei et al., 2011). One core component of depression is reduced hedonic behavior (Fava and Kendler, 2000; Pizzagalli et al., 2008), which can be evaluated using a two-bottle choice test in rodents (Liu et al., 2018). In this study, we specifically assessed whether the adult $PEE^{P0\text{-}P10}$ male and female progeny would prefer a sucrose solution (at two different concentrations) over water and failed to find any deficits. This allows us to draw two important conclusions: on the one hand, $PEE^{P0\text{-}P10}$ does not alter reward-processing mechanisms, and on the other, it implies that the adult male and female progeny do not show anhedonia-like behavior indicative of a depressive-like phenotype in this test. However, it is crucial to consider that in rodents, core components of depressive-like states can be assessed and revealed by using other behavioral tests, including the forced-swim task (Porsolt et al., 1978; Lopatynska-Mazurek et al., 2021b), the tail-suspension test (Cryan et al., 2005), the learned helplessness test (Seligman, 1972; Pryce et al., 2012), and the urine scent marking test (Lehmann et al., 2013). Whether depressive like-states might emerge in the male and female $PEE^{P0\text{-}P10}$ progeny during these tests remains a future investigation venue.

Beyond socioemotional impairments, FASD individuals and animals used as models of PEE display deficits in several aspects of executive function (Bariselli and Lovinger, 2021). As opposed to previous Y-Maze, Barnes Maze, and Morris Water Maze tasks conducted on the progeny of PEE rats and mice (O'Leary-Moore et al., 2006; Allan et al., 2014; Subbanna et al., 2018; Joshi et al., 2019; Gibula-Tarlowska et al., 2021; Shivakumar et al., 2021; Lopatynska-Mazurek et al., 2021a; Risbud et al., 2022), we failed to observe deficits in associative and reversal learning during operant training. Several factors may account for these discrepancies. For example, the developmental timing of alcohol exposure could be an important variable. While previous studies used a prenatal alcohol exposure paradigm (Allan et al., 2014; Marquardt et al., 2014), we utilized a post-natal alcohol exposure protocol. The type of behavioral assay may also underlie the difference in results. While previous authors assessed spatial navigation-based associative learning (O'Leary-Moore et al., 2006; Allan et al., 2014; Subbanna et al., 2018; Joshi et al., 2019; Gibula-Tarlowska et al., 2021; Shivakumar et al., 2021; Lopatynska-Mazurek et al., 2021a; Risbud et al., 2022) or cue-based reversal learning tasks (Marquardt et al., 2014), we examined self-paced instrumental reversal learning where non-cued active and inactive levers were switched. Finally, the age of the experimental subjects at testing is an important variable. Previous experiments showed reversal learning deficits in juvenile, but not adult, rats postnatally exposed to alcohol (O'Leary-Moore et al., 2006), while we used adult subjects only.

After reversal learning, adult female subjects were re-trained using a random ratio (RR) schedule that, in previous experiments, resulted in hyper-responding in mice exposed to ethanol throughout the

prenatal and early postnatal periods (Cuzon Carlson et al., 2020). In this study, we limited our PEE to postnatal periods that might not be enough to increase lever-pressing behavior. However, we noticed that reward omission during the extinction phase resulted in heightened lever-pressing behavior in the $PEE^{P0\text{-}P10}$ compared to the $CE^{P0\text{-}P10}$ adult female offspring, demonstrating the persistence of action-outcome responding. These defects highlight behavioral maladaptations to changes in environmental contingencies (Bouton, 2004) following PEE. Once again, the absence of extinction defects associated with reinstatement deficits reported in prenatally alcohol-exposed subjects (Olguin et al., 2019) might highlight fundamental differences in the teratogenic effects of alcohol on the developing brain.

Our experiments reveal specific behavioral deficits in the adult female progeny of a postnatal mouse model of $PEE^{P0\text{-}P10}$, mainly related to the social and behavioral adaptation domains. One limitation of this study is the need for more data on the phase of the estrous cycle of the female offspring, which influence both social (Ervin et al., 2015) and operant (Verharen et al., 2019) behavior in rodents. Together with the existing literature on different models of fetal alcohol exposure, these data highlight the importance of timing of exposure in mediating the teratogenic effects of alcohol on the developing brain. This approach will help to identify and tailor specific therapeutic interventions for subgroups of individuals affected by FASD.

Data availability statement

The raw data supporting the conclusions of this article will be made available by the authors, without undue reservation.

Ethics statement

The animal study was reviewed and approved by Animal Care and Use Committee of the NIAAA Division of Intramural Clinical and Biological Research.

Author contributions

SB, YM, and DL conceived the study. SB wrote the manuscript with the assistance of the other authors. NR performed instrumental learning experiments and helped with the generation of $PEE^{P0\text{-}P10}$ mice. NR and NW performed the sociability, elevated O-maze, and sucrose preference test. All authors contributed to the article and approved the submitted version.

Funding

This research was supported by the Intramural Research Program of the NIH (ZIAAA000416). SB is supported by the Center on Compulsive Behaviors at NIH.

Acknowledgments

The authors want to thank all the members of the Lovinger laboratory for discussing the data included in this work.

Conflict of interest

The authors declare that the research was conducted in the absence of any commercial or financial relationships that could be construed as a potential conflict of interest.

Publisher's note

All claims expressed in this article are solely those of the authors and do not necessarily represent those of their affiliated organizations, or those of the publisher, the editors and the reviewers. Any product that may be evaluated in this article, or claim that may be made by its manufacturer, is not guaranteed or endorsed by the publisher.

References

Allan, A. M., Goggin, S. L., and Caldwell, K. K. (2014). Prenatal alcohol exposure modifies glucocorticoid receptor subcellular distribution in the medial prefrontal cortex and impairs frontal cortex-dependent learning. *PLoS One* 9:e96200. doi: 10.1371/journal.pone.0096200

Autti-Rämö, I., Fagerlund, Å., Ervalahti, N., Loimu, L., Korkman, M., and Hoyme, H. E. (2006). Fetal alcohol spectrum disorders in Finland: clinical delineation of 77 older children and adolescents. *Am. J. Med. Genet.* 140A, 137–143. doi: 10.1002/ajmg.a.31037

Bariselli, S., and Lovinger, D. M. (2021). Corticostriatal circuit models of cognitive impairments induced by fetal exposure to alcohol. *Biol. Psychiatry* 90, 516–528. doi: 10.1016/j.biopsych.2021.05.014

Bariselli, S., Tzanoulinou, S., Glangetas, C., Prévost-Solié, C., Pucci, L., Viguié, J., et al. (2016). SHANK3 controls maturation of social reward circuits in the VTA. *Nat. Neurosci.* 19, 926–934. doi: 10.1038/nn.4319

Barr, H. (2006). Binge drinking during pregnancy as a predictor of psychiatric disorders on the structured clinical interview for DSM-IV in Young adult offspring. *Am. J. Psychiatry* 163, 1061–1065. doi: 10.1176/appi.ajp.163.6.1061

Barron, S., Kelly, S. J., and Riley, E. P. (1991). Neonatal alcohol exposure alters suckling behavior in neonatal rat pups. *Pharmacol. Biochem. Behav.* 39, 423–427. doi: 10.1016/0091-3057(91)90202-D

Bianco, C. D., Hübner, I. C., Bennemann, B., de Carvalho, C. R., and Brocardo, P. S. (2021). Effects of postnatal ethanol exposure and maternal separation on mood, cognition and hippocampal arborization in adolescent rats. *Behav. Brain Res.* 411:113372. doi: 10.1016/j.bbr.2021.113372

Boschen, K. E., Hamilton, G. F., Delorme, J. E., and Klintsova, A. Y. (2014). Activity and social behavior in a complex environment in rats neonatally exposed to alcohol. *Alcohol* 48, 533–541. doi: 10.1016/j.alcohol.2014.07.005

Bouton, M. E. (2004). Context and behavioral processes in extinction. *Learn. Mem.* 11, 485–494. doi: 10.1101/lm.78804

Braun, A. A., Skelton, M. R., Vorhees, C. V., and Williams, M. T. (2011). Comparison of the elevated plus and elevated zero mazes in treated and untreated male Sprague-Dawley rats: effects of anxiolytic and anxiogenic agents. *Pharmacol. Biochem. Behav.* 97, 406–415. doi: 10.1016/j.pbb.2010.09.013

Brodkin, E. S., Hagemann, A., Nemetski, S. M., and Silver, L. M. (2004). Social approach-avoidance behavior of inbred mouse strains towards DBA/2 mice. *Brain Res.* 1002, 151–157. doi: 10.1016/j.brainres.2003.12.013

Burd, L., Klug, M. G., Martsolf, J. T., and Kerbeshian, J. (2003). Fetal alcohol syndrome: neuropsychiatric phenomics. *Neurotoxicol. Teratol.* 25, 697–705. doi: 10.1016/j.ntt.2003.07.014

Caldwell, K. K., Sheema, S., Paz, R. D., Samudio-Ruiz, S. L., Laughlin, M. H., Spence, N. E., et al. (2008). Fetal alcohol spectrum disorder-associated depression: evidence for reductions in the levels of brain-derived neurotrophic factor in a mouse model. *Pharmacol. Biochem. Behav.* 90, 614–624. doi: 10.1016/j.pbb.2008.05.004

Carcea, I., Caraballo, N. L., Marlin, B. J., Ooyama, R., Mendoza Navarro, J. M., Opendak, M., et al. (2019). Oxytocin neurons enable social transmission of maternal behavior. bioRxiv. doi: 10.1101/845495,

Creighton-Taylor, J. A., and Rudeen, P. K. (1991). Prenatal ethanol exposure and opiatergic influence on puberty in the female rat. *Alcohol* 8, 187–191. doi: 10.1016/0741-8329(91)90790-4

Cryan, J. F., Mombereau, C., and Vassout, A. (2005). The tail suspension test as a model for assessing antidepressant activity: review of pharmacological and genetic studies in mice. *Neurosci. Biobehav. Rev.* 29, 571–625. doi: 10.1016/j.neubiorev.2005.03.009

Cullen, C. L., Burne, T. H. J., Lavidis, N. A., and Moritz, K. M. (2013). Low dose prenatal ethanol exposure induces anxiety-like behaviour and alters dendritic morphology in the Basolateral amygdala of rat offspring. *PLoS One* 8, e54924–e54912. doi: 10.1371/journal.pone.0054924

Cuzon Carlson, V. C., Gremel, C. M., and Lovinger, D. M. (2020). Gestational alcohol exposure disrupts cognitive function and striatal circuits in adult offspring. *Nat. Commun.* 11:2555. doi: 10.1038/s41467-020-16385-4

Dursun, I., Jakubowska-Doğru, E., and Uzbay, T. (2006). Effects of prenatal exposure to alcohol on activity, anxiety, motor coordination, and memory in young adult Wistar rats. *Pharmacol. Biochem. Behav.* 85, 345–355. doi: 10.1016/j.pbb.2006.09.001

Ericson, L., Magnusson, L., and Hovstadius, B. (2017). Societal costs of fetal alcohol syndrome in Sweden. *Eur. J. Health Econ.* 18, 575–585. doi: 10.1007/s10198-016-0811-4

Ervin, K. S. J., Lymer, J. M., Matta, R., Clipperton-Allen, A. E., Kavaliers, M., and Choleris, E. (2015). Estrogen involvement in social behavior in rodents: rapid and long-term actions. *Horm. Behav.* 74, 53–76. doi: 10.1016/j.yhbeh.2015.05.023

Famy, C., Streissguth, A. P., and Unis, A. S. (1998). Mental illness in adults with fetal alcohol syndrome or fetal alcohol effects. *Am. J. Psychiatry* 155, 552–554. doi: 10.1176/ajp.155.4.552

Fava, M., and Kendler, K. S. (2000). Major depressive disorder. *Neuron* 28, 335–341. doi: 10.1016/B978-012373947-6.00245-2

Flannigan, K., Poole, N., Cook, J., and Unsworth, K. (2023). Sex-related differences among individuals assessed for fetal alcohol spectrum disorder in Canada. *Alcohol. Clin. Exp. Res.* 47, 613–623. doi: 10.1111/acer.15017

Forray, A., Merry, B., Lin, H., Ruger, J. P., and Yonkers, K. A. (2015). Perinatal substance use: a prospective evaluation of abstinence and relapse. *Drug Alcohol Depend.* 150, 147–155. doi: 10.1016/j.drugalcdep.2015.02.027

Gabriel, K., Hofmann, C., Glavas, M., and Weinberg, J. (1998). The hormonal effects of alcohol use on the mother and fetus. *Alcohol Res. Heal.* 22, 170–177.

Gibula-Tarlowska, E., Korz, V., Lopatynska-Mazurek, M., Chlopas-Konowalek, A., Grochecki, P., Kalaba, P., et al. (2021). CE-123, a novel dopamine transporter inhibitor, attenuates locomotor hyperactivity and improves cognitive functions in rat model of fetal alcohol spectrum disorders. *Behav. Brain Res.* 410:113326. doi: 10.1016/j.bbr.2021.113326

Glass, L., Moore, E. M., and Mattson, S. N. (2023). Current considerations for fetal alcohol spectrum disorders: identification to intervention. *Curr. Opin. Psychiatry* 36, 249–256. doi: 10.1097/YCO.0000000000000862

Greenmyer, J. R., Klug, M. G., Kambeitz, C., Popova, S., and Burd, L. (2018). A multicountry updated assessment of the economic impact of fetal alcohol spectrum disorder: costs for psychiatry children and adults. *J. Addict. Med.* 12, 466–473. doi: 10.1097/ADM.0000000000000438

Guerri, C., Bazinet, A., and Riley, E. P. (2009). Foetal alcohol spectrum disorders and alterations in brain and behaviour. *Alcohol Alcohol.* 44, 108–114. doi: 10.1093/alcalc/agn105

Gursky, Z. H., Savage, L. M., and Klintsova, A. Y. (2021). Executive functioning-specific behavioral impairments in a rat model of human third trimester binge drinking implicate prefrontal-thalamo-hippocampal circuitry in fetal alcohol Spectrum disorders. *Behav. Brain Res.* 405:113208. doi: 10.1016/j.bbr.2021.113208

Harris, A. Z., Atsak, P., Bretton, Z. H., Holt, E. S., Alam, R., Morton, M. P., et al. (2018). A novel method for chronic social defeat stress in female mice. *Neuropsychopharmacology* 43, 1276–1283. doi: 10.1038/npp.2017.259

Hellemans, K. G. C., Verma, P., Yoon, E., Yu, W., and Weinberg, J. (2008). Prenatal alcohol exposure increases vulnerability to stress and anxiety-like disorders in adulthood. *Ann. N. Y. Acad. Sci.* 1144, 154–175. doi: 10.1196/annals.1418.016

Hellemans, K. G. C., Verma, P., Yoon, E., Yu, W. K., Young, A. H., and Weinberg, J. (2010). Prenatal alcohol exposure and chronic mild stress differentially alter depressive- and anxiety-like behaviors in male and female offspring. *Alcohol. Clin. Exp. Res.* 34, 633–645. doi: 10.1111/j.1530-0277.2009.01132.x

Heroux, N. A., Robinson-Drummer, P. A., Kawan, M., Rosen, J. B., and Stanton, M. E. (2019). Neonatal ethanol exposure impairs long-term context memory formation and prefrontal immediate early gene expression in adolescent rats. *Behav. Brain Res.* 359, 386–395. doi: 10.1016/j.bbr.2018.11.018

Hoffman, K. L. (2016). *Modeling neuropsychiatric disorders in laboratory animals*, 35–86.

Hoyme, H. E., Kalberg, W. O., Elliott, A. J., Blankenship, J., Buckley, D., Marais, A. S., et al. (2016). Updated clinical guidelines for diagnosing fetal alcohol spectrum disorders. *Pediatrics* 138. doi: 10.1542/peds.2015-4256

Jagodzinski, T., and Fleming, M. F. (2007). Postpartum and alcohol-related factors associated with the relapse of risky drinking. *J. Stud. Alcohol Drugs* 68, 879–885. doi: 10.15288/jsad.2007.68.879

Joshi, V., Subbanna, S., Shivakumar, M., and Basavarajappa, B. S. (2019). CB1R regulates CDK5 signaling and epigenetically controls Rac1 expression contributing to neurobehavioral abnormalities in mice postnatally exposed to ethanol. *Neuropsychopharmacology* 44, 514–525. doi: 10.1038/s41386-018-0181-y

Kasten, C. R., Carzoli, K. L., Sharfman, N. M., Henderson, T., Holmgren, E. B., Lerner, M. R., et al. (2020). Adolescent alcohol exposure produces sex differences in negative affect-like behavior and group I mGluR BNST plasticity. *Neuropsychopharmacology* 45, 1306–1315. doi: 10.1038/s41386-020-0670-7

Kelly, S. J., Dillingham, R. R., and Dillingham, R. R. (1994). Sexually dimorphic effects of perinatal alcohol exposure on social interactions and amygdala DNA and DOPAC concentrations. *Neurotoxicol. Teratol.* 16, 377–384. doi: 10.1016/0892-0362(94)90026-4

Koob, G. F., Arends, M. A., and Le Moal, M. (2014). Cellular mechanisms of liver fibrosis. *Front. Pharmacol.* 12:671640. doi: 10.1016/B978-0-12-386937-1.00006-4

Kully-Martens, K., Denys, K., Treit, S., Tamana, S., and Rasmussen, C. (2012). A review of social skills deficits in individuals with fetal alcohol Spectrum disorders and prenatal alcohol exposure: profiles, mechanisms, and interventions. *Alcohol. Clin. Exp. Res.* 36, 568–576. doi: 10.1111/j.1530-0277.2011.01661.x

Lehmann, M. L., Geddes, C. E., Lee, J. L., and Herkenham, M. (2013). Urine scent marking (USM): a novel test for depressive-like behavior and a predictor of stress resiliency in mice. *PLoS One* 8:e69822. doi: 10.1371/journal.pone.0069822

Little, R. E., Lambert, M. D., and Worthington-Roberts, B. (1990). Drinking and smoking at 3 months postpartum by lactation history. *Paediatr. Perinat. Epidemiol.* 4, 290–302. doi: 10.1111/j.1365-3016.1990.tb00653.x

Liu, M. Y., Yin, C. Y., Zhu, L. J., Zhu, X. H., Xu, C., Luo, C. X., et al. (2018). Sucrose preference test for measurement of stress-induced anhedonia in mice. *Nat. Protoc.* 13, 1686–1698. doi: 10.1038/s41596-018-0011-z

Lopatynska-Mazurek, M., Antolak, A., Grochecki, P., Gibula-tarlowska, E., Bodzon-kulakowska, A., Listos, J., et al. (2021a). Rapamycin improves spatial learning deficits, vulnerability to alcohol addiction and altered expression of the glun2b subunit of the nmda receptor in adult rats exposed to ethanol during the neonatal period. *Biomol. Ther.* 11, 1–23. doi: 10.3390/biom11050650

Lopatynska-Mazurek, M., Komsta, L., Gibula-tarlowska, E., and Kotlinska, J. H. (2021b). Aversive learning deficits and depressive-like behaviors are accompanied by an increase in oxidative stress in a rat model of fetal alcohol spectrum disorders: the protective effect of rapamycin. *Int. J. Mol. Sci.* 22. doi: 10.3390/ijms22137083

Maier, S. E., and West, J. R. (2001). Drinking patterns and alcohol-related birth defects. *Alcohol Res. Heal.* 25, 168–174.

Marlin, B. J., Mitre, M., D'Amour, J. A., Chao, M. V., and Froemke, R. C. (2015). Oxytocin enables maternal behaviour by balancing cortical inhibition. *Nature* 520, 499–504. doi: 10.1038/nature14402

Marquardt, K., and Brigman, J. L. (2016). The impact of prenatal alcohol exposure on social, cognitive and affective behavioral domains: insights from rodent models. *Alcohol* 51, 1–15. doi: 10.1016/j.alcohol.2015.12.002

Marquardt, K., Sigdel, R., Caldwell, K., and Brigman, J. L. (2014). Prenatal ethanol exposure impairs executive function in mice into adulthood. *Alcohol. Clin. Exp. Res.* 38, 2962–2968. doi: 10.1111/acer.12577

Mattson, S. N., Bernes, G. A., and Doyle, L. R. (2019). Fetal alcohol Spectrum disorders: a review of the neurobehavioral deficits associated with prenatal alcohol exposure. *Alcohol. Clin. Exp. Res.* 43, 1046–1062. doi: 10.1111/acer.14040

Mattson, S. N., Crocker, N., and Nguyen, T. T. (2011). Fetal alcohol spectrum disorders: neuropsychological and behavioral features. *Neuropsychol. Rev.* 21, 81–101. doi: 10.1007/s11065-011-9167-9

Mattson, S. N., and Riley, E. P. (1998). A review of the neurobehavioral deficits in children with fetal alcohol syndrome or prenatal exposure to alcohol. *Alcohol. Clin. Exp. Res.* 22, 279–294. doi: 10.1111/j.1530-0277.1998.tb03651.x

May, P. A., Baete, A., Russo, J., Elliott, A. J., Blankenship, J., Kalberg, W. O., et al. (2014). Prevalence and characteristics of fetal alcohol Spectrum disorders. *Pediatrics* 134, 855–866. doi: 10.1542/peds.2013-3319

May, P. A., Brooke, L., Gossage, J. P., Croxford, J., Adnams, C., Jones, K. L., et al. (2000). Epidemiology of fetal alcohol syndrome in a south African community in the Western Cape Province. *Am. J. Public Health* 90, 1905–1912. doi: 10.2105/AJPH.90.12.1905

May, P. A., and Gossage, J. P. (2011). Maternal risk factors for fetal alcohol spectrum disorders: not as simple as it might seem. *Alcohol Res. Heal.* 34, 15–26.

May, P. A., Hasken, J. M., Hooper, S. R., Hedrick, D. M., Jackson-Newsom, J., Mullis, C. E., et al. (2021). Estimating the community prevalence, child traits, and maternal risk factors of fetal alcohol spectrum disorders (FASD) from a random sample of school children. *Drug Alcohol Depend.* 227:108918. doi: 10.1016/j.drugalcdep.2021.108918

May, P. A., Tabachnick, B., Hasken, J. M., Marais, A. S., de Vries, M. M., Barnard, R., et al. (2017). Who is most affected by prenatal alcohol exposure: boys or girls? *Drug Alcohol Depend.* 177, 258–267. doi: 10.1016/j.drugalcdep.2017.04.010

Mcgivern, R. F., Raum, W. J., Handa, R. J., and Sokol, R. Z. (1992). Comparison of two weeks versus one week of prenatal ethanol exposure in the rat on gonadal organ weights,

sperm count, and onset of puberty. *Neurotoxicol. Teratol.* 14, 351–358. doi: 10.1016/0892-0362(92)90042-9

Meyer, L. S., and Riley, E. P. (1986). Social play in juvenile rats prenatally exposed to alcohol. *Teratology* 34, 1–7. doi: 10.1002/tera.1420340102

Muggli, E., O'Leary, C., Donath, S., Orsini, F., Forster, D., Anderson, P. J., et al. (2016). Did you ever drink more? A detailed description of pregnant women's drinking patterns. *BMC Public Health* 16:683. doi: 10.1186/s12889-016-3354-9

O'Leary-Moore, S. K., McMechan, A. P., Mathison, S. N., Berman, R. F., and Hannigan, J. H. (2006). Reversal learning after prenatal or early postnatal alcohol exposure in juvenile and adult rats. *Alcohol* 38, 99–110. doi: 10.1016/j.alcohol.2006.05.005

Olguin, S. L., Zimmerman, A., Zhang, H., Allan, A., Caldwell, K. C., and Brigman, J. L. (2019). Increased maternal care rescues altered reinstatement responding following moderate prenatal alcohol exposure. *Alcohol. Clin. Exp. Res.* 43, 1949–1956. doi: 10.1111/acer.14149

Oubraim, S., Wang, R., Hausknecht, K., Kaczocha, M., Shen, R. Y., and Haj-Dahmane, S. (2022). Prenatal ethanol exposure causes anxiety-like phenotype and alters synaptic nitric oxide and endocannabinoid signaling in dorsal raphe nucleus of adult male rats. *Transl. Psychiatry* 12, 440–412. doi: 10.1038/s41398-022-02210-7

Palmeter, S., Probert, A., and Lagacé, C. (2021). At-a-glance: fasd prevalence among children and youth: results from the 2019 Canadian health survey on children and youth. *Heal. Promot. Chronic Dis. Prev. Canada* 41, 272–276. doi: 10.24095/HPCDP.41.9.05

Patra, J., Bakker, R., Irving, H., Jaddoe, V. W. V., Malini, S., and Rehm, J. (2011). Dose-response relationship between alcohol consumption before and during pregnancy and the risks of low birthweight, preterm birth and small for gestational age (SGA)-a systematic review and meta-analyses. *BJOG An Int. J. Obstet. Gynaecol.* 118, 1411–1421. doi: 10.1111/j.1471-0528.2011.03050.x

Pei, J., Denys, K., Hughes, J., and Rasmussen, C. (2011). Mental health issues in fetal alcohol spectrum disorder. *J. Ment. Health* 20, 473–483. doi: 10.3109/09638237.2011.577113

Pizzagalli, D. A., Iosifescu, D., Hallett, L. A., Ratner, K. G., and Fava, M. (2008). Reduced hedonic capacity in major depressive disorder: evidence from a probabilistic reward task. *J. Psychiatr. Res.* 43, 76–87. doi: 10.1016/j.jpsychires.2008.03.001

Popova, S., Lange, S., Probst, C., Gmel, G., and Rehm, J. (2018). Global prevalence of alcohol use and binge drinking during pregnancy, and fetal alcohol spectrum disorder. *Biochem. Cell Biol.* 96, 237–240. doi: 10.1139/bcb-2017-0077

Porsolt, R. D., Anton, G., Blavet, N., and Jalfre, M. (1978). Behavioural despair in rats: a new model sensitive to antidepressant treatments. *Eur. J. Pharmacol.* 47, 379–391. doi: 10.1016/0014-2999(78)90118-8

Pryce, C. R., Azzinnari, D., Sigrist, H., Gschwind, T., Lesch, K. P., and Seifritz, E. (2012). Establishing a learned-helplessness effect paradigm in C57BL/6 mice: behavioural evidence for emotional, motivational and cognitive effects of aversive uncontrollability per se. *Neuropharmacology* 62, 358–372. doi: 10.1016/j.neuropharm.2011.08.012

Rein, B., Ma, K., and Yan, Z. (2020). A standardized social preference protocol for measuring social deficits in mouse models of autism. *Nat. Protoc.* 15, 3464–3477. doi: 10.1038/s41596-020-0382-9

Riley, E. P., Infante, M. A., and Warren, K. R. (2011). Fetal alcohol spectrum disorders: an overview. *Neuropsychol. Rev.* 21, 73–80. doi: 10.1007/s11065-011-9166-x

Risbud, R. D., Breit, K. R., and Thomas, J. D. (2022). Early developmental alcohol exposure alters behavioral outcomes following adolescent re-exposure in a rat model. *Alcohol. Clin. Exp. Res.* 46, 1993–2009. doi: 10.1111/acer.14950

Rouzer, S. K., Cole, J. M., Johnson, J. M., Varlinskaya, E. I., and Diaz, M. R. (2017). Moderate maternal alcohol exposure on gestational day 12 impacts anxiety-like behavior in offspring. *Front. Behav. Neurosci.* 11, 1–13. doi: 10.3389/fnbeh.2017.00183

Rouzer, S. K., and Diaz, M. R. (2022). Moderate prenatal alcohol exposure modifies sex-specific CRFR1 activity in the central amygdala and anxiety-like behavior in adolescent offspring. *Neuropsychopharmacology* 47, 2140–2149. doi: 10.1038/s41386-022-01327-z

Sanchez Vega, M. C., Chong, S., and Burne, T. H. J. (2013). Early gestational exposure to moderate concentrations of ethanol alters adult behaviour in C57BL/6J mice. *Behav. Brain Res.* 252, 326–333. doi: 10.1016/j.bbr.2013.06.003

Seligman, M. E. P. (1972). Learned helplessness. *Annu. Rev. Med.* 23, 407–412. doi: 10.1146/annurev.me.23.020172.002203

Semple, B. D., Blomgren, K., Gimlin, K., Ferriero, D. M., and Noble-Haeusslein, L. J. (2013). Brain development in rodents and humans: identifying benchmarks of maturation and vulnerability to injury across species. *Prog. Neurobiol.* 106-107, 1–16. doi: 10.1016/j.pneurobio.2013.04.001

Shivakumar, M., Subbanna, S., Joshi, V., and Basavarajappa, B. S. (2021). Postnatal ethanol exposure activates hdacmediated histone deacetylation, impairs synaptic plasticity gene expression and behavior in mice. *Int. J. Neuropsychopharmacol.* 23, 324–338. doi: 10.1093/IJNP/PYAA017

Subbanna, S., Nagre, N. N., Shivakumar, M., Joshi, V., Psychoyos, D., Kutlar, A., et al. (2018). CB1R-mediated activation of caspase-3 causes epigenetic and neurobehavioral abnormalities in postnatal ethanol-exposed mice. *Front. Mol. Neurosci.* 11, 1–20. doi: 10.3389/fnmol.2018.00045

Subramanian, M. G. (1992). Lactation and prolactin release in Foster dams suckling prenatally ethanol exposed pups. *Alcohol. Clin. Exp. Res.* 16, 891–894. doi: 10.1111/j.1530-0277.1992.tb01888.x

Terasaki, L. S., Gomez, J., and Schwarz, J. M. (2016). An examination of sex differences in the effects of early-life opiate and alcohol exposure. *Philos. Trans. R. Soc. B Biol. Sci.* 371:20150123. doi: 10.1098/rstb.2015.0123

Traccis, F., Frau, R., and Melis, M. (2020). Gender differences in the outcome of offspring prenatally exposed to drugs of abuse. *Front. Behav. Neurosci.* 14. doi: 10.3389/fnbeh.2020.00072

Verharen, J. P. H., Kentrop, J., Vanderschuren, L. J. M. J., and Adan, R. A. H. (2019). Reinforcement learning across the rat estrous cycle. *Psychoneuroendocrinology* 100, 27–31. doi: 10.1016/j.psyneuen.2018.09.016

Walf, A. A., and Frye, C. A. (2007). The use of the elevated plus maze as an assay of anxiety-related behavior in rodents. *Nat. Protoc.* 2, 322–328. doi: 10.1038/nprot.2007.44

Yang, M., Silverman, J. L., and Crawley, J. N. (2011). Automated three-chambered social approach task for mice. *Curr. Protoc. Neurosci.* 56:Unit 8.26. doi: 10.1002/0471142301.ns0826s56

Yu, Y., Xu, D., Cheng, S., Zhang, L., Shi, Z., Qin, J., et al. (2020). Prenatal ethanol exposure enhances the susceptibility to depressive behavior of adult offspring rats fed a high-fat diet by affecting BDNF-associated pathway. *Int. J. Mol. Med.* 45, 365–374. doi: 10.3892/ijmm.2019.4436

frontiers | Frontiers in Neuroscience

TYPE Original Research
PUBLISHED 02 June 2023
DOI 10.3389/fnins.2023.1174165

Check for updates

OPEN ACCESS

EDITED BY
Paola A. Haeger,
Catholic University of the North, Chile

REVIEWED BY
Daniele Corbo,
University of Brescia, Italy
Christopher D. Kroenke,
Oregon Health & Science University,
United States

*CORRESPONDENCE
Catherine Lebel
✉ clebel@ucalgary.ca

RECEIVED 25 February 2023
ACCEPTED 09 May 2023
PUBLISHED 02 June 2023

CITATION
Ostertag C, Reynolds JE, Kar P, Dewey D, Gibbard WB, Tortorelli C and Lebel C (2023) Arcuate fasciculus and pre-reading language development in children with prenatal alcohol exposure.
Front. Neurosci. 17:1174165.
doi: 10.3389/fnins.2023.1174165

COPYRIGHT
© 2023 Ostertag, Reynolds, Kar, Dewey, Gibbard, Tortorelli and Lebel. This is an open-access article distributed under the terms of the Creative Commons Attribution License (CC BY). The use, distribution or reproduction in other forums is permitted, provided the original author(s) and the copyright owner(s) are credited and that the original publication in this journal is cited, in accordance with accepted academic practice. No use, distribution or reproduction is permitted which does not comply with these terms.

Arcuate fasciculus and pre-reading language development in children with prenatal alcohol exposure

Curtis Ostertag[1,2], Jess E. Reynolds[2,3,4], Preeti Kar[1,2], Deborah Dewey[2,3,5,6], W. Ben Gibbard[2,5], Christina Tortorelli[7] and Catherine Lebel[2,3,8]*

[1]Cumming School of Medicine, University of Calgary, Calgary, AB, Canada, [2]Alberta Children's Hospital Research Institute, University of Calgary, Calgary, AB, Canada, [3]Hotchkiss Brain Institute, University of Calgary, Calgary, AB, Canada, [4]Telethon Kids Institute, The University of Western Australia, Perth, WA, Australia, [5]Department of Pediatrics, University of Calgary, Calgary, AB, Canada, [6]Department of Community Health Sciences, University of Calgary, Calgary, AB, Canada, [7]Department of Social Work, Mount Royal University, Calgary, AB, Canada, [8]Department of Radiology, University of Calgary, Calgary, AB, Canada

Introduction: Prenatal alcohol exposure (PAE) contributes to widespread neurodevelopmental challenges, including reading, and has been associated with altered white matter. Here, we aimed to investigate whether arcuate fasciculus (AF) development is associated with pre-reading language skills in young children with PAE.

Methods: A total of 51 children with confirmed PAE (25 males; 5.6 ± 1.1 years) and 116 unexposed controls (57 males; 4.6 ± 1.2 years) underwent longitudinal diffusion tensor imaging (DTI), for a total of 111 scans from participants with PAE and 381 scans in the unexposed control group. We delineated the left and right AF and extracted mean fractional anisotropy (FA) and mean diffusivity (MD). Pre-reading language ability was assessed using age-standardized phonological processing (PP) and speeded naming (SN) scores of the NEPSY-II. Linear mixed effects models were run to determine the relationship between diffusion metrics and age, group, sex, and age-by-group interactions, with subject modeled as a random factor. A secondary mixed effect model analysis assessed the influence of white matter microstructure and PAE on pre-reading language ability using diffusion metric-by-age-by-group interactions, with 51 age- and sex-matched unexposed controls.

Results: Phonological processing (PP) and SN scores were significantly lower in the PAE group ($p < 0.001$). In the right AF, there were significant age-by-group interactions for FA ($p < 0.001$) and MD ($p = 0.0173$). In the left AF, there was a nominally significant age-by-group interaction for MD that failed to survive correction ($p = 0.0418$). For the pre-reading analysis, a significant diffusion-by-age-by-group interaction was found for left FA ($p = 0.0029$) in predicting SN scores, and for the right FA ($p = 0.00691$) in predicting PP scores.

Discussion: Children with PAE showed altered developmental trajectories for the AF, compared with unexposed controls. Children with PAE, regardless of age, showed altered brain-language relationships that resembled those seen in

younger typically developing children. Our findings support the contention that altered developmental trajectories in the AF may be associated with functional outcomes in young children with PAE.

KEYWORDS

prenatal alcohol exposure, FASD, MRI, development, children, language, magnetic resonance imaging

1. Introduction

Prenatal alcohol exposure (PAE) contributes to widespread neurodevelopmental and health challenges including cognitive and behavioral deficits, growth deficiencies, and/or craniofacial abnormalities (Cook et al., 2016; Mattson et al., 2019). Children who experience complex impacts of PAE may go on to be diagnosed with fetal alcohol spectrum disorder (FASD), which has an estimated prevalence of approximately 4% in North America (Cook et al., 2016; Flannigan et al., 2018; May et al., 2018; Popova et al., 2019).

Previous diffusion magnetic resonance imaging (dMRI) studies have reported extensive alterations to white matter microstructure in school-aged children, youth, and young adults with PAE (Lebel et al., 2008; Donald et al., 2015a; Ghazi Sherbaf et al., 2019), including lower fractional anisotropy (FA) and higher mean diffusivity (MD) compared to unexposed controls (Ghazi Sherbaf et al., 2019). These findings appear to be reversed in younger children, with higher FA and/or lower diffusivity in young children and infants with PAE compared to unexposed controls (Donald et al., 2015b; Kar et al., 2021). There are few longitudinal neuroimaging studies of PAE; however, they suggest that patterns of brain development are also altered in children with PAE, with slower maturation seen in young children (Kar et al., 2022) and faster development in older children (Treit et al., 2013). Longitudinal research is critical to capture the nuances of brain development during early childhood, which is a period of rapid brain growth (Lebel and Deoni, 2018). A better understanding of brain development at early ages may help identify sensitive periods for targeted interventions in children with PAE.

Prenatal alcohol exposure (PAE) negatively impacts cognitive and behavioral domains of functioning, including but not limited to general intelligence, motor skills, attention, executive function, learning, memory, and language (Mattson et al., 2019). Language and reading are areas of particular interest as deficits emerge during early childhood and can significantly influence social and educational outcomes. Worse receptive and expressive language abilities have been noted in children with FASD, and linked to problems with learning (Wyper and Rasmussen, 2011). Children and adolescents with PAE show deficits in reading comprehension and verbal fluency (O'Leary et al., 2013; Lindinger et al., 2022). A recent study showed comparable single word reading and phonological processing (PP) skills in adolescents with FASD compared to controls, but poorer reading comprehension, suggesting that even though the mechanics of reading may be intact at older ages in individuals with FASD, comprehension continues to be a problem (Lindinger et al., 2022).

In typically developing children, reading is supported by a network of left-lateralized brain regions in frontal, parietal, and temporal areas, including the Sylvian-parietal-temporal (SPT) area (Hickok and Poeppel, 2007; Buchsbaum and D'Esposito, 2008). These regions are connected by white matter tracts, which enable communication among regions and facilitate reading (Pugh et al., 2001; Vandermosten et al., 2012). White matter tracts classically associated with reading include the superior longitudinal fasciculus (SLF), inferior longitudinal fasciculus (ILF), inferior fronto-occipital fasciculus (IFOF), corona radiata, and uncinate fasciculus (UF) (Vandermosten et al., 2012; Lebel et al., 2019a; Meisler and Gabrieli, 2022). Another important region is the arcuate fasciculus (AF), a subdivision of the SLF, which is a white matter tract that plays a critical role in language processing, connecting the speech comprehension (Wernicke's) area in the posterior temporal lobe to the speech production (Broca's) area in the frontal lobe (Hickok and Poeppel, 2004). In conjunction with the SPT area, it maps sound-motor integration and supports phonological aspects of reading and speech (Vigneau et al., 2006), making it an interesting target of study in the context of PAE. In the AF of typically developing children, FA increases with age while MD decreases with age (Reynolds et al., 2019b). Notably, AF macrostructure is left lateralized in adults and typically developing children as young as 2 years of age (Lebel and Beaulieu, 2009; Qiu et al., 2011; Reynolds et al., 2019b), whereas functional and microstructural lateralization of the AF appear to develop more gradually across childhood (Reynolds et al., 2019b). FA, MD, and lateralization of the AF have all been linked to reading skills in school-aged children (Lebel and Beaulieu, 2009; Cheema et al., 2018). Similar relationships have also been observed in younger children, with AF microstructure linked to pre-reading language skills (Saygin et al., 2013; Reynolds et al., 2019b).

The neural correlates of reading and language difficulties in individuals with PAE are not well understood. One fMRI study found greater activation in the right precentral gyrus during PP tasks, as well as more rightward lateralization of FA in the ILF in children and adolescents with FASD compared to children with PAE but without FASD diagnoses or typically developing controls (Yu et al., 2022); however, they found no group differences in arcuate or SLF FA. Studies of the whole SLF (including the arcuate) report no microstructural differences (Kar et al., 2021) or lower FA compared to unexposed controls (Lebel et al., 2008). These varying results suggest that the AF requires further study to pinpoint microstructural abnormalities and to better understand how they may relate to reading difficulties in children with FASD. This is especially important to understand in early childhood as pre-reading skills develop rapidly

and lay the foundation for later reading acquisition (Lonigan et al., 2000). Understanding the microstructural development of the AF and how this is associated with pre-reading skills in children with PAE will help in identifying the neurobiological correlates of reading difficulties in FASD and when they emerge.

The dynamic nature of brain maturation, especially during early childhood, makes longitudinal studies of white matter development critical in connecting brain alterations to functional outcomes in PAE. Early childhood is especially important to understand, as it is a time when many difficulties associated with PAE first become apparent, yet it remains largely unexplored in neuroimaging studies of PAE (Donald et al., 2015a). This study aimed to characterize development of AF microstructure in young children with PAE, and investigate its relationship to pre-reading language skills, using longitudinal MR imaging.

2. Materials and methods

2.1. Participants with PAE

A total of 57 children between 2 and 7 years of age with PAE were recruited through caregiver support groups, early intervention services, and the Ministry of Children's Services in Alberta, Canada. Exclusion criteria were: birth before 34 weeks' gestation, English not a primary language for the child, a history of head trauma, a diagnosis of autism spectrum disorder, cerebral palsy, epilepsy or any other medical or genetic disorder associated with serious motor or cognitive disability, and contraindications to MRI (e.g., metal implants, dental braces). Children with attention deficit hyperactivity disorder, learning disabilities, language delays, and/or mental health diagnoses were included, as these diagnoses are frequently comorbid with PAE. No participants had been diagnosed with FASD, as most clinics in Alberta do not assess children for FASD until age 7 years. Of the 57 children recruited, one was excluded for an incidental finding on MRI, 2 children did not feel comfortable participating in MRI scanning, and 3 children were excluded at analysis due to our inability to delineate the left and right arcuate. The final sample included in the analysis consists of 51 children (25 males/26 females; mean age for all scans: 5.65 ± 1.11 years) who provided a total of 111 diffusion tensor imaging (DTI) scans (2.2 ± 0.9 scans/participant); age at scan ranged from 3.13 to 8.07 years. The mean age at first scan was 5.3 ± 1.1 years. The distribution of number of scans per participant was as follows: 14 participants with 1 scan, 17 participants with 2 scans, 17 participants with 3 scans, and 3 participants with 4 scans (**Figure 1**). Other neuroimaging results from these children have been published previously (Kar et al., 2021, 2022).

All participants had PAE confirmed via medical, legal, or child welfare files, as well as interviews with biological and/or adoptive/foster families. A total of 33% (n = 17) of participants had confirmed PAE greater than or equal to the threshold indicated by the Canadian guidelines for diagnosing FASD (Cook et al., 2016): ≥ 7 drinks in 1 week and/or two or more binge episodes (≥ 4 drinks at one time) during pregnancy. A total of 67% (n = 34) had confirmed PAE of an unspecified amount.

2.2. Control participants

Typically developing participants were part of the Calgary Preschool MRI Study (Reynolds et al., 2020) and were recruited from Calgary and surrounding areas, as well as the Alberta Pregnancy Outcomes and Nutrition (APrON) study (Kaplan et al., 2014; Letourneau et al., 2022). Inclusion criteria were born > 36 weeks' gestation, English as the primary language, no contraindications to MRI scans, and no history of developmental disorders or brain trauma. From this cohort, there were 381 high quality scans in 116 participants (3.3 ± 2.7 scans/participant) ranging from 1.95 to 7.63 years (mean age for all scans: 4.61 ± 1.20 years). The mean age at first scan was 4.0 ± 1.0 years. The distribution of numbers of scans per participant ranged from 1 to 20 and is as follows: 39 participants with 1 scan, 22 participants with 2 scans, 8 participants with 3 scans, 11 participants with 4 scans, 14 participants with 5 scans, 12 participants with 6 scans, 8 participants with 7 scans, 1 participant with 12 scans, and 1 participant with 20 scans (**Figure 1**). Unexposed control participants had confirmed absence of PAE based on prospective questionnaires and interviews completed with the mothers during pregnancy that asked directly about alcohol consumption.

Parent/guardian written informed consent and child verbal assent were obtained for each participant. The University of Calgary Conjoint Health Research Ethics Board (CHREB) approved this study (REB14-2266, REB13-020).

2.3. Language assessments

Participants ≥ 3 years completed the PP and speeded naming (SN) subtests of the NEPSY-II (Korkman et al., 2007) at each MRI scan timepoint. Phonological processing (PP) Standard scores and SN Combined Scaled Scores were used for analysis. The population means for standard scores are 10, with scores below the 26th percentile (score of 8), reflecting deficits (Korkman et al., 2007).

2.4. MRI image acquisition

All imaging was conducted using the same General Electric 3T MR750w system and 32-channel head coil at the Alberta Children's Hospital, Calgary, Canada. Children were scanned either while awake and watching a movie of their choice or while sleeping without sedation. Foam padding was used to minimize head motion. Prior to scanning, parents were provided with detailed information of MRI procedures and were invited to an optional practice MRI session in an MRI mock scanner to familiarize the child with the scanning environment (Thieba et al., 2018). Whole-brain diffusion weighted images were acquired in 4:03 min using single shot spin echo echo-planar imaging sequence with: 1.6 mm × 1.6 mm × 2.2 mm resolution (resampled to 0.78 mm × 0.78 mm × 2.2 mm on scanner), TR = 6,750 ms; TE = 79 ms, 30 gradient encoding directions at b = 750 s/mm^2, and 5 interleaved images without diffusion encoding at b = 0 s/mm^2.

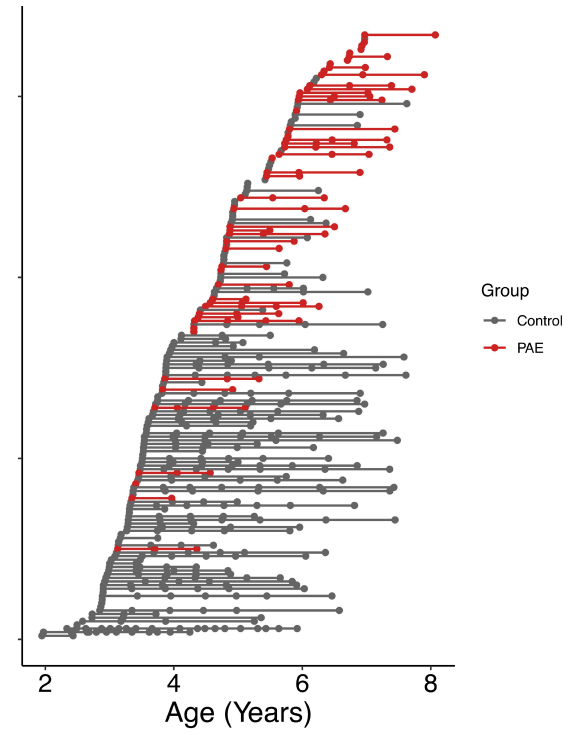


FIGURE 1
Age at MRI scans for all participants. Each row shows a different individual participant, ordered by age at first scan. Data points from the same participant are connected by a line. The PAE group is shown in red, and the unexposed control group is shown in gray.

TABLE 1 Participant characteristics for growth trajectories.

	PAE (n = 51; 111 datasets)	Control (n = 116; 381 datasets)	p
Mean age at first scan (years)	5.27 ± 1.06	3.97 ± 1.03	<0.001
Mean age across all scans (years)	5.65 ± 1.11	4.61 ± 1.20	<0.001
Age range (years)	3.13–8.07	1.95–7.63	
Mean number of scans per participant	2.18 ± 0.91	3.28 ± 2.71	0.005
Sex	25 M/26 F	57 M/59 F	0.828

PAE, prenatal alcohol exposure.

TABLE 2 Participant characteristics for the pre-reading language analysis subset.

	PAE (n = 51; 111 datasets)	Control (n = 51; 123 datasets)	p
Mean age at first scan (years)	5.27 ± 1.06	5.14 ± 0.99	0.54
Mean age across all scans (years)	5.65 ± 1.11	5.54 ± 1.04	0.42
Age range (years)	3.13–8.07	3.17–7.61	
Mean number of scans per participant	2.18 ± 0.91	2.35 ± 1.26	0.42
Sex	25 M/26 F	25 M/26 F	
Phonological processing std. score	9.94 ± 2.96	11.95 ± 2.66	< 0.001
Speeded naming combined scaled score	10.50 ± 3.26	11.96 ± 2.87	< 0.001

PAE, prenatal alcohol exposure.

2.5. Data processing

Diffusion tensor imaging (DTI) data was visually inspected for quality, and volumes with artifacts or motion corruption were removed, per our previous methods (Walton et al., 2018; Reynolds et al., 2019a). All datasets included in the analysis had ≥ 18 high-quality volumes. Following corrupted volume removal, data was pipelined through ExploreDTI (V4.8.6) for correction for signal drift, Gibbs ringing (non-DWIs), subject motion, and eddy current distortions (Leemans et al., 2009).

Fiber tracking was performed using a deterministic streamline method in ExploreDTI. A minimum FA threshold of 0.20 was set to initiate and continue tracking, with angle threshold set to 30°. Using *a priori* location information on AF anatomy (Wakana et al., 2004; Lebel and Beaulieu, 2009), inclusion and exclusion regions of interest (ROI) were drawn on the left and right hemisphere separately, in each subject, per our previously published methods (Reynolds et al., 2019b). The number of streamlines, and mean values of FA and MD (mm^2/s) were extracted for each tract. FA and MD mean values were calculated by computing an average of all voxels containing a portion of the tract, weighted by the number of streamlines intersecting with each voxel. Tracts with fewer than 10 streamlines were deemed unsuccessful and excluded from analysis. The left arcuate was successfully delineated in 111 of the 122 PAE datasets acquired (91%) and all 381 of the unexposed control datasets (100%). The mean number of streamlines for the left AF was 231 ± 144 in the PAE datasets and 295 ± 169 in the control datasets. The right arcuate could not be delineated in 31 of the 122 PAE datasets (25%) and 38 of the 381 unexposed control datasets (10%). The mean number of streamlines for the right AF was 151 ± 141 in the PAE datasets and 155 ± 122 in the control datasets.

2.6. Statistical analysis

RStudio version 1.4.1106 (R Core Team, 2020) and packages "lme4" (Bates et al., 2015), "lmerTest" (Kuznetsova et al., 2017) and "ggplot2" (Wickham, 2016) were used to carry out statistical analysis and plotting. Two-tailed t-tests were used to test group differences in pre-reading language scores (PP and SN), with a chi-square test used to test the distribution of scores below the < 26th percentile (Korkman et al., 2007) between each group. Linear mixed effects models were run to determine linear age-related changes in FA and MD for the left and right arcuate, as well as an asymmetry index [calculated as: (L-R)/(L + R)]. A positive asymmetry index for FA (higher FA in the left AF) and a negative asymmetry index for MD (lower FA in the left AF) indicate leftward asymmetry. Linear (y = age + sex + group + age*group + [1| Subject]) terms were modeled with age, sex, and age-group interactions as fixed factors

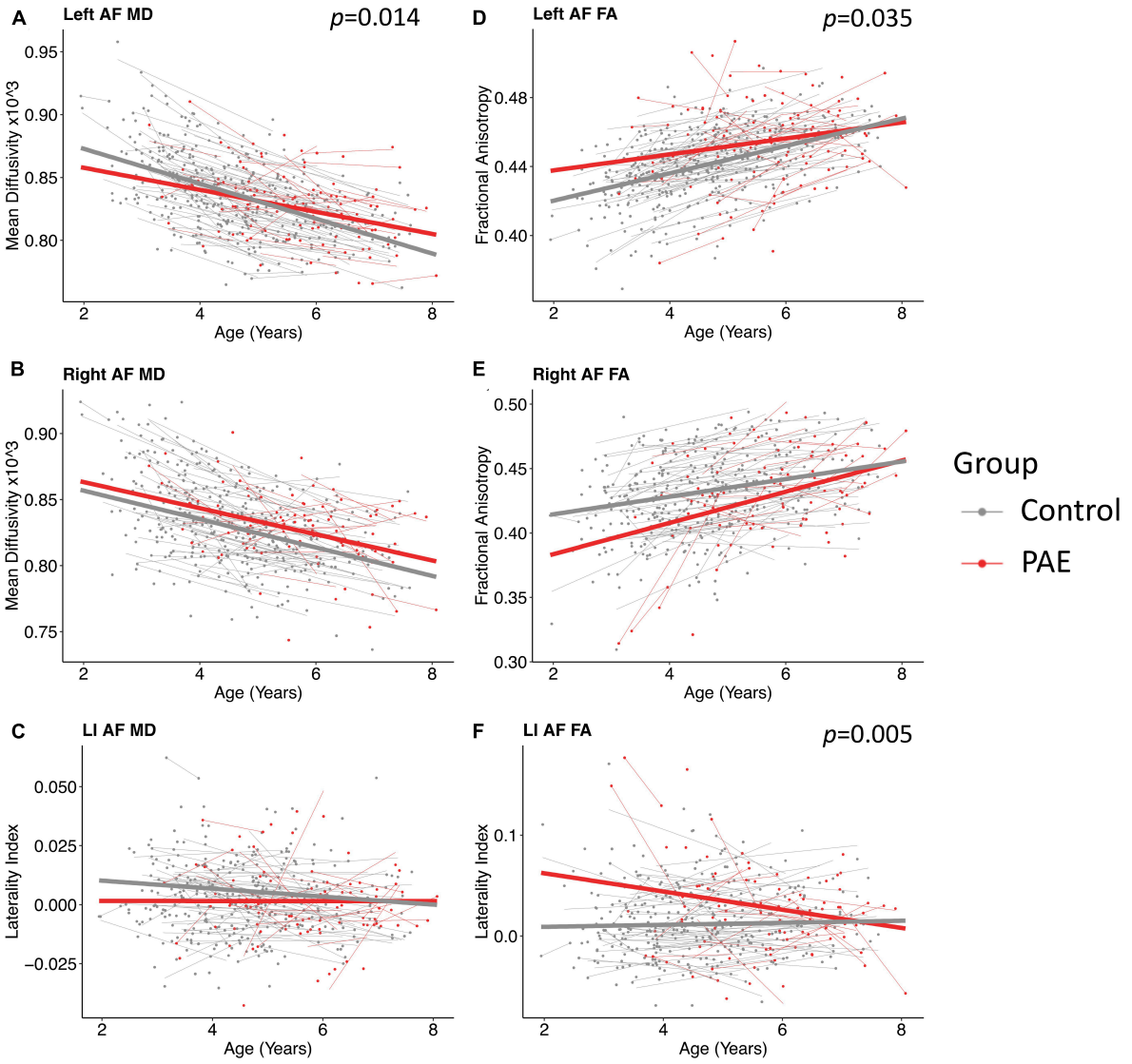


FIGURE 2
Linear growth trajectories for diffusion metrics in PAE and unexposed controls. Plots show individual data points as dots, with individual trajectories shown as thin lines, and the group trajectories displayed with thick lines. The PAE group is shown in red, while the unexposed control group is shown in gray. Plots **(A–C)** show the changes in mean diffusivity (MD) across ages. MD values in plots **(B,C)** are scaled up by 1,000. Plots **(D–F)** show the changes in fractional anisotropy across ages. Plots **(A)** and **(F)** show significant age-group interactions for MD in the left arcuate (p = 0.014; q = 0.043) and laterality index of FA (p = 0.005; q = 0.028), respectively. Plot **(D)** shows a nominally significant age-group interaction for FA in the left arcuate (p = 0.035), which failed to survive FDR correction (q = 0.07).

and subject as a random factor. Restricted maximum likelihood was set to false. The main measure of interest was age-group interactions, which indicates different linear growth trajectories between groups. MD values were scaled by 1,000 to make them like other values for analysis. False discovery rate (FDR) was used to correct for 6 multiple comparisons of interaction terms (2 diffusion parameters for the right and left arcuate, as well as laterality index), with significance set at $q < 0.05$ (Benjamini and Hochberg, 1995).

The NEPSY-II has two different age bands, split at 5 years. The age-standardized scores allow comparisons of children younger and older than 5 years; however, the control and PAE groups differed in their mean age (see above). Therefore, we age-matched groups for analysis of language assessments to ensure balance is maintained across the age bands. A total of 51 typically developing children were matched to the PAE group by age at first scan and sex. This subset of controls had a total of 123 scans (2.4 ± 1.3 scans/participant) ranging from 3.17 to 7.61 years, with a mean age at first scan was 5.1 ± 1.0 years.

We used linear mixed effects models to investigate the association between diffusion metrics (FA/MD), age, and group on pre-reading language ability (PP/SN) (y = diffusion metric + age + sex + group + diffusion metric*age*group + [1| Subject]). PP/SN scores, diffusion metrics, and age were included as continuous variables within the model, while sex and group were categorical. The key outcome of interest was the relationship between diffusion metrics and pre-reading language ability

TABLE 3 Linear mixed effects model parameters for MD.

Mean diffusivity (x10^3 mm^2/s)	Parameter estimate (SE)	*t*	*p* (*q*)
Left AF			
Intercept	0.905 (0.004)	209.112	<2E-16***
Age	−0.014 (0.001)	−19.72	<2E-16***
Sex	−0.010 (0.004)	−2.792	0.006
Group	−0.025 (0.012)	−.063	0.040*
Age*group	0.005 (0.002)	2.46	**0.014* (0.043)**
Right AF			
Intercept	0.884 (0.005)	169.982	<2E-16***
Age	−0.011 (0.001)	−11.948	<2E-16***
Sex	−0.011 (0.004)	−2.773	0.006**
Group	0.005 (0.015)	0.316	0.752
Age*group	0.001 (0.003)	0.335	0.738
Laterality index			
Intercept	0.013 (0.003)	3.518	0.0005***
Age	−0.002 (0.001)	−2.813	0.005**
Sex	0.001 (0.002)	0.545	0.587
Group	−0.012 (0.009)	−1.324	0.186
Age*group	0.002 (0.002)	1.067	0.287

Results are shown for linear mixed models comparing age-related brain changes between children with PAE and unexposed controls. Significant differences in the main effects are shown as: *($p < 0.05$), **($p < 0.01$), ***($p < 0.001$). Significant differences in the age-group interactions that survived multiple comparison ($q < 0.05$) are bolded, with the corresponding *q* value in parentheses. AF, arcuate fasciculus; SE, standard error.

TABLE 4 Linear mixed effects model parameters for FA.

Fractional anisotropy	Parameter estimate (SE)	*t*	*p*
Left AF			
Intercept	0.403 (0.003)	119.413	<2E-16***
Age	0.008 (0.001)	15.512	<2E-16***
Sex	0.002 (0.003)	0.764	0.446
Group	0.024 (0.009)	2.583	0.010*
Age*group	−0.003 (0.002)	−2.110	*0.035*(0.07)*
Right AF			
Intercept	0.397 (0.006)	71.182	<2E-16***
Age	0.007 (0.001)	7.407	1.1E-12***
Sex	0.007 (0.005)	1.575	0.117
Group	−0.042 (0.016)	−2.578	0.010*
Age*group	0.005 (0.003)	1.925	0.055
Laterality index			
Intercept	0.010 (0.007)	1.386	0.167
Age	0.001 (0.001)	0.812	0.418
Sex	−0.006 (0.005)	−1.040	0.300
Group	0.073 (0.021)	3.563	0.0004***
Age*group	−0.010 (0.004)	−2.840	**0.005****(0.028)**

Results are shown for linear mixed models comparing age-related brain changes between children with PAE and unexposed controls. Significant differences in the main effects are shown as: *($p < 0.05$), **($p < 0.01$), ***($p < 0.001$). Significant differences in the age-group interactions that survived multiple comparison correction ($q < 0.05$) are bolded, with the corresponding *q* value in parentheses. Nominally significant age-group interactions that failed to survive multiple comparison correction are italicized, with the corresponding *q* value in parentheses. AF, arcuate fasciculus; SE, standard error.

at different ages. FDR correction was used to correct for 6 comparisons (2 diffusion parameters for the right and left arcuate, as well as laterality index) for both PP and SN models.

For plotting the pre-reading language analysis results, diffusion metrics were residualized for age and sex, and data points were split at age 5 (in accordance with the NEPSY-II age bands) to create 4 main group trajectories: PAE young, PAE old, unexposed young, and unexposed old.

3. Results

3.1. Participant characteristics

Participant characteristics are displayed in Table 1 (for the growth trajectories) and Table 2 (for the pre-reading language analysis subset). The mean PP score was 9.9 ± 3.0 in the PAE group and 12.0 ± 2.7 in the control group. The mean SN score was 10.5 ± 3.3 in the PAE group and 12.0 ± 2.9 in the unexposed control group. PP and SN scores were significantly lower in the PAE group compared to the unexposed controls ($p < 0.001$) (Table 2), though the mean scores in the PAE group are at the population mean (10). The PAE group had a significantly higher proportion of low PP scores (19 vs. 3% of datasets; $p < 0.001$) and low SN scores (19 vs. 7% of datasets; $p = 0.016$) than the controls.

3.2. Growth trajectories

A significant age-group interaction was detected for MD in the left arcuate ($p = 0.014$, $q = 0.043$). There were no significant age-group interactions for MD in the right arcuate ($p = 0.74$) or for the laterality index ($p = 0.29$). For FA, there was a significant age-group interaction for laterality index ($p = 0.005$, $q = 0.028$). There was a nominally significant age-group interaction for FA in the left arcuate ($p = 0.035$) that failed to survive FDR correction ($q = 0.07$). The age-group interaction was not significant for FA in the right arcuate ($p = 0.055$). Growth trajectories are displayed in Figure 2, with model outputs in Tables 3, 4.

Group main effects were significant in several models, including FA in the left arcuate ($p = 0.010$), the right arcuate ($p = 0.010$), and the laterality index ($p = 0.0004$); and MD in the left arcuate ($p = 0.040$). The PAE group showed higher overall FA in the left arcuate and higher (more leftward) FA laterality than controls, with lower FA in the right arcuate and lower MD in the left arcuate.

3.3. Pre-reading language models

There were two significant three-way FA-age-group interactions detected: for PP and the right arcuate ($p = 0.008$, $q = 0.0495$) and for SN and the left arcuate ($p = 0.003$, $q = 0.017$)

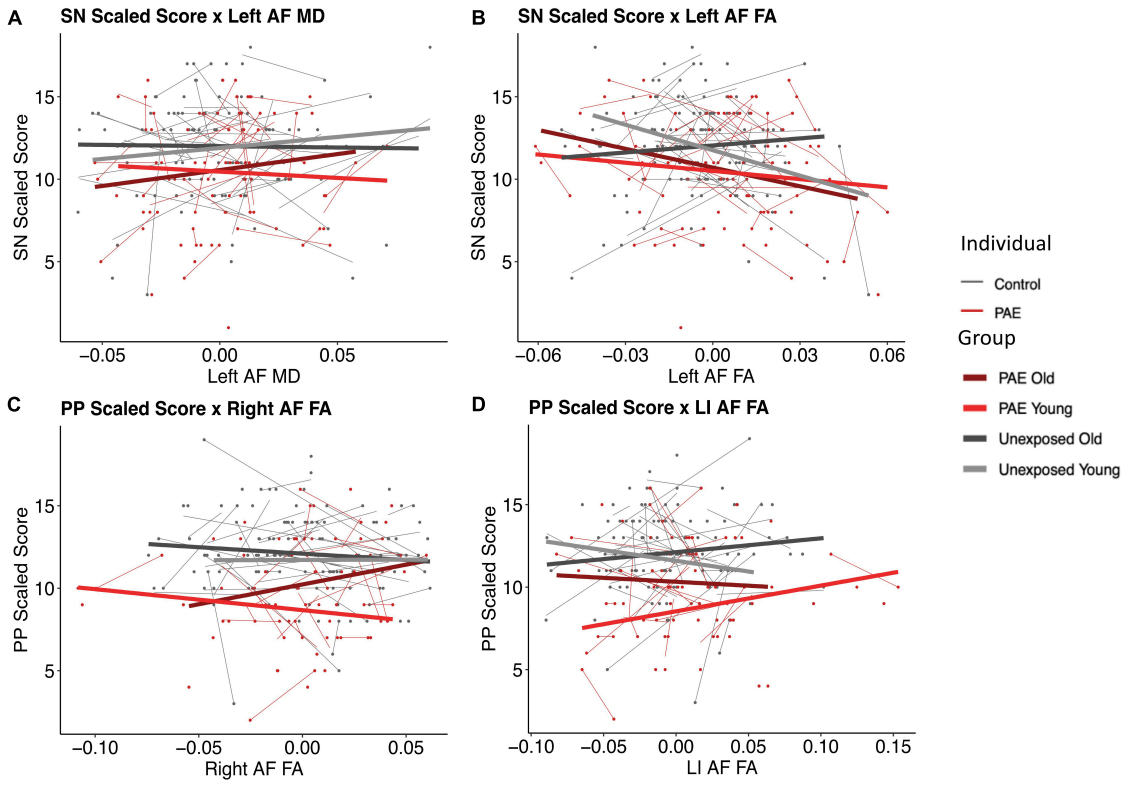


FIGURE 3
Plots of pre-reading scores by diffusion metrics. Diffusion metrics are shown as unstandardized residuals, controlled for age and sex. All plots shown display significant diffusion-age-group interactions. Individual data points are shown as dots, with individual trajectories fit by thin lines (PAE shown in red, unexposed controls shown in gray). Group fits are shown by the thicker lines, with the following color pattern: PAE old (dark red), PAE young (light red), unexposed old (dark gray), and unexposed young (light gray). Participants were split at age 5 to create the young and old plotting groups. Plots **(B)** and **(C)** show significant FA-age-group interactions for SN and the left arcuate (p = 0.003, q = 0.017) and PP and the right arcuate (p = 0.008, q = 0.0495), respectively. Plots **(A)** and **(D)** show nominally significant interactions that failed to survive FDR correction: an MD-age-group interaction for SN and the left arcuate (p = 0.031, q = 0.093) and a laterality index FA-age-group interaction for PP (p = 0.033, q = 0.098), respectively.

(Figure 3). There were two nominally significant interactions that failed to survive FDR correction: a laterality index FA-age-group interaction for PP (p = 0.033, q = 0.098) and an MD-age-group interaction for SN and the left arcuate (p = 0.031, q = 0.093) (Figure 3). All other three-way interactions were non-significant (see Tables 5, 6).

4. Discussion

Here, we show altered developmental trajectories of AF microstructure in young children with PAE compared to unexposed controls. Our study also found reduced pre-reading language abilities in children with PAE compared to unexposed controls. Although both group means are in line with population norms (scores of ~10), deficits (standard scores < 8) were more common in the PAE group.

The PAE group showed slower age-related decreases of MD in the AF than controls (see Tables 5, 6 for model interaction outputs and Supplementary Tables 1, 2 for model main effects). Initially, the PAE group had lower MD values than controls, but controls had steeper decreases of MD, leading to higher MD in the PAE group at the upper end of our age range. This aligns with our prior findings in the genu of the corpus callosum, the UF, the ILF, and the IFOF in the same participants (Kar et al., 2022). A similar pattern of slower development for FA was observed, although not significant, in the left AF. A recent study found no arcuate FA differences in adolescents with PAE-related facial dysmorphology (FASD/partial FASD) or heavy PAE non-FASD-diagnosed adolescents, compared to typically developing adolescents (Yu et al., 2022), perhaps suggesting these differences are more prominent at younger ages. These results are consistent with studies of other children at risk of reading disorders. For example, pre-reading children with a family history of dyslexia have lower FA and reduced leftward lateralization in the arcuate compared to children without a family history of dyslexia (Wang et al., 2017). Further, in both groups, the rate of FA development across the ILF, SLF, and arcuate positively correlated with reading development, suggesting that white matter development plays a role in both typical and atypical reading skill development (Wang et al., 2017). This may suggest children with PAE have similar neural correlates and developmental patterns to children at risk for other disorders associated with reading difficulties.

Lateralization of FA in the AF also showed significant group-by-age interactions. The PAE group began with strong leftward lateralization (higher FA in the left arcuate) and became more

TABLE 5 Phonological processing model interaction outputs.

Phonological processing standard score	Parameter estimate (SE)	*t*	*p* (*q*)
Left AF FA			
FA*age*group	8.34 (14.54)	0.574	0.567
FA*group	−24.35 (78.03)	−0.312	0.755
FA*age	−10.12 (10.51)	−0.962	0.337
Age*group	−3.50 (6.55)	−0.535	0.593
Intercept	−14.51 (24.77)	−0.586	0.559
Left AF MD			
MD*age*group	1.86 (11.88)	0.157	0.875
MD*group	−24.93 (65.06)	−0.383	0.702
MD*age	0.51 (8.43)	0.061	0.952
Age*group	−1.42 (9.86)	−0.144	0.886
Intercept	10.91 (37.52)	0.291	0.772
Right AF FA			
FA*age*group	25.58 (9.58)	2.67	**0.00825****(0.0495)**
FA*group	−125.96 (52.42)	−2.403	0.017*
FA*age	−10.48 (7.02)	−1.493	0.138
Age*group	−10.55 (4.09)	−2.577	0.011**
Intercept	−13.15 (17.22)	−0.764	0.446
Right AF MD			
MD*age*group	−2.30 (11.70)	−0.197	0.844
MD*group	9.71 (64.34)	0.151	0.880
MD*age	3.36 (6.76)	0.498	0.620
Age*group	2.20 (9.71)	0.227	0.821
Intercept	24.73 (31.09)	0.795	0.428
Laterality index FA			
LI*age*group	−18.00 (8.36)	−2.154	*0.0325*(0.0975)*
LI*group	94.12 (46.53)	2.023	0.0446*
LI*age	7.45 (6.65)	1.121	0.264
Age*group	0.94 (0.42)	2.242	0.0261*
Intercept	10.22 (1.56)	6.544	6.97E-10***
Laterality index MD			
LI*age*group	6.87 (23.53)	0.292	0.771
LI*group	−56.45 (126.26)	−0.447	0.655
LI*age	−9.61 (13.97)	−0.7688	0.493
Age*group	0.29 (0.35)	0.848	0.398
Intercept	9.10 (1.29)	7.070	3.46E-11***

Results are shown for the linear mixed effects models that compared diffusion-age-group interactions in predicting PP scores. Only the interaction terms and the intercept are shown. Stars correspond to the following *p*-values: *($p < 0.05$), **($p < 0.01$), ***($p < 0.001$). Significant three-way interactions that survived multiple comparison correction ($q < 0.05$) are bolded, with the corresponding *q* value in parentheses. Nominally significant three-way interactions that failed to survive multiple comparison correction are italicized, with the corresponding *q* value in parentheses. Significant two-way interactions and intercepts are starred, but not bolded, as these were not corrected for. AF, arcuate fasciculus; SE, standard error; FA, fractional anisotropy; MD, mean diffusivity; LI, laterality index.

TABLE 6 Speeded naming model interaction outputs.

Speeded naming combined scaled score	Parameter estimate (SE)	*t*	*p*
Left AF FA			
FA*age*group	−48.79 (16.16)	−3.019	**0.0029****(0.0174)**
FA*group	229.4 (86.73)	2.645	0.0088**
FA*age	43.62 (11.75)	3.714	0.00026***
Age*group	22.43 (7.28)	3.08	0.0023**
Left AF MD			
MD*age*group	29.40 (13.54)	2.172	*0.031*(0.093)*
MD*group	−141.75 (74.23)	−1.91	0.0576
MD*age	−24.24 (9.74)	−2.49	0.0139*
Age*group	−23.67 (11.23)	−2.11	0.0362*
Right AF FA			
FA*age*group	−10.49 (11.08)	−0.948	0.345
FA*group	63.82 (60.59)	1.053	0.294
FA*age	15.61 (8.17)	1.91	0.058
Age*group	5.12 (4.74)	1.081	0.281
Right AF MD			
MD*age*group	16.1 (13.38)	1.203	0.231
MD*group	−83.8 (73.9)	−1.133	0.259
MD*age	−3.7 (7.93)	−0.467	0.641
Age*group	−12.86 (11.11)	−1.158	0.248
Laterality index FA			
LI*age*group	−10.05 (9.75)	−1.031	0.3038
LI*group	37.17 (54.35)	0.685	0.494
LI*age	3.12 (7.79)	0.4	0.689
Age*group	0.77 (0.48)	1.595	0.112
Laterality index MD			
LI*age*group	15.03 (27.07)	0.555	0.579
LI*group	−65.72 (144.85)	−0.454	0.651
LI*age	−24.61 (16.14)	−1.525	0.130
Age*group	0.49 (0.39)	1.235	0.218

Results are shown for the linear mixed effects models that compared diffusion-age-group interactions in predicting SN scores. Only the interaction terms and the intercept are shown. Stars correspond to the following *p*-values: *($p < 0.05$), **($p < 0.01$), ***($p < 0.001$). Significant three-way interactions that survived multiple comparison correction ($q < 0.05$) are bolded, with the corresponding *q* value in parentheses. Nominally significant three-way interactions that failed to survive multiple comparison correction are italicized, with the corresponding *q* value in parentheses. Significant two-way interactions and intercepts are starred, but not bolded, as these were not corrected for. AF, arcuate fasciculus; SE, standard error; FA, fractional anisotropy; MD, mean diffusivity; LI, laterality index.

rightward lateralized over time; controls remained consistently left lateralized. The change in the PAE group was driven by steeper increases of FA in the right arcuate than in the left arcuate. Recent structural and functional MRI literature has demonstrated trends toward rightward lateralization of the language network in PAE and other disorders that impact reading. For example, adolescents with PAE show rightward laterality of FA in the ILF and greater activation of the right precentral gyrus during PP tasks than controls (Yu et al., 2022). Older children with dyslexia also show increased rightward laterality in white matter tracts associated with reading, including the IFOF

and the SLF, with lateralization patterns related to individual differences in dyslexic children's reading abilities (Zhao et al., 2016). Greater engagement of the right hemisphere in poor readers has been commonly noted across studies (Pugh et al., 2001; Shaywitz et al., 2002; Waldie et al., 2013), including in pre-readers at risk for reading difficulties (Ostertag et al., 2022), which suggests compensation mechanisms in which alternate pathways are recruited to process reading tasks in the context of dysfunctional left hemispheric reading networks. The altered trends in microstructural arcuate development found in this study may contribute to the development of atypical reading pathways and may underlie the reading impairments displayed in the PAE group.

Both pre-reading language scores were lower in the PAE group, and more participants with PAE had scores below the 26th percentile than controls (33 vs. 8%). Reading and language abilities are known to be reduced in older children and adolescents with PAE (O'Leary et al., 2013; Mattson et al., 2019; Lindinger et al., 2022). Here, we show that pre-reading language deficits are apparent in some children with PAE even before the emergence of fluent reading skills. This suggests an important link between brain and language development, similar to what has been previously observed in non-exposed children (Saygin et al., 2013; Wang et al., 2017; Reynolds et al., 2019b; De Vos et al., 2020).

The PAE group demonstrated an opposite relationship between SN scores and left arcuate FA compared to controls, such that better scores were associated with lower FA values. Interestingly, these trends mimic the younger age band of unexposed controls, suggesting that our findings may reflect brain immaturity. This is similar, although slightly less obvious, for the PP scores and right arcuate FA plot, such that both PAE groups (younger and older) showed trajectories of development of the arcuate similar to younger controls, with positive slopes, whereas the older controls show a negative slope. The faster development in the unexposed control group may represent a more dynamic period of establishing the expected brain-behavior relationships, which then are positively reflected in the older controls. The altered arcuate development in the PAE group could disrupt the organization of pre-reading language-microstructure relationships, thus reflecting the period of typical development where these relationships are theoretically weaker: younger ages. Considering the typical development of the AF where FA increases and MD decreases with age, with faster FA increases and MD decreases being related to better reading performance (Cheema et al., 2018), cohesiveness between white matter development and reading development is critical. Overall, these relationships suggest that the altered developmental trajectories in the arcuate could be associated with adverse functional pre-reading language outcomes.

5. Limitations and future directions

Brain alterations may depend on the timing, pattern, and amount of PAE, as well as exposures to other substances and experiences pre- or postnatally (Paintner et al., 2012; Lebel et al., 2019b; Hemingway et al., 2020; Flannigan et al., 2021). PAE was confirmed in all cases, however, precise information about dosage and timing is challenging to obtain retrospectively. Prospective studies that begin in the prenatal period and progress through childhood can capture more detail on PAE to compliment this work. Further, although pre-reading language skills have been linked to future reading outcomes (Wang et al., 2017), we cannot know which participants will go on to develop significant reading impairments. Future research should aim to pursue this issue longitudinally and identify early neural correlates of poor reading outcomes in children with PAE.

6. Conclusion

This was the first study to investigate microstructural development of the AF in young children with PAE. We found altered developmental trajectories for FA and MD in children with PAE when compared with unexposed controls. Pre-reading language skills were reduced in the PAE group, with scores low enough to be considered impaired significantly more prevalent in children with PAE. Relationships between pre-reading language skills and arcuate microstructure were altered in the PAE group, with children with PAE, regardless of age, displaying relationships that are more in line with a younger typically developing brain. This suggests that altered developmental trajectories are associated with adverse functional outcomes in young children with PAE.

Data availability statement

The healthy control datasets presented in this study can be found in online repositories at https://osf.io/axz5r/. The data on participants with PAE is available upon request from the corresponding author and with appropriate ethics approval.

Ethics statement

The studies involving human participants were reviewed and approved by the University of Calgary Conjoint Health Research Ethics Board. Written informed consent to participate in this study was provided by the participants' legal guardian/next of kin.

Author contributions

CO: conceptualization, methodology, data processing, analysis, investigation, writing the original draft, visualization, reviewing, and editing the draft. JR and PK: methodology, data collection and processing, investigation, reviewing, and editing the draft. DD: conceptualization, methodology, reviewing, editing the draft. WG: conceptualization, methodology, reviewing, editing the draft, and funding acquisition. CT: methodology, reviewing, and editing the draft. CL: conceptualization, methodology, writing the original draft, visualization, formal analysis, investigation, reviewing, editing the draft, project administration, funding acquisition, and overall

project supervision. All authors contributed to the article and approved the submitted version.

Funding

This work was funded by grants from the Canadian Institutes of Health Research (CIHR) (IHD-134090, MOP-123535, and MOP-136797), the US National Institutes of Health (Exploration/Development Grant 1R21ES021295-01R21), and the Alberta Children's Hospital Foundation. Funding to establish the APrON cohort was provided by a grant from Alberta Innovates-Health Solutions (AIHS). Salary support was provided by the Canada Research Chairs Program (CL) and an NSERC Undergraduate Student Research Award (CO).

Acknowledgments

We acknowledge the contributions of the APrON Study Team. We are extremely grateful to all the families who took part in this study and the whole APrON team (http://apronstudy.ca).

Conflict of interest

The authors declare that the research was conducted in the absence of any commercial or financial relationships that could be construed as a potential conflict of interest.

Publisher's note

All claims expressed in this article are solely those of the authors and do not necessarily represent those of their affiliated organizations, or those of the publisher, the editors and the reviewers. Any product that may be evaluated in this article, or claim that may be made by its manufacturer, is not guaranteed or endorsed by the publisher.

Supplementary material

The Supplementary Material for this article can be found online at: https://www.frontiersin.org/articles/10.3389/fnins.2023.1174165/full#supplementary-material

References

Bates, D., Mächler, M., Bolker, B., and Walker, S. (2015). Fitting linear mixed-effects models using lme4. *J. Stat. Softw.* 67, 1–48.

Benjamini, Y., and Hochberg, Y. (1995). Controlling the false discovery rate: A practical and powerful approach to multiple testing. *J. R. Stat. Soc. Series B Stat. Methodol.* 57, 289–300.

Buchsbaum, B. R., and D'Esposito, M. (2008). The search for the phonological store: From loop to convolution. *J. Cogn. Neurosci.* 20, 762–778.

Cheema, K., Cummine, J., and For the Pediatric Imaging, Neurocognition, and Genetics Study (2018). The relationship between white matter and reading acquisition, refinement and maintenance. *Dev. Neurosci.* 40, 209–222. doi: 10.1159/000489491

Cook, J. L., Green, C. R., Lilley, C. M., Anderson, S. M., Baldwin, M. E., Chudley, A. E., et al. (2016). Fetal alcohol spectrum disorder: A guideline for diagnosis across the lifespan. *CMAJ* 188, 191–197.

De Vos, A., Vanderauwera, J., Vanvooren, S., Vandermosten, M., Ghesquiere, P., and Wouters, J. (2020). The relation between neurofunctional and neurostructural determinants of phonological processing in pre-readers. *Dev. Cogn. Neurosci.* 46:100874. doi: 10.1016/j.dcn.2020.100874

Donald, K. A., Eastman, E., Howells, F. M., Adnams, C., Riley, E. P., Woods, R. P., et al. (2015a). Neuroimaging effects of prenatal alcohol exposure on the developing human brain: A magnetic resonance imaging review. *Acta Neuropsychiatr.* 27, 251–269. doi: 10.1017/neu.2015.12

Donald, K. A., Roos, A., Fouche, J. P., Koen, N., Howells, F. M., Woods, R. P., et al. (2015b). A study of the effects of prenatal alcohol exposure on white matter microstructural integrity at birth. *Acta Neuropsychiatr.* 27, 197–205.

Flannigan, K., Kapasi, A., Pei, J., Murdoch, I., Andrew, G., and Rasmussen, C. (2021). Characterizing adverse childhood experiences among children and adolescents with prenatal alcohol exposure and fetal alcohol spectrum disorder. *Child Abuse Negl* 112:104888. doi: 10.1016/j.chiabu.2020.104888

Flannigan, K., Unssorth, K., and Harding, K. (2018). *The prevalence of fetal alcohol spectrum disorder*. Canada: FASD Research Network.

Ghazi Sherbaf, F., Aarabi, M. H., Hosein Yazdi, M., and Haghshomar, M. (2019). White matter microstructure in fetal alcohol spectrum disorders: A systematic review of diffusion tensor imaging studies. *Hum. Brain Mapp.* 40, 1017–1036. doi: 10.1002/hbm.24409

Hemingway, S. J. A., Davies, J. K., Jirikowic, T., and Olson, E. M. (2020). What proportion of the brain structural and functional abnormalities observed among children with fetal alcohol spectrum disorder is explained by their prenatal alcohol exposure and their other prenatal and postnatal risks? *Adv. Pediatr. Res.* 7:41.

Hickok, G., and Poeppel, D. (2004). Dorsal and ventral streams: A framework for understanding aspects of the functional anatomy of language. *Cognition* 92, 67–99. doi: 10.1016/j.cognition.2003.10.011

Hickok, G., and Poeppel, D. (2007). The cortical organization of speech processing. *Nat. Rev. Neurosci.* 8, 393–402.

Kaplan, B. J., Giesbrecht, G. F., Leung, B. M., Field, C. J., Dewey, D., Bell, R. C., et al. (2014). The Alberta pregnancy outcomes and nutrition (APrON) cohort study: Rationale and methods. *Matern. Child Nutr.* 10, 44–60. doi: 10.1111/j.1740-8709.2012.00433.x

Kar, P., Reynolds, J. E., Gibbard, W. B., Mcmorris, C., Tortorelli, C., and Lebel, C. (2022). Trajectories of brain white matter development in young children with prenatal alcohol exposure. *Hum. Brain Mapp.* 43, 4145–4157.

Kar, P., Reynolds, J. E., Grohs, M. N., Gibbard, W. B., Mcmorris, C., Tortorelli, C., et al. (2021). White matter alterations in young children with prenatal alcohol exposure. *Dev. Neurobiol.* 81, 400–410.

Korkman, M., Kirk, U., and Kemp, S. (2007). *Nepsy-II*. San Antonio, TX: Pearson.

Kuznetsova, A., Brockhoff, B. P., and Christensen, R. (2017). lmerTest package: Tests in linear mixed effects models. *J. Stat. Softw.* 82, 1–26.

Lebel, C., and Beaulieu, C. (2009). Lateralization of the arcuate fasciculus from childhood to adulthood and its relation to cognitive abilities in children. *Hum. Brain Mapp.* 30, 3563–3573. doi: 10.1002/hbm.20779

Lebel, C., Benischek, A., Geeraert, B., Holahan, J., Shaywitz, S., Bakhshi, K., et al. (2019a). Developmental trajectories of white matter structure in children with and without reading impairments. *Dev. Cogn. Neurosci.* 36:100633.

Lebel, C., Mcmorris, C. A., Kar, P., Ritter, C., Andre, Q., Tortorelli, C., et al. (2019b). Characterizing adverse prenatal and postnatal experiences in children. *Birth Defects Res.* 111, 848–858.

Lebel, C., and Deoni, S. (2018). The development of brain white matter microstructure. *Neuroimage* 182, 207–218.

Lebel, C., Rasmussen, C., Wyper, K., Walker, L., Andrew, G., Yager, J., et al. (2008). Brain diffusion abnormalities in children with fetal alcohol spectrum disorder. *Alcohol. Clin. Exp. Res.* 32, 1732–1740.

Leemans, A., Jeurissen, B., Sijbers, J., and Jones, D. (2009). "ExploreDTI: A graphical toolbox for processing, analyzing, and visualizing diffusion MR data," in *Proceedings 17th scientific meeting, international society for magnetic resonance in medicine*, Honolulu, HI, 3537.

Letourneau, N., Aghajafari, F., Bell, R. C., Deane, A. J., Dewey, D., Field, C., et al. (2022). The Alberta pregnancy outcomes and nutrition (APrON) longitudinal study:

Cohort profile and key findings from the first three years. *BMJ Open* 12:e047503. doi: 10.1136/bmjopen-2020-047503

Lindinger, N. M., Jacobson, S. W., Davidson, L., Conradie, S., Dodge, N. C., Molteno, C. D., et al. (2022). Reading impairment in adolescents with fetal alcohol spectrum disorders. *Sci. Stud. Read.* 26, 469–488.

Lonigan, C. J., Burgess, S. R., and Anthony, J. L. (2000). Development of emergent literacy and early reading skills in preschool children: Evidence from a latent-variable longitudinal study. *Dev. Psychol.* 36, 596–613. doi: 10.1037/0012-1649.36.5.596

Mattson, S. N., Bernes, G. A., and Doyle, L. R. (2019). Fetal alcohol spectrum disorders: A review of the neurobehavioral deficits associated with prenatal alcohol exposure. *Alcohol. Clin. Exp. Res.* 43, 1046–1062.

May, P. A., Chambers, C. D., Kalberg, W. O., Zellner, J., Feldman, H., Buckley, D., et al. (2018). Prevalence of fetal alcohol spectrum disorders in 4 US communities. *JAMA* 319, 474–482.

Meisler, S. L., and Gabrieli, J. D. E. (2022). A large-scale investigation of white matter microstructural associations with reading ability. *Neuroimage* 249:118909. doi: 10.1016/j.neuroimage.2022.118909

O'Leary, C. M., Taylor, C., Zubrick, S. R., Kurinczuk, J. J., and Bower, C. (2013). Prenatal alcohol exposure and educational achievement in children aged 8-9 years. *Pediatrics* 132, e468–e475. doi: 10.1542/peds.2012-3002

Ostertag, C., Reynolds, J. E., Dewey, D., Landman, B., Huo, Y., and Lebel, C. (2022). Altered gray matter development in pre-reading children with a family history of reading disorder. *Dev. Sci.* 25:e13160.

Paintner, A., Williams, A. D., and Burd, L. (2012). Fetal alcohol spectrum disorders–implications for child neurology, part 1: Prenatal exposure and dosimetry. *J. Child Neurol.* 27, 258–263.

Popova, S., Lange, S., Poznyak, V., Chudley, A. E., Shield, K. D., Reynolds, J. N., et al. (2019). Population-based prevalence of fetal alcohol spectrum disorder in Canada. *BMC Public Health* 19:845. doi: 10.1186/s12889-019-7213-3

Pugh, K. R., Mencl, W. E., Jenner, A. R., Katz, L., Frost, S. J., Lee, J. R., et al. (2001). Neurobiological studies of reading and reading disability. *J. Commun. Disord.* 34, 479–492.

Qiu, D., Tan, L. H., Siok, W. T., Zhou, K., and Khong, P. L. (2011). Lateralization of the arcuate fasciculus and its differential correlation with reading ability between young learners and experienced readers: A diffusion tensor tractography study in a Chinese cohort. *Hum. Brain Mapp.* 32, 2054–2063. doi: 10.1002/hbm.21168

R Core Team (2020). *R: A language and environment for statistical computing*. Vienna: R Foundation for Statistical Computing.

Reynolds, J. E., Grohs, M. N., Dewey, D., and Lebel, C. (2019a). Global and regional white matter development in early childhood. *Neuroimage* 196, 49–58.

Reynolds, J. E., Long, X., Grohs, M. N., Dewey, D., and Lebel, C. (2019b). Structural and functional asymmetry of the language network emerge in early childhood. *Dev. Cogn. Neurosci.* 39:100682. doi: 10.1016/j.dcn.2019.100682

Reynolds, J. E., Long, X., Paniukov, D., Bagshawe, M., and Lebel, C. (2020). Calgary preschool magnetic resonance imaging (MRI) dataset. *Data Brief* 29:105224.

Saygin, Z. M., Norton, E. S., Osher, D. E., Beach, S. D., Cyr, A. B., Ozernov-Palchik, O., et al. (2013). Tracking the roots of reading ability: White matter volume and integrity correlate with phonological awareness in prereading and early-reading kindergarten children. *J. Neurosci.* 33, 13251–13258. doi: 10.1523/JNEUROSCI.4383-12.2013

Shaywitz, B. A., Shaywitz, S. E., Pugh, K. R., Mencl, W. E., Fulbright, R. K., Skudlarski, P., et al. (2002). Disruption of posterior brain systems for reading in children with developmental dyslexia. *Biol. Psychiatry* 52, 101–110.

Thieba, C., Frayne, A., Walton, M., Mah, A., Benischek, A., Dewey, D., et al. (2018). Factors associated with successful MRI scanning in unsedated young children. *Front. Pediatr.* 6:146. doi: 10.3389/fped.2018.00146

Treit, S., Lebel, C., Baugh, L., Rasmussen, C., Andrew, G., and Beaulieu, C. (2013). Longitudinal MRI reveals altered trajectory of brain development during childhood and adolescence in fetal alcohol spectrum disorders. *J. Neurosci.* 33, 10098–10109. doi: 10.1523/JNEUROSCI.5004-12.2013

Vandermosten, M., Boets, B., Wouters, J., and Ghesquiere, P. (2012). A qualitative and quantitative review of diffusion tensor imaging studies in reading and dyslexia. *Neurosci. Biobehav. Rev.* 36, 1532–1552.

Vigneau, M., Beaucousin, V., Herve, P. Y., Duffau, H., Crivello, F., Houde, O., et al. (2006). Meta-analyzing left hemisphere language areas: Phonology, semantics, and sentence processing. *Neuroimage* 30, 1414–1432. doi: 10.1016/j.neuroimage.2005.11.002

Wakana, S., Jiang, H., Nagae-Poetscher, L. M., Van Zijl, P. C., and Mori, S. (2004). Fiber tract-based atlas of human white matter anatomy. *Radiology* 230, 77–87.

Waldie, K. E., Haigh, C. E., Badzakova-Trajkov, G., Buckley, J., and Kirk, I. J. (2013). Reading the wrong way with the right hemisphere. *Brain Sci.* 3, 1060–1075.

Walton, M., Dewey, D., and Lebel, C. (2018). Brain white matter structure and language ability in preschool-aged children. *Brain Lang.* 176, 19–25.

Wang, Y., Mauer, M. V., Raney, T., Peysakhovich, B., Becker, B. L. C., Sliva, D. D., et al. (2017). Development of tract-specific white matter pathways during early reading development in at-risk children and typical controls. *Cereb. Cortex* 27, 2469–2485. doi: 10.1093/cercor/bhw095

Wickham, H. (2016). *ggplot2: Elegant graphics for data analysis*. New York, NY: Springer-Verlag.

Wyper, K. R., and Rasmussen, C. R. (2011). Language impairments in children with fetal alcohol spectrum disorders. *J. Popul. Ther. Clin. Pharmacol.* 18, e364–e376.

Yu, X., Dunstan, J., Jacobson, S. W., Molteno, C. D., Lindinger, N. M., Turesky, T. K., et al. (2022). Distinctive neural correlates of phonological and reading impairment in fetal alcohol-exposed adolescents with and without facial dysmorphology. *Neuropsychologia* 169:108188. doi: 10.1016/j.neuropsychologia.2022.108188

Zhao, J., Thiebaut De Schotten, M., Altarelli, I., Dubois, J., and Ramus, F. (2016). Altered hemispheric lateralization of white matter pathways in developmental dyslexia: Evidence from spherical deconvolution tractography. *Cortex* 76, 51–62. doi: 10.1016/j.cortex.2015.12.004

frontiers | Frontiers in Pediatrics

TYPE Review
PUBLISHED 08 June 2023
DOI 10.3389/fped.2023.1169570

Check for updates

OPEN ACCESS

EDITED BY
Carlos Fernando Valenzuela,
University of New Mexico, United States

REVIEWED BY
Michael Suttie,
University of Oxford, United Kingdom
Devi Sewvandini Atukorallaya,
University of Manitoba, Canada

*CORRESPONDENCE
Moritz Blanck-Lubarsch
✉ blancklubarsch@uni-muenster.de

RECEIVED 19 February 2023
ACCEPTED 23 May 2023
PUBLISHED 08 June 2023

CITATION
Blanck-Lubarsch M, Dirksen D, Feldmann R and Hohoff A (2023) A systematic review: facial, dental and orthodontic findings and orofacial diagnostics in patients with FASD.
Front. Pediatr. 11:1169570.
doi: 10.3389/fped.2023.1169570

COPYRIGHT
© 2023 Blanck-Lubarsch, Dirksen, Feldmann and Hohoff. This is an open-access article distributed under the terms of the Creative Commons Attribution License (CC BY). The use, distribution or reproduction in other forums is permitted, provided the original author(s) and the copyright owner(s) are credited and that the original publication in this journal is cited, in accordance with accepted academic practice. No use, distribution or reproduction is permitted which does not comply with these terms.

A systematic review: facial, dental and orthodontic findings and orofacial diagnostics in patients with FASD

Moritz Blanck-Lubarsch[1]*, Dieter Dirksen[2], Reinhold Feldmann[3] and Ariane Hohoff[1]

[1]Department of Orthodontics, University of Münster, Münster, Germany, [2]Department of Prosthodontics and Biomaterials, University of Münster, Münster, Germany, [3]Department of Pediatrics, University of Münster, Münster, Germany

Background: The fetal alcohol spectrum disorder is a group of developmental disorders caused by maternal alcohol consumption. Patients with fetal alcohol syndrome show abnormal orofacial features. This review presents an overview over the facial, oral, dental or orthodontic findings and diagnostic tools concerning these features.
Methods: For this systematic review Cochrane, Medline and Embase databases were considered and the review was performed according to the PRISMA checklist. Two independent reviewers evaluated all studies and recorded results in a summary of findings table. Risk of bias was analyzed via Quadas-2 checklist.
Results: 61 studies were eligible for inclusion. All included studies were clinical studies. Methods and results of the studies were not comparable, guidelines or methods for the detection of FASD varied across studies. Facial features most often measured or found as distinguishing parameter were: palpebral fissure length, interpupillary or innercanthal distance, philtrum, upper lip, midfacial hypoplasia or head circumference.
Conclusions: This review shows that to date a multitude of heterogeneous guidelines exists for the diagnosis of FASD. Uniform, objective diagnostic criteria and parameters for the orofacial region in FASD diagnosis are needed. A bio database with values and parameters for different ethnicities and age groups should be made available for diagnosis.

KEYWORDS
review, craniofacial anomalies, orofacial disorder, diagnostic methods, fetal alcohol syndrome (FAS)

1. Introduction

1.1. What is FASD?

FASD is a group of developmental disorders, which result from maternal alcohol exposure. Symptoms comprise growth deficiencies, aberrant facial features and damage or

Abbreviations
ARBD, Alcohol Related Birth Defects; ARND, Alcohol Related Neurodevelopmental Disorder; BMI, Body Mass Index; CNS, Central Nervous Systems; DDE, Developmental Defects of Enamel; dmft, decayed, missing, filled, teeth (deciduous dentition); DMFT, Decayed, Missing, Filled, Teeth (permanent dentition); DSM, Dense Surface Model; FAE, Fetal Alcohol Effects; FAS, Feta Alcohol Syndrome; FASD, Fetal Alcohol Spectrum Disorder; HE, Heavily Exposed; ICD, Innercanthal Distance; IOM, Institute Of Medicine; IPD, Interpupillary Distance; IQ, Intelligence Quotient; OCD, Outer Canthal Distance; OFC, Occipital Frontal Circumference; pFAE, partial Fetal Alcohol Effects; pFAS, partial Fetal Alcohol Syndrome; PFL, Palpebral Fissure Length.

dysfunction of the central nervous system (1–3). Individuals with FASD suffer from lifetime consequences, even more if the underlying disorder remains undiagnosed.

Different severity grades of the disorder are summarized by the term fetal alcohol spectrum disorder (FASD). The most severe form of FASD is the fetal alcohol syndrome (FAS), less severe forms are categorized as partial fetal alcohol syndrome (pFAS), alcohol-related birth defects (ARBD) or alcohol-related neurodevelopmental disorder (ARND) (4–6).

1.2. Prevalence of FASD, FAS, pFAS, ARND, ARBD

Unfortunately, the estimated worldwide prevalence of the fetal alcohol spectrum disorder is still very high (0,77%, Lange et al., 2017), although it should be common knowledge that any amount of alcohol consumption during pregnancy is harmful to the embryo. FASD shows regional differences ranging from up to 5% in first grade school children in the United States (7), 2%–3% in Canadian school children (8), 1.98% in Europe to 0.01% in the eastern Mediterranean region (9). According to a Canadian study by Popova et al. the estimated prevalence for school children aged 7–9 years is 1.2 per 1,000 for FAS, 2.0 per 1,000 for pFAS and 15 per 1,000 for ARND (8). There is no recent prevalence for ARBD in literature, a study from 1988 by Warren et al. mentions a high prevalence of 417 per 1,000 (10).

1.3. Diagnosis of FASD

FASD is a developmental disorder, which is, because of its complexity and variable severity, challenging to detect. Since Lemoine first described the distinctive features and established the disorder FAS, a great number of diagnostic systems have been developed (11).

The current variability of existing diagnostic methods concerning FASD impedes comparability and reproducibility (12, 13).

There seem to be four guidelines across the world, which are most commonly used but which contain differences in certain diagnostic parameters:

- The four-digit code by Astley et al.—not for the terms ARND/ARBD (14)
- The revised IOM by Hoyme (5)
- The Canadian guideline by Chudley (6)
- The CDC code—mainly for FAS, not for partial FAS/ARND/ARBD (15)

Most diagnostic guidelines for FASD include **four parameters: growth deficiency, facial phenotype, central nervous system (CNS) damage or dysfunction as well as gestational exposure to alcohol** (5, 16). The most uncertain parameter is in many cases the exposure to alcohol since many children with FASD live in foster care or mothers might not tell the truth about alcohol consumption during pregnancy (17).

Growth retardation is measured according to percentile curves and for the guidelines mentioned above, measurements should be below the 10th percentile to be considered relevant for FAS diagnosis. In the case of partial FAS this measurement is only required for the IOM guideline and not necessary for diagnosis in the other guidelines. For ARBD and ARND growth retardation is not part of the diagnosis (5, 6, 14, 15).

CNS involvement is measured differently in the mentioned guidelines. For FAS the four-digit code requires a head circumference, which is smaller by more than two standard deviations below the 2.5th percentile, whereas the revised IOM and the CDC require only measurements below the 10th percentile for FAS diagnosis. The Canadian guideline does not measure according to percentile curve but requires more than three impairments in the CNS domains, for example hard and soft neurologic signs, brain structure, cognition, academic achievement, memory. For partial FAS CNS involvement is the same as for FAS in the four-digit code and the Canadian guideline, not applicable for the CDC guideline and for the revised IOM head circumference should be below the 10th percentile or behavioral and cognitive abnormalities should be present. ARND requires neurobehavioral impairment for the IOM and for the Canadian guideline evidence of CNS neurodevelopmental abnormalities and/or evidence of a complex pattern of behavior or cognitive abnormalities. ARBD requires one or more specific cardiac, skeletal, renal, eye or ear malformation for both the IOM and the Canadian guideline (5, 6, 14, 15).

In all four diagnostic guidelines **alcohol exposure** must not necessarily be confirmed for FAS. For partial FAS the four-digit code and the Canadian guideline require confirmed alcohol exposure, whereas the revised IOM does not require confirmed alcohol exposure for diagnosis of partial FAS. For ARND and ARBD confirmed alcohol exposure is required in the revised IOM and Canadian Guideline (5, 6, 14, 15).

For the parameter **facial phenotype** a commonly used tool is the lip-philtrum guide by Astley and Clarren (18). Facial characteristics used in the diagnostic guidelines comprise short palpebral fissures, thin vermillion borders and a smooth philtrum. Short palpebral fissure lengths are measured using a ruler or are measured via computer using the FAS facial photographic analysis software by Astley et al. The smooth philtrum and thin vermillion border are diagnosed comparing the patient's facial features to pictures on the lip-philtrum guide by Astley and Clarren and then ranking them to a certain grade of the feature (14, 18, 19).

All currently available diagnostic guidelines for the detection of facial FASD-parameters are in parts based on subjective evaluation. Therefore, this requires a professional dysmorphologist with experience in this field and is otherwise another factor for possible bias in the FASD diagnosis.

1.4. Aim of the review

Newer methods for the evaluation of facial parameters have investigated shape analysis, morphometrics, 3D-facial scanning

and stereophotogrammetry with promising results for objectifying facial analysis in the future (20–35).

To improve the diagnostic process in patients with FASD it seems important to find facial characteristics for reproducible and objective measurements.

The aim of this review was to analyze, which facial, oral, orthodontic and dental parameters for the detection of FASD have been found so far and what kind of different diagnostic methods have been described for the diagnosis of FASD.

2. Materials and methods

2.1. Protocol and eligibility criteria

This review was performed according to the PRISMA guidelines. It was confined to articles in English, French or German that were published until January 2022.

Studies were considered eligible for inclusion if facial or oral structures in patients with FASD were investigated or if diagnostic methods for abnormal facial or oral structures in patients with FASD were described or tested.

Exclusion criteria were: Animal studies, scientific papers in which exposure of the study subjects to alcohol during pregnancy was not clear and studies concerning exclusively brain structures or ophthalmologic findings other than external ophthalmologic findings such as palpebral fissure length, innercanthal or interpupillary distance.

2.2. Search strategy

PICO Question was defined (**Table 1**).

Cochrane, Medline and Embase databases were considered. The search strategy was: [fetal alcohol syndrome OR "fetal alcohol spectrum disorders" (MESH)] AND ("Face" [MESH] OR "Mouth" [MESH] OR "Oral Health" [MESH] OR "orthodontics" [MESH] OR "dental" OR "Head" [MESH] OR "palpebral fissure length" OR "diagnostic" OR "diagnose").

2.3. Study selection

All studies were screened for eligibility criteria.

TABLE 1 Showing the PICO question.

PICOs	
Participants	Children with FASD, FAS, pFAS, ARND, ARBD
Intervention or exposure	Facial, dental or orthodontic findings or orofacial diagnostic methods
Comparison or control	Patients without prenatal alcohol exposure
Outcome measure(s)	Anatomic measurements of length, width or depth and/or dental/orthodontic score(s), diagnostic method(s)
Type of Studies included	Clinical studies

2.4. Data extraction

All studies were screened by two independent reviewers MBL, AH in a blinded manner and classified into "eligible" or "not eligible" for this review. All "eligible" studies were read in full-text by the two reviewers and evaluated according to the Quadas-2 checklist. Data concerning facial features in patients with FASD and FASD diagnostic methods for the orofacial region were extracted independently by the two reviewers and recorded in a summary of findings table.

After reading all eligible studies full-text the two reviewers discussed their results and re-read those studies for which results differed in order to find a consensus.

2.5. Data items

The following outcomes were extracted:

- FASD or subgroup (FAS, pFAS, ARND, ARBD) diagnosis
- Control group
- Ethnicity
- Age
- Results, metric facial measurements or diagnostic scores of
  - Head circumference (OFC = occipital frontal circumference)
  - Palpebral fissure length (PFL), distance of inner and other canthi of the eye
  - Innercanthal distance (ICD), distance between the inner canthi of right and left eye
  - Interpupillary distance (IPD), distance between the centers of the pupils or right and left eye
  - Philtrum anomalies in sagittal, vertical and transversal dimension
  - **d**ecayed **m**issing **f**illed **t**eeth index for deciduous teeth (dmft) and permanent teeth (DMFT), the sum of the number of decayed, missing due to caries and filled teeth
  - DDE index (classification of **d**evelopmental **d**efects of **e**namel),
  - facial or oral features associated with FASD
- applied/(new, for example 3D or computer aided) diagnostic methods for the orofacial region
- aim of the study

2.6. Synthesis

Synthesis of data was not possible due to inconsistent measuring methods and inhomogeneity across the studies.

2.7. Effect measures

Effect measures were not possible due to inhomogeneity across the studies.

2.8. Bias/quality assessment

To minimize bias, two reviewers independently selected eligible studies for this review according to afore defined criteria and did independent full-text reading and data extraction of all included studies.

The quality of the studies was assessed using the Quadas-2 checklist. The Quadas-2 checklist is supposed to evaluate the quality of diagnostic accuracy studies.

Possible bias for the synthesis of data was recorded if:

- the diagnostic guideline for FASD was unclear or not stated.
- the diagnosis FAS, FASD, pFAS, ARND or ARBD was not clearly defined.
- ethnicity was not described or unclear.
- the method was not fully described or unclear.
- the participants' ages did not match or were not clearly stated.

3. Results

3.1. Study selection (flow of studies)

The search strategy resulted in a total of 1,470 studies (**Figure 1**).

3.2. Study selection (excluded studies)

1,409 studies were excluded (**Figure 1**).

3.3. Study characteristics

All 61 included studies were clinical studies: 33 studies investigated diagnostic methods (**Figure 2A**) and 28 studies investigated the FASD phenotype (**Figure 3A**).

3.4. Risk of bias in studies

The Quadas-2 evaluation showed low risk of bias concerning flow and timing (diagnostic studies 75%, phenotype studies 86%), reference standard (diagnostic studies 81%, phenotype studies 79%) and index test (diagnostic studies 84%, phenotype studies 75%) (**Figures 2B**, **3B**). Risk of bias in patient selection was low for 39% of the diagnostic studies and for 54% of the phenotype studies. This was for example due to unclear or missing clarification of ethnicities or unclear verification of the FASD diagnosis.

None of the studies was rated with high concerns regarding applicability.

3.5. Results of individual studies

The results of the individual studies are displayed in **Table 2**.

3.6. Guidelines used for FASD diagnosis

The guidelines for FASD diagnosis used within the studies were the IOM (5 studies), the revised IOM (14 studies), the 4-digit diagnostic guide (4 studies), the German guideline (5 studies) and the Canadian guideline (1 study) (5, 6, 18, 36, 37).

Some studies only consulted expert dysmorphologists/pediatricians for FASD diagnosis (14 studies) or did not state which guideline was used (10 studies). For diagnosis, eight studies only considered the amount of alcohol consumed by pregnant women during pregnancy. 4 studies mentioned Hoyme as reference, two studies performed the Gestalt method. One study used the Chambers checklist, one study mentioned May et al. as reference and 1 study mentioned Clarren et al. as reference.

3.7. Age groups

The majority of studies only included infants or school children. Only three studies included adult patients. Three studies did not mention the patients' ages. 27 studies included children aged between 6 and 10 years, 10 studies included children 5 years or younger, 7 studies included children 10–14 years old. Only two studies included patients aged above 18 years. Some studies had a large age range (each 1 study: 0–27 years, 6–17 years, 1–17 years, 4–18 years, 12–40 years, 3–26 years, 8–16 years).

3.8. Group sizes

For FASD patients 7 studies included 20 subjects or less, 11 studies included 35 patients or less, 6 studies included 50 subjects or less, 16 studies included 100 patients or less and 19 studies included more than 100 participants.

For patients with FAS 10 studies included 20 patients or less, 14 studies included 35 patients or less, 4 studies included 50 subjects or less, 13 studies included 100 participants or less and 5 studies included more than 100 participants.

3.9. Ethnicities

Ten studies did not mention which ethnic group was analyzed. Many studies analyzed different ethnic populations. Some of these studies separately measured and analyzed these groups while other studies did not differentiate between different ethnicities.

3.10. Methods

Methods included direct facial measurements [7 studies (38–44)], 2D-photos [13 studies (20, 35, 45–52, 53–55)], 3D photographs [6 studies (27, 29, 33, 34, 56, 57)] and 3D-scans/stereophotogrammetry [9 studies (21–25, 28, 31, 32, 58)], landmark

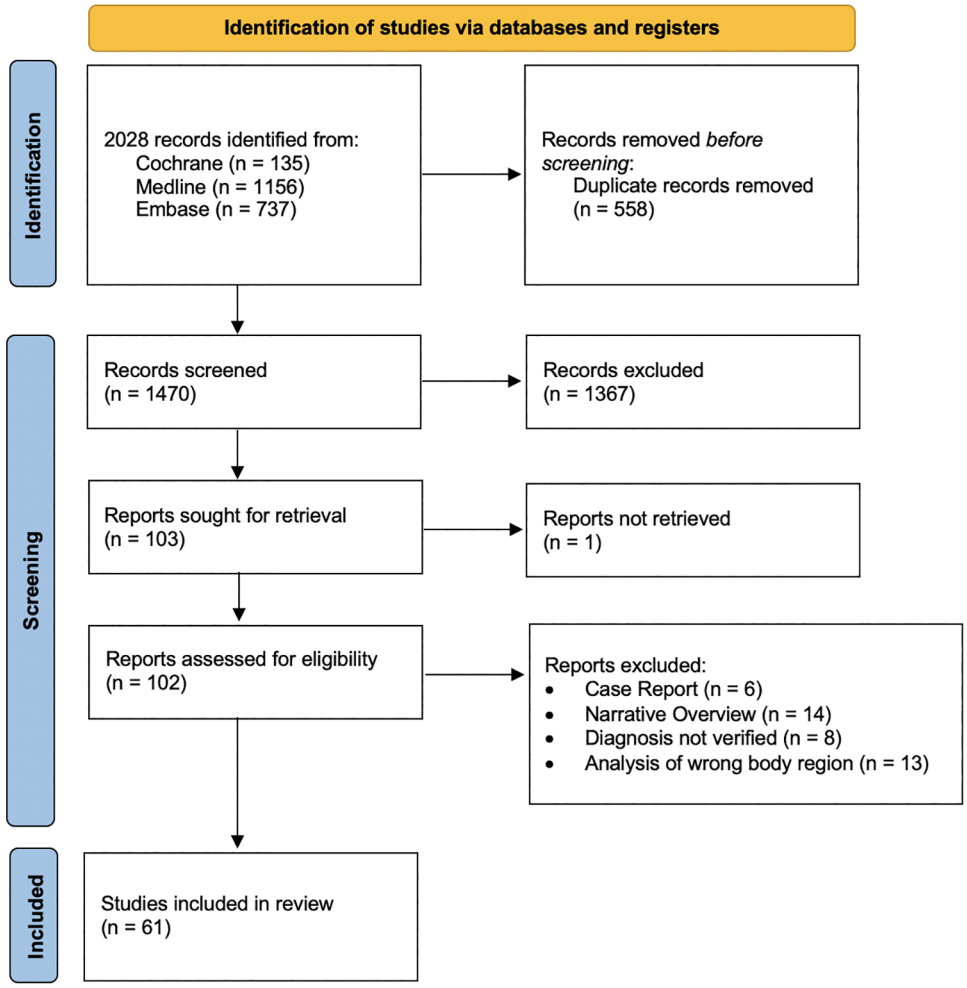


FIGURE 1
PRISMA flowchart. The search strategy resulted in 1,470 studies. A total of 1,409 studies were excluded. 61 studies were included in the review (84).

measurements, cephalometric measurements [2 studies (59, 60)], oral status [4 studies (61–64)], demographic and growth parameters [1 study (65)], heat maps [1 study (33)], telemedicine [1 study (66)], machine learning [1 study (21)] or automated diagnosis [7 studies (27, 31, 35, 50, 56, 58, 67)]. For decision trees the landmarks with highest scores for FAS detection in one study were midfacial length, palpebral fissure length and nose breadth at sulcus nasi (21).

3.11. Orofacial parameters

Small palpebral fissure length (PFL), smooth philtrum, upper lip circularity, thin vermillion border, midfacial hypoplasia, small head circumference and high dmft/DMFT (decayed, missing, filled teeth) score were the parameters, which were frequently found in the orofacial region.

3.11.1. Facial characteristics

Eyes

Reduced palpebral fissure length was found in 19 studies (20, 21, 23, 27, 29, 31, 38, 45, 46–48, 55, 57, 63, 65, 71). One study mentioned that higher alcohol exposure was not correlated with smaller PFLs and one study found that reduced PFLs were less frequently found in adult patients with FASD (42, 71). 4 studies found reduced IPD or ICD (43, 44, 63, 70). Epicanthal folds and ptosis were described by one study (70).

Lips and philtrum

12 studies (20, 24, 30, 38, 41, 42, 47, 49, 51, 55, 69, 70) found a smooth philtrum in patients with FASD and 12 studies (18, 30, 32, 38, 41, 47, 55, 68) reported a thin vermillion border or reduced upper lip thickness. Philtrum depth, when measured metrically on 3D-facial scans, significantly differed between patients with FAS and healthy controls (24).

Nose

One study found that nose breadth at the transition point of the sulcus alaris to the philtrum could be an indicator for FAS (23). Another study describes a flat nasal bridge (70).

Facial proportions

A hypoplastic or flat midface was mentioned in four studies (32, 43, 45, 70). Midfacial length was found to be significantly shorter when using profile analysis (22). Another study found overdevelopment of the upper and lower thirds in patients with FAS (60).

A

	PATIENT SELECTION	INDEX TEST	REFERENCE STANDARD	FLOW AND TIMING	PATIENT SELECTION	INDEX TEST	REFERENCE STANDARD
Diagnostic studies							
Clarren SK 1987	High	Low	Low	Low	Low	Low	Low
Sokol RJ 1987	Unclear	High	Low	Low	Low	Low	Low
Astley SJ1987a	Unclear	Low	Unclear	Low	Low	Low	Low
Astley SJ 1987b	Unclear	Low	Low	Low	Low	Low	Low
Astley SJ 2000	Unclear	Low	High	High	Unclear	Low	Unclear
Meintjes EM 2002	High	Low	High	Unclear	Low	Low	Low
Douglas TS 2003	High	Low	Low	Unclear	Low	Low	Low
Naidoo S 2005	Unclear	Low	Low	Low	Low	Low	Low
Hoyme HE 2006	Unclear	Low	Low	Low	Low	Low	Low
Naidoo S 2006a	Unclear	Low	Low	Low	Low	Low	Low
Naidoo S 2006b	Low	Low	Low	Low	Low	Low	Low
Grobbelaar R 2007	High	Unclear	Low	Low	Low	Low	Low
Moore ES 2007	Low	Low	Low	High	Low	Low	Low
Mutsvangwa TEM 2007	Low	Low	Low	Low	Low	Low	Low
Fang S 2008	Low	Low	Low	Low	Low	Low	Low
Mutsvangwa TEM 2009a	High	Low	Low	Low	Unclear	Low	Low
Mutsvangwa TEM 2009b	Low	Low	Low	Low	Low	Low	Low
Jones KL 2010	High	High	Low	Low	Unclear	Unclear	Low
Astley SJ 2011	Unclear	Low	Low	Unclear	Low	Low	Low
Douzgou S 2012	High	Low	High	High	Unclear	Low	Unclear
Suttie M 2013	Low	Low	Low	Low	Low	Low	Low
Avner M 2014	High	Low	Low	Low	Low	Low	Low
Hoyme HE 2015	Low	Low	Low	Low	Low	Low	Low
Abell K 2016	Low	High	Low	Low	Low	Unclear	Low
Suttie M 2017	Unclear	Unclear	Low	Unclear	Low	Low	Low
Valentine M 2017	Low	Low	Low	Low	Low	Low	Low
Suttie M 2018	Unclear	Low	Low	Low	Low	Low	Low
Blanck-Lubarsch M 2019a	Low	Low	Low	Low	Low	Low	Low
Blanck-Lubarsch M 2019b	Low	Low	Low	Low	Low	Low	Low
Blanck-Lubarsch M 2019c	Low	Low	Low	Low	Low	Low	Low
Del Campo M 2021	Unclear	Low	High	Low	Low	Low	Unclear
Fu Z 2021	Unclear	Low	Unclear	Unclear	Unclear	Low	Unclear
Blanck-Lubarsch M 2022	Low	Low	Low	Low	Low	Low	Low

B

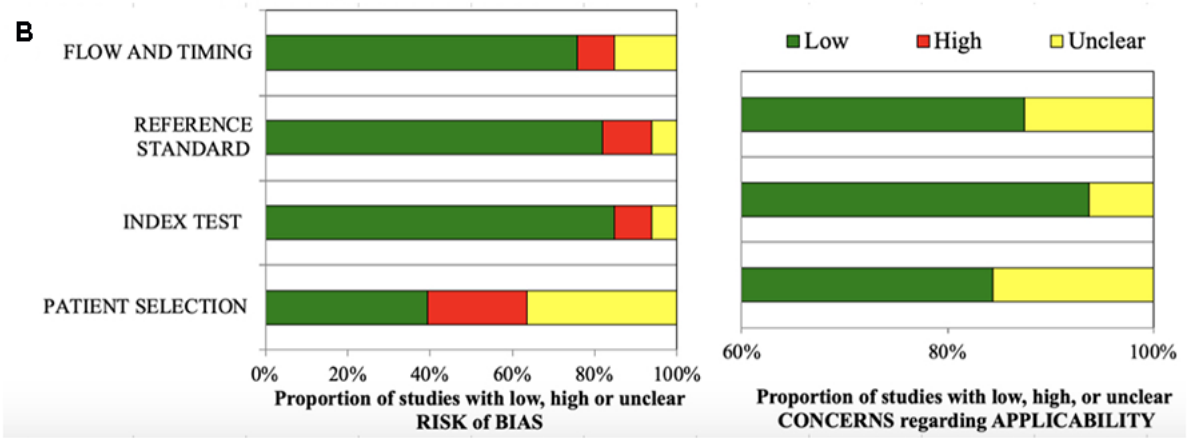


FIGURE 2
(A,B) Quadas-2 checklist for diagnostic studies. The evaluation showed low risk of bias concerning flow and timing, reference standard and index test. Risk of bias in patient selection was low for about 39% of the studies (85).

A

	PATIENT SELECTION	INDEX TEST	REFERENCE STANDARD	FLOW AND TIMING	PATIENT SELECTION	INDEX TEST	REFERENCE STANDARD
Phenotype studies							
Riekman GA 1984	Unclear	Low	Low	Unclear	Low	Low	Low
Gir AV 1989	Unclear	Low	Low	Low	Low	Low	Low
O'Leary CM 1990	Low	High	Unclear	Unclear	Low	Unclear	Unclear
Rostand A 1990	High	High	High	Low	Unclear	Low	Low
Streissguth AP 1991	High	Low	Low	Unclear	Low	Low	Low
Church MW 1997	High	High	High	Low	Low	Low	Low
Moore ES 2002	High	Low	Low	Low	Low	Low	Low
Autti-Rämö I 2006	Low	High	High	Low	Low	Unclear	Unclear
May PA 2007	Low	Low	Low	Low	Low	Low	Low
Ervalahti N 2007	Low	Low	High	Low	Low	Low	Unclear
Spohr HL 2007	Low	High	Unclear	Low	Low	Low	Unclear
Feldmann HS 2012	High	Unclear	Low	Unclear	Low	Low	Low
Foroud T 2012	Unclear	Low	Low	Low	Low	Low	Low
Nayak R 2012	Unclear	High	Low	Low	Unclear	Unclear	Low
Yang Y 2012a	Low	Low	Low	Low	Low	Low	Low
Yang Y 2012b	Low	Low	Low	Low	Low	Low	Low
May PA 2016a	Low	Low	Low	Low	Low	Low	Low
May PA 2016b	Low	Low	Low	Low	Low	Low	Low
Treit S 2016	High	Low	Low	Low	Low	Low	Low
May PA 2017	Low	Low	Low	Low	Low	Low	Low
Blanck-Lubarsch M 2019d	Unclear	Low	Low	Low	Low	Low	Low
Blanck-Lubarsch M 2019e	Low	Low	Low	Low	Low	Low	Low
Kesmodel US 2019	High	Low	Low	Low	Unclear	Low	Low
Landgren V 2019	Low	Low	Low	Low	Low	Low	Low
Gomez DA 2020	Low	Low	Low	Low	Low	Low	Low
Da Silva K 2021	Unclear	Low	Low	Low	Low	Low	Low
Jacobson SW 2021	Low	Low	Low	Low	Low	Low	Low
May PA 2021	Low	Low	Low	Low	Low	Low	Low

B

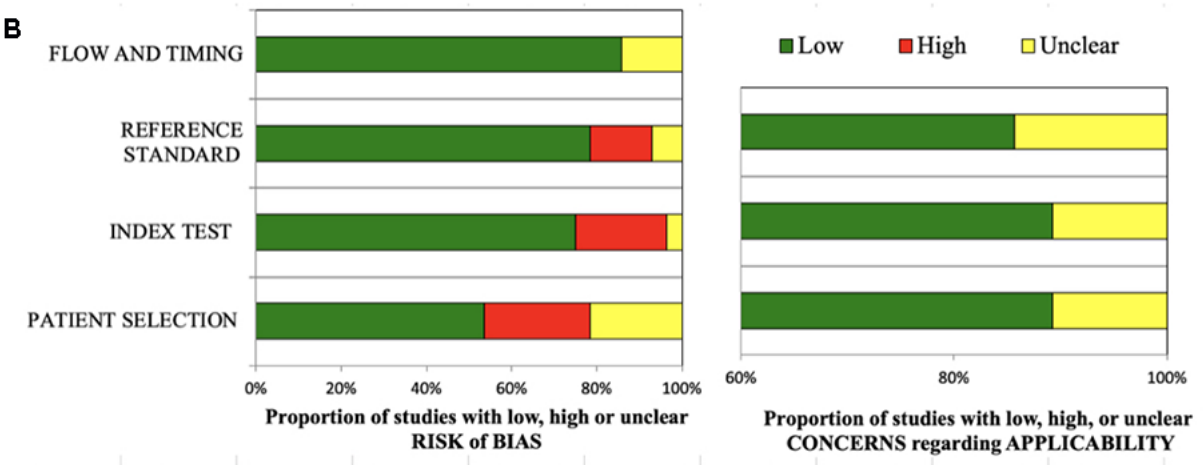


FIGURE 3
(A,B) Quadas-2 checklist for phenotype studies. The evaluation showed low risk of bias concerning flow and timing, reference standard and index test. Risk of bias in patient selection was low for about 54% of the studies (85).

Impact of age on facial parameters

One study describes a decreased proportion of patients exhibiting small palpebral fissures in adulthood (73). Another study also describes fading of short palpebral fissures, whereas a thin vermillion was still apparent and the flat philtrum was variable. This study also describes that the physical phenotype of FAS was most apparent during early childhood and least apparent during puberty (71). Another study describes fading of facial

TABLE 2 Showing the complete list of included studies and investigated parameters.

Author	Year	Ethnicity (nomenclature as mentioned in the respective study)	Population (Age)	Population (*n*=)	Control (*n*=)	Guideline used	Diagnosis FASD/FAS/PAE	Measurements	Results	Research Aim
Clarren SK	1987	White (15), Black (5), American Indian (1)	7.00	21 (2 FAS)	21	Alcohol consumption mother	FAS/probable FAE/possible FAE	2D photographs; landmarks face lateral/frontal	Short palpebral fissure length (PFL), long and flat midface, retrusive mandible	Expert diagnostics via photographs/facial morphometric analysis via landmarks
Sokol RJ	1991	Unclear	Newborn	21/25?	76	Alcohol consumption mother	FAS	Frontal/lateral Polaroid snapshots; landmarks face lateral/frontal	Short PFL, scoping out of the nasal bridge, thin vermilion	Facial features in neonates
Astley SJ	1995	African American; American Indian; Alaskan Native; Asian; other	5.20	194/27 FAS	no	Trained dysmorphologist, Gestalt diagnosis	FAS/pFAS	Expert evaluation	Screening tool parameters: PFL, philtrum smoothness, upper lip thinness, minimal influence by gender, race and age up to 10	Development of effective screening tool
Astley SJ	1996	White, Black, American Indian, Alaskan Native, Asian, Hispanic	6.50 (0–27)	42	84	expert	FAS	Frontal photographs	Parameters: Reduced PFL and innercanthal distance ratio, smooth philtrum, thin upper lip; unaffected by gender, race and age	Development of FAS diagnosis via photographic screening tool
Astley SJ	2000	Caucasian 57.5%; African American 9%; Native American/ Alaskan 14.1%; other 19.4%	Birth to 51 mth; mean: 10.1 (+/- 7)	454 (FAS 69, AFAS 41, PFAE 344)	no	Gestalt diagnosis	FAS/AFAS/ PFAE	Gestalt diagnosis vs. 4-digit diagnostic code	Classification with Gestalt and 4-digit diagnostic code is variable. Inter- and intrarater reliability of the 4-digit code (for 20/16 patients) was high	To describe and present preliminary assessments of the accuracy, precision and power of the 4-digit diagnostic code so that others can consider and evaluate its use
Meintjes EM	2002	Not mentioned	First grade children	0	44	Two dysmorphologists	Children with growth retardation	3D photographs vs. handheld ruler measurement, PFL, ICD and IPD	PFL is suitable for 3D analysis; 3D measurements for PFL, ICD and IPD are highly repeatable ICD and IPD	Evaluation of measurements on 3D photographs vs. measurements via handheld ruler
Douglas TS	2003	South Africa	6–7	0	46	FAS screening	Unclear/FAS screening	3D photographs; manual vs. automatic extraction of eye features	Values for PFL and IPD were within 1 mm, whereas ICD and OCD showed ICD and IPD greater differences	Comparison between the automatic vs. manual extraction of eye features in 3D photographs for PFL, IPD, ICD and OCD ICD and IPD
Naidoo S	2005	South Africa	8.90	90	90	Not mentioned	FAS	decayed missing filled teeth (dmft), DMFT, enamel opacities, plaque score, gingival bleeding	dmft FAS: 1.79 vs. control: 1.63; DMFT FAS 0.77 vs. control 0.94 anthropometry; 42% of the FAS sample manifested statistically significant growth retardation, more	Anthropometric measures and oral health

(*Continued*)

10.3389/fped.2023.1169570

TABLE 2 Continued

Author	Year	Ethnicity (nomenclature as mentioned in the respective study)	Population (Age)	Population (*n*=)	Control (*n*=)	Guideline used	Diagnosis FASD/FAS/ PAE	Measurements	Results	Research Aim
									plaque and gingival bleeding but not significant; no difference in enamel opacities; crowded incisors, maxillary overjet and openbite	
Hoyme HE	2006	Native American; South African	Not mentioned	164	Yes (matched control children)	Institute of Medicine (IOM)	FAS/pFAS/ ARND/ARBD	PFL, morphologic features of the philtral ridges and the upper lip	Revised IOM criteria	To present specific clarifications of the 1996 IOM criteria for the diagnosis of FASD, to facilitate their practical application in clinical pediatric practice
Naidoo S	2006[a]	Not mentioned	FAS: 8.90 Control: 9.1	90	90	IOM	FAS	Cephalometric analysis, cranial base, midface, mandible, soft tissue profile	Vertically and horizontally underdeveloped maxilla, longface syndrome with large gonial angle and a short ramus in relation to total face height; tendency anterior open bite	Cephalometric findings in patients with FAS
Naidoo S	2006[b]	coloured	FAS: 8.95 Control: 9.04	90	90	IOM	FAS	Panoramic radiographs, handwrist radiograph, dental maturaty, skeletal age, chronological age	Dental delay score was significantly lower for male children with FAS compared with control	Analysis of dental vs. skeletal age in patients with FAS
Grobbelaar R	2007	South African	6.50	0	48	Not mentioned	No FASD diagnosis	Eye measurements, upper lip circularity	Introduction of an approximation to the upper lip circularity, which replaces manual outlining of the lip on a digital image with more time-efficient selection of four points on the image; automated point selection is not suitable for eye measurements	Area based matching, stereophotogrammetry, manually vs. automatically selected reference points
Moore ES	2007	North American Caucasian, Finnish Caucasian, African American, Cape Coloured	NAC: FAS 10.9, control 11.1; AA: FAS 11.3, control 6.5; FC: FAS 13.1, control 13.8; CC FAS 5.6, control 5.3	124	152	Revised IOM	FAS	4 different populations (North American Caucasian, Finnish Caucasian, African American, Cape Coloured); 6 scans per participant, 3D images, customized software, 20 landmarks, 16 measurements	FAS can be effectively discriminated from controls in Caucasians and African admixture. The facial feature, which most effectively discriminates FAS and controls differed across the populations	The purpose of the study was to test whether computerized anthropometry can distinguish patients with FAS from controls across a wide age range as well as across ethnically disparate study populations

(*Continued*)

10.3389/fped.2023.1169570

TABLE 2 Continued

Author	Year	Ethnicity (nomenclature as mentioned in the respective study)	Population (Age)	Population (*n*=)	Control (*n*=)	Guideline used	Diagnosis FASD/FAS/PAE	Measurements	Results	Research Aim
Mutsvangwa TEM	2007	South African	FAS 7.11; controls 6.56	14	20	Expert/3 independent dysmorphologists	FAS	Procrustes, principal component analysis, face shape analysis, facial landmarks	No difference between control and FAS when using PFL, upper lip thinness and philtrum smoothness but significant difference with additional landmarks concerning the midfacial region	Morphometric analysis of facial landmark data to characterize the facial phenotype associated with FAS
Fang S	2008	South Africa and Finland	5.09 (South Africa) 13.12 (Finland)	86	63	Revised IOM	FAS	3D facial scan, facial feature analysis, feature computation, feature set identification, feature selection	Within the Finnish Caucasian group the automated technique correctly classified 88,2% of the FAS faces and 100% of the control faces; within the Cape Coloured sample 90,9% of FAS faces and 90% of control faces were classified correctly	To develop a computational model that can automatically compute facial features from 3D scans and use this data to identify children with FAS
Mutsvangwa TEM	2009	unclear	Infants/dummies	dummies	5 infants	–	–	Stereophotogrammetry, landmark distances were measured manually and in the software	The stereophotogrammetry precision results were better than those of the manual measurements; the manual measurements showed a higher degree of variability than the stereo-photogrammetry results; concerning stereophotogrammetry, landmarks with with low precision were: the distance from the middle of the philtrum to the crista philtri, pronasale to left subalare, pronasale to right pronasale, philtrum center to labiale superius	Testing of stereophotogrammetric tool for the diagnosis of FAS in infants
Mutsvangwa TEM	2010	Mixed ancestry	FAS 10.90; controls 7.99	17	17	dysmorphologist	FAS	Stereophotogrammetry; 3D coordinates of 26 landmarks, generalized Procrustes analysis, regression and discriminant function analysis were applied to stereophotogrammetrically derived 3D coordinates of landmarks	Analysis showed that the FAS face is characterized by small palpebral fissures, a thin upper lip, and midfacial hypoplasia 5-year old group cassified with 95.46% accuracy and the 12-year old group classified with 80.13% accuracy	Influence of age and size on shape; shape differences between FAS and controls

(*Continued*)

10.3389/fped.2023.1169570

TABLE 2 Continued

Author	Year	Ethnicity (nomenclature as mentioned in the respective study)	Population (Age)	Population (*n*=)	Control (*n*=)	Guideline used	Diagnosis FASD/FAS/PAE	Measurements	Results	Research Aim
Jones KL	2010	Native American, Alaskan Native, Asian, Hawaiian/Pacific Islander, Black/African American, White, Cape Coloured, multiracial, unknown ethnicity	Not mentioned	245 FAS	586	Key facial features	FAS	Dysmorphology assessment, additional features	For seven of the eight additional features, there was a „dose-response" relation with the children in the FAS group having the highest prevalence for each feature	Additional features of FAS, frequency of these features and variability concerning age, sex or race of the child
Astley SJ	2011	Caucasian, African American	6.0–16.9	822	90 6.0–16.9 years + 16 8.3–15.8 years	4-digit code	FASD	Palpebral fissure length, digital face photographs	The mean z-score of the healthy Caucasian group was in accordance with the mean growth curves on the Canadian charts (0.2 SDs) and were 1.6 SDs below the mean on the Hall chart; the mean PFL z-score for children with FAS was 2.4 SDs below the mean on the Canadian charts and 3.9 SDs below the mean on the Hall chart; The charts were not suitable for African Americans	Assess the goodness of two U.S. populations (healthy children & children with prenatal alcohol exposure) when plottet on the Canadian, Hall, and other published PFL charts
Douzgou S	2012	Not defined	5.50	42	?	Reported alcohol exposure	FASD	Genetic testing, e. g. routine karyotype, *in situ* fluorescence hybridisation, Fragile X	Genetic referral did not impact significantly on the general health of the child, the study highlighted that the most useful role of the geneticist was to identify and investigate alternative diagnoses	The study investigated the value of genetic assessment of children with suspected FASD
Suttie M	2013	Cape Coloured (mixed ancestry)		123	69	Hoyme	FAS/pFAS/HE	Dense surface modelling and signature analysis of 3D facial photographs	DSM-based representation of 3D face shape alone achieved perfect agreement for FAS and good agreement for FAS + pFAS; heat map comparison of dynamic morphing of faces to matched controls revealed facial dysmorphism, which was otherwise overlooked	Strategies to help detect facial dysmorphism across the fetal alcohol spectrum in children without classic facial characteristics

(*Continued*)

10.3389/fped.2023.1169570

TABLE 2 Continued

Author	Year	Ethnicity (nomenclature as mentioned in the respective study)	Population (Age)	Population (*n*=)	Control (*n*=)	Guideline used	Diagnosis FASD/FAS/ PAE	Measurements	Results	Research Aim
Avner M	2014	Not defined	4.8	40	no	Not defined	FASD?	PFL, philtrum smoothness; direct measurement vs. computer software measurement on photographs	Photographic measurements showed shorter PFL lengths than direct measurements; direct measurement scores for philtrum smoothness were different from the computer's measurements using the frontal view but not using the ¾ view	Validation of the computer assisted methods of photographic measurements by comparing the results to those by a trained physician performing direct measurements of the same child
Hoyme HE	2015	Cape Coloured (mixed race)	Not mentioned	400/1,057	no	Not defined	FASD	Two photographic views (frontal/45°); philtrum, vermillion border; Score 1–5 Testing of lip philtrum guide for Caucasian population vs. new lip philtrum guide for Cape Couloured population	New lip philtrum guide for Cape Coloured population; the results indicated more sensitivity of the new guide to detect the cardinal facial features of FASD in a coloured population	Introduction of a lip philtrum guide for a Cape Coloured population
Abell K	2016	South Africa, Italy, United States	5–9	273	981	lip philtrum/Hoyme	FAS/pFAS/ ARND	Extraoral mandibular and maxillary arc measurements with a flexible measuring tape, arc ratios	No significant differences in arc ratio measurements, except for males with FAS (ratio increased); female patients with FAS had significantly decreased maxillary arcs	Values for maxillary and mandibula arcs and maxillary to mandibular arc ratio
Suttie M	2017	Cape Coloured/ Caucasian	Cape Coloured FAS 10.6/ Highliuy Exposes (HE) 10.4; Caucasian FAS 11.8/HE 12.1	Cape Coloured 97 (22 FAS/75 HE)/ Caucasian (35 FAS + 73 HE)108	Cape Coloured 69 (mean age10.1)/ Caucasian141 (11.5)	Hoyme	FAS/HE	Curvature visualization and quantification; surface curvature-based delineations of the face form	Facial curvature assists the recognition of the effects of prenatal alcohol exposure and helps explain why different facial regions result in inconsistent control-FAS discrimination rates in disparate ethnic groups	Help clinicians detect the facial effects of prenatal alcohol exposure by developing computer-based tools for screening facial form
Valentine M	2017	South Africa, Italy and United States	5–9	89	50	According to May PA, Baete A, Russo J, et al. Prevalence and characteristics of fetal alcohol spectrum disorders. *Pediatrics*. 2014;134 (5):855–866. doi:10.1542/ peds.2013–3319	FAS/pFAS/ ARND	Manual examination, Dysmorphology scoring system vs. facial dysmorphology novel analysis—computer based recognition, 2D frontal images	Increased diagnostic accuracy for ARND via computer aided method	To compare detection of facial features by computer based recognition software of 2D images against manual examination in FASD

(*Continued*)

10.3389/fped.2023.1169570

TABLE 2 Continued

Author	Year	Ethnicity (nomenclature as mentioned in the respective study)	Population (Age)	Population (*n*=)	Control (*n*=)	Guideline used	Diagnosis FASD/FAS/PAE	Measurements	Results	Research Aim
Suttie M	2018	Caucasian/Latin American	13.00	72; (FAS 22; HE 50)	47	Hoyme	FAS/HE	3D image, MRI; facial growth delineations, caudate nucleus and corpus callosum	Combined morphology analysis of the caudate nucleus, and the corpus callosum, with the face better identify patients with FAS; caudate nucleus asymmetry was reduced for patients with FAS	To improve the understanding of the teratogenic effects of prenatal alcohol exposure by simultaneously considering face brain morphology and neurocognitive measures
Blanck-Lubarsch M	2019[a]	Caucasian	8.80 (control group: 8.2)	30	30	4-digit (German FAS Guideline, Landgraf)	FAS	Palatal depth; metric length measurement of the face in vertical dimension; 3D intraoral and facial scans	Palatal depth evaluation did not show significant differences; vertical facial measurements are suitable for FAS diagnosis with midfacial length being significantly shorter and the philtrum length being significantly longer in patients with FAS	To measure intraoral and extraoral dimensions of the maxilla and face in patients with FAS
Blanck-Lubarsch M	2019[b]	Caucasian	8.80 (control group: 8.1)	25	30	4-digit (German FAS Guideline, Landgraf)	FAS	3D facial scans; Philtrum depth measurements	Philtrum depth significantly differs between patients with FAS and healthy controls	To metrically assess philtrum depth in patients with FAS
Blanck-Lubarsch M	2019[c]	Caucasian	8.70 (control group:	28	30	4-digit (German FAS Guideline, Landgraf)	FAS	3D facial scans; inner canthal distance, mouth breadth, palpebral fissure length right/left, distance between alares nasi and sulcus alares nasi	Mouth breadth and breadth between nasal wings cannot be used for FAS diagnosis; nose breadth at the transition point of the sulcus alaris to the philtrum, inner canthal distance (only for males) and PFL are potential indicators for FAS	To investigate metrical difference concerning various facial features in the region of the eyes, nose and mouth
Del Campo M	2021	Not mentioned	1.67–17; mean: 8.33	56 (FAS/pFAS: 16; ARND: 50)	5	Revised IOM	FAS/pFAS/ARND	Telemedicine, face to face examination, 2 examiners	High agreement between telemedecine vs. face to face examination in identification of physical features of FAS	To compare telemedicine and face to face examinations of patients with FASD
Fu Z	2021	Not mentioned	4–18	1,549 facial scans	no	Not mentioned	FASD?	2D images; 14 FAS associated landmarks, regularized transfer learning framework	Results show that the proposed learning framework performs well with limited training samples	Facial anatomical landmark detection using regularized transfer learning with application to fetal alcohol syndrome recognition

(*Continued*)

10.3389/fped.2023.1169570

TABLE 2 Continued

Author	Year	Ethnicity (nomenclature as mentioned in the respective study)	Population (Age)	Population (*n*=)	Control (*n*=)	Guideline used	Diagnosis FASD/FAS/ PAE	Measurements	Results	Research Aim
Blanck-Lubarsch M	2022	Caucasian	FAS 8.8 Control 8.2	30	30	German FAS diagnostic guideline (Landgraf et al.)	FAS	3D-facial scans, decision trees, support vector machines, k-nearest neighbors, identification of suitable landmarks for FAS	Landmarks with highest scores were midfacial length, palpebral fissure length, nose breadth at sulcus nasi; all tested machine learning methods (k-nearest neighbors, decision trees and support vector machine) showed high accuracy of 89.5%	To identify machine learning methods from 3D facial scans to improve and objectify diagnosis of FAS
Riekman GA	1984	Native American	Not mentioned; primary dentition	19	20	Not mentioned	FAS	Oral hygiene status, dental caries and occlusion, arch length and circumference; full face profile photos, upper and lower dentition photos, teeth in occlusion photos, study models for the control group only study models were utilized	No significant differences were found	Oral findings in patients with FAS
Gir AV	1989	Urban American black chidren	Not mentioned	15	30 (age and ethnicity matched)	Not mentioned	FAS	Lateral cephalograms, 41 linear, angular and projected values were calculated	Forehead is unusually prominent in patients FAS, mandible is of normal overall size, the corpus of the mandible is significantly longer in patients with FAS, overdevelopment of the upper and lower thirds in patients with FAS	To quantitatively assess the craniofacial complex of children with FAS
O'Leary CM	1990	Australian, Aboriginal	Up to 5	84	yes	Prenatal alcohol exposure	FAS	Oral diseases	Children of mothers with alcohol diagnosis had increased odds of gingivitis and periodontal diseases, other diseases of the lip and oral mucosa and diseases of the salivary glands; the odds ratio for children with FAS having any dental admission by 5 years of age was 2.58, the number of children with FAS was too small to examine each of the dental diagnoses separately	Investigate the relationship between maternal alcohol-use disorder and dental hospital admissions in children up to 5 years of age
Rostand A	1990	French	Newborn, first week of life	202	no	Prenatal alcohol exposure	PAE	Standardized morphological examination, 17 craniofacial	Offspring of alcoholics and heavy drinkers in the first	

(*Continued*)

10.3389/fped.2023.1169570

TABLE 2 Continued

Author	Year	Ethnicity (nomenclature as mentioned in the respective study)	Population (Age)	Population (*n*=)	Control (*n*=)	Guideline used	Diagnosis FASD/FAS/ PAE	Measurements	Results	Research Aim
								characteristics, the number of characteristics was calculated for each infant	trimester had significantly more craniofacial characteristics than those of moderate and light drinkers; the authors conclude that craniofacial morphology might be a more sensitive and specific indicator of prenatal alcohol effect than other anomalies	Alcohol use in pregnancy, craniofacial features and fetal growth
Streissguth AP	1991	American Indian, White, Black	12–40	61	no	According to Clarren et al	FAS (70%)/ possible fetal alcohol exposed (30%)	IQ according to Wechsler, physical measurements, photographs, medical records, Vineland Adaptive Behaviour scale	Height and head circumference about 2 SDs below the population mean; less effect on weight; characteristic facies of patients with FAS became less distinctive with increasing age; reduced PFL, larger inner canthal distance, abnormalities of the philtrum, lips and misaligned teeth in patients with FAS	Follow- up study of adolescent and adult manifestations of FAS
Church MW	1997	African American, Caucasian	3.8–26.11	22	no	Expert dysmorphologist based on Rosett et al. (1980)	FAS	Hearing assessment, central auditory processing assessment, auditory brain stem response assessment, vestibular system assessment, language and speech assessment	All patients had continuing problems with recurrent serious otitis media throughout childhood; abnormal competing sentence test and abnormal word recognition with ipsilateral noise test; abnormally prolonged auditory brain stem response; normal vestibular function; significant receptive and expressive language deficits below the 5th percentile; dental malocclusions could be found but 52% of the patients had cleft palate	Assessment of patients with FAS for hearing disorders, evaluation of speech, language and vestibular problems, dentofacial anomalies

(*Continued*)

10.3389/fped.2023.1169570

TABLE 2 Continued

Author	Year	Ethnicity (nomenclature as mentioned in the respective study)	Population (Age)	Population (*n*=)	Control (*n*=)	Guideline used	Diagnosis FASD/FAS/ PAE	Measurements	Results	Research Aim
Moore ES	2002	Caucasian, African American, Other	Under the age of 18	100	31	IOM	FAS (41)/ pFAS (59)	Head breadth, minimal fronal breadth, bitragal breadth, bizygomatic breadth, bigonal breadth, interoccular breadth, biocular breadth, PFL, upper facial breadth; midfacial breadth, lower facial breadth, head length, nasal bridge length, nasal length, philtrum length, lower facial height, total facial height, ear length, maxillary arc, mandibular arc, head circumference	19 of 21 measurements differed significantly between FAS, pFAS and control, not significantly different were inner canthal distance and philtrum length; only seven of the measurements differed between pFAS and control, (head length, width, circumference; minimal frontal breadth, bitragal breadth, midfacial depth, total facial height)	Effects of alcohol exposure on the facial phenotype; to objectively describe the anthropometric facial gestalt of individuals diagnosed with FAS and pFAS
Autti-Rämö I	2006	Finnish	Mean 13.00 (8–20 years)	73	No (PFL was compared to American norms Thomas et al. 1987; anthropometric measures to Finnish norms, Sorva et al. 1990)	Revised IOM	FASD	Standard interview regarding family, medical and developmental history; anthropometric measurements, height, weight and head circumference, PFL, morphology of upper lip and philtrum, physical examination to assess major and minor anomalies	The results of the study indicate that the weighted dysmorphology score is a useful adjunctive tool in the clinical and/or research assessment.	To examine a cohort of Finnish children and adolescents with FAS and morphological, societal, cognitive and educational levels to compare the data to those previously published and to examine the utility of a weighted dysmorphology score
May PA	2007	Community in South Africa, other human populations	Different values in table vs. text; Values from table: FAS 10.28; pFAS 6.63; control: 6.29	73 (FAS 55, pFAS 18)	145	Revised IOM	FAS/pFAS	Demographic and growth parameters; dysmorphology score	Height, weight, BMI measures, head circumference, PFL was significantly different between FAS, pFAS and control including total dysmorphology scores, camptodactylie and altered palmar crease were significantly different between the groups	To further explore and summarize the epidemiology, the maternal risk, child characteristics, trends, and etiology of FAS and pFAS
Ervalahti N	2007	Not mentioned	8–16 (mean 11.8)	48 (30 FAS, 13 pFAS, 5 ARND)	No	Revised IOM	FAS/pFAS/ ARND	Complete physical examination, dysmorphology score according to Hoyme; cognitive capacity with abbreviated version of the Wechsler intelligence score	Performance on the Wechsler test was below average in all groups; significant difference in total dysmorphology score; more severe growth deficiencies and dysmorphic features were associated with poorer cognitive capacity	To clarify the extent to which dysmorphic features and growth deficiencies are associated with general cognitive capacity in a subsample of the participants

(*Continued*)

10.3389/fped.2023.1169570

TABLE 2 Continued

Author	Year	Ethnicity (nomenclature as mentioned in the respective study)	Population (Age)	Population (*n*=)	Control (*n*=)	Guideline used	Diagnosis FASD/FAS/ PAE	Measurements	Results	Research Aim
Spohr HL	2007	Caucasian	FAS: 24.7; fetal alcohol exosure (FAE): 21.6	37 (15 FAE; 22 FAS)	no	First examination: Expert in accordance with research society on alcoholism	FAS/FAE	Follow up: dysmorphologist, coded item list based on an interview, the young adult behaviour checklist	Despite substantial reduction of symptoms across time a sizeable number of subject still exhibited growth retardation, microcephaly, developmental delay and hyperactivity. In contrast the very marked craniofacial features mostly disappeared although elongated philtrum and thinner lip were still prominent;only 5% had ever held an ordinary job; young adult behaviour checklist: deviates significant for thought disorder, attention problems, intrusive behaviour, aggressive behaviour.	20-year follow up study
Feldmann HS	2012	White, otherethnicity, unknown	Newborn; 2.6 months	992	no	Alcohol mother, dysmorphologist; Chambers checklist	FASD	Dysmorphologist performed a blinded examination of all infants; patterns of drinking were evaluated by drinks per day, number of binge episodes and maximum number of drinks; timing of exposure was evaluated 0–6 week post conception, 6–12 weeks post conception, 1., 2.,3. trimester	Higher prenatal alcohol exposure in any pattern was significantly associated with the incidence of smooth philtrum but not with short palpebral fissures; strongest associations with timing of exposure were in the second half of the first trimester mostly for thin vermilion border; reduced birth length was increased with exposure in any trimester; the associations were linear and there was no evidence of a threshold	To examine how specific prenatal alcohol exposure patterns relate to characteristic alcohol related facial features and growth deficiencies

(*Continued*)

10.3389/fped.2023.1169570

TABLE 2 Continued

Author	Year	Ethnicity (nomenclature as mentioned in the respective study)	Population (Age)	Population (*n*=)	Control (*n*=)	Guideline used	Diagnosis FASD/FAS/PAE	Measurements	Results	Research Aim
Foroud T	2012	South Africa, Cape Coloured (mixed ancestry)	First clinic FAS/pFAS: 5.2; HE: 4.7; control 4.6 Second clinic: FAS/pFAS: 9.20; HE 8.6; control 8.6	76(FAS/pFAS: 35; HE: 41)	49	Revised IOM	FAS/pFAS/HE	3D facial images, 17 anthropometric measurements at 5 and 9 years, IQ; 3 groups (FAS/pFAS, HE and control), prenatal alcohol exposure	Upper facial width, ear length, lower facial depth and eye width were consistent predictors distinguishing those that were exposed from those that were not; prenatal alcohol exposure appears to have its primary effect on brain growth reflected by smaller forehead width; some measures were only predictive at certain ages	To present anthropometric measures that identify and best classify groups of children based on their alcohol exposure and accompanying facial dysmorphology
Nayak R	2012	India	6.21 (cases); 6.16 (controls)	26 (2 FAS; 4 pFAS; 2 neurobehavioural disorder, 18 static encephalopathy)	27 (controls with neurobehavioural disorder, static encephalopathy)	4-digit	FAS	Facial photographic analysis, Waldrop list of minor physical anomalies; child behaviour checklist for 4–16 yrs and 2–3 yrs; Mini international neuropsychiatric interview for children and adolescents; Vineland social maturity scale for below 6 yrs; Malin's intelligence for Indian children	Minor physical anomalies were more common in cases; among FAS facial features, only philtrum smoothness varied significantly; behavioural problems were more pronounced and intellectual functioning significantly poorer in cases	To evaluate the effects among children prenatally exposed to alcohol
Yang Y	2012[a]	Non Hispanic white; Asian; Native Hawaiians; African American; more than one ethnicity; Cape Coloured; European Whites	13.40 (FASD), 13.0 (non-exposed)	69	58	Alcohol mother; Dysmorphologist	FASD	MRI data acquisition, facial and cognitive evaluation	Subjects with FASD showed significantly thicker cortices in several frontal, temporal, and parietal regions; increased inferior frontal thickness correlated with reduced palpebral fissure length	To detect cortical thickness abnormalities in FASD and the association with facial dysmorphology

(*Continued*)

10.3389/fped.2023.1169570

TABLE 2 Continued

Author	Year	Ethnicity (nomenclature as mentioned in the respective study)	Population (Age)	Population (*n*=)	Control (*n*=)	Guideline used	Diagnosis FASD/FAS/ PAE	Measurements	Results	Research Aim
Yang Y	2012[b]	Non-Hispanic White; Asian, Native Hawaiian; African American; Cape Coloured (mixed ancestry); European Whites	12.80 (FASD); 12.3 (FASD)	82	71	Alcohol mother (maternal interview)	FASD	Facial and cognitive evaluation; MRI data acquisition	FASD subjects had smaller total brain and white matter volumes; FASD subjects consistently showed lower FSIQ (full scale IQ); FASD subjects showed significantly smaller PFL and increased Lipometer scores; significantly reduced callosal thickness in the anterior third and the splenium in FASD; no significant correlations between corpus callosum thickness or area measures and total number of drinks per week or average drinks per occasion in all three trimesters; callosal thickness and area measures were found significantly correlated with facial dysmorphology measures, specifically PFL scores were significantly correlated with callosal thickness (reduced cc thickness had smaller PFLs)	To investigate associations between facial dysmorphology and callosal thickness and area measures
May PA	2016[a]	92.9% Coloured (mixed race); 5.6% Black; 1.5% White	FAS 9.6; pFAS 8.5; ARND 8.7; controls 7.7	341(FAS 173, pFAS 109, ARND 59)	212	Revised IOM	FAS/pFAS/ ARND	Height, weight, head circumference; physical growth and dysmorphology score; assessment of cognitive and behavioural traits	Children with FASD were significantly smaller on height, weight, BMI; OFC; PFL, smooth philtrum and narrow vermillion; cognitive and behavioural traits were low, especially in ARND, followed by FAS and pFAS	Prevalence and characteristics of the continuum of diagnosis with FASD were researched in unstudied rural agricultural, lower socioeconomic populations in South Africa

(*Continued*)

10.3389/fped.2023.1169570

TABLE 2 Continued

Author	Year	Ethnicity (nomenclature as mentioned in the respective study)	Population (Age)	Population (*n*=)	Control (*n*=)	Guideline used	Diagnosis FASD/FAS/PAE	Measurements	Results	Research Aim
May PA	2016[b]	South Africa	FAS 7.5, pFAS 6.3; ARND 7.7; control 6.3	199 (FAS 69, pFAS 91, ARND 39)	207	Revised IOM	FAS/pFAS/ARND	Cognitive and behavioural traits	Significant differences concerning height, weight, BMI, OFC, PFL, smooth philtrum and narrow vermillion; head significance was a single trait which most distinguished one group from another; minor anomalies: maxillary and mandibular arcs, ICD, IPD; hypoplastic midface, epicanthal folds, ptosis, camptodactyly, flat nasal bridge, altered palmar creases, prognathism; cognitive testing and behaviour checklist low; correlation alcohol use with outcomes	The prevalence and characteristics of the continuum of diagnosis within FASD were researched in a fifth sample in a south African community
Treit S	2016	Caucasian, Aboriginal, other/unknown	12.50 (PAE); 11.9 (controls)	144 (33 FAS/pFAS; 79 ARND or FASD, 32 confirmed prenatal alcohol exposure)	145	Canadian and 4-digit code	PAE/FAS/pFAS	Head circumference and brain volumes from MRI, inter-site reliability; cognitive testing	High inter-site reliability of 0.994 for brain volume and head circumference 0.995; mean head circumference, brain volume and cognitive scores were significantly reduced in the prenatally exposure group, with overlap between groups; no significant correlations between head circumference and any cognitive scores	Relationship between head circumference an brain volume in children with PAE

(*Continued*)

10.3389/fped.2023.1169570

TABLE 2 Continued

Author	Year	Ethnicity (nomenclature as mentioned in the respective study)	Population (Age)	Population (*n*=)	Control (*n*=)	Guideline used	Diagnosis FASD/FAS/PAE	Measurements	Results	Research Aim
May PA	2017	Coloured (mixed ethnicity) 92.8%, Black 5.4%; White 1.6%, Other 0.1%	FAS 10.1; pFAS 8.7; ARND 9; controls 10.7	284 (FASD) (FAS 129, pFAS 100, ARND 55)	104	Revised IOM	FAS/pFAS/ARND	Maxillary/mandibular arc; inner canthal distance, interpupillary distance, hypoplastic midface, railroad track ears; ptosis; camptodactyly, altered palmar creases, anteverted nostrils	Shorter innercanthal and interpupillary distance, hypoplastic midface, ptosis, camptodactyly of the fingers, altered palmar creases were significantly more common among FASD groups and most common among children with FAS, even children with ARND have significantly more dysmorphology than controls	Prevalence rates, child characteristics and maternal risk factor in a rural community in South Africa
Blanck-Lubarsch M	2019[d]	Caucasian	8.80 (FAS); 8.2 (controls)	30	30	Specialist pediatrician	FAS	Swallowing pattern, oral habits, breast feeding, speech therapy, ergotherapy, physiotherapy, exfoliation of teeth, DMFT-index, modified DDE index and otitis media were recorded	Swallowing pattern, exfoliation of teeth and otitis media were not significantly different; significant differences could be found concerning mouth breathing, oral habits, age at termination of habits, speech treatment, ergotherapy, physiotherapy and breast feeding; DMFT and DDE-index showed significantly higher values for children with FAS	Tooth malformations, DMFT index, speech impairment and oral habits in children with FAS
Blanck-Lubarsch M	2019[e]	Caucasian	8.70 (FAS), 8.2 (controls)	28	30	4-digit; German Diagnostic Guideline (Landgraf et. al)	FAS	3D-facial scans, 3D-facial parameters at the mouth, nose and eye regions were measured	Significant differences could be found for the distance between left and right sulcus nasi, for the inner canthal distance, as well as for right and left palpebral fissure length; no significant differences for measurements of mouth breadth and breadth between the left and right alares nasi.	To find objective facial parameters for the verification of FAS(D).

(*Continued*)

10.3389/fped.2023.1169570

TABLE 2 Continued

Author	Year	Ethnicity (nomenclature as mentioned in the respective study)	Population (Age)	Population (*n*=)	Control (*n*=)	Guideline used	Diagnosis FASD/FAS/PAE	Measurements	Results	Research Aim
Kesmodel US	2019	Denmark	5.20	1,036?; 10 FASD	Not mentioned	4-digit?	FASD, alcohol exposure	Exposure assessment (interview concerning alcohol consumption); digital photos; measurement of three facial features (philtrum, upper lip, lip circularity) on 2D photographs; PFL	Children exposed to 1–4 drinks/week were 8.5 fold more likely to present with FAS/pFAS facial phenotypes, the risk was 2.5 fold increased in children with a single binge exposure in gestational weeks 3–4, the magnitude of expression of the FAS facial phenotype was significantly correlated with all other diagnostic features (growth deficiency, microcephaly and measures of CNS dysfunction)	To use the lifestyle during pregnancy study to assess potential effects of low to moderate weekly alcohol consumption and binge drinking in early pregnancy on facial features associated with FAS
Landgren V	2019	Russia, Poland, Romania, Latvia, Estonia	22	36 (FASD)	No	IOM	FASD	Clinical evaluation of social, medical, psychiatric, neuropsychological, adaptive and ophtamological status by a physician ophthalmologist, orthoptist and psychologist	Follow-up study of 15.5 years; in 21 individuals with FAS growth restriction in height and head circumference of approximately 1.8 SD persisted into adulthood; 56% were dependent on social support; 69 had gross motor coordination abnormalities; ophtamological abnormalities in 29/30; median IQ of 86 in childhood had declined significantly to 71 in adulthood; psychiatric disorders in 88%, most commonly attention deficit hyperactivity disorder; BMI steadily increased from start to adulthood; the proportion exhibiting small palpebral fissures had decreased considerably by adulthood (76% vs. 47%)	To characterize young adult outcome of FASD in a socially favourable rearing environment and to evaluate the diagnostic stability of FASD in the adulthood

(*Continued*)

10.3389/fped.2023.1169570

TABLE 2 Continued

Author	Year	Ethnicity (nomenclature as mentioned in the respective study)	Population (Age)	Population (*n*=)	Control (*n*=)	Guideline used	Diagnosis FASD/FAS/PAE	Measurements	Results	Research Aim
Gomez DA	2020	Cape Coloured (mixed ethnicity)	6.93	1,395; FAS 582; pFAS 481; ARND 332	604	Revised IOM	FAS/pFAS/ARND	Plastic ruler; ICD, IPD; OCD	Reductions in all three centiles ICD, IPD and OCD could be observed	We investigated how inner canthal distance, inter pupillary distance and outer canthal distance centiles differed between FASD and non-FASD individuals
Da Silva K	2021	Not mentioned	FASD 8.37; control 8.34	68	184	Guideline not mentioned, information from medical intake form, medical records	FASD	Retrospective study, oral health status	Children with FASD were significantly older at their first dental visit, had significantly higher DMFT/dmft. (score: 7.18 vs. 2.93); children with FASD were 4.71 times more likely to be referred for treatment under general anaesthesia	To investigate differences in oral health status indicators, treatment outcomes and risk factors for treatment under general anaesthesia for children with FASD compared to healthy controls
Jacobson SW	2021	Cape Coloured (mixed ancestry)	Early childhood (2005): FAS 6.5; pFAS 6.4; highly exposed 4.6; controls 5.1 School age (2009;+4 years) Puberty (2013; +4 years) Adolescence (2016;+3 years)	96; FAS 18; pFAS 27; highly exposed 51	59	Revised IOM	FAS/pFAS	Evaluation by dysmorphologists; weighted dysmorphology according to Hoyme	Prevalence of the physical phenotype was stable across the four ages for about half of the children with FAS and about one third of those with pFAS; the physical phenotype was most apparent during early childhood and least apparent during puberty, due to differences in timing of the growth spurt and evolving adult face; short palpebral features and small head circumference diminished with age, flat philtrum fluctuated while thin vermillion, weight and height restriction were stable	Findings from longitudinal study on the evolution of the physical phenotype of FAS and pFAS from early childhood to adolescence

(*Continued*)

10.3389/fped.2023.1169570

TABLE 2 Continued

Author	Year	Ethnicity (nomenclature as mentioned in the respective study)	Population (Age)	Population (*n*=)	Control (*n*=)	Guideline used	Diagnosis FASD/FAS/PAE	Measurements	Results	Research Aim
May PA	2021	Cape Coloured (mixed ethnicity) 68%; black African 16%; White 15%; Other 1%	7.2 (FAS); 7.1 (pFAS); 7.1 (ARND); 6.9 (controls)	181 FASD; (48 FAS, pFAS 65; ARND 67; ARBD 1)	137	Revised IOM	FAS/pFAS/ ARND/ARBD	2D photographs; dysmorphology examination; mother interview; cognitive and behavioural traits; OFC; BMI; height; weight; PFL; smooth philtrum; narrow vermillion of upper lip	Children with FAS, pFAS, ARND were significantly different from controls on all cardinal variables, multiple dysmorphology traits and neurobehavioural performance; women reporting first trimester drinking of 2 drinks per drinking day were 13 times more likely to having a child with FASD and those who reported drinking throughout pregnancy were 19.4 times more likely to having a child with FASD	Analysis of the common physical and neurobehavioural traits; association between alcohol and physical features

parameters with age with the exception of elongated philtrum and thinner lips (72).

Impact of alcohol on facial findings

One study found that the offspring of alcoholics and heavy drinkers in the first trimester had significantly more craniofacial characteristics than those of moderate and light drinkers (40). Another study describes that higher prenatal alcohol exposure in any pattern was significantly associated with the incidence of a smooth philtrum but not with short palpebral fissures (42). In one study, children exposed to 1–4 drinks/week were 8.5-fold more likely to present with FAS phenotypes and the risk was 2.5-fold increased in children with a single binge exposure in gestational week 3–4 (52).

3.11.2. Findings of the dentition

Three studies found significantly higher dmft/DMFT scores in patients with FASD (1 of these studies could only find higher dmft and not DMFT scores) (61, 63, 64). One study found that the DDE-index measuring structural tooth anomalies was significantly higher in patients with FAS (63). Another study describes misaligned teeth (55).

3.11.3. Findings of the upper and lower jaw bones

Differences in mandibular and maxillary arcs were found in two studies (39, 43), abnormal vertical facial measurements, such as vertically and horizontally underdeveloped maxilla, large gonial angle and a short ramus, tendency to anterior open bite were found in three studies (22, 61, 74). One study found that the mandible was of normal overall size whereas the corpus of the mandible was significantly longer in patients with FAS (60). Another study described prognathism (43).

3.11.4. General oral health

Two studies found increased odds for gingivitis or periodontal diseases (60, 62). The odds ratio for children with FAS of having any dental admission by 5 years of age was 2.58 (62). Patients with FASD were 4.71 times more likely to be referred for treatment under general anaesthesia in one study (64). Additionally, one study found significantly higher rates of mouth breathing and habits in patients with FASD (63).

4. Discussion

This review shows that various parameters in the orofacial region for the diagnosis for FASD have been found so far. However different diagnostic methods or differing landmarks (for example manual/automated vs. 2D/3D measurements) for the same characteristic were used, which leads to difficulties in matching study results into uniform criteria.

In parts this is due to a multitude of heterogeneous diagnostic guidelines, which exist for the diagnosis of FASD. These diagnostic guidelines have in parts similarities but are not comparable or universal (12, 13). Riley et al. compared four different guidelines and could show that they are comparable in the sense that they all use facial characteristics, growth retardation, CNS involvement

and alcohol exposure as the cardinal features (13). However, different cut-off values for diagnosis are used, for example the four-digit code requires a head circumference which is smaller by more than two standard deviations below the 2.5th percentile, whereas the revised IOM and the CDC require only measurements below the 10th percentile for FAS diagnosis.

The studies analyzed in this review most often used the IOM or revised IOM criteria, as well as the 4-digit diagnostic code or the German diagnostic guideline (5, 6, 14, 36, 37). Many studies however, only stated the verification of FASD via diagnosis by an expert dysmorphologist or reported alcohol consumption of the mother during pregnancy.

This lack in comparability and diagnostic standard concerning verification of a FASD diagnosis shows the importance of further clarification and standardization of this process. Another difficulty is that most studies included different ethnicities and therefore are not comparable. In addition, values or parameters for adults are not available. Only three studies investigated facial features in adult patients and Streissguth et al. concluded that characteristic facial features became less distinctive with increasing age (55, 72, 73).

Much progress seems to have been made concerning the investigation of new, objective and innovative diagnostic methods such as 3D-facial scans, stereophotogrammetry and machine learning approaches, which could facilitate and improve the diagnostic process in the future (20–35).

Many studies used 2D photographs in combination with the lip-philtrum guide as well as ruler measurements for the palpebral fissure length. Even if these are well-established methods in FASD detection, it seems that 3D measurements may be more accurate. Many studies used 3D-facial scans or 3D-photographs for further landmark analysis (21–25, 27, 29, 30, 32–34, 56–58).

Astley et al. compared accuracy of measurements of fissure length with a ruler with using the FAS facial photographic analysis software and found that the software was more accurate in comparison with a handheld ruler, which showed high interrater variability (75).

Meintjes et al. found high repeatability of PFL, ICD and IPD for 3D measurements in comparison with measurements with a handheld ruler (29).

A study by Mutsvangwa et al. could show that stereophotogrammetry precision results were better than those of manual measurements (31). Fang et al. found high precision for correct classification of FAS faces via automated techniques (59).

Suttie et al. found that facial curvature method assists the recognition of the effects of prenatal alcohol exposure (67). Another study by Suttie et al. could show that dense surface modelling achieved good agreement for FAS and pFAS and that heat map comparison of faces to matched controls revealed facial dysmorphisms with were otherwise overlooked (33). Valentine et al. also found an increased diagnostic accuracy for ARND via computer aided methods (35).

Machine learning methods such as decision trees, support vector machines and k-nearest neighbors proved to be accurate methods in detecting certain facial features in a study by Blanck-Lubarsch et al. (21). The above study results support that research is needed towards using 3D measurements as well as computer aided analysis methods or machine learning techniques since these methods seem to be accurate for FASD diagnosis.

Concerning the FASD phenotype, there were some parameters, which were repeatedly measured and mentioned as diagnostic features in FASD. These parameters comprise reduced palpebral fissure length, smooth philtrum, thin vermillion border and upper circularity, abnormal interpupillary or innercanthal distance and hypoplastic or flat midface (22, 23, 46, 48, 49, 70).

Unfortunately, the measuring or detection methods for most parameters were not metrically comparable between different studies because of different methodology (for 2D vs. 3D measurements) so that it was not possible to extract definite values for certain FASD parameters. For future research standardized measuring would improve comparability and enable the documentation of norm values for FASD diagnosis.

To date palpebral fissure length, smooth philtrum and thin vermillion border are cardinal parameters for the diagnostics of facial parameters in FASD diagnosis of most FASD guidelines (5, 6, 14, 15).

However, studies found that not all parameters are detectable in adulthood and another difficulty is that comparing facial parameters of patients to photographs in the lip-philtrum guide needs an expert dysmorphologist in the field of FASD (71–73).

Study results in various studies showed that multiple facial characteristics such as interpupillary or innercanthal distances, vertical measurements in x-rays or 3D-photographs, as well as nasal, maxillary or mandibular measurements could be used for FASD diagnosis (5, 6, 14, 15, 18, 21, 67, 74).

In addition, patients with FASD seem to have more dental and orthodontic treatment needs in comparison with healthy controls. Studies found higher dmft/DMFT values and more anomalies of the enamel structure (DDE-index) for FASD patients. Orthodontic findings included anterior open bite, horizontally and vertically underdeveloped maxilla, as well as prognathism. Mouth breathing and higher rates of habits were also found and can contribute to orthodontic problems such as open-bites, crossbites or increased sagittal distances between upper and lower front teeth (76). One study found a higher prevalence of crossbites and dental crowding in patients with FASD. These orthodontic problems need early treatment since dental crowding tends to aggravate with age and crossbites lead to asymmetric growth of the mandible or growth restriction of the upper jaw (77–83). Therefore, these dental and orthodontic parameters could not only contribute to the detection of FASD but also need to be kept in mind as these findings show the necessity for interdisciplinary treatment and early referral of the FASD patients to the dentist and/or orthodontist for prevention (43, 55, 61, 63, 64, 83). The included studies did not investigate dental findings in the deciduous dentition apart from dmft scores. In addition, it might be interesting to investigate, whether dental findings concerning crossbites or dental crowding are still characteristic parameters in the permanent dentition or whether these factors might be less frequent in adults because of orthodontic treatment in adolescence. Dental crowding is a malocclusion, which becomes worse with age even in healthy subjects (78), which in turn could result in dental crowding not being a distinguishing characteristic for FASD in adults. Therefore, these orofacial findings should be investigated for different age groups.

Further research should aim at finding values for abnormal parameters in FASD and defining universal, favorably digital measuring methods. The latter would help to store the data more easily and provide it to bio databanks, that should be accessible worldwide.

Once homogeneous and easy to apply measuring methods for the detection of FASD are defined, a routine screening of small patients could be applied by pediatricians within routine check-ups, or to for example kindergarten or primary school children, thus enabling early developmental care for patients with FASD. Early detection of FASD seems even more important since studies found a possible fading of facial parameters with age and in adult patients thus making diagnosis at older ages more difficult (55, 71, 73). If the applied methods were universal across different countries, this would allow for comparability and improvement of the diagnostic process. In addition, routine screening procedures in early childhood could reduce the number of undetected FASD patients which is suspected to be high across the world.

Furthermore, finding additional facial parameters could improve the development of machine learning methods in FASD screening.

Further studies investigating facial features in adults could find helpful parameters for the diagnosis of patients with FASD, which were not diagnosed in childhood or adolescence.

The results of this review stress the need for uniform diagnostic criteria and measuring methods. Comparable values are necessary in order to create bio databases with values for different degrees, ethnicities and ages.

5. Conclusion

This review could show that uniform diagnostic criteria and parameters for the orofacial region in FASD diagnosis are needed. Many facial parameters in the orofacial region for the detection of FASD have been found so far but only few of them are part of the diagnostic processes or current guidelines.

Further research should aim:

- to find among the existing characteristics the most comparable parameters
- to find parameters which are easy to measure for routine pediatric screenings as it is important to detect patients at young ages, even more since there seems to be a fading in facial parameters with age
- to examine larger groups of different ethnicities to find objective and uniform criteria
- to create a bio database with values and parameters for different ethnicities, degrees and age groups
- to address machine learning and 3D-facial measurement approaches as these seem to be more accurate and might facilitate the diagnostic process
- to find a consensus for one globally valid guideline with special consideration of different ethnicities and age groups

In addition, several orofacial findings hint at a higher need for dental and orthodontic treatment. This stresses the need for early referral to a dentist or orthodontist.

Author contributions

Conceptualization, MB and AH; methodology, MB, DD; software, DD; validation, MB, RF, AH and DD; formal analysis, MB, DD; investigation, MB, AH; resources, AH; data curation, MB, DD; writing—original draft preparation, MB; writing—review and editing, MB, RF, DD, AH; visualization, MB; supervision, AH; project administration, MB, AH. All authors have read and agreed to the published version of the manuscript. All authors contributed to the article and approved the submitted version.

Acknowledgments

We acknowledge Open Access support from the University of Muenster.

Conflict of interest

The authors declare that the research was conducted in the absence of any commercial or financial relationships that could be construed as a potential conflict of interest.

Publisher's note

All claims expressed in this article are solely those of the authors and do not necessarily represent those of their affiliated organizations, or those of the publisher, the editors and the reviewers. Any product that may be evaluated in this article, or claim that may be made by its manufacturer, is not guaranteed or endorsed by the publisher.

References

1. Popova S, Lange S, Probst C, Gmel G, Rehm J. Estimation of national, regional, and global prevalence of alcohol use during pregnancy and fetal alcohol syndrome: a systematic review and meta-analysis. *Lancet Glob Health*. (2017) 5(3):e290–e9. doi: 10.1016/S2214-109X(17)30021-9

2. Jones KL, Smith DW. Recognition of the fetal alcohol syndrome in early infancy. *Lancet*. (1973) 302(7836):999–1001. doi: 10.1016/S0140-6736(73)91092-1

3. Jones KL, Smith DW. The fetal alcohol syndrome. *Teratology*. (1975) 12(1):1–10. doi: 10.1002/tera.1420120102

4. May PA, Baete A, Russo J, Elliott AJ, Blankenship J, Kalberg WO, et al. Prevalence and characteristics of fetal alcohol spectrum disorders. *Pediatrics*. (2014) 134 (5):855–66. doi: 10.1542/peds.2013-3319

5. Hoyme HE, Kalberg WO, Elliott AJ, Blankenship J, Buckley D, Marais AS, et al. Updated clinical guidelines for diagnosing fetal alcohol Spectrum disorders. *Pediatrics*. (2016) 138(2). doi: 10.1542/peds.2015-4256

6. Chudley AE, Conry J, Cook JL, Loock C, Rosales T, LeBlanc N, et al. Fetal alcohol spectrum disorder: canadian guidelines for diagnosis. *Can Med Assoc J*. (2005) 172(5 Suppl):S1–S21. doi: 10.1503/cmaj.1040302

7. May PA, Chambers CD, Kalberg WO, Zellner J, Feldman H, Buckley D, et al. Prevalence of fetal alcohol Spectrum disorders in 4 US communities. *JAMA*. (2018) 319(5):474–82. doi: 10.1001/jama.2017.21896

8. Popova S, Lange S, Chudley AE, Reynolds JN, Rehm J. World Health Organization International Study on the Prevalence of Fetal Alcohol Spectrum Disorder (FASD) (2018).

9. Lange S, Probst C, Gmel G, Rehm J, Burd L, Popova S. Global prevalence of fetal alcohol Spectrum disorder among children and youth: a systematic review and meta-analysis. *JAMA Pediatr*. (2017) 171(10):948–56. doi: 10.1001/jamapediatrics.2017.1919

10. Warren KR, Bast RJ. Alcohol-related birth defects: an update. *Public Health Rep*. (1988) 103(6):638–42.

11. Lemoine P, Harousseau H, Borteyru JP, Menuet JC. Children of alcoholic parents—anomalies in 127 cases. *Arch Fr Pediatr*. (1968) 25(7):830.

12. Coles CD, Gailey AR, Mulle JG, Kable JA, Lynch ME, Jones KL. A comparison among 5 methods for the clinical diagnosis of fetal alcohol Spectrum disorders. *Alcohol Clin Exp Res*. (2016) 40(5):1000–9. doi: 10.1111/acer.13032

13. Riley EP, Infante MA, Warren KR. Fetal alcohol spectrum disorders: an overview. *Neuropsychol Rev*. (2011) 21(2):73–80. doi: 10.1007/s11065-011-9166-x

14. Astley SJ. *Diagnostic guide for fetal alcohol Spectrum disorders: The 4- digit diagnostic code*. Seattle WA: University of Washington Publication Services (2004).

15. Bertrand JFR, Weber MK, O'Connor M, Riley EP, Johnson KA, Cohen DE, et al. Fetal Alcohol Syndrome: Guidelines for Referral and Diagnosis. (2004). Available at: https://www.cdc.gov/ncbddd/fasd/documents/FAS_guidelines_accessible-P.pdf

16. Clarren SK, Chudley AE, Wong L, Friesen J, Brant R. Normal distribution of palpebral fissure lengths in Canadian school age children. *Can J Clin Pharmacol*. (2010) 17(1):e67–78.

17. Greenbaum R, Koren G. Fetal alcohol spectrum disorder—new diagnostic initiatives. *Paediatr Child Health*. (2002) 7(3):139–41. doi: 10.1093/pch/7.3.139

18. Astley SJ, Clarren SK. Diagnosing the full spectrum of fetal alcohol-exposed individuals: introducing the 4-digit diagnostic code. *Alcohol Alcohol*. (2000) 35 (4):400–10. doi: 10.1093/alcalc/35.4.400

19. Astley SJ, Stachowiak J, Clarren SK, Clausen C. Application of the fetal alcohol syndrome facial photographic screening tool in a foster care population. *J Pediatr*. (2002) 141(5):712–7. doi: 10.1067/mpd.2002.129030

20. Avner M, Henning P, Koren G, Nulman I. Validation of the facial photographic in fetal alcohol spectrum disorder screening and diagnosis. *J Popul Ther Clin Pharmacol*. (2014) 21(1):e106–13.

21. Blanck-Lubarsch M, Dirksen D, Feldmann R, Bormann E, Hohoff A. Simplifying diagnosis of fetal alcohol syndrome using machine learning methods. *Front Pediatr*. (2022) 9. doi: 10.3389/fped.2021.707566

22. Blanck-Lubarsch M, Dirksen D, Feldmann R, Sauerland C, Hohoff A. Children with fetal alcohol syndrome (FAS): 3D-analysis of palatal depth and 3D-metric facial length. *Int J Environ Res Public Health*. (2019) 17(1). doi: 10.3390/ijerph17010095

23. Blanck-Lubarsch M, Dirksen D, Feldmann R, Sauerland C, Hohoff A. 3D-Analysis of mouth, nose and eye parameters in children with fetal alcohol syndrome (FAS). *Int J Environ Res Public Health*. (2019) 16(14). doi: 10.3390/ijerph16142535

24. Blanck-Lubarsch M, Dirksen D, Feldmann R, Sauerland C, Kirschneck C, Hohoff A. 3D Analysis of philtrum depth in children with fetal alcohol syndrome. *Alcohol Alcohol*. (2019) 54(2):152–8. doi: 10.1093/alcalc/agy088

25. Blanck-Lubarsch M, Dirksen D, Feldmann R, Sauerland C, Kirschneck C, Hohoff A. Asymmetry-index and orthodontic facial analysis of children with foetal alcohol syndrome using 3D-facial scans. *Pediatr Res*. (2019) 88(2):243–9. doi: 10.1038/s41390-019-0559-5

26. Chik L, Sokol RJ, Martier SS, editors. *Computer aided morphometry of the neonatal fetal alcohol syndrome face*. Bellingham, WA, United States: Publ by Society of Photo-Optical Instrumentation Engineers (1993).

27. Douglas TS, Martinez F, Meintjes EM, Vaughan CL, Viljoen DL. Eye feature extraction for diagnosing the facial phenotype associated with fetal alcohol syndrome. *Med Biol Eng Comput*. (2003) 41(1):101–6. doi: 10.1007/BF02343545

28. Grobbelaar R, Douglas TS. Stereo image matching for facial feature measurement to aid in fetal alcohol syndrome screening. *Med Eng Phys*. (2007) 29 (4):459–64. doi: 10.1016/j.medengphy.2006.06.005

29. Meintjes EM, Douglas TS, Martinez F, Vaughan CL, Adams LP, Stekhoven A, et al. A stereo-photogrammetric method to measure the facial dysmorphology of children in the diagnosis of fetal alcohol syndrome. *Med Eng Phys*. (2002) 24 (10):683–9. doi: 10.1016/S1350-4533(02)00114-5

30. Mutsvangwa T, Douglas TS. Morphometric analysis of facial landmark data to characterize the facial phenotype associated with fetal alcohol syndrome. *J Anat*. (2007) 210(2):209–20. doi: 10.1111/j.1469-7580.2006.00683.x

31. Mutsvangwa TE, Smit J, Hoyme HE, Kalberg W, Viljoen DL, Meintjes EM, et al. Design, construction, and testing of a stereo-photogrammetric tool for the diagnosis of fetal alcohol syndrome in infants. *IEEE Trans Med Imaging*. (2009) 28(9):1448–58. doi: 10.1109/TMI.2009.2017375

32. Mutsvangwa TEM, Meintjes EM, Viljoen DL, Douglas TS. Morphometric analysis and classification of the facial phenotype associated with fetal alcohol syndrome in 5- and 12-year-old children. *Am J Med Genet A*. (2010) 152(1):32–41. doi: 10.1002/ajmg.a.33137

33. Suttie M, Foroud T, Wetherill L, Jacobson JL, Molteno CD, Meintjes EM, et al. Facial dysmorphism across the fetal alcohol spectrum. *Pediatrics*. (2013) 131(3): e779–e88. doi: 10.1542/peds.2012-1371

34. Suttie M, Wozniak JR, Parnell SE, Wetherill L, Mattson SN, Sowell ER, et al. Combined face–brain morphology and associated neurocognitive correlates in fetal alcohol Spectrum disorders. *Alcohol Clin Exp Res*. (2018) 42(9):1769–82. doi: 10.1111/acer.13820

35. Valentine M, Bihm DCJ, Wolf L, Hoyme HE, May PA, Buckley D, et al. Computer-Aided recognition of facial attributes for fetal alcohol Spectrum disorders. *Pediatrics*. (2017) 140(6). doi: 10.1542/peds.2016-2028

36. Hoyme HE, May PA, Kalberg WO, Kodituwakku P, Gossage JP, Trujillo PM, et al. A practical clinical approach to diagnosis of fetal alcohol spectrum disorders: clarification of the 1996 institute of medicine criteria. *Pediatrics*. (2005) 115 (1):39–47. doi: 10.1542/peds.2004-0259

37. Landgraf MN, Nothacker M, Heinen F. Diagnosis of fetal alcohol syndrome (FAS): german guideline version 2013. *Eur J Paediatr Neurol*. (2013) 17(5):437–46. doi: 10.1016/j.ejpn.2013.03.008

38. Astley SJ, Clarren SK. A fetal alcohol syndrome screening tool. *Alcohol Clin Exp Res*. (1995) 19(6):1565–71. doi: 10.1111/j.1530-0277.1995.tb01025.x

39. Abell K, May W, May PA, Kalberg W, Hoyme HE, Robinson LK, et al. Fetal alcohol spectrum disorders and assessment of maxillary and mandibular arc measurements. *Am J Med Genet A*. (2016) 170(7):1763–71. doi: 10.1002/ajmg.a.37656

40. Rostand A, Kaminski M, Lelong N, Dehaene P, Delestret I, Klein-Bertrand C, et al. Alcohol use in pregnancy, craniofacial features, and fetal growth. *J Epidemiol Community Health*. (1990) 44(4):302–6. doi: 10.1136/jech.44.4.302

41. Autti-Rämö I, Fagerlund A, Ervalahti N, Loimu L, Korkman M, Hoyme HE. Fetal alcohol spectrum disorders in Finland: clinical delineation of 77 older children and adolescents. *Am J Med Genet A*. (2006) 140(2):137–43. doi: 10.1002/ajmg.a.31037

42. Feldman HS, Jones KL, Lindsay S, Slymen D, Klonoff-Cohen H, Kao K, et al. Prenatal alcohol exposure patterns and alcohol-related birth defects and growth deficiencies: a prospective study. *Alcohol Clin Exp Res*. (2012) 36(4):670–6. doi: 10.1111/j.1530-0277.2011.01664.x

43. May PA, De Vries MM, Marais AS, Kalberg WO, Buckley D, Adnams CM, et al. Replication of high fetal alcohol spectrum disorders prevalence rates, child characteristics, and maternal risk factors in a second sample of rural communities in South Africa. *Int J Environ Res Public Health*. (2017) 14(5). doi: 10.3390/ijerph14050522

44. Gomez DA, May PA, Tabachnick BG, Hasken JM, Lyden ER, Kalberg WO, et al. Ocular measurements in fetal alcohol spectrum disorders. *Am J Med Genet A*. (2020) 182(10):2243–52. doi: 10.1002/ajmg.a.61759

45. Clarren SK, Sampson PD, Larsen J, Donnell DJ, Barr HM, Bookstein FL, et al. Facial effects of fetal alcohol exposure: assessment by photographs and morphometric analysis. *Am J Med Genet*. (1987) 26(3):651–66. doi: 10.1002/ajmg.1320260321

46. Sokol RJ, Chik L, Martier SS, Salari V. Morphometry of the neonatal fetal alcohol syndrome face from "snapshots". *Alcohol Alcohol Suppl*. (1991) 1:531–4.

47. Astley SJ, Clarren SK. A case definition and photographic screening tool for the facial phenotype of fetal alcohol syndrome. *J Pediatr*. (1996) 129(1):33–41. doi: 10.1016/S0022-3476(96)70187-7

48. Astley SJ. Canadian Palpebral fissure length growth charts reflect a good fit for two school and fasd clinic-based U.S. Populations. *J Clin Pharmacol*. (2011) 18(2): e231–e41.

49. Hoyme HE, Hoyme DB, Elliott AJ, Blankenship J, Kalberg WO, Buckley D, et al. A South African mixed race lip/philtrum guide for diagnosis of fetal alcohol spectrum disorders. *Am J Med Genet A*. (2015) 167(4):752–5. doi: 10.1002/ajmg.a.37023

50. Fu Z, Jiao J, Suttie M, Noble JA. Facial anatomical landmark detection using regularized transfer learning with application to fetal alcohol syndrome recognition. *IEEE J Biomed Health Inform*. (2021) 26(4):1591–601. doi: 10.1109/JBHI.2021.3110680

51. Nayak R, Murthy P, Girimaji S, Navaneetham J. Fetal alcohol spectrum disorders–a case-control study from India. *J Trop Pediatr*. (2012) 58(1):19–24. doi: 10.1093/tropej/fmr015

52. Kesmodel US, Nygaard SS, Mortensen EL, Bertrand J, Denny CH, Glidewell A, et al. Are low-to-moderate average alcohol consumption and isolated episodes of binge drinking in early pregnancy associated with facial features related to fetal alcohol syndrome in 5-year-old children? *Alcohol Clin Exp Res*. (2019) 43 (6):1199–212. doi: 10.1111/acer.14047

53. May PA, Marais AS, De Vries MM, Buckley D, Kalberg WO, Hasken JM, et al. The prevalence, child characteristics, and maternal risk factors for the continuum of fetal alcohol spectrum disorders: a sixth population-based study in the same South African community. *Drug Alcohol Depend*. (2021) 218:108408. doi: 10.1016/j.drugalcdep.2020.108408

54. Riekman GA. Oral findings of fetal alcohol syndrome patients. *J Can Dent Assoc*. (1984) 50(11):841–2.

55. Streissguth AP, Aase JM, Clarren SK, Randels SP, Ladue RA, Smith DF. Fetal alcohol syndrome in adolescents and adults. *J Am Med Assoc*. (1991) 265 (15):1961–7. doi: 10.1001/jama.1991.03460150065025

56. Moore ES, Ward RE, Wetherill LF, Rogers JL, Autti-Rämö I, Fagerlund A, et al. Unique facial features distinguish fetal alcohol syndrome patients and controls in diverse ethnic populations. *Alcohol Clin Exp Res*. (2007) 31(10):1707–13. doi: 10.1111/j.1530-0277.2007.00472.x

57. Foroud T, Wetherill L, Vinci-Booher S, Moore ES, Ward RE, Hoyme HE, et al. Relation over time between facial measurements and cognitive outcomes in fetal alcohol-exposed children. *Alcohol Clin Exp Res*. (2012) 36(9):1634–46. doi: 10.1111/j.1530-0277.2012.01750.x

58. Fang S, McLaughlin J, Fang J, Huang J, Autti-Rämö I, Fagerlund A, et al. Automated diagnosis of fetal alcohol syndrome using 3D facial image analysis. *Orthod Craniofacial Res*. (2008) 11(3):162–71. doi: 10.1111/j.1601-6343.2008.00425.x

59. Naidoo S, Norval G, Swanevelder S, Lombard C. Foetal alcohol syndrome: a dental and skeletal age analysis of patients and controls. *Eur J Orthod*. (2006) 28 (3):247–53. doi: 10.1093/ejo/cji109

60. Gir AV, Aksharanugraha K, Harris EF. A cephalometric assessment of children with fetal alcohol syndrome. *Am J Orthod Dentofac*. (1989) 95(4):319–26. doi: 10.1016/0889-5406(89)90165-0

61. Naidoo S, Chikte U, Laubscher R, Lombard C. Fetal alcohol syndrome: anthropometric and oral health status. *J Contemp Dent Pract*. (2005) 6(4):101–15. doi: 10.5005/jcdp-6-4-101

62. O'Leary CM, Slack-Smith LM. Dental hospital admissions in the children of mothers with an alcohol-related diagnosis: a population-based, data-linkage study. *J Pediatr*. (2013) 163(2):515–20.e1. doi: 10.1016/j.jpeds.2013.02.020

63. Blanck-Lubarsch M, Dirksen D, Feldmann R, Sauerland C, Hohoff A. Tooth malformations, dmft index, speech impairment and oral habits in patients with fetal alcohol syndrome. *Int J Environ Res Public Health*. (2019) 16(22). doi: 10.3390/ijerph16224401

64. Da Silva K, Wood D. The oral health status and treatment needs of children with fetal alcohol spectrum disorder. *Clin Oral Investig*. (2021) 25(6):3497–503. doi: 10.1007/s00784-020-03671-0

65. May PA, Gossage JP, Marais AS, Adnams CM, Hoyme HE, Jones KL, et al. The epidemiology of fetal alcohol syndrome and partial FAS in a South African community. *Drug Alcohol Depend*. (2007) 88(2–3):259–71. doi: 10.1016/j.drugalcdep.2006.11.007

66. del Campo M, Beach D, Wells A, Jones KL. Use of telemedicine for the physical examination of children with fetal alcohol Spectrum disorders. *Alcohol Clin Exp Res*. (2021) 45(2):409–17. doi: 10.1111/acer.14533

67. Suttie M, Wetherill L, Jacobson SW, Jacobson JL, Hoyme HE, Sowell ER, et al. Facial curvature detects and explicates ethnic differences in effects of prenatal alcohol exposure. *Alcohol Clin Exp Res*. (2017) 41(8):1471–83. doi: 10.1111/acer.13429

68. Yang Y, Phillips OR, Kan E, Sulik KK, Mattson SN, Riley EP, et al. Callosal thickness reductions relate to facial dysmorphology in fetal alcohol Spectrum disorders. *Alcohol Clin Exp Res*. (2012) 36(5):798–806. doi: 10.1111/j.1530-0277.2011.01679.x

69. May PA, de Vries MM, Marais AS, Kalberg WO, Adnams CM, Hasken JM, et al. The continuum of fetal alcohol spectrum disorders in four rural communities in South Africa: prevalence and characteristics. *Drug Alcohol Depend*. (2016) 159:207–18. doi: 10.1016/j.drugalcdep.2015.12.023

70. May PA, Marais AS, de Vries MM, Kalberg WO, Buckley D, Hasken JM, et al. The continuum of fetal alcohol spectrum disorders in a community in South Africa: prevalence and characteristics in a fifth sample. *Drug Alcohol Depend*. (2016) 168:274–86. doi: 10.1016/j.drugalcdep.2016.09.025

71. Jacobson SW, Hoyme HE, Carter RC, Dodge NC, Molteno CD, Meintjes EM, et al. Evolution of the physical phenotype of fetal alcohol Spectrum disorders from childhood through adolescence. *Alcohol Clin Exp Res*. (2021) 45(2):395–408. doi: 10.1111/acer.14534

72. Spohr HL, Willms J, Steinhausen HC. Fetal alcohol spectrum disorders in young adulthood. *J Pediatr*. (2007) 150(2):175–9. 9 e1. doi: 10.1016/j.jpeds.2006.11.044

73. Landgren V, Svensson L, Gyllencreutz E, Aring E, Gronlund MA, Landgren M. Fetal alcohol spectrum disorders from childhood to adulthood: a Swedish population-based naturalistic cohort study of adoptees from Eastern Europe. *BMJ Open*. (2019) 9 (10):e032407. doi: 10.1136/bmjopen-2019-032407

74. Naidoo S, Harris A, Swanevelder S, Lombard C. Foetal alcohol syndrome: a cephalometric analysis of patients and controls. *Eur J Orthod*. (2006) 28(3):254–61. doi: 10.1093/ejo/cji110

75. Astley SJ. Palpebral fissure length measurement: accuracy of the FAS facial photographic analysis software and inaccuracy of the ruler. *J Popul Ther Clin Pharmacol*. (2015) 22(1):e9–e26.

76. Festa P, Mansi N, Varricchio AM, Savoia F, Cali C, Marraudino C, et al. Association between upper airway obstruction and malocclusion in mouth-breathing children. *Acta Otorhinolaryngol Ital*. (2021) 41(5):436–42. doi: 10.14639/0392-100X-N1225

77. Lippold C, Stamm T, Meyer U, Vegh A, Moiseenko T, Danesh G. Early treatment of posterior crossbite–a randomised clinical trial. *Trials*. (2013) 14:20. doi: 10.1186/1745-6215-14-20

78. Lombardo G, Vena F, Negri P, Pagano S, Barilotti C, Paglia L, et al. Worldwide prevalence of malocclusion in the different stages of dentition: a systematic review and meta-analysis. *Eur J Paediatr Dent*. (2020) 21(2):115–22. doi: 10.23804/ejpd.2020.21.02.05

79. McNamara JA. Maxillary transverse deficiency. *Am J Orthod Dentofacial Orthop*. (2000) 117(5):567–70. doi: 10.1016/s0889-5406(00)70202-2

80. McNamara JA Jr. Early intervention in the transverse dimension: is it worth the effort? *Am J Orthod Dentofacial Orthop*. (2002) 121(6):572–4. doi: 10.1067/mod.2002.124167

81. Melink S, Vagner MV, Hocevar-Boltezar I, Ovsenik M. Posterior crossbite in the deciduous dentition period, its relation with sucking habits, irregular orofacial functions, and otolaryngological findings. *Am J Orthod Dentofacial Orthop*. (2010) 138(1):32–40. doi: 10.1016/j.ajodo.2008.09.029

82. Pinto AS, Buschang PH, Throckmorton GS, Chen P. Morphological and positional asymmetries of young children with functional unilateral posterior crossbite. *Am J Orthod Dentofacial Orthop*. (2001) 120(5):513–20. doi: 10.1067/mod.2001.118627a

83. Blanck-Lubarsch M, Flieger S, Feldmann R, Kirschneck C, Sauerland C, Hohoff A. Malocclusion can give additional hints for diagnosis of fetal alcohol spectrum disorder. *Alcohol Alcohol*. (2019) 54(1):56–61. doi: 10.1093/alcalc/agy071

84. Page MJ, Moher D, Bossuyt PM, Boutron I, Hoffmann TC, Mulrow CD, et al. PRISMA 2020 explanation and elaboration: updated guidance and exemplars for reporting systematic reviews. *BMJ (OPEN ACCESS)*. (2021) 372:n160. doi: 10.1136/bmj.n160

85. Whiting PF, Rutjes AWS, Westwood ME, Mallett S, Deeks JJ, Reitsma JB, et al. QUADAS-2: a revised tool for the quality assessment of diagnostic accuracy studies. *Ann Intern Med*. (2011) 155(8):529–36. doi: 10.7326/0003-4819-155-8-201110180-00009

frontiers | Frontiers in Neuroscience

TYPE Original Research
PUBLISHED 09 June 2023
DOI 10.3389/fnins.2023.1188367

Check for updates

OPEN ACCESS

EDITED BY
Kirsten A. Donald,
University of Cape Town, South Africa

REVIEWED BY
Anish Kumar Simhal,
Memorial Sloan Kettering Cancer Center, United States
Lijia Zhang,
Duke University, United States

*CORRESPONDENCE
Justine Fraize
✉ justine.fraize@inserm.fr
David Germanaud
✉ david.germanaud@cea.fr

†These authors have contributed equally to this work

RECEIVED 17 March 2023
ACCEPTED 17 May 2023
PUBLISHED 09 June 2023

CITATION
Fraize J, Convert G, Leprince Y, Sylvestre-Marconville F, Kerdreux E, Auzias G, Lefèvre J, Delorme R, Elmaleh-Bergès M, Hertz-Pannier L and Germanaud D (2023) Mapping corpus callosum surface reduction in fetal alcohol spectrum disorders with sulci and connectivity-based parcellation. *Front. Neurosci.* 17:1188367. doi: 10.3389/fnins.2023.1188367

COPYRIGHT
© 2023 Fraize, Convert, Leprince, Sylvestre-Marconville, Kerdreux, Auzias, Lefèvre, Delorme, Elmaleh-Bergès, Hertz-Pannier and Germanaud. This is an open-access article distributed under the terms of the Creative Commons Attribution License (CC BY). The use, distribution or reproduction in other forums is permitted, provided the original author(s) and the copyright owner(s) are credited and that the original publication in this journal is cited, in accordance with accepted academic practice. No use, distribution or reproduction is permitted which does not comply with these terms.

Mapping corpus callosum surface reduction in fetal alcohol spectrum disorders with sulci and connectivity-based parcellation

Justine Fraize[1,2*†], Gabrielle Convert[1,2†], Yann Leprince[1], Florent Sylvestre-Marconville[1,2], Eliot Kerdreux[1,2], Guillaume Auzias[3], Julien Lefèvre[3], Richard Delorme[4], Monique Elmaleh-Bergès[5], Lucie Hertz-Pannier[1,2] and David Germanaud[1,2,6*]

[1]UNIACT, NeuroSpin, Frederic Joliot Institute, Centre d'études de Saclay, CEA Paris-Saclay, Gif-sur-Yvette, France, [2]InDEV, NeuroDiderot, Inserm, Université Paris Cité, Paris, France, [3]Institut de Neurosciences de La Timone, CNRS, Aix-Marseille Université, Marseille, France, [4]Department of Child and Adolescent Psychiatry, Robert-Debré Hospital, AP-HP, Centre of Excellence InovAND, Paris, France, [5]Department of Pediatric Radiologic, Robert-Debré Hospital, AP-HP, Centre of Excellence InovAND, Paris, France, [6]Department of Genetics, Robert-Debré Hospital, AP-HP, Centre de Référence Déficiences Intellectuelles de Causes Rares, Centre of Excellence InovAND, Paris, France

Introduction: Fetal alcohol spectrum disorders (FASD) range from fetal alcohol syndrome (FAS) to non-syndromic non-specific forms (NS-FASD) that are still underdiagnosed and could benefit from new neuroanatomical markers. The main neuroanatomical manifestation of prenatal alcohol exposure on developmental toxicity is the reduction in brain size, but repeated imaging observations have long driven the attention on the corpus callosum (CC), without being all convergent. Our study proposed a new segmentation of the CC that relies on both a sulci-based cortical segmentation and the "hemispherotopic" organization of the transcallosal fibers.

Methods: We collected a monocentric series of 37 subjects with FAS, 28 with NS-FASD, and 38 with typical development (6 to 25 years old) using brain MRI (1.5T). Associating T1- and diffusion-weighted imaging, we projected a sulci-based cortical segmentation of the hemispheres on the midsagittal section of the CC, resulting in seven homologous anterior–posterior parcels (frontopolar, anterior and posterior prefrontal, precentral, postcentral, parietal, and occipital). We measured the effect of FASD on the area of callosal and cortical parcels by considering age, sex, and brain size as linear covariates. The surface proportion of the corresponding cortical parcel was introduced as an additional covariate. We performed a normative analysis to identify subjects with an abnormally small parcel.

Results: All callosal and cortical parcels were smaller in the FASD group compared with controls. When accounting for age, sex, and brain size, only the postcentral ($\eta^2 = 6.5\%$, $p_{FDR} = 0.032$) callosal parcel and % of the cortical parcel ($\eta^2 = 8.9\%$, $p_{FDR} = 0.007$) were still smaller. Adding the surface proportion (%) of the corresponding cortical parcel to the model, only the occipital parcel was persistently reduced in the FASD group ($\eta^2 = 5.7\%$, $p_{FDR} = 0.014$). In the normative analysis, we found an excess of subjects with FASD with abnormally small precentral and postcentral (peri-isthmic) and posterior–splenial parcels ($p_{FDR} < 0.05$).

Conclusion: The objective sulcal and connectivity-based method of CC parcellation proved to be useful not only in confirming posterior–splenial

damage in FASD but also in the narrowing of the peri-isthmic region strongly associated with a specific size reduction in the corresponding postcentral cortical region (postcentral gyrus). The normative analysis showed that this type of callosal segmentation could provide a clinically relevant neuroanatomical endophenotype, even in NS-FASD.

KEYWORDS

fetal alcohol spectrum disorder (FASD), corpus callosum, segmentation, cortical sulci, connectivity, microcephaly

1. Introduction

The pathological consequences of prenatal alcohol exposure (PAE) are grouped under the diagnosis of fetal alcohol spectrum disorders (FASD) that range from fetal alcohol syndrome (FAS) to non-syndromic, non-specific forms (NS-FASD) (Astley, 2004; Cook et al., 2016; Hoyme et al., 2016). The positive diagnosis of FAS is based on a consensual set of clinical features, including facial dysmorphia, growth retardation, and microcephaly, while the positive diagnosis of NS-FASD remains probabilistic. One of the main targets of the teratogenic effects of ethanol is the brain; subjects with FASD tend to have not only a smaller brain but also recurrent focal brain abnormalities detectable with magnetic resonance imaging (MRI). However, no specific neuroanatomical criterion has been added to the diagnostic guidelines.

One of the more frequently reported of these focal brain abnormalities occurs in the corpus callosum (CC) (for reviews, see: Lebel et al., 2011; Donald et al., 2015; Nguyen et al., 2017; Moore and Xia, 2021). In Astley et al.'s cohort of 65 children with FASD (6 to 16 years old), two had hypoplasia or agenesis of the CC (Astley et al., 2009). Autti-Rämö et al. described two adolescents of approximately 14 years among the 17 adolescents who were prenatally exposed to alcohol with anomalies of the CC (one thinning and one hypoplasia) (Autti-Rämö et al., 2002). Similarly, Boronat et al. (2017) listed among the 62 subjects aged between 4 and 18 years old with FASD, 24 with hypoplasia of the CC, and two with partial agenesis. Recently, Treit et al. (2020) described five subjects with dysmorphic CC, associated with the asymmetry of the lateral ventricles among 124 subjects with FASD from school age to adulthood. In a previous radiological-clinical study, we reported two cases of partial agenesis of the CC over 89 subjects with FASD from school age to early adulthood and described, with manual measurements and normative scaling analysis, an isthmus narrowing as a recurrent abnormality in both FAS and non-syndromic FASD (Fraize et al., 2022). In addition to these radiological descriptions, computational neuroimaging has searched for more subtle anomalies or more objective morphometric descriptions. Several studies of the CC in the FASD population recommended a reduction in the midsagittal CC area (Riley et al., 1995; Sowell et al., 2001; Astley et al., 2009; Dodge et al., 2009), thickness (Yang et al., 2012), volume (Gautam et al., 2014; Biffen et al., 2020; Inkelis et al., 2020), or shape with a flattened or misshapen appearance (Sowell et al., 2001; Bookstein et al., 2002) that could be correlated to the amount of prenatal alcohol consumption (Biffen et al., 2017; Jacobson et al., 2017). Within the callosal structure itself, it appears that the size reduction affected the posterior region more severely, notably the isthmus and the splenium size (Sowell et al., 2001; Dodge et al., 2009; Fraize et al., 2022) or position (Sowell et al., 2001; Bookstein et al., 2002). Note that while several studies of the last 20 years, mostly in children and young adults, tend to converge toward a global reduction in the size of the CC, affecting its posterior part in particular, this result has proved difficult to fully or systematically replicate, even within large cohorts (Sowell et al., 2001; Yang et al., 2012; Marshall et al., 2022).

The CC is a large white matter fiber bundle consisting of axonal projections between homologous cortical regions and crossing the interhemispheric plane as a compact well-individualized midsagittal structure. Midsagittal CC fibers mainly have a "hemispherotopic" organization and two adjacent CC fibers corresponding to two adjacent points on the hemisphere (Pandya et al., 1971; Friedrich et al., 2020), and the frontal connectivity is largely overrepresented, accounting for the anterior two-third of the structure (Park et al., 2008; Chao et al., 2009; Wang et al., 2020). At first approximation, the midsagittal section of the CC is often proposed as a proxy for the much larger and more complex 3D whole CC bundle. It can be divided into several regions to be compared across subjects in terms of area, length, or thickness. These divisions are commonly determined by neuroradiologists based on the arbitrary geometrical processes deemed to guarantee homology between subjects (Witelson, 1989; Hofer and Frahm, 2006). Relying only on the midsagittal anatomy or geometry, such approaches are not related to the actual anatomical connectivity. In fact, they may be not only irrelevant in the case of the pathological shortening (partial agenesis of the CC) that occurs in FASD but also insensitive to the interindividual variations of relative cortical representation in the midsagittal section. Even if the results are still ambiguous concerning FASD-associated regional anomalies of hemispheric volume (Archibald et al., 2001; Astley et al., 2009), cortical thickness (Sowell et al., 2008; Zhou et al., 2011; Yang et al., 2012; Treit et al., 2014; Marshall et al., 2022), or

Abbreviations: PAE, prenatal alcohol exposure; FASD, fetal alcohol spectrum disorders; FAS, fetal alcohol syndrome; NS-FASD, non-syndromic fetal alcohol spectrum disorders; MRI, magnetic resonance imaging; CC, corpus callosum; CxPS, cortical parcel surface area; TCxS, total cortical surface area; CcPS, callosal parcel surface area.

extension (Rajaprakash et al., 2014; Hendrickson et al., 2018), any midsagittal anomaly of the CC should raise questions about either cortical or white matter damage (Gautam et al., 2014; Fan et al., 2016; Ghazi Sherbaf et al., 2019; Kar et al., 2022), prompting a conjoint analysis of both cortical and callosal anatomy. Hence, it appears important to introduce and use parcellation of the CC into as many parcels as relevant in the regions defined on the cortical surface anatomy and projected on the midsagittal section through the real hemispherotopic callosal–cortical connectivity. A few implementations have been proposed during the past 20 years (Huang et al., 2005; Styner et al., 2005; Chao et al., 2009) without resulting in a consensual use for callosal parcellation and morphometry, but they have never been applied to the study of developmental conditions, let alone FASD.

Therefore, we aimed to describe the anatomy of the midsagittal section of the CC in a large monocentric cohort of FASD and typically developing control subjects, by means of its automatic anterior–posterior parcellation into seven parcels, achieved at the individual level from T1- and diffusion-weighted images, reflecting a fan-shaped segmentation of the cortex along six major sulcal meridians. The comparison between FASD or FAS and typical callosal anatomy was performed not only by considering covariates, including the cortical extension, as a brain size proxy but also a relative representation of the reference cortical parcel to better disentangle pathological phenomena and increase sensitivity in the detection of FASD singularity. In addition to the group comparison, we completed the analysis of our models of the callosal surfaces by a normative approach to show the detectability at the individual level of likely focal callosal anomalies.

2. Material and methods

2.1. Population and MRI data

A total of 65 subjects with FASD, aged between 6 and 25 years, were included retrospectively from a clinical series of patients with neurodevelopmental disorders who were admitted to the Child Neurology Department at Robert-Debré University Hospital between 2014 and 2020. FASD diagnosis was established using the two main guidelines (Astley, 2004; Hoyme et al., 2016), and a full differential diagnosis work-up was completed, notably a systematic brain MRI. The exclusion criteria were participants who were prenatally exposed to another embryo-fetotoxic agent or who explicitly disagreed with the study participation. Finally, subjects with FASD were separated into two groups: the syndromic or FAS (including partial FAS) and the non-syndromic or NS-FASD. The clinical and radiological characteristics of the 65 subjects with FASD are detailed in Table 1. This cohort and the diagnostic procedure were already described in a previous study (Fraize et al., 2022, 2023).

A total of 38 typically developing subjects, aged between 6 and 25 years, with no report of PAE, developmental delay, or family history of the neurological or psychiatric condition (1st degree) were included for comparison (control group), as part of a research program on autism in the Department of Child and Adolescent Psychiatry of Robert-Debré University Hospital. There were no significant sex or age differences in the control groups compared with the FASD group ($p = 0.813$ and $p = 0.479$ respectively) (Table 2).

MRI data acquisition was performed in the Department of Pediatric Radiology of Robert-Debré University Hospital on the same 1.5T scanner (Ingenia, Philips Healthcare, Amsterdam, the Netherlands) including a 3D T1-weighted FFE-TFE sequence (1 mm isotropic; TR = 8.2ms; TE = 3.8ms; TI = 0.8s; Flip = 8°; SENSE = 2), a 2D diffusion-weighted SE-EPI (2.5 mm isotropic, b1,000 s/mm2, 32 directions), and a field map. A visual quality check was systematically performed to exclude images of insufficient quality.

TABLE 1 Sociodemographic, clinical, radiological data of subjects with FASD.

	FAS	NS-FASD	*p*-value
n =	**37**	**28**	
Sociodemographic assessment			
Sex: male *n* (%)	17 (47.2)	15 (57.7)	0.578
Age at MRI, mean in years (SD)	11.17 (3.72)	13.06 (4.97)	0.098
Clinical assessment, *n* (%)			
(1) Prenatal alcohol exposure			
4.Confirmed, severe	15 (40.5)	13 (46.4)	0.825
3.Confirmed, moderate or unquantified	20 (54.1)	13 (46.4)	0.720
2.Not documented	2 (5.4)	2 (7.1)	1.000
1.No exposition	0 (0.0)	0 (0.0)	-
(2) FAS facial features			
4.Severe	22 (59.5)	2 (7.1)	**<0.001**
3.Moderate	15 (40.5)	0 (0.0)	**<0.001**
2.Mild	0 (0.0)	23 (82.1)	**<0.001**
1.None	0 (0.0)	3 (10.7)	0.075
(3) Growth deficiency			
4.Significant	14 (37.8)	3 (10.7)	**0.020**
3.Moderate	8 (21.6)	2 (7.1)	0.175
2.Mild	6 (16.2)	6 (21.4)	1.000
1.None	9 (24.3)	17 (60.7)	**0.012**
Brain anatomy			
(4) Structural central nervous system damage	29 (78.4)	17 (60.7)	0.097
Head circumference, smallest known			
(4) ≤ - 2 SD: microcephaly	26 (70.3)	14 (50.0)	0.086

Diagnostic criteria of the 4-Digit Diagnostic Code are numbered from (1) to (4). FAS, fetal alcohol syndrome; FASD, fetal alcohol spectrum disorder; NS-FASD, non-syndromic FASD; SD, standard deviation. In bold, *p*-values <5%.

TABLE 2 Clinical characteristics of the two groups of subjects.

	Controls	FASD	*p*-value
n	**38**	**65**	
Sex: male *n* (%)	17 (0.45)	32 (0.49)	0.813†
Age at MRI, mean in years (SD)	12.63 (4.15)	12.02 (4.37)	0.479††

FASD, fetal alcohol spectrum disorder; SD, standard deviation. †*p*-value of the comparison of proportions for sex, ††*p*-value of the comparison of means by Student's *t*-test.

2.2. Image processing

We combined the existing tools for sulcal-based cortical segmentation and tractography to perform an original parcellation of the midsagittal section of the CC into seven parcels along the anterior–posterior axis, achieved at the individual level in the native space without any template-based normalization process. The delineation and further inter-individual homology of the cortical and callosal parcels rely on the identification of major sulcal landmarks previously described as "sulcal meridians" (Auzias et al., 2013).

T1-weighted MRI data were processed within the *BrainVISA/Anatomist* (RRID:SCR_007354), using *Morphologist2015* (Rivière et al., 2009; Perrot et al., 2011) for tissue segmentation, inner cortical surface meshing, sulci modeling, and identification. All the MRI processing steps explained below are summed up in Figure 1.

2.2.1. Midsagittal section of the corpus callosum

The mask of the midsagittal section of the CC was obtained within the *Morphologist2015* framework after oversampling of the T1-weighted images at 0.5 mm isotropic resolution, by intersecting the white matter mask with the midsagittal plane in the Talairach space, localizing the section in the interhemispheric plane. The mask was checked systematically for any obvious segmentation error that could be manually corrected.

2.2.2. Sulcal-based parcellation of the cortical surface

The cortical parcellation was obtained individually for each subject in its own image space, with an adaptation of the *MarsAtlas* parcellation (Auzias et al., 2016), which is based on the *Hip-Hop* model (Auzias et al., 2013) of the geodesic representation of the cortex, where the CC wraps around a cingular pole and a set of well-identified major sulci are used as "meridians," linking the cingular pole to the insular pole, and others as orthogonal "parallels." We added the anterior (*aka* horizontal) ramus of the lateral fissure and anterior perpendicular ramus of the cingular sulcus (*aka* anterior vertical paracingulate sulcus) (Amiez et al., 2019) to the original *Hip-Hop* model to increase the constraints on the first and second sulcal meridian, respectively. The *Morphologist2015* identification and projection on the inner cortical surface of all the meridian sulci were systematically quality-checked and corrected for obvious errors by an expert (GD). Seven cortical parcels separated by the sulcal meridians were obtained by fusion of the original *MarsAtlas* parcels along the parallels, schematically corresponding to the following classical lobar and sub-lobar hemispheric regions: frontopolar, anterior prefrontal, posterior prefrontal, precentral, postcentral, parietal, and occipital. The corresponding cortical parcel surface area (CxPS, cm^2) was computed, as well as the total cortical surface area (TCxS, cm^2). The cortical parcellation and the binary mask of the midsagittal section of the CC were realigned to the diffusion space using FSL FLIRT (Jenkinson et al., 2002).

2.2.3. Diffusion-weighted image processing and whole-brain tractography

Preprocessing of the diffusion-weighted image data was performed using tools from *FSL* (RRID:SCR_002823) (Jenkinson et al., 2012) and *MRtrix3* (RRID:SCR_006971) (Tournier et al., 2019). FSL *eddy* (Andersson and Sotiropoulos, 2016; Andersson et al., 2016) corrects for motion, eddy currents, and susceptibility distortions related to the magnetic field B_0, based on a field map acquired along with the diffusion. Fiber orientation distributions were estimated using the constrained spherical deconvolution method (Tournier et al., 2007). With the orientation distribution functions (ODF) thus obtained, the iFOD2 algorithm was used to perform probabilistic tractography (Tournier et al., 2010). We imposed biological constraints to optimize the quality of the tractograms, reducing the number of biologically aberrant "fibers" based on the segmentation of five distinct tissues of the T1-weighted image (Anatomically Constrained Tractography) (Zhang et al., 2001; Smith et al., 2012). A dynamic seeding strategy was used to generate 10^7 streamlines (or fibers) per subject, and the *SIFT2* filter was employed to weigh streamlines according to their density (Smith et al., 2015).

2.2.4. Hemispherotopic parcellation of the midsagittal section of the CC

The entire CC bundle was automatically extracted from the whole-brain tractography using the crossing of the midsagittal section of the CC as the positive selection criterion. Any CC fiber connecting two homologous parcels from our seven sulcal-based cortical parcellations was labeled accordingly, resulting in the segmentation of the CC into seven sub-bundles corresponding to its bilateral homologous interhemispheric connectivity. A volumetric fiber density map was then computed and restricted to the midsagittal section of the CC for each of the seven CC sub-bundles. Finally, a subdivision of the midsagittal section of the CC was obtained by assigning to each of its voxels the label of the cortical parcel that sent the most fibers by majority voting on density maps. A weighting of the vote by the eight nearest neighbors (half weight for the concerned voxel, a twelfth for the neighbors) was implemented to regularize a few isolated voxels observed with simple majority voting. The final parcellation of all subjects was quality-checked visually: No aberrant segmentation was observed, and no manual correction was performed. The final metric was the callosal surface area for the total CC surface and the frontopolar, anterior prefrontal, posterior prefrontal, precentral, postcentral, parietal, and occipital callosal parcel surface (CcPS, mm^2). The code used to perform the selection of the CC bundle

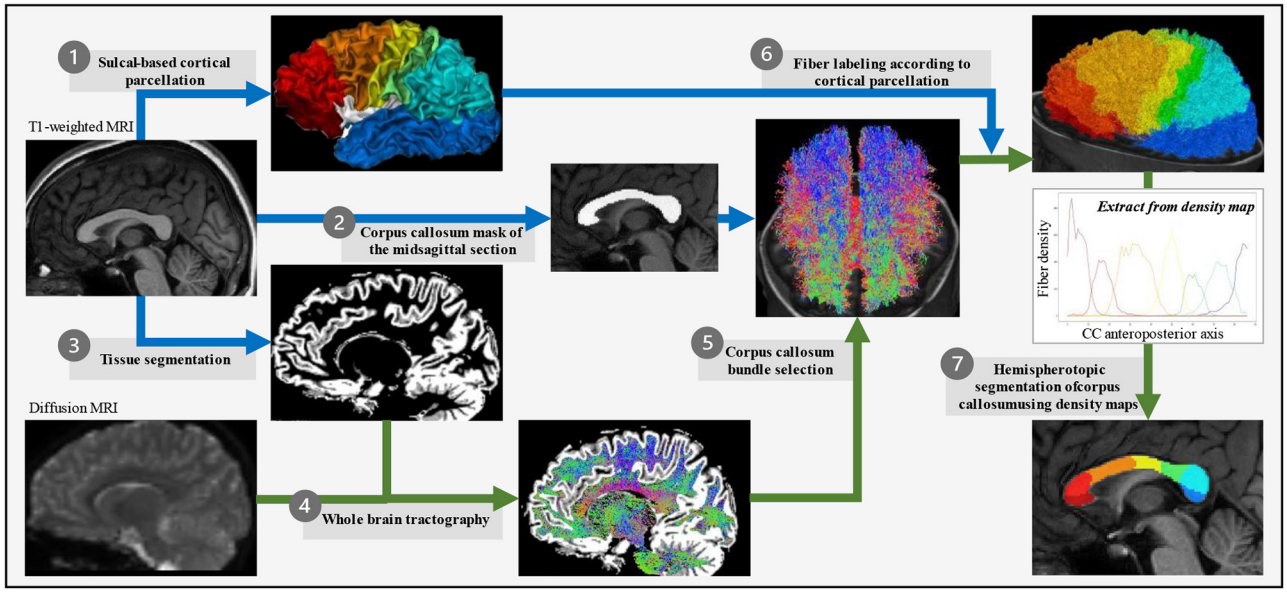


FIGURE 1
Corpus callosum parcellation pipeline. For each subject in its own image space, T1-weighted images were used to obtain the cortical surface (*Morphologist*) that was then divided into seven parcels based on the *Hip-Hop* model of geodesic representation of the cortex (adapted from *MarsAtlas*) **(1)**, the mask of the midsagittal section of the corpus callosum (*Morphologist*) **(2),** and the white *vs.* gray matter segmentation (*FSL*) **(3)**. Diffusion-weighted images were used to generate the whole-brain tractography (*MRtrix3*) **(4)** from which the corpus callosum fiber bundle was selected for passing through the midsagittal section of the corpus callosum (*MRtrix3*) **(5)**, and then its fibers connecting two homologous parcels of the sulcal-based cortical parcellation labeled according to this bilateral homologous interhemispheric connectivity (*MRtrix3*) **(6)**. Finally, a regularized majority vote on the labeled-fibers density map allowed to assign a cortical-based label to each voxel of the midsagittal section of the corpus callosum **(7)**.

and the parcellation of the midsagittal section is released on https://github.com/neurospin/CC-parcellation-from-tractography.

2.3. Statistical analysis

Statistics were performed using R Project for Statistical Computing (RRID:SCR_001905), with a 5% alpha risk with both uncorrected (*p*-value) and corrected (*q*-value) FDR for multiple comparisons (Benjamini and Hochberg, 1995).

Group differences in clinical characteristics and callosal and cortical surface areas (CcPS and CxPS) were evaluated using two-sample *t*-tests for continuous variables and a chi-squared test for categorical variables.

To examine the surface area reduction in the callosal parcels (CcPS) in FASD subjects by comparison to typically developing controls, we performed multiple regression, including age at MRI, sex, and the TCxS as a proxy of brain size, using the following model (1):

$$CcPS = DIAG^{*}b_{DIAG} + SEX{*}b_{SEX} + AGE{*}b_{AGE} + TCxS{*}b_{TCxS} + b_0 \quad (1)$$

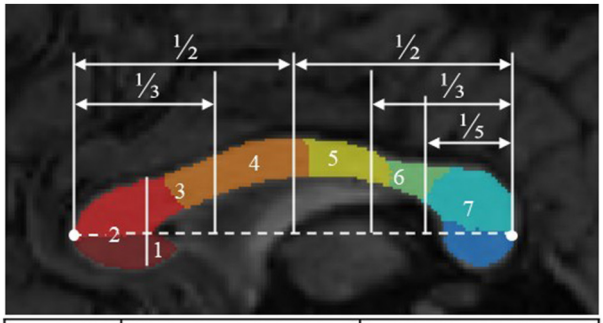
where b is the unstandardized regression coefficient for each predictor.

Given the potential effect of FASD on the size of each cortical parcel surface area (CxPS), expressed in model (2) and their mechanical correlation with the corresponding callosal parcel surface area (CcPS), an additional model (3) was also tested, which included the CxPS expressed as a percentage of the total surface ($\%CxSP = CxPS/TCxS$) as a covariate. The *p*-values and *t*-values associated with the unstandardized regression coefficients were used to assess the effect of each covariate and the eta-squared (η^2) for the effect size.

$$\%CxPS = DIAG{*}b_{DIAG} + SEX{*}b_{SEX} + AGE{*}b_{AGE} + TCxS{*}b_{TCxS} + b_0 \quad (2)$$

$$CcPS = DIAG{*}b_{DIAG} + SEX{*}b_{SEX} + AGE{*}b_{AGE} + TCxS{*}b_{TCxS} + \%\boldsymbol{CxPS}{*}\boldsymbol{b}_{\%\boldsymbol{CxPS}} + b_0 \quad (3)$$

For the normative analysis at the individual level, the model of CcPS as a function of sex, age, and brain size was regressed in the control group (4). The values of the regression coefficients ($b_{AGE/control}$, $b_{SEX/control}$, $b_{TCxS/control}$) thus obtained were applied to the two FASD populations to obtain "residues" or deviations from the control model.



N° of the labels	Name of anatomical label (*Witelson, 1989*)	Correspondence with the labels of our study
1	*Rostrum*	Frontopolar and anterior prefrontal
2	*Genu*	
3	*Rostral body*	Mainly posterior prefrontal
4	*Anterior midbody*	
5	*Posterior midbody*	Mainly precentral and postcentral
6	*Isthmus*	
7	*Splenium*	Parietal and occipital

FIGURE 2
Qualitative comparison between arbitrary geometric parcellation of Witelson in 1989 with seven anatomical labels (delimitation appearing in white) and the parcels of our final segmentation (in color). Label numbers and names with a correspondence table.

$$CcPS\left[control\right] = SEX{*}b_{SEX/control} + AGE{*}b_{AGE/control} + TCxS{*}b_{TCxS/control} + b_0 \quad (4)$$

Finally, the numbers of subjects with FASD below the 10th percentile of the control distribution, a threshold deemed of clinical relevance for potential anomaly detection, were tagged and counted and compared to the number of controls (Fisher's exact test).

3. Results

3.1. Anatomical analysis of CC parcellation

For all the FASD and control subjects, the parcellation process resulted in one-piece parcels which were comparable in size (from ~10% to 25% of the total callosal surface), with clear-cut radial boundaries, regularly sampling the whole midsagittal section of the CC along its anterior–posterior axis. The parcellation was not similar but consistent with more classical geometric segmentations (Witelson, 1989), highlighting the large representation of frontal and pericentral projections (Figure 2). It was also successfully applied to the cases of partial agenesis, with the process being robust to the reductional abnormalities, showing which parcels still occupy the residual CC (Figures 3C–H).

3.2. Group comparison

3.2.1. FASD vs. controls

Mean callosal and cortical parcel surface areas were all significantly different between FASD and control groups (q-value< 0.05) (Figure 4).

When age, sex, and brain size (TCxS) covariates were included in the analysis of callosal surfaces (*model* 1), a negative effect of FASD was found on the total CC surface, the precentral, postcentral, and occipital CcPS areas (η^2 = 2.7, 2.3, 6.5, and 4.1%, respectively), that remained significant after FDR correction only for the postcentral one (q-value = 0.032). With the same covariates (*model* 2), a strong negative effect of FASD was found on the postcentral %CxPS (η^2 = 8.9%, q-value = 0.007). Adding the corresponding %CxPS to the analysis of each CcPS (*model* 3), a negative effect of FASD was observed on the anterior and posterior prefrontal, the precentral and postcentral CcPS areas, increasing from η^2 = 1.9 to 2.6%, but not remaining after FDR correction and a stronger negative effect on the occipital CcPS area (η^2 = 5.7%, q-value = 0.014) (Figure 5, Table 3). Note that no effect at all was observed in the frontopolar and parietal callosal or cortical parcels.

3.2.2. FAS vs. controls

In the FAS group, the effect of the FAS diagnosis was also found only on the postcentral CcPS area using (*model* 1) (η^2 = 12.8%, q-value = 0.008). A strong negative effect of FAS was observed on the postcentral CxPS area (η^2 = 20.4%, q-value< 0.001). In *model* 3, the effect of FAS on CcPS followed the same prefrontal to postcentral gradient (from η^2 = 3.3% to 4.2%) and affected the occipital CcPS (η^2 = 4.9%, p = 0.014, q-value = 0.059) but did not remain significant after FDR correction (Figure 5, Table 4).

3.3. Normative analysis

This last step aimed at identifying subjects with one or other of the parcels abnormally small (10th centile threshold) considering the distribution in controls. The distribution of the "residues" from *model 4* fitted in controls (age, sex, and brain size as covariates) is presented in Figure 6, in each group (controls, FAS, and NS-FASD) for each parcel, identifying the subjects below the 10th percentile and comparing their proportion between patients and controls.

Subjects with FAS were significantly in excess below the 10th percentile, for total CC surface (n = 11, q = 0.006), precentral CcSP (n = 10, q = 0.025), postcentral CcSP (n = 19, q = 0.004), and occipital CcSP (n = 12, q = 0.008) (Figure 6). The two subjects with FAS showing radiologically evident callosal agenesis, whose corresponding CcSP areas were equal to zero, were counted (Figures 3C, D). In a *post hoc* analysis excluding these two subjects, these results persisted except for the precentral CcSP (q>0.05). Subjects with NS-FASD were significantly in excess below the 10th percentile, for total CC surface (n=9, q = 0.005), anterior prefrontal CcSP (n = 10, q = 0.028), precentral CcSP (n = 11, q = 0.005), postcentral CcSP (n=13, q = 0.009), and occipital CcSP (10, q = 0.007).

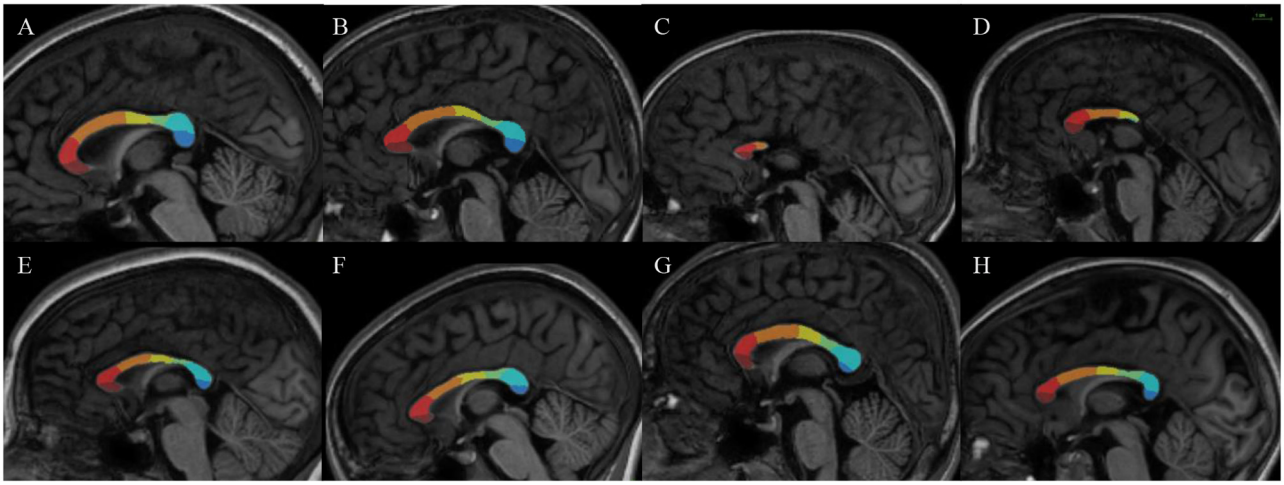


FIGURE 3
Results of our new segmentation pipeline of the corpus callosum in selected subjects, with the seven parcels (antero-posterior): frontopolar (dark red), anterior prefrontal (red), posterior prefrontal (orange), precentral (yellow) postcentral (green), parietal (light blue), occipital (dark blue). **(A, B)** Parcellation on control subjects. **(C, D)** Subjects with FAS with partial agenesis of the corpus callosum. **(E)** Subject with FAS. **(F–H)**. Subjects with NS-FASD. The scale common to all images appears at the top right.

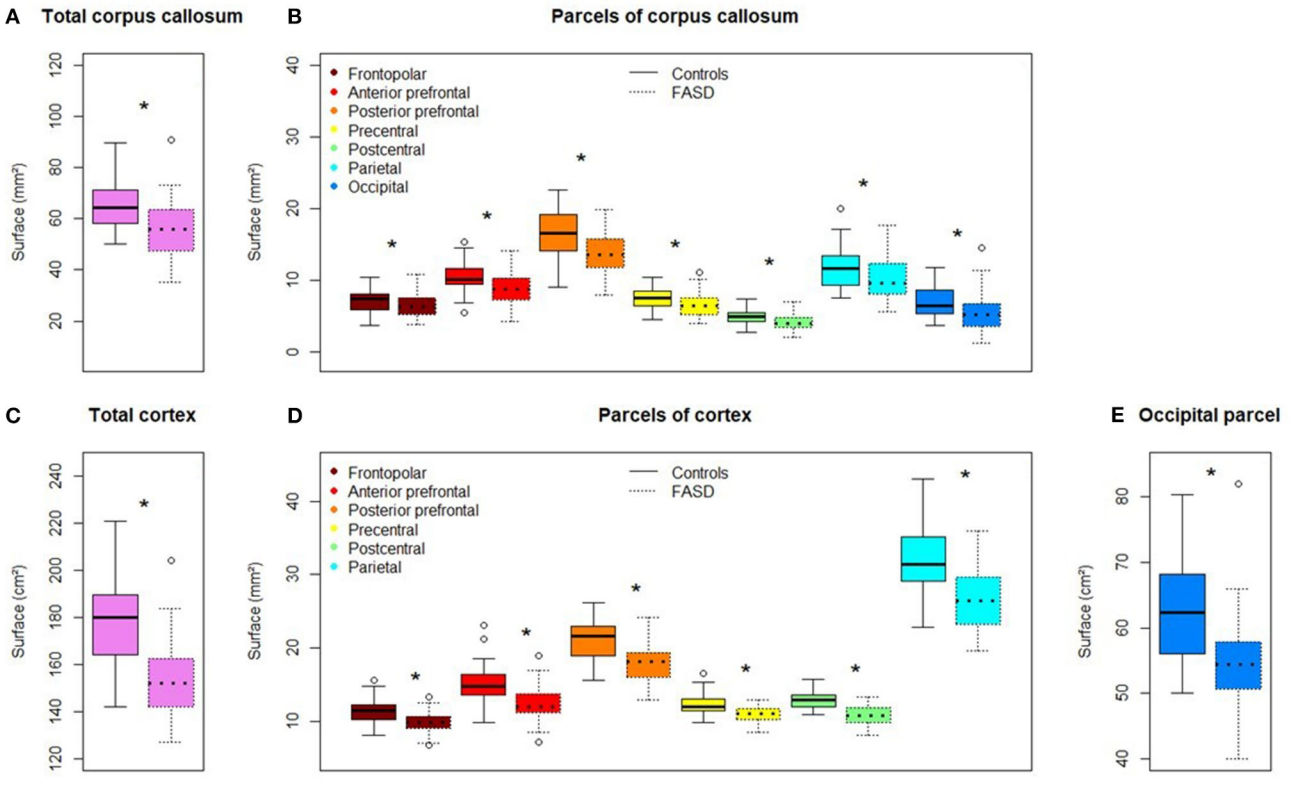


FIGURE 4
Comparison of callosal and cortical parcel surface areas of controls (left) and subjects with FASD (right, dotted line). **(A)** Total corpus callosum surface area. **(B)** All parcels, right to left: frontopolar, anterior prefrontal, posterior prefrontal, precentral, postcentral, parietal, occipital. **(C)** Total cortical surface area. **(D)** Frontopolar, anterior prefrontal, posterior prefrontal, precentral, postcentral, parietal cortical surface area. **(E)** Occipital cortical surface area. *Significantly different between FASD and control group (FDR corrected p-value: q-value < 0.05).

The reduction in the size of the postcentral CcSP was the most frequent. We tagged in blue the subjects presenting with this abnormally small postcentral CcPS on all other parcel plots to see whether they presented or not with other abnormally small CcSP. The subjects with FAS showing an abnormally small precentral CcSP had also too small a postcentral one (dark blue), but it was not the case for all those with an abnormally small occipital CsSP (Figure 6). We can also note that there

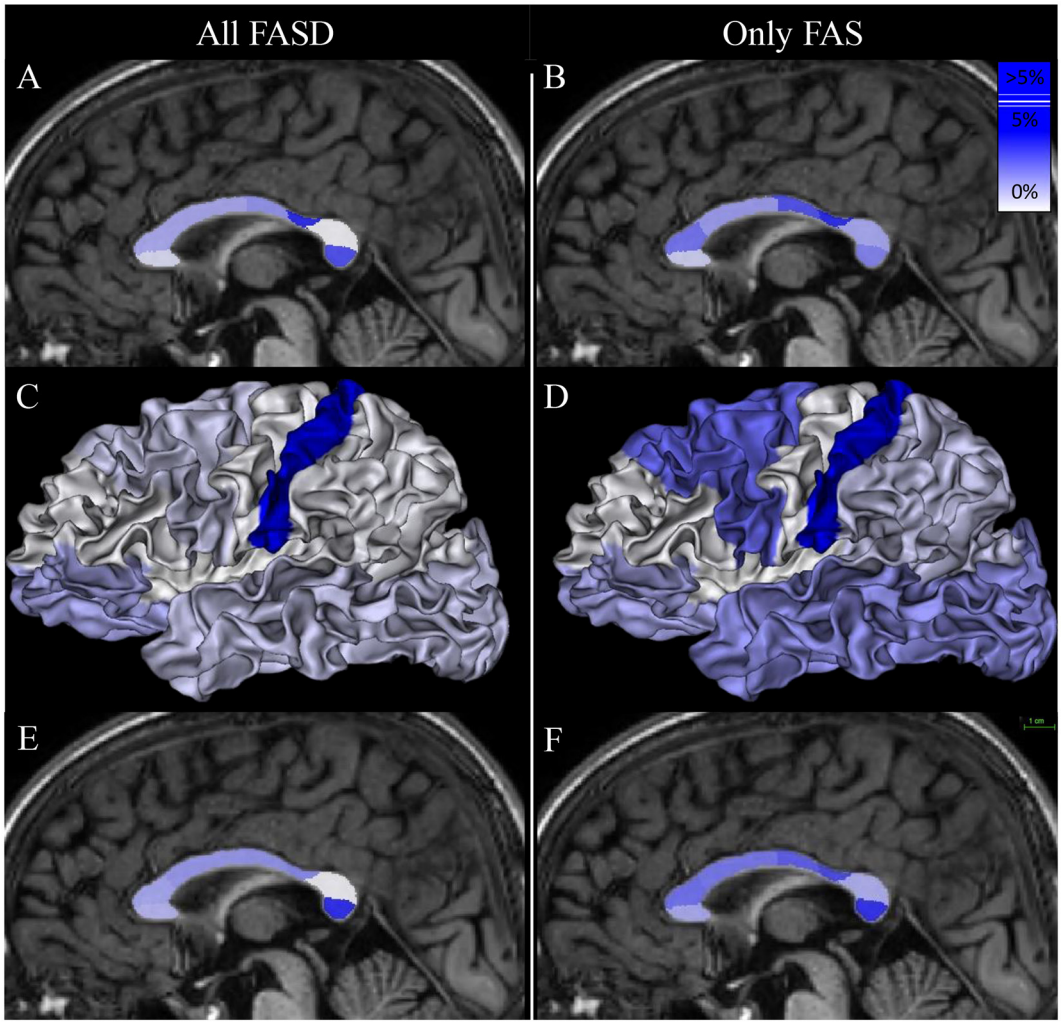


FIGURE 5
Mapping of the group effect size (FASD vs. control on the left and FAS vs. control on the right) on callosal parcel surface area [**(A, B, E, F)**, respectively] and cortical parcel surface area **(C, D)**. Eta-squared (η^2) associated with b_{DIAG} in each model are listed in Tables 3, 4. The scale appears at the top right of **(F)**.

were more subjects with FASD identified below the 10th for the postcentral CcSP than for the global CC size reduction (20 vs. 32).

4. Discussion

Our study compared the morphology of the CC between 65 subjects with FASD and 38 typically developing controls, aged between 6 and 25 years old, by means of a sulci and connectivity-based segmentation of its midsagittal section into seven parcels. We were able to show two main significant spots of surface reduction in the callosal section, one in the peri-isthmic and especially post-isthmic region (precentral and postcentral parcels), the other in the posterior terminal end (occipital parcel). Though mainly posterior, these focal shrinkages were separated by a more preserved section (parietal parcel) and our results suggested progressive damage from the more anterior regions corresponding to the prefrontal parcels to the much reduced post-isthmic region. Furthermore, the hemispherotopic segmentation allowed for an increased understanding of the nature of this callosal section damage showing that the post-isthmic reduction is highly associated with a shrinkage of the corresponding postcentral cortical surface parcel, while, conversely, the very terminal posterior reduction was all the more visible considering the relative preservation of the corresponding occipital–temporal cortical surface parcel. Finally, we suggested how such group results could translate to individual analysis through normative identification of subjects with post-isthmic and terminal callosal parcels that were too small compared to the control distribution, the two markers being not always redundant to each other, and in any case more sensitive than the whole callosal section reduction alone.

4.1. Bimodal damage mostly in the posterior half of the corpus callosum

4.1.1. Considering the callosal section only

The surface of the midsagittal section of the CC was globally reduced in our FASD population compared with controls (Figure 4), which is consistent with previous reports, a reduction

TABLE 3 Group effect (FASD vs. control) on callosal parcel surface area (CcPS in models 1 and 3) and cortical parcel surface area (CxPS in model 2).

All subjects with FASD	b_{DIAG} in model 1 (CcPS)				b_{DIAG} in model 2 (CxPS)				b_{DIAG} in model 3 (CcPS)			
	η^2	t (98)	p-value	q-value	η^2	t (98)	p-value	q-value	η^2	t (97)	p-value	q-value
Total CC	2.7	−1.90	**0.030**	0.080	-	-	-	-	-	-	-	-
Frontopolar	0.6	−0.81	0.211	0.241	1.4	1.20	0.116	0.333	1.5	−1.36	0.088	0.103
Anterior prefrontal	1.8	−1.49	0.070	0.093	0.0	0.05	0.480	0.492	1.9	−1.73	**0.044**	0.062
Posterior prefrontal	1.8	−1.54	0.064	0.093	0.7	0.89	0.187	0.333	2.2	−1.72	**0.044**	0.062
Precentral	2.3	−1.72	**0.044**	0.088	0.0	0.02	0.492	0.492	2.3	−1.77	**0.040**	0.062
Postcentral	6.5	−2.75	**0.004**	**0.032**	8.9	−3.17	**0.001**	**0.007**	2.6	−1.82	**0.036**	0.062
Parietal	0.0	−0.14	0.445	0.445	0.2	−0.50	0.308	0.431	0.0	−0.04	0.486	0.486
Occipital	4.1	−2.17	**0.016**	0.064	0.8	0.88	0.190	0.333	5.7	−2.87	**0.002**	**0.014**

Eta-squared (η^2), t-value, p-value, and q-value (FDR corrected p-value) associated with b_{DIAG} in each model. In bold, p-value and FDR-corrected p-value (q-value) <0.05. Effect sizes (η^2) are mapped in Figures 5A, C, E.

TABLE 4 Group effect (FAS vs. control) on callosal parcel surface area (CcPS in models 1 and 3) and cortical parcel surface area (CxPS in model 2).

All subjects with FAS	b_{DIAG} in model 1 (CcPS)				b_{DIAG} in model 2 (CxPS)				b_{DIAG} in model 3 (CcPS)			
	η^2	t (98)	p-value	q-value	η^2	t (98)	p-value	q-value	η^2	t (97)	p-value	q-value
Total CC	4.6	−2.09	**0.020**	0.069	-	-	-	-	-	-	-	-
Frontopolar	0.9	−0.84	0.202	0.202	1.4	1.03	0.154	0.270	1.8	−1.28	0.103	0.114
Anterior prefrontal	3.2	−1.65	0.052	0.102	0.0	0.05	0.479	0.479	3.3	−1.85	**0.034**	0.059
Posterior prefrontal	2.1	−1.42	0.081	0.108	2.8	1.57	0.061	0.214	3.0	−1.73	**0.044**	0.062
Precentral	4.0	−1.97	**0.026**	0.069	0.1	−0.31	0.378	0.441	3.7	−1.94	**0.028**	0.059
Postcentral	12.8	−3.36	**0.001**	**0.008**	20.4	−4.40	**<0.001**	**<0.001**	4.2	−1.98	**0.026**	0.059
Parietal	1.9	−1.30	0.100	0.114	0.8	−0.76	0.224	0.314	1.7	−1.21	0.114	0.114
Occipital	2.8	−1.54	0.064	0.102	1.9	1.18	0.120	0.270	4.9	−2.24	**0.014**	0.059

Eta-squared (η^2), t-value, p-value, and q-value (FDR-corrected p-value) associated with b_{DIAG} in each model. In bold, p-value and FDR-corrected p-value (q-value) <0.05. Effect sizes (η^2) are mapped in Figures 5B, D, F.

that affected all the parcels we defined on the anterior–posterior axis. In the first step of our analysis, we searched for an effect that was independent of obvious confounding factors, including age, sex, and a brain size parameter reflecting the amount of hemispheric cortex to be connected through the CC (here TCxS), to detect any heterogeneous damage. The main effect is an anterior–posterior U-shape gradient of surface reduction, bottoming around the isthmus, and is more precisely posterior to the typical narrowing in the postcentral parcel. In fact, this gradient is very probably not unimodal as this first analysis strongly demonstrated another spot of focal surface reduction at the very end of the CC in the terminal occipital parcel, with the parietal parcel being fully preserved in between (Figure 5, Table 3). We found similar results in the FAS-only subgroup even if the terminal reduction was not significant (Figure 5, Table 4).

Hence, we confirmed the previous data of the literature that pointed out a reduction in the midsagittal CC area (Riley et al., 1995; Sowell et al., 2001; Dodge et al., 2009; Jacobson et al., 2017), affecting the posterior isthmic and splenial regions more severely (Sowell et al., 2001; Dodge et al., 2009; Fraize et al., 2022) but demonstrating a more complex landscape of surface reduction in the posterior half of the CC with the preservation of the anterior part of the splenium in between a post isthmic nadir and a terminal splenial dip.

We were able to replicate our previous results (Fraize et al., 2022), which highlighted the narrowing of the isthmus as a recurrent FAS anomaly in a subset of the original MRI dataset, but with a computational automatic imaging approach. Consistently, we showed a major reduction in the callosal surface in the post-isthmic parcel (postcentral) controlling for brain size. At the same time and with simple manual measurements, we failed to show an effect of the FASD on the splenium thickness, incriminating the necessarily noisy measurement of this plump object that is highly variable in shape. The difference with the present study is twofold: First, we have a better proxy of the splenium with surface measurement than only a middle thickness, but more importantly, the splenium is now divided into an anterior part (parietal parcel) and a posterior one (occipital parcel), revealing a differential involvement.

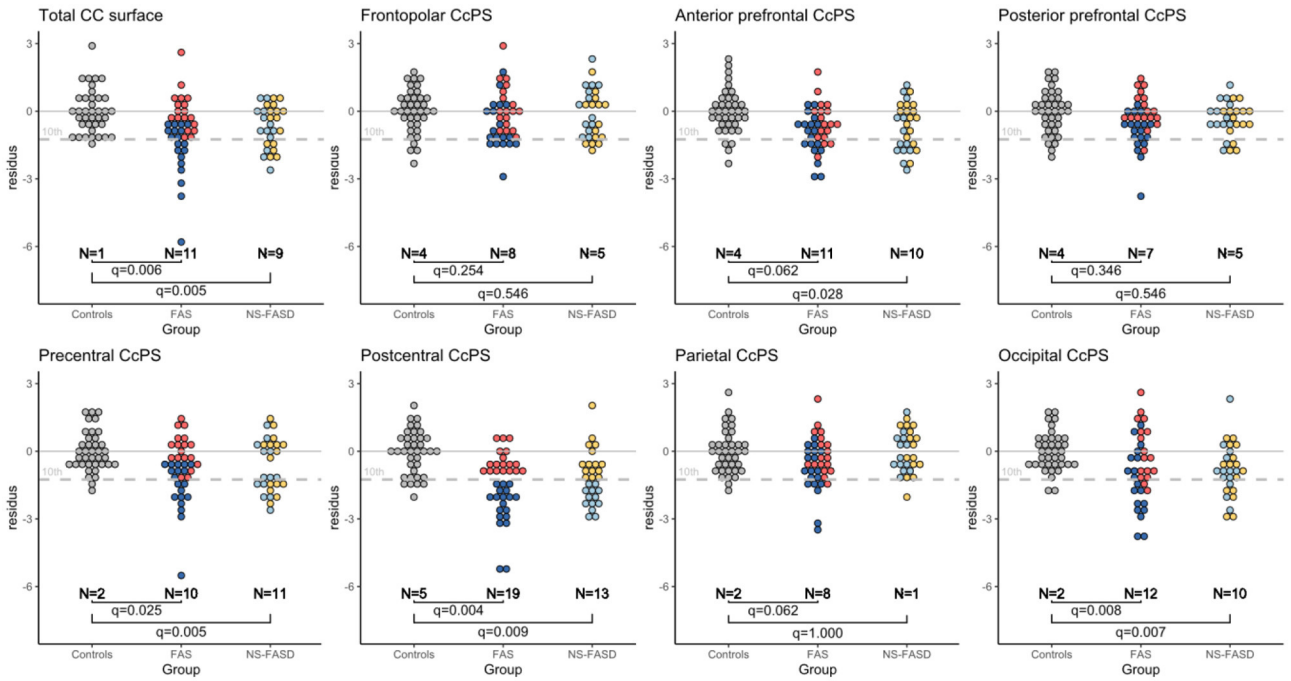


FIGURE 6
Normative analysis of callosal parcel surface area. Distribution of "residue" of each subject according to regression fitted in the control group, adjusting for age, sex, and brain size (TCxS). Number of subjects below the 10th percentile (dotted gray line) of the control distribution. FDR correction *p*-value of the Fisher test (*q*-value). Subjects identified as "too small" for the postcentral CcPS are tagged in blue so as to be easily identifiable on each plot.

4.1.2. Considering cortical–callosal surface correlations

One main contribution of our callosal parcellation based on sulci landmarks and cortical–callosal connectivity was to allow for the analysis of the focal surface variations of the midsagittal section not only according to the global hemispheric size (TCxS) but more precisely according to the focal extension of the connectivity-related cortical surfaces, with two outcomes for the study.

The primary outcome was that a second step of analysis of the callosal parcel surfaces, including the relative cortical parcel surface as a covariate, emphasized the relative terminal reduction in the callosal section while mitigating the post-isthmic one, both in the FASD group and, to a lesser extent, in the FAS group. Within the limits of statistical power, this analysis also revealed a potential prefrontal-postcentral gradient of relative callosal reduction that could be tackled in a larger study, conducted perhaps at a higher resolution (more parcels or even continuous shape analysis).

A secondary outcome of this parcellation strategy was that, our study, designed to target the CC, revealed a very significant focal cortical surface reduction in FASD and FAS, electively affecting the postcentral gyrus. To our knowledge, this has not been reported yet. The two studies of cortical surface extension in FASD reported discordant observations in other regions: It was decreased in the right temporal surface area in 36 participants with ARND (equivalent to NS-FASD) compared to 52 controls (Rajaprakash et al., 2014), whereas a larger surface area of the right precentral gyrus was observed in a large cohort of exposed subjects but without PAE threshold (Marshall et al., 2022). An indirect insight could also come from gyrification studies: For instance, a reduced sulcal depth was found in the intraparietal sulci, including the postcentral one, of 24 children with FASD correlating with the level of PAE (De Guio et al., 2014), and a reduction in local gyrification was observed in bilateral parietal clusters, including the superior part of the postcentral gyrus and the inferior part of the right one in 30 alcohol-exposed adolescents (Infante et al., 2015). However, in both studies, the postcentral involvement was neither elective nor exclusive, and it would, in any case, only be an indirect correlate of postcentral cortical surface reduction. The heterogeneity of the populations and analyses makes it difficult to put our cortical result further in perspective. Regarding the structure and shape of the CC, the question of the directionality of the observed correlation between the reduction in callosal and cortical parcels also remains open, as it would make sense not only if a defect in interhemispheric connectivity affected the size of the concerned gyrus but also if a primary defect in the cortical extension of this gyrus led to a reduction in the size of the associated callosal sub-bundle.

4.1.3. Insight from preclinical models with callosal damage

The profile of damage in the midsagittal section of the CC that we report should be compared with what has been observed in animal models of PAE, mostly in rodents, even if the choice of species, strain, type of exposure, and measurements are likely to trigger different results (Parnell et al., 2014; Zhang et al., 2019; Milbocker et al., 2022). Interestingly, we found reports not only of global and recurrent terminal reduction in the midsagittal corpus callosum in rats (Moreland et al., 2002) but also of global and middle "isthmic" thinning in mice (O'Leary-Moore et al., 2011), both consistent with our bimodal mostly terminal profile.

4.2. Quantitative anomalies of the corpus callosum as a potential diagnostic marker

Pragmatically, we also sought to identify callosal abnormalities that could be found at the individual level. We looked for FASD subjects with callosal parcels that could be considered too small once the appropriate covariates were taken into account. We performed a normative-like analysis by computing the residual for each subject and each callosal surface to the model fitted in the controls while considering all the covariates of interest. We were then able to identify the subjects with FAS or NS-FASD with values below the 10th percentile of the control distribution. Though exploratory due to the limited size of our control group, this individual analysis found global, peri-isthmic (pre and postcentral), and terminal anomalies ($<10^{th}$ percentile) to be recurrent (in excess) not only in FAS but also in NS-FASD. More interestingly, this individual analysis showed that anomalies in the postcentral or occipital callosal parcel surfaces were more frequent than in the total callosal section alone (for instance in the FAS group, 19+2 vs. 11 subjects), making them better candidate markers of the disease. Besides, if all the patients with FAS showing abnormal precentral values had a postcentral anomaly, this was not the case for the occipital value that tended to add new subjects (Figure 6). This phenomenon appeared to be even more complex in NS-FASD in any case, highlighting the probably multimodal nature of the callosal damage already illustrated by our study.

The question of the specificity of our findings as of any callosal marker in the FASD population is worth raising. Agenesis of the CC is not extremely rare in the general population (0.02%−0.7%) (Glass et al., 2008) and could be as high as approximately 1% in a population of subjects with neurodevelopmental disorders (Jeret et al., 1985). One could therefore expect an additional comparison group of subjects with neurodevelopmental disorders or microcephaly without PAE for a better assessment of specificity. Even in the absence of this type of study, the sheer number of subjects with FAS concerned by at least one peri-isthmic or terminal quantitative anomaly of the CC gives our result a much broader potential for clinical use than visually assessed agenesis of the CC. Indeed, with a reduction in the midsagittal callosal section following the bimodal profile, we found that positively diagnosed FAS could be a relevant feature to strengthen the probabilistic diagnosis of non-syndromic non-specific FASD. In that respect, our result argues for more precise and meaningful neuroanatomical criteria in FASD diagnostic guidelines.

4.3. Interest and limitations of the sulci and connectivity-based parcellation

The intrinsic limitations of the purely geometric parcellations in the midsagittal section of the CC, such as Witelson's (Witelson, 1989), have prompted the use of connectivity-based ones, relying on objective and anatomically grounded cortical segmentations (Huang et al., 2005; Styner et al., 2005; Chao et al., 2009; Friedrich et al., 2020). These methods are relevant even when there is no guarantee of the integrity of the extremities, especially the posterior one which is difficult to verify morphologically, and ensure an adequate proxy of inter-individual variations in the relative representation of the different cortical regions at the level of the medial CC. However, there were very few implementations in the field of neurodevelopmental imaging (Lebel et al., 2010), and to our knowledge, our study is the first in a neurodevelopmental condition such as FASD. Relying on the *Hip-Hop* and *MarsAtlas* cortical parcellation, with the homology of the parcels being supported by the reasonable assumption of homology between the large sulci that define the geodesic meridians, our implementation proved to be highly appropriate to sample the anterior–posterior axis of the CC. It also allowed, as previously discussed, the conjoint analysis of cortical and callosal parcels.

Other methodological limitations could be discussed, such as the use of a segmentation tool as *MarsAtlas* initially developed for a healthy adult cohort. The first steps of the *MarsAtlas/Hip-Hop* process rely on the *Morphologist* segmentation pipeline that has currently been successfully used in typically developing or impaired children and adolescents (Borst et al., 2014; Cachia et al., 2016; Kersbergen et al., 2016). Then, the *MarsAtlas* method is essentially based on the identification of homologous sulci in each subject space, without any normalization step. Our cohort was composed of children above 6 years of age whose gyrification has been shown to be very similar to that of adults (White et al., 2010). However, the use of such a method in a pathological population raises the question of the integrity of the main cortical sulci in FASD. Indeed, we lack the knowledge of any reports on FASD, showing that the sulcal pattern may be so impaired as to prevent the use of sulcal landmarks, with the few sulcal modifications reported being mostly quantitative and small-sized (Infante et al., 2015; Hendrickson et al., 2017; Kilpatrick et al., 2021). Besides, the parcellation process was carefully quality checked to avoid mis-segmentation or misclassification of the sulci that would affect the final callosal parcellation (Figure 1). Finally, it should be emphasized that the proposed method is purely object-based morphometry and thus does not rely on any template normalization or averaging in the image domain, which may have unpredictable consequences in pathological populations and raise methodological questions in dysgenetic CC.

Our implementation of this strategy led to a sampling of the midsagittal section of the CC into seven parcels, with subdivisions that proved to be quite relevant in some regions (for instance, isthmus and splenium), but this may still be insufficient. Much more subtle spatial resolution could be achieved with the same rationale using higher resolution cortical atlases, not only in both the large parcels (for instance prefrontal ones) and possibly complex regions, such as the splenium, but also within the thickness of the CC (Park et al., 2008). Provided that a dataset with sufficient statistical power is available, such an increase in spatial resolution and a number of parcels might have revealed a more subtle pattern of surface area reduction.

4.4. Other limitations and future directions

With hundred subjects and only a third of typically developing controls, the size of our dataset may have limited the power of the study and the scope of the results, at least because of the risk of sampling bias. However, it can be recalled that the relatively small number of subjects allowed a particularly thorough

quality control that would not have been possible with a larger data set, mitigating, in part, the disadvantage of the limitation in group size and that this is a homogeneous monocentric study in terms of both clinical recruitment and MRI acquisitions. However, some potentially interesting results are still exploratory as they did not remain after FDR correction to limit type I risk (for instance, the prefrontal–postcentral gradient) and that, conversely, some interesting small-sized effects may have been missed due to insufficient power.

Our choice of a linear model to regress the data, and in particular, the effect of brain size is debatable since the use of a power model in which the proportions can vary with the size (allometry) (de Jong et al., 2017; Fraize et al., 2023) is more correct and less prone to mismodeling (covering the linear one). The small size of the control group and the low-shared variance share between brain size and callosal section area led us to consider that non-linear modeling was not appropriate for our dataset and to apply only an affine approximation of the scaling effect. A more complex non-linear account for scaling could be used in a replication study with a larger sample.

Last, it is also an understandable but real limitation not to be able to analyze the observed variance with respect to the level of PAE. While PAE is documented to be above a relatively consensual threshold in our population, we do not have further insight into the timing and extent of this exposure.

Hence, in light of our results, we considered that there is a real interest for future studies to implement our segmentation or any similar cortical and connectivity-based one, with a high FAS to NS-FASD ratio to ensure specificity of the findings and a large control group to provide normative data for potential clinical use at the individual level. It could also be of interest to focus on younger samples or even a prenatal population, as to the authors' knowledge, only one ultrasound imaging study has suggested the early damage of the splenium as a diagnostic or prognostic marker of the consequences of PAE in neonates (Bookstein et al., 2005).

5. Conclusion

Our study described the surface reduction in the midsagittal section of the corpus callosum in a series of 65 patients with FASD. A unique combination of anatomical and diffusion tensor imaging was used to provide a sulci and connectivity-based parcellation into seven regions, designed to account for the cortical connectivity of the structure and its possible partial agenesis or marked dysgenesis. We demonstrated bimodal damage mostly in the posterior half of the corpus callosum, with a strong post-isthmic narrowing and relative terminal splenium damage, of which only the latter was independent of the reduction in the connected cortical parcel. These anomalies were more frequently and sensitively observed than the reduction in the whole section area and, interestingly, were frequent not only in FAS but also in NS-FASD, opening the field for a clinical application as a diagnostic marker.

Data availability statement

The datasets presented in this article are not readily available because the data that support the findings of this study are available on request from the corresponding author. The data are not publicly available due to privacy or ethical restrictions. Requests to access the datasets should be directed to JF, justine.fraize@inserm.fr.

Ethics statement

This study was conducted in accordance with the principles of the Declaration of Helsinki. Subjects' data were studied in accordance with French regulation (MR-004, declaration of conformity n 2059980v0), following approval by the Paris-Saclay research ethics committee (CER-Paris-Saclay-2020-094). Written informed consent from the FASD participants' legal guardian/next of kin was not required to participate in this study in accordance with the national legislation and the institutional requirements. Controls' data were used within the framework of the ethical authorizations of the primary studies (Gene and autism, Inserm C07-33). Written informed consent from the control participants' legal guardian/next of kin was required to participate in the initial study in accordance with the national legislation and the institutional requirements.

Author contributions

JF, GC, and DG contributed to the conception and design of the study. JF and EK collected and organized the database. GC, FS-M, and YL ensured data processing. JF performed the statistical analysis. JF and DG wrote the manuscript. All authors contributed to manuscript revision, read, and approved the submitted version.

Funding

This study was supported by the French National Agency for Research (ANR-19-CE17-0028-01) and the French National Institute for Public Health Research (IRESP-19-ADDICTIONS-08).

Acknowledgments

The authors would like to thank the volunteers, patients and families, and the French supportive association for FASD-affected families *Vivre avec le SAF*.

Conflict of interest

The authors declare that the research was conducted in the absence of any commercial or financial relationships that could be construed as a potential conflict of interest.

Publisher's note

All claims expressed in this article are solely those of the authors and do not necessarily represent those of their affiliated organizations, or those of the publisher, the editors and the reviewers. Any product that may be evaluated in this article, or claim that may be made by its manufacturer, is not guaranteed or endorsed by the publisher.

References

Amiez, C., Sallet, J., Hopkins, W. D., Meguerditchian, A., Hadj-Bouziane, F., Ben Hamed, S., et al. (2019). Sulcal organization in the medial frontal cortex provides insights into primate brain evolution. *Nat. Commun.* 10, 3437. doi: 10.1038/s41467-019-11347-x

Andersson, J. L. R., Graham, M. S., Zsoldos, E., and Sotiropoulos, S. N. (2016). Incorporating outlier detection and replacement into a non-parametric framework for movement and distortion correction of diffusion MR images. *Neuroimage* 141, 556–572. doi: 10.1016/j.neuroimage.06058

Andersson, J. L. R., and Sotiropoulos, S. N. (2016). An integrated approach to correction for off-resonance effects and subject movement in diffusion MR imaging. *Neuroimage* 125, 1063–1078. doi: 10.1016/j.neuroimage.10019

Archibald, S. L. Fennema-Notestine, C., Gamst, A., Riley, E. P., Mattson, S. N., and Jernigan, T. L. (2001). Brain dysmorphology in individuals with severe prenatal alcohol exposure. *Dev. Med. Child Neurol.* 43, 148–154. doi: 10.1111/j.1469-8749.2001.tb00179.x

Astley, S. J. (2004). Diagnostic guide for fetal alcohol spectrum disorders: The 4-digit diagnostic code. Astley SJ. Diagnostic Guide for Fetal Alcohol Spectrum Disorders: The 4-Digit Diagnostic Code. 3rd edition University of Washington Publication Services, Seattle, WA: 2004. Available online at: http://depts.washington.edu/fasdpn/pdfs/guide04.pdf,123

Astley, S. J., Aylward, E. H., Olson, H. C., Kerns, K., Brooks, A., Coggins, T. E., et al. (2009). Magnetic resonance imaging outcomes from a comprehensive magnetic resonance study of children with fetal alcohol spectrum disorders. *Alcohol. Clin. Exp. Res.* 33, 1671–1689. doi: 10.1111/j.1530-0277.2009.01004.x

Autti-Rämö, I., Autti, T., Korkman, M., Kettunen, S., Salonen, O., Valanne, L., et al. (2002). MRI findings in children with school problems who had been exposed prenatally to alcohol. *Dev. Med. Child Neurol.* 44, 98–106. doi: 10.1017/s0012162201001748

Auzias, G., Coulon, O., and Brovelli, A. (2016). MarsAtlas: A cortical parcellation atlas for functional mapping. *Hum. Brain Mapp.* 37, 1573–1592. doi: 10.1002/hbm.23121

Auzias, G., Lefèvre, J., Le Troter, A., Fischer, C., Perrot, M., Régis, J., et al. (2013). Model-driven harmonic parameterization of the cortical surface: HIP-HOP. *IEEE Trans. Med. Imaging* 32, 873–887. doi: 10.1109/TMI.2013.2241651

Benjamini, Y., and Hochberg, Y. (1995). Controlling the false discovery rate: a practical and powerful approach to multiple testing. *J. Royal Stat. Soc. Series B (Methodol.)* 57, 289–300. doi: 10.1111/j.2517-6161.1995.tb02031.x

Biffen, S. C., Warton, C. M. R., Dodge, N. C., Molteno, C. D., Jacobson, J. L., Jacobson, S. W., et al. (2020). Validity of automated FreeSurfer segmentation compared to manual tracing in detecting prenatal alcohol exposure-related subcortical and corpus callosal alterations in 9- to 11-year-old children. *Neuroimage Clin.* 28, 102368. doi: 10.1016/j.nicl.2020.102368

Biffen, S. C., Warton, C. M. R., Lindinger, N. M., Randall, S. R., Lewis, C. E., Molteno, C. D., et al. (2017). Reductions in corpus callosum volume partially mediate effects of prenatal alcohol exposure on IQ. *Front. Neuroanat.* 11, 132. doi: 10.3389/fnana.2017.00132

Bookstein, F. L., Connor, P. D., Covell, K. D., Barr, H. M., Gleason, C. A., Sze, R. W., et al. (2005). (2005). Preliminary evidence that prenatal alcohol damage may be visible in averaged ultrasound images of the neonatal human corpus callosum. *Alcohol* 36, 151–160. doi: 10.1016/j.alcohol.07007

Bookstein, F. L., Sampson, P. D., Connor, P. D., and Streissguth, A. P. (2002). Midline corpus callosum is a neuroanatomical focus of fetal alcohol damage. *Anat. Rec.* 269, 162–174. doi: 10.1002/ar.10110

Boronat, S., Sánchez-Montañez, A., Gómez-Barros, N., Jacas, C., Martínez-Ribot, L., Vázquez, E., et al. (2017). Correlation between morphological MRI findings and specific diagnostic categories in fetal alcohol spectrum disorders. *Eur. J. Med. Genet.* 60, 65–71. doi: 10.1016/j.ejmg.09003

Borst, G., Cachia, A., Vidal, J., Simon, G., Fischer, C., Pineau, A., et al. (2014). Folding of the anterior cingulate cortex partially explains inhibitory control during childhood: a longitudinal study. *Dev. Cogn. Neurosci.* 9, 126–135. doi: 10.1016/j.dcn.02006

Cachia, A., Borst, G., Tissier, C., Fisher, C., Plaze, M., Gay, O., et al. (2016). Longitudinal stability of the folding pattern of the anterior cingulate cortex during development. *Dev. Cogn. Neurosci.* 19, 122–127. doi: 10.1016/j.dcn.02011

Chao, Y-. P., Cho, K-. H., Yeh, C-. H., Chou, K-. H., Chen, J-. H., Lin, C-. P., et al. (2009). Probabilistic topography of human corpus callosum using cytoarchitectural parcellation and high angular resolution diffusion imaging tractography. *Hum. Brain Mapp.* 30, 3172–3187. doi: 10.1002/hbm.20739

Cook, J. L., Green, C. R., Lilley, C. M., Anderson, S. M., Baldwin, M. E., Chudley, A. E., et al. (2016). Fetal alcohol spectrum disorder: a guideline for diagnosis across the lifespan. *Can. Med. Assoc. J.* 188, 191–197. doi: 10.1503/cmaj.141593

De Guio, Mangin, F., Rivière, J-. F., Perrot, D., Molteno, M., Jacobson, C. D., et al. S. W., et al. (2014). A study of cortical morphology in children with fetal alcohol spectrum disorders: cortical morphology in fetal alcohol spectrum disorders. *Hum. Brain Mapp.* 35, 2285–2296. doi: 10.1002/hbm.22327

de Jong, Vidal, L. W., Forsberg, J-. S., Zijdenbos, L. E., and Haight, A. P. T., Alzheimer's Disease Neuroimaging Initiative, et al. (2017). Allometric scaling of brain regions to intra-cranial volume: an epidemiological MRI study. *Hum. Brain Mapp.* 38, 151–164. doi: 10.1002/hbm.23351

Dodge, N. C., Jacobson, J. L., Molteno, C. D., Meintjes, E. M., Bangalore, S., Diwadkar, V., et al. (2009). Prenatal alcohol exposure and interhemispheric transfer of tactile information: detroit and cape town findings. *Alcohol. Clin. Exp. Res.*33, 1628–1637. doi: 10.1111/j.1530-0277.2009.00994.x

Donald, K. A., Eastman, E., Howells, F. M., Adnams, C., Riley, E. P., Woods, R. P., et al. (2015). Neuroimaging effects of prenatal alcohol exposure on the developing human brain: a magnetic resonance imaging review. *Acta Neuropsychiatr.* 27, 251–269. doi: 10.1017/neu.2015.12

Fan, J., Jacobson, S. W., Taylor, P. A., Molteno, C. D., Dodge, N. C., Stanton, M. E., et al. (2016). White matter deficits mediate effects of prenatal alcohol exposure on cognitive development in childhood. *Hum. Brain Mapp.* 37, 2943–2958. doi: 10.1002/hbm.23218

Fraize, J., Fischer, C., Elmaleh-Bergès, M., Kerdreux, E., Beggiato, A., Ntorkou, A., et al. (2023). Enhancing fetal alcohol spectrum disorders diagnosis with a classifier based on the intra-cerebellar gradient of volume reduction. *Hum. Brain Mapp.* doi: 10.1002/hbm.26348. [Epub ahead of print].

Fraize, J., Garzón, P., Ntorkou, A., Kerdreux, E., Boespflug-Tanguy, O., Beggiato, A., et al. (2022). Combining neuroanatomical features to support diagnosis of fetal alcohol spectrum disorders. *Dev. Med. Child Neurol.* 3, 5411. doi: 10.1111./dmcn.15411

Friedrich, P., Fraenz, C., Schlüter, C., Ocklenburg, S., Mädler, B., Güntürkün, O., et al. (2020). The relationship between axon density, myelination, and fractional anisotropy in the human corpus callosum. *Cerebral Cortex* 30, 2042–2056. doi: 10.1093/cercor/bhz221

Gautam, P., Nuñez, S. C., Narr, K. L., Kan, E. C., and Sowell, E. R. (2014). Effects of prenatal alcohol exposure on the development of white matter volume and change in executive function. *NeuroImage: Clinical* 5, 19–27. doi: 10.1016/j.nicl.05010

Ghazi Sherbaf, F., Aarabi, M. H., Hosein Yazdi, M., and Haghshomar, M. (2019). White matter microstructure in fetal alcohol spectrum disorders: a systematic review of diffusion tensor imaging studies. *Hum. Brain Mapp.* 40, 1017–1036. doi: 10.1002/hbm.24409

Glass, H. C., Shaw, G. M., Ma, C., and Sherr, E. H. (2008). Agenesis of the corpus callosum in California 1983–2003: a population-based study. *Am. J. Med. Genet. A* 146A, 2495–2500. doi: 10.1002./ajmg.a.32418

Hendrickson, T. J., Mueller, B. A., Sowell, E. R., Mattson, S. N., Coles, C. D., Kable, J. A., et al. (2017). (2017). Cortical gyrification is abnormal in children with prenatal alcohol exposure. *Neuroimage Clin* 15, 391–400. doi: 10.1016/j.nicl.05015

Hendrickson, T. J., Mueller, B. A., Sowell, E. R., Mattson, S. N., Coles, C. D., Kable, J. A., et al. (2018). 2-year cortical trajectories are abnormal in children and adolescents with prenatal alcohol exposure. *Dev. Cogn. Neurosci.* 30, 123–133. doi: 10.1016/j.dcn.02008

Hofer, S., and Frahm, J. (2006). (2006). Topography of the human corpus callosum revisited—Comprehensive fiber tractography using diffusion tensor magnetic resonance imaging. *Neuroimage* 32, 989–994. doi: 10.1016/j.neuroimage.05044

Hoyme, H. E., Kalberg, W. O., Elliott, A. J., Blankenship, J., Buckley, D., Marais, A. S., et al. (2016). Updated clinical guidelines for diagnosing fetal alcohol spectrum disorders. *Pediatrics* 138, 4256. doi: 10.1542./peds.2015-4256

Huang, H., Zhang, J., Jiang, H., Wakana, S., Poetscher, L., Miller, M. I., et al. (2005). (2005). DTI tractography based parcellation of white matter: application to the mid-sagittal morphology of corpus callosum. *Neuroimage* 26, 195–205. doi: 10.1016/j.neuroimage.01019

Infante, M. A., Moore, E. M., Bischoff-Grethe, A., Migliorini, R., Mattson, S. N., Riley, E. P., et al. (2015). (2015). Atypical cortical gyrification in adolescents with histories of heavy prenatal alcohol exposure. *Brain Res.* 1624, 446–454. doi: 10.1016/j.brainres.08002

Inkelis, S. M., Moore, E. M., Bischoff-Grethe, A., and Riley, E. P. (2020). Neurodevelopment in adolescents and adults with fetal alcohol spectrum disorders (FASD): a magnetic resonance region of interest analysis. *Brain Res.* 1732, 146654. doi: 10.1016/j.brainres.2020.146654

Jacobson, S. W., Jacobson, J. L., Molteno, C. D., Warton, C. M. R., Wintermark, P., Hoyme, H. E., et al. (2017). Heavy prenatal alcohol exposure is related to smaller corpus callosum in newborn MRI scans. *Alcohol. Clin. Exp. Res.* 41, 965–975. doi: 10.1111/acer.13363

Jenkinson, M., Bannister, P., Brady, M., and Smith, S. (2002). Improved optimization for the robust and accurate linear registration and motion correction of brain images. *Neuroimage* 17, 825–841. doi: 10.1016/s1053-8119(02)91132-8

Jenkinson, M., Beckmann, C. F., Behrens, T. E. J., Woolrich, M. W., and Smith, S. M. (2012). FSL. *Neuroimage* 62, 782–790. doi: 10.1016/j.neuroimage.09015

Jeret, J. S., Serur, D., Wisniewski, K., and Fisch, C. (1985). Frequency of agenesis of the corpus callosum in the developmentally disabled population as determined by computerized tomography. *Pediatr. Neurosci.* 12, 101–103. doi: 10.1159/000120229

Kar, P., Reynolds, J. E., Gibbard, W. B., McMorris, C., Tortorelli, C., Lebel, C., et al. (2022). Trajectories of brain white matter development in young children with prenatal alcohol exposure. *Hum. Brain Mapp.* 43, 4145–4157. doi: 10.1002/hbm.25944

Kersbergen, K. J., Leroy, F., Išgum, I., Groenendaal, F., Vries, d. e., Claessens, L. S., et al. (2016). Relation between clinical risk factors, early cortical changes, and neurodevelopmental outcome in preterm infants. *Neuroimage* 142, 301–310. doi: 10.1016/j.neuroimage.07010

Kilpatrick, L. A., Joshi, S. H., O'Neill, J., Kalender, G., Dillon, A., Best, K. M., et al. (2021). Cortical gyrification in children with attention deficit-hyperactivity disorder and prenatal alcohol exposure. *Drug Alcohol. Depend.* 225, 108817. doi: 10.1016/j.drugalcdep.2021.108817

Lebel, C., Caverhill-Godkewitsch, S., and Beaulieu, C. (2010). Age-related regional variations of the corpus callosum identified by diffusion tensor tractography. *Neuroimage* 52, 72. doi: 10.1016/j.neuroimage.03072

Lebel, C., Roussotte, F., and Sowell, E. R. (2011). Imaging the impact of prenatal alcohol exposure on the structure of the developing human brain. *Neuropsychol. Rev.* 21, 102–118. doi: 10.1007/s11065-011-9163-0

Marshall, A. T., Bodison, S. C., Uban, K. A., Adise, S., Jonker, D., Charles, W., et al. (2022). The impact of prenatal alcohol and/or tobacco exposure on brain structure in a large sample of children from a South African birth cohort. *Alcohol. Clin. Exp. Res.* 46, 1980–1992. doi: 10.1111/acer.14945

Milbocker, K. A. LeBlanc, G. L., Brengel, E. K., Hekmatyar, K. S., Kulkarni, P., Ferris, C. F., et al. (2022). Reduced and delayed myelination and volume of corpus callosum in an animal model of fetal alcohol spectrum disorders partially benefit from voluntary exercise. *Sci. Rep.* 12, 10653. doi: 10.1038/s41598-022-14752-3

Moore, E. M., and Xia, Y. (2021). neurodevelopmental trajectories following prenatal alcohol exposure. *Front. Hum. Neurosci.* 15, 695855. doi: 10.3389/fnhum.2021.695855

Moreland, N., La Grange, L., and Montoya, R. (2002). Impact of in utero exposure to EtOH on corpus callosum development and paw preference in rats: protective effects of silymarin. *BMC Complement. Altern. Med.* 2, 10. doi: 10.1186/1472-6882-2-10

Nguyen, V. T., Chong, S., Tieng, Q. M., Mardon, K., Galloway, G. J., Kurniawan, N. D., et al. (2017). (2017). Radiological studies of fetal alcohol spectrum disorders in humans and animal models: an updated comprehensive review. *Magn. Reson. Imaging* 43, 10–26. doi: 10.1016/j.mri.06012

O'Leary-Moore, S. K., Parnell, S. E., Lipinski, R. J., and Sulik, K. K. (2011). Magnetic resonance-based imaging in animal models of fetal alcohol spectrum disorder. *Neuropsychol. Rev.* 21, 167–185. doi: 10.1007/s11065-011-9164-z

Pandya, D. N., Karol, E. A., and Heilbronn, D. (1971). The topographical distribution of interhemispheric projections in the corpus callosum of the rhesus monkey. *Brain Res.* 32, 31–43. doi: 10.1016/0006-8993(71)90153-3

Park, H-. J., Kim, J. J., Lee, S-. K., Seok, J. H., Chun, J., Kim, D. I., et al. (2008). Corpus callosal connection mapping using cortical gray matter parcellation and DT-MRI. *Hum. Brain Mapp.* 29, 503–516. doi: 10.1002/hbm.20314

Parnell, S. E., Holloway, H. E., Baker, L. K., Styner, M. A., and Sulik, K. K. (2014). Dysmorphogenic effects of first trimester-equivalent ethanol exposure in mice: a magnetic resonance microscopy-based study. *Alcohol. Clin. Exp. Res.* 38, 2008–2014. doi: 10.1111/acer.12464

Perrot, M., Rivière, D., and Mangin, J-. F. (2011). (2011). Cortical sulci recognition and spatial normalization. *Med. Image Anal.* 15, 529–550. doi: 10.1016/j.media.02008

Rajaprakash, M., Chakravarty, M. M., Lerch, J. P., and Rovet, J. (2014). Cortical morphology in children with alcohol-related neurodevelopmental disorder. *Brain Behav.* 4, 41–50. doi: 10.1002/brb3.191

Riley, E. P., Mattson, S. N., Sowell, E. R., Jernigan, T. L., Sobel, D. F., Jones, K. L., et al. (1995). Abnormalities of the corpus callosum in children prenatally exposed to alcohol. *Alcohol. Clin. Exp. Res.* 19, 1198–1202. doi: 10.1111/j.1530-0277.1995.tb01600.x

Rivière, D., Geffroy, D., Denghien, I., Souedet, N., and Cointepas, Y. (2009). BrainVISA: an extensible software environment for sharing multimodal neuroimaging data and processing tools. *Neuroimage* 47, 3. doi: 10.1016./S1053-8119(09)71720-3

Smith, R. E., Tournier, J-. D., Calamante, F., and Connelly, A. (2012). (2012). Anatomically-constrained tractography: improved diffusion MRI streamlines tractography through effective use of anatomical information. *Neuroimage* 62, 1924–1938. doi: 10.1016/j.neuroimage.06005

Smith, R. E., Tournier, J-. D., Calamante, F., and Connelly, A. (2015). (2015). SIFT2: enabling dense quantitative assessment of brain white matter connectivity using streamlines tractography. *Neuroimage* 119, 338–351. doi: 10.1016/j.neuroimage.06092

Sowell, E. R., Mattson, S. N., Kan, E., Thompson, P. M., Riley, E. P., Toga, A. W., et al. (2008). Abnormal cortical thickness and brain-behavior correlation patterns in individuals with heavy prenatal alcohol exposure. *Cereb. Cortex* 18, 136–144. doi: 10.1093/cercor/bhm039

Sowell, E. R., Mattson, S. N., Thompson, P. M., Jernigan, T. L., Riley, E. P., Toga, A. W., et al. (2001). Mapping callosal morphology and cognitive correlates: effects of heavy prenatal alcohol exposure. *Neurology* 57, 235–244. doi: 10.1212/wnl.57.2.235

Styner, M. A., Oguz, I., Smith, R. G., Cascio, C., and Jomier, M. (2005). Corpus callosum subdivision based on a probabilistic model of inter-hemispheric connectivity. *Med. Image Comput. Comput. Assist. Interv.* 8, 765–772. doi: 10.1007/11566489_94

Tournier, J-. D., Calamante, F., and Connelly, A. (2007). (2007). Robust determination of the fibre orientation distribution in diffusion MRI: non-negativity constrained super-resolved spherical deconvolution. *Neuroimage* 35, 1459–1472. doi: 10.1016/j.neuroimage.02016

Tournier, J. D., Calamante, F., and Connelly, A. (2010). Improved probabilistic streamlines tractography by 2nd order integration over fibre orientation distributions. *Proc. Intl. Soc. Mag. Reson. Med. (ISMRM).* 18, 25.

Tournier, J-. D., Smith, R., Raffelt, D., Tabbara, R., Dhollander, T., Pietsch, M., et al. (2019). MRtrix3: A fast, flexible and open software framework for medical image processing and visualisation. *Neuroimage* 202, 116137. doi: 10.1016/j.neuroimage.2019.116137

Treit, S., Jeffery, D., Beaulieu, C., and Emery, D. (2020). Radiological findings on structural magnetic resonance imaging in fetal alcohol spectrum disorders and healthy controls. *Alcohol. Clin. Exp. Res.* 44, 455–462. doi: 10.1111/acer.14263

Treit, S., Zhou, D., Lebel, C., Rasmussen, C., Andrew, G., Beaulieu, C., et al. (2014). Longitudinal MRI reveals impaired cortical thinning in children and adolescents prenatally exposed to alcohol. *Hum. Brain Mapp.* 35, 4892–4903. doi: 10.1002/hbm.22520

Wang, X., Cuzon Carlson, V. C., Studholme, C., Newman, N., Ford, M. M., Grant, K. A., et al. (2020). In utero MRI identifies consequences of early-gestation alcohol drinking on fetal brain development in rhesus macaques. *Proc. Natl. Acad. Sci. USA.* 117, 10035–10044. doi: 10.1073/pnas.1919048117

White, T., Su, S., Schmidt, M., Kao, C-. Y., and Sapiro, G. (2010). The development of gyrification in childhood and adolescence. *Brain Cogn.* 72, 36–45. doi: 10.1016/j.bandc.10009

Witelson, S. F. (1989). Hand and sex differences in the isthmus and genu of the human corpus callosum. A postmortem morphological study. *Brain* 112(Pt 3), 799–835. doi: 10.1093./brain/112.3.799

Yang, Y., Phillips, O. R., Kan, E., Sulik, K. K., Mattson, S. N., Riley, E. P., et al. (2012). Callosal thickness reductions relate to facial dysmorphology in fetal alcohol spectrum disorders. *Alcohol. Clin. Exp. Res.* 36, 798–806. doi: 10.1111/j.1530-0277.2011.01679.x

Zhang, C. R., Kurniawan, N. D., Yamada, L., Fleming, W., Kaminen-Ahola, N., Ahola, A., et al. (2019). Early gestational ethanol exposure in mice: effects on brain structure, energy metabolism and adiposity in adult offspring. *Alcohol* 75, 1–10. doi: 10.1016/j.alcohol.04008

Zhang, Y., Brady, M., and Smith, S. (2001). Segmentation of brain MR images through a hidden Markov random field model and the expectation-maximization algorithm. *IEEE Trans. Med. Imaging* 20, 45–57. doi: 10.1109/42.906424

Zhou, D., Lebel, C., Lepage, C., Rasmussen, C., Evans, A., Wyper, K., et al. (2011). Developmental cortical thinning in fetal alcohol spectrum disorders. *Neuroimage* 58, 16–25. doi: 10.1016/j.neuroimage.06026

frontiers | Frontiers in Neuroscience

TYPE Original Research
PUBLISHED 09 June 2023
DOI 10.3389/fnins.2023.1180308

Check for updates

OPEN ACCESS

EDITED BY
Hermes H. Yeh,
Dartmouth College, United States

REVIEWED BY
Alexander Skorput,
Dartmouth Hitchcock Medical Center, United States
Ania K. Majewska,
University of Rochester, United States

*CORRESPONDENCE
Shahani Noor
snoor@salud.unm.edu

†These authors have contributed equally to this work

RECEIVED 06 March 2023
ACCEPTED 09 May 2023
PUBLISHED 09 June 2023

CITATION
Noor S, Pritha AN, Pasmay AA, Sanchez JE, Sanchez JJ, Fernandez-Oropeza AK, Sun MS, Dell'Orco M, Davies S, Savage DD, Mellios N and Milligan ED (2023) Prenatal alcohol exposure dysregulates spinal and circulating immune cell circular RNA expression in adult female rats with chronic sciatic neuropathy.
Front. Neurosci. 17:1180308.
doi: 10.3389/fnins.2023.1180308

COPYRIGHT
© 2023 Noor, Pritha, Pasmay, Sanchez, Sanchez, Fernandez-Oropeza, Sun, Dell'Orco, Davies, Savage, Mellios and Milligan. This is an open-access article distributed under the terms of the Creative Commons Attribution License (CC BY). The use, distribution or reproduction in other forums is permitted, provided the original author(s) and the copyright owner(s) are credited and that the original publication in this journal is cited, in accordance with accepted academic practice. No use, distribution or reproduction is permitted which does not comply with these terms.

Prenatal alcohol exposure dysregulates spinal and circulating immune cell circular RNA expression in adult female rats with chronic sciatic neuropathy

Shahani Noor*†, Ariana N. Pritha†, Andrea A. Pasmay, Jacob E. Sanchez, Joshua J. Sanchez, Annette K. Fernandez-Oropeza, Melody S. Sun, Michela Dell'Orco, Suzy Davies, Daniel D. Savage, Nikolaos Mellios and Erin D. Milligan

Department of Neurosciences, School of Medicine, University of New Mexico, Albuquerque, NM, United States

Alcohol consumption during pregnancy is associated with Fetal Alcohol Spectrum Disorders (FASD) that results in a continuum of central nervous system (CNS) deficits. Emerging evidence from both preclinical and clinical studies indicate that the biological vulnerability to chronic CNS disease in FASD populations is driven by aberrant neuroimmune actions. Our prior studies suggest that, following minor nerve injury, prenatal alcohol exposure (PAE) is a risk factor for developing adult-onset chronic pathological touch sensitivity or allodynia. Allodynia in PAE rats occurs concurrently with heightened proinflammatory peripheral and spinal glial-immune activation. However, minor nerve-injured control rats remain non-allodynic, and corresponding proinflammatory factors are unaltered. A comprehensive molecular understanding of the mechanism(s) that underlie PAE-induced proinflammatory bias during adulthood remains elusive. Non-coding circular RNAs (circRNAs) are emerging as novel modulators of gene expression. Here, we hypothesized that PAE induces dysregulation of circRNAs that are linked to immune function under basal and nerve-injured conditions during adulthood. Utilizing a microarray platform, we carried out the first systematic profiling of circRNAs in adult PAE rats, prior to and after minor nerve injury. The results demonstrate a unique circRNA profile in adult PAE rats without injury; 18 circRNAs in blood and 32 spinal circRNAs were differentially regulated. Following minor nerve injury, more than 100 differentially regulated spinal circRNAs were observed in allodynic PAE rats. Bioinformatic analysis identified that the parental genes of these circRNAs are linked to the NF-κB complex, a central transcription factor for pain-relevant proinflammatory cytokines. Quantitative real-time PCR was employed to measure levels of selected circRNAs and linear mRNA isoforms. We have validated that *circVopp1* was significantly downregulated in blood leukocytes in PAE rats, concurrent with downregulation of *Vopp1* mRNA levels. Spinal *circVopp1* levels were upregulated in PAE rats, regardless of nerve injury. Additionally, PAE downregulated levels of *circItch* and *circRps6ka3*, which are linked to immune regulation. These results demonstrate that PAE exerts long-lasting dysregulation of circRNA expression in blood leukocytes and the spinal cord. Moreover, the spinal circRNA expression profile following peripheral nerve

injury is differentially modulated by PAE, potentially contributing to PAE-induced neuroimmune dysregulation.

KEYWORDS

prenatal alcohol exposure, neuroimmune, circular RNA, nerve injury, biomarker, NF-kB, blood leukocytes, TLR4

1. Introduction

Exposure to alcohol during gestation can cause mild to severe cognitive and behavioral deficits, representing a continuum referred to as Fetal Alcohol Spectrum Disorders (FASD). While FASD occurs worldwide, the prevalence in the US is as high as 5% in some regions (England et al., 2020), indicating it is a significant public health problem with increasing medical costs to support the health and well-being of these populations. Prenatal alcohol exposure (PAE), which leads to FASD, confers well-characterized long-term physical health problems that impact central nervous system (CNS) function (Panczakiewicz et al., 2016; Reid et al., 2021). Altered immune system function in individuals with FASD (Tominaga and Caterina, 2004; Topiwala et al., 2017) has been implicated in chronic disease, as evidenced by a 4.9-fold greater incidence of autoimmune disorders (Himmelrich et al., 2000). Evidence of immune dysfunction as a consequence of PAE is also linked with Type II diabetes, allergy, and asthma in clinical studies (Zhang et al., 2005; Salmon, 2018). Several preclinical studies reported heightened brain proinflammatory cytokines due to PAE (Drew et al., 2015; Terasaki and Schwarz, 2016; Pascual et al., 2017). Both animal and clinical studies show that the underlying biological vulnerability due to PAE that extends to chronic CNS disease is driven by dysfunctional CNS-immune interactions (Drew and Kane, 2014; Wilhelm and Guizzetti, 2015; Terasaki and Schwarz, 2017; Bodnar et al., 2018, 2020; Ruyak et al., 2022). Little is known about how PAE-related changes lead to chronic CNS dysfunction triggered by challenges in adulthood.

Sensory processing disorders such as touch hypersensitivity are one of the comorbid conditions observed in children with FASD (Franklin et al., 2008; Moore and Riley, 2015; Fjeldsted and Xue, 2019). Notably, hypersensitivity to light touch referred to as mechanical allodynia, is a manifestation of peripheral neuropathy from chronic CNS dysfunction (Milligan and Watkins, 2009). Our recent reports demonstrate that moderate PAE is a risk factor for developing allodynia, following minor, peripheral sciatic nerve chronic constriction injury (CCI) in adult rats (Sanchez et al., 2017; Noor et al., 2020). Strikingly, a PAE-generated heightened susceptibility to develop allodynia is unmasked *only after* a minor nerve injury. Allodynia in PAE offspring occurs concurrently with augmented production of well-defined pain-relevant proinflammatory immune signaling in the spinal cord (Noor et al., 2017, 2020; Sanchez et al., 2017), where damaged peripheral axon terminals communicate with spinal pain neurons. Moreover, inhibiting peripheral and spinal proinflammatory immune activation is sufficient to reverse chronic allodynia in nerve-injured PAE rats (Sanchez et al., 2019; Noor et al., 2020). Similarly, our prior report and others described a PAE-induced proinflammatory bias with increased levels of Interleukin (IL)-1β and tumor necrosis factor (TNF)-α production from peripheral leukocytes upon immune stimulation with lipopolysaccharide (LPS) (Terasaki and Schwarz, 2016; Sanchez et al., 2017). These data are suggestive of PAE-induced long-term immune dysregulation. However, the overt basal identification of key peripheral and central immune modulators as a consequence of PAE is yet to be determined (Noor and Milligan, 2018).

The mechanism of long-term modulatory effects of PAE on neuroimmune interactions during adulthood remains poorly understood (Sanchez et al., 2019; Noor et al., 2020). Emerging evidence suggests that epigenetic mechanisms involving non-coding RNAs are strong mediators of long-lasting effects of PAE (Savage et al., 2010; Balaraman et al., 2013, 2014, 2016; Tseng et al., 2019; Mahnke et al., 2021). Although several studies have focused on the roles of non-coding RNAs in neuronal function, their roles within the context of PAE-induced neuroinflammatory consequences are not known. Circular RNAs (circRNAs) are a novel category of long non-coding RNAs that are derived from the circularization and covalent joining of back-spliced exons and/or introns (Barrett and Salzman, 2016; Haque and Harries, 2017), where the 3′ terminus of a downstream exon ligates to the 5′ terminus of an upstream exon, compared to linear mRNA transcripts generated from canonical splicing. Recent advances in high-throughput RNA sequencing and bioinformatic analysis approaches have revealed the existence of tens of thousands circRNAs in multiple species (Barrett and Salzman, 2016; Haque and Harries, 2017; Ng et al., 2018). CircRNAs exhibit high abundance, stability, tissue specificity and expression during discrete developmental stages of the CNS (Peng Peng et al., 2021). More recently, Mellios et al., reported evidence of circRNA alterations in developing and postnatal brains in a mouse model of PAE (Paudel et al., 2020; Papageorgiou et al., 2023). In the current set of studies, we hypothesized that PAE induces dysregulation of circRNAs under basal and nerve-injured conditions that are associated with immune function during adulthood. Utilizing a microarray-based technology, we evaluated levels of circRNAs in the spinal cord in adult non-PAE and PAE rats with or without minor nerve injury. Additionally, we investigated whether PAE-induced dysregulation of circRNAs was detectable in circulating immune cells from the blood in adult rats. A comprehensive bioinformatic analysis and additional validation studies of selected circRNAs, along with mRNA levels of these parental or host genes (i.e., genes giving rise to a specific circRNA), was carried out to explore circRNAs concurrent with PAE-related neuropathic pain susceptibility in adult rats.

2. Materials and methods

2.1. Animals

All procedures were approved by the Institutional Animal Care and Use Committee (IACUC) of The University of New Mexico Health Sciences Center. All animal experiments were carried out in accordance with ARRIVE (Animal Research: Reporting of *In Vivo* Experiments) guidelines and National Institutes of Health guide for the care and use of laboratory animals (NIH Publications No. 8023, revised 1978). Long-Evans rat breeders were purchased from Harlan Industries (Indianapolis, IN) and were maintained in a breeding colony on a 12:12-h reverse light/dark schedule (lights on from 2,100 to 0900 h), and fed Teklad 2,920X rodent chow and tap water, available *ad libitum*. For all experiments, 6- to 7-month-old female prenatal alcohol-exposed (PAE) or age-matched Saccharin control (Sac control) rat offspring were used. Offspring were habituated to a standard light/dark cycle (lights on from 0600 h to 1800 h) for at least 28 days and kept in these conditions for the duration of the study.

2.2. Moderate prenatal alcohol exposure paradigm

Pregnant female rat dams were given either ethanol or saccharin throughout pregnancy until birth according to the well-established drinking paradigm described in prior reports (Hamilton et al., 2010; Noor et al., 2017; Sanchez et al., 2017, 2019; Davies et al., 2019). Briefly, after 1 week of acclimation to the animal facility, all 3 month-old female breeders were single housed and allowed to drink tap water containing 0.066% (w/v) Saccharin that gradually increased in ethanol content from 0% (v/v) on Days 1–2, to 2.5% (v/v) on Days 3–4, to 5% (v/v) on Day 5 and thereafter for 2 weeks. Females were allowed to drink for 4 h each day from 1,000 to 1,400 h. Regular drinking water was freely available from 1,400 h to 1,000 h the next morning. Daily, 4-h ethanol consumption was monitored for 2 weeks after which the mean daily ethanol consumption was determined for each female. Females, whose mean daily ethanol consumption was greater than one standard deviation below the group mean, typically about 10–15% of the entire group, were removed from the study at this point. Subsequently, the remainder of the females were assigned to either a Saccharin control (Sac) or 5% ethanol drinking group and matched such that the mean pre-pregnancy ethanol consumption by each group was similar. Subsequently, females were placed with proven male rat breeders until pregnant. No alcohol was consumed during the breeding period, which averaged between 1 and 2 days.

Beginning on gestational day 1 (GD1), rat dams were given either 0% (Sac) or 5% ethanol (PAE) in Sac water (4 h/day). Sac control group rats were given a volume of 0% ethanol in Sac water that was matched to the mean volume consumed by the PAE group. The amount of ethanol consumed was determined 4 h after the drinking tubes were introduced into the cages for each dam through GD21. Ethanol consumption was discontinued at birth. Offspring were weaned at 24 days of age and offspring were pair-housed. Serum ethanol concentrations were measured from a separate set of rat dams. Blood samples were collected from tail veins and trunk blood, and average values from these samples are reported.

Our prior study unmasked unique signatures of immune-related factors underlying the risk of neuropathy from PAE in female rodent offspring. Critical contributions of peripheral immune cells were identified underlying spinal glial-immune proinflammatory activation (Noor et al., 2020). To further characterize the underlying factors leading to neuroimmune activation during nerve injury, we have carried out these studies in females. The potential effect of different phases of the estrous cycle on hindpaw threshold responses was not systematically examined. However, despite that all female offspring were housed in the same colony room, characterization of hindpaw response thresholds demonstrated <10% variance at baseline and after surgical manipulation. These observations were consistent despite female rats entering experiments at different phases of the estrous cycle, suggesting that hindpaw responses remained independent of the estrus cycle phase. Consequently, the stage of the estrous cycle was not a controlled variable, and female rats were randomly entered into and examined throughout the chronic neuropathy paradigm. It should be noted that none of the experimental groups contained more than one subject from a given litter in order to avoid "litter effects."

2.3. Minor chronic constriction injury

Chronic constriction injury (CCI) is a well-established model of mechanical allodynia (Bennett and Xie, 1988) involving the application of 4 segments of 4-0 chromic gut sutures around the sciatic nerve. The material of the chromic gut induces peri-neural inflammation, causing edema and slight compression of the nerve. This model of experimental neuropathy is an ideal model to reflect peripheral neuropathy, as about 50% of all peripheral neuropathies in humans involve both direct nerve damage and peri-neural inflammation. In contrast to other models of peripheral neuropathy that cause a complete disruption of the peripheral nerves (Menorca et al., 2013; Challa, 2015), the sciatic nerve CCI model allows a systematic reduction of the degree of sciatic nerve damage. In our prior reports, we modified the standard CCI model to produce a minor CCI injury that applies a *single suture,* rather than 4 suture segments, to minimize the magnitude of nerve injury (Sanchez et al., 2017, 2019; Noor et al., 2020). This modification was developed to unmask the greater risk of PAE offspring developing neuropathy, compared to Sac-exposed control rats. All surgical procedures were performed under aseptic techniques as previously described (Noor et al., 2017, 2020; Sanchez et al., 2017, 2019). Briefly, under isoflurane anesthesia, the sciatic nerve was carefully isolated and loosely ligated with 1 segment of 4–0 chromic gut suture (Ethicon, Somerville, NJ) without pinching into the nerve. Sham surgery involved isolation of the sciatic nerve, without nerve ligation. The overlying muscle was sutured closed with two 3-0 sterile silk sutures (Ethicon, Somerville, NJ). All rats fully recovered from anesthesia within approximately 5 min. Animals were monitored daily after surgery.

2.4. Behavioral assessment of allodynia

Hindpaw touch threshold was measured utilizing the von Frey fiber test method, as described in our prior reports (Milligan et al., 2000; Sanchez et al., 2017, 2019; Noor et al., 2020). Briefly, rats were habituated to the testing environment atop 2-mm thick parallel bars

spaced 8-mm apart allowing full access to the plantar hindpaw. Habituation occurred for approximately 45 min per day for 4 sequential days within the first 3 h of the light cycle (inactive phase) in a sound- and temperature-controlled dimly lit section of the home colony room. Baseline (BL) responses were then assessed. A total of 13 calibrated monofilaments (touch-test sensory evaluator, North Coast Medical, United States) were used in these studies, with the range from 3.61 to 5.18 log stimulus intensity. Following our previously published protocol (Noor et al., 2017; Sanchez et al., 2017, 2019), fibers were applied to the plantar surface of the left and right hindpaw for a maximum of 8 s per application. Random order between left and right hindpaw assessment was conducted. A metronome placed in the room provided guidance at 1 tick/s. Lifting, licking, or shaking the paw was considered a response. In a similar manner to BL evaluation, all rats were re-assessed following CCI or Sham surgery on Days 3, 10, 17, 24, and 28. The experimental testers were blinded to the treatment groups.

2.5. Blood leukocyte and spinal cord tissue collection and RNA extraction

Immediately following behavioral analysis on Day 28 after CCI surgery, rats were deeply anesthetized under isoflurane, 8–10 min, 5% vol in oxygen. 1 mL blood sample was collected through cardiac puncture using a $25G^{5/8}$ needle, and a 3 mL syringe (Becton Dickinson, United States). Blood samples were immediately processed to isolate blood circulating peripheral leukocytes (peripheral blood mononuclear cells) utilizing Ficoll density gradient centrifugation (GE Healthcare, IL, United States), as described in our prior report (Sanchez et al., 2017). Following blood collection, rats went through rapid transcardiac perfusion with ice-cold 0.1 M phosphate-buffered saline (PBS; pH = 7.4; flow rate 10 mL/min). Rats were placed on a frozen gel refrigerant pack (Glacier Ice, Pelton Shepherd Industries) and the lumbar spinal cord (LSC; L3-L6) was dissected ipsilateral to the sciatic lesion, the relevant spinal cord region where primary neurons synapse with the secondary pain projection neurons. All tissues and blood leukocytes were immediately placed in DNase/RNase/Protease-free microtubes (VWR International; Cat#: 47747–358), frozen on dry ice, and stored at −80°C for future analysis.

Total RNA was isolated using the miRNeasy RNA isolation kit (Qiagen, Hilden, Germany) according to the manufacturer's instructions, as described previously. Samples were randomly pooled from 2 to 3 biological replicates and 1 ug total RNA material per sample was shipped to Arraystar company under frozen conditions. The following groups were sent for circRNA profiling from the spinal cord: (1) Sac control + Sham surgery, (2) PAE + Sham surgery, (3) Sac control + minor CCI surgery, (4) PAE + minor CCI surgery. For peripheral blood samples, Sac + Sham or PAE + Sham leukocytes were used to examine whether PAE alone modulated basal levels of circRNAs. Individual RNA samples remaining from these tissues were utilized for validating circRNAs and analyzing mRNA levels. Blood RNA samples were purified with Monarch RNA clean-up kit (New England Biolabs, Germany). Due to the limited amount of RNA materials from blood leukocytes, additional blood leukocyte samples were collected from age-matched PAE and Sac rats, without any nerve injury.

2.6. CircRNA expression profiling from peripheral leukocytes and spinal cord

CircRNA expression was profiled using Arraystar Rat Circular RNA Microarray service (Arraystar Inc., Rockville, MD). The circRNA array platform consisted of 14,145 probes designed by the manufacturer to detect unique circular junction-specific probes and quantify circular RNA targets at high sensitivity and specificity (Guo et al., 2014; Paudel et al., 2020). Briefly, samples were quantified using a NanoDrop ND-1000. The integrity of RNA samples was assessed by electrophoresis on a denaturing agarose gel. 1 ug of extracted total RNA was treated with RnaseR (3 h at 37°C of ribonuclease R, 20 U/μL, Epicenter, Madison WI) to digest linear RNA and enrich circRNA. Random primers were then used to amplify and transcribe the enriched circRNAs into fluorescent cRNAs per the Arraystar Super RNA Labelling protocol (Arraystar Inc.). Using Arraystar Rat Circular RNA arrays, the labeled cRNAs were hybridized and incubated in an Agilent hybridization oven for 17 h at 65°C (Agilent Technologies, Santa Clara, CA). The slides were washed and scanned using the Agilent Scanner G2505C (Agilent Technologies). The array image was analyzed, and quantile normalization, and subsequent data processing were performed using the LIMMA (implemented with the R software package). Both raw and normalized circRNA levels were then compared to identify differentially altered circRNAs. Heatmap and hierarchical cluster analysis were used to demonstrate the expression patterns of these differentially expressed circRNAs. All these datasets are made publicly available (see below).

2.7. Quantification of circRNA and mRNA expression

CircRNAs were validated with custom-designed primers to amplify back-spliced junctions specific to circRNA, as described in prior reports from our group, Mellios (Paudel et al., 2020; Zimmerman et al., 2020) and (Dell'Orco et al., 2020). Briefly, reverse transcription was performed using the SuperScript IV First-Strand Synthesis System (ThermoFisher Scientific) with random hexamers for circRNA and separately, with oligo-dT primers for linear mRNA detection. For circRNA detection, cDNA was then used together with custom-made, validated, and sequence-verified circRNA primers and PowerUp SYBR green master mix (Thermo Fisher Scientific). The following formula was used to calculate normalized or relative values of circRNAs: Relative value = 2^Ct-normalizer/A^Ct-circRNA, where A = 10^ (−1/primer slope). All circRNA primers were tested for their resistance to RNase R and reduced abundance in oligo-dT reverse-transcribed cDNA, together with melting curve and primer slope analysis, as described in prior studies (Paudel et al., 2020; Zimmerman et al., 2020). For qRT-PCR quantification for mRNA, commercially available TaqMan probes were used, as described in our prior reports (Vanderwall et al., 2017; Noor et al., 2020). The following formula was used: Relative value = 2^Ct-normalizer/2^Ct-mRNA. 18 s ribosomal RNA or GAPDH was used as a normalizer. All samples were run in triplicates. Data were acquired and melt curves were analyzed using QuantStudio 7 Flex system (Themofisher Scientific, United States).

2.8. Ingenuity pathway analysis (IPA)

For comparisons, normalized circRNA expression levels that were significantly altered (>1.5-fold, $p < 0.05$) were used for further bioinformatic analyses (see detail below) to identify potential immune or neuroimmune regulatory effects of the genes that generate these circRNAs. Ingenuity Pathway Analysis (IPA) (Krämer et al., 2014) online software (IPA, QIAGEN Redwood City, CA, United States) was employed to conduct unbiased Core Analysis using the Arraystar microarray data (Arraystar Inc.). IPA identified canonical signaling pathways and their categories, associated diseases and functions, and top molecular networks associated with these genes. Gene IDs associated with significantly dysregulated circRNAs and the fold changes ("+" indicating upregulation, "−" indicating downregulation) were included for IPA analysis. IPA analysis calculated the *p*-values using a right-tailed Fisher's Exact Test. The *p*-values ≤0.05 (−log = 1.3) indicated a statistically significant, non-random association with the molecules from the dataset being compared with the IPA-listed pathways or diseases and functions. The z-score provides the direction and magnitude of the enrichment. An absolute z-score ≥ 2 or ≤ −2 was considered significant.

2.9. Statistical analysis

SPSS (IBM, Chicago, IL, United States) or GraphPad Prism was used for statistical analyses. For behavioral data analysis, at baseline (BL), a 2-way (2 × 2) analysis of variance (ANOVA) to assess differences between prenatal exposure (Sac vs. PAE) and surgical treatment (Sham vs. minor CCI). Additionally, a 2-way (2 × 2) repeated measures ANOVA was used for the analysis of the between-subject factors of prenatal exposure, surgery, and for days post-surgery. To control the type I error rate, Tukey's test was applied for *post hoc* examination and adjusted *p*-values are reported. mRNA and circRNA levels were analyzed using a 2-way ANOVA, with Tukey's test for multiple group comparisons. For comparisons between the two groups, unpaired *t*-tests were performed. The threshold for statistical significance was set *a priori* at $p < 0.05$ for all comparisons. Outliers were removed following Grubbs' *Z*-test (Grubbs, 1950). In all cases, the data are presented as the mean ± SEM. All figures are created in GraphPad Prism version 9 software (GraphPad Software Inc., San Diego, CA, United States).

3. Results

3.1. Paradigm outcome measures

Rat dams in the 5% ethanol group consumed a mean of 1.96 ± 0.06 grams of ethanol each day during gestation (Table 1). In a separate set of rat dams, this level of consumption produced a low to moderate level of mean serum ethanol concentration of 25.1 ± 3.3 mg/dL, when sampled 2 h after the introduction of drinking tubes (Davies et al., 2023). This prenatal ethanol exposure paradigm resulted in a 7.5% reduction in maternal weight gain that was statistically significant. However, this reduction in maternal weight gain did not affect offspring litter size or offspring birth weight (Table 1).

TABLE 1 Prenatal alcohol exposure paradigm outcomes.

	Saccharin control	5% ethanol group
Daily 4 h 5% ethanol consumption	NA	1.96 ± 0.06[a] (23)
Maternal serum ethanol concentration	NA	25.1 ± 3.3[b] (14)
Maternal weight gain during pregnancy	110.8 ± 2.3[c] (25)	102.5 ± 3.1* (23)
Litter size	11.1 ± 0.5[d] (25)	11.0 ± 0.4 (23)
Pup birth weight	8.22 ± 0.32[e] (25)	7.95 ± 0.27 (23)

[a]Mean ± S.E.M. grams ethanol consumed/kg body weight/day.
[b]Mean ± S.E.M. mg ethanol/dL in serum. Serum samples were collected 2 h after the introduction of the drinking tubes from a separate set of rat dams. This time point is at or near the peak blood ethanol concentration as ethanol consumption reduces significantly in the third and fourth hours of the drinking session (Davies et al., 2023).
[c]Mean ± S.E.M. grams increase in body weight from GD 1 through GD 21. Asterisk denotes maternal weight gain data significantly less than control rats ($t = 2.10$, $p = 0.042$).
[d]Mean ± S.E.M. number of live births/litter.
[e]Mean ± S.E.M. grams pup birth weight.
NA, not applicable, (*n*)-Group sample.

3.2. A minor nerve injury model to unmask PAE-induced susceptibility to chronic allodynia

A minor nerve injury model was utilized to unmask the susceptibility to develop allodynia in PAE adult offspring. Under baseline conditions (BL), light touch sensory thresholds demonstrated no significant differences in all rat groups, with responses occurring at approximately 10 g of touch stimuli (Figures 1A,B). Following Sham surgery, non-PAE control (Sac) and PAE groups maintained normal sensitivity throughout the time course in the ipsilateral and contralateral (opposite hindpaw of the site of nerve injury site) hindpaws. These data suggest that PAE without injury, did not alter hindpaw sensitivity. Following a minor sciatic nerve injury, ipsilateral hindpaw responses remained close to their BL values in Sac rats, with sensory thresholds measured on all post-CCI time-points overlapping with Sham-injured rats. However, following this minor nerve injury, striking allodynia was observed only in PAE rats, as measured by increased sensitivity of the ipsilateral hindpaw developed by Day 3 post-CCI and displayed persistent allodynia up to 28 days-post CCI (Figure 1A). Contralateral hindpaw responses remained stably near BL values (Figure 1B) in all Sham and minor-nerve injured rats, regardless of prenatal exposure treatment. These data replicate our prior study in adult female PAE rat offspring with minor CCI (Noor et al., 2020) supporting that the role of proinflammatory spinal glia and peripheral immune activation under PAE conditions are key factors that lead to chronic allodynia. These data demonstrate that the persistent insidious effects of prenatal alcohol exposure, even at low to moderate levels, on immune priming are unmasked following a minor challenge. Following testing on Day 28 after induction of CCI, tissues were collected to examine circRNA expression during allodynia in these PAE rats. Samples from Sham-injured rats served as control tissue to compare against the circRNA changes modulated by PAE, as described in sections 3.3 and 3.6.

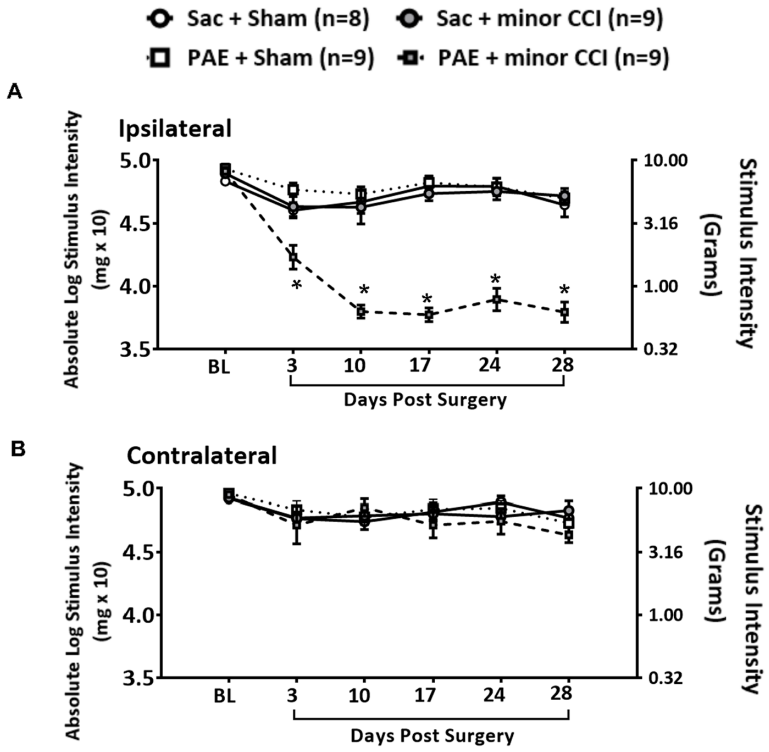


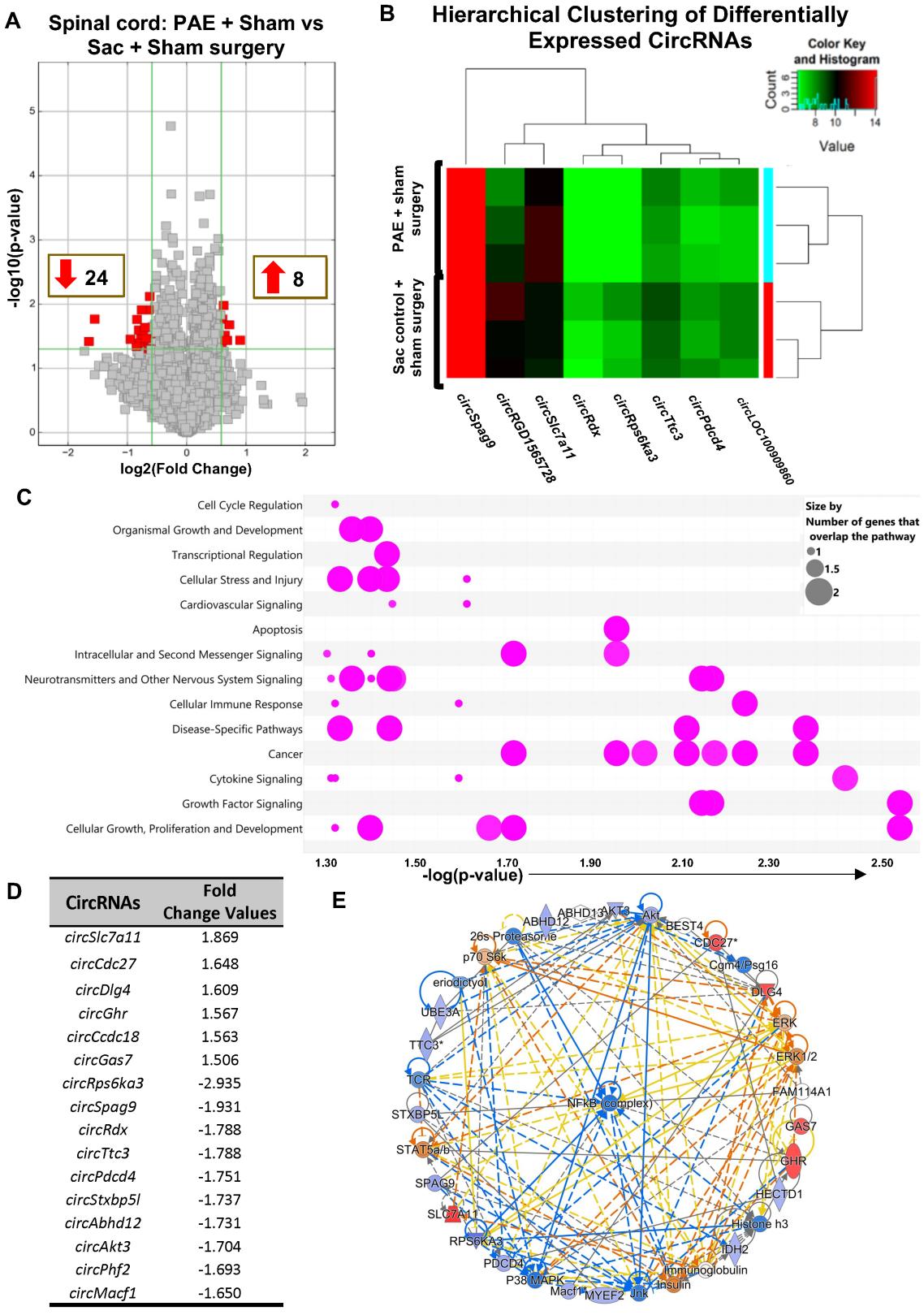
FIGURE 1
A minor chronic constriction injury (CCI) establishes chronic allodynia in PAE rats. Age-matched adult Sac and PAE rats were subjected to a minor sciatic nerve chronic constriction injury (CCI) to reveal the PAE-induced risk of neuropathy. Hindpaw light touch thresholds were measured using calibrated monofilaments applied to the planter hindpaw. **(A)** Hindpaw responses of PAE vs. Sac control rats showed no significant differences at the pre-surgery baseline (BL) in the ipsilateral hindpaw ($F_{3,31}$=2.587, p=0.071). Following minor CCI, a main effect of prenatal exposure (ipsilateral, $F_{1,31}$=42.477, p<0.001) and surgery (ipsilateral, $F_{1,31}$=69.783, p<0.001) and an interaction between prenatal exposure and surgery (ipsilateral, $F_{1,31}$=77.001, p<0.001) was observed in the ipsilateral hindpaw. Hindpaw responses to light touch were significantly increased in PAE+minor CCI group compared to Sac+minor CCI group at D3 (p=0.003), D10 through D28 (p<0.0001). *Denotes p values with significance. **(B)** For contralateral hindpaw responses, no effect of prenatal exposure and nerve injury at any time point was observed. Error bars represent SEM (standard error of mean). Number of rats used: N=8 in Sac+Sham group, Sac+minor CCI, PAE+Sham, PAE+minor CCI, N=9 in each group.

3.3. PAE causes long-term alterations in spinal cord circRNA expression

CircRNA microarray profiles in non-injured PAE and Sac rats were compared to explore whether PAE influenced the basal levels of circRNAs. Data suggested that more than 30 circRNAs were differentially expressed due to PAE. 24 circRNAs were found downregulated and 8 circRNAs were upregulated in PAE spinal cord, displayed as colored dots in Figure 2A. A heatmap expression pattern was generated displaying selective differentially expressed circRNAs, up- or down-regulated by a factor of greater than 1.75 (Figure 2B). Using IPA, an unbiased approach was taken to determine the pathways and molecular networks associated with these parental genes, with a cut-off at 1.5-fold change with $p < 0.05$, including both up-regulated and down-regulated circRNAs. This bioinformatics analysis platform suggested that these genes were related to canonical cellular signaling pathways regulating critical CNS and immune functions including transcriptional regulation, cytokine and neurotransmitter signaling, cellular stress and injury, and cellular immune responses (Figure 2C and Supplementary Figure S1E, the list of the top 5 pathways). IPA analysis also detected top up- or down-regulated circRNAs, with a cut-off value of 1.5 (Figure 2D). Additionally, "top networks" of the genes associated with these differentially expressed circRNAs were analyzed. Interestingly, this analysis demonstrated that the top molecular network of parental genes was related to a key transcription factor, nuclear factor-kappa B (NF-kB), which is a central driver for the transcription of several pain-relevant proinflammatory cytokines (Figure 2E).

3.4. Minor nerve injury results in an overlapping yet distinct circRNA expression profile in PAE rats compared to control rats

The effect of minor nerve injury on spinal cord circRNA expression profile was examined in Sac and PAE rats separately in comparison to their corresponding sham-surgery controls. Minor nerve injury dysregulated more than a thousand circRNAs from spinal cords of either Sac or PAE rats. Minor nerve injury upregulated 837 circRNAs in Sac rats and 1,017 circRNAs in PAE rats. Additionally, minor nerve injury downregulated 516 circRNAs in Sac rats and 1,533 circRNAs in PAE rats (Figure 3A). However, only about 350 circRNAs were common in both Sac and PAE rats that were either upregulated or downregulated, as a result of nerve injury (Figure 3B). Comparing the ratio of the fold regulations of these circRNAs that were common in these two datasets, about 27%



CircRNAs	Fold Change Values
circSlc7a11	1.869
circCdc27	1.648
circDlg4	1.609
circGhr	1.567
circCcdc18	1.563
circGas7	1.506
circRps6ka3	-2.935
circSpag9	-1.931
circRdx	-1.788
circTtc3	-1.788
circPdcd4	-1.751
circStxbp5l	-1.737
circAbhd12	-1.731
circAkt3	-1.704
circPhf2	-1.693
circMacf1	-1.650

FIGURE 2
PAE results in altered spinal circRNAs from genes related to the proinflammatory transcription factor NF-κB in the absence of chronic neuropathy. **(A)** Volcano plots displaying differentially expressed circRNAs between PAE and Sac spinal cord, without nerve injury. X-axis represents log2 fold change (dotted line=1.5-fold), Y-axis represents −log10 *p*-value (dotted line: $p=0.05$). The red points in the plot represent the differentially expressed (both upregulated and downregulated) circRNAs with 1.5-fold changes ($p<0.05$). **(B)** Heat map of the circRNA microarray profiles (selected for fold changes of 1.75 or more) in the PAE+Sham surgery and Sac control+Sham surgery groups. The expression of circRNAs is hierarchically clustered on

(Continued)

FIGURE 2 (Continued)
the Y-axis, and spinal cord biological replicates from these two groups are hierarchically clustered on the X-axis. Green and red represent lower higher expression levels of the circRNAs, respectively. **(C)** Ingenuity Pathway Analysis (IPA) of host genes associated with differentially expressed circRNAs. The bubble chart plots the pathway categories (Y-axis) related to these genes vs. the negative log of the *p*-values (X-axis), the smaller the *p*-values (a larger −log of that value) indicates a more significant association. This plot demonstrates the major functional categories of various associated canonical signaling pathways (as indicated by bubbles) regulating critical functions such as cell cycle regulation, cellular stress and injury, neurotransmitters and other nervous system signaling, and cytokine signaling, amongst many more. The associations with signaling pathways are selected for IPA analysis (pink color), the size refers to the number of genes that overlap with a pathway. **(D)** Top upregulated and downregulated circRNAs, parental or host gene symbol and fold changes, the absolute ratio of normalized intensities between two conditions. **(E)** The comprehensive molecular networks are generated using IPA Canonical Pathways' top network function. The network comparing PAE to the control group in the spinal cord is generated from the primary top network (z-score=47). Molecules in blue and red are downregulated and upregulated, respectively. Three different biological replicates (each sample pooled from 2 to 3 rats per group, from Figure 1) per treatment group were used to generate the circRNA microarray data.

of the circRNAs that were upregulated in Sac rats, were further upregulated in PAE rats. Among the commonly downregulated circRNAs following minor never injury, more than 70% circRNAs revealed a more pronounced downregulation in PAE rats (Figure 3B). Additionally, more than a thousand differentially regulated circRNAs were detected in PAE rats, which were not modulated in nerve-injured Sac rats. These data suggested that PAE not only influenced the fold regulations of circRNAs that were dysregulated by nerve injury in control conditions, but PAE also generated unique circRNA changes as a result of nerve injury. IPA analysis of the circRNA host genes in nerve-injured Sac rats and nerve-injured PAE rats detected relevance to multiple diseases and biological functions in common, such as neurological diseases, developmental disorders, immunological diseases, cell-to-cell interactions and psychological disorders. However, an overall stronger association, with higher −log (*p*-values), was observed in PAE rats (Figure 3C). The top 50 canonical signaling pathways associated with CNS function were compared between minor nerve injury-induced circRNAs in PAE vs. Sac rats (Tables 2, 3). In both groups, a number of common and pain-relevant pathways, such as in dorsal horn neurons and glutamate receptor signaling or circadian rhythm signaling, were associated with these genes. However, increased −log (*p*-values) indicated a stronger association with these pathways in PAE rats (Table 2). Additionally, G-protein receptor signaling, neurovascular coupling, corticotropin-releasing hormone signaling, chemokine CXCR4 signaling were noted among the top 50 pathways only in PAE rats, indicating a stronger association of these pathways under PAE conditions. The top 50 pathways in Sac rats included PPAR signaling, integrin, and JAK/STAT signaling pathways. Although these pathways were not in the top 50 associated pathways in PAE rats, a similar or weaker association (lower −log *p*-values) of these pathways was observed (Table 3). Together, these data suggest that following minor nerve injury, differentially regulated circRNAs are derived from genes that are highly associated with a number of common pathways in both Sac and PAE conditions. However, a number of additional canonical signaling pathways are found to be strongly associated with circRNA changes in PAE rats.

3.5. Significantly differentially expressed circRNAs are observed between nerve-injured sac and PAE rats

To explore minor nerve injury-induced differential pattern of circRNA expression in PAE rats, which may be linked to key modulators of PAE-related aberrant immune interactions causing allodynia (Figure 1A), circRNA profiles in the nerve-inured PAE (allodynic) vs. nerve-injured Sac rats (non-allodynic) were compared. Data revealed that 36 circRNAs were significantly up-regulated and 78 circRNAs significantly down-regulated in PAE spinal cord compared to minor-nerve injured Sac rats (Figure 4A). A clustered heatmap exhibited a differential pattern of spinal circRNAs between these two groups of rats (Figure 4B). The top 10 up- or down-regulated circRNAs were listed in Figure 4D. IPA was utilized to determine the signaling pathways and molecular networks associated with these parental genes, with a cut-off at 1.5-fold change with $p < 0.05$, including both up-regulated and down-regulated circRNAs. Interestingly, IPA results showed that these differentially expressed circRNAs were preferentially linked to genes related to neuropathic pain signaling, as indicated by the lowest *p*-values for this pathway (Figure 4C; Supplementary Figure S2E). Involvement of other relevant pathways such as nuclear receptor signaling or neurotransmitter signaling and disease-specific pathways and the relation to xenobiotics and ingenuity toxicity pathways were noted. Moreover, focusing on the molecular networks that were formed from these genes, two networks with a z-score greater than 40 suggested relevance to categories such as cell–cell interactions and nervous system function and indicated involvement of these parental genes with the NF-κB immune complex (Figure 4E; Supplementary Figure S2C).

3.6. PAE produces a unique signature pattern of circRNAs detected in blood-circulating immune cells

Given substantial evidence that peripheral immune activation contributes to PAE-induced deficits (Bodnar et al., 2016; Terasaki and Schwarz, 2016; Sanchez et al., 2017; Noor et al., 2020; Bake et al., 2021) during adulthood and its potential relevance to biomarker development, we carried out an analysis of circRNAs that are specifically present in peripheral immune cells. Although far fewer in numbers compared to our observations in the spinal cord tissues, circRNAs were detected in the peripheral leukocytes. Comparing these circRNAs between uninjured PAE and Sac rats revealed a unique circRNA signature profile due to PAE (Figures 5A–D). Hierarchical clustering analysis indicated that circRNA expression patterns were distinguishable between PAE and Sac blood leukocytes (Figure 5B). Some of these differentially expressed circRNAs were derived from genes including those associated with glucocorticoid receptor signaling (*Smarcc1*), Rho GTPase activating protein (*Arhgap10*), ATP/GTP binding Carboxypeptidase (*Agtpbp1*) and Vesicular, Overexpressed in

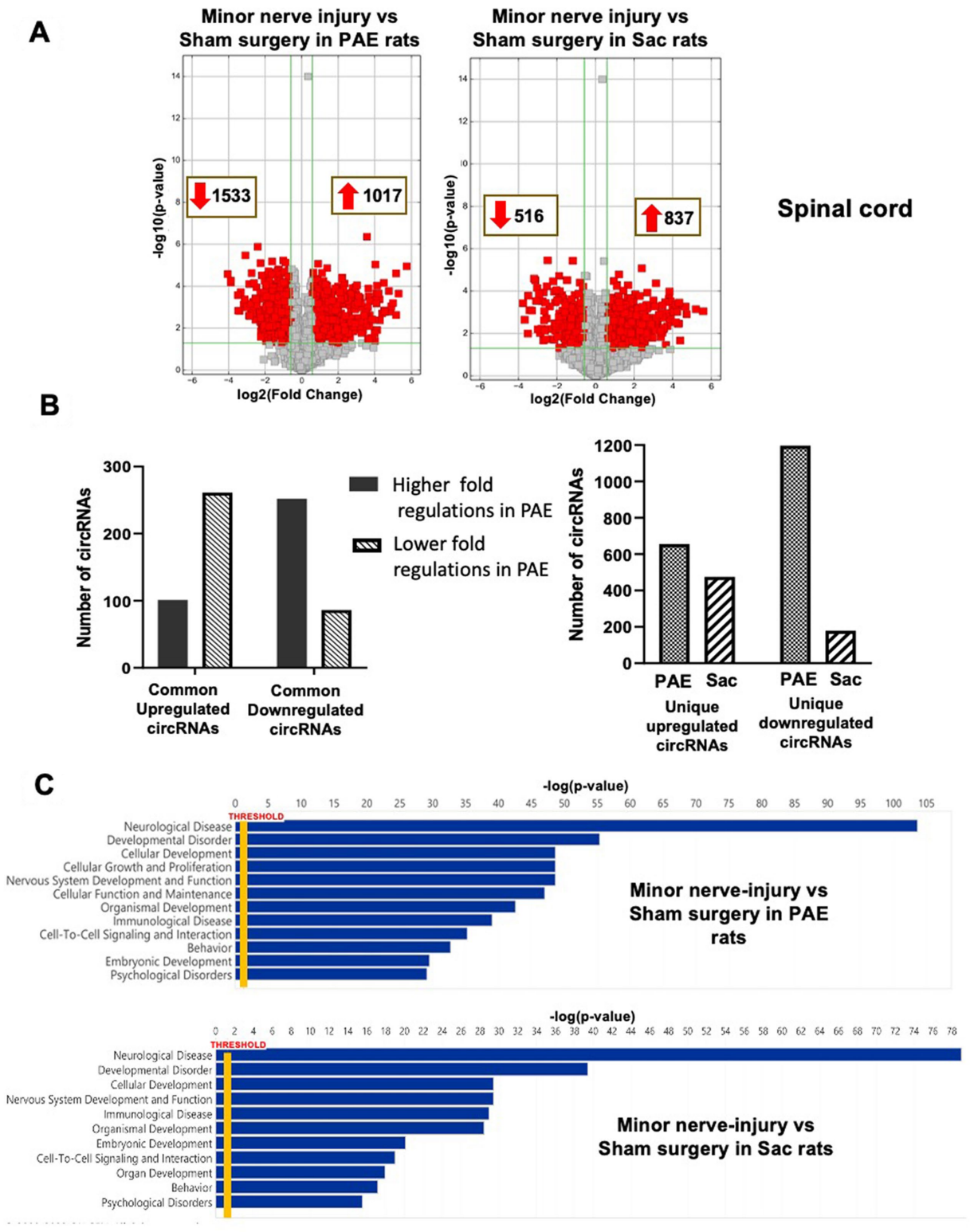


FIGURE 3
PAE differentially modulates spinal circRNA expression following a minor nerve injury. **(A)** Volcano plots of differentially expressed circRNAs between nerve-injured PAE and Sac spinal cord, compared to their corresponding control tissues. X-axis represents log2 fold change (dotted line=1.5-fold), Y-axis represents −log10 *p*-value (dotted line: $p=0.05$). The red points in the plot represent the differentially expressed circRNAs, with 1.5-fold changes ($p<0.05$). **(B)** The bar graphs represent the number of differentially expressed circRNAs as a result of injury, that are common or unique in PAE and Sac control rats. Among the altered circRNAs that are common in Sac control and PAE rats, the numbers of circRNAs that are further up or down-regulated in PAE conditions as a result of nerve injury are shown. **(C)** Ingenuity Pathway Analysis (IPA) from the host genes of the differentially expressed circRNAs is used to generate the list of associated diseases or functions (Y-axis) with associated −log *p*-values (X-axis).

Cancer, and Prosurvival Protein 1 (*Vopp1*). CircRNAs were generated from genes involved in cell–cell interactions, immune cell trafficking, inflammatory response, and genes linked to psychological and neurological diseases (Supplementary Figures S3D,E). Notably, no overlap was observed among the differentially expressed circRNAs detected in blood compared to the spinal cord, between PAE and Sac rats under non-injured conditions. Although driven by a different set of host genes observed in blood relative to spinal cord, the top molecular network with the highest z-score from these peripheral circRNA host genes further suggested the involvement of the NF-κB pathway (Figure 5D).

3.7. Exploring circRNAs and mRNA levels of host genes potentially relevant to neuroimmune function

Based on our circRNA array results and prior studies suggesting NF-κB signaling is a key immune modulator in PAE-related immune sensitization, we speculated that some of these circRNAs may have a direct or indirect influence on the mRNA levels of their corresponding host/parent genes (Figure 6A), hence contributing to proinflammatory bias under PAE conditions observed in our prior studies (Noor et al., 2020). Therefore, we further explored the

TABLE 2 Common canonical pathways associated with circRNA host genes in both PAE and Sac rats following minor nerve injury.

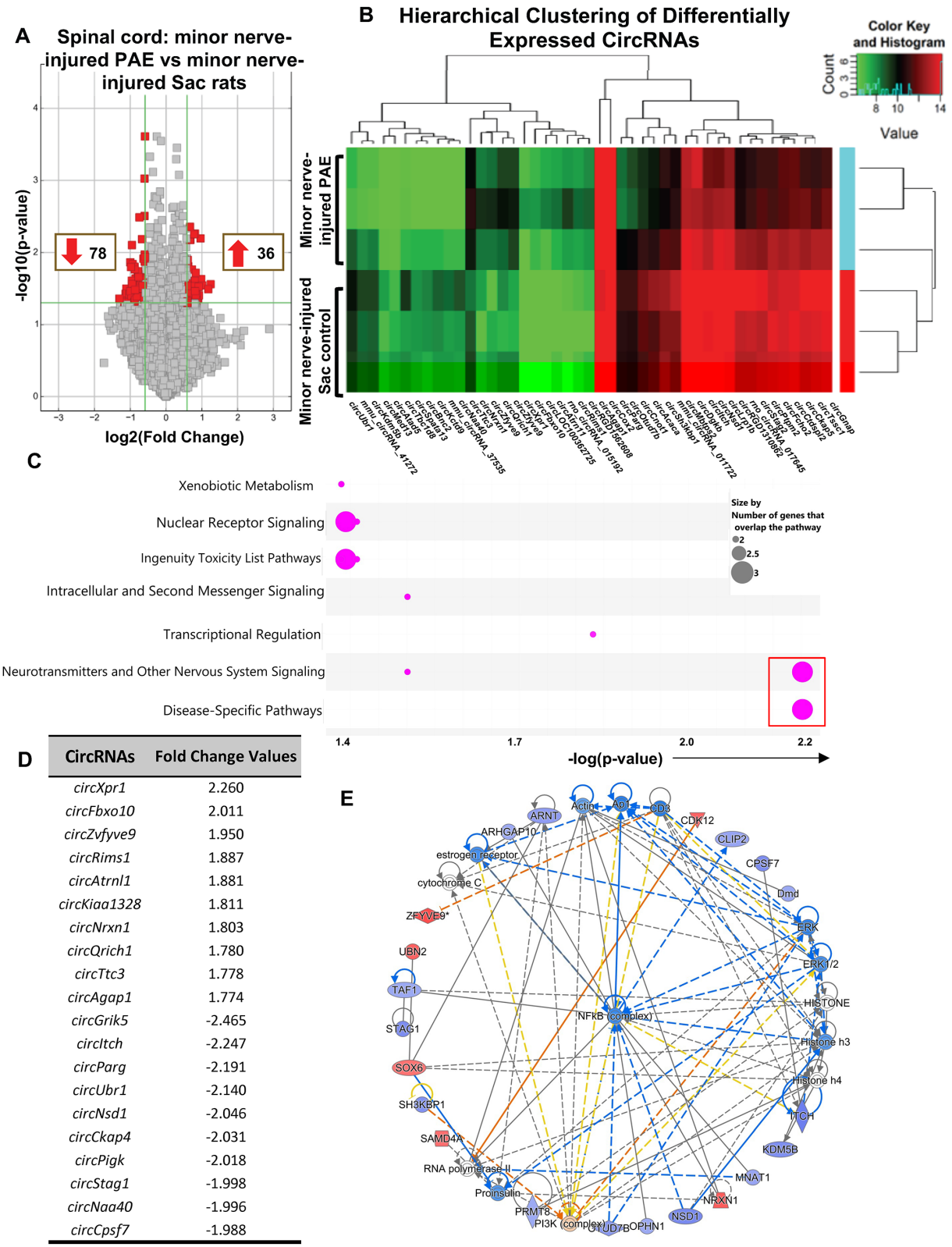
Ingenuity canonical pathways that are included in the top 50 pathways in both PAE and Sac rats	−log(*p*-value), minor nerve injury vs. sham surgery in PAE rats	−log(*p*-value), minor nerve injury vs. sham surgery in Sac rats
Synaptogenesis signaling pathway	16	9.58
Protein kinase A signaling	11.7	4.42
Opioid signaling pathway	10.1	4.53
Neuropathic pain signaling in dorsal horn neurons	6.05	3
Circadian rhythm signaling	9.14	2.76
cAMP-mediated signaling	6.7	3.04
Amyotrophic lateral sclerosis signaling	10.3	6.77
Gap junction signaling	4.64	4
TR/RXR activation	7.44	6.56
Dopamine-DARPP32 feedback in cAMP signaling	9.45	4.89
Insulin secretion signaling pathway	5.66	3.45
Calcium signaling	10.8	4.81
CLEAR signaling pathway	5.6	4.85
Glutamate receptor signaling	8.58	3.94
Myelination signaling pathway	5.35	3.1
Synaptic long-term potentiation	7.62	4.67
Autophagy	6.17	5.46
Adrenomedullin signaling pathway	4.17	3.5
Molecular mechanisms of cancer	5.64	4.39
NGF signaling	4.32	2.89
Oxytocin signaling pathway	5.29	3.63
IL-15 production	6.39	3.87
Sphingosine-1-phosphate signaling	4.32	3.42
PPARα/RXRα activation	4.32	6.23
Endocannabinoid neuronal synapse pathway	8.92	5.76
Synaptic long-term depression	7.05	2.66
Estrogen receptor signaling	6.9	4.85
Huntington's disease signaling	5.67	4.46
Axonal guidance signaling	5.39	4.02
SNARE signaling pathway	5.06	3.41
RAR activation	4.8	4.78
Senescence pathway	4.36	2.9
Ephrin A signaling	4.29	3.62

top molecules (Figures 2D, 4D, 5C) through databases, Gene Cards and Gene, NCBI, and consequently selected some genes to examine their mRNA levels. Selected genes from these differentially regulated circRNAs that are known to contribute to immune function or pathological pain processing are listed in Table 4. Additionally, utilizing custom-designed splice-junction-specific primers, we have validated one circRNA from each comparison category (Figures 2–4). Supporting the microarray data presented in Figure 2, we have validated that *circRp6ka3* levels were down-regulated (Figure 6B) in PAE-Sham spinal cord compared to Sac-Sham spinal cord. Comparing *circItch* levels, we have validated that *circItch* levels were down-regulated (Figure 6C) following nerve injury in PAE rats. However, this downregulation was also observed at the baseline, and a main effect of PAE and surgery was observed. We did not observe changes in mRNA levels of *Itch* or *Rp6ka3* mRNA levels (Figures 6B,C).

To explore circRNA changes due to PAE that could be detected in the peripheral immune system, we prioritized validating *circVopp1*

TABLE 3 List of other top 50 pathways associated with circRNA host genes in either PAE or Sac rats following minor nerve injury.

	−log(*p*-value)
Ingenuity canonical pathways in minor-nerve injury vs. sham surgery in PAE rats	
Neurovascular coupling signaling pathway	7.38
Apelin endothelial signaling pathway	4.31
Netrin signaling	8.69
GPCR-mediated nutrient sensing in enteroendocrine cells	5.53
Endocannabinoid cancer inhibition pathway	4.51
GABA receptor signaling	5.27
CXCR4 signaling	4.07
Epithelial adherens junction signaling	5.03
GNRH signaling	5.87
Corticotropin releasing hormone signaling	6.9
Reelin signaling in neurons	5.48
Gα12/13 signaling	5.22
Gαq signaling	4.44
Semaphorin neuronal repulsive signaling pathway	3.91
Cholecystokinin/gastrin-mediated signaling	3.87
Type II diabetes mellitus signaling	3.79
Relaxin signaling	3.71
Ingenuity canonical pathways in minor nerve injury vs. sham surgery in Sac rats	
GM-CSF signaling	3.72
nNOS signaling in neurons	3.62
Renin-angiotensin signaling	3.38
Glioblastoma multiforme signaling	3.34
PPAR signaling	3.34
HIF1α signaling	3.27
Integrin signaling	3.17
Ephrin receptor signaling	2.99
Insulin receptor signaling	2.79
ERBB signaling	2.73
IL-3 signaling	2.69
Serotonin receptor signaling	1.66
IL-2 signaling	1.63
IL-23 signaling pathway	1.62
JAK/STAT signaling	1.56
D-myo-inositol (1,4,5,6)-tetrakisphosphate biosynthesis	1.55
D-myo-inositol (3,4,5,6)-tetrakisphosphate biosynthesis	1.55



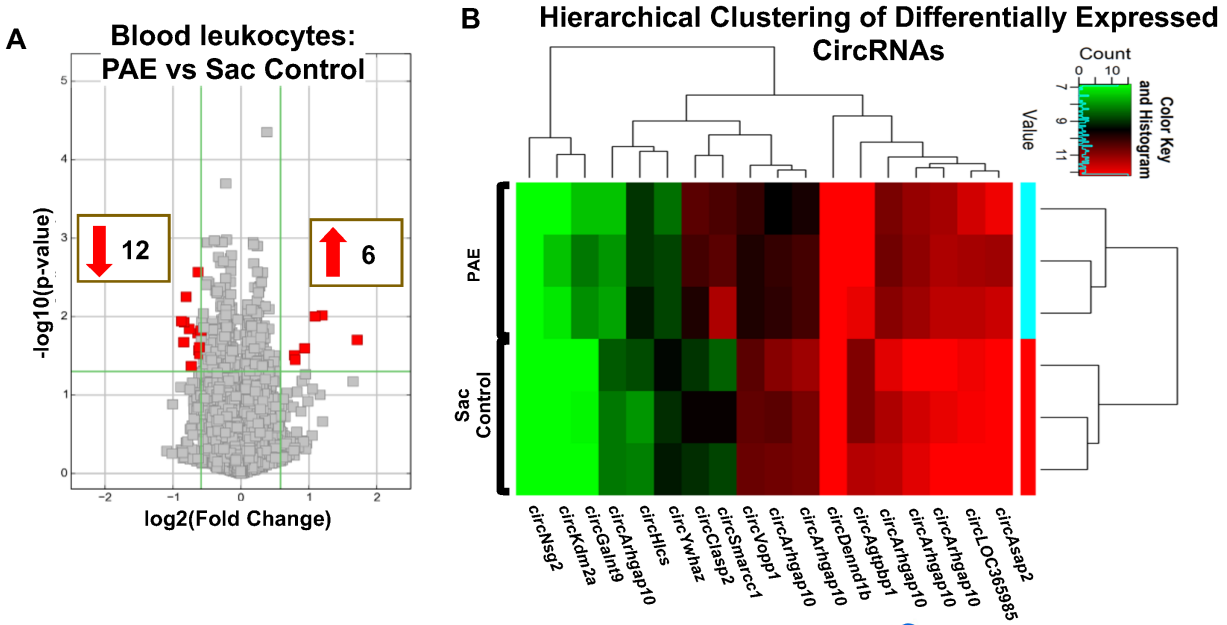
D

CircRNAs	Fold Change Values
circXpr1	2.260
circFbxo10	2.011
circZvfyve9	1.950
circRims1	1.887
circAtrnl1	1.881
circKiaa1328	1.811
circNrxn1	1.803
circQrich1	1.780
circTtc3	1.778
circAgap1	1.774
circGrik5	-2.465
circItch	-2.247
circParg	-2.191
circUbr1	-2.140
circNsd1	-2.046
circCkap4	-2.031
circPigk	-2.018
circStag1	-1.998
circNaa40	-1.996
circCpsf7	-1.988

FIGURE 4
Differential circRNA expression was observed in the spinal cord in PAE rats during allodynia, compared to non-allodynic control rats. **(A)** Volcano plots of differentially expressed circRNAs between PAE and Sac spinal cord, following nerve injury. X-axis represents log2 fold change (dotted line=1.5-fold), Y-axis represents −log10 *p*-value (dotted line: $p=0.05$). The red points in the plot represent the differentially expressed circRNAs, with 1.5-fold changes ($p<0.05$). **(B)** Heat map of the circRNA microarray profiles in the minor nerve-injured PAE (allodynic) and minor nerve-injured Sac control groups (non-allodynic), more than 1.75-fold changes. The expression of circRNAs is hierarchically clustered on the Y-axis, and spinal cord samples are hierarchically clustered on the X-axis. Green and red represent lower and higher expression levels of the circRNAs. **(C)** Ingenuity Pathway Analysis (IPA) from the host

(Continued)

FIGURE 4 (Continued)
genes of the differentially expressed circRNAs is used to generate the bubble plot. The bubble chart plots the pathway categories (Y-axis) related to these genes vs. the negative log of the *p*-values (X-axis), demonstrating the involvement of these genes with important canonical pathway categories such as nuclear receptor signaling, neurotransmitters and nervous system signaling and disease-specific pathways. The red square indicates bubbles referring to the neuropathic pain signaling pathway as the most significantly associated pathway. **(D)** Top upregulated and downregulated spinal circRNAs in minor nerve injured PAE rats compared to minor nerve injured control rats, parental or host gene symbol and fold changes with a cut off at 1.5-fold. **(E)** The three comprehensive networks are generated using IPA Canonical Pathways' top network function. The network compares minor nerve-injured PAE to minor nerve-injured control in the spinal cord and uses the secondary top network (z-score=46). Molecules in blue and red are downregulated and upregulated, respectively. Three separate biological replicates per treatment group were used to generate these data.



C

CircRNAs	Fold Change Value
circSmarcc1	3.270
circAgtpbp1	2.288
circGalnt9	2.132
circClasp2	1.915
circHlcs	1.736
circKdm2a	1.726
circArhgap10	-1.835
circAsap2	-1.661
circVopp1	-1.550
circYwhaz	-1.537
circDennd1b	-1.528
circNsg2	-1.503

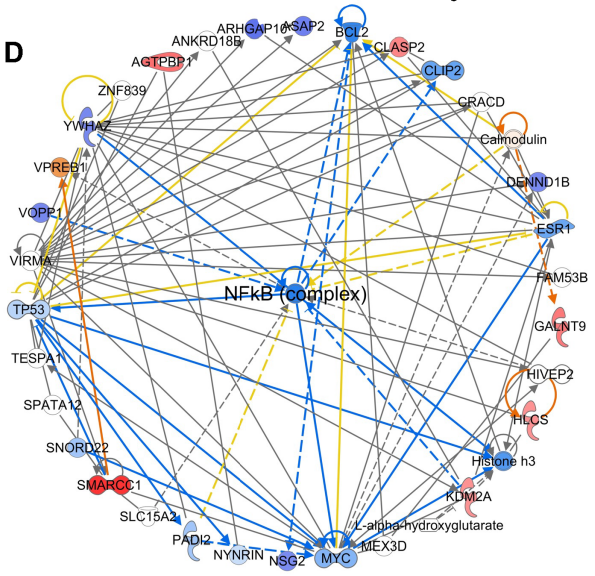


FIGURE 5
PAE-induced dysregulation of circRNAs is evident in blood leukocytes and is related to NF-κB-associated genes. **(A)** Volcano plots of differentially expressed circRNAs between PAE and Sac blood leukocytes without nerve injury. X-axis represents Log2 fold change (dotted line=1.5-fold), Y-axis represents −log10 *p*-value (dotted line: *p*=0.05). The red points in the plot represent the differentially expressed circRNAs, with 1.5-fold changes ($p<0.05$). **(B)** Heat map of the differentially expressed circRNAs in the PAE and control groups with fold changes of 1.5 or more. The expression of circRNAs is hierarchically clustered on the Y-axis, and biological replicates in different groups are hierarchically clustered on the X-axis. Green represents a lower and red represents a higher expression level of the circRNAs. **(C)** Top upregulated and downregulated circRNAs in PAE vs. Sac control leukocytes **(D)** The comprehensive networks are generated using IPA Canonical Pathways' top network function. The network graph's primary top network compares PAE vs. control in the blood leukocyte (z-score=37). Three separate biological replicates (each sample was pooled from 2 to 3 rats from Figure 1) per treatment group were used to generate these data.

levels based on prior studies of *Vopp1* as a regulator of nuclear translocation of NF-κB (Park and James, 2005). We have validated the levels of *circVopp1* and supporting our array data, *circVopp1* levels were significantly downregulated in PAE leukocytes (Figure 6D) compared to Sac control leukocytes. More interestingly, we found that *Vopp1* linear mRNA levels were also downregulated due to PAE. In contrast to our peripheral leukocyte data, spinal *circVopp1* levels were up-regulated due to PAE (Figure 6E). Although a trend of higher levels ($p = 0.08$) of linear *Vopp1* levels was observed in the PAE spinal cord following minor nerve injury, statistical significance was not observed across the different treatment groups.

4. Discussion

To our knowledge, this is the first study to provide preclinical evidence that prenatal alcohol exposure, at low to moderate levels, induces long-lasting modulation of circRNA expression profiles that are detectable during adulthood. Our data suggest that: (1) PAE itself dysregulates circRNAs in peripheral blood leukocytes and in the spinal cord without injury. Alterations in circRNA detected from blood-derived immune cells during adulthood can act as novel biomarkers to identify adult populations with FASD (Lu and Xu, 2016; Liu et al., 2020, 2021; Ravanidis et al., 2021). (2) Dysregulation of circRNAs displays a distinct pattern, which is dependent on tissue/sample type, and is further regulated by subsequent immune insult, as evidenced by the application of a minor nerve injury model. Although minor nerve injury resulted in dysregulated circRNAs that are common in PAE and Sac rats, a unique profile of circRNA modulation was also observed in PAE rats due to minor nerve injury. (3) Our comprehensive analysis of all these datasets from PAE relative to non-PAE, with or without nerve injury, demonstrate that the host genes of these circRNAs are related to NF-κB-related immune signaling. Together with our prior observations, the data are supportive of the idea that targeting NF-κB signaling and downstream immune molecules may be effective for mitigating FASD-related CNS pathologies (Doremus-Fitzwater et al., 2020). (4) Multiple circRNAs that are known to play modulatory roles in neuroimmune function are found to be dysregulated following nerve injury in PAE rats (discussed below). (5) Our data suggest that PAE dysregulates levels of *circVopp1* concurrent with changes in the levels of linear *Vopp1*, supporting *Vopp1* as a potential mechanism of neuroimmune dysfunction under PAE conditions.

Animal models of PAE demonstrate many similar manifestations of FASD that likewise reflect CNS dysfunction (Panczakiewicz et al., 2016; Reid et al., 2021) involving heightened immune reactivity (Topiwala et al., 2017; Himmelrich et al., 2020). Several animal studies support the emerging hypothesis that underlying CNS dysfunction from PAE may not manifest until a second challenge is encountered, such as from adult-onset nerve injury or typical immune stimulation (Terasaki and Schwarz, 2016; Sanchez et al., 2017). Our prior reports compared the effects of adult-onset nerve injury utilizing both standard CCI (4 sutures) and minor (a single suture) CCI models in PAE rats (Noor et al., 2017; Sanchez et al., 2017). Allodynia in PAE rats was found to be positively correlated with the degree of CCI; that is the standard CCI resulted in much greater allodynia compared to the minor CCI in PAE rats. Additionally, the degree of spinal cord astrocyte and microglial activation increased as the level of sciatic nerve damage increased, from a minor CCI to a standard CCI (Noor et al., 2017; Sanchez et al., 2017). Our prior published reports support that the underlying mechanism that causes a risk of developing allodynia in PAE rats is linked to heightened neuroimmune signaling (Sanchez et al., 2019). Specifically, the role of the proinflammatory cytokine, IL-1β, was critical in the maintenance of neuropathy in adult rats with PAE and minor injury. Together, both standard CCI and minor CCI model is expected to involve similar pathophysiology of perineural inflammation driving the spinal glial-immune activation and neuronal sensitization leading to chronic allodynia. However, due to heightened immune response as a consequence of PAE, only PAE rats but not the control rats, demonstrate allodynia despite a reduction of the degree of nerve damage with the minor CCI model. Other models of neuropathic pain caused by peripheral nerve injury, such as sciatic nerve ligation or sciatic nerve transection, or spared nerve injury do not allow the experimenter to systematically reduce the injury to a minor insult. Consequently, exploring susceptibility to developing neuropathy in PAE rats is not readily attainable when utilizing these other models. In addition, other suture materials, such as silk sutures that induce peri-neural inflammation may cause increased susceptibility to develop allodynia under PAE conditions, although different onset, magnitude and resolution of allodynia may occur (Dowdall et al., 2005; Grace et al., 2010).

The underlying molecular regulators and key immune pathways driving neuroimmune dysfunction upon adult-inset immune challenges are still under investigation. The well-characterized immune cell surface receptor, toll-like 4 (TLR4) is emerging as the nexus for immune dysregulation from PAE that impacts CNS function (Terasaki and Schwarz, 2016; Pascual et al., 2017) despite that spinal TLR4 gene expression remained unaltered from PAE (Noor et al., 2020). These observations suggest that other regulators may be involved underlying this heightened TLR4 signaling. While speculative, PAE may create a "silent" immune sensitization via changes in circRNA expression in the peripheral immune system and in the CNS. The immune sensitization by alterations in specific circRNAs may act as a "priming" factor that precipitates expression of exaggerated TLR4-related mRNA and protein only after the secondary challenge (e.g., a minor nerve injury) underlying heightened CNS glia and peripheral immune responses as a long-term consequence of PAE (Chen, 2020; Chen et al., 2021). One interesting aspect of this study is the compelling evidence of dysregulated circRNAs preferentially arising from genes that are linked to NF-κB immune complex, which is one of the most studied downstream regulators of the TLR4 signaling pathway. NF-κB is also a downstream effector of other proinflammatory cytokine receptor signaling, such as signaling through IL-1β and TNF-α receptors (Verstrepen et al., 2008; Mitchell et al., 2016). CircRNA biogenesis is paired with active transcription of their parental genes. Thus, these data support prior transcriptome studies in alcohol and PAE literature suggesting NF-κB-responsive genes are potential key modulators of PAE-related CNS dysfunction. Moreover, these bioinformatic analyses of these parental genes provided new NF-κB-related target genes that may contribute to long-term neuroimmune dysregulation due to PAE.

Additionally, our data identified a discrete subset of differentially expressed spinal circRNAs following minor nerve injury. Among these differentially expressed circRNAs are some circRNAs that are proven to be critical regulators of immune and neuroimmune function by recent studies. To be noted, we have

10.3389/fnins.2023.1180308

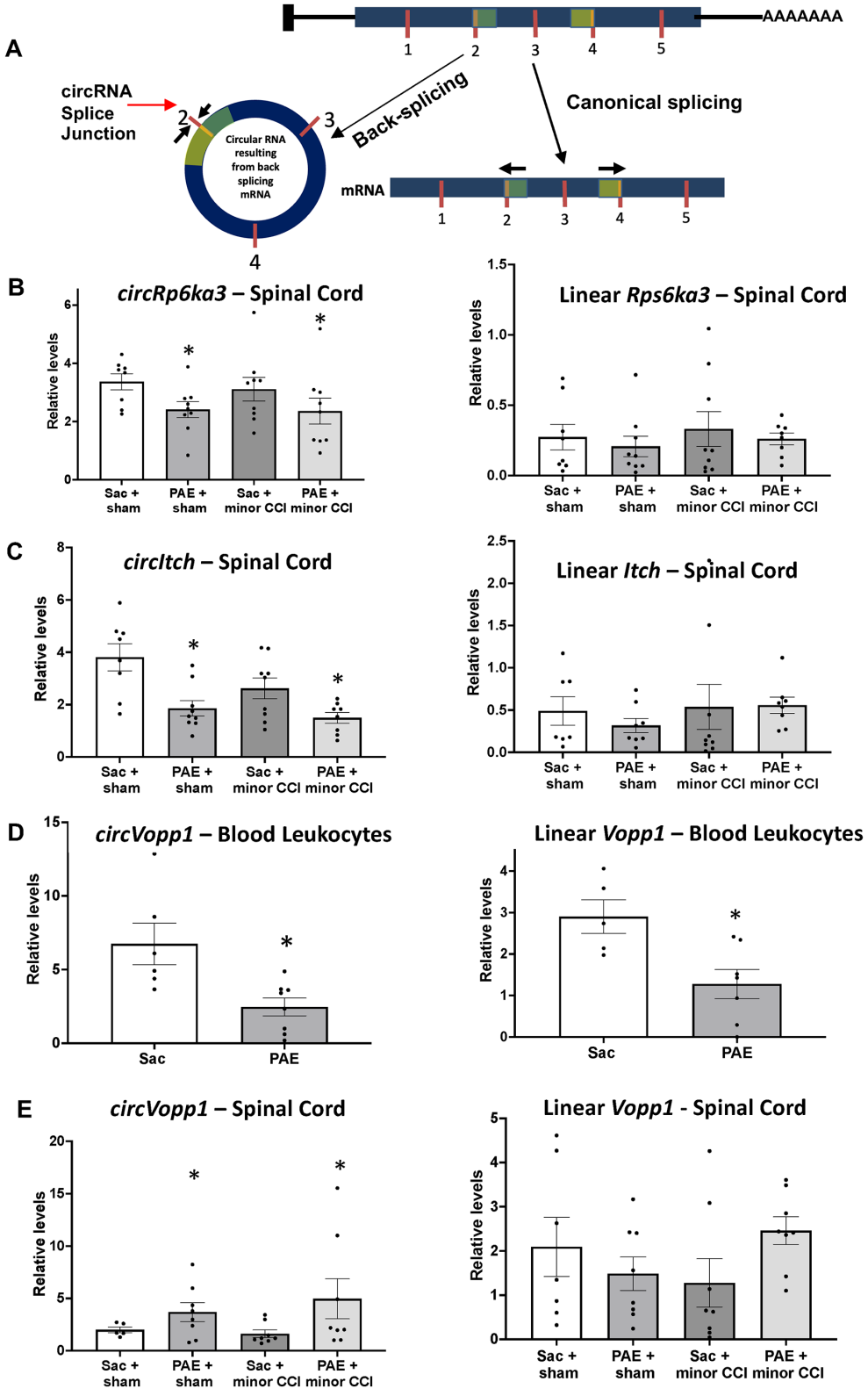


FIGURE 6
Quantitative real-time PCR validated dysregulated levels of circRNAs and their linear isoforms. **(A)** Schematic representation of an example circRNA biogenesis resulting from back-splicing events of Exon 2 and Exon 4 from a hypothetical precursor mRNA. The divergent primers for circRNA qRT-PCR validation were designed such that only the back-spliced and not linear junction was amplified. **(B)** Spinal *circRps6ka3* and linear *Rps6ka3* levels were measured. A main effect of PAE ($F_{1,31}$=5.53, p=0.025) was observed in *circRps6ka3* levels. An unpaired t-test revealed a significant downregulation of *circRps6ka3* levels (p<0.03) between PAE vs. Sac control, Sham injured rats. mRNA levels were not different across treatment groups. **(C)** *CircItch* levels were downregulated with PAE, a main effect ($F_{1,29}$=4.58, p=0.004) was observed. A main effect of surgery ($F_{1,29}$=15.66, p<0.05) was also observed. Post-doc test revealed a significant difference between PAE to Sac control (p<0.005), Sham-injured groups. Although the levels were not significantly

(Continued)

FIGURE 6 (Continued)
different with 2-way ANOVA, an unpaired t-test revealed significant downregulation of *circItch* levels ($p<0.05$) between nerve-injured PAE vs. nerve injure Sac control rats. mRNA levels were not different across treatment groups. **(D)** Blood leukocytes from additional adult Sac ($N=6$) and PAE ($N=8$) female rats were used for validation. A significant decrease of both *circVopp1* ($p<0.01$) and linear *Vopp1* ($p<0.02$) levels was observed in PAE. **(E)** A main effect of PAE ($F_{1,25}=4.25$, $^*p<0.05$) was observed on *circVopp1* levels in the spinal cord, however, multiple comparisons were not significant between groups. mRNA levels were not different across treatment groups, however, a trend of increased *Vopp1* mRNA levels in nerve-injured PAE rats was observed compared to the nerve-injured Sac rats. *Denotes *p* values with significance.

TABLE 4 Selected circRNAs arising from genes that are associated with immune signaling and/or allodynia.

CircRNA	Tissue	Comparison Category	Fold changes (up or down)	Role in the genes in immune signaling or pathological pain	References
CircRps6ka3	Spinal	PAE vs. Sac, no nerve injury	−2.93	Serine/threonine kinase that phosphorylates various substrates, including members of the mitogen-activated kinase (MAPK) signaling pathway. Related to Activated TLR4 signaling	Kakugawa et al. (2009)
CircSlc7a11	Spinal	PAE vs. Sac, no nerve injury	1.86	Inverse relationship of SLC7A11 and inflammatory cytokines are observed during CNS injury	Sprimont et al. (2021)
CircOtud7b	Spinal	PAE vs. Sac, nerve injured	−1.82	Negative regulator of the non-canonical NF-κB pathway	Hu et al. (2013)
CircGrik5	Spinal	PAE vs. Sac, nerve injured	−2.46	Glutamate-gated ion channel, involved in sensitization in nociceptive neurons	
CircItch	Spinal	PAE vs. Sac, nerve injured	−2.24	Ubiquitin ligase, connected to MAPK and Wnt signaling, a negative regulator of NF-κB signaling	Su et al. (2022) and Kong et al. (2020)
CircFkbp9	Spinal	PAE vs. Sac, nerve injured	−1.58	FK506-binding protein 9, involved in preventing stress-induced cell death	Gan et al. (2022)
CircVopp1	Blood	PAE vs. Sac, no nerve injury	−1.55	Regulates NF-κB1 translocation to nucleus to initiate its transcriptional activity	Park and James, (2005)

found that *circItch* (Liu et al., 2022; Su et al., 2022) is downregulated in PAE spinal cord following nerve injury. Interestingly, *circItch* has been characterized to be involved in several biological functions such as regulating cell proliferation, inflammation, and neovascularization. *CircItch* is proven to act as an anti-inflammatory agent in humans. *Circ-Itch* regulates proinflammatory cytokines such as IL-1β and TNF-α *via* regulating mRNA or *via* interacting with miRNAs (Liu et al., 2022; Su et al., 2022). *CircItch* levels are downregulated in multiple disease models and overexpression of *CircItch* can relieve proinflammatory cytokines in an intervertebral disc degeneration model (Kong et al., 2020). Additionally, *CircItch* may regulate drug resistance or toxicity which could be an area of interest to study the differential effects of drugs under PAE conditions (Hausknecht et al., 2017; Rangmar et al., 2017; Cantacorps et al., 2020). We have also detected altered levels of circRNAs such as *circTttc3* which has been implicated in playing modulatory roles in endogenous stress response or CNS injury (Ma et al., 2021; Yang et al., 2021). Based on these data, our future studies will focus on specific manipulations of circRNA expression *via* knockdown or overexpression studies to determine the necessary roles of these circRNAs underlying PAE-related chronic CNS dysfunction.

CircRNAs and their putative function is an emerging area of research. CircRNAs can regulate gene expression *via* multiple and diverse mechanisms such as interacting with RNA binding proteins and sponging miRNAs (Barrett and Salzman, 2016; Chen, 2020; Chen et al., 2021). Dysregulation of circRNAs can occur with up-regulation, down-regulation, or no change in the host gene expression (Wang et al., 2020; Xu et al., 2020; Shao et al., 2021). A majority of the host gene mRNA levels we have examined in this study appear similar across the different treatment groups suggesting that these circRNAs may act *via* other mechanisms such as interacting with pain-relevant miRNA or other mRNA molecules. Interestingly, we have found that linear levels of *Vopp1* and *circVopp1* are dysregulated by PAE. Interpretation of whether or how *circVopp1* regulates linear *Vopp1* levels is limited at this point, our data suggest that dysregulated circ- and linear *Vopp1* levels may contribute to aberrant NF-κB signaling affecting immune function in PAE offspring. Moreover, peripheral blood-identified circRNAs may serve as potential biomarkers for CNS pathologies (Lu and Xu, 2016; Liu et al., 2020; Piscopo et al., 2022), often an indicator of disease prognosis (Gaffo et al., 2019; Ravanidis et al., 2021). Although opposite to what was observed in blood, our real-time PCR data suggesting the altered *circVopp1* levels in both the periphery and CNS tissue may identify *circVopp1* as an ideal marker of PAE-related CNS dysfunction. Although a minimal overlap of PAE-induced circular RNA molecules was observed in the periphery and in the spinal cord in the absence of injury, differentially expressed circRNAs may overlap in the spinal cord and in the peripheral blood samples following subsequent immune challenges. Future studies from clinical samples will address whether these newly identified blood leukocyte-derived circRNAs are viable biomarkers for FASD populations.

Overall, this study provides preclinical evidence that PAE results in dysregulated circRNAs during adulthood. These data demonstrate that PAE-induced neuropathic pain susceptibility is concurrent with an altered profile of circular RNA expression. Data presented here encourage the scientific premise of studying circRNAs as potential clinical biomarkers and as novel therapeutic targets in adults with FASD. Considering only a limited number of studies focused on utilizing female rodents and our prior knowledge on associated proinflammatory glia and peripheral immune factors in minor nerve-injured PAE female rats (Noor et al., 2020), we have prioritized these studies in females. However, multiple reports from our group established that PAE-related neuropathic pain susceptibility is evident in male rats that follow a comparable timeline of allodynia development and reversal with PAE female rats (Sanchez et al., 2017, 2019). Therefore, we anticipate that dysregulation of circRNAs will be present in male rats, although sex-specific patterns of PAE-induced circRNA dysregulation may occur (Paudel et al., 2020; Papageorgiou et al., 2023). Future studies will examine sex-specific differences in circRNA expression during adulthood under PAE conditions.

Data availability statement

The datasets presented in this study can be found online: https://data.mendeley.com/datasets/mt4fwkzh77/draft?a=8aa0ba.

Ethics statement

The animal study was reviewed and approved by Institutional Animal Care and Use Committee (IACUC) of The University of New Mexico Health Sciences Center.

Author contributions

SN, EM, and NM contributed to the conception and design of the study and edited the manuscript. JES, JJS, and EM collected allodynia behavior data. SN, ANP, JES, JJS, and EM collected tissues. SN, MS, and ANP processed the tissues. NM guided designing circRNA-specific primers and primer slope analysis. ANP, AAP, AKF-O, and SN performed the real-time PCRs and statistical analysis. ANP carried out that IPA analysis. SN and MD assisted IPA analysis. ANP and SN wrote the first draft of the manuscript. SD and DS generated Saccharin control and moderate PAE rat offspring and assisted with manuscript preparation. All authors contributed to the article and approved the submitted version.

Funding

This work was supported by National Institute of Health (NIH) grants R01 AA025967, R21 AA023051, T32 AA014127, P50 AA022534, R01 AA029694, and R01 AA026583.

Acknowledgments

The authors would like to thank Bill Shuttleworth, David L. Linsenbardt, Nora Perrone-Bizzozero, and Karin High at UNM, for providing the laboratory facilities for RNA extraction, qRT-PCR, and data analysis.

Conflict of interest

NM has a financial interest in Circular Genomics Inc., a company focused on the use of circRNAs as biomarkers for psychiatric disorders.

The remaining authors declare that the research was conducted in the absence of any commercial or financial relationships that could be construed as a potential conflict of interest.

Publisher's note

All claims expressed in this article are solely those of the authors and do not necessarily represent those of their affiliated organizations, or those of the publisher, the editors and the reviewers. Any product that may be evaluated in this article, or claim that may be made by its manufacturer, is not guaranteed or endorsed by the publisher.

Supplementary material

The Supplementary material for this article can be found online at: https://www.frontiersin.org/articles/10.3389/fnins.2023.1180308/full#supplementary-material

References

Bake, S., Pinson, M. R., Pandey, S., Chambers, J. P., Mota, R., Fairchild, A. E., et al. (2021). Prenatal alcohol-induced sex differences in immune, metabolic and neurobehavioral outcomes in adult rats. *Brain Behav. Immun.* 98, 86–100. doi: 10.1016/j.bbi.2021.08.207

Balaraman, S., Lunde, E. R., Sawant, O., Cudd, T. A., Washburn, S. E., and Miranda, R. C. (2014). Maternal and neonatal plasma microRNA biomarkers for fetal alcohol exposure in an ovine model. *Alcohol. Clin. Exp. Res.* 38, 1390–1400. doi: 10.1111/acer.12378

Balaraman, S., Schafer, J. J., Tseng, A. M., Wertelecki, W., Yevtushok, L., Zymak-Zakutnya, N., et al. (2016). Plasma miRNA profiles in pregnant women predict infant outcomes following prenatal alcohol exposure. *PLoS One* 11:e0165081. doi: 10.1371/journal.pone.0165081

Balaraman, S., Tingling, J. D., Tsai, P. C., and Miranda, R. C. (2013). Dysregulation of microRNA expression and function contributes to the etiology of fetal alcohol spectrum disorders. *Alcohol Res.* 35, 18–24.

Barrett, S. P., and Salzman, J. (2016). Circular RNAs: analysis, expression and potential functions. *Development* 143, 1838–1847. doi: 10.1242/dev.128074

Bennett, G. J., and Xie, Y. K. (1988). A peripheral mononeuropathy in rat that produces disorders of pain sensation like those seen in man. *Pain* 33, 87–107. doi: 10.1016/0304-3959(88)90209-6

Bodnar, T. S., Hill, L. A., and Weinberg, J. (2016). Evidence for an immune signature of prenatal alcohol exposure in female rats. *Brain Behav. Immun.* 58, 130–141. doi: 10.1016/j.bbi.2016.05.022

Bodnar, T. S., Raineki, C., Wertelecki, W., Yevtushok, L., Plotka, L., Granovska, I., et al. (2020). Immune network dysregulation associated with child neurodevelopmental delay: modulatory role of prenatal alcohol exposure. *J. Neuroinflammation* 17:39. doi: 10.1186/s12974-020-1717-8

Bodnar, T. S., Raineki, C., Wertelecki, W., Yevtushok, L., Plotka, L., Zymak-Zakutnya, N., et al. (2018). Altered maternal immune networks are associated with adverse child neurodevelopment: impact of alcohol consumption during pregnancy. *Brain Behav. Immun.* 73, 205–215. doi: 10.1016/j.bbi.2018.05.004

Cantacorps, L., Montagud-Romero, S., Luján, M. Á., and Valverde, O. (2020). Prenatal and postnatal alcohol exposure increases vulnerability to cocaine addiction in adult mice. *Br. J. Pharmacol.* 177, 1090–1105. doi: 10.1111/bph.14901

Challa, S. R. (2015). Surgical animal models of neuropathic pain: pros and cons. *Int. J. Neurosci.* 125, 170–174. doi: 10.3109/00207454.2014.922559

Chen, L. L. (2020). The expanding regulatory mechanisms and cellular functions of circular RNAs. *Nat. Rev. Mol. Cell Biol.* 21, 475–490. doi: 10.1038/s41580-020-0243-y

Chen, M., Lai, X., Wang, X., Ying, J., Zhang, L., Zhou, B., et al. (2021). Long non-coding RNAs and circular RNAs: insights into microglia and astrocyte mediated neurological diseases. *Front. Mol. Neurosci.* 14:745066. doi: 10.3389/fnmol.2021.745066

Davies, S., Ballesteros-Merino, C., Allen, N. A., Porch, M. W., Pruitt, M. E., Christensen, K. H., et al. (2019). Impact of moderate prenatal alcohol exposure on histaminergic neurons, histidine decarboxylase levels and histamine H2 receptors in adult rat offspring. *Alcohol* 76, 47–57. doi: 10.1016/j.alcohol.2018.07.007

Davies, S., Nelson, D. E., and Savage, D. D. (2023). (in press)). Impact of two different rodent diets on maternal ethanol consumption, serum ethanol concentration and pregnancy outcome measures. *Alcohol*. doi: 10.2139/ssrn.4161442

Dell'Orco, M., Oliver, R. J., and Perrone-Bizzozero, N. (2020). HuD binds to and regulates circular RNAs derived from neuronal development- and synaptic plasticity-associated genes. *Front. Genet.* 11:790. doi: 10.3389/fgene.2020.00790

Doremus-Fitzwater, T. L., Youngentob, S. L., Youngentob, L., Gano, A., Vore, A. S., and Deak, T. (2020). Lingering effects of prenatal alcohol exposure on basal and ethanol-evoked expression of inflammatory-related genes in the CNS of adolescent and adult rats. *Front. Behav. Neurosci.* 14:82. doi: 10.3389/fnbeh.2020.00082

Dowdall, T., Robinson, I., and Meert, T. F. (2005). Comparison of five different rat models of peripheral nerve injury. *Pharmacol. Biochem. Behav.* 80, 93–108. doi: 10.1016/j.pbb.2004.10.016

Drew, P. D., Johnson, J. W., Douglas, J. C., Phelan, K. D., and Kane, C. J. M. (2015). Pioglitazone blocks ethanol induction of microglial activation and immune responses in the hippocampus, cerebellum, and cerebral cortex in a mouse model of fetal alcohol spectrum disorders. *Alcohol. Clin. Exp. Res.* 39, 445–454. doi: 10.1111/acer.12639

Drew, P. D., and Kane, C. J. (2014). Fetal alcohol spectrum disorders and neuroimmune changes. *Int. Rev. Neurobiol.* 118, 41–80. doi: 10.1016/B978-0-12-801284-0.00003-8

England, L. J., Bennett, C., Denny, C. H., Honein, M. A., Gilboa, S. M., Kim, S. Y., et al. (2020). Alcohol use and co-use of other substances among pregnant females aged 12-44 years - United States, 2015-2018. *MMWR Morb. Mortal. Wkly Rep.* 69, 1009–1014. doi: 10.15585/mmwr.mm6931a1

Fjeldsted, B., and Xue, L. (2019). Sensory processing in Young children with fetal alcohol Spectrum disorder. *Phys. Occup. Ther. Pediatr.* 39, 553–565. doi: 10.1080/01942638.2019.1573775

Franklin, L., Deitz, J., Jirikowic, T., and Astley, S. (2008). Children with fetal alcohol spectrum disorders: problem behaviors and sensory processing. *Am. J. Occup. Ther.* 62, 265–273. doi: 10.5014/ajot.62.3.265

Gaffo, E., Boldrin, E., Dal Molin, A., Bresolin, S., Bonizzato, A., Trentin, L., et al. (2019). Circular RNA differential expression in blood cell populations and exploration of circRNA deregulation in pediatric acute lymphoblastic leukemia. *Sci. Rep.* 9:14670. doi: 10.1038/s41598-019-50864-z

Gan, Y. L., Wang, C. Y., He, R. H., Hsu, P. C., Yeh, H. H., Hsieh, T. H., et al. (2022). FKBP51 mediates resilience to inflammation-induced anxiety through regulation of glutamic acid decarboxylase 65 expression in mouse hippocampus. *J. Neuroinflammation* 19:152. doi: 10.1186/s12974-022-02517-8

Grace, P. M., Hutchinson, M. R., Manavis, J., Somogyi, A. A., and Rolan, P. E. (2010). A novel animal model of graded neuropathic pain: utility to investigate mechanisms of population heterogeneity. *J. Neurosci. Methods* 193, 47–53. doi: 10.1016/j.jneumeth.2010.08.025

Grubbs, F. (1950). Sample criteria for testing outlying observations. *Ann. Math. Statist.* 21, 27–58. doi: 10.1214/aoms/1177729885

Guo, J. U., Agarwal, V., Guo, H., and Bartel, D. P. (2014). Expanded identification and characterization of mammalian circular RNAs. *Genome Biol.* 15:409. doi: 10.1186/s13059-014-0409-z

Hamilton, D. A., Akers, K. G., Rice, J. P., Johnson, T. E., Candelaria-Cook, F. T., Maes, L. I., et al. (2010). Prenatal exposure to moderate levels of ethanol alters social behavior in adult rats: relationship to structural plasticity and immediate early gene expression in frontal cortex. *Behav. Brain Res.* 207, 290–304. doi: 10.1016/j.bbr.2009.10.012

Haque, S., and Harries, L. W. (2017). Circular RNAs (circRNAs) in health and disease. *Genes (Basel)* 8:353. doi: 10.3390/genes8120353

Hausknecht, K., Shen, Y. L., Wang, R. X., Haj-Dahmane, S., and Shen, R. Y. (2017). Prenatal ethanol exposure persistently alters endocannabinoid signaling and endocannabinoid-mediated excitatory synaptic plasticity in ventral tegmental area dopamine neurons. *J. Neurosci.* 37, 5798–5808. doi: 10.1523/JNEUROSCI.3894-16.2017

Himmelrich, H., Lo-Man, R., Winter, N., Guermonprez, P., Sedlik, C., Rojas, M., et al. (2000). Immune responses induced by recombinant BCG strains according to level of production of a foreign antigen: malE. *Vaccine* 18, 2636–2647. doi: 10.1016/S0264-410X(00)00070-0

Himmelrich, M., Lutke, C. J., and Hargrave, E. T. (2020). "The lay of the land: fetal alcohol spectrum disorder (FASD) as a whole body diagnosis" in *The Routledge handbook of social work and addictive behaviors*. eds. A. L. Begun and M. M. Murray (London: Routledge)

Hu, H., Brittain, G. C., Chang, J. H., Puebla-Osorio, N., Jin, J., Zal, A., et al. (2013). OTUD7B controls non-canonical NF-κB activation through deubiquitination of TRAF3. *Nature* 494, 371–374. doi: 10.1038/nature11831

Kakugawa, S., Shimojima, M., Goto, H., Horimoto, T., Oshimori, N., Neumann, G., et al. (2009). Mitogen-activated protein kinase-activated kinase RSK2 plays a role in innate immune responses to influenza virus infection. *J. Virol.* 83, 2510–2517. doi: 10.1128/JVI.02416-08

Kong, D., Gu, R., Zhang, C., and Yin, R. (2020). Knockdown of hsa_circ_0059955 induces apoptosis and cell cycle arrest in nucleus pulposus cells via inhibiting. *Drug Des. Devel. Ther.* 14, 3951–3963. doi: 10.2147/DDDT.S253293

Krämer, A., Green, J., Pollard Jr, J., and Tugendreich, S. (2014). Causal analysis approaches in ingenuity pathway analysis. *Bioinformatics* 30, 523–530. doi: 10.1093/bioinformatics/btt703

Liu, L., Chen, X., Chen, Y. H., and Zhang, K. (2020). Identification of circular RNA hsa_Circ_0003391 in peripheral blood is potentially associated with Alzheimer's disease. *Front. Aging Neurosci.* 12:601965. doi: 10.3389/fnagi.2020.601965

Liu, T., Huang, T., Shang, M., and Han, G. (2022). CircRNA ITCH: insight into its role and clinical application Prospect in tumor and non-tumor diseases. *Front. Genet.* 13:927541. doi: 10.3389/fgene.2022.927541

Liu, J., Zhu, X., Yan, M., and Li, H. (2021). Development of a two-circular RNA panel as potential prognostic biomarker for gastric cancer. *J. Transl. Med.* 19:412. doi: 10.1186/s12967-021-03075-y

Lu, D., and Xu, A. D. (2016). Mini review: circular RNAs as potential clinical biomarkers for disorders in the central nervous system. *Front. Genet.* 7:53. doi: 10.3389/fgene.2016.00053

Ma, X., Zhu, G., Jiao, T., and Shao, F. (2021). Effects of circular RNA Ttc3/miR-148a/Rcan2 axis on inflammation and oxidative stress in rats with acute kidney injury induced by sepsis. *Life Sci.* 272:119233. doi: 10.1016/j.lfs.2021.119233

Mahnke, A. H., Sideridis, G. D., Salem, N. A., Tseng, A. M., Carter, R. C., Dodge, N. C., et al. (2021). Infant circulating MicroRNAs as biomarkers of effect in fetal alcohol spectrum disorders. *Sci. Rep.* 11:1429. doi: 10.1038/s41598-020-80734-y

Menorca, R. M., Fussell, T. S., and Elfar, J. C. (2013). Nerve physiology: mechanisms of injury and recovery. *Hand Clin.* 29, 317–330. doi: 10.1016/j.hcl.2013.04.002

Milligan, E. D., Mehmert, K. K., Hinde, J. L., Harvey, L. O. Jr., Martin, D., Tracey, K. J., et al. (2000). Thermal hyperalgesia and mechanical allodynia produced by intrathecal administration of the human immunodeficiency virus-1 (HIV-1) envelope glycoprotein, gp120. *Brain Res.* 861, 105–116. doi: 10.1016/S0006-8993(00)02050-3

Milligan, E. D., and Watkins, L. R. (2009). Pathological and protective roles of glia in chronic pain. *Nat. Rev. Neurosci.* 10, 23–36. doi: 10.1038/nrn2533

Mitchell, S., Vargas, J., and Hoffmann, A. (2016). Signaling via the NFκB system. *Wiley Interdiscip. Rev. Syst. Biol. Med.* 8, 227–241. doi: 10.1002/wsbm.1331

Moore, E. M., and Riley, E. P. (2015). What happens when children with fetal alcohol Spectrum disorders become adults? *Curr. Dev. Disord. Rep.* 2, 219–227. doi: 10.1007/s40474-015-0053-7

Ng, W. L., Mohd Mohidin, T. B., and Shukla, K. (2018). Functional role of circular RNAs in cancer development and progression. *RNA Biol.* 15, 995–1005. doi: 10.1080/15476286.2018.1486659

Noor, S., and Milligan, E. D. (2018). Lifelong impacts of moderate prenatal alcohol exposure on Neuroimmune function. *Front. Immunol.* 9:1107. doi: 10.3389/fimmu.2018.01107

Noor, S., Sanchez, J. J., Sun, M. S., Pervin, Z., Sanchez, J. E., Havard, M. A., et al. (2020). The LFA-1 antagonist BIRT377 reverses neuropathic pain in prenatal alcohol-exposed female rats via actions on peripheral and central neuroimmune function in discrete pain-relevant tissue regions. *Brain Behav. Immun.* 87, 339–358. doi: 10.1016/j.bbi.2020.01.002

Noor, S., Sanchez, J. J., Vanderwall, A. G., Sun, M. S., Maxwell, J. R., Davies, S., et al. (2017). Prenatal alcohol exposure potentiates chronic neuropathic pain, spinal glial and immune cell activation and alters sciatic nerve and DRG cytokine levels. *Brain Behav. Immun.* 61, 80–95. doi: 10.1016/j.bbi.2016.12.016

Panczakiewicz, A. L., Glass, L., Coles, C. D., Kable, J. A., Sowell, E. R., Wozniak, J. R., et al. (2016). Neurobehavioral deficits consistent across age and sex in youth with prenatal alcohol exposure. *Alcohol. Clin. Exp. Res.* 40, 1971–1981. doi: 10.1111/acer.13153

Papageorgiou, G., Amoah, S. K., Pierotti, C., Otero, M., Eckel, S., Coffey, K., et al. (2023). Prenatal alcohol exposure results in brain region- and sex-specific changes in circHomer1 expression in adult mouse brain. *Front. Neurosci.* 17:1087950. doi: 10.3389/fnins.2023.1087950

Park, S., and James, C. D. (2005). ECop (EGFR-coamplified and overexpressed protein), a novel protein, regulates NF-kappaB transcriptional activity and associated apoptotic response in an IkappaBalpha-dependent manner. *Oncogene* 24, 2495–2502. doi: 10.1038/sj.onc.1208496

Pascual, M., Montesinos, J., Montagud-Romero, S., Forteza, J., Rodríguez-Arias, M., Miñarro, J., et al. (2017). TLR4 response mediates ethanol-induced neurodevelopment alterations in a model of fetal alcohol spectrum disorders. *J. Neuroinflammation* 14:145. doi: 10.1186/s12974-017-0918-2

Paudel, P., Pierotti, C., Lozano, E., Amoah, S. K., Gardiner, A. S., Caldwell, K. K., et al. (2020). Prenatal alcohol exposure results in sex-specific alterations in circular RNA expression in the developing mouse brain. *Front. Neurosci.* 14:581895. doi: 10.3389/fnins.2020.581895

Peng, P., Yu, H., Yongjin Li, , Huang, J., Yao, S., Xing, C., et al. (2021). The emerging role of circular RNAs in spinal cord injury. *J. Orthop. Translat.* 30, 1–5. doi: 10.1016/j.jot.2021.06.001

Piscopo, P., Manzini, V., Rivabene, R., Crestini, A., le Pera, L., Pizzi, E., et al. (2022). A plasma circular RNA profile differentiates subjects with Alzheimer's disease and mild cognitive impairment from healthy controls. *Int. J. Mol. Sci.* 23:13232. doi: 10.3390/ijms232113232

Rangmar, J., Dahlgren Sandberg, A., Aronson, M., and Fahlke, C. (2017). Self-reported health, use of alcohol and illicit drugs, and criminality among adults with foetal alcohol syndrome. *Nordisk Alkohol Nark* 34, 255–266. doi: 10.1177/1455072517707887

Ravanidis, S., Bougea, A., Karampatsi, D., Papagiannakis, N., Maniati, M., Stefanis, L., et al. (2021). Differentially expressed circular RNAs in peripheral blood mononuclear cells of patients with Parkinson's disease. *Mov. Disord.* 36, 1170–1179. doi: 10.1002/mds.28467

Reid, N., Hayes, N., Young, S. B., Akison, L. K., and Moritz, K. M. (2021). Caregiver-reported physical health status of children and young people with fetal alcohol spectrum disorder. *J. Dev. Orig. Health Dis.* 12, 420–427. doi: 10.1017/S2040174420000537

Ruyak, S. L., Noor, S., DiDomenico, J., Sun, M. S., Fernandez Oropeza, A. K., Rodriguez, D. E., et al. (2022). Effects of prenatal opioid and alcohol exposures on immune and serotonin factors in human placenta. *Exp. Neurol.* 353:114057. doi: 10.1016/j.expneurol.2022.114057

Salmon, J. (2018). Fetal alcohol Spectrum disorder: risk for diabetes and congenital heart defects. *Integr. Diab. Cardiovasc. Dis.* 2, 48–55. doi: 10.18314/idcd.v1i1.1080

Sanchez, J. J., Noor, S., Davies, S., Savage, D., and Milligan, E. D. (2017). Prenatal alcohol exposure is a risk factor for adult neuropathic pain via aberrant neuroimmune function. *J. Neuroinflammation* 14:254. doi: 10.1186/s12974-017-1030-3

Sanchez, J. J., Sanchez, J. E., Noor, S., Ruffaner-Hanson, C. D., Davies, S., Wagner, C. R., et al. (2019). Targeting the beta2-integrin LFA-1, reduces adverse neuroimmune actions in neuropathic susceptibility caused by prenatal alcohol exposure. *Acta Neuropathol. Commun.* 7:54. doi: 10.1186/s40478-019-0701-y

Savage, D. D., Rosenberg, M. J., Wolff, C. R., Akers, K. G., el-Emawy, A., Staples, M. C., et al. (2010). Effects of a novel cognition-enhancing agent on fetal ethanol-induced learning deficits. *Alcohol. Clin. Exp. Res.* 34, 1793–1802. doi: 10.1111/j.1530-0277.2010.01266.x

Shao, T., Pan, Y. H., and Xiong, X. D. (2021). Circular RNA: an important player with multiple facets to regulate its parental gene expression. *Mol. Ther. Nucleic Acids* 23, 369–376. doi: 10.1016/j.omtn.2020.11.008

Sprimont, L., Janssen, P., de Swert, K., van Bulck, M., Rooman, I., Gilloteaux, J., et al. (2021). Cystine-glutamate antiporter deletion accelerates motor recovery and improves histological outcomes following spinal cord injury in mice. *Sci. Rep.* 11:12227. doi: 10.1038/s41598-021-91698-y

Su, K., Yi, Q., Dai, X., and Liu, O. (2022). Circular RNA ITCH: an emerging multifunctional regulator. *Biomol. Ther.* 12:359. doi: 10.3390/biom12030359

Terasaki, L. S., and Schwarz, J. M. (2016). Effects of moderate prenatal alcohol exposure during early gestation in rats on inflammation across the maternal-fetal-immune Interface and later-life immune function in the offspring. *J. Neuroimmune Pharmacol.* 11, 680–692. doi: 10.1007/s11481-016-9691-8

Terasaki, L. S., and Schwarz, J. M. (2017). Impact of prenatal and subsequent adult alcohol exposure on pro-inflammatory cytokine expression in brain regions necessary for simple recognition memory. *Brain Sci.* 7:125. doi: 10.3390/brainsci7100125

Tominaga, M., and Caterina, M. J. (2004). Thermosensation and pain. *J. Neurobiol.* 61, 3–12. doi: 10.1002/neu.20079

Topiwala, A., Allan, C. L., Valkanova, V., Zsoldos, E., Filippini, N., Sexton, C., et al. (2017). Moderate alcohol consumption as risk factor for adverse brain outcomes and cognitive decline: longitudinal cohort study. *BMJ* 357:j2353. doi: 10.1136/bmj.j2353

Tseng, A. M., Mahnke, A. H., Wells, A. B., Salem, N. A., Allan, A. M., Roberts, V. H. J., et al. (2019). Maternal circulating miRNAs that predict infant FASD outcomes influence placental maturation. *Life Sci. Alliance* 2:e201800252. doi: 10.26508/lsa.201800252

Vanderwall, A. G., Noor, S., Sun, M. S., Sanchez, J. E., Yang, X. O., Jantzie, L. L., et al. (2017). Effects of spinal non-viral interleukin-10 gene therapy formulated with d-mannose in neuropathic interleukin-10 deficient mice: behavioral characterization, mRNA and protein analysis in pain relevant tissues. *Brain Behav. Immun.* 69, 91–112. doi: 10.1016/j.bbi.2017.11.004

Verstrepen, L., Bekaert, T., Chau, T. L., Tavernier, J., Chariot, A., and Beyaert, R. (2008). TLR-4, IL-1R and TNF-R signaling to NF-kappaB: variations on a common theme. *Cell. Mol. Life Sci.* 65, 2964–2978. doi: 10.1007/s00018-008-8064-8

Wang, X., Li, H., Lu, Y., and Cheng, L. (2020). Regulatory effects of circular RNAs on host genes in human Cancer. *Front. Oncol.* 10:586163. doi: 10.3389/fonc.2020.586163

Wilhelm, C. J., and Guizzetti, M. (2015). Fetal alcohol Spectrum disorders: an overview from the glia perspective. *Front. Integr. Neurosci.* 9:65. doi: 10.3389/fnint.2015.00065

Xu, X., Zhang, J., Tian, Y., Gao, Y., Dong, X., Chen, W., et al. (2020). CircRNA inhibits DNA damage repair by interacting with host gene. *Mol. Cancer* 19:128. doi: 10.1186/s12943-020-01246-x

Yang, B., Zang, L., Cui, J., and Wei, L. (2021). Circular RNA TTC3 regulates cerebral ischemia-reperfusion injury and neural stem cells by miR-372-3p/TLR4 axis in cerebral infarction. *Stem Cell Res Ther* 12:125. doi: 10.1186/s13287-021-02187-y

Zhang, X., Sliwowska, J. H., and Weinberg, J. (2005). Prenatal alcohol exposure and fetal programming: effects on neuroendocrine and immune function. *Exp. Biol. Med. (Maywood)* 230, 376–388. doi: 10.1177/15353702-0323006-05

Zimmerman, A. J., Hafez, A. K., Amoah, S. K., Rodriguez, B. A., Dell'Orco, M., Lozano, E., et al. (2020). A psychiatric disease-related circular RNA controls synaptic gene expression and cognition. *Mol. Psychiatry* 25, 2712–2727. doi: 10.1038/s41380-020-0653-4

frontiers | Frontiers in Neuroscience

TYPE Original Research
PUBLISHED 09 June 2023
DOI 10.3389/fnins.2023.1154621

Check for updates

OPEN ACCESS

EDITED BY
Carlos Fernando Valenzuela,
University of New Mexico, United States

REVIEWED BY
Paola A. Haeger,
Catholic University of the North,
Coquimbo, Chile
James Alan Marrs,
Indiana University–Purdue University
Indianapolis, United States
Rebecca McLennan,
Children's Mercy Hospital, United States

*CORRESPONDENCE
Rayna Mazumdar
✉ rayna.mazumdar@utexas.edu

RECEIVED 30 January 2023
ACCEPTED 10 April 2023
PUBLISHED 09 June 2023

CITATION
Mazumdar R and Eberhart JK (2023) Loss of *Nicotinamide nucleotide transhydrogenase* sensitizes embryos to ethanol-induced neural crest and neural apoptosis via generation of reactive oxygen species.
Front. Neurosci. 17:1154621.
doi: 10.3389/fnins.2023.1154621

COPYRIGHT
© 2023 Mazumdar and Eberhart. This is an open-access article distributed under the terms of the Creative Commons Attribution License (CC BY). The use, distribution or reproduction in other forums is permitted, provided the original author(s) and the copyright owner(s) are credited and that the original publication in this journal is cited, in accordance with accepted academic practice. No use, distribution or reproduction is permitted which does not comply with these terms.

Loss of *Nicotinamide nucleotide transhydrogenase* sensitizes embryos to ethanol-induced neural crest and neural apoptosis via generation of reactive oxygen species

Rayna Mazumdar[1,2]* and Johann K. Eberhart[1,2]

[1]Department of Molecular Biosciences, School of Natural Sciences, University of Texas at Austin, Austin, TX, United States, [2]Waggoner Center for Alcohol and Addiction Research, School of Pharmacy, University of Texas at Austin, Austin, TX, United States

Fetal alcohol spectrum disorders (FASD) are a continuum of birth defects caused by prenatal alcohol exposure. FASD are the most common environmentally induced birth defect and are highly variable. The genetics of an individual influence the severity of their FASD phenotype. However, the genes that sensitize an individual to ethanol-induced birth defects are largely unknown. The ethanol-sensitive mouse substrain, C57/B6J, carries several known mutations including one in *Nicotinamide nucleotide transhydrogenase* (*Nnt*). Nnt is a mitochondrial transhydrogenase thought to have an important role in detoxifying reactive oxygen species (ROS) and ROS has been implicated in ethanol teratogenesis. To directly test the role of Nnt in ethanol teratogenesis, we generated zebrafish *nnt* mutants via CRISPR/Cas9. Zebrafish embryos were dosed with varying concentrations of ethanol across different timepoints and assessed for craniofacial malformations. We utilized a ROS assay to determine if this could be a contributing factor of these malformations. We found that exposed and unexposed mutants had higher levels of ROS compared to their wildtype counterparts. When treated with ethanol, *nnt* mutants experienced elevated apoptosis in the brain and neural crest, a defect that was rescued by administration of the antioxidant, N-acetyl cysteine (NAC). NAC treatment also rescued most craniofacial malformations. Altogether this research demonstrates that ethanol-induced oxidative stress leads to craniofacial and neural defects due to apoptosis in *nnt* mutants. This research further supports the growing body of evidence implicating oxidative stress in ethanol teratogenesis. These findings suggest that antioxidants can be used as a potential therapeutic in the treatment of FASD.

KEYWORDS

FASD, neural crest cells, oxidative stress, *nnt*, ethanol, brain, gene–environment interactions

Introduction

Fetal alcohol spectrum disorder (FASD) encompasses the full range of birth defects caused by prenatal alcohol exposure. FASD is thought to be the most widespread of environmentally-induced birth defects in humans, affecting between 2 and 5% of all live births in the U.S (May et al., 2014a). While alcohol exposure is necessary to induce this spectrum of deleterious effects, the outcomes of these exposures are highly variable. FASD can range in severity from neurodevelopmental deficits and behavioral abnormalities as seen in Alcohol Related

Neurodevelopmental Disorder, to craniofacial defects such as microphthalmia, microcephaly, smoothened philtrum, and hypoplastic mandible typical of Fetal Alcohol Syndrome (Stratton et al., 1996).

While exposure to alcohol is necessary to give rise to these developmental defects, genetics modulate the sensitivity to ethanol. Of pregnancies with known heavy alcohol exposure, only 4.3% of children develop Fetal Alcohol Syndrome (Abel, 1995). Twin studies have provided further evidence for the role of genetics in modulating the outcomes of alcohol exposures. Studies of monozygotic and dizygotic twins have shown that monozygotic twins were 100% concordant in their FAS diagnosis, while dizygotic twins were only 56–64% concordant despite experiencing the same prenatal environment (Streissguth and Dehaene, 1993; Astley Hemingway et al., 2018). We continue to make strides toward understanding the genetic influence on ethanol teratogenesis, but our comprehension remains extremely limited.

Strain differences within animal model systems provided some of the early evidence for the importance of genetics in ethanol-induced birth defects. C57BL/6J mice are sensitized to ethanol-induced teratogenesis compared to their C57BL/6N counterparts. Among other substrain differences, C57BL/6J mice have a 5-exon deletion in *Nicotinamide nucleotide transhydrogenase* (*Nnt*) (Freeman et al., 2006). Nnt is a transhydrogenase in the inner mitochondrial membrane that is important in ATP synthesis and the reduction of NADP+ to NADPH (Hoek and Rydström, 1988). C57BL/6J experience with the *Nnt* mutation have a nondetectable level of the protein and impaired glucose clearance and H_2O_2 metabolism (Huang et al., 2006; Ronchi et al., 2013).

Nnt can sequester reactive oxygen species (ROS) via NADPH-mediated reduction of the oxidized form of glutathione (Rush et al., 1985). Failure to sequester ROS can lead to oxidative stress. Oxidative stress can induce apoptosis in cells through the increased production of free radicals, peroxidation of membranes, and mitochondrial dysfunction (Zamzami et al., 1995). The metabolism of ethanol by alcohol dehydrogenase (ADH) creates acetaldehyde, which itself can lead to overproduction of ROS (Chu et al., 2007; Yan and Zhao, 2020) Reduction of NNT activity leads to lower NADPH concentration and lower oxidized glutathione/reduced glutathione conversion (Sheeran et al., 2010). When *NNT* is knocked down in cell culture, proliferation is decreased and the NADH/NAD+ ratio is increased relative to the control, likely because this oxidation step is coupled with the reduction of NADP+ to NADPH (Ho et al., 2017). Thus, loss of *Nnt* may sensitize embryos to ethanol teratogenesis.

While *NNT* dysfunction has been implicated in human diseases such as glucocorticoid deficiency 1, there has yet to be a direct exploration of its interaction with ethanol during development (Meimaridou et al., 2012). Zebrafish provide an excellent system to study ethanol teratogenesis due to external fertilization, ease of determining developmental age, large clutch sizes, rapid development, availability of transgenic approaches, and a high level of conservation to the human genome. Thus, the zebrafish serves as an exceptional model to explore the effects and mechanisms of ethanol-induced birth defects.

Here, we demonstrate that loss of *nnt* sensitizes embryos to ethanol-induced teratogenesis. Ethanol induces a range of craniofacial phenotypes ranging in severity across ethanol concentration, dosing windows, and genotype, with ethanol-exposed *nnt* mutants having the most severe defects in the facial skeleton. Mutants appear most sensitive to ethanol from 6 to 24 h post-fertilization (hpf). Apoptosis was significantly elevated in the neural crest of control and ethanol-treated *nnt* mutants compared to their wildtype siblings, although proliferation was not significantly changed across genotype or treatment. Apoptosis was also significantly increased in the brains of ethanol-exposed *nnt* mutants. Levels of ROS predictably increased across treatment and genotype, with ethanol-exposed mutants having the highest levels. Apoptosis and craniofacial abnormalities were largely rescued by concurrent antioxidant administration using N-acetyl cysteine (NAC). Our findings demonstrate that *nnt* modifies susceptibility to embryonic ethanol exposure, providing more evidence for the role of oxidative stress in ethanol teratogenesis.

Materials and methods

Zebrafish husbandry

All animal research was performed in accordance with a protocol approved by the University of Texas at Austin Institutional Animal Care and Use Committee. Embryos were incubated at 28°C in embryo media (Westerfield, 1993). Zebrafish were staged according to the zebrafish developmental staging series (Kimmel et al., 1995). All zebrafish stocks used were derived from the AB wild-type genetic background.

CRISPR-Cas9

We utilized ZiFiT Targeter[1] to identify gRNA binding sites for *nnt*. We made *nnt* gRNA via MEGAscript T7 Kit (Invitrogen) using a described protocol (Jao et al., 2013). The oligo used to generate the gRNA is aattaatacgactcactataGGCCTCATGAACTCCTAGAGgttttta gagctagaaatagc (capitalized nucleotides code for the gRNA). We injected embryos with a 2 nl bolus of a cocktail containing: 500 ng/µl *Cas9* protein (IDT) and 250 ng/µl *nnt* gRNA in water with 0.2% phenol red.

One F1 individual, with a 74 base pair deletion in *nnt* (designated nnt^{au111} and we refer to the allele as nnt^{-} for clarity), was backcrossed to AB to produce a stable line. To assess whether *nnt* expression was absent in the mutant embryos, fluorescent *in situ* hybridization was performed using a Molecular Instruments probe on 24 hpf zebrafish embryos according to manufacturer's protocol (Choi et al., 2018).

Chemical treatments

Embryos were treated with ethanol at various timepoints from 6 to 24 hpf, 24–48 hpf, 48–72 hpf, and 6 hpf-5 days post-fertilization (dpf), as well as with different ethanol concentrations in embryo medium (0.5, 0.75, 1, 1.25, and 1.5% ethanol). Embryos were also treated with 1 mM NAC (Sigma-Aldrich) and 1% ethanol concurrently from 6 to 24 hpf. Previous studies have shown that tissue levels are 1/4–1/3 of the dose of ethanol, meaning a dose of 1% ethanol is approximately equivalent to a

1 http://zifit.partners.org/ZiFiT/

blood alcohol concentration of 0.18 to 0.21 (Lovely et al., 2014). NAC has been used in animal models and the 1 mM dosage is based on previous literature (Ni et al., 2020).

Skeletal analyses

Zebrafish were stained at 5 dpf with Alcian Blue and Alizarian Red (Walker and Kimmel, 2007). Whole and flat-mount craniofacial images were then taken on the Zeiss AxioImager.A1 compound microscope with a Zeiss AxioCam HRc camera. Whole body images were taken on an Olympus SZX7 microscope with an Olympus DP22 camera.

TUNEL staining

Cell death was assessed using the Biotium *CF*® 640R TUNEL Assay Apoptosis Detection Kit. Following chemical treatment, embryos were fixed at 36 hpf in 4% paraformaldehyde (PFA) overnight at 4°C with gentle agitation. Embryos were dehydrated and rehydrated with serial dilutions of methanol (MeOH) and Phosphate Buffered Saline with 0.5% Triton-X (PBTx) at room temperature. Embryos were permeabilized with a 25 µg/ml solution of proteinase K for 5 min and fixed with 4% PFA for 20 min. After washing with PBTx, embryos were incubated with the TUNEL solution (5 µl of enzyme in 45 µl buffer) for 3 h at 37°C with gentle agitation. Embryos were washed with PBTx and postfixed with 4% PFA for 30 min. Embryos were washed with PBTx and stored in 1X Phosphate buffered saline (PBS) for imaging.

Phospho-histone H3 (pHH3) staining

Cell proliferation was assessed using the pHH3 (Ser10) (D2C8) XP® Rabbit mAb (Cell Signaling Technology). Embryos were fixed at 36 hpf in 4% PFA overnight at 4°C with gentle agitation. Embryos were dehydrated and rehydrated with serial dilutions of MeOH and PBTx at room temperature. Embryos were washed 4 times for 30 min each in IB buffer (1% BSA, 0.5% TritonX100, and 1% DMSO in 1X PBS). Embryos were incubated with IB containing 5% Normal goat serum (NGS) for 30 min. Embryos were then incubated with the primary antibody in IB + 5% NGS at a 1:250 dilution overnight at 4°C with gentle agitation. Embryos were washed with IB once for 30 min, then with IB +5% NGS for 30 min. Embryos were incubated with the Invitrogen Goat anti-Rabbit IgG (H + L) Secondary Antibody, Alexa Fluor™ 568 in IB + 5% NGS at a 1:500 dilution overnight at 4°C with gentle agitation. Embryos were washed 3 times with PBTx for 15 min each and postfixed in 4% PFA for 30 min. Embryos were washed 3 times with 1X PBS for 5 min each and stored in 1X PBS for imaging.

ROS assay

ROS concentration was assessed in embryos using the CellROX® ROS Assay kit (Thermo Scientific). 24 hpf embryos were incubated with a 2.5 µM enzyme solution for 30 min at 28°C, while 48 hpf embryos were incubated with a 5 µM enzyme solution for 15 min at 28°C. Embryos were washed with 1X PBS and imaged.

Image analysis

Fluorescent embryos were imaged on a Zeiss LSM 710 Confocal. ImageJ was used to quantify apoptotic and proliferating cells, ROS fluorescence, and craniofacial and body length measurements.

Statistical analysis

A two-tailed Fisher's exact test of independence was used to determine if the occurrence of craniofacial defects between genotypes was statistically significant. Two-way ANOVA with Tukey's multiple comparisons correction was used for analysis of the ROS assay, TUNEL data, craniofacial measurements, proliferation, and body length. All graphs and statistical analyses were run using Graphpad Prism 9.

Results

Zebrafish *nnt* mutants are sensitized to ethanol teratogenesis

To generate zebrafish *nnt* mutants, we injected CRISPR/Cas9 reagents into 1 cell-stage embryos and raised them to adulthood. The gRNA targeted exon 4, out of 22 (Figures 1A,B). One F0 fish gave rise to progeny harboring a 74 base pair deletion (Figure 1A) resulting in a frame shift and premature termination sequence.

Such an early stop codon would be anticipated to trigger nonsense-mediated decay of the mutant transcript. To determine if there was a loss of *nnt* mRNA, fluorescent *in situ* hybridization was performed on 24 hpf embryos. All wildtype and heterozygote embryos displayed bright and ubiquitous expression consistent with previous data (Thisse and Thisse, 2004). However, no transcript was detected in the *nnt* mutant, confirming that *nnt* expression is absent in the mutant embryos (Figures 1C,D).

To assess whether *nnt* mutation predisposes embryos to ethanol-induced defects, embryos were dosed with 1% ethanol from 6 hpf-5 dpf (Figures 2A,D). As we have shown previously, ethanol-exposed wild-type fish are not discernable from unexposed wild-types (Figures 2A,B, $n = 22$ and $n = 29$, respectively). Similarly, unexposed *nnt* mutants are indistinguishable from wild-types (Figure 2C, $n = 24$). Indeed, unexposed *nnt* mutants are viable and fertile. In contrast, 74% (17/23) of ethanol-exposed mutant zebrafish had profound craniofacial defects (Figure 2D). This is a significant increase compared to wildtypes ($p < 0.0001$) (Figure 2E). These defects include reduced jaw (Meckel's cartilage) and ceratohyal (Figure 2D). Ethanol-exposed mutants also have smaller eyes and heads as quantified in Supplementary 1 respectively. Ethanol-exposed mutants had significantly smaller eyes ($p < 0.0001$), consistent with data showing ethanol-exposed C57/B6J mice have smaller eyes compared to untreated embryos (Parnell et al., 2010). Ethanol-exposed fish survived to 5 dpf, indicating that there was not elevated embryonic mortality in the mutants. This demonstrates that *nnt* mutants are more susceptible to ethanol teratogenesis.

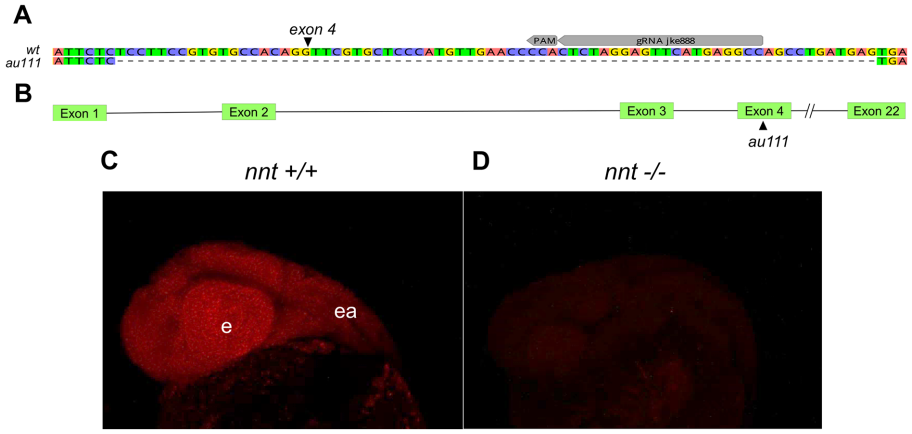


FIGURE 1
Generation of a zebrafish *nnt mutation*. **(A)** Schematic depicting the 74bp deletion in exon 4 of *nnt*. The gRNA binding site (gRNA jke888) and PAM sequence are noted. **(B)** Location of the mutation (designated *au111*) relative to the 22 exon long gene. **(C)** Confocal images of fluorescent *in situ* hybridization staining for *nnt*-specific probe in 24 hpf wildtype and **(D)** mutant embryos, demonstrating a lack of transcript in *nnt* mutants, suggesting extensive non-sense mediated decay of the mutant transcript. Anterior is left, dorsal is up, e: eye, ea: ear.

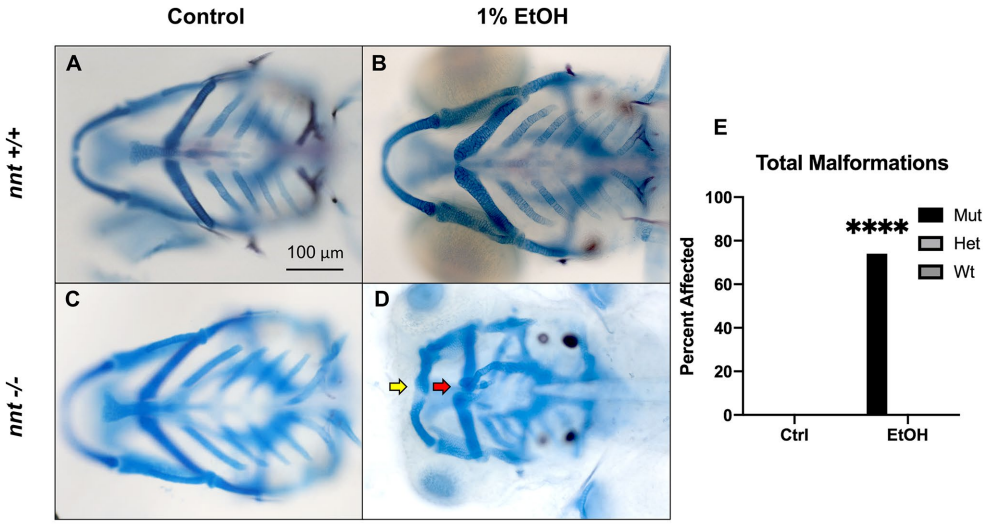


FIGURE 2
Loss of *nnt* sensitizes embryos to ethanol teratogenesis. **(A–D)** Alcian Blue/Alizarian Red-stained zebrafish at 5 dpf treated from 6 hpf- 5 dpf. All images are ventral views with anterior to the left. **(A,B)** Control and ethanol-treated wildtypes and **(C,D)** *nnt* mutants. Both the untreated and 1% ethanol dosed wt embryos appear phenotypically normal. **(C)** Untreated *nnt* mutant with a typical phenotype akin to wt. **(D)** Ethanol-exposed *nnt* mutant zebrafish with aberrant craniofacial phenotype consisting of a hypoplastic Meckel's cartilage (yellow arrow), deformed ceratohyal (red arrow), microphthalmia, and microcephaly. **(E)** Quantification of the percentage of fish with craniofacial defects in each group (Fischer's exact test, n ≥ 20 per group, ****p<.0001). Only ethanol-treated mutants displayed craniofacial defects, a statistically significant increase. EtOH: ethanol, Ctrl: control, mut: mutant, het: heterozygote, Wt: wildtype.

The effects of the of *nnt* mutation on ethanol teratogenicity is dependent on time and dosage

To identify the critical period of exposure, zebrafish embryos were dosed with 1% ethanol at different timepoints (Figures 3A–H). Of the mutants exposed from 6 to 24 hpf, 76% (16/21) had craniofacial abnormalities similar to those observed within the longer treatment window, a significant increase from the respective wildtype ($p < 0.0001$) (Figures 3F,I). In the larvae treated from 24 to 48 hpf, there was not a gross craniofacial phenotype, but 29% (9/31) had cardiac edema and smaller than average faces (Figure 3G). The incidence of these phenotypes was significantly higher in the mutants relative to exposed wildtype ($p = 0.0020$) (Figure 3I). Finally, in the 48–72 hpf treatment group, all 29 embryos appeared craniofacially typical and were otherwise indistinguishable from the wildtype (Figure 3H). Thus, the critical period of ethanol exposure for *nnt* mutants is between gastrulation and the onset of the pharyngula period.

To further characterize and quantify the sensitivity of *nnt* mutants to ethanol, embryos were dosed with a range of ethanol concentrations. Embryos from heterozygous crosses were treated with 0, 0.5, 0.75, 1,

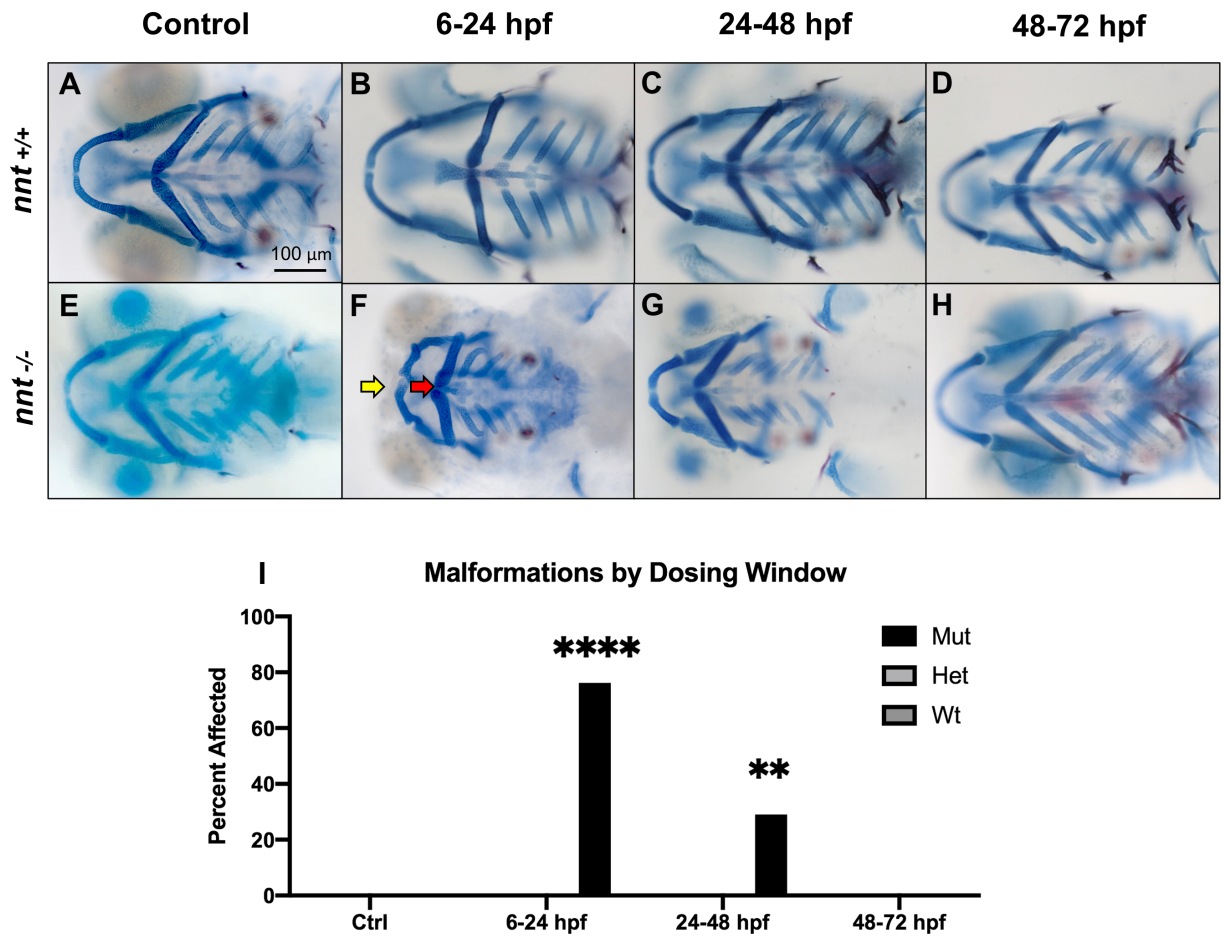


FIGURE 3
nnt mutants appear sensitized to ethanol teratogenesis from 6 to 24 hpf. Embryos were treated with 1% ethanol at different timepoints **(A–H)** to establish a critical period of ethanol teratogenesis. All images are ventral views with anterior to the left. Control (unexposed) wildtype and mutant **(A, E)** appear phenotypically normal. Wildtype embryos dosed across all timepoints **(B–D)** appear phenotypically normal. **(F)** Mutant embryos dosed at 6–24 hpf had stark craniofacial defects consisting of a hypoplastic Meckel's cartilage (yellow arrow), deformed ceratohyal (red arrow), microphthalmia, and microcephaly. **(G)** Mutant embryos dosed at 24–48 hpf had no apparent defects in craniofacial morphology, but did have microcephaly and reductions in the size of skeletal elements. **(H)** Mutant embryos dosed at 48–72 hpf had no apparent defects. **(I)** Quantification of the percentage of fish with craniofacial defects in each group. (Fischer's exact test, $n \geq 20$ per group, $^{**}p < 0.01$, $^{****}p < .0001$). The most highly statistical difference was observed at 6–24 hpf. Mut: mutant, Het: heterozygote, Wt: wildtype.

1.25%, or 1.5% ethanol solutions from 6 to 24 hpf (Figures 4A–L). In wildtype and heterozygous fish, there were no phenotypic defects observed at doses below 1.25% ethanol. At 1.25% ethanol, 8.70% (2/23) of wildtype and 13.6% (6/44) of heterozygous fish had craniofacial defects (Figures 4E,K,M). These percentages rose to 11.54% (3/26) and 25% (10/40), at 1.5% ethanol (Figures 4F,L,M). Thus, consistent with previous studies, 1% ethanol does not cause gross craniofacial defects in wildtypes, and it appears that *nnt* heterozygosity does not significantly sensitize embryos to this dose of ethanol (McCarthy et al., 2013; Swartz et al., 2014; Everson et al., 2020; Fish et al., 2021).

There was a range of phenotypes across most concentrations of ethanol in *nnt* mutants. While there were no craniofacial defects at 0.5% ethanol, at 0.75% ethanol, there was a significantly higher amount of craniofacial defects in the mutants compared to the 0.75% ethanol treated wildtypes ($p = 0.0219$) (Figures 4C,I,M). 21.74% (5/23) of treated *nnt* mutant larvae had craniofacial malformations. In all of these fish the malformation was the same: the ceratohyal cartilages fail to meet appropriately at the midline and do not angle anteriorly. This suggests that the ceratohyal is the most easily perturbed skeletal element in *nnt* mutants (Figure 4N).

At 1% ethanol, craniofacial malformations in *nnt* mutants increased substantially in penetrance and severity, with total malformations being significantly higher in the mutant compared to the wildtype ($p < 0.0001$) (Figures 4D,J,M). The ceratohyal defect, described above, was present in all fish with malformations 82.22% (37/45). Additionally, a subset of these fish, 46.67% (21/45), also had a reduced Meckel's cartilage (Figure 4N). The reduced Meckel's phenotype consisted of a Meckel's cartilage that was shorter and wider than the typical anteriorly elongated structure in wildtype.

In the mutants treated with 1.25% ethanol, 100% (21/21) treated embryos had craniofacial defects, a significant amount compared to

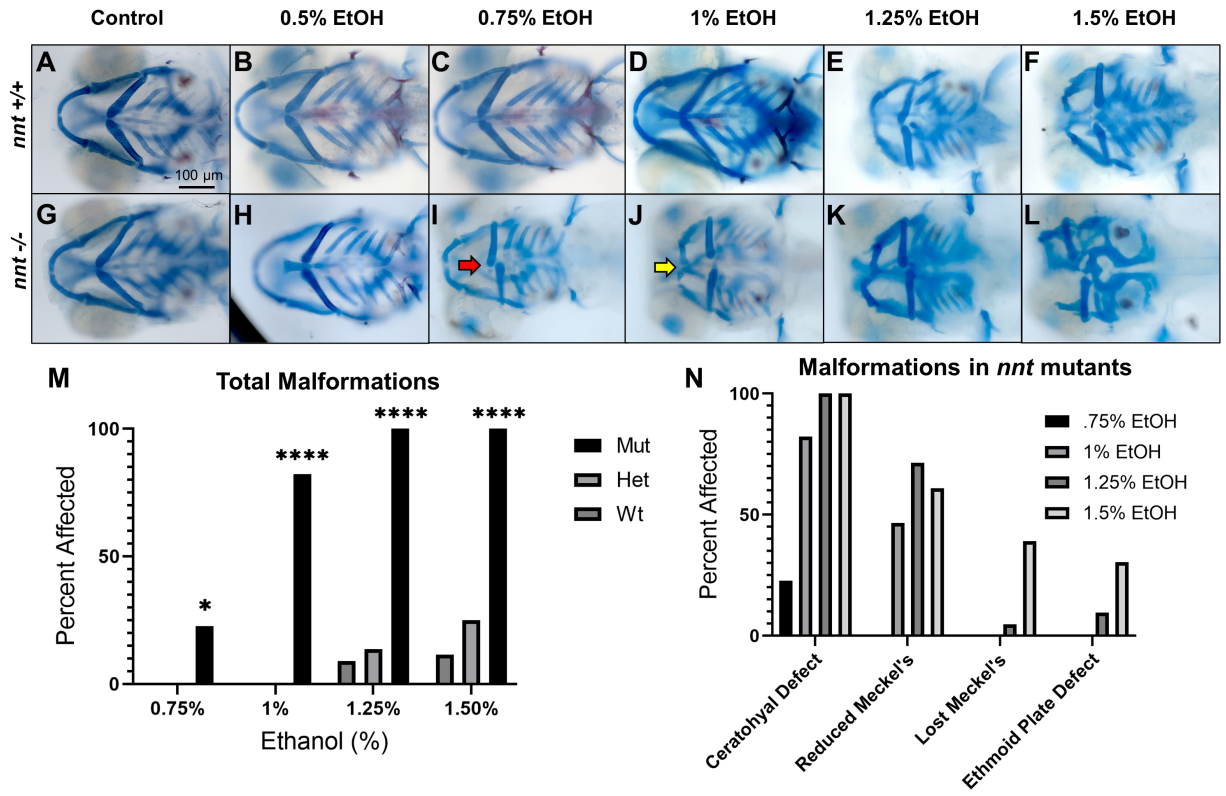


FIGURE 4
Severity of *nnt* malformations increases with ethanol concentration. **(A–L)** Untreated and ethanol-exposed Alcian Blue/ Alizarian Red-stained zebrafish embryos at 5 dpf treated from 6 hpf- 24 hpf. All images are ventral views with anterior to the left. **(A,B,G,H)** Wildtypes and mutants appear phenotypically normal at concentrations of 0 and 0.5% ethanol. **(C,I)** At 0.75% ethanol, wildtypes still appear normal, but 22.7% of mutants have ceratohyal cartilages that do not extend anteriorly (red arrow). **(D,J)** At 1% ethanol, the wildtypes remain normal, but 82.2% of nnt mutants had gross craniofacial defects, including a hypoplastic Meckel's cartilage (yellow arrow). **(E,F,K,L)**.. At 1.25 and 1.5% craniofacial defects become apparent in the wildtypes, and there is increased severity of the craniofacial defects in the mutants. **(M)** A bar chart depicting total craniofacial malformations across genotype and ethanol concentration (Fisher's exact test, $n \geq 20$ per group, *$p<0.05$, ****$p<0.0001$). **(N)** A bar chart depicting the types of craniofacial malformations seen in mutants at different ethanol concentrations. EtOH: ethanol, Mut: mutant, Het: heterozygote, Wt: wildtype.

their wildtype counterparts ($p < 0.0001$) (Figures 4E,K,M). Again, the ceratohyal defect was the most common 100% (21/21). 71.4% (15/21) also had a reduced Meckel's and 4.8% (1/21) having a loss of Meckel's on one side of the face. At this dose, phenotypes were expanded to the neurocranium with 9.5% (2/21) having ethmoid plate defects (Figure 4N). These ethmoid plate defects were characterized by a small, pointed ethmoid plate replacing the typically wide and triangular ethmoid plate seen in wildtypes. Of the 2 embryos with ethmoid plate defects, one had a loss of Meckel's and the other had a reduced Meckel's. At lower doses there were no discernable defects in the wildtype, however at 1.25% ethanol, defects were seen in the wildtypes as well, with 8.70% (2/23) embryos displaying ceratohyal and reduced Meckel's phenotype.

Finally, in the mutant group that was treated with 1.5% ethanol from 6 to 24 hpf, there was an even wider range of phenotypes, with the total malformations in mutants remaining significantly higher than the wildtype ($p < 0.0001$) (Figures 4F,L,M). 100% (23/23) of treated mutants had ceratohyal defects. All fish also had defects to Meckel's cartilage, with 60.9% (14/23) having reduced Meckel's and 39.1% (9/23) having lost Meckel's. The number of fish with the ethmoid plate defect also rose, to 30.4% (7/23) (Figure 4N). Wildtypes at this dose were also disrupted, as 11.54% (3/26) embryos had the ceratohyal and reduced Meckel's phenotype.

ROS elevation underlies ethanol-induced defects in *nnt* mutants

We hypothesize that *nnt* mutants are more susceptible to the deleterious effects of ethanol exposure due to an inability to tolerate increased oxidative stress. Therefore, we quantified the levels of ROS and apoptosis and we tested the effects of antioxidant (NAC) administration on *nnt* mutant phenotypes.

NAC is a powerful antioxidant and, together with glycine and glutamate, is one of the precursors of glutathione (White et al., 2003). Cysteine is the rate-limiting substrate of glutathione production, revealing an important role for NAC in replenishing these stores (Sen, 2001). Indeed, NAC administration directly increases production of glutathione (Atkuri et al., 2007). We believe *nnt* mutants are unable to effectively reduce NADP+ to NADPH, leading to fewer stores of reduced glutathione. Thus, NAC was chosen as a means of compensating for this potential decrease in reduction capacity.

To assess ROS concentration in *nnt* mutants compared to wildtypes, the CellROX ROS Assay Kit was used to stain 24 hpf and 48 hpf embryos (Figure 5). Embryos were untreated, dosed with 1% ethanol, dosed with 1 mM NAC, or treated with 1 mM NAC + 1% ethanol from 6 to 24 hpf. There was a significant increase in the basal concentration of ROS at 24 hpf in both unexposed and ethanol treated

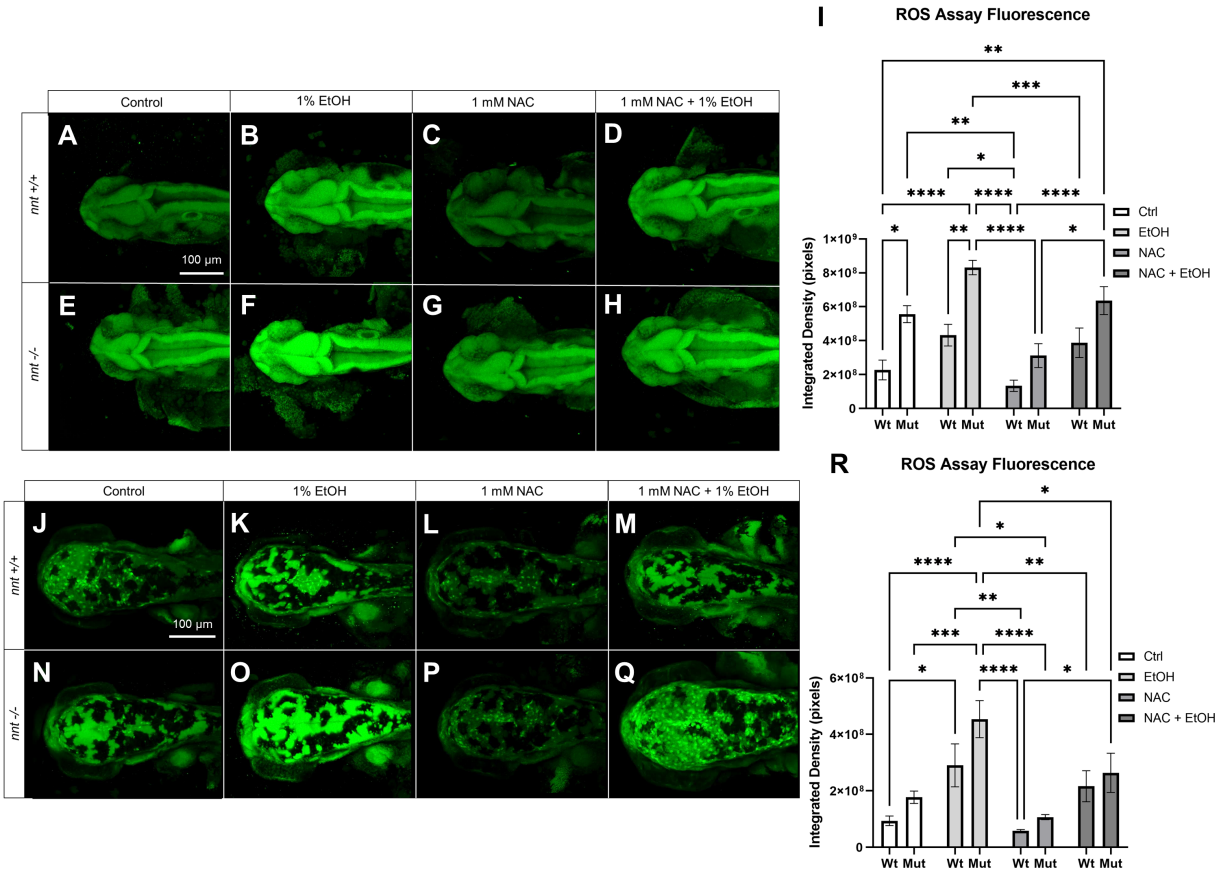


FIGURE 5
ROS concentration is elevated in *nnt* mutants exposed to ethanol. **(A–H)** CellROX Assay-stained 24 hpf fish that were unexposed, exposed to 1% EtOH from 6–24 hpf, exposed to NAC from 6–24 hpf, or exposed to 1% EtOH +1mM NAC from 6–24 hpf. All images are dorsal views of the head with anterior to the left. **(A)** Unexposed wildtype embryos have lower basal levels of ROS than **(E)** unexposed mutants ($p=0.0175$). **(B)** 1% EtOH exposed wildtypes have lower ROS levels than **(F)** EtOH-exposed mutants ($p=0.0022$). **(C)** 1mM NAC treated wildtypes were not significantly different from **(G)** NAC treated mutants. **(D)** Wildtypes treated with 1mM NAC and 1% EtOH were not significantly different from the **(H)** NAC and EtOH-treated mutant, but these mutants had significantly elevated ROS compared to the wildtype control ($p=0.0016$). **(I)** Graph depicting ROS concentration across all groups in 24 hpf zebrafish (Two-way ANOVA with multiple comparisons, black bars depict mean±SEM, $n=5$ per group, *$p<0.05$, **$p<0.01$, ***$p<0.001$, ****$p<0.0001$). **(J–Q)** CellROX Assay-stained 48 hpf fish. Dorsal views, anterior to the left. **(J)** Unexposed wildtypes were not significantly different in ROS concentration than **(N)** unexposed mutants. **(K)** 1% EtOH-exposed wildtypes were not significantly different from **(O)** EtOH-exposed mutants. **(L)** Wildtypes treated with 1mM NAC were not significantly different from **(P)** NAC-treated mutants. **(M)** Wildtypes treated with 1mM NAC and 1% EtOH were not significantly different from the **(Q)** NAC and EtOH-treated mutant, though these mutants had significantly lower ROS concentration compared to the EtOH-treated mutants ($p=0.0337$). **(R)** Graph depicting ROS concentration across all groups in 48 hpf zebrafish (Two-way ANOVA with multiple comparisons, black bars depict mean±SEM, $n=5$ per group, *$p<0.05$, **$p<0.01$, ***$p<0.001$, ****$p<0.0001$). Ctrl: control, EtOH: ethanol, NAC: N-acetyl Cysteine, Mut: mutant, Wt: wildtype.

mutants compared to the respective wildtypes ($p=0.0175$, $p=0.0022$, respectively) (Figures 5A,B,E,F,I). While there was a decrease in ROS level in the *nnt* mutants treated with NAC + EtOH compared to those treated solely with ethanol, this change did not reach $p<0.05$ ($p=0.3915$) (Figures 5F,H,I). We note though that this level of ROS was similar to that in ethanol-exposed wildtypes, which develop no profound defects. When treated with NAC alone however, the mutant has a significantly lower level of ROS than the NAC + EtOH treated mutant ($p=0.0201$) (Figures 5G–I). At 48 hpf, there were still significantly elevated levels of ROS in ethanol-exposed *nnt* mutants compared to untreated mutants and wildtypes ($p=0.0005$, $p<0.0001$) (Figures 5J,N,O,R). There was a significant difference between the ethanol-treated *nnt* mutant and the NAC + EtOH treated mutant ($p=0.0337$) (Figures 5O,Q,R). Mutants treated solely with NAC were not significantly different from the control mutants, but they had significantly lower levels of ROS compared to the ethanol-treated mutants ($p=0.9067$, $p<0.0001$, respectively) (Figures 5N–P,R). Collectively, these data show that ethanol exposure further exacerbates an elevation in ROS levels in *nnt* mutants and that NAC can partially restore the level of ROS.

Elevated ROS can lead to apoptosis. We performed TUNEL in a *nnt;fli1a:eGFP* transgenic line to quantify cell death (Figure 6). TUNEL was performed on 36 hpf embryos that were untreated or dosed with 1% ethanol from 6 to 24 hpf. We counted apoptotic neural crest cells (GFP positive) and cells within the brain (evident in the PMT channel). Interestingly, unexposed *nnt* mutants had significantly increased basal level of cell death in the pharyngeal arches relative to the unexposed *nnt* wildtypes ($p=0.0230$) (Figures 6A,D,K). When treated with ethanol, *nnt* mutants experience significantly elevated levels of apoptosis in the arches relative to the wildtype ethanol group ($p<0.0001$) (Figures 6B,E,K). The most significant elevation in apoptosis in the arches occurs

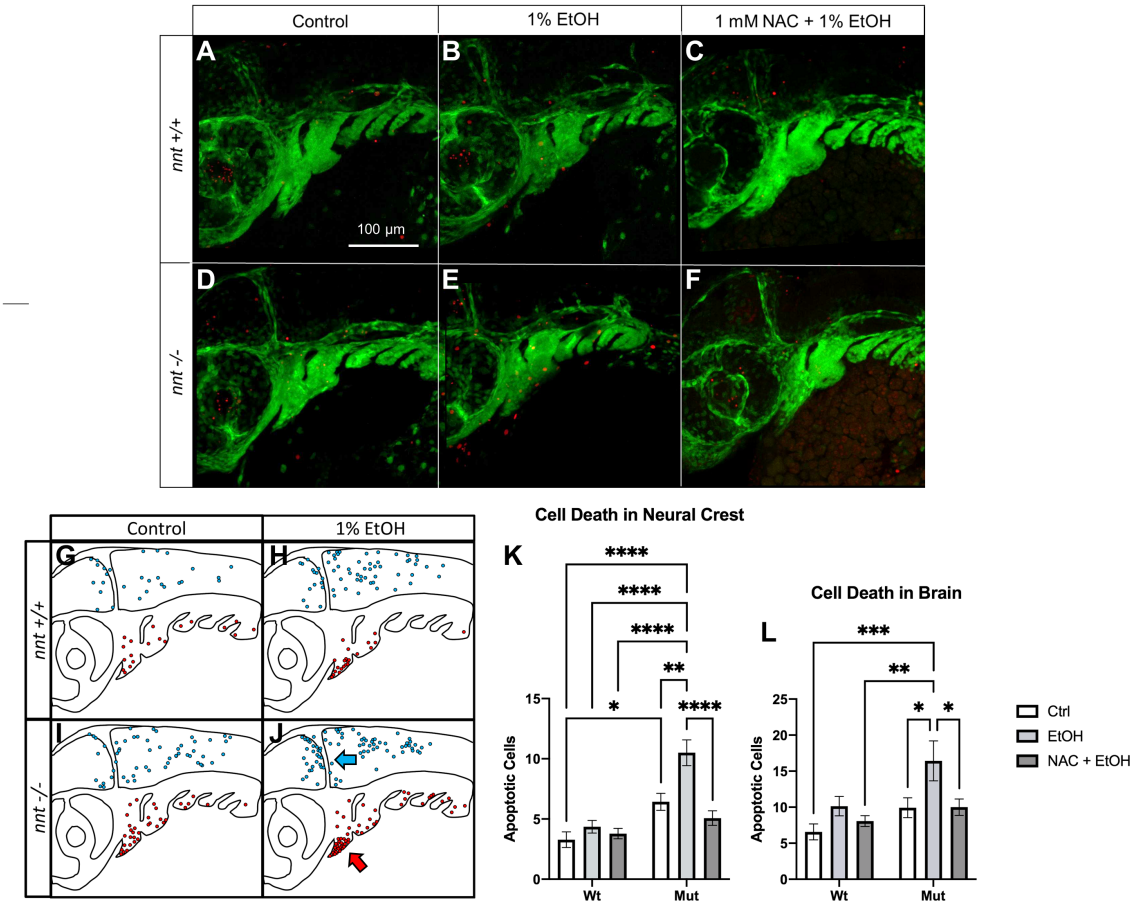


FIGURE 6
Aberrant ethanol-induced apoptosis in *nnt* mutants is rescued by antioxidant treatment. **(A–F)** 36 hpf *nnt;fli1a:eGFP* (green) embryos stained with TUNEL (red) (n=14 per group). Lateral views, anterior to the left, dorsal up. **(A)** Unexposed wildtypes had significantly lower apoptosis in the pharyngeal arches compared to **(D)** unexposed mutants (p=0.0230). **(B)** 1% ethanol-dosed wildtypes had significantly less apoptosis in the arches and brain compared to **(E)** ethanol-treated mutants (p=<0.0001 and p=0.0003). **(C)** 1mM NAC+1% EtOH dosed wildtypes were not significantly different from **(F)** NAC+EtOH-treated mutants (p=0.7775), but NAC+EtOH mutants had significantly lower apoptosis in the arches and brain compared to ethanol-dosed mutants (p=<0001 and p=0.0491, respectively). **(G–J)** Schematic of the spatial distribution of apoptosis in the brains (blue arrow) and pharyngeal arches (red arrow) of untreated and ethanol-treated mutants and wildtypes (n=5 per group). **(G)** The wildtype control had fewer apoptotic cells that were more widely distributed across the brain and arches compared to the **(H,I)** unexposed mutants and ethanol-treated wildtypes that had higher levels of apoptosis in both regions. **(J)** Ethanol-treated mutants had more apoptosis than all other groups and had cell death localized to the ventral portion of the arches and clustered around the midbrain-hindbrain boundary. **(K)** Graph depicting apoptotic cells in the neural crest across all groups (Two-way ANOVA with multiple comparisons, black bars depict mean±SEM, n=14 per group, *p<0.05, **p<0.01, ****p<0.0001). **(L)** Graph depicting apoptotic cells in the brain across all groups (Two-way ANOVA with multiple comparisons, black bars depict mean±SEM, n=14 per group, *p<0.05, **p<0.01, ***p<0.001). Ctrl: control, EtOH: ethanol, NAC: N-acetyl Cysteine, Mut: mutant, Wt: wildtype.

largely in arches 1 and 2, consistent with cartilages derived from these arches being most sensitive to disruption (Supplementary Figure S2). Cell death also appears localized to the ventral portions of arches 1 and 2 where progenitor cells for Meckel's cartilage and the ceratohyal are localized (Figure 6J). In the brain, there is not a significant difference between the unexposed *nnt* mutant and wildtype (p = 0.6465) (Figures 5A,D,L). With the addition of ethanol, there is a significant increase in apoptosis in the brains of *nnt* mutants relative to unexposed *nnt* wildtypes (p = 0.0003) (Figures 6A,E,L). As in the neural crest, there appears to be a spatially restricted distribution of cell death, with an abundance of cell death that appears to be localized around the midbrain-hindbrain boundary (MHB) (Figure 6J).

We hypothesize that if elevated ROS is causing this increase in apoptosis, antioxidant administration may then be able to rescue this defect. To test this prediction, we performed TUNEL on 36 hpf embryos from the *nnt;fli1a;eGFP* transgenic line that were treated with 1 mM NAC + 1% ethanol from 6–24 hpf (Figures 6C,F,K,L). There was a significant decrease in the apoptosis of the arches in ethanol + NAC-treated *nnt* mutants compared to those treated with ethanol alone (p < 0.0001) (Figures 6E,F,K). In the brain, there is also a significant decrease of cell death in ethanol + NAC-treated *nnt* mutants compared to those treated with ethanol (p = 0.0491) (Figures 6E,F,L). We conclude that nnt function protects sensitive cell types, such as neural crest cells and neurons, from ROS-induced apoptosis.

An additional cellular mechanism for the observed craniofacial defects could be reduced neural crest cell proliferation. Thus, we also analyzed proliferation in these embryos using the proliferation marker pHH3 (Figure 7). Embryos were untreated or dosed with 1% ethanol

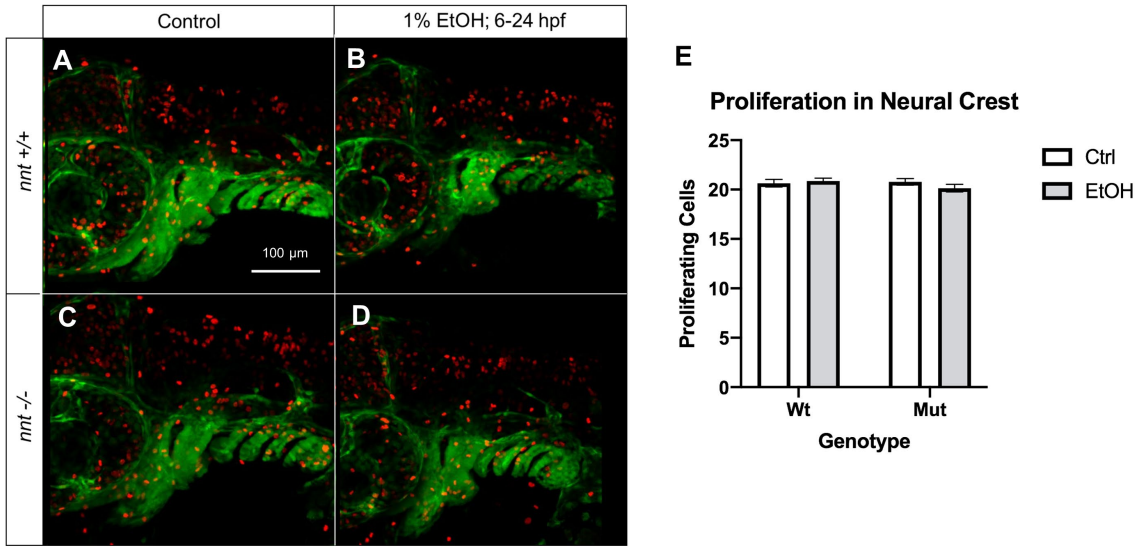


FIGURE 7
Proliferation is not significantly altered in neural crest of *nnt* mutants. **(A–D)** 36 hpf *nnt;fli1a:eGFP* (green) embryos stained with pHH3 (red). Lateral views, anterior to the left, dorsal up. **(A)** Unexposed wildtypes and **(C)** mutants have similar levels of proliferating cells compared to **(B)** ethanol-treated wildtypes and **(D)** mutants. **(E)** Graph depicting proliferating cells in the neural crest (Twoway ANOVA with multiple comparisons, black bars depict mean±SEM, *n*=14 per group). Ctrl: control, EtOH: ethanol, Mut: mutant, Wt: wildtype.

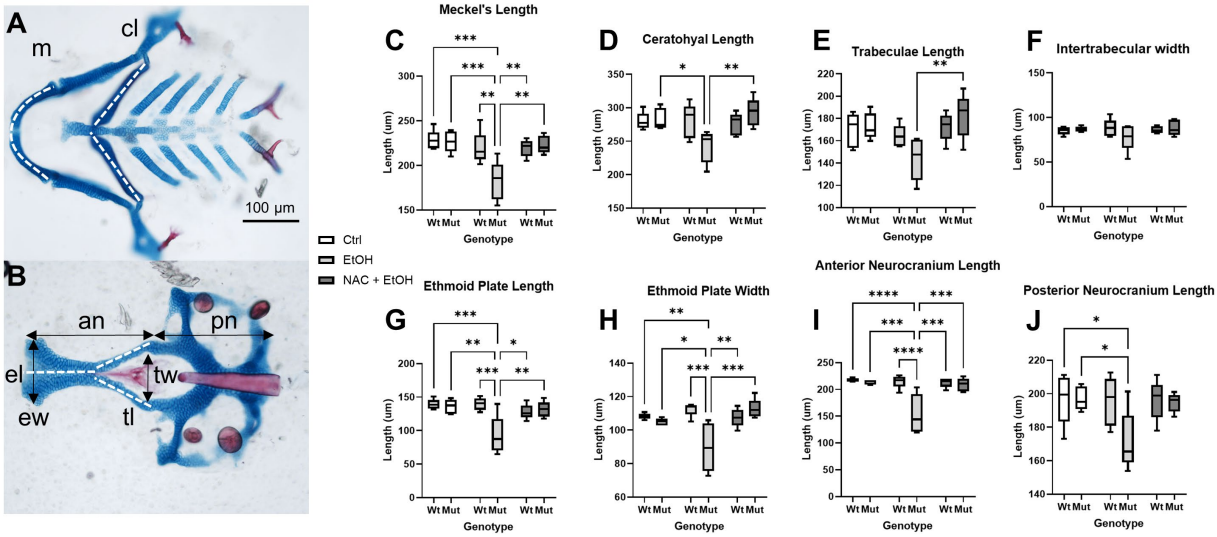


FIGURE 8
Ethanol-induced craniofacial abnormalities are rescued by concurrent NAC dosage. **(A,B)** Flatmounts of 5 dpf wildtype craniofacial skeleton displaying the linear measurements used with anterior to the left. **(A)** Viscerocranium and **(B)** neurocranium. The cartilaginous elements that were measured: m: Meckel's length, cl: ceratohyal length, tl: Trabeculae length, tw: Intertrabecular width, el: Ethmoid plate length, ew: Ethmoid plate width, an: Anterior neurocranium length, pn: Posterior neurocranium length. **(C–J)** Embryo were unexposed, exposed to 1% EtOH from 6–24 hpf, or exposed to 1% EtOH +1mM NAC from 6–24 hpf. Fish were then grown to 5 dpf for morphometric analyses. Graphs depict craniofacial measurements across each cartilaginous element in all groups (Two-way ANOVA with multiple comparisons, black bars depict range, *n*=5 per group, **p*<0.05, ***p*<0.01, ****p*<0.001, *****p*<0.0001). In nearly every instance in which ethanol caused a significant reduction in length or width in *nnt* mutants, the co-exposure with NAC restored the size back to that of wildtype **(C,D,G-I)**. The only exception being posterior neurocranium length, where the co-exposure is not significantly different from wildtype or ethanol-exposed *nnt* mutants. Ctrl: control, EtOH: ethanol, NAC: N-acetyl Cysteine, Mut: mutant, Wt: wildtype.

from 6–24 hpf and fixed for staining at 36 hpf. We found no differences across any of the treatment or genotype groups. Collectively, these results demonstrate that *nnt* mutants are sensitized to ethanol-induced cell death.

Our model further predicts that this ROS-induced apoptosis causes craniofacial defects in *nnt* mutants. Therefore, we quantified cartilaginous defects in the face to determine the extent to which antioxidant treatment ameliorates the craniofacial defects in ethanol-exposed *nnt* mutants. We took linear measurements of the neural crest-derived Meckel's cartilage, ceratohyal, trabeculae, ethmoid plate and anterior neurocranium (Figure 8). We also measured the mesoderm-derived posterior neurocranium and quantified

inter-trabeculae width as a midface measure. None of these measures varied between untreated wildtype, untreated mutant, ethanol-treated wildtype fish and ethanol + NAC-treated wildtype fish. No differences were found across groups for inter-trabeculae width. For all other measures except trabeculae length, ethanol-exposure significantly reduced the size of the cartilage element, although we note the strong trend in trabeculae length. The reduction in overall head size (noted in Figure 2) would be explained by the reduction of both neural crest-derived and mesodermally-derived portions of the skull. There was no significant difference in body length among any of the groups (Supplementary Figure S3). For all of these measures, NAC treatment restored the size of the skeletal element relative to control. For a complete list of comparisons, see Supplementary Table S1. These results demonstrate that antioxidant treatment protects *nnt* mutants from ethanol teratogenesis.

Discussion

Our findings have demonstrated that loss of Nnt function in and of itself leads to increased susceptibility to alcohol teratogenesis. In addition, exposed mutants display severe craniofacial defects at normally subteratogenic doses of alcohol. We have shown that *nnt* mutants have greatly elevated levels of ROS following ethanol exposure. This elevated ROS leads to elevated levels of apoptosis in sensitive cell types and causes the observed craniofacial defects. Our findings have broad implications not only for researchers using C57 mice, but for humans as well, due to high level of conservation of *nnt*. Factors that elevate ROS, environmentally or genetically, could interact and lead to defects. Any phenotype that could be modified by ROS could be affected in a C57/B6J background and should be considered in future research.

Role of Nnt in oxidative stress

The primary function of Nnt is in reducing NADP+ to NADPH. NADPH is an important cofactor in many metabolic pathways such as cellular respiration and ATP production. This reducing agent also plays a critical role in detoxifying ROS (Zamzami et al., 1995). NADPH reduces the oxidized form of glutathione (GSSG) into a reduced state (GSH) such that glutathione is now able to directly sequester and reduce ROS.

We hypothesize that in an embryo where the initial reduction of NADP+ to NADPH is compromised, inadequate stores of GSH will be present to reduce ROS. The administration of ethanol is known to increase ROS (Henderson et al., 1995, 1999; Chu et al., 2007; Brocardo et al., 2011; Yan and Zhao, 2020). Thus, in a *nnt* mutant background, this ROS would lead to elevated levels of oxidative stress and subsequent apoptosis. Based on our ROS assay, we do observe significantly higher basal levels of ROS in mutants at 24 hpf. With the addition of ethanol, mutants have significantly elevated ROS concentration. The elevation at 48 hpf, 24 h after the embryos were last exposed to ethanol was surprising, but demonstrates that the ROS induced by ethanol is having a lasting effect. The concurrent dosage of NAC + EtOH in mutants was found to significantly decrease ROS concentration at 48 hpf. Dosage of NAC alone did not significantly lower ROS concentration relative to the control, however there does appear to be a trend toward reduction. In the 24 hpf embryos however, the NAC treated mutants have significantly lower levels of ROS compared to the NAC + EtOH treated mutants ($p = 0.0201$). NAC appears to reduce the basal level of ROS, likely due to its ability to directly upregulate glutathione. To better define the mechanism of *nnt* in mitigating oxidative stress, direct measurements of the GSH/GSSG ratio and levels of NADP+/NADPH could be performed.

We utilized NAC to mitigate the deleterious effects of this increased oxidative stress. Studies on diet during pregnancy suggest antioxidants such as vitamin E, beta-carotene, selenium, choline and folic acid protect against ethanol-induced birth defects (Mitchell et al., 1999; Ojeda et al., 2009; May et al., 2014b). Though NAC use in pregnant mothers with alcohol-exposed fetuses has not been well-characterized, human data suggests that NAC during pregnancy has neuroprotective effects (Wiest et al., 2014). The existing literature and our experimentation provide evidence for the amelioration of ethanol-induced birth defects via antioxidant administration.

Cellular mechanism and craniofacial defects

Unexposed *nnt* mutants experienced higher levels of apoptosis in the pharyngeal arches relative to their wildtype counterparts. This is a surprising phenotype given that they do not appear to have an aberrant craniofacial phenotype in the absence of ethanol. We have previously shown that ethanol increases cell death in wildtype zebrafish (McCarthy et al., 2013). However, this level of apoptosis is not elevated to the point of causing craniofacial defects. We believe that there may be a threshold effect where there is a certain level of cell death that needs to occur for craniofacial development to be perturbed. The localization of the cell death at the most ventral portions of arches 1 and 2 is consistent with the craniofacial phenotype as these cells give rise to the most anterior craniofacial elements which are disrupted in exposed mutants (Eberhart et al., 2006). Apoptosis of the neural crest is thought to contribute to the craniofacial phenotype of FASD as shown by various animal studies (Cartwright and Smith, 1995; Dunty et al., 2001). The morphology of these fish is consistent with FASD-associated malformations, such as an underdeveloped jaw and microcephaly (Jones et al., 1973; Jackson and Hussain, 1990).

In addition to recapitulating the craniofacial phenotype associated with FASD, ethanol-exposed mutants also exhibited apoptosis in areas of the brain affected by prenatal ethanol exposure. When mutants were exposed to ethanol, clustering of apoptotic cells occurred, particularly around the MHB. The MHB gives rise to the cerebellum, a structure responsible for motor function. Children with FASD often experience cerebellar defects (West, 1993; Swayze et al., 1997; Norman et al., 2009). Prenatally exposed children often experience a decrease in volume of both the cerebellum and the vermis (Autti-Rämö et al., 2002). An interesting future experiment could be to track this cell death in the developed cerebellum to determine if specific subpopulations of cells are lost.

Role of Nicotinamide nucleotide transhydrogenase across vertebrate species

The NNT transhydrogenase is highly conserved across species, with zebrafish and human having 82.23% identity

(Cunningham et al., 2022). The high conservation of this gene is likely due to the critical function of NNT. Loss of function of this gene in humans is predicted to be strongly selected against as the loss-of-function observed/expected upper bound fraction (LOEUF) is quite low at 0.311 (Karczewski et al., 2020). Thus, the fact that loss of Nnt is tolerated in laboratory-raised mouse and zebrafish is somewhat surprising. The critical function of Nnt is only revealed when mutants are environmentally challenged. Thus, as we have found with *platelet-derived growth factor receptor alpha* (*pdgfra*) mutants, environmental exposures can reveal requirements for gene function not demonstrated in neutral laboratory conditions (McCarthy et al., 2013).

While associations between FASD and *NNT* in humans have not been characterized, *NNT* dysfunction in humans is associated with heart failure. In human cardiac tissue derived from donors with chronic severe heart failure, NNT activity was 18% lower than donors who did not experience heart failure (Sheeran et al., 2010). This change was accompanied by lower GSH/GSSG ratio, lower NADPH levels, and higher levels of oxidized glutathione. This may be due to the heart's inability to maintain proper metabolic function and antioxidant defense.

Mutations in *NNT* are also associated with glucocorticoid deficiency 1 (GCCD1) (Meimaridou et al., 2012; Weinberg-Shukron et al., 2015). GCCD1 is characterized by inability of the adrenal cortex to respond to adrenocorticotropin hormone and produce cortisol. SNPs in *NNT* were found in 15 kindreds with GCCD1 (Meimaridou et al., 2012). In a human adrenocortical cell line, loss of *NNT* resulted in increased superoxide concentration as well as lower GSH/GSSG ratios, suggesting that inability to properly regulate oxidative stress may contribute to adrenal dysfunction.

C57BL/6J mice also experience redox abnormalities, with 6J mice exhibiting increase superoxide production (Leskov et al., 2017). 6J mice also have increased mitochondrial membrane permeability, spontaneous NADPH oxidation, and lower GSH/GSSG ratios compared to a 6J strain with wildtype *Nnt* (Huang et al., 2006). Collectively, these studies demonstrate the importance of Nnt in modulating ROS and subsequent cellular functions.

Our research has demonstrated that loss of *nnt* sensitizes embryos to ethanol-induced defects. The importance of this gene across multiple species strongly suggests that NNT function may be involved in FASD. Our findings demonstrate that nnt is a critical modulator of ROS levels following ethanol exposure, to prevent apoptosis of sensitive cell types. Our findings provide insight into the genesis of FASD and will help to guide treatments to prevent FASD.

Data availability statement

The raw data supporting the conclusions of this article will be made available by the authors, without undue reservation.

Ethics statement

The animal study was reviewed and approved by the University of Texas at Austin Institutional Animal Care and Use Committee.

Author contributions

JKE and RM conceived and designed the study and wrote the manuscript. JKE generated the CRISPR mutants. RM carried out all subsequent experiments and analyses. All authors contributed to the article and approved the submitted version.

Funding

This work was funded by NIH/NIAAA R01AA023426, NIH/NIDCR R35DE029086, and NIH/NIAAA 5U01AA021651 to JKE, and NIH/NIAAA 2T32AA007471–36 to RM.

Acknowledgments

We would like to thank Mary Swartz (lab manager) and Angela Martinez, Cadianna Garcia, Kathryn Thompson, and Nika Sarraf (fish facility technicians) for their support of this research. We also thank Scott Parnell for his insight into this project. We thank the Waggoner Center for Alcohol and Addiction Research for their insight and assistance. Finally, we thank Mary Swartz, Joshua Everson, and Ritika Ghosal for their edits and support in writing the manuscript.

Conflict of interest

The authors declare that the research was conducted in the absence of any commercial or financial relationships that could be construed as a potential conflict of interest.

Publisher's note

All claims expressed in this article are solely those of the authors and do not necessarily represent those of their affiliated organizations, or those of the publisher, the editors and the reviewers. Any product that may be evaluated in this article, or claim that may be made by its manufacturer, is not guaranteed or endorsed by the publisher.

Supplementary material

The Supplementary material for this article can be found online at: https://www.frontiersin.org/articles/10.3389/fnins.2023.1154621/full#supplementary-material

References

Abel, E. L. (1995). An update on incidence of FAS: FAS is not an equal opportunity birth defect. *Neurotoxicol. Teratol.* 17, 437–443. doi: 10.1016/0892-0362(95)00005-C

Astley Hemingway, S. J., Bledsoe, J. M., Brooks, A., Davies, J. K., Jirikowic, T., Olson, E. M., et al. (2018). Twin study confirms virtually identical prenatal alcohol exposures can lead to markedly different fetal alcohol spectrum disorder outcomes-

fetal genetics influences fetal vulnerability. *Adv. Pediatr. Res.* 5:23. doi: 10.24105/apr.2019.5.23

Atkuri, K. R., Mantovani, J. J., Herzenberg, L. A., and Herzenberg, L. A. (2007). N-acetylcysteine--a safe antidote for cysteine/glutathione deficiency. *Curr. Opin. Pharmacol.* 7, 355–359. doi: 10.1016/j.coph.2007.04.005

Autti-Rämö, I., Autti, T., Korkman, M., Kettunen, S., Salonen, O., and Valanne, L. (2002). MRI findings in children with school problems who had been exposed prenatally to alcohol. *Dev. Med. Child Neurol.* 44, 98–106. doi: 10.1017/S0012162201001748

Brocardo, P. S., Gil-Mohapel, J., and Christie, B. R. (2011). The role of oxidative stress in fetal alcohol spectrum disorders. *Brain Res. Rev.* 67, 209–225. doi: 10.1016/j.brainresrev.2011.02.001

Cartwright, M. M., and Smith, S. M. (1995). Increased cell death and reduced neural crest cell numbers in ethanol exposed embryos: partial basis for the fetal alcohol syndrome phenotype. *Alcohol. Clin. Exp. Res.* 19, 378–386. doi: 10.1111/j.1530-0277.1995.tb01519.x

Choi, H. M., Schwarzkopf, M., Fornace, M. E., Acharya, A., Artavanis, G., Stegmaier, J., et al. (2018). Third-generation in situ hybridization chain reaction: multiplexed, quantitative, sensitive, versatile, robust. *Development* 145:dev165753. doi: 10.1242/dev.165753

Chu, J., Tong, M., and de la Monte, S. M. (2007). Chronic ethanol exposure causes mitochondrial dysfunction and oxidative stress in immature central nervous system neurons. *Acta Neuropathol.* 113, 659–673. doi: 10.1007/s00401-007-0199-4

Cunningham, F., Allen, J. E., Allen, J., Alvarez-Jarreta, J., Amode, M. R., Armean, I. M., et al. (2022). Ensembl 2022. *Nucleic Acids Res.* 50, D988–D995. doi: 10.1093/nar/gkab1049

Dunty, W. C. Jr., Chen, S. Y., Zucker, R. M., Dehart, D. B., and Sulik, K. K. (2001). Selective vulnerability of embryonic cell populations to ethanol-induced apoptosis: implications for alcohol-related birth defects and neurodevelopmental disorder. *Alcohol. Clin. Exp. Res.* 25, 1523–1535. doi: 10.1111/j.1530-0277.2001.tb02156.x

Eberhart, J. K., Swartz, M. E., Crump, J. G., and Kimmel, C. B. (2006). Early hedgehog signaling from neural to oral epithelium organizes anterior craniofacial development. *Development* 133, 1069–1077. doi: 10.1242/dev.02281

Everson, J. L., Batchu, R., and Eberhart, J. K. (2020). Multifactorial genetic and environmental hedgehog pathway disruption sensitizes embryos to alcohol-induced craniofacial defects. *Alcohol. Clin. Exp. Res.* 44, 1988–1996. doi: 10.1111/acer.14427

Fish, E. W., Tucker, S. K., Peterson, R. L., Eberhart, J. K., and Parnell, S. E. (2021). Loss of tumor protein 53 protects against alcohol-induced facial malformations in mice and zebrafish. *Alcohol. Clin. Exp. Res.* 45, 1965–1979. doi: 10.1111/acer.14688

Freeman, H. C., Hugill, A., Dear, N. T., Ashcroft, F. M., and Cox, R. D. (2006). Deletion of nicotinamide nucleotide transhydrogenase: a new quantitive trait locus accounting for glucose intolerance in C57BL/6J mice. *Diabetes* 55, 2153–2156. doi: 10.2337/db06-0358

Henderson, G. I., Chen, J., and Schenker, S. (1999). Ethanol, oxidative stress, reactive aldehydes, and the fetus. *Front. Biosci.* 4, 541–550. doi: 10.2741/A450

Henderson, G. I., Devi, B. G., Perez, A., and Schenker, S. (1995). In utero ethanol exposure elicits oxidative stress in the rat fetus. *Alcohol. Clin. Exp. Res.* 19, 714–720. doi: 10.1111/j.1530-0277.1995.tb01572.x

Ho, H. Y., Lin, Y. T., Lin, G., Wu, P. R., and Cheng, M. L. (2017). Nicotinamide nucleotide transhydrogenase (NNT) deficiency dysregulates mitochondrial retrograde signaling and impedes proliferation. *Redox Biol.* 12, 916–928. doi: 10.1016/j.redox.2017.04.035

Hoek, J. B., and Rydström, J. (1988). Physiological roles of nicotinamide nucleotide transhydrogenase. *Biochem. J.* 254, 1–10. doi: 10.1042/bj2540001

Huang, T. T., Naeemuddin, M., Elchuri, S., Yamaguchi, M., Kozy, H. M., Carlson, E. J., et al. (2006). Genetic modifiers of the phenotype of mice deficient in mitochondrial superoxide dismutase. *Hum. Mol. Genet.* 15, 1187–1194. doi: 10.1093/hmg/ddl034

Jackson, I. T., and Hussain, K. (1990). Craniofacial and oral manifestations of fetal alcohol syndrome. *Plast. Reconstr. Surg.* 85, 505–512. doi: 10.1097/00006534-199004000-00003

Jao, L. E., Wente, S. R., and Chen, W. (2013). Efficient multiplex biallelic zebrafish genome editing using a CRISPR nuclease system. *Proc. Natl. Acad. Sci.* 110, 13904–13909. doi: 10.1073/pnas.1308335110

Jones, K. L., Smith, D. W., Ulleland, C. N., and Streissguth, A. P. (1973). Pattern of malformations in offspring of chronic alcoholic mothers. *Lancet* 301, 1267–1271. doi: 10.1016/S0140-6736(73)91291-9

Karczewski, K. J., Francioli, L. C., Tiao, G., Cummings, B. B., Alföldi, J., Wang, Q., et al. (2020). The mutational constraint spectrum quantified from variation in 141,456 humans. *Nature* 581, 434–443. doi: 10.1038/s41586-020-2308-7

Kimmel, C. B., Ballard, W. W., Kimmel, S. R., Ullmann, B., and Schilling, T. F. (1995). Stages of embryonic development of the zebrafish. *Dev. Dyn.* 203, 253–310. doi: 10.1002/aja.1002030302

Leskov, I., Neville, A., Shen, X., Pardue, S., Kevil, C. G., Granger, D. N., et al. (2017). Nicotinamide nucleotide transhydrogenase activity impacts mitochondrial redox balance and the development of hypertension in mice. *J. Am. Soc. Hypertens.* 11, 110–121. doi: 10.1016/j.jash.2016.12.002

Lovely, C. B., Nobles, R. D., and Eberhart, J. K. (2014). Developmental age strengthens barriers to ethanol accumulation in zebrafish. *Alcohol* 48, 595–602. doi: 10.1016/j.alcohol.2014.06.003

May, P. A., Baete, A., Russo, J., Elliott, A. J., Blankenship, J., Kalberg, W. O., et al. (2014a). Prevalence and characteristics of fetal alcohol spectrum disorders. *Pediatrics* 134, 855–866. doi: 10.1542/peds.2013-3319

May, P. A., Hamrick, K. J., Corbin, K. D., Hasken, J. M., Marais, A. S., Brooke, L. E., et al. (2014b). Dietary intake, nutrition, and fetal alcohol spectrum disorders in the Western Cape Province of South Africa. *Reprod. Toxicol.* 46, 31–39. doi: 10.1016/j.reprotox.2014.02.002

McCarthy, N., Wetherill, L., Lovely, C. B., Swartz, M. E., Foroud, T. M., and Eberhart, J. K. (2013). Pdgfra protects against ethanol-induced craniofacial defects in a zebrafish model of FASD. *Development* 140, 3254–3265. doi: 10.1242/dev.094938

Meimaridou, E., Kowalczyk, J., Guasti, L., Hughes, C. R., Wagner, F., Frommolt, P., et al. (2012). Mutations in NNT encoding nicotinamide nucleotide transhydrogenase cause familial glucocorticoid deficiency. *Nat. Genet.* 44, 740–742. doi: 10.1038/ng.2299

Mitchell, J. J., Paiva, M., and Heaton, M. B. (1999). The antioxidants vitamin E and beta-carotene protect against ethanol-induced neurotoxicity in embryonic rat hippocampal cultures. *Alcohol* 17, 163–168. doi: 10.1016/s0741-8329(98)00051-2

Ni, J., Wang, H., Wei, X., Shen, K., Sha, Y., Dong, Y., et al. (2020). Isoniazid causes heart looping disorder in zebrafish embryos by the induction of oxidative stress. *BMC Pharmacol. Toxicol.* 21, 1–9. doi: 10.1186/s40360-020-0399-2

Norman, A. L., Crocker, N., Mattson, S. N., and Riley, E. P. (2009). Neuroimaging and fetal alcohol spectrum disorders. *Dev. Disabil. Res. Rev.* 15, 209–217. doi: 10.1002/ddrr.72

Ojeda, M. L., Nogales, F., Jotty, K., Barrero, M. J., Murillo, M. L., and Carreras, O. (2009). Dietary selenium plus folic acid as an antioxidant therapy for ethanol-exposed pups. *Birth Defects Res. B Dev. Reprod. Toxicol.* 86, 490–495. doi: 10.1002/bdrb.20211

Parnell, S. E., Sulik, K. K., Dehart, D. B., and Chen, S. Y. (2010). Reduction of ethanol-induced ocular abnormalities in mice through dietary administration of N-acetylcysteine. *Alcohol* 44, 699–705. doi: 10.1016/j.alcohol.2010.05.006

Ronchi, J. A., Figueira, T. R., Ravagnani, F. G., Oliveira, H. C., Vercesi, A. E., and Castilho, R. F. (2013). A spontaneous mutation in the nicotinamide nucleotide transhydrogenase gene of C57BL/6J mice results in mitochondrial redox abnormalities. *Free Radic. Biol. Med.* 63, 446–456. doi: 10.1016/j.freeradbiomed.2013.05.049

Rush, G. F., Gorski, J. R., Ripple, M. G., Sowinski, J., Bugelski, P., and Hewitt, W. R. (1985). Organic hydroperoxide-induced lipid peroxidation and cell death in isolated hepatocytes. *Toxicol. Appl. Pharmacol.* 78, 473–483. doi: 10.1016/0041-008x(85)90255-8

Sen, C. K. (2001). Antioxidant and redox regulation of cellular signaling: introduction. *Med. Sci. Sports Exerc.* 33, 368–370. doi: 10.1097/00005768-200103000-00005

Sheeran, F. L., Rydström, J., Shakhparonov, M. I., Pestov, N. B., and Pepe, S. (2010). Diminished NADPH transhydrogenase activity and mitochondrial redox regulation in human failing myocardium. *Biochim. Biophys. Acta* 1797, 1138–1148. doi: 10.1016/j.bbabio.2010.04.002

Stratton, K, Howe, C, and Battaglia, F. *Fetal alcohol syndrome diagnosis, epidemiology, prevention and treatment*. Washington, DC: Institute of Medicine, National Academy Press; (1996).

Streissguth, A. P., and Dehaene, P. (1993). Fetal alcohol syndrome in twins of alcoholic mothers: concordance of diagnosis and IQ. *Am. J. Med. Genet.* 47, 857–861. doi: 10.1002/ajmg.1320470612

Swartz, M. E., Wells, M. B., Griffin, M., McCarthy, N., Lovely, C. B., McGurk, P., et al. (2014). A screen of zebrafish mutants identifies ethanol-sensitive genetic loci. *Alcohol. Clin. Exp. Res.* 38, 694–703. doi: 10.1111/acer.12286

Swayze, V. W. 2nd, Johnson, V. P., Hanson, J. W., Piven, J., Sato, Y., Giedd, J. N., et al. (1997). Magnetic resonance imaging of brain anomalies in fetal alcohol syndrome. *Pediatrics* 99, 232–240. doi: 10.1542/peds.99.2.232

Thisse, B., and Thisse, C. (2004). Fast release clones: a high throughput expression analysis. ZFIN Direct Data Submission. Available at: http://zfin.org.

Walker, M. B., and Kimmel, C. B. (2007). A two-color acid-free cartilage and bone stain for zebrafish larvae. *Biotech. Histochem.* 82, 23–28. doi: 10.1080/10520290701333558

Weinberg-Shukron, A., Abu-Libdeh, A., Zhadeh, F., Carmel, L., Kogot-Levin, A., Kamal, L., et al. (2015). Combined mineralocorticoid and glucocorticoid deficiency is caused by a novel founder nicotinamide nucleotide transhydrogenase mutation that alters mitochondrial morphology and increases oxidative stress. *J. Med. Genet.* 52, 636–641. doi: 10.1136/jmedgenet-2015-103078

West, J. R. (1993). Acute and long-term changes in the cerebellum following developmental exposure to ethanol. *Alcohol Alcohol. Suppl.* 2, 199–202.

Westerfield, M. (1993). *A guide to the laboratory use of the zebrafish (Brachydanio rerio). The Zebrafish Book*. Eugene: Univ. of Oregon Press.

White, C. C., Viernes, H., Krejsa, C. M., Botta, D., and Kavanagh, T. J. (2003). Fluorescence-based microtiter plate assay for glutamate–cysteine ligase activity. *Anal. Biochem.* 318, 175–180. doi: 10.1016/S0003-2697(03)00143-X

Wiest, D. B., Chang, E., Fanning, D., Garner, S., Cox, T., and Jenkins, D. D. (2014). Antenatal pharmacokinetics and placental transfer of N-acetylcysteine in chorioamnionitis for fetal neuroprotection. *J. Pediatr.* 165, 672–677.e2. doi: 10.1016/j.jpeds.2014.06.044

Yan, T., and Zhao, Y. (2020). Acetaldehyde induces phosphorylation of dynamin-related protein 1 and mitochondrial dysfunction via elevating intracellular ROS and Ca2+ levels. *Redox Biol.* 28:101381. doi: 10.1016/j.redox.2019.101381

Zamzami, N., Marchetti, P., Castedo, M., Decaudin, D., Macho, A., Hirsch, T., et al. (1995). Sequential reduction of mitochondrial transmembrane potential and generation of reactive oxygen species in early programmed cell death. *J. Exp. Med.* 182, 367–377. doi: 10.1084/jem.182.2.367

frontiers | Frontiers in Neuroscience

TYPE Original Research
PUBLISHED 13 June 2023
DOI 10.3389/fnins.2023.1192786

Check for updates

OPEN ACCESS

EDITED BY
Carlos Fernando Valenzuela,
University of New Mexico, United States

REVIEWED BY
Ricardo Marcos Pautassi,
Medical Research Institute Mercedes and Martín Ferreyra (INIMEC), Argentina
Jonathan L. Brigman,
University of New Mexico School of Medicine, United States
Marvin Rafael Diaz,
Binghamton University, United States

*CORRESPONDENCE
Jennifer D. Thomas
✉ thomas3@sdsu.edu

RECEIVED 23 March 2023
ACCEPTED 15 May 2023
PUBLISHED 13 June 2023

CITATION
Lei A, Breit KR and Thomas JD (2023) Prenatal alcohol and tetrahydrocannabinol exposure: Effects on spatial and working memory. *Front. Neurosci.* 17:1192786. doi: 10.3389/fnins.2023.1192786

COPYRIGHT
© 2023 Lei, Breit and Thomas. This is an open-access article distributed under the terms of the Creative Commons Attribution License (CC BY). The use, distribution or reproduction in other forums is permitted, provided the original author(s) and the copyright owner(s) are credited and that the original publication in this journal is cited, in accordance with accepted academic practice. No use, distribution or reproduction is permitted which does not comply with these terms.

Prenatal alcohol and tetrahydrocannabinol exposure: Effects on spatial and working memory

Annie Lei[1], Kristen R. Breit[1,2] and Jennifer D. Thomas[1]*

[1]Department of Psychology, Center for Behavioral Teratology, San Diego State University, San Diego, CA, United States, [2]Department of Psychology, West Chester University of Pennsylvania, West Chester, PA, United States

Introduction: Alcohol and cannabis are widely used recreational drugs that can negatively impact fetal development, leading to cognitive impairments. However, these drugs may be used simultaneously and the effects of combined exposure during the prenatal period are not well understood. Thus, this study used an animal model to investigate the effects of prenatal exposure to ethanol (EtOH), Δ-9-tetrahydrocannabinol (THC), or the combination on spatial and working memory.

Methods: Pregnant Sprague–Dawley rats were exposed to vaporized ethanol (EtOH; 68ml/h), THC (100mg/ml), the combination, or vehicle control during gestational days 5–20. Adolescent male and female offspring were evaluated using the Morris water maze task to assess spatial and working memory.

Results: Prenatal THC exposure impaired spatial learning and memory in female offspring, whereas prenatal EtOH exposure impaired working memory. The combination of THC and EtOH did not exacerbate the effects of either EtOH or THC, although subjects exposed to the combination were less thigmotaxic, which might represent an increase in risk-taking behavior.

Discussion: Our results highlight the differential effects of prenatal exposure to THC and EtOH on cognitive and emotional development, with substance- and sex-specific patterns. These findings highlight the potential harm of THC and EtOH on fetal development and support public health policies aimed at reducing cannabis and alcohol use during pregnancy.

KEYWORDS

cannabis, alcohol, combined exposure, spatial memory, working memory, pregnancy, vaping, rodents

1. Introduction

Prenatal alcohol exposure presents a substantial risk to the developing fetus, leading to a variety of adverse outcomes in physical, cognitive, and behavioral development collectively known as fetal alcohol spectrum disorders (FASD). Prevalence of FASD is alarmingly high, estimated at 2–5% in the US and several Western European countries (May et al., 2009, 2018). Despite the known risks, it is estimated that 11–14% of expectant individuals are currently drinking, with 5% engaging in binge drinking (Gosdin, 2022; Substance Abuse and Mental Health Services Administration, 2022); thus, FASD represents a serious and persistent public health problem. However, prenatal alcohol exposure does not always occur alone. In fact,

cannabis is the most commonly used illicit substance during pregnancy (Alpár et al., 2016), with 8% of pregnant individuals reporting use within the past month (Substance Abuse and Mental Health Services Administration, 2022). Pregnant individuals who use cannabis typically perceive no risk, are early in their pregnancy, and frequently co-use with tobacco and/or alcohol (Odom et al., 2020). This frequent co-use with alcohol is of great concern.

Co-use of alcohol and cannabis may be reflected in two distinct patterns of substance use: SAM (simultaneous alcohol and marijuana use) and CAM (concurrent alcohol and marijuana use). SAM involves using both substances close in time so that their effects overlap, whereas CAM refers to using both substances, but not necessarily on the same occasions (Bravo et al., 2021; Gonçalves et al., 2022). Both patterns of use increase the vulnerability to negative consequences (Jackson et al., 2020; Bravo et al., 2021), but SAM, with almost twice the prevalence of CAM (Subbaraman and Kerr, 2015), is more deleterious and associated with more severe consequences than those related to CAM or alcohol-only use (Jackson et al., 2020; Bravo et al., 2021; Gonçalves et al., 2022; Salguero et al., 2022).

Simultaneous use of alcohol and cannabis is associated with increased frequency of use for both substances and an increase in the quantity of alcohol consumed (Subbaraman and Kerr, 2015; Crummy et al., 2020). Furthermore, individuals who engage in simultaneous use demonstrate increased negative consequences related to alcohol (i.e., physical altercations, legal issues, car accidents, risky sexual behavior, negative academic outcomes, hangovers) potentially due to their propensity for binge-drinking behavior (Salguero et al., 2022), while also reporting more subjective alcohol-related positive consequences (i.e., relaxation, sociability, feeling buzzed; Lee et al., 2022).

With the legalization of recreational cannabis, prevalence of simultaneous co-use has increased in adults (Gonçalves et al., 2022). Recent estimates indicate that 20% percent of females who are current non-heavy drinkers use both alcohol and cannabis, whereas almost 50% of female heavy drinkers consume both drugs (Substance Abuse and Mental Health Services Administration, 2022). The high levels of co-use of alcohol and cannabis is concerning, particularly given that approximately half of all pregnancies are unplanned (Finer and Zolna, 2016) which can result in unintended prenatal drug exposure. In fact, among pregnant individuals consuming cannabis, half also report consuming alcohol (Substance Abuse and Mental Health Services Administration, 2015). Notably, these data are based on self-reports and given the possibility that stigma and legal implications may influence responses, use rates of either alcohol or cannabis may be much higher (Sharma et al., 2016; Chiandetti et al., 2017; England, 2020).

Prenatal exposure to either alcohol or cannabis can influence a range of behavioral domains (Fontaine et al., 2016; Mattson et al., 2019; Little et al., 2021; De Genna et al., 2022). For example, cognitive dysfunction associated with prenatal alcohol exposure can contribute to life-long challenges in school and independent living (McLachlan et al., 2020), negatively affecting an individual's quality of life (Mattson et al., 2019). Specifically, clinical studies have shown that prenatal alcohol exposure disrupts learning and memory on a variety of tasks, including spatial memory (Dodge et al., 2019) and spatial working memory (Moore et al., 2021). Prenatal alcohol exposure can lead to difficulties in efficiently encoding information (Lewis et al., 2021), which is associated with slower information processing and/or utilization of inefficient and ineffective memory strategies (Lewis et al., 2021). Similarly, preclinical research confirms that prenatal alcohol exposure leads to spatial learning (Schambra et al., 2017; Aglawe et al., 2021) and working memory deficits (Schambra et al., 2017; Waddell et al., 2020; Gursky et al., 2021), consistent with the vulnerability of the developing hippocampus, a brain region important for learning and memory (Fontaine et al., 2016; Mattson et al., 2019; Dodge et al., 2020), and the prefrontal cortex, a brain region important in executive functioning including working memory (Mattson et al., 2019; Waddell et al., 2020; Gursky et al., 2021).

The effects of prenatal cannabis exposure on memory and other cognitive functions are less understood. Although some clinical studies report only weak associations or a lack of clinically relevant impairments (Sharapova et al., 2018; Navarrete et al., 2020; Torres et al., 2020; Murnan et al., 2021; Betts et al., 2022; De Genna et al., 2022), others report that prenatal cannabis exposure is related to memory deficits (Sharapova et al., 2018; Grant et al., 2020; Navarrete et al., 2020; De Genna et al., 2022). Notably, one fMRI study found heightened neural activity among subjects prenatally exposed to cannabis when performing a working memory task, despite no group differences in task performance (Smith et al., 2016). This suggests a possible compensatory response for equivalent task completion compared to non-exposed individuals, although others have failed to replicate this finding (Cioffredi et al., 2022). Importantly, the adverse effects of cannabis use during pregnancy are most often seen with comorbid substance use (Basavarajappa, 2015; Forray, 2016), and so effects on memory may be more severe with combined exposure to alcohol.

Similar to clinical studies, preclinical studies also vary, with some studies finding no effects of prenatal cannabis (Breit et al., 2019b), whereas others finding persistent deficits in learning and memory which may be due to alterations in the prefrontal cortex and hippocampus (Beggiato et al., 2017, 2020; de Salas-Quiroga et al., 2020; Grant et al., 2020; De Genna et al., 2022). Variation in findings may be due to the type of cannabinoid used. For example, prenatal CBD exposure may actually improve spatial working memory (Wanner et al., 2021). Thus, the effects of prenatal cannabis on learning and memory are still unclear.

Moreover, the effects of prenatal exposure to the combination of alcohol and cannabis is also not well understood, although given that ethanol can interact with the endogenous cannabinoid system (ECS) (Basavarajappa, 2015), the likelihood that the two drugs interact is high. Prenatal exposure to either substance separately can disrupt development of the hippocampus and prefrontal cortex by interfering with the endocannabinoid system (Basavarajappa, 2015; Smith et al., 2016; Beggiato et al., 2020; Manduca et al., 2020). THC exposure may weaken the developing nervous system, possibly acting as a "first hit" to the ECS, making the nervous system more vulnerable to other drug insults, as suggested by the "double hit hypothesis" (Richardson et al., 2016; Little et al., 2021). In fact, preclinical studies have found interactive effects of prenatal alcohol and cannabis on physical birth defects (specifically malformations of the eyes, face, and brain), even at low doses of both drugs (Fish et al., 2019). Our lab found that developmental exposure to the cannabinoid receptor agonist CP-55,940, which mimics the effects of THC, in combination with ethanol led to higher mortality rates, more severe growth deficits, and more severe behavioral deficits than exposure to either substance alone (Breit et al., 2019a,b). Additionally, the combination of prenatal THC and prenatal EtOH leads to more severe open field hyperactivity, specifically among males (Breit et al., 2022). In contrast, the Maternal Health Practices and Child Development (MHPCD) longitudinal study found that either prenatal exposure to ethanol or cannabis was an independent predictor of school performance, but found no

interaction between prenatal marijuana and prenatal alcohol exposure (Goldschmidt et al., 2004). However, the MHPCD project began before the rapid rise in THC levels, not representing the levels consumed today.

To model ethanol and cannabis simultaneous co-exposure, the present study used an animal model with THC exposure via electronic cigarettes (e-cigarettes) vapor. The use of e-cigarettes for cannabis consumption is becoming more prevalent, particularly as more states legalize cannabis (Borodovsky et al., 2016). In fact, pregnant women perceive e-cigarettes as safer alternatives to use during pregnancy than combustible cigarettes (Baeza-Loya et al., 2014; Kahr et al., 2015), which is concerning because vaporized cannabis may lead to higher THC concentrations and greater pharmacodynamic effects compared to the traditional route of smoking (Spindle et al., 2018). Pregnant dams were exposed to alcohol, THC, or the combination throughout gestation (gestational days [GD] 5–20, a period of development equivalent to the first and second trimester for humans; Dobbing and Sands, 1979; Patten et al., 2014), and both spatial and working memory were examined in the offspring using the Morris water maze.

2. Materials and methods

All procedures included in this study were approved by the San Diego State University Institutional Animal Care and Use Committee and are in accordance with the National Institute of Health Guide for Care and Use of Laboratory Animals.

2.1. Subjects

Breeding took place in the mating colony at the Center for Behavioral Teratology, San Diego State University, as previously described in detail (Breit et al., 2020). Briefly, adult Sprague–Dawley females were housed with adult Sprague–Dawley males overnight until a seminal plug, indicating mating, was found and designated GD 0. The SAM model used in this study was developed to model human consumption patterns (Hartman et al., 2015; Andrenyak et al., 2017), generating low to moderate THC exposure, with peak alcohol and THC levels overlapping in time. The model has been previously described in detail in Breit et al. (2020). Pregnant dams were randomly assigned to receive vaporized EtOH (68 mL/h; Sigma-Aldrich), THC via e-cigarette (100 mg/mL using SMOK V8 X-Baby Q2; NIDA Drug Supply Program), the combination of EtOH and THC, or Vehicle (propylene glycol; Sigma-Aldrich). Dams were exposed daily from gestational days (GD) 5–20 via a vapor inhalation system (La Jolla Alcohol Research Inc.) for 3 h, 30 min. The first 3 h were EtOH or air and the last 30-min session were THC or vehicle delivered in 6-s puffs every 5 min. This co-exposure paradigm produced maternal plasma levels of 150–200 mg/dL for alcohol and 20 ng/mL for THC (Breit et al., 2020) and did not significantly impact maternal food or water intake.

There were no effects of EtOH, THC, or the combination on gestation duration, number of offspring, birth weight, or male to female litter ratio (Breit et al., 2020). Following birth, litters (EtOH + THC: 10; EtOH + Vehicle: 12; Air + THC: 13; Air + Vehicle: 12) were randomly culled to 8 pups (4 males and 4 females whenever possible) on PD 2. Subjects were tattooed for identification purposes on PD 7, to keep experimenters blind to treatment condition. To control for possible litter effects, only one sex pair per litter was randomly assigned to the Morris water maze spatial learning and working memory tasks (EtOH + THC: 9 females, 10 males; EtOH + Vehicle: 12 females, 12 males; Air + THC: 12 females, 14 males; Air + Vehicle: 12 females, 12 males).

2.2. Behavioral testing

2.2.1. Morris water maze visuospatial learning

The Morris water maze apparatus consisted of a large circular tank (178-cm diameter, 61-cm height) painted black and filled with 26°C water. A Plexiglas escape platform (4-in diameter) was placed randomly in 1 of 4 quadrants and the location remained constant for each subject throughout the trials. The escape platform was 4 cm under the surface of the water, hidden from view of the subjects. The room contained a number of extra-maze cues mounted on the room walls. A video tracking system interfaced with the computer running the Water2020 software (HVS Image) was placed above the tank to record data.

Subjects were tested for 4 trials/day with a 3–5 min intertrial interval (ITI) for 6 consecutive days during PD 40–45. At the start of each trial, each subject was placed in the water, facing the edge of the tank at 12 potential random starting locations. If the subject could not locate the platform within 60 s, the experimenter manually guided the subject to the platform. The rat remained on the platform for 10 s before being removed. Path length, latency, heading angle, swimming speed and thigmotaxis served as outcome measures. Heading angle is the difference between initial swimming direction and direction of the escape platform and serves as a measure of spatial accuracy as it reflects the subject's ability to select the most direct and efficient path to the target. Thigmotaxis (swimming along the outer perimeter of the tank) serves as a measure of anxiety. On the 7th day (PD 46), subjects were tested on a probe test trial, where the platform was removed and subjects were allowed to swim for 60 s. Time spent and passes through the target quadrants, as well as the target area (3 times the diameter of the platform), served as a measure of spatial memory.

2.2.2. Working memory

From PD 55–60, the same subjects were then tested on a working memory version of the Morris water maze task (D'Hooge and De Deyn, 2001; Vorhees and Williams, 2006; Schulteis et al., 2008; Schneider and Thomas, 2016). For this task, subjects were tested for 2 sessions per day, one in the morning and one in the afternoon (6 h apart). Each session consisted of 1 acquisition trial and 1 test trial. During the acquisition trial, the Plexiglas escape platform was placed randomly in 1 of 8 positions. Once the subject found the platform, where they remained for 20 s, they were removed for either a 0-s ITI (first 3 days) or a 60-s ITI (last 3 days), before being placed back into the tank for the test trial. If subjects failed to find the platform with 60 s, they were guided to the platform. During each session, the location of the platform was moved to a novel location, placing a demand on working memory. Path length, latency, heading angle, swimming speed and thigmotaxis served as outcome measures.

2.3. Data analyses

Data were analyzed using SPSS software (SPSS Inc., Chicago, IL) with a significance value set at $p < 0.05$. All data were analyzed using

3-way (EtOH, Air) × (THC, Vehicle) × (Female, Male) ANOVAs. When applicable, data were also analyzed by Group (EtOH + THC, EtOH + Vehicle, Air + THC, Air + Vehicle), with Fisher's Least Significant Difference *post hoc* tests as follow-up, given complex higher-order interactions. All working memory data were initially analyzed separately for 0-s ITI and 60-s ITI training and testing trials using 3 (Day) × 2 (Sex) × 2 (EtOH) × 2 (THC) ANOVAs. Day, Session, and Trial were used as repeated measures. Data were also analyzed separated by sex due to previous findings on sex differences (Breit et al., 2022). Means and standard errors of the mean (M ± SEM) are reported for data described but not shown graphically. Power analyses were conducted with power 0.80. Effect sizes for both the Morris Water Maze visuospatial learning data and for the working memory version of the task ranged from moderate to large (0.05–0.2).

3. Results

3.1. Body weight

During the Morris water maze testing, all groups gained weight across Days ($F[6,510] = 293.4$, $p < 0.01$). Although offspring exposed to prenatal THC weighed less than those not exposed to THC on each day ($F[1,85] = 11.0$, $p < 0.01$; Figure 1), there were interactions of Day*Sex*THC ($F[6,510] = 4.0$, $p < 0.01$) and Day*Sex ($F[6,510] = 40.4$, $p < 0.01$), as body weight deficits became less severe among the THC groups over days, particularly among males. In addition, females weighed less than males ($F[1,85] = 296.1$, $p < 0.01$) on each day. This pattern continued during the working memory testing {PD55-60; THC ($F[1,85] = 5.3$, $p < 0.05$); Sex ($F[1,85] = 77.0$, $p < 0.01$); Day*Sex*THC ($F[5,425] = 2.4$, $p < 0.05$); Day*Sex ($F[5,425] = 35.5$, $p < 0.01$)}.

3.2. Morris water maze

3.2.1. Acquisition

Although performance improved in all groups across acquisition days ($F[5,425] = 106.9$, $p < 0.01$), female subjects exposed to prenatal THC alone showed spatial learning deficits. There were no group differences in path length to find the platform on the first day of testing; however, THC-exposed females exhibited slower acquisition than non-THC exposed females, taking significantly longer paths to find the platform (Figure 2C). This produced an interaction of THC*Sex*Day ($F[5,425] = 2.3$, $p < 0.05$), and a main effect of Sex ($F[1,85] = 6.6$, $p = 0.01$). Although the interaction of EtOH and THC did not reach statistical significance, these effects were most robust within the THC only group. Females exposed only to prenatal THC took significantly longer path lengths compared to controls ($p < 0.05$; Figure 2A), whereas the combination group did not differ significantly from any other group. There were no significant group differences in performance among males (Figures 2B,D).

Similar findings were observed in the latency to find the hidden platform (data not shown), despite differences in swimming speed. Prenatal THC exposure tended to reduce swimming speed among the males ($F[1,44] = 3.6$, $p = 0.07$; EtOH + THC: $M = 0.18 \pm 0.01$ m/s; EtOH: $M = 0.20 \pm 0.01$ m/s; THC: $M = 0.19 \pm 0.01$ m/s; Air + Vehicle: $M = 0.20 \pm 0.01$ m/s), but not females. There was also a main effect of Sex ($F[1,85] = 5.3$, $p < 0.05$).

Interestingly, there were main effects of Sex ($F[1,85] = 4.5$, $p < 0.05$), Day ($F[5,425] = 8.0$, $p < 0.01$) and Trial ($F[3,255] = 8.3$, $p < 0.01$) on heading angle. Given the main effect of Sex, analyses were conducted for each sex separately. Among females, the EtOH- only exposed group displayed significantly larger heading angles compared to controls, producing an EtOH*THC interaction ($F[1,41] = 4.7$, $p < 0.05$), as seen in Figures 3A,C. Heading angle was not significantly affected by prenatal THC or EtOH in males (Figures 3B,D).

Larger heading angle could indicate impaired spatial accuracy but could also be affected by differences in thigmotaxis (swimming along the outer perimeter of the tank due to anxiety). Interestingly, prenatal exposure to either THC or EtOH increased thigmotaxis among female offspring, leading to significant interactions of Sex*EtOH*THC ($F[1,85] = 4.5$, $p < 0.05$) and EtOH*Day ($F[5,425] = 2.6$, $p < 0.05$). Exposure to either THC or EtOH alone produced more thigmotaxis compared to the combination for the first 4 days of acquisition in females (Figure 4C). When collapsed across days (EtOH*THC, $F[1,41] = 9.9$, $p < 0.01$), females exposed to THC only were more thigmotaxic compared to controls and the combination group, whereas the EtOH group was more thigmotaxic than the combination group (p's < 0.05), as seen in Figure 4A. These effects on thigmotaxis were not seen in the male subjects (Figures 4B,D).

3.2.2. Spatial memory

Consistent with acquisition deficits, females exposed to prenatal THC showed significant impairments on spatial memory during the probe trial. THC-exposed females spent less time in the platform quadrant ($F[1,41] = 7.0$, $p < 0.01$, Figure 5A) leading to a main effect of sex ($F[1,85] = 4.2$, $p < 0.05$) and interaction of Sex*THC ($F[1,85] = 4.0$, $p < 0.05$). Conversely, females exposed to prenatal THC increased time spent in the opposite quadrant ($F[1,41] = 10.8$, $p < 0.01$), which also led to an interaction of Sex*THC ($F[1,85] = 5.4$, $p < 0.05$) and a main effect of THC ($F[1,85] = 6.7$, $p < 0.05$). In fact, female subjects exposed to THC did not discriminate among the quadrants, spending roughly 25% time in each quadrant, as seen in Figure 5A. Females with prenatal THC exposure also spent less time ($F[1,41] = 4.1$, $p < 0.05$; Figure 6A) and made fewer passes ($F[1,41] = 4.7$, $p < 0.05$; Figure 6C) in the platform area.

Collapsed across sex, subjects exposed to EtOH alone exhibited greater thigmotaxis during the probe trial than the Combination ($p < 0.05$) group, resulting in a significant interaction between EtOH*THC ($F[1,85] = 5.1$, $p < 0.05$). However, analyses also revealed an EtOH*Sex interaction ($F[1,85] = 4.9$, $p < 0.05$) and a main effect of sex ($F[1,85] = 4.2$, $p < 0.05$). Upon separating the data by sex, it was found that females exposed to the combination of EtOH and THC spent less time in thigmotaxis than either drug exposure alone, resulting in an EtOH*THC interaction ($F[1,41] = 4.4$, $p < 0.05$; Figure 6E), a result that was consistent with acquisition (Figures 6B,D,F).

3.3. Working memory

During the working memory task, the location of the platform changes with each session, so during the training trials, subjects have no prior knowledge of the platform location. However, during the 0-s ITI training trials, there was a three-way interaction of Day*EtOH*THC ($F[2,170] = 3.7$, $p < 0.05$) and a main effect of Sex ($F[1,85] = 8.7$, $p < 0.01$), as females took longer path lengths than males. Females exposed to prenatal EtOH took shorter path lengths

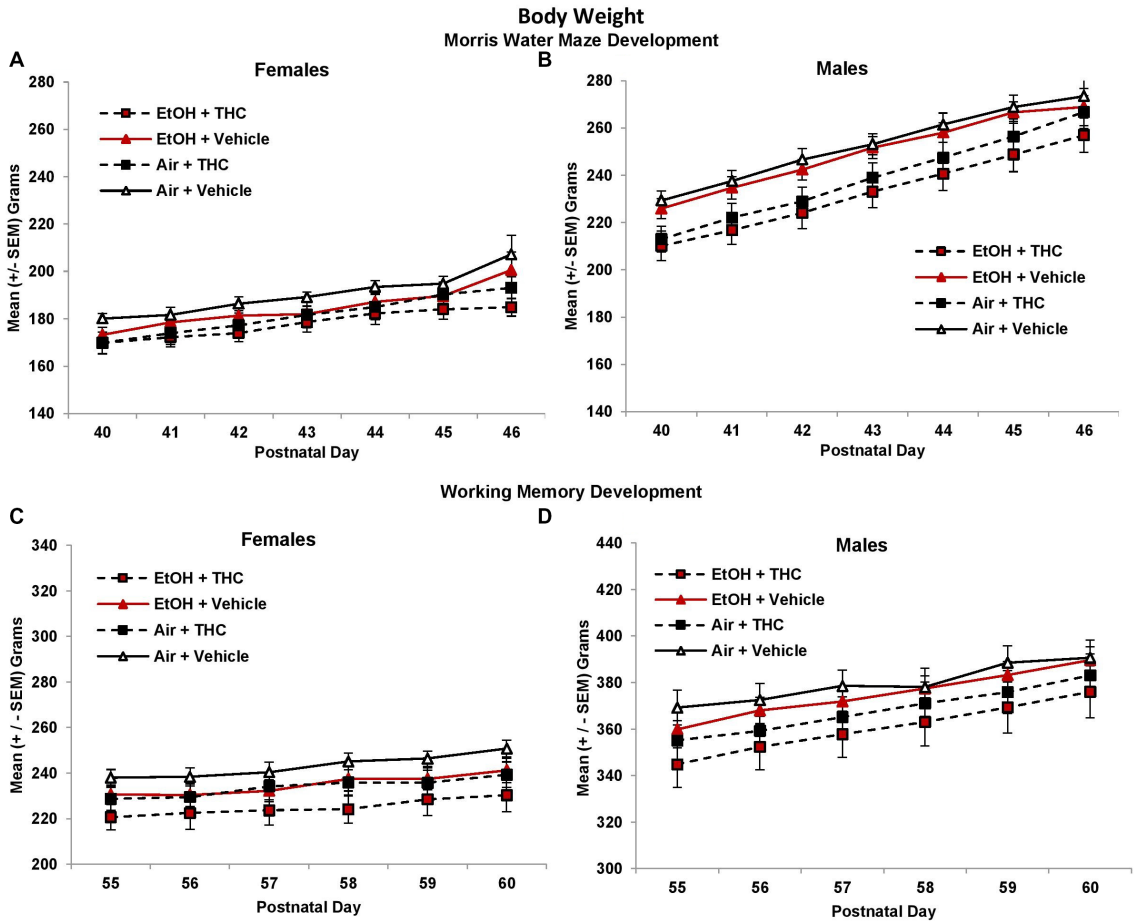


FIGURE 1
Offspring exposed to prenatal THC weighed less than those not exposed to prenatal THC throughout behavioral testing, although these effects became less pronounced with age [females **(A,C)**; males **(B,D)**].

to find the platform compared to those not exposed to EtOH (EtOH + THC: $M = 8.44 \pm 0.82$ m; EtOH: $M = 8.44 \pm 0.66$; THC: $M = 9.63 \pm 0.60$; Vehicle: $M = 9.67 \pm 0.41$), although this effect failed to reach statistical significance ($F[1,41] = 3.8$, $p = 0.06$). Nevertheless, this suggests that females exposed to ethanol may utilize a different search strategy. There were no other effects of prenatal drug exposure or sex during training trials.

During the 0-s ITI testing sessions, an interaction of Day*Sex was observed ($F[2,170] = 4.3$, $p < 0.05$). Males prenatally exposed to EtOH required longer path lengths to find the platform on Day 1 ($F[1,44] = 5.4$, $p < 0.05$; Figure 7B). Consistent with memory impairments, males exposed to alcohol prenatally also had significantly larger heading angles during the 0-s ITI testing days ($F[1,44] = 6.00$, $p < 0.05$; EtOH + THC: $M = 50.68 \pm 4.73$; EtOH: $M = 47.37 \pm 5.48$; THC: $M = 38.28 \pm 3.21$; Vehicle: $M = 39.39 \pm 2.95$) producing an interaction of Sex*EtOH ($F[1,85] = 5.0$, $p < 0.05$). There were no effects among females (Figure 7A).

When the ITI was increased to 60-s, there was a main effect of Sex ($F[1,85] = 4.2$, $p < 0.05$), as well as a trending interaction of Day*EtOH*Sex ($F[2,170] = 2.8$, $p = 0.06$)Given the main effect of sex, data were analyzed separately for males and females. Among females, subjects exposed to prenatal EtOH took shorter path lengths to find the platform ($F[1,41] = 5.7$, $p < 0.05$; Figure 7A), particularly on Day 5 ($F[1,41] = 9.3$, $p < 0.01$) and 6 ($F[1,41] = 3.5$, $p = 0.06$). In contrast, female offspring exposed to THC had smaller heading angles on Day 5 only ($F[1,41] = 4.1$, $p < 0.05$; EtOH + THC: $M = 34.91 \pm 8.70$; EtOH: $M = 50.55 \pm 7.19$; THC: $M = 45.00 \pm 4.12$; Vehicle: $M = 61.80 \pm 10.48$). No significant differences were observed among male offspring (Figure 7B).

Memory performance is best measured as savings (testing minus training path lengths), which takes into account individual differences in training trial performance. Offspring exposed to prenatal EtOH exhibited less savings during the 0-s ITI sessions ($F[1,85] = 4.8$, $p < 0.05$). Although this effect was seen in both sexes, follow-up analyses indicated that EtOH impaired memory among female offspring ($F[1,41] = 4.8$, $p < 0.05$), but failed to reach statistical significance among males (Figures 7C,D). During the 60-s ITI sessions, despite a significant interaction of Day*Sex*EtOH ($F[2,170] = 2.9$, $p = 0.05$), follow-up analyses did not yield any meaningful or significant effects on individual Days (data not shown).

Similar to the Morris water maze spatial learning task, prenatal THC exposure reduced swimming speed among males during working memory training. Overall, all offspring increased their speed over Days ($F[2,170] = 3.3$, $p < 0.05$; data not shown), but offspring exposed to prenatal THC swam slower than those exposed to the Vehicle ($F[1,85] = 5.8$, $p < 0.05$). Given there was a significant effect of sex

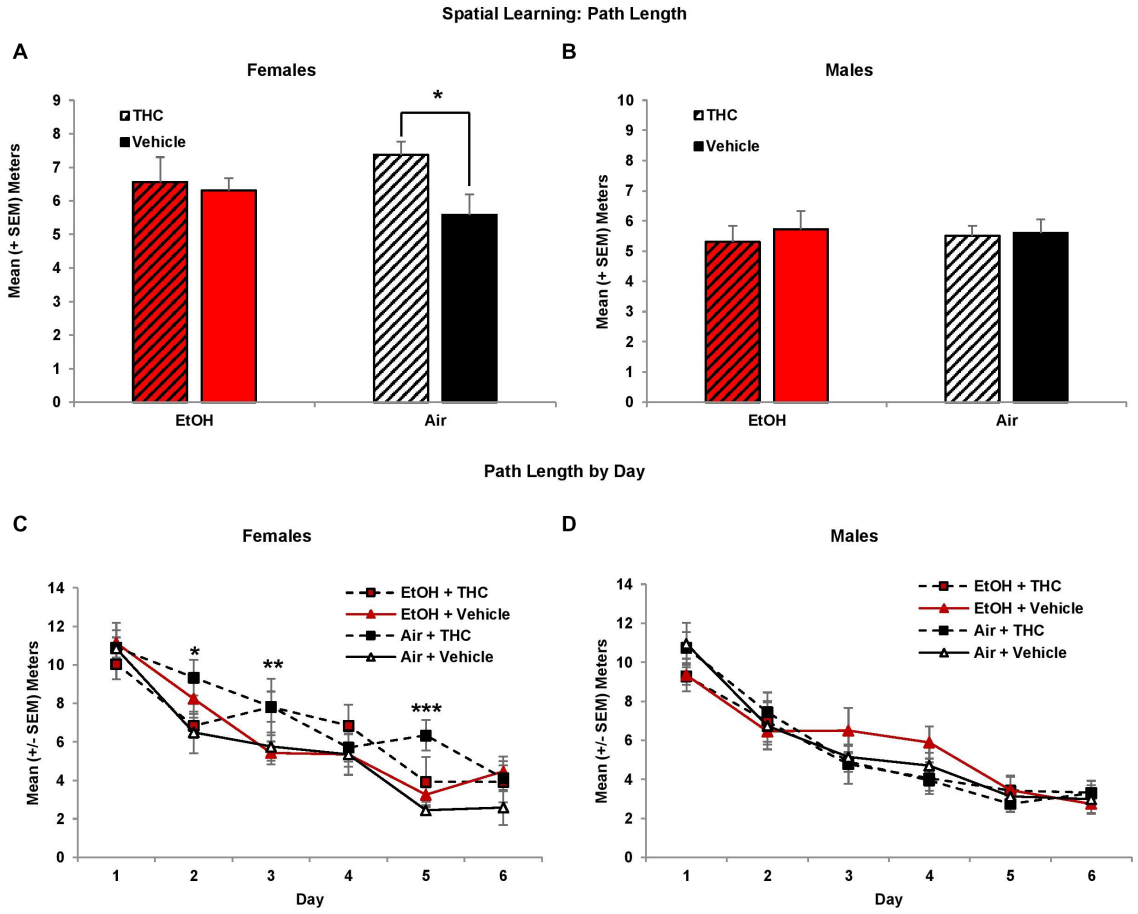


FIGURE 2
Female offspring prenatally exposed to THC alone required longer path lengths to find the hidden platform during the visuospatial memory task **(A,C)**. There were no effects of prenatal exposure on performance among male offspring **(B,D)**. *Air+THC>Air+Vehicle, $p<0.05$; **Air+THC>EtOH+Vehicle, $p<0.05$; ***Air+THC>all other groups, $p<0.01$.

($F[1,85]=6.3$, $p<0.05$), data were examined separately by sex. Reductions in speed among prenatal THC-exposed offspring during the 0-s training sessions were driven by the males ($F[1,44]=4.9$, $p<0.05$), not females (Figures 8A,B). A similar trend was also observed during the 60-s ITI training sessions among the male offspring ($F[1,44]=3.7$, $p=0.06$; Figures 8A,B). By the testing sessions, there were no meaningful group differences in swimming speed (data not shown). Thus, prenatal THC may influence motor function in males.

To determine if anxiety and/or alternative search strategies affected working memory performance, thigmotaxis was also examined. During the 0-s ITI training and testing sessions, female offspring spent more time in thigmotaxis than males (Training: $F[1,85]=4.1$, $p<0.05$; Testing: $F[1,85]=3.7$, $p=0.05$, Figures 9A,B). Among female offspring, an interaction of Day*EtOH*THC ($F[2,82]=4.8$, $p<0.05$) indicated females prenatally exposed to either EtOH ($F[1,19]=4.9$, $p<0.05$) alone or THC alone ($F[1,22]=4.1$, $p=0.05$) spent significantly more time in thigmotaxis than those exposed to the combination (EtOH + THC) or the Vehicle on the 1st day of 0-s ITI training (Figure 9A).

When the ITI was increased to 60 s, a Day*THC interaction was observed ($F[2,170]=7.5$, $p<0.01$) and a Sex*EtOH interaction approached significance ($F[1,85]=3.4$, $p=0.06$). Females exposed to the combination of prenatal EtOH + THC spent less time in thigmotaxis during the first 60-s ITI training session (Day 4) compared to those exposed to EtOH alone ($F[1,19]=4.2$, $p=0.05$, Figure 9A). During the 60-s ITI testing sessions, interactions of Day*Sex*THC ($F[2,170]=3.0$, $p=0.05$), and EtOH*THC ($F[1,85]=5.1$, $p<0.05$) were observed. Although female offspring exposed to prenatal THC generally spent more time in thigmotaxis, whereas males in the control group (Air + Vehicle) spent less time in thigmotaxis, effects were not significant (Figures 9C,D).

4. Discussion

The present study investigated the impact of combined prenatal exposure to EtOH and THC, delivered via an e-cigarette, on spatial and working memory. The results revealed sex-specific effects of THC and EtOH exposure on cognitive and emotional domains. Cognitively, prenatal THC exposure adversely impacted spatial learning and memory in female offspring, whereas prenatal EtOH exposure impaired working memory. Notably, the combination of prenatal exposure to THC and EtOH did not intensify the cognitive effects of either substance.

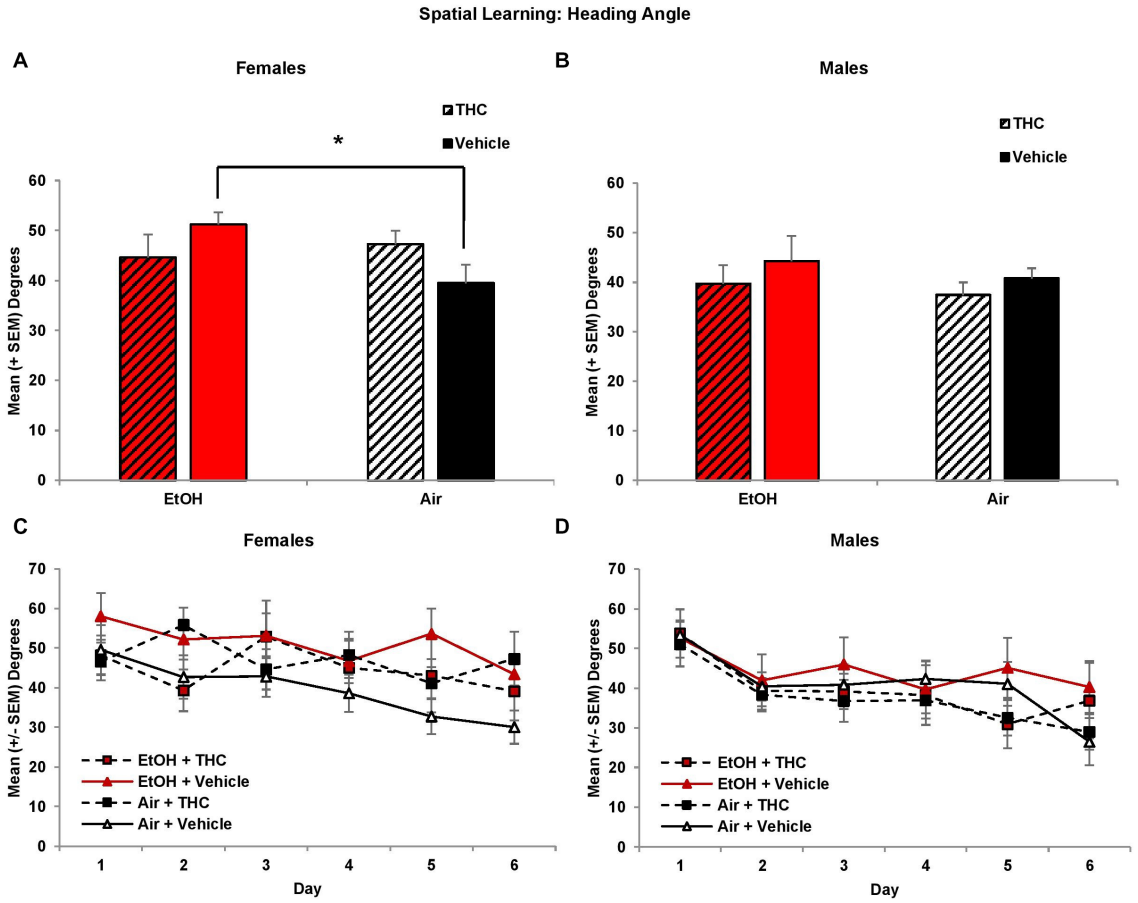


FIGURE 3
Female offspring prenatally exposed to alcohol alone had significantly larger heading angles (impaired performance) compared to controls **(A,C)**. Heading angle did not differ among groups of male offspring **(B,D)**. *EtOH+Vehicle>Air+Vehicle, $p<0.05$.

Surprisingly, our findings showed that ethanol exposure during gestation did not produce deficits in spatial learning and memory, in contrast to other preclinical studies using prenatal models (Patten et al., 2014; Brancato et al., 2020; Aglawe et al., 2021; Mahdinia et al., 2021) and 3rd trimester equivalent models (Thomas et al., 2007; Ryan et al., 2008; Breit et al., 2019b). Variation in outcome may be related to route of administration and/or developmental timing. However, our failure to find effects may be related to the lower peak BACs compared to previous studies. Specifically, spatial learning deficits are more often observed when peak BACs are over 200 mg/dl, whereas the peak BACs in the current study were around 150 mg/dl (albeit see below).

Clinical studies have shown that prenatal alcohol exposure can have dose-dependent negative impacts on learning, memory, and academic attainment in children and adults. For example, frequent episodes of binge drinking during the first and second trimester predict learning and memory deficits, including deficits in spatial memory, in children (Richardson et al., 2002). A recent study suggests that heavy, but not moderate, prenatal EtOH exposure impairs spatial learning and memory (Dodge et al., 2019). Importantly, in the Dodge et al. (2019) study, there was a confound of age, as the moderately exposed group was older, so there may be a developmental delay in performance that was missed in the moderately exposed group. Nevertheless, the amount of alcohol consumed per occasion was related to spatial navigation; thus, the absence of prenatal alcohol effect in the current study could be attributed to the failure to attain a threshold BAC.

In contrast, prenatal EtOH did impair spatial working memory. Females exposed to prenatal EtOH showed memory impairments during the 0-s ITI sessions, whereas males showed only transient impairments during the early stages of learning, as evidenced by longer path lengths and larger heading angles on the initial days of testing. Previous preclinical studies have also reported that prenatal alcohol exposure impairs spatial working memory (Schambra et al., 2017; Lucia et al., 2019; Waddell et al., 2020; Gursky et al., 2021), even at low to moderate ethanol doses (Schambra et al., 2017; Waddell et al., 2020) and across different gestational periods (Schambra et al., 2017; Lucia et al., 2019; Waddell et al., 2020; Gursky et al., 2021). Similar working memory deficits have been reported in clinical populations (Kodituwakku et al., 1995; Moore et al., 2021; Chetty-Mhlanga et al., 2022). This deficit is likely related to dysfunction of the prefrontal cortex (Waddell et al., 2020; Gursky et al., 2021), and our data suggest that the alcohol levels achieved in the current study may disrupt development of this brain area.

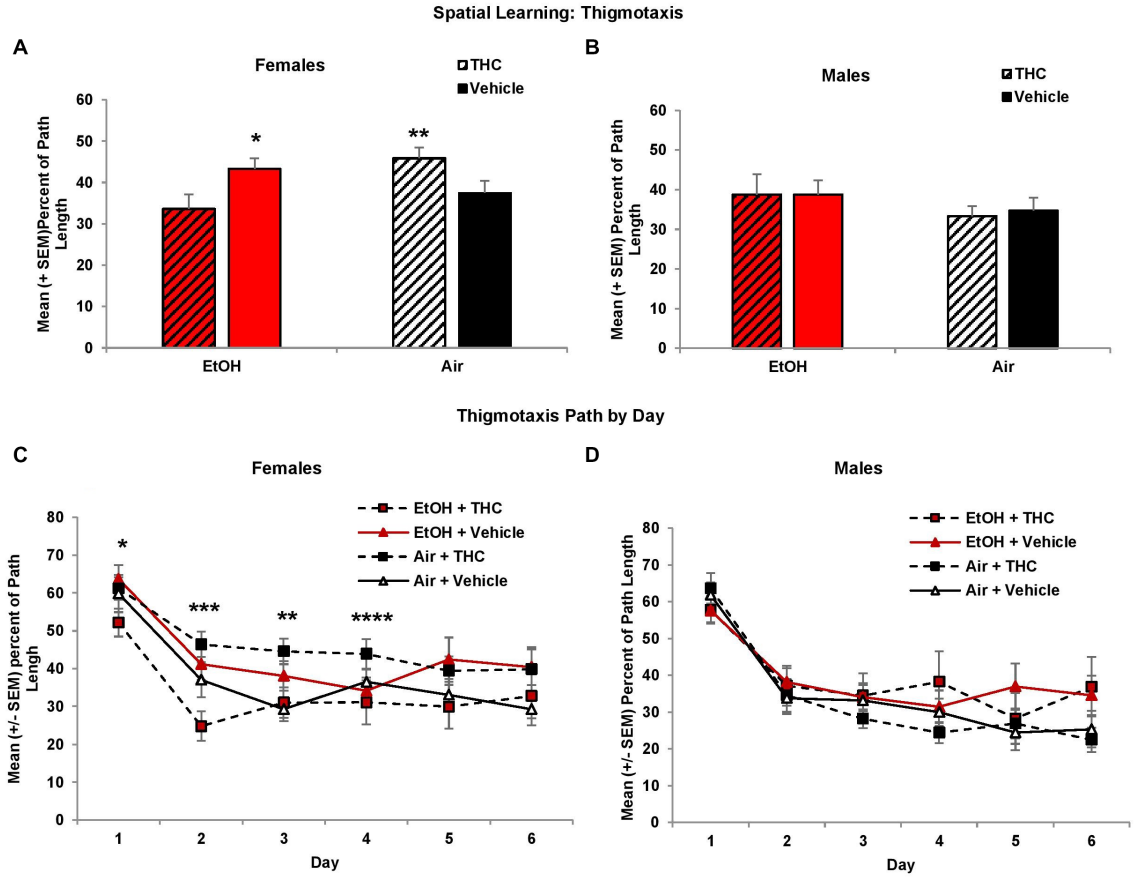


FIGURE 4
Female offspring exposed to either THC alone or alcohol alone were more thigmotaxic compared to those exposed to the combination or controls **(A,C)**. No differences were observed among male offspring **(B,D)**. *EtOH+Vehicle>EtOH+THC, $p<0.05$; **Air+THC>EtOH+THC and Air+Vehicle, p's<0.05; ***all other groups>EtOH+THC, p's<0.05; ****Air+THC>EtOH+THC, p's<0.05.

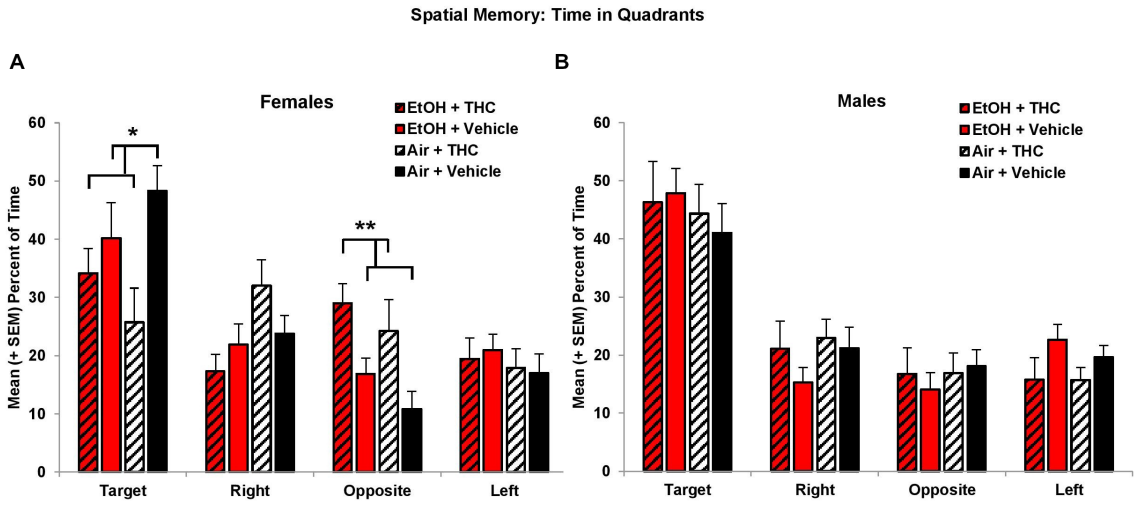


FIGURE 5
Female offspring exposed to THC spent less time in the Target quadrant and more time in the Opposite quadrant than non-exposed offspring **(A)**. Neither prenatal THC nor alcohol significantly affected spatial memory among male offspring **(B)**. *THC<no THC, $p<0.05$; **THC>no THC, $p<0.01$.

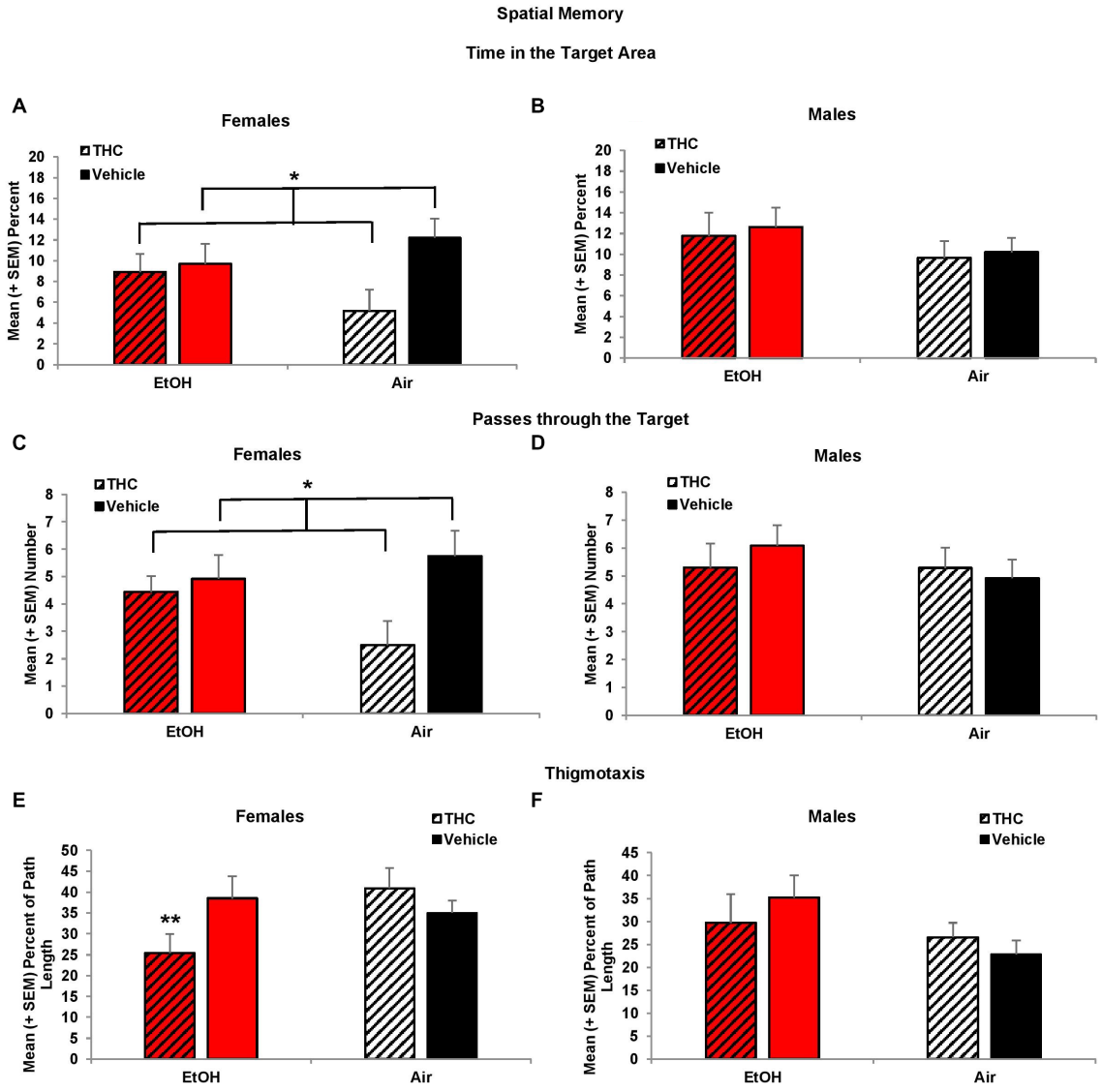


FIGURE 6
Female offspring exposed to prenatal THC showed impaired performance during the probe trial, spending less time in the target area **(A)** and fewer passes through the target **(C)**. Female offspring exposed to combined alcohol and THC prenatally were less thigmotaxic **(E)**. No differences were observed among male offspring **(B,D,F)**. *THC<no THC, $p<0.01$; **EtOH+THC<EtOH+Vehicle and Air+THC, p's<0.05.

Unlike prenatal EtOH, our study found that exposure to prenatal THC did alter spatial learning and memory, but only in females. This sex effect contrasts with previous studies reporting that prenatal THC exposure impairs spatial memory in males (de Salas-Quiroga et al., 2020; Castelli et al., 2023), but not females (de Salas-Quiroga et al., 2020). Prenatal cannabinoid exposure has also been found to impact CB1 receptors and GABAergic transmission in the hippocampus of adult male rats, potentially affecting long-lasting learning and memory performance (Castelli et al., 2007; Beggiato et al., 2017; de Salas-Quiroga et al., 2020), whereas others report that prenatal THC exposure may not alter hippocampal function in females (de Salas-Quiroga et al., 2020). Interestingly, previous research within our own lab using a synthetic cannabinoid found no significant effects on spatial learning (Breit et al., 2019b). However, it is important to note that exposure in that study occurred during postnatal days 4–9, equivalent to the human third trimester, rather than prenatal exposure used in the current study. Importantly, differential effects of prenatal THC and EtOH on memory are consistent with individual and opposing effects each drug has on the hippocampus (Reid et al., 2021).

Despite deficits in spatial learning and memory, there was no effect of prenatal THC on working memory. Research on the effects of prenatal THC on working memory has yielded mixed findings in both preclinical (Silva et al., 2012; Beggiato et al., 2020; Castelli et al., 2023) and clinical studies (Smith et al., 2016; Murnan et al., 2021; Cioffredi et al., 2022). Studies have reported poorer performance on learning and memory tasks in children exposed to marijuana in the first trimester (Richardson et al., 2002) and an increased risk of educational underachievement for children of mothers with cannabis use disorder (Betts et al., 2022). However,

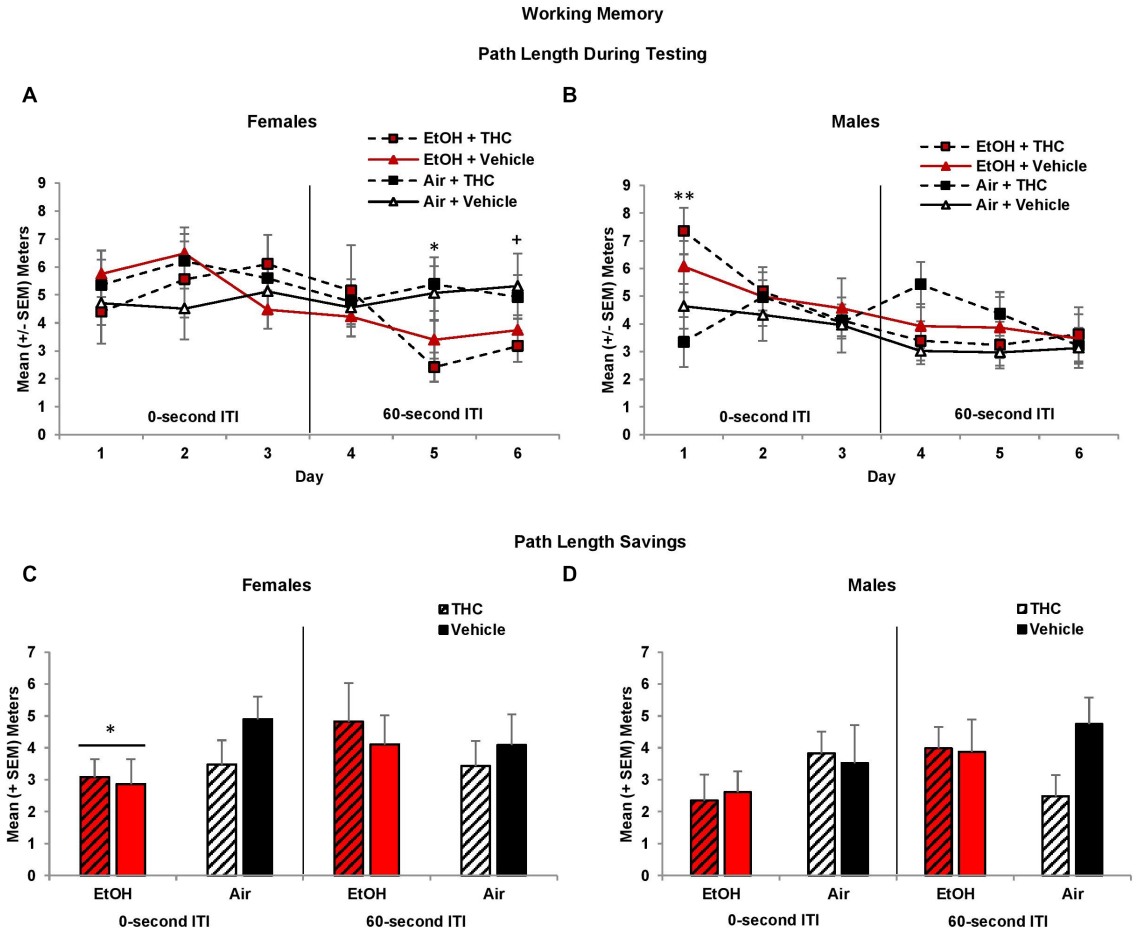


FIGURE 7
Male offspring exposed to prenatal alcohol exposure traveled longer path lengths on the first day of testing **(B)**, whereas female offspring with prenatal alcohol exposure traveled shorter path lengths during the latter 60-s ITI test trials **(A)**. However, offspring prenatally exposed to alcohol had less memory savings between the training and test trials, an effect driven by the female offspring **(C,D)**. *EtOH<no EtOH, *p*'s<0.05; **EtOH>no EtOH, *p*<0.05; ⁺EtOH<no EtOH, *p*=0.06.

adjusting for socioeconomic status and other comorbidities attenuated this association, suggesting that additional environmental factors may contribute to learning and memory outcomes. The inconsistencies in findings may be attributed to various factors such as the form of administration (injections, gavage), type of drug (THC, synthetic cannabinoids), dose, timing of exposure, and age of outcome measurement.

Unexpectedly, the combination of prenatal THC and EtOH did not produce more severe cognitive deficits than either drug alone. This was particularly surprising given pharmacokinetic interactions of prenatal EtOH and THC, which led to higher BACs (EtOH + THC = 200 mg/dl vs. EtOH = 150 mg/dl) and transiently elevated plasma THC levels (Breit et al., 2020). Moreover, both prenatal THC and alcohol exposure can disrupt endocannabinoid function, making offspring more vulnerable to stressors and impairing memory and learning processes (Trezza et al., 2012; Richardson et al., 2016; Little et al., 2021). The ECS plays a crucial role in various developmental processes, including movement, memory, and emotions; changes in its activity during periods of high brain plasticity, such as prenatal development, can lead to long-term problems in behavior and brain function (Pinky et al., 2019; Navarrete et al., 2020; Little et al., 2021; De Genna et al., 2022). For example, prenatal alcohol exposure is associated with increased EC activity and increased CB1 receptor activation (Nagre et al., 2015; Subbanna et al., 2015; Rodrigues et al., 2017), and prenatal alcohol exposure is associated with long-lasting changes in the ECS, which may contribute to some of the behavioral deficits observed in FASD (Basavarajappa, 2015; Hungund, 2017). In contrast, prenatal cannabinoid exposure actually reduces CB1 activation (de Salas-Quiroga et al., 2015, 2020). However, when consumed together, combined exposure increases the bioavailability of each drug (Abel and Subramanian, 1990; Hartman et al., 2015, 2016), which may lead to greater alterations in the ECS.

Both the hippocampus and prefrontal cortex are rich in CB1 receptors and, in fact, combined exposure to THC and alcohol can lead to more severe neuronal degeneration and altered neuronal circuitry in the hippocampus (Hansen et al., 2008; Basavarajappa, 2015). The lack of combination effects on cognitive functioning are also surprising given findings in other behavioral domains. For example, the combination of EtOH and CP-55,940 produces more severe motor deficits and hyperactivity (Breit et al., 2019a), as well thigmotaxis (Breit et al., 2019b). Even littermates from the present study exposed to the combination illustrated more severe open field

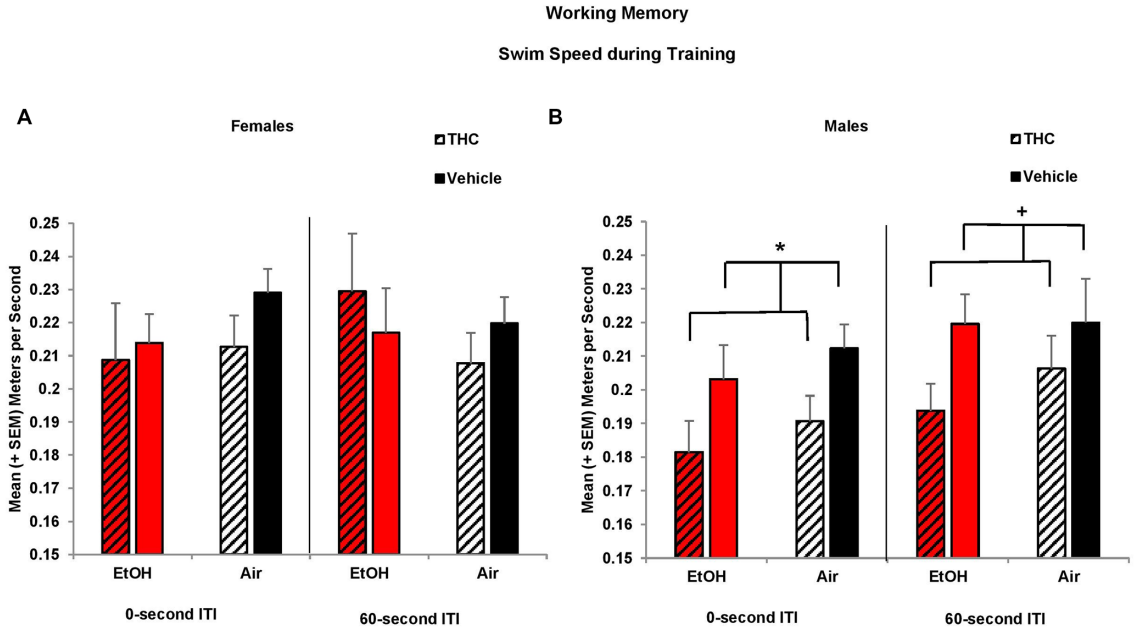


FIGURE 8
Male offspring exposed to prenatal THC swam slower during training sessions than those not exposed to THC **(B)**. Swim speed did not differ among groups of female offspring **(A)**. *THC<no THC, $p<0.05$; ⁺THC<no THC, $p=0.06$.

hyperactivity compared to either substance alone (Breit et al., 2022). Thus, the combination of ethanol and THC at the doses used in the present study affects behavioral domains outside of cognitive functioning.

In fact, the combination EtOH and THC did reduce thigmotaxis among female subjects compared to either prenatal EtOH or THC alone, suggesting that the combination may impact emotional processing, reducing anxiety and increasing risk-taking behavior. Interestingly, zebrafish exposed to a low-dose CB1R agonist during development exhibit increased risk-taking behavior, but only when combined with alcohol (Boa-Amponsem et al., 2019). Moreover, littermates from the current study exposed to the combination of prenatal EtOH and THC were less thigmotaxic in the open field, spending more time in the center (Breit et al., 2022), although this effect was seen in males, but not females. Together, these data suggest that the combination of prenatal EtOH and THC may produce unique effects on emotional development.

In contrast to the combination, exposure to either prenatal EtOH or THC alone increased thigmotaxis, suggesting increased anxiety. For example, female subjects exposed prenatally to THC exhibited increased thigmotaxis during both spatial and working memory tasks. The effects of prenatal cannabis exposure on emotional development have been diverse and dependent on various factors, including the age of testing, cannabinoid type, and sex of the subjects. For instance, prenatal exposure to whole-plant cannabis extract increased anxiety-like behavior in juveniles but not in adults (Weimar et al., 2020), whereas studies of prenatal exposure to synthetic cannabinoids have reported mixed results, including no effects (Manduca et al., 2020), decreased anxiety/increased risk-taking (Boa-Amponsem et al., 2019; Breit et al., 2019b) and elevated anxiety-like behaviors (Traccis et al., 2021; Lallai et al., 2022). Interestingly, in littermates prenatally exposed to THC alone, there were no effects on open field thigmotaxis, although subjects were tested during pre-adolescence (Breit et al., 2022). Clinically, cannabis exposure has been associated with increased frequency of depression and anxiety in children (Goldschmidt et al., 2004; Leech et al., 2006; Eiden et al., 2018; Grant et al., 2020); thus, prenatal cannabis may impact emotional development in complex ways.

Similarly, prenatal EtOH exposure produced modest increases in thigmotaxis among females. As with prenatal THC, the effects of prenatal EtOH exposure on emotional development are highly variable, with some reporting increased anxiety (Balaszczuk et al., 2019; Aglawe et al., 2021), while others report decreased anxiety/more risk-taking behavior (Breit et al., 2019b), and with variable sex-dependent effects (Weinberg et al., 2008; Muñoz-Villegas et al., 2017; Bake et al., 2021) related to alterations in the hypothalamic–pituitary–adrenal axis (Weinberg et al., 2008). Clinical studies have also reported mixed results (Goldschmidt et al., 2004; O'Leary et al., 2010).

Interestingly, the effects of prenatal EtOH and THC on cognitive and emotional functioning in the present study were more robust among females. However, prenatal THC did reduce swimming speed among males. We previously reported that prenatal THC exposure can delay sensorimotor development and impair motor function in adolescents, although we did not see sex-specific effects on those outcomes (Breit et al., 2022). Thus, motor coordination deficits induced by prenatal THC exposure may persist in males, but not females, as they age. Although clinical research has found varied effects of prenatal THC on motor development, including no impairments (Chandler et al., 1996; Richardson et al., 2002; Huizink, 2014), impairments (Richardson et al., 1995), and advanced motor skills (Fried and Watkinson, 1990; Huizink, 2014), further investigation is required to

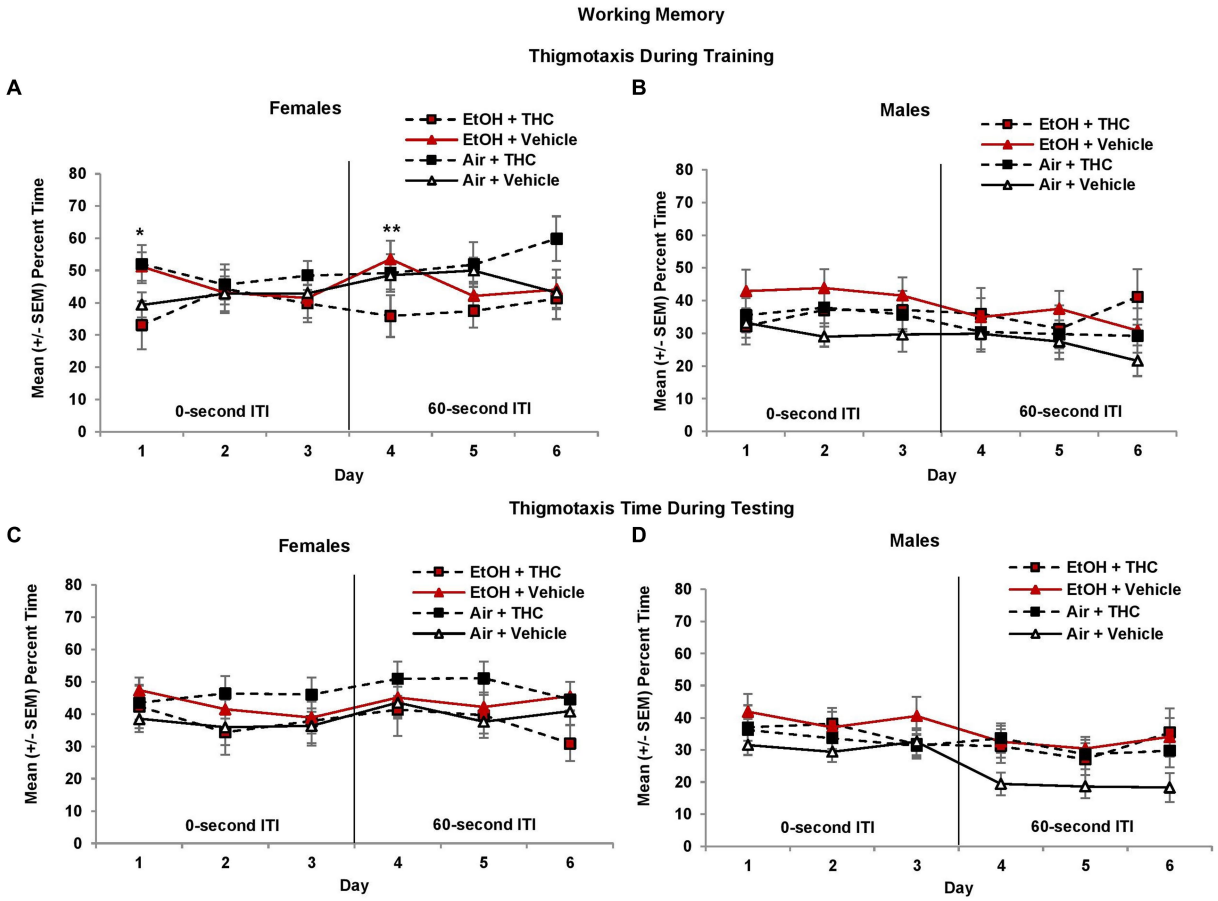


FIGURE 9
Female offspring exposed to either alcohol or THC prenatally spent more time in thigmotaxis on the 1st day of 0-s ITI training **(A)**. In contrast, females exposed to the combination of prenatal alcohol and THC spent less time in thigmotaxis on the 1st day of 60-s ITI training (4th day; **A**). There were no significant differences during testing in females **(C)**. No significant differences were observed among male offspring **(B,D)**. *EtOH+Vehicle and Air+THC>EtOH+THC and Air+Vehicle, $p<0.05$; **EtOH+THC<all other groups, $p=0.05$.

discern the impact of cannabis on motor development and coordination, and to identify any possible sex differences.

Notably, in addition to behavioral effects, offspring prenatally exposed to THC exhibited lower weight compared to those not exposed to THC. These results illustrate that even low levels of prenatal THC exposure can impair growth and that growth impairments extend beyond early life (Breit et al., 2022) into adolescence. Importantly, this growth impairment was seen in both sexes. Given the sex- and task-dependent behavioral effects of prenatal THC, body weight reductions do not relate to behavioral outcome. Nevertheless, long-lasting effects of prenatal THC on physical development represent another adverse outcome associated with prenatal cannabis exposure.

The current study illustrates that prenatal exposure to EtOH and THC can alter cognitive and emotional development, but there are several limitations to consider. First, the effects of only one dose of THC and EtOH were examined, and consequences of either drug alone or in combination are likely dose-dependent. This is particularly critical to investigate, as the lack of regulation of THC products and the dramatic variation in THC potencies (Giroud et al., 2015; Kahr et al., 2015) create challenges in establishing dose–response effects in clinical studies. Second, only THC was administered, but cannabis products include many constituents which may impact outcome. By solely focusing on one constituent of cannabis, THC, the potential interactive effects of other cannabinoids present in various cannabis products, such as CBD, are not considered.

Third, the study focused primarily on learning and memory during late adolescence, without follow-up testing as they transitioned into adulthood. The age range was chosen because rats have typically reached the ontological stage of hippocampal maturation and spatial learning ability (Morterá and Herculano-Houzel, 2012), and are capable of navigating and swimming efficiently in the maze (D'Hooge and De Deyn, 2001; Albani et al., 2014). It is possible that performance could be affected by factors such as pubertal hormones. For instance, the onset of puberty has been associated with improved cognitive performance in the Morris Water Maze, possibly due to prefrontal cortex maturation and changes in learning strategy (Willing et al., 2016). Performance in females can also be affected by differences in the estrous cycle, while alterations in sex hormones can impact spatial ability in males (D'Hooge and De Deyn, 2001; Moradpour et al., 2013). However, recent data suggest that hormonal factors may not necessarily induce large changes in behavior (Levy et al., 2023). Importantly, we do not know if prenatal alcohol or THC is affecting

pubertal onset in the current study; thus, future studies should examine whether alterations in maturation contribute to behavioral outcomes.

Fourth, there is a possibility that the subjects' performance on the initial Morris water maze task could affect subsequent performance on the working memory version of the task. For example, if the memory for the initial spatial location of the escape platform is strong, subjects may become biased towards a particular strategy or location and have more difficulty adapting to the changing demands of the working memory task. Importantly, subjects were tested on the working memory version 1 week after spatial memory testing to reduce carryover effects and all subjects showed improvement in performance. Moreover, even if prior spatial learning impacted performance on the working memory task, impaired performance would still reflect deficits in cognitive flexibility. Nevertheless, testing subjects on only the working memory version would determine whether interference influenced performance.

Finally, the control subjects in his study were exposed to propylene glycol vehicle, a well-known e-cigarette vehicle commonly used in e-liquids alongside various flavorings. The effects of inhaling e-cigarette vehicles by themselves, as well as the effects of mixing various commonly used flavorings, remain poorly understood. In fact, a recent study discovered that e-cigarette vehicles can dysregulate gene expression in the lungs and that adding flavorings can increase toxicity and alter immune lung cells, potentially leading to reduced lung function (Szafran et al., 2020).

In summary, our findings suggest that prenatal exposure to THC and EtOH can have differential effects on cognitive functions, with sex-specific and substance-specific patterns. Our results suggest that even low doses of THC delivered through e-cigarettes during pregnancy can lead to learning and memory deficits, whereas exposure to EtOH can impair working memory. Co-administration of THC and EtOH did not magnify the adverse effects of either substance on cognitive function, but may influence anxiety-like behavior and risk-taking tendencies. Overall, our findings underscore the potential harm of THC and EtOH on fetal development and reinforce the importance of educating pregnant individuals and promoting public health policies and interventions to minimize the risk of drug-related cognitive deficits in offspring.

Data availability statement

The raw data supporting the conclusions of this article will be made available by the authors, without undue reservation.

Ethics statement

The animal study was reviewed and approved by Institutional Animal Care and Use Committee at San Diego State University.

Author contributions

AL contributed as first authorship based on roles in study design, project organization, data collection, data analyses, and writing of the manuscript. KB contributed to study design, data collection, analyses, and writing of the manuscript. JT contributed as last authorship based on roles in study design, funding acquisition, supervision, data analyses, and writing of the manuscript. All authors contributed significantly to the preparation of this submission.

Funding

This work was supported by NIAAA grants AA025425 and AA012446 to JT, the NIAAA training grant T32 AA007456-38 and the NIH Loan Repayment Program award to KB.

Acknowledgments

THC was obtained from the NIDA Drug Supply Program. Special thanks to Maury Cole at La Jolla Alcohol Research, Inc. (San Diego, CA) for building the vapor inhalation equipment and for co-exposure advisement. We also want to recognize Michael Taffe for his aid and advisement in the implementation of this vapor inhalation paradigm. Lastly, we want to recognize the member of the Center for Behavioral Teratology at San Diego State University for assisting in data collection and interpretation, particularly the instrumental efforts of Cristina G. Rodriguez. We would like to acknowledge that some of the content of this manuscript has previously appeared in Lei's Master's thesis entitled "The effects of combined prenatal alcohol and cannabis vapor exposure on spatial learning." The source has been listed in the reference list as Lei (2022). That aided the efforts of the authors.

Conflict of interest

The authors declare that the research was conducted in the absence of any commercial or financial relationships that could be construed as a potential conflict of interest.

Publisher's note

All claims expressed in this article are solely those of the authors and do not necessarily represent those of their affiliated organizations, or those of the publisher, the editors and the reviewers. Any product that may be evaluated in this article, or claim that may be made by its manufacturer, is not guaranteed or endorsed by the publisher.

References

Abel, E. L., and Subramanian, M. G. (1990). Effects of low doses of alcohol on delta-9-tetrahydrocannabinol's effects in pregnant rats. *Life Sci.* 47, 1677–1682. doi: 10.1016/0024-3205(90)90374-z

Substance Abuse and Mental Health Services Administration (2022). *2020 National Survey on drug use and health: Women | CBHSQ data*. Rockville, MD: Center for Behavioral Health Statistics and Quality.

Aglawe, M. M., Kale, M. B., Rahangdale, S. R., Kotagale, N. R., Umekar, M. J., and Taksande, B. G. (2021). Agmatine improves the behavioral and cognitive impairments associated with chronic gestational ethanol exposure in rats. *Brain Res. Bull.* 167, 37–47. doi: 10.1016/j.brainresbull.2020.11.015

Albani, S. H., McHail, D. G., and Dumas, T. C. (2014). Developmental studies of the hippocampus and hippocampal-dependent behaviors: insights from interdisciplinary studies and tips for new investigators. *Neurosci. Biobehav. Rev.* 43, 183–190. doi: 10.1016/j.neubiorev.2014.04.009

Alpár, A., Di Marzo, V., and Harkany, T. (2016). At the tip of an iceberg: prenatal marijuana and its possible relation to neuropsychiatric outcome in the offspring. *Biol. Psychiatry* 79, e33–e45. doi: 10.1016/j.biopsych.2015.09.009

Andrenyak, D. M., Moody, D. E., Slawson, M. H., O'Leary, D. S., and Haney, M. (2017). Determination of Δ-9-Tetrahydrocannabinol (THC), 11-hydroxy-THC, 11-nor-9-carboxy-THC and cannabidiol in human plasma using gas chromatography–tandem mass spectrometry. *J. Anal. Toxicol.* 41, 277–288. doi: 10.1093/jat/bkw136

Baeza-Loya, S., Viswanath, H., Carter, A., Molfese, D. L., Velasquez, K. M., Baldwin, P. R., et al. (2014). Perceptions about e-cigarette safety may lead to e-smoking during pregnancy. *Bull. Menn. Clin.* 78, 243–252. doi: 10.1521/bumc.2014.78.3.243

Bake, S., Pinson, M. R., Pandey, S., Chambers, J. P., Mota, R., Fairchild, A. E., et al. (2021). Prenatal alcohol-induced sex differences in immune, metabolic and neurobehavioral outcomes in adult rats. *Brain Behav. Immun.* 98, 86–100. doi: 10.1016/j.bbi.2021.08.207

Balaszczuk, V., Salguero, J. A., Villarreal, R. N., Scaramuzza, R. G., Mendez, S., and Abate, P. (2019). Hyperlocomotion and anxiety- like behavior induced by binge ethanol exposure in rat neonates. Possible ameliorative effects of omega 3. *Behav. Brain Res.* 372:112022. doi: 10.1016/j.bbr.2019.112022

Basavarajappa, B. S. (2015). Fetal alcohol Spectrum disorder: potential role of endocannabinoids signaling. *Brain Sci.* 5, 456–493. doi: 10.3390/brainsci5040456

Beggiato, S., Borelli, A. C., Tomasini, M. C., Morgano, L., Antonelli, T., Tanganelli, S., et al. (2017). Long-lasting alterations of hippocampal GABAergic neurotransmission in adult rats following perinatal Δ9-THC exposure. *Neurobiol. Learn. Mem.* 139, 135–143. doi: 10.1016/j.nlm.2016.12.023

Beggiato, S., Ieraci, A., Tomasini, M. C., Schwarcz, R., and Ferraro, L. (2020). Prenatal THC exposure raises kynurenic acid levels in the prefrontal cortex of adult rats. *Prog. Neuro Psychopharmacol. Biol. Psychiatry* 100:109883. doi: 10.1016/j.pnpbp.2020.109883

Betts, K. S., Kisely, S., and Alati, R. (2022). Prenatal cannabis use disorders and offspring primary and secondary educational outcomes. *Addiction* 117, 425–432. doi: 10.1111/add.15629

Boa-Amponsem, O., Zhang, C., Mukhopadhyay, S., Ardrey, I., and Cole, G. J. (2019). Ethanol and cannabinoids interact to alter behavior in a zebrafish fetal alcohol spectrum disorder model. *Birth Defects Res.* 111, 775–788. doi: 10.1002/bdr2.1458

Borodovsky, J. T., Crosier, B. S., Lee, D. C., Sargent, J. D., and Budney, A. J. (2016). Smoking, vaping, eating: is legalization impacting the way people use cannabis? *Int. J. Drug Policy* 36, 141–147. doi: 10.1016/j.drugpo.2016.02.022

Brancato, A., Castelli, V., Lavanco, G., and Cannizzaro, C. (2020). Environmental enrichment during adolescence mitigates cognitive deficits and alcohol vulnerability due to continuous and intermittent perinatal alcohol exposure in adult rats. *Front. Behav. Neurosci.* 14:583122. doi: 10.3389/fnbeh.2020.583122

Bravo, A. J., Prince, M. A., Pilatti, A., Mezquita, L., Keough, M. T., and Hogarth, L. (2021). Young adult concurrent use and simultaneous use of alcohol and marijuana: a cross-national examination among college students in seven countries. *Addict. Behav. Rep.* 14:100373. doi: 10.1016/j.abrep.2021.100373

Breit, K. R., Rodriguez, C. G., Lei, A., Hussain, S., and Thomas, J. D. (2022). Effects of prenatal alcohol and delta-9-tetrahydrocannabinol exposure via electronic cigarettes on motor development. *Alcohol Clin. Exp. Res.* 46, 1408–1422. doi: 10.1111/acer.14892

Breit, K. R., Rodriguez, C. G., Lei, A., and Thomas, J. D. (2020). Combined vapor exposure to THC and alcohol in pregnant rats: maternal outcomes and pharmacokinetic effects. *Neurotoxicol. Teratol.* 82:106930. doi: 10.1016/j.ntt.2020.106930

Breit, K. R., Zamudio, B., and Thomas, J. D. (2019a). Altered motor development following late gestational alcohol and cannabinoid exposure in rats. *Neurotoxicol. Teratol.* 73, 31–41. doi: 10.1016/j.ntt.2019.03.005

Breit, K. R., Zamudio, B., and Thomas, J. D. (2019b). The effects of alcohol and cannabinoid exposure during the brain growth spurt on behavioral development in rats. *Birth Defects Res.* 111, 760–774. doi: 10.1002/bdr2.1487

Castelli, V., Lavanco, G., Feo, S., D'Amico, C., Micale, V., Kuchar, M., et al. (2023). Prenatal exposure to Δ9-tetrahydrocannabinol affects hippocampus-related cognitive functions in the adolescent rat offspring: focus on specific markers of neuroplasticity. *Pharmaceutics* 15:692. doi: 10.3390/pharmaceutics15020692

Castelli, M. P., Paola Piras, A., D'Agostino, A., Pibiri, F., Perra, S., Gessa, G. L., et al. (2007). Dysregulation of the endogenous cannabinoid system in adult rats prenatally treated with the cannabinoid agonist WIN 55,212-2. *Eur. J. Pharmacol.* 573, 11–19. doi: 10.1016/j.ejphar.2007.06.047

Chandler, L. S., Richardson, G. A., Gallagher, J. D., and Day, N. L. (1996). Prenatal exposure to alcohol and marijuana: effects on motor development of preschool children. *Alcohol Clin. Experiment. Res.* 20, 455–461. doi: 10.1111/j.1530-0277.1996.tb01075.x

Chetty-Mhlanga, S., Viglietti, P., Röösli, M., and Dalvie, M. A. (2022). Maternal drinking behaviour and co-exposure from smoking during and after pregnancy in relation to the neurocognitive function of school-children in the rural Western cape. *Neurotoxicology* 88, 36–43. doi: 10.1016/j.neuro.2021.10.010

Chiandetti, A., Hernandez, G., Mercadal-Hally, M., Alvarez, A., Andreu-Fernandez, V., Navarro-Tapia, E., et al. (2017). Prevalence of prenatal exposure to substances of abuse: questionnaire versus biomarkers. *Reprod. Health* 14:137. doi: 10.1186/s12978-017-0385-3

Cioffredi, L.-A., Anderson, H., Loso, H., East, J., Nguyen, P., Garavan, H., et al. (2022). Prenatal cannabis exposure predicts attention problems, without changes on fMRI in adolescents. *Neurotoxicol. Teratol.* 91:107089. doi: 10.1016/j.ntt.2022.107089

Crummy, E. A., O'Neal, T. J., Baskin, B. M., and Ferguson, S. M. (2020). One is not enough: understanding and modeling polysubstance use. *Front. Neurosci.* 14:569. doi: 10.3389/fnins.2020.00569

D'Hooge, R., and De Deyn, P. P. (2001). Applications of the Morris water maze in the study of learning and memory. *Brain Res. Rev.* 36, 60–90. doi: 10.1016/S0165-0173(01)00067-4

De Genna, N. M., Willford, J. A., and Richardson, G. A. (2022). Long-term effects of prenatal cannabis exposure: pathways to adolescent and adult outcomes. *Pharmacol. Biochem. Behav.* 214:173358. doi: 10.1016/j.pbb.2022.173358

de Salas-Quiroga, A., Díaz-Alonso, J., García-Rincón, D., Remmers, F., Vega, D., Gómez-Cañas, M., et al. (2015). Prenatal exposure to cannabinoids evokes long-lasting functional alterations by targeting CB1 receptors on developing cortical neurons. *Proc. Natl. Acad. Sci. U. S. A.* 112, 13693–13698. doi: 10.1073/pnas.1514962112

de Salas-Quiroga, A., García-Rincón, D., Gómez-Domínguez, D., Valero, M., Simón-Sánchez, S., Paraíso-Luna, J., et al. (2020). Long-term hippocampal interneuronopathy drives sex-dimorphic spatial memory impairment induced by prenatal THC exposure. *Neuropsychopharmacology* 45, 877–886. doi: 10.1038/s41386-020-0621-3

Dobbing, J., and Sands, J. (1979). Comparative aspects of the brain growth spurt. *Early Hum. Dev.* 3, 79–83. doi: 10.1016/0378-3782(79)90022-7

Dodge, N. C., Thomas, K. G. F., Meintjes, E. M., Molteno, C. D., Jacobson, J. L., and Jacobson, S. W. (2019). Spatial navigation in children and young adults with fetal alcohol spectrum disorders. *Alcohol. Clin. Exp. Res.* 43, 2536–2546. doi: 10.1111/acer.14210

Dodge, N. C., Thomas, K. G. F., Meintjes, E. M., Molteno, C. D., Jacobson, J. L., and Jacobson, S. W. (2020). Reduced hippocampal volumes partially mediate effects of prenatal alcohol exposure on spatial navigation on a virtual water maze task in children. *Alcohol Clin. Experiment. Res.* 44, 844–855. doi: 10.1111/acer.14310

Eiden, R. D., Zhao, J., Casey, M., Shisler, S., Schuetze, P., and Colder, C. R. (2018). Pre- and postnatal tobacco and cannabis exposure and child behavior problems: bidirectional associations, joint effects, and sex differences. *Drug Alcohol Depend.* 185, 82–92. doi: 10.1016/j.drugalcdep.2017.11.038

England, L. J. (2020). Alcohol use and co-use of other substances among pregnant females aged 12–44 years — United States, 2015–2018. *MMWR Morb. Mortal. Wkly Rep.* 69, 1009–1014. doi: 10.15585/mmwr.mm6931a1

Finer, L. B., and Zolna, M. R. (2016). Declines in unintended pregnancy in the United States, 2008–2011. *N. Engl. J. Med.* 374, 843–852. doi: 10.1056/NEJMsa1506575

Fish, E. W., Murdaugh, L. B., Zhang, C., Boschen, K. E., Boa-Amponsem, O., Mendoza-Romero, H. N., et al. (2019). Cannabinoids exacerbate alcohol teratogenesis by a CB1-hedgehog interaction. *Sci. Rep.* 9:16057. doi: 10.1038/s41598-019-52336-w

Fontaine, C. J., Patten, A. R., Sickmann, H. M., Helfer, J. L., and Christie, B. R. (2016). Effects of pre-natal alcohol exposure on hippocampal synaptic plasticity: sex, age and methodological considerations. *Neurosci. Biobehav. Rev.* 64, 12–34. doi: 10.1016/j.neubiorev.2016.02.014

Forray, A. (2016). Substance use during pregnancy. *F1000Res* 5:887. doi: 10.12688/f1000research.7645.1

Fried, P. A., and Watkinson, B. (1990). 36- and 48-month neurobehavioral follow-up of children prenatally exposed to marijuana, cigarettes, and alcohol. *J. Dev. Behav. Pediatr.* 11, 49–58. doi: 10.1097/00004703-199004000-00003

Giroud, C., de Cesare, M., Berthet, A., Varlet, V., Concha-Lozano, N., and Favrat, B. (2015). E-cigarettes: a review of new trends in cannabis use. *Int. J. Environ. Res. Public Health* 12, 9988–10008. doi: 10.3390/ijerph120809988

Goldschmidt, L., Richardson, G. A., Cornelius, M. D., and Day, N. L. (2004). Prenatal marijuana and alcohol exposure and academic achievement at age 10. *Neurotoxicol. Teratol.* 26, 521–532. doi: 10.1016/j.ntt.2004.04.003

Gonçalves, P. D., Levy, N. S., Segura, L. E., Bruzelius, E., Boustead, A. E., Hasin, D. S., et al. (2022). Cannabis recreational legalization and prevalence of simultaneous cannabis and alcohol use in the United States. *J. Gen. Intern. Med.* 38, 1493–1500. doi: 10.1007/s11606-022-07948-w

Gosdin, L. K. (2022). Alcohol consumption and binge drinking during pregnancy among adults aged 18–49 years — United States, 2018–2020. *MMWR Morb. Mortal. Wkly Rep.* 71, 10–13. doi: 10.15585/mmwr.mm7101a2

Grant, K. S., Conover, E., and Chambers, C. D. (2020). Update on the developmental consequences of cannabis use during pregnancy and lactation. *Birth Defects Res.* 112, 1126–1138. doi: 10.1002/bdr2.1766

Gursky, Z. H., Savage, L. M., and Klintsova, A. Y. (2021). Executive functioning-specific behavioral impairments in a rat model of human third trimester binge drinking implicate prefrontal-thalamo-hippocampal circuitry in fetal alcohol Spectrum disorders. *Behav. Brain Res.* 405:113208. doi: 10.1016/j.bbr.2021.113208

Hansen, H. H., Krutz, B., Sifringer, M., Stefovska, V., Bittigau, P., Pragst, F., et al. (2008). Cannabinoids enhance susceptibility of immature brain to ethanol neurotoxicity. *Ann. Neurol.* 64, 42–52. doi: 10.1002/ana.21287

Hartman, R. L., Brown, T. L., Milavetz, G., Spurgin, A., Gorelick, D. A., Gaffney, G., et al. (2015). Controlled cannabis vaporizer administration: blood and plasma cannabinoids with and without alcohol. *Clin. Chem.* 61, 850–869. doi: 10.1373/clinchem.2015.238287

Hartman, R. L., Brown, T. L., Milavetz, G., Spurgin, A., Gorelick, D. A., Gaffney, G., et al. (2016). Controlled vaporized cannabis, with and without alcohol: subjective effects and oral fluid-blood cannabinoid relationships. *Drug Test. Anal.* 8, 690–701. doi: 10.1002/dta.1839

Huizink, A. C. (2014). Prenatal cannabis exposure and infant outcomes: overview of studies. *Prog. Neuro-Psychopharmacol. Biol. Psychiatry* 52, 45–52. doi: 10.1016/j.pnpbp.2013.09.014

Hungund, B. L. (2017). Drinking during pregnancy: potential role of endocannabinoid signaling in fetal alcohol effects. *World J. Neurol.* 7, 1–5. doi: 10.5316/wjn.v7.i1.1

Jackson, K. M., Sokolovsky, A. W., Gunn, R. L., and White, H. R. (2020). Consequences of alcohol and marijuana use among college students: prevalence rates and attributions to substance-specific versus simultaneous use. *Psychol. Addict. Behav.* 34, 370–381. doi: 10.1037/adb0000545

Kahr, M. K., Padgett, S., Shope, C. D., Griffin, E. N., Xie, S. S., Gonzalez, P. J., et al. (2015). A qualitative assessment of the perceived risks of electronic cigarette and hookah use in pregnancy. *BMC Public Health* 15:1273. doi: 10.1186/s12889-015-2586-4

Kodituwakku, P. W., Handmaker, N. S., Cutler, S. K., Weathersby, E. K., and Handmaker, S. D. (1995). Specific impairments in self-regulation in children exposed to alcohol prenatally. *Alcohol. Clin. Exp. Res.* 19, 1558–1564. doi: 10.1111/j.1530-0277.1995.tb01024.x

Lallai, V., Manca, L., Sherafat, Y., and Fowler, C. D. (2022). Effects of prenatal nicotine, THC or co-exposure on cognitive behaviors in adolescent male and female rats. *Nicotine Tob. Res.* 24, 1150–1160. doi: 10.1093/ntr/ntac018

Lee, C. M., Calhoun, B. H., Abdallah, D. A., Blayney, J. A., Schultz, N. R., Brunner, M., et al. (2022). Simultaneous alcohol and marijuana use among young adults: a scoping review of prevalence, patterns, psychosocial correlates, and consequences. *Alcohol Res.* 42:8. doi: 10.35946/arcr.v42.1.08

Leech, S. L., Larkby, C. A., Day, R., and Day, N. L. (2006). Predictors and correlates of high levels of depression and anxiety symptoms among children at age 10. *J. Am. Acad. Child Adolesc. Psychiatry* 45, 223–230. doi: 10.1097/01.chi.0000184930.18552.4d

Lei, A. (2022). *The effects of combined prenatal alcohol and cannabis vapor exposure on spatial learning*. [Master's thesis, San Diego State University]. SDSU Theses and Dissertations. Available at: https://digitallibrary.sdsu.edu/islandora/object/sdsu%3A200242

Levy, D. R., Hunter, N., Lin, S., Robinson, E. M., Gillis, W., Conlin, E. B., et al. (2023). Mouse spontaneous behavior reflects individual variation rather than estrous state. *Curr. Biol.* 33, 1358–1364.e4. doi: 10.1016/j.cub.2023.02.035

Lewis, C. E., Thomas, K. G. F., Ofen, N., Warton, C. M. R., Robertson, F., Lindinger, N. M., et al. (2021). An fMRI investigation of neural activation predicting memory formation in children with fetal alcohol spectrum disorders. *NeuroImage: Clinical* 30:102532. doi: 10.1016/j.nicl.2020.102532

Little, B., Sud, N., Nobile, Z., and Bhattacharya, D. (2021). Teratogenic effects of maternal drug abuse on developing brain and underlying neurotransmitter mechanisms. *Neurotoxicology* 86, 172–179. doi: 10.1016/j.neuro.2021.08.007

Lucia, D., Burgess, D., Cullen, C. L., Dorey, E. S., Rawashdeh, O., and Moritz, K. M. (2019). Periconceptional maternal alcohol consumption leads to behavioural changes in adult and aged offspring and alters the expression of hippocampal genes associated with learning and memory and regulators of the epigenome. *Behav. Brain Res.* 362, 249–257. doi: 10.1016/j.bbr.2019.01.009

Mahdinia, R., Goudarzi, I., Lashkarbolouki, T., and Salmani, M. E. (2021). Vitamin E attenuates alterations in learning, memory and BDNF levels caused by perinatal ethanol exposure. *Nutr. Neurosci.* 24, 747–761. doi: 10.1080/1028415X.2019.1674523

Manduca, A., Servadio, M., Melancia, F., Schiavi, S., Manzoni, O. J., and Trezza, V. (2020). Sex-specific behavioural deficits induced at early life by prenatal exposure to the cannabinoid receptor agonist WIN55, 212-2 depend on mGlu5 receptor signalling. *Br. J. Pharmacol.* 177, 449–463. doi: 10.1111/bph.14879

Mattson, S. N., Bernes, G. A., and Doyle, L. R. (2019). Fetal alcohol spectrum disorders: a review of the neurobehavioral deficits associated with prenatal alcohol exposure. *Alcohol Clin. Experiment. Res.* 43, 1046–1062. doi: 10.1111/acer.14040

May, P. A., Chambers, C. D., Kalberg, W. O., Zellner, J., Feldman, H., Buckley, D., et al. (2018). Prevalence of fetal alcohol spectrum disorders in 4 US communities. *JAMA* 319, 474–482. doi: 10.1001/jama.2017.21896

May, P. A., Gossage, J. P., Kalberg, W. O., Robinson, L. K., Buckley, D., Manning, M., et al. (2009). Prevalence and epidemiologic characteristics of FASD from various research methods with an emphasis on recent in-school studies. *Dev. Disabil. Res. Rev.* 15, 176–192. doi: 10.1002/ddrr.68

McLachlan, K., Flannigan, K., Temple, V., Unsworth, K., and Cook, J. L. (2020). Difficulties in daily living experienced by adolescents, transition-aged youth, and adults with fetal alcohol spectrum disorder. *Alcohol Clin. Experiment. Res.* 44, 1609–1624. doi: 10.1111/acer.14385

Moore, E. M., Glass, L., Infante, M. A., Coles, C. D., Kable, J. A., Jones, K. L., et al. (2021). Cross-sectional analysis of spatial working memory development in children with histories of heavy prenatal alcohol exposure. *Alcohol Clin. Experiment. Res.* 45, 215–223. doi: 10.1111/acer.14506

Moradpour, F., Naghdi, N., Fathollahi, Y., Javan, M., Choopani, S., and Gharaylou, Z. (2013). Pre-pubertal castration improves spatial learning during mid-adolescence in rats. *Prog. Neuro Psychopharmacol. Biol. Psychiatry* 46, 105–112. doi: 10.1016/j.pnpbp.2013.07.005

Morterá, P., and Herculano-Houzel, S. (2012). Age-related neuronal loss in the rat brain starts at the end of adolescence. *Front. Neuroanat.* 6:45. doi: 10.3389/fnana.2012.00045

Muñoz-Villegas, P., Rodríguez, V. M., Giordano, M., and Juárez, J. (2017). Risk-taking, locomotor activity and dopamine levels in the nucleus accumbens and medial prefrontal cortex in male rats treated prenatally with alcohol. *Pharmacol. Biochem. Behav.* 153, 88–96. doi: 10.1016/j.pbb.2016.12.011

Murnan, A. W., Keim, S. A., Yeates, K. O., Boone, K. M., Sheppard, K. W., and Klebanoff, M. A. (2021). Behavioral and cognitive differences in early childhood related to prenatal marijuana exposure. *J. Appl. Dev. Psychol.* 77:101348. doi: 10.1016/j.appdev.2021.101348

Nagre, N. N., Subbanna, S., Shivakumar, M., Psychoyos, D., and Basavarajappa, B. S. (2015). CB1-receptor knockout neonatal mice are protected against ethanol-induced impairments of DNMT1, DNMT3A, and DNA methylation. *J. Neurochem.* 132, 429–442. doi: 10.1111/jnc.13006

Navarrete, F., García-Gutiérrez, M. S., Gasparyan, A., Austrich-Olivares, A., Femenía, T., and Manzanares, J. (2020). Cannabis use in pregnant and breastfeeding women: behavioral and neurobiological consequences. *Front. Psych.* 11:586447. doi: 10.3389/fpsyt.2020.586447

O'Leary, C. M., Nassar, N., Zubrick, S. R., Kurinczuk, J. J., Stanley, F., and Bower, C. (2010). Evidence of a complex association between dose, pattern and timing of prenatal alcohol exposure and child behaviour problems. *Addiction* 105, 74–86. doi: 10.1111/j.1360-0443.2009.02756.x

Odom, G. C., Cottler, L. B., Striley, C. W., and Lopez-Quintero, C. (2020). Perceived risk of weekly cannabis use, past 30-Day cannabis use, and frequency of cannabis use among pregnant women in the United States. *IJWH* 12, 1075–1088. doi: 10.2147/IJWH.S266540

Patten, A. R., Fontaine, C. J., and Christie, B. R. (2014). A comparison of the different animal models of fetal alcohol spectrum disorders and their use in studying complex behaviors. *Front. Pediatr.* 2:93. doi: 10.3389/fped.2014.00093

Pinky, P. D., Bloemer, J., Smith, W. D., Moore, T., Hong, H., Suppiramaniam, V., et al. (2019). Prenatal cannabinoid exposure and altered neurotransmission. *Neuropharmacology* 149, 181–194. doi: 10.1016/j.neuropharm.2019.02.018

Reid, H. M. O., Snowden, T. M., Shkolnikov, I., Breit, K. R., Rodriguez, C., Thomas, J. D., et al. (2021). Prenatal alcohol and cannabis exposure can have opposing and region-specific effects on parvalbumin interneuron numbers in the hippocampus. *Alcohol. Clin. Exp. Res.* 45, 2246–2255. doi: 10.1111/acer.14708

Richardson, G., Day, N. L., and Goldschmidt, L. (1995). Prenatal alcohol, marijuana, and tobacco use: infant mental and motor development. *Neurotoxicol. Teratol.* 17, 479–487. doi: 10.1016/0892-0362(95)00006-D

Richardson, K., Hester, A. K., and McLemore, G. L. (2016). Prenatal cannabis exposure – the "first hit" to the endocannabinoid system. *Neurotoxicol. Teratol.* 58, 5–14. doi: 10.1016/j.ntt.2016.08.003

Richardson, G., Ryan, C., Willford, J., Day, N. L., and Goldschmidt, L. (2002). Prenatal alcohol and marijuana exposure: effects on neuropsychological outcomes at 10 years. *Neurotoxicol. Teratol.* 24, 309–320. doi: 10.1016/S0892-0362(02)00193-9

Rodrigues, R. S., Ribeiro, F. F., Ferreira, F., Vaz, S. H., Sebastião, A. M., and Xapelli, S. (2017). Interaction between cannabinoid type 1 and type 2 receptors in the modulation of subventricular zone and dentate Gyrus neurogenesis. *Front. Pharmacol.* 8:516. doi: 10.3389/fphar.2017.00516

Ryan, S. H., Williams, J. K., and Thomas, J. D. (2008). Choline supplementation attenuates learning deficits associated with neonatal alcohol exposure in the rat: effects of varying the timing of choline administration. *Brain Res.* 1237, 91–100. doi: 10.1016/j.brainres.2008.08.048

Salguero, A., Pilatti, A., Michelini, Y., Rivarola Montejano, G., and Pautassi, R. M. (2022). Factors associated with simultaneous or concurrent use of alcohol and marijuana in Argentina. *Subst. Use Misuse* 57, 1062–1071. doi: 10.1080/10826084.2022.2063895

Schambra, U. B., Lewis, C. N., and Harrison, T. A. (2017). Deficits in spatial learning and memory in adult mice following acute, low or moderate levels of prenatal ethanol exposure during gastrulation or neurulation. *Neurotoxicol. Teratol.* 62, 42–54. doi: 10.1016/j.ntt.2017.05.001

Schneider, R. D., and Thomas, J. D. (2016). Adolescent choline supplementation attenuates working memory deficits in rats exposed to alcohol during the third trimester equivalent. *Alcohol. Clin. Exp. Res.* 40, 897–905. doi: 10.1111/acer.13021

Schulteis, G., Archer, C., Tapert, S. F., and Frank, L. R. (2008). Intermittent binge alcohol exposure during the periadolescent period induces spatial working memory deficits in young adult rats. *Alcohol* 42, 459–467. doi: 10.1016/j.alcohol.2008.05.002

Sharapova, S. R., Phillips, E., Sirocco, K., Kaminski, J. W., Leeb, R. T., and Rolle, I. (2018). Effects of prenatal marijuana exposure on neuropsychological outcomes in children aged 1-11 years: a systematic review. *Paediatr. Perinat. Epidemiol.* 32, 512–532. doi: 10.1111/ppe.12505

Sharma, G., Oden, N., VanVeldhuisen, P. C., and Bogenschutz, M. P. (2016). Hair analysis and its concordance with self-report for drug users presenting in emergency department. *Drug Alcohol Depend.* 167, 149–155. doi: 10.1016/j.drugalcdep.2016.08.007

Silva, L., Zhao, N., Popp, S., and Dow-Edwards, D. (2012). Prenatal Tetrahydrocannabinol (THC) alters cognitive function and amphetamine response from weaning to adulthood in the rat. *Neurotoxicol. Teratol.* 34, 63–71. doi: 10.1016/j.ntt.2011.10.006

Smith, A. M., Mioduszewski, O., Hatchard, T., Byron-Alhassan, A., Fall, C., and Fried, P. A. (2016). Prenatal marijuana exposure impacts executive functioning into young adulthood: an fMRI study. *Neurotoxicol. Teratol.* 58, 53–59. doi: 10.1016/j.ntt.2016.05.010

Spindle, T. R., Cone, E. J., Schlienz, N. J., Mitchell, J. M., Bigelow, G. E., Flegel, R., et al. (2018). Acute effects of smoked and vaporized cannabis in healthy adults who infrequently use cannabis: a crossover trial. *JAMA Netw. Open* 1:e184841. doi: 10.1001/jamanetworkopen.2018.4841

Subbanna, S., Nagre, N. N., Umapathy, N. S., Pace, B. S., and Basavarajappa, B. S. (2015). Ethanol exposure induces neonatal neurodegeneration by enhancing CB1R Exon1 histone H4K8 acetylation and up-regulating CB1R function causing neurobehavioral abnormalities in adult mice. *Int. J. Neuropsychopharmacol.* 18:pyu028. doi: 10.1093/ijnp/pyu028

Subbaraman, M. S., and Kerr, W. C. (2015). Simultaneous versus concurrent use of alcohol and cannabis in the National Alcohol Survey. *Alcohol. Clin. Exp. Res.* 39, 872–879. doi: 10.1111/acer.12698

Substance Abuse and Mental Health Services Administration (2015). *Behavioral health trends in the United States: Results from the 2014 National Survey on drug use and health*. Rockville, MD: Center for Behavioral Health Statistics and Quality.

Szafran, B. N., Pinkston, R., Perveen, Z., Ross, M. K., Morgan, T., Paulsen, D. B., et al. (2020). Electronic-cigarette vehicles and flavoring affect lung function and immune responses in a murine model. *Int. J. Mol. Sci.* 21:6022. doi: 10.3390/ijms21176022

Thomas, J. D., Biane, J. S., O'Bryan, K. A., O'Neill, T. M., and Dominguez, H. D. (2007). Choline supplementation following third-trimester-equivalent alcohol exposure attenuates behavioral alterations in rats. *Behav. Neurosci.* 121, 120–130. doi: 10.1037/0735-7044.121.1.120

Torres, C. A., Medina-Kirchner, C., O'Malley, K. Y., and Hart, C. L. (2020). Totality of the evidence suggests prenatal cannabis exposure does not lead to cognitive impairments: a systematic and critical review. *Front. Psychol.* 11:816. doi: 10.3389/fpsyg.2020.00816

Traccis, F., Serra, V., Sagheddu, C., Congiu, M., Saba, P., Giua, G., et al. (2021). Prenatal THC does not affect female mesolimbic dopaminergic system in preadolescent rats. *Int. J. Mol. Sci.* 22:1666. doi: 10.3390/ijms22041666

Trezza, V., Campolongo, P., Manduca, A., Morena, M., Palmery, M., Vanderschuren, L. J. M. J., et al. (2012). Altering endocannabinoid neurotransmission at critical developmental ages: impact on rodent emotionality and cognitive performance. *Front. Behav. Neurosci.* 6:2. doi: 10.3389/fnbeh.2012.00002

Vorhees, C. V., and Williams, M. T. (2006). Morris water maze: procedures for assessing spatial and related forms of learning and memory. *Nat. Protoc.* 1, 848–858. doi: 10.1038/nprot.2006.116

Waddell, J., Hill, E., Tang, S., Jiang, L., Xu, S., and Mooney, S. M. (2020). Choline plus working memory training improves prenatal alcohol-induced deficits in cognitive flexibility and functional connectivity in adulthood in rats. *Nutrients* 12:3513. doi: 10.3390/nu12113513

Wanner, N. M., Colwell, M., Drown, C., and Faulk, C. (2021). Developmental cannabidiol exposure increases anxiety and modifies genome-wide brain DNA methylation in adult female mice. *Clin. Epigenetics* 13:4. doi: 10.1186/s13148-020-00993-4

Weimar, H. V., Wright, H. R., Warrick, C. R., Brown, A. M., Lugo, J. M., Freels, T. G., et al. (2020). Long-term effects of maternal cannabis vapor exposure on emotional reactivity, social behavior, and behavioral flexibility in offspring. *Neuropharmacology* 179:108288. doi: 10.1016/j.neuropharm.2020.108288

Weinberg, J., Sliwowska, J. H., Lan, N., and Hellemans, K. G. C. (2008). Prenatal alcohol exposure: foetal programming, the hypothalamic-pituitary-adrenal axis and sex differences in outcome. *J. Neuroendocrinol.* 20, 470–488. doi: 10.1111/j.1365-2826.2008.01669.x

Willing, J., Drzewiecki, C. M., Cuenod, B. A., Cortes, L. R., and Juraska, J. M. (2016). A role for puberty in water maze performance in male and female rats. *Behav. Neurosci.* 130, 422–427. doi: 10.1037/bne0000145

frontiers | Frontiers in Neuroscience

TYPE Review
PUBLISHED 15 June 2023
DOI 10.3389/fnins.2023.1182635

Check for updates

OPEN ACCESS

EDITED BY
Hermes H. Yeh,
Dartmouth College, United States

REVIEWED BY
Marina Guizzetti,
Oregon Health and Science University, United States
Verginia Cuzon Carlson,
Oregon Health and Science University, United States

*CORRESPONDENCE
Amanda H. Mahnke
✉ mahnke@tamu.edu

†These authors have contributed equally to this work

RECEIVED 09 March 2023
ACCEPTED 23 May 2023
PUBLISHED 15 June 2023

CITATION
Upreti D, Rouzer SK, Bowring A, Labbe E, Kumar R, Miranda RC and Mahnke AH (2023) Microbiota and nutrition as risk and resiliency factors following prenatal alcohol exposure. *Front. Neurosci.* 17:1182635. doi: 10.3389/fnins.2023.1182635

COPYRIGHT
© 2023 Upreti, Rouzer, Bowring, Labbe, Kumar, Miranda and Mahnke. This is an open-access article distributed under the terms of the Creative Commons Attribution License (CC BY). The use, distribution or reproduction in other forums is permitted, provided the original author(s) and the copyright owner(s) are credited and that the original publication in this journal is cited, in accordance with accepted academic practice. No use, distribution or reproduction is permitted which does not comply with these terms.

Microbiota and nutrition as risk and resiliency factors following prenatal alcohol exposure

Deepa Upreti†, Siara K. Rouzer†, Abigail Bowring, Emma Labbe, Rosaline Kumar, Rajesh C. Miranda and Amanda H. Mahnke*

Department of Neuroscience and Experimental Therapeutics, Texas A&M University School of Medicine, Bryan, TX, United States

Alcohol exposure in adulthood can result in inflammation, malnutrition, and altered gastroenteric microbiota, which may disrupt efficient nutrient extraction. Clinical and preclinical studies have documented convincingly that prenatal alcohol exposure (PAE) also results in persistent inflammation and nutrition deficiencies, though research on the impact of PAE on the enteric microbiota is in its infancy. Importantly, other neurodevelopmental disorders, including autism spectrum and attention deficit/hyperactivity disorders, have been linked to gut microbiota dysbiosis. The combined evidence from alcohol exposure in adulthood and from other neurodevelopmental disorders supports the hypothesis that gut microbiota dysbiosis is likely an etiological feature that contributes to negative developmental, including neurodevelopmental, consequences of PAE and results in fetal alcohol spectrum disorders. Here, we highlight published data that support a role for gut microbiota in healthy development and explore the implication of these studies for the role of altered microbiota in the lifelong health consequences of PAE.

KEYWORDS

nutrition, gut-brain axis, gut microbiota, ethanol, FASD, non-protein-coding RNA, extracellular vesicles

1. Introduction

Alcohol use is common among adults of reproductive age, and moreover, as with other psychotropic drugs, alcohol can be addictive and abstention aversive. In 2020 it was estimated that 60.7% of young adults (ages 18–25) and 55.1% of adults (26 years of age or older) consumed alcohol within the last month, with 44.4% of all alcohol consumers engaging in binge drinking (Substance Abuse and Mental Health Services Administration, 2021). Alongside these high rates of alcohol use in individuals of child-bearing age, the United States also has high rates of unintended pregnancy. Data from 2008 to 2011 show that for individuals between the ages of 18–29 years, i.e., the peak reproductive years, between 66 and 81% of all pregnancies are unintended (Finer and Zolna, 2016). More recent estimates, from the Center for Disease Control's Pregnancy Risk Assessment Monitoring System 2020 data, indicated that 28.5% of pregnancies resulting in live births were unintended (America's Health Rankings, 2023), which is comparable to the 22% of live births occurring from unintended pregnancies from the 2008–2011 dataset (Finer and Zolna, 2016). Rates of unintended pregnancy can vary widely across states, ranging from 19.4 to 41.0% of live births (America's Health Rankings, 2023). These data collectively suggest that pregnancy awareness varies, particularly during early pregnancy and peak reproductive years, when alcohol use occurs at the highest rates, resulting in the common

occurrence of prenatal alcohol exposure (PAE). Several North American state-wide assessments of alcohol metabolites in neonatal blood (Bakhireva et al., 2017; Umer et al., 2020; DiBattista et al., 2022), indicate that between 8 and 15% of infants in the general population are exposed to alcohol in the last month of pregnancy. Binge alcohol exposures, the pattern of drinking for almost half of alcohol consumers, can be particularly harmful for *in utero* fetal development (Bonthius and West, 1990), although cessation of this drinking pattern can be moderately protective against negative neurobehavioral outcomes compared to consumption throughout pregnancy, even at low, albeit sustained, levels (Bandoli et al., 2022). Therefore, it is not surprising that fetal alcohol spectrum disorders (FASDs), the collection of neurodevelopmental and growth deficits that can occur following PAE (Popova et al., 2023), are prevalent, occurring in a conservatively estimated 1.1–5% (weighted estimate of 3.1–9.9%) of school-aged children in the United States (May et al., 2018). The implications are that PAE constitutes a health risk factor for up to 1 in 10 of all US children and adults.

While the neurodevelopmental impacts of PAE have historically been well studied, there are also a large number of co-morbid conditions that can also occur, as has been shown by a systematic review with meta-analysis (Popova et al., 2016) and by a self-report survey of adults with FASDs (Himmelreich et al., 2020). Not all individuals with FASDs will develop these co-morbidities nor will all individuals with PAE develop a FASD. Preclinical research has shown that multiple factors, including nutrition, genetics, stress, and the timing of alcohol exposure during pregnancy (Petrelli et al., 2018), can confer risk or resiliency to the negative consequence of PAE. Critically, for other neurodevelopmental disorders, microbiota have been shown to not only be at the intersection of a number of these risk/resiliency factors, but also directly contribute to neurodevelopment through the gut-brain axis and, potentially, through the placenta-brain axis. Here, we provide a framework for the potential role of microbiota as a risk/resiliency factor following PAE, by integrating the literature on the known impacts of PAE on nutritional insufficiencies and microbiota with the more robust findings for the role of microbiota in other neurodevelopmental disorders. We also extrapolate what alterations to microbiota could mean for plasma biomarkers/mediators of PAE's effects, long-term health for individuals with FASDs, and the therapeutic potential of targeting PAE-induced alterations to microbiota (Figure 1).

2. Microbiota and the developing brain

2.1. Gut microbiota

The microbiome is the genomic content of the community of microbes, known as the microbiota, that colonize human body surfaces, such as the skin, respiratory tract, genitourinary tract, and gastrointestinal tract. The gastrointestinal tract is extensively colonized with microbiota, with human gut flora estimated to contain greater than 10^{13} microbial cells, resulting in approximately a 1:1 microbial: human cell ratio (reviewed in Sender et al., 2016). Gut microbiota are predominantly bacteria, but also include archaea, viruses, and unicellular eukaryotes (reviewed in Sender et al., 2016; Thursby and Juge, 2017). Bacteria belonging to the Firmicutes and Bacteroidetes phyla make up the majority of the gut bacteria, whereas other phyla that are present in minor proportions include, but are not limited to, Fusobacteria, Verrucomicrobia, Proteobacteria, and Actinobacteria (reviewed in Sekirov et al., 2010).

The human gut microbiota is shaped by early life events such as the delivery method (vaginal delivery vs. cesarean section), maternal use of antibiotics, and feeding modality, e.g., breast-, formula-, or mixed-feeding (Niu et al., 2020). In a study that examined fecal microbial content from individuals across the lifespan (0–70 years of age) in three geographically, culturally, and nutritionally distinct communities, individuals ≤3 years of age had the greatest interindividual microbial variability (Yatsunenko et al., 2012). The adults in this study had less interindividual and intercommunity variability than the ≤3 years of age group. The intercommunity variability identified in this study was attributed to differences in nutrition, as the microbial content for the community with a predominantly carnivorous diet could be statistically segregated from the other two communities with predominantly herbivorous diets. A recent study has shown that for adults, microbial content can be stable over time (Frost et al., 2021). When microbial content was assessed from matched fecal samples, acquired at a median interval of 5 years, the three most abundant genera, *Bacteroides*, *Prevotella,* and *Faecalibacterium*, were maintained across this ~5 year time span. Variability in microbiota was almost entirely attributable to interpersonal differences, with intraindividual variability across the time span associated with the development of metabolic disorders. For adults, dietary changes can be a potent modifier of gut microbiota. For healthy adults administered a controlled high-fat/low-fiber or low-fat/high-fiber diet, although interindividual differences were the largest contributor to microbiota variability, all subjects showed a change in microbial content within the first 24 h (Wu et al., 2011). Similarly, 5 days of an animal product-based diet, labeled with a food-tracking dye, increased microbiome diversity within 24 h of the diet reaching the distal gut compared to baseline microbiome diversity (David et al., 2014). This effect was not seen with a plant-based diet. Additionally, the increase in microbiome diversity from the animal product-based diet was normalized 2 days after returning to their normal diet. Therefore, gut microbiota can stabilize across the lifespan but are sensitive to alterations due to dietary and physiological changes, suggesting that gut microbiota can be targeted for rapid intervention.

2.2. Gut-brain axis

The gut-brain axis is a complex bidirectional communication network between gut microbiota and the central nervous system. For example, through the autonomic nervous system signaling, the central nervous system can affect gut motility and secretion of bile and mucous, which can alter microbial colonization in the gut. Reciprocally, gut microbiota can shape human health through the production and release of metabolites into human circulation, impacting metabolic, immune, and neuroendocrine networks (Rhee et al., 2009).

Metabolic products released by gut microbiota include short-chain fatty acids (SCFAs), indole derivatives, choline metabolites, polyamines, and lipopolysaccharides (reviewed in Anand and Mande, 2018). SCFAs, such as acetate, propionate, and butyrate, are the major metabolic products of gut microbial anerobic fermentation. They can enter gut endothelial cells or actively be transported across the basement membrane to blood capillaries and into circulation

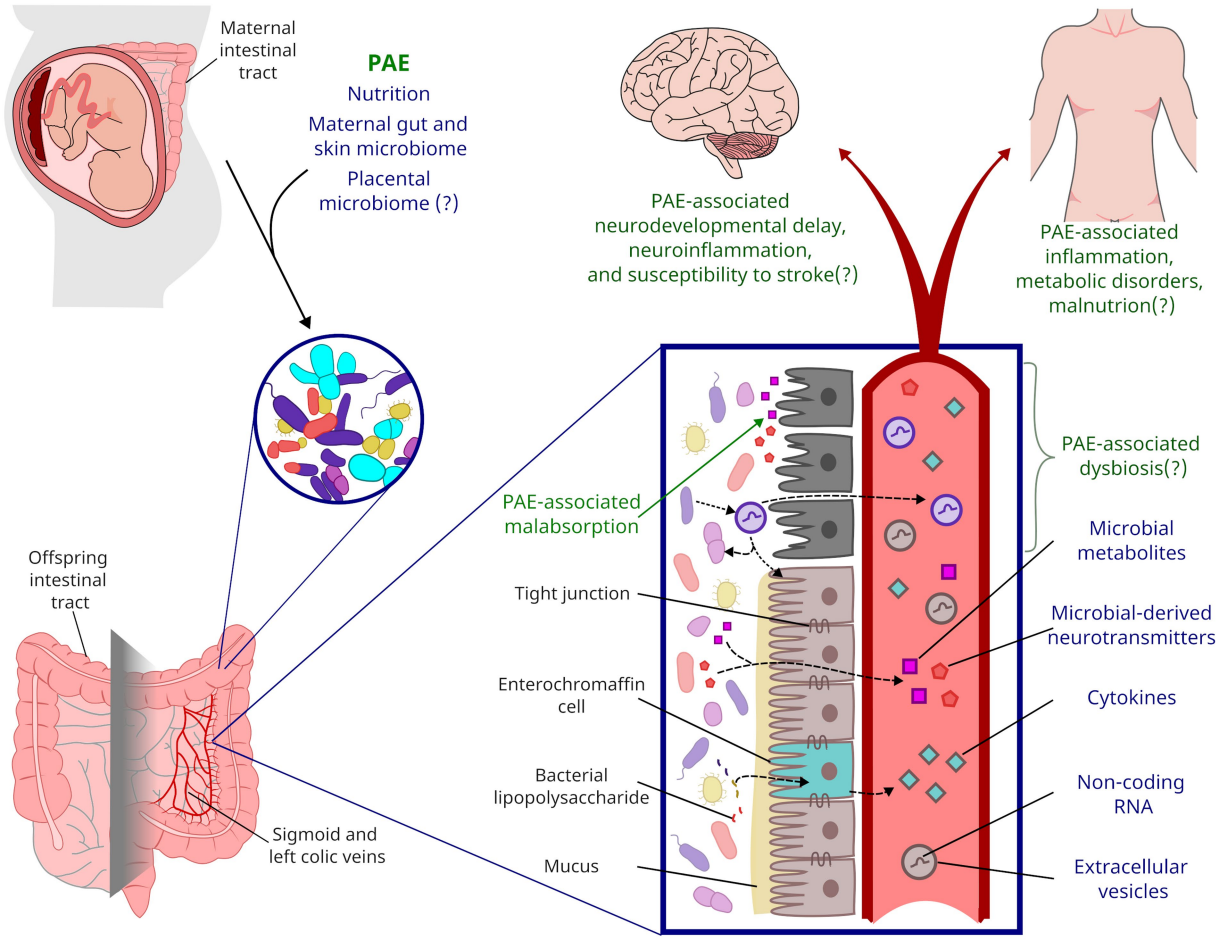


FIGURE 1
Framework for the life-long impact of PAE on gut microbiota. During parturition, a neonate's gastrointestinal microbiota is colonized from maternal sources. PAE likely shapes the neonatal microbiome through alcohol's impacts on maternal microbiota and nutrient absorption. PAE has been shown to impact microbial metabolites present in offspring circulation, but PAE may also impact inflammation and other endocrine factors through altered microbiota and gut function. Affectors and effectors of changes to microbiota discussed in this review are indicated by blue text while the potential life-long consequences of PAE are indicated by green text.

(reviewed in van der Hee and Wells, 2021). A number of bacteria can also produce a range of mammalian neurotransmitters (reviewed in Strandwitz, 2018), release tryptophan and other indole derivatives that promote synthesis of neurotransmitters and neuropeptides by the endocrine enterochromaffin cells (reviewed in Gao et al., 2020). Microbiota also release byproducts, such as polyamines and lipopolysaccharides, that impact immune function both within the gut and throughout the body through the release of cytokines both by enterochromaffin cells and resident intestinal immune cells (Zheng et al., 2020).

The products released by microbiota can have systemic effects, including in the central nervous system, through multiple pathways. Microbiota-released SCFAs, as well as neurotransmitters and peptides synthesized by the endocrine enterochromaffin cells, can signal through G-protein coupled receptors on a variety of cells, including vagal nerve afferents (reviewed in Husted et al., 2017; van der Hee and Wells, 2021). This signaling through the vagal nerve can directly impact brain chemistry and neurobehavioral outcomes (Bravo et al., 2011; Goswami et al., 2018). Additionally, along with cytokines made by the local immune and endocrine cell populations, SCFAs can act as endocrine factors, signaling systemically in the host (Cryan and Dinan, 2012). Materials released by microbiota can cross the blood brain barrier, including extracellular vesicles (see 5.2, Cuesta et al., 2021) and some metabolites (reviewed by Cryan and Dinan, 2012; e.g. Needham et al., 2022). Gut microbiota can also alter blood brain barrier integrity, thereby making the brain more (or less) susceptible to microbial metabolites. In a germ-free mouse model, which has normally-occurring blood brain barrier permeability, colonization with SCFA-producing bacteria improved blood brain barrier integrity (Braniste et al., 2014). Therefore, not only can secreted factors from microbiota act peripherally to impact brain function, but some can also cross the blood brain barrier to act directly on the CNS.

Gut microbiota metabolites can also impact host gene expression through epigenetic mechanisms. Butyrate can inhibit histone deacetylase, thereby promoting histone acetylation and subsequent chromatin relaxation and gene expression (reviewed in Stilling et al., 2016). A recent clinical study found that reduced amounts of fecal butyrate, and butyrate-producing bacteria, were associated with increased depression symptoms in individuals with Parkinson's disease (Xie et al., 2022). This study also identified leukocyte genes

whose methylation correlated with fecal butyrate levels in patients. To connect these butyrate-associated changes in peripheral methylation to changes within the brain, the researchers compared the identified leukocyte genes to previous work that identified genes with altered methylation in prefrontal cortical neurons (Li et al., 2020). They found significant overlap and correlated likelihood of methylation in Parkinson's disease patients for the leukocyte and neuronal genes, suggesting the potential for decreased butyrate levels to contribute to neurological changes through effects on brain DNA methylation (Xie et al., 2022). Choline is a dietary source of one-carbon units for DNA methylation. Gut microbiota can decrease choline bioavailability by metabolizing choline. When germ-free mice were colonized with *Escherichia coli* that use choline as a nutrition source, serum choline levels and DNA methylation were decreased, even with high choline supplementation in the diet (Romano et al., 2017). These choline-deficit mice also exhibited elevated markers of metabolic disorders, e.g., serum and live triglycerides (for choline deficits following PAE, see 4.1.2.1). Additionally, as discussed below (see 5.3.2), microbiota-derived extracellular vesicles can carry small RNA molecules that can potentially act like long-non-coding RNAs in recipient cells to impact gene expression.

2.3. Placenta-brain axis

Appropriate placental development and function is critical for fetal development and, ultimately, for the offspring's long-term health. The placenta exchanges nutrients, gasses, and waste between the mother and the fetus, in addition to producing the hormones needed to support the fetus and maintain pregnancy (Godfrey, 2002). The placenta can also directly contribute to neurodevelopment by placental release of neurotransmitters including norepinephrine/epinephrine, dopamine, and serotonin, a relationship termed the "placenta-brain-axis" (Hodyl et al., 2017; Rosenfeld, 2021). Disturbances or pathophysiological shifts in placenta, and therefore *in utero* environment, can contribute to a variety of neurological disorders (Mir et al., 2021; Gardella et al., 2022; Parenti et al., 2022; Williams and LaSalle, 2022). For example, an analysis of the placental metabolome at birth following prenatal exposure to the teratogen phthalate revealed a correlation between the placental metabolome and ASD-associated neurodevelopmental outcomes in male, but not female, children (Parenti et al., 2022).

A controversial component of the placenta-brain axis is the possibility that the placenta also supports microbiota. Contrary to the dominant conceptual model that the uterus is free from pathogens (Blaser et al., 2021) and that the microbial colonization begins only during delivery, several studies have suggested the infant microbiome is initially colonized in fetal life, through vertical transmission by the uterus of maternal microbiota through the placenta, and subsequently amniotic fluid (Collado et al., 2016). Early studies demonstrated the presence of bacterial communities in the placenta and documented their impact on pregnancy outcomes and fetal health (Fardini et al., 2010; Stout et al., 2013; Aagaard et al., 2014; Collado et al., 2016). Placental colonization includes both commensal and pathogenic bacteria from the vaginotropic non-infectious microflora, oral cavity, and maternal intestinal lumen, likely *via* translocation through maternal circulation (Aagaard et al., 2014; Bangma et al., 2021). Pathogenic microbes' invasion in the uterine environment, specifically within the placenta, has been linked with premature birth, epigenetic changes in the placenta and other tissues, and adverse neurological effects during fetal brain development and later in life (Goldenberg et al., 2000; Tomlinson et al., 2019, 2020). Microorganism invasion in the placenta has been suggested to disrupt fetal brain development through the activation of inflammatory pathways by bacteria-related pathogen associated molecular patterns and by changing placental function through epigenetic changes, such as placental DNA methylation (Tomlinson et al., 2019, 2020). However, it should be noted that the presence of fetal placental microbiota is not settled science, and some researchers have suggested that technical sources of contamination may have contributed to faulty study outcomes (Theis et al., 2019; Blaser et al., 2021; Sterpu et al., 2021). As the occurrence of placental microbiota is still controversial, additional studies in this field and analyses of placental microbial metabolites are required to fully understand the placental microbiota's contribution to the placenta-brain axis.

2.4. Impact of maternal microbiota on neonatal colonization

In addition to the vertical transmission, i.e., direct colonization of the neonate's gastrointestinal (GI) tract by maternal microbiota during delivery, environmental factors can significantly shape GI colonization during the neonatal period. These environmental factors include method of delivery, breastfeeding, prematurity, antibiotic exposure, maternal infection, and stress (Khan et al., 2016; Kalbermatter et al., 2021; Bolte et al., 2022; Miko et al., 2022). For example, vaginal deliveries transmit particular family-specific strains, and higher numbers of bacteria, to the neonate's gut in comparison to cesarian section (Makino et al., 2013; Rutayisire et al., 2016; Kim et al., 2020). In a preclinical study on the impact of maternal stress on offspring microbiota and neurodevelopment, maternal stress decreased both vaginal *Lactobacillus* in pregnant mouse dams and decreased *Lactobacillus* colonization in the offspring (Jašarević et al., 2015). Additionally, the effects of early bacterial colonization of the neonate can be long-lived, even if the bacterial colonization is subsequently normalized. For instance, in one study, cesarean-delivered pathogen-free mouse pups were exposed to human vaginal microbiota by gastric gavage and compared to pups gavaged with microbe-free transport media (Jašarević et al., 2021). By adulthood the microbial population differences in treated and control offspring GI were no longer apparent, with similar measures of microbiome diversity and membership across groups. However, there were lasting impacts on the immune system and neural gene expression, as adult males had altered proportions of immune cells and hypothalamic gene expression across the neonatal microbial colonized and control groups. The data from this study indicate that alterations in the maternal environment not only shape their own microbiota, but also change neonatal colonization, which can have lasting consequences for offspring health.

2.5. Known role of gut microbiota in the etiology of neurodevelopmental disorders

Gut microbiota have been implicated in neurodevelopment and cognitive function. Studies have used microbial treatments and assessed the impact of microbiota alterations on behavioral outcomes.

In a study examining the relationship between gut microbiota and memory formation, wild-type mice and germ-free mice were infected with pathogenic *Citrobacter rodentium* and cognitive performance was evaluated using the novel object recognition test and the T-maze in the presence or absence of acute stress (Gareau et al., 2011). Infection alone did not impair novel object exploration, but following acute stress, infected mice were unable to discriminate the novel object from the familiar object. This effect persisted 30d after infection by which time the active infection had been resolved. Similarly, active infection with acute stress decreased spontaneous alternation when exploring a T-maze. These stress-induced cognitive impairments were ameliorated with antibiotic treatment, indicating a causal link between gut microbiota and cognitive impairment. Gut microbiota have also been associated with anxiety behavior. Male mice were infected with pathogenic *Campylobacter jejuni* and evaluated for anxiety-like behaviors using a holeboard assay (Goehler et al., 2008). In the holeboard assay, the central middle hole, in an array of evenly spaced holes, is baited with a food reward. Each subject is evaluated for its time spent in the center of the assay, as well as the quantity of nose pokes into central vs. peripheral holes, with less time/nose pokes in the center indicating greater anxiety-like behavior. Mice with active infection spent significantly less time in the center and had fewer nose pokes in the center, baited hole. Anxiety-like behavior in infected mice was associated with aberrant regional cell activation, as demonstrated by c-Fos expression. Several stress-related brain regions were correlated with time in center (including basolateral amygdala and medial prefrontal cortex, among others) in non-infected mice, whereas a few brain regions largely associated with viscerosensory signal processing (bed nucleus of the striata terminalis, central amygdala, and nucleus of the solitary tract) were correlated with time spent in the center for infected mice.

Impacts of microbiota on anxiety-like behaviors may be transmissible from pregnant dams to their offspring. As previously mentioned, germ-free mice colonized with choline-consuming *Escherichia coli* have decreased DNA methylation (Romano et al., 2017). In this study, the researchers also examined germ-free pregnant mouse dams colonized with choline-consuming *Escherichia coli* and fed a high choline diet. Serum of colonized pregnant dams had lower levels of choline, while the fetuses had decreased DNA methylation in the brain but not in the liver. When a strain of knockout animals known to develop memory impairments and stereotyped behaviors (*Apoe*$^{-/-}$) underwent the same treatment (colonized and fed a choline-supplemented diet), pregnant dams displayed elevated anxiety-like behaviors, including significantly increased rates of barbering and infanticide, compared to non-colonized pregnant dams. Moreover, offspring of the colonized pregnant dams had elevated rates of marble burying than the offspring of non-colonized dams, indicating increased anxiety-like behavior in the offspring. Several studies in rodent models have shown that probiotics can (a) improve cognitive function or prevent cognitive dysfunction, and (b) reduce stress-induced anxiety as well as depressive behaviors (Eastwood et al., 2021; Mindus et al., 2021; Natale et al., 2021). Collectively, these data emphasize a crucial role of gut microbiota in cognitive function and neurobehavioral outcomes, and the potential to target microbiota for therapeutic interventions.

Alterations to gut microbiota have also been implicated in neurodevelopmental disorders. Gut microbiome in children with ASD has been shown to be less diverse compared to children with neurotypical development (Kang et al., 2018). The authors of this study also hypothesized that a relationship may exist between altered fecal metabolites present in children with ASD, including increased levels of the neurotoxin isopropanol and decreased levels of the neurotransmitter γ-aminobutyric acid (GABA), which may contribute to altered neurodevelopment. This connection between gut microbiota and GABA signaling-related microbial metabolites is further supported in a preclinical study wherein germ-free (GF) mice were colonized with fecal microbiota from children with ASD or neurotypical development (TD) (Sharon et al., 2019). These colonized mice were then mated and offspring examined for neurobehavioral, microbial, and neural transcriptomic changes. In adolescence (postnatal day [PND] 45), offspring mice from ASD microbiota-colonized parents exhibited greater ASD-like behaviors than offspring mice from TD-colonized parents including increased repetitive behaviors, decreased vocalizations, and decreased social interaction, shown by the marble burying task, quantification of ultrasonic vocalizations, and the direct social interaction test, respectively. Not only could these offspring be separated by gut bacterial taxa, but the behavioral deficits were correlated with the expression of four species of bacteria. Using untargeted metabolomics analyses to determine the expression of microbial metabolites in the colon, the offspring from ASD microbiota-colonized mice had lower amounts of weak GABA receptor agonists 5-aminovaleric acid and taurine. However, while the expression of these agonists was not altered in serum, oral administration of 5-aminovaleric acid or taurine to the pregnant dam improved ASD-like behaviors in a separate ASD mouse model.

Attention-deficit/hyperactivity disorder (ADHD), is another neurodevelopmental disorder with a gut microbiota linkage. A systematic review of clinical literature found that, while numerous differences in microbiota have been reported, there were no overarching differences in microbiome diversity between children with ADHD and children with neurotypical development (Gkougka et al., 2022). In one study, *Faecalibacterium* content was inversely correlated with parental-reported ADHD severity in treatment-naïve children (Jiang et al., 2018). It should be noted that FASD and ADHD have a high co-morbidity. For example, a study that examined the association of adverse childhood experiences and neurodevelopmental disorders with FASD made an incidental observation regarding the comorbidity of ADHD and FASD (Kambeitz et al., 2019). In this study of individuals <22 years of age, seen at a regional FASD center, of those diagnosed with FASD, 85.7% were also diagnosed with ADHD, while 63.8% of those with suspected FASD, but nevertheless did not reach criteria for FASD diagnosis, were diagnosed with ADHD. It is possible that individuals who did not meet criteria for a FASD diagnosis may have sub-clinical impacts of PAE that are associated with increased rates of ADHD. Contrastingly, for 3–17-year-olds across the US, an estimated 9.6–9.8% have received an ADHD diagnosis (Bitsko et al., 2022). Notably, the neurobehavioral profile and brain structure alterations of PAE-associated ADHD are distinct from non-PAE-associated ADHD (Coles et al., 1997; Mattson et al., 2019; O'Neill et al., 2022) and, due to barriers in obtaining FASD diagnoses (Burd, 2016, see 4.1), these differences are not typically assessed. Therefore, the relationship between ADHD and microbiota is likely confounded by undiagnosed comorbid conditions, such as FASD, that can shape the profile of ADHD and, consequently, ADHD-related microbiome diversity.

There are overlaps in symptoms between neurological and neurodevelopmental diseases. ASD and ADHD are often co-morbid

and share many common features, with one study at a tertiary center for ASD finding that 63% of ASD patients also displayed ADHD symptoms (Avni et al., 2018). Overlapping symptoms include anxiety, cognitive impairment, inattentiveness, and social difficulties (Avni et al., 2018). More importantly, ADHD and ASD patients both share common gastrointestinal disorders (Buie et al., 2010; Vargason et al., 2019) and for individuals with ASD, the severity of these gastrointestinal disorders positively correlate with the severity of the neurological disorders (McElhanon et al., 2014). Overall, many neurodevelopmental and neurological disorders appear to overlap both in symptoms and in the role of microbiota in shaping disorder outcomes and symptom severity.

3. Alcohol exposure affects maternal and infant gut microbiota

Although gut microbiota and their metabolites have been associated with neurodevelopmental disorders, we are currently just beginning to understand the relationship between PAE and gut microbiota in both the mother and fetus. Recent research found that ethanol exposure alters the plasma metabolite profile, both microbial and non-microbial, in pregnant mouse dams (Virdee et al., 2021). Principal component analysis of metabolites from ethanol-exposed and control exposure dams showed that metabolite profile well-segregated these groups. In particular, the first principal component segregated the alcohol-exposed and control dams, explaining ~23% of the overall variance between samples. In that study, microbial-derived metabolites were a major contributor to the separation between alcohol-exposed and control dams. Critically, microbial-derived metabolites were also found in fetal tissues, including the fetal brain. However, while microbial-derived metabolites in maternal plasma were promising biomarkers of ethanol exposure due to their ability to separate groups, microbial metabolites altered in fetal brain did not exhibit similar discriminatory power. Nevertheless, changes in fetal brain metabolites may have longer term consequences for neurodevelopment and need further investigation. Another preclinical study reported that PAE altered the fecal microbiota of adult offspring in a sex-specific manner (Bodnar et al., 2022). Pregnant Sprague–Dawley rats were fed ethanol containing liquid diet or a nutritionally matched chow throughout gestation (gestational day [GD] 1-GD 21).[1] PAE offspring (at PND 80) exhibited more diverse microbial communities than control offspring. When stratified by offspring sex, this difference was found to be attributable to male, and not female, offspring. Intriguingly, in control offspring, males and females segregated in an analysis of microbial community composition while the PAE offspring, the microbial composition of males and female overlapped, suggesting that PAE may minimize sex differences. This study also showed that the effects of PAE on fecal microbiota are long-lasting and differences can be documented in adult offspring. The relevance of these preclinical findings are supported by a self-report survey by adults with FASDs, who reported intestinal complications (e.g., irritable bowel syndrome, chronic diarrhea, chronic constipation) at rates 1.8–2.5 times higher than the general population (Himmelreich et al., 2020), which can be attributed to altered gut microbial composition and function (Barbara et al., 2016).

The impact of alcohol exposure on gut microbiota has also been documented in individuals with alcohol use disorders (AUDs). Individuals with AUDs were found to have decreased bacterial community diversity and statistical analyses indicated these altered microbiota could be biomarkers of both amount of alcohol consumed and decreased cognitive function associated with alcohol consumption (Du et al., 2022). A systematic review of alterations to gut microbiota in individuals with AUD showed that a common outcome was a reduction in *Ruminococcus, Collinsella,* and *Prevotella* genera and an increase in Proteobacteria phylum (Litwinowicz et al., 2020). Anti-inflammatory and SCFA-producing species are decreased, which may contribute to decreased gut barrier function and increased inflammatory tone found in preclinical models of chronic alcohol use (reviewed in Leclercq et al., 2017). Moreover, as the above review noted, this inflammatory profile may further contribute to alcohol seeking behavior. Thus, several microbiota normalization strategies have recently been proposed and used as preventatives and therapeutics for AUDs by lowering systemic inflammation and restoring the gut barrier function. Fecal microbiota transplantation may be one method for treating AUDs by increasing beneficial microbiota (Bajaj et al., 2021). Bajaj and colleagues, in a double-blind randomized clinical trial, treated patients with AUD-associated cirrhosis and active AUD with fecal microbiota enriched in *Lachnospiraceae* and *Ruminococcaceae* or placebo. Fecal microbiota transfer decreased alcohol craving and increased microbiome diversity and plasma butyrate (a microbial-derived SCFA) levels in patients with AUDs 15 days after transplantation. Additionally, 6 months after the transfer, fewer AUD-related serious adverse events occurred in fecal microbial transfer patients compared to the placebo group.

For fetal microbial colonization, maternal diet is a major driver of microbiota composition (Miko et al., 2022). Alcohol exposure has been shown to drastically shape nutrition, including by altering both maternal and infant nutrient absorption which has been associated with neurodevelopmental delays in children with PAE.

4. Nutrition as a driver and consequence of PAE-altered microbiota

4.1. PAE-induced alterations to maternal and fetal nutrition

The consumption of recreational and illicit substances during pregnancy can contribute to nutrient malabsorption, especially micronutrients like zinc, choline, iron, copper, and selenium (May et al., 2016). This malnutrition has been associated with impaired GI absorption of nutrients in consumers, as well as drug-induced changes in food-intake preferences and behaviors, which contribute to unhealthy weight fluctuation and nutrient deficiency. Alcohol, particularly chronic alcohol consumption in adults has long been associated with malnutrition [for example, documented in early studies by Lieber

1 In rodent models, the *in utero* period (gestational days 1–18 for mice and 1–21 for rats) is roughly equivalent to the first and second trimesters of human development while the early postnatal period (post-natal days 1–10) is roughly equivalent to the third trimester of human development (Workman et al., 2013).

(1975)]. Notably, changes in nutritional levels are directly associated with immune function, with poor nutrition serving as the leading cause of immunodeficiency worldwide (Chandra, 1997).

However, a body of literature conversely suggests that alcohol consumption can also stimulate food consumption (Caton et al., 2004, 2005) and that heavy consumption in particular is a risk factor for obesity (reviewed in Yeomans, 2010). Since deficiencies in essential nutrients can readily occur in individuals with obesity (Kobylinska et al., 2022), due in part to the consumption of calorie-dense foods low in essential nutrients, and to altered microbiota associated with obesity, this stimulation of food consumption may paradoxically lead to malnutrition. Eating patterns can, conversely, impact alcohol consumption behavior. For instance, dieters and mindful eaters surprisingly demonstrate greater instances of binge-drinking than non-dieters, specifically when dieting to achieve weight loss (reviewed in Caton et al., 2015). These effects may be further influenced by the physique and sex of drinkers (Colditz et al., 1991; Clevidence et al., 1995; Caton et al., 2007), as well as their age and racial identity (Wannamethee et al., 2004).

Ongoing studies in clinical and preclinical settings are investigating the effects of alcohol exposure during pregnancy on maternal and fetal nutritional profiles. In this section, we will highlight current literature describing the role of multiple common nutrients in either preventing or augmenting deficits associated with PAE.

4.1.1. Metal ions

Metal ions, including iron, manganese and zinc among others, form core constituents of catalytic proteins and are critically important for maintaining cellular physiology including redox states in cells, but can also be toxic at high levels (Jomova et al., 2022). Therefore, destabilization of metal ion homeostasis may have significant consequences for tissue growth and toxicity.

4.1.1.1. Iron

Preclinical studies have shown that PAE can impact fetal iron homeostasis, independent of maternal iron status. In a rat PAE model (Huebner et al., 2016), pregnant Long-Evans rats, following evidence of successful mating (GD 0.5) were provided iron sufficient (100 mg/kg) or deficient (<4 mg/kg) diets, and exposed either to 5 g/kg ethanol or isocaloric maltodextrin, via oral gavage, from GD 13.5 – GD 19.5. On GD 20.5, fetuses in the PAE-alone group had decreased body, liver, and brain weight. Following hematological assessment, the authors determined PAE disrupted iron distribution throughout the fetal body, sequestering iron in the liver with decreased iron in the brain. Although alcohol exposure did not affect overall maternal liver iron concentrations or transporters important for liver iron storage, alcohol exposure did significantly increase maternal gene expression of hepcidin. Hepcidin is a critical hormone for iron metabolism and elevated levels may reflect decreased ability for iron absorption in the gut. Notably, maternal iron levels were not predictive of fetal iron levels, and increased anemia observed in PAE offspring was not mediated by maternal iron status, suggesting that fetal iron absorption was directly inhibited by PAE. Further work in this model (Huebner et al., 2018), which examined an iron-fortified group (500 ppm) alongside the iron-sufficient group, found that PAE decreased fetal body weight, independent of maternal iron diet. In maternal and fetal subjects, PAE increased hepcidin levels beyond healthy levels (50–175 mcg/dL). When PAE was supplemented with an iron-fortified diet, hepcidin expression was normalized to non-PAE controls. Furthermore, hepcidin levels in PAE offspring corresponded to increased iron levels in the liver compared to maltodextrin controls, and increased iron levels in the brain compared to PAE without iron supplementation.

In a follow-up study, rat dams were fed an iron sufficient diet and further supplementation of iron through oral gavage (6 mg/kg, doubling daily intake) during the ethanol/maltodextrin exposure window had a positive impact on iron metabolism in PAE fetuses compared to vehicle-treated PAE fetuses (Helfrich et al., 2022). Compared to the maltodextrin-exposed controls, PAE fetuses without iron supplementation had decreased brain weight, body weight, and number of red blood cells, and increased levels of hepatic iron and rates of fetal anemia. With iron supplementation, PAE animals had no fetal anemia, normalized red blood cell counts, and increased brain weight, although only males experienced a recovery equivalent to non-exposed controls. These effects are conserved across species, as this group recently found that iron deficiency with concomitant PAE also reduces hemoglobin and red blood cells in a PAE mouse model (Helfrich et al., 2023). In this study, they further found that the underlying mechanisms for this change in hemoglobin are likely, surprisingly, changes in ribosome biogenesis and not hemoglobin synthesis or iron metabolism.

Clinical investigations have further validated the relationship between PAE and iron dysregulation (Bradley et al., 2022). Pregnant women in Cape Town, South Africa were recruited and categorized by their drinking patterns during the first trimester of pregnancy (Carter et al., 2007). If they reported two or more instances of binge drinking alcohol during pregnancy, or consumed ≥1.0 oz. of absolute alcohol (AA) per day, they were qualified as heavy drinkers. Light drinkers included women who averaged <1.0 oz. AA, the equivalent of 2 standard drinks, or reported ≤2 incidents of binge drinking (≥5 standard drinks per occasion). At 6.5 and 12 months of age, infant blood samples were collected to determine iron status. At 6.5 months, PAE was not associated with iron-deficiency anemia. However, PAE infants exhibited reduced birth weight and body length. In contrast, at 12 months of age, infants exposed to PAE in the binge drinking group experienced higher rates of iron-deficiency anemia diagnosis compared to abstinent/light drinking-exposed infants. Although PAE was associated with low infant weights independent of iron deficiency, iron levels moderated this relationship, with iron deficiency leading to the lowest birth weights among PAE offspring.

In the same population, the longitudinal impacts of iron deficiency were also examined (Carter et al., 2012). In this study, consumption of two drinks per day, or 4 drinks per occasion, was classified as "heavy drinking" while consumption of one drink per day without binging, or alcohol abstinence, was classified as abstaining/light-drinking controls. PAE was associated with lower offspring heights and weights at 6.5 months, 12 months, 5 years, and 9 years. Moreover, PAE was also associated with higher rates of iron deficiency across all age groups, with five-year-old children in the PAE group 6.5 times more likely to exhibit iron deficiency than the age-matched controls. A follow-up investigation in this cohort further determined that children with a history of PAE experienced different growth-deficit recoveries (Carter et al., 2016). Children born small for their age were classified as experiencing either catch-up growth, or long-term postnatal growth restriction, through the age of 13 years old. In children without a history of PAE, all but one child born small for

their age (98.3%) experienced postnatal catch-up growth. This percentage was considerably lower for children born small for their age with PAE (58.5%). Furthermore, degree of gestational alcohol exposure corresponded with whether children experienced catch-up growth; specifically, children with the highest degree of PAE were the least likely to experience growth recovery. It is yet unknown whether iron deficiency contributes to and/or predicts growth trajectories in children with PAE throughout early life.

Decreased iron in offspring may be attributable, in part, to impaired maternal iron absorption, which has been implicated by elevated hepcidin levels in rodent models PAE (Huebner et al., 2016, 2018), as discussed above. In a separate investigation, pregnant women ($n = 206$) were interviewed during three prenatal visits, in which their drug-taking habits were recorded (Carter et al., 2021). Blood samples from infants (either 2 or 6.5 months old) and mothers, and tissue samples from corresponding placentas in control (non-drinking) and heavy-alcohol-drinking groups were later examined and compared. Heavy drinking during pregnancy was associated with increased maternal hepcidin, increased fetal iron sequestration in fetal blood samples, and decreased placental ferroportin and transferrin, which decreased maternal and neonate red blood cell synthesis (erythropoiesis). These restrictions in iron transport were associated with decreased fetal hemoglobin levels and increased iron-deficiency anemia diagnoses in 6.5-month-old infants. Maternal decreases in hemoglobin were positively correlated with neonatal hemoglobin deficits, which increased rates of infant iron-deficiency anemia.

Taken together, these studies indicate that PAE may impair maternal-fetal iron transportation across the placental barrier and result in persistent fetal iron deficiency and greater risk for childhood anemia. While iron supplementation serves as a promising therapeutic intervention for children with a history of PAE, it is important to note that negative side effects for iron supplementation have been reported, including constipation and bloating following oral administration, likely due to effects on gut microbiota (Bloor et al., 2021).

4.1.1.2. Zinc

In a preclinical study (Keppen et al., 1985), pregnant CBA/J mouse dams on GD 1 were randomly assigned to treatment groups receiving liquid diet containing 15%, or 20% ethanol, or maltose dextran-containing isocaloric control from either GD 1–18 or GD 6–18. The liquid diet also contained low levels of zinc (0.3 μg zinc/ml) or a concentration of zinc that is the recommended dietary amount for reproduction in laboratory mice (8.5 μg zinc/ml). Low-zinc diet significantly reduced fetal weight on GD 18 compared to adequate zinc exposure. Low zinc with PAE (15 or 20%) co-exposure significantly increased fetal resorption (37–52%) compared to low zinc diet without PAE and adequate zinc diet with PAE (0–2%). With increasing levels of PAE, there were increased numbers of fetal malformations (e.g., precocious opening of eyelids, mild limb hypoplasia). This effect was most pronounced in the low-zinc/20% ethanol group where all fetuses exhibited malformations.

Prenatal alcohol exposure has additionally been associated with deficits in placental zinc transport (Ghishan et al., 1982). *In vivo* assessments of zinc transport revealed that PAE was associated with reduced zinc in the placenta and fetus, compared to pair-fed controls. In the first study, Sprague Dawley dams received ethanol (4 g/kg) via nasogastric intubation on GD 20 as a model of acute ethanol exposure. In the second study, Sprague Dawley dams received a liquid diet of either 5% ethanol or calorically-matched maltodextrin (controls) from GD 4-GD 20 as a model of chronic ethanol exposure. In both exposure paradigms, pregnant rats were anesthetized on GD 20 and administered radioisotope zinc-65 chloride injections (2 μCi/100 mg body weight) via an exposed femoral vein. Compared to control subjects, acute ethanol exposure reduced placental uptake of zinc-65 by 40%, while reducing fetal absorption by 30%, but did not impact overall placental and fetal tissue weights. In contrast, chronic ethanol exposure significantly decreased fetal weights at the time of tissue collection, while simultaneously increasing placental weights, compared to pair-fed controls. Similar to acute ethanol exposure, this chronic paradigm decreased zinc-65 placental uptake by 40% compared to controls. Ethanol-exposed dams also exhibited lower steady-state, non-radioactive zinc concentrations in their serum, although non-radioactive zinc levels in maternal femurs did not differ by exposure. Unsurprisingly, PAE fetuses also demonstrated significantly lower (−13%) zinc concentrations than alcohol-free controls, consistent with the reduction in placental uptake. This study importantly emphasizes that, even when mothers consume the daily recommended levels of zinc through diet, alcohol-exposed fetuses may require additional supplementation due to impaired placental transport.

Zinc deficiency has also been reported in children with a history of PAE. Infants with fetal alcohol syndrome (FAS, average 8.8 months old), a FASD diagnostic category characterized by facial anomalies, growth deficiencies including brain growth anomalies, and neurobehavioral impairment (Hoyme et al., 2016), had lower levels of zinc in their plasma than the control group, which contained slightly younger infants (average 6.9 months old) that were, nevertheless, on average, not significantly different from the FAS infants for height and weight (Assadi and Ziai, 1986). Yet, infants with FAS excreted significantly higher levels of zinc in urine than the control group, indicating that the decreased plasma levels of zinc may be due to increased excretion in the FAS infants.

4.1.1.3. Selenium

Sufficient levels of selenium in pregnant individuals have been linked to healthy neurodevelopment of the neonatal cerebellum (Močenić et al., 2019). In contrast, deficient maternal selenium levels have been associated with increased risk of neurodevelopmental disorders, including ASD and ADHD (Lee et al., 2021). Selenium deficiency has previously been investigated in maternal and fetal tissues following gestational alcohol exposure (Ojeda et al., 2009). In this preclinical study, female Wistar rats were split into three experimental groups: control, alcohol, and pair-fed dams, who served as controls for alcohol-based malnutrition. Dams drank 20% ethanol *ad libitum* through the exposure paradigm, beginning 4 weeks before mating and continuing up to 21 days post-parturition. As established by many other models of FASD, PAE was associated with fewer viable pups/litter and lower body weights in PND 21 juveniles. In both the pair-fed and alcohol exposed groups, dams consumed less selenium, due to overall decreased dietary intake, and ethanol-exposed dams had decreased overall selenium balance, indicating increased excretion of selenium, compared to the pair-fed controls. These patterns were mimicked in offspring, with PAE offspring receiving less selenium from dams, but also eliminating more selenium than pair-fed controls. PAE-associated selenium deficits were specifically found within tissues of the liver, kidney, and heart in offspring, although future

investigations of brain-specific changes in selenium would elucidate whether selenium malnutrition contributes to aberrant neurodevelopment in FASD.

4.1.2. Other essential dietary nutrients

Vitamins A and E, the polyunsaturated fatty acid docosahexaenoic acid (DHA), and the micronutrient choline are only a few of the many nutrients essential for fetal development (Cortes-Albornoz et al., 2021). These nutrients support many cellular functions including: antioxidant capacity, cell membrane integrity, and one-carbon metabolism/methyl donor formation (Ducker and Rabinowitz, 2017; Blaner et al., 2021; Cortes-Albornoz et al., 2021). Therefore, undernutrition with regards to these nutrients can inhibit growth and development.

4.1.2.1. Choline

Maternal choline insufficiency is associated with neural tube deficits while choline supplementation is associated with improved childhood cognitive function in infancy and potentially early childhood (Obeid et al., 2022). Preclinical, as well as clinical, research consistently shows that choline insufficiency increases risk of negative outcomes following PAE while choline supplementation promotes resiliency (for a systematic review see Akison et al., 2018). Additional research has further supported the use of choline as a therapeutic for PAE/FASD. In a rat model, the impact of choline insufficiency on the effects of PAE was investigated (Idrus et al., 2017). Pregnant Sprague–Dawley rats received diets with 40, 70%, or 100% of the daily recommended choline levels alongside exposure to ethanol (intragastric intubation, 6.0 g/kg/day) or two control groups, one that had caloric intake matched to that of the ethanol group (pair-fed) and one that was normally fed (*ad libitum*). These exposures occurred from GD 5 to GD 20. On PND 5–6, PAE was found to impair motor development, reduce body weight, and increase hyperactive behavior compared to both pair-fed and *ad libitum* groups. Notably, when PAE was concomitant with the highest choline deficit, 40% of the recommended daily intake, offspring experienced the most severe deficits in motor development and increases in activity compared to all other exposure groups.

Additional preclinical models have shown that choline supplementation can ameliorate PAE-induced negative outcomes. In a model of periconceptional alcohol exposure, Sprague–Dawley rats received 12.5% ethanol or 0% ethanol in liquid diet from 4 days pre-conception through GD 4. On GD 5, dams began a diet of either standard, 1.6 g choline/kg chow, or a choline-enriched diet of 2.6 g choline/kg chow (Steane et al., 2021, 2022). Fetal tissue samples were collected and analyzed on GD 20. Choline supplementation increased fetal liver weight and decreased fetal brain:liver ratio, a marker for fetal growth restriction (Westen et al., 2019), independent of alcohol exposure (Steane et al., 2021). Choline supplementation dose-dependently decreased placental and increased fetal plasma acetylcholine levels (Steane et al., 2022). Periconceptional alcohol co-exposure abrogated the impact of choline on acetylcholine levels for placentae of fetuses of both sexes and reduced acetylcholine levels in the plasma of female offspring only. Given that acetylcholine is one of the neurotransmitters in the placenta-brain axis (Rosenfeld, 2021), these findings indicate that periconceptional alcohol can interfere with this critical placenta-derived neurodevelopmental signaling.

The therapeutic potential of choline supplementation has been further demonstrated in clinical studies. Pregnant women who self-reported heavy alcohol consumption (time-line follow back, ≥2 standard drinks [1.0 oz. AA]/day, or ≥ 2 binge-drinking episodes) self-administered either 2 g packets of choline or placebo twice daily from 23 gestational weeks until birth (Jacobson et al., 2018; Warton et al., 2021). While PAE infants were small at birth, choline supplementation facilitated catch-up gains in weight and head circumference at 6.5 months and 12 months and increased the volume of brain regions, including the left and right thalamus, left and right caudate, right putamen, and corpus callosum. Moreover, the PAE infants with choline supplementation had improved performance on infant learning and memory tests, namely eyeblink conditioning and the Fagan test of infant intelligence.

A separate research group has similarly investigated the effects of choline supplementation on cognitive performance in children. A cohort of 60 children with FASD diagnoses (2.5–5 years old) were randomly assigned to receive 500 mg choline or a placebo daily for 9 months (Wozniak et al., 2015). Children received cognitive assessments prior to and following treatment, including an elicited imitation memory test, an assessment of explicit memory ability using hippocampal-supported behavioral imitation. Choline treatment was found to improve elicited imitation performance specifically in children under 4 years old, indicating a potential window of early development that is most beneficial for memory-recovery *via* choline treatment. In a follow-up study performed 4 years later, children were assessed on a multitude of cognitive and behavioral domains to look at long-term outcomes associated with the initial choline supplementation paradigm (Wozniak et al., 2020). Compared to children in the placebo group, children with FASD who received choline treatments exhibited greater aptitude for non-verbal visual spatial reasoning and working memory. The choline-receiving group also exhibited fewer behaviors associated with ADHD, according to parental self-reports. Unlike acute assessments in this cohort, the age of choline treatment did not affect overall outcomes in older children, indicating that long-term improvements were possible as long as children with FASD received choline between 2.5–5 years of age. To identify a possible mechanism underlying the benefits of choline supplementation on FASD symptomology, blood samples were collected from 52 children in this cohort and genotyped for ~400 single nucleotide polymorphisms (SNPs) associated with choline status and/or choline metabolism (Smith et al., 2021). Although baseline serum levels of choline did not differ between treatment groups, 14 SNPs associated with the choline transporter gene *SLC44A1*, were correlated with improved cognitive performance exclusively in children with FASD who received choline treatments. Although further research is needed, this may implicate a role for PAE in inhibiting proper choline transport, which is exacerbated by genetic risk factors, leading to FASD-associated cognitive impairment.

Although choline supplementation demonstrates promise for treatment in children with FASD, supplementation can also result in the adverse side effect of producing a fishy body odor. This effect can be common and increases in frequency with increasing doses of choline. In a randomized, placebo-controlled trial of choline supplementation, 56% of participants in the choline supplementation arm developed a fishy body odor that was noticeable during parental caregiving during the study, with 100% of participants in the top quartile of choline dose developing this body odor (Wozniak et al., 2013).

4.1.2.2. Vitamin A/retinoic acid

Vitamin A and retinoids, the active metabolites of vitamin A, are required for appropriate embryonic development (Ross et al., 2000), including neurodevelopment (Haushalter et al., 2017). As some tissues are responsive to low levels of the most active retinoid, retinoic acid (RA, Ross et al., 2000), the use of retinoids is associated with teratogenic effects on fetal development. In these cases, fetuses were exposed to a vitamin A derivative 13-*cis*-retonic acid, the type commonly found in the treatment of cystic acne, psoriasis, skin diseases, or skin cancer (isotretinoin, brand name: Accutane), resulting in birth defects (Draghici et al., 2021). Notably, retinoic acid deficiency during pregnancy has also been associated with fetotoxic outcomes and birth deficiencies, including microphthalmia, respiratory distress, and abnormal cardiac, lung, and urogenital system function (Azaïs-Braesco and Pascal, 2000). However, at sub-teratogenic levels, vitamin A supplementation may protect against some PAE-associated negative outcomes. In one study, zebrafish embryos were exposed to ethanol (100 or 150 mM) during somitogenesis (2–24 h post fertilization [hpf][2]) *via* the embryo medium (Muralidharan et al., 2015). At 48 hpf, embryos exposed to either ethanol concentration had microphthalmia, retinal lamination delay, and significantly decreased optic nerve width, compared to control counterparts. RA supplementation (1 nM, 2–24 hpf) ameliorated the effect of ethanol exposure on optic nerve width. Importantly, RA supplementation was less effective prior to RA biosynthesis period (2–16 hpf) compared to supplementation during RA biosynthesis (16–24 hpf), implicating an important window of development for improving supplementation treatment efficacy.

In a separate study, zebrafish were exposed to ethanol (150 mM) during a smaller early window of exposure, the period of gastrulation (5.25–10.75 hpf), with or without RA supplementation (1 nM) (Ferdous et al., 2017). At 2 days post fertilization, ethanol exposure significantly decreased zebrafish body length, an effect that was prevented by RA supplementation. RA supplementation improved the survival rates of ethanol-exposed embryos to the levels of the control exposure group. PAE during gastrulation also disrupted neuronal development, decreasing the cell body size, axon diameter, and frequency of synaptic response to excitatory innervation in Mauthner cells (M-cells) (Ferdous et al., 2017), a pair of neurons that mediate the escape response in fish (Pereda and Faber, 2011). RA supplementation prevented ethanol-induced decreases in cell body size and axon diameter and improved synaptic excitatory signaling, although not to control levels. Correspondingly, ethanol-induced increases in the angular velocity of the tail flip escape response, indicating an aberrant over-response, were prevented by RA supplementation.

The utility of vitamin A/retinoid supplementation to improve outcomes following PAE may be due, in part, to an amelioration of PAE-induced deficits in normally occurring retinol production. In a study of Sprague–Dawley rats (Kim et al., 2015), ethanol exposure altered the metabolism of vitamin A and its derivative retinoids, contributing to inappropriate retinol levels. Pregnant dams were fed a liquid diet of ethanol, an isocaloric liquid diet without ethanol (pair-fed), or access to typical rat chow. Ethanol-treated dams were given increasing percentages of ethanol from GD 7-GD 21 (2.2% on GD 7, 4.4% on GD 8, 6.7% on GD 9-GD 21). Independent of the exposure group, at PND 60–75, males demonstrated overall higher retinol levels than females. In males, PAE increased retinol levels in serum, while producing no significant effect in serum from female offspring. Additionally, PAE decreased retinol levels in male liver, lung, and prostate tissue compared to both control groups. In females, PAE increased retinol levels in liver and lung tissue compared to chow-fed controls, without producing a change in levels from pair-fed controls, suggesting this effect may be primarily driven by caloric intake. PAE lowered vitamin A (retinyl ester) levels in male and female lung tissues compared to pair-fed controls, without affecting the gene expression of the acyltransferase responsible for retinyl ester synthesis in mammals. These findings are particularly meaningful for potential PAE-induced effects on the microbiota, as the mammalian microbiota works symbiotically with the body to synthesize retinol from beta-carotene and prevent vitamin A deficiency (Srinivasan and Buys, 2019).

4.1.2.3. Vitamin E

Vitamin E, which is exclusively available through diet, has well-established health benefits, including: antioxidant and anti-inflammatory actions, stabilization of cell membrane integrity, and promotion of immune function (Rizvi et al., 2014). Two preclinical studies in rat PAE models have demonstrated cognitive and metabolic benefits of vitamin E supplementation (Shirpoor et al., 2015; Mahdinia et al., 2021). In one of these studies, pregnant Wistar rats received 4 g/kg ethanol and a daily gavage of 100, 200, or 400 mg/kg vitamin E in sunflower oil from GD 0-PND 28 (Mahdinia et al., 2021). These perinatal ethanol exposed offspring were compared against two control groups that were not significantly different from one another and collapsed for analysis: an all treatment naïve group and a saline (ethanol vehicle) gavage group. Due to a lack of significant changes between an ethanol-alone exposure group and an ethanol with vitamin E vehicle (sunflower oil) control, these groups were also collapsed for analysis (ethanol-alone control group). At the end of this exposure period, offspring were tested on the Morris Water Maze for ethanol-induced deficits in memory and learning abilities. Perinatal ethanol exposure increased escape latency during the training, or learning, portion of the Morris Water Maze compared to controls, indicating diminished task learning. Vitamin E supplementation at both 100 and 400 mg/kg significantly decreased escape latency in ethanol-exposed rats compared to the ethanol-alone control group. During the probe trial, a test of memory, perinatal ethanol exposed offspring had significantly longer escape latency; concomitant 400 mg/dL vitamin E supplementation restored this impaired performance to non-PAE proficiency. An additional study that examined perinatal ethanol exposure (GD 7 – PND 21), during which pregnant Wistar rat dams were administered 4.5 g ethanol/kg and/or 300 mg of vitamin E by oral gavage (Shirpoor et al., 2015). In male offspring, PAE lowered body weight and disrupted lipid profiles at PND 21 and PND 90. Vitamin E supplementation during the period of ethanol exposure recovered ethanol-induced reductions in body weight and partially recovered lipid profiles. Perinatal ethanol-exposure also resulted in disrupted heart structure, with increased cellular proliferation in cardiac tissue and disrupted endothelial cell structure in the coronary artery, both of which were improved with concomitant vitamin E supplementation. Ethanol exposure also significantly elevated plasma

2 For zebrafish development 24 hpf is roughly equivalent to up to 8 gestational weeks in humans and 48 hpf is roughly equivalent to 16 gestational weeks (Walter et al., 2019).

pro-inflammatory markers, including cytokines. Vitamin E supplementation along with ethanol exposure significantly increased antioxidant capabilities in cardiac tissues; however, vitamin E was unable to fully ameliorate the impact of ethanol exposure on plasma pro-inflammatory cytokine levels.

4.1.2.4. Docosahexaenoic acid

Docosahexaenoic acid (DHA) is an omega-3 (ω-3) fatty acid critical in the growth and functional development of the neonatal brain and deficits are well-associated with learning and memory difficulties (Richard and Calder, 2016). In a preclinical study of PAE in guinea pigs, researchers investigated how PAE affects fatty acid and phospholipid levels in the liver and brain (Burdge et al., 1997). Pregnant dams received either 6 g/kg/day ethanol, 0.5 g/kg/day of tuna oil (a nutritional supplement high in DHA), or a combination of both, for 2 weeks prior to and throughout pregnancy. Phosphatidylcholine (PC) and phosphatidylethanolamine (PE) levels in the liver and brain were quantified in exposed offspring. In several cases, tuna oil supplementation recovered fatty acid levels in PAE offspring to the levels of non-exposed controls. In the fetal brain, ethanol exposure alone significantly reduced stearic acid and DHA fatty acid levels, which were completely recovered in PAE offspring with DHA supplementation. Furthermore, PAE increased the ratio of overall brain PC:PE levels from control animals, a ratio that was re-established with the addition of tuna oil treatment. In the fetal liver, PAE was significantly associated with reductions in DHA, and increased levels of ω-6 fatty acids, namely γ-linoleic acid, arachidonic acid, and docosapentanoic acid, all of which were recovered when alcohol exposure was combined with DHA administration. These data highlight a possible correlation between ethanol exposure and the biosynthesis of brain phospholipids PC and PE, which may underly cognitive challenges experienced by individuals with FASD.

DHA supplementation can also improve PAE-induced deficits in social behavior and somatosensory performance (Wellmann et al., 2015). In this study, pregnant Long-Evans rat dams were assigned to one of three exposure groups: ethanol exposure or pair-fed controls, both of which received a liquid diet from GD 6 – GD 21, or an *ad libitum* chow control group. For ethanol-exposed dams, ethanol concentrations in the liquid diet were escalated from 2.1 to 6.3% for GD 11- GD 21. Later, male offspring (PND 11 – PND 20) were randomly assigned to receive either artificial milk alone or supplemented with 10 g/kg DHA, or received no treatment as an additional control. Along with other reported deficits, PAE offspring, compared to pair-fed and chow controls, engaged in significantly less play fighting during adolescence, had fewer ultrasonic vocalizations in response to social isolation on PND 14, and had worse somatosensory performance on a gap crossing test, with PAE offspring crossing shorter gaps. Importantly, these deficits in play, vocalizations, and somatosensory performance were recovered by postnatal DHA administration, supporting the role of DHA in facilitating healthy offspring behavior.

4.2. The reciprocal relationship between nutrition and microbiota

As ongoing research continues to explore the relationship between PAE and malnutrition, it is important for scientists and clinical practitioners to consider how nutrient imbalance affects microbiota function in pregnant individuals and their offspring. Dysregulated choline levels, for instance, contribute to unhealthy levels of trimethylamine-*N*-oxide in serum, which are associated with the onset of non-alcoholic steatohepatitis, cardiovascular disease, and chronic kidney disease (Arias et al., 2020). Gut bacteria rely on iron stores to replicate and survive; however, iron over-abundance in the gut produces reactive oxygen species, inducing oxidative stress and intestinal damage (Yilmaz and Li, 2018). The retinoic acid derived from vitamin A consumption stimulates immune cell migration to the intestines and maintains the health of the gut barrier (Iyer and Vaishnava, 2019). Vitamin A deficiency, in contrast, impairs the immune response to intestinal challenge, and can increase risk for colorectal cancer (Jijon et al., 2018). Changes in vitamin A, zinc and vitamin E levels are each associated with altered gut bacteria composition (Chen et al., 2020; Choi et al., 2020; Skalny et al., 2021), while selenium deficiency contributes to a gut environment that is more susceptible to thyroid, inflammatory, and cardiovascular dysfunction (Ferreira et al., 2021). Finally, DHA supplementation in mice was recently associated with reduced adipose inflammation and the reversal of insulin resistance following consumption of a high-fat diet (Zhuang et al., 2020). Thus, future research into PAE-induced changes in the microbiota would benefit from investigating nutrient levels as a moderating factor in alcohol-associated changes in gut-microbiota associated health outcomes.

5. Potential contribution of microbiota plasma biomarkers for FASDs

5.1. Plasma markers of PAE vulnerability

Fetal alcohol spectrum disorders are difficult to diagnose, as they require a team of physicians/pediatricians with specialized training (Jones et al., 2006; Burd, 2016; Bernes et al., 2021). Moreover, for diagnosis by clinicians, we are woefully under capacity, with the estimated ability to diagnose only ~1% of FASD cases worldwide (Burd and Popova, 2019). Critically, while metabolite biomarkers of ethanol can be used to assay PAE, they are limited by the time frame of exposure they can reflect and can be difficult to collect, e.g., meconium collection to assay fatty acid ethyl esters (Bakhireva and Savage, 2011). Research by our group and others have identified biomarkers in plasma that are able to risk stratify offspring and indicate vulnerability for future FASD development and/or neurodevelopmental delay. However, the origin of these biomarkers is currently unknown. Altered gut (and potentially placenta) microbiota likely contribute to and shape the profile of plasma biomarkers.

5.2. Extracellular vesicles

Extracellular vesicles (EVs) are membrane-bound vesicles that are released by cells and carry nucleic acids, proteins, lipids, and metabolites (van Niel et al., 2018). EVs that are released from one cell can fuse with, and release cargo into, other cells and impact the recipient cell's physiology as a form of endocrine signaling. Work in adults who consume alcohol has shown that EVs can be part of the endocrine signaling of alcohol use, including increased inflammatory

tone. In healthy adults, binge alcohol consumption increases the amount of a sub-type of EVs, namely exosomes, present in blood serum (Momen-Heravi et al., 2015). In the same study, serum exosome number was also elevated in mice following binge-like ethanol exposure. Moreover, the levels of microRNA (miRNA) cargo, miR-122, was increased in exosomes following alcohol exposure in both systems, and this elevation was found in culture to reprogram monocyte cells resulting in aberrant elevation of proinflammatory cytokines following immune challenge. Along with miR-122, additional EV cargo has been identified as potential biomarkers for alcohol-associated liver damage and disease (Cho et al., 2018).

Altered EV dynamics and cargo have been implicated in diseases with developmental origins, for which prenatal exposure to stress and drugs of abuse, including PAE, may act as an "initial hit" to promote the development of these diseases (Pinson et al., 2021). In preclinical models, PAE has been shown to alter EVs in the developing brain. In an *in vitro* neural stem cell culture model, ethanol exposure altered neural stem cell-derived EV cargo (Tseng et al., 2019a; Pinson et al., 2022) and proteome (Chung et al., 2022). These alterations to EV cargo can have functional consequences for recipient cells. When ethanol-naïve neural stem cells were exposed to EVs from other ethanol-naïve neural stem cells, the recipient neural stem cells had significantly decreased oxidative metabolism and proportion of cells in S-phase (Chung et al., 2022). However, when EVs were added that were derived from stem cells exposed to 320 mg/dl ethanol, these effects on ethanol-naïve neural stem cell metabolism and cell cycle were decreased, suggesting that changes in EV composition following PAE have a biologically relevant impact for the recipient cells. Similarly, hypothalamic microglia-derived EVs have altered cargo following ethanol exposure in a rat early postnatal/third trimester-equivalent exposure model (Mukherjee et al., 2020). These microglia-derived EVs contributed to the PAE-induced death of hypothalamic β-endorphin neurons *in vivo* and *in vitro*, potentially through increased complement-protein induced apoptosis.

Clinically, a subset of EVs in maternal circulation, carrying markers that were interpreted as suggestive of fetal origin, were found to carry potential biomarkers of early deficits associated with PAE (Darbinian et al., 2022). Within these potential fetally-derived EVs, molecules associated with brain development, including proteins myelin basic protein and synaptic protein synapsin-2 and miRNA miR-9, were significantly correlated with eye size, and therefore could be biomarkers of PAE-induced growth deficits (see 5.3 for more about miRNA biomarkers). Preclinically, in a rat model of PAE, amniotic fluid EVs had altered miRNA content following PAE (Tavanasefat et al., 2020). *In vitro*, these PAE-altered EVs had functional consequences for stem cell development, reprogramming bone marrow stem cells to reduce osteogenic differentiation. The effects of the PAE-altered EVs on stem cells were similar to effects seen following low dose ethanol exposure, indicating that PAE may directly and indirectly, through EVs, impact stem cell biology *in vivo*. This anti-osteogenic effect was attributed to the upregulation of three miRNAs within the EVs, as overexpression of these miRNAs in the bone marrow stem cells was sufficient to decrease pro-osteogenic RNA transcript expression. These amniotic fluid EVs may also play a key role in gut development, as amniotic fluid is digested by the fetus and provides trophic factors for intestinal growth (Dasgupta et al., 2016). Amniotic fluid may also be the primary source for fetal microbial colonization of the intestinal tract (e.g., Stinson et al., 2019; He et al., 2020), although this route of colonization is debated (Perez-Munoz et al., 2017).

Microbiota, including both gram-positive and gram-negative bacteria, can also release EVs. These microbiota EVs are taken up by intestinal epithelial cells and their cargo can: impact barrier function; promote cytokine release by epithelial cells; and be repackaged into epithelial cell EVs and released into host circulation (reviewed in Kaparakis-Liaskos and Ferrero, 2015). For example, in an *in vitro* model of the gut endothelial barrier, EVs, but not cell lysates, from probiotic, gram-negative *Escherichia coli*, stimulated cytokine release from intestinal epithelial cells (Fábrega et al., 2016). These endothelial cells were in a co-culture system that also contained peripheral blood mononuclear cells (PBMCs), which were spatially segregated from the endothelial cells. The EV-stimulated cytokines released by the endothelial cells induced TNFα expression in PBMCs. In disorders with intestinal barrier disruption, microbiota-EVs can also be released into circulation. Clinical subjects with disrupted endothelial barrier function show higher levels of microbiota-derived EVs, with more plasma EVs containing lipopolysaccharide (LPS) (Tulkens et al., 2020). In these subjects, the amount of LPS activity in the EVs was positively correlated with a plasma marker of increased intestinal permeability. LPS was also detected in EVs from some control subjects, albeit at lower levels, indicating that additional mechanisms may exist to allow microbiota EVs into circulation, including sub-chronic or transient gut dysbiosis. These microbial EVs can stimulate immune response; however, when derived from probiotic bacterial strains, they may also be beneficial. In a mouse model of colitis, in which intestinal inflammation is induced by administration of dextran sodium sulfate (DSS), the profile of bacterial contributors to the fecal EV milieu was altered to a greater degree than the change seen in microbial taxa diversity in the DSS animals (Kang et al., 2013). For the strain *Akkermansia muciniphila*, DSS did not alter the representation of *A. muciniphila* in the gut flora but significantly reduced the amount of fecal EVs from *A. muciniphila*. Oral administration of *A. muciniphila* EVs alongside DSS was able to recover DSS-induced weight loss, damage to colon epithelial cells, and inflammatory cell infiltration in the colon. None of these symptoms were improved when *A. muciniphila* bacteria was co-administered with DSS.

As briefly mentioned, microbiota-derived EVs and EVs released from endothelial cells containing microbiota-derived EV cargo play a role in the gut-brain axis, in part, by modulating inflammation (reviewed in Cuesta et al., 2021). Previous work indicates that cytokines, a key modulator of inflammation, are not only altered by PAE but can also serve as biomarkers of prenatal exposure and child outcomes. For example, in a clinical study, cytokines were assessed in maternal plasma during the second and third trimesters (Bodnar et al., 2018). Not only were individual cytokines altered by maternal alcohol exposure status, but altered cytokines were also associated with future offspring neurocognitive outcomes, i.e., whether a child showed neurodevelopmental delay. Moreover, statistical modeling identified unique groups, or networks, of cytokines that were associated with alcohol-dependent or alcohol-independent offspring neurodevelopmental delay, indicating that cytokines could discriminate PAE effects from other sources of neurodevelopmental delay. Similarly, in the offspring, networks of plasma cytokines were also able to indicate previous PAE as well as neurodevelopmental status (Bodnar et al., 2020). Preclinically, a number of factors have been shown to shape

these cytokine profiles including additional endocrine molecules (Bodnar et al., 2016), environmental factors like early life stress (Raineki et al., 2017), and genetic sex (Raineki et al., 2017). Given the known roles of gut microbiota, both through EVs and other mechanisms, to shape host inflammatory tone and cytokine profiles (Mendes et al., 2019), further work needs to be done to understand the contribution of gut microbiota to PAE-altered cytokines.

A few preclinical studies have indicated that microbiota-derived EVs can cross the blood–brain barrier. For example, two studies using *in vivo* fluorescent computed tomography imaging of mice found labeled EVs from *Escherichia coli* (Jang et al., 2015) and *Staphylococcus aureus* (Choi et al., 2015) in the mouse heads, although the overall distribution within the brain was not assessed. A similar study that examined *Heliobacter pylori*-derived EVs did not find similar localization to the head (Choi et al., 2017), suggesting that trafficking to the head, and potential subsequent crossing of the blood–brain barrier, by these microbial EVs may be species-of-origin specific. One study examined the brain distribution of *Aggregatibacter actinomycetemcomitans*-derived EVs as a potential link between periodontitis and neuroinflammation (Han et al., 2019). *A. actinomycetemcomitans* EVs with fluorescently labelled membrane and RNA cargo were injected into the heart of 6-week-old male mice. Acutely following the injection (4 h), the EVs were localized within brain blood vessels. After 24 h, diffuse fluorescent signal for both the EV membrane label and the RNA cargo label was found in brain parenchyma, indicating that the microbiota-derived EVs crossed the blood brain barrier and released their RNA cargo.

While microbiota-derived EVs have not been studied in the context of PAE, these data suggest that microbiota likely shape host EVs, including their miRNA and long non-protein-coding RNA (lncRNA) cargo. Critically, these non-protein-coding RNAs have also been implicated in the etiology of FASDs.

5.3. Non-protein-coding RNAs

Non-protein-coding RNAs (ncRNAs) are RNAs that are transcribed but not translated into proteins (Mattick and Makunin, 2006). ncRNAs include multiple RNAs that can range in size, from small, e.g., miRNAs that are 18–22 nucleotides in length, to large, e.g., lncRNAs that are >200 nucleotides in length. These ncRNAs are multi-functional and impact developmental biology, including stem cell biology (Tseng et al., 2018), and are implicated in PAE and FASD (Mahnke et al., 2018). Microbiota can shape both peripheral and brain expression of miRNAs and lncRNAs, indicating a critical role for microbiota in ncRNA biology.

5.3.1. miRNAs

miRNAs act within the cell to fine-tune translation (Bushati and Cohen, 2007), and in the nucleus to control transcription (Roberts, 2014). miRNAs can be released from cells into extracellular fluids, including blood plasma, where they can act as endocrine molecules. We (Balaraman et al., 2016; Salem et al., 2020), and others (Gardiner et al., 2016), found that alcohol exposure during pregnancy can alter the circulating miRNA profile, i.e., miRNAs present in blood plasma and serum. Plasma miRNAs in pregnant women were found to be indicative of future child outcomes (Balaraman et al., 2016; Tseng et al., 2019b), including growth restriction and neurodevelopmental delay. Moreover, in a preclinical mouse model, tail vein injection of these human-identified predictive miRNAs resulted in decreased fetal and placental growth in the absence of ethanol exposure (Tseng et al., 2019b). These data indicate that circulating miRNAs can be biomarkers of effect following PAE as well as endocrine mediators of negative health outcomes, including growth deficits.

Plasma miRNAs present during the neonatal and early infancy periods can also predict future health outcomes. miRNAs in umbilical cord plasma were found to predict neonatal opioid withdrawal syndrome development and severity in neonates prenatally exposed to medications for opioid use disorders (Mahnke et al., 2022). These withdrawal symptoms can develop from 24 h to 7 days after birth (Hudak et al., 2012); indicating that plasma miRNAs can predict short-term neonatal outcomes. Similarly, infant plasma miRNA profile at 2 weeks and 6.5 months of age was altered by PAE (Mahnke et al., 2021). Groups of PAE-altered miRNAs, which were likely biologically related, were identified. The groups of miRNAs in each age group that were associated with inflammation were found to statistically mediate PAE-induced growth deficits and neurodevelopmental delay, indicating that the variance in expression of these miRNAs is related to the PAE-associated outcomes. These data suggest that miRNAs have the potential to predict longer term changes that arise from prenatal exposures. It is likely that a number of tissues secrete miRNAs that contribute to the overall plasma miRNA profile, and gut microbiota are key regulators of the intestinal contribution.

Appropriate miRNA expression in intestinal epithelial cells is critical for intestinal barrier function. Mice with intestinal epithelial cell specific knockout of *Dicer1*, an obligatory gene for the generation of miRNAs, have substantially decreased miRNA content, aberrant intestinal epithelium structure, increased trans-epithelium transport, disrupted expression of genes associated with immune-related pathways, and increased invasion of immune cells into the lamina propria (McKenna et al., 2010). An additional study in intestinal endothelial cell *Dicer1* knockout (KO) mice found that miRNAs had predominantly decreased fecal expression compared to *Dicer1*-expressing control animals (Liu et al., 2016). The *Dicer1* KO mice also had greater between-mouse microbiome diversity and Proteobacteria as the dominant phyla. In contrast, *Dicer1*-expressing mice that had greater between-mouse microbiota similarity and Firmicutes as the dominant phyla. Fecal miRNA can: shape microbiota profile, as fecal miRNA from *Dicer1* expressing mice shifted the microbiome diversity in *Dicer1* KO mice to a higher similarity/lower diversity; and alter intestinal barrier function, as fecal miRNAs from *Dicer1* expressing mice ameliorated weight loss and colon damage in *Dicer1* KO animals in response to DSS-induced colitis. Additional research demonstrated that microbiota induce miRNA expression in intestinal epithelial cells, and thereby regulate gut barrier permeability. In this study, intestinal epithelial cells from conventional mice were found to have 1.5- to 3-fold higher levels of miR-21-5p than germ-free mice, indicating that microbiota regulate intestinal epithelial cell miRNA expression (Nakata et al., 2017). *In vitro*, the elevation of miR-21-5p was implicated with increased barrier permeability, as inhibition of miR-21-5p expression in intestinal epithelial cells increased intestinal barrier electrical resistance, indicating decreased permeability. The researchers further found that miR-21-5p inhibited expression of second messenger signaling pathway members, leading to increased expression of ARF4 which suppressed tight junction proteins.

The relationship between microbiota and miRNAs is not limited to intestinal epithelial cells. Altered circulating miRNAs and gut microbiota were found in human subjects with body mass index in the "obesity" range compared to subjects in the "normal" range (Assmann et al., 2020). A subset of the altered miRNAs and microbiota were correlated across samples, including miRNAs with mRNA targets that include pathways associated with mineral and vitamin absorption. These data suggest a relationship between circulating miRNAs and the microbiota that could be direct, e.g., circulating miRNAs can be in the gut lumen and directly alter microbiota, or indirect, e.g., similar biological mechanisms contribute both to the altered miRNAs and microbiota, which could include responses to altered adiponectin or insulin levels. It is also known that microbiota can shape circulating miRNA profile (Monaghan et al., 2021), which could also explain the correlation between circulating miRNAs and microbiota in these patients.

5.3.2. Long non-coding RNAs

lncRNAs have multiple functions within the cell, including regulating transcription, translation, chromatin remodeling, and protein activity (Mahnke et al., 2018; Sanchez Calle et al., 2018). lncRNAs are important for neurodevelopment, including neurogenesis, cell proliferation, and synaptic pruning (Arzua et al., 2021).

Neural lncRNAs are altered following PAE. In murine neural stem cells, expression of *Oct4pg9*, a lncRNA that arose from a gene duplication event of the pluripotency gene *Oct4*, is increased by ethanol exposure (Salem et al., 2021b). The increased expression of *Oct4pg9* was associated with decreased expression of *Oct4*, which may reflect a reciprocal relationship between the parent gene and the lncRNA as single cell RNA sequencing revealed that *Oct4* and *Oct4pg9* were only co-expressed in ~2% of cells expressing either transcript. In the early murine developing neocortex, single cell RNA sequencing showed that ethanol-exposed female fetuses had decreased X-chromosome inactivation, with decreased expression of the lncRNA *Xist*, increased expression of the reciprocally regulatory lncRNA *Tsix*, and increased expression of genes on the X-chromosome that are typically within the inactivation regions (Salem et al., 2021a). Additional studies using post-mortem tissues of patient with AUDs also indicate that alcohol can impact lncRNAs as a mechanism to disrupt cellular function (reviewed in Mahnke et al., 2018).

Emerging evidence supports a role for intracellular epithelial cell lncRNAs in regulating intestinal epithelium integrity (reviewed in Xiao et al., 2021). The lncRNA *H19* can regulate epithelial health and recovery. In a mouse model of intestinal inflammation, the expression of *H19* was increased in intestinal epithelial cells following systemic administration of LPS (Geng et al., 2018). In genetically modified mice, deletion of the first exon of *H19* impaired crypt epithelial cell proliferation and impaired intestinal recovery following colitis. Moreover, intestinal cell lncRNA content is affected by microbial content. In a comparison between conventional mice, which have commensal gut bacteria, and germ-free mice, which are not exposed to microorganisms, conventional mice had >900 lncRNAs differentially expressed compared to germ-free mice in intestinal tissues (Dempsey et al., 2018). Furthermore, intestinal cell lncRNA content can be shaped in a microbial strain-specific manner. Existing intestinal transcriptome data (Joyce et al., 2014) were reanalyzed to compare lncRNA content between germ-free mice and germ-free mice that were colonized with either commensal microbiota or *Escherichia coli* with or without bile salt hydrolase (Liang et al., 2015). Colonization of germ-free mice upregulated 612 lncRNAs, but only 70 of these lncRNAs were upregulated in more than one group, indicating strain-specific modulation of intestinal lncRNA expression. Intriguingly, microbial colonization of germ-free mice altered lncRNA expression in other organs, including immune related organs (Liang et al., 2015), adipose tissue (Dempsey et al., 2018), liver (Liang et al., 2015; Dempsey et al., 2018), and, critically, the hippocampus (Liang et al., 2015). Additional research has implicated lncRNAs in neurological impacts of altered microbiota. *In silico* analysis of existing mouse transcriptomics data sets found that *Pten* and *Vegfa* were implicated as hub genes for altered gene expression in both the hippocampus and ileum in chronic stress-induced depression models (Abedpoor et al., 2022). Four lncRNAs were identified that were associated with both *Pten* and *Vegfa* and three of these lncRNAs (*Hotair*, *Meg3*, *Gas5*) had similarly altered expression in the hippocampus and ileum of depressed mice. Following an intervention of exercise and leucine, which ameliorated depression-related behaviors, the expression of *Pten, Vegfa*, and the three lncRNAs were partially recovered in both the hippocampus and ileum. In an additional study, germ-free mice were colonized with microbiota from patients with major depressive disorder or contrast patients without depression (Liu et al., 2021). Following fecal transplant, two mRNA-lncRNA-miRNA gene networks were identified in the hippocampus that were significantly different between the two groups. Both of these studies identified hippocampal ncRNA/mRNA networks associated with the gut-brain axis in depression.

One potential contributor to microbiota-altered lncRNA expression across tissues is microbial EVs. Bacteria create small RNAs (sRNAs) that range from 70 and 500 nucleotides in length (Gomez-Lozano et al., 2014), a size range that partially overlaps that for lncRNAs. These sRNAs can be packaged into microbial EVs and affect recipient cell function (Koeppen et al., 2016). As EVs can be found in blood circulation following intestinal barrier disruption, these lncRNA-like cargo may regulate cell biology throughout the host in a similar manner to the host's lncRNAs.

6. Microbial contribution to risks for later-in-life health outcomes

The gut microbiota that is established very early during a newborn's life has a significant and long-lasting impact on the overall health and well-being of the individual. A healthy gut microbiota provides a good start for the offspring's metabolism and immune system that can reduce the risk of adverse secondary conditions later in life. Disruption of the gut by PAE may be part of an initial hit that can lead to increased risk for secondary conditions throughout the lifespan for individuals with FASDs. Preclinically, in an PAE rat model, increased amounts of inflammatory cytokines were found in the mesenteric adipose tissue of adult offspring (Bake et al., 2021) which could be due, in part, to altered microbiota and/or intestinal barrier function. There are also known reciprocal relationships between gut microbiota and metabolic disease (Cani and Delzenne, 2009), and there is clinical evidence for higher rates of multiple metabolic abnormalities in males and an increased risk of being overweight/obese in females with FASDs (Weeks et al., 2020). In this study, effects were conserved across species, as male zebrafish exposed to ethanol embryonically were also predisposed to metabolic disorders and

altered visceral adipose content. In a rat model, adult PAE animals experience worse acute stroke outcomes and impaired long-term recovery following an ischemic stroke, with evidence for increased gut permeability following stroke (Bake et al., 2022). Recent work has shown that gut health is an important therapeutic focus for stroke recovery, as intestinal epithelial stem cell transplant has been shown to improve both acute and long-term recovery following ischemic stroke in a rat model (Mani et al., 2023).

Therefore, early interventions targeting microbiota could lead to improvements not only in neurodevelopment, but health across the lifespan following PAE.

7. Probiotics/prebiotics as a potential therapeutic approach for FASD

As nutritional interventions can directly impact gut microbiota, and nutritional interventions have been efficacious in decreasing negative outcomes following PAE (see section 4), the question becomes whether directly targeting gut microbial communities can have similar positive impacts following PAE. Furthermore, can interventions targeting gut health improve outcomes for secondary conditions which have worse outcomes following PAE, such as stroke, metabolic disorders, and cancer (Burd et al., 2014; Upreti et al., 2022)? In medical and clinical contexts, manipulation of gut microbiota is achieved through the use of pre-, pro-, and syn-biotics. Probiotics contain live microorganisms, whereas prebiotics containing nutritional components (usually non-digestible food fibers) that shape the gut microbial profile and synbiotics contain both probiotics and prebiotics (Pandey et al., 2015). As only a few studies to date have investigated the impact of PAE on gut microbiota, it is yet unknown whether pre/pro/synbiotics could be used as a therapeutic strategy for FASD. However, the administration of the pre/post/synbiotics has been shown preclinically to improve outcomes in neurobehavioral and neurodegenerative disorders, including depression, stress and anxiety-like behaviors (Bravo et al., 2011; Abildgaard et al., 2017), Alzheimer's disease (Rezaei Asl et al., 2019), Parkinson's disease (Rocha et al., 2015). Notably, preclinical research also shows these therapies can improve outcomes in neurodevelopmental disorders, such as ASD (Rocha et al., 2015; Siniscalco et al., 2018). In a randomized, double-blind, placebo-controlled clinical study, *Lactobacillus plantarum 299v* was used as a probiotic bacteria to enhance cognitive functioning in depressed patients (Rudzki et al., 2019). Compared to the placebo group, there was a significant decrease in kynurenine concentration, a tryptophan metabolite made in the liver that negatively affects mood and cognition, in the probiotic-treatment group. Another randomized controlled trial (Santocchi et al., 2020) used a patented and marketed multiple probiotic mixture, Vivomixx®, to investigate the efficacy of probiotic therapy for ASDs. Preschoolers with ASDs were administered either Vivomixx® or placebo based on their daily weight for 6 months. While probiotic supplementation had no statistically significant impact on the severity of ASD in the overall sample, an exploratory secondary analysis compared outcomes in children with ASDs between those who did and did not experience GI symptoms. Probiotic treatment significantly reduced the severity of ASDs in children without GI symptoms, and improved some GI symptoms, adaptive functioning, and sensory profiles in children with GI symptoms.

Given the growing body of evidence for the contribution of maternal-fetal microbiota to neurodevelopment, more research is needed to learn how PAE affects the microbiota, and how pre/pro/synbiotics can be used as a therapeutic approach for FASDs.

8. Conclusion and future directions

The gut microbiota is likely a critical contributor to negative outcomes following PAE, particularly with self-reported rates of gut disturbances in adults with FASDs (Himmelreich et al., 2020) and recent preclinical studies showing dysbiosis in PAE offspring (Bodnar et al., 2022) as well as alterations to bacterial metabolites in the maternal and fetal compartments following alcohol exposure (Virdee et al., 2021). More research is needed to understand how PAE may impact systemic function through the microbiota, including investigation of microbial contribution to biomarkers present in circulation, and how these microbiota impacts may differ by age, genetic, sex, and other key biological variables. Research of other neurodevelopmental disorders has implicated microbiota as a contributing factor to symptom development and severity and have demonstrated promising efficacy of microbial-based interventions. There is likely a reciprocal relationship between the nutritional deficits found following PAE and alterations to the gut microbiota, indicating that probiotic and prebiotic therapies could ameliorate negative outcomes following PAE and improve the quality of life for individuals with FASDs.

Notably, many of the studies implicating the microbiota and nutrition in FASDs and other neurodevelopmental diseases are correlational. In addition to the needed experiments and gaps in knowledge highlighted throughout this review, further experiments are required to interrogate where microbiota and nutrition are mechanistically linked to FASDs and determine systemic locations for therapeutic intervention. Rigorous experiments should be designed to account for subject variables that influence microbiota composition, including chromosomal and gonadal sex, diet, medication usage, age, and, in animal research, species. Gender, or the ways the presentation of genetic sex is impacted by sociocultural factors, is likely also a critical variable, particularly as receipt of gender-affirming care has been shown to alter the microbiome (reviewed in Krakowsky et al., 2022), but is drastically understudied. Sex is a particularly important factor for consideration, as sex-specific microbiotas have been identified in human and animal research, and has been the subject of recent review articles (Kim and Benayoun, 2020; Valeri and Endres, 2021). Although investigations of sexually-dimorphic FASD outcomes mediated by microbiota are currently lacking, biological sex has been shown to influence the gut-brain axis in individuals with other neurodevelopmental disorders. One research group has argued that the relationship between ASD and microbiota is heavily influenced by reduced variability in food preference (Yap et al., 2021). Others have found that the degree of microbiome diversity between individuals with and without ASD is mediated by sex, in humans (Wang et al., 2019) and rodents (Coretti et al., 2017), further supporting the need to investigate the interactions between multiple subject factors in individuals with FASDs. The role of biological sex underlying gut-brain axis function in individuals with other neurodevelopmental and neuropsychiatric disorders, including ADHD, anxiety, and depression, has been interrogated in a separate review article (Shobeiri et al., 2022). Given the comorbidity of FASD and other neurodevelopmental and

neuropsychiatric disorders (e.g., Kambeitz et al., 2019; Coles et al., 2022), as well as common physical and behavioral symptoms across these disorders, it is likely that sex contributes to distinct microbiota alterations in individuals with FASDs.

Author contributions

DU, SR, and AM contributed to conception and design of the review. DU, SR, AB, EL, RK, and AM wrote sections of the manuscript. RM and AM revised the work critically for important intellectual content. All authors contributed to manuscript revision, read, and approved the submitted version.

Funding

This work was supported by the National Institute on Alcohol Abuse and Alcoholism (F32AA029866, SR) and by Texas A&M University's Accountability, Climate, Equity, and Scholarship (ACES) Faculty Fellows Program (AM).

Conflict of interest

The authors declare that the research was conducted in the absence of any commercial or financial relationships that could be construed as a potential conflict of interest.

Publisher's note

All claims expressed in this article are solely those of the authors and do not necessarily represent those of their affiliated organizations, or those of the publisher, the editors and the reviewers. Any product that may be evaluated in this article, or claim that may be made by its manufacturer, is not guaranteed or endorsed by the publisher.

References

Aagaard, K., Ma, J., Antony, K. M., Ganu, R., Petrosino, J., and Versalovic, J. (2014). The placenta harbors a unique microbiome. *Sci. Transl. Med.* 6:237ra265. doi: 10.1126/scitranslmed.3008599

Abedpoor, N., Taghian, F., and Hajibabaie, F. (2022). Cross brain-gut analysis highlighted hub genes and LncRNA networks differentially modified during leucine consumption and endurance exercise in mice with depression-like behaviors. *Mol. Neurobiol.* 59, 4106–4123. doi: 10.1007/s12035-022-02835-1

Abildgaard, A., Elfving, B., Hokland, M., Wegener, G., and Lund, S. (2017). Probiotic treatment reduces depressive-like behaviour in rats independently of diet. *Psychoneuroendocrinology* 79, 40–48. doi: 10.1016/j.psyneuen.2017.02.014

Akison, L. K., Kuo, J., Reid, N., Boyd, R. N., and Moritz, K. M. (2018). Effect of choline supplementation on neurological, cognitive, and behavioral outcomes in offspring arising from alcohol exposure during development: a quantitative systematic review of clinical and preclinical studies. *Alcohol. Clin. Exp. Res.* 42, 1591–1611. doi: 10.1111/acer.13817

America's Health Rankings (2023). Analysis of CDC, pregnancy risk assessment monitoring system or state equivalent, (ed.) U.H. Foundation. Available at: AmericasHealthRankings.org

Anand, S., and Mande, S. S. (2018). Diet, microbiota and gut-lung connection. *Front. Microbiol.* 9:2147. doi: 10.3389/fmicb.2018.02147

Arias, N., Arboleya, S., Allison, J., Kaliszewska, A., Higarza, S. G., Gueimonde, M., et al. (2020). The relationship between choline bioavailability from diet, intestinal microbiota composition, and its modulation of human diseases. *Nutrients* 12:2340. doi: 10.3390/nu12082340

Arzua, T., Jiang, C., Yan, Y., and Bai, X. (2021). The importance of non-coding RNAs in environmental stress-related developmental brain disorders: a systematic review of evidence associated with exposure to alcohol, anesthetic drugs, nicotine, and viral infections. *Neurosci. Biobehav. Rev.* 128, 633–647. doi: 10.1016/j.neubiorev.2021.06.033

Assadi, F. K., and Ziai, M. (1986). Zinc status of infants with fetal alcohol syndrome. *Pediatr. Res.* 20, 551–554. doi: 10.1203/00006450-198606000-00014

Assmann, T. S., Cuevas-Sierra, A., Riezu-Boj, J. I., Milagro, F. I., and Martinez, J. A. (2020). Comprehensive analysis reveals novel interactions between circulating MicroRNAs and gut microbiota composition in human obesity. *Int. J. Mol. Sci.* 21:9509. doi: 10.3390/ijms21249509

Avni, E., Ben-Itzchak, E., and Zachor, D. A. (2018). The presence of comorbid ADHD and anxiety symptoms in autism spectrum disorder: clinical presentation and predictors. *Front. Psych.* 9:717. doi: 10.3389/fpsyt.2018.00717

Azaïs-Braesco, V., and Pascal, G. (2000). Vitamin a in pregnancy: requirements and safety limits. *Am. J. Clin. Nutr.* 71, 1325S–1333S. doi: 10.1093/ajcn/71.5.1325s

Bajaj, J. S., Gavis, E. A., Fagan, A., Wade, J. B., Thacker, L. R., Fuchs, M., et al. (2021). A randomized clinical trial of fecal microbiota transplant for Alcohol use disorder. *Hepatology* 73, 1688–1700. doi: 10.1002/hep.31496

Bake, S., Hurst, D. A., Miranda, R. C., and Sohrabji, F. (2022). Prenatal alcohol exposure exacerbates acute sensorimotor deficits and impedes long-term behavioral recovery from the effects of an adult-onset cerebrovascular ischemic stroke. *Alcohol. Clin. Exp. Res.* 46, 2267–2279. doi: 10.1111/acer.14952

Bake, S., Pinson, M. R., Pandey, S., Chambers, J. P., Mota, R., Fairchild, A. E., et al. (2021). Prenatal alcohol-induced sex differences in immune, metabolic and neurobehavioral outcomes in adult rats. *Brain Behav. Immun.* 98, 86–100. doi: 10.1016/j.bbi.2021.08.207

Bakhireva, L. N., and Savage, D. D. (2011). Focus on: biomarkers of fetal alcohol exposure and fetal alcohol effects. *Alcohol Res. Health* 34, 56–63.

Bakhireva, L. N., Sharkis, J., Shrestha, S., Miranda-Sohrabji, T. J., Williams, S., and Miranda, R. C. (2017). Prevalence of prenatal alcohol exposure in the state of Texas as assessed by phosphatidylethanol in newborn dried blood spot specimens. *Alcohol. Clin. Exp. Res.* 41, 1004–1011. doi: 10.1111/acer.13375

Balaraman, S., Schafer, J. J., Tseng, A. M., Wertelecki, W., Yevtushok, L., Zymak-Zakutnya, N., et al. (2016). Plasma miRNA profiles in pregnant women predict infant outcomes following prenatal alcohol exposure. *PLoS One* 11:e0165081. doi: 10.1371/journal.pone.0165081

Bandoli, G., Kable, J. A., Coles, C. D., Del Campo, M., Suttie, M., and Chambers, C. D. (2022). Trajectories of prenatal alcohol exposure and behavioral outcomes: findings from a community-based sample. *Drug Alcohol Depend.* 233:109351. doi: 10.1016/j.drugalcdep.2022.109351

Bangma, J. T., Hartwell, H., Santos, H. P. Jr., O'Shea, T. M., and Fry, R. C. (2021). Placental programming, perinatal inflammation, and neurodevelopment impairment among those born extremely preterm. *Pediatr. Res.* 89, 326–335. doi: 10.1038/s41390-020-01236-1

Barbara, G., Feinle-Bisset, C., Ghoshal, U. C., Quigley, E. M., Santos, J., Vanner, S., et al. (2016). The intestinal microenvironment and functional gastrointestinal disorders. *Gastroenterology.* 150, 1305–1318. doi: 10.1053/j.gastro.2016.02.028

Bernes, G. A., Villodas, M., Coles, C. D., Kable, J. A., May, P. A., Kalberg, W. O., et al. (2021). Validity and reliability of executive function measures in children with heavy prenatal Alcohol exposure: correspondence between multiple raters and laboratory measures. *Alcohol. Clin. Exp. Res.* 45, 596–607. doi: 10.1111/acer.14547

Bitsko, R. H., Claussen, A. H., Lichstein, J., Black, L. I., Jones, S. E., Danielson, M. L., et al. (2022). Mental health surveillance among children - United States, 2013-2019. *MMWR Suppl* 71, 1–42. doi: 10.15585/mmwr.su7102a1

Blaner, W. S., Shmarakov, I. O., and Traber, M. G. (2021). Vitamin a and vitamin E: will the real antioxidant please stand up? *Annu. Rev. Nutr.* 41, 105–131. doi: 10.1146/annurev-nutr-082018-124228

Blaser, M. J., Devkota, S., McCoy, K. D., Relman, D. A., Yassour, M., and Young, V. B. (2021). Lessons learned from the prenatal microbiome controversy. *Microbiome* 9:8. doi: 10.1186/s40168-020-00946-2

Bloor, S. R., Schutte, R., and Hobson, A. R. (2021). Oral Iron supplementation—gastrointestinal side effects and the impact on the gut microbiota. *Microbiol. Res.* 12, 491–502. doi: 10.3390/microbiolres12020033

Bodnar, T. S., Hill, L. A., and Weinberg, J. (2016). Evidence for an immune signature of prenatal alcohol exposure in female rats. *Brain Behav. Immun.* 58, 130–141. doi: 10.1016/j.bbi.2016.05.022

Bodnar, T. S., Lee, C., Wong, A., Rubin, I., Wegener Parfrey, L., and Weinberg, J. (2022). Evidence for long-lasting alterations in the fecal microbiota following prenatal alcohol exposure. *Alcohol. Clin. Exp. Res.* 46, 542–555. doi: 10.1111/acer.14784

Bodnar, T. S., Raineki, C., Wertelecki, W., Yevtushok, L., Plotka, L., Granovska, I., et al. (2020). Immune network dysregulation associated with child neurodevelopmental delay: modulatory role of prenatal alcohol exposure. *J. Neuroinflammation* 17:39. doi: 10.1186/s12974-020-1717-8

Bodnar, T. S., Raineki, C., Wertelecki, W., Yevtushok, L., Plotka, L., Zymak-Zakutnya, N., et al. (2018). Altered maternal immune networks are associated with adverse child neurodevelopment: impact of alcohol consumption during pregnancy. *Brain Behav. Immun.* 73, 205–215. doi: 10.1016/j.bbi.2018.05.004

Bolte, E. E., Moorshead, D., and Aagaard, K. M. (2022). Maternal and early life exposures and their potential to influence development of the microbiome. *Genome Med.* 14:4. doi: 10.1186/s13073-021-01005-7

Bonthius, D. J., and West, J. R. (1990). Alcohol-induced neuronal loss in developing rats: increased brain damage with binge exposure. *Alcohol. Clin. Exp. Res.* 14, 107–118. doi: 10.1111/j.1530-0277.1990.tb00455.x

Bradley, R., Lakpa, K. L., Burd, M., Mehta, S., Katusic, M. Z., and Greenmyer, J. R. (2022). Fetal alcohol Spectrum disorder and Iron homeostasis. *Nutrients* 14:4223 doi: 10.3390/nu14204223

Braniste, V., Al-Asmakh, M., Kowal, C., Anuar, F., Abbaspour, A., Toth, M., et al. (2014). The gut microbiota influences blood-brain barrier permeability in mice. *Sci. Transl. Med.* 6:263ra158. doi: 10.1126/scitranslmed.3009759

Bravo, J. A., Forsythe, P., Chew, M. V., Escaravage, E., Savignac, H. M., Dinan, T. G., et al. (2011). Ingestion of Lactobacillus strain regulates emotional behavior and central GABA receptor expression in a mouse via the vagus nerve. *Proc. Natl. Acad. Sci. U. S. A.* 108, 16050–16055. doi: 10.1073/pnas.1102999108

Buie, T., Campbell, D. B., Fuchs, G. J. 3rd, Furuta, G. T., Levy, J., Vandewater, J., et al. (2010). Evaluation, diagnosis, and treatment of gastrointestinal disorders in individuals with ASDs: a consensus report. *Pediatrics* 125, S1–S18. doi: 10.1542/peds.2009-1878C

Burd, L. (2016). FASD and ADHD: are they related and how? *BMC Psychiatry* 16:325. doi: 10.1186/s12888-016-1028-x

Burd, L., Peterson, L., and Kobrinsky, N. (2014). Fetal alcohol spectrum disorders and childhood cancer: a concise review of case reports and future research considerations. *Pediatr. Blood Cancer* 61, 768–770. doi: 10.1002/pbc.24886

Burd, L., and Popova, S. (2019). Fetal alcohol spectrum disorders: fixing our aim to aim for the fix. *Int. J. Environ. Res. Public Health* 16:3978. doi: 10.3390/ijerph16203978

Burdge, G. C., Wright, S. M., Warner, J. O., and Postle, A. D. (1997). Fetal brain and liver phospholipid fatty acid composition in a guinea pig model of fetal alcohol syndrome: effect of maternal supplementation with tuna oil. *J. Nutr. Biochem.* 8, 438–444. doi: 10.1016/S0955-2863(97)00051-X

Bushati, N., and Cohen, S. M. (2007). microRNA functions. *Annu. Rev. Cell Dev. Biol.* 23, 175–205. doi: 10.1146/annurev.cellbio.23.090506.123406

Cani, P. D., and Delzenne, N. M. (2009). The role of the gut microbiota in energy metabolism and metabolic disease. *Curr. Pharm. Des.* 15, 1546–1558. doi: 10.2174/138161209788168164

Carter, R. C., Georgieff, M. K., Ennis, K. M., Dodge, N. C., Wainwright, H., Meintjes, E. M., et al. (2021). Prenatal alcohol-related alterations in maternal, placental, neonatal, and infant iron homeostasis. *Am. J. Clin. Nutr.* 114, 1107–1122. doi: 10.1093/ajcn/nqab165

Carter, R. C., Jacobson, J. L., Molteno, C. D., Dodge, N. C., Meintjes, E. M., and Jacobson, S. W. (2016). Fetal Alcohol growth restriction and cognitive impairment. *Pediatrics* 138. doi: 10.1542/peds.2016-0775

Carter, R. C., Sandra, W., Molteno, J.C. D., and Jacobson, J. L. (2007). FFetal Alcohol Exposure, Iron-Deficiency Anemia, and Infant Growth. Pediatrics September. 120, 559–567. doi: 10.1542/peds.2007-0151

Carter, R. C., Jacobson, J. L., Molteno, C. D., Jiang, H., Meintjes, E. M., Jacobson, S. W., et al. (2012). Effects of heavy prenatal Alcohol exposure and Iron deficiency Anemia on child growth and body composition through age 9 years. *Alcohol* 36, 1973–1982. doi: 10.1111/j.1530-0277.2012.01810.x

Caton, S. J., Ball, M., Ahern, A., and Hetherington, M. M. (2004). Dose-dependent effects of alcohol on appetite and food intake. *Physiol. Behav.* 81, 51–58. doi: 10.1016/j.physbeh.2003.12.017

Caton, S. J., Bate, L., and Hetherington, M. M. (2007). Acute effects of an alcoholic drink on food intake: aperitif versus co-ingestion. *Physiol. Behav.* 90, 368–375. doi: 10.1016/j.physbeh.2006.09.028

Caton, S. J., Marks, J. E., and Hetherington, M. M. (2005). Pleasure and alcohol: manipulating pleasantness and the acute effects of alcohol on food intake. *Physiol. Behav.* 84, 371–377. doi: 10.1016/j.physbeh.2004.12.013

Caton, S. J., Nolan, L. J., and Hetherington, M. M. (2015). Alcohol, appetite and loss of restraint. *Curr. Obes. Rep.* 4, 99–105. doi: 10.1007/s13679-014-0130-y

Chandra, R. K. (1997). Nutrition and the immune system: an introduction. *Am. J. Clin. Nutr.* 66, 460S–463S. doi: 10.1093/ajcn/66.2.460S

Chen, B., Liu, S., Feng, D., Xiao, L., Yang, T., Li, T., et al. (2020). Vitamin a deficiency in the early-life periods alters a diversity of the colonic mucosal microbiota in rats. *Front. Nutr.* 7:580780. doi: 10.3389/fnut.2020.580780

Cho, Y. E., Song, B. J., Akbar, M., and Baek, M. C. (2018). Extracellular vesicles as potential biomarkers for alcohol- and drug-induced liver injury and their therapeutic applications. *Pharmacol. Ther.* 187, 180–194. doi: 10.1016/j.pharmthera.2018.03.009

Choi, H. I., Choi, J. P., Seo, J., Kim, B. J., Rho, M., Han, J. K., et al. (2017). Helicobacter pylori-derived extracellular vesicles increased in the gastric juices of gastric adenocarcinoma patients and induced inflammation mainly via specific targeting of gastric epithelial cells. *Exp. Mol. Med.* 49:e330. doi: 10.1038/emm.2017.47

Choi, S. J., Kim, M. H., Jeon, J., Kim, O. Y., Choi, Y., Seo, J., et al. (2015). Active immunization with extracellular vesicles derived from Staphylococcus aureus effectively protects against staphylococcal lung infections, mainly via Th1 cell-mediated immunity. *PLoS One* 10:e0136021. doi: 10.1371/journal.pone.0136021

Choi, Y., Lee, S., Kim, S., Lee, J., Ha, J., Oh, H., et al. (2020). Vitamin E (alpha-tocopherol) consumption influences gut microbiota composition. *Int. J. Food Sci. Nutr.* 71, 221–225. doi: 10.1080/09637486.2019.1639637

Chung, D. D., Pinson, M. R., Mahnke, A. H., Salem, N. A., Le, K. T., Payne, E. A., et al. (2022). Dose-related shifts in proteome and function of extracellular vesicles secreted by fetal neural stem cells following chronic alcohol exposure. *Heliyon* 8:e11348. doi: 10.1016/j.heliyon.2022.e11348

Clevidence, B. A., Taylor, P. R., Campbell, W. S., and Judd, J. T. (1995). Lean and heavy women may not use energy from alcohol with equal efficiency. *J. Nutr.* 125, 2536–2540. doi: 10.1093/jn/125.10.2536

Colditz, G. A., Giovannucci, E., Rimm, E. B., Stampfer, M. J., Rosner, B., Speizer, F. E., et al. (1991). Alcohol intake in relation to diet and obesity in women and men. *Am. J. Clin. Nutr.* 54, 49–55. doi: 10.1093/ajcn/54.1.49

Coles, C. D., Grant, T. M., Kable, J. A., Stoner, S. A., and Perez, A.Collaborative Initiative on Fetal Alcohol Spectrum (2022). Prenatal alcohol exposure and mental health at midlife: a preliminary report on two longitudinal cohorts. *Alcohol. Clin. Exp. Res.* 46, 232–242. doi: 10.1111/acer.14761

Coles, C. D., Platzman, K. A., Raskind-Hood, C. L., Brown, R. T., Falek, A., and Smith, I. E. (1997). A comparison of children affected by prenatal alcohol exposure and attention deficit, hyperactivity disorder. *Alcohol. Clin. Exp. Res.* 21, 150–161. doi: 10.1111/j.1530-0277.1997.tb03743.x

Collado, M. C., Rautava, S., Aakko, J., Isolauri, E., and Salminen, S. (2016). Human gut colonisation may be initiated in utero by distinct microbial communities in the placenta and amniotic fluid. *Sci. Rep.* 6:23129. doi: 10.1038/srep23129

Coretti, L., Cristiano, C., Florio, E., Scala, G., Lama, A., Keller, S., et al. (2017). Sex-related alterations of gut microbiota composition in the BTBR mouse model of autism spectrum disorder. *Sci. Rep.* 7:45356. doi: 10.1038/srep45356

Cortes-Albornoz, M. C., Garcia-Guaqueta, D. P., Velez-van-Meerbeke, A., and Talero-Gutierrez, C. (2021). Maternal nutrition and neurodevelopment: a scoping review. *Nutrients* 13:3530. doi: 10.3390/nu13103530

Cryan, J. F., and Dinan, T. G. (2012). Mind-altering microorganisms: the impact of the gut microbiota on brain and behaviour. *Nat. Rev. Neurosci.* 13, 701–712. doi: 10.1038/nrn3346

Cuesta, C. M., Guerri, C., Urena, J., and Pascual, M. (2021). Role of microbiota-derived extracellular vesicles in gut-brain communication. *Int. J. Mol. Sci.* 22:4235. doi: 10.3390/ijms22084235

Darbinian, N., Darbinyan, A., Sinard, J., Tatevosian, G., Merabova, N., D'Amico, F., et al. (2022). Molecular markers in maternal blood exosomes allow early detection of fetal alcohol spectrum disorders. *Int. J. Mol. Sci.* 24:135. doi: 10.3390/ijms24010135

Dasgupta, S., Arya, S., Choudhary, S., and Jain, S. K. (2016). Amniotic fluid: source of trophic factors for the developing intestine. *World J Gastrointest Pathophysiol* 7, 38–47. doi: 10.4291/wjgp.v7.i1.38

David, L. A., Maurice, C. F., Carmody, R. N., Gootenberg, D. B., Button, J. E., Wolfe, B. E., et al. (2014). Diet rapidly and reproducibly alters the human gut microbiome. *Nature* 505, 559–563. doi: 10.1038/nature12820

Dempsey, J., Zhang, A., and Cui, J. Y. (2018). Coordinate regulation of long non-coding RNAs and protein-coding genes in germ-free mice. *BMC Genomics* 19:834. doi: 10.1186/s12864-018-5235-3

DiBattista, A., Ogrel, S., MacKenzie, A. E., and Chakraborty, P. (2022). Quantitation of phosphatidylethanols in dried blood spots to determine rates of prenatal alcohol exposure in Ontario. *Alcohol. Clin. Exp. Res.* 46, 243–251. doi: 10.1111/acer.14766

Draghici, C.-C., Miulescu, R.-G., Petca, R.-C., Petca, A., Dumitrașcu, M. C., and Șandru, F. (2021). Teratogenic effect of isotretinoin in both fertile females and males. *Exp. Ther. Med.* 21, 1–5. doi: 10.3892/etm.2021.9966

Du, Y., Li, L., Gong, C., Li, T., and Xia, Y. (2022). The diversity of the intestinal microbiota in patients with alcohol use disorder and its relationship to alcohol consumption and cognition. *Front. Psych.* 13:1054685. doi: 10.3389/fpsyt.2022.1054685

Ducker, G. S., and Rabinowitz, J. D. (2017). One-carbon metabolism in health and disease. *Cell Metab.* 25, 27–42. doi: 10.1016/j.cmet.2016.08.009

Eastwood, J., Walton, G., Van Hemert, S., Williams, C., and Lamport, D. (2021). The effect of probiotics on cognitive function across the human lifespan: a systematic review. *Neurosci. Biobehav. Rev.* 128, 311–327. doi: 10.1016/j.neubiorev.2021.06.032

Fábrega, M. J., Aguilera, L., Giménez, R., Varela, E., Alexandra Cañas, M., Antolín, M., et al. (2016). Activation of immune and defense responses in the intestinal mucosa by outer membrane vesicles of commensal and probiotic *Escherichia coli* strains. *Front. Microbiol.* 7:705. doi: 10.3389/fmicb.2016.00705

Fardini, Y., Chung, P., Dumm, R., Joshi, N., and Han, Y. W. (2010). Transmission of diverse oral bacteria to murine placenta: evidence for the oral microbiome as a potential source of intrauterine infection. *Infect. Immun.* 78, 1789–1796. doi: 10.1128/IAI.01395-09

Ferdous, J., Mukherjee, R., Ahmed, K. T., and Ali, D. W. (2017). Retinoic acid prevents synaptic deficiencies induced by alcohol exposure during gastrulation in zebrafish embryos. *Neurotoxicology* 62, 100–110. doi: 10.1016/j.neuro.2017.05.011

Ferreira, R. L. U., Sena-Evangelista, K. C. M., de Azevedo, E. P., Pinheiro, F. I., Cobucci, R. N., and Pedrosa, L. F. C. (2021). Selenium in human health and gut microflora: bioavailability of selenocompounds and relationship with diseases. *Front. Nutr.* 8:685317. doi: 10.3389/fnut.2021.685317

Finer, L. B., and Zolna, M. R. (2016). Declines in unintended pregnancy in the United States, 2008-2011. *N. Engl. J. Med.* 374, 843–852. doi: 10.1056/NEJMsa1506575

Frost, F., Kacprowski, T., Ruhlemann, M., Pietzner, M., Bang, C., Franke, A., et al. (2021). Long-term instability of the intestinal microbiome is associated with metabolic liver disease, low microbiota diversity, diabetes mellitus and impaired exocrine pancreatic function. *Gut* 70, c–530. doi: 10.1136/gutjnl-2020-322753

Gao, K., Mu, C. L., Farzi, A., and Zhu, W. Y. (2020). Tryptophan metabolism: a link between the gut microbiota and brain. *Adv. Nutr.* 11, 709–723. doi: 10.1093/advances/nmz127

Gardella, B., Dominoni, M., Scatigno, A. L., Cesari, S., Fiandrino, G., Orcesi, S., et al. (2022). What is known about neuroplacentology in fetal growth restriction and in preterm infants: a narrative review of literature. *Front Endocrinol* 13:936171. doi: 10.3389/fendo.2022.936171

Gardiner, A. S., Gutierrez, H. L., Luo, L., Davies, S., Savage, D. D., Bakhireva, L. N., et al. (2016). Alcohol use during pregnancy is associated with specific alterations in microRNA levels in maternal serum. *Alcohol. Clin. Exp. Res.* 40, 826–837. doi: 10.1111/acer.13026

Gareau, M. G., Wine, E., Rodrigues, D. M., Cho, J. H., Whary, M. T., Philpott, D. J., et al. (2011). Bacterial infection causes stress-induced memory dysfunction in mice. *Gut* 60, 307–317. doi: 10.1136/gut.2009.202515

Geng, H., Bu, H. F., Liu, F., Wu, L., Pfeifer, K., Chou, P. M., et al. (2018). In inflamed intestinal tissues and epithelial cells, interleukin 22 signaling increases expression of H19 Long noncoding RNA, Which Promotes Mucosal Regeneration. *Gastroenterology* 155, 144–155. doi: 10.1053/j.gastro.2018.03.058

Ghishan, F. K., Patwardhan, R., and Greene, H. L. (1982). Fetal alcohol syndrome: inhibition of placental zinc transport as a potential mechanism for fetal growth retardation in the rat. *J. Lab. Clin. Med.* 100, 45–52.

Gkougka, D., Mitropoulos, K., Tzanakaki, G., Panagouli, E., Psaltopoulou, T., Thomaidis, L., et al. (2022). Gut microbiome and attention deficit/hyperactivity disorder: a systematic review. *Pediatr. Res.* 92, 1507–1519. doi: 10.1038/s41390-022-02027-6

Godfrey, K. M. (2002). The role of the placenta in fetal programming-a review. *Placenta* 23 Suppl A, S20–S27. doi: 10.1053/plac.2002.0773

Goehler, L. E., Park, S. M., Opitz, N., Lyte, M., and Gaykema, R. P. (2008). Campylobacter jejuni infection increases anxiety-like behavior in the holeboard: possible anatomical substrates for viscerosensory modulation of exploratory behavior. *Brain Behav. Immun.* 22, 354–366. doi: 10.1016/j.bbi.2007.08.009

Goldenberg, R. L., Hauth, J. C., and Andrews, W. W. (2000). Intrauterine infection and preterm delivery. *N. Engl. J. Med.* 342, 1500–1507. doi: 10.1056/NEJM200005183422007

Gomez-Lozano, M., Marvig, R. L., Molin, S., and Long, K. S. (2014). Identification of bacterial small RNAs by RNA sequencing. *Methods Mol. Biol.* 1149, 433–456. doi: 10.1007/978-1-4939-0473-0_34

Goswami, C., Iwasaki, Y., and Yada, T. (2018). Short-chain fatty acids suppress food intake by activating vagal afferent neurons. *J. Nutr. Biochem.* 57, 130–135. doi: 10.1016/j.jnutbio.2018.03.009

Han, E. C., Choi, S. Y., Lee, Y., Park, J. W., Hong, S. H., and Lee, H. J. (2019). Extracellular RNAs in periodontopathogenic outer membrane vesicles promote TNF-alpha production in human macrophages and cross the blood-brain barrier in mice. *FASEB J.* 33, 13412–13422. doi: 10.1096/fj.201901575R

Haushalter, C., Asselin, L., Fraulob, V., Dolle, P., and Rhinn, M. (2017). Retinoic acid controls early neurogenesis in the developing mouse cerebral cortex. *Dev. Biol.* 430, 129–141. doi: 10.1016/j.ydbio.2017.08.006

He, Q., Kwok, L. Y., Xi, X., Zhong, Z., Ma, T., Xu, H., et al. (2020). The meconium microbiota shares more features with the amniotic fluid microbiota than the maternal fecal and vaginal microbiota. *Gut Microbes* 12:1794266. doi: 10.1080/19490976.2020.1794266

Helfrich, K. K., Saini, N., Kwan, S. T. C., Rivera, O. C., Hodges, R., and Smith, S. M. (2022). Gestational iron supplementation improves fetal outcomes in a rat model of prenatal alcohol exposure. *Nutrients* 14:1653. doi: 10.3390/nu14081653

Helfrich, K. K., Saini, N., Kwan, S. T. C., Rivera, O. C., Mooney, S. M., and Smith, S. M. (2023). Fetal anemia and elevated hepcidin in a mouse model of fetal alcohol spectrum disorder. *Pediatr. Res.* doi: 10.1038/s41390-023-02469-6

Himmelreich, M., Lutke, C. J., and Hargrove, E. T. (2020). "The lay of the land" in *The Routledge handbook of social work and addictive behaviors* (London, UK: Routledge).

Hodyl, N. A., Aboustate, N., Bianco-Miotto, T., Roberts, C. T., Clifton, V. L., and Stark, M. J. (2017). Child neurodevelopmental outcomes following preterm and term birth: what can the placenta tell us? *Placenta* 57, 79–86. doi: 10.1016/j.placenta.2017.06.009

Hoyme, H. E., Kalberg, W. O., Elliott, A. J., Blankenship, J., Buckley, D., Marais, A. S., et al. (2016). Updated clinical guidelines for diagnosing Fetal Alcohol Spectrum disorders. *Pediatrics* 138. doi: 10.1542/peds.2015-4256

Hudak, M. L., Tan, R. C., Committee On, D., and Committee On, F.Newborn, and American Academy of, P (2012). Neonatal drug withdrawal. *Pediatrics* 129, e540–e560. doi: 10.1542/peds.2011-3212

Huebner, S. M., Blohowiak, S. E., Kling, P. J., and Smith, S. M. (2016). Prenatal alcohol exposure alters fetal iron distribution and elevates hepatic hepcidin in a rat model of fetal alcohol spectrum disorders. *J. Nutr.* 146, 1180–1188. doi: 10.3945/jn.115.227983

Huebner, S. M., Helfrich, K. K., Saini, N., Blohowiak, S. E., Cheng, A. A., Kling, P. J., et al. (2018). Dietary iron fortification normalizes fetal hematology, hepcidin, and iron distribution in a rat model of prenatal alcohol exposure. *Alcohol. Clin. Exp. Res.* 42, 1022–1033. doi: 10.1111/acer.13754

Husted, A. S., Trauelsen, M., Rudenko, O., Hjorth, S. A., and Schwartz, T. W. (2017). GPCR-mediated signaling of metabolites. *Cell Metab.* 25, 777–796. doi: 10.1016/j.cmet.2017.03.008

Idrus, N. M., Breit, K. R., and Thomas, J. D. (2017). Dietary choline levels modify the effects of prenatal alcohol exposure in rats. *Neurotoxicol. Teratol.* 59, 43–52. doi: 10.1016/j.ntt.2016.11.007

Iyer, N., and Vaishnava, S. (2019). Vitamin a at the interface of host-commensal-pathogen interactions. *PLoS Pathog.* 15:e1007750. doi: 10.1371/journal.ppat.1007750

Jacobson, S. W., Carter, R. C., Molteno, C. D., Stanton, M. E., Herbert, J. S., Lindinger, N. M., et al. (2018). Efficacy of maternal choline supplementation during pregnancy in mitigating adverse effects of prenatal Alcohol exposure on growth and cognitive function: a randomized, double-blind, placebo-controlled clinical trial. *Alcohol. Clin. Exp. Res.* 42, 1327–1341. doi: 10.1111/acer.13769

Jang, S. C., Kim, S. R., Yoon, Y. J., Park, K. S., Kim, J. H., Lee, J., et al. (2015). In vivo kinetic biodistribution of nano-sized outer membrane vesicles derived from bacteria. *Small* 11, 456–461. doi: 10.1002/smll.201401803

Jašarević, E., Hill, E. M., Kane, P. J., Rutt, L., Gyles, T., Folts, L., et al. (2021). The composition of human vaginal microbiota transferred at birth affects offspring health in a mouse model. *Nat. Commun.* 12:6289. doi: 10.1038/s41467-021-26634-9

Jašarević, E., Howerton, C. L., Howard, C. D., and Bale, T. L. (2015). Alterations in the vaginal microbiome by maternal stress are associated with metabolic reprogramming of the offspring gut and brain. *Endocrinology* 156, 3265–3276. doi: 10.1210/en.2015-1177

Jiang, H. Y., Zhou, Y. Y., Zhou, G. L., Li, Y. C., Yuan, J., Li, X. H., et al. (2018). Gut microbiota profiles in treatment-naive children with attention deficit hyperactivity disorder. *Behav. Brain Res.* 347, 408–413. doi: 10.1016/j.bbr.2018.03.036

Jijon, H. B., Suarez-Lopez, L., Diaz, O. E., Das, S., De Calisto, J., Parada-kusz, M., et al. (2018). Intestinal epithelial cell-specific RARα depletion results in aberrant epithelial cell homeostasis and underdeveloped immune system. *Mucosal Immunol.* 11, 703–715. doi: 10.1038/mi.2017.91

Jomova, K., Makova, M., Alomar, S. Y., Alwasel, S. H., Nepovimova, E., Kuca, K., et al. (2022). Essential metals in health and disease. *Chem. Biol. Interact.* 367:110173. doi: 10.1016/j.cbi.2022.110173

Jones, K. L., Robinson, L. K., Bakhireva, L. N., Marintcheva, G., Storojev, V., Strahova, A., et al. (2006). Accuracy of the diagnosis of physical features of fetal alcohol syndrome by pediatricians after specialized training. *Pediatrics* 118, e1734–e1738. doi: 10.1542/peds.2006-1037

Joyce, S. A., MacSharry, J., Casey, P. G., Kinsella, M., Murphy, E. F., Shanahan, F., et al. (2014). Regulation of host weight gain and lipid metabolism by bacterial bile acid modification in the gut. *Proc. Natl. Acad. Sci. U. S. A.* 111, 7421–7426. doi: 10.1073/pnas.1323599111

Kalbermatter, C., Fernandez Trigo, N., Christensen, S., and Ganal-Vonarburg, S. C. (2021). Maternal microbiota, early life colonization and breast Milk drive immune development in the newborn. *Front. Immunol.* 12:683022. doi: 10.3389/fimmu.2021.683022

Kambeitz, C., Klug, M. G., Greenmyer, J., Popova, S., and Burd, L. (2019). Association of adverse childhood experiences and neurodevelopmental disorders in people with fetal alcohol spectrum disorders (FASD) and non-FASD controls. *BMC Pediatr.* 19:498. doi: 10.1186/s12887-019-1878-8

Kang, C. S., Ban, M., Choi, E. J., Moon, H. G., Jeon, J. S., Kim, D. K., et al. (2013). Extracellular vesicles derived from gut microbiota, especially Akkermansia muciniphila, protect the progression of dextran sulfate sodium-induced colitis. *PLoS One* 8:e76520. doi: 10.1371/journal.pone.0076520

Kang, D. W., Ilhan, Z. E., Isern, N. G., Hoyt, D. W., Howsmon, D. P., Shaffer, M., et al. (2018). Differences in fecal microbial metabolites and microbiota of children with autism spectrum disorders. *Anaerobe* 49, 121–131. doi: 10.1016/j.anaerobe.2017.12.007

Kaparakis-Liaskos, M., and Ferrero, R. L. (2015). Immune modulation by bacterial outer membrane vesicles. *Nat. Rev. Immunol.* 15, 375–387. doi: 10.1038/nri3837

Keppen, L. D., Pysher, T., and Rennert, O. M. (1985). Zinc deficiency acts as a co-teratogen with alcohol in fetal alcohol syndrome. *Pediatr. Res.* 19, 944–947. doi: 10.1203/00006450-198509000-00016

Khan, I., Azhar, E. I., Abbas, A. T., Kumosani, T., Barbour, E. K., Raoult, D., et al. (2016). Metagenomic analysis of antibiotic-induced changes in gut microbiota in a pregnant rat model. *Front. Pharmacol.* 7:104. doi: 10.3389/fphar.2016.00104

Kim, G., Bae, J., Kim, M. J., Kwon, H., Park, G., Kim, S. J., et al. (2020). Delayed establishment of gut microbiota in infants delivered by cesarean section. *Front. Microbiol.* 11:2099. doi: 10.3389/fmicb.2020.02099

Kim, M., and Benayoun, B. A. (2020). The microbiome: an emerging key player in aging and longevity. *Transl Med Aging* 4, 103–116. doi: 10.1016/j.tma.2020.07.004

Kim, Y.-K., Zuccaro, M. V., Zhang, C., Sarkar, D., and Quadro, L. (2015). Alcohol exposure in utero perturbs retinoid homeostasis in adult rats. *Hepatob Surg Nutr* 4, 268–277. doi: 10.3978/j.issn.2304-3881.2015.01.06

Kobylinska, M., Antosik, K., Decyk, A., and Kurowska, K. (2022). Malnutrition in obesity: is it possible? *Obes. Facts* 15, 19–25. doi: 10.1159/000519503

Koeppen, K., Hampton, T. H., Jarek, M., Scharfe, M., Gerber, S. A., Mielcarz, D. W., et al. (2016). A novel mechanism of host-pathogen interaction through sRNA in bacterial outer membrane vesicles. *PLoS Pathog.* 12:e1005672. doi: 10.1371/journal.ppat.1005672

Krakowsky, Y., Potter, E., Hallarn, J., Monari, B., Wilcox, H., Bauer, G., et al. (2022). The effect of gender-affirming medical care on the vaginal and Neovaginal microbiomes of transgender and gender-diverse people. *Front. Cell. Infect. Microbiol.* 11:769950. doi: 10.3389/fcimb.2021.769950

Leclercq, S., de Timary, P., Delzenne, N. M., and Stärkel, P. (2017). The link between inflammation, bugs, the intestine and the brain in alcohol dependence. *Transl. Psychiatry* 7:e1048. doi: 10.1038/tp.2017.15

Lee, A. S. E., Ji, Y., Raghavan, R., Wang, G., Hong, X., Pearson, C., et al. (2021). Maternal prenatal selenium levels and child risk of neurodevelopmental disorders: a prospective birth cohort study. *Autism Res.* 14, 2533–2543. doi: 10.1002/aur.2617

Li, P., Ensink, E., Lang, S., Marshall, L., Schilthuis, M., Lamp, J., et al. (2020). Hemispheric asymmetry in the human brain and in Parkinson's disease is linked to divergent epigenetic patterns in neurons. *Genome Biol.* 21:61. doi: 10.1186/s13059-020-01960-1

Liang, L., Ai, L., Qian, J., Fang, J. Y., and Xu, J. (2015). Long noncoding RNA expression profiles in gut tissues constitute molecular signatures that reflect the types of microbes. *Sci. Rep.* 5:11763. doi: 10.1038/srep11763

Lieber, C. S. (1975). Alcohol and malnutrition in the pathogenesis of liver disease. *JAMA* 233, 1077–1080. doi: 10.1001/jama.1975.03260100047019

Litwinowicz, K., Choroszy, M., and Waszczuk, E. (2020). Changes in the composition of the human intestinal microbiome in alcohol use disorder: a systematic review. *Am. J. Drug Alcohol Abuse* 46, 4–12. doi: 10.1080/00952990.2019.1669629

Liu, S., da Cunha, A. P., Rezende, R. M., Cialic, R., Wei, Z., Bry, L., et al. (2016). The host shapes the gut microbiota via fecal MicroRNA. *Cell Host Microbe* 19, 32–43. doi: 10.1016/j.chom.2015.12.005

Liu, L., Wang, H., Chen, X., Zhang, Y., Li, W., Rao, X., et al. (2021). Integrative analysis of Long non-coding RNAs, messenger RNAs, and MicroRNAs indicates the neurodevelopmental dysfunction in the Hippocampus of gut microbiota-dysbiosis mice. *Front. Mol. Neurosci.* 14:745437. doi: 10.3389/fnmol.2021.745437

Mahdinia, R., Goudarzi, I., Lashkarbolouki, T., and Salmani, M. E. (2021). Vitamin E attenuates alterations in learning, memory and BDNF levels caused by perinatal ethanol exposure. *Nutr. Neurosci.* 24, 747–761. doi: 10.1080/1028415X.2019.1674523

Mahnke, A. H., Roberts, M. H., Leeman, L., Ma, X., Bakhireva, L. N., and Miranda, R. C. (2022). Prenatal opioid-exposed infant extracellular miRNA signature obtained at birth predicts severity of neonatal opioid withdrawal syndrome. *Sci. Rep.* 12:5941. doi: 10.1038/s41598-022-09793-7

Mahnke, A. H., Salem, N. A., Tseng, A. M., Chung, D. D., and Miranda, R. C. (2018). Nonprotein-coding RNAs in Fetal Alcohol Spectrum disorders. *Prog. Mol. Biol. Transl. Sci.* 157, 299–342. doi: 10.1016/bs.pmbts.2017.11.024

Mahnke, A. H., Sideridis, G. D., Salem, N. A., Tseng, A. M., Carter, R. C., Dodge, N. C., et al. (2021). Infant circulating MicroRNAs as biomarkers of effect in fetal alcohol spectrum disorders. *Sci. Rep.* 11:1429. doi: 10.1038/s41598-020-80734-y

Makino, H., Kushiro, A., Ishikawa, E., Kubota, H., Gawad, A., Sakai, T., et al. (2013). Mother-to-infant transmission of intestinal bifidobacterial strains has an impact on the early development of vaginally delivered infant's microbiota. *PLoS One* 8:e78331. doi: 10.1371/journal.pone.0078331

Mani, K. K., El-Hakim, Y., Branyan, T. E., Samiya, N., Pandey, S., Grimaldo, M. T., et al. (2023). Intestinal epithelial stem cell transplants as a novel therapy for cerebrovascular stroke. *Brain Behav. Immun.* 107, 345–360. doi: 10.1016/j.bbi.2022.10.015

Mattick, J. S., and Makunin, I. V. (2006). Non-coding RNA. *Hum Mol Genet* 15 Spec No 1, R17–R29. doi: 10.1093/hmg/ddl046

Mattson, S. N., Bernes, G. A., and Doyle, L. R. (2019). Fetal Alcohol Spectrum disorders: a review of the neurobehavioral deficits associated with prenatal Alcohol exposure. *Alcohol. Clin. Exp. Res.* 43, 1046–1062. doi: 10.1111/acer.14040

May, P. A., Chambers, C. D., Kalberg, W. O., Zellner, J., Feldman, H., Buckley, D., et al. (2018). Prevalence of Fetal Alcohol Spectrum disorders in 4 US communities. *JAMA* 319, 474–482. doi: 10.1001/jama.2017.21896

May, P. A., Hamrick, K. J., Corbin, K. D., Hasken, J. M., Marais, A.-S., Blankenship, J., et al. (2016). Maternal nutritional status as a contributing factor for the risk of fetal alcohol spectrum disorders. *Reprod. Toxicol.* 59, 101–108. doi: 10.1016/j.reprotox.2015.11.006

McElhanon, B. O., McCracken, C., Karpen, S., and Sharp, W. G. (2014). Gastrointestinal symptoms in autism spectrum disorder: a meta-analysis. *Pediatrics* 133, 872–883. doi: 10.1542/peds.2013-3995

McKenna, L. B., Schug, J., Vourekas, A., McKenna, J. B., Bramswig, N. C., Friedman, J. R., et al. (2010). MicroRNAs control intestinal epithelial differentiation, architecture, and barrier function. *Gastroenterology* 139:1654-1664, 1664 e1651. doi: 10.1053/j.gastro.2010.07.040

Mendes, V., Galvao, I., and Vieira, A. T. (2019). Mechanisms by which the gut microbiota influences cytokine production and modulates host inflammatory responses. *J. Interf. Cytokine Res.* 39, 393–409. doi: 10.1089/jir.2019.0011

Miko, E., Csaszar, A., Bodis, J., and Kovacs, K. (2022). The maternal-fetal gut microbiota axis: physiological changes, dietary influence, and modulation possibilities. *Life* 12:, 424. doi: 10.3390/life12030424

Mindus, C., Ellis, J., van Staaveren, N., and Harlander-Matauschek, A. (2021). Lactobacillus-based probiotics reduce the adverse effects of stress in rodents: a meta-analysis. *Front. Behav. Neurosci.* 15:642757. doi: 10.3389/fnbeh.2021.642757

Mir, I. N., Leon, R., and Chalak, L. F. (2021). Placental origins of neonatal diseases: toward a precision medicine approach. *Pediatr. Res.* 89, 377–383. doi: 10.1038/s41390-020-01293-6

Močenić, I., Kolić, I., Nišević, J. R., Belančić, A., Tratnik, J. S., Mazej, D., et al. (2019). Prenatal selenium status, neonatal cerebellum measures and child neurodevelopment at the age of 18 months. *Environ. Res.* 176:108529. doi: 10.1016/j.envres.2019.108529

Momen-Heravi, F., Bala, S., Kodys, K., and Szabo, G. (2015). Exosomes derived from alcohol-treated hepatocytes horizontally transfer liver specific miRNA-122 and sensitize monocytes to LPS. *Sci. Rep.* 5:9991. doi: 10.1038/srep09991

Monaghan, T. M., Seekatz, A. M., Markham, N. O., Yau, T. O., Hatziapostolou, M., Jilani, T., et al. (2021). Fecal microbiota transplantation for recurrent Clostridioides difficile infection associates with functional alterations in circulating microRNAs. *Gastroenterology* 161, 255–270 e254. doi: 10.1053/j.gastro.2021.03.050

Mukherjee, S., Cabrera, M. A., Boyadjieva, N. I., Berger, G., Rousseau, B., and Sarkar, D. K. (2020). Alcohol increases exosome release from microglia to promote complement C1q-induced cellular death of proopiomelanocortin neurons in the hypothalamus in a rat model of fetal alcohol spectrum disorders. *J. Neurosci.* 40, 7965–7979. doi: 10.1523/JNEUROSCI.0284-20.2020

Muralidharan, P., Sarmah, S., and Marrs, J. A. (2015). Zebrafish retinal defects induced by ethanol exposure are rescued by retinoic acid and folic acid supplement. *Alcohol* 49, 149–163. doi: 10.1016/j.alcohol.2014.11.001

Nakata, K., Sugi, Y., Narabayashi, H., Kobayakawa, T., Nakanishi, Y., Tsuda, M., et al. (2017). Commensal microbiota-induced microRNA modulates intestinal epithelial permeability through the small GTPase ARF4. *J. Biol. Chem.* 292, 15426–15433. doi: 10.1074/jbc.M117.788596

Natale, N. R., Kent, M., Fox, N., Vavra, D., and Lambert, K. (2021). Neurobiological effects of a probiotic-supplemented diet in chronically stressed male Long-Evans rats: evidence of enhanced resilience. *IBRO Neurosci Rep* 11, 207–215. doi: 10.1016/j.ibneur.2021.10.004

Needham, B. D., Funabashi, M., Adame, M. D., Wang, Z., Boktor, J. C., Haney, J., et al. (2022). A gut-derived metabolite alters brain activity and anxiety behaviour in mice. *Nature* 602, 647–653. doi: 10.1038/s41586-022-04396-8

Niu, J., Xu, L., Qian, Y., Sun, Z., Yu, D., Huang, J., et al. (2020). Evolution of the gut microbiome in early childhood: a cross-sectional study of Chinese children. *Front. Microbiol.* 11:439. doi: 10.3389/fmicb.2020.00439

Obeid, R., Derbyshire, E., and Schon, C. (2022). Association between maternal choline, Fetal brain development, and child Neurocognition: systematic review and Meta-analysis of human studies. *Adv. Nutr.* 13, 2445–2457. doi: 10.1093/advances/nmac082

Ojeda, M. L., Vázquez, B., Nogales, F., Murillo, M. L., and Carreras, O. (2009). Ethanol consumption by wistar rat dams affects selenium bioavailability and antioxidant balance in their progeny. *Int. J. Environ. Res. Public Health* 6, 2139–2149. doi: 10.3390/ijerph6082139

O'Neill, J., O'Connor, M. J., Kalender, G., Ly, R., Ng, A., Dillon, A., et al. (2022). Combining neuroimaging and behavior to discriminate children with attention deficit-hyperactivity disorder with and without prenatal alcohol exposure. *Brain Imaging Behav.* 16, 69–77. doi: 10.1007/s11682-021-00477-w

Pandey, K. R., Naik, S. R., and Vakil, B. V. (2015). Probiotics, prebiotics and synbiotics-a review. *J. Food Sci. Technol.* 52, 7577–7587. doi: 10.1007/s13197-015-1921-1

Parenti, M., Schmidt, R. J., Ozonoff, S., Shin, H. M., Tancredi, D. J., Krakowiak, P., et al. (2022). Maternal serum and placental metabolomes in association with prenatal phthalate exposure and neurodevelopmental outcomes in the MARBLES cohort. *Meta* 12:829. doi: 10.3390/metabo12090829

Pereda, A. E., and Faber, D. S. (2011). "Brain and nervous system | physiology of the Mauthner cell: discovery and properties" in *Encyclopedia of fish physiology*. ed. A. P. Farrell (San Diego: Academic Press), 66–72.

Perez-Munoz, M. E., Arrieta, M. C., Ramer-Tait, A. E., and Walter, J. (2017). A critical assessment of the "sterile womb" and "in utero colonization" hypotheses: implications for research on the pioneer infant microbiome. *Microbiome* 5:48. doi: 10.1186/s40168-017-0268-4

Petrelli, B., Weinberg, J., and Hicks, G. G. (2018). Effects of prenatal alcohol exposure (PAE): insights into FASD using mouse models of PAE. *Biochem. Cell Biol.* 96, 131–147. doi: 10.1139/bcb-2017-0280

Pinson, M. R., Chung, D. D., Adams, A. M., Scopice, C., Payne, E. A., Sivakumar, M., et al. (2021). Extracellular vesicles in premature aging and diseases in adulthood due to developmental exposures. *Aging Dis.* 12, 1516–1535. doi: 10.14336/AD.2021.0322

Pinson, M. R., Chung, D. D., Mahnke, A. H., Salem, N. A., Osorio, D., Nair, V., et al. (2022). Gag-like proteins: novel mediators of prenatal alcohol exposure in neural development. *Alcohol. Clin. Exp. Res.* 46, 556–569. doi: 10.1111/acer.14796

Popova, S., Charness, M. E., Burd, L., Crawford, A., Hoyme, H. E., Mukherjee, R. A. S., et al. (2023). Fetal alcohol spectrum disorders. *Nat. Rev. Dis. Primers.* 9:11. doi: 10.1038/s41572-023-00420-x

Popova, S., Lange, S., Shield, K., Mihic, A., Chudley, A. E., Mukherjee, R. A. S., et al. (2016). Comorbidity of fetal alcohol spectrum disorder: a systematic review and meta-analysis. *Lancet* 387, 978–987. doi: 10.1016/S0140-6736(15)01345-8

Raineki, C., Bodnar, T. S., Holman, P. J., Baglot, S. L., Lan, N., and Weinberg, J. (2017). Effects of early-life adversity on immune function are mediated by prenatal environment: role of prenatal alcohol exposure. *Brain Behav. Immun.* 66, 210–220. doi: 10.1016/j.bbi.2017.07.001

Rezaei Asl, Z., Sepehri, G., and Salami, M. (2019). Probiotic treatment improves the impaired spatial cognitive performance and restores synaptic plasticity in an animal model of Alzheimer's disease. *Behav. Brain Res.* 376:112183. doi: 10.1016/j.bbr.2019.112183

Rhee, S. H., Pothoulakis, C., and Mayer, E. A. (2009). Principles and clinical implications of the brain-gut-enteric microbiota axis. *Nat. Rev. Gastroenterol. Hepatol.* 6, 306–314. doi: 10.1038/nrgastro.2009.35

Richard, C., and Calder, P. C. (2016). Docosahexaenoic acid. *Adv. Nutr.* 7, 1139–1141. doi: 10.3945/an.116.012963

Rizvi, S., Raza, S. T., Ahmed, F., Ahmad, A., Abbas, S., and Mahdi, F. (2014). The role of vitamin e in human health and some diseases. *Sultan Qaboos Univ. Med. J.* 14, e157–e165.

Roberts, T. C. (2014). The MicroRNA biology of the mammalian nucleus. *Mol Ther Nucleic Acids* 3:e188. doi: 10.1038/mtna.2014.40

Rocha, N. P., de Miranda, A. S., and Teixeira, A. L. (2015). Insights into Neuroinflammation in Parkinson's disease: from biomarkers to anti-inflammatory based therapies. *Biomed. Res. Int.* 2015:628192. doi: 10.1155/2015/628192

Romano, K. A., Martinez-Del Campo, A., Kasahara, K., Chittim, C. L., Vivas, E. I., Amador-Noguez, D., et al. (2017). Metabolic, epigenetic, and transgenerational effects of gut bacterial choline consumption. *Cell Host Microbe* 22, 279–290 e277. doi: 10.1016/j.chom.2017.07.021

Rosenfeld, C. S. (2021). The placenta-brain-axis. *J. Neurosci. Res.* 99, 271–283. doi: 10.1002/jnr.24603

Ross, S. A., McCaffery, P. J., Drager, U. C., and De Luca, L. M. (2000). Retinoids in embryonal development. *Physiol. Rev.* 80, 1021–1054. doi: 10.1152/physrev.2000.80.3.1021

Rudzki, L., Ostrowska, L., Pawlak, D., Malus, A., Pawlak, K., Waszkiewicz, N., et al. (2019). Probiotic Lactobacillus Plantarum 299v decreases kynurenine concentration and improves cognitive functions in patients with major depression: a double-blind, randomized, placebo controlled study. *Psychoneuroendocrinology* 100, 213–222. doi: 10.1016/j.psyneuen.2018.10.010

Rutayisire, E., Huang, K., Liu, Y., and Tao, F. (2016). The mode of delivery affects the diversity and colonization pattern of the gut microbiota during the first year of infants' life: a systematic review. *BMC Gastroenterol.* 16:86. doi: 10.1186/s12876-016-0498-0

Salem, N. A., Mahnke, A. H., Konganti, K., Hillhouse, A. E., and Miranda, R. C. (2021a). Cell-type and fetal-sex-specific targets of prenatal alcohol exposure in developing mouse cerebral cortex. *iScience* 24:102439. doi: 10.1016/j.isci.2021.102439

Salem, N. A., Mahnke, A. H., Tseng, A. M., Garcia, C. R., Jahromi, H. K., Geoffroy, C. G., et al. (2021b). A novel Oct4/Pou5f1-like non-coding RNA controls neural maturation and mediates developmental effects of ethanol. *Neurotoxicol. Teratol.* 83:106943. doi: 10.1016/j.ntt.2020.106943

Salem, N. A., Mahnke, A. H., Wells, A. B., Tseng, A. M., Yevtushok, L., Zymak-Zakutnya, N., et al. (2020). Association between fetal sex and maternal plasma microRNA responses to prenatal alcohol exposure: evidence from a birth outcome-stratified cohort. *Biol. Sex Differ.* 11:51. doi: 10.1186/s13293-020-00327-2

Sanchez Calle, A., Kawamura, Y., Yamamoto, Y., Takeshita, F., and Ochiya, T. (2018). Emerging roles of long non-coding RNA in cancer. *Cancer Sci.* 109, 2093–2100. doi: 10.1111/cas.13642

Santocchi, E., Guiducci, L., Prosperi, M., Calderoni, S., Gaggini, M., Apicella, F., et al. (2020). Effects of probiotic supplementation on gastrointestinal, sensory and Core symptoms in autism Spectrum disorders: a randomized controlled trial. *Front. Psych.* 11:550593. doi: 10.3389/fpsyt.2020.550593

Sekirov, I., Russell, S. L., Antunes, L. C., and Finlay, B. B. (2010). Gut microbiota in health and disease. *Physiol. Rev.* 90, 859–904. doi: 10.1152/physrev.00045.2009

Sender, R., Fuchs, S., and Milo, R. (2016). Revised estimates for the number of human and bacteria cells in the body. *PLoS Biol.* 14:e1002533. doi: 10.1371/journal.pbio.1002533

Sharon, G., Cruz, N. J., Kang, D. W., Gandal, M. J., Wang, B., Kim, Y. M., et al. (2019). Human gut microbiota from autism spectrum disorder promote behavioral symptoms in mice. *Cells* 177, 1600–1618 e1617. doi: 10.1016/j.cell.2019.05.004

Shirpoor, A., Nemati, S., Ansari, M. H. K., and Ilkhanizadeh, B. (2015). The protective effect of vitamin E against prenatal and early postnatal ethanol treatment-induced heart abnormality in rats: a 3-month follow-up study. *Int. Immunopharmacol.* 26, 72–79. doi: 10.1016/j.intimp.2015.03.008

Shobeiri, P., Kalantari, A., Teixeira, A. L., and Rezaei, N. (2022). Shedding light on biological sex differences and microbiota–gut–brain axis: a comprehensive review of its roles in neuropsychiatric disorders. *Biol. Sex Differ.* 13:12. doi: 10.1186/s13293-022-00422-6

Siniscalco, D., Schultz, S., Brigida, A. L., and Antonucci, N. (2018). Inflammation and neuro-immune dysregulations in autism Spectrum disorders. *Pharmaceuticals* 11:56. doi: 10.3390/ph11020056

Skalny, A. V., Aschner, M., Lei, X. G., Gritsenko, V. A., Santamaria, A., Alekseenko, S. I., et al. (2021). Gut microbiota as a mediator of essential and toxic effects of zinc in the intestines and other tissues. *Int. J. Mol. Sci.* 22:13074. doi: 10.3390/ijms222313074

Smith, S. M., Virdee, M. S., Eckerle, J. K., Sandness, K. E., Georgieff, M. K., Boys, C. J., et al. (2021). Polymorphisms in SLC44A1 are associated with cognitive improvement in children diagnosed with fetal alcohol spectrum disorder: an exploratory study of oral choline supplementation. *Am. J. Clin. Nutr.* 114, 617–627. doi: 10.1093/ajcn/nqab081

Srinivasan, K., and Buys, E. M. (2019). Insights into the role of bacteria in vitamin a biosynthesis: future research opportunities. *Crit. Rev. Food Sci. Nutr.* 59, 3211–3226. doi: 10.1080/10408398.2018.1546670

Steane, S. E., Fielding, A. M., Kent, N. L., Andersen, I., Browne, D. J., Tejo, E. N., et al. (2021). Maternal choline supplementation in a rat model of periconceptional alcohol exposure: impacts on the fetus and placenta. *Alcohol. Clin. Exp. Res.* 45, 2130–2146. doi: 10.1111/acer.14685

Steane, S. E., Kumar, V., Cuffe, J. S. M., Moritz, K. M., and Akison, L. K. (2022). Prenatal choline supplementation alters one carbon metabolites in a rat model of Periconceptional Alcohol exposure. *Nutrients* 14:1874. doi: 10.3390/nu14091874

Sterpu, I., Fransson, E., Hugerth, L. W., Du, J., Pereira, M., Cheng, L., et al. (2021). No evidence for a placental microbiome in human pregnancies at term. *Am. J. Obstet. Gynecol.* 224, 296 e291–296 e223. doi: 10.1016/j.ajog.2020.08.103

Stilling, R. M., van de Wouw, M., Clarke, G., Stanton, C., Dinan, T. G., and Cryan, J. F. (2016). The neuropharmacology of butyrate: the bread and butter of the microbiota-gut-brain axis? *Neurochem. Int.* 99, 110–132. doi: 10.1016/j.neuint.2016.06.011

Stinson, L. F., Boyce, M. C., Payne, M. S., and Keelan, J. A. (2019). The not-so-sterile womb: evidence that the human fetus is exposed to Bacteria prior to birth. *Front. Microbiol.* 10:1124. doi: 10.3389/fmicb.2019.01124

Stout, M. J., Conlon, B., Landeau, M., Lee, I., Bower, C., Zhao, Q., et al. (2013). Identification of intracellular bacteria in the basal plate of the human placenta in term and preterm gestations. *Am. J. Obstet. Gynecol.* 208:226 e221-227. doi: 10.1016/j.ajog.2013.01.018

Strandwitz, P. (2018). Neurotransmitter modulation by the gut microbiota. *Brain Res.* 1693, 128–133. doi: 10.1016/j.brainres.2018.03.015

Substance Abuse and Mental Health Services Administration (2021). *Key substance uses and mental health indicators in the United States: Results from the 2020 National Survey on drug use and health*. Rockville, MD: Center for Behavioral Health and Statistics Quality.

Tavanasefat, H., Li, F., Koyano, K., Gourtani, B. K., Marty, V., Mulpuri, Y., et al. (2020). Molecular consequences of fetal alcohol exposure on amniotic exosomal miRNAs with functional implications for stem cell potency and differentiation. *PLoS One* 15:e0242276. doi: 10.1371/journal.pone.0242276

Theis, K. R., Romero, R., Winters, A. D., Greenberg, J. M., Gomez-Lopez, N., Alhousseini, A., et al. (2019). Does the human placenta delivered at term have a microbiota? Results of cultivation, quantitative real-time PCR, 16S rRNA gene sequencing, and metagenomics. *Am. J. Obstet. Gynecol.* 220, 267 e261–267 e239. doi: 10.1016/j.ajog.2018.10.018

Thursby, E., and Juge, N. (2017). Introduction to the human gut microbiota. *Biochem. J.* 474, 1823–1836. doi: 10.1042/BCJ20160510

Tomlinson, M. S., Lu, K., Stewart, J. R., Marsit, C. J., O'Shea, T. M., and Fry, R. C. (2019). Microorganisms in the placenta: links to early-life inflammation and neurodevelopment in children. *Clin. Microbiol. Rev.* 32, e00103–18. doi: 10.1128/CMR.00103-18

Tomlinson, M. S., Santos, H. P., Stewart, J. R., Joseph, R., Leviton, A., Onderdonk, A. B., et al. (2020). Neurocognitive and social-communicative function of children born very preterm at 10 years of age: associations with microorganisms recovered from the placenta parenchyma. *J. Perinatol.* 40, 306–315. doi: 10.1038/s41372-019-0505-8

Tseng, A. M., Chung, D. D., Pinson, M. R., Salem, N. A., Eaves, S. E., and Miranda, R. C. (2019a). Ethanol exposure increases miR-140 in extracellular vesicles: implications for Fetal neural stem cell proliferation and maturation. *Alcohol. Clin. Exp. Res.* 43, 1414–1426. doi: 10.1111/acer.14066

Tseng, A. M., Mahnke, A. H., Salem, N. A., and Miranda, R. C. (2018). "Chapter 30 – noncoding RNA regulatory networks, epigenetics, and programming stem cell renewal and differentiation: implications for stem cell therapy" in *Epigenetics in human disease (second edition)*. ed. T. O. Tollefsbol (Cambridge, MA: Academic Press), 903–933.

Tseng, A. M., Mahnke, A. H., Wells, A. B., Salem, N. A., Allan, A. M., Roberts, V. H., et al. (2019b). Maternal circulating miRNAs that predict infant FASD outcomes influence placental maturation. *Life Sci Alliance* 2. doi: 10.26508/lsa.201800252

Tulkens, J., Vergauwen, G., Van Deun, J., Geeurickx, E., Dhondt, B., Lippens, L., et al. (2020). Increased levels of systemic LPS-positive bacterial extracellular vesicles in patients with intestinal barrier dysfunction. *Gut* 69, 191–193. doi: 10.1136/gutjnl-2018-317726

Umer, A., Lilly, C., Hamilton, C., Baldwin, A., Breyel, J., Tolliver, A., et al. (2020). Prevalence of alcohol use in late pregnancy. *Pediatr. Res.* 88, 312–319. doi: 10.1038/s41390-019-0731-y

Upreti, D., Ishiguro, S., Robben, N., Nakashima, A., Suzuki, K., Comer, J., et al. (2022). Oral administration of water extract from Euglena gracilis alters the intestinal microbiota and prevents lung carcinoma growth in mice. *Nutrients* 14:678. doi: 10.3390/nu14030678

Valeri, F., and Endres, K. (2021). How biological sex of the host shapes its gut microbiota. *Front. Neuroendocrinol.* 61:100912. doi: 10.1016/j.yfrne.2021.100912

van der Hee, B., and Wells, J. M. (2021). Microbial regulation of host physiology by short-chain fatty acids. *Trends Microbiol.* 29, 700–712. doi: 10.1016/j.tim.2021.02.001

van Niel, G., D'Angelo, G., and Raposo, G. (2018). Shedding light on the cell biology of extracellular vesicles. *Nat. Rev. Mol. Cell Biol.* 19, 213–228. doi: 10.1038/nrm.2017.125

Vargason, T., McGuinness, D. L., and Hahn, J. (2019). Gastrointestinal symptoms and Oral antibiotic use in children with autism Spectrum disorder: retrospective analysis of a privately insured U.S Population. *J Autism Dev Disord* 49, 647–659. doi: 10.1007/s10803-018-3743-2

Virdee, M. S., Saini, N., Kay, C. D., Neilson, A. P., Kwan, S. T. C., Helfrich, K. K., et al. (2021). An enriched biosignature of gut microbiota-dependent metabolites characterizes maternal plasma in a mouse model of fetal alcohol spectrum disorder. *Sci. Rep.* 11:248. doi: 10.1038/s41598-020-80093-8

Walter, K. M., Dach, K., Hayakawa, K., Giersiefer, S., Heuer, H., Lein, P. J., et al. (2019). Ontogenetic expression of thyroid hormone signaling genes: an in vitro and in vivo species comparison. *PLoS One* 14:e0221230. doi: 10.1371/journal.pone.0221230

Wang, M., Zhou, J., He, F., Cai, C., Wang, H., Wang, Y., et al. (2019). Alteration of gut microbiota-associated epitopes in children with autism spectrum disorders. *Brain Behav. Immun.* 75, 192–199. doi: 10.1016/j.bbi.2018.10.006

Wannamethee, S. G., Field, A. E., Colditz, G. A., and Rimm, E. B. (2004). Alcohol intake and 8-year weight gain in women: a prospective study. *Obes. Res.* 12, 1386–1396. doi: 10.1038/oby.2004.175

Warton, F. L., Molteno, C. D., Warton, C. M. R., Wintermark, P., Lindinger, N. M., Dodge, N. C., et al. (2021). Maternal choline supplementation mitigates alcohol exposure effects on neonatal brain volumes. *Alcohol. Clin. Exp. Res.* 45, 1762–1774. doi: 10.1111/acer.14672

Weeks, O., Bosse, G. D., Oderberg, I. M., Akle, S., Houvras, Y., Wrighton, P. J., et al. (2020). Fetal alcohol spectrum disorder predisposes to metabolic abnormalities in adulthood. *J. Clin. Invest.* 130, 2252–2269. doi: 10.1172/JCI132139

Wellmann, K. A., George, F., Brnouti, F., and Mooney, S. M. (2015). Docosahexaenoic acid partially ameliorates deficits in social behavior and ultrasonic vocalizations caused by prenatal ethanol exposure. *Behav. Brain Res.* 286, 201–211. doi: 10.1016/j.bbr.2015.02.048

Westen, E. A., Lynch, T. A., Glantz, J. C., Taggar, A., Katzman, P. J., Drennan, K., et al. (2019). 194: Fetal brain to liver weight ratio as a marker of uteroplacental insufficiency in stillbirths. *Am. J. Obstetr. Gynecol.* 220:S141. doi: 10.1016/j.ajog.2018.11.215

Williams, L. A., and LaSalle, J. M. (2022). Future prospects for epigenetics in autism spectrum disorder. *Mol. Diagn. Ther.* 26, 569–579. doi: 10.1007/s40291-022-00608-z

Workman, A. D., Charvet, C. J., Clancy, B., Darlington, R. B., and Finlay, B. L. (2013). Modeling transformations of neurodevelopmental sequences across mammalian species. *J. Neurosci.* 33, 7368–7383. doi: 10.1523/JNEUROSCI.5746-12.2013

Wozniak, J. R., Fink, B. A., Fuglestad, A. J., Eckerle, J. K., Boys, C. J., Sandness, K. E., et al. (2020). Four-year follow-up of a randomized controlled trial of choline for neurodevelopment in fetal alcohol spectrum disorder. *J. Neurodev. Disord.* 12:9. doi: 10.1186/s11689-020-09312-7

Wozniak, J. R., Fuglestad, A. J., Eckerle, J. K., Fink, B. A., Hoecker, H. L., Boys, C. J., et al. (2015). Choline supplementation in children with fetal alcohol spectrum disorders: a randomized, double-blind, placebo-controlled trial. *Am. J. Clin. Nutr.* 102, 1113–1125. doi: 10.3945/ajcn.114.099168

Wozniak, J. R., Fuglestad, A. J., Eckerle, J. K., Kroupina, M. G., Miller, N. C., Boys, C. J., et al. (2013). Choline supplementation in children with fetal alcohol spectrum disorders has high feasibility and tolerability. *Nutr. Res.* 33, 897–904. doi: 10.1016/j.nutres.2013.08.005

Wu, G. D., Chen, J., Hoffmann, C., Bittinger, K., Chen, Y. Y., Keilbaugh, S. A., et al. (2011). Linking long-term dietary patterns with gut microbial enterotypes. *Science* 334, 105–108. doi: 10.1126/science.1208344

Xiao, L., Rao, J. N., and Wang, J. Y. (2021). RNA-binding proteins and long noncoding RNAs in intestinal epithelial autophagy and barrier function. *Tissue Barriers* 9:1895648. doi: 10.1080/21688370.2021.1895648

Xie, A., Ensink, E., Li, P., Gordevicius, J., Marshall, L. L., George, S., et al. (2022). Bacterial butyrate in Parkinson's disease is linked to epigenetic changes and depressive symptoms. *Mov. Disord.* 37, 1644–1653. doi: 10.1002/mds.29128

Yap, C. X., Henders, A. K., Alvares, G. A., Wood, D. L. A., Krause, L., Tyson, G. W., et al. (2021). Autism-related dietary preferences mediate autism-gut microbiome associations. *Cells* 184, 5916–5931.e5917. doi: 10.1016/j.cell.2021.10.015

Yatsunenko, T., Rey, F. E., Manary, M. J., Trehan, I., Dominguez-Bello, M. G., Contreras, M., et al. (2012). Human gut microbiome viewed across age and geography. *Nature* 486, 222–227. doi: 10.1038/nature11053

Yeomans, M. R. (2010). Alcohol, appetite and energy balance: is alcohol intake a risk factor for obesity? *Physiol. Behav.* 100, 82–89. doi: 10.1016/j.physbeh.2010.01.012

Yilmaz, B., and Li, H. (2018). Gut microbiota and Iron: the crucial actors in health and disease. *Pharmaceuticals* 11:98. doi: 10.3390/ph11040098

Zheng, D., Liwinski, T., and Elinav, E. (2020). Interaction between microbiota and immunity in health and disease. *Cell Res.* 30, 492–506. doi: 10.1038/s41422-020-0332-7

Zhuang, P., Zhang, Y., Shou, Q., Li, H., Zhu, Y. E., He, L., et al. (2020). Eicosapentaenoic and docosahexaenoic acids differentially alter gut microbiome and reverse high-fat diet–induced insulin resistance. *Mol. Nutr. Food Res.* 64:1900946. doi: 10.1002/mnfr.201900946

frontiers | Frontiers in Neuroscience

TYPE Original Research
PUBLISHED 21 June 2023
DOI 10.3389/fnins.2023.1193304

Check for updates

OPEN ACCESS

EDITED BY
Paola A. Haeger,
Catholic University of the North,
Coquimbo, Chile

REVIEWED BY
Fernando Faunes,
Andres Bello University, Chile
Johann Eberhart,
The University of Texas at Austin, United States

*CORRESPONDENCE
Joel G. Hashimoto
✉ hashimoj@ohsu.edu
Marina Guizzetti
✉ guizzett@ohsu.edu

RECEIVED 24 March 2023
ACCEPTED 22 May 2023
PUBLISHED 21 June 2023

CITATION
Hashimoto JG, Zhang X and Guizzetti M (2023) Ethanol-induced transcriptional and translational changes in Aldh1l1-Egfp/Rpl10a cortical astrocyte cultures.
Front. Neurosci. 17:1193304.
doi: 10.3389/fnins.2023.1193304

COPYRIGHT
© 2023 Hashimoto, Zhang and Guizzetti. This is an open-access article distributed under the terms of the Creative Commons Attribution License (CC BY). The use, distribution or reproduction in other forums is permitted, provided the original author(s) and the copyright owner(s) are credited and that the original publication in this journal is cited, in accordance with accepted academic practice. No use, distribution or reproduction is permitted which does not comply with these terms.

Ethanol-induced transcriptional and translational changes in Aldh1l1-Egfp/Rpl10a cortical astrocyte cultures

Joel G. Hashimoto[1,2]*, Xiaolu Zhang[1,2] and Marina Guizzetti[1,2]*

[1]Department of Behavioral Neuroscience, Oregon Health and Science University, Portland, OR, United States, [2]Research Service, VA Portland Health Care System, Portland, OR, United States

The role astrocytes play in brain development and function has garnered greater attention as the diversity of roles they are involved in has become apparent. We have previously shown that ethanol-exposed astrocytes alter neuronal neurite outgrowth in an *in vitro* co-culture system and that ethanol alters the astrocyte-produced extracellular matrix (ECM) *in vitro*, with similar alterations *in vivo*. In this study, we utilized the translating ribosome affinity purification (TRAP) procedure in *Aldh1l1*-EGFP/Rpl10a transgenic mouse primary cortical astrocyte cultures to transcriptionally and translationally profile the astrocyte response to ethanol. We found a large number of differences between the total RNA pool and the translating RNA pool, indicating that the transcriptional state of astrocytes may not always reflect the translational state of astrocytes. In addition, there was a considerable overlap between ethanol-dysregulated genes in the total RNA pool and the translating RNA pool. Comparisons to published datasets indicate the *in vitro* model used here is most similar to PD1 or PD7 *in vivo* cortical astrocytes, and the ethanol-regulated genes showed a significant overlap with models of chronic ethanol exposure in astrocytes, a model of third-trimester ethanol exposure in the hippocampus and cerebellum, and an acute model of ethanol exposure in the hippocampus. These findings will further our understanding of the effects of ethanol on astrocyte gene expression and protein translation and how these changes may alter brain development and support the use of *in vitro* astrocyte cultures as models of neonatal astrocytes.

KEYWORDS

astrocyte, FASD, translating RNA affinity purification (TRAP), alcohol, *in vitro*

Introduction

The significance of astrocytes as key players in brain development and function has been growing as the variety and number of crucial functions played by astrocytes have been discovered. Astrocytes are the main producers of the brain extracellular matrix (ECM), provide key structural and chemical cues for proper neuronal connections during brain development, stabilize and regulate synapses, and facilitate the creation and maintenance of the blood–brain barrier (Abbott et al., 2006; Santello et al., 2019; Kane and Drew, 2021), among other functions (Wilhelm and Guizzetti, 2016).

Recent advances in single-cell and single-nuclei RNA sequencing (RNA-Seq) and cell-type-specific expression profiling have further improved our understanding of the roles astrocytes play in the brain (Erickson et al., 2018; Brenner et al., 2020). However, studying astrocytes *in vivo* creates challenges based on the heterogeneity of the brain's cellular

makeup and the complex feedback and cross-talk between different cell types. The use of *in vitro* models to study neurotoxic insults has provided a crucial understanding of the mechanistic underpinnings of complex diseases (Guttenplan et al., 2021; Kane and Drew, 2021). Mechanistic studies are particularly well suited to *in vitro* models, in which individual cell types can be manipulated in complex ways that would be untenable in whole tissues. However, one of the challenges associated with using *in vitro* models is interpreting how these models relate to *in vivo* processes.

Prenatal alcohol exposure (PAE) can lead to fetal alcohol spectrum disorders (FASD), resulting in brain and behavioral effects caused by a wide range of neurodevelopmental perturbations (Williams et al., 2015). PAE resulting in FASD impacts many different aspects of brain development and represents the largest type of preventable intellectual disability (Williams et al., 2015). Understanding the role of astrocytes in FASD-related brain dysfunction has been bolstered by *in vitro* studies in which astrocytes have been found to produce neuroinflammatory molecules, have altered extracellular protease expression, and have altered the production of chondroitin sulfate proteoglycans after ethanol exposure (Kane and Drew, 2021; Zhang et al., 2021; Goeke et al., 2022).

Gene expression studies utilizing high-throughput RNA-Seq typically analyze all RNA present in a given cell or tissue. Newer approaches have been developed to enrich cell-type-specific mRNA that is physically attached to the ribosome during the process of protein translation using the translating ribosome affinity-purification (TRAP) technology and the RiboTag system (Heiman et al., 2008; Sanz et al., 2009). These transgenic models result in cell-type-specific expression of tagged ribosomal proteins that, after incorporation into ribosomes, allow for the pull-down of cell-type-specific polysomes via immunoprecipitation methods and the assessment of mRNA abundance either by qRT-PCR or RNA-Seq. These approaches complement traditional RNA-Seq studies as the mRNA pool is enriched for specific cell types and actively translated, which is more closely linked to protein abundance (Heiman et al., 2014).

We have used both *in vitro* and *in vivo* methods to study the effects of developmental ethanol exposure. In our *in vivo* studies, we employed third trimester-equivalent human gestation models by exposing rats and mice to ethanol neonatally during the "brain growth spurt," when astrocytes proliferate and provide crucial support and pathfinding cues to neurons (Goeke et al., 2018, 2022; Wilhelm et al., 2018; Zhang et al., 2021). To further understand how ethanol alters astrocyte functions during early brain development, we used the Aldh1l1-EGFP/Rpl10a transgenic mouse line, which allows for the analysis of astrocyte-specific mRNA translation. Here, we generated primary cortical astrocyte cultures from the Aldh1l1-EGFP/Rpl10a transgenic mouse line to assess translational and transcriptional changes caused by ethanol. Our data showed large differences in the total RNA vs. translating RNA pools.

However, the ethanol-induced alterations are very similar in terms of gene ontology (GO) and pathway enrichment analysis in the total RNA and translating RNA pools. A comparison of our datasets with published data indicates that our *in vitro* astrocytes were most similar to *in vivo* cortical astrocytes at postnatal days (PD) 1–7. In addition, broad similarities in the ethanol responses were observed in our datasets when compared to a neonatal model of ethanol exposure at PD10 in the hippocampus and the cerebellum, the hippocampus of PD7 mice administered a single dose of ethanol, and the medial prefrontal cortex (mPFC) following chronic ethanol exposure in adult mice. These comparisons provide context for our *in vitro* results on the adult and developmental impacts of ethanol exposure.

Materials and methods

Animals

Hemizygous B6;FVB-Tg(Aldh1l1-EGFP/Rpl10a)JD130Htz/J mice, originally generated by Nathaniel Heintz (Doyle et al., 2008), were obtained from The Jackson Laboratory (JAX, Bar Harbor, ME; Strain # 030247) and were bred with C57BL/6J mice to produce hemizygous offspring. Genotyping was carried out on a tail biopsy using a rapid DNA isolation protocol (Conner, 2002) and qPCR for eGFP and *Gapdh* for transgene presence and positive control, respectively, as previously described (Goeke et al., 2022). All animals were housed in the VA Portland Health Care System Veterinary Medical Unit on a 12-h light/dark cycle at an ambient temperature of 22 ± 1°C. All animal-related procedures were carried out in accordance with the National Institutes of Health Guidelines for the Care and Use of Laboratory Animals and were approved by the VA Portland Health Care System's Institutional Animal Care and Use Committee (Protocol # 4331).

Primary astrocyte cultures and ethanol treatments

Primary mouse astrocyte cultures were created as previously described (Zhang et al., 2021; Goeke et al., 2022) using an equal number of transgenic male and female postnatal day (PD) 0 cortices. As the successful isolation and culturing of astrocytes are time-sensitive, the presence of the Aldh1l1-EGFP/Rpl10a transgene was detected using the Nightsea DFP-1 fluorescent protein flashlight and glasses in the dissected brain, with subsequent confirmation by qPCR for eGFP. In addition, sex determination was based on the anogenital distance and confirmed by qPCR for *Sry,* as previously described (Wilhelm et al., 2016). Astrocyte cultures were maintained in Dulbecco's Modified Eagle Medium (DMEM; Thermo Fisher Scientific, 11885092) with 10% fetal bovine serum (Atlanta Biologicals, S12450) and 1,000 U/ml penicillin-streptomycin (pen-strep, Thermo Fisher Scientific, 15140122) in a humidified incubator at 37°C under 5% CO_2/95% air atmosphere for 14 days *in vitro* (DIV) to reach confluence. Astrocytes were subcultured onto 100 mm dishes at a density of 2.5×10^6. After 6 days, the serum-containing medium was replaced with serum-free medium for 24 h, followed by 50 mM ethanol treatment in serum-free medium or control serum-free medium. To limit the effect of ethanol evaporation on culture conditions, dishes were placed in sealed chambers containing 5% CO_2/95% air atmosphere with an open dish containing either 50 mM ethanol or water, as previously described by Goeke et al. (2018). After 24 h in the 50 mM ethanol or control medium, the

medium was removed, and adherent astrocyte cells were processed for the TRAP procedure.

Translating RNA affinity purification

TRAP was carried out on six control and six ethanol-treated 100 mm dishes, as previously described by Heiman et al. (2014) with modifications (Sanz et al., 2009). Briefly, homogenization buffer (HB) was used as described in Sanz et al., with heparin omitted. Lysed cells in HB were centrifuged at 10,000 g for 10 min at 4°C to remove insoluble debris, and the supernatant was used for all subsequent steps. Input samples, equivalent to 5% of the initial HB volume, were saved from the supernatant prior to the immunoprecipitation, and RNA was extracted at the same time as TRAP samples. This beginning clause is confusing 50 μg of two GFP antibodies (bioreactor supernatant, clones 19C8 and 19F7 from the Memorial Sloan-Kettering Institute Monoclonal Antibody Facility) was added to each sample for 4 h at 4°C under gentle end-over-end rotation. Samples were transferred to tubes containing 200 μl of Pierce Protein A/G Magnetic Beads (Thermo Fisher Scientific; 88803; lot VF298063) and incubated overnight at 4°C with end-over-end rotation. The following day, beads were washed in high-salt buffer as described in Sanz et al., and RNA was isolated from the beads and input samples using TRIzol (Thermo Fisher Scientific, 15596018) and the Direct-zol RNA Microprep Kit (Zymo Research, R2062). RNA concentration was determined using the Quant-iT RiboGreen RNA Assay (Thermo Fisher Scientific, R11490) using a CLARIOstar Plus plate reader (BMG Labtech). TRAP controls with either no antibody or using wild-type tissue result in no measurable RNA based on the RiboGreen assay and only trace amounts of RNA detected using qRT-PCR.

RNA-Seq and analysis

TRAP (IP) samples from all 12 (six control and six ethanol) dishes and six input (three control and three ethanol) samples (selected arbitrarily) were submitted for RNA-sequencing at the OHSU Massively Parallel Sequencing Shared Resource. RNA quality was assessed using an Agilent Bioanalyzer, with all samples having a RIN of $\geq$8.8 (range 8.8–9.8). RNA-seq libraries were profiled on a 4200 Tapestation (Agilent) and quantified by real-time PCR using a commercial kit (Kapa Biosystems/Roche) on a StepOnePlus Real-Time PCR Workstation (ABI/Thermo). Libraries were then sequenced on a NovaSeq 6000 (Illumina). Fastq files were assembled from the base call files using bcl2fastq (Illumina). The fastq files were trimmed with Trimmomatic (Bolger et al., 2014; Bioinformatics 30, 2114) using the built-in filters for Illumina adapters. After trimming, sequence files were aligned with the STAR aligner (Dobin et al., 2013). The reference genome was Mus musculus GRCm38, downloaded with annotations from Ensembl. Following the alignment, the SAM files were converted to BAM format using SAMtools (Li et al., 2009). Short-read sequencing assays were performed using the OHSU Massively Parallel Sequencing Shared Resource (OHSU MPSSR). Raw read count data were analyzed using the R package DESeq2 (Love et al., 2014). Genes with less than a total of 10 reads across the 18 samples were excluded from the analysis. Clustering and principal component analysis were conducted on all 18 samples (inputs and IP), as well as an analysis of differential expression between the IP and input fractions. Differential expression/translation caused by ethanol treatment was carried out separately with each fraction. The significance of RNA-Seq data was determined using DESeq2 FDR-adjusted Wald test p-values of <0.05. All processed and raw sequencing reads are publicly accessible at the Gene Expression Omnibus (GEO; https://www.ncbi.nlm.nih.gov/geo/) using accession number GSE227891.

Validation of RNA-Seq by qRT-PCR

Confirmation of differential regulation by ethanol was carried out with qRT-PCR, as previously described by Goeke et al. (2022). Primers for mouse *Bcan* (Forward: 5′-CTGCGCGTCAAGGTAAACG-3′; Reverse: 5′-AGAGACACATCCGTGAGCGAT-3′), *Ncan* (Forward: 5′-GCTGGGGATCAGGACACAC-3′; Reverse: 5′-CAGTCTGAACCTTAGTCCACTTG-3′), and *Serpine1* (Forward: 5′-GCCACCGACTTCGGAGTAAA-3′; Reverse: 5′-TGAGCTGTGCCCTTCTCATT-3′) were used with 5 ng of RNA and the Luna Universal One-Step RT-qPCR Kit (NEB) with SYBR Green detection on the CFX96 Real-Time System (Bio-Rad). Cycle threshold data were normalized to total RNA using RiboGreen (ThermoFisher) and expressed as $\log_2$ transformed data relative to the input control samples, with significance determined by the Student's t-test.

Bioinformatics analysis

Gene Ontology (GO) and pathway enrichment analysis was carried out using the enrichR package in R to query the enrichR database (Chen et al., 2013; Kuleshov et al., 2016). We limited the analysis to the following databases to focus our results on GO categories and known gene pathways: "GO_Molecular_Function_2021," "GO_Cellular_Component_2021," "GO_Biological_Process_2021," "BioPlanet_2019," "Elsevier_Pathway_Collection," "KEGG_2021_Human," "MSigDB_Hallmark_2020," and "WikiPathway_2021_Human." Significant gene categories were determined by unadjusted p-values <0.01.

Results

To understand the differences in gene transcription and translation caused by ethanol treatments in primary astrocyte cultures, we performed the TRAP procedure on primary Aldh1l1-EGFP/Rpl10a astrocytes (Figure 1). The astrocytes were cultured for a total of 20 DIV, with a single pass at 14 DIV. Ethanol (50 mM) treatments were carried out in serum-free conditions, as we and others have done to model the *in vivo* environment of astrocytes (Prah et al., 2019; Zhang et al., 2021). An average of 103 million paired-end reads were obtained for each sample (standard deviation: 15.9 million, range 88.9–157.2 million), with

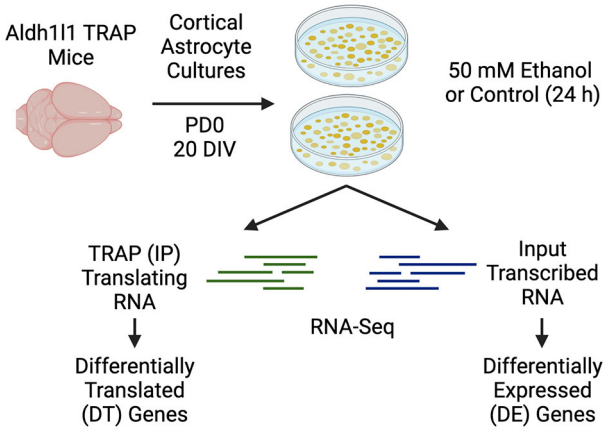


FIGURE 1
Experimental design. Primary cortical astrocyte cultures were generated from PD0 Aldh1l1-EGFP/Rpl10a transgenic mice. Astrocytes were cultured for 14 DIV before replating and were cultured for an additional 6 days. Serum was removed for 24 h prior to ethanol or control treatments for an additional 24 h. Following ethanol or control treatments, media was removed from the dishes, and the samples were processed for TRAP (IP), or input RNA, followed by RNA-Seq. Created with BioRender.com.

a unique mapping average of 92.0% to the reference genome (range 89.7%–93.5%). Principle component analysis (PCA) of all RNA-Seq samples showed separation based on fraction (IP vs. input), which accounted for 97% of the variance (PC1), and ethanol treatment (PC2), which accounted for 1% of the variance (Figure 2A). Hierarchical clustering of all samples was conducted, resulting in the initial division of samples by fraction, followed by treatment (Figure 2B).

Differential expression/translation analysis

Comparing IP vs. input fractions, we identified 12,313 (6,045 genes with higher read counts in IP vs. input and 6,268 genes with lower read counts in IP vs. input) genes using an adjusted (FDR) p-value cutoff of 0.05 (Supplementary Tables 1, 2). These results indicate that over half of the detected transcripts showed differential partitioning between the cytosol and the ribosome, as only transcripts being actively translated were pulled down during the TRAP procedure. The TRAP samples were from six independent dishes per treatment, while the RNA for the input samples was from aliquots taken from three of the control and three of the ethanol-treated IP (TRAP) samples; therefore, experimental variation due to differences in treatment conditions was minimized. The remaining three control and three ethanol-treated input samples were not sequenced due to design and cost considerations and were not excluded due to low yield or other technical issues.

Using DESeq2 to explore ethanol-induced differential expression/translation (DE and DT) within each fraction, we identified 5,581 DT genes in the TRAP (IP) fraction and 3,125 DE genes in the input fraction (Supplementary Tables 3, 4, respectively). A comparison of the direction of ethanol regulation between the fractions showed that 1,179 genes were upregulated by ethanol in the IP and input fractions, and 1,345 genes were downregulated in both the IP and input fractions. In addition, we identified 1,659 genes that were only upregulated by ethanol in the IP fraction and 1,394 genes that were only downregulated in the IP fraction. We also found 330 genes that were only upregulated by ethanol in the input fraction and 267 genes that were downregulated by ethanol in the input fraction (Figure 2C). Four genes were differentially regulated by ethanol in opposite directions based on the fraction, with three upregulated by ethanol in IP and downregulated by ethanol in input (*Chd3*, *Meg3*, and *Ndst1*) and one gene downregulated by ethanol in IP and upregulated by ethanol in input (*Sumo1*).

RNA-Seq results were validated by qRT-PCR utilizing the same samples used for RNA-Seq. We confirmed the upregulation of *Bcan* [input: $t_{(10)} = 2.732$, $p = 0.021$; TRAP: $t_{(9)} = 4.982$, $p = 0.0008$] and *Ncan* [input: $t_{(10)} = 2.603$, $p = 0.026$; TRAP: $t_{(9)} = 5.133$, $p = 0.0006$] by ethanol in both input and TRAP fractions (Figures 2D, E). In addition, we confirmed the downregulation of *Serpine1* [input: $t_{(10)} = 0.7059$, $p = 0.496$; TRAP: $t_{(9)} = 2.325$, $p = 0.045$] in the TRAP fraction by ethanol (Figure 2F). We have previously shown that brevican (encoded by the gene *Bcan*) and neurocan (encoded by the gene *Ncan*) protein levels are upregulated by ethanol and that plasminogen activator inhibitor 1 (PAI-1; encoded by the gene *Serpine1*) protein levels are downregulated by ethanol in astrocyte cultures measured by Western blot and/or ELISA (Wilhelm et al., 2018; Zhang et al., 2021), indicating that changes in translating RNA levels in our TRAP fraction result in corresponding changes in protein abundance.

Due to the differences in the number of samples processed between fractions and the large difference in the number of ethanol-regulated genes we identified in the IP vs. input fraction, we investigated how the difference in sample sizes impacted the number of ethanol-regulated genes. Because our samples are matched with IP samples immunoprecipitated from the lysate sampled for the input, we limited our analysis to the three control and three ethanol-treated samples with both input and IP RNA-Seq results. We re-ran the same data analysis pipeline with the limited IP data and found a similar number of ethanol-regulated genes in the limited data set of the IP fraction and in the input fraction (3,317 DT genes in the limited dataset compared to 3125 DE genes in the input samples). This indicates that most of the difference in the number of ethanol-regulated genes identified in each fraction was due to the higher number of samples in the IP comparison (Supplementary Table 5). For all subsequent analyses and discussions, we will refer to the analysis of the full complement of IP samples unless explicitly indicated.

Bioinformatics analysis: gene category enrichment

Ethanol-regulated DE and DT genes were used to query the Enrichr database to identify GO and pathway enrichment (Chen et al., 2013; Xie et al., 2021). In the IP samples, we identified 1,111 categories as enriched at an unadjusted enrichment

10.3389/fnins.2023.1193304

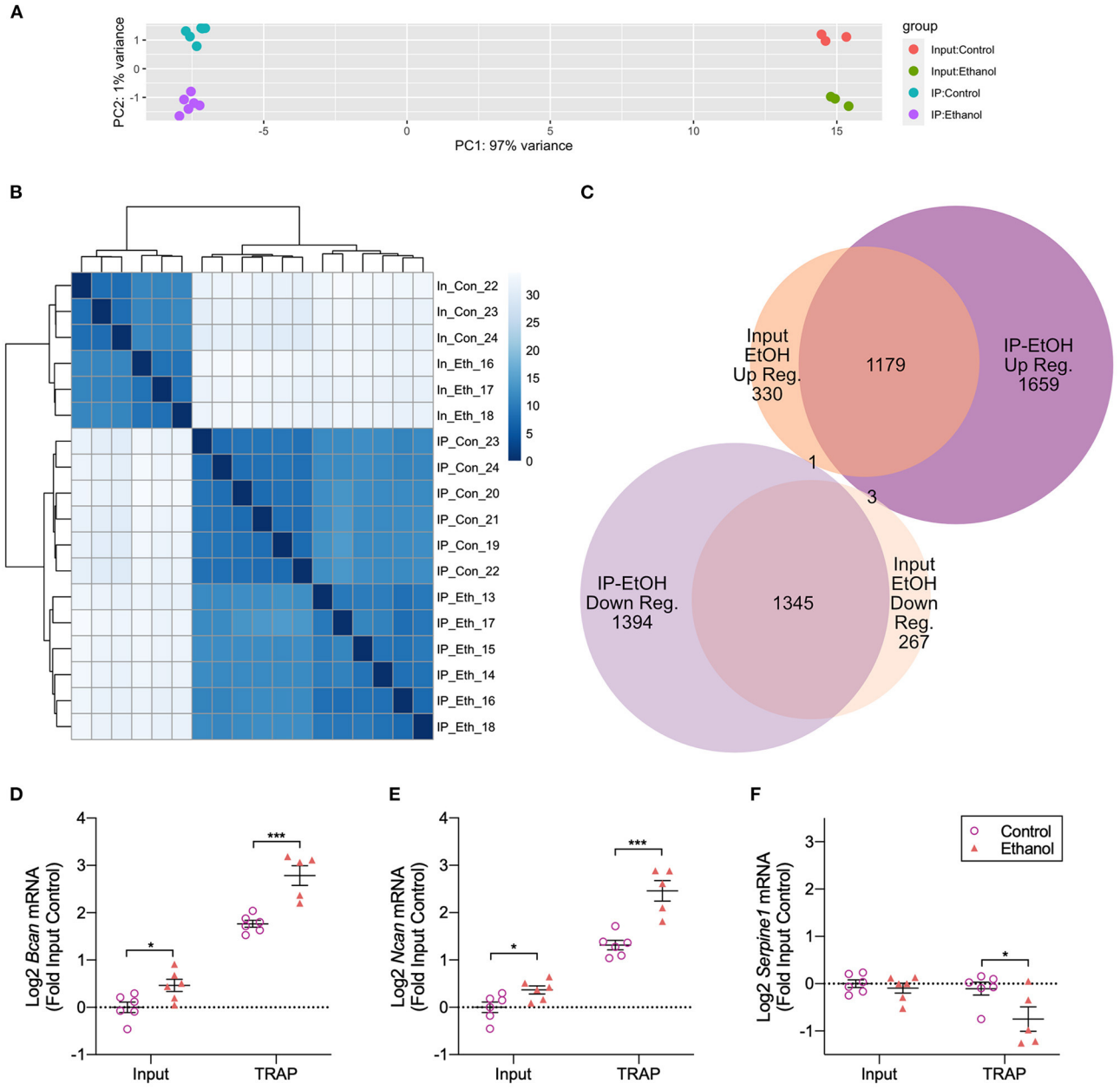


FIGURE 2
Translatome and transcriptome analyses of *in vitro* astrocytes following ethanol treatment. **(A)** Principal Component Analysis (PCA) of RNA-Seq data shows PC1 accounting for 97% of the variance separating IP and input samples. PC2 accounting for 1% of the variance separates control samples from ethanol-treated samples. **(B)** Hierarchical cluster analysis shows clear separation based on the fraction (input vs. IP) and treatment [control vs. ethanol (EtOH)]. **(C)** More genes were differentially regulated by ethanol in the IP fraction compared to the input fraction [5,581 (IP) vs. 3,125 (input)]. A comparison of ethanol-regulated genes in each fraction shows a large overlap between fractions, with 1,179 genes upregulated by ethanol in common between IP and input fractions and 1,345 genes in common between fractions that were downregulated by ethanol. **(D)** Confirmation of RNA-Seq results by qRT-PCR for *Bcan* showed increased *Bcan* mRNA in both input and TRAP fractions. The Log_2 transformed data expressed relative to the input control with the mean ± SEM are shown. *$p < 0.05$; ***$p < 0.001$ ($n = 5–6$). **(E)** Confirmation of RNA-Seq results by qRT-PCR for *Ncan* showed increased *Ncan* mRNA in both input and TRAP fractions. The Log_2 transformed data expressed relative to the input control with the mean ± SEM are shown. *$p < 0.05$; ***$p < 0.001$ ($n = 5–6$). **(F)** Confirmation of RNA-Seq results by qRT-PCR for *Serpine1*, which is the gene encoding PAI-1, showed decreased *Serpine1* mRNA in the TRAP fraction. The Log_2 transformed data expressed relative to the input control with the mean ± SEM are shown. *$p < 0.05$ ($n = 5–6$).

p-value of < 0.01. When sub-setting the genes based on the direction of ethanol regulation, we identified 711 and 1,120 significant gene categories in upregulated and downregulated genes, respectively (Supplementary Table 6). The top 25 categories in each comparison, based on *p*-value, are shown in Figures 3A–C. Of note, we identified several categories related to RNA and ribosomes ("RNA binding," "ribosome biogenesis," "rRNA processing") in ethanol-regulated and ethanol-downregulated

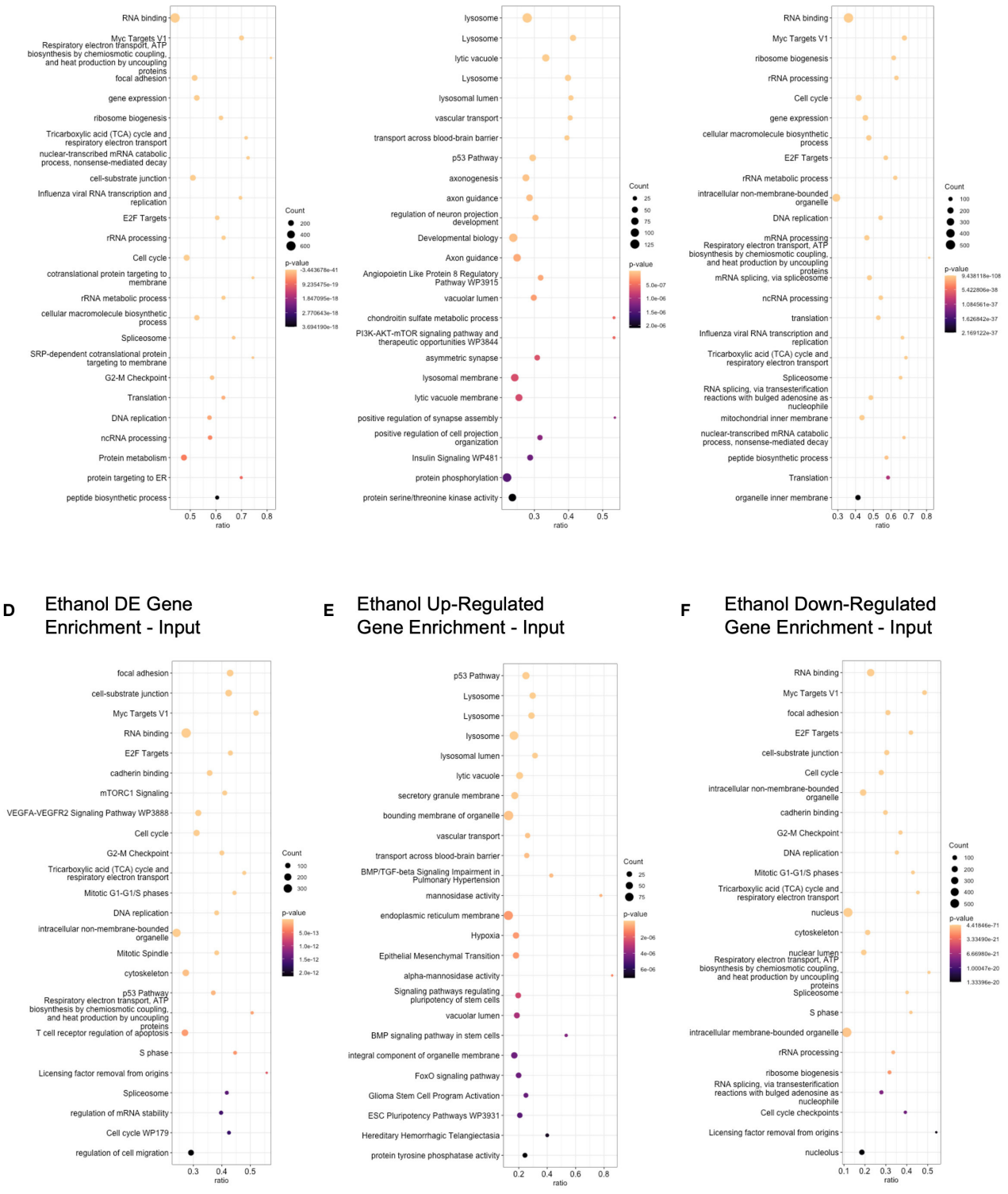


FIGURE 3 (Continued)

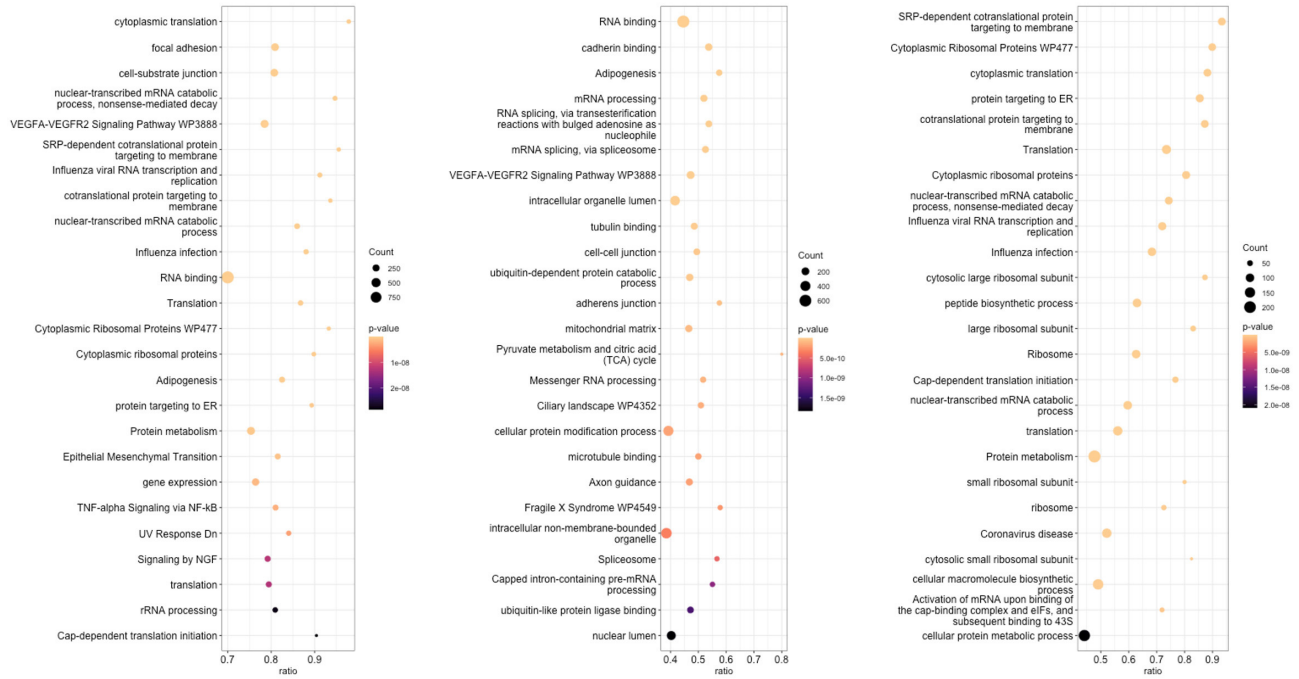


FIGURE 3 (Continued)
Top 25 enrichR results (based on enrichment *p*-value) for each comparison. **(A)** Ethanol DT genes in the IP fraction were analyzed using enrichR to identify enriched GO categories or pathways. **(B)** Ethanol-upregulated DT genes were used to query the enrichR database. **(C)** Ethanol-downregulated DT genes were used to query the enrichR database. **(D)** Ethanol DE genes in the input fraction were analyzed using enrichR to identify enriched GO categories or pathways. **(E)** Ethanol-upregulated DE genes in the input fraction were used to query the enrichR database. **(F)** Ethanol-downregulated DE genes in the input fraction were used to query the enrichR database. **(G)** Genes with different read counts between IP and input fractions were analyzed using enrichR to identify enriched GO categories and pathways. **(H)** Genes with higher read counts in IP compared to input were analyzed using enrichR to identify enriched GO categories and pathways. **(I)** Genes with higher read counts in input compared to IP were analyzed using enrichR to identify enriched GO categories and pathways.

genes in the IP fraction. Of the 140 genes that were ethanol regulated in the "Myc Targets V1" category in the IP fraction, 135 were downregulated by ethanol, indicating that Myc may be a primary target of ethanol. Similarly, of the 17 genes in the "Chondroitin sulfate metabolic process," which was highly significant in the ethanol-upregulated genes in the IP fraction ($p = 5.26 \times 10^{-7}$), and all ethanol-regulated genes ($p = 8.69 \times 10^{-4}$), 16 were upregulated by ethanol, suggesting that this process was highly upregulated in ethanol-exposed astrocytes. In addition, we identified 16 other glycosaminoglycan/chondroitin sulfate proteoglycan-related categories that were upregulated by ethanol in the IP fraction, which showed few to no genes in the ethanol-downregulated group in the IP fraction (Supplementary Table 6). Other categories with highly skewed makeup between upregulated and downregulated genes by ethanol include lysosome-related functions/cellular components, "transport across the blood–brain barrier," and axonogenesis/axon guidance, with more genes upregulated than downregulated by ethanol.

In the input samples, we identified 1,142 enriched gene categories, with 657 and 1,277 gene categories in ethanol upregulated and downregulated genes, respectively (Figures 3D–F and Supplementary Table 6). Mirroring the results from the IP analysis, "Myc Targets V1," "RNA binding," and "cell cycle" were significant only in the ethanol-downregulated genes in the input fraction. Lysosome-related categories ("lysosome," "lysosomal lumen"), "transport across the blood–brain barrier," and "vascular transport" were significant only in the ethanol-upregulated genes in the input fraction.

Comparing these analyses, we found that only 15 categories were significant in all of the analyses of genes upregulated, downregulated, and regulated in either direction in the IP fraction, indicating that these 15 pathways were impacted irrespective of the direction of ethanol regulation (Supplementary Table 7). The categories include the "androgen receptor signaling pathway," the "integrin signaling pathway," and "BDNF signaling pathway." In the input fraction, we found 59 significant categories for genes that were upregulated, downregulated, and ethanol regulated in either direction (Supplementary Table 7). The categories with significant enrichment in up, down, and both directions in the input fraction include "focal adhesion," "TGF-beta signaling pathway," and "cell-substrate junction." The four categories were enriched in all six comparisons across IP, and input fractions (ethanol-regulated IP, ethanol-upregulated IP, ethanol-downregulated IP, ethanol-regulated input, ethanol-upregulated input, ethanol-downregulated input) were "PI3/AKT/mTOR signaling," "BDNF signaling pathway," "UV Response Up," and "Apical Junction."

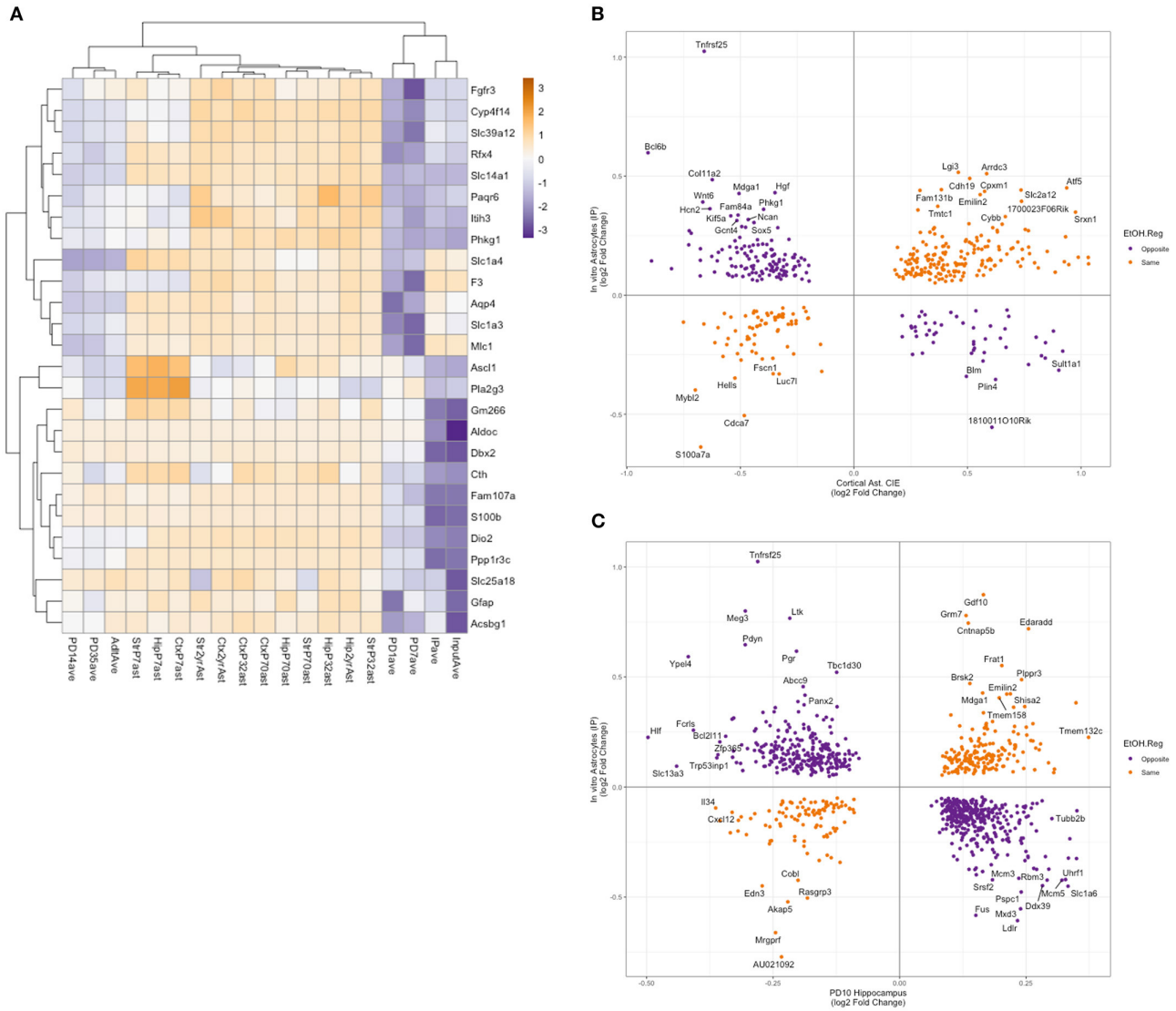


FIGURE 4
Comparison of *in vitro* astrocyte TRAP RNA-Seq to published datasets of *in vivo* astrocyte expression. **(A)** Astrocyte-enriched genes identified as altered during development (as in Rurak et al., 2022) were clustered using the percentile rank of each gene to account for differences between the experiments (Clarke et al., 2018; Rurak et al., 2022). The clustering of these genes indicates that our *in vitro* RNA-Seq expression is more similar to PD1 and PD7 cortical astrocyte expression. **(B)** An overlap of ethanol-regulated genes in *in vivo* astrocytes after chronic intermittent ethanol exposure and DT genes in the IP fraction from *in vitro* astrocytes. Genes with the same direction of regulation by ethanol are shown in orange, and genes with the opposite direction of regulation by ethanol are shown in purple. Genes with a $\log_2$ fold change greater than abs 0.3 are labeled with the gene symbol. **(C)** An overlap of ethanol-regulated genes in PD10 hippocampus after ethanol exposure and DT genes in the IP fraction from *in vitro* astrocytes. Genes with the same direction of regulation by ethanol are shown in orange, and genes with the opposite direction of regulation by ethanol are shown in purple. Genes with a $\log_2$ fold-change greater than abs 0.35 in the PD10 hippocampus or abs 0.4 in the *in vitro* astrocytes are labeled with the gene symbol.

A comparison of the significant GO and pathway categories identified in ethanol-regulated genes in the IP and input fractions shows 732 categories as significant in both the input and IP fractions. The high proportion (66 and 64% in IP and input, respectively) of gene category similarity is expected based on the high number of overlapping regulated genes in each fraction.

We also conducted pathway and GO enrichment analysis on the genes that were identified as significantly different between the input and IP fractions, with the top 25 categories enriched in the analysis of upregulated and downregulated genes, upregulated in IP, and upregulated in input shown in Figures 3G–I, respectively. Enriched categories, irrespective of direction, included "cytoplasmic translation," "cell-substrate junction," "VEGFA-VEGFR2 Signaling Pathway," "cotranslational protein targeting to the membrane," and "RNA binding." Top categories in genes that were higher in the IP fraction compared to the input that were not also significant in genes that were higher in the input fraction compared to IP (which can be characterized as gene categories that are actively translated)

included "RNA binding," "cadherin binding," "VEGFA-VEGFR2 Signaling Pathway," and "Axon guidance." Top categories in genes that were higher in the input fraction compared to the IP fraction that were not also significant in genes that were higher in the IP fraction compared to input (which can be characterized as gene categories related to RNAs that are present in the cell but not actively translated) included "SRP-dependent cotranslational protein targeting to membrane," "Cytoplasmic Ribosomal Proteins," and "Translation."

Comparison to developmental astrocyte TRAP studies

To better understand the relevance of *in vitro* astrocyte transcription and translation to the *in vivo* setting, we compared our results to previously published studies on the Aldh1l1-EGFP/Rpl10a mice. Clarke et al. (2018) profiled astrocyte translation in the striatum, hippocampus, and cortex at PD7, PD32, 10 weeks, 9.5 months, and 2 years using TRAP, followed by RNA-Seq. Rurak et al. (2022) profiled the cortex in males and females at PD1, PD4, PD7, PD14, PD35, and adult time points using TRAP followed by RNA-Seq. To observe what developmental stage and brain region(s) our *in vitro* astrocytes are most similar to in *in vivo* astrocytes, we conducted a hierarchical cluster analysis on 26 genes identified as being astroglial-specific and developmentally regulated (Rurak et al., 2022). As our data were from mixed-sex cultures, we collapsed sex data based on time points for the Rurak et al. analysis. In addition, to account for differences in library preparation and sequencing protocols, we calculated the average percentile for each gene in each age and tissue. Inspection of the cluster dendrogram showed that our *in vitro* astrocytes (both input and IP fractions) cluster most closely with the PD1 and PD7 cortical astrocytes (Figure 4).

Comparison to chronic intermittent ethanol effects on *in vivo* astrocytes

We then compared the genes that were identified as DE or DT in our input and IP fractions to an analysis of astrocytes isolated via magnetic bead/antibody complexes targeting an astrocyte-specific surface marker (*Acsa2*) from mice that had undergone chronic intermittent ethanol exposure (CIE). The CIE model is well established in the literature as a model of binge exposure, which can cause increased drinking and dependence. Erickson et al. (2018) identified 1,153 differentially expressed genes in astrocytes after CIE. We compared our DT and DE genes to these genes regulated *in vivo* and saw 434 and 253 genes in common, respectively (Figures 4B, C). Hypergeometric analysis, using the R package GeneOverlap (Shen, 2022), showed a significant overlap between the *in vivo* astrocytes and both fractions (IP: $p = 1.8 \times 10^{-17}$, input: $p = 2.9 \times 10^{-11}$), indicating that the similarity of the gene sets was unlikely to be random. As observed in Figure 4B, there was a significant proportion of the genes that were regulated by ethanol in the opposite direction between the *in vivo* and *in vitro* astrocytes, and hypergeometric testing of the genes based on the direction of regulation did not show a significant overlap. An analysis of GO and pathway enrichment of the ethanol-regulated genes in common between the *in vivo* and *in vitro* data showed categories related to the lysosome, pre- and post-synapse, and extracellular matrix, which in many ways is consistent with what we observed in the GO and pathway enrichment analysis of DT and DE genes (Figure 3 and Supplementary Table 8). While conducting the enrichment analysis on genes that were regulated in opposite directions between *in vitro* and *in vivo* datasets, gene categories that potentially relate to the cross-talk between astrocytes and other brain cell types or the extracellular matrix were overrepresented, with "regulation of synapse assembly," "positive regulation of cell junction assembly," and "nervous system development" enriched in IP genes regulated in the opposite direction from *in vivo* astrocytes, and "regulation of cell migration," "Dermatan sulfate biosynthesis," and "extracellular matrix organization" enriched in input genes regulated in the opposite direction from *in vivo* astrocytes (Supplementary Table 8).

Comparison to neonatal ethanol-treated mice

We also sought to compare our DT and DE genes with a neonatal model of third-trimester equivalent ethanol exposure in mice. Key developmental processes that occur in the third trimester of human gestation, occur in the first two post-natal weeks in mice (Clancy et al., 2001). Pinson et al. (2021) administered 4 g/kg of ethanol from PD4-PD9 and examined ethanol-induced changes in hippocampal and cerebellar gene expression at PD10 24 h after the last dose of ethanol administered using RNA-Seq. After neonatal ethanol exposure, they found 2,150 DE genes in the hippocampus and 2,017 DE genes in the cerebellum (Pinson et al., 2021). Comparison of our DT and DE genes from *in vitro* astrocytes showed an overlap of 903 genes in common between DT (IP) and PD10 DE genes from the hippocampus, 596 genes in common between DE (input) and PD10 DE genes from the hippocampus, 777 genes in common between DT (IP) and PD10 DE genes from the cerebellum, and 497 genes in common between DE (input) and PD10 DE genes from the cerebellum (Supplementary Table 9). Hypergeometric analysis showed a significant overlap in all four comparisons (IP vs. hippocampus: $p = 1.5 \times 10^{-60}$, input vs. hippocampus: $p = 5.6 \times 10^{-60}$; IP vs. cerebellum: $p = 3.5 \times 10^{-35}$, input vs. cerebellum: $p = 4.1 \times 10^{-34}$). GO and pathway enrichment analysis showed enriched categories relating to "RNA binding," "Myc Targets V1," and "Protein metabolism" in the overlapping genes between both the IP and input ethanol-regulated genes in our analyses and the PD10 hippocampus (Supplementary Table 10). GO and pathway enrichment analysis of overlapping genes between the IP and input ethanol-regulated genes from our analysis with the PD10 cerebellum ethanol-regulated genes showed enrichment in categories relating to "cytoplasmic translation," "cytoplasmic ribosomal proteins," and "SRP-dependent cotranslational protein targeting to the membrane." While examining the direction of

regulation in the overlapping genes, we observed that a higher number of genes were regulated by ethanol in opposite directions between *in vitro* astrocytes and the whole hippocampus or cerebellum [IP vs. hippocampus: 283 (same), 620 (opposite); input vs. hippocampus: 155 (same), 441 (opposite); IP vs. cerebellum: 232 (same), 545 (opposite); input vs. cerebellum: 145 (same), 352 (opposite)]. Moreover, hypergeometric analysis of the overlap of genes regulated by ethanol in the same direction showed no significant overlap. This is likely due to many factors, including the difference between *in vivo* and *in vitro* ethanol treatments (with a major difference being that in the study by Pinson et al., tissue samples were collected 24 h after the last administration of ethanol, corresponding to an alcohol withdrawal time point, while in our experiments, samples were collected immediately after alcohol exposure), the difference in brain areas (*in vitro* astrocytes were generated from the cortex while the *in vivo* study examined the hippocampus and the cerebellum), and the presence of multiple cell types in the whole tissue expression profiles. GO and pathway enrichment analyses of overlapping genes in the same direction in IP and the hippocampus showed pathways related to "cell-cell adhesion via plasma-membrane adhesion molecules," "proteoglycans in cancer," and "axon guidance," while overlapping genes in the same direction in IP and the cerebellum showed pathways related to "wound healing," "positive regulation of cell migration," and "signaling events mediated by focal adhesion kinase." GO and pathway enrichment analysis of genes that were regulated in opposite directions between IP and the hippocampus returned categories "RNA binding," "Myc Targets V1," and "protein metabolism," while oppositely regulated genes between IP and the cerebellum returned categories "cytoplasmic ribosomal proteins," "cytoplasmic translation," and "cotranslational protein targeting the membrane."

As our *in vitro* exposure is a single 24 h exposure, we wanted to compare our data to a recently published dataset from C57BL/6J mice that were administered a single dose of ethanol on PD7 (Baker et al., 2022). Baker et al. (2022) used a microarray platform to identify ethanol-regulated genes in males and females of several different recombinant inbred BXD lines and the parental C57BL/6J (B6) and DBA/2J lines. A comparison of the ethanol-regulated genes from our *in vitro* astrocytes to the ethanol-regulated genes in the B6 hippocampus from either males or females shows a large number of genes in common, with 158 genes in the IP fraction and 113 genes in the input fraction. Hypergeometric analysis shows a significant overlap in both comparisons (IP vs. B6: 1.2×10^{-20}; input vs. B6: 2.4×10^{-21}). Interestingly, in this comparison, we observed that the vast majority of the ethanol regulation *in vitro* and in the hippocampus after a single ethanol exposure was in the same direction. We found 142 genes regulated in the same direction in the IP fraction (hypergeometric overlap: $p = 1.4 \times 10^{-13}$), with only 16 genes regulated in the opposite direction, and 104 genes regulated in the same direction in the input fraction (hypergeometric overlap: $p = 8.1^{-17}$), while only nine were regulated in opposite directions (Supplementary Table 11). This suggests that the exposure model used in our *in vitro* studies more closely resembled a single exposure *in vivo*.

Discussion

In this study, we utilized the TRAP procedure to generate transcriptional (input) and translational (IP) profiles of Aldh1l1-EGFP/Rpl10a primary cortical astrocyte cultures following ethanol treatment that showed broad similarities between the ethanol response in each fraction. In addition, we identified many genes that were differentially expressed between the input and IP (TRAP) fractions, highlighting the different makeup of the total mRNA pool vs. translating mRNA pools in a given cell type. Our primary goal in these studies was to identify ethanol-regulated genes in an *in vitro* model that was similar to what we have used in the past using rat cortical astrocytes. By using astrocytes isolated from Aldh1l1-EGFP/Rpl10a mice, we could also identify genes that were differentially translated vs. differentially expressed in a single cell type. These data will be valuable in analyzing our ongoing studies of *in vivo* astrocyte responses to ethanol exposure in Aldh1l1-EGFP/Rpl10a mice. In addition, by leveraging published datasets using the Aldh1l1-EGFP/Rpl10a mice, we can better understand how our i*n vitro* model relates to *in vivo* astrocytes from a developmental time-point perspective. This study also compared our data sets to the *in vivo* astrocyte response to ethanol using published data from *in vivo* astrocytes isolated using a cell-surface antibody-enrichment method following a chronic model of ethanol consumption as well as whole tissue gene expression analysis in the FASD models of ethanol exposure.

In the brain, multiple cell types and heterogeneity within each cell type add complexity to studying the effects of a neurodevelopmental perturbation such as ethanol. Significant progress has been made recently using single-cell and single-nucleus RNA-Seq, but these approaches can be limited by the cost and the ability to detect treatment differences (Ofengeim et al., 2017; Brenner et al., 2020). The use of *in vitro* models has been a valuable tool for understanding complex mechanisms occurring in the brain, allowing the study of individual cell types' responses to alcohol exposure (Goeke et al., 2022). However, there are limitations (Slanzi et al., 2020).

The first question our study addresses is how the total RNA pool and translational RNA pool (mRNA physically associated with ribosomes during translation) differ in a single cell type. We found that approximately half of all detected genes were differentially partitioned between the input and IP fractions (12,313 out of 24,495), with 6,045 genes with higher levels in the IP vs. input and 6,268 genes with higher levels in the input vs. IP. The IP fraction was enriched for genes related to cadherin binding, axon guidance, RNA binding, and VEGFA-VEGFR2 signaling (Supplementary Table 6). Cadherins are cell adhesion molecules that are known to be essential in neuronal development and neurite outgrowth (Tomaselli et al., 1988; Martinez-Garay, 2020). Astrocytes are known to facilitate neuronal development, including axon guidance (Rigby et al., 2020). VEGFA-VEGFR2 signaling is essential for endothelial cell differentiation during angiogenesis, and astrocytes are key facilitators in the process of angiogenesis during early postnatal brain development (Puebla et al., 2022).

It should be noted that the input fraction in the TRAP procedure is a sampling of all RNA present, so it contains both translating RNA and RNA that is not being actively translated. We

observed categories related to ribosomes, translation, and protein targeting to the membrane as enriched in the input fraction, suggesting that astrocytes are primed for the translation of these processes and functions. Astrocytes need to respond rapidly to changes in the local environment, and many of the responses elicited in astrocytes occur extracellularly. Therefore, it would be logical to have a pool of translational capacity and membrane-targeting machinery in the form of mRNA that is ready to be translated.

As observed in Figure 2, samples in our data separate most strongly based on the fraction (IP vs. input) in both PCA and hierarchical clustering, but ethanol treatment also clearly separates the samples in the second principal component (PC2) and within each fraction of the hierarchical clustering. Gene pathway and GO enrichment analyses show broad similarities between ethanol-regulated genes from the two fractions (IP and input). Interestingly, the genes downregulated by ethanol appear to be more cohesive in that the enrichment analysis *p*-values are lower and the number of genes in the top enriched categories is larger in both fractions (Figure 3), even though the number of genes that are identified as upregulated vs. downregulated in each fraction is similar (i.e., there is no bias toward one direction of regulation). This indicates that ethanol is upregulating genes in a greater number or a variety of smaller categories, while genes that are downregulated are clumped into a smaller, more concentrated number of categories. Many early transcriptional surveys of gene expression in brain tissue in response to ethanol exposure noted a bias toward downregulated genes (Lewohl et al., 2000; Saito et al., 2002). While we did not observe a bias in the direction of regulation in either of our datasets, the coordinated downregulation caused by ethanol in bulk tissue may reflect a large-scale transcriptional response, while our use of a single cell type allows the identification of the targeted groups of genes that are upregulated and obscured when looking at the bulk tissue with many different cell types and transcriptional responses.

The top GO and pathway categories that were identified in ethanol-downregulated genes in IP and input fractions include broad generic categories such as "RNA binding" and "cell cycle," as well as the pathway "Myc Targets V1." Myc-related signaling has been observed in the acute response to ethanol (Kerns et al., 2005) and is differentially expressed in the rodent models of alcohol preferences and avoidance (Sommer et al., 2006). We observed enrichment in lysosome-related genes upregulated by ethanol in both the input and IP fractions (Figure 3). The involvement of lysosomal-related function in the astrocyte response to ethanol has previously been shown. Pla et al. (2016) showed autophagy induction and lysosome enlargement after ethanol treatment in primary astrocyte cultures that were blocked in astrocytes cultured from *Tlr4* knock-out mice, implicating a TLR4-autophagy-lysosome pathway in the astrocyte response to ethanol (Pla et al., 2016). While the TLR4 pathway was not enriched in our ethanol-regulated analyses, *Tlr4* mRNA was upregulated by ethanol in both input and IP fractions (Supplementary Tables 3, 4), and the GO molecular process "regulation of autophagy" is enriched in ethanol-regulated genes from input and IP fractions (Supplementary Table 6).

Our lab is interested in the role astrocytes play in brain development, with a particular emphasis on the extracellular matrix (ECM). During the brain growth spurt, which occurs in the third trimester of human gestation and during the first two postnatal weeks in mice, astrocytes proliferate and provide structural and chemical cues to neurons as they make connections (Clarke and Barres, 2013; Kane and Drew, 2021). In our *in vitro* TRAP data, we noticed that ethanol-upregulated genes were enriched in categories related to axon guidance and chondroitin sulfate-related categories, which provide important extracellular guideposts to developing neurons (Kwok et al., 2012).

One of the challenges in the utilization of *in vitro* models of complex *in vivo* systems is understanding how the *in vitro* model is a good representation of the *in vivo* system and where the models diverge. We utilized both *in vivo* and *in vitro* systems to understand the interaction of astrocytes and neurons in response to ethanol and to model the effects of third-trimester ethanol exposure on brain development. To these ends, we sought to contextualize our *in vitro* data by comparing our translational and transcriptional data to published reports using the same Aldh1l1-EGFP/Rpl10a mouse model we utilized for our cultures. Recent publications studying astrocyte functions in the brain during development and aging allowed us to compare the expression profiles of astrocytes *in vivo* with our *in vitro* data. While examining genes that were identified as altered during development (i.e., the genes that change based on the developmental age of the mice), our *in vitro* data clustered most closely with samples from the cortex of PD1 and PD7 mice (Figure 4). Our astrocytes are isolated from the neocortex of PD0 mice, and we use the cultures to model astrocytes from the early postnatal period of PD7.

We also sought to compare our *in vitro* data to ethanol regulation of gene expression in astrocytes *in vivo*. A method to study cell-type-specific expression profiles involves disruption of the tissue to generate single-cell suspensions and purification of cells by antibody-magnetic bead complexes directed to cell surface proteins. For astrocytes, Acsa2 is commonly used to enrich astrocytes from single-cell suspensions (Erickson et al., 2018; Pan and Wan, 2020). Comparison of our *in vitro* astrocyte data to the medial prefrontal cortex (mPFC) astrocytes following a chronic ethanol exposure paradigm showed many of the same genes as dysregulated by ethanol (Figure 4B), providing support for the relevance of our *in vitro* observations to astrocyte *in vivo* responses.

As our astrocyte cultures are most similar to PD1-PD7 cortical astrocytes, and given our interest in the role astrocytes play during brain development, we also compared our data to recent studies exploring the effects of neonatal ethanol on hippocampal and cerebellar gene expression. We observed a significant overlap in DE and DT genes with both hippocampal and cerebellar ethanol-induced changes. However, compared to the *in vivo* astrocyte comparison above, we observed a greater number of genes with opposite regulation by ethanol in the overlapping genes. There are many potential reasons for the different directions of ethanol regulation, including the presence of multiple cell types in bulk hippocampal or cerebellar RNA, the difference

in brain areas examined, differences in the ethanol treatments, the timing of ethanol exposure and when RNA was collected, and the lack of astrocyte-neuron communication in our *in vitro* data, to name a few. However, it is striking that the genes that showed the same direction of regulation by ethanol were enriched in categories related to known astrocyte functions such as cell adhesion, axon guidance, and proteoglycan synthesis and signaling (Wiese et al., 2012; Rigby et al., 2020; Saint-Martin and Goda, 2022). In addition, a comparison of our *in vitro* astrocyte DT and DE genes to a recently published dataset from the hippocampus of C57BL/6J mice administered a single dose of ethanol on PD7 showed that ∼90% of genes were regulated in the same direction by ethanol, indicating that our model more closely resembled an acute exposure *in vivo* model (Baker et al., 2022).

Taken together, we found that primary astrocyte cultures isolated from PD0 mice showed the highest similarity in the expression profile of developmentally regulated genes to PD1 and PD7 astrocytes *in vivo* (Figure 4A), indicating that our method of culturing astrocytes is more representative of the early neonatal period than other developmental stages. We observed a significant overlap of DT and DE genes with published reports of ethanol-regulated genes using various models of ethanol exposure. It was somewhat concerning that the direction of ethanol regulation was not always the same. However, it should be noted that some of the comparisons we made were to adult expression profiles after prolonged chronic ethanol exposure (Figure 4B) or in neonatal animals after 24 h of withdrawal from ethanol (Figure 4C). Furthermore, the cellular heterogeneity of intact tissues adds complexity to the interpretation of expression changes as to astrocyte-specific responses to ethanol vs. compensatory changes to alterations in other cell types. Interestingly, the greatest correspondence of our data based on the direction of ethanol regulation was to a recent report in neonatal mice in which expression profiling occurred while alcohol was still in the system (Baker et al., 2022), indicating that our *in vitro* model was most similar to neonatal studies of single ethanol exposures or while ethanol was still present in the system.

Conclusion

We analyzed the transcriptional and translational pools of primary astrocyte cultures generated from Aldh1l1-EGFP/Rpl10a mice following ethanol treatment to better understand how our *in vitro* model compared to *in vivo* astrocyte responses to ethanol during the early postnatal period in mice. While a large number of differences were observed between the total RNA pool and translating RNA, we observed broad similarities in the GO and pathways enriched in the ethanol-regulated genes in the two fractions. A comparison of our data to recently published reports of developmental astrocyte gene translation showed that our cultures were most similar to PD1 and PD7 cortical astrocytes. In addition, we observed many similarities in our *in vitro* astrocyte response to ethanol to a published report of the *in vivo* astrocyte response to chronic ethanol exposure. Finally, comparing our data to neonatal models of ethanol exposure showed many similarities in genes and pathways that were dysregulated by ethanol.

Data availability statement

The datasets presented in this study can be found in online repositories. The names of the repository/repositories and accession number(s) can be found in the article/Supplementary material.

Ethics statement

The animal study was reviewed and approved by VA Portland Health Care System Institutional Animal Care and Use Committee (IACUC).

Author contributions

MG conceived the project and designed the experiments. JH and XZ contributed to data collection and performed experiments. JH performed the data analysis and wrote the first draft of the manuscript. All authors contributed to the final manuscript.

Funding

This study was supported by NIH P60AA010760, R01AA029486, and U01AA029965, VA Merit Review Award I01BX001819, and by facilities and resources at the Portland VA Health Care System. The contents of this article do not represent the views of the United States Department of Veterans Affairs or the United States government.

Conflict of interest

The authors declare that the research was conducted in the absence of any commercial or financial relationships that could be construed as a potential conflict of interest.

Publisher's note

All claims expressed in this article are solely those of the authors and do not necessarily represent those of their affiliated organizations, or those of the publisher, the editors and the reviewers. Any product that may be evaluated in this article, or claim that may be made by its manufacturer, is not guaranteed or endorsed by the publisher.

Supplementary material

The Supplementary Material for this article can be found online at: https://www.frontiersin.org/articles/10.3389/fnins.2023.1193304/full#supplementary-material

References

Abbott, N. J., Rönnbäck, L., and Hansson, E. (2006). Astrocyte–endothelial interactions at the blood–brain barrier. *Nat. Rev. Neurosci.* 7, 41–53. doi: 10.1038/nrn1824

Baker, J. A., Brettin, J. T., Mulligan, M. K., and Hamre, K. M. (2022). Effects of genetics and sex on acute gene expression changes in the hippocampus following neonatal ethanol exposure in BXD recombinant inbred mouse strains. *Brain Sci.* 12, 1634. doi: 10.3390/brainsci12121634

Bolger, A. M., Lohse, M., and Usadel, B. (2014). Trimmomatic: a flexible trimmer for Illumina sequence data. *Bioinformatics.* 30, 2114–2120. doi: 10.1093/bioinformatics/btu170

Brenner, E., Tiwari, G. R., Kapoor, M., Liu, Y., Brock, A., and Mayfield, R. D. (2020). Single cell transcriptome profiling of the human alcohol-dependent brain. *Hum. Mol. Genet.* 29, 1144–1153. doi: 10.1093/hmg/ddaa038

Chen, E. Y., Tan, C. M., Kou, Y., Duan, Q., Wang, Z., Meirelles, G. V., et al. (2013). Enrichr: interactive and collaborative HTML5 gene list enrichment analysis tool. *BMC Bioinformatics* 14, 128. doi: 10.1186/1471-2105-14-128

Clancy, B., Darlington, R. B., and Finlay, B. L. (2001). Translating developmental time across mammalian species. *Neuroscience* 105, 7–17. doi: 10.1016/S0306-4522(01)00171-3

Clarke, L. E., and Barres, B. A. (2013). Emerging roles of astrocytes in neural circuit development. *Nat. Rev. Neurosci.* 14, 311–321. doi: 10.1038/nrn3484

Clarke, L. E., Liddelow, S. A., Chakraborty, C., Münch, A. E., Heiman, M., and Barre, B. A. (2018). Normal aging induces A1-like astrocyte reactivity. *Proc. Nat. Acad. Sci. USA.* 115, E1896–E1905. doi: 10.1073/pnas.1800165115

Conner, D. A. (2002). Mouse colony management. *Curr. Protoc. Mol. Biol.* 57, 23.8.1–23.8.11. doi: 10.1002/0471142727.mb2308s57

Dobin, A., Davis, C. A., Schlesinger, F., Drenkow, J., Zaleski, C., Jha, S., et al. (2013). STAR: ultrafast universal RNA-seq aligner. *Bioinformatics* 29, 15–21. doi: 10.1093/bioinformatics/bts635

Doyle, J. P., Dougherty, J. D., Heiman, M., Schmidt, E. F., Stevens, T. R., Ma, G., et al. (2008). Application of a translational profiling approach for the comparative analysis of CNS cell types. *Cell* 135, 749–762. doi: 10.1016/j.cell.2008.10.029

Erickson, E. K., Farris, S. P., Blednov, Y. A., Mayfield, R. D., and Harris, R. A. (2018). Astrocyte-specific transcriptome responses to chronic ethanol consumption. *Pharmacogenomics J.* 18, 578–589. doi: 10.1038/s41397-017-0012-2

Goeke, C. M., Roberts, M. L., Hashimoto, J. G., Finn, D. A., and Guizzetti, M. (2018). Neonatal ethanol and choline treatments alter the morphology of developing rat hippocampal pyramidal neurons in opposite directions. *Neuroscience* 374, 13–24. doi: 10.1016/j.neuroscience.2018.01.031

Goeke, C. M., Zhang, X., Hashimoto, J. G., and Guizzetti, M. (2022). Astrocyte tissue plasminogen activator expression during brain development and its role in pyramidal neuron neurite outgrowth. *Neurosci. Lett.* 769, 136422. doi: 10.1016/j.neulet.2021.136422

Guttenplan, K. A., Weigel, M. K., Prakash, P., Wijewardhane, P. R., Hasel, P., Rufen-Blanchette, U., et al. (2021). Neurotoxic reactive astrocytes induce cell death via saturated lipids. *Nature* 599, 102–107. doi: 10.1038/s41586-021-03960-y

Heiman, M., Kulicke, R., Fenster, R. J., Greengard, P., and Heintz, N. (2014). Cell type-specific mRNA purification by translating ribosome affinity purification (TRAP). *Nat. Protoc.* 9, 1282–1291. doi: 10.1038/nprot.2014.085

Heiman, M., Schaefer, A., Gong, S., Peterson, J. D., Day, M., Ramsey, K. E., et al. (2008). A translational profiling approach for the molecular characterization of CNS cell types. *Cell* 135, 738–748. doi: 10.1016/j.cell.2008.10.028

Kane, C. J. M., and Drew, P. D. (2021). Neuroinflammatory contribution of microglia and astrocytes in fetal alcohol spectrum disorders. *J. Neurosci. Res.* 99, 1973–1985. doi: 10.1002/jnr.24735

Kerns, R. T., Ravindranathan, A., Hassan, S., Cage, M. P., York, T., Sikela, J. M., et al. (2005). Ethanol-responsive brain region expression networks: implications for behavioral responses to acute ethanol in DBA/2J versus C57BL/6J mice. *J. Neurosci.* 25, 2255–2266. doi: 10.1523/JNEUROSCI.4372-04.2005

Kuleshov, M. V., Jones, M. R., Rouillard, A. D., Fernandez, N. F., Duan, Q., Wang, Z., et al. (2016). Enrichr: a comprehensive gene set enrichment analysis web server 2016 update. *Nucleic Acids Res.* 44, W90–W97. doi: 10.1093/nar/gkw377

Kwok, J. C. F., Warren, P., and Fawcett, J. W. (2012). Chondroitin sulfate: a key molecule in the brain matrix. *Int. J. Biochem. Cell Biol.* 44, 582–586. doi: 10.1016/j.biocel.2012.01.004

Lewohl, J. M., Wang, L., Miles, M. F., Zhang, L., Dodd, P. R., and Harris, R. A. (2000). Gene Expression in human alcoholism: microarray analysis of frontal cortex. *Alcohol. Clin. Exp. Res.* 24, 1873–1882. doi: 10.1111/j.1530-0277.2000.tb01993.x

Li, H., Handsaker, B., Wysoker, A., Fennell, T., Ruan, J., Homer, N., et al. (2009). The sequence alignment/map format and SAMtools. *Bioinformatics* 25, 2078–2079. doi: 10.1093/bioinformatics/btp352

Love, M. I., Huber, W., and Anders, S. (2014). Moderated estimation of fold change and dispersion for RNA-seq data with DESeq2. *Genome Biol.* 15, 550. doi: 10.1186/s13059-014-0550-8

Martinez-Garay, I. (2020). Molecular mechanisms of cadherin function during cortical migration. *Front. Cell Dev. Biol.* 8, 588152. doi: 10.3389/fcell.2020.588152

Ofengeim, D., Giagtzoglou, N., Huh, D., Zou, C., and Yuan, J. (2017). Single-cell RNA sequencing: unraveling the brain one cell at a time. *Trends Mol. Med.* 23, 563–576. doi: 10.1016/j.molmed.2017.04.006

Pan, J., and Wan, J. (2020). Methodological comparison of FACS and MACS isolation of enriched microglia and astrocytes from mouse brain. *J. Immunol. Methods* 486, 112834. doi: 10.1016/j.jim.2020.112834

Pinson, M. R., Holloway, K. N., Douglas, J. C., Kane, C. J. M., Miranda, R. C., and Drew, P. D. (2021). Divergent and overlapping hippocampal and cerebellar transcriptome responses following developmental ethanol exposure during the secondary neurogenic period. *Alcohol. Clin. Exp. Res.* 45, 1408–1423. doi: 10.1111/acer.14633

Pla, A., Pascual, M., and Guerri, C. (2016). Autophagy constitutes a protective mechanism against ethanol toxicity in mouse astrocytes and neurons. *PLoS ONE* 11, e0153097. doi: 10.1371/journal.pone.0153097

Prah, J., Winters, A., Chaudhari, K., Hersh, J., Liu, R., and Yang, S.-H. (2019). A novel serum free primary astrocyte culture method that mimic quiescent astrocyte phenotype. *J. Neurosci. Methods* 320, 50–63. doi: 10.1016/j.jneumeth.2019.03.013

Puebla, M., Tapia, P. J., and Espinoza, H. (2022). Key role of astrocytes in postnatal brain and retinal angiogenesis. *IJMS* 23, 2646. doi: 10.3390/ijms23052646

Rigby, M. J., Gomez, T. M., and Puglielli, L. (2020). Glial cell-axonal growth cone interactions in neurodevelopment and regeneration. *Front. Neurosci.* 14, 203. doi: 10.3389/fnins.2020.00203

Rurak, G. M., Simard, S., Freitas-Andrade, M., Lacoste, B., Charih, F., Van Geel, A., et al. (2022). Sex differences in developmental patterns of neocortical astroglia: a mouse translatome database. *Cell Rep.* 38, 110310. doi: 10.1016/j.celrep.2022.110310

Saint-Martin, M., and Goda, Y. (2022). Astrocyte–synapse interactions and cell adhesion molecules. *FEBS J.* 16540. doi: 10.1111/febs.16540

Saito, M., Smiley, J., Toth, R., and Vadasz, C. (2002). Microarray analysis of gene expression in rat hippocampus after chronic ethanol treatment. *Neurochem. Res.* 27, 1221–1229. doi: 10.1023/A:1020937728506

Santello, M., Toni, N., and Volterra, A. (2019). Astrocyte function from information processing to cognition and cognitive impairment. *Nat. Neurosci.* 22, 154–166. doi: 10.1038/s41593-018-0325-8

Sanz, E., Yang, L., Su, T., Morris, D. R., McKnight, G. S., and Amieux, P. S. (2009). Cell-type-specific isolation of ribosome-associated mRNA from complex tissues. *Proc. Natl. Acad. Sci. USA* 106, 13939. doi: 10.1073/pnas.0907143106

Shen, L. (2022). *GeneOverlap: Test and Visualize Gene Overlaps. R package version 1.34.0.* Available online at: https://github.com/shenlab-sinai/GeneOverlap (accessed June 05, 2023).

Slanzi, A., Iannoto, G., Rossi, B., Zenaro, E., and Constantin, G. (2020). *In vitro* models of neurodegenerative diseases. *Front. Cell Dev. Biol.* 8, 328. doi: 10.3389/fcell.2020.00328

Sommer, W., Hyytiä, P., and Kiianmaa, K. (2006). The alcohol-preferring AA and alcohol-avoiding ANA rats: neurobiology of the regulation of alcohol drinking. *Addict. Biol.* 11, 289–309. doi: 10.1111/j.1369-1600.2006.00037.x

Tomaselli, K. J., Neugebauer, K. M., Bixby, J. L., Lilien, J., and Reichard, L. F. (1988). N-cadherin and integrins: two receptor systems that mediate neuronal process outgrowth on astrocyte surfaces. *Neuron* 1, 33–43. doi: 10.1016/0896-6273(88)90207-3

Wiese, S., Karus, M., and Faissner, A. (2012). Astrocytes as a source for extracellular matrix molecules and cytokines. *Front. Pharmacol.* 3, 120. doi: 10.3389/fphar.2012.00120

Wilhelm, C. J., and Guizzetti, M. (2016). Fetal alcohol spectrum disorders: an overview from the glia perspective. *Front. Integr. Neurosci.* 9, 65. doi: 10.3389/fnint.2015.00065

Wilhelm, C. J., Hashimoto, J. G., Roberts, M. L., Bloom, S. H., Andrew, M. R., and Wiren, K. M. (2016). Astrocyte dysfunction induced by alcohol in females but not males: alcohol-induced astrocyte dysfunction in females. *Brain Pathol.* 26, 433–451. doi: 10.1111/bpa.12276

Wilhelm, C. J., Hashimoto, J. G., Roberts, M. L., Zhang, X., Goeke, C. M., Bloom, S. H., et al. (2018). Plasminogen activator system homeostasis and its dysregulation by ethanol in astrocyte cultures and the developing brain. *Neuropharmacology* 138, 193–209. doi: 10.1016/j.neuropharm.2018.06.004

Williams, J. F., Smith, V. C., and the Committee On Substance Abuse (2015). Fetal alcohol spectrum disorders. *Pediatrics* 136, e20153113. doi: 10.1542/peds.2015-3113

Xie, Z., Bailey, A., Kuleshov, M. V., Clarke, D. J. B., Evangelista, J. E., Jenkins, S. L., et al. (2021). Gene set knowledge discovery with enrichr. *Curr. Protoc.* 1, e90. doi: 10.1002/cpz1.90

Zhang, X., Hashimoto, J. G., Han, X., Zhang, F., Linhardt, R. J., and Guizzetti, M. (2021). Characterization of glycosaminoglycan disaccharide composition in astrocyte primary cultures and the cortex of neonatal rats. *Neurochem. Res.* 46, 595–610. doi: 10.1007/s11064-020-03195-9

frontiers | Frontiers in Neuroscience

TYPE Review
PUBLISHED 21 June 2023
DOI 10.3389/fnins.2023.1176695

Check for updates

OPEN ACCESS

EDITED BY
Lisa Akison,
The University of Queensland, Australia

REVIEWED BY
Carlos Fernando Valenzuela,
The University of New Mexico, United States
Carson Kautz-Turnbull,
University of Rochester, United States

*CORRESPONDENCE
James N. Reynolds
✉ jnr@queensu.ca

RECEIVED 28 February 2023
ACCEPTED 09 May 2023
PUBLISHED 21 June 2023

CITATION
Champagne M, McCrossin J, Pei J and Reynolds JN (2023) A tornado in the family: fetal alcohol spectrum disorder and aggression during childhood and adolescence: a scoping review. *Front. Neurosci.* 17:1176695. doi: 10.3389/fnins.2023.1176695

COPYRIGHT
© 2023 Champagne, McCrossin, Pei and Reynolds. This is an open-access article distributed under the terms of the Creative Commons Attribution License (CC BY). The use, distribution or reproduction in other forums is permitted, provided the original author(s) and the copyright owner(s) are credited and that the original publication in this journal is cited, in accordance with accepted academic practice. No use, distribution or reproduction is permitted which does not comply with these terms.

A tornado in the family: fetal alcohol spectrum disorder and aggression during childhood and adolescence: a scoping review

Maude Champagne[1], Jeffrey McCrossin[2], Jacqueline Pei[3] and James N. Reynolds[1]*

[1]Centre for Neuroscience Studies, Queen's University, Kingston, ON, Canada, [2]School of Social Work, McGill University, Montreal, PQ, Canada, [3]Department of Educational Psychology, University of Alberta, Edmonton, AB, Canada

Background: Aggression exhibited by children and youth with Fetal Alcohol Spectrum Disorder (FASD) toward family members is a major cause of stress and anxiety for caregivers, but relatively little attention has been directed toward designing interventions specific to this phenomenon. In light of the serious negative impact of this issue for families, a scoping review was undertaken to summarize the evidence available on psychosocial interventions that may mitigate the frequency and severity of aggression exhibited by children and youth with FASD toward family members.

Methods: This review was designed using PRISMA-SCR and JBI scoping review guidelines. Three databases were searched in August 2021: EMBASE, PsychINFO, and Medline.

Results: A total of 1,061 studies were imported for screening with only five studies meeting full eligibility criteria. None of the interventions were aimed at specifically targeting aggression and instead reported on broader constructs of externalizing behaviors such as hyperactivity. The interventions were limited to school-aged children. Studies reported primarily on child outcomes while only one reported on family related outcomes.

Conclusion: Following from this review of the literature, we argue that aggression is a related but separate construct from other behavioral problems most frequently targeted by parenting interventions. Given the often dire consequence of aggression displayed by children and youth with FASD and the limited number of studies, there is an urgent need for research on how to support families to manage this specific type of behavior in this population.

KEYWORDS

aggression, intervention, fetal alcohol spectrum disorder (FASD), scoping review, child, adolescent

1. Introduction

Fetal Alcohol Spectrum Disorder (FASD) encompasses a range of neurodevelopmental outcomes that may occur as a consequence of prenatal alcohol exposure (PAE). A recent prevalence study estimated that the rate of FASD in the general population of Canada is approximately 4% (Popova et al., 2019). FASD is associated with deficits in multiple behavioral domains, including executive and adaptive functioning skills, emotional regulation, and learning and communication (Cook et al., 2016). Families raising children and youth with FASD report experiencing high levels of stress specifically in relation to dealing with maladaptive behaviors (Watson et al., 2013) and caregivers have reported that childhood aggression, violence and temper tantrums are the most difficult challenges for families to manage (Green et al., 2014). In a meta-analysis, Tsang et al. (2016) found aggression to be among the most reported concerns of parents and teachers of children with FASD, and that children with FASD exhibited higher levels of aggressive behavior compared to children diagnosed with attention-deficit/hyperactivity disorder (ADHD) without PAE (Tsang et al., 2016). Families experiencing aggression from their child with FASD in adoptive homes have reported placement instability—a situation aggravated by the COVID-19 pandemic (Champagne et al., 2023).

A recent report from the National Consortium on Aggression toward Family/Caregivers in Childhood and Adolescence, that included interviews with families raising children and youth with FASD in Canada, highlighted this issue as an urgent matter (AFCCA, 2021). Child-related impacts that were reported included exclusion from school and community settings, damaged relationships, adverse mental health outcomes and diminished self-esteem. The impacts reported for caregivers and siblings encompassed a range of issues from physical injury to psychological trauma, financial strain, and negative mental health. Furthermore, families experiencing aggression reported receiving very little support to assist them and their child which led, in some instances, to involvement with the justice system or the child being removed from the home. These difficult situations were compared to a tornado striking the family, leaving damage and devastation behind; a storm needing to be weathered with support and understanding from those around. That is, caregivers need to be supported in their role to provide a safe environment for the affected child and for the whole family (AFCCA, 2021). If the appropriate support is provided, the evidence suggests that children and youth with FASD can thrive, live safely and enjoy a good quality of life (Pei et al., 2019). The strengths of youth with FASD have been reported in several studies based on a recent review such as their kindness, loyalty, forgiveness, and many creative talents (Flannigan et al., 2021).

Recently, Canadian researchers completed a synthesizing review of aggressive behavior and violence in the context of FASD (Joseph et al., 2022). The authors argue that understanding the mechanisms underlying the behavioral presentation of a child/youth with FASD requires a consideration of the convergence of genetic, environmental and neurophysiological developmental factors. In particular, the authors point to the importance of the interaction between prenatal alcohol exposure and the postnatal environment, especially exposure to trauma, violence and other adverse childhood experiences, as key factors driving the occurrence of aggression in children/youth with FASD (Joseph et al., 2022). To further our understanding of aggression in FASD, this scoping review was developed to identify how aggression is addressed in the context of psychosocial interventions for children and adolescents living with FASD to promote healthy outcomes.

Aggression is defined as the delivery of any form of definite and observable harm-giving behavior toward any target (Ramirez and Andreu, 2006). Although most often aggression in children is thought of as physical in nature (e.g., hitting, kicking, biting, or throwing objects) other types of aggression include psychological (e.g., shaming, threatening) and relational aggression (e.g., malicious gossiping). Aggression can be reactive or proactive in nature (Kempes et al., 2005). Reactive aggression refers to the combative reaction to a perceived threat, while proactive aggression refers to behavior in expectation of achieving some goal, such as domination or control (Kempes et al., 2005). This dichotomous model of reactive-proactive aggression has been critiqued for oversimplifying a complex issue (Bushman and Anderson, 2001). Additional subtypes of aggression have been defined in the psychiatry literature to better understand the phenomenon and plan treatment accordingly (Connor et al., 2019). For example, impulsive aggression (IA) is a reactive and maladaptive subtype of aggression that usually is expressed in individuals with an impaired central nervous system (Waltes et al., 2016). IA is a common form of aggression reported in relation to several neurodevelopmental disorders such as autism spectrum disorder (ASD) and ADHD, as well as traumatic brain injury and mental health disorders (Connor et al., 2019). Given the applicability in related neurodevelopmental disorders, IA may be of interest in the context of FASD as well. IA may be identified by common characteristics that describe the unplanned nature of the aggression, challenges in regaining composure, and demonstration of remorse: "Characteristics include sudden, intense aggression inappropriately expressed in relationship to environmental precipitants. The individual may have frequent aggressive episodes, difficulty terminating aggression, and remorse when the episode ends" (Connor et al., 2019).

Aggression during childhood and adolescence occurring in the general population has several proposed etiologies that have been described in the scientific literature based on interactional models. The model describing IA suggests that central nervous system dysfunction interacts with other factors such as social adversity and genetics (Connor et al., 2019). Little is currently known about possible etiological factors of aggression specifically in the FASD population but research on other neurodevelopmental disorders, such as autism spectrum disorder (ASD), found that risk factors included greater impairment in cognition, language, and adaptive behavior (Politte et al., 2019). Nevertheless, it has yet to be determined which factors could play a role in the issue of aggression for the FASD population. Understanding the etiology of aggression in FASD is important to plan the proper course of intervention to improve the quality of life of these children and their caregivers.

Aggression is not well understood in children and youth with FASD, and there are no published reviews of psychosocial interventions addressing aggression in this population. Given the emotional and physical consequences of aggression on the quality of life of children and their caregivers, it is imperative to address

this issue. For these reasons, a scoping review methodology was selected to explore the interventions for the issue of aggression in children and youth with FASD, map the current evidence, better understand the key concepts, and identify knowledge gaps related to this topic.

The initial aim of this scoping review was to assess the evidence available on psychosocial interventions addressing the impact of aggression by children and youth with FASD toward family members. However, the initial search of the literature did not yield data specific to the family context. Therefore, we adapted the review to instead summarize more broadly the evidence available on psychosocial interventions for aggression displayed by children and youth with FASD or Prenatal Alcohol Exposure (PAE) as well as the gaps in knowledge. We formulated the following research questions: (1) What are the terms most used in the intervention literature to describe aggression displayed by children and youth with FASD or PAE? (2) What are the current psychosocial interventions reported in the literature that are used to respond to this issue? (3) What are the current gaps and limitations in the literature regarding psychosocial intervention for aggression displayed by this population? This study is a preliminary step in developing a richer conceptualization for aggression in the context of children and youth living with FASD or PAE.

2. Methods

2.1. Design

This scoping review was designed using the PRISMA-SCR (Tricco et al., 2018) and JBI scoping review guidelines (Peters et al., 2015).

2.2. Search strategy

Databases were determined in collaboration with a professional librarian at Queen's University and a search protocol was designed for each database. Key search terms were determined by three researchers in the field of FASD (James Reynolds, Jacqueline Pei, and Maude Champagne) and informed through an iterative process in the early stages of preparing for this review. Terms related to FASD, PAE, and aggression, violence or disruptive behaviors were used to identify articles that may contain data related to the research questions. The search process took place in August 2021 and included Embase, Medline and PsychINFO databases.

2.3. Article screening

The PRISMA- Scoping Review Extension was used to guide the screening process (Tricco et al., 2018). Search results were exported to the systematic review software Covidence[1] and duplicates were removed. In the first stage of screening, the first author screened titles and abstracts to remove any articles unrelated to psychosocial issues in FASD. During the second stage of screening, the first and second authors identified the inclusion and exclusion criteria through an iterative process of team discussion as authors became more familiar with the available literature. To be included in our review, articles needed to report on the evaluation of a psychosocial intervention targeting aggression or other externalizing behavior problems in children or youth with FASD or PAE under the age of 18. We placed no restrictions on study design, and as such, we included qualitative, quantitative, and mixed-methods studies. Review papers, book chapters, and gray literature were excluded. Only articles published in English or French were included. No restrictions were placed on the date of publication. The first and second authors conducted a third screening phase, reviewing the full-text of articles to assess eligibility based on the inclusion and exclusion criteria. Consensus was reached on all disagreements through team discussion. A PRISMA flow diagram is provided (see **Figure 1**).

2.4. Data extraction and analysis

A data extraction tool was created by the first author based on the research questions and the JBI Scoping Review guidelines (Peters et al., 2015). The tool included study characteristics, measurement tools, parental involvement in the intervention, and key findings. The tool was tested and modified through an iterative process by the first and second authors using three articles. Data from all five articles included in the review were extracted using the final extraction tool. Data extracted from two articles that used the same dataset were merged (Petrenko et al., 2017, 2019).

3. Results

The initial search resulted in 1,061 studies from which 280 duplicates were removed (**Figure 1**). Subsequently, 627 studies were removed from the remaining 781 studies during the initial screening process by the first author. The full texts of the remaining 154 articles were screened for eligibility. Approximately one third of the studies screened at this stage were not related to aggression ($n = 58$), and several were not related to psychosocial interventions but focused instead on etiology (e.g., brain imaging or medication), adults with FASD, or were review articles. A total of five studies met full eligibility criteria and were included in the data extraction phase of the review.

3.1. Intervention characteristics

Four interventions were identified in this review for children and youth with FASD (**Table 1**). The *GoFAR*, *Families on Track*, and *Alert Program* interventions all aimed to improve child behaviors by targeting either executive functioning or emotional regulation (Coles et al., 2015; Nash et al., 2015; Petrenko et al., 2017). The *Math Interactive Learning Experience* (MILE) intervention program aims to improve math performance and behaviors (Coles et al., 2009). None of the interventions described in the

1 https://www.covidence.org/

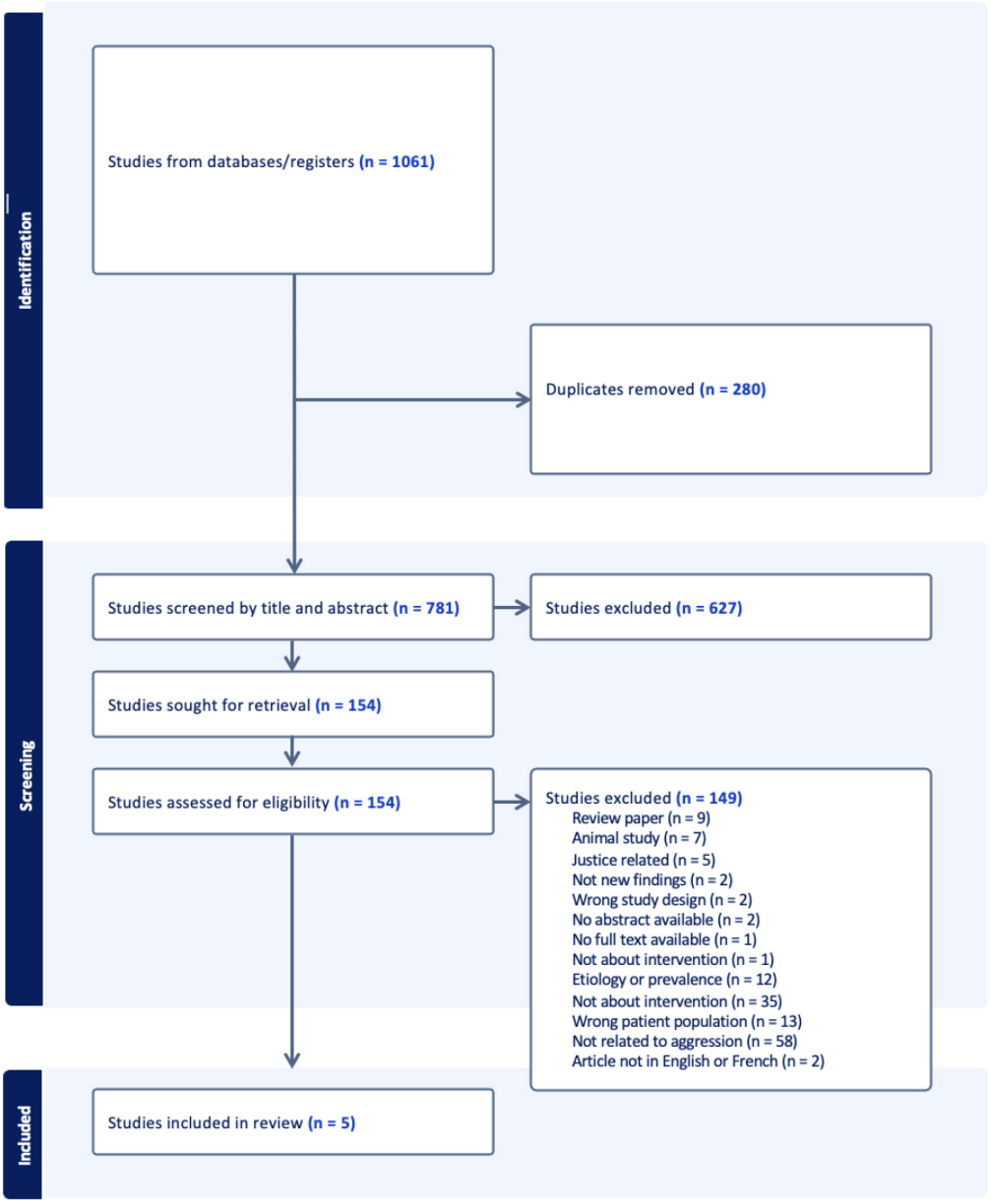


FIGURE 1
PRISMA flow diagram.

articles were designed specifically to modify patterns of aggression. Similarly, none of the studies measured aggression as a construct. Instead, each study reported on other behavior-related constructs, such as disruptive behaviors, externalized behaviors, emotion regulation, temper tantrums, frustration tolerance, impulsivity, and destructiveness.

The MILE program consists of 6 weeks of math interventions and two parent workshops (Coles et al., 2009). Families were also provided with behavior problem case management, social work, psychiatric consultations, and strategies to foster child self-regulation skills.

The *GoFAR* videogame teaches children metacognitive strategies to focus, plan, act and reflect (Coles et al., 2015). This program has several caregiver-focused elements such as psychoeducation training and dyadic sessions. *GoFAR* consists of 15 sessions; 5 sessions for the children, 5 individual sessions with the parent and 5 dyadic sessions.

The *Alert Program* is child-focused and uses a car analogy to teach the child to use strategies for modulation of sensory and cognitive processing (Nash et al., 2015). The impact of the program is tested on the child's executive functioning skills, behaviors and social skills. The program consisted of 12 sessions with the child and 1 parent workshop.

Families on Track has two published manuscripts (pilot and 6 months follow-up) assessing the impact of the intervention on the emotional and social development of the child (Petrenko et al., 2017, 2019). The 30-week program described by Petrenko et al. (2017) centered on preventing secondary conditions and

TABLE 1 Intervention characteristics.

References	Intervention description	Target of intervention parent involvement in length of intervention	Parent involvement in intervention	Length of intervention
Coles et al., 2009	MILE math intervention, caregiver education, if needed case management, social work or psychiatric services were provided.	Evaluating the persistence of the effect of an intervention on math performance and behaviors.	Parents were given workshops and weekly assignments	6 weeks of math intervention and two parent workshops
Coles et al., 2015	The first element of the intervention included a psychoeducational workshop for parents on the neurobehavioral implications of prenatal alcohol exposure. The second element lasted for 5 weeks and include the GoFAR videogame for children where they learn a metacognitive strategy to focus and plan, act, and reflect; and a simultaneous parent training program on supporting children to develop behavioral regulation skills. The third element of the intervention involved 5 weekly behavior analog therapy sessions where parent-child dyads learn to implement the metacognitive strategy in the context of problem behavior observed at home.	To test the impact of a metacognitive, video game based intervention, parent psychoeducation and training on emotion regulation and disruptive behaviors.	Parents were involved in dyadic therapy sessions and individual psychoeducational workshops	15 sessions: 5 GoFAR for the children 5 individual sessions with the parent, 5 dyadic session
Nash et al., 2015	Alert Program for Self-Regulation targets improvement in self-regulation through sensory and cognitive processing. The therapy involves three successive stages organized around a car analogy of car engine speeds representing recognition and modulation of sensory and cognitive processing.	To evaluate the impact of the Alert intervention on aspects of executive functioning in children with FASD such as behaviors and social skills.	one parent session	12 sessions of therapy with the child
Petrenko et al., 2017	Families on Track: This intervention involved a neuropsychological and diagnostic evaluation and two treatment components. The caregiver treatment involved 1.5 h in-home sessions with a facilitator reviewing skills taught in the child group sessions to encourage generalization of skills to the home environment. The child treatment involved a small group (6–10 children) of which a portion (3–4) had diagnoses of FASD while the remainder were typically developing children in the target age range. The child group sessions targeted social and emotional skill development.	To pilot an intervention program targeting social and emotional development in children with both a child focused intervention and concurrent parent-focused intervention. The program targets key risk factors and protective factor.	Parents received training to support generalization of child skills in the home environment	30 weeks long

TABLE 2 Study characteristics.

	References	Country	Context	Study design	Sample size
1	Coles et al., 2009	United States	Pediatric neurodevelopmental exposure clinic	RCT[1]	54
2	Coles et al., 2015	United States	Pediatric neurodevelopmental exposure clinic	3-arm RCT	30
3	Nash et al., 2015	Canada	Pediatric hospital or accredited FASD diagnostic clinic	RCT	25
4	Petrenko et al., 2017	United States	University clinic	RCT	30

[1]Randomized control trial.

improving family functioning, rather than improvement of child behavior problems. FASD diagnostic services were offered. Children received group therapy and caregivers received training to help the child generalize the skills at home.

3.2. Study characteristics

Out of the five articles eligible for this scoping review, four were from the USA and one was from Canada (Table 2). Studies

TABLE 3 Sample characteristics.

	Coles et al. (2009)	Coles et al. (2015)	Nash et al. (2015)	Petrenko et al. (2017)
Age of child	Range: 5–10 years old Mean (SD): 6.5 (2.0)	Range: 5–10 years old Mean (SD): 7.5 (1.4)	Range: 8–12 years old Mean (SD): 10.3 (1.7)	Range: 4–8 years old Mean (SD): 6.52 (1.31)
Relationship to caregivers	71.4% adopted by non-relatives	100% legal guardianship or adoptive caregiver	Adopted: 75% Foster: 17% Kinship: 8%	Adopted or foster: 81.3% Kinship: 18.8%
Age of caregiver	Mean (SD): 43.9 (7.2)	Not reported	Not reported	Mean (SD):45.77 (8.97)
Race and culture	64% white (intervention group)	40% Caucasian 40% Mixed -raced 10% Black	Not reported	87.5% white
Gross household income or socioeconomic status	Range of household income: $35,000-$49,000	Not reported	Socio-economic status: Low:42% Medium: 42% High: 16%	Family income: mean (SD) $90,312$ ($49,378$)

TABLE 4 Outcomes measures and findings.

References	Descriptive words for aggression	Child measures of behavior	Key findings for constructs related to aggression	Parent outcome measures
Coles et al., 2009	Externalized behavior problems	CBCL[2] Teacher report form	Aggressive behaviors continued to decline over time and showed a significant difference between Post-tests 1 and 2. For the teacher which had a smaller sample, the summary showed significant differences in externalized behavior	Not reported
Coles et al., 2015	Disruptive behavior, temper tantrums, frustration tolerance, impulsivity destructiveness, aggression,	Disruptive behavior record form	The intervention groups appeared to have improved scores on the disruptive behavior aggregate score with a medium to large effect. However, the results are limited by the small sample size.	Not reported
Nash et al., 2015	Externalizing behavior problems as measured by the CBCL externalizing behavior problems scale and BRIEF behavioral regulation scale.	CBCL BRIEF[3]	At 12 weeks follow-up parents were reporting significant improvement in inhibitory control and social cognition. Reduction in externalized behaviors, and improvements in behavioral and emotional regulation was reported. Behavioral improvements were maintained at 6 months follow-up.	Not reported
Petrenko et al., 2017	Disruptive behavior	Eyberg Child Behavior Inventory Emotion regulation checklist Impairment rating scale	Medium to large size improvement in emotion regulation, significant group difference. A moderate decrease in behavior intensity for the treatment group was noted from pre to post-test, which was maintained at follow-up. No difference between treatment and comparison groups were noted when considering change from pre-test to follow-up. No specific mention of aggressive behavior.	Measures of Caregiver Functioning Knowledge and Advocacy Parenting Practices Interviews Family Needs Met Parenting Sense of Competence Parenting Stress Index Perceived Social Support Scale Self-care Parent Evaluation Inventory Intervention Satisfaction
Petrenko et al., 2019	Same as Petrenko et al. (2017)	Same as Petrenko et al. (2017)	Follow-up data was available for 24 out of the 30 families and showed continued gained for the intervention group in parent self-efficacy and parent knowledge of FASD compared to the comparison group. Decrease in disruptive behaviors in both groups although improvement in child self-esteem and emotional regulation were diminished.	Measures of Caregiver Functioning Knowledge and Advocacy Family Needs Met Parenting Stress Index
Petrenko et al., 2019	*idem*	*idem*	Follow-up data was available for 24 out of the 30 families and showed continued gained for the intervention group in parent self-efficacy and parent knowledge of FASD compared to the comparison group. Decrease in disruptive behaviors in both groups although improvement in child self-esteem and emotional regulation were diminished.	Measures of Caregiver Functioning Knowledge and Advocacy Family Needs Met Parenting Stress Index

[2]Child behavior checklist (CBCL). [3]Behavior rating inventory of executive function.

were published between 2009 and 2019 with four published in the past 6 years. All were randomized control trials conducted in universities or pediatric clinics using quantitative methodologies. All studies had relatively small sample sizes between 25 and 54 and two of the studies were pilots.

3.3. Sample characteristics

Participating children were all diagnosed with FASD (Canadian guidelines) (Cook et al., 2016), FAS or pFAS (United States guidelines) (Astley, 2013) (**Table 3**). The age range of the children or youth was between 5 and 12 years, and studies included predominantly children living with foster, adoptive or kinship carers. Three studies included child race, two of which reported that the majority of participants were of Caucasian descent.

3.4. Outcomes and tools

Child behaviors were assessed using the Child Behavior Checklist (CBCL) (n = 2), Eyberg Child Behavior Inventory, Emotion Regulation Checklist, Impairment Rating Scale, Disruptive Behavior Record Form, or Behavior Rating Inventory of Executive Function (BRIEF) (**Table 4**). Only one study included parental outcomes measures (Petrenko et al., 2017).

3.5. Key findings for aggression-related construct

The MILE intervention study reported a decline in aggressive behaviors over time that achieved statistical significance between Post-tests 1 and 2 (**Table 4**). Teacher reports also showed significant improvements in externalized behaviors over time (Coles et al., 2009). In the *GoFAR* intervention, the intervention group exhibited improved scores on the disruptive behavior aggregate score with a medium to large effect size (Coles et al., 2015). In the *Alert Program* for self-regulation, parents reported significant improvements in inhibitory control and social cognition at the 12-week followup, accompanied by a reduction in externalized behaviors and improvements in behavioral and emotional regulation. At the 6-month follow-up assessment these behavioral improvements were maintained (Nash et al., 2015). The *Families on Track Program* showed an improvement in emotion regulation with medium to large effect size and a statistically significant group difference. A moderate decrease in behavior intensity for the treatment group was noted from pre- to post-test, which was maintained at follow-up. Follow-up data was available for 24 out of the 30 families and showed continued gains for the intervention group in parent self-efficacy and parent knowledge of FASD compared to the control group. There was a decrease in disruptive behaviors in the control and intervention groups although improvement in child self-esteem and emotional regulation were diminished (Petrenko et al., 2017, 2019).

4. Discussion

The limited number of articles eligible for inclusion in this review demonstrates that psychosocial interventions specifically targeting aggression in children and youth with FASD have not been on the research agenda serving this community. Very few psychosocial interventions exist for behavioral challenges in this population, let alone specific to aggression. This despite the fact that families identify aggression and externalizing behaviors as a major concern (Green et al., 2014; Tsang et al., 2016; Champagne et al., 2023). It is difficult to know the prevalence and the extent of the problem with any certainty as this is an issue that often goes unreported due to the stigma associated with aggression in children. This is a field that has not yet been adequately explored. However, from the evidence of positive changes in behavior, cognition, and self-regulation reported in the interventions of this review, it is reasonable to suggest that providing psychosocial interventions targeting aggression in children and youth with FASD is a worthwhile investment that will benefit these individuals and their families.

4.1. Family outcomes vs. child outcomes

Our review reveals the relative paucity of evidence for family outcomes in intervention studies targeting aggression and related constructs (e.g., externalized behaviors, disruptive behaviors) in children and youth with FASD. This is a significant knowledge gap given the impact of aggression toward caregivers during childhood and adolescence (AFCCA, 2021). While 3 out of the 4 studies examined in this review included caregivers in their intervention, only one study provided data on caregiver and family outcomes (Petrenko et al., 2017). More recent developments in caregiver training for children with neurodevelopmental disabilities have brought an increased focus on caregiver wellbeing and on the family as a whole (Sikora et al., 2013; Factor et al., 2019). These advances in research priorities acknowledge the importance of caregiver wellbeing on their efficacy in providing care, and the value of the family as an important context in which the child develops (Dykens, 2015). Family cohesion was also a factor identified to promote healthy outcomes in individuals with FASD (Pei et al., 2019).

Including family input and outcomes in intervention studies can provide rich data on family resilience processes that involve risk and protective factors at the level of the child, caregiver, and family (Gunty, 2020). Such data can help improve the design of interventions by identifying pathways through which families thrive in the face of adversity without being limited to child-level factors. Given that impulsive aggression likely stems from impaired brain function compounded by other environmental risk factors, management of this issue should be personalized and multifactorial (Connor et al., 2019). Understanding contributing factors to aggression and its management within the family system could help tailor the treatment by leveraging a broader set of resources beyond interventions that focus solely on child input. Moreover, outcomes should also be measured at the family level rather than solely on the child's outcome given the importance

of caregiver wellbeing and family cohesiveness as mediators of positive outcomes.

There are multiple approaches to assessing family level outcomes available to researchers to measure the impact of interventions on families, including impact of the child's disability on the family (Trute and Hiebert-Murphy, 2002), family functioning (Epstein et al., 1983; Olson, 2011) quality of life (Hoffman et al., 2006), self-efficacy (Hohlfeld et al., 2018), and resilience (Duncan et al., 2021). Several reviews are available that describe additional family level outcomes and measures for families of children with neurodevelopmental disabilities (Alderfer et al., 2008; Bogossian et al., 2012; Ketelaar et al., 2017) that are highly relevant to the context of children and youth with FASD and aggressive behaviors.

4.2. Increasing accessibility and diversity

The studies included in this review were limited in terms of accessibility (i.e., context of delivery) of the interventions and lack of diversity among participants. All studies included in the current review were conducted in-person by clinicians in universities or pediatric centers. Future research should prioritize identifying effective interventions that can be more widely accessible, including consideration of issues such as flexible scheduling according to family availability, location of intervention delivery (e.g., in-person or online), as well as minimizing costs to the family. For example, both GoFAR (do2learn.org) and a subsequent version of Families on Track (Families Moving Forward) (Petrenko et al., 2017, 2019) have been modified for remote/virtual delivery. However, the potential impact of these online interventions for mitigating aggressive behaviors in children and youth with FASD has not been established. The COVID-19 pandemic caused many services to be moved from in-person to online delivery, which created an opportunity for new innovations in intervention delivery methods. Even prior to the pandemic, online parent training interventions were available for children with disruptive behavior (Olthuis et al., 2018), ADHD (DuPaul et al., 2018), and conduct problems (Sanders et al., 2012). Such interventions have many advantages, including offering increased flexibility for caregivers to attend groups at a distance or complete modules on their own time at a fraction of the cost (Olthuis et al., 2018). These programs are, however, exclusively caregiver focused.

Accessibility should also be considered in the context of diversity. The demographic data available for this review were fairly limited but showed a lack of diversity among participants. Most studies included adoptive or foster families, primarily Caucasian and school-age children. Intervention planning should also consider ethnic and racial minorities, Indigenous families, and gender diversity. Biological families are also less inclined to access services due to the stigma attached to the etiology of FASD (Bell et al., 2016). Anti-oppression frameworks could be explored when planning research interventions to ensure accessibility to these groups. Corneau and Stergiopoulos (2012) describe strategies to promote anti-oppression practices in social services such as using self-reflexivity, empowerment and alliance building (Corneau and Stergiopoulos, 2012). Further psychosocial intervention research in FASD for a diverse population is needed.

4.3. Future directions

The aim of this scoping review was to map the evidence for psychosocial interventions related to aggression and is a preliminary step in developing a richer conceptualization for aggression in the context of children and youth living with FASD. Many questions remain regarding the prevalence of the issue, the impacts on the children and their caregivers as well as the mechanism of aggression in this population. Meanwhile, interventions specific to the issue of child-to-parent aggression have been developed for other clinical populations (Toole-Anstey et al., 2021). Research is needed to test the efficacy of some of these programs in the FASD population.

Caregivers raising children and youth with FASD who display aggression are facing a highly stressful situation that frequently engenders feelings of isolation and helplessness (AFCCA, 2021; Champagne et al., 2023). The National Consortium on Aggression toward Family/Caregivers in Childhood and Adolescence (AFCCA) made several systemic recommendations (AFCCA, 2021). Among them was the importance of raising awareness about AFCCA in the general population and providing education to professionals and first responders who are often managing these crises when they arise. Educating medical and social services professionals on aggression in this population is also crucial to creating safety for families when accessing support. Furthermore, building a network of peer support for family members and the youth themselves was identified by participants. Finally, creating a system of support for all family members in facing and recovering from the "tornado" that may have hit their family may avoid the entrenchment of these children and youth in the child welfare and youth justice systems. Recommendations were also made to develop multisectoral and personalized interventions that are strength-based and non-stigmatizing as well as delivered in a timely manner. Consulting with caregivers and individuals who have lived-with experience is essential for guidance on ways forward.

4.4. Strengths and limitations

A strength of the current review is the collaboration with two national experts in the field of FASD, one clinician-scientist and a professional librarian who advised the search criteria. A limitation of this review is the lack of the term "aggression" in our search. However, most researchers use other terms to describe the problematic behaviors they are aiming at targeting with their intervention. Scoping reviews are also very broad, and it is possible that the search strategy employed may have missed interventions that could provide additional insight into the conceptualization of aggression in FASD. Interventions aimed at other problems commonly associated with FASD such as sleep disturbance, sensory integration disorder, and developmental trauma may also reveal potentially interesting clues to the problem

of aggression. For instance, sleep disturbance is associated with increased externalizing behavior problems, thus sleep intervention could possibly be part of the solution for some individuals.

5. Conclusion

While caregivers have described aggression as an area of great concern to help them care for their children and youth with FASD, no intervention has been designed to specifically target outcomes related to this construct. The very limited number of interventions identified in this review were all aimed at changing the child's behavior, improving self-regulation, and other cognitive skills. More research is needed on the etiology of aggression in this population to advance the development of evidence-based interventions.

Author contributions

MC, JM, and JP developed the search strategy. MC conducted the search and screening of articles retrieved, conducted the analysis, and drafted the first version of the manuscript. All authors contributed to the conceptualization of this scoping review and reviewed drafts of the manuscript.

Conflict of interest

The authors declare that the research was conducted in the absence of any commercial or financial relationships that could be construed as a potential conflict of interest.

Publisher's note

All claims expressed in this article are solely those of the authors and do not necessarily represent those of their affiliated organizations, or those of the publisher, the editors and the reviewers. Any product that may be evaluated in this article, or claim that may be made by its manufacturer, is not guaranteed or endorsed by the publisher.

References

AFCCA (2021). *National consortium on aggression toward family/caregivers in childhood & adolescence (AFCCA)*. AFCCA: Washington, MD.

Alderfer, M. A., Fiese, B. H., Gold, J. I., Cutuli, J. J., Holmbeck, G. N., Goldbeck, L., et al. (2008). Evidence-based assessment in pediatric psychology: family measures. *J. Pediatr. Psychol.* 33, 1046–1061. doi: 10.1093/jpepsy/jsm083

Astley, S. (2013). Validation of the fetal alcohol spectrum disorder (FASD) 4-digit diagnostic code. *J. Population Ther. Clin. Pharmacol.* 20, e416–e467.

Bell, E., Andrew, G., Di Pietro, N., Chudley, A. E., Reynolds, J., and Racine, E. (2016). It's a shame! Stigma against fetal alcohol spectrum disorder: examining the ethical implications for public health practices and policies. *Public Health Ethics* 9, 65–77. doi: 10.1093/phe/phv012

Bogossian, A., Lach, L., and Saini, M. (2012). "Environmental factors: support and relationships," in *Measures for children with developmental disability: an ICF-CY approach*, ed. A. Majnemer (London: Mac Keith Press), E310–E399.

Bushman, B. J., and Anderson, C. A. (2001). Is it time to pull the plug on hostile versus instrumental aggression dichotomy? *Psychol. Rev.* 108, 273–279. doi: 10.1037/0033-295x.108.1.273

Champagne, M., Willis, R., and Reynolds, J. (2023). COVID-19 pandemic challenges for families of children and youth impacted by fetal alcohol spectrum disorder. *J. Dev. Disabil.* 28.

Coles, C. D., Kable, J. A., and Taddeo, E. (2009). Math performance and behavior problems in children affected by prenatal alcohol exposure: intervention and follow-up. *J. Dev. Behav. Pediatr.* 30, 7–15. doi: 10.1097/DBP.0b013e3181966780

Coles, C. D., Kable, J. A., Taddeo, E., and Strickland, D. C. (2015). A metacognitive strategy for reducing disruptive behavior in children with fetal alcohol spectrum disorders: GoFAR pilot. *Alcohol. Clin. Exp. Res.* 39, 2224–2233. doi: 10.1111/acer.12885

Connor, D. F., Newborn, J. H., Saylor, B. H., Lawrence Scahill, A. S., Robb, A., Jensen, P., et al. (2019). Maladaptive aggression: with a focus on impulsive aggression in children and adolescents. *J. Child Adolesc. Psychopharmacol.* 29, 576–591.

Cook, J. L., Green, C. R., Lilley, C. M., Anderson, S. M., Baldwin, M. E., Chudley, A. E., et al. (2016). Fetal alcohol spectrum disorder: a guideline for diagnosis across the lifespan. *Cana. Med. Assoc. J.* 188, 191–197. doi: 10.1503/cmaj.141593

Corneau, S., and Stergiopoulos, V. (2012). More than being against it: anti-racism and anti-oppression in mental health services. *Trans. Psychiatry* 49, 261–282. doi: 10.1177/1363461512441594

Duncan, J. M., Garrison, M. E., and Killian, T. S. (2021). Measuring family resilience: evaluating the walsh family resilience questionnaire. *Fam. J.* 29, 80–85. doi: 10.1177/1066480720956641

DuPaul, G. J., Kern, L., Belk, G., Custer, B., Daffner, M., Hatfield, A., et al. (2018). Face-to-face versus online behavioral parent training for young children at risk for ADHD: treatment engagement and outcomes. *J. Clinical Child Adoles. Psychol.* 47(Suppl. 1), S369–S383. doi: 10.1080/15374416.2017.1342544

Dykens, E. M. (2015). Family adjustment and interventions in neurodevelopmental disorders. *Curr. Opin. Psychiatry* 28, 121–126. doi: 10.1097/YCO.0000000000000129

Epstein, N. B., Baldwin, L. M., and Bishop, D. S. (1983). The mcmaster family assessment device. *J. Mar. Fam. Ther.* 9, 171–180. doi: 10.1111/j.1752-0606.1983.tb01497.x

Factor, R. S., Ollendick, T. H., Cooper, L. D., Dunsmore, J. C., Rea, H. M., and Scarpa, A. (2019). All in the family: a systematic review of the effect of caregiver-administered Autism Spectrum Disorder interventions on family functioning and relationships. *Clin. Child Fam. Psychol. Rev.* 22, 433–457. doi: 10.1007/s10567-019-00297-x

Flannigan, K., Wrath, A., Ritter, C., McLachlan, K., Harding, K. D., Campbell, A., et al. (2021). Balancing the story of fetal alcohol spectrum disorder: a narrative review of the literature on strengths. *Alcohol* 45, 2448–2464. doi: 10.1111/acer.14733

Green, C. R., Hewitt, A., Reynolds, J. N., Roane, J., Muhajarine, N., Mushquash, C., et al. (2014). Frequent behavioural challenges in children with fetal alcohol spectrum disorder: A needs-based assessment reported by caregivers and clinicians. *J. Popul. Ther. Clin. Pharmacol.* 21, e405–e420.

Gunty, A. L. (2020). Rethinking resilience in families of children with autism spectrum disorders. *Couple Fam. Psychol.* 10, 87–102. doi: 10.1037/cfp0000155

Hoffman, L., Marquis, J., Poston, D., Summers, J. A., and Turnbull, A. (2006). Assessing family outcomes: psychometric evaluation of the beach center family quality of life scale. *J. Marr. Fam.* 68, 1069–1083. doi: 10.1111/j.1741-3737.2006.00314.x

Hohlfeld, A., Harty, M., and Engel, M. (2018). Parents of children with disabilities: a systematic review of parenting intervention and self-efficacy. *Afri. J. Disabil.* 7:437.

Joseph, J. J., Mela, M., and Pei, J. (2022). Aggressive behaviour and violence in children and adolescents with FASD: a synthesizing review. *Clin. Psychol. Rev.* 94:102155. doi: 10.1016/j.cpr.2022.102155

Kempes, M., Matthys, W., de Vries, H., and van Engeland, H. (2005). Reactive and proactive aggression in children A review of theory, findings and the relevance for child and adolescent psychiatry. *Eur. Child Adoles. Psychiatry* 14, 11–19. doi: 10.1007/s00787-005-0432-4

Ketelaar, M., Bogossian, A., Saini, M., Visser-Meily, A., and Lach, L. (2017). Assessment of the family environment in pediatric neurodisability: a state-of-the-art review. *Dev. Med. Child Neurol.* 59, 259–269. doi: 10.1111/dmcn.13287

Nash, K., Stevens, S., Greenbaum, R., Weiner, J., Koren, G., and Rovet, J. (2015). Improving executive functioning in children with fetal alcohol spectrum disorders. *Child Neuropsychol.* 21, 191–209. doi: 10.1080/09297049.2014.889110

Olson, D. H. (2011). FACES IV and the circumplex model: validation study. *J. Mar. Fam. Ther.* 37, 64–80. doi: 10.1111/j.1752-0606.2009.00175.x

Olthuis, J. V., McGrath, P. J., Cunningham, C. E., Boyle, M. H., Lingley-Pottie, P., Reid, G. J., et al. (2018). Distance-delivered parent training for childhood disruptive behavior (Strongest Families^{TM}): a randomized controlled trial and economic analysis. *J. Abnor. Child Psychol.* 46, 1613–1629. doi: 10.1007/s10802-018-0413-y

Pei, J., Kapasi, A., Kennedy, A. E., and Joly, V. (2019). *Towards healthy outcomes for individuals with fetal alcohol spectrum disorder. Canada FASD research network in collaboration with the University of Alberta*. Edmonton, AB: University of Alberta.

Peters, M. D. J., Godfrey, C. M., Khalil, H., McInerney, P., Parker, D., and Soares, C. B. (2015). Guidance for conducting systematic scoping reviews. *JBI Evidence Implement.* 13, 141–146.

Petrenko, C. L. M., Demeusy, E. M., and Alto, M. E. (2019). Six-month follow-up of the families on track intervention pilot trial for children with fetal alcohol spectrum disorders and their families. *Alcohol. Clin. Exp. Res.* 43, 2242–2254. doi: 10.1111/acer.14180

Petrenko, C. L. M., Pandolfino, M. E., and Robinson, L. K. (2017). Findings from the families on track intervention pilot trial for children with fetal alcohol spectrum disorders and their families. *Alcohol. Clin. Exp. Res.* 41, 1340–1351. doi: 10.1111/acer.13408

Politte, L. C., Fitzpatrick, S. E., and Erickson, C. (2019). *Aggression in autism spectrum Disorder and other Neurodevelopmental Disorders. In Aggression: Clinical Features and Treatment across the lifespan*. Washington, DC: American Psychiatry Association Publishing.

Popova, S., Lange, S., Poznyak, V., Chudley, A. E., Shield, K. D., Reynolds, J. N., et al. (2019). Population-based prevalence of fetal alcohol spectrum disorder in Canada. *BMC Public Health* 19:845. doi: 10.1186/s12889-019-7213-3

Ramirez, J., and Andreu, J. (2006). Aggression, and some related psychological constructs (anger, hostility, and impulsivity) some comments from a research project. *Neurosci. Biobehav. Rev.* 30, 276–291. doi: 10.1016/j.neubiorev.2005.04.015

Sanders, M. R., Baker, S., and Turner, K. M. T. (2012). A randomized controlled trial evaluating the efficacy of Triple P Online with parents of children with early-onset conduct problems. *Behav. Res. Ther.* 50, 675–684. doi: 10.1016/j.brat.2012.07.004

Sikora, D., Moran, E., Orlich, F., Hall, T. A., Kovacs, E. A., Delahaye, J., et al. (2013). The relationship between family functioning and behavior problems in children with autism spectrum disorders. *Res. Autism Spect. Dis.* 7, 307–315. doi: 10.1016/j.rasd.2012.09.006

Toole-Anstey, C., Keevers, L., and Townsend, M. (2021). A systematic review of child to parent violence interventions. *Trauma Violence Abuse* 24, 1157–1171. doi: 10.1177/15248380211053618

Tricco, A. C., Lillie, E., Zarin, W., O'Brien, K. K., Colquhoun, H., Levac, D., et al. (2018). PRISMA extension for scoping reviews (PRISMA-SCR): checklist and explanation. *Ann. Internal Med.* 169, 467–473. doi: 10.7326/M18-0850

Trute, B., and Hiebert-Murphy, D. (2002). Family adjustment to childhood developmental disability: a measure of parent appraisal of family impacts. *J. Pediatric Psychol.* 27, 271–280. doi: 10.1093/jpepsy/27.3.271

Tsang, T. W., Lucas, B. R., Olson, H. C., Pinto, R. Z., and Elliott, E. J. (2016). Prenatal alcohol exposure, FASD, and child behavior: a meta-analysis. *Pediatrics* 137:e20152542. doi: 10.1542/peds.2015-2542

Waltes, R., Chiocchetti, A., and Freitag, C. (2016). The neurobiological basis of human aggression: a review on genetic and epigenetic mechanisms. *Am. J. Med. Genet.* 171, 650–675. doi: 10.1002/ajmg.b.32388

Watson, S. L., Coons, K. D., and Hayes, S. A. (2013). Autism spectrum disorder and fetal alcohol spectrum disorder. Part I: a comparison of parenting stress. *J. Intell. Dev. Disabil.* 38, 95–104. doi: 10.3109/13668250.2013.788136

frontiers | Frontiers in Neuroscience

TYPE Original Research
PUBLISHED 23 June 2023
DOI 10.3389/fnins.2023.1203557

Check for updates

OPEN ACCESS

EDITED BY
Claire-Marie Vacher,
Columbia University, United States

REVIEWED BY
Helene Lacaille,
Columbia University, United States
Marvin Rafael Diaz,
Binghamton University, United States

*CORRESPONDENCE
Erin D. Milligan
✉ EMilligan@salud.unm.edu

RECEIVED 10 April 2023
ACCEPTED 24 May 2023
PUBLISHED 23 June 2023

CITATION
Ruffaner-Hanson CD, Fernandez-Oropeza AK, Sun MS, Caldwell KK, Allan AM, Savage DD, Valenzuela CF, Noor S and Milligan ED (2023) Prenatal alcohol exposure alters mRNA expression for stress peptides, glucocorticoid receptor function and immune factors in acutely stressed neonatal brain. *Front. Neurosci.* 17:1203557. doi: 10.3389/fnins.2023.1203557

COPYRIGHT
© 2023 Ruffaner-Hanson, Fernandez-Oropeza, Sun, Caldwell, Allan, Savage, Valenzuela, Noor and Milligan. This is an open-access article distributed under the terms of the Creative Commons Attribution License (CC BY). The use, distribution or reproduction in other forums is permitted, provided the original author(s) and the copyright owner(s) are credited and that the original publication in this journal is cited, in accordance with accepted academic practice. No use, distribution or reproduction is permitted which does not comply with these terms.

Prenatal alcohol exposure alters mRNA expression for stress peptides, glucocorticoid receptor function and immune factors in acutely stressed neonatal brain

Chaselyn D. Ruffaner-Hanson, Annette K. Fernandez-Oropeza, Melody S. Sun, Kevin K. Caldwell, Andrea M. Allan, Daniel D. Savage, C. Fernando Valenzuela, Shahani Noor and Erin D. Milligan*

Department of Neurosciences, University of New Mexico School of Medicine, Albuquerque, New Mexico

Background: The amygdala, hippocampus and hypothalamus are critical stress regulatory areas that undergo functional maturation for stress responding initially established during gestational and early postnatal brain development. Fetal alcohol spectrum disorder (FASD), a consequence of prenatal alcohol exposure (PAE), results in cognitive, mood and behavioral disorders. Prenatal alcohol exposure negatively impacts components of the brain stress response system, including stress-associated brain neuropeptides and glucocorticoid receptors in the amygdala, hippocampus and hypothalamus. While PAE generates a unique brain cytokine expression pattern, little is known about the role of Toll-like receptor 4 (TLR4) and related proinflammatory signaling factors, as well as anti-inflammatory cytokines in PAE brain stress-responsive regions. We hypothesized that PAE sensitizes the early brain stress response system resulting in dysregulated neuroendocrine and neuroimmune activation.

Methods: A single, 4-h exposure of maternal separation stress in male and female postnatal day 10 (PND10) C57Bl/6 offspring was utilized. Offspring were from either prenatal control exposure (saccharin) or a limited access (4h) drinking-in-the-dark model of PAE. Immediately after stress on PND10, the hippocampus, amygdala and hypothalamus were collected, and mRNA expression was analyzed for stress-associated factors (CRH and AVP), glucocorticoid receptor signaling regulators (GAS5, FKBP51 and FKBP52), astrocyte and microglial activation, and factors associated with TLR4 activation including proinflammatory interleukin-1β (IL-1β), along with additional pro- and anti-inflammatory cytokines. Select protein expression analysis of CRH, FKBP and factors associated with the TLR4 signaling cascade from male and female amygdala was conducted.

Results: The female amygdala revealed increased mRNA expression in stress-associated factors, glucocorticoid receptor signaling regulators and all of the factors critical in the TLR4 activation cascade, while the hypothalamus revealed blunted mRNA expression of all of these factors in PAE following stress. Conversely, far fewer mRNA changes were observed in males, notably in the hippocampus and hypothalamus, but not the amygdala. Statistically significant increases in CRH protein, and a strong trend in increased IL-1β were observed in male offspring with PAE independent of stressor exposure.

Conclusion: Prenatal alcohol exposure creates stress-related factors and TLR-4 neuroimmune pathway sensitization observed predominantly in females, that is unmasked in early postnatal life by a stress challenge.

KEYWORDS

prenatal alcohol exposure, TLR4, amygdala, maternal separation, stress, FKBP5, Gas5, glucocorticoid receptor

Introduction

Maternal consumption of alcohol during pregnancy results in a broad constellation of outcomes known as fetal alcohol spectrum disorder (FASD) and includes central nervous system (CNS) deficits manifesting as cognitive, behavioral and emotional dysregulation (Moore and Xia, 2021). Alcohol can interact with CNS systems such as the hypothalamic–pituitary–adrenal (HPA) axis that regulate stress responses. Published data show that, as a consequence of alcohol consumption during pregnancy, increased maternal glucocorticoids lead to detrimental exposure levels to the fetus (O'Connor et al., 1998; Przybycien-Szymanska et al., 2011). Further, alcohol can alter the expression of corticotropin-releasing hormone (CRH), a factor that initiates HPA activation in response to alcohol or stress, and is released within several key brain regions involved in stress regulation such as the periventricular nucleus within the hypothalamus (O'Connor et al., 1998), the amygdala, and the hippocampus (Tsigos et al., 2000; Charney, 2004; Zhou and Fang, 2018). In addition to fetal exposure to deleterious levels of maternal stress hormones, maternal consumption of alcohol poses direct developmental risks to the fetus, as alcohol is capable of crossing the placenta to interact directly with ongoing fetal CNS maturation including HPA axis regulation (Gabriel et al., 1998). That is, prenatal alcohol exposure (PAE) results in elevated glucocorticoids in fetal blood and acts in brain, altering glucocorticoid receptor expression and signaling in the hypothalamus, amygdala and hippocampus (Caldwell et al., 2014; Lam et al., 2018; Lu et al., 2018; Raineki et al., 2019). Importantly, the consequence of elevated glucocorticoid levels during CNS maturation results in reduced CNS neural development and myelination (De Kloet et al., 1988). While the changes and the impact of initial biochemical factors/receptors resulting from direct alcohol exposure from maternal alcohol consumption differ from maternal stress, the downstream consequences of fetal exposure to elevated glucocorticoids (Gabriel et al., 1998; Lan et al., 2017) converge resulting in an enduring dysregulation of the brain stress-response and HPA axis in offspring (Rash et al., 2016; Gartstein and Skinner, 2018; McGowan and Matthews, 2018).

A large body of evidence demonstrates an extensive interface of the neuro-immune-endocrine systems, with bi-directional communication and regulation (Elenkov et al., 2000; Haddad et al., 2002) through the actions of common ligands including cytokines/chemokines and their receptors in brain regions such as, but not limited to, the hypothalamus, amygdala and hippocampus. While glucocorticoids inhibit the production of several potent proinflammatory cytokines including interleukin (IL)-1β (Páez Pereda et al., 1996; Goujon et al., 1997; Plagemann et al., 1998), conversely, brain proinflammatory cytokines induce HPA activation through multiple mechanisms including reducing glucocorticoid receptor sensitivity (Pariante et al., 1999; Daun et al., 2000). More recent studies have extended the role of the neuro-immune-endocrine interface in underlying CNS dysregulation as a consequence of PAE (Bodnar et al., 2016), emphasizing the critical influence that a variety of cytokines exert in the developing CNS, particularly in offspring following PAE.

Prenatal alcohol exposure negatively impacts the delicate balance of neuroimmune factors. Increases in glial (microglia and astrocytes) activation, proinflammatory cytokines IL-1β and tumor necrosis factor-a (TNF-α), and the chemokine known as C–C motif chemokine ligand-2 (CCL2) are observed in the brain from offspring with PAE, along with decreases in the anti-inflammatory cytokine, interleukin-10 (IL-10; Drew et al., 2015; Topper et al., 2015) and in the spinal cord following peripheral nerve damage (Noor et al., 2017, 2020; Sanchez et al., 2017, 2019). Additionally, PAE female rat pups at postnatal day (PND) 8 reveal IL-1β and TNF-α protein are decreased in the hypothalamus and increased in the hippocampus (Bodnar et al., 2016). However, it remains poorly understood how altered early-life neuroendocrine-immune function may impact factors that initiate the brain stress response system (i.e., CRH) in neonatal brain regions where glucocorticoid receptors are expressed.

Given PAE exerts strong influences on the brain neuroimmune-neuroendocrine interface, the goal of the current study was to examine whether PAE alters early-life transcriptional (mRNA) expression of CRH and arginine vasopressin (AVP), which play critical roles in initiating the HPA stress responses, in addition to basal and stress-induced neuroimmune factors generated by stimulation of the Toll-like Receptor 4 (TLR4). Activated TLR4 results in a proinflammatory cellular signaling cascade of cytokines, chemokines, and transcription factors (Chen and Jiang, 2013). The stress-integrative and responsive brain regions, the hypothalamus, amygdala and hippocampus, following maternal separation stress at PND10 are examined. Interestingly, growth arrest specific 5 (GAS5) is characterized to occupy the nuclear DNA-binding domain of the glucocorticoid receptor and FK506-binding protein 51 (FKBP51) binds to the glucocorticoid receptor in the cytoplasm resulting in reduced nuclear translocation of the glucocorticoid-glucocorticoid receptor complex (Davies et al., 2002; Petta et al., 2016). Consequently, GAS5 and FKBP51 may act to reduce glucocorticoid receptor signaling. Conversely, FKBP52 acts to promote glucocorticoid receptor high affinity for glucocorticoids, thus enhancing glucocorticoid nuclear translocation of the glucocorticoid receptor complex (Schiene-Fischer and Yu, 2001). Thus, we speculate that PAE reduces glucocorticoid receptor function and ultimately signaling through the dysregulated increase in GAS5, FKBP51, and FKBP52 in limbic regions critical for stress regulation. We hypothesized that PAE acts to sensitize stress neuropeptides, endogenous glucocorticoid receptor signaling

regulators and TLR4- related and -independent proinflammatory factors in the hippocampus, amygdala and hypothalamus in response to an acute stressor during early postnatal life.

Materials and methods

Animals

All procedures adhered to the ethical guidelines for laboratory animals in research (Council, N.R, 2011), which required approval by the Institutional Animal Care and Use Committee (IACUC) of the University of New Mexico Health Sciences Center, and are reported according to ARRIVE Guidelines (Kilkenny et al., 2010). All mice were housed in a temperature (22°C) and light-controlled (reverse light/dark; lights on at 20:00 h) rooms, with standard rodent chow and water available *ad libitum* prior to and during experimentation. Male and female 60-day-old mice (C57BL/6 J; Jackson laboratories, Bar Harbor, ME) were group-housed and acclimated for 1 week prior to single-housing females 1 week prior to initiating the alcohol paradigm. Male mice were grouped two per cage approximately, 1 week prior to initiating breeding.

Ethanol exposure model

Thirty-two female mice were allowed limited access to ethanol identically as previously described (Brady et al., 2012). Briefly, female mice were randomly assigned to saccharin sweetened water (SAC; saccharin was obtained from Sigma-Aldrich, St. Louis, MO), used as the control, or a SAC-sweetened ethanol solution (ethanol was obtained from Deacon Labs, King of Prussia, PA). Two hours into the dark cycle (10:00), mice were provided access to a solution of either 10% (*w*/*v*) ethanol and 0.066% (*w*/*v*) saccharin or 0.066% (*w*/*v*) saccharin (control) offered in replacement of standard water for a period of 4 h and replaced by water thereafter. On days 1–2, the ethanol concentration (*w*/*v*) was 0%, and increased to 5% on days 3–4 and further increased to 10% on days 5–6. Mice continued to be offered either SAC or 10% ethanol for a 4-h period for ~ 1 week prior to initiating the breeding period. After establishing consistent drinking, a 5-day breeding period commenced, whereby immediately following the 4-h drinking period, females were placed with 2 males and at 08:00 and returned to their individual cages. Access to SAC or 10% ethanol was available throughout gestation. Females were weighed every 3–4 days to confirm pregnancy by weight gain. Following parturition, solutions were decreased to 0% in a stepwise fashion over a period of 6 days. The currently used PAE model has been fully characterized previously (Brady et al., 2012).

Maternal separation stress

On PND10, pups were subjected to a 4-h maternal separation stress. For the majority of litters (30 of 32), whole litters were randomly assigned to control or maternal separation. All pups from the litter remained in the same cage that was placed in a separate room for 4 h starting at 10:00. Control mice stayed in the home cage with their dams, undisturbed, for 4 h.

Tissue collection

Immediately following stress or control conditions, pups were sexed by visual examination of external genitalia and then euthanized by rapid decapitation followed by brain removal and dissection on ice of the hypothalamus (HYP), bilateral hippocampus (HPC), and amygdala (AMG) that were placed into homogenization DNase/RNase/Protease-free 1.5 mL disposable pellet mixer microtubes (VWR International; Cat#47747-358), briefly spun down, and immediately snap frozen in liquid nitrogen. All samples were stored at − 80° C until the time of assay. Tissue samples were selected from different litters to achieve up to an $N = 10$ / study group for each sex. The experimental conditions for males and females were as follows: PAE unstressed, SAC unstressed, PAE stressed, SAC stressed. Final numbers for each group were between 4 and 10.

RNA extraction and RT-qPCR assay

RNA extraction and RT-qPCR procedures were conducted similarly to that previously described (Noor et al., 2019). Briefly, frozen tissues were retrieved on dry ice and scraped into homogenization tubes or onto a petri dish on dry ice for cutting, ensuring that tissues remained frozen. Total RNA was extracted using the miRNeasy micro kit (Qiagen, catalog # 217084). The petri dish, cutting blade, and forceps were thoroughly cleaned with ethanol, RNAse zap, and DNAse away (Thermo Scientific, MA, United States). The entire tissue sample from the HYP and AMG was processed. A randomly selected half of the HPC within each experimental condition was processed for RNA extraction. Qiazol (200 µl) was added to homogenization tubes containing the frozen tissue, homogenized on ice for 90 s followed by further addition of Qiazol (500 µl), vortexed for 30 s, and incubated at RT for 7-min, which allows dissociation of nucleoprotein complexes, and finally adding 140 µL of chloroform (Sigma-Aldrich; Cat#C2432). The samples were then mixed vigorously for 15 s, incubated for 4 min at RT, mixed vigorously for 10 s, and then centrifuged at 4°C at 12000 × *g* for 15 min. Approximately 300 µl of the aqueous layer was retrieved from the samples and the final elution of RNA was in 20 µl of RNAse/DNase free sterile water. RNA concentration was assessed using NanoDrop (Thermo Scientific, MA, United States). The remaining sample (~300ul) was aliquoted into homogenization DNase/RNase/Protease-free 1.5 mL disposable pellet mixer microtubes (VWR International; Cat#47747-358), briefly spun down and frozen at − 80° C until protein assay from the AMG.

RT-qPCR assay

The extracted RNA was diluted to a standardized concentration of 200 ng/ µl (+/− 10 ng/ µl) for all tissues except male hypothalamus. The male hypothalamus was standardized to a concentration of 100 ng/ µl (+/− 5 ng/ µl). The reduced concentration relative to all of the other tissues was due to proportion of samples having been previously processed with compromised sample integrity and consequently, reduced sample material. Half of the male hypothalamus RNA samples had been extracted separately with these resultant lower levels of RNA. For the current experiment, we chose a concentration

of 100 ng/μl to ensure adequate sample material collected from each pup. For the cDNA synthesis reaction, the RNA concentration for the reaction was 2.4 μg for all tissues except for male hypothalamus, which was 1.1 ug. cDNA synthesis was performed using the SuperScript™ IV VILO™ cDNA Synthesis Kit (Invitrogen; Cat#:11754250) per manufacturer's instructions.

mRNA expression levels were measured and analyzed as previously described (2) with the following modifications. Dilution factors were determined to allow for C_T values between 17 and 33, as estimated by prior publications from our lab (Noor et al., 2019) based on their estimated abundance under non-pathological conditions. The housekeeping gene used as an internal control for each reaction was 18 s, and the cDNA required a dilution factor of 1:1,000 for all tissues due to its high abundance in cells. However, for all of the target genes of interest, the following cDNA dilution factors were adjusted down, ranging from 50 to 400-fold dilutions, to account for their relative reduced abundance in cells (Noor et al., 2019). For the amygdala and hippocampus for both males and females, a dilution of 1:8 was used for Gas5, FKBP5, FKBP4, GFAP, and HMGB1, and a dilution of 1:4 was used for TLR4, NLRP3, IκBα, IL-1β, TNF-α, CCL2, IL-10, IL-1R, CRH, AVP, and Tmem119. For female hypothalamus, a dilution of 1:4 was used for targets Gas5, FKBP5, FKBP4, GFAP, HMGB1, TLR4, NLRP3, IL-1β, TNF-α, CCL2, IL-10 and Tmem119. A 1:8 dilution was used CRH, AVP, IL-1R, and IκBα. For male hypothalamus, a dilution of 1:2.5 was used for NLRP3, IL-1β, TNF-α, CCL2, and IL-10, a dilution of 1:5 was used for IκBα. IL-1R, CRH, and AVP, a dilution of 1:10 was used for TLR4 and Tmem119, and a dilution of 1:20 was used for Gas5, FKBP5, FKBP4, GFAP, and HMGB1. All targets were run in triplicate and data are presented as 2^CTnorm/2^CTtarget as previously detailed (Noor et al., 2019).

For the amygdala and hippocampus, all male and female samples were run on the same plate for both the cDNA synthesis reaction and each PCR reaction for each target.

RT-qPCR validation of results for hypothalamus

A significant majority of the samples from male and female hypothalamus were conducted with standardized RNA inputs for the cDNA reactions *within* male and female groups, but different *between* males (100 ng/μl) and females (200 ng/μl). Additionally, the PCR assays for females were run on separate assay plates from the male samples. Therefore, to ensure that potential sex differences were not due to different RNA concentration (males 100 ng/μl) and on separate plates at the time of assay, we conducted a validation of qRT-PCR reflecting target mRNA levels of males and females using a subset of samples from each experimental group and examined a subset of gene targets, *with cDNA diluted identically*, and males and females assayed together on the same qPCR plate for each target. This separate, smaller experiment using a subset of samples from the hypothalamus was composed of all experimental groups ($n = 4$/group) *with cDNA diluted identically*, at 100 ng/μl for males and females, and assayed together for the following subset of the gene targets: CRH, GAS5, GFAP, NFKBIA and IL1B. All other tissues were assayed using identical standardized RNA inputs for the cDNA reactions as well as run on the same assay plates.

Protein extraction and analysis

Frozen pellets of amygdalae samples (~300 μl), which were derived from the samples created at the time of total RNA extraction (see above), were thawed on ice and treated with 100% ethanol, 0.3 M of guanidium hydrochloride to recover proteins from a denaturing environment (prior Qiazol-chloroform). Pellets were homogenized, sonicated, and incubated in BSA solution and cell lysis buffer 2 (R&D Systems; Cat# 895347) for purified protein isolation. The supernatant containing the proteins were transferred to final tubes and stored at −20°C until further assay using the *RC–DC Protein Assay* which is reducing-agent and detergent-agent compatible (Bio-Rad Cat#500-0122). All procedures were performed according the manufacturer's instructions for RC/DC Protein assay. Briefly, a six-point standard curve in the range 1.25–500 ng/μl was performed using the BSA solution and cell lysis buffer 2 (R&D Systems; Cat# 895347). Samples were diluted 1:15 in cell lysis buffer 2. Standards and samples were added to RC Reagent I (BioRad; Cat# 500-0117) and RC Reagent II (BioRad; Cat# 500-0118) and centrifuged at 12,758 rpm for 5 min, followed by discarding the supernatant. RC Reagent A', which was prepared by combining Reagent A (BioRad; Cat#500-0113) with Reagent S (BioRad; Cat # 500-0115), was added to the pellet and vortexed. The mixture was then added to DC Reagent B (BioRad; Cat# 500-0114), vortexed and incubated in the dark at RT for 15 min. Triplicate standards and samples (200μl/well) were prepared. Absorbance was measured at 750 nm in Biotek-Syngery-Neo2 plate reader.

Enzyme-linked immunosorbent assays (ELISA)

The protein expression of CRH, IL-1β, FKBP5 and NLRP3, in mouse amygdala was detected using enzyme-linked immunosorbent assay (ELISA) kits (CRH: Cat#MBS2020732; FKBP5: Cat#MBS2705556; NLRP3: Cat#MBS920134 MyBiosource, United States; IL-1β Cat#MHSLB00 R&D Systems, United States). The relative concentrations for IL-1β and NLRP3 were acquired according to the standard curve generated by microplate reading at 450 nm; wavelength corrections at 540 nm and 570 nm. The relative concentrations for CRH and FKBP5 were acquired according to the standard curve generated by microplate reading at 450 nm.

Statistical analysis

All statistical analyses were conducted using GraphPad Prism Version 8.4.3 (GraphPad Software Inc.; RRID: SCR002798) as previously described (Noor et al., 2019). Briefly, results were graphed as normalized values ($2^{Ct\ normalizer}/2^{Ct\ target}$) and analyzed using a 3-way ANOVA to identify main effects and interactions of sex, stress, and/or prenatal alcohol exposure in AMG and HPC. Importantly, prior work established that results from qRT-PCR can be utilized to compare mRNA expression levels from different groups when identical RNA amounts are used for the cDNA synthesis reaction (Ståhlberg et al., 2004).

For the validation experiment of hypothalamus tissue, a 3-way ANOVA was conducted to determine if mRNA levels of chosen target

TABLE 1 Three-way ANOVA: validation of methods from a subset of samples from the hypothalamus with cDNA identically diluted to detect sex differences.

	CRH	GAS5	GFAP	NFKBIA	IL1B
Significance	ns	ns	ns	**	*
Sex with higher expression	–	–	–	F	F

A significant majority of the samples from male and female hypothalamus were conducted with standardized RNA inputs for the cDNA reactions within male and female groups, but different between males (100 ng/μl) and females (200 ng/μl). To address potential sex differences due to different RNA concentrations, a separate and smaller experiment was performed with a subset of samples from the hypothalamus from each experimental group ($n = 4$/group) with cDNA diluted identically; that is at 100 ng/ul for males and females, which were assayed together for a subset of gene targets. No sex differences were detected in mRNA levels for CRH, GAS5 or GFAP, but females demonstrated significantly greater mRNA expression for NFKBIA and IL1B. These results support that the pattern of sex differences observed for hypothalamic CRH, GAS5, GFAP, NFKBIA and IL1B mRNA levels from the much larger study (Figures 1–5; $n = 10$) reflect true mRNA levels of despite applying different RNA concentrations between male and female samples for assay. CRH, corticotropin releasing hormone; GAS5, growth arrest specific 5; GFAP, glial fibrillary acid protein; NFKBIA, NF-κB inhibitor alpha; IL1B, interleukin-1 beta. * = $p \leq 0.05$, ** = $p \leq 0.01$.

genes between males and females were significantly different when utilizing identical RNA concentration inputs. Similar to that for the validation experiment, mRNA derived from the AMG and the HPC were analyzed using 3-way ANOVA procedures to make direct comparisons between males and females of all target genes. Two-way ANOVA procedures were applied to identify within-sex effects of stress and/or prenatal alcohol exposure in HYP, AMG, and HPC. The results were graphed as fold change using the $2^{-\Delta\Delta CT}$ method (Livak and Schmittgen, 2001). All graphs represent mean +/− standard error of the mean. The Fisher's LSD test was used for *post hoc* analysis of between-group differences as determined *a priori*. Within-group outliers were excluded from all analyses as determined by the Grubb's test (Grubbs, 1969; Iglewicz and Hoaglin, 1993), and applied to the data using the GraphPad online outlier calculator[1] with $\alpha = 0.05$. Grubb's test could not be applied to data derived from the HYP validation experiments due to low sample sizes.

Results

Validation of mRNA levels between sex in the hypothalamus: comparison of levels when RNA extracted material is utilized at different concentrations (100 vs. 200 ng)

Only tissue from the hypothalamus (HYP) for males and females was assayed differently relative to the amygdala (AMG) and hippocampus (HPC). Specifically, male and female hypothalamic tissue were not assayed on the same plate at the same time, and RNA concentrations between males and females were not the same, which can lead to potential spurious effects caused by differences in PCR amplification efficiencies. Such artificial results can include differences in male relative to female mRNA expression levels. To address this possibility, a validation of qRT-PCR reflecting selected target mRNAs from each stress and neuroimmune category was conducted. The data demonstrate significant sex differences were identified, with significantly greater mRNA expression in female hypothalamus for NFKBIA ($F_{1,15} = 8.750$, $p = 0.0098$), and IL1B ($F_{1,15} = 5.948$, $p = 0.0276$), mRNA (Table 1). A strong trend toward an interaction between sex and PAE in elevated IL1B in was revealed, albeit lacking statistical significance ($F_{1,15} = 5.730$, $p = 0.0741$). No sex differences were detected in mRNA levels for CRH, GAS5 or GFAP (Table 1).

These data show a similar pattern of sex comparability observed for hypothalamic CRH, GAS5, GFAP, NFKBIA and IL1B mRNA levels relative to those levels observed from the much larger study reflected in Figures 1B, 2C–5C, despite lower RNA concentrations between male and female samples for the hypothalamic assay. Hence, while results of mRNA levels from the larger study between males and females were either on similar y-axis scales, or were 2–10 -fold different, or 40-fold different with CRH (Figures 1B, 2C, 3C, 4C, 5C), the *pattern* of sex differences remained very similar relative to the smaller validation study represented in Table 1. The selected mRNA factors from the smaller validation study represent 1–2 targets from each of the following categories: the stress peptide, CRH; the glucocorticoid receptor signaling regulator, GAS5; a glial activation marker, astrocyte GFAP; the TLR4-related activation factors, NFKBIA and IL1B, as represented in Table 1. Thus, no additional analyses for main effects of sex on other targets were conducted for hypothalamus.

Characterization of stress-associated mRNA levels of CRH and AVP

Sex differences in the amygdala

Clear sex differences in mRNA levels for AVP from the amygdala were observed, with significantly greater levels in females than males ($F_{1,36} = 5.730$, $p = 0.022$), with significant increases observed from PAE and following stress ($F_{1,36} = 4.445$, $p = 0.042$; Figure 1A; Table 2). It is notable that a strong trend toward elevated CRH mRNA levels in females was observed ($F_{1,39} = 2.849$, $p = 0.099$), with notable increases from PAE and following stress ($F_{1,39} = 3.266$, $p = 0.078$). No sex differences were identified in the CRH:AVP ratio. Additionally, both PAE and stress robustly increased mRNA CRH ($F_{1,39} = 4.901$, $p = 0.033$) and AVP ($F_{1,36} = 5.206$, $p = 0.029$; Figure 1A; Table 2). The robust changes in mRNA levels as a consequence of both PAE and stress prompted additional analyses for potential within sex differences, as noted below and in Table 3.

Impact of PAE and/or stress in the amygdala

Two-way ANOVAs were conducted to address potential PAE and/or stress induced gene expression (Table 3) within males and females. PAE, stress or the interaction of PAE and stress on target gene expression are represented in Figure 1A, and demonstrate that CRH and AVP expression within male AMG were not altered by PAE or stress. However, in females with PAE and following stress, CRH ($F_{1,19} = 4.717$, $p = 0.043$) and AVP ($F_{1,18} = 4.827$, $p = 0.041$) mRNA levels were increased in female AMG. Robust impact of PAE ($F_{1,18} = 5.237$, $p = 0.034$) and stress ($F_{1,18} = 5.305$, $p = 0.033$) on AVP mRNA levels were observed. The ratio of CRH to AVP mRNA levels revealed no effects of PAE or stress within male or female AMG (Figure 1A; Table 3).

1 https://www.graphpad.com/quickcalcs/grubbs1/

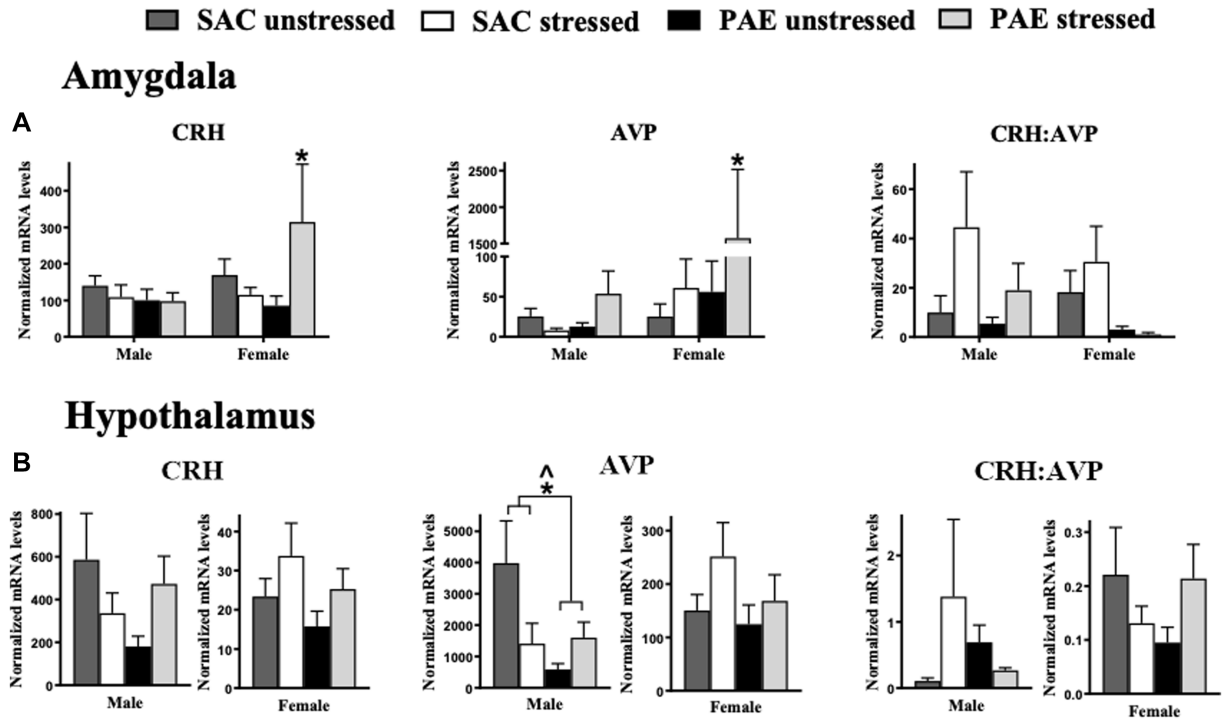


FIGURE 1
The influence of prenatal alcohol exposure (PAE) and stress exposure on corticotropin releasing hormone (CRH) and arginine vasopressin (AVP) mRNA in the amygdala (AMG) and hypothalamus (HYP). **(A)** In the male amygdala, CRH, AVP, and the ratio of CRH:AVP mRNA levels were not altered by PAE or stress. In females, a significant interaction between PAE and stress results in increased CRH and AVP mRNA levels; *Indicates an interaction between PAE and stress. The ratio of CRH to AVP mRNA are not altered by PAE and/or stress in females. **(B)** In the hypothalamus, CRH mRNA levels and the ratio of CRH:AVP mRNA levels are not altered by PAE or stress in either sex. A main effect of PAE reduces AVP mRNA levels in males. Additionally in males, an interaction of PAE and stress is revealed with lower AVP levels in PAE relative to SAC mice, with disparate responses to stress. No reliable differences are observed in AVP mRNA levels from PAE or stress in female HYP. All results reflect 2-way ANOVA main effects and interactions. *Interaction of PAE and stress=$p \leq 0.05$. ^main effect of PAE=$p \leq 0.05$.

Impact of PAE and/or stress in the hypothalamus

CRH mRNA levels were not influenced by PAE or stress in either males or females (Figure 1B; Table 3). However, AVP mRNA levels in males was lower as a consequence of PAE ($F_{1,19} = 4.396$, $p = 0.049$) as well as an impact of both PAE and stress ($F_{1,21} = 5.542$, $p = 0.029$). Relative to unstressed conditions, AVP mRNA levels were divergent following stress in PAE and SAC male HYP. That is, stress decreased SAC AVP expression and increased PAE AVP expression. Neither PAE nor stress influenced the expression of AVP in female HYP or of the ratio of CRH to AVP in male or female HYP. Two-way ANOVA within males and females was utilized to determine these main effects of PAE and/or stress on the expression of stress-associated genes within the HYP (Table 3).

Characterization of regulators of glucocorticoid receptor signaling: levels of lncRNA for GAS5, and mRNA for FKBP5 and FKBP4

Sex differences in the hippocampus and amygdala

For the HPC, sex contributed significantly in observed differences in mRNA levels in mice with PAE for GAS5 ($F_{1,58} = 10.94$, $p = 0.0016$), FKBP5 ($F_{1,57} = 5.138$, $p = 0.027$), FKBP4 ($F_{1,57} = 9.642$, $p = 0.003$), as revealed by an interaction between sex and PAE (Figure 2A; Table 2). In general, female HPC reveals greater changes than observed in males.

For the AMG, there were no significant differences between male and female levels of GAS5 lncRNA and FKBP5, FKBP4, and the ratio of FKBP5 to FKBP4 mRNA, as indicated by 3-way ANOVA analyses (Figure 2B; Table 2). However, further analyses were performed within males and females, as detailed below.

Impact of PAE and/or stress in the hippocampus

In male HPC, greater levels of GAS5 lncRNA levels were observed in PAE relative to SAC mice ($F_{1,26} = 4.741$, $p = 0.039$), but in female HPC, lower levels of GAS5 lncRNA levels were observed in PAE relative to SAC mice ($F_{1,32} = 6.367$, $p = 0.017$; Figure 2A; Table 3). Among females, stress resulted in increased GAS5 lncRNA levels ($F_{1,32} = 6.932$, $p = 0.013$; Table 3). In male HPC, FKBP5 mRNA levels were not altered by PAE or stress, but female HPC FKBP5 mRNA levels increase in response to stress ($F_{1,31} = 21.75$, $p < 0.0001$), an effect that was driven by FKBP5 mRNA elevations in PAE but not SAC mice following stress ($F_{1,31} = 9.979$, $p = 0.004$). Within males, PAE led to higher levels of FKBP4 expression ($F_{1,26} = 5.500$, $p = 0.027$). Neither PAE nor stress did not influence the expression of FKBP4 mRNA in female HPC or of the ratio of FKBP5 to FKBP4 mRNA in male HPC. The ratio of FKBP5 to FKBP4 mRNA levels increased in response to stress in female HPC ($F_{1,32} = 4.951$, $p = 0.033$; Figure 2A; Table 3).

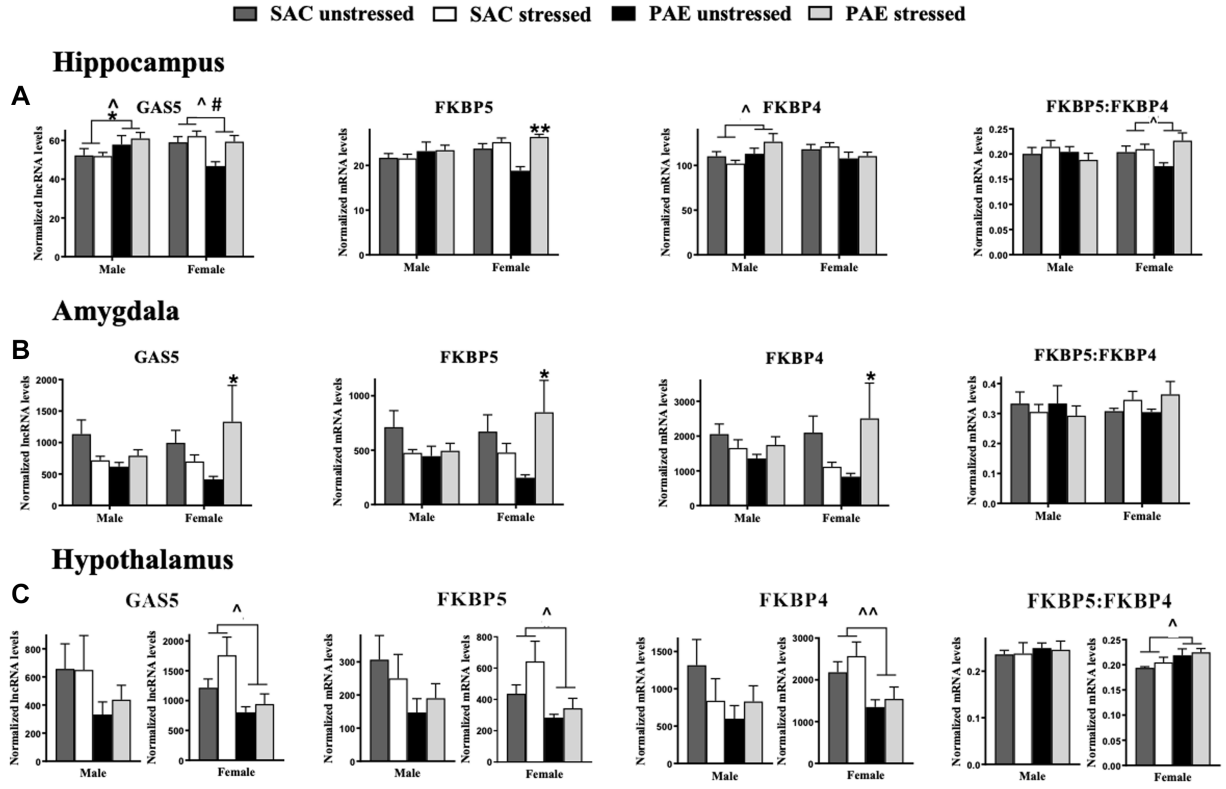


FIGURE 2
The mRNA of glucocorticoid receptor signaling regulators are altered by PAE and stress in the hippocampus amygdala and hypothalamus
(A) Hippocampus (HPC): a main effect of PAE results in increased GAS5 lncRNA levels in male mice and decreased GAS5 lncRNA levels in female mice, as well as a main effect of stress that increases Gas5 expression in females. In males, FKBP5 mRNA levels are not altered by PAE or stress, but in females with PAE, a main effect of stress increases FKBP5 expression. In males, a main effect of PAE increases FKBP4 expression. Neither PAE nor stress do not alter FKBP4 mRNA levels in females. The ratio of FKBP5 to FKBP4 mRNA levels were not affected by PAE or stress in males. In females, a main effect of PAE reveals increases in FKBP5: FKBP4. **(B)** Amygdala (AMG): In the male amygdala, GAS5, FKBP5, FKBP4, and FKBP5:FKBP4 ratio mRNA levels were not influenced by PAE or stress. In females with PAE, an interaction with stress increases expression of GAS5, FKBP5, and FKBP4. Stress and/or PAE does not alter FKBP5:FKBP4 mRNA in females. **(C)** Hypothalamus (HYP): For the male hypothalamus, GAS5, FKBP5, FKBP4, and the ratio of FKBP5 to FKBP4 mRNA levels are not influenced by PAE or stress. However, a main effect of PAE in females results in blunted levels of GAS5, FKBP5, and FKBP4 mRNA independent of stress exposure, and FKBP5:FKBP4 mRNA is increased by PAE. GAS5 lncRNA: growth arrest specific 5 long non-coding RNA; FKBP5: FK506-binding protein 51; FKBP4: FK506-binding protein 52. All results reflect 2-way ANOVA main effects of PAE and stress and interactions of PAE and stress. *Interaction=$p \leq 0.05$, interaction **=$p \leq 0.01$. ^main effect of PAE=$p<0.05$, ^^main effect of PAE=$p<0.005$, #main effect of stress=$p<0.05$.

Impact of PAE and/or stress in the amygdala

We explored whether the gene expression of glucocorticoid receptor signaling regulators were influenced by PAE and/or stress within males or females in the AMG utilizing 2-way ANOVA procedures (Table 3). In the males, GAS5 lncRNA expression levels were not altered by PAE or stress, however, in females, PAE increased GAS5 lncRNA expression following stress that was not observed SAC mice ($F_{1,20} = 6.097$, $p = 0.023$). Strikingly, stress-driven elevations of FKBP5 and FKBP4 expression only in female mice with PAE was observed ($F_{1,20} = 6.545$, $p = 0.019$; $F_{1,19} = 6.953$, $p = 0.016$), while FKBP5 and FKBP4 expression was not reliably altered by PAE or stress in male mice (Figure 2B; Table 3). Additionally, the ratio of FKBP5 to FKBP4 mRNA levels was not altered by PAE or stress within either sex.

Impact of PAE and/or stress in the hypothalamus

In females, expression levels of GAS, FKBP5, and FKBP4 were consistently lower in mice with PAE relative to SAC-treated mice ($F_{1,31} = 7.169$, $p = 0.012$; $F_{1,31} = 5.868$, $p = 0.022$; $F_{1,30} = 9.260$, $p = 0.005$, respectively). The ratio of FKBP5 to FKBP4 mRNA levels was additionally increased in female offspring with PAE ($F_{1,31} = 6.474$, $p = 0.016$; Figure 2C; Table 3). In males, there were no effects of PAE or stress on the expression of GAS5, FKBP5, FKBP4, or the ratio of FKBP5 to FKBP4.

Characterization of astrocyte and microglial mRNA levels of GFAP and TMEM119, respectively

Sex differences in the hippocampus and amygdala

The mRNA expression levels of the astrocyte activation marker, GFAP and the microglial activation marker, TMEM119, did not consistently and significantly differ between males and females in either the HPC or AMG (Figures 3A,B; Table 2).

Impact of PAE and/or stress in the hippocampus

While GFAP mRNA levels increased in response to stress in females ($F_{1,32} = 4.534$, $p = 0.041$), in the males, GFAP mRNA expression was not influenced by either PAE or stress. TMEM119 mRNA levels

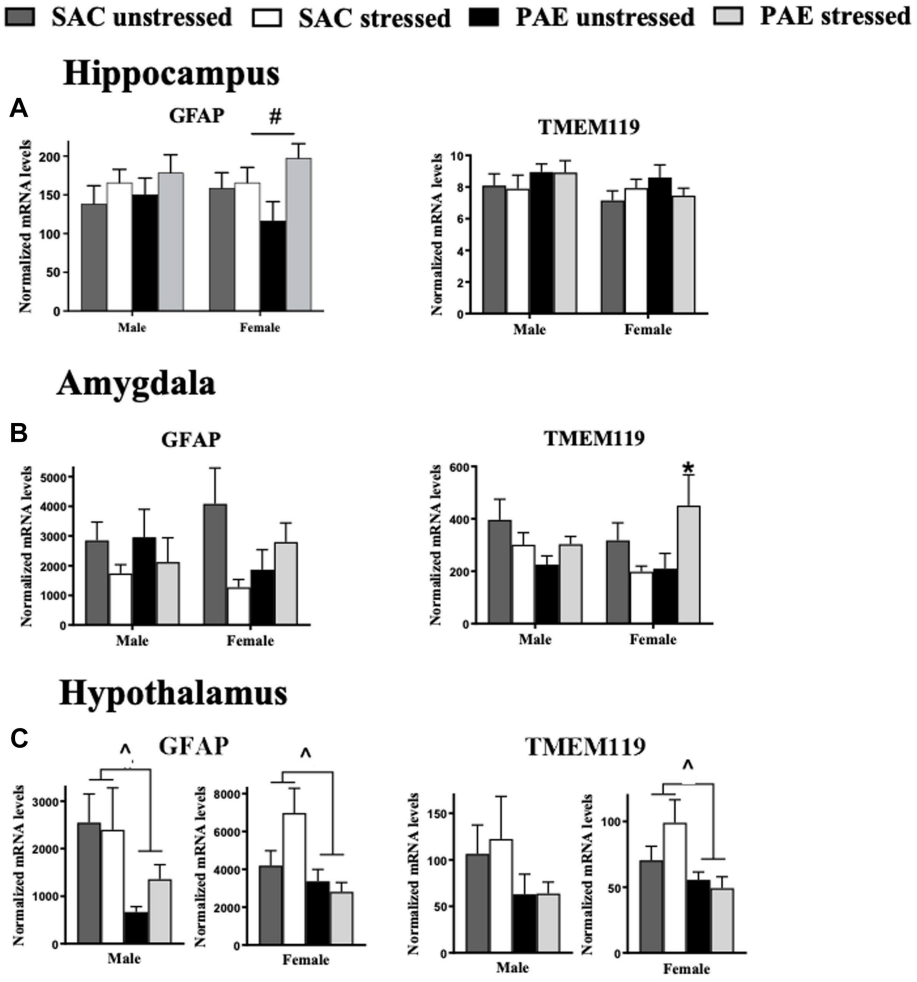


FIGURE 3
Glial activation markers for astrocytes and microglia mRNA expression in the hippocampus, amygdala, and hypothalamus. **(A)** Hippocampus (HPC): male GFAP and TMEM119 mRNA levels are not altered by prenatal alcohol exposure (PAE) or stress. In females with PAE, an interaction with stress increases GFAP expression, while no changes in TMEM119 expression between groups are observed. **(B)** Amygdala (AMG): For the amygdala, male and female GFAP mRNA levels are not altered as a result of PAE or stress. In males, TMEM119 expression is similarly unaffected by PAE or stress. However, females with PAE revealed a significant interaction with stress leading to elevated TMEM119 mRNA levels. **(C)** Hypothalamus (HYP): For the hypothalamus, a main effect of PAE induced blunted GFAP mRNA levels in both male and females. While no significant changes in TMEM119 expression between groups are observed in males, a main effect of PAE blunted TMEM119 expression observed in females independent of stress exposure. Astrocytes, glial fibrillary acid protein (GFAP); microglia, transmembrane protein 119 (TMEM119). All results reflect 2-way ANOVA main effects and interactions. #main effect of stress=$p<0.05$, ^main effect of PAE=$p<0.05$, *Interaction of PAE and stress=$p<0.05$.

were not influenced by PAE or stress in either sex, as examined by applying a 2-way ANOVA procedures (Figure 3A; Table 3).

Impact of PAE and/or stress in the amygdala

A striking interaction between PAE and stress induced elevated microglial TMEM119 mRNA levels in females ($F_{1,19} = 7.273$, $p = 0.014$) with no such changes observed in males. Astrocyte GFAP mRNA expression levels were not altered by either PAE or stress in either males or females, as revealed by 2-way ANOVA procedures to explore possible within-sex effects in the AMG (Figure 3B).

Impact of PAE and/or stress in the hypothalamus

While differences in GFAP mRNA levels in the HYP were not dependent on sex (Figure 3C), as shown by a 3-way ANOVA for GFAP in the smaller validation experiment ($p = 0.067$; Table 1), PAE on glial activation markers within sex in the HYP revealed robust differences. Astrocyte GFAP mRNA expression in male mice was blunted by PAE ($F_{1,17} = 5.525$, $p = 0.031$) as well as within females ($F_{1,30} = 6.374$, $p = 0.017$). Microglial TMEM119 expression was blunted in female mice by PAE ($F_{1,31} = 5.687$, $p = 0.023$), while TMEM119 mRNA levels were not significantly changed by PAE or stress in males (Figure 3C; Table 3).

Characterization of TLR4 activation pathway markers: mRNA levels of HMGB1, TLR4, NFKBIA, NLRP3, and IL1B

Sex differences in the hippocampus and amygdala

For the HPC, a significant impact of sex and stress lead to alterations in HMGB1, with females demonstrating greater HMGB1

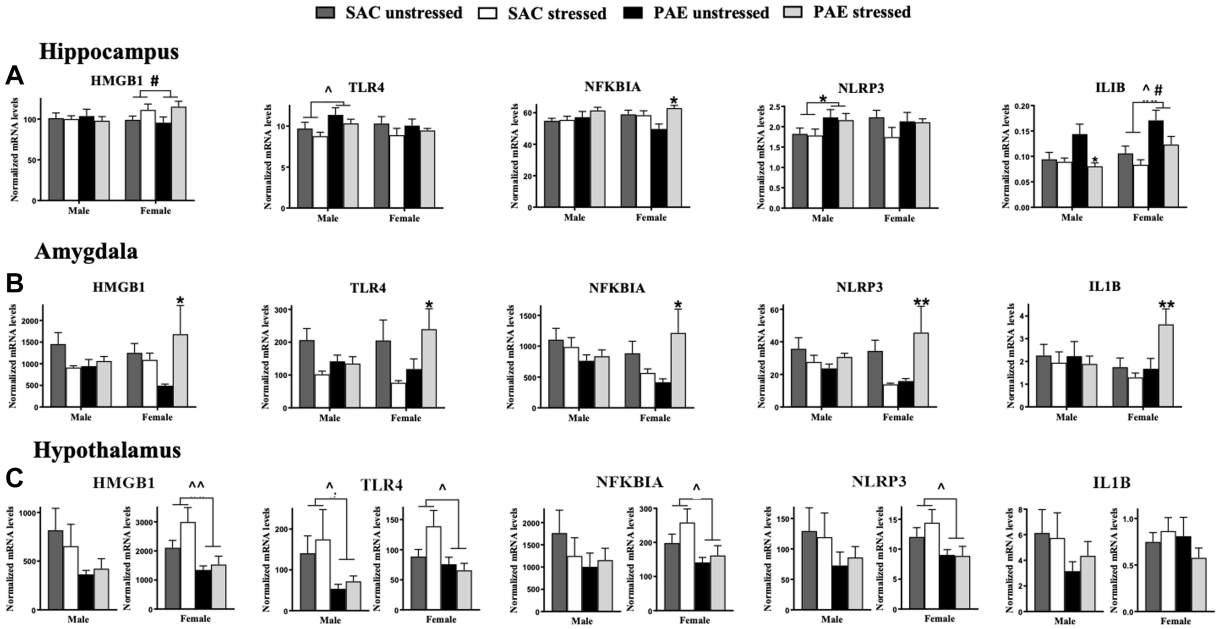


FIGURE 4
mRNA alterations in factors related to the TLR4 signaling cascade HMGB1, TLR4, NFKBIA, NLRP3, and ILIB. **(A)** Hippocampus (HPC): HMGB1 mRNA levels are not altered by prenatal alcohol exposure (PAE) or stress in males. A main effect of stress in females results in elevated HMGB1 expression. A main effect of PAE results in increased TLR4 expression, while no group differences are observed in TLR4 expression levels in females. While no changes are observed in male NFKBIA, females with PAE reveal an interaction with stress that leads to increases NFKBIA mRNA levels. Male offspring reveal a main effect of PAE that increases NLRP3 expression, with no meaningful differences observed between groups in females. In females, main effects of stress and PAE result in increased IL1B mRNA levels while in males, an interaction between PAE and stress result in decreased IL1B mRNA levels relative to SAC male mice. **(B)** Amygdala (AMG): In females, a significant interaction of PAE and stress increases expression of HMGB1, TLR4, NFKBIA, NLRP3, and IL1B while no alterations in mRNAs from SAC female mice were observed. No reliable mRNA changes were observed in male amygdala. **(C)** Hypothalamus (HYP): In males, levels of HMGB1 are not significantly different between treatment groups, while blunted HMGB1 levels are observed in females due to a main effect of PAE independent of stress exposure. Similarly, TLR4 expression is significantly blunted due to a main effect of PAE males and females. Additionally in females, but not males, PAE blunted NFKBIA, and NLRP3 mRNA levels independent of stress exposure. HMGB1, high mobility group box 1; TLR4, toll-like receptor 4; NFKBIA, NF-κB inhibitor alpha; NLRP3, NOD-, LRR- and pyrin domain-containing protein 3; ILIB, interleukin-1 beta. All results reflect 2-way ANOVA main effects and interactions. #main effect of stress=p<0.05, ^main effect of PAE=p<0.05, ^^main effect of PAE=p<0.01, *Interaction of PAE and stress=p<0.05, **=p<0.01.

mRNA levels following stress, but independent of PAE ($F_{1,58} = 4.341$, $p = 0.042$; Figure 4A; Table 2). The mRNA levels of the remaining TLR4-related factors;TLR4, NFKBIA, NLRP3, and IL1B were not impacted by sex, as revealed by 3-way ANOVA analyses procedures (Figure 4A; Table 3).

For the AMG, a significant impact of sex and stress lead to alterations in HMGB1, with females demonstrating greater HMGB1 mRNA levels following stress, but independent of PAE ($F_{1,40} = 4.415$, $p = 0.0420$; Figure 4B; Table 2). Additionally, sex interacted with PAE and stress, which increased NLRP3 mRNA levels in females, but not males ($F_{1,38} = 4.101$, $p = 0.0499$; Figure 4B; Table 2).

Impact of PAE and/or stress in the hippocampus

The impact of PAE and/or stress on TLR4-associated mRNA expression in the HPC within sex was analyzed using 2-way ANOVA (Figure 4A; Table 3). While the expression of HMGB1 was not altered by PAE or stress in males, HMGB1 mRNA levels were increased by stress treatment in female HPC ($F_{1,32} = 5.783$, $p = 0.022$). TLR4 expression was increased by PAE in males ($F_{1,26} = 5.062$, $p = 0.033$), while in females, TLR4 expression remained unaltered by PAE or stress. In males, NFKBIA expression was also not influenced by PAE or stress, while in females, stress increased NFKBIA expression ($F_{1,32} = 5.847$, $p = 0.022$), an effect that reflected stress-induced elevations of NFKBIA mRNA by PAE but not SAC female mice ($F_{1,32} = 6.856$, $p = 0.013$). NLRP3 mRNA levels were greater by PAE in males ($F_{1,26} = 5.130$, $p = 0.032$), while NLRP3 remained unchanged in females. In males, stress-induced decreased IL1B expression ($F_{1,24} = 6.055$, $p = 0.021$) was observed in mice with PAE, with an interaction between PAE and stress revealed in males ($F_{1,24} = 4.453$, $p = 0.046$; Figure 4A; Table 3). No changes in IL-1B expression were detected from SAC-exposed offspring under basal or following stressed conditions. In females, PAE increased the overall IL1B expression ($F_{1,32} = 11.99$, $p = 0.001$), with stress exposure resulting in decreased IL1B mRNA a ($F_{1,32} = 5.396$, $p = 0.027$; Figure 4A; Table 3).

Impact of PAE and/or stress in the amygdala

Alterations in TLR4-associated factors in mRNA expression of the AMG as a consequence of PAE and/or stress were analyzed within sex using 2-way ANOVA (Figure 4B; Table 3). In male offspring, significant differences as a consequence of PAE and stress in HMGB1, TLR4, NFKBIA, and IL1B mRNA expression levels were absent. Conversely, in females, a striking interaction of mice with PAE that were exposed to stress produced a consistent increase in all of the TLR4-related factors measured. That is, increased HMGB1 ($F_{1,20} = 5.721$, $p = 0.027$), TLR4 ($F_{1,19} = 6.848$, $p = 0.017$), NFKBIA ($F_{1,18} = 8.264$, $p = 0.010$), NLRP3 ($F_{1,18} = 11.96$, $p = 0.003$), and IL1B (F

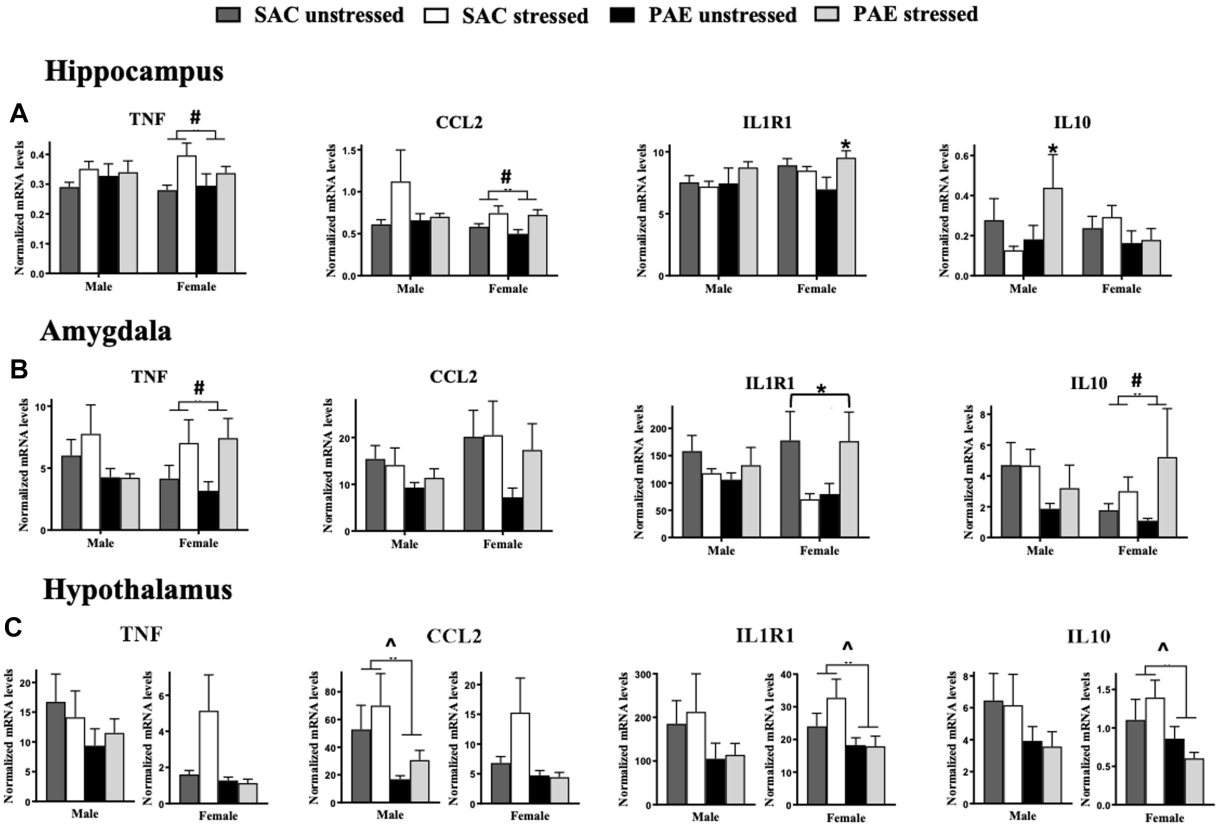


FIGURE 5
Alterations in mRNA expression of TNF, CCL2, IL1R1, and IL10. **(A)** Hippocampus (HPC): In females, a main effect of stress increases TNF and CCL2 mRNA levels, while no changes between treatment groups are observed in males. A significant interaction of PAE and stress results in elevated IL1R1 mRNA expression levels in females, while no changes between treatment groups are observed in males. Levels of IL10 mRNA expression are significantly elevated in males as a result of a PAE and stress interaction, while no changes in IL-10 levels are observed between treatment groups in females. **(B)** Amygdala (AMG): In females, but not males, a main effect of stress results in increased TNF and IL-10 mRNA levels, independent of PAE. An interaction of PAE and stress differentially alters in IL1R1 expression in females. Levels of CCL2 mRNA are not significantly different between treatment groups in males and females. While no meaningful differences are observed between groups in males **(C)** Hypothalamus (HYP): Despite strong trends for diminished TNF and CCL2 expression levels in females, mRNA levels were not significantly influenced by PAE, while PAE significantly reduced CCL2 in males. Additionally, a main effect of PAE consistently blunted IL1R1 and IL10 mRNA levels in females, with strong trends of blunted IL1R1 and IL-10 mRNA levels in males with PAE. TNF, tumor necrosis factor alpha; CCL2, chemokine ligand 2; IL1R1, interleukin-1 receptor 1; IL10, interleukin-10. All results reflect 2-way ANOVA main effects and interactions. ^main effect of PAE=$p<0.05$, #main effect of stress=$p<0.05$, *main interaction of stress and PAE=$p\leq0$.

$_{1,20}=8.144$, $p=0.010$) mRNA expression was observed (Figure 4B; Table 3).

Impact of PAE and/or stress in the hypothalamus

The impact of PAE and/or stress on TLR4-assoicated inflammatory factors were examined within sex in the HYP by 2-way ANOVA (Figure 4C; Table 3). In males, while mRNA levels for HMGB1, NFKBIA, NLRP3, or IL1B were not impacted by PAE and/or stress, TLR4 mRNA levels were blunted in male by PAE ($F_{1,23}=4.651$, $p=0.041$). However, the mRNA expression pattern analyzed in females was remarkably different. Females with PAE revealed a significant and robustly different pattern, with blunted expression of HMGB1 ($F_{1,31}=8.629$, $p=0.006$), TLR4 ($F_{1,30}=5.005$, $p=0.033$), NFKBIA ($F_{1,30}=5.503$, $p=0.026$), and NLRP3 ($F_{1,31}=5.079$, $p=0.031$) compared to SAC treated females. IL1B expression in the female was not significantly influenced by PAE or stress (Figure 4C; Table 3).

Characterization of mRNA levels of neuroimmune factors that influence TLR4 actions; proinflammatory cytokine TNF, chemokine CCL2, cytokine receptor IL1R1, and anti-inflammatory cytokine IL10

Sex differences in the hippocampus and amygdala

While sex alone did not impact mRNA levels of TNF, CCL2, IL1R1, or IL10 in the HPC or AMG, a significant impact of sex with PAE and stress induced increases in the anti-inflammatory cytokine, IL-10 in male HPC ($F_{1,56}=4.209$, $p=0.045$), as revealed by a 3-way ANOVA (Figure 5A; Table 2). The levels of IL-10 mRNA in females are observed lowest in females with PAE (Figure 5A). No other interactions with sex were observed between male and female mRNA expression levels of TNF, CCL2, or IL1R1, in the HPC or AMG.

TABLE 2 Summary of 3-way ANOVA: hippocampus and amygdala for effects of sex, prenatal exposure and stress.

	CRH	AVP	CRH: AVP	GAS5	FKBP5	FKBP4	FKBP5: FKBP4	GFAP	TMEM119	HMGB1	TLR4	IκBα	NLRP3	IL-1β	TNF-α	CCL2	IL-1R	IL-10
Main effect of sex																		
Hippocampus																		
Amygdala		*																
Main effect of prenatal exposure																		
Hippocampus						**							*	**				
Amygdala		*																
Main effect of stress exposure																		
Hippocampus				*	**			*				*		**	*			
Amygdala		*																
Main interaction between sex and prenatal exposure																		
Hippocampus				**	*	**												
Amygdala		*																
Main interaction between sex and stress exposure																		
Hippocampus					**					*								
Amygdala		*								*								
Main interaction between prenatal exposure and stress exposure																		
Hippocampus					*							*					*	
Amygdala	*	*		**	**	**			**	**	**	*	***				**	
Main interaction between sex, prenatal exposure, and stress exposure																		
Hippocampus																		*
Amygdala		*											*					

The table represents a summary of 3-way ANOVA analyses procedures of all targets examined in the hippocampus and the amygdala for (1) main effects of sex, (2) prenatal exposure and (3) Stress and interactions between (4) sex and prenatal exposure, (5) sex and stress exposure, (6) prenatal exposure and stress exposure, and (7) sex, prenatal exposure and stress exposure. CRH, corticotropin releasing hormone; AVP, arginine vasopressin; GAS5, growth arrest specific 5; FKBP5, FK506-binding protein 51; FKBP4, FK506-binding protein 52; GFAP, glial fibrillary acid protein; TMEM119, transmembrane protein 119; HMGB1, high mobility group box 1; TLR4, toll-like receptor 4; NFKBIA, NF-κB inhibitor alpha; NLRP3, NOD-like receptor family pyrin domain-containing protein 3; IL1B, interleukin-1 beta; TNF, tumor necrosis factor alpha; CCL2, C-C motif chemokine ligand 2; IL1R1, interleukin-1 receptor 1; IL10, interleukin-10. All main effects and interactions are indicated by *, * = $p \leq 0.05$, ** = $p \leq 0.01$, *** = $p \leq 0.001$.

10.3389/fnins.2023.1203557

TABLE 3 Two-way ANOVA: hippocampus, amygdala, and hypothalamus for prenatal exposure and stress.

		CRH	AVP	CRH: AVP	GAS5	FKBP51	FKBP52	FKBP51: FKBP52	GFAP	TMEM119	HMGB1	TLR4	IκBα	NLRP3	IL-1β	TNF-α	CCL2	IL-1R	IL-10
Within-sex main interaction between prenatal and stress exposure																			
Male	Hipp														*				*
	Amygdala																		
	Hypothal		*																
Fem	Hipp					**							*					*	
	Amygdala	*	*		*	*	*			*	*	*	*	**	**			*	
	Hypothal																		
Within-sex main effect of prenatal exposure																			
Male	Hipp				*		*							*					
	Amygdala																		
	Hypothal		*						*			*					*		
Fem	Hipp				*										**				
	Amygdala		*												*				
	Hypothal				*	*	**	*	*	*	**	*	*	*				*	*
Within-sex main effect of stress exposure																			
Male	Hipp											*			*				
	Amygdala																		
	Hypothal																		
Fem	Hipp				*	****		*	*		*		*		*	*	**		
	Amygdala		*													*			*
	Hypothal																		

The table represents a summary of within-sex analyses using 2-way ANOVA procedures of all targets examined in the hippocampus, amygdala, and the hypothalamus. For all tissue regions, main effects of (1) prenatal exposure and (2) stress exposure, and an interaction between prenatal exposure and stress exposure are reported. CRH, corticotropin releasing hormone; AVP, arginine vasopressin; GAS5, growth arrest specific 5; FKBP5, FK506-binding protein 51; FKBP4, FK506-binding protein 52; GFAP, glial fibrillary acid protein; TMEM119, transmembrane protein 119; HMGB1, high mobility group box 1; TLR4, toll-like receptor 4; NFKBIA, NF-κB inhibitor alpha; NLRP3, NOD-like receptor family pyrin domain-containing protein 3; IL1B, interleukin-1 beta; TNF, tumor necrosis factor alpha; CCL2, C-C motif chemokine ligand 2; IL1R1, interleukin-1 receptor 1; IL10, interleukin-10. All main effects and interactions are indicated by *, * = $p \leq 0.05$, ** = $p \leq 0.01$, *** = $p \leq 0.001$, **** = $p \leq 0.0001$.

10.3389/fnins.2023.1203557

Impact of PAE and/or stress in the hippocampus

Within sex comparisons were examined to identify the influence of PAE and/or stress on the mRNA expression of pro- and anti-inflammatory factors in the HPC (Figure 5A; Table 3), as analyzed by 2-way ANOVA procedures. While significant increases in IL10 mRNA levels were observed in male offspring with PAE exposed to stress relative to mRNA changes in SAC offspring ($F_{1,25} = 4.558$, $p = 0.043$), TNF, CCL2, and IL1R1 mRNA levels were not altered by either PAE or stress. However, in females, increases in mRNA levels as a consequence of stress were observed for TNF ($F_{1,32} = 6.440$, $p = 0.016$), and CCL2 ($F_{1,30} = 8.815$, $p = 0.006$). A robust interaction was revealed in female mice with PAE exposed to stress as observed by significant increases in IL1R1 expression ($F_{1,31} = 6.275$, $p = 0.018$; Figure 5A; Table 3).

Impact of PAE and/or stress in the amygdala

Within sex examination of the effects of PAE and/or stress on mRNA expression in the AMG applying 2-way ANOVA procedures revealed main effects of stress and an interaction between PAE and stress (Figure 5B; Table 3). Specifically in females, TNF ($F_{1,20} = 5.966$, $p = 0.024$), and IL-10 ($F_{1,20} = 4.875$, $p = 0.039$) expression increased as a consequence of stress exposure while no changes in CCL2 and IL1R1 from stress alone were observed. Additionally, no main effects of PAE were revealed for TNF, CCL2, IL1R1, or IL10 mRNA levels. However, in female mice with PAE and exposed to stress, divergent IL1R1 mRNA expression levels were observed ($F_{1,20} = 5.761$, $p = 0.026$; Figure 5B; Table 3).

Impact of PAE and/or stress in the hypothalamus

For within sex, the impact of PAE and/or stress on mRNA expression levels were examined in the HYP of males and females by applying 2-way ANOVAs (Figure 5C; Table 3). Although strong trends of blunted mRNA expression levels were observed in females, TNF and CCL2 mRNA levels were not significantly influenced by PAE or stress in females, while in males, CCL2 mRNA expression was significantly decreased only in PAE mice ($F_{1,18} = 4.466$, $p = 0.049$). While no IL-1R1 and IL-10 expression level differences were observed in males between groups, females with PAE revealed blunted IL1R1 and IL10 mRNA expression levels independent of stress exposure ($F_{1,31} = 4.868$, $p = 0.035$; $F_{1,31} = 5.465$, $p = 0.026$, respectively).

Characterization of protein in the amygdala for CRH, IL-1b, FKBP5 and NLRP3

For within sex, the impact of PAE and/or stress on protein levels from the amygdala were examined for the stress peptide, CRH, and pro inflammatory *IL-1β and NLRP3, and the glucocorticoid receptor signaling regulator, FKBP5* by applying 2-way ANOVAs (Table 4). Within sex protein analysis from samples that were left over from mRNA extraction yielded low total protein levels. Despite these low yields, either significant differences or strong trends were detected in CRH ($F_{(1,18)} = 4.617$, $p < 0.05$), and IL-1β ($F_{(1,19)} = 4.132$, $p = 0.05$) levels, respectively, from PAE-treated male offspring independent of stress exposure. While it was predicted that protein analyses from the amygdala would reveal group differences that would mirror changes observed in mRNA expression levels, it was not surprising that most of the protein analyses did not result in significant differences between treatment groups, mainly due to the exceptionally low protein yields.

Discussion

Accumulating evidence supports the adverse impact of PAE on CNS function that often goes unnoticed until a secondary challenge occurs after birth and well into adulthood, typically from direct immune activation or from direct peripheral tissue damage. Significant PAE-induced susceptibility of the CNS to dysregulation may involve sensitized inflammatory cytokines/chemokines and transcriptional factors (Drew et al., 2015; Bodnar et al., 2016, 2020; Terasaki and Schwarz, 2016; Noor et al., 2017, 2020; Sanchez et al., 2017, 2019). The current report extends these observations by demonstrating that a secondary challenge can include non-tissue damaging stressors occurring in early life, and supports that both neuroimmune and neuroendocrine dysregulation may underlie early programing that leads to adult CNS vulnerabilities. In support of prior studies, a striking demonstration is made in the current report that the amygdala reveals significant mRNA upregulation of the stress-associated factors CRH and AVP (Figure 1A; Table 2), disruptors of glucocorticoid receptor signaling GAS5 and FKBP5 (Figure 2B; Table 2), the microglial activation marker transmembrane protein 119 (TMEM119; Figure 3B; Table 2), and factors that initiate or are induced downstream of TLR4 activation (Figure 4B; Table 2) by PAE in offspring treated with a single session of maternal separation stress at PND10.

Other proinflammatory factors measured in the amygdala that are not necessarily dependent on TLR4 activation, but can impact TLR4 downstream effects and are critical for mediating aspects of innate immune proinflammatory progression are altered in females as a consequence of stress (TNF), or with disparate IL1R1 stress-response changes between SAC and PAE (Figure 5B and Table 3). IL-10, as an endogenous anti-inflammatory cytokine showing compensatory upregulation upon inflammatory cytokine signaling, is robustly increased in females with PAE that are also exposed to maternal separation stress (Figure 5B; Table 3).

In the hypothalamus, blunted CCL2 (in males), IL1R1 and IL-10 (in females) with strong trends toward blunted TNF levels as a consequence of PAE are observed (Figure 5C; Table 3). The extent of low hypothalamic mRNA neuroimmune factors under basal conditions and blunted in response to stress in offspring with PAE consistently extends to a large number of proinflammatory indicators, as shown by blunted glial activation (astrocytes and microglia; Figure 3C; Table 3), factors associated with the TLR4 signaling cascade (HMGB1, TLR4, NFKBIA, and NLRP3; Figure 4C; Table 3), that were revealed predominantly in female offspring. Even strong trends in reduced CCL2 expression are shown in females (Figure 5C). The observed data from hypothalamic tissue are remarkably consistent, and while speculative, suggest that the underlying hypothalamic process may involve an exaggerated stress *hypo*responsive period. That is, during later life stressors, the hypothalamus may be reprogramed as less responsive to elevated circulating glucocorticoids, with diminished glucocorticoid receptor function until elevated glucocorticoid levels at longer-durations are achieved before the activation and downstream impact by glucocorticoids occur.

10.3389/fnins.2023.1203557

TABLE 4 Protein from amygdala (pg/100ng).

		CRH						IL-β						FKBP5						NLRP3					
		SAC			PAE			SAC			PAE			SAC			PAE			SAC			PAE		
		AVE	SD	N	AVE	SD	N	P	AVE	SD	N	P	AVE	SD	N	AVE	SD	N	p	AVE	SD	N	AVE	SD	N	p
M	No stress	734.6	539.8	7	1243.5	906.3	6	*	0.9	0.9	7	# 1.5	0.98	6	#	16.6	10.5	5	NS	30.2	26.6	6	NS	51.0	33.7	7	73.7	49.7	6	NS
M	Stress	654.8	202.8	6	1320.1	538	3	*	0.7	0.3	7	# 1.5	0.6	3	#	12.6	7.6	6	NS	17.6	10.2	3	NS	44.7	27.4	7	61.3	1.8	2	NS
F	No stress	1171.2	935.0	9	773.3	209.4	6	NS	0.9	0.9	10	0.7	0.3	6	NS	15.3	14.3	9	NS	12.3	5.9	6	NS	41.2	23.0	9	46.7	21.4	6	NS
F	Stress	630.9	602.4	8	558.6	346.9	4	NS	0.7	0.4	8	0.6	0.3	4	NS	12.2	7.6	8	NS	9.2	6.1	4	NS	38.2	18.7	8	44.4	35.2	4	NS

Within sex protein analysis (2-way ANOVAs) from pre-processed samples remaining from mRNA extraction from the amygdala. Select targets were analyzed: corticotropin releasing hormone (CRH); interleukin-1 beta (IL-1β), FK506-binding protein 51 (FKBP5), and NOD-like receptor family pyrin domain-containing protein 3 (NLRP3). Prenatal alcohol exposure (PAE) resulted in elevated CRH protein in male offspring independent of stress exposure ($F_{(1,18)} = 4.617$, $p < 0.05$), with a strong trend toward a significant elevation of IL-1β protein in male offspring with PAE independent of stress exposure ($F_{(1,19)} = 4.132$, $p = 0.05$) was revealed. NS, not significant; *$p < 0.05$, #$p = 0.05$. * Main effect of PAE: $F(1,18) = 4.617$, $p = 0.045$. # Main effect of PAE: $F(1,19) = 4.132$, $p = 0.056$. AVP, arginine vasopressin; GAS5, growth arrest specific 5; FKBP4, FK506-binding protein 52; GFAP, glial fibrillary acid protein; TMEM119, transmembrane protein 119; HMGB1, high mobility group box 1; TLR4, toll-like receptor 4; NFKBIA, NF-κB inhibitor alpha; NLRP3; IL1B; TNF, tumor necrosis factor alpha; CCL2, C–C motif chemokine ligand 2; IL1R1, interleukin-1 receptor 1; IL10, interleukin-10.

While an earnest attempt was made to measure protein levels of CRH, FKBP5, NLRP3 and IL-1β from the amygdala, only CRH protein from males revealed significant increases relative to controls without PAE (Table 4). Considering the pattern of CRH mRNA together with protein CRH in the male amygdala, the data suggest that protein levels retrieved from these samples are too low to achieve interpretable results. Moreover, due to loss of material, large discrepancies in samples sizes for various targets resulted, and the resultant data analyses are limited in this respect. No additional changes in protein levels were observed.

The amygdala is uniquely positioned to regulate responses to psychogenic stressors, as cortical association areas project to the amygdala, and in turn, the amygdala influences the function of critical stress-integrative brain areas such as the hippocampus and hypothalamus through direct amygdala-hippocampal (Stefanacci et al., 1996; Leal et al., 2017; Zheng et al., 2019) and amygdala-hypothalamic circuitry (Alexander et al., 2012). In addition, the amygdala is characterized as the fundamental brain area supporting fear-related behaviors such that a perceived threat is immediately processed as dangerous (Murison, 2016; Godoy et al., 2018) with amygdaloid activation being important for emotional retrieval and analysis of any given stressor. The amygdala can directly stimulate components of brain stress-response circuits via CRH neuropeptide release in (a) an autocrine manner within the amygdala and also (b) at more distant sites such as in the hippocampus (Tsigos et al., 2000). Notably, CRH peptidergic neurons in the amygdala are activated by glucocorticoids and upon activation, lead to the stimulation of the stress circuitry and fear/anxiety (Kolber et al., 2008). The amygdala-hippocampus circuit is bidirectional, and under normal conditions, the hippocampus can exert a tonic and evoked inhibitory effect on CRH neurons of the amygdala. Indeed, the hippocampus plays an important role in shutting off the HPA stress response [(Tsigos et al., 2000) for Review].

In light of this background concerning hippocampal influences on amygdala function, one aspect of the CNS stress-response system examined by the current report is the potential impact that PAE exerts on general amygdaloid responses to a single, acute stress (maternal separation). The current data demonstrate pronounced changes in mRNA expression of CRH and AVP, both of which are significantly elevated in the amygdala (Figure 1A). Unexpectedly, these changes are observed from tissue derived from females with PAE and not from males.

Under non-pathological conditions, the ventral hippocampus has been characterized to influence hypothalamic responses resulting in activation of hypothalamic subnuclei. The present data show that blunted AVP mRNA expression is observed in males (Figure 1B), which may be a consequence of dysregulated ventral hippocampal influences on hypothalamic subnuclei (e.g., lateral hypothalamic area) by PAE. However, meaningful mRNA changes of CRH in the hypothalamus were not observed in neither males nor females.

The current data also show that not only are stress-associated factors elevated in the amygdala following PND10 maternal separation, but also factors that disrupt glucocorticoid receptor signaling. Glucocorticoid receptors are a key effector element of the HPA stress response (De Kloet et al., 1988; Oakley and Cidlowski, 2013). Glucocorticoid receptors interact with factors that function to fine tune the HPA stress response, thereby regulating glucocorticoid receptor signaling or its sensitivity. GAS5 is a long non-coding RNA

expressed throughout the body originally found to have tumor suppressor activity by arresting the growth cycle of stressed cells, but also promotes apoptosis and acts to remove micro-RNA, ultimately decreasing glucocorticoid-dependent transcription of genes; it essentially acts as a decoy glucocorticoid response element (GRE) within the cell nucleus (Petta et al., 2016; Yu and Hann, 2019). The current report reveals that transcriptional expression of GAS5 is elevated in the male hippocampus, and to a much greater degree, in the female amygdala of PAE offspring following maternal separation stress (Figures 2A,B). The data support the possibility that glucocorticoid receptor signaling is reduced only in PAE offspring, which is unmasked by the secondary challenge of an acute maternal separation stress in females.

Interestingly, prenatal arsenic exposure induced sex-specific differences in the expression of GAS5 mRNA bound to the glucocorticoid receptor in the developing telencephalon (gestational days 14–18) (Caldwell et al., 2018), which includes the neocortex and the hippocampus (Hebert and Fishell, 2008). Arsenic has been characterized to impact the glucocorticoid and HPA axis system (Tyler and Allan, 2014). The data by Caldwell and colleagues (Caldwell et al., 2018) demonstrate that arsenic-exposed female telencephalon revealed relatively lower bound GAS5-to-glucocorticoid receptor compared to males, suggesting that males undergo reduced control over telencephalic glucocorticoid signaling and/or regulation during this critical gestational period. That is, during late gestational periods, glucocorticoids facilitate fetal neuronal maturation, axon remodeling and cell survival (De Kloet et al., 1988). Note that in the current report, GAS5 in female hippocampus with PAE is significantly lower (Figure 2A; Table 3) compared to the opposite trend observed in male hippocampus. While speculative, reduced glucocorticoid receptor signaling during this late gestational period may impact postnatal corticolimbic development resulting altered responses to stress during later life, particularly in males.

However, while lower, presumably protective GAS5 mRNA levels are demonstrated in the female hippocampus from PAE, a striking elevation of GAS5 in the female amygdala with PAE is revealed upon stress exposure (Figure 2B). The data are additionally striking in that no significant alterations are observed in the male amygdala of any glucocorticoid receptor signaling regulator examined in the current report (GAS5, FKBP5, and FKBP4), suggesting that adverse stress responses between males and females are regulated by different corticolimbic areas. Prior reports have demonstrated sex differences in glucocorticoid dysregulation involving hippocampal pathways, and a discussion of the data considers the possibility that PAE impacts glucocorticoid signaling in different pathways of the female brain (Caldwell et al., 2018). Our current data support and extend the differential impact of PAE between male and female limbic pathways, and especially following stress.

Glucocorticoid receptors are present in the cytoplasm in a complex with other proteins including chaperone proteins and FKBP51 (encoded by FKBP5) (Schiene-Fischer and Yu, 2001; Oakley and Cidlowski, 2013) that ultimately reduces glucocorticoid receptor signaling (Zannas et al., 2016). In further support that PAE dysregulates glucocorticoid receptor signaling, elevated levels of FKBP5 are observed in the hippocampus and, again to a greater magnitude, in the amygdala following stress (Figures 2A,B; Table 3). Significantly increased FKBP5 may act to further reduce the affinity of glucocorticoid receptor-glucocorticoid ligand binding, as has been previously considered (Schiene-Fischer and Yu, 2001). An additional mechanism by which FKBP51 may alter glucocorticoid receptor signaling is via FKBP51's direct interaction with the IKK complex (scaffold and isomerase activity) that ultimately increases NF-kB activation (Romano et al., 2015). NF-kB is a pivotal transcription factor that regulates the expression of several potent proinflammatory cytokines such as IL-1β, which is increased in the hippocampus and amygdala following stress and reduces glucocorticoid receptor signaling (Sugama et al., 2011; Wohleb et al., 2011).

The current study additionally examined the transcriptional expression of FKBP52, encoded by the FKBP4 gene, as it promotes high affinity binding of glucocorticoid receptors with glucocorticoids through interactions with microtubule proteins and thus facilitates the nuclear translocation of this complex (Schiene-Fischer and Yu, 2001; Davies et al., 2002). While FKBP51 and FKBP52 compete for binding to the glucocorticoid receptor in the cytoplasm, evidence demonstrates that in the presence of both FKBP52 and FKBP51, the glucocorticoid receptor preferentially associates with FKBP51 (Barent et al., 1998). The data from the current report demonstrate that elevated transcriptional expression of FKBP4 is present in male hippocampus from offspring with PAE and maternal separation stress (Figure 2A; Table 3), and to a large degree in female amygdala from offspring with PAE and stress exposure (Figure 2B; Table 3). Given that elevated FKBP51 binds glucocorticoid receptors reducing glucocorticoid ligand binding and preferential glucocorticoid receptor-FKBP51 occurs in the presence of FKBP52, an examination of the FKBP5:FKBP4 ratio was additionally performed. The data show that significantly elevated FKBP5:FKBP4 is present only in the hypothalamus of PAE female offspring, further supporting the possibility that PAE reduces glucocorticoid receptor signaling. Together, the observation that increased GAS5 with concurrent elevations of FKBP5 in the hippocampus, and to a much greater degree, in the amygdala of PAE offspring following maternal separation stress support the possibility that PAE dysregulates CRH/AVP actions and glucocorticoid receptor signaling in the amygdaloid-hippocampal circuit response to early life stress.

Evidence is mounting that adverse CNS function from PAE offspring is due to elevated expression of brain proinflammatory cytokines, chemokines, and increased activation of related immune receptors and glia (Drew and Kane, 2014; Drew et al., 2015; Noor and Milligan, 2018). Further, the possibility that dysregulated neuroimmune function may adversely impact the brain stress-response and neuroendocrine system has been emerging for a number of years (Weinberg, 1989; Zhang et al., 2005; Hellemans et al., 2008, 2010; Bodnar et al., 2016; Raineki et al., 2017; Lam et al., 2018). Given cytokines are now characterized to act as important contributors to healthy brain development (Smith et al., 2007; Jakovcevski et al., 2009; Stephan et al., 2012), alterations in the levels and regulation of a number of immune-related factors can wreak havoc on brain function, including the brain stress-response system. The current report extends this prior work demonstrating that significantly increased amygdaloid microglial activation is present in female offspring with PAE following maternal separation stress (Figure 3B; Table 3), suggesting that the consistent interaction of PAE and early life stress on glucocorticoid signaling blockers, and proinflammatory signaling factors may be mediated by microglial activation. However, not all brain areas examined demonstrated consistent microglial activation, as blunted hypothalamic microglial activation is observed in female PAE

offspring (Figure 3C; Tables 2, 3), with no such changes occurring in male PAE offspring.

Activated TLR4 results in the synthesis of a number of proinflammatory factors even following non-tissue damaging stressors. For example, non-physiological stress (i.e., maternal separation) can induce the release of classic immune danger-associated molecular patterns (DAMPs) such as the high-mobility group box 1 (HMGB1) independently of cell necrosis (Fleshner et al., 2017; Johnson et al., 2019). HMGB1 released from neurons, glia and immune cells activates TLR4. Following TLR4 activation by DAMPs, intracellular signaling mediated by myeloid differentiation factor 88 (MyD88) that ultimately induces activation of the NFkB transcription factor that initiates the synthesis of a number of proinflammatory cytokines including tumor necrosis factor-α (TNF-α, encoded by TNF), and precursor proteins pro-IL-1β (encoded by IL1B), pro-caspase-1 and the inflammasome, Nod-like receptor family pyrin domain containing 3 (NLRP3). Activated NLRP3 interacts with pro-caspase-1 to form the NLRP3 inflammasome protein complex, allowing for caspase-1 activation and consequent conversion of pro-IL-1β to mature, active IL-1β (Liu et al., 2017). Termination of active NFkB transcription is based on NFkB-dependent gene transcription of I kappa B-alpha (IkBa), an inhibitory subunit encoded by the NFKBIA gene (Bottero et al., 2003). Thus, quantification of NFkB activity is best captured by assessing gene synthesis encoding the protein IκB-α because induction of NFkB is reliably followed by NFKBIA mRNA synthesis, and a reduction in NFkB transcriptional activity is reflected in a reduction in NFKBIA mRNA. Notably, stabilization and accumulation of NFKBIA does not occur, which allows for the real time examination of NFKBIA mRNA levels to indirectly assess NFkB activity (Bottero et al., 2003).

In support of this background, the data from the current report reveals a striking increase in factors characterized to be induced following TLR4 activation predominantly in amygdala of female PAE offspring in response to maternal separation stress (Figure 4B; Table 3). Compared to prenatal control exposed offspring, reliable increases in mRNA for HMGB1, TLR4, NFKBIA, NLRP3 as well as IL1B are observed in the amygdala of offspring with PAE in response to stress, suggesting a primed proinflammatory state is created by PAE that is triggered by the acute stressor. It is notable that the significant alterations in these factors are observed predominantly in females rather than males. However, significant TLR4 and NLRP3 mRNA increases are observed in hippocampus of male PAE offspring regardless of stress exposure (Figure 4A; Table 3), while no changes in TLR4-associated factors were present in the male amygdala, consistent with a lack of astrocyte and microglial activation. Further, the hypothalamus from male offspring with PAE reveals blunted astrocyte activation as well as a non-significant trend toward blunted microglial activation. Combined, the data suggest that during early postnatal life, stress-induced increases in TLR4-related factors are observed different limbic structures between males and females, with some factors altered in the male hippocampus, and a large majority of these factors altered in female hippocampus and amygdala. One possibility may be that with regard to neuroimmune dysregulation, males may have greater protection against stress-induced neuroimmune dysregulation, but may be more vulnerable to stress-induced glucocorticoid receptor insensitivity.

The pathophysiology of PAE that is mediated by proinflammatory factors that can influence TLR4 activation and downstream cellular signaling. These factors include TNFα, CCL2, IL-1R1 alterations, and compensatory production of the and the anti-inflammatory cytokine, IL-10 (Noor and Milligan, 2018). Brain TNFα and CCL2 are upregulated as a consequence of TLR4 activation following alcohol exposure (Alfonso-Loeches et al., 2010; Montesinos et al., 2016; Pascual et al., 2017), and other recent reports suggest that PAE leads to suppressed anti-inflammatory IL-10 expression in peripheral and central nervous tissue (Noor et al., 2017; Sanchez et al., 2019; Noor et al., 2020). Notably, IL-10 is well-characterized to limit the actions of IL-1β, TNFα and CCL2, in addition to a number of other proinflammatory factors (Foey et al., 1998). The data from the current report demonstrate elevated IL1R1 mRNA is unmasked in the hippocampus of female offspring with PAE due to a stressor, in support of IL-1R1 brain elevations from inflammatory insults (Andre et al., 2005). Hippocampal IL10 mRNA elevations are observed only in stressed PAE male offspring (Figure 5A; Tables 2, 3), suggesting that IL-10 in males may be one mechanism conferring protection from stress-induced neuroimmune alterations.

Sex-specific outcomes as a consequence of PAE have been documented demonstrating sexually dimorphic effects of activity-dependent hippocampal glucocorticoid receptor protein levels (Caldwell et al., 2018), as well as HPA activity in PAE offspring (Weinberg et al., 2008; Lam et al., 2018; Lussier et al., 2021). While the inflammatory effects between PAE and/or stress on placental cytokines are similar (Ruffaner-Hanson et al., 2022), the levels of these inflammatory factors are distinctly different in male versus female fetuses (Terasaki and Schwarz, 2016). While speculative, the current data demonstrating consistent elevations in stress-associated and immune-related factors in the amygdala of PAE females, and blunted hypothalamic expression of many of these same markers suggests that PAE predisposes females to dysregulated limbic stress responses (e.g., CRH, AVP, GAS5, FKBP5 and FKBP4) as a consequence of altered glial and TLR4-assoicated factors. Interestingly, females often demonstrate an increased incidence of immune disorders and increased brain proinflammatory cytokine gene activation in animal models also expressing depressive-like behaviors (Whitacre, 2001; Tonelli et al., 2008). Thus, the sensitized female limbic pathways from PAE due to underlying alterations in the stress and neuroimmune axis may be of particular relevance to understanding the development of mood disorders later in life in individuals with an FASD (Hellemans et al., 2008; Hagan et al., 2016; van Bodegom et al., 2017; Wang et al., 2019). If dysregulated limbic cytokine expression is ultimately found to be critical in the neuropathology of mood disorders, the intriguing possibility emerges that treatment strategies can be identified that target re-balancing the brain cytokine milieu in individuals living with FASD.

In conclusion, our sex-specific findings of robustly elevated transcriptional expression of key stress-related neuropeptides as well as TLR4 signaling pathway factors in the female amygdala that is unmasked by early postnatal maternal separation stress provides new insight into how PAE may remodel developing brain areas responsible for integrating the stress response during early and adult life. The data further reveal that PAE *per se*, is insufficient to alter basal transcription of stress-related neuropeptides and TLR4 neuroimmune factors, but instead, changes in gene expression are unmasked only following stressor exposure. Thus, together the results support our hypothesis that PAE sensitizes key stress-integrative limbic circuits such that significant exaggerated responses in the amygdala and blunted

responses in the hypothalamus are unmasked due to early life stress. Prior work demonstrates a unique cytokine profile such as IL-1β and TNFα, from PAE occurs in the hippocampus, prefrontal cortex and the hypothalamus depending on early postnatal age, with blunted patterns of expression observed in the hypothalamus (Bodnar et al., 2016). This work suggests that even subtle changes in brain cytokine expression levels may act to alter the course of normal brain development. It is possible that in the PAE brain, even minor stressors during early postnatal life may be sufficient to exert enduring developmental changes.

Data availability statement

The original contributions presented in the study are included in the article/supplementary material, further inquiries can be directed to the corresponding author.

Ethics statement

The animal study was reviewed and approved by University of New Mexico Animal Care and Use Committee.

Author contributions

CR–H performed all the real-time PCRs and statistical analysis, and prepared the first draft of the manuscript. AF-O performed the protein ELISAs and statistical analyses. MS participated in tissue collection. KC and AA contributed to conception and design of the study, generated the mouse model of prenatal alcohol exposure, and collected tissue. EM contributed to conception and design of the study, participated in collection of tissues, assisted in statistical analyses, and prepared the manuscript. DS and CV supported the generation of the mouse model of prenatal alcohol exposure. SN contributed to tissue collection, real-time PCR data collection, statistical analysis and edited the manuscript. All authors contributed to the article and approved the submitted version.

Funding

The experiments conducted to generate this manuscript were funded by the NIH NIAAA 2P50 AA022534, and R01-AA025967.

Acknowledgments

We thank Nikolaos Mellios, Associate Professor of Neuroscience at the University of New Mexico, Health Sciences Center for access to equipment for our group to perform real time PCR, and providing expertise related to trouble-shooting mRNA data when needed.

Conflict of interest

The authors declare that the research was conducted in the absence of any commercial or financial relationships that could be construed as a potential conflict of interest.

Publisher's note

All claims expressed in this article are solely those of the authors and do not necessarily represent those of their affiliated organizations, or those of the publisher, the editors and the reviewers. Any product that may be evaluated in this article, or claim that may be made by its manufacturer, is not guaranteed or endorsed by the publisher.

References

Alexander, N., Klucken, T., Koppe, G., Osinsky, R., Walter, B., Vaitl, D., et al. (2012). Interaction of the serotonin transporter-linked polymorphic region and environmental adversity: increased amygdala-hypothalamus connectivity as a potential mechanism linking neural and endocrine Hyperreactivity. *Biol. Psychiatry* 72, 49–56. doi: 10.1016/j.biopsych.2012.01.030

Alfonso-Loeches, S., Pascual-Lucas, M., Blanco, A. M., Sanchez-Vera, I., and Guerri, C. (2010). Pivotal role of TLR4 receptors in alcohol-induced neuroinflammation and brain damage. *J. Neurosci. Off. J. Soc. Neurosci.* 30, 8285–8295. doi: 10.1523/JNEUROSCI.0976-10.2010

Andre, R., Lerouet, D., Kimber, I., Pinteaux, E., and Rothwell, N. J. (2005). Regulation of expression of the novel IL-1 receptor family members in the mouse brain. *J. Neurochem.* 95, 324–330. doi: 10.1111/j.1471-4159.2005.03364.x

Barent, R. L., Nair, S. C., Carr, D. C., Ruan, Y., Rimerman, R. A., Fulton, J., et al. (1998). Analysis of FKBP51/FKBP52 chimeras and mutants for Hsp90 binding and association with progesterone receptor complexes. *Mol. Endocrinol. (Baltimore, MD)* 12, 342–354. doi: 10.1210/mend.12.3.0075

Bodnar, T. S., Hill, L. A., and Weinberg, J. (2016). Evidence for an immune signature of prenatal alcohol exposure in female rats. *Brain Behav. Immun.* 58, 130–141. doi: 10.1016/j.bbi.2016.05.022

Bodnar, T. S., Raineki, C., Wertelecki, W., Yevtushok, L., Plotka, L., et al. (2020). Immune network dysregulation associated with child neurodevelopmental delay: modulatory role of prenatal alcohol exposure. *J. Neuroinflammation* 17:39. doi: 10.1186/s12974-020-1717-8

Bottero, V., Imbert, V., Frelin, C., Formento, J. L., and Peyron, J. F. (2003). Monitoring NF-kappa B transactivation potential via real-time PCR quantification of I kappa B-alpha gene expression. *Mol. Diagn.* 7, 187–194. doi: 10.2165/00066982-200307030-00008

Brady, M. L., Allan, A. M., and Caldwell, K. K. (2012). A limited access mouse model of prenatal alcohol exposure that produces long-lasting deficits in hippocampal-dependent learning and memory. *Alcohol. Clin. Exp. Res.* 36, 457–466. doi: 10.1111/j.1530-0277.2011.01644.x

Caldwell, K. K., Goggin, S. L., Tyler, C. R., and Allan, A. M. (2014). Prenatal alcohol exposure is associated with altered subcellular distribution of glucocorticoid and mineralocorticoid receptors in the adolescent mouse hippocampal formation. *Alcohol. Clin. Exp. Res.* 38, 392–400. doi: 10.1111/acer.12236

Caldwell, K. K., Hafez, A., Solomon, E., Cunningham, M., and Allan, A. M. (2018). Arsenic exposure during embryonic development alters the expression of the long noncoding RNA growth arrest specific-5 (Gas5) in a sex-dependent manner. *Neurotoxicol. Teratol.* 66, 102–112. doi: 10.1016/j.ntt.2017.11.003

Caldwell, K. K., Solomon, E. R., Smoake, J. J. W., Djatche de Kamgaing, C. D., and Allan, A. M. (2018). Sex-specific deficits in biochemical but not behavioral responses to delay fear conditioning in prenatal alcohol exposure mice. *Neurobiol. Learn. Mem.* 156, 1–16. doi: 10.1016/j.nlm.2018.10.002

Charney, D. S. (2004). Psychobiological mechanisms of resilience and vulnerability: implications for successful adaptation to extreme stress. *Am. J. Psychiatr.* 161, 195–216. doi: 10.1176/appi.ajp.161.2.195

Chen, H., and Jiang, Z. (2013). The essential adaptors of innate immune signaling. *Protein Cell* 4, 27–39. doi: 10.1007/s13238-012-2063-0

Council, N.R Guide for the care and use of laboratory animals. (2011); National Academies Press: Washington (DC).

Daun, J. M., Ball, R. W., and Cannon, J. G. (2000). Glucocorticoid sensitivity of interleukin-1 agonist and antagonist secretion: the effects of age and gender. *Am. J. Phys. Regul. Integr. Comp. Phys.* 278, R855–R862. doi: 10.1152/ajpregu.2000.278.4.R855

Davies, T. H., Ning, Y.-M., and Sánchez, E. R. (2002). A new first step in activation of steroid receptors. *J. Biol. Chem.* 277, 4597–4600. doi: 10.1074/jbc.C100531200

de Kloet, E. R., Rosenfeld, P., Van Eekelen, J. A. M., Sutanto, W., and Levine, S. (1988). "Stress, glucocorticoids and development" in *Biochemical Basis of Functional Neuroteratology -permanent Effects of Chemicals on the Developing Brain*. eds. G. J. Boer et al. (Elsevier), 73, 101–120.

Drew, P. D., Johnson, J. W., Douglas, J. C., Phelan, K. D., and Kane, C. J. M. (2015). Pioglitazone blocks ethanol induction of microglial activation and immune responses in the hippocampus, cerebellum, and cerebral cortex in a mouse model of fetal alcohol spectrum disorders. *Alcohol. Clin. Exp. Res.* 39, 445–454. doi: 10.1111/acer.12639

Drew, P. D., and Kane, C. J. (2014). Fetal alcohol spectrum disorders and neuroimmune changes. *Int. Rev. Neurobiol.* 118, 41–80. doi: 10.1016/B978-0-12-801284-0.00003-8

Elenkov, I. J., Wilder, R. L., Chrousos, G. P., and Vizi, E. S. (2000). The sympathetic nerve--an integrative interface between two supersystems: the brain and the immune system. *Pharmacol. Rev.* 52, 595–638.

Fleshner, M., Frank, M., and Maier, S. F. (2017). Danger signals and Inflammasomes: stress-evoked sterile inflammation in mood disorders. *Neuropsychopharmacology* 42, 36–45. doi: 10.1038/npp.2016.125

Foey, A. D., Parry, S. L., Williams, L. M., Feldmann, M., Foxwell, B. M. J., and Brennan, F. M. (1998). Regulation of monocyte IL-10 synthesis by endogenous IL-1 and TNF-alpha: role of the p38 and p42/44 mitogen-activated protein kinases. *J. Immunol.* 160, 920–928. doi: 10.4049/jimmunol.160.2.920

Gabriel, K., Hofmann, C., Glavas, M., and Weinberg, J. (1998). The hormonal effects of alcohol use on the mother and fetus. *Alcohol Health Res. World* 22, 170–177.

Gartstein, M. A., and Skinner, M. K. (2018). Prenatal influences on temperament development: the role of environmental epigenetics. *Dev. Psychopathol.* 30, 1269–1303. doi: 10.1017/S0954579417001730

Godoy, L. D., Rossignoli, M. T., Delfino-Pereira, P., Garcia-Cairasco, N., and de Lima Umeoka, E. H. (2018). A comprehensive overview on stress neurobiology: basic concepts and clinical implications. *Front. Behav. Neurosci.* 12:127. doi: 10.3389/fnbeh.2018.00127

Goujon, E., Layé, S., Parnet, P., and Dantzer, R. (1997). Regulation of cytokine gene expression in the central nervous system by glucocorticoids: mechanisms and functional consequences. *Psychoneuroendocrinology* 22, S75–S80. doi: 10.1016/S0306-4530(97)00009-7

Grubbs, F. E. (1969). Procedures for detecting outlying observations in samples. *Technometrics* 11, 1–21. doi: 10.1080/00401706.1969.10490657

Haddad, J. J., Saadé, N. E., and Safieh-Garabedian, B. (2002). Cytokines and neuro–immune–endocrine interactions: a role for the hypothalamic–pituitary–adrenal revolving axis. *J. Neuroimmunol.* 133, 1–19. doi: 10.1016/S0165-5728(02)00357-0

Hagan, J. F., Balachova, T., Bertrand, J., Chasnoff, I., Dang, E., Fernandez-Baca, D., et al. (2016). Neurobehavioral disorder associated with prenatal alcohol exposure. *Pediatrics* 138. doi: 10.1542/peds.2015-1553

Hebert, J. M., and Fishell, G. (2008). The genetics of early telencephalon patterning: some assembly required. *Nat. Rev. Neurosci.* 9, 678–685. doi: 10.1038/nrn2463

Hellemans, K. G. C., Sliwowska, J. H., Verma, P., and Weinberg, J. (2010). Prenatal alcohol exposure: fetal programming and later life vulnerability to stress, depression and anxiety disorders. *Neurosci. Biobehav. Rev.* 34, 791–807. doi: 10.1016/j.neubiorev.2009.06.004

Hellemans, K. G., Verma, P., Yoon, E., Yu, W., and Weinberg, J. (2008). Prenatal alcohol exposure increases vulnerability to stress and anxiety-like disorders in adulthood. *Ann. N. Y. Acad. Sci.* 1144, 154–175. doi: 10.1196/annals.1418.016

Iglewicz, B., and Hoaglin, D. C. *How to Detect and Handle Outliers. ASQC Basic References in Quality Control*. (1993), Milwaukee: ASQC Quality Press, 87.

Jakovcevski, I., Filipovic, R., Mo, Z., Rakic, S., and Zecevic, N. (2009). Oligodendrocyte development and the onset of myelination in the human fetal brain. *Front. Neuroanat.* 3:5. doi: 10.3389/neuro.05.005.2009

Johnson, J. D., Barnard, D. F., Kulp, A. C., and Mehta, D. M. (2019). Neuroendocrine regulation of brain cytokines after psychological stress. *J. Endocr. Soc.* 3, 1302–1320. doi: 10.1210/js.2019-00053

Kilkenny, C., Browne, W. J., Cuthill, I. C., Emerson, M., and Altman, D. G. (2010). Improving bioscience research reporting: the ARRIVE guidelines for reporting animal research. *J. Pharmacol. Pharmacother.* 1, 94–99. doi: 10.4103/0976-500X.72351

Kolber, B. J., Roberts, M. S., Howell, M. P., Wozniak, D. F., Sands, M. S., and Muglia, L. J. (2008). Central amygdala glucocorticoid receptor action promotes fear-associated CRH activation and conditioning. *Proc. Natl. Acad. Sci. U. S. A.* 105, 12004–12009. doi: 10.1073/pnas.0803216105

Lam, V. Y. Y., Raineki, C., Ellis, L., Yu, W., and Weinberg, J. (2018). Interactive effects of prenatal alcohol exposure and chronic stress in adulthood on anxiety-like behavior and central stress-related receptor mRNA expression: sex- and time-dependent effects. *Psychoneuroendocrinology* 97, 8–19. doi: 10.1016/j.psyneuen.2018.06.018

Leal, S. L., Noche, J. A., Murray, E. A., and Yassa, M. A. (2017). Age-related individual variability in memory performance is associated with amygdala-hippocampal circuit function and emotional pattern separation. *Neurobiol. Aging* 49, 9–19. doi: 10.1016/j.neurobiolaging.2016.08.018

Liu, T., Zhang, L., Joo, D., and Sun, S. C. (2017). NF-κB signaling in inflammation. *Signal Transduct. Target. Ther.* 2:17023. doi: 10.1038/sigtrans.2017.23

Livak, K. J., and Schmittgen, T. D. (2001). Analysis of relative gene expression data using real-time quantitative PCR and the 2(-Delta Delta C(T)) method. *Methods* 25, 402–408. doi: 10.1006/meth.2001.1262

Lu, J., Jiao, Z., Yu, Y., Zhang, C., He, X., Li, Q., et al. (2018). Programming for increased expression of hippocampal GAD67 mediated the hypersensitivity of the hypothalamic–pituitary–adrenal axis in male offspring rats with prenatal ethanol exposure. *Cell Death Dis.* 9, 1–17. doi: 10.1038/s41419-018-0663-1

Lussier, A. A., Bodnar, T. S., Moksa, M., Hirst, M., Kobor, M. S., and Weinberg, J. (2021). Prenatal adversity alters the epigenetic profile of the prefrontal cortex: sexually dimorphic effects of prenatal alcohol exposure and food-related stress. *Genes (Basel)* 12, 1773. doi: 10.3390/genes12111773

McGowan, P. O., and Matthews, S. G. (2018). Prenatal stress, glucocorticoids, and developmental programming of the stress response. *Endocrinology* 159, 69–82. doi: 10.1210/en.2017-00896

Montesinos, J., Alfonso-Loeches, S., and Guerri, C. (2016). Impact of the innate immune response in the actions of ethanol on the central nervous system. *Alcohol. Clin. Exp. Res.* 40, 2260–2270. doi: 10.1111/acer.13208

Moore, E. M., and Xia, Y. (2021). "Neurodevelopmental Trajectories Following Prenatal Alcohol Exposure." *Front. Hum. Neurosci.* 15:695855.

Murison, R. (2016). "Chapter 2–The Neurobiology of Stress" in *Neuroscience of Pain, Stress, and Emotion*. eds. M. al'Absi and M. A. Flaten (San Diego: Academic Press), 29–49.

Noor, S., and Milligan, E. D. (2018). Lifelong impacts of moderate prenatal alcohol exposure on Neuroimmune function. *Front. Immunol.* 9:1107. doi: 10.3389/fimmu.2018.01107

Noor, S., Sanchez, J. J., Sun, M. S., Pervin, Z., Sanchez, J. E., Havard, M. A., et al. (2020). The LFA-1 antagonist BIRT377 reverses neuropathic pain in prenatal alcohol-exposed female rats via actions on peripheral and central neuroimmune function in discrete pain-relevant tissue regions. *Brain Behav. Immun.* 87, 339–358. doi: 10.1016/j.bbi.2020.01.002

Noor, S., Sanchez, J. J., Vanderwall, A. G., Sun, M. S., Maxwell, J. R., Davies, S., et al. (2017). Prenatal alcohol exposure potentiates chronic neuropathic pain, spinal glial and immune cell activation and alters sciatic nerve and DRG cytokine levels. *Brain Behav. Immun.* 61, 80–95. doi: 10.1016/j.bbi.2016.12.016

Noor, S., Sun, M. S., Vanderwall, A. G., Havard, M. A., Sanchez, J. E., Harris, N. W., et al. (2019). LFA-1 antagonist (BIRT377) similarly reverses peripheral neuropathic pain in male and female mice with underlying sex divergent peripheral immune proinflammatory phenotypes. *Neuroimmunol. Neuroinflamm.* 2019, 1–32. doi: 10.20517/2347-8659.2019.18

Oakley, R. H., and Cidlowski, J. A. (2013). The biology of the glucocorticoid receptor: new signaling mechanisms in health and disease. *J. Allergy Clin. Immunol.* 132, 1033–1044. doi: 10.1016/j.jaci.2013.09.007

O'Connor, S., Morzorati, S., Christian, J., and Li, T. K. (1998). Alcohol-seeking behavior: the roles of the hypothalamic-pituitary-adrenal axis and the endogenous opioid system. *Alcohol Health Res. World* 22, 202–210. doi: 10.1111/j.1530-0277.1998.tb03639.x

Páez Pereda, M., Perez Castro, C., Costas, M., Nahmod, V. E., Stalla, G. K., Holsboer, F., et al. (1996). Glucocorticoids inhibit the autoregulatory induction of interleukin-1 in monocytes after endotoxin stimulation. *Neuroimmunomodulation* 3, 227–232. doi: 10.1159/000097275

Pariante, C. M., Pearce, B. D., Pisell, T. L., Sanchez, C. I., Po, C., Su, C., et al. (1999). The Proinflammatory cytokine, interleukin-1α, reduces glucocorticoid receptor translocation and function. *Endocrinology* 140, 4359–4366. doi: 10.1210/endo.140.9.6986

Pascual, M., Montesinos, J., Montagud-Romero, S., Forteza, J., Rodríguez-Arias, M., Miñarro, J., et al. (2017). TLR4 response mediates ethanol-induced neurodevelopment alterations in a model of fetal alcohol spectrum disorders. *J. Neuroinflammation* 14:145. doi: 10.1186/s12974-017-0918-2

Petta, I., Dejager, L., Ballegeer, M., Lievens, S., Tavernier, J., de Bosscher, K., et al. (2016). The Interactome of the glucocorticoid receptor and its influence on the actions of glucocorticoids in combatting inflammatory and infectious diseases. *Microbiol. Mol. Biol. Rev.* 80, 495–522. doi: 10.1128/MMBR.00064-15

Plagemann, A., Staudt, A., Gotz, F., Malz, U., Rohde, W., Rake, A., et al. (1998). Long-term effects of early postnatally administered Interleukin-1-beta on the hypothalamic-pituitary-adrenal (HPA) Axis in rats. *Endocr. Regul.* 32, 77–85.

Przybycien-Szymanska, M. M., Mott, N. N., and Pak, T. R. (2011). Alcohol dysregulates corticotropin-releasing-hormone (CRH) promoter activity by interfering with the negative glucocorticoid response element (nGRE). *PLoS One* 6:e26647. doi: 10.1371/journal.pone.0026647

Raineki, C., Bodnar, T. S., Holman, P. J., Baglot, S. L., Lan, N., and Weinberg, J. (2017). Effects of early-life adversity on immune function are mediated by prenatal environment: role of prenatal alcohol exposure. *Brain Behav. Immun.* 66, 210–220. doi: 10.1016/j.bbi.2017.07.001

Raineki, C., Morgan, E. J., Ellis, L., and Weinberg, J. (2019). Glucocorticoid receptor expression in the stress-limbic circuitry is differentially affected by prenatal alcohol exposure and adolescent stress. *Brain Res.* 1718, 242–251. doi: 10.1016/j.brainres.2019.05.019

Rash, J. A., Thomas, J. C., Campbell, T. S., Letourneau, N., Granger, D. A., Giesbrecht, G. F., et al. (2016). Developmental origins of infant stress reactivity profiles: a multi-system approach. *Dev. Psychobiol.* 58, 578–599. doi: 10.1002/dev.21403

Romano, S., Xiao, Y., Nakaya, M., D'Angelillo, A., Chang, M., Jin, J., et al. (2015). FKBP51 employs both scaffold and isomerase functions to promote NF-κB activation in melanoma. *Nucleic Acids Res.* 43, 6983–6993. doi: 10.1093/nar/gkv615

Ruffaner-Hanson, C., Noor, S., Sun, M. S., Solomon, E., Marquez, L. E., Rodriguez, D. E., et al. (2022). The maternal-placental-fetal interface: adaptations of the HPA axis and immune mediators following maternal stress and prenatal alcohol exposure. *Exp. Neurol.* 355:114121. doi: 10.1016/j.expneurol.2022.114121

Sanchez, J. J., Noor, S., Davies, S., Savage, D., and Milligan, E. D. (2017). Prenatal alcohol exposure is a risk factor for adult neuropathic pain via aberrant neuroimmune function. *J. Neuroinflammation* 14:254. doi: 10.1186/s12974-017-1030-3

Sanchez, J. J., Sanchez, J. E., Noor, S., Ruffaner-Hanson, C. D., Davies, S., Wagner, C. R., et al. (2019). Targeting the beta2-integrin LFA-1, reduces adverse neuroimmune actions in neuropathic susceptibility caused by prenatal alcohol exposure. *Acta Neuropathol. Commun.* 7:54. doi: 10.1186/s40478-019-0701-y

Schiene-Fischer, C., and Yu, C. (2001). Receptor accessory folding helper enzymes: the functional role of peptidyl prolyl cis/trans isomerases. *FEBS Lett.* 495, 1–6. doi: 10.1016/S0014-5793(01)02326-2

Smith, S. E. P., Li, J., Garbett, K., Mirnics, K., and Patterson, P. H. (2007). Maternal immune activation alters fetal brain development through Interleukin-6. *J. Neurosci.* 27, 10695–10702. doi: 10.1523/JNEUROSCI.2178-07.2007

Ståhlberg, A., Håkansson, J., Xian, X., Semb, H., and Kubista, M. (2004). Properties of the reverse transcription reaction in mRNA quantification. *Clin. Chem.* 50, 509–515. doi: 10.1373/clinchem.2003.026161

Stefanacci, L., Suzuki, W. A., and Amaral, D. G. (1996). Organization of connections between the amygdaloid complex and the perirhinal and parahippocampal cortices in macaque monkeys. *J. Comp. Neurol.* 375, 552–582. doi: 10.1002/(SICI)1096-9861(19961125)375:4<552::AID-CNE2>3.0.CO;2-0

Stephan, A. H., Barres, B. A., and Stevens, B. (2012). The complement system: an unexpected role in synaptic pruning during development and disease. *Annu. Rev. Neurosci.* 35, 369–389. doi: 10.1146/annurev-neuro-061010-113810

Sugama, S., Takenouchi, T., Sekiyama, K., Kitani, H., and Hashimoto, M. (2011). Immunological responses of astroglia in the rat brain under acute stress: interleukin 1 beta co-localized in astroglia. *Neuroscience* 192, 429–437. doi: 10.1016/j.neuroscience.2011.06.051

Terasaki, L. S., and Schwarz, J. M. (2016). Effects of moderate prenatal alcohol exposure during early gestation in rats on inflammation across the maternal-fetal-immune Interface and later-life immune function in the offspring. *J. Neuroimmune Pharmacol.* 11, 680–692. doi: 10.1007/s11481-016-9691-8

Tonelli, L. H., Holmes, A., and Postolache, T. T. (2008). Intranasal immune challenge induces sex-dependent depressive-like behavior and cytokine expression in the brain. *Neuropsychopharmacology* 33, 1038–1048. doi: 10.1038/sj.npp.1301488

Topper, L. A., Baculis, B. C., and Valenzuela, C. F. (2015). Exposure of neonatal rats to alcohol has differential effects on neuroinflammation and neuronal survival in the cerebellum and hippocampus. *J. Neuroinflammation* 12:160. doi: 10.1186/s12974-015-0382-9

Tsigos, C., Kyrou, I., Kassi, E., and Chrousos, G. P. (2000). "Stress, Endocrine Physiology and Pathophysiology" in *Endotext*. eds. K. R. Feingoldet al. (South Dartmouth (MA): MDText.com, Inc)

Tyler, C. R., and Allan, A. M. (2014). The effects of arsenic exposure on neurological and cognitive dysfunction in human and rodent studies: a review. *Curr. Environ. Health Rep.* 1, 132–147. doi: 10.1007/s40572-014-0012-1

van Bodegom, M., Homberg, J. R., and Henckens, M. J. A. G. (2017). Modulation of the hypothalamic-pituitary-adrenal Axis by early life stress exposure. *Front. Cell. Neurosci.* 11:87. doi: 10.3389/fncel.2017.00087

Wang, T., Wang, H. L., Liu, R., Wang, H., Zhang, Y., Sun, Y. X., et al. (2019). Early-life stress alters sleep structure and the excitatory-inhibitory balance in the nucleus accumbens in aged mice. *Chin. Med. J.* 132, 1582–1590. doi: 10.1097/CM9.0000000000000279

Weinberg, J. (1989). Prenatal ethanol exposure alters adrenocortical development of offspring. *Alcohol. Clin. Exp. Res.* 13, 73–83. doi: 10.1111/j.1530-0277.1989.tb00287.x

Weinberg, J., Sliwowska, J. H., Lan, N., and Hellemans, K. G. C. (2008). Prenatal alcohol exposure: foetal programming, the hypothalamic-pituitary-adrenal axis and sex differences in outcome. *J. Neuroendocrinol.* 20, 470–488. doi: 10.1111/j.1365-2826.2008.01669.x

Whitacre, C. C. (2001). Sex differences in autoimmune disease. *Nat. Immunol.* 2, 777–780. doi: 10.1038/ni0901-777

Wohleb, E. S., Hanke, M. L., Corona, A. W., Powell, N. D., Stiner, L. T. M., Bailey, M. T., et al. (2011). β-Adrenergic receptor antagonism prevents anxiety-like behavior and microglial reactivity induced by repeated social defeat. *J. Neurosci.* 31, 6277–6288. doi: 10.1523/JNEUROSCI.0450-11.2011

Yu, Y., and Hann, S. S. (2019). Novel tumor suppressor lncRNA growth arrest-specific 5 (GAS5) in human Cancer. *Onco. Targets. Ther.* 12, 8421–8436. doi: 10.2147/OTT.S221305

Zannas, A. S., Wiechmann, T., Gassen, N. C., and Binder, E. B. (2016). Gene–stress–epigenetic regulation of FKBP5: clinical and translational implications. *Neuropsychopharmacology* 41, 261–274. doi: 10.1038/npp.2015.235

Zhang, X., Sliwowska, J. H., and Weinberg, J., *Prenatal Alcohol Exposure and Fetal Programming: Effects on Neuroendocrine and Immune Function. Experimental Biology and Medicine*. Maywood, NJ, (2005); 230:376–388.

Zheng, J., Stevenson, R. F., Mander, B. A., Mnatsakanyan, L., Hsu, F. P. K., Vadera, S., et al. (2019). Multiplexing of Theta and alpha rhythms in the amygdala-hippocampal circuit supports pattern separation of emotional information. *Neuron* 102, 887–898.e5. doi: 10.1016/j.neuron.2019.03.025

Zhou, J.-N., and Fang, H. (2018). Transcriptional regulation of corticotropin-releasing hormone gene in stress response. *IBRO Reports* 5, 137–146. doi: 10.1016/j.ibror.2018.08.003

frontiers | Frontiers in Neuroscience

TYPE Original Research
PUBLISHED 28 June 2023
DOI 10.3389/fnins.2023.1192096

Check for updates

OPEN ACCESS

EDITED BY
Paola Tognini,
University of Pisa, Italy

REVIEWED BY
Sebastiano Bariselli,
National Institute on Alcohol Abuse and Alcoholism (NIH), United States
Rajesh Miranda,
Texas A&M University, United States

*CORRESPONDENCE
Daniel D. Savage
✉ dsavage@salud.unm.edu

RECEIVED 22 March 2023
ACCEPTED 30 May 2023
PUBLISHED 28 June 2023

CITATION
Davies S, Lujan KS, Rappaport EJ, Valenzuela CF and Savage DD (2023) Effect of moderate prenatal ethanol exposure on the differential expression of two histamine H3 receptor isoforms in different brain regions of adult rat offspring.
Front. Neurosci. 17:1192096.
doi: 10.3389/fnins.2023.1192096

COPYRIGHT
© 2023 Davies, Lujan, Rappaport, Valenzuela and Savage. This is an open-access article distributed under the terms of the Creative Commons Attribution License (CC BY). The use, distribution or reproduction in other forums is permitted, provided the original author(s) and the copyright owner(s) are credited and that the original publication in this journal is cited, in accordance with accepted academic practice. No use, distribution or reproduction is permitted which does not comply with these terms.

Effect of moderate prenatal ethanol exposure on the differential expression of two histamine H3 receptor isoforms in different brain regions of adult rat offspring

Suzy Davies, Kiana S. Lujan, Ella J. Rappaport, Carlos F. Valenzuela and Daniel D. Savage*

Department of Neurosciences, University of New Mexico School of Medicine, Albuquerque, NM, United States

We have reported that prenatal alcohol exposure (PAE) elevates histamine H_3 receptor (H3R) agonist-mediated inhibition of glutamatergic neurotransmission in the dentate gyrus. Here, we hypothesized that PAE alters the expression of two prominent H3R isoforms namely, the rH_{3A} and rH_{3C} isoforms, which have differing intrinsic activities for H3R agonists, in a manner that may contribute to heightened H3R function in PAE rats. In contrast to our predictions, we found different effects of sex and PAE in various brain regions with significant interactions between sex and PAE in dentate gyrus and entorhinal cortex for both isoforms. Subsequently, to confirm the PAE-and sex-induced differences on H3R isoform mRNA expression, we developed a polyclonal antibody selective for the rH_{3A} inform. Western blots of rH_{3A} mRNA-transfected HEK-293 cells identified a ~48kDa band of binding consistent with the molecular weight of rH_{3A}, thus confirming antibody sensitivity for rH_{3A} protein. In parallel, we also established a pan-H3R knockout mice line to confirm antibody specificity in rodent brain membranes. Both qRT-PCR and H3R agonist-stimulated [^{35}S]-GTPγS binding confirmed the absence of mH_{3A} mRNA and H3 receptor-effector coupling in H3R knockout (KO) mice. Subsequent western blotting studies in both rat and mouse brain membranes were unable to detect rH_{3A} antibody binding at ~48kDa. Rather, the H3RA antibody bound to a ~55kDa band in both rat and mouse membranes, including H3R KO mice, suggesting H3RA binding was not specific for H3Rs in rodent membranes. Subsequent LC/MS analysis of the ~55kDa band in frontal cortical membranes identified the highly abundant beta subunit of ATPase in both WT and KO mice. Finally, LC/MS analysis of the ~48kDa band from rH_{3A} mRNA-transfected HEK-293 cell membranes was able to detect rH_{3A} protein, but its presence was below the limits of quantitative reliability. We conclude that PAE alters rH_{3A} and rH_{3C} mRNA expression in some of the same brain regions where we have previously reported PAE-induced alterations in H3R-effector coupling. However, interpreting the functional consequences of altered H3R isoform expression was limited given the technical challenges of measuring the relatively low abundance of rH_{3A} protein in native membrane preparations.

KEYWORDS

prenatal alcohol (ethanol), histamine H3 receptor, *in situ* hybridization, western blotting, dentate gyrus, cerebral cortex

1. Introduction

Our laboratory has reported spatial and associative learning deficits in adult rat offspring whose mothers consumed moderate quantities of ethanol during pregnancy. These prenatal alcohol exposure (PAE)-induced learning deficits were more apparent with increasingly challenging versions of the behavioral tasks (Sutherland et al., 2000; Weeber et al., 2001; Savage et al., 2002, 2010). Further, baseline input/output physiological responses appeared intact in our PAE rat offspring, whereas more complex activity-dependent changes in synaptic plasticity were more sensitive to PAE (Sutherland et al., 1997; Savage et al., 1998; Varaschin et al., 2010). A series of combined neurochemical and physiologic studies (Perrone-Bizzozero et al., 1998; Savage et al., 2002; Galindo et al., 2004) provided evidence that PAE impairs presynaptic mechanisms associated with activity-dependent potentiation of glutamate release from perforant path terminals in dentate gyrus as one mechanism contributing to the synaptic plasticity and learning deficits observed in PAE rats.

We have since pursued the acquisition of agents with mechanisms of action that target the regulation of neurotransmitter release as potential therapeutic interventions for the synaptic plasticity and learning deficits we had observed in our PAE rats. One such class of so-called "cognition-enhancing" agents are the histamine H3 receptor (H3R) inverse agonists. H3Rs reside primarily on nerve terminals where they inhibit the release of a variety of transmitters including histamine (Arrang et al., 1983), other monoamines (Schlicker et al., 1988, 1989, 1993), acetylcholine (Clapham and Kilpatrick, 1992) and glutamate (Garduño-Torres et al., 2007). Collectively, H3R inverse agonists have been shown to interfere with H3R function, leading to enhanced neurotransmitter release, as well as to exhibit procognitive effects in a variety of animal models of learning and memory [see reviews by Esbenshade et al. (2008), Haas et al. (2008), Brioni et al. (2011), and Nikolic et al. (2014)].

Similar to these prior studies, we reported that the H3R inverse agonist ABT-239 ameliorated both contextual fear conditioning deficits and spatial memory deficits in PAE rats (Savage et al., 2010). Concurrently, in separate groups of control and PAE rats, we reported that ABT-239 reversed PAE-induced deficits in perforant path-dentate gyrus long-term potentiation (LTP) (Varaschin et al., 2010). Further, treatment of saccharin control rats with the selective H3R agonist methimepip mimicked the LTP deficit observed in saline-treated PAE rats (Varaschin et al., 2014). Currently, there is no evidence indicating that H3R function is altered in patients with FASD or that drugs acting at H3Rs affect patients with FASD differently than other patients. However, given our preclinical observations with ABT-239, the ongoing objective of our research program has been to establish a preclinical rationale for considering clinical trials in patients with FASD based on how PAE alters H3R function in our model of moderate prenatal alcohol exposure. Subsequently, our lab investigated whether PAE alters histamine H3R number or function in various regions. Radio-histochemical studies employing the selective H3R antagonist [^{3}H]-A349821 indicated that moderate PAE did not affect H3R density in any brain region measured (Varaschin et al., 2018). However, using the selective H3R agonist methimepip to stimulate [^{35}S]-GTPγS (GTP) binding as a measure of H3R receptor-effector coupling, we observed a significant enhancement of GTP binding in hippocampal and cerebrocortical regions of PAE rats, particularly at higher agonist concentrations (Varaschin et al., 2018). The functional significance of this heightened H3 receptor-effector coupling response in PAE rats was examined in dentate gyrus slices. The ability of methimepip to decrease the probability of glutamate release from dentate gyrus slices, noted as an increase in the paired-pulse ratio measure, was significantly elevated in PAE rats (Varaschin et al., 2018). Further, the concentrations of methimepip that lowered the probability of glutamate release were similar to the methimepip concentrations that enhanced GTP binding in dentate gyrus of PAE rats.

A closer examination of methimepip's stimulation of GTP binding indicated that binding increased over a nearly four-order-of-magnitude elevation in agonist concentration in both control and PAE rats (Varaschin et al., 2018). In contrast to agonist concentration-response curves occurring over roughly two orders of magnitude of increasing agonist concentration, which reflect the presence of a single non-interacting receptor binding site, agonist-response curves greater than two orders of magnitude suggest the presence of at least two non-interacting subpopulations of binding sites with differing affinities for binding agonist. Based on prior studies of H3R isoforms measured in expression systems (Drutel et al., 2001; Bakker, 2004; Bongers et al., 2007), we suspected that two functional rH3R isoforms namely, the rH_{3A} and the rH_{3C} isoforms, may be responsible for the methimepip-stimulated GTP binding concentration-response study described above. These two functional H3R isoforms, which are prominent in various higher brain regions (Drutel et al., 2001; Morisset et al., 2001), are splice variants of the same gene. However, due to alternative gene splicing, they differ in their size and pharmacologic properties. The rH_{3A}, the full-length (445 amino acid) isoform in rat, displays relatively lower agonist affinity, but higher intrinsic agonist activity, whereas the rH_{3C} isoform (397 amino acids) contains a 48 amino acid deletion in the middle of the third intracellular loop and exhibits higher agonist affinity, but lower intrinsic activity relative to the rH_{3A} (Drutel et al., 2001).

Given that H3R receptor-effector coupling was elevated in PAE rats in the absence of changes in the total H3R number (Varaschin et al., 2018), we hypothesized that PAE causes a net increase in the expression of the lower affinity, but higher intrinsic activity rH_{3A} isoform relative to the higher affinity, but lower intrinsic activity rH_{3C} isoform in PAE rat brain. We first tested this hypothesis by employing *in situ* hybridization to measure the binding density of radiolabeled cDNA probes for each of these two H3R isoforms in various brain regions. However, given the limitations of relating mRNA quantity with protein function (Allen et al., 2013; Moritz et al., 2019), we subsequently developed and characterized a polyclonal antibody to selectively target the rH_{3A} protein and attempted to measure rH_{3A} protein in various brain regions with the prediction that rH_{3A} protein would be elevated in the same brain regions of PAE rats where elevations in H3R agonist-stimulated GTP binding had been observed previously (Varaschin et al., 2018).

2. Materials and methods

2.1. Housing for Long-Evan rats

The University of New Mexico Health Sciences Center (UNM HSC) Institutional Animal Care and Use Committee (IACUC) approved all of the procedures involving the use of live rodents. All experiments were in compliance with the ARRIVE guidelines. The

Long-Evans rats used in these studies were purchased from Envigo Corporation (Indianapolis, IN, USA). Upon arrival at our UNM HSC Animal Resource Facility, the rats were single housed in static micro isolator cages with Envigo Tek-Fresh bedding at 22°C on a reverse 12-h dark/12-h light schedule (lights on from 2100 to 0900 h). They were provided irradiated Teklad Global 2920 Soy Protein Free rodent diet (Envigo) and water (chlorine dioxide treated in water bottles, autoclaved prior to use) *ad libitum*. Female rats arrived at around 6–7 weeks of age (125–150 g) and were approximately 9–10 weeks old at the time of breeding. The males were established breeders, 12 weeks old upon arrival, and 15 to 16 weeks old at the start of the breeding protocol. After one-week acclimation to the animal facility, baseline body weights for each female were obtained prior to the start of the pre-pregnancy drinking phase of the PAE paradigm.

2.2. Moderate prenatal ethanol exposure paradigm

The breeding and prenatal alcohol exposure (PAE) procedures for rats employed in this study were the same as described previously (Hamilton et al., 2014; Davies et al., 2023). Pre-pregnancy drinking levels in female rats were evaluated by gradually acclimating them to drinking 5% ethanol in 0.066% saccharin in tap water 4 h each day. The saccharin water contained 0% ethanol on the first and second day, 2.5% ethanol (v/v) on the third and fourth day, and 5% ethanol on the fifth day and thereafter. The drinking tubes were placed in the cages 1 h. after the onset of the dark phase. Daily ethanol consumption was measured using 55 mL volume conical beaded glass test tubes (25 mm × 150 mm; Fisher Scientific International, Waltham, MA, USA) with millimeter graduated markings, topped with a metal sipper tube with a stainless steel ball (Ancare Corporation, Bellmore, NY, USA) inserted in a white #4 rubber stopper (The Plasticoid Company, Elkton, MD, USA). Drinking tubes were filled daily to the 20 mm mark. At the end of each drinking session, the volume consumed was noted as a net change in the mm scale and converted to the volume consumed. The amount of ethanol consumed, expressed as g/kg body weight, was calculated using a daily weight extrapolated from weight data collected at the start and the end of each week. Upon completion of the pre-pregnancy drinking phase, the mean and standard deviation in 5% ethanol consumption from pre-pregnancy Day 5 to Day 14 was calculated. Any females whose drinking was more than one standard deviation below the group mean (usually less than 10% of the group) was removed from the study at this point.

Subsequently, females were assigned to either a saccharin control or 5% ethanol drinking group and matched such that the mean pre-pregnancy ethanol consumption by each group was similar. Females were then placed with alcohol-naïve proven male breeders until pregnant, as indicated by the presence of a vaginal plug. Female rats did not consume ethanol during the breeding procedure, which averaged about 2 days in length. Beginning on Gestational Day 1 (GD1), rat dams were provided saccharin water containing either 0% or 5% ethanol for 4 h each day, from 1000 to 1400 h. The volume of saccharin water provided to the control group (16 mL) was matched to the mean volume of 5% ethanol in saccharin water consumed by the ethanol prenatal treatment group during gestation. Daily four-hour ethanol consumption was recorded for each dam through GD21, after which ethanol consumption was discontinued. Rats were weighed weekly to assess maternal weight gain. At birth, the number of live births were recorded and the pups weighed. Subsequently the litters were culled to 10 pups by Postnatal Day 2 (PD2). Offspring were weaned at PD 23–26, at which time the numbers of each sex was confirmed.

2.3. *In situ* hybridization (ISH) studies

Seven pairs of seven-month-old control and PAE rats of each sex were sacrificed by decapitation and their brains dissected, frozen in isopentane chilled in a dry ice/methanol bath, and then stored in airtight containers at −80°C until sectioning. Sixteen-µm-thick horizontal sections were collected at Figure 107 (Bregma: – 4.60 mm; Interaural: 5.40 mm) according to the Paxinos and Watson rat stereotaxic atlas (Paxinos and Watson, 1998) and stored in airtight containers at-80°C until incubation. Oligonucleotide probes (Thermo Fisher Scientific, Waltham, MA, USA) were designed to specifically recognize rH_{3A} and rH_{3C} mRNA, as previously described (Drutel et al., 2001). The probes (2.5–5 pmol) were labeled with 62.5 µCi of [^{35}S]-deoxyadenosine 5′-α (−thio) triphosphate (Perkin Elmer Inc. Boston, MA, USA), at their 3′ ends using terminal deoxynucleotidyl transferase for 2 h. Non-incorporated nucleotides were removed by purification through QIAquick columns (Qiagen Sciences, Germantown, MD, USA). Hybridization was carried out using quintuplicate sections from each rat brain at 52°C for 20 h in a humidified chamber. After post-hybridization washing, the sections were dried and then placed along with ^{14}C standards in x-ray cassettes to expose Hyperfilm (GE HealthCare Technologies Inc. Chicago, IL, USA) for 14 days at 4°C. The film was then developed manually in Kodak D-19 (1:1, 18°C) for 2 min, fixed and then mounted onto microscope glass slides. Microdensitometric measurements of rH_{3A} and rH_{3C} mRNA were performed using Media Cybernetics Image Pro Plus® on an Olympus BH-2 microscope. An optical density standard curve, expressed in picoCuries/10^5µm^2, was established based on autoradiograms of ^{14}carbon standards. Measurements were made in six different brain regions (see Figure 1) at 3.125X total magnification. The density of rH_{3A} mRNA expression and rH_{3C} mRNA expression were each corrected against an off-section background density in each brain region measured in each rat.

2.4. Rat H3A polyclonal antibody design and characterization in HEK-293 cells

We contracted GenScript (Piscataway, NJ, USA) to develop a polyclonal antibody against a fourteen amino acid sequence within the third cytoplasmic loop of the rH_{3A} isoform, a sequence not present in other functional rH3 isoforms (see Figure 2). A FASTA search indicated this sequence is only present in rH_{3A} of different species and not present in other receptors. Antibody specificity was characterized using human HEK-293 cells cultured in T175 cell culture flasks (Avantor™, Radnor, PA, USA) in DMEM media containing 0.584 g/L glutamine (Sigma-Aldrich, Inc., St. Louis, MO, USA) 5% penicillin–streptomycin (Thermo Fisher Scientific) and 10% Fetal Bovine Serum (FBS, Sigma-Aldrich, Inc.) in a humidified atmosphere with 5% CO_2 until 65–75% confluence on the day of transfection. As described by Bakker et al. (2006), the cells were transfected with cDNAs encoding

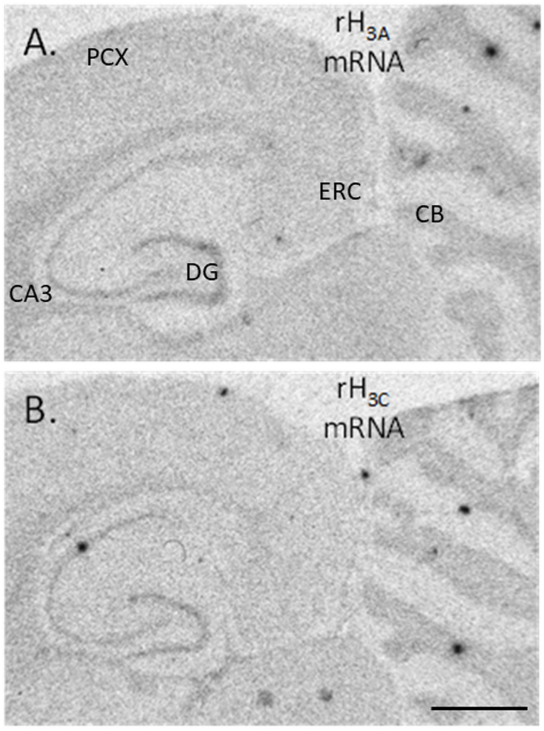


FIGURE 1
Autoradiograms of hybridized cDNA probes to rH_{3A} mRNA **(A)** and to rH_{3C} mRNA **(B)** present in horizontal sections collected from an unexposed control rat brain. Areas where densitometric measurements were collected are DG – dentate gyrus stratum granulosum, CA3 – hippocampal CA3 stratum pyramidale, CB – cerebellar stratum granulosum, ERC – medial entorhinal cortical layers 2/3, PCX – parietal cortex layers 2/3 (An image of the medial frontal cortex is not shown here, but the pattern of hybridization was identical to the distribution of H3R agonist-simulated GTP binding shown in Figure 5A). The horizontal black line in the bottom right corner of panel **(B)** denotes a distance of 2,500μm.

each of six rH3 isoforms (A-F) from GenScript (cDNA sequences are provided at the GenScript website: www.genscript.com/search?q=rat+histamine+receptor+isoforms&g=orf), labeled with a C-terminal DYKDDDK tag (FLAG tag) detectable *via* immunoblotting, using the LipofectaminePlus method, according to the manufacturer's protocol (Thermo Fisher Scientific). Briefly, on the day of transfection, the cells were trypinized with 0.05% trypsin–EDTA (Gibco™, Thermo Fisher Scientific) and washed with media to collect the HEK-293 cells and centrifuged for 5 min at 300×*g* to pellet the cells. The cDNAs ($rH_{3A\text{-}C}$: 46 μg and $rH3_{D\text{-}F}$: 90 μg) and Lipofectamine (92–180 μL) were diluted in Opti-MEM media without serum (Sigma-Aldrich, Inc.) and, after 5 min incubation, were mixed together and incubated for 20 min at room temperature to allow complex formation to occur. The complex was added directly to each well containing cells and mixed gently by rocking the plate back and forth. The media was changed after 6 h. The cells were incubated for 24–48 h and harvested by centrifugation.

Protein was extracted from the transfected HEK 293 cells with isotonic homogenization buffer (320 mM sucrose, 10 mM Tris HCl, 1 mM $NaVO_4$, 5 mM NaF, 1 mM EDTA, 1 mM EGTA, 1 mM DTT) containing 1× protease and phosphatase inhibitors (Sigma-Aldrich, Inc.). The cells were then homogenized in a glass Dounce homogenizer with six up and down strokes each using a loose fitting and then a tight fitting pestle. The resulting homogenate was then centrifuged at 1000×*g* for 6 min at 4°C. The supernatant (S1) was then centrifuged again at 10,000×*g* for 15 min at 4°C. The resulting P2 fraction was resuspended in homogenization buffer. Proteins were quantified using a BCA Protein Assay Kit (Pierce, Rockford, IL, USA) according to manufacturer's instructions. The fraction was aliquoted, flash frozen in liquid nitrogen and stored at −80°C until use.

Subsequently, 5 μg of sample protein were loaded onto a 4–12% NuPage gradient gel (Invitrogen™, Thermo Fisher Scientific Inc.) and run at 150 V for 2 h. The proteins were transferred onto a PVDF membrane (Millipore Sigma, Burlington, MA, USA). The membranes were blocked using I-block (Applied Biosystems, Foster City, CA, USA) in 1X PBS at room temperature for 1 h, then incubated with the GenScript anti-rH_{3A} (H3RA) polyclonal antibody (1:5000) and the GenScript anti-FLAG tag (1:2500, A00187) overnight at 4°C in I-block plus 0.1% Tween-20. Membranes were then washed three times for 10 min in 1X PBS-T, incubated in secondary antibodies at 1:15,000–1:20,000 dilution (LI-COR Biosciences, Lincoln, NE, USA) in I-block containing PBS plus 0.1% Tween-20 and 0.01% SDS for 1 h at room temperature. Membranes were then scanned using the LI-COR Odyssey Infrared Imaging System using the 700 nm wavelength channel to visualize the Tag and Actin and the 800 nm channel for H3RA antibody binding. The optical densities were quantitated using LI-COR Odyssey Application Software version 3.0.

2.5. Breeding of H3R knockout mice

As another strategy for confirming H3AR specificity, we acquired the B6.129P2-*Hrh3*^{tm1Tw}*/J* line of transgenic mice from The Jackson Laboratory (JAX stock #023433; Bar Harbor, ME, USA). These mice carry a targeted mutation of the *Hrh3*, histamine receptor H3R gene, with a cassette containing a neomycin resistance gene replacing a 0.7-kilobase region covering part of the first intron and the 5′ end of the second exon of the gene (Toyota et al., 2002). Jackson Labs provided male and female heterozygote breeding pairs for our experiments. Breeding pairs were maintained in the UNM HSC Breeding Barrier. The mice were kept in ventilated standard cages with autoclaved recycled cardboard bedding with low lights on from 0600 to 1800 h and provided irradiated Teklad Global 2920 Soy Protein Free rodent diet (Envigo) and sterilized water pouches *ad libitum*. Offspring mouse genotype was determined with tail biopsies using real-time PCR with specific probes designed for HrH3 (Transnetyx, Cordova, TN, USA). The three genotypes generated were Wild type (WT – $mH3R^{+/+}$), heterozygous (HT – $mH3R^{+/-}$) and pan H3R Knockout (KO – $mH3R^{-/-}$).

2.6. RNA extraction and qRT-PCR from mouse frontal cortex

Medial frontal cortex was collected from five pairs of ~five-month-old adult WT (all female) and KO (two male and three female) mice, flash frozen and stored at −80°C until RNA extraction. Total RNA was extracted using TRIzol™ (Invitrogen™, Thermo Fisher Scientific). RNA quality was determined using a NanoDrop 2000 (Thermo Fisher Scientific), using absorbance at 260, 280 and 230 nm. One μg of total RNA was reverse-transcribed using SuperScript III

10.3389/fnins.2023.1192096

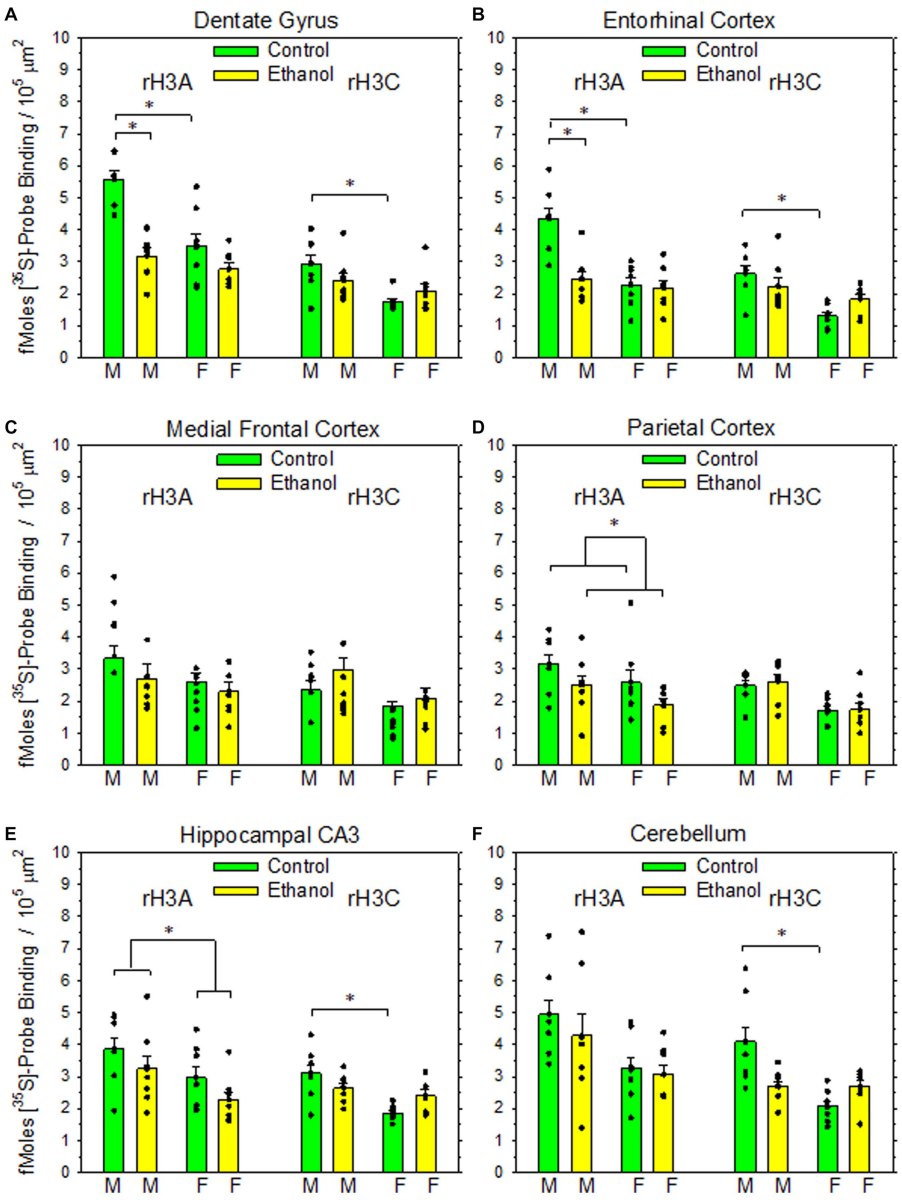


FIGURE 2
Impact of PAE on rH_{3A} mRNA and rH_{3C} mRNA expression in six rat brain regions. Data bars represent the mean±SEM density of [^{35}S]-labelled cDNA probe binding, expressed as fMoles bound/$10^5\mu m^2$ from seven pairs of control and PAE rats of each sex. **(A)** A two-way ANOVA of rH3A probe binding in dentate gyrus revealed a significant interaction between prenatal treatment group and sex ($F_{1,27}$=9.02, p=0.006). A Holm-Sidak All Pairwise Multiple Comparisons Procedure indicated a significant effect of sex within the control group (t=5.30, p<0.001), but not within the PAE group (t=1.05, p=0.303). A significant effect of prenatal treatment group was also observed between males (t=6.08, p<0.001) but not between females (t=1.84, p=0.077). A Kruskal-Wallis One-Way ANOVA on Ranks on the rH3C probe binding data indicated a significant difference based on sex with the control group (q=4.52, p<0.05). **(B)** A two-way ANOVA of rH3A probe binding in entorhinal cortex revealed a significant interaction between prenatal treatment group and sex ($F_{1,27}$=12.2, p=0.002). The Holm-Sidak procedure indicated a significant effect of sex within the control group (t=5.67, p<0.001), but not within the PAE group (t=0.737, p=0.467). A significant effect of prenatal treatment group was also observed between males (t=5.23, p<0.001), but not between females (t=0.297, p=0.768). A two-way ANOVA of rH3C probe binding revealed a significant interaction between prenatal treatment group and sex ($F_{1,27}$=5.45, p=0.027). The Holm-Sidak procedure indicated a significant effect of sex within the control group (t=4.73, p<0.001), but not within the PAE group (t=1.431, p=0.163). The comparisons between prenatal treatment within sex were not significant for either sex. **(C)** A two-way ANOVA of rH3A probe binding in medial frontal cortex revealed no significant effect of prenatal treatment ($F_{1,27}$=1.65, p=0.209), sex ($F_{1,27}$=2.34, p=0.138) or a significant interaction ($F_{1,27}$=0.222, p=0.641). Likewise, a two-way ANOVA of rH3C binding revealed no significant effect of prenatal treatment ($F_{1,27}$=3.96, p=0.057), sex ($F_{1,27}$=0.003, p=0.955) or significant interaction ($F_{1,27}$=0.075, p=0.786). **(D)** A two-way ANOVA of rH3A probe binding in parietal cortex revealed a significant main effect of prenatal treatment ($F_{1,27}$=5.09, p=0.032) but not sex ($F_{1,27}$=3.78, p=0.062). A K-W ANOVA on Ranks on the rH3C probe binding data indicated no significant effects based on prenatal treatment or sex. **(E)** A two-way ANOVA of rH3A probe binding in hippocampal CA3 revealed a significant main effect of sex ($F_{1,27}$=7.53, p=0.010), but not prenatal treatment ($F_{1,27}$=3.73, p=0.064). A two-way ANOVA of rH3C probe binding data revealed a significant interaction between prenatal treatment and sex ($F_{1,27}$=7.32, p<0.001). A H-S Comparisons procedure indicated a significant effect of sex within the control group (t=4.708, p<0.001), but not within the PAE group (t=0.880, p=0.386). No effects based on prenatal treatment were observed in either males (t=1.787, p<0.085) or females (t=2.04, p=0.051). **(F)** A K-W ANOVA on Ranks on the rH3A probe binding data in cerebellum indicated no significant differences based on prenatal treatment or sex. A K-W ANOVA on Ranks on the rH3C probe binding data indicated a significant effect of sex within the control group (q=5.65, p<0.05).

reverse transcriptase (Invitrogen™, Thermo Fisher Scientific) following the manufacturer's protocol and qRT-PCR carried out with a Model 7500 fast real-time PCR system (Applied Biosystems™, Thermo Fisher Scientific) using PowerUp SYBR Green master mix (Thermo Fisher Scientific). Primer sequences for qRT-PCR for mouse mRNAs were made by Invitrogen (Thermo Fisher Scientific) to detect mouse H3R Transcript Variant 1 (Forward primer sequence: CTTCCTCGTGGGTGCCTTC, Reverse primer sequence: CAGCTCGAGTGACTGACAGG) and the GAPDH gene (Forward primer sequence: TGTGATGGGTGTGAACCACGAGAA, Reverse primer sequence: GAGCCCTTCCACAATGCCAAAGT). For each sample, the GAPDH cycling time (CT) was subtracted from mH3R CT and then the relative expression of mH3R was determined using the comparative 2-ΔCt method (Livak and Schmittgen, 2001). All 2-ΔCt values were normalized to the mean of WT mH3R expression and the normalized values expressed as the mean ± SEM.

2.7. Immethridine-stimulated [^{35}S]-GTPγS (GTP) binding studies In mouse brain

As described above for the ISH studies in Section 2.3, four ~ten-week-old mice, two male and two females from each of the three genotypes, were sacrificed, their whole brains dissected, frozen in isopentane and stored in airtight containers at −80°C until sectioning. Eight-μm-thick cryostat sections were collected in the sagittal plane corresponding to Figure 113 (Lateral: - 1.44 mm) in the Paxinos & Franklin stereotaxic atlas of mouse brain (Paxinos and Franklin, 2013), thaw-mounted onto pre-cleaned Superfrost-Plus® microscope slides and stored at −80°C in airtight containers until incubation. Tissue sections were pre-incubated for 10 min in incubation buffer (50 mM Tris–HCl, 100 mM NaCl, 5 mM $MgCl_2$, 0.2 mM EGTA, 2 mM GDP, 1 mM DTT, and 100 nM DPCPX; pH 7.4 at 25°C), and then incubated with 100 pM [^{35}S]-GTPγS (Perkin Elmer, specific activity = 1,250 Ci/mmole) for 90 min at 25°C with the H3R agonist immethridine (3 μM) in the absence or presence of 30 μM unlabeled iodopotentidine (IPP), a H3R antagonist. After incubation, sections were rinsed twice for 15 s each in ice-cold incubation buffer, dipped in ice-cold distilled water, air-dried, and vacuum desiccated overnight. Sections were then exposed to Kodak Biomax MR film for 4 days, and the film developed in Kodak D-19 (1:1, 18°C), fixed and then mounted onto microscope glass slides. Measurements of [^{35}S]-GTPγS binding were performed using Media Cybernetics Image Pro Plus® on an Olympus BH-2 microscope at 3.125X total magnification. An optical density standard curve, expressed in picoCuries/10^5 μm^{2,} was established based on autoradiograms of ^{14}carbon standards. Immethridine-stimulated [^{35}S]-GTPγS binding was expressed as percent of GTP binding above GTP binding in the presence of iodopotentidine. The mean ± the SEM percent agonist-stimulated GTP binding was computed for each brain region for each genotype.

2.8. Western blotting of P2 membranes from rat and mouse frontal cortex

Protein was extracted from frontal cortical brain tissue of ~seven-week-old female untreated control rats or from ~eleven-week-old WT and H3R KO mice of both sexes using isotonic homogenization buffer containing protease and phosphatase inhibitors as described for HEK-293 cells in Section 2.4. We ran varying amounts of sample protein (2–50 μg) on 4–12% gradient gels and optimized the primary antibody concentrations as follows: GenScript H3RA (1:5000), and β-Actin (1:80,000, Sigma-Aldrich Inc.) as the reference protein. Secondary antibodies used were donkey anti-rabbit IRDye® 800CW (1:20,000, LI-COR Biosciences) for H3RA, and goat anti-mouse IRDye® 630RD (1:40,000, LI-COR Biosciences) for β-actin. The fluorescence images of the western blots were analyzed as described previously (Section 2.4).

2.9. Western blotting and LC/MS of the ~55kDa band of P2 membranes from frontal cortex

2.9.1. Western blotting

Frontal cortical tissue was dissected from a seven-week-old-female rat, and eleven-week-old WT and KO mice of both sexes, and protein extracted using isotonic homogenization buffer containing protease and phosphatase inhibitors as described for HEK-293 cells in Section 2.4. The resulting P2 pellet was kept at −80°C until shipment to Kendrick Laboratories (Madison, WI, USA). Upon arrival, the pellets were dissolved in 250 μL of SDS Boiling Buffer without reducing agents. All samples were heated in a dry bath for 10 min at 95°C before the sample protein concentrations were determined using the BCA assay (Smith et al., 1985). Samples were then diluted to 3.0 μg/μl in SDS Boiling Buffer with reducing agents and heated in a digital dry bath at 95°C for 10 min. Samples were then further diluted to 1.5 mg/mL in SDS Boiling Buffer with reducing agents before loading. One dimensional SDS slab gel electrophoresis was carried out under reducing conditions according to the method of Laemmli (1970) as modified by O'Farrell (1975). Twenty-five μg of sample were loaded into wells in 10% acrylamide slab gels (0.75 mm thick). SDS slab gel electrophoresis was carried out for about 4 h at 15 mA/gel. The following proteins (Millipore Sigma) were used as molecular weight standards: Myosin (220,000), phosphorylase A (94,000), catalase (60,000), actin (43,000), carbonic anhydrase (29,000), and lysozyme (14,000). These standards are visible in lanes on images of the Coomassie blue-stained PVDF membranes (images not shown).

After slab gel electrophoresis, the gels for blotting were placed in transfer buffer (10 mM Caps, pH 11.0, 10% methanol) and transblotted onto PVDF membranes overnight at 200 mA. The blot was stained with Coomassie Brilliant Blue R-250. The blot was then blocked for 2 h in 5% non-fat dry milk (NFDM) diluted in Tween-20 tris buffer saline (TTBS). The blot was then incubated overnight in primary antibody (GenScript H3RA, 1:25,000) in 2% NFDM TTBS and rinsed 3 × 10 min in TTBS. The blot was then placed in secondary antibody (anti-Rabbit IgG-HRP [SeraCare, Milford, MA, USA, Cat# 5220–0337, Lot# 10440068] diluted 1:20,000 in 2% NFDM TTBS) for 2 h, rinsed as above, treated with ECL, and exposed to x-ray film for 3 min. The ~55 kDa bands of interest were excised from the corresponding gel and sent to Dr. Costel Darie at the Clarkson University Protein Core Facility (Potsdam, NY, USA) for protein identification by LC MS/MS.

2.9.2. Protein digestion and peptide extraction

Proteins that were separated by SDS-PAGE/2D-PAGE and stained by Coomassie dye were excised, washed and the proteins from the gel were treated according to published protocols (Channaveerappa et al., 2017; Aslebagh et al., 2018; Mihăşan et al., 2018; Wormwood et al., 2018; Lux et al., 2019). Briefly, the gel pieces were washed in high purity, high performance liquid chromatography HPLC grade water, dehydrated and cut into small pieces and destained by incubating in 50 mM ammonium bicarbonate, 50 mM ammonium bicarbonate/50% acetonitrile, and 100% acetonitrile under moderate shaking, followed by drying in a speed-vac concentrator. The gel bands were then rehydrated with 50 mM ammonium bicarbonate. The procedure was repeated twice. The gel bands were then rehydrated in 50 mM ammonium bicarbonate containing 10 mM DTT and incubated at 56°C for 45 min. The DTT solution was then replaced with 50 mM ammonium bicarbonate containing 100 mM iodoacetamide for 45 min in the dark, with occasional vortexing. The gel pieces were then re-incubated in 50 mM ammonium bicarbonate/50% acetonitrile, and 100% acetonitrile under moderate shaking, followed by drying in speed-vac concentrator. The dry gel pieces were then rehydrated using 50 mM ammonium bicarbonate containing 10 ng/μL trypsin and incubated overnight at 37°C under low shaking. The resulting peptides were extracted twice with 5% formic acid/50 mM ammonium bicarbonate/50% acetonitrile and once with 100% acetonitrile under moderate shaking. Peptide mixture was then dried in a speed-vac, solubilized in 20 μL of 0.1% formic acid / 2% acetonitrile.

2.9.3. NanoLC–MS/MS

The peptides mixture was analyzed by reverse phase nanoliquid chromatography (LC) and MS (LC–MS/MS) using a NanoAcuity UPLC (Micromass/Waters, Milford, MA) coupled to a Q-TOF Xevo G2 mass spectrometer (Micromass/Waters, Milford, MA), according to published procedures (Channaveerappa et al., 2017; Aslebagh et al., 2018; Mihăşan et al., 2018; Wormwood et al., 2018; Lux et al., 2019). Briefly, the peptides were loaded onto a 100 μm x 10 mm NanoAquity BEH130 C18 1.7 μm UPLC column (Waters, Milford, MA) and eluted over a 60 min gradient of 2–80% organic solvent (ACN containing 0.1% FA) at a flow rate of 400 nL/min. The aqueous solvent was 0.1% FA in HPLC water. The column was coupled to a Picotip Emitter Silicatip nano-electrospray needle (New Objective, Woburn, MA). MS data acquisition involved survey MS scans and automatic data dependent analysis (DDA) of the top six ions with the highest intensity ions with the charge of 2+, 3+ or 4+ ions. The MS/MS was triggered when the MS signal intensity exceeded 250 counts/s. In survey MS scans, the three most intense peaks were selected for collision-induced dissociation (CID) and fragmented until the total MS/MS ion counts reached 10,000 or for up to 6 s each. The entire procedure used was previously described (Channaveerappa et al., 2017; Aslebagh et al., 2018; Mihăşan et al., 2018; Wormwood et al., 2018; Lux et al., 2019). Calibration was performed for both precursor and product ions using 1 pmol GluFib (Glu1-Fibrinopeptide B) standard peptide with the sequence EGVNDNEEGFFSAR and the monoisotopic doubly-charged peak with m/z of 785.84.

2.9.4. Data processing and protein identification

The raw data were processed using ProteinLynx Global Server (PLGS, version 2.4) software as previously described (Channaveerappa et al., 2017; Aslebagh et al., 2018; Mihăşan et al., 2018; Wormwood et al., 2018; Lux et al., 2019). The following parameters were used: background subtraction of polynomial order 5 adaptive with a threshold of 30%, two smoothings with a window of three channels in Savitzky–Golay mode and centroid calculation of top 80% of peaks based on a minimum peak width of 4 channels at half height. The resulting pkl files were submitted for database search and protein identification to the in-house Mascot server (Matrix Science, London, UK)[1] for database search using the following parameters: databases from NCBI (*mouse and histamine H3A receptor*), parent mass error of 0.5 Da with 1 ^{13}C, product ion error of 0.8 Da, enzyme used: trypsin, three missed cleavages, propionamide as cysteine fixed modification and Methionine oxidized as variable modification. To identify the false negative results, we used additional parameters such as different databases or organisms, a narrower error window for the parent mass error (1.2 and then 0.2 Da) and for the product ion error (0.6 Da), and up to two missed cleavage sites for trypsin. In addition, the pkl files were also searched against in-house PLGS database version 2.4[2] using searching parameters similar to the ones used for Mascot search. The Mascot and PLGS database search provided a list of proteins for each gel band. To eliminate false positive results, for the proteins identified by either one peptide or a mascot score lower than 25, we verified the MS/MS spectra that led to identification of a protein.

2.10. Western blotting and LC/MS of the ~48kDa band of P2 membranes from HEK-293 cells

HEK-293 cells were transfected with rH_{3A} mRNA and Lipofectamine only, as described in Section 2.4. Protein was extracted and varying concentrations of protein (20–50 μg) were run on a 4–12% gel which was stained with Coomassie Brilliant blue R-250. Western blotting was conducted as described above in Section 2.4 and the ~48 kDa band was excised from the corresponding gel and sent for LC–MS analysis as described in Section 2.9 above.

2.11. Statistical procedures

All statistical procedures and graphical illustrations were performed using SigmaPlot® 11 (Systat Software Inc., San Jose, CA, USA). All data are expressed as the mean ± SEM with a p value <0.05 deemed as statistically significant. A Mann–Whitney Rank Student's two-tailed t-tests was used to compare differences in maternal weight gain and pup birthweight and Mann–Whitney rank sum test was used to test differences in litter size (Table 1). Two-way ANOVAs were used to test for differences in the individual rH3A mRNA and rH3C mRNA expression data in each brain region unless the data was not normally distributed, in which case a Kruskal-Wallis ANOVA on ranks was employed

1 www.matrixscience.com
2 www.waters.com

TABLE 1 Daily ethanol consumption by dams in the 5% ethanol group, resulting serum ethanol concentration and impact of moderate prenatal ethanol exposure on pregnancy outcome measures.

	Saccharin control	5% Ethanol
Number of dams (*n*)	11	10
Daily gestational ethanol consumption (g/kg)	NA	1.81 ± 0.05
Serum ethanol concentration (mg/dL)	NA	25.1 ± 3.3[a]
Maternal weight gain (g)	103 ± 5	88 ± 4*
Number of live births (n)	10.9 ± 0.2	9.6 ± 0.6
Pup birthweight (g)	7.85 ± 0.33	8.61 ± 0.45

[a]Samples collected 2 h after the introduction of drinking tubes (Davies et al., 2023).
*Denotes maternal weight gain data significantly less that control ($t = 2.66$, $p = 0.015$).

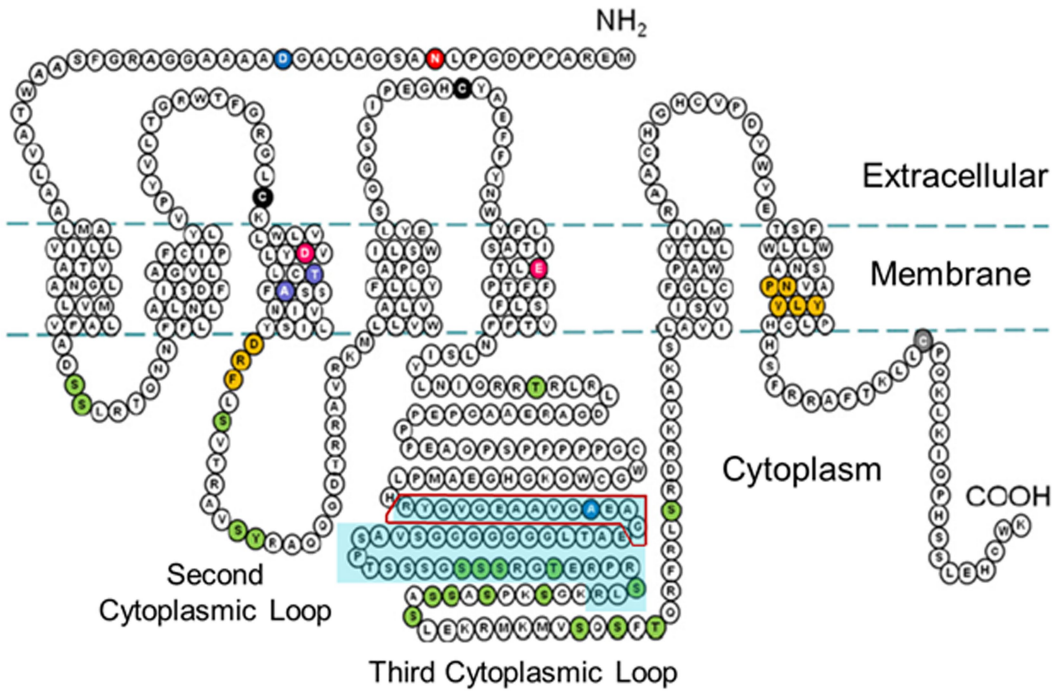


FIGURE 3
Two-dimensional schematic diagram of the amino acid sequence of the rH3A isoform [adapted from the amino acid sequence diagram in Nieto-Alamilla et al., 2016] illustrating the seven transmembrane spanning regions and the three cytoplasmic loops. The turquoise-shaded area within the third cytoplasmic loop denotes the 48 amino acid region not present in the rH_{3B} and rH_{3C} isoforms. The red box outline within that region denotes the 14 amino acid sequence used to raise the GenScript polyclonal antibody to the rH3A isoform.

(Figure 3). A Mann–Whitney rank sum test was used to compare the qRT-PCR data (Figure 4). A two-way ANOVA was used to test differences in GTP binding data in the absence and presence of the H3R antagonist iodopotentidine (Figure 5).

3. Results

3.1. Paradigm outcome measures

Rat dams in the 5% ethanol group consumed a mean of 1.81 ± 0.05 grams of ethanol each day during gestation (Table 1). In a separate set of rat dams, this level of consumption produced a mean serum ethanol concentration of 25.1 ± 3.3 mg/dL when sampled 2 h after the introduction of drinking tubes (Davies et al., 2023). This moderate prenatal ethanol exposure paradigm resulted in a 14% reduction in maternal weight gain that was statistically significant. However, the reduction in maternal weight gain did not significantly affect offspring litter size or offspring birth weight (Table 1).

3.2. *In situ* hybridization studies in rat brain

As illustrated in Figure 1, both rH_{3A} mRNA and rH_{3C} mRNA were heterogeneously distributed across brain regions in patterns similar to the distribution of H3Rs and H3R agonist-stimulated [^{35}S]-GTPγS binding (Varaschin et al., 2018). The density of rH_{3A} binding appears to be greater than the rH_{3C} signal. Figure 3 summarizes the impact of PAE and sex on the expression of rH_{3A} mRNA and rH_{3C} mRNA in six brain regions. No prenatal

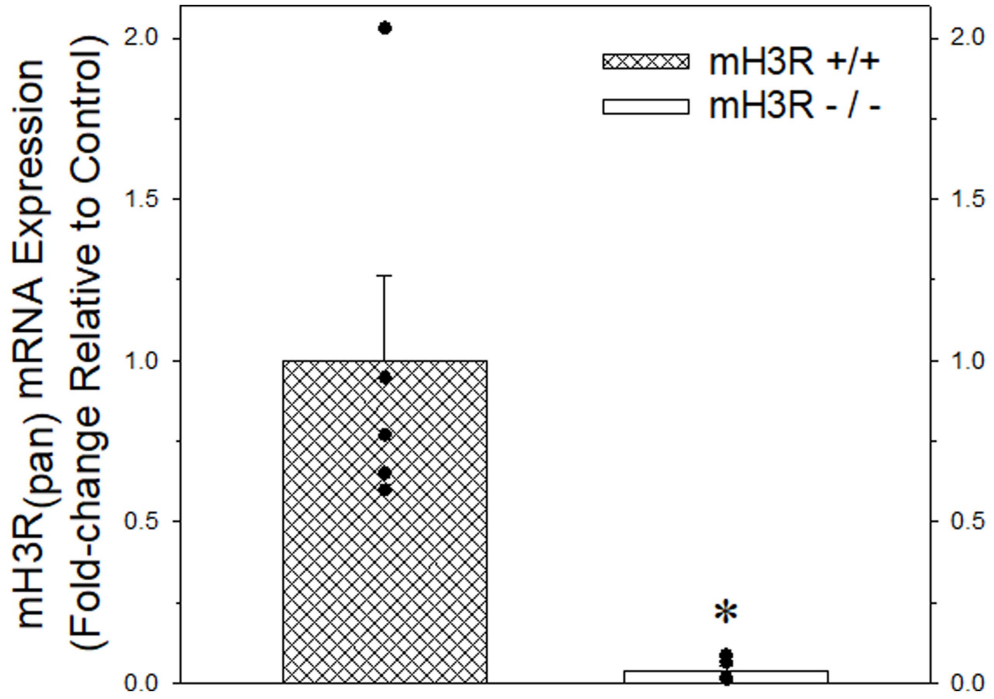


FIGURE 4
Quantitative real-time PCR analysis of pan-mH3R mRNA expression in P2 membranes prepared from frontal cortex of five pairs of WT (course cross hatching bar) and mH3R KO (white bar) mice. Data bars represent the mean±SEM of mRNA expression normalized to the mean of the WT group. A Mann–Whitney Rank Sum Test indicated a significant reduction in pan-H3R mRNA expression, denoted by the asterisk, in the mH3R KO group compared to the WT control group (T=40.0, p=0.008).

treatment or sex-related effects were consistently observed across the six brain regions analyzed. Significant interactions between prenatal treatment and sex were observed for rH_{3A} mRNA expression in the dentate gyrus (3A) and entorhinal cortex (3B) and for rH_{3C} RNA expression in entorhinal cortex (3B) and hippocampal CA3 region (3E). In each of these four cases, along with non-parametric assessments of rH_{3C} mRNA in dentate gyrus (3A) and cerebellum (3F), a sex-related effect was detected in control but not PAE offspring. Further, a significant main effect of sex was noted for rH_{3A} mRNA in the hippocampal CA3 region (3E). A significant main effect of prenatal treatment was only observed in the parietal cortex (3D) and a significant difference based on prenatal treatment was observed for males but not females in dentate gyrus (3A) and entorhinal cortex (3B). No significant effects were observed in the medial frontal cortex (3C).

3.3. Characterization of rH3A antibody specificity in HEK-293 cells

We developed a polyclonal antibody against a fourteen amino acid sequence within the third cytoplasmic loop of the rH_{3A} isoform, a sequence not present in other functional rH3 isoforms (Figure 2) for use in our Western blotting studies. Figure 6 illustrates a representative western blot of HEK-293 P2 samples prepared from six different overexpressing H3R isoform derived cell lines (A–F). Green bands represent H3RA antibody binding, red bands are binding by the Tag peptide, and the yellow band represents binding by both the H3RA antibody and the Tag peptide. The yellow band detected at ~48 kDa in Lane A representing the rH3A-overexpressing HEK-293 cells of Figure 6, confirms the specificity of the GenScript polyclonal antibody for detecting rH_{3A} protein. While sufficient H3R protein was available to visualize Tag peptide binding (red bands) for rH_{3B} (Lane B) and kDa for rH_{3C} (Lane C), the H3RA antibody did not recognize these proteins, as evidenced by the absence of yellow bands. Note that the band positions in Lane B and Lane C are consistent with the shorter amino acid sequences for rH_{3B} (413 aa) and for rH_{3C} (397 aa). However, as the non-functional rH_{3D} (Bakker et al., 2006) has a similar amino acid sequence to rH_{3A}, a faint green band of H3RA antibody binding was noted. Anti-FLAG tag antibody labeling was not observed for H3R isoforms D–F (Lanes D–F) due to the relatively low abundance of these isoforms compared to the A, B, and C isoforms.

3.4. Quantitative RT-PCR analysis of pan mH3R expression in mouse frontal cortex

As a second approach for confirming antibody specificity, we obtained heterozygote pan H3R transgenic mouse breeding pairs and then generated and confirmed mouse offspring with the WT ($mH3R^{+/+}$), HT ($mH3R^{+/-}$) and KO ($mH3R^{-/-}$) genotypes. Subsequently, we conducted a qRT-PCR analysis of pan-mH3R mRNA expression in medial frontal cortical membranes prepared from WT and KO mice. GAPDH mRNA expression, whose expression

10.3389/fnins.2023.1192096

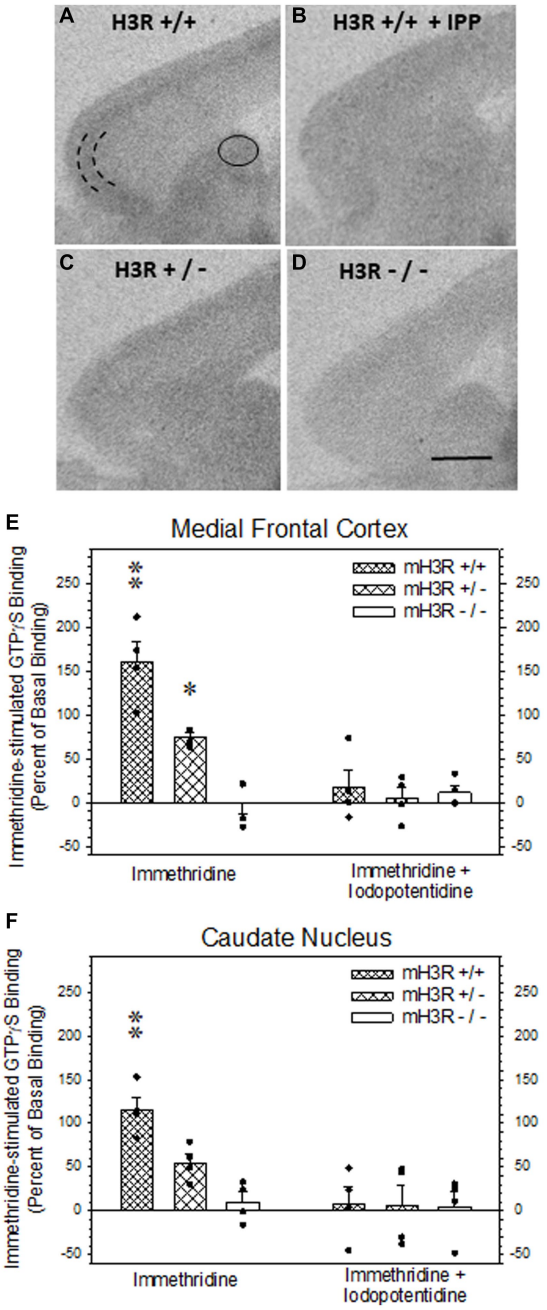


FIGURE 5
H3R agonist-stimulated [^{35}S]-GTPγS (GTP) binding in sagittal sections of frontal mouse brain. **(A,B)** H3R agonist (3μM immethridine)-stimulated GTP binding in WT mH3R$^{+/+}$ mouse in the absence **(A)** and in the presence of 30μM of the H3R antagonist iodopotentidine (IPP, **B**). **(C,D)** H3R agonist-stimulated GTP binding in the absence of IPP in HT mH3R$^{+/-}$ **(C)** and the KO mH3R$^{-/-}$ mouse genotypes. The curved parallel lines in panel **(A)** denote where microdensitometric measurements were performed in the external pyramidal layer of the medial frontal cortex **(D)** and within the oval circle in dorsal medial caudate nucleus **(A)**. **(E,F)** Effects of genotype and incubation condition on immethridine stimulated GTP binding in mouse brain. The data bars in each graph represent the mean±SEM H3R agonist-simulated GTP binding, expressed as percent of binding above the GTP binding in the presence of added IPP, from four mice in each of the three genotypes. A two-way ANOVA of the GTP binding data in medial frontal cortex **(E)** revealed a significant interaction between genotype and the presence of H3R antagonist IPP in the incubation medium ($F_{2,23}$=13.6, p<0.001). A Holm-Sidak All Pairwise Multiple Comparisons Procedure indicated a significant effect of incubation condition in the WT group (t=6.80, p<0.001) and the HT group (t=3.33, p=0.004) but not in the KO group (t=0.582, p=0.568). Within genotype in the absence of IPP, there was a significant difference between WT and HT (t=4.08, p<0.001) and between WT and KO (t=7.66, p<0.001), denoted by the double asterisk, and between HT and KO (t=3.59, p=0.002), denoted by the single asterisk. No differences between genotypes were noted in the presence of IPP. A two-way ANOVA of the GTP binding data in dorsal medial caudate nucleus **(F)** also indicated a significant interaction between genotype and the presence of H3R antagonist IPP in the incubation medium ($F_{2,23}$=4.64, p=0,024). The Holm-Sidak procedure indicated a significant effect of incubation condition in the WT group (t=4.52, p<0.001), but not the HT group (t=2.06, p=0.054) or the KO group (t=0.221, p=0.828). Within genotype in the absence of IPP, there was a significant difference between WT and HT (t=2.53, p=0.021) and between WT and KO (t=4,42, <0.001), denoted by the double asterisk, but not between HT and KO (t=1.89, p=0.075). Again, there were no differences between genotype in the presence of IPP.

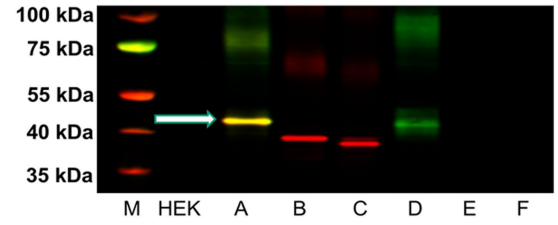


FIGURE 6
Western blot analysis of five μg of P2 membrane fractions of HEK-293 cells transfected with cDNA for each of the six rH3 isoforms (Lanes A–F). The GenScript antibody recognized protein at ~48kDa for both rH_{3A} (yellow band in Lane A) and rH_{3D} (green band in Lane D). The red bands in lanes B and C correspond to the anti-FLAG Tag antibody binding to the lower molecular weight rH_{3B} and rH_{3C} isoforms. The non-functional $rH3_{D-F}$ isoforms were present in too low an abundance to be detected by the anti-FLAG tag (Lanes D–F). The yellow band in lane A denotes that both rH3A and the FLAG Tag were detected. M denotes the molecular weight marker bands.

was not different between WT and KO mice, was used as the reference gene. However, as shown in Figure 4, we observed a significant 25-fold reduction in pan H3R mRNA expression in KO mice compared to WT mice.

3.5. Immethridine-stimulated [^{35}S]-GTPγS (GTP) binding in mouse brain

We also employed H3R agonist-stimulated [^{35}S]-GTPγS (GTP) binding as a measure of H3R function in all three genotypes. Autoradiograms of immethridine-stimulated GTP binding in sagittal sections of WT mice (Figure 5A) showed a relatively higher level of agonist-stimulated GTP binding in external pyramidal layer of medial frontal cortex with more moderate and diffuse levels of binding in the dorsomedial caudate nucleus, as well as other regions of the cerebral cortex (Figure 5A) and hippocampal formation (not shown). H3R agonist-stimulated GTP binding was virtually abolished in the presence of the H3R antagonist iodopotentidine (IPP; Figure 5B). A fainter degree of agonist-stimulated GTP binding was noted in the medial frontal cortex and caudate nucleus of sections collected from a H3R HT mouse (Figure 5C) and was not present in sections from H3R KO mice (Figure 5D). The H3R agonist-stimulated GTP binding data, expressed as percent increase in GTP binding above the mean binding in the presence of IPP from four mice of each of the three genotypes is summarized for medial frontal cortex (Figure 5E) and caudate nucleus (Figure 5F). A two-way ANOVA of the GTP binding in medial frontal cortex revealed a significant interaction between genotype and the presence of IPP in the incubation medium (Figure 5E). Agonist-stimulated GTP binding was not different among the three genotypes in the presence of IPP nor between the GTP binding in the absence and presence of IPP in the H3R KO group, indicating the absence of H3R agonist-stimulated GTP binding in the H3R KO mice. However, agonist-stimulated GTP binding was significantly greater in the HT group compared to the KO group and significantly greater in the WT group compared to the two other genotypes. Similar results were observed in the caudate nucleus except the agonist-stimulated GTP binding in the HT group was not significantly greater than the H3R KO group (Figure 5F).

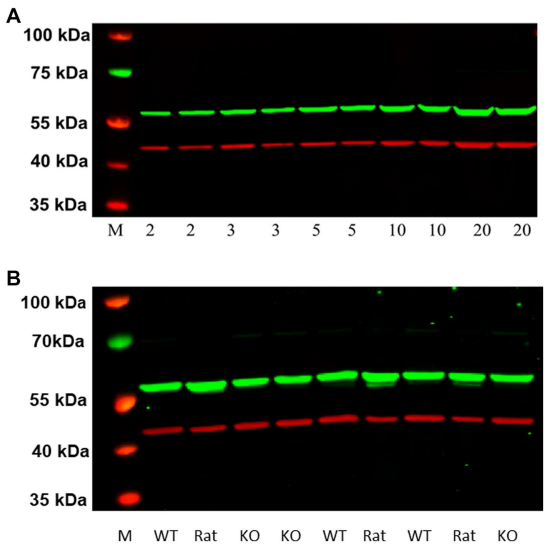


FIGURE 7
(A) Western blot analysis of increasing protein concentrations of P2 membranes from rat frontal cortical tissue **(A)**. Visualization of the GenScript antibody (green band at ~55kDa) and the reference protein β actin (red band at ~42kDa) can be seen. M denotes the molecular weight marker bands. We did not detect a~48kDa band of H3RA antibody binding here, as seen in HEK-293 cells (Figure 6). **(B)** Comparison of western blots of frontal cortical membranes from rat, and WT and H3R KO mice. As observed before for rat membranes, the green band at ~55kDa was also observed in both WT and KO mice, suggesting that the ~55kDa band is not H3R protein.

3.6. Western blotting of P2 membranes from rat frontal cortex

As illustrated in Figure 7A, western blots of increasing protein concentrations of P2 membranes prepared from rat frontal cortical tissue identified a single higher molecular weight band (~55 kDa) in contrast to the ~48 kDa band observed with HEK-293 cells overexpressing rH_{3A} (Figure 6). Subsequent studies employing higher quantities of protein (30, 50 and 100 μg) along with higher concentrations of the primary (1:5,000–1:500) or secondary (1:20,000–1:5,000) antibody failed to detect a ~ 48 kDa band in rat frontal cortex. Our preliminary interpretation of these results was that either the rH_{3A} isoform undergoes post-translational modifications in native membranes that increase its molecular weight or, that the H3RA antibody was binding to another, possibly higher abundance, protein. Subsequently, with confirmation of the mouse H3R phenotypes, we repeated this experiment comparing frontal cortical membranes from rat as well as WT and KO mice. As illustrated in Figure 7B, we observed that the H3RA antibody labeled a ~ 55 kDa band in all three sample types suggesting the ~55 kDa band was not rH_{3A} protein.

3.7. LC/MS analysis of the ~55kDa band of P2 membranes from rodent frontal cortex

Subsequently, frontal cortical membranes of rat and H3R WT and KO mice were prepared and sent to Kendrick Laboratories along with our GenScript H3RA antibody. Western blotting was

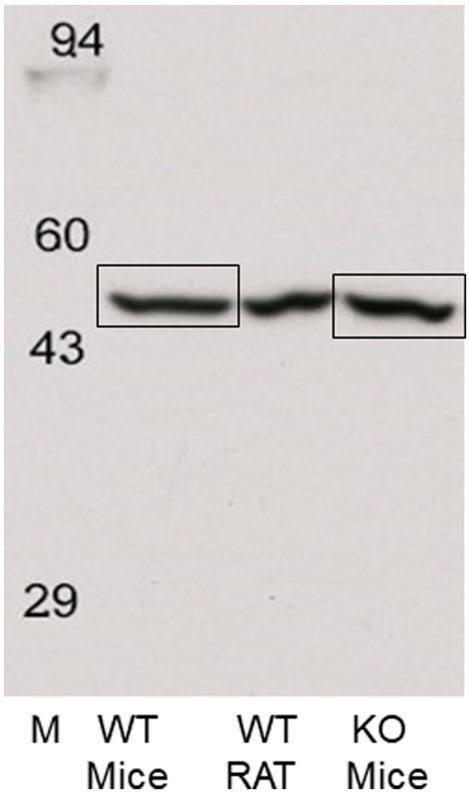


FIGURE 8
Western blots of rat and WT and H3R KO mouse frontal cortical membranes performed by Kendrick Laboratories using chemiluminescence to visualize the ~55kDa band. The ~55kDa bands from the WT and H3R KO mice, denoted by the boxes, were excised from their corresponding gels and sent to the Clarkson Proteomic Facility for LC/MS identification. The ~55kDa in both WT and KO samples was identified as the beta-subunit of the highly abundant ATPase protein. No mH3A protein was detectable in these samples.

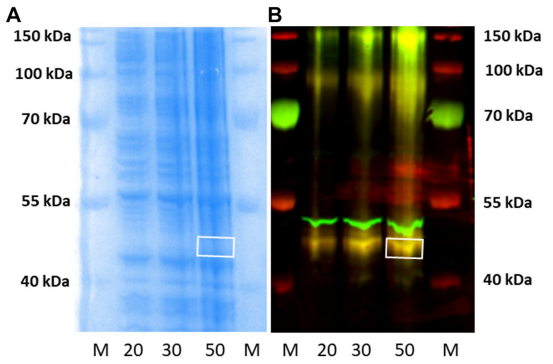


FIGURE 9
Western blotting of P2 membranes from HEK-293 cells overexpressing rH_{3A} were run in our laboratory, as before. Panel **(A)** is the Coomassie-stained gel corresponding to the western blot shown in panel **(B)**. M denotes the molecular weight marker lanes, and the numbers (20, 30, and 50) denote the μg amount of P2 membranes applied to the gels. Yellow bands, denoting H3RA antibody binding to rH3A protein was observed in all three tissue lanes, not only at ~48kDa but also at ~100kDa and~150kDa suggesting the presence of dimers and trimers of rH3A protein **(B)** Another protein, not observed previously using lower amounts of HEK-293 sample protein, appeared above the rH3A band, but below the ~55kDa band of non-specific binding observed in rodent membranes (Figures 7, 8). This band was not labeled by anti-FLAG antibody. The ~48kDa band from the 50μg lane was excised from the corresponding gel [denoted by the white box in panel **(A)**] and subsequently confirmed by LC/MS to be rH_{3A} protein. However, its detection was below the limit of quantitative reliability (LOQ).

performed as before except that Enhanced chemiluminescence (ECL) was used to detect the bands on X-ray film. As before, a single band of antibody binding was observed at ~55 kDa in all three tissue types. The ~55 kDa bands were excised from the mouse WT and KO samples, as illustrated in Figure 8, and sent to the Clarkson Proteomic Facility for protein identification. LC/MS analysis of the ~55 kDa band identified the presence of the highly abundant β-subunit of ATPase in both WT and KO mice, with no evidence of the rH_{3A} protein isoform.

3.8. LC/MS analysis of the ~48kDa band of P2 membranes from HEK-293 cells

Subsequently, western blotting experiments were repeated in our laboratory, as described in Section 3.3 above, using higher amounts (20–50 μg) of P2 membranes from rH_{3A} mRNA-transfected HEK 293 cells than used in earlier studies (Figure 6). Figure 9A illustrates a Coomassie-stained gel of increasing amounts of protein. Figure 9B is the fluorescence image of the western blot illustrating increasing amounts of rH_{3A} protein at ~48 kDa (yellow bands). In addition, we noted yellow bands near the ~100 kDa and ~ 150 kDa molecular weight markers, suggesting the possibility of rH_{3A} dimers and trimers in this preparation (Figure 9B). Finally, the antibody also bound to another protein (green band) just above the ~48 kDa rH_{3A} band, but below the ~55 kDa band observed in western blots of rodent membranes (Figure 7). This protein, whose identity is uncertain at this point, had not been observed in earlier studies using lower amounts (5 μg) of HEK-293 membrane protein. Subsequently, the ~48 kDa band was excised from the 50 μg lane of the gel (white box in Figure 9A) and sent to the Clarkson Laboratory where LC/MS analysis detected the presence of rH_{3A} protein from the excised band. However, the level of rH_{3A} protein detected was below the limit of quantitative reliability (LOQ), even in rH_{3A} overexpressing HEK-293 cells, suggesting that it would not be possible to quantitate rH_{3A} in rodent membranes.

4. Discussion

The salient observation from this study is that moderate PAE is associated with variable alterations in the expression of two H3R mRNA isoforms in dentate gyrus and some cerebral cortical and cerebellar brain regions of adult offspring. While no consistent pattern of mRNA alterations were noted for either H3R mRNA isoform, a prevailing sex-related effect was noted for one or both isoforms in five of the six brain regions studied. In all of these cases, mRNA expression was significantly greater in males than females and, with the exception of the hippocampal CA3 region (Figure 3E), only in control rats. A significant main effect of prenatal treatment was only observed in the parietal cortex (Figure 3D), but significant

treatment differences were also observed in the dentate gyrus (Figure 3A) and entorhinal cortex (Figure 3B) in males only.

Examining whether the H3R mRNA alterations were consistent with what would have been predicted based on prior H3R agonist-stimulated GTP binding data in some of these brain regions (Varaschin et al., 2018) is problematic at this point. First, the H3R-agonist-stimulated GTP binding data reported previously was based entirely on studies in female rats. Nevertheless, given that elevations in GTP binding were noted previously in dentate gyrus, parietal cortex, medial frontal cortex and cerebellum, one prediction based on the greater intrinsic activity of rH_{3A} compared to rH_{3C} would have been a PAE-induced elevation in rH_{3A} relative to rH_{3C} in these four brain regions, at least in female rat brain. However, prenatal treatment effects were not observed in any of the six brain regions of female rats. Prenatal treatment effects were observed for males in dentate gyrus and parietal cortex, but not medial frontal cortex. However, the elevation in rH_{3A} mRNA expression occurred in control rats, not PAE rats, as would have been predicted from the H3R agonist-stimulated GTP binding data. Whether the effect of sex on rH_{3A} and rH_{3C} expression could have been predicted based on H3R agonist-stimulated GTP binding in male rats awaits completion of ongoing studies of H3R agonist-stimulated GTP binding in male control and PAE offspring. Thus, whether a PAE-induced shift in H3R mRNA isoform expression relates to diminished H3R agonist responsiveness is unclear. Further, there are many cases where there are either no or even negative correlations between mRNA expression and protein expression data (Moritz et al., 2019) that limit interpreting the functional implications of these alterations in mRNA expression.

Given the limitations of interpreting changes in mRNA expression relative to measures of H3R function, it was critically important to quantitate H3R isoform protein expression in brain regions where PAE altered H3R mRNA expression (Figure 3) as well as "downstream" measures of H3R function (Varaschin et al., 2018). While there are a number of commercially available pan-H3R antibodies, our goal, given our working hypothesis, was to design an antibody that specifically binds to rH_{3A} protein without detecting the other two functional rH3Rs, namely the rH_{3B} and rH_{3C}. To this end, we developed a polyclonal antibody based on a fourteen amino acid segment in the third cytoplasmic loop of the rH_{3A} that is not present in either the rH_{3B} or rH_{3C} isoforms (see Figure 2). Subsequently, we were able to demonstrate H3RA specificity for binding rH_{3A} protein in membranes prepared from overexpressing HEK-293 cells (Figure 6). In addition to H3RA antibody development, we generated a transgenic line of pan-mH3R knockout mice to further test H3RA antibody specificity and confirmed the virtual absence of pan-H3R mRNA (Figure 4) and H3 agonist receptor-effector coupling (Figure 5) in H3R KO mouse brain.

Going forward, we predicted that rH_{3A} protein expression would be elevated in PAE rat brain, consistent with the original hypothesis of this study. However, extensive efforts to visualize rH_{3A} protein expression in rat membranes by western blotting were frustrated by the inability to detect the same ~48 kDa band of antibody binding as had been seen in rH_{3A} mRNA-overexpressing HEK-293 cells (Figure 6). Increasing the amount of protein sample or the concentrations of primary and secondary antibody were not successful. We also acquired a pan-H3R antibody from MyBioSource that was used in conjunction with the GenScript H3RA antibody to explore, different immunoprecipitation procedures for enriching H3R protein from tissue preparations using a protocol modified from Cotney and Noonan (2015), and tried to visualize protein both by fluorescence and chemiluminescence detection procedures. We also switched from β-actin (~42 kDa) to the α-$_1$ subunit of Na^+/K^+ ATPase (110 kDa), as a better reference protein for membrane-associated proteins given that β-actin labeling may have interfered with visualization of H3 receptor isoforms. However, none of these manipulations were successful for detecting the rH_{3A} protein isoform in rat brain membrane preparations. Our tentative conclusion from these studies was that rH_{3A} protein may exist in relatively low abundance in comparison to other receptor proteins and not amenable to quantitation by standard immunological techniques.

While we were unable to visualize H3RA antibody binding to a ~ 48 kDa band in rat membranes, the antibody did label a different band at ~55 kDa (Figure 7A). We subsequently ran western blots of medial frontal cortex from rat, and WT and H3R KO mice which showed the presence of the ~55 kDa band in all three preparations (Figure 7B), indicating that the ~55 kDa the band was not H3R protein. A subsequent LC/MS analysis of the ~55 kDa bands excised from WT and KO mice gels (Figure 8) confirmed no detectable H3R protein in the WT mouse, but identified the highly abundant beta subunit of ATPase protein in both genotypes.

These latter results highlight one of the challenges concerning antibody specificity, particularly when attempting to quantitate relatively low-abundance proteins in native tissues. At the outset of this study, we opted to develop a polyclonal antibody, which are generally less expensive and faster to produce, and they can also recognize multiple epitopes of a single protein antigen, thus providing higher sensitivity for detecting lower abundance proteins. However, polyclonal antibodies can have problems with batch to batch variability. They also have a higher chance of cross-reactivity due to recognition of multiple epitopes that can also cause antibody binding to other protein antigens of lower affinity but present in higher concentrations; such as with the beta subunit of ATPase in the ~55 kDa band from rodent membranes in our studies (Figures 7, 8) and an as yet unidentified protein observed with higher sample protein amounts from HEK-293 cells (Figure 9). The issue of specificity becomes more problematic when increasing the amount of sample protein, primary or secondary antibody in an attempt to detect the protein of interest.

Two alternative approaches for detecting rH_{3A} were considered in lieu of a polyclonal antibody. The first was to consider developing a monoclonal antibody to rH_{3A}. In general, monoclonal antibodies are more specific for target protein antigens, given that only a single epitope of an antigen is recognized, thus, they have lower cross-reactivity and also greater homogeneity between batches. However, monoclonal antibodies require significantly more time to produce and, thus, are more expensive to manufacture. Given the relatively lower sensitivity for protein detection with a single binding epitope coupled with the low relative abundance of H3R protein, we were not confident of greater success at visualizing rH_{3A} protein with a monoclonal antibody than we had been with the rH_{3A} polyclonal antibody. A second alternative approach that was considered, given that we have visualized pan-H3R binding with the H3R antagonist [^{3}H]-A349821 (Varaschin et al., 2018), and routinely measure H3R

function by H3R agonist-stimulated [^{35}S]-GTPγS binding (Figure 5), was to radiolabel our GenScript polyclonal antibody. Such an approach would have greatly increased the sensitivity of antibody binding reaction providing the radiolabeling procedure did not affect antibody affinity or specificity. However, significant disadvantages to this approach include the relatively short half-lives of radioisotopes that could be employed in these studies along with the prohibitively high cost of purchasing many radioisotopes in recent years.

In conclusion, we demonstrate here sex-and/or moderate PAE-related alterations in the expression of at least two H3R mRNA isoforms in rat brain regions where we have previously demonstrated elevated H3R function (Varaschin et al., 2018). However, the mRNA alterations observed in Figure 3 were variable across brain regions, were sex-related in some cases and, where present, the prenatal treatment effects were in the opposite direction from what had been predicted from H3R agonist-stimulated GTP binding data reported previously. Further, interpreting the functional consequences of altered H3R mRNA isoform expression in PAE rats is limited given the inability to assess these changes at the receptor isoform protein level. Thus, we were unable to confirm whether a PAE-induced alteration in the differential expression of specific H3R isoforms is one mechanism contributing to the heightened H3 receptor-effector coupling and H3R function in dentate gyrus and cerebral cortex of PAE rats. Our studies here also highlight the challenge of quantitating proteins that exist in very low abundance of native tissues. Indeed, while the rH_{3A} protein isoform was detectable in rH_{3A}-overexpressing HEK-293 cells, rH_{3A} protein was present in too low of an abundance in rodent membranes to be reliably quantitated by the methods employed here. Further, most all prior reports measuring H3R isoform expression and examining the function of different H3R isoforms have relied on overexpression systems, such as HEK-293 cells, to generate enough H3R protein to conduct studies using standard biochemical approaches.

While we were unable to confirm whether PAE differentially alters different H3R isoforms in a manner that would alter H3R function, it is important to point out that PAE may alter a variety of other "downstream mechanisms" that could modify H3R receptor affinity and/or H3 receptor-effector coupling in a manner that alters H3R receptor function, independent of whether H3R number or isoform expression have been altered. For example, H3Rs, like other G protein-coupled receptors (Gainetdinov et al., 2004; Gurevich et al., 2012), undergo desensitization and downregulation in the presence of H3R agonists (Garduño-Torres and Arias-Montaño, 2006; Osorio-Espinoza et al., 2014; Montejo-López et al., 2016). While the mechanisms that mediate desensitization have not been investigated with H3Rs, other GPCRs are desensitized via multiple mechanisms including the activation of phospholipases, protein kinases and protein phosphatases, which can modulate receptor affinity and function of GPCRs (Sorensen et al., 2002; Suh et al., 2013). It is interesting to note that prior studies have shown reductions in the activity of phospholipase β1 and phospholipase A2 (Allan et al., 1997), protein kinase C (Perrone-Bizzozero et al., 1998) and extracellular signal-regulated kinase (Samudio-Ruiz et al., 2009) in hippocampal formation of PAE rodents. Whether any of these enzymes regulate H3R function in general or after PAE is unknown, but one question is whether protein kinase-mediated capacity to desensitize H3Rs is diminished in PAE rats in a manner that may contribute to the heightened H3 receptor coupling we have observed in PAE rats.

Another mechanism for modulating H3R function that may be altered after PAE relates to receptor regulation by interactions with other transmitter receptors and other modulatory proteins. Consistent with our observations of rH_{3A} mRNA-overexpressing HEK-293 cells (Figure 9B), a number of studies have reported that H3Rs can dimerize with a variety of other neurotransmitter receptors (Shenton et al., 2005; Márquez-Gómez et al., 2018) as well as form trimers combining with dopamine D1 and NMDA-glutamate receptors (Rodríguez-Ruiz et al., 2017). Typically, these reports show how H3Rs modulate the function of its dimer / trimer partner, but do not report whether activation of the partner receptors alters H3R function. Whether or not PAE alters the heterodimerization of receptors or changes the function of H3R-containing dimers is unknown. However, one regulatory protein that may be of particular interest here is the Sigma 1 receptor (S1R) which acts as a "chaperone protein" modifying the activity of many protein targets, including GPCRs in membranes and cytoplasm of different cell types (Mishra et al., 2015; Pasternak, 2017), including H3Rs (Moreno et al., 2014). Curiously, many different classes of clinically-used neuroactive agents have representatives that, in addition to their primary mechanism of action, also act either as S1R agonists or antagonists (Cobos et al., 2008). One such class of agents is the H3R inverse agonists (Riddy et al., 2019; Szczepańska et al., 2021). Indeed, Riddy and colleagues reported that ABT-239, the agent that reversed both LTP and learning deficits in our PAE rats (Savage et al., 2010; Varaschin et al., 2010), has similar affinity for both H3Rs and S1Rs. As ABT-239 reversed PAE-induced LTP deficits without affecting LTP in control rats, one possible interpretation of this differential effect of ABT-239 may be a difference in how S1Rs modulate H3R function in PAE rats compared to control, a question currently under investigation in our laboratory.

Data availability statement

The raw data supporting the conclusions of this article will be made available by the authors, without undue reservation.

Ethics statement

The animal study was reviewed and approved by University of New Mexico Health Sciences Center Institutional Animal Care and Use Committee.

Author contributions

SD, CV, and DS conceived and contributed to the experimental design of the study. KL, ER, SD, and DS generated moderate PAE rat offspring for the *in situ* hybridization studies. KL, SD, and DS conducted and analyzed the *in situ* hybridization studies in rat. SD harvested and transfected HEK-293 cells with

different rH3 mRNA isoforms for western blotting studies, conducted the qRT-PCR studies in H3R transgenic mice, and processed them for the western blotting studies. SD and CV supervised the management of the H3R transgenic mouse colony. ER and DS conducted and analyzed the GTP binding studies in H3R transgenic mice. SD and DS harvested brain tissues and prepared the manuscript. All authors read and approved the submitted version of the manuscript.

Funding

This work was supported by NIH-NIAAA 1 P50 AA022534.

Acknowledgments

The authors thank Nicole Crandall, Victoria Sugita, April Sweeney, Jennifer Wagner and Kevin O'Hair for their outstanding animal husbandry support. We also thank Jason Weick for kindly providing us HEK-293 cells. We thank Michela Dell'Orco for her advice on the qRT-PCR analysis and Elizabeth Solomon for sharing the immunoprecipitation procedures. We also thank Jon Johansen and Matt Hoelter of Kendrick Laboratories Inc. for conducting western blot studies to confirm our results and Costel Darie for conducting the LS/MS analysis of the ~55 kDa and ~ 48 kDa bands from western blots.

Conflict of interest

The authors declare that the research was conducted in the absence of any commercial or financial relationships that could be construed as a potential conflict of interest.

Publisher's note

All claims expressed in this article are solely those of the authors and do not necessarily represent those of their affiliated organizations, or those of the publisher, the editors and the reviewers. Any product that may be evaluated in this article, or claim that may be made by its manufacturer, is not guaranteed or endorsed by the publisher.

References

Allan, A. M., Weeber, E. J., Savage, D. D., and Caldwell, K. K. (1997). Effect of prenatal ethanol exposure on phospholipase C-beta 1 and phospholipase A_2 in hippocampus and medial frontal cortex of adult rat offspring. *Alcohol. Clin. Exp. Res.* 21, 1534–1541.

Allen, M., Bird, C., Feng, W., Liu, G., Li, W., Perrone-Bizzozero, N. I., et al. (2013). HuD promotes BDNF expression in brain neurons via selective stabilization of the BDNF long 3'UTR mRNA. *PLoS One* 8:e55718. doi: 10.1371/journal.pone.0055718

Arrang, J. M., Garbarg, M., and Schwartz, J. C. (1983). Auto-inhibition of brain histamine release mediated by a novel class (H3) of histamine receptor. *Nature* 302, 832–837. doi: 10.1038/302832a0

Aslebagh, R., Channaveerappa, D., Arcaro, F. K., and Darie, C. C. (2018). Comparative two-dimensional polyacrylamide gel electrophoresis (2D-PAGE) of human milk to identify dysregulated proteins in breast cancer. *Electrophoresis*. doi: 10.1002/elps.201800025

Bakker, R. A. (2004). Histamine H3-receptor isoforms. *Inflamm. Res.* 53, 509–516. doi: 10.1007/s00011-004-1286-9

Bakker, R. A., Lozada, A. F., van Marle, A., Shenton, F. C., Drutel, G., Karlstedt, K., et al. (2006). Discovery of naturally occurring splice variants of the rat histamine H3 receptor that act as dominant-negative isoforms. *Mol. Pharmacol.* 69, 1194–1206. doi: 10.1124/mol.105.019299

Bongers, G., Krueger, K. M., Miller, T. R., Baranowski, J. L., Estvander, B. R., Witte, D. G., et al. (2007). An 80-amino acid deletion in the third intracellular loop of a naturally occurring human histamine H3 isoform confers pharmacological differences and constitutive activity. *J. Pharmacol. Exp. Ther.* 323, 888–898. doi: 10.1124/jpet.107.127639

Brioni, J. D., Esbenshade, T., Garrison, T., Bitner, S., and Cowart, M. (2011). H_3 receptor miniseries: discovery of histamine H_3 antagonists for the treatment of cognitive disorders and Alzheimer's disease. *J. Pharmacol. Exp. Ther.* 336, 38–46. doi: 10.1124/jpet.110.166876

Channaveerappa, D., Lux, J. C., Wormwood, K. L., Heintz, T. A., McLerie, M., Treat, J. A., et al. (2017). Atrial electrophysiological and molecular remodeling induced by obstructive sleep apnea. *J. Cell. Mol. Med.* 21, 2223–2235. doi: 10.1111/jcmm.13145

Clapham, J., and Kilpatrick, G. J. (1992). Histamine H_3 receptors modulate the release of [^{3}H]-acetylcholine from slices of rat entorhinal cortex: evidence for the possible existence of H_3 receptor subtypes. *Br. J. Pharmacol.* 107, 919–923. doi: 10.1111/j.1476-5381.1992.tb13386.x

Cobos, E. J., Entrena, J. M., Nieto, F. R., Cendán, C. M., and Del Pozo, E. (2008). Pharmacology and therapeutic potential of sigma (1) receptor ligands. *Curr. Neuropharmacol.* 6, 344–366. doi: 10.2174/157015908787386113

Cotney, J. L., and Noonan, J. P. (2015). Chromatin immunoprecipitation with fixed animal tissues and preparation for high-throughput sequencing. *Cold Spring Harb. Protoc.* 419. doi: 10.1101/pdb.err087585, Erratum for: *Cold Spring Harb Protoc*. 2015 Feb; 2015 (2):191–9

Davies, S., Nelson, D. E., and Savage, D. D. (2023). Impact of two different rodent diets on maternal ethanol consumption, serum ethanol concentration and pregnancy outcome measures. *Alcohol* 22, S0741-8329(23)00219–7. doi: 10.1016/j.alcohol.2023.05.002

Drutel, G., Peitsaro, N., Karlstedt, K., Wieland, K., Smit, M. J., Timmerman, H., et al. (2001). Identification of rat H3 receptor isoforms with different brain expression and signaling properties. *Mol. Pharmacol.* 59, 1–8.

Esbenshade, T. A., Browman, K. E., Bitner, R. S., Strakhova, M., Cowart, M. D., and Brioni, J. D. (2008). The histamine H_3 receptor: an attractive target for the treatment of cognitive disorders. *Br. J. Pharmacol.* 154, 1166–1181. doi: 10.1038/bjp.2008.147

Gainetdinov, R. R., Premont, R. T., Bohn, L. M., Lefkowitz, R. J., and Caron, M. G. (2004). Desensitization of G protein-coupled receptors and neuronal functions. *Annu. Rev. Neurosci.* 27, 107–144. doi: 10.1146/annurev.neuro.27.070203.144206

Galindo, R., Frausto, S., Wolff, C., Caldwell, K. K., Perrone-Bizzozero, N. I., and Savage, D. D. (2004). Prenatal ethanol exposure reduces $mGluR_5$ receptor number and function in the dentate gyrus of adult offspring. *Alcohol. Clin. Exp. Res.* 28, 1587–1597. doi: 10.1097/01.alc.0000141815.21602.82

Garduño-Torres, B., and Arias-Montaño, J. A. (2006). Homologous down-regulation of histamine H3 receptors in rat striatal slices. *Synapse* 60, 165–171. doi: 10.1002/syn.20288

Garduño-Torres, B., Treviño, M., Gutiérrez, R., and Arias-Montaño, J. A. (2007). Presynaptic histamine H3 receptors regulate glutamate, but not GABA release in rat thalamus. *Neuropharmacology* 52, 527–535. doi: 10.1016/j.neuropharm.2006.08.001

Gurevich, E. V., Tesmer, J. J., Mushegian, A., and Gurevich, V. V. (2012). G protein-coupled receptor kinases: more than just kinases and not only for GPCRs. *Pharmacol. Ther.* 133, 40–69. doi: 10.1016/j.pharmthera.2011.08.001

Haas, H. L., Sergeeva, O. A., and Selbach, O. (2008). Histamine in the nervous system. *Physiol. Rev.* 88, 1183–1241. doi: 10.1152/physrev.00043.2007

Hamilton, D. A., Magcalas, C. M., Barto, D., Bird, C. W., Rodriguez, C. I., Fink, B. C., et al. (2014). Moderate prenatal alcohol exposure and quantification of social behavior in adult rats. *J. Vis. Exp.* 94:52407. doi: 10.3791/52407

Laemmli, U. K. (1970). Cleavage of structural proteins during the assembly of the head of bacteriophage T4. *Nature* 227, 680–685. doi: 10.1038/227680a0

Livak, K. J., and Schmittgen, T. D. (2001). Analysis of relative gene expression data using real-time quantitative PCR and the 2-ΔΔCT method. *Methods* 25, 402–408. doi: 10.1006/meth.2001.1262

Lux, J. C., Channaveerappa, D., Aslebagh, R., Heintz, T. A., McLerie, M., Panama, B. K., et al. (2019). Identification of dysregulation of atrial proteins in rats with chronic obstructive apnea using two-dimensional polyacrylamide gel

electrophoresis and mass spectrometry. *J. Cell. Mol. Med.* 23, 3016–3020. doi: 10.1111/jcmm.14131

Márquez-Gómez, R., Robins, M. T., Gutiérrez-Rodelo, C., Arias, J. M., Olivares-Reyes, J. A., van Rijn, R. M., et al. (2018). Functional histamine H3 and adenosine A2A receptor heteromers in recombinant cells and rat striatum. *Pharmacol. Res.* 129, 515–525. doi: 10.1016/j.phrs.2017.11.036

Mihăşan, M., Babii, C., Aslebagh, R., Channaveerappa, D., Dupree, E., and Darie, C. C. (2018). Proteomics based analysis of the nicotine catabolism in *Paenarthrobacter nicotinovorans* pAO1. *Sci. Rep.* 8 16239, 1–9. doi: 10.1038/s41598-018-34687-y

Mishra, A. K., Mavlyutov, T., Singh, D. R., Biener, G., Yang, J., Oliver, J. A., et al. (2015). The sigma-1 receptors are present in monomeric and oligomeric forms in living cells in the presence and absence of ligands. *Biochem. J.* 466, 263–271. doi: 10.1042/BJ20141321

Montejo-López, W., Rivera-Ramírez, N., Escamilla-Sánchez, J., García-Hernández, U., and Arias-Montaño, J. A. (2016). Heterologous, PKC-mediated desensitization of human histamine H3 receptors expressed in CHO-K1 cells. *Neurochem. Res.* 41, 2415–2424. doi: 10.1007/s11064-016-1954-5

Moreno, E., Moreno-Delgado, D., Navarro, G., Hoffmann, H. M., Fuentes, S., Rosell-Vilar, S., et al. (2014). Cocaine disrupts histamine H3 receptor modulation of dopamine D1 receptor signaling: σ1-D1-H3 receptor complexes as key targets for reducing cocaine's effects. *J. Neurosci.* 34, 3545–3558. doi: 10.1523/JNEUROSCI.4147-13.2014

Morisset, S., Sasse, A., Gbahou, F., Héron, A., Ligneau, X., Tardivel-Lacombe, J., et al. (2001). The rat H3 receptor: gene organization and multiple isoforms. *Biochem. Biophys. Res. Commun.* 280, 75–80. doi: 10.1006/bbrc.2000.4073

Moritz, C. P., Mühlhaus, T., Tenzer, S., Schulenborg, T., and Friauf, E. (2019). Poor transcript-protein correlation in the brain: negatively correlating gene products reveal neuronal polarity as a potential cause. *J. Neurochem.* 149, 582–604. doi: 10.1111/jnc.14664

Nieto-Alamilla, G., Márquez-Gómez, R., García-Gálvez, A. M., Morales-Figueroa, G. E., and Arias-Montaño, J. A. (2016). The histamine H3 receptor: structure, pharmacology, and function. *Mol. Pharmacol.* 90, 649–673. doi: 10.1124/mol.116.104752

Nikolic, K., Filipic, S., Agbaba, D., and Stark, H. (2014). Procognitive properties of drugs with single and multitargeting H3 receptor antagonist activities. *CNS Neurosci. Ther.* 20, 613–623. doi: 10.1111/cns.12279

O'Farrell, P. H. (1975). High resolution two-dimensional electrophoresis of proteins. *J. Biol. Chem.* 250, 4007–4021.

Osorio-Espinoza, A., Escamilla-Sánchez, J., Aquino-Jarquin, G., and Arias-Montaño, J. A. (2014). Homologous desensitization of human histamine H_3 receptors expressed in CHO-K1 cells. *Neuropharmacology* 77, 387–397. doi: 10.1016/j.neuropharm.2013.09.011

Pasternak, G. W. (2017). Allosteric modulation of opioid G-protein coupled receptors by sigma 1 receptors. *Handb. Exp. Pharmacol.* 244, 163–175. doi: 10.1007/164_2017_34

Paxinos, G., and Franklin, K.B.J. (2013). *The mouse brain in stereotaxic coordinates*. Academic Press, San Diego.

Paxinos, G., and Watson, C. (1998) *The rat brain in stereotaxic coordinates*. Academic Press, San Diego.

Perrone-Bizzozero, N. I., Isaacson, T. V., Keidan, G. M., Eriqat, C., Meiri, K. F., Savage, D. D., et al. (1998). Prenatal ethanol exposure decreases GAP-43 phosphorylation and protein kinase C activity in the hippocampus of adult rat offspring. *J. Neurochem.* 71, 2104–2111. doi: 10.1046/j.1471-4159.1998.71052104.x

Riddy, D. M., Cook, A. E., Shackleford, D. M., Pierce, T. L., Mocaer, E., Mannoury la Cour, C., et al. (2019). Drug-receptor kinetics and sigma-1 receptor affinity differentiate clinically evaluated histamine H_3 receptor antagonists. *Neuropharmacology* 144, 244–255. doi: 10.1016/j.neuropharm.2018.10.028

Rodríguez-Ruiz, M., Moreno, E., Moreno-Delgado, D., Navarro, G., Mallol, J., Cortés, A., et al. (2017). Heteroreceptor complexes formed by dopamine D1, histamine H3, and N-methyl-D-aspartate glutamate receptors as targets to prevent neuronal death in Alzheimer's disease. *Mol. Neurobiol.* 54, 4537–4550. doi: 10.1007/s12035-016-9995-y

Samudio-Ruiz, S. L., Allan, A. M., Valenzuela, C. F., Perrone-Bizzozero, N. I., and Caldwell, K. K. (2009). Prenatal ethanol exposure persistently impairs NMDA receptor-dependent activation of extracellular signal-regulated kinase in the mouse dentate gyrus. *J. Neurochem.* 109, 1311–1323. doi: 10.1111/j.1471-4159.2009.06049.x

Savage, D. D., Becher, M., de la Torre, A. J., and Sutherland, R. J. (2002). Dose-dependent effects of prenatal ethanol exposure on synaptic plasticity and learning in mature offspring. *Alcohol. Clin. Exp. Res.* 26, 1752–1758. doi: 10.1097/01.ALC.0000038265.52107.20

Savage, D. D., Cruz, L. L., Duran, L. M., and Paxton, L. L. (1998). Prenatal ethanol exposure diminishes activity-dependent potentiation of amino acid neurotransmitter release in adult rat offspring. *Alcohol. Clin. Exp. Res.* 22, 1771–1777. doi: 10.1111/j.1530-0277.1998.tb03978.x

Savage, D. D., Rosenberg, M. J., Wolff, C. R., Akers, K. G., el-Emawy, A., Staples, M. C., et al. (2010). Effects of a novel cognition-enhancing agent on fetal ethanol-induced learning deficits. *Alcohol. Clin. Exp. Res.* 34, 1793–1802. doi: 10.1111/j.1530-0277.2010.01266.x

Schlicker, E., Betz, R., and Gothert, M. (1988). Histamine H_3 receptor-medicated inhibition of serotonin release in the rat brain cortex. *Naunyn Schmiedeberg's Arch. Pharmacol.* 337, 588–590. doi: 10.1007/BF00182737

Schlicker, E., Fink, K., Detzner, M., and Göthert, M. (1993). Histamine inhibits dopamine release in the mouse striatum via presynaptic H3 receptors. *J. Neural Transm. Gen. Sect.* 93, 1–10. doi: 10.1007/BF01244933

Schlicker, E., Fink, K., Hinterhaner, M., and Gothert, M. (1989). Inhibition of noradrenaline release in the rat brain cortex via presynaptic H_3 receptors. *Naunyn Schmiedeberg's Arch. Pharmacol.* 340, 633–638. doi: 10.1007/BF00717738

Shenton, F. C., Hann, V., and Chazot, P. L. (2005). Evidence for native and cloned H3 histamine receptor higher oligomers. *Inflamm. Res.* 54, S48–S49. doi: 10.1007/s00011-004-0422-x

Smith, P. K., et al. (1985). Measurement of protein using bicinchoninic acid. *Anal. Biochem.* 150, 76–85. doi: 10.1016/0003-2697(85)90442-7

Sorensen, S. D., Macek, T. A., Cai, Z., Saugstad, J. A., and Conn, P. J. (2002). Dissociation of protein kinase-mediated regulation of metabotropic glutamate receptor 7 (mGluR7) interactions with calmodulin and regulation of mGluR7 function. *Mol. Pharmacol.* 61, 1303–1312. doi: 10.1124/mol.61.6.1303

Suh, Y. H., Park, J. Y., Park, S., Jou, I., Roche, P. A., and Roche, K. W. (2013). Regulation of metabotropic glutamate receptor 7 (mGluR7) internalization and surface expression by Ser/Thr protein phosphatase 1. *J. Biol. Chem.* 288, 17544–17551. doi: 10.1074/jbc.M112.439513

Sutherland, R. J., McDonald, R. J., and Savage, D. D. (1997). Prenatal exposure to moderate levels of ethanol can have long-lasting effects on hippocampal synaptic plasticity in adult offspring. *Hippocampus* 7, 232–238. doi: 10.1002/(SICI)1098-1063(1997)7:2<232::AID-HIPO9>3.0.CO;2-O

Sutherland, R. J., McDonald, R. J., and Savage, D. D. (2000). Prenatal exposure to moderate levels of ethanol can have long-lasting effects on learning and memory of adult rat offspring. *Psychobiology* 28, 532–539. doi: 10.3758/BF03332012

Szczepańska, K., Kuder, K. J., and Kieć-Kononowicz, K. (2021). Dual-targeting approach on histamine H3 and Sigma-1 receptor ligands as promising pharmacological tools in the treatment of CNS-linked disorders. *Curr. Med. Chem.* 28, 2974–2995. doi: 10.2174/0929867327666200806103144

Toyota, H., Dugovic, C., Koehl, M., Laposky, A. D., Weber, C., Ngo, K., et al. (2002). Behavioral characterization of mice lacking histamine H (3) receptors. *Mol. Pharmacol.* 62, 389–397. Erratum in: Mol Pharmacol 2002 Sep; 62(3):763. doi: 10.1124/mol.62.2.389

Varaschin, R. K., Akers, K. G., Rosenberg, M. J., Hamilton, D. A., and Savage, D. D. (2010). Effects of the cognition-enhancing agent ABT-239 on fetal ethanol-induced deficits in dentate gyrus synaptic plasticity. *J. Pharmacol. Exp. Ther.* 334, 191–198. doi: 10.1124/jpet.109.165027

Varaschin, R. K., Allen, N. A., Rosenberg, M. J., Valenzuela, C. F., and Savage, D. D. (2018). Prenatal alcohol exposure increases histamine H3 receptor-mediated inhibition of glutamatergic neurotransmission in rat dentate gyrus. *Alcohol. Clin. Exp. Res.* 42, 295–305. doi: 10.1111/acer.13574

Varaschin, R. K., Rosenberg, M. J., Hamilton, D. A., and Savage, D. D. (2014). Differential effects of the histamine H (3) receptor agonist methimepip on dentate granule cell excitability, paired-pulse plasticity and long-term potentiation in prenatal alcohol-exposed rats. *Alcohol. Clin. Exp. Res.* 38, 1902–1911. doi: 10.1111/acer.12430

Weeber, E. J., Savage, D. D., Sutherland, R. J., and Caldwell, K. K. (2001). Fear conditioning-induced alterations of phospholipase C-beta 1a protein level and enzyme activity in rat hippocampal formation and medial frontal cortex. *Neurobiol. Learn. Mem.* 76, 151–182. doi: 10.1006/nlme.2000.3994

Wormwood, K. L., Ngounou Wetie, A. G., Gomez, M. V., Ju, Y., Kowalski, P., Mihasan, M., et al. (2018). Structural characterization and disulfide assignment of spider peptide Phα1β by mass spectrometry. *J. Am. Soc. Mass Spectrom.* 29, 827–841. doi: 10.1007/s13361-018-1904-3

frontiers | Frontiers in Neuroscience

TYPE Original Research
PUBLISHED 06 July 2023
DOI 10.3389/fnins.2023.1187220

Check for updates

OPEN ACCESS

EDITED BY
Hermes H. Yeh,
Dartmouth College, United States

REVIEWED BY
Katherine Nautiyal,
Dartmouth College, United States
Johann Eberhart,
The University of Texas at Austin, United States

*CORRESPONDENCE
Sandra M. Mooney
✉ sandra_mooney@unc.edu

RECEIVED 15 March 2023
ACCEPTED 14 June 2023
PUBLISHED 06 July 2023

CITATION
Mooney SM, Billings E, McNew M, Munson CA, Shaikh SR and Smith SM (2023) Behavioral changes in *FPR2/ALX* and *Chemr23* receptor knockout mice are exacerbated by prenatal alcohol exposure.
Front. Neurosci. 17:1187220.
doi: 10.3389/fnins.2023.1187220

COPYRIGHT
© 2023 Mooney, Billings, McNew, Munson, Shaikh and Smith. This is an open-access article distributed under the terms of the Creative Commons Attribution License (CC BY). The use, distribution or reproduction in other forums is permitted, provided the original author(s) and the copyright owner(s) are credited and that the original publication in this journal is cited, in accordance with accepted academic practice. No use, distribution or reproduction is permitted which does not comply with these terms.

Behavioral changes in *FPR2/ALX* and *Chemr23* receptor knockout mice are exacerbated by prenatal alcohol exposure

Sandra M. Mooney[1,2]*, Elanaria Billings[1], Madison McNew[1], Carolyn A. Munson[1], Saame R. Shaikh[2] and Susan M. Smith[1,2]

[1]Nutrition Research Institute, University of North Carolina at Chapel Hill, Kannapolis, NC, United States, [2]Department of Nutrition, University of North Carolina at Chapel Hill, Kannapolis, NC, United States

Introduction: Prenatal alcohol exposure (PAE) causes neuroinflammation that may contribute to the pathophysiology underlying Fetal Alcohol Spectrum Disorder. Supplementation with omega-3 polyunsaturated fatty acids (PUFAs) has shown success in mitigating effects of PAE in animal models, however, the underlying mechanisms are unknown. Some PUFA metabolites, specialized pro-resolving mediators (SPMs), play a role in the resolution phase of inflammation, and receptors for these are in the brain.

Methods: To test the hypothesis that the SPM receptors FPR2 and ChemR23 play a role in PAE-induced behavioral deficits, we exposed pregnant wild-type (WT) and knockout (KO) mice to alcohol in late gestation and behaviorally tested male and female offspring as adolescents and young adults.

Results: Maternal and fetal outcomes were not different among genotypes, however, growth and behavioral phenotypes in the offspring did differ and the effects of PAE were unique to each line. In the absence of PAE, ChemR23 KO animals showed decreased anxiety-like behavior on the elevated plus maze and FPR2 KO had poor grip strength and low activity compared to age-matched WT mice. WT mice showed improved performance on fear conditioning between adolescence and young adulthood, this was not seen in either KO.

Discussion: This PAE model has subtle effects on WT behavior with lower activity levels in young adults, decreased grip strength in males between test ages, and decreased response to the fear cue indicating an effect of alcohol exposure on learning. The PAE-mediated decreased response to the fear cue was also seen in ChemR23 KO but not FPR2 KO mice, and PAE worsened performance of adolescent FPR2 KO mice on grip strength and activity. Collectively, these findings provide mechanistic insight into how PUFAs could act to attenuate cognitive impairments caused by PAE.

KEYWORDS

prenatal alcohol exposure, brain development, cognition, behavior, omega-3 polyunsaturated fatty acid, specialized pro-resolving mediator, Fetal Alcohol Spectrum Disorder, inflammation

1. Introduction

At least 13.5% of pregnant women report using alcohol and ~5% report binge drinking (Gosdin et al., 2022). The incidence of Fetal Alcohol Spectrum Disorders (FASDs), a potential consequence of alcohol exposure, in the US is estimated at 2–5% (May et al., 2018). Prenatal alcohol exposure (PAE) causes behavioral effects in humans and in animal models including in learning and memory (Hoyme et al., 2016; Marquardt and Brigman, 2016); these outcomes persist through the lifespan but may present differently at different ages (e.g., Day and Richardson, 2004; Goldschmidt et al., 2019; Jacobson et al., 2021; Smith et al., 2022). At this time, little is known about mechanisms that underlie the risk and resilience factors affecting PAE, including nutrition.

Supplementation with omega-3 polyunsaturated fatty acids (PUFAs) has shown success in mitigating effects of PAE in animal models. We showed that postnatal supplementation with the omega-3 PUFA docosahexaenoic acid (DHA) improved prenatal alcohol-induced deficits in social behaviors in a rat model of FASD (Wellmann et al., 2015). Others have shown that maternal supplementation with lipids enriched with combinations of omega-3 PUFAs improve alcohol effects on sensory development, hyperactivity, and hippocampal synaptic plasticity (Wainwright et al., 1990; Patten et al., 2013; Balaszczuk et al., 2019). Interestingly, in a study in humans with FASDs we identified a SNP in the fatty acid desaturase gene *FADS2* that was associated with better performance on a memory test, supporting the idea that PUFAs may also modulate outcomes in humans following PAE (Smith et al., 2021). However, it is unknown how omega-3 PUFAs might confer such a benefit.

Candidate mechanisms include through their anti-inflammatory and/or pro-resolution activities. Alcohol is a potent pro-inflammatory agent, and PAE causes both systemic and neuroinflammation, and in animal models this inflammation can be persistent (Cantacorps et al., 2017; Komada et al., 2017; Bodnar et al., 2020; Gano et al., 2020). With respect to the brain, PAE elicits an activated microglial phenotype, astrogliosis, and pro-inflammatory cytokine production in the pre-weaning rat (Topper et al., 2015; Bodnar et al., 2016; García-Baos et al., 2021). PAE can also prime the brain for persistent neuroinflammation and hypersensitivity to microglial and astrocytic activation later in life (Cantacorps et al., 2017; Pascual et al., 2017; Chastain et al., 2019; García-Baos et al., 2021), and loss-of-function in the Toll-like receptor 4 (TLR4) that activates these inflammatory responses normalizes these behavioral deficits in the PAE offspring (Pascual et al., 2017). We recently reported that hippocampal microglial morphology indicative of greater microglial activation was still apparent at ~1 year of age in a mouse PAE model, and that this shows a trend to correlate with poorer performance on a recognition memory test (Walter et al., 2022).

Recent discoveries show that omega-3 PUFAs can also resolve inflammation (see review Dyall et al., 2022). Oxy-metabolites of long-chain PUFAs, especially those derived from eicosapentanoic acid (EPA) and DHA, act as short-lived, short-range lipid mediators that both initiate and resolve the intensity and duration of an inflammatory response (Serhan, 2014). Whereas prostaglandins, leukotrienes, and cytokines generally promote inflammation, the small molecules collectively known as specialized pro-resolving mediators (SPMs), serve to actively resolve that response. SPMs include resolvins, protectins, maresins, and lipoxins, all of which are derived from either omega-3 or omega-6 PUFAs. SPMs bind to specific G-protein coupled membrane receptors to suppress inflammatory signals and activate anti-inflammatory signaling cascades (Han et al., 2021). Of these, the formyl peptide receptor 2 (FPR2, aka FPR2/ALX) and the chemerin receptor (chemokine-like receptor 1 (CMKLR1) aka Chemerin1 aka ChemR23) play pivotal roles in mediating this "resolution pharmacology" (Mastromarino et al., 2020; Perretti and Godson, 2020; Qin et al., 2022). Ligands for both are derived from omega-3 PUFAs; ligands for FPR2 include the D-series resolvin 1, RvD1, derived from DHA (Krishnamoorthy et al., 2010) and for ChemR23 the E-series resolvin 1, RvE1 derived from EPA (Arita et al., 2005). Although their downstream signaling cascades are incompletely understood, resolvin binding to its receptor is shown to be both anti-inflammatory and pro-resolving of inflammation (Li et al., 2020; Anand et al., 2022).

Little is known about SPM actions in the brain. The Allen Brain Atlas shows that FPR2 and ChemR23 are expressed in multiple regions in adult mouse brain[1],[2] (see also Zhang et al., 2014) and that they are primarily found in microglia, consistent with these cells' inflammatory role. They are also detected in neurons, oligodendrocytes, and astrocytes, albeit at much lower levels. In adult rat brain FPR2 has differential expression across brain regions and is highly expressed in regions important for cognitive behaviors, including prefrontal cortex and hippocampus (Ho et al., 2018) but differential localization of ChemR23 in the rodent brain has not been reported. Relatively little is known about the potential role of these receptors in behavior. In one study FPR2 KO animals show increased activity, increased time in the light side of the light–dark box, and increased recognition memory (using the novel object recognition test) than WT, interpreted as evidence of lower anxiety (Gallo et al., 2014).

To test the hypothesis that the SPM receptors FPR2 and ChemR23 play a role in PAE-induced behavioral deficits, we exposed pregnant wild-type and knockout mice to alcohol for 5 days in late gestation and tested male and female offspring on a variety of behavior tests as adolescents and young adults.

2. Methods

2.1. Animals

Wild-type (WT) C57BL/6J from Jackson Labs (Bar Harbor, ME) and FPR2 KO and ChemR23 KO mouse strains were used. KO strains were generated by the UNC Animal Models Core from WT (C57BL/6J) mice using CRISPR/Cas9-mediated genome editing. Exon 3 was deleted from ChemR23 KO mice and exon 2 from FPR2 KOs. The guide RNAs used in the genome editing for ChemR23 KO mice were 5sg81T (protospacer sequence 5′-GAGATCGTTCACAACCC-3′) and 3sg81T (protospacer sequence 5′-gCGGCCCAGGGACGCCTA-3′) and for FPR2 KO were 5sg74B (protospacer sequence 5′-gATACCACCTGCTACTAC-3′) and 3sg47T (protospacer sequence

1 mouse.brain-map.org

2 brainrnaseq.org

5′-GAGCAATGCATATTCTC-3′). All other methods (cloning, transformation, progeny screening) were the same as described (Pal et al., 2020). Deletion of the relevant exon for each strain was verified by PCR using the primers described in Supplementary Figure S1. Mice were bred as WT-WT or KO-KO crosses to avoid potential competition between neonates of differing genotypes and to assure sufficient offspring of both sexes for the behavioral testing.

Dams consumed a fixed-nutrient diet (AIN-93G, TD. 94,045, Teklad Envigo, Indianapolis, IN; Reeves et al., 1993) from 3 weeks prior to mating through lactation. This diet contains 0.48% by weight of the omega-3 precursor alpha-linolenic acid but no EPA or DHA. Offspring consumed the same diet after weaning. Animals were kept in a temperature- and humidity-controlled environment with a 12:12 light-dak cycle (lights on at 7 a.m.). All procedures were approved by the David H. Murdock Research Institute.

Female mice were mated to genotype-matched males overnight with plug day designated embryonic day (E)0.5. On E13.5 through E17.5 dams received two daily oral gavages of 2.25 g/kg body weight alcohol given 2 h apart (total daily exposure 4.5 g/kg; alcohol-exposed, ALC) or iso-caloric maltodextrin (control, CON). After weaning on postnatal day (P)28, mice were housed with 2–3 same-sex littermates where possible.

Dam body weight was recorded at E0.5, E13.5, and E17.5; weight gain over the whole pregnancy and during the gavage period was calculated. Offspring were weighed and underwent behavior testing in adolescence (6 weeks of age; 6 wk) and again at young adulthood (14 wk). Mice were euthanized at ~16 wk by cardiac puncture under isoflurane anesthesia; body, brain, and liver weights were recorded. Final sample sizes are 8–16 animals from 5 to 10 litters and are shown in Table 1.

2.2. Blood alcohol concentrations

BACs were determined in FPR2 KO and ChemR23 KO non-pregnant females. Samples were analyzed using the Analox GM7 Micro-Stat (Analox Technologies, Atlanta, GA) and compared with published WT data (Kwan et al., 2020).

2.3. Behavior testing

Testing was typically performed in the order described. A maximum of two animals of each sex were used from a given litter, our previous work shows that litter contributes significant variability to body weight (~25%) but not to behavior outcomes (typically <10%) (Smith et al., 2022). Animals were tested at both 6 and 14 wk.

TABLE 1 Number of animals that underwent behavior testing (number of litters).

Genotype	Male CON	Male ALC	Female CON	Female ALC
WT	13 (7)	9 (5)	12 (7)	10 (5)
FPR2 KO	9 (5)	11 (6)	8 (5)	12 (6)
ChemR23 KO	16 (10)	11 (8)	12 (9)	11 (8)

ALC, alcohol-exposed; CON, control; FPR2, formyl peptide receptor 2; KO, knockout; WT, wild type.

2.3.1. Elevated plus maze

The elevated plus maze (EPM) has 4 arms (35 cm in length and 5 cm in width) and a center area (5 cm × 5 cm). Two arms have walls that are 20 cm high and two arms are open. The maze stand is 61 cm high. The mouse is placed in the center of the maze facing an open arm and the center-point is tracked for 5 min using Ethovision XT software (Noldus, Leesburg, VA). The software records time spent in each of the arms and in the center. Distance traveled in the maze, percent time in closed arms, and number of entries into open arms are reported.

2.3.2. Grip strength

The assessment is done using a grip strength meter (Harvard Apparatus, Holliston, MA) that has a grid that is connected to a sensor. The animal is allowed to grab the grid with its forelimbs and is then pulled gently backwards. The force reading right before the animal loses grip is recorded as highest tension (grams). Three successive trials are measured and the highest tension recorded is normalized to the animal's body weight.

2.3.3. Accelerating rotarod

Mice were placed on a rotarod (BioSeb, Pinellas Park, FL) which accelerates from 3 revolutions per minute (rpm) to 30 rpm over 5 min (300 s). Mice were given an initial training trial and after a 45 s intertrial interval, the 5 min test trial. Latency (s) to fall from the rotating barrel was recorded.

2.3.4. Novel object recognition

Mice were placed facing the wall in a rectangular arena (40 cm × 40 cm × 29.5 cm) and allowed to explore for 5 min. Total distance traveled during this time was determined using Ethovision software and is reported as activity. For the NOR test, two of the same object were introduced in the arena and the mice were left to explore for 3 min. Twenty four hour later, mice were placed in the arena where one of the familiar objects was substituted with a novel object, and the mouse was left to explore the objects for 3 min. Time exploring objects was determined by Ethovision software when the mouse's nose was within 2 cm of the object. Percent time exploring the novel object was calculated as time spent with novel/total time with objects.

2.3.5. Auditory cued fear conditioning

This is a 3-day procedure performed as previously described (Video Fear Sound Attenuating Cubicles, Med Associates, Fairfax, VT) (Mooney et al., 2021; Smith et al., 2022; Walter et al., 2022). Briefly, on Day 1 animals acquire fear conditioning through 4 exposures to a 30 s tone that co-terminates with a 2 s foot shock. Day 2 is a test of contextual conditioning in which animals are in the same chamber as Day 1 for 5 min. Day 3 tests cued conditioning; animals are in a chamber with different features for 5 min but hear the tone (cue) used on Day 1 at beginning at 2 min. For all outcomes, percent time freezing is determined by Ethovision software.

2.4. Statistical analysis

Group means and standard deviations were generated for each dependent measure. Between-group differences in maternal and litter outcomes and post-mortem tissue weights were tested using two-way

analysis of variance (ANOVA; genotype and group). Because we know that body and organ weights differ by sex, two-way ANOVAs (genotype, exposure) were used for analysis of these data. To directly test for sex differences in behavior, three-way repeated measures (RM) ANOVAs (genotype, exposure, sex) were applied to those data. Alpha was set at <0.05, Bonferroni post-hoc tests were performed where significance was found, and trends are reported where $p < 0.1$. Associations between behavior and body weight and between grip strength and other behaviors were assessed using Pearson correlation analysis of the whole dataset and separately for each genotype to determine if associations were ubiquitous or unique. Analyses were done using SigmaPlot (Systat Software Inc., version 14.0, Palo Alto, CA) and SPSS (IBM SPSS Statistics, version 28, Armonk, NY).

3. Results

3.1. Dam and litter outcomes

Two-way ANOVA showed there was no difference among genotypes in dam weight gain through pregnancy, in the mean number of pups per litter at weaning, or the percent that were male (largest $F = 1.895$, smallest $p = 0.177$; Table 2). Weight gain during the gavage period showed a trend to be lower for ALC dams ($F_{1,35} = 3.865$, $p = 0.057$) across the genotypes. Dam body weights were different among genotypes ($F_{2,35} = 9.385$, $p < 0.001$) and exposure groups at E0.5 ($F_{1,35} = 4.473$, $p = 0.042$); ChemR23 KO dams weighed more than WT ($p = 0.002$) or FPR2 KO ($p = 0.003$), likely because they were older at initiation of breeding, and dams assigned to CON were heavier than those assigned to ALC. There was an effect of genotype at E13.5 ($F_{2,35} = 3.705$, $p = 0.035$); ChemR23 KO dams showed a trend to weigh more than WT ($p = 0.073$) and FPR2 KO ($p = 0.070$) mice. No differences were seen at E17.5.

3.2. Blood alcohol concentration

BAC in WT animals 30 min after the second gavage was 217 ± 21 mg/dL (Kwan et al., 2020), in FPR2 KO mice this was 261 ± 50 mg/dL and in ChemR23 KO was 243 ± 15 mg/dL. One way ANOVA showed no significant differences among genotypes ($F_{2,6} = 1.384$, $p = 0.320$). Comparison of BACs in pregnant and non-pregnant FPR2 KO mice showed no differences (Mooney, unpublished data).

3.3. Body weights of experimental animals

In males, the two-way RM ANOVA identified a significant interaction for age × genotype ($F_{2,63} = 6.861$, $p = 0.002$), as well as main effect of age ($F_{1,63} = 1995.348$, $p < 0.001$; Table 3). Male ChemR23 KO mice weighed less than WT at 6 wk ($p < 0.001$) and 14 wk ($p = 0.005$) and weighed less than FPR2 KO males at 6 wk ($p < 0.001$). As expected, all animals gained weight between 6 and 14 wk ($F_{2,63} = 6.861$, $p = 0.002$), but FPR2 KO mice gained significantly less weight during that period than did WT ($p = 0.008$) and ChemR23 KO ($p = 0.004$).

For females, there were significant interactions for age × exposure ($F_{1,59} = 5.022$, $p = 0.029$), age × genotype ($F_{2,59} = 47.770$, $p < 0.001$), and a main effect of age ($F_{1,59} = 1585.674$, $p < 0.001$; Table 3). At 14 wk there was a trend for ALC animals to weigh less than CON ($p = 0.067$). ChemR23 KO females weighed less than FPR2 KO at 6 wk ($p = 0.005$) but neither were different to WT, and at 14 wk FPR2 KO or ChemR23 KO females weighed less than WT ($p < 0.001$ and $p = 0.004$, respectively). As expected, all animals gained weight between 6 and 14 wk ($p < 0.001$). There were significant effects of genotype ($F_{2,59} = 47.803$, $p < 0.001$) and exposure ($F_{1,59} = 5.020$, $p = 0.029$) on weight gain; KO mice animals gained less weight than WT (FPR2 $p < 0.001$, ChemR23 $p = 0.005$), ChemR23 KO mice gained more weight than FPR2 KO ($p < 0.001$), and ALC animals gained less weight than CON ($p = 0.029$).

3.4. Tissue weights of experimental animals

Tissues were collected at ~16 wk (Table 3). In males, the brains of ALC animals weighed more than CON ($F_{1,63} = 9.323$, $p = 0.003$). Body weight at the time of collection was not different among the groups, neither was the brain weight to body weight ratio, or the liver weight. In females, brain weight was significantly different among the genotypes ($F_{2,58} = 8.155$, $p < 0.001$); it was lower in ChemR23 KO mice than either FPR2 KO ($p = 0.042$) or WT ($p < 0.001$). Body weight at collection showed a trend to be lower in ALC animals than CON

TABLE 2 Dam and litter outcomes.

Group (n)	Dam weight E0.5 (g)	Dam weight E13.5 (g)	Dam weight E17.5 (g)	Pregnancy weight gain (g)	Gavage weight gain (g)	Number of pups	% male
WT CON (7)	19.67 ± 1.16[a]	26.48 ± 1.57[a]	32.50 ± 2.06	12.84 ± 2.36	5.86 ± 2.04	5.9 ± 2.0	52.2 ± 16.6
WT ALC (5)	19.05 ± 1.24[a]	26.72 ± 1.17[a]	30.79 ± 1.91	11.75 ± 1.45	4.07 ± 1.57	5.0 ± 1.2	44.0 ± 18.8
FPR2 CON (5)	19.47 ± 0.66[a]	26.41 ± 1.41[a]	32.30 ± 2.16	12.83 ± 2.12	5.89 ± 1.16	5.2 ± 1.3	53.8 ± 21.1
FPR2 ALC (6)	19.36 ± 0.76[a]	26.96 ± 1.39[a]	32.40 ± 2.25	13.04 ± 1.58	5.47 ± 0.91	5.5 ± 1.1	47.7 ± 17.8
ChemR23 CON (10)	**21.77 ± 1.41[b]**	**28.47 ± 1.04[b]**	33.35 ± 1.33	11.58 ± 2.32	4.88 ± 1.33	5.7 ± 2.5	59.0 ± 22.2
ChemR23 ALC (8)	**20.16 ± 1.17[b]**	**27.37 ± 2.10[b]**	32.17 ± 2.82	12.01 ± 2.41	4.79 ± 1.41	4.7 ± 1.0	45.8 ± 24.0

ALC, alcohol-exposed; CON, control; FPR2, formyl peptide receptor 2; KO, knockout; WT, wild type. Means that do not share a common superscript letter differ at $p < 0.05$. Significant p-values are bold.

TABLE 3 Offspring outcomes.

Males	6wk body weight (g)	14wk body weight (g)	Weight gain (g)	16wk body weight (g)	Liver weight (g)	Brain weight (g)*	Ratio brain weight to body weight
WT CON	20.26 ± 1.18[a]	27.08 ± 0.98[a]	6.82 ± 0.84[a]	27.73 ± 1.33	1.16 ± 0.18	0.42 ± 0.02	0.015 ± 0.001
WT ALC	21.15 ± 2.15[a]	27.81 ± 2.31[a]	6.66 ± 0.81[a]	27.29 ± 1.57	1.23 ± 0.08	0.44 ± 0.02	0.016 ± 0.001
FPR2 CON	21.12 ± 0.98[a]	26.48 ± 1.96[a]	**5.36 ± 1.59[b]**	27.11 ± 2.06	1.17 ± 0.13	0.42 ± 0.01	0.016 ± 0.001
FPR2 ALC	21.19 ± 0.58[a]	27.05 ± 1.23[a]	**5.86 ± 1.02[b]**	27.45 ± 1.39	1.13 ± 0.09	0.42 ± 0.02	0.015 ± 0.001
ChemR23 CON	**19.08 ± 0.96[b]**	**25.94 ± 1.14[b]**	6.86 ± 1.39[a]	26.51 ± 1.33	1.14 ± 0.09	0.41 ± 0.01	0.016 ± 0.001
ChemR23 ALC	**19.18 ± 2.15[b]**	**25.88 ± 2.01[b]**	6.70 ± 1.09[a]	26.95 ± 1.95	1.22 ± 0.09	0.43 ± 0.01	0.016 ± 0.001
Females	6 wk body weight (g)	14 wk body weight (g)	Weight gain (g)	16 wk body weight (g)	Liver weight (g)	Brain weight (g)	Ratio brain weight to body weight
WT CON	16.57 ± 0.87[a]	**21.17 ± 0.87[a]**	**4.60 ± 0.69[a]**	21.08 ± 0.98	0.83 ± 0.13[a]	0.45 ± 0.01[a]	0.021 ± 0.001
WT ALC	16.50 ± 1.03[a]	**20.45 ± 1.53[a]**	**3.95 ± 1.06[a]**	20.17 ± 1.80	0.85 ± 0.11[a]	0.45 ± 0.02[a]	0.022 ± 0.002
FPR2 CON	17.22 ± 0.68[a]	19.47 ± 0.69[b]	2.25 ± 0.46[b]	20.12 ± 0.91	0.77 ± 0.11[a]	0.44 ± 0.02[a]	0.022 ± 0.002
FPR2 ALC	16.93 ± 0.83[a]	19.16 ± 0.70[b]	2.23 ± 0.40[b]	19.61 ± 0.79	0.78 ± 0.03[a]	0.44 ± 0.02[a]	0.022 ± 0.001
ChemR23 CON	**16.12 ± 0.78[b]**	19.96 ± 0.88[b]	**3.84 ± 0.74[c]**	20.19 ± 1.03	**0.90 ± 0.08[b]**	**0.42 ± 0.03[b]**	0.021 ± 0.002
ChemR23 ALC	**16.17 ± 1.22[b]**	19.54 ± 1.29[b]	**3.38 ± 0.47[c]**	19.98 ± 1.54	0.78 ± 0.13[a]	**0.42 ± 0.02[b]**	0.021 ± 0.002

ALC, alcohol-exposed; CON, control; FPR2, formyl peptide receptor 2; KO, knockout; WT, wild type. Means that do not share a common superscript letter differ at $p < 0.05$. Significant p-values are bold. See text for more information.
*Significant difference between exposure groups.

($p = 0.082$), but there were no effects on the brain weight to body weight ratio. Liver weight showed a genotype × exposure interaction ($F_{2,58} = 3.249$, $p = 0.046$); in ChemR23 KO mice, ALC animals had lower liver weight than CON ($p = 0.006$).

3.5. Behavior testing

3.5.1. Elevated plus maze

Percent time in closed arms: Three-way RM ANOVA identified significant interactions for age × genotype × sex ($F_{2,122} = 4.908$, $p = 0.009$), age × genotype ($F_{2,122} = 7.363$, $p < 0.001$), age × sex ($F_{1,122} = 5.034$, $p = 0.027$), and significant effects of exposure ($F_{1,122} = 7.771$, $p = 0.006$) and age ($F_{1,122} = 124.553$, $p < 0.001$) (Figure 1). Overall, percent time in closed arms was higher in ALC mice than CON ($p = 0.006$) and was higher at 14 wk than 6 wk ($p < 0.001$). All genotypes and both sexes showed the decrease at 14 wk (all ps <0.001). No genotype differences were seen at 6 wk, but at 14 wk female ChemR23 KO mice spent less time in the closed arms than WT ($p = 0.004$) or FPR2 KO ($p < 0.001$) females.

Number of entries into open arms: The three-way RM ANOVA identified a significant effect of age ($F_{1,122} = 109.591$, $p < 0.001$) and genotype ($F_{2,122} = 6.922$, $p = 0.001$). The number of entries into open arms decreased between 6 and 14 wk ($p < 0.001$) and was lower in FPR2 KO compared with WT ($p = 0.001$) and ChemR23 KO ($p = 0.023$) but was not different between WT and ChemR23 KO mice.

Activity in EPM: Three-way RM ANOVA identified significant interactions for age × genotype ($F_{2,122} = 4.588$, $p = 0.012$), age × sex ($F_{1,122} = 5.473$, $p = 0.012$), exposure × genotype ($F_{2,122} = 5.012$, $p = 0.008$), a trend for age × exposure ($F_{1,122} = 3.024$, $p = 0.085$), and significant effects of genotype ($F_{2,122} = 8.338$, $p < 0.001$) and age ($F_{1,122} = 441.426$, $p < 0.001$). Animals from all genotypes and both sexes traveled further at 6 wk than 14 wk (all ps <0.001). In the CON group, there were no genotype differences, but in the ALC group FPR2 KO mice traveled less than WT ($p < 0.001$) and ChemR23 KO ($p = 0.002$).

3.5.2. Grip strength

Three-way RM ANOVA identified significant interactions for age × genotype × exposure ($F_{2,122} = 5.304$, $p = 0.006$) and genotype × sex ($F_{2,122} = 4.607$, $p = 0.012$), trends for interaction of age × genotype × sex ($F_{2,122} = 2.734$, $p = 0.069$) and genotype × exposure ($F_{2,122} = 2.752$, $p = 0.068$), and significant effects of age ($F_{1,122} = 22.902$, $p < 0.001$) and genotype ($F_{2,122} = 56.184$, $p < 0.001$) (Figure 2).

For all groups, mice did better on grip strength at 6 wk than 14 wk ($p < 0.001$), possibly reflecting a higher body weight at the latter age. All genotypes were different to each other; ChemR23 KO animals did better than WT, and both did better than FPR2 KO animals (all ps <0.001).

ALC interacted with genotype and age; for WT ALC animals, grip strength was higher than CON at 6 wk ($p = 0.003$) but did not differ from WT CON at 14 wk. FPR2 KO mice showed a trend for effect of exposure at 6 wk ($p = 0.059$) where ALC mice did worse than CON; this was not seen at 14 wk. ChemR23 KO mice did not show effects of exposure at either age.

Investigation of the genotype × sex effect showed that FPR2 KO males did better than FPR2 KO females ($p = 0.022$) and WT females showed a trend to do better than WT males ($p = 0.098$). ChemR23 KO mice did not show sex differences at either age.

3.5.3. Rotarod

Three-way RM ANOVA identified a trend for an interaction between age × genotype × sex ($F_{2,122} = 2.927$, $p = 0.057$) and effects of age ($F_{1,122} = 16.591$, $p < 0.001$), genotype ($F_{2,122} = 10.417$, $p < 0.001$), and sex ($F_{1,122} = 5.045$, $p = 0.026$) (Figure 2). Mice spent more time on the rotarod at 14 wk than 6 wk ($p < 0.001$), females outperformed males ($p = 0.026$), and ChemR23 KO mice did better than WT ($p < 0.001$) or FPR2 KO ($p = 0.001$). The time WT animals spent on

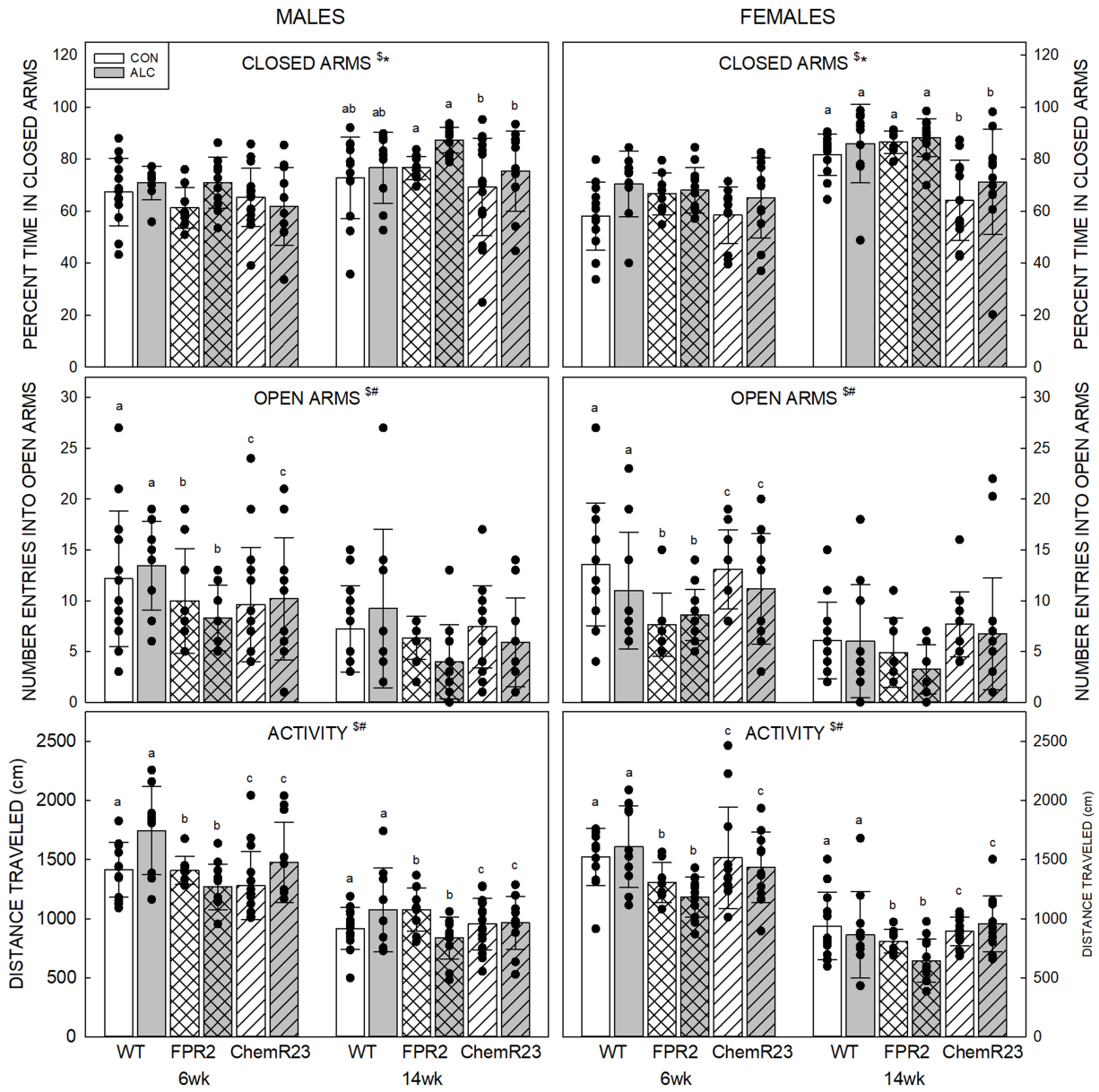


FIGURE 1
Elevated plus maze. (Top) Older animals spent more time in the closed arms than younger animals and ALC animals spent more time in the closed arms than CON. At 14wk, ChemR23 females spent less time in closed arms than WT or FPR2 KO. (Middle) The number of entries into open arms was lower at 14wk than 6wk and was lower in FPR2 KO mice compared to WT or ChemR23 KO. (Bottom) Activity in the EPM (distance traveled during the test) decreased with age for all groups. Differences between genotypes were only seen in ALC mice where FPR2 KO-ALC mice moved less than WT or ChemR23 ALC mice. Data shown are mean and standard deviation. Comparisons across age are only made within genotype. Dots represent individual animals with N =8–16 mice per group. Experimental group means that do not share a common superscript letter differ at p <0.05; omission of superscript indicates no difference by genotype or exposure at that age. *Significant difference between exposure groups. #Significant difference among genotypes. $Significant difference between ages. ALC, alcohol-exposed; CON, control; EPM, elevated plus maze; FPR2, formyl peptide receptor 2; KO, knockout; WT, wild type.

the rotarod did not change with age, but FPR2 females ($p = 0.008$) and ChemR23 males ($p < 0.001$) significantly improved their performance between 6 and 14 wk.

3.5.4. Novel object recognition

For activity in the NOR arena, three-way RM ANOVA identified a significant interaction between age × genotype × exposure ($F_{2,122} = 4.056$, $p = 0.020$), trends for genotype × sex ($F_{2,122} = 2.839$, $p = 0.062$) and age × sex ($F_{1,122} = 3.067$, $p = 0.082$) interactions, significant effects of age ($F_{1,122} = 213.628$, $p < 0.001$), genotype ($F_{2,122} = 3.930$, $p = 0.022$), and exposure ($F_{1,122} = 3.929$, $p = 0.050$), and a trend for an effect of sex ($F_{1,122} = 2.839$, $p = 0.069$) (Figure 3).

Distance traveled was less in ALC mice than CON ($p = 0.050$), less at 14 wk than 6 wk for all groups ($p < 0.001$) and showed a trend to be less in males than females ($p = 0.069$). FPR2 KO animals were significantly less active than WT ($p = 0.027$) and showed a trend to be less active than ChemR23 KO mice ($p = 0.092$). Sex differences were apparent at 14 wk ($p = 0.010$), where females traveled further than males.

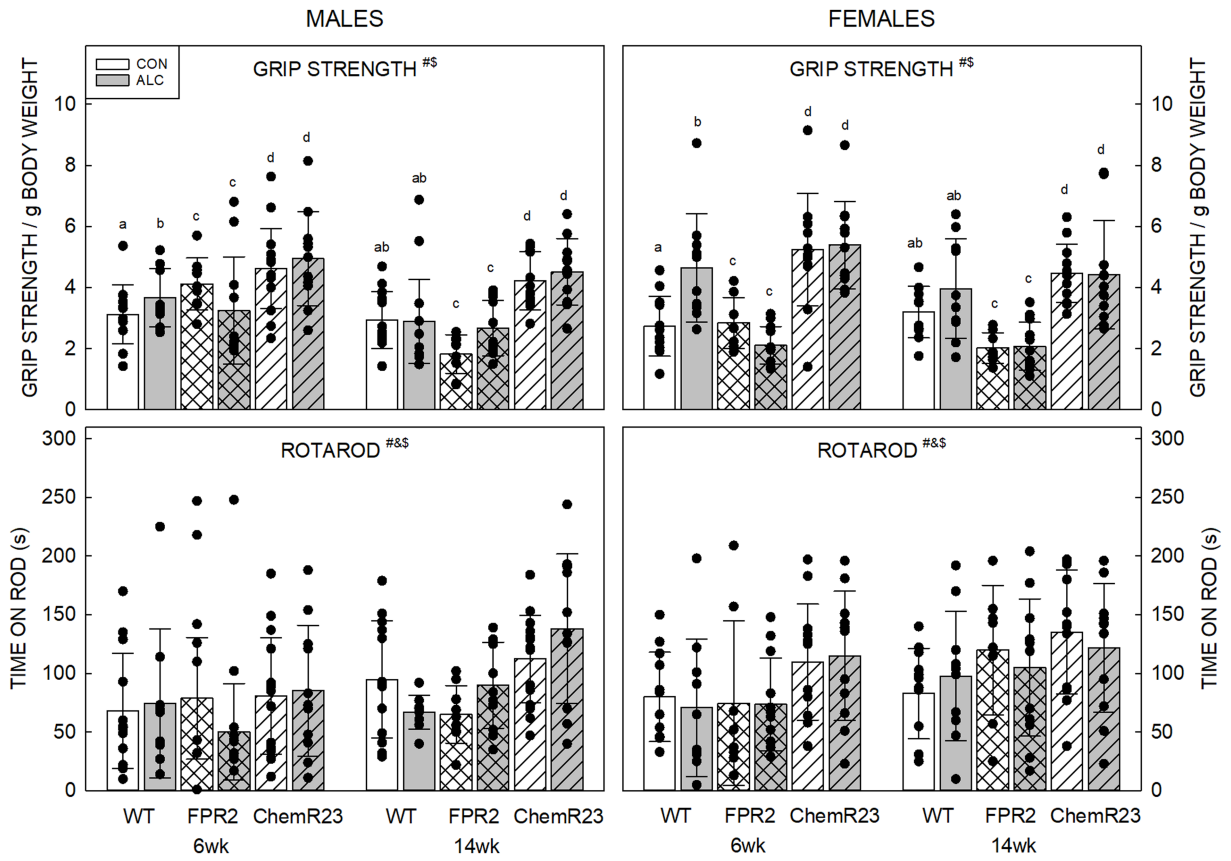


FIGURE 2
Motor outcomes. (Top) There were significant effects of age ($F_{1,122}$=22.902, p<0.001) and genotype ($F_{2,122}$=56.184, p<0.001), and interactions of age×genotype×exposure ($F_{2,122}$=5.304, p=0.006) and genotype × sex ($F_{2,122}$=4.607, p=0.012). Grip strength decreased with age and differed among the genotypes. Overall, grip strength was highest in ChemR23 KO and was not affected by ALC in these KOs. In WT mice, grip strength was higher in ALC mice than CON at 6wk. FPR2 KO mice had the lowest grip strength and showed a trend for this to be lower in ALC mice than CON at 6wk. (Bottom) There were significant effects of age ($F_{1,122}$=16.591, p<0.001), genotype ($F_{2,122}$=10.417, p<0.001), and sex ($F_{1,122}$=5.045, p=0.026). Females spent more time on the rod than males, and ChemR23 KO mice did better than WT or FPR2 KO. Both KO lines spent more time on the rod at 14wk than at 6wk, this was not seen in WT mice. Data shown are mean and standard deviation. Comparisons across age are only made within genotype. Dots represent individual animals with N =8–16 mice per group. Experimental group means that do not share a common superscript letter differ at p <0.05; omission of superscript indicates no difference by genotype or exposure at that age. *Significant difference between exposure groups. #Significant difference among genotypes. &Significant difference between sexes. $Significant difference between ages. ALC, alcohol-exposed; CON, control; FPR2, formyl peptide receptor 2; KO, knockout; WT, wild type.

CON animals did not show effects of age or exposure, but ALC animals did. At 6 wk, ALC FPR2 KO mice were less active than ALC WT (p = 0.016), and both ALC WT (p = 0.052) and ALC FPR2 KO (p = 0.059) showed trends for less activity at 14 wk than 6 wk.

For percent time with the novel object, three-way RM ANOVA identified a significant interaction between age × genotype × sex ($F_{2,122}$ = 3.460, p = 0.035). In 6 wk males, ChemR23 KO mice spent significantly less time with the novel object than FPR2 KO (p = 0.030) and show a trend to less compared with WT (p = 0.087). In 6 wk females, ChemR23 KO mice spend more time with the novel object than WT animals (p = 0.031). No differences among groups were seen at 14 wk but there was an overall weak trend for females to spend more time with the novel object than males ($F_{1,122}$ = 3.049, p = 0.083).

3.5.5. Auditory cued fear conditioning

Context: Three-way RM ANOVA identified a significant age × genotype interaction ($F_{2,122}$ = 20.761, p < 0.001) as well as trends for an interaction between age × genotype × exposure × sex ($F_{2,122}$ = 2.954, p = 0.056) and effect of genotype ($F_{2,122}$ = 2.461, p = 0.090) (Figure 4).

At 6 wk FPR2 KO (p < 0.001) and ChemR23 KO (p = 0.001) mice freeze more than WT, and the KO strains did not different to each other. Both WT and FPR2 KO animals show changes in freezing with age; this decreased in FPR2 KO (p < 0.001) but increased in WT (p < 0.001) at 14 wk compared with 6 wk.

At 6 wk CON ChemR23 KO males freeze more than WT (p = 0.010), and CON FPR2 KO females show a trend to freeze more than WT (p = 0.083), but there were no differences at 14 wk. In ALC animals, 6 wk FPR2 KO (p < 0.001) or ChemR23 KO (p = 0.028) males freeze more than WT, and at 14 wk, there is a trend for more freezing in ChemR23 KO males than FPR2 KO (p = 0.073). At 6 wk ALC ChemR23 KO females show a trend for less freezing than FPR2 KO (p = 0.091) and there are no differences among female groups at 14 wk.

Cue: Three-way RM ANOVA identified significant interactions for age × genotype ($F_{2,122}$ = 22.566, p < 0.001) and genotype × exposure ($F_{2,122}$ = 3.110, p = 0.048), and effects of age ($F_{1,122}$ = 116.489, p < 0.001)

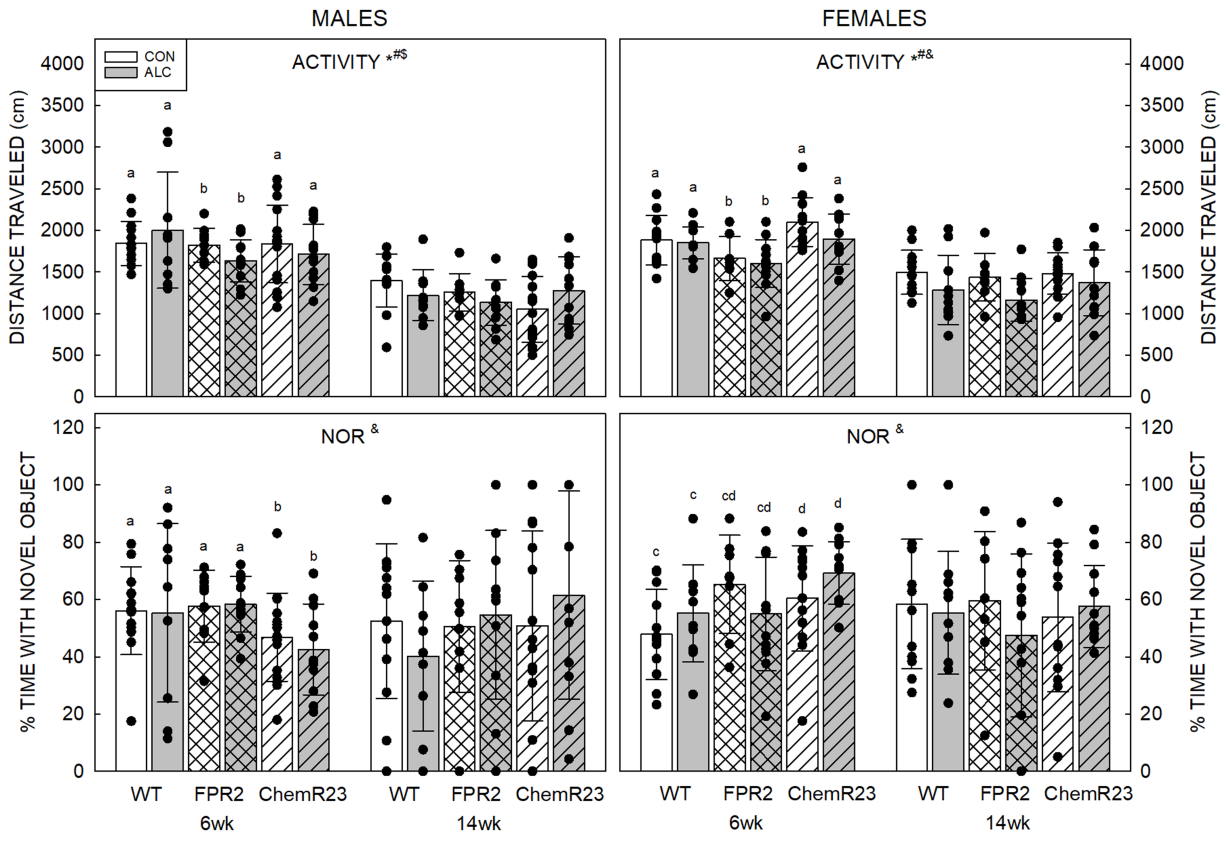


FIGURE 3
Activity and novel object recognition. (Top) There were significant effects of age ($F_{1,122}$=213.628, p<0.001), genotype ($F_{2,122}$=3.930, p=0.022), and exposure ($F_{1,122}$=3.929, p=0.050), and an interaction between age×genotype×exposure ($F_{2,122}$=4.056, p=0.020). Distance traveled in an empty arena was less in ALC animals than CON, less at 14wk than 6wk, and less in FPR2 KO mice than WT. Activity at 14wk was not affected by genotype or exposure. (Bottom) There was a significant interaction between age×genotype×sex ($F_{2,122}$=3.460, p=0.035). At 6wk, ChemR23 KO males spent less time with the novel object than FPR2 KO and showed a trend (p=0.087) to spend less time than WT males, whereas 6wk ChemR23 KO females spent more time with the novel object than WT females. There was an overall trend for females to spend more time with the novel object than did males. Data shown are mean and standard deviation. Comparisons across age are only made within genotype. Dots represent individual animals with N =8–16 mice per group. Experimental group means that do not share a common superscript letter differ at p <0.05; omission of superscript indicates no difference by genotype or exposure at that age. *Significant difference between exposure groups. #Significant difference among genotypes. $Significant difference between sexes. $Significant difference between ages. ALC, alcohol-exposed; CON, control; FPR2, formyl peptide receptor 2; KO, knockout; WT, wild type.

and exposure ($F_{1,122}$ = 4.659, p = 0.033) (Figure 4). Overall, younger animals freeze less than older (p < 0.001) and ALC mice freeze less than CON mice (p = 0.033). At 6 wk, KO mice freeze more than WT mice (both ps <0.001), and the KO were not different to each other, but at 14 wk there are trends for FPR2 KO (p = 0.062) and ChemR23 KO (p = 0.085) animals to freeze less than WT.

There were no differences among genotypes in CON animals, but in ALC animals there was a trend for FPR2 KO to freeze more than WT or ChemR23 KO (p = 0.080 and p = 0.094, respectively). Within genotype, only ChemR23 KO animals showed an effect of exposure with less freezing in ALC compared with CON (p = 0.004).

There was a positive correlation between percent time freezing in context and percent time freezing to the cue across all animals (r = 0.384, p < 0.001). Within genotypes, this was seen in WT (r = 0.417, p < 0.001) and ChemR23 KO (r = 0.509, p < 0.001), but not in FPR2 KO mice.

3.5.6. Correlations

Correlations between body weight and behavior: For the whole dataset, body weight positively correlated with percent time in closed arms of EPM (r = 0.346, p < 0.001) and percent time freezing to the cue (r = 0.30, p < 0.001) and negatively correlated with distance traveled in EPM (r = −0.181, p = 0.003), grip strength (r = −0.189, p = 0.002), and activity in NOR (r = −0.44, p < 0.001). For three of these, the correlations were significant or trends in all genotypes: the positive correlations with percent time in closed arms of EPM and percent time freezing to the cue, and the negative correlation with activity in NOR (see Table 4 for r- and p-values).

Grip strength is a non-invasive test of muscle strength (e.g., Takeshita et al., 2017), therefore we used Pearson correlation analysis to assess whether genotype differences in muscle strength were associated with other behavioral outcomes. When all animals were assessed together, grip strength positively associated with distance traveled in the EPM (r = 0.147, p = 0.016) and activity in NOR (r = 0.24, p < 0.001) and negatively correlated with percent time in closed arms of EPM (r = −0.276, p < 0.001). Only the positive association with activity in NOR was apparent in all genotypes (see Table 4 for r- and p-values).

Because the poor performance of FPR2 KO mice on grip strength may reflect an effect on skeletal muscle, we tested

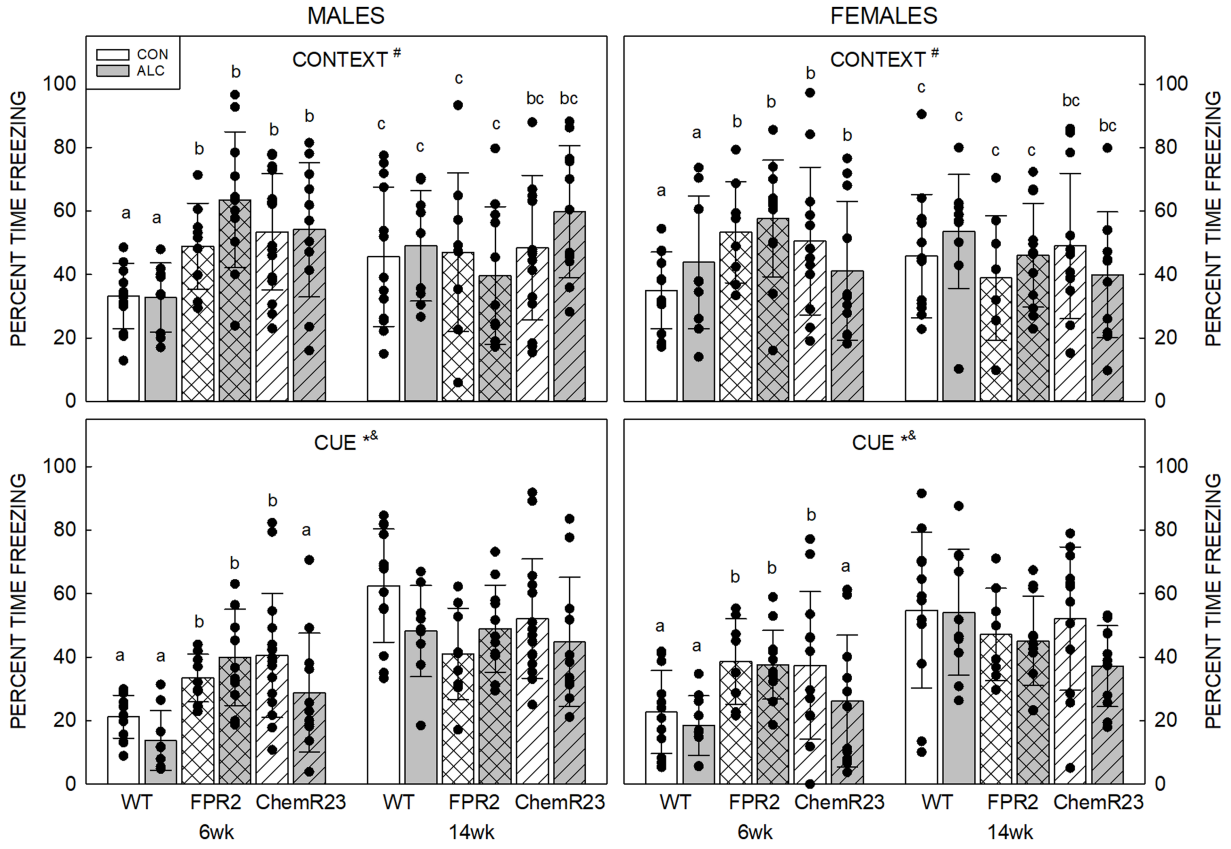


FIGURE 4
Auditory cued fear conditioning. (Top) Context. There is an age×genotype interaction ($F_{2,122}$=20.761, p<0.001), such that at 6wk, FPR2 and ChemR23 KO mice show more freezing to the context compared to WT. WT mice show an age-related increase in freezing at 14wk; however, FPR2 KO mice show a decrease in freezing with age, and there is no age-related change in ChemR23 KO mice. (Bottom) In response to the cue, there were significant effects of age ($F_{1,122}$=116.489, p<0.001) and exposure ($F_{1,122}$=4.659, p=0.033), and interactions between age×genotype ($F_{2,122}$=22.566, p<0.001) and genotype×exposure ($F_{2,122}$=3.110, p=0.048). ALC animals freeze less than CON and younger animals freeze less than older. KO mice freeze more than WT at 6wk and this shows a trend to be lower in KO than WT at 14wk. ALC ChemR23 KO mice freeze less than their CON. There was no significant effect of genotype or exposure at 14wk. Data shown are mean and standard deviation. Comparisons across age are only made within genotype. Dots represent individual animals with N =8–16 mice per group. Experimental group means that do not share a common superscript letter differ at p <0.05; omission of superscript indicates no difference by genotype or exposure at that age. *Significant difference between exposure groups. #Significant difference among genotypes. &Significant difference between sexes. $Significant difference between ages. ALC, alcohol-exposed; CON, control; FPR2, formyl peptide receptor 2; KO, knockout; WT, wild type.

associations between grip strength and other behaviors for this genotype. When both ages were assessed together, grip strength positively correlated with movement in the EPM and activity in NOR, and negatively associated with percent time in closed arms of EPM, time on rotarod, and freezing in response to the cue (see Table 4 for r- and p-values). When each age was examined separately, grip strength positively correlated with movement in the EPM (r = 0.431, p = 0.005) and showed a trend to positively correlate with activity in NOR (r = 0.302, p = 0.058) at 6 wk but not at 14 wk. Similarly, the negative correlation between grip strength and freezing in response to the cue was apparent at 6 wk (r = −0.343, p = 0.031) but not 14 wk.

4. Discussion

To date, studies of FPR2 and ChemR23 and their ligands have emphasized their resolution activities in diverse acute and chronic inflammatory diseases and little attention has been given to their potential influences on cognition and behavioral outcomes despite their presence in the brain. We report here that both FPR2 and ChemR23 are essential for healthy brain development, and their loss-of-function leads to greater measures of anxiety and perhaps deficits in memory. Moreover, this is the first demonstration that they interact with alcohol to further alter behavioral performance, thus supporting their importance in attenuating the behavioral deficits associated with PAE. These alterations differ between the two knock-out lines, further highlighting that these receptors make distinct mechanistic contributions to these processes. Taken together, these findings emphasize the importance of FPR2 and ChemR23 in the brain and offer mechanistic insight into how omega-3 PUFAs support healthy brain development and may act to improve the behavioral defects that characterize PAE.

With respect to behavior, adolescent female ChemR23 KO mice froze more than WT animals in a fear conditioning test. Although the WT animals showed more freezing in the fear conditioning test as young adults compared with adolescence, this age- or experience-dependent improvement was not observed in ChemR23 KOs and may

TABLE 4 Pearson correlation outcomes.

Correlations with body weight	All mice	WT	FPR2 KO	ChemR23 KO
% time in closed arms of EPM	$r = 0.266$, $p < 0.001$	$r = 0.190$, $p = 0.08^{T}$	$r = 0.294$, $p = 0.008$	$r = 0.295$, $p = 0.003$
% time freezing to cue	$r = 0.310$, $p < 0.001$	$r = 0.510$, $p < 0.001$	$r = 0.186$, $p = 0.099^{T}$	$r = 0.189$, $p = 0.059^{T}$
Correlations with grip strength				
% time in closed arms of EPM	$r = -0.224$, $p < 0.001$		$r = -0.387$, $p < 0.001$	
Distance in EPM	$r = 0.205$, $p < 0.001$	$r = -0.223$, $p = 0.037$	$r = 0.392$, $p < 0.001$	
Time on rotarod			$r = -0.221$, $p = 0.049$	
Activity in NOR	$r = 0.240$, $p < 0.001$	$r = 0.227$, $p = 0.033$	$r = 0.324$, $p = 0.003$	$r = 0.203$, $p = 0.043$
% time freezing to cue			$r = -0.268$, $p = 0.016$	

EPM, elevated plus maze; FPR2, formyl peptide receptor 2; KO, knockout; NOR, novel object recognition test; WT, wild type. T denotes trend, $0.05 < p < 0.1$.

suggest problems with long-term memory in those animals. The adolescent FPR2 KO animals froze more than WT in the fear conditioning test and did not show increased freezing between adolescence and young adulthood. ChemR23 KO females showed less anxiety-like behavior in the elevated plus maze in young adulthood; they spent less time in closed arms than other mice but did not show any difference in the number of entries into open arms or greater activity in the maze. Unlike a previous report (Gallo et al., 2014), there was no evidence of differences in anxiety-like behavior or changes in NOR in FPR2 KO males compared with WT mice. Moreover, the young adult FPR2 KOs performed poorly on a test of grip strength which suggested an effect on skeletal muscle, and they had the lowest activity in both EPM and NOR, however, they performed normally on the rotarod and were not different to the ChemR23 KO mice in fear conditioning. Correlation analyses were performed to try to understand whether the potential skeletal muscle effect altered other behaviors in the FPR2 KO mice; correlations between grip strength and other behaviors were age-dependent and were only seen in adolescent mice even though grip strength worsened with age suggesting that at least some of the behavior deficits were independent of grip strength.

Interestingly, FPR1 loss-of-function is associated with reduced anxiety and fear behaviors (Gao et al., 2011), suggesting that FPR1 and FPR2 receptors serve complementary roles. Although the mice tested here are global knock-outs, insight into the affected population emerges from the well-mapped neurocircuitry of fear-conditioning, which involves the amygdala, medial prefrontal cortex, and hippocampus (Shin and Liberzon, 2010), regions where microglia express both FPR2 and ChemR23. Microglia are known to affect neurobehaviors and their function can be influenced by diet (see review by Paolicelli and Ferretti, 2017); for example, deficiency of omega-3 PUFAs during development alters microglial motility and expression of phenotypic markers and increases expression of pro-inflammatory cytokines in hippocampus at P21 (Madore et al., 2014).

Alcohol, including in the context of prenatal exposure, is strongly pro-inflammatory, and this inflammation is a significant driver of alcohol-related pathologies including the behavioral deficits that typify FASD (Cantacorps et al., 2017; Komada et al., 2017; Bodnar et al., 2020; Gano et al., 2020). Both FPR2 and ChemR23 are implicated in inflammatory brain disorders including ischemic stroke and Alzheimer's (Valente et al., 2022), and findings herein extend those actions to PAE. Loss of either receptor further altered PAE's impact in select domains involving anxiety, learning, and activity. That alcohol's impact was a function of genotype suggests the involvement of different cell types and/or different functions. The relatively modest changes reported here reflects our use of a relatively moderate exposure to avoid basement effects in the alcohol × genotype interaction; genotype did not affect alcohol levels *per se*.

Where and how FPR2 and ChemR23 act to affect behavior, and how they interact with PAE, is unclear. Using whole transcriptome sequencing, we find that FPR2 is present in fetal liver but not fetal brain or placenta (Petry et al., unpublished), suggesting it may affect behavior indirectly through peripheral inflammation. Alcohol increases gut permeability and the entry of pro-inflammatory bacterial products including LPS and cytolysin (Duan et al., 2019); in our model alcohol increases the content of microbial products in both dam and fetus (Virdee et al., 2021). A loss of FPR2 would heighten the inflammatory responses to these products, thereby exacerbating alcohol's damage and limiting the capacity for recovery (Dufton and Perretti, 2010; Sansbury and Spite, 2016). In contrast, we detected ChemR23 in the E17.5 WT mouse brain and liver, and in the placenta, and alcohol induced its brain expression 1.17-fold (Padj = 0.032). ChemR23 loss-of-function leads to a similar pro-inflammatory environment (Cash et al., 2008; Zhang et al., 2018) that is accompanied by cognitive impairment (Zhang et al., 2022). In the brain it acts to recruit and activate microglia and promotes their transition to a pro-resolving phenotype in models of brain injury (Zhang et al., 2018). Thus, ChemR23 may serve to limit alcohol's pro-inflammatory actions on microglia.

Limitations of this study include the global nature of these knockouts, which precludes identification of the cell population mediating these behavioral deficits. Although all mice used the same background strain (C57BL/6J), each line was generated independently from WT-WT or KO-KO breedings. As such, it is possible that environmental differences, including maternal care or litter effects, could contribute to genotype-related differences in growth or behavior. Off-target CRISPR effects also would not be detected. Similarly, it is unclear whether these receptors are acting within the fetus, maternal compartment, or both at the time of alcohol exposure. Also unknown is the identity of the ligands that stimulate these receptors' protective actions in response to alcohol; however, the

candidate lipoxins, cytokines, and formylated microbial peptides are consistent with alcohol's known actions, and it is possible that multiple signals act in concert. Future studies could also examine other ligands for these receptors, such as chemerin and annexins. It should also be noted that animals underwent all behavioral testing at both ages which can add a test–retest confound, however, tests were administered with at least 5 weeks between them and studies in rodents find that a 4-week intertrial interval restores the baseline behavior for EPM and that NOR is repeatable regardless of the length of the intertrial interval (Cnops et al., 2022).

In summary, we validate and expand the range of behavioral domains influenced by FPR2 and ChemR23, consistent both with the role of inflammation in affecting behavioral performance and offering insight into the mechanism by which essential fatty acids support brain development. Findings also inform how supplemental PUFAs attenuate the cognitive impairments caused by PAE, and suggest that strategies that activate these receptors, such as RvD and RvE resolvins, could limit or improve recovery from alcohol's damage.

Data availability statement

The raw data supporting the conclusions of this article will be made available by the authors, without undue reservation.

Ethics statement

The animal study was reviewed and approved by the Institutional Animal Care and Use Committee, David H. Murdock Research Institute.

Author contributions

SM and SMS designed the study and wrote the first draft of the manuscript. SM, SRS, and SMS contributed to the conception of the study. EB, MM, and CM performed the study. SM performed the statistical analysis. All authors contributed to manuscript revision, read, and approved the submitted version.

Funding

This work was supported by the NRI internal grant funds to SM and SMS, and by NIH (R01AA024980) to SM, (R01AA011085) to SMS, (R01ES031378) to SRS. The UNC Animal Models Core Facility was supported in part by P30 CA016086 Cancer Center Core Support Grant to the UNC Lineberger Comprehensive Cancer Center.

Conflict of interest

The authors declare that the research was conducted in the absence of any commercial or financial relationships that could be construed as a potential conflict of interest.

Publisher's note

All claims expressed in this article are solely those of the authors and do not necessarily represent those of their affiliated organizations, or those of the publisher, the editors and the reviewers. Any product that may be evaluated in this article, or claim that may be made by its manufacturer, is not guaranteed or endorsed by the publisher.

Supplementary material

The Supplementary material for this article can be found online at: https://www.frontiersin.org/articles/10.3389/fnins.2023.1187220/full#supplementary-material

References

Anand, S., Azam Ansari, M., Kumaraswamy Sukrutha, S., Alomary, M. N., Anwar Khan, A., and Elderdery, A. Y. (2022). Resolvins lipid mediators: potential therapeutic targets in Alzheimer and Parkinson disease. *Neuroscience* 507, 139–148. doi: 10.1016/J.NEUROSCIENCE.2022.11.001

Arita, M., Bianchini, F., Aliberti, J., Sher, A., Chiang, N., Hong, S., et al. (2005). Stereochemical assignment, antiinflammatory properties, and receptor for the omega-3 lipid mediator resolvin E1. *J. Exp. Med.* 201, 713–722. doi: 10.1084/JEM.20042031

Balaszczuk, V., Salguero, J. A., Villarreal, R. N., Scaramuzza, R. G., Mendez, S., and Abate, P. (2019). Hyperlocomotion and anxiety- like behavior induced by binge ethanol exposure in rat neonates. Possible ameliorative effects of omega 3. *Behav. Brain Res.* 372:112022. doi: 10.1016/J.BBR.2019.112022

Bodnar, T. S., Hill, L. A., and Weinberg, J. (2016). Evidence for an immune signature of prenatal alcohol exposure in female rats. *Brain Behav. Immun.* 58, 130–141. doi: 10.1016/j.bbi.2016.05.022

Bodnar, T. S., Raineki, C., Wertelecki, W., Yevtushok, L., Plotka, L., Granovska, I., et al. (2020). Immune network dysregulation associated with child neurodevelopmental delay: modulatory role of prenatal alcohol exposure. *J. Neuroinflammation* 17:39. doi: 10.1186/S12974-020-1717-8

Cantacorps, L., Alfonso-Loeches, S., Moscoso-Castro, M., Cuitavi, J., Gracia-Rubio, I., López-Arnau, R., et al. (2017). Maternal alcohol binge drinking induces persistent neuroinflammation associated with myelin damage and behavioural dysfunctions in offspring mice. *Neuropharmacology* 123, 368–384. doi: 10.1016/j.neuropharm.2017.05.034

Cash, J. L., Hart, R., Russ, A., Dixon, J. P. C., Colledge, W. H., Doran, J., et al. (2008). Synthetic chemerin-derived peptides suppress inflammation through ChemR23. *J. Exp. Med.* 205, 767–775. doi: 10.1084/JEM.20071601

Chastain, L. G., Franklin, T., Gangisetty, O., Cabrera, M. A., Mukherjee, S., Shrivastava, P., et al. (2019). Early life alcohol exposure primes hypothalamic microglia to later-life hypersensitivity to immune stress: possible epigenetic mechanism. *Neuropsychopharmacology* 44, 1579–1588. doi: 10.1038/s41386-019-0326-7

Cnops, V., Iyer, V. R., Parathy, N., Wong, P., and Dawe, G. S. (2022). Test, rinse, repeat: a review of carryover effects in rodent behavioral assays. *Neurosci. Biobehav. Rev.* 135:104560. doi: 10.1016/J.NEUBIOREV.2022.104560

Day, N. L., and Richardson, G. A. (2004). An analysis of the effects of prenatal alcohol exposure on growth: a teratologic model. *Am. J. Med. Genet. C Semin. Med. Genet.* 127C, 28–34. doi: 10.1002/AJMG.C.30013

Duan, Y., Llorente, C., Lang, S., Brandl, K., Chu, H., Jiang, L., et al. (2019). Bacteriophage targeting of gut bacterium attenuates alcoholic liver disease. *Nature* 575, 505–511. doi: 10.1038/S41586-019-1742-X

Dufton, N., and Perretti, M. (2010). Therapeutic anti-inflammatory potential of formyl-peptide receptor agonists. *Pharmacol. Ther.* 127, 175–188. doi: 10.1016/J.PHARMTHERA.2010.04.010

Dyall, S. C., Balas, L., Bazan, N. G., Brenna, J. T., Chiang, N., da Costa Souza, F., et al. (2022). Polyunsaturated fatty acids and fatty acid-derived lipid mediators: recent advances in the understanding of their biosynthesis, structures, and functions. *Prog. Lipid Res.* 86:101165. doi: 10.1016/J.PLIPRES.2022.101165

Gallo, I., Rattazzi, L., Piras, G., Gobbetti, T., Panza, E., Perretti, M., et al. (2014). Formyl peptide receptor as a novel therapeutic target for anxiety-related disorders. *PLoS One* 9:e114626. doi: 10.1371/JOURNAL.PONE.0114626

Gano, A., Prestia, L., Middleton, F. A., Youngentob, S. L., Ignacio, C., and Deak, T. (2020). Gene expression profiling reveals a lingering effect of prenatal alcohol exposure on inflammatory-related genes during adolescence and adulthood. *Cytokine* 133:155126. doi: 10.1016/J.CYTO.2020.155126

Gao, J. L., Schneider, E. H., Dimitrov, E. L., Haun, F., Pham, T. M., Mohammed, A. H., et al. (2011). Reduced fear memory and anxiety-like behavior in mice lacking formylpeptide receptor 1. *Behav. Genet.* 41, 724–733. doi: 10.1007/S10519-011-9467-0

García-Baos, A., Puig-Reyne, X., García-Algar, Ó., and Valverde, O. (2021). Cannabidiol attenuates cognitive deficits and neuroinflammation induced by early alcohol exposure in a mice model. *Biomed. Pharmacother.* 141:111813. doi: 10.1016/j.biopha.2021.111813

Goldschmidt, L., Richardson, G. A., De Genna, N. M., Cornelius, M. D., and Day, N. L. (2019). Prenatal alcohol exposure and offspring alcohol use and misuse at 22 years of age: a prospective longitudinal study. *Neurotoxicol. Teratol.* 71, 1–5. doi: 10.1016/J.NTT.2018.11.001

Gosdin, L. K., Deputy, N. P., Kim, S. Y., Dang, E. P., and Denny, C. H. (2022). Alcohol consumption and binge drinking during pregnancy among adults aged 18-49 years - United States, 2018-2020. *MMWR Morb. Mortal. Wkly Rep.* 71, 10–13. doi: 10.15585/MMWR.MM7101A2

Han, Y. H., Lee, K., Saha, A., Han, J., Choi, H., Noh, M., et al. (2021). Specialized Proresolving mediators for therapeutic interventions targeting metabolic and inflammatory disorders. *Biomol. Ther.* 29, 455–464. doi: 10.4062/BIOMOLTHER.2021.094

Ho, C. F. Y., Ismail, N. B., Koh, J. K. Z., Gunaseelan, S., Low, Y. H., Ng, Y. K., et al. (2018). Localisation of formyl-peptide receptor 2 in the rat central nervous system and its role in axonal and dendritic outgrowth. *Neurochem. Res.* 43, 1587–1598. doi: 10.1007/S11064-018-2573-0

Hoyme, H. E., Kalberg, W. O., Elliott, A. J., Blankenship, J., Buckley, D., Marais, A.-S., et al. (2016). Updated clinical guidelines for diagnosing fetal alcohol spectrum disorders. *Pediatrics* 138:e20154256. doi: 10.1542/peds.2015-4256

Jacobson, S. W., Hoyme, H. E., Carter, R. C., Dodge, N. C., Molteno, C. D., Meintjes, E. M., et al. (2021). Evolution of the physical phenotype of fetal alcohol spectrum disorders from childhood through adolescence. *Alcohol. Clin. Exp. Res.* 45, 395–408. doi: 10.1111/ACER.14534

Komada, M., Hara, N., Kawachi, S., Kawachi, K., Kagawa, N., Nagao, T., et al. (2017). Mechanisms underlying neuro-inflammation and neurodevelopmental toxicity in the mouse neocortex following prenatal exposure to ethanol. *Sci. Rep.* 7:4934. doi: 10.1038/s41598-017-04289-1

Krishnamoorthy, S., Recchiuti, A., Chiang, N., Yacoubian, S., Lee, C. H., Yang, R., et al. (2010). Resolvin D1 binds human phagocytes with evidence for proresolving receptors. *Proc. Natl. Acad. Sci. U. S. A.* 107, 1660–1665. doi: 10.1073/PNAS.0907342107

Kwan, S. T. C., Presswood, B. H., Helfrich, K. K., Baulch, J. W., Mooney, S. M., and Smith, S. M. (2020). An interaction between fetal sex and placental weight and efficiency predicts intrauterine growth in response to maternal protein insufficiency and gestational exposure window in a mouse model of FASD. *Biol. Sex Differ.* 11:40. doi: 10.1186/S13293-020-00320-9

Li, C., Wu, X., Liu, S., Shen, D., Zhu, J., and Liu, K. (2020). Role of Resolvins in the inflammatory resolution of neurological diseases. *Front. Pharmacol.* 11:612. doi: 10.3389/FPHAR.2020.00612

Madore, C., Nadjar, A., Delpech, J.-C., Sere, A., Aubert, A., Portal, C., et al. (2014). Nutritional n-3 PUFAs deficiency during perinatal periods alters brain innate immune system and neuronal plasticity-associated genes. *Brain Behav. Immun.* 41, 22–31. doi: 10.1016/J.BBI.2014.03.021

Marquardt, K., and Brigman, J. L. (2016). The impact of prenatal alcohol exposure on social, cognitive and affective behavioral domains: insights from rodent models. *Alcohol* 51, 1–15. doi: 10.1016/j.alcohol.2015.12.002

Mastromarino, M., Lacivita, E., Colabufo, N. A., and Leopoldo, M. (2020). G-protein coupled receptors involved in the resolution of inflammation: ligands and therapeutic perspectives. *Mini-Rev. Med. Chem.* 20, 2090–2103. doi: 10.2174/1389557520666200719014433

May, P. A., Chambers, C. D., Kalberg, W. O., Zellner, J., Feldman, H., Buckley, D., et al. (2018). Prevalence of fetal alcohol spectrum disorders in 4 US communities. *JAMA* 319, 474–482. doi: 10.1001/jama.2017.21896

Mooney, S. M., Pjetri, E., Friday, W. B., and Smith, S. M. (2021). Growth and behavioral differences in a C56BL/6J mouse model of prenatal alcohol exposure. *Alcohol* 97, 51–57. doi: 10.1016/J.ALCOHOL.2021.09.031

Pal, A., Al-Shaer, A. E., Guesdon, W., Torres, M. J., Armstrong, M., Quinn, K., et al. (2020). Resolvin E1 derived from eicosapentaenoic acid prevents hyperinsulinemia and hyperglycemia in a host genetic manner. *FASEB J.* 34, 10640–10656. doi: 10.1096/FJ.202000830R

Paolicelli, R. C., and Ferretti, M. T. (2017). Function and dysfunction of microglia during brain development: consequences for synapses and neural circuits. *Front. Synapt. Neurosci.* 9:9. doi: 10.3389/FNSYN.2017.00009

Pascual, M., Montesinos, J., Montagud-Romero, S., Forteza, J., Rodríguez-Arias, M., Miñarro, J., et al. (2017). TLR4 response mediates ethanol-induced neurodevelopment alterations in a model of fetal alcohol spectrum disorders. *J. Neuroinflammation* 14:145. doi: 10.1186/s12974-017-0918-2

Patten, A. R., Sickmann, H. M., Dyer, R. A., Innis, S. M., and Christie, B. R. (2013). Omega-3 fatty acids can reverse the long-term deficits in hippocampal synaptic plasticity caused by prenatal ethanol exposure. *Neurosci. Lett.* 551, 7–11. doi: 10.1016/J.NEULET.2013.05.051

Perretti, M., and Godson, C. (2020). Formyl peptide receptor type 2 agonists to kick-start resolution pharmacology. *Br. J. Pharmacol.* 177, 4595–4600. doi: 10.1111/bph.15212

Qin, C. X., Norling, L. V., Vecchio, E. A., Brennan, E. P., May, L. T., Wootten, D., et al. (2022). Formylpeptide receptor 2: nomenclature, structure, signalling and translational perspectives: IUPHAR review 35. *Br. J. Pharmacol.* 179, 4617–4639. doi: 10.1111/BPH.15919

Reeves, P. G., Nielsen, F. H., and Fahey, G. C. Jr. (1993). AIN-93 purified diets for laboratory rodents: final report of the American Institute of Nutrition ad hoc writing committee on the reformulation of the AIN-76A rodent diet. *J Nutr.* 123:1939–51. doi: 10.1093/jn/123.11.1939

Sansbury, B. E., and Spite, M. (2016). Resolution of acute inflammation and the role of Resolvins in immunity, thrombosis, and vascular biology. *Circ. Res.* 119, 113–130. doi: 10.1161/CIRCRESAHA.116.307308

Serhan, C. N. (2014). Pro-resolving lipid mediators are leads for resolution physiology. *Nature* 510, 92–101. doi: 10.1038/NATURE13479

Shin, L. M., and Liberzon, I. (2010). The neurocircuitry of fear, stress, and anxiety disorders. *Neuropsychopharmacology* 35, 169–191. doi: 10.1038/NPP.2009.83

Smith, S. M., Pjetri, E., Friday, W. B., Presswood, B. H., Ricketts, D. K., Walter, K. R., et al. (2022). Aging-related behavioral, adiposity, and glucose impairments and their association following prenatal alcohol exposure in the C57BL/6J mouse. *Nutrients* 14:1438. doi: 10.3390/NU14071438

Smith, S. M., Virdee, M. S., Eckerle, J. K., Sandness, K. E., Georgieff, M. K., Boys, C. J., et al. (2021). Polymorphisms in SLC44A1 are associated with cognitive improvement in children diagnosed with fetal alcohol spectrum disorder: an exploratory study of oral choline supplementation. *Am. J. Clin. Nutr.* 114, 617–627. doi: 10.1093/AJCN/NQAB081

Takeshita, H., Yamamoto, K., Nozato, S., Inagaki, T., Tsuchimochi, H., Shirai, M., et al. (2017). Modified forelimb grip strength test detects aging-associated physiological decline in skeletal muscle function in male mice. *Sci. Rep.* 7:42323. doi: 10.1038/SREP42323

Topper, L. A., Baculis, B. C., and Valenzuela, C. F. (2015). Exposure of neonatal rats to alcohol has differential effects on neuroinflammation and neuronal survival in the cerebellum and hippocampus. *J. Neuroinflammation* 12:160. doi: 10.1186/s12974-015-0382-9

Valente, M., Dentoni, M., Bellizzi, F., Kuris, F., and Gigli, G. L. (2022). Specialized pro-resolving mediators in neuroinflammation: overview of studies and perspectives of clinical applications. *Molecules* 27:4836. doi: 10.3390/MOLECULES27154836

Virdee, M. S., Saini, N., Kay, C. D., Neilson, A. P., Kwan, S. T. C., Helfrich, K. K., et al. (2021). An enriched biosignature of gut microbiota-dependent metabolites characterizes maternal plasma in a mouse model of fetal alcohol spectrum disorder. *Sci. Rep.* 11:248. doi: 10.1038/S41598-020-80093-8

Wainwright, P. E., Ward, G. R., Winfield, D., Huang, Y. S., Mills, D. E., Ward, R. P., et al. (1990). Effects of prenatal ethanol and long-chain n-3 fatty acid supplementation on development in mice. 1. Body and brain growth, sensorimotor development, and water T-maze reversal learning. *Alcohol. Clin. Exp. Res.* 14, 405–412. doi: 10.1111/j.1530-0277.1990.tb00495.x

Walter, K. R., Ricketts, D. R., Presswood, B. H., Smith, S. M., and Mooney, S. M. (2022). Prenatal alcohol exposure causes persistent neuroinflammation and age- and sex-specific effects on cognition and metabolic outcomes in an Alzheimer's disease mouse model. *Am. J. Drug Alcohol Abuse*, 1–19. doi: 10.1080/00952990.2022.2119571

Wellmann, K. A., George, F., Brnouti, F., and Mooney, S. M. (2015). Docosahexaenoic acid partially ameliorates deficits in social behavior and ultrasonic vocalizations caused by prenatal ethanol exposure. *Behav. Brain Res.* 286, 201–211. doi: 10.1016/j.bbr.2015.02.048

Zhang, Y., Chen, K., Sloan, S. A., Bennett, M. L., Scholze, A. R., O'Keeffe, S., et al. (2014). An RNA-sequencing transcriptome and splicing database of glia, neurons, and vascular cells of the cerebral cortex. *J. Neurosci.* 34, 11929–11947. doi: 10.1523/JNEUROSCI.1860-14.2014

Zhang, J., Liu, L., Zhang, Y., Yuan, Y., Miao, Z., Lu, K., et al. (2022). ChemR23 signaling ameliorates cognitive impairments in diabetic mice via dampening oxidative stress and NLRP3 inflammasome activation. *Redox Biol.* 58:102554. doi: 10.1016/J.REDOX.2022.102554

Zhang, Y., Xu, N., Ding, Y., Zhang, Y., Li, Q., Flores, J., et al. (2018). Chemerin suppresses neuroinflammation and improves neurological recovery via CaMKK2/AMPK/Nrf2 pathway after germinal matrix hemorrhage in neonatal rats. *Brain Behav. Immun.* 70, 179–193. doi: 10.1016/J.BBI.2018.02.015

frontiers | Frontiers in Neuroscience

TYPE Original Research
PUBLISHED 19 July 2023
DOI 10.3389/fnins.2023.1214100

Check for updates

OPEN ACCESS

EDITED BY
Lisa Akison,
The University of Queensland, Australia

REVIEWED BY
Danielle J. Burgess,
The University of Queensland, Australia
Erin Milligan,
University of New Mexico, United States

*CORRESPONDENCE
Tamara S. Bodnar
✉ tamara.bodnar@ubc.ca

RECEIVED 28 April 2023
ACCEPTED 14 June 2023
PUBLISHED 19 July 2023

CITATION
Bodnar TS, Chao A, Holman PJ, Ellis L, Raineki C and Weinberg J (2023) Impact of the COVID-19 pandemic on adults with Fetal Alcohol Spectrum Disorder: linking immune function to mental health status.
Front. Neurosci. 17:1214100.
doi: 10.3389/fnins.2023.1214100

COPYRIGHT
© 2023 Bodnar, Chao, Holman, Ellis, Raineki and Weinberg. This is an open-access article distributed under the terms of the Creative Commons Attribution License (CC BY). The use, distribution or reproduction in other forums is permitted, provided the original author(s) and the copyright owner(s) are credited and that the original publication in this journal is cited, in accordance with accepted academic practice. No use, distribution or reproduction is permitted which does not comply with these terms.

Impact of the COVID-19 pandemic on adults with Fetal Alcohol Spectrum Disorder: linking immune function to mental health status

Tamara S. Bodnar[1]*, Amanda Chao[1], Parker J. Holman[1], Linda Ellis[1], Charlis Raineki[2] and Joanne Weinberg[1]

[1]Department of Cellular and Physiological Sciences, Faculty of Medicine, University of British Columbia, Vancouver, BC, Canada, [2]Department of Psychology, Brock University, St. Catharines, ON, Canada

Prenatal alcohol exposure (PAE) is known to cause a variety of cognitive, behavioral, and neurological changes. Importantly, mental health problems are also overrepresented in individuals with Fetal Alcohol Spectrum Disorder (FASD), the group of neurodevelopmental conditions that can occur following PAE. Approximately 90% of individuals with FASD report experiencing mental health problems over their lifespan, compared to approximately 30% in the overall population. Individuals with FASD also display impairments in coping skills and increased vulnerability to stress. Here, we investigated whether the COVID-19 pandemic would have a differential impact on mental health and inflammation-to-mood associations in adults with FASD, compared to unexposed controls (no PAE). We capitalized on our pre-pandemic study examining health and immune function and invited past-participants to enroll in the current study. Participants completed mental health assessments and COVID-related questionnaires by phone. In addition, blood samples collected at baseline (pre-pandemic) were used to probe for inflammation-to-mood associations. Overall, our results indicate that lower SES was predictive of higher coronavirus anxiety scores, with no differences between adults with FASD and controls. In addition, while there were no differences in depression or anxiety measures at baseline (pre-pandemic) or during the pandemic, examination of inflammation-to-mood associations identified differential relationships in adults with FASD compared to unexposed controls. Specifically, there was a positive association between baseline neutrophil counts and both baseline and pandemic mental health scores in unexposed controls only. In addition, for unexposed controls there was also a negative association between baseline interferon-ɣ (IFN-ɣ) and pandemic mental health scores. By contrast, only adults with FASD showed positive associations between baseline interleukin-12p70 (IL-12p70), IL-8, soluble intercellular adhesion molecule-1 (sICAM-1), and soluble vascular cell adhesion molecule-1 (sVCAM-1) and pandemic mental health scores. Taken together, to our knowledge, this study is the first to examine the impact of the pandemic in adults with FASD. And while it may be too soon to predict the long-term effects of the pandemic on mental health, our data suggest that it will be important that future work also takes into account how immune function may be modulating mental health outcomes in this population.

KEYWORDS

prenatal alcohol exposure (PAE), cytokines, immune system, white blood cells, depression, anxiety

1. Introduction

The COVID-19 pandemic has resulted in unprecedented changes to daily life worldwide (Haleem et al., 2020). Public health measures aimed at decreasing the spread of coronavirus, including cancelation of events and social distancing from friends and family, have resulted in unfortunate consequences such as increased loneliness and impaired psychological well-being (Okruszek et al., 2020). It has been established that rates of mental health problems, such as depression and anxiety, increased substantially during the pandemic (Kwong et al., 2021; Hawes et al., 2022; Wettstein et al., 2022). In addition, there are subgroups within the general population known to be especially vulnerable to poor mental health as a result of the COVID-19 pandemic including women (Almeida et al., 2020), people in low-income households (Kwong et al., 2021), and individuals with a previous history of mental health problems (Neelam et al., 2021). Another group shown to be at higher risk are those with neurodevelopmental disorders (NDDs) (Guller et al., 2022). Notably, the majority of this work has been conducted in children, with reasons for the increased risk of mental health problems attributed to changes in routines (e.g., disruptions to schooling and extracurricular activities) and increased fear of infection (Ehrler et al., 2021; Guller et al., 2022). Adults with NDDs, including attention deficit hyperactivity disorder (ADHD) and autism spectrum disorder (ASD), also experienced increased rates of depression and anxiety during the pandemic (Shakeshaft et al., 2023). However, it is important to note that not all of the impacts of the pandemic on mental health were negative for these populations. For example, one study reported that, for adult females with ASD, depressive symptoms *decreased* during the pandemic, potentially due to the reduced demands/opportunities for social interactions (Shakeshaft et al., 2023). Similarly, decreased sensory and social overloading were also reported as positive impacts of the pandemic on mental health for adults with NDDs (Oomen et al., 2021).

Much less is known regarding the impact of the pandemic on mental health in individuals with Fetal Alcohol Spectrum Disorder (FASD), the group of neurodevelopmental conditions that can occur following prenatal alcohol exposure (PAE). Importantly, FASD is the most common neurodevelopmental disorder, with current North American prevalence estimates at approximately 4–7% (Flannigan et al., 2018; May et al., 2021), which is higher than that of ASD, cerebral palsy and down syndrome combined (Cook, 2021). Of relevance, individuals with FASD may be at particularly high risk of impairments to mental wellbeing during the pandemic for reasons including the high rate of existing mental health problems in this population (Pei et al., 2011; Coles et al., 2022), as approximately 90% of individuals with FASD experience a mental health disorder in their lifetime (Famy et al., 1998), as well as an apparent link between lower socioeconomic status (SES) and FASD (Bingol et al., 1987; Abel and Hannigan, 1995; May and Gossage, 2011). Despite the high prevalence of FASD and the added mental health risk factors, very little is known in terms of how the pandemic impacted mental health in these individuals.

Pre-clinical and clinical studies have demonstrated that *in utero* alcohol-exposure has significant negative impacts on immune development and function [reviewed in Bodnar and Weinberg (2013), Reid et al. (2019), Lussier et al. (2021)]. Specifically, children with FASD broadly exhibit increased rates of infection (Johnson et al., 1981; Gauthier et al., 2005) and atopic conditions (Linneberg et al., 2004; Wada et al., 2016), as well as altered immune cell counts (Johnson et al., 1981; Gottesfeld and Abel, 1991; Oleson et al., 1998) and cytokine levels (Ahluwalia et al., 2000; Bodnar et al., 2020). Much less is known regarding immune function in adults with FASD; however, preliminary results from our ongoing research suggest that immune system disruptions persist into adulthood, including alterations in cytokine levels (Raineki et al., 2021; McMahan et al., 2023). Importantly, positive associations between inflammatory cytokines and mood symptoms have been consistently reported (Anisman et al., 2005; Raison et al., 2006; Kohler et al., 2017; Leighton et al., 2018). In addition, pre-clinical and clinical evidence indicates that cytokine increases can precipitate depressive-like symptomology (Reichenberg et al., 2001; Dunn et al., 2005; Liang and Ghany, 2013). While inflammation-to-mood associations have been generally well-established, the specific cytokines involved vary based on factors including the health status and environment of the individual (Rosenblat et al., 2014). For example, psychological stress has generally been shown to increase levels of C-reactive protein (CRP), interleukin (IL)-6, IL-1β, and tumour necrosis factor (TNF)-α in otherwise healthy individuals (Steptoe et al., 2007), whereas for obese individuals, elevated levels of IL-5, IL-12, and interferon-ɣ (IFN-ɣ) have been associated with depression (Schmidt et al., 2014). By contrast, inflammation-to-mood relationships have yet to be explored in individuals with FASD. A better understanding of inflammation-to-mood relationships could highlight opportunities for early-recognition, prevention and treatment of mood disorders (Rosenblat et al., 2014).

In the current study, we examined the impact of the pandemic on mental health in adults with FASD, as well as the link between immune function and mental health outcomes. We capitalized on our ongoing, pre-pandemic study examining health and immune function in adults with FASD, re-contacting study participants and inviting them to participate in the current study to re-examine their mental health during the pandemic. Overall, we hypothesized that mental health would be impaired in adults with FASD as a result of the pandemic and specifically, that higher scores than unexposed controls (no PAE) on anxiety and depression assessments would be identified. In addition, we hypothesized that inflammation-to-mood associations would differ between adults with FASD and unexposed controls due to differential impacts of pandemic-related stress on these two populations. Specifically, we hypothesized that, given the known immune dysregulation in individuals with FASD, the pandemic would act as a stressor such that mood dysregulation would be higher in adults with FASD who had a higher immunological set-point pre-pandemic.

2. Materials and methods

2.1. Cohort description

Participants were recruited from our ongoing Collaborative Initiative on Fetal Alcohol Spectrum Disorders (CIFASD) study examining health and immune outcomes in adults with FASD, which was paused in March 2020 due to the pandemic. Briefly, for this broader CIFASD study, inclusion criteria included: adults (19+) with a diagnosis of FASD (i.e., Fetal Alcohol Syndrome

[FAS], partial FAS [pFAS], Alcohol-Related Birth Defects [ARBD], Alcohol-Related Neurodevelopmental Disorder [ARND] or a related diagnosis) living in British Columbia (BC), Canada. Participants were asked to provide details regarding their diagnosis (i.e., year of diagnosis, clinic/doctor who performed the diagnosis, etc.) and participants who did not have a diagnosis of FASD were unable to participate in the study. Participants with FASD were recruited through social media, advertising at events and conferences related to FASD, and through flyers posted at FASD diagnostic clinics. A matched group of unexposed controls (no PAE) was also recruited from the community through social media, online advertisements, and posting study flyers in libraries, coffee shops and other community locations. Potential participants were excluded if they could not provide informed consent, were currently pregnant or breastfeeding, or had HIV/AIDS.

Of the 46 adults with FASD and 26 unexposed controls who had been recruited and had completed the broader CIFASD study by March 2020, and who had provided consent to be re-contacted, a total of 19 adults with FASD and 17 unexposed controls participated in the current pandemic study, carried out over the phone, from January 2021 – May 2021. This timeframe was recognized by the Public Health Agency of Canada as a peak of COVID infections, with 2,800 - 9,000+ daily cases of COVID-19 documented in BC, representing the largest peak in infections in BC up to that point (Statistics Canada, 2023). Study questionnaires administered pre-pandemic (during in-person testing for our broader CIFASD study) were repeated for the current pandemic study (by phone), with the addition of the COVID-19 assessments.

2.2. Demographic information

Questionnaires were used to collect demographic information including race/ethnicity, income, education, employment status, neighborhood characteristics etc. (Table 1). Demographic information was also used to generate a composite measure of socioeconomic status (SES), as has been previously reported (Gilman et al., 2017). Briefly, this SES measure combined information regarding: (1) education (incomplete high school, high school graduate, post-high school education); (2) income relative to the Canadian 2021 low-income cut-off (LICO), adjusted for family size (<LICO, 100–150% of LICO, >150% of LICO); (3) occupation [unemployed, employed – manual/part-time, employed (non-manual/full-time]); (4) neighborhood safety (is it safe to walk alone at night in your neighborhood? [mostly unsafe, somewhat safe, safe]). For each of the four factors, a score of 0, 1, or 2 was assigned, with higher scores, indicating a higher degree of socioeconomic advantage and the score for each of the four factors summed to produce a composite measure of SES (Supplementary Table 1).

2.3. Mental health and stress assessments

Mental health was assessed using the Beck Depression Inventory 2 (BDI-2; Pearson, Canada) and the Beck Anxiety Inventory (BAI; Pearson, Canada). The BDI is a 21-item, self-report questionnaire that assesses characteristic attitudes and symptoms of depression (Beck et al., 1961). A total score on the BDI ranging from 0 to 63 is obtained by adding the scores for each item. Total scores are classified as either: normal mood or minimal depression (score 0–13), mild depression (score 14–19), moderate depression (score 20–28), or severe depression (score 29–63). The BDI has been shown to have high reliability (Cronbach $\alpha = 0.92$), with a 1-week test–retest reliability of $r = 0.93$ (Wang and Gorenstein, 2013), and to have the capacity to discriminate between individuals with and without depression, in a wide variety of populations (Osman et al., 2004; Wang and Gorenstein, 2013; Garcia-Batista et al., 2018; Toledano-Toledano and Contreras-Valdez, 2018). The BAI is a 21-item, self-report questionnaire assessing common somatic and cognitive symptoms of anxiety (Beck et al., 1988). A total score on the BAI ranging from 0–63 is obtained by adding the scores for each item. Total scores are classified as either: low anxiety (score 0–21), moderate anxiety (score 22–35), or high anxiety (score ≥ 36). The BAI has been reported to be highly reliable (Cronbach $\alpha = 0.92$), with a 1-week test–retest reliability of $r = 0.75$ (Beck et al., 1988; Fydrich et al., 1992). The BAI has also been shown to be able to discriminate between anxious and non-anxious diagnostic groups (Beck et al., 1988). The BDI and BAI were administered at baseline (pre-pandemic) during the in-person study visit and again during the pandemic, over the phone by trained study personnel. In addition to total scores for the BDI and BAI, a combined BDI/BAI score was generated by adding the BDI and BAI total scores, to examine mental health, in general.

2.4. Blood collection

Blood samples were drawn at the initial study visit for our CIFASD study (pre-pandemic/baseline) using EDTA-coated vacutainers, with separate tubes used to collect samples for cytokine and hematology analysis. Samples for cytokine analysis were placed on ice, centrifuged at 4°C, and plasma stored at −80°C. Samples for hematological analysis were kept at room temperature and analysis performed within 6 h of blood collection.

2.5. Hematology analysis and cytokine assays

Hematological analyses were performed using the Sysmex XN-550 automated hematology analyzer (Sysmex Canada, Mississauga, ON). Measures included a complete blood count (CBC), routine white blood cell differential, platelet counts, and hemoglobin level. Cytokine/chemokine and related inflammatory markers were measured in plasma samples using the Meso Scale Discovery (MSD) VLEX Human Biomarker 40-Plex kit (K15209D-1, MSD, Rockville, MD). Plates were read using a MESO QuickPlex SQ120 and data analyzed using the MSD Discovery Workbench software v.4.0. For the lower limit of detection and unabbreviated cytokine list, see Supplementary Table 2.

2.6. COVID-19 assessments

Self-report screeners including the Obsession with COVID-19 Scale (OCS), the Coronavirus Anxiety Scale (CAS) and the

TABLE 1 Demographic information.

Variable		Unexposed control (*n*=17)	FASD (*n*=19)	*p* value
Age (years)		36.1 ± 3.0	37.2 ± 2.4	0.350[1]
Diagnosis (self-report)	Fetal Alcohol Syndrome (FAS)	–	42.1% (8)	–
	Partial FAS (pFAS)	–	10.5% (2)	
	Alcohol Related Neurodevelopmental Disorder (ARND)	–	5.3% (1)	
	FASD (specific diagnosis unknown)	–	42.1% (8)	
Current gender identity	Man	23.5% (4)	21.1% (4)	0.586[2]
	Woman	76.5% (13)	78.9% (15)	
Ethnicity	Indigenous	11.8% (2)	57.9% (11)**	**0.010**[3]
	White	35.3% (6)	26.3% (5)	
	Other ethnicities	52.9% (9)	5.3% (3)*	
Education level	Incomplete high school	5.9% (1)	31.6% (6)	0.107[2]
	Graduated high school	11.8% (2)	26.3% (5)	
	Partial college	11.8% (2)	15.8% (3)	
	College or University graduate	23.5% (4)	15.8% (3)	
	Graduate professional training	47.0% (8)	10.5% (2)	
Employment status	Employed	70.6% (12)	42.1% (8)	0.287[2]
	Full-time student (or vocational training)	0% (0)	5.3% (1)	
	Volunteer work	0% (0)	10.5% (2)	
	Unemployed	29.4% (5)	36.8% (7)	
	Missing	0% (0)	5.3% (1)	
Current income	<$20,000	23.5% (4)	57.9% (11)	0.080[2]
	$20,000–$49,999	23.5% (4)	26.3% (5)	
	$50,000–$99,999	17.6% (3)	5.3% (1)	
	>$100,000	29.4% (5)	5.3% (1)	
	Missing	5.9% (1)	5.3% (1)	

Questionnaires (self-report) were used to collect demographic information including: age, diagnosis (FASD group only), current gender identity, ethnicity, education level, employment status, and current income. The continuous variable (age) was reported as the mean value ± standard error of the mean (SEM). Categorical variables were reported as the percentage of the group followed by the *n* in parentheses. [1]Mann Whitney *U* test, [2]Fisher's Exact Test, [3]Chi Square Test.
Bolded *p*-values are significant; *post-hoc* testing – ** ($p < 0.01$): FASD > unexposed control; *($p < 0.05$): FASD < unexposed control. FASD: Fetal Alcohol Spectrum Disorder.

Coronavirus Reassurance Seeking Behaviors Scale (CRBS) were administered over the phone to assess COVID-related mental health problems. Specifically, the OCS identifies persistent and disturbed thinking related to COVID-19 (Lee, 2020), the CRBS measures reassurance-seeking behaviors associated with concerns over COVID-19 infection (Lee et al., 2020), and the CAS assesses dysfunctional anxiety related to the COVID-19 pandemic (Lee, 2020). Participants were also asked to self-report whether they had experienced a previous COVID-19 infection.

2.7. Statistical modeling

Analysis of demographic variables was performed using Mann–Whitney U test (age), Chi Square test (ethnicity), or the Fisher's Exact test (gender, education level, employment status, current income, SES composite). The mental health assessments (BDI, BAI, BDI/BAI) and the COVID-19 assessments were analyzed by analysis of covariance (ANCOVA), having met the homogeneity of regression assumption. Repeated measures ANOVAs were also conducted to examine BDI, BAI, and BDI/BAI from baseline to pandemic. The rate of COVID-19 infection (self-report COVID-19 infection) was analyzed by Fisher's Exact Test. Cytokine levels below the lower limit of detection of the assay were assigned a value of zero and outlier values were Winsorized (transformed to limit extreme outliers) (Tukey, 1962). The following cytokines were undetectable in >15% of the samples and were excluded from the analyses: Granulocyte-macrophage colony stimulating factor (GM-CSF; 78%), IL-17 (19%), IL-5 (75%), tumor necrosis factor-β (TNF-β; 19%), macrophage inflammatory protein-1α (MIP-1α; 44%), IL-13 (72.2%), IL-1β (63.9%), IL-2 (25%), IL-4 (75%). Cytokine values were non-normally distributed and were Blom transformed for statistical analyses. Hierarchical linear regression models were fit to examine the relationship between the SES composite and the COVID-19 assessments. To explore the relationship between cytokine levels (baseline) and mental health (baseline and pandemic), separate hierarchical linear regression models were fit for each cytokine. In addition, hierarchical linear

regression was also performed to examine the relationship between baseline white blood cell counts and mental health (baseline and pandemic). For all hierarchical regression analyses, self-reported gender and age at the time of blood collection were controlled for in the model. p values were considered significant at $p \leq 0.05$. Statistical analyses were conducted using IBM SPSS Statistics version 25.0.

3. Results

3.1. Sample characteristics

There were no group differences in the age of study participants, education level, employment status, or current income (Table 1). For self-reported ethnicity [X^2 (2, $n = 36$) = 9.24, $p = 0.010$], however, more adults with FASD reported their ethnicity as Indigenous, compared to unexposed controls ($p = 0.004$). In addition, unexposed controls reported higher rates of "other ethnicities" (e.g., South Asian/East Indian, Asian, other) compared to adults with FASD ($p = 0.018$) (Table 1). In the FASD group, 42.1% were diagnosed with Fetal Alcohol Syndrome (FAS), 10.5% were diagnosed with partial FAS (pFAS), and 5.3% were diagnosed with Alcohol Related Neurodevelopmental Disorder (ARND) (Table 1). In addition, 42.1% of adults with FASD could not recall their specific diagnosis; however, confirmation that the participant was, in fact, diagnosed with FASD was performed by research staff (through confirmation of details including diagnostic clinic and/or physician who performed the diagnosis). Finally, examination of the composite measure of SES showed that adults with FASD had lower SES (greater socioeconomic disadvantage), compared to unexposed adults [X^2 (8, $n = 36$) = 15.71, $p = 0.017$; Figure 1].

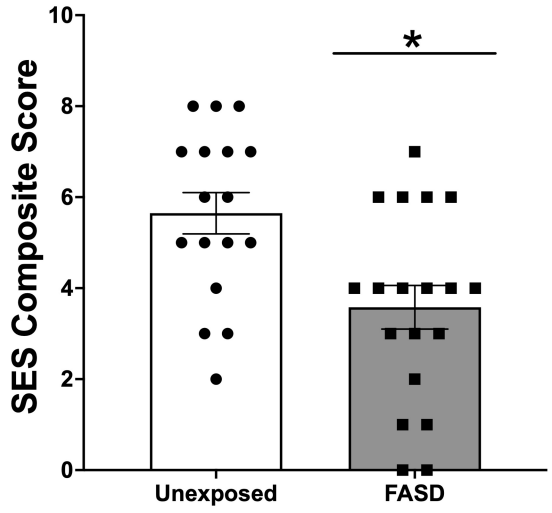


FIGURE 1
Socioeconomic status (SES) composite score generated from measures of education, income relative to the Canadian 2021 low income cut-off (adjusted for family size), occupation, and neighborhood. Higher scores indicated higher SES (and lower degree of socioeconomic disadvantage). SES was lower in adults with Fetal Alcohol Spectrum Disorder (FASD) compared to unexposed controls *p<0.05.

A comparison of demographic variables, including age, gender, ethnicity, education level, employment status, current income, and baseline mental health (BDI, BAI) between the current COVID study participants ($n = 36$) and the overall CIFASD study sample recruited pre-pandemic ($n = 72$) revealed no differences between the two samples (Supplementary Table 3).

3.2. COVID-19 assessments

There were no differences in the self-reported rates of COVID-19 infection or scores on the CAS, the CRBS, or the OCS between adults with FASD and unexposed controls (Table 2). However, regression analysis revealed that lower SES was predictive of higher coronavirus anxiety on the CAS [ΔR^2: 0.289, β: −0.379, $F(1, 32) = 5.18$, $p = 0.030$] in the overall sample (no group differences). No associations were identified between SES and the CRBS or the OCS.

3.3. Mental health and immune function

There were no differences between adults with FASD and unexposed adults on the BDI, BAI or overall mental health (BDI/BAI) either at baseline or during the pandemic, with the exception of a trend for increased pre-pandemic BAI in adults with FASD compared to unexposed controls [$F(1, 32) = 3.388$, $p = 0.075$; Figure 2]. In addition, repeated measures ANOVA of baseline to pandemic BDI and BAI similarly revealed no differences over time or by group.

To examine the relationship between immune function and mental health, hierarchical regression analyses were performed between baseline white blood cell counts and overall mental health (BDI/BAI). Regression analyses identified a positive association between neutrophil counts and pre-pandemic BDI/BAI score in unexposed controls [ΔR^2: 0.307, β: 0.575, $F(1, 12) = 5.65$, $p = 0.035$] but

TABLE 2 COVID-19 assessments.

Variable	Unexposed control (n =17)	FASD (n=19)	Value of p
Do you think you have previously had a COVID-19 infection?	Yes: 23.5% (4)	Yes: 21.1% (4)	0.586[1]
Coronavirus Anxiety Scale (CAS)	2.0 ± 0.56	3.6 ± 1.1	0.215[2]
Coronavirus Reassurance Seeking Behaviors Scale (CRBS)	1.4 ± 0.7	2.3 ± 0.8	0.392[2]
Obsession with COVID-19 Scale (OCS)	2.0 ± 0.7	2.9 ± 1.0	0.471[2]

Participants were asked to report previous COVID-19 infection(s) and questionnaires were used to assess COVID-19-related anxieties/stressors. COVID-19 infection rates were reported as the percentage of the group followed by the n in parentheses. The COVID-19 scales are reported as the mean ± standard error of the mean (SEM). [1]Fisher's Exact Test, [2]Analysis of covariance (ANCOVA). There were no differences between groups.

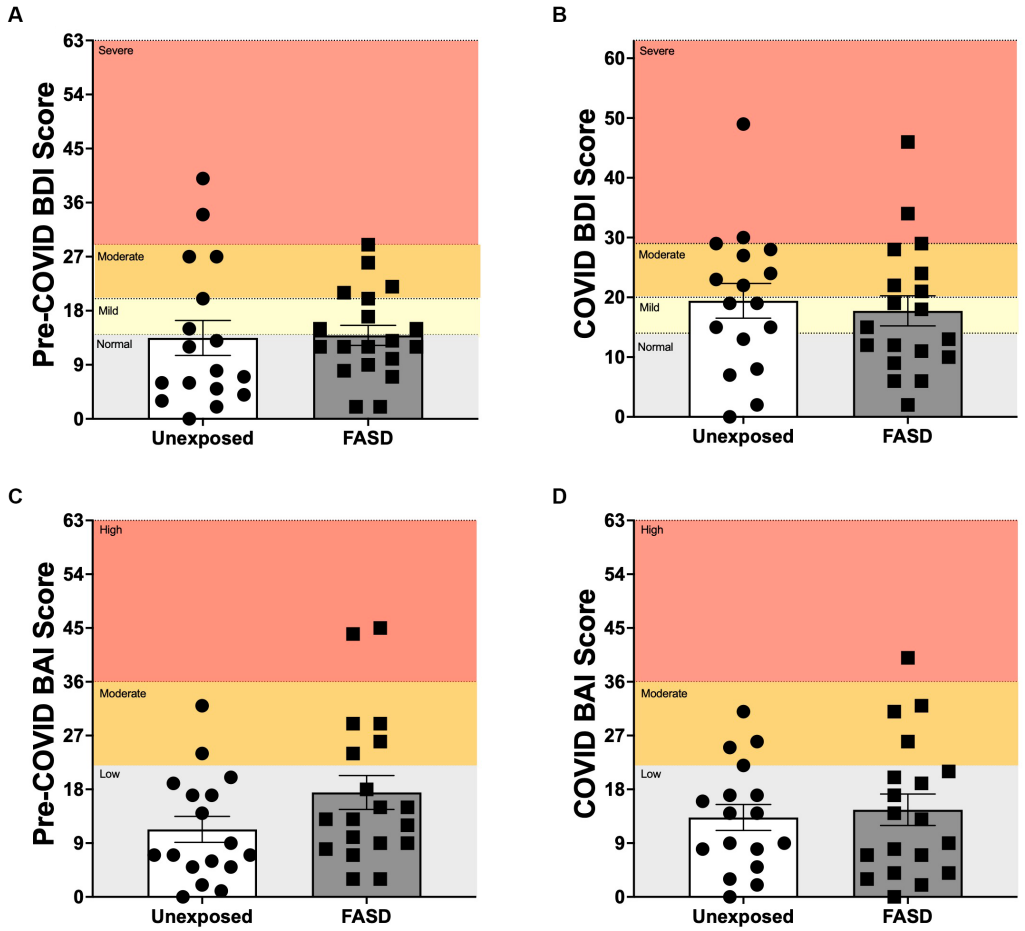


FIGURE 2
Beck Depression Inventory 2 (BDI), and Beck Anxiety Inventory (BAI) scores pre-COVID (baseline) and during the COVID-19 pandemic. **(A,B)** Normal: normal mood; Mild: mild mood disturbance; Moderate: moderate depression; Severe: severe depression. **(C,D)** Low: low anxiety; Moderate: moderate anxiety; High: high anxiety. There were no group differences between adults with FASD and unexposed adults on the BDI or BAI at baseline or during the pandemic, with the exception of a trend for higher pre-pandemic BAI in adults with FASD, compared to unexposed controls [$F(1, 32)=3.388$, $p=0.075$].

not in adults with FASD. Similarly, a positive association was also identified between baseline neutrophil counts and pandemic BDI/BAI scores again in unexposed adults only [ΔR^2: 0.268, β: 0.548, $F(1, 12)=4.49$, $p=0.05$]. No associations between lymphocyte and monocyte counts and baseline or pandemic BDI/BAI scores were identified.

To further explore the link between immune function and mental health, hierarchical regression analyses were performed between baseline cytokine levels and BDI/BAI scores (baseline and pandemic) (Table 3). Interestingly, baseline cytokine levels failed to predict current (pre-pandemic) BDI/BAI scores. However, associations between baseline cytokines and pandemic BDI/BAI scores were identified. In unexposed controls, there was a negative association between pre-pandemic IFN-ɣ and pandemic BDI/BAI scores [ΔR^2: 0.411, β: −0.664, $F(1, 12)=8.59$, $p=0.013$]. In adults with FASD, there were positive associations between baseline levels of IL-12p70 [ΔR^2: 0.231, β: 0.471, $F(1, 15)=4.53$, $p=0.050$], IL-8 [ΔR^2: 0.368, β: 0.738, $F(1, 15)=8.76$, $p=0.010$], soluble intercellular adhesion molecule-1 (sICAM-1) [ΔR^2: 0.273, β: 0.781, $F(1, 15)=5.65$, $p=0.031$], and soluble vascular cell adhesion molecule-1 (sVCAM-1) [ΔR^2: 0.235, β: 0.587, $F(1, 15)=4.62$, $p=0.048$] and pandemic BDI/BAI scores (see Supplementary Tables 4A,B for non-significant results).

4. Discussion

The goal of the current study was to examine the impact of the COVID-19 pandemic on mental health in adults with FASD and to probe for inflammation-to-mood associations. Overall, while there were no differences between adults with FASD and unexposed controls on COVID-19 assessments, lower SES was predictive of higher coronavirus anxiety scores on the CAS in the overall study sample. Perhaps surprisingly, there were no differences in depression and anxiety measures at baseline or during the pandemic between adults with FASD and unexposed controls. However, for unexposed controls but *not* adults with FASD, we identified a positive association between baseline neutrophil counts and both baseline and pandemic mental health scores. Moreover, we found differential associations between baseline cytokines and mental health scores during the pandemic in unexposed controls versus adults with FASD. Specifically,

TABLE 3 Summary of hierarchical regression analyses between pre-pandemic cytokine levels and pandemic BDI/BAI scores.

	IFN-ɣ	IL-12p70	IL-8	sICAM-1	sVCAM-1
Unexposed control (n=17)					
ΔR^2	0.411	n.s	n.s	n.s	n.s
β	−0.664				
F	8.59				
p	0.013				
FASD (n=19)					
ΔR^2	n.s	0.231	0.368	0.273	0.235
β		0.471	0.738	0.781	0.587
F		4.53	8.76	5.65	4.62
p		0.050	0.010	0.031	0.048

Hierarchical regression analyses were performed between baseline cytokine levels and mental health scores (combined Beck Depression Inventory [BDI] and Beck Anxiety Inventory [BAI] score) during the pandemic. For unexposed controls, there was a negative association between pre-pandemic IFN-ɣ and pandemic BDI/BAI scores. For adults with FASD, there were positive associations between baseline levels of interleukin (IL)-12p70, IL-8, soluble intercellular adhesion molecule-1 (sICAM-1), and soluble vascular cell adhesion molecule-1 (sVCAM-1) and pandemic BDI/BAI scores. Unexposed control: df: 1, 12; FASD: df: 1, 15; n.s. non-significant.

a negative association between baseline IFN-ɣ and pandemic mental health scores was observed in controls while positive associations between baseline IL-12p70, IL-8, sICAM-1, and sVCAM-1 and pandemic mental health scores were identified in adults with FASD. Taken together, these data highlight that while mental health scores were not different between adults with FASD and unexposed adults during the pandemic, differential inflammation-to-mood relationships were identified, suggesting a possible role for altered immune function in these differential mental health outcomes. Future work is needed to explore the long-terms impacts of the COVID-19 pandemic on these associations.

The observed link between SES and anxiety around coronavirus—specifically lower SES being predictive of higher coronavirus anxiety scores on the CAS—is in line with other studies in which financial difficulties, unemployment, and lower levels of education were correlated with poor mental health during the pandemic (Smith et al., 2020; Wang et al., 2020; Nagasu et al., 2021). Importantly, while we replicated these previous findings, demonstrating a relationship between SES and anxiety around coronavirus in our full sample, adults with FASD make up a higher proportion of those with low SES and thus may be at disproportionately high risk of anxiety related to coronavirus. Similar findings have been reported in other NDDs where, for example, individuals with ASD may experience a higher rate of confusion around the pandemic, which in turn impacts their mental health (Oomen et al., 2021). While not explicitly examined, many of our participants with FASD reported confusion around public health measures and repeated misinformation related to coronavirus spread and symptoms of illness. Moving forward, it will be important that messaging around societal crises takes into account the specific needs of individuals with NDDs, including FASD.

The current study did not identify differences in depression or anxiety scores between adults with FASD and unexposed controls, with the exception of a trend for higher anxiety scores at baseline in adults with FASD. This was perhaps surprising as adults with FASD were predicted to be at higher risk of mental health problems during the pandemic as a result of risk factors including lower SES (May and Gossage, 2011; Kwong et al., 2021) and higher rates of existing mental health problems (Famy et al., 1998; Pei et al., 2011; Neelam et al., 2021). However, it has been recognized that the pandemic afforded some positive effects for individuals with NDDs, including reduced sensory and social overloading (Oomen et al., 2021). As FASD is associated with impaired social abilities (Thomas et al., 1998; Tsang et al., 2016), it stands to reason that the reduction in social demands during the pandemic could have had some beneficial impact for adults with FASD. Clearly, however, the pandemic also impacted the availability of social supports and programming that many adults with FASD rely on, which underscores the need for future work to examine the long-term impacts of the pandemic on mental health in this population, as well as underlying factors contributing to these impacts.

The association between immune function and mental health has been well established (Raison et al., 2006) such that at the extreme end, major depressive disorder (MDD) is associated with a proinflammatory bias and impaired adaptive immune functioning (Irwin et al., 1990; Leday et al., 2018; Beurel et al., 2020). And neutrophils, being the most abundant leukocyte and important cytokine secretors, are well-positioned to modulate the inflammation-to-mood relationship. Thus, the identification of a positive association between baseline neutrophil counts and mental health scores (baseline and pandemic) was expected. Additionally, previous work has shown positive correlations between depression scores and neutrophil counts during the pandemic (Li et al., 2021). However, in the current study, the association between neutrophils and mental health scores was only detected in unexposed controls. By contrast, the lack of a relationship between mental health status and neutrophil counts in adults with FASD may represent altered immune-to-brain communication in these adults, or differential immune cell and/or cytokine responses driving inflammation-to-mood associations.

The current study also identified a link between inflammatory mediators and mood in individuals with FASD, consisting of positive associations between baseline IL-12, IL-8, sICAM-1, and sVCAM-1 and pandemic mental health scores. IL-12 in particular, has been strongly linked to depression in the literature. In a meta-analysis involving 82 studies, IL-12 was shown to be higher in individuals with MDD (Kohler et al., 2018). IL-8, which can have both pro- and anti-inflammatory functions, has been less consistently identified in individuals with mood disorders (Kohler et al., 2018); however, elevated IL-8 has been suggested as an acute biomarker of a variety of psychiatric conditions (Gariup et al., 2015), as well as other chronic conditions (Shahzad et al., 2010). Moreover, cell adhesion molecules (CAMs), including ICAM-1 and VCAM-1, transmembrane adhesion proteins expressed predominantly in endothelial cells, are critical to the integrity of the blood brain barrier, with dysregulation linked to immune-mediated trafficking to the central nervous system and neuroinflammation (Muller et al., 1999; Sheikh et al., 2023). Soluble isoforms (e.g., sICAM-1, sVCAM-1) reflect an indirect plasma measure, with increases in sICAM-1 shown in conditions including depression and dementia, as well as aging [reviewed in Muller (2019)] and increases in sVCAM-1 identified in inflammatory disorders (Park and Jeen, 2018). Thus, in the current study, higher levels of sICAM-1 and sVCAM-1 may be contributing to neuroinflammatory processes in individuals with FASD and subsequently, driving increasing scores on mental health assessments. By contrast only a single association between baseline cytokines and mental health scores was identified in unexposed

controls – a negative association between baseline IFN-ɣ and pandemic mental health scores. It is possible that the stress of the pandemic, acting on a dysregulated immune system in adults with FASD, may have had a bigger impact on the inflammatory environment and subsequently mood, than it did in unexposed controls.

Finally, it is important to consider possible limitations of the current study. First, re-examining mental health in a vulnerable population during a global pandemic was challenging and it is possible that the study sample reflected some degree of selection bias. For example, it stands to reason that the study sample could have been biased towards more resilient individuals, potentially explaining the lack of a detectable impact of the pandemic on mental health outcomes. A comparison of pre-pandemic mental health scores between current study participants and the full cohort, however, showed no differences, suggesting that at least with regards to mental health, the current cohort was representative of the overall sample. However, it is possible that despite no baseline differences in mental health scores, individuals who did not participate in the current study could have been experiencing more life difficulties/stressors during the pandemic. To this end, it was more difficult to re-recruit adults with FASD from our overall study sample, as compared to controls, resulting in the small sample size, which must be acknowledged. More research in this area, and research involving other populations of adults with FASD will be needed to confirm the generalizability of the current findings. Finally, it is important to consider the time frame in which this study was completed. Major closures and establishment of public health measures aimed at decreasing the spread of COVID-19 were implemented in Canada beginning in March 2020. This study began 10 months later and while this timing coincided with the biggest peak to that point in time in COVID-19 infections in BC, "pandemic fatigue," referring to waning of precautionary behaviors, was also emerging (Brankston et al., 2022), which may also have impacted mental health outcomes.

In conclusion, our findings are important as there has been minimal research examining the impact of the COVID-19 pandemic on individuals with FASD and, to our knowledge, this is the first study to investigate outcomes in adults with FASD. While it may be too soon to predict the impact this pandemic will have on long-term mental health, our research suggests that the pandemic differentially impacted inflammation-to-mood relationships between adults with FASD and unexposed controls and highlights the need for longitudinal research in this area.

Data availability statement

The raw data supporting the conclusions of this article will be made available by the authors, without undue reservation.

Ethics statement

The studies involving human participants were reviewed and approved by the University of British Columbia Children's and Women's Research Ethics Board. The patients/participants provided their written informed consent to participate in this study.

Author contributions

TSB contributed to the conception and design of the study and funding acquisition, performed the statistical analyses, and wrote the first draft of the manuscript. AC contributed to testing study participants, data management, and project administration. PJH contributed to testing study participants and assisted with the ethics submission. LE assisted with the ethics submission and data and study administration. CR contributed to the conception and design of the study, interpretation of the data, and funding acquisition. JW contributed to the conception and design of the study and funding acquisition. All authors contributed to manuscript revisions and approved the submitted version.

Funding

All or part of this work was done in conjunction with the Collaborative Initiative on Fetal Alcohol Spectrum Disorders (CIFASD), which is funded by grants from the National Institute on Alcohol Abuse and Alcoholism (NIAAA). Additional information about CIFASD can be found at www.cifasd.org. Funded by NIH/NIAAA U01 AA026101 to JW and NIH/NIAAA R01 AA022460 to JW, CR, and TSB.

Acknowledgments

We wish to acknowledge the members of the Weinberg lab who assisted with this study. We would also like to thank Dr. Timothy Kieffer for generously providing access to the QuickPlex and Travis Webber for his assistance. Finally, we would like to thank the individuals who generously participated in this study.

Conflict of interest

The authors declare that the research was conducted in the absence of any commercial or financial relationships that could be construed as a potential conflict of interest.

Publisher's note

All claims expressed in this article are solely those of the authors and do not necessarily represent those of their affiliated organizations, or those of the publisher, the editors and the reviewers. Any product that may be evaluated in this article, or claim that may be made by its manufacturer, is not guaranteed or endorsed by the publisher.

Supplementary material

The Supplementary material for this article can be found online at: https://www.frontiersin.org/articles/10.3389/fnins.2023.1214100/full#supplementary-material

References

Abel, E. L., and Hannigan, J. H. (1995). Maternal risk factors in fetal alcohol syndrome: provocative and permissive influences. *Neurotoxicol. Teratol.* 17, 445–462. doi: 10.1016/0892-0362(95)98055-6

Ahluwalia, B., Wesley, B., Adeyiga, O., Smith, D. M., Da-Silva, A., and Rajguru, S. (2000). Alcohol modulates cytokine secretion and synthesis in human fetus: an in vivo and in vitro study. *Alcohol* 21, 207–213. doi: 10.1016/S0741-8329(00)00076-8

Almeida, M., Shrestha, A. D., Stojanac, D., and Miller, L. J. (2020). The impact of the COVID-19 pandemic on women's mental health. *Arch. Womens Ment. Health* 23, 741–748. doi: 10.1007/s00737-020-01092-2

Anisman, H., Merali, Z., Poulter, M. O., and Hayley, S. (2005). Cytokines as a precipitant of depressive illness: animal and human studies. *Curr. Pharm. Des.* 11, 963–972. doi: 10.2174/1381612053381701

Beck, A. T., Epstein, N., Brown, G., and Steer, R. A. (1988). An inventory for measuring clinical anxiety: psychometric properties. *J. Consult. Clin. Psychol.* 56, 893–897. doi: 10.1037/0022-006X.56.6.893

Beck, A. T., Ward, C. H., Mendelson, M., Mock, J., and Erbaugh, J. (1961). An inventory for measuring depression. *Arch. Gen. Psychiatry* 4, 561–571. doi: 10.1001/archpsyc.1961.01710120031004

Beurel, E., Toups, M., and Nemeroff, C. B. (2020). The bidirectional relationship of depression and inflammation: double trouble. *Neuron* 107, 234–256. doi: 10.1016/j.neuron.2020.06.002

Bingol, N., Schuster, C., Fuchs, M., Iosub, S., Turner, G., Stone, R. K., et al. (1987). The influence of socioeconomic factors on the occurrence of fetal alcohol syndrome. *Adv. Alcohol Subst. Abuse* 6, 105–118. doi: 10.1300/J251v06n04_08

Bodnar, T. S., Raineki, C., Wertelecki, W., Yevtushok, L., Plotka, L., Granovska, I., et al. (2020). Immune network dysregulation associated with child neurodevelopmental delay: modulatory role of prenatal alcohol exposure. *J. Neuroinflammation* 17:39. doi: 10.1186/s12974-020-1717-8

Bodnar, T., and Weinberg, J. (2013). "Prenatal alcohol exposure: impact on neuroendocrine-neuroimmune networks" in *Neural-immune interactions in brain function and alcohol related disorders*. eds. C. Cui, L. Grandison and A. Noronha (New York: Springer), 312–362.

Brankston, G., Merkley, E., Loewen, P. J., Avery, B. P., Carson, C. A., Dougherty, B. P., et al. (2022). Pandemic fatigue or enduring precautionary behaviours? Canadians' long-term response to COVID-19 public health measures. *Prev. Med. Rep.* 30:101993. doi: 10.1016/j.pmedr.2022.101993

Coles, C. D., Grant, T. M., Kable, J. A., Stoner, S. A., and Perez, A.Collaborative Initiative on Fetal Alcohol Spectrum, D (2022). Prenatal alcohol exposure and mental health at midlife: a preliminary report on two longitudinal cohorts. *Alcohol. Clin. Exp. Res.* 46, 232–242. doi: 10.1111/acer.14761

Cook, J. L. (2021). Alcohol use during pregnancy and fetal alcohol spectrum disorder in Canada: who, what, where? *Health Promot. Chronic Dis. Prev. Can.* 41, 264–266. doi: 10.24095/hpcdp.41.9.03

Dunn, A. J., Swiergiel, A. H., and de Beaurepaire, R. (2005). Cytokines as mediators of depression: what can we learn from animal studies? *Neurosci. Biobehav. Rev.* 29, 891–909. doi: 10.1016/j.neubiorev.2005.03.023

Ehrler, M., Werninger, I., Schnider, B., Eichelberger, D. A., Naef, N., Disselhoff, V., et al. (2021). Impact of the COVID-19 pandemic on children with and without risk for neurodevelopmental impairments. *Acta Paediatr.* 110, 1281–1288. doi: 10.1111/apa.15775

Famy, C., Streissguth, A. P., and Unis, A. S. (1998). Mental illness in adults with fetal alcohol syndrome or fetal alcohol effects. *Am. J. Psychiatry* 155, 552–554. doi: 10.1176/ajp.155.4.552

Flannigan, K., Unsworth, K., and Harding, K. (2018). *The prevalence of fetal alcohol spectrum disorder*. Canada FASD Research Network. Available at: https://canfasd.ca/wp-content/uploads/publications/Prevalence-1-Issue-Paper-FINAL.pdf

Fydrich, T., Dowdall, D., and Chambless, D. L. (1992). Reliability and validity of the beck anxiety inventory. *J. Anxiety Disord.* 6, 55–61. doi: 10.1016/0887-6185(92)90026-4

Garcia-Batista, Z. E., Guerra-Pena, K., Cano-Vindel, A., Herrera-Martinez, S. X., and Medrano, L. A. (2018). Validity and reliability of the Beck Depression Inventory (BDI-II) in general and hospital population of Dominican Republic. *PLoS One* 13:e0199750. doi: 10.1371/journal.pone.0199750

Gariup, M., Gonzalez, A., Lazaro, L., Torres, F., Serra-Pages, C., and Morer, A. (2015). IL-8 and the innate immunity as biomarkers in acute child and adolescent psychopathology. *Psychoneuroendocrinology* 62, 233–242. doi: 10.1016/j.psyneuen.2015.08.017

Gauthier, T. W., Drews-Botsch, C., Falek, A., Coles, C., and Brown, L. A. (2005). Maternal alcohol abuse and neonatal infection. *Alcohol. Clin. Exp. Res.* 29, 1035–1043. doi: 10.1097/01.ALC.0000167956.28160.5E

Gilman, S. E., Hornig, M., Ghassabian, A., Hahn, J., Cherkerzian, S., Albert, P. S., et al. (2017). Socioeconomic disadvantage, gestational immune activity, and neurodevelopment in early childhood. *Proc. Natl. Acad. Sci. U. S. A.* 114, 6728–6733. doi: 10.1073/pnas.1617698114

Gottesfeld, Z., and Abel, E. L. (1991). Maternal and paternal alcohol use: effects on the immune system of the offspring. *Life Sci.* 48, 1–8. doi: 10.1016/0024-3205(91)90419-C

Guller, B., Yaylaci, F., and Eyuboglu, D. (2022). Those in the shadow of the pandemic: impacts of the COVID-19 outbreak on the mental health of children with neurodevelopmental disorders and their parents. *Int. J. Dev. Disabil.* 68, 943–955. doi: 10.1080/20473869.2021.1930827

Haleem, A., Javaid, M., and Vaishya, R. (2020). Effects of COVID-19 pandemic in daily life. *Curr. Med. Res. Pract.* 10, 78–79. doi: 10.1016/j.cmrp.2020.03.011

Hawes, M. T., Szenczy, A. K., Klein, D. N., Hajcak, G., and Nelson, B. D. (2022). Increases in depression and anxiety symptoms in adolescents and young adults during the COVID-19 pandemic. *Psychol. Med.* 52, 3222–3230. doi: 10.1017/S0033291720005358

Irwin, M., Patterson, T., Smith, T. L., Caldwell, C., Brown, S. A., Gillin, J. C., et al. (1990). Reduction of immune function in life stress and depression. *Biol. Psychiatry* 27, 22–30. doi: 10.1016/0006-3223(90)90016-U

Johnson, S., Knight, R., Marmer, D. J., and Steele, R. W. (1981). Immune deficiency in fetal alcohol syndrome. *Pediatr. Res.* 15, 908–911. doi: 10.1203/00006450-198106000-00005

Kohler, C. A., Freitas, T. H., Maes, M., de Andrade, N. Q., Liu, C. S., Fernandes, B. S., et al. (2017). Peripheral cytokine and chemokine alterations in depression: a meta-analysis of 82 studies. *Acta Psychiatr. Scand.* 135, 373–387. doi: 10.1111/acps.12698

Kohler, C. A., Freitas, T. H., Stubbs, B., Maes, M., Solmi, M., Veronese, N., et al. (2018). Peripheral alterations in cytokine and chemokine levels after antidepressant drug treatment for major depressive disorder: systematic review and Meta-analysis. *Mol. Neurobiol.* 55, 4195–4206. doi: 10.1007/s12035-017-0632-1

Kwong, A. S. F., Pearson, R. M., Adams, M. J., Northstone, K., Tilling, K., Smith, D., et al. (2021). Mental health before and during the COVID-19 pandemic in two longitudinal UK population cohorts. *Br. J. Psychiatry* 218, 334–343. doi: 10.1192/bjp.2020.242

Leday, G. G. R., Vertes, P. E., Richardson, S., Greene, J. R., Regan, T., Khan, S., et al. (2018). Replicable and coupled changes in innate and adaptive immune gene expression in two case-control studies of blood microarrays in major depressive disorder. *Biol. Psychiatry* 83, 70–80. doi: 10.1016/j.biopsych.2017.01.021

Lee, S. A. (2020). Coronavirus anxiety scale: a brief mental health screener for COVID-19 related anxiety. *Death Stud.* 44, 393–401. doi: 10.1080/07481187.2020.1748481

Lee, S. A., Jobe, M. C., Mathis, A. A., and Gibbons, J. A. (2020). Incremental validity of coronaphobia: coronavirus anxiety explains depression, generalized anxiety, and death anxiety. *J. Anxiety Disord.* 74:102268. doi: 10.1016/j.janxdis.2020.102268

Leighton, S. P., Nerurkar, L., Krishnadas, R., Johnman, C., Graham, G. J., and Cavanagh, J. (2018). Chemokines in depression in health and in inflammatory illness: a systematic review and meta-analysis. *Mol. Psychiatry* 23, 48–58. doi: 10.1038/mp.2017.205

Li, X., Cai, Q., Jia, Z., Zhou, Y., Liu, L., Zhou, Y., et al. (2021). The correlation between mental health status, sleep quality, and inflammatory markers, virus negative conversion time among patients confirmed with 2019-nCoV during the COVID-19 outbreak in China: an observational study. *Medicine (Baltimore)* 100:e26520. doi: 10.1097/MD.0000000000026520

Liang, T. J., and Ghany, M. G. (2013). Current and future therapies for hepatitis C virus infection. *N. Engl. J. Med.* 368, 1907–1917. doi: 10.1056/NEJMra1213651

Linneberg, A., Petersen, J., Gronbaek, M., and Benn, C. S. (2004). Alcohol during pregnancy and atopic dermatitis in the offspring. *Clin. Exp. Allergy* 34, 1678–1683. doi: 10.1111/j.1365-2222.2004.02101.x

Lussier, A. A., Bodnar, T. S., and Weinberg, J. (2021). Intersection of epigenetic and immune alterations: implications for fetal alcohol spectrum disorder and mental health. *Front. Neurosci.* 15:788630. doi: 10.3389/fnins.2021.788630

May, P. A., and Gossage, J. P. (2011). Maternal risk factors for fetal alcohol spectrum disorders: not as simple as it might seem. *Alcohol Res. Health* 34, 15–26.

May, P. A., Hasken, J. M., Hooper, S. R., Hedrick, D. M., Jackson-Newsom, J., Mullis, C. E., et al. (2021). Estimating the community prevalence, child traits, and maternal risk factors of fetal alcohol spectrum disorders (FASD) from a random sample of school children. *Drug Alcohol Depend.* 227:108918. doi: 10.1016/j.drugalcdep.2021.108918

McMahan, R. H., Anton, P., Coleman, L. G. Jr., Cresci, G. A. M., Crews, F. T., Crotty, K. M., et al. (2023). Alcohol and immunology: mechanisms of multi-organ damage. Summary of the 2022 alcohol and immunology research interest group (AIRIG) meeting. *Alcohol* 110, 57–63. doi: 10.1016/j.alcohol.2023.04.002

Muller, N. (2019). The role of intercellular adhesion Molecule-1 in the pathogenesis of psychiatric disorders. *Front. Pharmacol.* 10:1251. doi: 10.3389/fphar.2019.01251

Muller, N., Riedel, M., Hadjamu, M., Schwarz, M. J., Ackenheil, M., and Gruber, R. (1999). Increase in expression of adhesion molecule receptors on T helper cells during antipsychotic treatment and relationship to blood-brain barrier permeability in schizophrenia. *Am. J. Psychiatry* 156, 634–636. doi: 10.1176/ajp.156.4.634

Nagasu, M., Muto, K., and Yamamoto, I. (2021). Impacts of anxiety and socioeconomic factors on mental health in the early phases of the COVID-19 pandemic in the general population in Japan: a web-based survey. *PLoS One* 16:e0247705. doi: 10.1371/journal.pone.0247705

Neelam, K., Duddu, V., Anyim, N., Neelam, J., and Lewis, S. (2021). Pandemics and pre-existing mental illness: a systematic review and meta-analysis. *Brain Behav. Immun. Health* 10:100177. doi: 10.1016/j.bbih.2020.100177

Okruszek, L., Aniszewska-Stanczuk, A., Piejka, A., Wisniewska, M., and Zurek, K. (2020). Safe but lonely? Loneliness, anxiety, and depression symptoms and COVID-19. *Front. Psychol.* 11:579181. doi: 10.3389/fpsyg.2020.579181

Oleson, D. R., Magee, R. M., Donahoe, R. M., Falek, A., and Coles, C. D. (1998). Immunity and prenatal alcohol exposure. A pilot study in human adolescents. *Adv. Exp. Med. Biol.* 437, 255–264. doi: 10.1007/978-1-4615-5347-2_28

Oomen, D., Nijhof, A. D., and Wiersema, J. R. (2021). The psychological impact of the COVID-19 pandemic on adults with autism: a survey study across three countries. *Mol. Autism.* 12:21. doi: 10.1186/s13229-021-00424-y

Osman, A., Kopper, B. A., Barrios, F., Gutierrez, P. M., and Bagge, C. L. (2004). Reliability and validity of the Beck Depression Inventory--II with adolescent psychiatric inpatients. *Psychol. Assess.* 16, 120–132. doi: 10.1037/1040-3590.16.2.120

Park, S. C., and Jeen, Y. T. (2018). Anti-integrin therapy for inflammatory bowel disease. *World J. Gastroenterol.* 24, 1868–1880. doi: 10.3748/wjg.v24.i17.1868

Pei, J., Denys, K., Hughes, J., and Rasmussen, C. (2011). Mental health issues in fetal alcohol spectrum disorder. *J. Ment. Health* 20, 438–448. doi: 10.3109/09638237.2011.577113

Raineki, C., Bodnar, T. S., Holman, P. J., and Weinberg, J. (2021). From animal models to humans: role of early-life adversity on emotional regulation and immune function following prenatal alcohol exposure. *ACER* 45, 64–65A.

Raison, C. L., Capuron, L., and Miller, A. H. (2006). Cytokines sing the blues: inflammation and the pathogenesis of depression. *Trends Immunol.* 27, 24–31. doi: 10.1016/j.it.2005.11.006

Reichenberg, A., Yirmiya, R., Schuld, A., Kraus, T., Haack, M., Morag, A., et al. (2001). Cytokine-associated emotional and cognitive disturbances in humans. *Arch. Gen. Psychiatry* 58, 445–452. doi: 10.1001/archpsyc.58.5.445

Reid, N., Moritz, K. M., and Akison, L. K. (2019). Adverse health outcomes associated with fetal alcohol exposure: a systematic review focused on immune-related outcomes. *Pediatr. Allergy Immunol.* 30, 698–707. doi: 10.1111/pai.13099

Rosenblat, J. D., Cha, D. S., Mansur, R. B., and McIntyre, R. S. (2014). Inflamed moods: a review of the interactions between inflammation and mood disorders. *Prog. Neuro-Psychopharmacol. Biol. Psychiatry* 53, 23–34. doi: 10.1016/j.pnpbp.2014.01.013

Schmidt, F. M., Lichtblau, N., Minkwitz, J., Chittka, T., Thormann, J., Kirkby, K. C., et al. (2014). Cytokine levels in depressed and non-depressed subjects, and masking effects of obesity. *J. Psychiatr. Res.* 55, 29–34. doi: 10.1016/j.jpsychires.2014.04.021

Shahzad, A., Knapp, M., Lang, I., and Kohler, G. (2010). Interleukin 8 (IL-8) – a universal biomarker? *Int. Arch. Med.* 3:11. doi: 10.1186/1755-7682-3-11

Shakeshaft, A., Blakey, R., Kwong, A. S. F., Riglin, L., Davey Smith, G., Stergiakouli, E., et al. (2023). Mental-health before and during the COVID-19 pandemic in adults with neurodevelopmental disorders. *J. Psychiatr. Res.* 159, 230–239. doi: 10.1016/j.jpsychires.2023.01.029

Sheikh, M. A., O'Connell, K. S., Lekva, T., Szabo, A., Akkouh, I. A., Osete, J. R., et al. (2023). Systemic cell adhesion molecules in severe mental illness: potential role of intercellular CAM-1 in linking peripheral and neuroinflammation. *Biol. Psychiatry* 93, 187–196. doi: 10.1016/j.biopsych.2022.06.029

Smith, L., Jacob, L., Yakkundi, A., McDermott, D., Armstrong, N. C., Barnett, Y., et al. (2020). Correlates of symptoms of anxiety and depression and mental wellbeing associated with COVID-19: a cross-sectional study of UK-based respondents. *Psychiatry Res.* 291:113138. doi: 10.1016/j.psychres.2020.113138

Statistics Canada (2023). *Preliminary dataset on confirmed cases of COVID-19, Public Health Agency of Canada, 2020–2023*. Canada, P.H.A.o. (Ed.). Statistics Canada. Available at: https://www150.statcan.gc.ca/n1/pub/13-26-0003/132600032020001-eng.htm

Steptoe, A., Hamer, M., and Chida, Y. (2007). The effects of acute psychological stress on circulating inflammatory factors in humans: a review and meta-analysis. *Brain Behav. Immun.* 21, 901–912. doi: 10.1016/j.bbi.2007.03.011

Thomas, S. E., Kelly, S. J., Mattson, S. N., and Riley, E. P. (1998). Comparison of social abilities of children with fetal alcohol syndrome to those of children with similar IQ scores and normal controls. *Alcohol. Clin. Exp. Res.* 22, 528–533. doi: 10.1111/j.1530-0277.1998.tb03684.x

Toledano-Toledano, F., and Contreras-Valdez, J. A. (2018). Validity and reliability of the Beck Depression Inventory II (BDI-II) in family caregivers of children with chronic diseases. *PLoS One* 13:e0206917. doi: 10.1371/journal.pone.0206917

Tsang, T. W., Lucas, B. R., Carmichael Olson, H., Pinto, R. Z., and Elliott, E. J. (2016). Prenatal alcohol exposure, FASD, and child behavior: a meta-analysis. *Pediatrics* 137:e20152542. doi: 10.1542/peds.2015-2542

Tukey, J. (1962). The future of data analysis. *Ann. Math. Stat.* 33, 1–67. doi: 10.1214/aoms/1177704711

Wada, K., Konishi, K., Tamura, T., Shiraki, M., Iwasa, S., and Nagata, C. (2016). Alcohol intake during pregnancy and offspring's atopic eczema risk. *Alcohol. Clin. Exp. Res.* 40, 1037–1043. doi: 10.1111/acer.13048

Wang, Y. P., and Gorenstein, C. (2013). Psychometric properties of the Beck Depression Inventory-II: a comprehensive review. *Braz. J. Psychiatry* 35, 416–431. doi: 10.1590/1516-4446-2012-1048

Wang, Y., Kala, M. P., and Jafar, T. H. (2020). Factors associated with psychological distress during the coronavirus disease 2019 (COVID-19) pandemic on the predominantly general population: a systematic review and meta-analysis. *PLoS One* 15:e0244630. doi: 10.1371/journal.pone.0244630

Wettstein, M., Nowossadeck, S., and Vogel, C. (2022). Well-being trajectories of middle-aged and older adults and the corona pandemic: no "COVID-19 effect" on life satisfaction, but increase in depressive symptoms. *Psychol. Aging* 37, 175–189. doi: 10.1037/pag0000664

frontiers | Frontiers in Public Health

TYPE Brief Research Report
PUBLISHED 24 July 2023
DOI 10.3389/fpubh.2023.1195484

Check for updates

OPEN ACCESS

EDITED BY
Brian A. Coffman,
University of Pittsburgh, United States

REVIEWED BY
Mauro Ceccanti,
Sapienza University of Rome, Italy
Jia Yan,
National Institutes of Health (NIH), United States

*CORRESPONDENCE
Kirsten R. Panton
✉ kirsten.panton@uwa.edu.au

RECEIVED 29 March 2023
ACCEPTED 05 July 2023
PUBLISHED 24 July 2023

CITATION
Panton KR, Fitzpatrick JP and Pestell CF (2023) An evaluation of a multi-site fetal alcohol spectrum disorder models of care project. *Front. Public Health* 11:1195484. doi: 10.3389/fpubh.2023.1195484

COPYRIGHT
© 2023 Panton, Fitzpatrick and Pestell. This is an open-access article distributed under the terms of the Creative Commons Attribution License (CC BY). The use, distribution or reproduction in other forums is permitted, provided the original author(s) and the copyright owner(s) are credited and that the original publication in this journal is cited, in accordance with accepted academic practice. No use, distribution or reproduction is permitted which does not comply with these terms.

An evaluation of a multi-site fetal alcohol spectrum disorder models of care project

Kirsten R. Panton[1]*, James P. Fitzpatrick[1,2] and Carmela F. Pestell[1]

[1]School of Psychological Science, The University of Western Australia, Perth, WA, Australia, [2]Patches Assessment Services, Subiaco, WA, Australia

Fetal alcohol spectrum disorder (FASD) continues to be underdiagnosed in Australia, partly due to the lack of trained clinicians and diagnostic services. This project aimed to help increase FASD knowledge and diagnostic capacity across Australia. Six sites across Australia formed part of a national consortium, delivering training clinics, diagnostic clinics and community education sessions. The number of FASD diagnoses significantly increased across the project. Additionally, the number of community education sessions steadily increased across the project, with largely positive feedback. Participants attending the training clinics demonstrated increased knowledge of and confidence in FASD diagnosis. This evaluation showcases the benefits of a coordinated approach to prevention, assessment, diagnosis and training in FASD.

KEYWORDS

fetal alcohol spectrum disorder, prenatal alcohol exposure, FASD, training, diagnosis

1. Introduction

Fetal alcohol spectrum disorder (FASD) is a diagnostic term that captures the neurodevelopmental and physical impairments resulting from alcohol exposure *in utero* (1). FASD continues to be underrecognized and underdiagnosed (2, 3), with general prevalence estimates between 0.01 and 0.68 per 1,000 live births in Australia (4, 5). However, the current prevalence rates are considered to be underestimates, as we have largely relied on passive surveillance systems to monitor FASD (4). Several studies have also attempted to estimate the prevalence of FASD in specific populations in Australia through active case ascertainment, with higher prevalence rates found in these sub-populations (6, 7).

The Australian FASD diagnostic guide was released in 2016; however, we have long since known about the potential harm of alcohol on the developing fetus (8–10). It has taken time for FASD to gain recognition in Australia, though we have seen positive movement toward change, with the Department of Health releasing the 2018–2028 National FASD Strategic Action Plan (11). The Action Plan (11) advocates for activities centered around FASD prevention, screening and diagnosis, and support and management.

FASD tends to be recognized as a diagnostic term, though individuals working closely with FASD (including health professionals) are often less familiar with the common behaviors associated with FASD (12–15). Similarly, individuals in the general public are likely to have heard of FASD but are less clear on key characteristics (16, 17). Even though it is promising that FASD continues to grow in recognition, in order to prevent, diagnose and manage FASD, it is important that both the general public and health professionals have a better understanding of FASD.

There continue to be significant barriers to obtaining a FASD diagnosis, and through this project, we aimed to reduce some of the existing service-level barriers (18, 19). One of the major issues is a lack of appropriately trained clinicians (20, 21). Clinicians are also fearful to ask about alcohol use during pregnancy due to concerns around stigma and the emotional burden it may bring for the parent or caregiver [e.g., blame, guilt, anger (18, 22)]. However, without a diagnosis, individuals will have difficulty accessing the appropriate supports to best meet their needs (23).

The current study examines the success of a national FASD prevention, assessment and diagnosis effort from 6 sites across Australia. Each site conducted community education sessions (CES) and FASD training clinics for health professionals to build relevant FASD knowledge. Additionally, each site assessed and diagnosed FASD within multidisciplinary (MDT) clinics. It was predicted that the number of FASD diagnoses would increase from the start (i.e., before these FASD clinics were established) to the end of the project. Similarly, the number of community education sessions and attendants was expected to increase as the consortium sites built their local FASD networks. Finally, it was predicted that individuals would see an increase in knowledge and diagnostic confidence following FASD-specific training.

2. Methods

2.1. Project design

This project had two broad aims of increasing diagnostic capacity and increasing FASD awareness, knowledge and advocacy through various activities. This paper evaluates the outcomes of the training and prevention activities and diagnostic service outcomes. The accompanying qualitative study describes the process of opening five new FASD MDT clinics and developing local models of care (24).

2.1.1. Sites

There were 6 sites involved from across the country, including Patches Assessment Services [Western Australia (WA) and Northern Territory (NT)], Central Australian Aboriginal Congress (CAAC; NT), Danila Dilba Health Service (DDHS; NT), Child Development Unit, Women's Children Hospital [CDU WCH; South Australia (SA)], Goulburn Valley Health Service [GVHS; Victoria (VIC)], and FASD Tasmania [Tasmania (TAS)]. The University of Western Australia Site Lead and Project Officer led the evaluation of the project (authors CP and KP respectively).

2.1.2. Diagnostic and training clinics

Diagnostic activity was tracked with the number of clients assessed, number of clients diagnosed with FASD and number of clients diagnosed with FASD that identified as Aboriginal and Torres Strait Islander. There was some discrepancy in the reporting of Aboriginal and Torres Strait Islander clients, with some sites reporting the total number assessed, and others reporting the total number diagnosed with FASD. Additionally, the number of clients assessed was a diluted metric, as some sites (e.g., CAAC) assessed a range of neurodevelopmental disorders (e.g., ADHD, ASD).

At each site, diagnostic training clinics were delivered to local clinicians to help upskill and build local diagnostic capacity. All clinicians within the project received direct training from experienced practitioners in FASD assessment and diagnosis, Dr. Pestell (clinical neuropsychologist), and Dr. Fitzpatrick (paediatrician). The training included structured training in-person across multiple days, covering all aspects of FASD assessment and diagnosis, namely: effects of prenatal alcohol exposure on the developing fetus, prevalence and patterns of FASD in various populations, medical aspects of assessment (diagnostic history, ascertaining PAE, growth assessment, facial feature assessment, physical assessment), and comprehensive training in the assessment of the ten brain domains within the framework of the Australian Guide to the Assessment and Diagnosis of FASD. Training often included the opportunity for direct observation of clinical assessment through regular training clinics, where trainees observed the testing and assessment, formulation and case conferencing, and report writing aspects of a comprehensive multidisciplinary FASD assessment. Training clinic activity was measured by the number of training clinics, number of clinic attendees and attendee profession.

2.1.3. Community education sessions

Each site was expected to deliver at least eight CES annually to help build FASD knowledge and awareness in local communities. CES activity was measured by the number of CES and number of CES attendees. The CES were primarily delivered by the Site Coordinator, which had varied clinical backgrounds, including nurse/midwife ($n = 3$), social worker ($n = 1$) and occupational therapist ($n = 1$). The CES broadly covered FASD prevalence, FASD diagnostic features, the importance of FASD diagnosis and FASD intervention.

2.2. Participants and measures

2.2.1. CES and training clinic feedback

A proportion of training clinic participants ($n = 273$) and CES participants ($n = 621$) provided formal feedback for the sessions. The CES and training clinic feedback forms were primarily distributed in the early stages of the project and prior to the COVID-19 pandemic. Although participants provided some qualitative feedback which was used to improve the training clinics, only quantitative feedback was approved to be used for research purposes. The four questions were: (1) "What is your overall assessment of the session"?; (2) "Were the learning objectives clearly stated"?; (3) "Did the knowledge and information gained from participation at this session meet your expectations?"; and (4) "Will the information covered be useful/applicable in your future clinical practice"?. Questions were rated from 1 (insufficient) to 5 (excellent). Questions 2–4 were coded as "definitely" = 5, "mostly" = 4, "somewhat" = 3 and "not at all" = 2. This coding was chosen to match most closely to the coding in question 1. The training clinics were mostly attended by pediatricians ($n = 72$), clinical neuropsychologists or psychologists ($n = 69$), speech pathologists ($n = 31$) and nurses ($n = 29$). Several clinics also hosted students from psychology ($n = 16$) and medical ($n = 13$) disciplines. In comparison, CE sessions were mostly attended by community workers, including education/childcare workers ($n = 81$), nurses/midwives ($n = 74$), social workers ($n = 60$) and speech pathologists ($n = 40$).

2.2.2. FASD confidence and knowledge survey

For a small proportion of training clinic participants ($n = 21$), a pre-and post-knowledge survey was administered, which included a more qualitative and quantitative appraisal of their FASD knowledge. The first portion of the survey asked participants to rate their confidence in FASD knowledge (e.g., "I have a good understanding of the cognitive features of FASD") on a five-point Likert scale ("strongly agree" to "strongly disagree"). The second part of the survey tested participants' specific knowledge of FASD with forced multiple choice (e.g., "The three sentinel facial features are"), multiple answer [selecting all that apply, e.g., "According to Australian diagnostic guidelines for FASD, which of the following are considered evidence of severe impairment in affect regulation? (select all that apply)"] and true or false ("There is no known safe level of alcohol consumption during pregnancy") questions. For the training clinic, there were 15 confidence and 10 knowledge questions (see Appendix 1). The questions were identical from pre-training/course to post-training/course. The training course participants completed the questionnaire directly before and after the training clinic.

The training clinic participants were primarily clinical neuropsychologists (including one registrar; $n = 18$), with other participants identifying as clinical psychologist ($n = 1$), postgraduate psychology student ($n = 1$) and undergraduate psychology student ($n = 1$), with an average of 14.05 years of clinical experience across participants (SD = 11.09 years). A proportion of the neuropsychologists also identified as clinical psychologists ($n = 5$) and forensic psychologist ($n = 1$).

2.3. Procedure

Ethics approval for this project was obtained through The University of Western Australia (RA/4/20/5792). Diagnostic services were launched at each site further details can be found in (24). Each site was asked to distribute feedback surveys at the end of each training and CES. Each site was required to report on its activity quarterly from August 2017 to August 2020. The lead researcher entered the relevant data into a master spreadsheet, tracking activity for each site over the government reporting periods for the project (6 monthly).

2.4. Data analysis

2.4.1. Diagnostic clinic, training clinic and CES

The diagnostic clinic, training clinic, and CES data were organized by six 6 monthly periods for each site. Due to the inconsistency in the reporting of training clinics by each site, it was difficult to meaningfully compare this data across the project, and as such, no formal statistical analyses were conducted on this data.

The diagnostic clinics and CES data were non-normally distributed and as such were analyzed using non-parametric tests. The Wilcoxon signed-rank test was chosen to compare data at two different time points (i.e., the start and end of the project). As most sites had to cancel or reschedule diagnostic clinics, training clinics and CES, the 6 months period pre-COVID was chosen as the final comparison point. As Patches was an established clinic, it was not included in the diagnostic activity data.

2.4.2. Feedback

The feedback data is presented as frequencies, as this data was only collected at one time point.

2.4.3. Knowledge surveys

The knowledge and confidence survey data were normally distributed, and were analyzed using paired samples *t*-tests, comparing FASD knowledge and confidence before the start of training and after training.

3. Results

3.1. Diagnostic activity

The number of individuals diagnosed with FASD was used as the metric for diagnostic success at each site. By rolling out FASD diagnostic clinics across the country, Wilcoxon signed rank tests revealed that diagnostic activity significantly increased from the first reporting period (July 2017–December 2017; $M = 0$, SD = 0) to the final (pre-COVID) reporting period (July 19–December 19; $M = 4.00$, SD = 4.58), $Z = -2.06$, $p = 0.04$ (Figure 1). Patches (WA & NT) was not included in this analysis, as Patches was already an established FASD diagnostic clinic.

3.2. CES

There was a steady increase in the delivery of community education across the project, however, there was a notable decrease in the delivery of CES in the final reporting periods (Figure 2). This is partly attributable to the global pandemic, which saw some sites cancelling sessions rather than opting for online alternatives. However, Wilcoxon signed ranks test revealed that the increase in CES sessions was not statistically significant when comparing the first reporting period ($M = 0.40$, SD = 0.89) compared to the final ($M = 6.20$, SD = 6.89) reporting period, $Z = -1.75$, $p = 0.08$.

3.3. CES and training clinic feedback

Feedback was obtained from a small portion of participants attending the community education and training clinics, as most sites stopped administering feedback forms after the first two reporting periods (Figure 3). Of these participants, most rated the sessions as "excellent" (4 or 5, 87.51%), meeting the learning objectives (68.91%), meeting expectations (70.73%) and applicable to clinical practice (83.03%). There was missing data on each of the items, as follows: "overall assessment of the workshop" = 5.53%, "learning objectives clearly stated" 26.03%, "workshop meets expectation" = 22.26% and "workshop is applicable to clinical practice" = 8.93%.

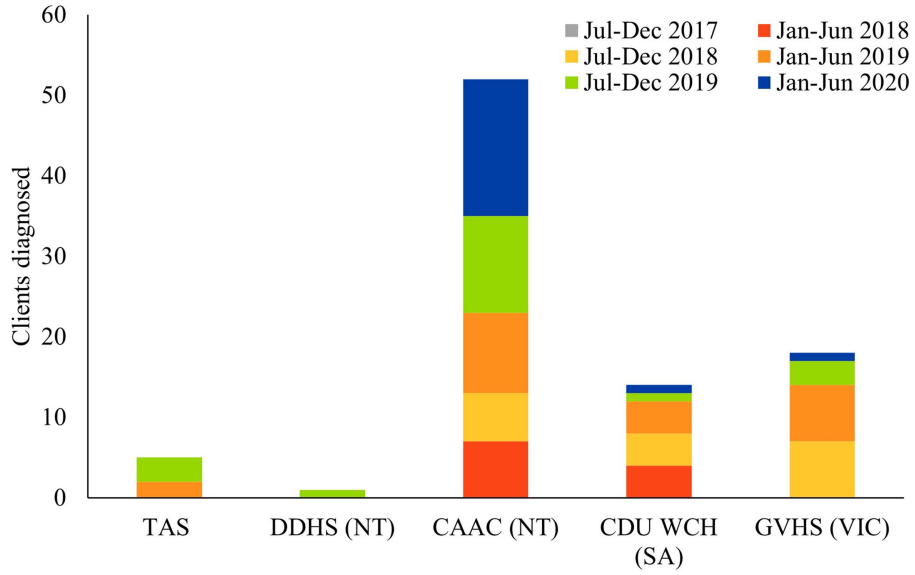


FIGURE 1
This figure represents the number of FASD diagnoses made across the 6 reporting periods for each state (excluding Patches WA & NT).

3.4. FASD confidence and knowledge surveys

A paired-sample *t*-test was used to compare pre and post training clinic knowledge of FASD, and found that FASD knowledge significantly increased from 50.00% pre-training to 78.5% post-training, $t\ (19) = -7.14$, $p < 0.001$. A separate paired samples *t*-test revealed an increase in participants confidence in FASD knowledge from pre-training ($M = 2.67$) to post-training ($M = 4.12$), $t\ (18) = -10.7$, $p < 0.001$ (Figure 4).

4. Discussion

This project aimed to increase diagnostic service capacity within Australia and improve FASD awareness among health professionals and local communities. Overall, there was a marked increase in FASD diagnostic activity, training activity and community education. Diagnostic activity significantly increased over the course of the project, with over 1,000 individuals assessed, and 425 individuals diagnosed with FASD. The number of FASD diagnoses made by this consortium comprised 81% of FASD cases reported the FASD Australian Registry (FASDAR), and 73% of cases recorded under the National Disability Insurance Scheme (NDIS) as a primary or secondary diagnosis during this reporting period (within the consortium states) (25, 26). Together this suggests that this consortium made a significant contribution to FASD diagnostic activity across Australia during this reporting period. It is acknowledged that the number of FASD cases reported to the FASDAR is likely to be an underestimate, as it requires manual entry by already overburdened clinicians (4), and only captures cases under 15 years old. As part of this consortium, the clinical teams were reminded quarterly to update their FASD cases to FASDAR, and explore methods for embedding this into their regular processes (24).

There was also an increase in community education activity (though not statistically significant). FASD knowledge was also disseminated to over 5,000 attendants across Australia (TAS, WA, NT, SA, VIC), to various community workers, such as education/childcare workers, nurses/midwives, social workers and speech pathologists. The FASD training clinics were successful in increasing FASD knowledge in the attendants, and over 400 clinicians received specialized FASD diagnostic training. Although pre-and post-knowledge surveys were not delivered to the community education session participants, the feedback indicated that participants found the session valuable. In the accompanying qualitative study examining the success of developing FASD models of care at each site (24), each site indicated that one of the key successes was increasing FASD knowledge and interest within their local community. Increasing local knowledge and interest around FASD has the potential to increase FASD prevention, as well as early diagnosis and intervention.

It has been recognized that health professionals play a vital role in FASD prevention efforts (12, 27). Through this study, we demonstrated that a short training session was adequate to significantly increase health professional's knowledge about FASD. Health professionals have the opportunity to be FASD advocates within the community, and as such, it will be important that they are aware of the lifelong impacts associated with alcohol use during pregnancy, and are consistent with messaging around the impact of prenatal alcohol exposure (16, 28, 29).

Due to the limited diagnostic capacity in Australia (21), it was a key aim of the current study to further train multidisciplinary clinicians to assess and diagnose FASD. It is recognized that although an MDT is the gold standard for assessment and diagnosis of FASD, a more flexible diagnostic approach may be required, which includes

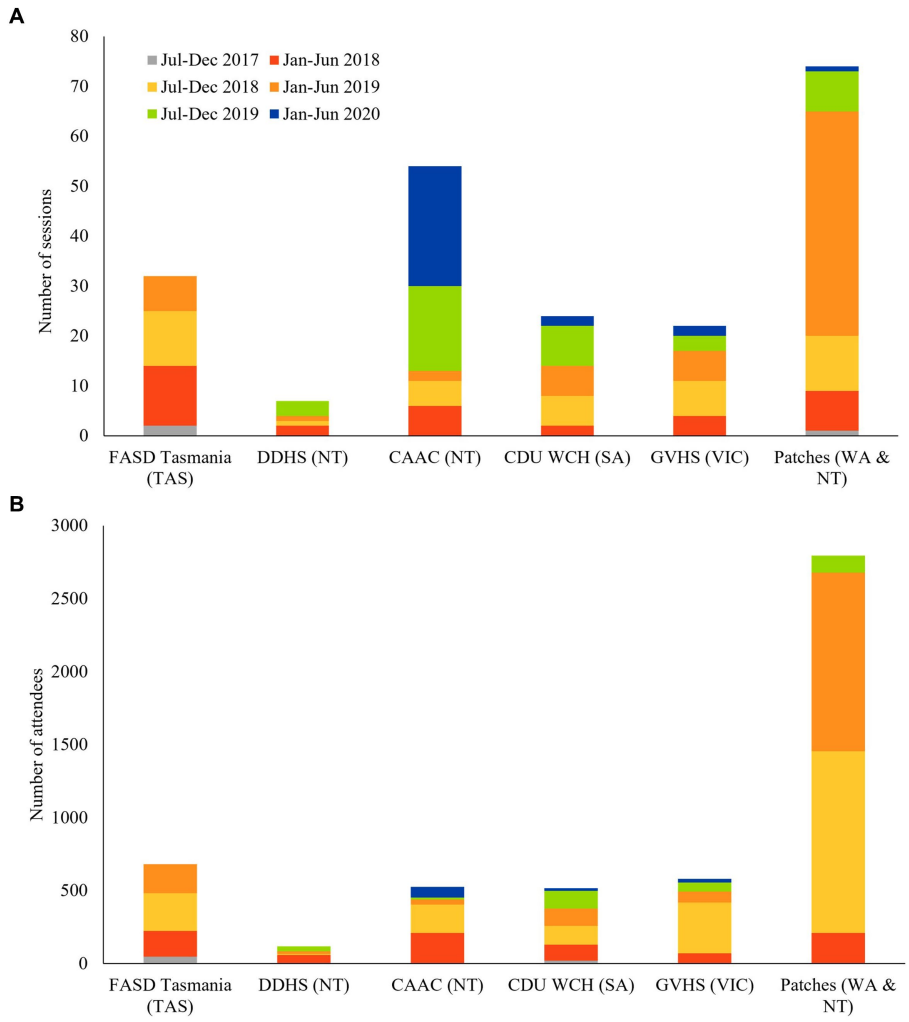


FIGURE 2
Number of CES **(A)** and attendees **(B)** per site.

further educating a wide range of clinicians, to help provide timely access to services (28). A FASD diagnosis provides an opportunity for individuals and their families to better understand their own strengths and weaknesses and gain access to further support and management for FASD (23, 30). Despite the stigma surrounding FASD as a diagnosis (31, 32), it is important for clinicians to be aware of the positive impact that a FASD diagnosis can have (30, 33). A recent systematic review of the qualitative evidence on FASD lived experience emphasized the impact of receiving a FASD diagnosis (30). The review also highlighted the difficulty in seeking recognition and validation for FASD and related concerns, reinforcing the need for health professionals to receive adequate FASD training.

4.1. Limitations and future research directions

This study evaluated the success of rolling out a FASD diagnostic service using a small sample, within a local context, limiting the generalizability of this study. Due to the small sample, we were limited in making inferences about the relative success of each site, though this is further explored in the accompanying qualitative paper (24). Although this study did not directly gather demographic information, most sites were predominantly youth-based. As such, further work is needed to develop appropriate models of care and diagnostic services for adults seeking FASD diagnostic clarity (34). This project focused on improving community knowledge and FASD diagnostic capacity across Australia, however, it is widely acknowledged that further efforts are needed to improve FASD therapy services (35). Future research should also explore the FASD training needs for clinicians, particularly since clinicians attitudes towards FASD (12) and lack of confidence 36 (which is still under review) 37 be a major barrier for diagnosis.

5. Conclusion

This paper demonstrated the positive impact of a coordinated approach to FASD prevention, assessment and diagnosis within

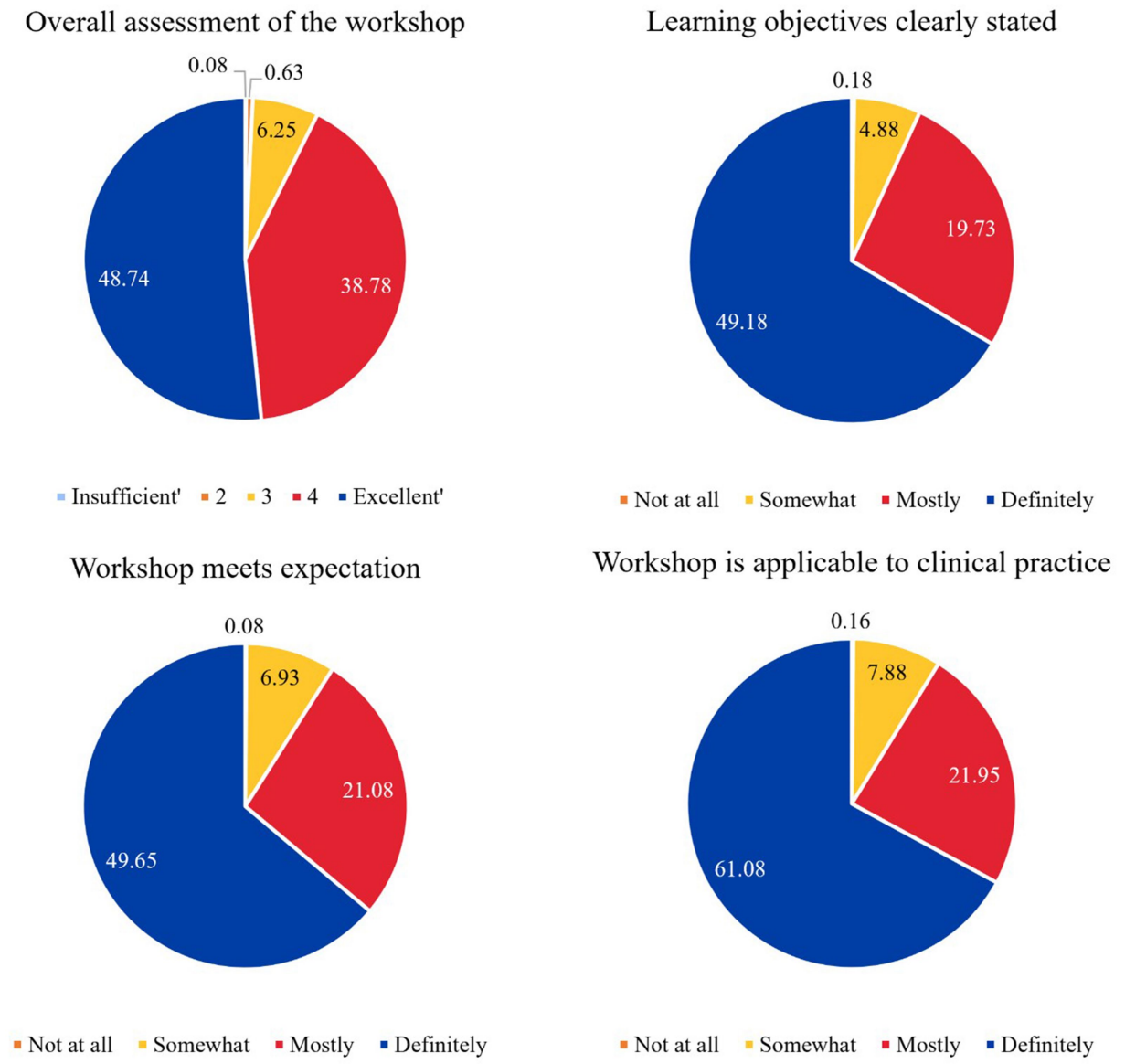


FIGURE 3
Participant feedback on training clinic and community education sessions.

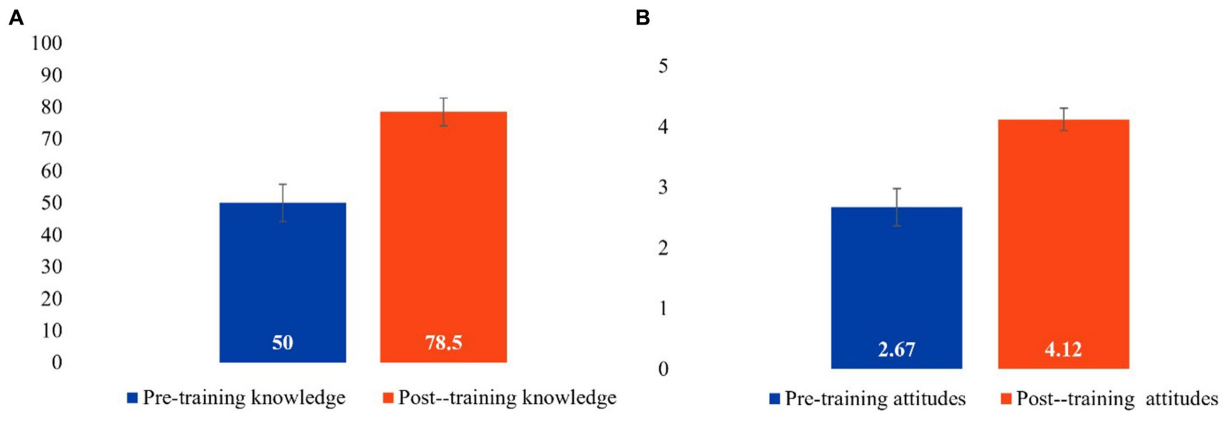


FIGURE 4
Pre and post training knowledge **(A)** and confidence **(B)**.

Australia. Increasing FASD knowledge among clinicians and community members will help to improve FASD prevention and identification efforts.

Data availability statement

The raw data supporting the conclusions of this article will be made available by the authors, without undue reservation.

Ethics statement

The studies involving human participants were reviewed and approved by The University of Western Australia Human Research Ethics Committee. The ethics committee waived the requirement of written informed consent for participation in the community education sessions.

Author contributions

JF and CP conceived the project design and supported the training, opening of the new FASD clinics, and reviewed and edited the manuscript. KP collated and analyzed the data and developed the first manuscript. All authors contributed to the article and approved the submitted version.

Funding

This work was supported by the Australian Government Department of Health Grant Opportunity—Fetal Alcohol Spectrum Disorder (FASD) Diagnostic Services and Models of Care Project (H1617G038).

Acknowledgments

The authors want to acknowledge the valued contributions from our consortium partners, including Patches Assessment Services, Central Australian Aboriginal Congress, Danila Dilba Health Service, Child Development Unit, Women's Children Hospital, FASD Tasmania and Goulburn Valley Health Service. This project was funded by the Australian Government Department of Health Drug and Alcohol Program. The consortium would like to acknowledge the guidance of Departmental Officials and Grant Managers across the life of the project.

Conflict of interest

The authors declare that the research was conducted in the absence of any commercial or financial relationships that could be construed as a potential conflict of interest.

Publisher's note

All claims expressed in this article are solely those of the authors and do not necessarily represent those of their affiliated organizations, or those of the publisher, the editors and the reviewers. Any product that may be evaluated in this article, or claim that may be made by its manufacturer, is not guaranteed or endorsed by the publisher.

Supplementary material

The Supplementary material for this article can be found online at: https://www.frontiersin.org/articles/10.3389/fpubh.2023.1195484/full#supplementary-material

References

1. Bower C, Elliott EJOn behalf of the Steering Group. (2016). *Report to the Australian Government Department of Health: "Australian Guide to the Diagnosis of Fetal Alcohol Spectrum Disorder (FASD)"*.

2. Elliott EJ, Bower C. Fetal alcohol spectrum disorder in Australia: from fiction to fact and to the future In: . *Fetal alcohol spectrum disorder: advances in research and practice*. New York: Springer (2022). 263–310.

3. Shelton D, Reid N, Till H, Butel F, Moritz K. Responding to fetal alcohol spectrum disorder in Australia. *J Paediatr Child Health*. (2018) 54:1121–6. doi: 10.1111/jpc.14152

4. Burns L, Breen C, Bower C, O'Leary C, Elliott EJ. Counting fetal alcohol spectrum disorder in Australia: the evidence and the challenges. *Drug Alcohol Rev*. (2013) 32:461–7. doi: 10.1111/dar.12047

5. Mutch RC, Watkins R, Bower C. Fetal alcohol spectrum disorders: notifications to the Western Australian register of developmental anomalies. *J Paediatr Child Health*. (2015) 51:433–6. doi: 10.1111/jpc.12746

6. Bower C, Watkins RE, Mutch RC, Marriott R, Freeman J, Kippin NR, et al. Fetal alcohol spectrum disorder and youth justice: a prevalence study among young people sentenced to detention in Western Australia. *BMJ Open*. (2018) 8:e019605. doi: 10.1136/bmjopen-2017-019605

7. Fitzpatrick JP, Latimer J, Ferreira ML, Carter M, Oscar J, Martiniuk ALC, et al. Prevalence and patterns of alcohol use in pregnancy in remote Western Australian communities: the Lililwan Project. *Drug Alcohol Rev*. (2015) 34:329–39. doi: 10.1111/dar.12232

8. Jones KL, Smith DW. Recognition of the fetal alcohol syndrome in early infancy. *Lancet*. (1973) 302:999–1001. doi: 10.1016/S0140-6736(73)91092-1

9. Lemoine D. Les enfants de parents alcoholiques Anomalies, observees de 127 cas. *Quest Méd*. (1968) 25:477–82.

10. Sullivan WC. A note on the influence of maternal inebriety on the offspring. *J Ment Sci*. (1899) 45:489–503. doi: 10.1192/bjp.45.190.489

11. Department of Health. *National fetal alcohol spectrum disorder stategic action plan*. Canberra, Australia: Department of Health (2018).

12. McCormack JC, Chu JTW, Marsh S, Bullen C. Knowledge, attitudes, and practices of fetal alcohol spectrum disorder in health, justice, and education professionals: a systematic review. *Res Dev Disabil*. (2022) 131:104354. doi: 10.1016/j.ridd.2022.104354

13. Passmore HM, Mutch RC, Burns S, Watkins R, Carapetis J, Hall G, et al. Fetal alcohol spectrum disorder (FASD): knowledge, attitudes, experiences and practices of the Western Australian youth custodial workforce. *Int J Law Psychiatry*. (2018) 59:44–52. doi: 10.1016/j.ijlp.2018.05.008

14. Payne J, Elliott E, D'Antoine H, O'Leary C, Mahony A, Haan E, et al. Health professionals' knowledge, practice and opinions about fetal alcohol syndrome and alcohol consumption in pregnancy. *Aust N Z J Public Health*. (2005) 29:558–64. doi: 10.1111/j.1467-842x.2005.tb00251.x

15. Payne J, France KE, Henley N, D'antoine HA, Bartu AE, Mutch RC, et al. Paediatricians' knowledge, attitudes and practice following provision of educational resources about prevention of prenatal alcohol exposure and fetal alcohol spectrum disorder. *J Paediatr Child Health*. (2011) 47:704–10. doi: 10.1111/j.1440-1754.2011.02037.x

16. Mukherjee RAS, Wray E, Hollins S, Curfs L. What does the general public in the UK know about the risk to a developing foetus if exposed to alcohol in pregnancy?

Findings from a UK mixed methodology study. *Child Care Health Dev*. (2015) 41:467–74. doi: 10.1111/cch.12187

17. Peadon E, Payne J, Henley N, D'antoine H, Bartu A, O'Leary C, et al. Women's knowledge and attitudes regarding alcohol consumption in pregnancy: a national survey. *BMC Public Health*. (2010) 10:510. doi: 10.1186/1471-2458-10-510

18. Oni Helen T, Buultjens Melissa, Abdel-Latif Mohamed E, and (2019). Islam MM. Barriers to screening pregnant women for alcohol or other drugs: a narrative synthesis. *Women Birth*. 32 479–486, doi: 10.1016/j.wombi.2018.11.009

19. Petrenko CLM, Tahir N, Mahoney EC, Chin NP. Prevention of secondary conditions in fetal alcohol spectrum disorders: identification of systems-level barriers. *Matern Child Health J*. (2014) 18:1496–505. doi: 10.1007/s10995-013-1390-y

20. Doherty E, Kingsland M, Wiggers J, Anderson AE, Elliott EJ, Symonds I, et al. Barriers to the implementation of clinical guidelines for maternal alcohol consumption in antenatal services: a survey using the theoretical domains framework. *Health Promot J Austr*. (2019) 31:133–9. doi: 10.1002/hpja.258

21. Reid N. Fetal alcohol spectrum disorder in Australia: what is the current state of affairs? *Drug Alcohol Rev*. (2018) 37:827–30. doi: 10.1111/dar.12855

22. France K, Henley N, Payne J, D'Antoine H, Bartu A, O'Leary C, et al. Health professionals addressing alcohol use with pregnant women in Western Australia: barriers and strategies for communication. *Subst Use Misuse*. (2010) 45:1474–90. doi: 10.3109/10826081003682172

23. Chamberlain K, Reid N, Warner J, Shelton D, Dawe S. A qualitative evaluation of caregivers' experiences, understanding and outcomes following diagnosis of FASD. *Res Dev Disabil*. (2017) 63:99–106. doi: 10.1016/j.ridd.2016.06.007

24. Panton KR, Fitzpatrick JP, Jeyaseelan D, Hill S, Pestell CF. Developing local fetal alcohol spectrum disorder diagnostic services and models of care in Australia. *J Fetal Alcoh Spect Disord*. (2022) 4:e1–e15. doi: 10.22374/jfasrp.v4i1.17

25. Fetal Alcohol Spectrum Disorder Australian Registry. *FASD notification summary tables—April 2023*. Westmead, Australia: University of Sydney (2023).

26. National Disability Insurance Scheme. *Counts of active NDIS participants diagnosied with Foetal Alcohol Syndrome or Foetal Alcohol Spectrum Disorder (FASD)*. split by state/territory (2023).

27. Commonwealth of Australia. *Effective approaches to prevention, diagnosis and support for fetal alcohol spectrum disorder*. Canberra, ACT, Australia: Community Affairs References Committee (2021).

28. Burd L, Popova S. Fetal alcohol spectrum disorders: fixing our aim to aim for the fix. *Int J Environ Res Public Health*. (2019) 16:3978. doi: 10.3390/ijerph16203978

29. Lyall V, Wolfson L, Reid N, Poole N, Moritz KM, Egert S, et al. "The problem is that we hear a bit of everything…": a qualitative systematic review of factors associated with alcohol use, reduction, and abstinence in pregnancy. *Int J Environ Res Public Health*. (2021) 18:3445. doi: 10.3390/ijerph18073445

30. Hayes N, Bagley K, Hewlett N, Elliott EJ, Pestell CF, Gullo MJ, et al. Lived experiences of the diagnostic assessment process for fetal alcohol spectrum disorder: a systematic review of qualitative evidence. *Alcoholism*. (2023):1–15. doi: 10.1111/acer.15097

31. Bell E, Andrew G, Di Pietro N, Chudley AE, Reynolds JN, Racine E. It's a shame! Stigma against fetal alcohol spectrum disorder: examining the ethical implications for public health practices and policies. *Public Health Ethics*. (2016) 9:65–77. doi: 10.1093/phe/phv012

32. Corrigan PW, Lara JL, Shah BB, Mitchell KT, Simmes D, Jones KL. The public stigma of birth mothers of children with fetal alcohol spectrum disorders. *Alcohol Clin Exp Res*. (2017) 41:1166–73. doi: 10.1111/acer.13381

33. Panton KR, Fitzpatrick JP, Pestell CPon behalf of the Fetal Alcohol Spectrum Disorder (FASD) Diagnostic Services and Model of Care Steering Committee. (2020). *Report to the Australian Government Department of Health: FASD diagnostic services and models of care project*.

34. Mukherjee RAS. Service delivery: organisation and models of care In: RAS Mukherjee and N Aiton, editors. *Prevention, recognition and management of fetal alcohol spectrum disorders*. Springer Nature: Switzerland (2021)

35. Doak J, Katsikitis M, Webster H, Wood A. A fetal alcohol spectrum disorder diagnostic service and beyond: outcomes for families. *Res Dev Disabil*. (2019) 93:103428. doi: 10.1016/j.ridd.2019.103428

36. Kerimofski K, Panton KR, Pestell C. Australian psychologists' knowledge, confidence and practices in fetal alcohol spectrum disorder diagnostic assessment, *Int J Disabil Dev Educ*Under review

37. Rojmahamongkol P, Cheema-Hasan A, Weitzman C. Do pediatricians recognize fetal alcohol spectrum disorders in children with developmental and behavioral problems? *J Dev Behav Pediatr*. (2015) 36:197–202. doi: 10.1097/DBP.0000000000000146

frontiers | Frontiers in Neuroscience

TYPE Original Research
PUBLISHED 26 July 2023
DOI 10.3389/fnins.2023.1197292

Check for updates

OPEN ACCESS

EDITED BY
Hermes H. Yeh,
Dartmouth College, United States

REVIEWED BY
Enrico Sanna,
University of Cagliari, Italy
Amanda Mahnke,
Texas A and M University, United States

*CORRESPONDENCE
Kristin M. Hamre
✉ khamre@uthsc.edu

RECEIVED 30 March 2023
ACCEPTED 11 July 2023
PUBLISHED 26 July 2023

CITATION
Baker JA, Mulligan MK and Hamre KM (2023) Effects of genetics and sex on adolescent behaviors following neonatal ethanol exposure in BXD recombinant inbred strains.
Front. Neurosci. 17:1197292.
doi: 10.3389/fnins.2023.1197292

COPYRIGHT
© 2023 Baker, Mulligan and Hamre. This is an open-access article distributed under the terms of the Creative Commons Attribution License (CC BY). The use, distribution or reproduction in other forums is permitted, provided the original author(s) and the copyright owner(s) are credited and that the original publication in this journal is cited, in accordance with accepted academic practice. No use, distribution or reproduction is permitted which does not comply with these terms.

Effects of genetics and sex on adolescent behaviors following neonatal ethanol exposure in BXD recombinant inbred strains

Jessica A. Baker[1,2], Megan K. Mulligan[3] and Kristin M. Hamre[1]*

[1]Department of Anatomy and Neurobiology, University of Tennessee Health Science Center, Memphis, TN, United States, [2]Center for Behavioral Teratology, San Diego State University, San Diego, CA, United States, [3]Department of Genetics, Genomics, and Informatics, University of Tennessee Health Science Center, Memphis, TN, United States

Introduction: Fetal alcohol spectrum disorders (FASD) are the leading preventable neurodevelopmental disorders and two hallmark symptoms of FASD are abnormal behavior, and cognitive and learning deficits. The severity of alcohol's teratogenic effects on the developing brain is influenced by genetics and sex. We previously identified recombinant inbred BXD mouse strains that show differential vulnerability to ethanol-induced cell death in the developing hippocampus, a brain region important in learning and memory. The present study aimed to test the hypothesis that strains with increased vulnerability to ethanol-induced cell death in the hippocampus have concomitant deficits in multiple hippocampal-related behaviors during adolescence.

Methods: The current study evaluated the effects of developmental ethanol exposure on adolescent behavior in two BXD strains that show high cell death (BXD48a, BXD100), two that show low cell death (BXD60, BXD71), and the two parental strains (C57BL/6 J (B6), DBA/2 J (D2)). On postnatal day 7, male and female neonatal pups were treated with ethanol (5.0 g/kg) or saline given in two equal doses 2 h apart. Adolescent behavior was assessed across multiple behavioral paradigms including the elevated plus maze, open field, Y-maze, and T-maze.

Results: Our results demonstrate that the effects of developmental ethanol exposure on adolescent behavioral responses are highly dependent on strain. The low cell death strains, BXD60 and BXD71, showed minimal effect of ethanol exposure on all behavioral measures but did present sex differences. The parental –B6 and D2–strains and high cell death strains, BXD48a and BXD100, showed ethanol-induced effects on activity-related or anxiety-like behaviors. Interestingly, the high cell death strains were the only strains that showed a significant effect of postnatal ethanol exposure on hippocampal-dependent spatial learning and memory behaviors.

Discussion: Overall, we identified effects of ethanol exposure, strain, and/or sex on multiple behavioral measures. Interestingly, the strains that showed the most effects of postnatal ethanol exposure on adolescent behavior were the BXD strains that show high ethanol-induced cell death in the neonatal hippocampus, consistent with our hypothesis. Additionally, we found evidence for interactions among strain and sex, demonstrating that these factors have a complex effect on alcohol responses and that both are important considerations.

KEYWORDS
alcohol, genetics, hippocampus, behavior, FASD, BXD RI strains

1. Introduction

Ethanol consumption during pregnancy can cause abnormal development and has been shown to be particularly detrimental to the developing brain (Moore et al., 2004; Riley and McGee, 2005; Guerri et al., 2009). Neurodevelopmental disorders associated with exposure to alcohol during prenatal development are referred to as fetal alcohol spectrum disorders (FASD) (Bertrand et al., 2005). In the United States, it is estimated that 2–5% of live births are adversely affected by prenatal alcohol exposure (May et al., 2014, 2018; Wozniak et al., 2019). Children with FASD exhibit long-lasting cognitive impairments such as deficits in learning and memory (Astley et al., 2009; Guerri et al., 2009; Mattson et al., 2011, 2019). Additionally, many individuals with FASD also exhibit other neurobehavioral symptoms such as hyperactivity, attention problems, and emotional dysregulation (Mattson and Riley, 2000; Riley and McGee, 2005; Hellemans et al., 2010; Mattson et al., 2011; Glass et al., 2014; Mattson et al., 2019). Interestingly, early twin studies established that an important factor in both the presence and severity of FASD is genetics, as a higher concordance of deficits are seen in human monozygotic twins compared to dizygotic twins (Christoffel and Salafsky, 1975; Chasnoff, 1985). In addition, evidence shows that children exposed to approximately equivalent amounts of alcohol at similar developmental timepoints, show variations in the severity of alcohol-induced deficits (Astley, 2010).

Similar cognitive impairments and behavioral abnormalities are seen in animal models of prenatal alcohol exposure and these models are a useful tool to investigate the underlying mechanisms behind alcohol-induced neurobehavioral alterations [as reviewed in (Chokroborty-Hoque et al., 2014; Patten et al., 2014; Fontaine et al., 2016)]. In addition, animal models are a useful tool for studying the role of genetics in the effects of alcohol exposure on the developing central nervous system. Numerous studies have examined differential vulnerability to ethanol's teratogenic effects across differing genetic backgrounds (Goodlett et al., 1989; Ogawa et al., 2005; Green et al., 2007; Downing et al., 2009; Chen et al., 2011; Goldowitz et al., 2014; Lossie et al., 2014). Most studies examining multiple strains have focused on malformations and brain abnormalities in embryos or neonates while fewer studies have examined differential behavioral responses to developmental alcohol exposure. The handful of studies that have focused on differential behavioral responses to perinatal ethanol exposure have used either selectivity bred strains that show differential alcohol-related traits such as alcohol preference or typically only compared two or three strains (Gilliam et al., 1987; Riley et al., 1993; Thomas et al., 1998, 2000). These studies identified differential behavioral responses to perinatal ethanol exposure such as hyperactivity, deficits in motor coordination, and learning and memory deficits (Gilliam et al., 1987; Riley et al., 1993; Thomas et al., 1998, 2000). Another tool for studying genetic variation and differential behavioral responses is the BXD recombinant inbred (RI) strains of mice which have been generated by crossing C57BL/6J (B6) and DBA/2J (D2) strains and inbreeding progeny for over 20 generations (Taylor et al., 1999; Wang et al., 2016). The BXD strains differ in alcohol responses in adults and show differential vulnerabilities to several malformations and developmental abnormalities after exposure to alcohol during development (Crabbe and Belknap, 1992; Downing et al., 2012; Goldowitz et al., 2014; Cook et al., 2015; Baker et al., 2017; Théberge et al., 2019). However, the behavioral effects of developmental alcohol exposure have yet to be examined in the BXD RI panel.

Using one strain, a number of animal studies have examined the effects of developmental alcohol exposure on activity-related and anxiety-like behaviors. Many of these studies report hyperactivity and/or increased anxiety-like behaviors though these results can vary depending on species, level of alcohol exposure, and time of exposure (Dursun et al., 2006; Kim et al., 2013; Fish et al., 2016; Xu et al., 2018). These preclinical results are similar to clinical findings in children with FASD who can present internalizing behavior problems such as anxiety or mood disorders as well as attention deficit hyperactivity disorder (ADHD) (Khoury et al., 2018). Importantly, these symptoms are not just present in childhood but continue throughout adulthood (Coles et al., 2022).

The hippocampus is of particular interest as it plays a large role in many of the cognitive and behavioral abnormalities present in FASD, specifically impairments in learning, memory, and attention. In humans, hippocampal abnormalities and dysfunctions have been associated with impaired spatial working memory performance (Coles et al., 1991; Hamilton et al., 2003; Willoughby et al., 2008; Moore et al., 2021). Impaired hippocampal-dependent behaviors are also seen in animal models using several different behavioral paradigms [as reviewed in (Patten et al., 2014; Marquardt and Brigman, 2016)] that assessed multiple hippocampal-dependent behaviors such as spatial learning and memory (Kelly et al., 1988; Wozniak et al., 2004) and fear conditioning (Wagner and Hunt, 2006; Hunt et al., 2009; Brady et al., 2012; Hamilton et al., 2014). Deficits in working memory have been assessed using the standard Y-Maze and impairments in spatial recognition memory have been examined using a modified Y-Maze (Sarnyai et al., 2000; Subbanna et al., 2013; Basavarajappa et al., 2014; Subbanna and Basavarajappa, 2014; Cantacorps et al., 2017). Importantly, ethanol-induced cell death during early postnatal development has been associated with memory impairments later in life (Wozniak et al., 2004; Subbanna et al., 2013; Subbanna and Basavarajappa, 2014). Moreover, the hippocampus, specifically the CA1 region has been linked to anxiety-like behavior (Cha et al., 2016; Jimenez et al., 2018; Ghasemi et al., 2022; Wang et al., 2022).

Interestingly, recent studies report sex-related differences in a number of behaviors including emotional regulation, hyperactivity, and cognition in individuals with FASD (Sayal et al., 2007; Herman et al., 2008; Flannigan et al., 2018) and animal models (Kelly et al., 1988; Wozniak et al., 2004; Hellemans et al., 2010; Fidalgo et al., 2017). Moreover, our previous analysis identified a strong effect of sex on changes in hippocampal gene expression following neonatal ethanol exposure (Baker et al., 2022). One advantage of using multiple strains is that we have the ability to investigate genotype-by-sex interactions

and recent evidence suggests that this interaction is crucial in a number of neurological disorders (Plummer et al., 2013; Schaafsma and Pfaff, 2014; Zhao et al., 2020; Blokland et al., 2022) but has not been fully investigated in relation to FASD. Many studies using rodent models investigate the effects of ethanol exposure on brain development and administer the ethanol exposure during the early postnatal period (Hamilton et al., 2011; Risbud et al., 2022). For mice, PD 7 is the middle of the brain growth spurt, a time during which neurons are completing migration and differentiation, establishing connections through synaptogenesis, dendritic arborization is ongoing, and natural programmed cell death is occurring, and is part of the third trimester-equivalent in humans (Gil-Mohapel et al., 2010; Alfonso-Loeches and Guerri, 2011; Marquardt and Brigman, 2016).

In the present study, we examined the effects of developmental ethanol exposure on adolescent behavior using selected BXD RI strains to assess whether cell death and behavior alterations co-occur as discussed below. Strains were selected based on previous work which identified BXD strains that showed increased vulnerability to ethanol-induced cell death in the neonatal hippocampus after exposure to postnatal ethanol while other BXD strains were resistant to these effects (Goldowitz et al., 2014). In addition, these BXD strains were shown to have differential gene expression changes in the neonatal hippocampus after exposure to alcohol during development (Baker et al., 2022). Using the same postnatal ethanol exposure paradigm that identified the BXD strains, we aim to further investigate the long-term effects of developmental alcohol exposure on cognition and behavior in these selected strains. We hypothesize that BXD strains that show increased vulnerability to ethanol-induced cell death in the hippocampus have concomitant deficits in multiple behavioral domains. Adolescent animals exposed to postnatal ethanol (equivalent to the third trimester in humans) were tested across a battery of behavioral tests to examine the effects of developmental alcohol exposure on activity, anxiety-like behavior, working memory, and spatial recognition memory. Both males and females were examined to investigate possible genotype-by-sex interactions and address the effect of sex on these behavioral measures as sex-specific behavioral impairments have been found in both humans and animal models (Ieraci and Herrera, 2007; Sayal et al., 2007; Herman et al., 2008; Kelly et al., 2009; Hellemans et al., 2010; May et al., 2017; Woods et al., 2018; Xu et al., 2018).

2. Materials and methods

2.1. Subjects

Original breeders were obtained from Dr. Robert Williams at the University of Tennessee Health Science Center (UTHSC) and the Jackson Laboratory (Bar Harbor, ME). All treatments and experiments were approved by the Institutional Animal Care and Use Committee at UTHSC. The present study aims to better understand the long-term effects of postnatal ethanol exposure in strains that show differential vulnerability to ethanol-induced cell death in the hippocampus of male and female mice. To test this, mouse strains were examined including, C57BL/6J (B6), DBA/2J (D2), and select BXD recombinant inbred (RI) strains that showed differential susceptibility to ethanol-induced cell death in the developing hippocampus (Goldowitz et al., 2014). BXD48a (previously named BXD96) and BXD100 showed higher susceptibility to ethanol-induced cell death in the hippocampus while BXD60 and BXD71 showed lower vulnerability.

Once all strains were acquired, breeding was conducted at UTHSC. Breeders were the products of on-site mating and thus breeders were not affected by excess stressors such as travel and relocation. Mice were maintained on a 12:12 hour light:dark cycle and given food and water *ad libitum*. Environmental enrichments (igloo house and Nestlets) were placed in each mouse cage throughout all experiments. Breeding cages were maintained with multiple male and female mice over 60 days of age. Breeders were checked several times per week and when female mice appeared pregnant, they were placed alone in a clean cage and monitored daily for pups. Pregnant dams were separated to (1) acclimate the dam to a new cage and reduce stress (2) control for differences in pup rearing with other adult male and female mice in original breeding cages and (3) to allow for close monitoring of pups without disturbing other breeders. On average dams were placed in a cage alone 1 week prior to birth. The date of birth was defined as postnatal day 0 (PD 0). In order to control for potential differences in maternal care, the first litter from each mother was not used for experiments. Only litters of 4 or more were kept while large litters were culled to 8 pups. Half of the pups in each litter were assigned to the ethanol groups and the other half the control group. If a litter contained more than one animal per treatment group, per sex, the litter mean for each treatment group and sex were calculated and used for statistical analysis.

2.2. Ethanol exposure

Neonatal mice were treated on postnatal day (PD) 7 which is a developmental time point during the third trimester-equivalent in humans. For mice, PD 7 is the middle of the brain growth spurt, a time during which neurons are completing migration and differentiation, establishing connections through synaptogenesis, dendritic arborization is ongoing programmed cell death is occurring (Gil-Mohapel et al., 2010; Alfonso-Loeches and Guerri, 2011; Marquardt and Brigman, 2016). For treatment, pups were brought to a separate testing room in their cage with their mother between 9:00 AM and 10:00 AM. Pups were placed in a clean cage on a heating pad while they were weighed, dosed, and then promptly placed back in their home cage with their mother. Litters were split with half of the pups in the ethanol group and half in the control group. As in previous studies (Goldowitz et al., 2014), ethanol treated animals received 20% ethanol in sterile saline though subcutaneous injection. The total dose of ethanol was 5.0 g/kg split in two 2.5 g/kg doses, given 2 h apart while controls received an isovolumetric volume of sterile saline (Goldowitz et al., 2014). This ethanol exposure represents an acute neonatal binge which has been shown to produce BACs of approximately 350 mg/dL in P7 neonatal mice (Goldowitz et al., 2014; Schaffner et al., 2020). Early prenatal and postnatal rodent studies of blood alcohol concentrations found no differences in BAC levels across multiple strains including B6 and D2 mouse strains (Goodlett et al., 1989; Boehm II et al., 1997). At the time of the first injection, pups were toe clipped for identification purposes during early development. On postnatal day 28, animals were weaned, separated by sex, and ear punched for easier identification purposes, as toe clip reading prior to behavioral testing can be an additional stressor (Castelhano-Carlos et al., 2010; Schaefer et al., 2010; Paluch et al., 2014).

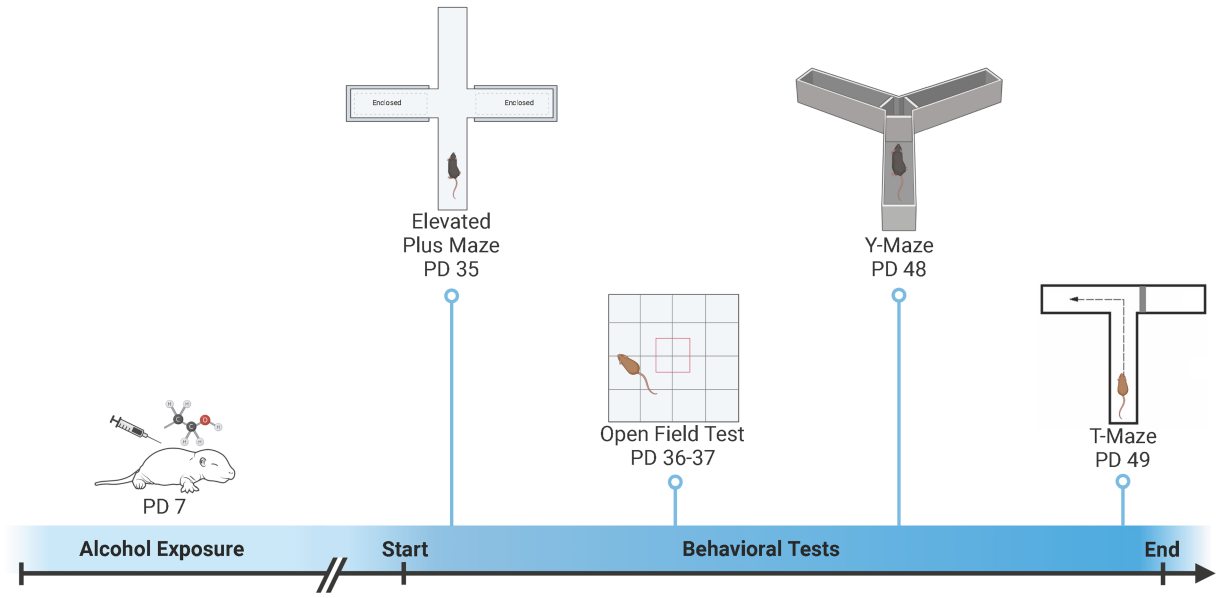


FIGURE 1
Overview of developmental ethanol exposure and behavioral testing. On postnatal day (PD) 7, pups were exposed to ethanol or saline vehicle via subcutaneous injection. Pups were then left undisturbed until behavioral testing. Activity-related and anxiety-like behaviors were measured during early adolescence (PD 35 – PD 37) using an Elevated Plus Maze (EPM) and Open Field (OF). Spatial learning and memory were measured during late adolescence (PD 48 – PD 49) using a Y-Maze and T-Maze. Created with BioRender.com.

2.3. Behavioral testing procedure and schedule

The elevated plus maze (EPM) and open field (OF) were used to examine activity and anxiety-like behaviors and the Y-Maze and T-Maze were used to examine spatial learning and memory (Figure 1). All mice were examined in all behaviors (Fish et al., 2016; Fidalgo et al., 2017), however, some subjects were excluded from analysis due to technical issues (see Supplemental Table S1). The EPM and OF were conducted during early adolescence (EPM: PD 35.8 ± 1.1; OF Day 1: PD 36.8 ± 1.1; OF Day 2: PD 37.8 ± 1.1). Approximately, two-weeks later animals were tested in the Y-Maze and T-Maze during late adolescence (Y-Maze: PD 49.1 ± 1.3; T-Maze: PD 50.1 ± 1.3). The testing order was designed to test anxiety first using the elevated plus maze and open field, as anxiety is the most likely to be impacted by prior experience followed by the learning and memory tasks (i.e., Y-Maze and T-Maze) (Thomas et al., 2010; Risbud et al., 2022). In addition, we chose the learning tasks of the Y-Maze and T-Maze, that were different shapes and sizes in order to minimize carry-over effects.

All behavioral testing was performed in the Behavioral Core of the Neuroscience Institute at the University of Tennessee Health Science Center. Animals were acclimated for 1 h prior to testing which began between 10:00 AM −11:00 AM with noise level and lighting tightly controlled. Animals were placed in clean cages after testing and each apparatus was cleaned with 70% ethanol.

All behavior was tracked and recorded using ANY-maze Software version 4.99z (Stoelting Co., Wood Dale Illinois, and United States). For all behaviors, the number of entries is defined as 85% of the animal's body, i.e., all four paws, to enter the zone, while their exit out of a zone requires 70% of the animal's body to leave the zone (Any-maze Manual, Stoelting). If a litter contained more than one animal per treatment group, per sex, the litter mean for each treatment group and sex were calculated and used for statistical analysis. A minimum of 7 animals (from a minimum of 7 litters) per strain, per treatment group, per sex was used. The complete summary of animal numbers by strain, treatment, and sex are recorded in Supplementary Table S1.

2.3.1. Elevated plus maze

The elevated plus maze (EPM) was used to examine anxiety-like behavior and locomotor activity as previously described (Bailey and Crawley, 2009; Fish et al., 2016; Xu et al., 2018). Mice were placed near the center of an EPM which is a plus-shaped (+) maze consisting of four arms (30 cm X 6 cm), two of which are open and two of which are enclosed with clear 15 cm walls. The runway was elevated 84 cm from the floor. Animals were tested for 5 min. The purpose of this test is to measure anxiety-like behavior and activity in mice. Therefore, total distance travelled in the maze and total number of line crossings as well as number of entries and percent time spent in each of the open and closed arms of the maze was determined.

2.3.2. Open field

The open field (OF) was used to examine anxiety-like behavior and locomotor activity as previously described (Ieraci and Herrera, 2007; Bailey and Crawley, 2009; Fish et al., 2016; Xu et al., 2018). Mice were placed in a clear OF (40 cm X 40 cm X 40 cm) and allowed to explore the arena for 15 min. Animals were tested twice in the OF, each session 24 h apart. For each session, analysis was conducted at the following time bins: 0 min to 5 min (Bin 1), 5 min to 10 min (Bin 2), 10 min to 15 min (Bin 3), and total 15 min (Total). Activity was examined in the whole maze area, in the center of the maze (286 cm^2), and in the edge of the maze (800 cm^2) as a measure of thigmotaxis (Bailey and Crawley, 2009). The following measures were recorded in the entire maze area, center of the maze or edge of the maze: total

distance travelled, time spent, and number of entries were evaluated across all time bins on day 1 and day 2.

2.3.3. Y-maze

The Y-Maze was used to examine hippocampal-dependent spatial working memory as previously described (Holcomb et al., 1998; Subbanna et al., 2013; Basavarajappa et al., 2014; Cantacorps et al., 2017). The Y-Maze consists of three enclosed arms (12 cm X 5 cm X 5 cm) in the shape of a Y. To orient the animal to the location of each arm, shapes of various colors were placed on the walls around the Y-Maze. Each mouse was placed in the entry arm and allowed to explore freely through the maze for an 8-min session. The sequence of arms entered was recorded to measure spontaneous alternations. Correct alternation was recorded as three consecutive choices of the three different arms. Spontaneous alternations are calculated by dividing the total number of alternations by the total number of choices minus 2 (Holcomb et al., 1998; Subbanna et al., 2014; Cantacorps et al., 2017). Total distance travelled in the Y-Maze was also examined. Additionally, distance travelled, number of entries, and time spent in each arm was also examined.

2.3.4. T-maze

The T-Maze was used to examine spatial working memory as previously described (Subbanna et al., 2014; Shivakumar et al., 2020). Briefly, the T-Maze consisted of three arms, one entry arm (50 cm X 10 cm) and two top arms (28 cm X 10 cm). As before, various shapes were placed around the maze. Mice were placed in the entry arm and allowed to freely explore for an 8-min training session. During the training session, one of the top arms was blocked and the mouse was only able to assess one of the top arms. The location of the blocked arm was randomized. After a 3-h interval, short-term memory was assessed, during which both top arms of the T-Maze were accessible. Mice were placed into the entry arm and allowed to explore both top arms for 3 min. The animal's ability to discriminate between the two top arms was measured by examining time in the novel (previously blocked armed) compared to total time between both the novel and familiar, previously opened arm. The discrimination ratio [novel arm/(novel arm + familiar arm)] was used to calculate the time spent between both arms and the number of entries into both arms. Other measures recorded during both the training and short-term memory sessions included: total distance travelled in the whole maze as well as number of entries and time spent in the entry arm and opened arm. Additionally, during the short-term memory session the following measures were recorded in the novel (previously blocked arm): number of entries, time spent, and latency to enter.

2.4. Behavioral analysis

All behavior was exported from ANY-maze and analyzed using the following packages in the R (version 4.1) software environment: plyr package (version 1.8.6), ggplot2 package (version 3.3.3) (Wickham, 2016), and effectsize package (version 0.4.5). The effect of strain, sex, treatment, strain x sex interaction, strain x treatment interaction, sex x treatment interaction, and strain x sex x treatment interaction were examined across the six strains (BXD48a, BXD60, BXD71, BXD100, B6, and D2), two sexes (male and females), and two treatments (controls and ethanol). ANOVAs were used to examine multiple measures in R using the following input: measure.model<−lm(data = Dat,measure~Strain*Sex*Treatment), anova(measure.model). The effect size was calculated using Omega Squared confidence intervals in R using the following input: omega_squared(measure.model, partial = TRUE, ci = 0.09) (Lakens, 2013). Further analysis within each strain was calculated by two-way ANOVAs for effects of sex, treatment, and sex x treatment interactions in GraphPad Prism 7 (GraphPad Software Inc., San Diego, California). Additional descriptive statistics can be found in Supplementary materials.

3. Results

3.1. Adolescent body weights

Body weight was measured after the animal completed the EPM and again after the Y-Maze in all strains and both males and females. Body weights after both the EPM and Y-Maze showed significant effects of strain [EPM: $F_{5,183} = 15.96$, $p < 0.001$, $\omega^2 = 0.36$, 90% CI (0.26, 0.43); Y-Maze: $F_{5,186} = 24.22$, $p < 0.001$ $\omega^2 = 0.27$, 90% CI (0.17, 0.34)] and sex [EPM: $F_{1,183} = 74.98$, $p < 0.001$ $\omega^2 = 0.49$, 90% CI (0.41, 0.56); Y-Maze: $F_{1,186} = 1999.89$, $p < 0.001$ $\omega^2 = 0.26$, 90% CI (0.18, 0.35)]. However, there was no significant difference in body weight between control and ethanol animals at either age.

3.2. Strain effects

There were robust effects of strain on almost every measure across all four behavioral tests, (Table 1). Activity-related behavior such as total distance travelled, showed significant effects of strain across the elevated plus maze, open field, Y-Maze, and T-Maze. Anxiety-related behaviors such as number of entries into the closed arms of the elevated plus maze and time in thigmotaxis during the open field also showed significant effects of strain. Similarly, learning and memory measures showed significant effects of strain such as spontaneous alternations in the Y-Maze and time in novel arm of the T-Maze during the short-term memory trial. Since there were such robust effects of strains across all behavioral tests, each strain was analyzed separately for effects of treatment, sex, or treatment by sex interactions. Therefore, we further analyzed the effects of developmental ethanol exposure and sex in each strain separately while paying attention to cell death status.

3.3. Moderate cell death strains: B6 and D2

For the EPM, there were no significant effects of ethanol exposure or sex for the B6 parental strain. In contrast, the D2 parental strain showed a significant interaction between ethanol exposure and sex for distance travelled [$F_{(1, 30)} = 4.20$, $p < 0.05$; Figure 2A] and number of line crossings [$F_{(1, 30)} = 3.94$, $p < 0.05$]. Ethanol exposure showed sex specific effects in activity-related measures in the D2 strain with increased distance travelled and number of line crossings in ethanol-exposed females compared to control females. In contrast,

TABLE 1 Significant effects of strain on body weight and behavioral measures.

	F-value (Dfm, DFd)	value of *p*	ω^2	90% CI [,]
Body weight				
Weight at elevated plus maze	15.96 (5, 183)	0.001	0.36	[0.26, 0.43]
Weight at Y-maze	24.22 (5, 186)	0.001	0.27	[0.17, 0.34]
Elevated plus maze				
Total distance travelled	52.02 (5,195)	0.001	0.54	[0.46, 0.60]
Number of entries to the open arms	14.90 (5, 195)	0.001	0.24	[0.15, 0.31]
Distance travelled in the open arms	53.74 (5, 195)	0.001	0.55	[0.47, 0.60]
Number of entries to the closed arms	13.21 (5, 195)	0.001	0.22	[0.13, 0.29]
Distance travelled in the closed arms	27.21 (5, 195)	0.001	0.37	[0.28, 0.44]
Open field				
Day 1- Total distance travelled	18.23 (5, 189)	0.001	0.29	[0.19, 0.36]
Day 1- Time in center	8.34 (5, 189)	0.001	0.15	[0.06, 0.21]
Day 1-Time in edge	8.80 (5, 189)	0.001	0.16	[0.07, 0.22]
Day 1-Number of entries to center	10.48 (5, 189)	0.001	0.18	[0.09, 0.25]
Day 1-Number of entries to edge	9.94 (5, 189)	0.001	0.17	[0.08, 0.24]
Day 2-Total distance travelled	30.42 (5, 189)	0.001	0.41	[0.31, 0.48]
Day 2-Time in center	6.60 (5, 189)	0.001	0.12	[0.04, 0.17]
Day 2-Time in edge	8.50 (5, 189)	0.001	0.15	[0.06, 0.21]
Day 2-Number of entries to center	11.05 (5, 189)	0.001	0.19	[0.10, 0.26]
Day 2-Number of entries to edge	13.05 (5, 189)	0.001	0.22	[0.13, 0.29]
Y-maze				
Spontaneous alternations	13.01 (5, 189)	0.001	0.22	[0.12, 0.28]
Total distance travelled	43.01 (5, 189)	0.001	0.50	[0.41, 0.26]
T-maze				
Training trial-total distance travelled	36.31 (5, 191)	0.001	0.45	[0.36, 0.52]
Training trial-number of entries to open arm	29.78 (5, 191)	0.001	0.40	[0.31, 0.74]
Training trial-latency to enter open arm	3.41 (5, 191)	0.01	0.05	[0.00, 0.09]
Short-term memory trial-total distance travelled	12.70 (5, 191)	0.001	0.21	[0.12, 0.28]
Short-term memory trial-number of entries to familiar arm	7.70 (5, 191)	0.001	0.13	[0.05, 0.20]
Short-term memory trial-time in familiar arm	4.10 (5, 191)	0.001	0.04	[0.01, 0.11]
Short-term memory trial-number of entries to novel arm	11.21 (5, 191)	0.001	0.19	[0.10, 0.26]
Short-term memory trial-time in novel arm	3.78 (5, 191)	0.001	0.06	[0.00, 0.10]
Short-term memory trial-latency to enter novel arm	2.33 (5, 191)	0.05	0.03	[0.00, 0.06]
Short-term memory trial-discrimination ratio-time	2.73 (5, 191)	0.05	0.04	[0.00, 0.07]

ethanol-exposed males showed decreased distance travelled and number of line crossings compared to control males.

In the OF, there was a significant interaction between ethanol exposure and sex in the B6 strains for distance travelled during the first 5 min on day 1 [$F_{(1, 41)} = 5.24$, $p < 0.05$; Figure 3A] and day 2 [$F_{(1, 41)} = 4.70$, $p < 0.05$; Figure 3B]. For both days, ethanol-exposed females showed increased distance travelled compared to control females. Ethanol-exposed males showed decreased distance travelled compared to control males on day one but there was no effect of ethanol-exposure in males on day 2. Non-sex-specific effects of ethanol exposure were present in the D2 strain with both males and females showing increased distance travelled during the first 5 min in the OF on day 1 [$F_{(1, 26)} = 6.19$, $p < 0.05$; Figure 3A] and day 2 [$F_{(1, 26)} = 7.46$, $p < 0.05$, Figure 3B].

Neither the B6 nor D2 strain showed any significant effects of ethanol-exposure or sex on spatial learning and memory measures in either the Y-Maze or the T-Maze.

3.4. Low cell death strains: BXD60 and BXD71

The low cell death strains, BXD60 and BXD71, showed no significant effects of developmental ethanol exposure or sex activity-or

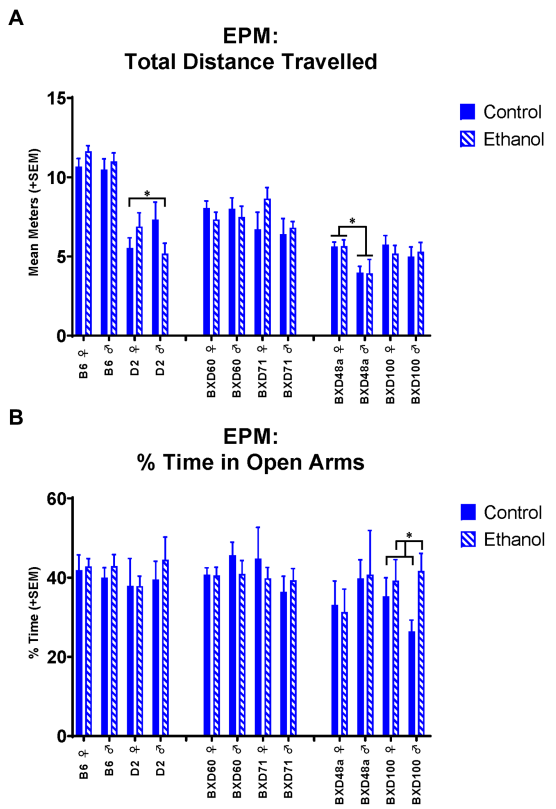


FIGURE 2
Effects of strain, ethanol, and sex on activity-related and anxiety-like behaviors in the Elevated Plus Maze (EPM). **(A)** There was a significant effect of strain ($p < 0.001$) on activity-related behaviors as measured by total distance travelled in the EPM. The D2 parental strain showed a significant ethanol-by-sex interaction (*$p < 0.05$; D2 ♀ Ethanol > D2 ♀ Control; D2 ♂ Ethanol < D2 ♂ Control). The high cell death strain, BXD48a, showed a significant effect of sex (*$p < 0.01$; BXD48a ♀ > BXD48a ♂). **(B)** The high cell death strain, BXD100, showed a significant effect of ethanol on anxiety-like behavior as measured by percent of time in the open arms of the EPM (*$p < 0.05$; BXD100 Ethanol > BXD100 Control). Striped bars represent animals exposed to postnatal ethanol while solid bars represent non-exposed control animals. Graphs are organized by parental strains (left), low cell death strains (middle), and high cell death strains (right). ♀, female, ♂, male.

anxiety-related measures in the EPM. In the OF, the BXD60 strain showed a significant effect of sex on distance travelled [$F_{(1, 28)} = 7.85$, $p < 0.01$; Figure 3B] and number of line crossings [$F_{(1, 28)} = 4.93$, $p < 0.05$] during the first 5 min that was only present on day 2 but not day 1. On day 2, BXD60 females showed greater levels of activity-related behaviors compared to BXD60 males, regardless of ethanol exposure. In contrast, the BXD71 strain showed no effect of sex or ethanol exposure on activity-related behaviors in the open field on day 1 or day 2; however, there was an effect of ethanol exposure on anxiety-related behaviors. Specifically, both male and female BXD71 animals exposed to ethanol during development spent significantly less time in the center of the OF on day 1 [$F_{(1, 31)} = 5.14$, $p < 0.05$; Figure 4A] with similar trends present on day 2 [$F_{(1, 31)} = 3.32$, $p = 0.07$].

In behavioral experiments related to spatial learning and memory, i.e., the Y-Maze and T-Maze, there were no effects of ethanol exposure or sex in the BXD60 strain. Similarly, the BXD71 strain showed no effects of ethanol or sex on learning and memory-related behavior. However, there was a significant effect of sex in the BXD71 strain on activity-related behaviors in both the Y-Maze and T-Maze (p's < 0.05). BXD71 females showed greater distance travelled and number of line crossings compared to BXD71 males.

3.5. High cell death strains: BXD48a and BXD100

The high cell death strains, BXD48a and BXD100, showed effects of ethanol and/or sex in multiple behavioral measures. The high cell death strain, BXD48a, showed a significant effect of sex [$F_{(1, 29)} = 8.74$, $p < 0.01$] on activity-related measures in the EPM with females showing greater total distance travelled compared to males (Figure 2A). The BXD100 strain, showed a significant effect of ethanol exposure [$F_{(1, 34)} = 4.78$, $p < 0.05$] on anxiety-related measures in the EPM with ethanol-exposed subjects spending significantly more time in the open arms than the closed arms of the EPM compared to control subjects (Figure 2B).

On Day 1 of the OF, the BXD48a strain showed a significant effect of ethanol exposure [$F_{(1, 30)} = 4.30$, $p < 0.05$] and sex [$F_{(1, 30)} = 5.28$, $p < 0.05$] on thigmotaxis for the total 15 min. BXD48a females showed increased anxiety-like behavior with greater time in the edge compared to males (Figure 4B). However, ethanol-exposure decreased time spent in the edge in both sexes compared to controls (Figure 4B). On Day 2 of the OF, there was a significant treatment by sex interaction [$F_{(1, 30)} = 4.51$, $p < 0.05$] in activity-related behaviors where BXD48a males and females showed opposing effects of ethanol on number of line crossings during the whole 15 min. Ethanol-exposed males showed increased activity-like behavior compared to control males, while ethanol-exposed females showed decreased activity-related behavior compared to control females. Although not significant, there was a similar trend for ethanol by sex interaction [$F_{(1, 30)} = 3.24$, $p = 0.08$] for total distance travelled on Day 2 during the whole 15 min of the OF in the BXD48a strain.

For the BXD100 strain, there were significant treatment by sex interactions in both activity-related [$F_{(1, 33)} = 4.83$, $p < 0.05$] and anxiety-like [$F_{(1, 33)} = 3.17$, $p < 0.05$] behaviors during the first 5 min of the OF on Day 1. Similar to that seen in BXD48a, BXD100 males and females showed opposite effects of ethanol-exposure. BXD100 males exposed to ethanol during development showed increased number of line crossings (Figure 3C) and time spent in the center of the open field (Figure 3D) compared to control BXD100 males. In contrast, ethanol exposure decreased these behaviors in females. However, these ethanol and sex effects were only present in the first 5 min on Day 1 and not seen on Day 2 of the OF.

Both high cell death strains showed significant interactions between ethanol exposure and sex on spatial learning and memory. There were significant ethanol by sex interactions in spontaneous alternations in the Y-Maze (Figure 5) for the BXD48a [$F_{(1, 29)} = 3.96$, $p < 0.05$] and BXD100 [$F_{(1, 34)} = 4.75$, $p < 0.05$] with males and females displaying opposite effects of ethanol exposure. In the BXD48a strain, males showed decreases in ethanol-induced spontaneous alternations while ethanol exposed females showed increases. However, the opposite was seen in BXD100, with ethanol exposure increasing spontaneous alternations in males and decreasing in females.

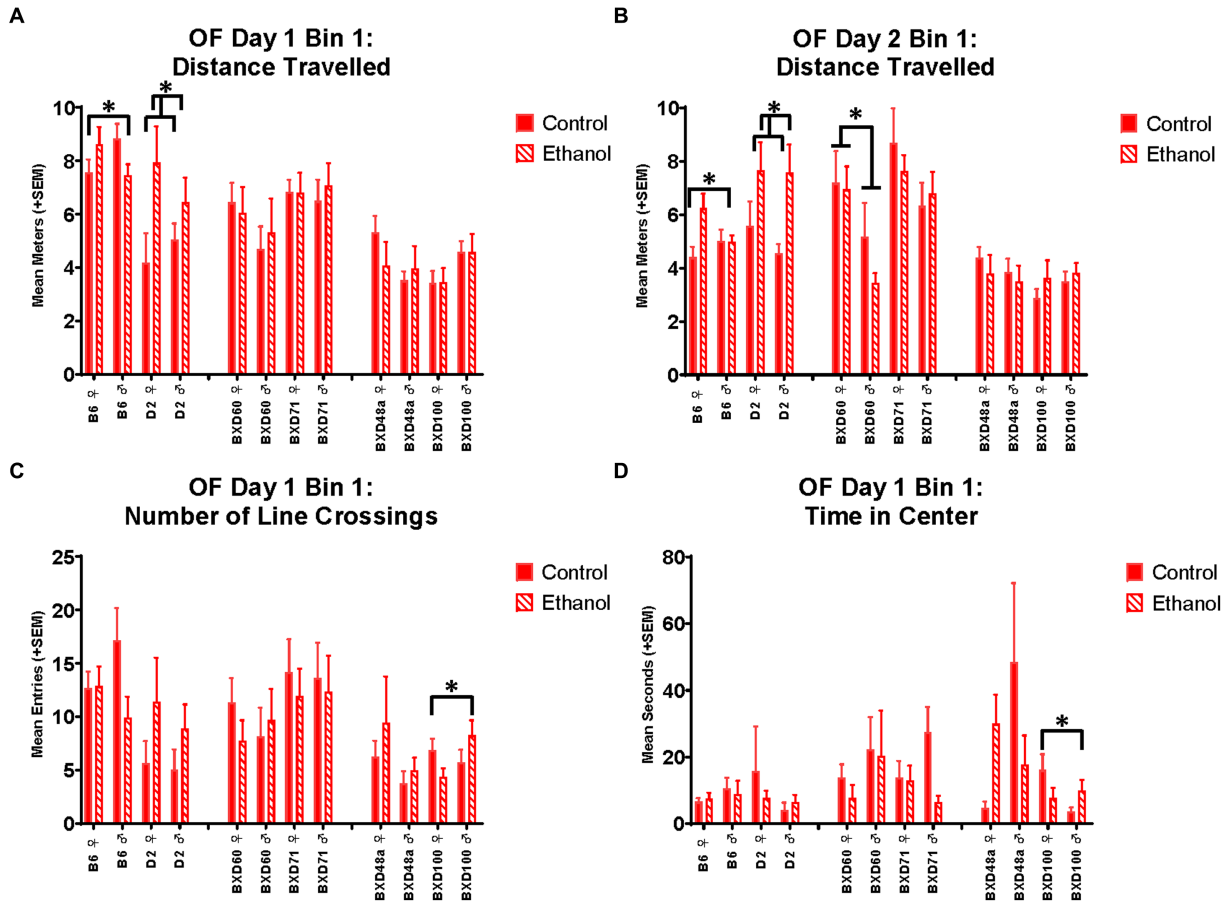


FIGURE 3
Effects of strain, ethanol, and sex on activity-related and anxiety-like behaviors during the first 5 min of the Open Field (OF). There was a significant effect of strain on distance travelled during the first 5 min (Bin 1) on **(A)** Day 1 ($p < 0.001$) and **(B)** Day 2 ($p < 0.001$). The parental B6 strain showed a significant ethanol-by-sex interaction (*$p < 0.05$; B6 ♀ Ethanol > B6 ♀ Control; B6 ♂ Ethanol < B6 ♂ Control) on distance travelled during the first 5 min. Additionally, the parental D2 strain showed a significant effect of ethanol (*$p < 0.05$; D2 Ethanol > D2 Control), regardless of sex, on Day 1 and Day 2. For the low cell death strain, BXD60, there was a significant effect of sex (*$p < 0.01$; BXD60 ♀ > BXD60 ♂) on distance travelled during the first 5 min of Day 2 but not Day 1. **(C)** There was also a significant effect of strain on number of line crossings during the first 5 min on Day 1 ($p < 0.001$) with the high cell death strain, BXD100 demonstrating a significant ethanol-by-sex interaction (*$p < 0.05$; BXD100 ♀ Ethanol < BXD100 ♀ Control; BXD100 ♂ Ethanol > BXD100 ♂ Control). **(D)** There were significant effects of strain ($p < 0.01$) on anxiety-like measures including time spent in the center of the Open Field on Day 1. For this measure, BXD100 strain showed similar ethanol-by-sex interactions (*$p < 0.05$; BXD100 ♀ Ethanol < BXD100 ♀ Control; BXD100 ♂ Ethanol > BXD100 ♂ Control). Striped bars represent animals exposed to postnatal ethanol while solid bars represent non-exposed control animals. Graphs are organized by parental strains (left), low cell death strains (middle), and high cell death strains (right). ♀, female, ♂, male.

The high cell death strains also showed differences in spatial learning and memory measures in the T-Maze. During the short-term memory trial in the T-Maze, the BXD48a strain showed ethanol-induced impairments in learning and memory. Specifically, ethanol exposed subjects entered the novel arm of the maze significantly [$F_{(1, 28)} = 4.89$, $p < 0.05$; Figure 6A] less than control subjects. Importantly, there were no significant differences on entries into the familiar arm during the short-term memory trial. This is also seen by a trend ($p < 0.1$) in the discrimination ratio for number of line crossings during the short-term memory trial. In addition, there was also showed a significant effect of sex [$F_{(1, 28)} = 4.89$, $p < 0.05$] for number of entries into the novel arm of the maze with BXD48a males showing reduced entries overall compared to females. For the BXD100 strain, there was a significant effect of ethanol exposure [$F_{(1, 32)} = 6.32$, $p < 0.05$; Figure 6B] on latency to enter the novel arm during the short-term memory trial with ethanol-exposed subjects entering the novel arm sooner during the trial compared to controls.

4. Discussion

This study was designed to investigate the hypothesis that strains with relatively higher levels of cell death in the hippocampus after postnatal ethanol exposure will display alterations in behavioral responses in adolescence compared to low cell death strains, especially in tasks relevant to learning and memory that are reliant on the hippocampus (Baker et al., 2022). Previous work in adult animals has shown that there are baseline behavioral differences between strains using multiple behavioral paradigms (Chesler et al., 2005; Philip et al., 2010; Knoll et al., 2016; Neuner et al., 2016) and we replicate those findings by showing that there are significant strain difference in almost every behavioral measure in all four tests during adolescence. Furthermore, we show significant effects of sex for a number of behavioral measures among the strains. Although there were less effects of ethanol exposure compared to strain and sex effects, there were several treatment interactions between strain and/or sex in our

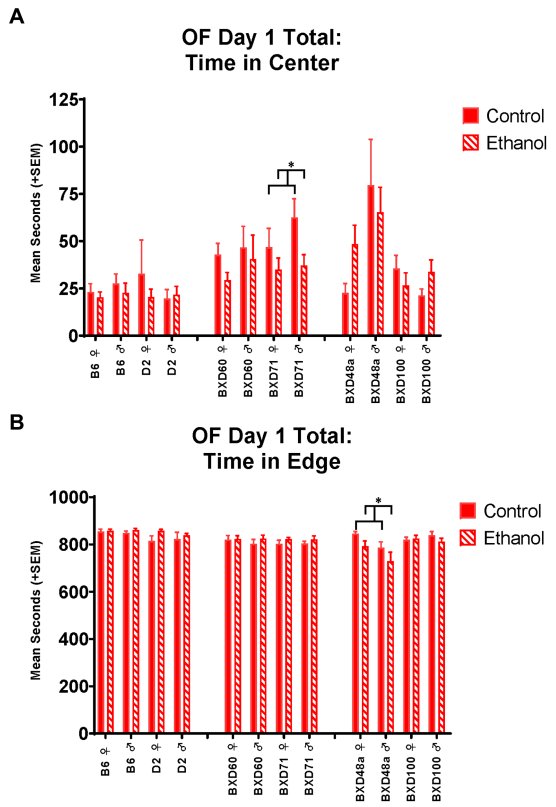


FIGURE 4
Effects of strain, ethanol, and sex on anxiety-like behaviors during the total 15 min of the Open Field (OF). **(A)** There was a significant effect of strain ($p < 0.001$) on time in center of the Open Field on Day 1. The low cell death strain, BXD71, showed a significant ethanol-by-sex interaction (*$p < 0.05$; BXD71 ♀ Ethanol < BXD71 ♀ Control; BXD71 ♂ Ethanol < BXD71 ♂ Control) in time in the center of the Open Field. **(B)** While there was not an overall effect of strain on time in edge of the Open Field on Day 1, there was a significant strain-by-ethanol interaction ($p < 0.01$). The high cell death strain, BXD48a, showed a significant effect of sex ($p < 0.05$; ♀ > BXD48a ♂) and ethanol (*$p < 0.05$; BXD48a Ethanol < BXD48a Control) on thigmotaxic behavior as measured by time in the edge of the Open Field. Striped bars represent animals exposed to postnatal ethanol while solid bars represent non-exposed control animals. Graphs are organized by parental strains (left), low cell death strains (middle), and high cell death strains (right). ♀, female, ♂, male.

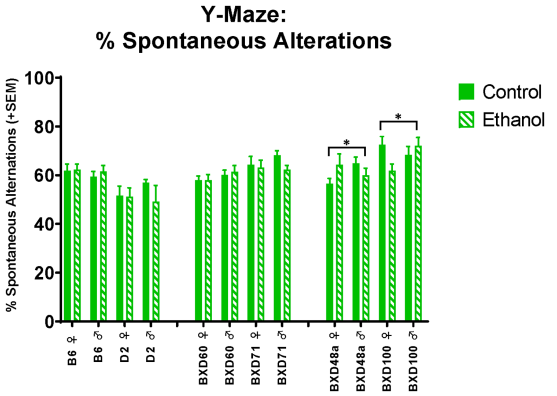


FIGURE 5
Effects of strain, ethanol, and sex spatial learning and memory in the Y-Maze. There was a significant effect of strain ($p < 0.001$) on percent of spontaneous alternations in the Y-Maze. Both high cell death strains, BXD48a and BXD100, showed significant ethanol-by-sex interactions, although effects were in opposing direction (*$p < 0.05$; BXD48a ♀ Ethanol > BXD48a ♀ Control; BXD48a ♂ Ethanol < BXD48a ♂ Control and *$p < 0.05$; BXD100 ♀ Ethanol < BXD100 ♀ Control; BXD100 ♂ Ethanol > BXD100 ♂ Control). Striped bars represent animals exposed to postnatal ethanol while solid bars represent non-exposed control animals. The graph is organized by parental strains (left), low cell death strains (middle), and high cell death strains (right). ♀, female, ♂, male.

behavioral measures, and several behaviors that showed ethanol-induced behavioral differences within specific strains. Interestingly, the strains that showed the most effects of postnatal ethanol exposure were the high cell death strains, BXD48a and BXD100 (Figure 7). In fact, these were the only strains to show effects of postnatal ethanol exposure on learning and memory tasks. Taken together these results emphasize the effects of genetics and sex on ethanol-induced behavioral alterations while at the same time underscoring the complex nature of these effects.

Developmental alcohol exposure has been shown to affect a wide-range of behavioral measures related to activity, emotional regulation, and learning and memory, though the presence or severity of these behavioral phenotypes vary depending on the level and timing of alcohol exposure as well as the age of behavioral testing [as reviewed in (Chokroborty-Hoque et al., 2014; Patten et al., 2014; Marquardt and Brigman, 2016)]. While molecular dysfunction and developmental abnormalities such as synaptic activity and apoptosis have been extensively studied in animals exposed to postnatal ethanol (equivalent to the third trimester in humans), behavioral responses to exposure at this developmental time point have been understudied in comparison. Many behavioral studies have examined the effects of chronic exposure to prenatal ethanol (Chokroborty-Hoque et al., 2014; Patten et al., 2014; Marquardt and Brigman, 2016) while fewer studies have examined behavioral effects to postnatal alcohol exposure (Marquardt and Brigman, 2016). In addition, many of the studies that do investigate the effects of postnatal ethanol exposure on behavioral responses use a chronic exposure paradigm across multiple postnatal days with fewer studies examining the behavioral effects of acute postnatal alcohol exposure. In our current model, we used an acute one-day ethanol exposure paradigm which could explain why we did not replicate some previous studies that examine the effects of ethanol treatment on adolescent behavior (Hunt et al., 2009; Patten et al., 2014; Marquardt and Brigman, 2016).

The overall statistical analysis comparing all strains, sexes, and treatment groups found little significant differences, however, further investigation within each strain revealed effects of treatment and/or sex by treatment interactions for many behavioral measures in almost all strains. We propose that the overwhelmingly large effects of strain, followed by sex in many measures may have obscured the effects of ethanol treatment in the overall analyses. This is not unexpected based on previous literature that has shown large strain effects in the BXD recombinant inbred strains in behavioral measures without drug exposure during adulthood (Chesler et al., 2005; Philip et al., 2010; Knoll et al., 2016; Neuner et al., 2016). We have expanded previous results by investigating the effects of sex and strain during adolescence. Moreover, this is the first study to evaluate the long-term effects of ethanol exposure during brain development on adolescent behaviors in our genetic reference population.

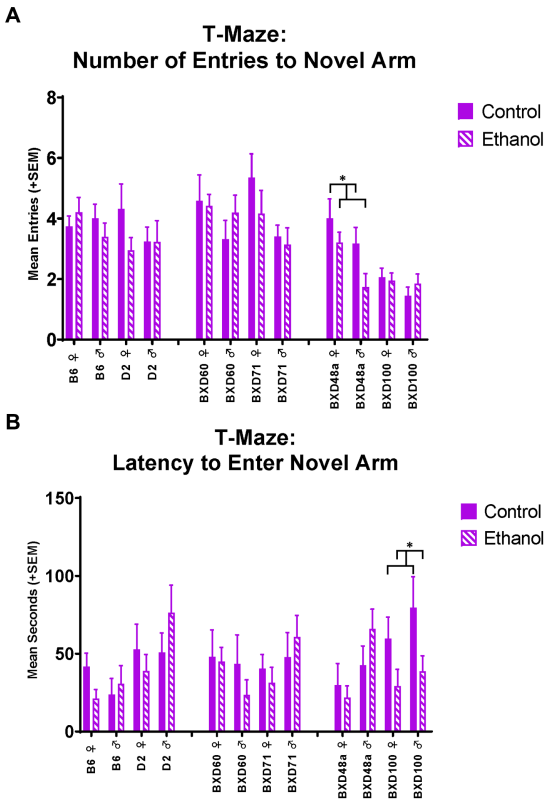


FIGURE 6
Effects of strain, ethanol, and sex on spatial learning and memory in the T-maze. **(A)** There was a significant effect of strain ($p < 0.001$) on number of entries to the novel, previously blocked, arm of the T-Maze during the short-term memory trial. The high cell death strain, BXD48a, showed a significant effect of ethanol in both sexes (*$p < 0.05$; BXD48a Ethanol < BXD48a Control) on number of entries to the novel arm. **(B)** In addition, there was also a significant effect of strain ($p < 0.05$) on latency to enter the novel arm of the T-Maze during the short-term memory trial. The other high cell death strain, BXD100, demonstrated a significant effect of ethanol (*$p < 0.05$; BXD100 Ethanol < BXD100 Control) on latency to enter the novel arm. Striped bars represent animals exposed to postnatal ethanol while solid bars represent non-exposed control animals. Graphs are organized by parental strains (left), low cell death strains (middle), and high cell death strains (right). ♀, Female, ♂, Male.

The BXD strains used in the current study were selected for their differential vulnerability to hippocampal cell death after exposure to postnatal ethanol (Goldowitz et al., 2014). The BXD100 and BXD48a strains were susceptible to high levels of ethanol induced cell death in the CA1 region of the hippocampus while the BXD60 and BXD71 strains were resistant to ethanol-induced cell death showing little to no difference compared to control animals (Goldowitz et al., 2014). This previous study also included the B6 and D2 parental strains which showed moderate levels of hippocampal cell death after postnatal ethanol exposure (Goldowitz et al., 2014).

While almost all strains showed effects of postnatal ethanol exposure in at least one measure of behavioral response, the strains that showed the most behavioral alterations after developmental ethanol exposure were the B6 and D2 parental strains as well as the high cell death strains, BXD100 and BXD48a (Figure 7). In these four strains, we observed many anxiety-like and/or activity-related behaviors that were significantly affected by postnatal ethanol exposure and in many of these measures there were sex-specific differences within the strain. The low cell death strains, BXD60 and BXD71, showed minimal effects of treatment in all behavioral tests. In the BXD60 strain, we did not observe effects of postnatal ethanol exposure on any of our behavioral measures. The BXD71 strain did show significant treatment effects in limited activity-related and anxiety-like behaviors.

The high cell death strains, BXD100 and BXD48a, were the only strains that showed significant effects of postnatal ethanol exposure in hippocampal-dependent spatial learning and memory assessments. The treatment effects in the BXD100 and BXD48a were often sex-specific and the direction of the behavioral response after postnatal ethanol exposure did not always indicate impairments in spatial learning. For example, spontaneous alternations in the Y-Maze showed significant treatment by sex interactions with ethanol-exposed BXD100 females and BXD48a males demonstrating impaired spatial memory. However, ethanol exposure had the opposite effects in the other sex of each strain: BXD100 male and BXD48a females. For the T-Maze, BXD100 ethanol-exposed males and females showed faster exploratory behavior in the novel arm during the short-term memory trial, indicative of enhanced short-term memory. In contrast, both male and female BXD48a mice exposed to postnatal ethanol showed reduced entries into the novel arm of the T-Maze indicative of impaired short-term memory. In addition, there was a trend toward significant effect of treatment for BXD48a ethanol-exposed discrimination between the arms of the T-Maze, indicating impaired short-term memory compared to non-exposed control BXD48a. While the high cell death strains did show effects of postnatal ethanol exposure on learning and memory behaviors, the relationship is more complex, not always indicating impairments. However, we want to emphasize that the only strains that showed effects in learning and memory tasks were the high cell death strains. More complex tasks that measure hippocampal related behaviors in a more in-depth manner and are less confounded by movement, may better clarify this in the future.

Our current study focused on examining strains that show differential cell death in the hippocampus after ethanol exposure during development as well as hippocampal-dependent learning and memory. However, the effects of ethanol-induced cell death during postnatal development in other brain regions can also affect long-term behavioral and cognitive measurements. For example, our previous study also identified differential susceptibility to ethanol-induced cell death in the cortex of BXD mice after postnatal alcohol exposure (Goldowitz et al., 2014). Interestingly, the level of cell death in each brain region showed uniformity in some strains while other strains showed regional specificity. For example, while the BXD100 strain was identified as a vulnerable strain for cell death in the hippocampus as well as the cortex, the BXD71 strain was resistant to cell death in the hippocampus but showed high susceptibility to cell death in layers 2/3 of the cortex (Goldowitz et al., 2014). Ethanol-induced cell death in other brain regions involved in cognition and attention, such as the cerebral cortex, could also impair learning and memory and may have had a strong impact on the results.

Previously, we examined gene expression differences in the neonatal hippocampus after acute ethanol exposure in the same

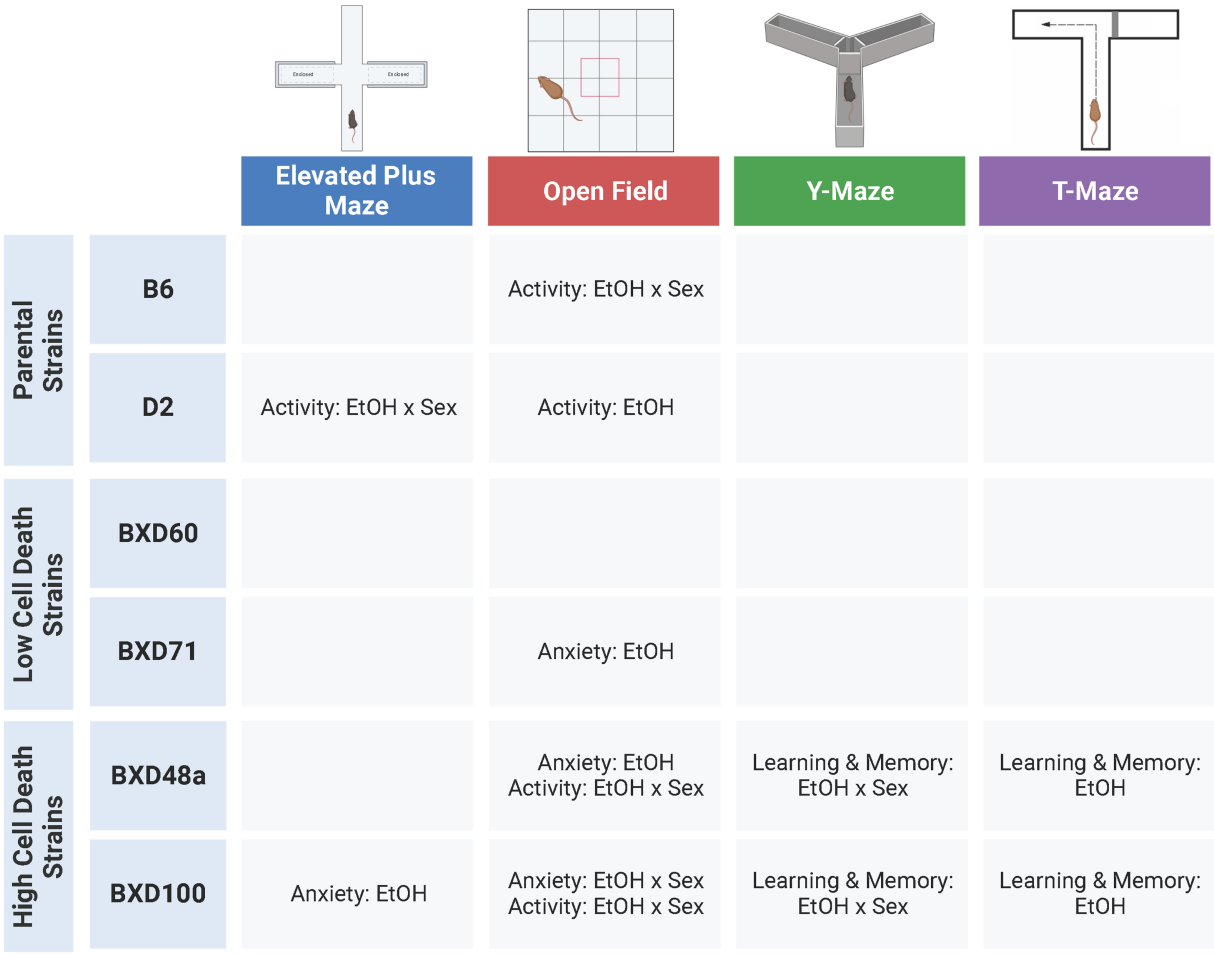


FIGURE 7
Summary of significant effects of ethanol across six strains and four behavioral tests. Adolescent behaviors were more effected by postnatal ethanol exposure in parental strains (B6, D2) and high cell death strains (BXD48a, BXD100). There were limited effects of ethanol exposure on adolescent behavior in the low cell death strains (BXD60, BXD71). Ethanol-induced alterations in learning and memory were only present in the high cell death strains. EtOH, Ethanol. Created with BioRender.com.

mouse strains used in the current study (Baker et al., 2022). Similar to the present findings, we found sex-specific effects of ethanol within each strain although few effects of sex were consistent across all strains. In addition, we previously identified ethanol-induced gene expression changes related to learning and memory that were unique in the high cell death strains, BXD48a and BXD100, such as, *Gadd45g* [growth arrest and DNA damage inducible gamma (Sultan and Sweatt, 2013; Sepp et al., 2017)], *Elavl2* [ELAV like RNA binding protein (Ustaoglu et al., 2021)], *Igf2r* [insulin like growth factor 2 receptor (Beletskiy et al., 2021)], and *Vegfa* [vascular endothelial growth factor A (Ping et al., 2019)]. Future studies could further investigate the role of these genes on long-term behavioral alterations induced by early developmental alcohol exposure.

We observed significant effects of sex and/or interactions between sex and ethanol exposure in many behavioral analyses. Every one of the six strains examined showed an effect of sex or interaction of sex and treatment in at least one of our behavioral measures. Interestingly, more sex-specific behaviors were seen in the anxiety-like and activity-related behaviors. However, for any given behavioral measure the effects of sex were often strain-specific and not seen across all strains. Likewise, the direction of sex-specific differences was not consistent across all behavioral measures and/or strains. This suggests a complex relationship between developmental ethanol exposure, sex, and strain on adolescent behavior. It is important to note that the original paper that identified the BXD strains did not report the sex of the subjects examined for the CA1 hippocampal cell death analysis but did use both male and female subjects (Goldowitz et al., 2014). Moreover, age-related sex-specific differences in the hippocampus have been identified (Nunez and McCarthy, 2007). Interestingly in our previous gene expression study on these strains (Baker et al., 2022), we found significant effects of sex on ethanol-induced gene expression in the neonatal hippocampus within each strain. However, there were significant ethanol-induced gene expression changes across all strains and sex-dependent effects were only observed within a strain (Baker et al., 2022).

While we saw an effect of ethanol exposure within strains, our treatment effect on hippocampal learning and memory were not as robust as previous studies have found. While part of this could be strain-specific, we did not observe impaired spatial learning and memory in the B6 strains which is a highly used strain in behavioral

studies assessing the effects of developmental alcohol exposure. An explanation for why we did not have a larger ethanol effect on behavioral responses could be due to the type of behavioral tests performed and the age of behavioral testing. For example, behavioral studies in adolescent animals exposed to acute postnatal ethanol have observed learning and memory impairments using more complex behavioral measures such as the Morris water maze, object recognition test, fear conditioning, and radial arm maze (Wozniak et al., 2004; Wagner and Hunt, 2006; Ieraci and Herrera, 2007; Wagner et al., 2014). Many of these experimental tests also included either a positive component such as a food pellet reward or a negative component such as a foot shock or forced water placement (Wozniak et al., 2004; Ieraci and Herrera, 2007; Wagner et al., 2014). In addition, all animals were tested in all behavioral tasks and while the order of the task was chosen to limit carry-over effects based on prior literature (Thomas et al., 2010; Risbud et al., 2022), this is still a limitation. Also, it is important to note that the behavioral tests used in the current study were highly dependent on activity. Since there were such robust effects of strain on activity levels, this could be overriding some of our ethanol-related effects. Future studies examining differential behavioral responses after exposure to developmental alcohol in these strains should take into account the significant strain effect on activity.

In addition, our behavioral results did show large individual variability within a strain, sex, and exposure group for many of our measures, especially in ethanol-exposed animals. This large variation could be due to the age of behavioral testing, as adolescent mice tend to show more behavioral variability than adult mice (Brust et al., 2015). Future studies could address large variation in behavioral measures by adding more subjects per group and running additional analyses to identify outliers. Although our study found large variability in animal behavior, we were still able to identify multiple behavioral measures effected by acute postnatal ethanol exposure including differences in activity, anxiety, and learning and memory behaviors in the BXD strains and B6 and D2 parental strains. Moreover, we assessed behavior on strains that showed differential cell death in the CA1 region of the hippocampus after ethanol exposure on postnatal day 7 and further studies can address cell counts in adult animals after behavioral testing.

This study emphasizes the importance of the role of genetics in ethanol-induced behavioral alterations. Moreover, the results are further influenced by sex as shown by strain-specific effects of sex. Our results support our hypothesis that adolescent behaviors were most affected by acute neonatal ethanol exposure in BXD strains that showed high ethanol-induced cell death in the postnatal hippocampus, particularly in behaviors related to learning and memory, which are highly dependent on the hippocampus. In contrast, BXD strains that showed low vulnerability to ethanol-induced cell death demonstrated limited effects of ethanol exposure on adolescent behavior. In conclusion, we found evidence for interactions among strain and sex, demonstrating that these factors have a complex effect on ethanol-induced responses and that both are important considerations for evaluating ethanol's effects. These results support the inclusion of multiple strains and the evaluation of both males and females in behavioral studies examining the effects of developmental alcohol exposure. By evaluating multiple strains and both sexes, we can better understand the effects of genetic background and sex on alcohol-induced neurobehavioral abnormalities.

Data availability statement

The raw data supporting the conclusions of this article will be made available by the authors, without undue reservation.

Ethics statement

The animal study protocol was approved by the Institutional Animal Care and Use Committee of the University of Tennessee Health Science Center.

Author contributions

JB, MM, and KH contributed to conception and design of the study. JB organized the database and performed the analyses under guidance of MM and KH. JB wrote the first draft of the manuscript with guidance from KH. All authors contributed to manuscript revisions, read, and approved the submitted version.

Funding

This research was funded by the National Institute on Alcohol Abuse and Alcoholism R01AA023508 (KH), F31AA026498 (JB), T32AA013525–21 (JB) and University of Tennessee Health Science Center CORNET Award.

Acknowledgments

The authors would like to thank the Neuroscience Institute and the Behavioral Core at the University of Tennessee Health Science Center for the use of behavioral equipment.

Conflict of interest

The authors declare that the research was conducted in the absence of any commercial or financial relationships that could be construed as a potential conflict of interest.

Publisher's note

All claims expressed in this article are solely those of the authors and do not necessarily represent those of their affiliated organizations, or those of the publisher, the editors and the reviewers. Any product that may be evaluated in this article, or claim that may be made by its manufacturer, is not guaranteed or endorsed by the publisher.

Supplementary material

The Supplementary material for this article can be found online at: https://www.frontiersin.org/articles/10.3389/10.3389/fnins.2023.1197292/full#supplementary-material

References

Alfonso-Loeches, S., and Guerri, C. (2011). Molecular and behavioral aspects of the actions of alcohol on the adult and developing brain. *Crit. Rev. Clin. Lab. Sci.* 48, 19–47. doi: 10.3109/10408363.2011.580567

Astley, S. J. (2010). Profile of the first 1,400 patients receiving diagnostic evaluations for fetal alcohol spectrum disorder at the Washington state fetal alcohol syndrome diagnostic & prevention network. *Can. J. Clin. Pharmacol.* 17, e132–e164.

Astley, S. J., Aylward, E. H., Olson, H. C., Kerns, K., Brooks, A., Coggins, T. E., et al. (2009). Functional magnetic resonance imaging outcomes from a comprehensive magnetic resonance study of children with fetal alcohol spectrum disorders. *J. Neurodev. Disord.* 1, 61–80. doi: 10.1007/s11689-009-9004-0

Bailey, K.R., and Crawley, J.N. (2009). *Anxiety-related behaviors in mice, in methods of behavior analysis in neuroscience, nd and J.J. Buccafusco, editors*. Boca Raton, FL: Taylor & Francis.

Baker, J. A., Brettin, J. T., Mulligan, M. K., and Hamre, K. M. (2022). Effects of genetics and sex on acute gene expression changes in the Hippocampus following neonatal ethanol exposure in BXD recombinant inbred mouse strains. *Brain Sci.* 12, 1–23. doi: 10.3390/brainsci12121634

Baker, J. A., Li, J., Zhou, D., Yang, M., Cook, M. N., Jones, B. C., et al. (2017). Analyses of differentially expressed genes after exposure to acute stress, acute ethanol, or a combination of both in mice. *Alcohol* 58, 139–151. doi: 10.1016/j.alcohol.2016.08.008

Basavarajappa, B. S., Nagre, N. N., Xie, S., and Subbanna, S. (2014). Elevation of endogenous anandamide impairs LTP, learning, and memory through CB1 receptor signaling in mice. *Hippocampus* 24, 808–818. doi: 10.1002/hipo.22272

Beletskiy, A., Chesnokova, E., and Bal, N. (2021). Insulin-like growth factor 2 as a possible neuroprotective agent and memory enhancer-its comparative expression, processing and signaling in mammalian CNS. *Int. J. Mol. Sci.* 22, 1–44. doi: 10.3390/ijms22041849

Bertrand, J., Floyd, L. L., and Weber, M. K.Fetal Alcohol Syndrome Prevention Team, Division of Birth Defects and Developmental Disabilities, National Center on Birth Defects and Developmental Disabilities, Centers for Disease Control and Prevention (CDC) (2005). Guidelines for identifying and referring persons with fetal alcohol syndrome. *MMWR Recomm. Rep.* 54, 1–14.

Blokland, G. A. M., Grove, J., Chen, C. Y., Cotsapas, C., Tobet, S., Handa, R., et al. (2022). Sex-dependent shared and nonshared genetic architecture across mood and psychotic disorders. *Biol. Psychiatry* 91, 102–117. doi: 10.1016/j.biopsych.2021.02.972

Boehm II, S. L., Lundahl, K. R., Caldwell, J., and Gilliam, D. M. (1997). Ethanol teratogenesis in the C57BL/6J, DBA/2J, and a/J inbred mouse strains. *Alcohol* 14, 389–395. doi: 10.1016/S0741-8329(97)87950-5

Brady, M. L., Allan, A. M., and Caldwell, K. K. (2012). A limited access mouse model of prenatal alcohol exposure that produces long-lasting deficits in hippocampal-dependent learning and memory. *Alcohol. Clin. Exp. Res.* 36, 457–466. doi: 10.1111/j.1530-0277.2011.01644.x

Brust, V., Schindler, P. M., and Lewejohann, L. (2015). Lifetime development of behavioural phenotype in the house mouse (*Mus musculus*). *Front. Zool.* 12:S17. doi: 10.1186/1742-9994-12-S1-S17

Cantacorps, L., Alfonso-Loeches, S., Moscoso-Castro, M., Cuitavi, J., Gracia-Rubio, I., López-Arnau, R., et al. (2017). Maternal alcohol binge drinking induces persistent neuroinflammation associated with myelin damage and behavioural dysfunctions in offspring mice. *Neuropharmacology* 123, 368–384. doi: 10.1016/j.neuropharm.2017.05.034

Castelhano-Carlos, M. J., Sousa, N., Ohl, F., and Baumans, V. (2010). Identification methods in newborn C57BL/6 mice: a developmental and behavioural evaluation. *Lab. Anim.* 44, 88–103. doi: 10.1258/la.2009.009044

Cha, J., Greenberg, T., Song, I., Blair Simpson, H., Posner, J., and Mujica-Parodi, L. R. (2016). Abnormal hippocampal structure and function in clinical anxiety and comorbid depression. *Hippocampus* 26, 545–553. doi: 10.1002/hipo.22566

Chasnoff, I. J. (1985). Fetal alcohol syndrome in twin pregnancy. *Acta Genet. Med. Gemellol.* 34, 229–232. doi: 10.1017/S0001566000004797

Chen, Y., Ozturk, N. C., Ni, L., Goodlett, C., and Zhou, F. C. (2011). Strain differences in developmental vulnerability to alcohol exposure via embryo culture in mice. *Alcohol. Clin. Exp. Res.* 35, 1293–1304. doi: 10.1111/j.1530-0277.2011.01465.x

Chesler, E. J., Lu, L., Shou, S., Qu, Y., Gu, J., Wang, J., et al. (2005). Complex trait analysis of gene expression uncovers polygenic and pleiotropic networks that modulate nervous system function. *Nat. Genet.* 37, 233–242. doi: 10.1038/ng1518

Chokroborty-Hoque, A., Alberry, B., and Singh, S. M. (2014). Exploring the complexity of intellectual disability in fetal alcohol spectrum disorders. *Front. Pediatr.* 2:90. doi: 10.3389/fped.2014.00090

Christoffel, K. K., and Salafsky, I. (1975). Fetal alcohol syndrome in dizygotic twins. *J. Pediatr.* 87, 963–967. doi: 10.1016/S0022-3476(75)80919-X

Coles, C. D., Brown, R. T., Smith, I. E., Platzman, K. A., Erickson, S., and Falek, A. (1991). Effects of prenatal alcohol exposure at school age. I. Physical and cognitive development. *Neurotoxicol. Teratol.* 13, 357–367. doi: 10.1016/0892-0362(91)90084-A

Coles, C. D., Grant, T. M., Kable, J. A., Stoner, S. A., and Perez, A.the Collaborative Initiative on Fetal Alcohol Spectrum Disorders (2022). Prenatal alcohol exposure and mental health at midlife: a preliminary report on two longitudinal cohorts. *Alcohol. Clin. Exp. Res.* 46, 232–242. doi: 10.1111/acer.14761

Cook, M. N., Baker, J. A., Heldt, S. A., Williams, R. W., Hamre, K. M., and Lu, L. (2015). Identification of candidate genes that underlie the QTL on chromosome 1 that mediates genetic differences in stress-ethanol interactions. *Physiol. Genomics* 47, 308–317. doi: 10.1152/physiolgenomics.00114.2014

Crabbe, J. C., and Belknap, J. K. (1992). Genetic approaches to drug dependence. *Trends Pharmacol. Sci.* 13, 212–219. doi: 10.1016/0165-6147(92)90066-F

Downing, C., Balderrama-Durbin, C., Broncucia, H., Gilliam, D., and Johnson, T. E. (2009). Ethanol teratogenesis in five inbred strains of mice. *Alcohol. Clin. Exp. Res.* 33, 1238–1245. doi: 10.1111/j.1530-0277.2009.00949.x

Downing, C., Balderrama-Durbin, C., Kimball, A., Biers, J., Wright, H., Gilliam, D., et al. (2012). Quantitative trait locus mapping for ethanol teratogenesis in BXD recombinant inbred mice. *Alcohol. Clin. Exp. Res.* 36, 1340–1354. doi: 10.1111/j.1530-0277.2012.01754.x

Dursun, I., Jakubowska-Dogru, E., and Uzbay, T. (2006). Effects of prenatal exposure to alcohol on activity, anxiety, motor coordination, and memory in young adult Wistar rats. *Pharmacol. Biochem. Behav.* 85, 345–355. doi: 10.1016/j.pbb.2006.09.001

Fidalgo, S., Skipper, C., Takyi, A., McIver, A., Tsiligkaridis, T., Quadir, A., et al. (2017). Low-dose chronic prenatal alcohol exposure abolishes the pro-cognitive effects of angiotensin IV. *Behav. Brain Res.* 329, 140–147. doi: 10.1016/j.bbr.2017.04.042

Fish, E. W., Holloway, H. T., Rumple, A., Baker, L. K., Wieczorek, L. A., Moy, S. S., et al. (2016). Acute alcohol exposure during neurulation: behavioral and brain structural consequences in adolescent C57BL/6J mice. *Behav. Brain Res.* 311, 70–80. doi: 10.1016/j.bbr.2016.05.004

Flannigan, K., Unsworth, K., and Harding, K. (2018). *The prevalence of fetal alcohol Spectrum disorder*. Vancouver, British Columbia, Canada: FASD Research Network, 1–4.

Fontaine, C. J., Patten, A. R., Sickmann, H. M., Helfer, J. L., and Christie, B. R. (2016). Effects of pre-natal alcohol exposure on hippocampal synaptic plasticity: sex, age and methodological considerations. *Neurosci. Biobehav. Rev.* 64, 12–34. doi: 10.1016/j.neubiorev.2016.02.014

Ghasemi, M., Navidhamidi, M., Rezaei, F., Azizikia, A., and Mehranfard, N. (2022). Anxiety and hippocampal neuronal activity: relationship and potential mechanisms. *Cogn. Affect. Behav. Neurosci.* 22, 431–449. doi: 10.3758/s13415-021-00973-y

Gilliam, D. M., Stilman, A., Dudek, B. C., and Riley, E. P. (1987). Fetal alcohol effects in long- and short-sleep mice: activity, passive avoidance, and in utero ethanol levels. *Neurotoxicol. Teratol.* 9, 349–357. doi: 10.1016/0892-0362(87)90030-4

Gil-Mohapel, J., Boehme, F., Kainer, L., and Christie, B. R. (2010). Hippocampal cell loss and neurogenesis after fetal alcohol exposure: insights from different rodent models. *Brain Res. Rev.* 64, 283–303. doi: 10.1016/j.brainresrev.2010.04.011

Glass, L., Graham, D. M., Deweese, B. N., Jones, K. L., Riley, E. P., and Mattson, S. N. (2014). Correspondence of parent report and laboratory measures of inattention and hyperactivity in children with heavy prenatal alcohol exposure. *Neurotoxicol. Teratol.* 42, 43–50. doi: 10.1016/j.ntt.2014.01.007

Goldowitz, D., Lussier, A. A., Boyle, J. K., Wong, K., Lattimer, S. L., Dubose, C., et al. (2014). Molecular pathways underpinning ethanol-induced neurodegeneration. *Front. Genet.* 5:203. doi: 10.3389/fgene.2014.00203

Goodlett, C. R., Gilliam, D. M., Nichols, J. M., and West, J. R. (1989). Genetic influences on brain growth restriction induced by development exposure to alcohol. *Neurotoxicology* 10, 321–334.

Green, M. L., Singh, A. V., Zhang, Y., Nemeth, K. A., Sulik, K. K., and Knudsen, T. B. (2007). Reprogramming of genetic networks during initiation of the fetal alcohol syndrome. *Dev. Dyn.* 236, 613–631. doi: 10.1002/dvdy.21048

Guerri, C., Bazinet, A., and Riley, E. P. (2009). Foetal alcohol Spectrum disorders and alterations in brain and behaviour. *Alcohol Alcohol.* 44, 108–114. doi: 10.1093/alcalc/agn105

Hamilton, D. A., Kodituwakku, P., Sutherland, R. J., and Savage, D. D. (2003). Children with fetal alcohol syndrome are impaired at place learning but not cued-navigation in a virtual Morris water task. *Behav. Brain Res.* 143, 85–94. doi: 10.1016/S0166-4328(03)00028-7

Hamilton, D. A., Magcalas, C. M., Barto, D., Bird, C. W., Rodriguez, C. I., Fink, B. C., et al. (2014). Moderate prenatal alcohol exposure and quantification of social behavior in adult rats. *J. Vis. Exp.* 94, 274–290. doi: 10.3791/52407-v

Hamilton, G. F., Murawski, N. J., St Cyr, S. A., Jablonski, S. A., Schiffino, F. L., Stanton, M. E., et al. (2011). Neonatal alcohol exposure disrupts hippocampal neurogenesis and contextual fear conditioning in adult rats. *Brain Res.* 1412, 88–101. doi: 10.1016/j.brainres.2011.07.027

Hellemans, K. G., Verma, P., Yoon, E., Yu, W. K., Young, A. H., and Weinberg, J. (2010). Prenatal alcohol exposure and chronic mild stress differentially alter depressive- and anxiety-like behaviors in male and female offspring. *Alcohol. Clin. Exp. Res.* 34, 633–645. doi: 10.1111/j.1530-0277.2009.01132.x

Herman, L. E., Acosta, M. C., and Chang, P. N. (2008). Gender and attention deficits in children diagnosed with a fetal alcohol Spectrum disorder. *Can. J. Clin. Pharmacol.* 15, e411–e419.

Holcomb, L., Gordon, M. N., McGowan, E., Yu, X., Benkovic, S., Jantzen, P., et al. (1998). Accelerated Alzheimer-type phenotype in transgenic mice carrying both mutant amyloid precursor protein and presenilin 1 transgenes. *Nat. Med.* 4, 97–100. doi: 10.1038/nm0198-097

Hunt, P. S., Jacobson, S. E., and Torok, E. J. (2009). Deficits in trace fear conditioning in a rat model of fetal alcohol exposure: dose-response and timing effects. *Alcohol* 43, 465–474. doi: 10.1016/j.alcohol.2009.08.004

Ieraci, A., and Herrera, D. G. (2007). Single alcohol exposure in early life damages hippocampal stem/progenitor cells and reduces adult neurogenesis. *Neurobiol. Dis.* 26, 597–605. doi: 10.1016/j.nbd.2007.02.011

Jimenez, J. C., Su, K., Goldberg, A. R., Luna, V. M., Biane, J. S., Ordek, G., et al. (2018). Anxiety cells in a hippocampal-hypothalamic circuit. *Neuron* 97, 670–683.e6. doi: 10.1016/j.neuron.2018.01.016

Kelly, S. J., Goodlett, C. R., Hulsether, S. A., and West, J. R. (1988). Impaired spatial navigation in adult female but not adult male rats exposed to alcohol during the brain growth spurt. *Behav. Brain Res.* 27, 247–257. doi: 10.1016/0166-4328(88)90121-0

Kelly, S. J., Leggett, D. C., and Cronise, K. (2009). Sexually dimorphic effects of alcohol exposure during development on the processing of social cues. *Alcohol Alcohol.* 44, 555–560. doi: 10.1093/alcalc/agp061

Khoury, J. E., Jamieson, B., and Milligan, K. (2018). Risk for childhood internalizing and externalizing behavior problems in the context of prenatal alcohol exposure: a meta-analysis and comprehensive examination of moderators. *Alcohol. Clin. Exp. Res.* 42, 1358–1377. doi: 10.1111/acer.13805

Kim, P., Park, J. H., Choi, C. S., Choi, I., Joo, S. H., Kim, M. K., et al. (2013). Effects of ethanol exposure during early pregnancy in hyperactive, inattentive and impulsive behaviors and MeCP2 expression in rodent offspring. *Neurochem. Res.* 38, 620–631. doi: 10.1007/s11064-012-0960-5

Knoll, A. T., Halladay, L. R., Holmes, A., and Levitt, P. (2016). Quantitative trait loci and a novel genetic candidate for fear learning. *J. Neurosci.* 36, 6258–6268. doi: 10.1523/JNEUROSCI.0177-16.2016

Lakens, D. (2013). Calculating and reporting effect sizes to facilitate cumulative science: a practical primer for t-tests and ANOVAs. *Front. Psychol.* 4:863. doi: 10.3389/fpsyg.2013.00863

Lossie, A. C., Muir, W. M., Lo, C. L., Timm, F., Liu, Y., Gray, W., et al. (2014). Implications of genomic signatures in the differential vulnerability to fetal alcohol exposure in C57BL/6 and DBA/2 mice. *Front. Genet.* 5:173. doi: 10.3389/fgene.2014.00173

Marquardt, K., and Brigman, J. L. (2016). The impact of prenatal alcohol exposure on social, cognitive and affective behavioral domains: insights from rodent models. *Alcohol* 51, 1–15. doi: 10.1016/j.alcohol.2015.12.002

Mattson, S. N., Bernes, G. A., and Doyle, L. R. (2019). Fetal alcohol Spectrum disorders: a review of the neurobehavioral deficits associated with prenatal alcohol exposure. *Alcohol. Clin. Exp. Res.* 43, 1046–1062. doi: 10.1111/acer.14040

Mattson, S. N., Crocker, N., and Nguyen, T. T. (2011). Fetal alcohol spectrum disorders: neuropsychological and behavioral features. *Neuropsychol. Rev.* 21, 81–101. doi: 10.1007/s11065-011-9167-9

Mattson, S. N., and Riley, E. P. (2000). Parent ratings of behavior in children with heavy prenatal alcohol exposure and IQ-matched controls. *Alcohol. Clin. Exp. Res.* 24, 226–231. doi: 10.1111/j.1530-0277.2000.tb04595.x

May, P. A., Baete, A., Russo, J., Elliott, A. J., Blankenship, J., Kalberg, W. O., et al. (2014). Prevalence and characteristics of fetal alcohol spectrum disorders. *Pediatrics* 134, 855–866. doi: 10.1542/peds.2013-3319

May, P. A., Chambers, C. D., Kalberg, W. O., Zellner, J., Feldman, H., Buckley, D., et al. (2018). Prevalence of fetal alcohol Spectrum disorders in 4 US communities. *JAMA* 319, 474–482. doi: 10.1001/jama.2017.21896

May, P. A., Tabachnick, B., Hasken, J. M., Marais, A. S., de Vries, M. M., Barnard, R., et al. (2017). Who is most affected by prenatal alcohol exposure: boys or girls? *Drug Alcohol Depend.* 177, 258–267. doi: 10.1016/j.drugalcdep.2017.04.010

Moore, E. M., Glass, L., Infante, M. A., Coles, C. D., Kable, J. A., Jones, K. L., et al. (2021). Cross-sectional analysis of spatial working memory development in children with histories of heavy prenatal alcohol exposure. *Alcohol. Clin. Exp. Res.* 45, 215–223. doi: 10.1111/acer.14506

Moore, D. B., Madorsky, I., Paiva, M., and Barrow Heaton, M. (2004). Ethanol exposure alters neurotrophin receptor expression in the rat central nervous system: effects of neonatal exposure. *J. Neurobiol.* 60, 114–126. doi: 10.1002/neu.20010

Neuner, S. M., Garfinkel, B. P., Wilmott, L. A., Ignatowska-Jankowska, B. M., Citri, A., Orly, J., et al. (2016). Systems genetics identifies Hp1bp3 as a novel modulator of cognitive aging. *Neurobiol. Aging* 46, 58–67. doi: 10.1016/j.neurobiolaging.2016.06.008

Nunez, J. L., and McCarthy, M. M. (2007). Evidence for an extended duration of GABA-mediated excitation in the developing male versus female hippocampus. *Dev. Neurobiol.* 67, 1879–1890. doi: 10.1002/dneu.20567

Ogawa, T., Kuwagata, M., Ruiz, J., and Zhou, F. C. (2005). Differential teratogenic effect of alcohol on embryonic development between C57BL/6 and DBA/2 mice: a new view. *Alcohol. Clin. Exp. Res.* 29, 855–863. doi: 10.1097/01.ALC.0000163495.71181.10

Paluch, L. R., Lieggi, C. C., Dumont, M., Monette, S., Riedel, E. R., and Lipman, N. S. (2014). Developmental and behavioral effects of toe clipping on neonatal and preweanling mice with and without vapocoolant anesthesia. *J. Am. Assoc. Lab. Anim. Sci.* 53, 132–140.

Patten, A. R., Fontaine, C. J., and Christie, B. R. (2014). A comparison of the different animal models of fetal alcohol spectrum disorders and their use in studying complex behaviors. *Front. Pediatr.* 2:93. doi: 10.3389/fped.2014.00093

Philip, V. M., Duvvuru, S., Gomero, B., Ansah, T. A., Blaha, C. D., Cook, M. N., et al. (2010). High-throughput behavioral phenotyping in the expanded panel of BXD recombinant inbred strains. *Genes Brain Behav.* 9, 129–159. doi: 10.1111/j.1601-183X.2009.00540.x

Ping, S., Qiu, X., Kyle, M., Hughes, K., Longo, J., and Zhao, L. R. (2019). Stem cell factor and granulocyte colony-stimulating factor promote brain repair and improve cognitive function through VEGF-A in a mouse model of CADASIL. *Neurobiol. Dis.* 132:104561. doi: 10.1016/j.nbd.2019.104561

Plummer, J. T., Evgrafov, O. V., Bergman, M. Y., Friez, M., Haiman, C. A., Levitt, P., et al. (2013). Transcriptional regulation of the MET receptor tyrosine kinase gene by MeCP2 and sex-specific expression in autism and Rett syndrome. *Transl. Psychiatry* 3:e316. doi: 10.1038/tp.2013.91

Riley, E. P., Barron, S., Melcer, T., and Gonzalez, D. (1993). Alterations in activity following alcohol administration during the third trimester equivalent in P and NP rats. *Alcohol. Clin. Exp. Res.* 17, 1240–1246. doi: 10.1111/j.1530-0277.1993.tb05236.x

Riley, E. P., and McGee, C. L. (2005). Fetal alcohol spectrum disorders: an overview with emphasis on changes in brain and behavior. *Exp. Biol. Med.* 230, 357–365. doi: 10.1177/15353702-0323006-03

Risbud, R. D., Breit, K. R., and Thomas, J. D. (2022). Early developmental alcohol exposure alters behavioral outcomes following adolescent re-exposure in a rat model. *Alcohol. Clin. Exp. Res.* 46, 1993–2009. doi: 10.1111/acer.14950

Sarnyai, Z., Sibille, E. L., Pavlides, C., Fenster, R. J., McEwen, B. S., and Tóth, M. (2000). Impaired hippocampal-dependent learning and functional abnormalities in the hippocampus in mice lacking serotonin(1A) receptors. *Proc. Natl. Acad. Sci.* 97, 14731–14736. doi: 10.1073/pnas.97.26.14731

Sayal, K., Heron, J., Golding, J., and Emond, A. (2007). Prenatal alcohol exposure and gender differences in childhood mental health problems: a longitudinal population-based study. *Pediatrics* 119, e426–e434. doi: 10.1542/peds.2006-1840

Schaafsma, S. M., and Pfaff, D. W. (2014). Etiologies underlying sex differences in autism Spectrum disorders. *Front. Neuroendocrinol.* 35, 255–271. doi: 10.1016/j.yfrne.2014.03.006

Schaefer, D. C., Asner, I. N., Seifert, B., BÜRki, K., and Cinelli, P. (2010). Analysis of physiological and behavioural parameters in mice after toe clipping as newborns. *Lab. Anim.* 44, 7–13. doi: 10.1258/la.2009.009020

Schaffner, S. L., Lussier, A. A., Baker, J. A., Goldowitz, D., Hamre, K. M., and Kobor, M. S. (2020). Neonatal alcohol exposure in mice induces select differentiation- and apoptosis-related chromatin changes both independent of and dependent on sex. *Front. Genet.* 11:35. doi: 10.3389/fgene.2020.00035

Sepp, M., Vihma, H., Nurm, K., Urb, M., Page, S. C., Roots, K., et al. (2017). The intellectual disability and schizophrenia associated transcription factor TCF4 is regulated by neuronal activity and protein kinase a. *J. Neurosci.* 37, 10516–10527. doi: 10.1523/JNEUROSCI.1151-17.2017

Shivakumar, M., Subbanna, S., Joshi, V., and Basavarajappa, B. S. (2020). Postnatal ethanol exposure activates HDAC-mediated histone deacetylation, impairs synaptic plasticity gene expression and behavior in mice. *Int. J. Neuropsychopharmacol.* 23, 324–338. doi: 10.1093/ijnp/pyaa017

Subbanna, S., and Basavarajappa, B. S. (2014). Pre-administration of G9a/GLP inhibitor during synaptogenesis prevents postnatal ethanol-induced LTP deficits and neurobehavioral abnormalities in adult mice. *Exp. Neurol.* 261, 34–43. doi: 10.1016/j.expneurol.2014.07.003

Subbanna, S., Nagre, N. N., Shivakumar, M., Umapathy, N. S., Psychoyos, D., and Basavarajappa, B. S. (2014). Ethanol induced acetylation of histone at G9a exon1 and G9a-mediated histone H3 dimethylation leads to neurodegeneration in neonatal mice. *Neuroscience* 258, 422–432. doi: 10.1016/j.neuroscience.2013.11.043

Subbanna, S., Shivakumar, M., Psychoyos, D., Xie, S., and Basavarajappa, B. S. (2013). Anandamide-CB1 receptor signaling contributes to postnatal ethanol-induced neonatal neurodegeneration, adult synaptic, and memory deficits. *J. Neurosci.* 33, 6350–6366. doi: 10.1523/JNEUROSCI.3786-12.2013

Sultan, F. A., and Sweatt, J. D. (2013). The role of the Gadd45 family in the nervous system: a focus on neurodevelopment, neuronal injury, and cognitive neuroepigenetics. *Adv. Exp. Med. Biol.* 793, 81–119. doi: 10.1007/978-1-4614-8289-5_6

Taylor, B. A., Wnek, C., Kotlus, B. S., Roemer, N., MacTaggart, T., and Phillips, S. J. (1999). Genotyping new BXD recombinant inbred mouse strains and comparison of BXD and consensus maps. *Mamm. Genome* 10, 335–348. doi: 10.1007/s003359900998

Théberge, E. T., Baker, J. A., Dubose, C., Boyle, J. K., Balce, K., Goldowitz, D., et al. (2019). Genetic influences on the amount of cell death in the neural tube of BXD mice exposed to acute ethanol at Midgestation. *Alcohol. Clin. Exp. Res.* 43, 439–452. doi: 10.1111/acer.13947

Thomas, J. D., Burchette, T. L., Dominguez, H. D., and Riley, E. P. (2000). Neonatal alcohol exposure produces more severe motor coordination deficits in high alcohol sensitive rats compared to low alcohol sensitive rats. *Alcohol* 20, 93–99. doi: 10.1016/S0741-8329(99)00080-4

Thomas, J. D., Idrus, N. M., Monk, B. R., and Dominguez, H. D. (2010). Prenatal choline supplementation mitigates behavioral alterations associated with prenatal alcohol exposure in rats. *Birth Defects Res. A Clin. Mol. Teratol.* 88, 827–837. doi: 10.1002/bdra.20713

Thomas, J. D., Melcer, T., Weinert, S., and Riley, E. P. (1998). Neonatal alcohol exposure produces hyperactivity in high-alcohol-sensitive but not in low-alcohol-sensitive rats. *Alcohol* 16, 237–242. doi: 10.1016/S0741-8329(98)00008-1

Ustaoglu, P., Gill, J. K., Doubovetzky, N., Haussmann, I. U., Dix, T. C., Arnold, R., et al. (2021). Dynamically expressed single ELAV/Hu orthologue elavl2 of bees is required for learning and memory. *Commun Biol* 4:1234. doi: 10.1038/s42003-021-02763-1

Wagner, A. F., and Hunt, P. S. (2006). Impaired trace fear conditioning following neonatal ethanol: reversal by choline. *Behav. Neurosci.* 120, 482–487. doi: 10.1037/0735-7044.120.2.482

Wagner, J. L., Zhou, F. C., and Goodlett, C. R. (2014). Effects of one-and three-day binge alcohol exposure in neonatal C57BL/6 mice on spatial learning and memory in adolescence and adulthood. *Alcohol* 48, 99–111. doi: 10.1016/j.alcohol.2013.12.001

Wang, G., Chen, L., Chen, H., Li, Y., Xu, Y., Xing, Y., et al. (2022). Glutamate receptor interacting protein 1 in the dorsal CA1 drives alpha-amino-3-hydroxy-5-methyl-4-Isoxazolepropionic acid receptor endocytosis and exocytosis Bidirectionally and mediates forgetting, exploratory, and anxiety-like behavior. *Neuroscience* 498, 235–248. doi: 10.1016/j.neuroscience.2022.07.009

Wang, X., Pandey, A. K., Mulligan, M. K., Williams, E. G., Mozhui, K., Li, Z., et al. (2016). Joint mouse-human phenome-wide association to test gene function and disease risk. *Nat. Commun.* 7:10464. doi: 10.1038/ncomms10464

Wickham, H. (2016). *ggplot2: Elegant graphics for data analysis, in use R!*. New York City, New York, United States: Springer International Publishing.

Willoughby, K. A., Sheard, E. D., Nash, K., and Rovet, J. (2008). Effects of prenatal alcohol exposure on hippocampal volume, verbal learning, and verbal and spatial recall in late childhood. *J. Int. Neuropsychol. Soc.* 14, 1022–1033. doi: 10.1017/S1355617708081368

Woods, K. J., Thomas, K. G. F., Molteno, C. D., Jacobson, J. L., Jacobson, S. W., and Meintjes, E. M. (2018). Prenatal alcohol exposure affects brain function during place learning in a virtual environment differently in boys and girls. *Brain Behav.* 8:e01103. doi: 10.1002/brb3.1103

Wozniak, J. R., Riley, E. P., and Charness, M. E. (2019). Clinical presentation, diagnosis, and management of fetal alcohol spectrum disorder. *Lancet Neurol.* 18, 760–770. doi: 10.1016/S1474-4422(19)30150-4

Wozniak, D. F., Hartman, R. E., Boyle, M. P., Vogt, S. K., Brooks, A. R., Tenkova, T., et al. (2004). Apoptotic neurodegeneration induced by ethanol in neonatal mice is associated with profound learning/memory deficits in juveniles followed by progressive functional recovery in adults. *Neurobiol. Dis.* 17, 403–414. doi: 10.1016/j.nbd.2004.08.006

Xu, W., Hawkey, A. B., Li, H., Dai, L., Brim, H. H., Frank, J. A., et al. (2018). Neonatal ethanol exposure causes behavioral deficits in Young mice. *Alcohol. Clin. Exp. Res.* 42, 743–750. doi: 10.1111/acer.13598

Zhao, N., Ren, Y., Yamazaki, Y., Qiao, W., Li, F., Felton, L. M., et al. (2020). Alzheimer's risk factors age, APOE genotype, and sex drive distinct molecular pathways. *Neuron* 106, 727–742.e6. doi: 10.1016/j.neuron.2020.02.034

frontiers | Frontiers in Neuroscience

TYPE Original Research
PUBLISHED 09 August 2023
DOI 10.3389/fnins.2023.1214958

Check for updates

OPEN ACCESS

EDITED BY
Hermes H. Yeh,
Dartmouth College, United States

REVIEWED BY
Amy Gardiner,
University of New Mexico, United States
Mathias Zink,
University of Heidelberg, Germany

*CORRESPONDENCE
Nune Darbinian
✉ nsarkiss@temple.edu
Michael E. Selzer
✉ mselzer@temple.edu

RECEIVED 30 April 2023
ACCEPTED 24 July 2023
PUBLISHED 09 August 2023

CITATION
Darbinian N, Darbinyan A, Merabova N, Kassem M, Tatevosian G, Amini S, Goetzl L and Selzer ME (2023) *In utero* ethanol exposure induces mitochondrial DNA damage and inhibits mtDNA repair in developing brain. *Front. Neurosci.* 17:1214958. doi: 10.3389/fnins.2023.1214958

COPYRIGHT
© 2023 Darbinian, Darbinyan, Merabova, Kassem, Tatevosian, Amini, Goetzl and Selzer. This is an open-access article distributed under the terms of the Creative Commons Attribution License (CC BY). The use, distribution or reproduction in other forums is permitted, provided the original author(s) and the copyright owner(s) are credited and that the original publication in this journal is cited, in accordance with accepted academic practice. No use, distribution or reproduction is permitted which does not comply with these terms.

In utero ethanol exposure induces mitochondrial DNA damage and inhibits mtDNA repair in developing brain

Nune Darbinian[1]*, Armine Darbinyan[2], Nana Merabova[1,3], Myrna Kassem[1,4], Gabriel Tatevosian[1], Shohreh Amini[4], Laura Goetzl[5] and Michael E. Selzer[1,6]*

[1]Center for Neural Repair and Rehabilitation (Shriners Hospitals Pediatric Research Center), Lewis Katz School of Medicine, Temple University, Philadelphia, PA, United States, [2]Department of Pathology, Yale University School of Medicine, New Haven, CT, United States, [3]Medical College of Wisconsin-Prevea Health, Green Bay, WI, United States, [4]Department of Biology, College of Science and Technology, Temple University, Philadelphia, PA, United States, [5]Department of Obstetrics and Gynecology, University of Texas, Houston, TX, United States, [6]Department of Neurology, Lewis Katz School of Medicine at Temple University, Philadelphia, PA, United States

Introduction: Mitochondrial dysfunction is postulated to be a central event in fetal alcohol spectrum disorders (FASD). People with the most severe form of FASD, fetal alcohol syndrome (FAS) are estimated to live only 34 years (95% confidence interval, 31 to 37 years), and adults who were born with any form of FASD often develop early aging. Mitochondrial dysfunction and mitochondrial DNA (mtDNA) damage, hallmarks of aging, are postulated central events in FASD. Ethanol (EtOH) can cause mtDNA damage, consequent increased oxidative stress, and changes in the mtDNA repair protein 8-oxoguanine DNA glycosylase-1 (OGG1). Studies of molecular mechanisms are limited by the absence of suitable human models and non-invasive tools.

Methods: We compared human and rat EtOH-exposed fetal brain tissues and neuronal cultures, and fetal brain-derived exosomes (FB-Es) from maternal blood. Rat FASD was induced by administering a 6.7% alcohol liquid diet to pregnant dams. Human fetal (11–21 weeks) brain tissue was collected and characterized by maternal self-reported EtOH use. mtDNA was amplified by qPCR. OGG1 and Insulin-like growth factor 1 (IGF-1) mRNAs were assayed by qRT-PCR. Exosomal OGG1 was measured by ddPCR.

Results: Maternal EtOH exposure increased mtDNA damage in fetal brain tissue and FB-Es. The damaged mtDNA in FB-Es correlated highly with small eye diameter, an anatomical hallmark of FASD. OGG1-mediated mtDNA repair was inhibited in EtOH-exposed fetal brain tissues. IGF-1 rescued neurons from EtOH-mediated mtDNA damage and OGG1 inhibition.

Conclusion: The correlation between mtDNA damage and small eye size suggests that the amount of damaged mtDNA in FB-E may serve as a marker to predict which at risk fetuses will be born with FASD. Moreover, IGF-1 might reduce EtOH-caused mtDNA damage and neuronal apoptosis.

KEYWORDS

mitochondria, brain development, FASD, exosomes, mtDNA damage, IGF-1, mtDNA repair, 8-oxoguanine DNA glycosylase-1 (OGG1)

1. Introduction

Fetal ethanol (EtOH) exposure during pregnancy is the leading cause of preventable cognitive impairment. Alterations of grey and white matter integrity are consistent findings in fetal alcohol spectrum disorders (FASD), and their most severe form, fetal alcohol syndrome (FAS), although the molecular mechanisms involved in these abnormalities are still not well understood (May et al., 2009, 2014, 2018; Valenzuela et al., 2011; Hoyme et al., 2016). Unfortunately, many women use alcohol before they know they are pregnant Not all exposed fetuses develop FASD, but there is no way to predict which children will be born with FASD because imaging methods currently lack sufficient resolution, particularly early in pregnancy, when the pathogenesis most likely begins, and there are no established *in utero* molecular markers for FASD, even for FAS. Recently, it was demonstrated that EtOH exposure downregulated the expression of neuronal markers and markers of mature oligodendrocytes (OLs) in fetal brain in the mid-second trimester (Darbinian et al., 2021a, 2023). People with FAS may experience early aging, like people with some genetic disorders, and thus have reduced life spans (Moore and Riley, 2015). Mitochondrial dysfunction and mitochondrial DNA (mtDNA) damage, the hallmarks of aging, are postulated to be a central event in FASD (Hoek et al., 2002; Bukiya, 2019). If mtDNA damage is not repaired, oxidative stress and cell damage are increased, and mitochondrial function is impaired. Quantitative or qualitative alterations in mtDNA repair proteins, particularly 8-oxoguanine DNA glycosylase-1 (OGG1), may inhibit mtDNA repair. Biomarkers that can detect FASD early in pregnancy might suggest strategies that can improve the quality of life and life expectancy of affected people as they age.

1.1. Mitochondrial injury

Mitochondria are sources of increased levels of reactive oxygen species (ROS) in age-related neurodegenerative disorders (Kaarniranta et al., 2019; Gyllenhammer et al., 2022). ROS increase is correlated with mtDNA damage (Zhao and Sumberaz, 2020). Further, Human Immunodeficiency Virus 1 (HIV-1) Tat inhibits neuronal cell survival through a mitochondrial pathway, and impaired mitochondrial oxidative phosphorylation is an important feature of HIV-1 pathogenesis (Côté et al., 2002; Casula et al., 2005; De Simone et al., 2016; Darbinian et al., 2020). The mitochondrial genome encodes only 37 genes, whereas most mitochondrial proteins are regulated by nuclear DNA (nDNA) (Abdullaev et al., 2020). Old mitochondria are replaced by autophagy (mitophagy) (Thangaraj et al., 2018). The mitochondrial genome is 16.5 kb. Each cell has several thousand copies of mitochondrial DNA. In age-related neurodegenerative diseases, nDNA is less susceptibile to DNA-damaging agents tthan is mtDNA (Cline, 2012). After oxidative stress in human cells, damage to nDNA also is less extensive than to mtDNA (Zhao and Sumberaz, 2020). Damage of mtDNA is reversed by the base excision repair (BER) pathway. There is a correlation between ROS-induced mtDNA damage and reductions in activity of BER, including OGG1 (Kaarniranta et al., 2019).

1.2. Mitochondrial DNA

mtDNA impacts the central nervous system (CNS) and peripheral nervous system (PNS) (Carelli and Chan, 2014), and is involved in neurodegenerative disorders (Yang et al., 2008). Mitochondrial DNA copy numbers were reduced in pyramidal neurons, and mitochondrial biogenesis signaling was disrupted in hippocampuses of patients with Alzheimer's disease (Rice et al., 2014). Mitochondrial changes also were detected in the aging human placenta (Bartho et al., 2020). HIV-1 and HIV-1-Tat can induce mtDNA damage in human neurons (Darbinian et al., 2020). Placental mtDNA content during development influences childhood intelligence (Bijnens et al., 2019). Prenatal exposures to cigarette smoke can alter nuclear and mitochondrial DNA in newborns (Pirini et al., 2015), and can increase oxidative stress and mitochondrial damage in non-human primates (Westbrook et al., 2010). In human cells, oxidative stress leads to more extensive and prolonged damage to mtDNA compared to nDNA (Yakes and Van Houten, 1997). Developmental changes in mtDNA also were found in human cord blood leukocytes during gestation (Pejznochová et al., 2008).

1.3. mtDNA damage and BER by OGG1

BER repairs oxidatively induced DNA base lesions in mitochondria, and consists of long and short patch pathways, involving multiple enzymes (Prakash and Doublié, 2015; Dizdaroglu et al., 2017). For example, OGG1 can protect against methamphetamine-enhanced fetal brain oxidative DNA damage (Wong et al., 2008). The first steps in the repair of 8-oxoG through the BER pathway are catalyzed by OGG1. OGG1 was expressed and activated in adult rodent brain tissues (Verjat et al., 2000). The oxidative DNA damage levels in the brain depend on the ability of OGG1 to remove 8-oxoG in mouse brain (Cardozo-Pelaez et al., 2000). BER of 8-hydroxyguanine protects DNA from endogenous oxidative stress (Boiteux and Radicella, 1999). Two major forms of human OGG1 are encoded by alternatively spliced OGG1 mRNAs (Nishioka et al., 1999). ROS can induce DNA damage, the product of OGG1 gene activation involved in this process is 8-hydroxyguanine (8-OH-G). OGG1 inactivation can cause spontaneous mutation, such as an increase in GC to TA transversions (Boiteux and Radicella, 2000). Another enzyme that regulates oxidative stress and aging is a longevity determing catalase (Cutler, 2005).

1.4. Exosomes

The brain cells of fetuses release small vesicles, exosomes, which carry cell components, and find their way into the mother's blood, from which they can be isolated without disturbing the fetus. Circulating exosomes are strongly implicated in FASD (Goetzl et al., 2016, 2019a; Darbinian et al., 2023). Studies in rats and human tissues showed increased apoptosis, cytokine dysregulation and maturational defects in neurons and OLs. These molecular abnormalities are detectable in cell type-specific (i.e., OLs and neurons) FB-E isolated from maternal blood. The contents of these cell type-specific exosomes can serve as biomarkers for neuronal and OL damage in FASD. Not only mRNA (Valadi et al., 2007; Skog et al., 2008; Batagov and Kurochkin, 2013), but even double-stranded DNA can be found in exosomes (Thakur et al., 2014; Witwer et al., 2017), and exosomes secreted by OLs (Fruhbeis et al., 2012) contain major myelin and stress-protective proteins (Kramer-Albers et al., 2007), lipids (Skotland et al., 2017) and miRNAs (Ebrahimkhani et al., 2017). Recently

mtDNA was found in exosomes (Vaidya et al., 2022), which also carry genomic and cytoplasmic DNA. Cells exposed to pathological conditions may secrete exosomes containing abnormal mtDNA (Vaidya et al., 2022), and this might also apply to damage from EtOH exposure. Considering the previous data (Darbinian et al., 2021a, 2023; Darbinian and Selzer, 2022), it would be possible that increased release of soluble factors may be involved in the dysregulation of OL and neuronal growth and survival. Changes in differentiation and chemokine secretion by OLs are associated with activation of apoptotic signaling in differentiated rat OL O2A cells and neurons (Darbinyan et al., 2013a,b; Darbinian et al., 2021a).

1.5. Fetal brain-derived exosomes (FB-Es) to study mitochondrial repair genes

Neurons and OLs are damaged in FASD, and either fail to develop, or undergo excessive apoptosis. Fetal brain tissue examination is not possible in ongoing human pregnancies, and non-invasive use of the fetal brain has been limited to expensive and technically challenging *in utero* imaging studies. Maternal plasma miRNAs have been used to predict infant outcomes and may be helpful to diagnose FASD subpopulations (Balaraman et al., 2014, 2016; Tseng et al., 2019). Previously, we determined the effect of prenatal EtOH exposure on human fetal neuronal and OL apoptosis (Amini et al., 2009; Darbinyan et al., 2013a; Darbinian et al., 2021a,b). Here we extend these studies to the effects of EtOH on mtDNA in FB-Es.

2. Methods

2.1. Clinical samples

We established a biobank that included 155 women who consumed EtOH, but no other drugs, during pregnancy, and had elective termination of their pregnancy due to economic or family conditions, and not because of adverse events, acute or chronic disease, or concerns about the health of the fetus. These were designated "clean EtOH-exposed" cases. We also incorporated 75 controls. EtOH-exposed and control cases were numbered in order of acquisition. For the present study, we selected the first 20 subjects and compared them to the first 20 carefully matched unexposed controls. Cases and controls were matched for sex and gestational age (GA) between 11- and 21-weeks GA (Table 1) under a protocol approved by our Institutional Review Board (IRB). All assays were performed in triplicates. Data from both sexes were combined. Details of the clinical samples, fetal brain tissues from elective termination of pregnancy, and matching maternal blood samples used in this study were reported earlier (Goetzl et al., 2016, 2019a; Darbinian et al., 2021a, 2023).

TABLE 1 Human subjects: Clinical characteristics.

	EtOH consumers (n = 20)	Controls (EtOH Non-consumers; n = 20)
Maternal Age (years ±SD)	28.0 ± 2.7	24.15 ± 2.3
Gestational Age (weeks ±SD)	15.22 ± 1.6	14.92 ± 1.58
Gestational Age range (weeks)	11.5 to 21	11.1 to 21
Ethnicity: Hispanic (%)	15	15
Race: White (%)	50	50
Race: Black (%)	50	50
Fetal Sex, Male (%)	50	50
Fetal Sex, Female (%)	50	50

2.1.1. Subject recruitment

Women reporting alcohol use (or no alcohol use) since conception were grouped in GA windows: 11–21 weeks (1st - 2nd Trimester) (Darbinian et al., 2023). GA was determined by a dating ultrasound performed immediately prior to recruitment (Spong et al., 2011). Blood samples of 20 "clean EtOH-consuming" subjects and 20 matched controls were collected. For EtOH-consuming mothers, the total cumulative alcohol dose in 1st trimester pregnancy terminations ranged from 57–168 drinks (or 12–30 drinks/month), and for 2nd trimester terminations was from 54.4 to 1827.5 drinks (or 6–320 drinks/month). A drink was estimated as the equivalent of one shot [1.5 oz. of brandy or 5 oz. of wine (Darbinian et al., 2023)]. Due to the limited nature of this study, and for the need to match EtOH-exposed fetuses with appropriate controls, it was not possible to carry out the study in a completely blinded way. However, moment by moment, the samples were identified only by their accession number, and most of the tissue handling and testing was automated so as to analyze all the EtOH-exposed and control samples simultaneously on the same devices.

2.1.2. Eligibility criteria

The brain and blood samples were obtained according to NIH Guidelines through a trained Study Coordinator. Samples were collected regardless of ethnic background, sex, and race.

2.1.3. Treatment plan

Each patient signed a separate consent form for research on blood and tissue samples. Collected blood was processed for collection of plasma. No invasive procedures were performed on the mother, other than those used in her routine medical care. Fetal tissues were processed for RNA or protein isolation.

2.1.4. Risk and benefits

There are very small risks of loss of privacy as with any research study where protected health information is viewed. The samples were depersonalized before they were sent to the lab for analysis. There was little anticipated risk from obtaining approximately 2–3 cc of blood, but a well-trained Study Coordinator.

There was no direct benefit to the research subjects from participation, but there is significant potential benefit for the future FASD subjects.

2.1.5. Informed consent

Consent forms and the de-identified log sheets and IRB protocol were sent by the Study Coordinator to Principal Investigator with each blood and tissue sample. Except for an assigned accession number, no

identification was kept on the blood and tissue samples (Darbinian et al., 2023).

2.1.6. Assessment of alcohol exposure in pregnancy

Maternal EtOH exposure was determined with a face-to-face questionnaire (Goetzl et al., 2016, 2019a; Darbinian et al., 2021a, 2023; Darbinian and Selzer, 2022). EtOH exposure was assessed using a detailed questionnaire adapted from the NICHD PASS study (Dukes et al., 2014). Women admitting to EtOH use were classified as EtOH exposed (see all details in Darbinian et al., 2023).

2.1.7. Tissue collection

Fetal brain tissue from subjects undergoing elective termination of pregnancy was collected according to an IRB-approved protocol (Goetzl et al., 2016; Darbinian et al., 2021a, 2023).

2.2. Animal studies

Female time-pregnant Sprague–Dawley rats were maintained on a LieberDeCarli EtOH liquid Diet (Bio-Serv) (containing 6.7% EtOH v/v) or isocaloric Maltose Dextrin Control liquid diet (Bio-Serv) for 6 days until delivery. Dams and pups were maintained according to the Temple University Institutional Animal Care and Use Committee (IACUC)-approved protocol. Rats were given Liquid Rat Diet for Pregnant Dams, High Protein (BioServ) with addition of either enough 95% EtOH to reach a concentration of 6.7% concentration (for the EtOH group), or Maltose Dextrin (for the control group). Alcohol blood levels were not measured, but both groups consumed the same volume of food. The alcohol diet was stopped immediately after delivery. Rats were then monitored carefully through delivery and the first 15 postnatal days. Controls as well as ethanol-exposed pups were studied on their 2nd, 5th, 8th, and 15th postnatal day. Pups were weighed, measured for crown-to-rump length (using a soft measuring tape, forceps, and a ruler), analyzed for ocular and mtDNA abnormalities. Four rat pups (2 male and 2 female) were used for each timepoint (Figure 1). Hemi-brains were dissected for DNA studies. Eye globe diameter (lateral), eye length (anterior–posterior), and pupil diameter and shape were noted for both the right and left eyes of all fetuses and informative comparisons were made.

2.3. Cell culture

Human primary cortical neurons were prepared in our laboratory by Darbinyan et al. (2013a,b), Darbinian et al. (2014), De Simone et al. (2016), and Darbinian et al. (2021c). In brief, 16-weeks fetal brain (approx 13 g) was collected under an approved Temple University IRB protocol and was treated with Tryple Express enzyme (Invitrogen, CA), DNase I (10 U/mL; Sigma, St. Louis, MO) and maintained at 37°C.

2.3.1. Cell treatment

Neuronal cells were incubated with 50 mM EtOH (Darbinian et al., 2021b), Insulin-like growth factor 1 (IGF-1, 50 ng/mL) or tumor necrosis factor α (TNFα, 50 ng/mL) for a total of 48 h.

2.4. RNA preparation and real-time qRT-PCR

Total RNA was isolated using the RNeasy kit (Qiagen, Valencia, CA) with on-column DNA digestion (Darbinian-Sarkissian et al., 2006). The RT-PCR reaction was performed with 1 μg total RNA, using One-Step FAST RT-PCR SYBR Green PCR Master Mix (Qiagen). StepOnePlus Real-Time PCR system was used (Applied Biosystems). PCR conditions were performed according (Darbinyan et al., 2013a, 2020). The amplified DNA was analyzed by gel electrophoresis using 2.0% agarose gel.

2.4.1. cDNA synthesis

One μg of RNA and reverse transcriptase (Roche Molecular Biochemicals, Indianapolis, IN, United States) were used.

RT-PCR. The SuperScript III One-Step RT-PCR System with Platinum *Taq* (Invitrogen, Carlsbad, CA, United States) was used. One microgram of total RNA and primers specific to *ogg1* gene were used to amplify OGG1 (Darbinian et al., 2020).

2.5. Analysis of mtDNA damage by qPCR

qPCR for nuclear and mitochondrial DNA integrity was carried out with GeneAmp XL-PCR kit (Applied Biosystems, Darbinian et al., 2020).

2.6. Estimation of DNA damage

Quantification of PCR products and calculation of lesion frequency were done by using PicoGreen (Ahn, 1996; Kovalenko and Santos, 2009; Hunter et al., 2010; Gureev et al., 2017; Darbinian et al., 2020). DNA damage is indicated by lower signal for DNA (lower amplification).

2.7. DNA isolation and qPCR

Genomic DNA was purified using the QIAamp DNA isolation kit (Qiagen, Chatsworth, CA) to perform long PCR (Meyer, 2010; Furda et al., 2014; Darbinian et al., 2020). qPCRs was done in a GeneAmp PCR System 2,400 using the GeneAmp XL PCR kit. Fifteen ng of genomic DNA was used to perform long qPCR (see all details in Darbinian et al., 2020).

2.8. Primers (IDT Inc.)

See details in Darbinian et al., 2020: β-actin: S: 5'-CTACAAT GAGCTGCG TGTGGC-3′,

AS: 5'-CAGGTCCAGACGCAGGATGGC-3′,

Primer nucleotide sequences for the 17.7-kb β-globin gene (GenBank: J00179J00179),

5′-TTGAGACGCATGAGACGTGCAG-3′, and 5′-GCACTGGCT TAGGAGTTGGACT-3′; and for the 16.2-kb fragment of the mitochondrial genome,

5′-TGAGGCCAAATATCATTCTGAGGGGC-3′ and.

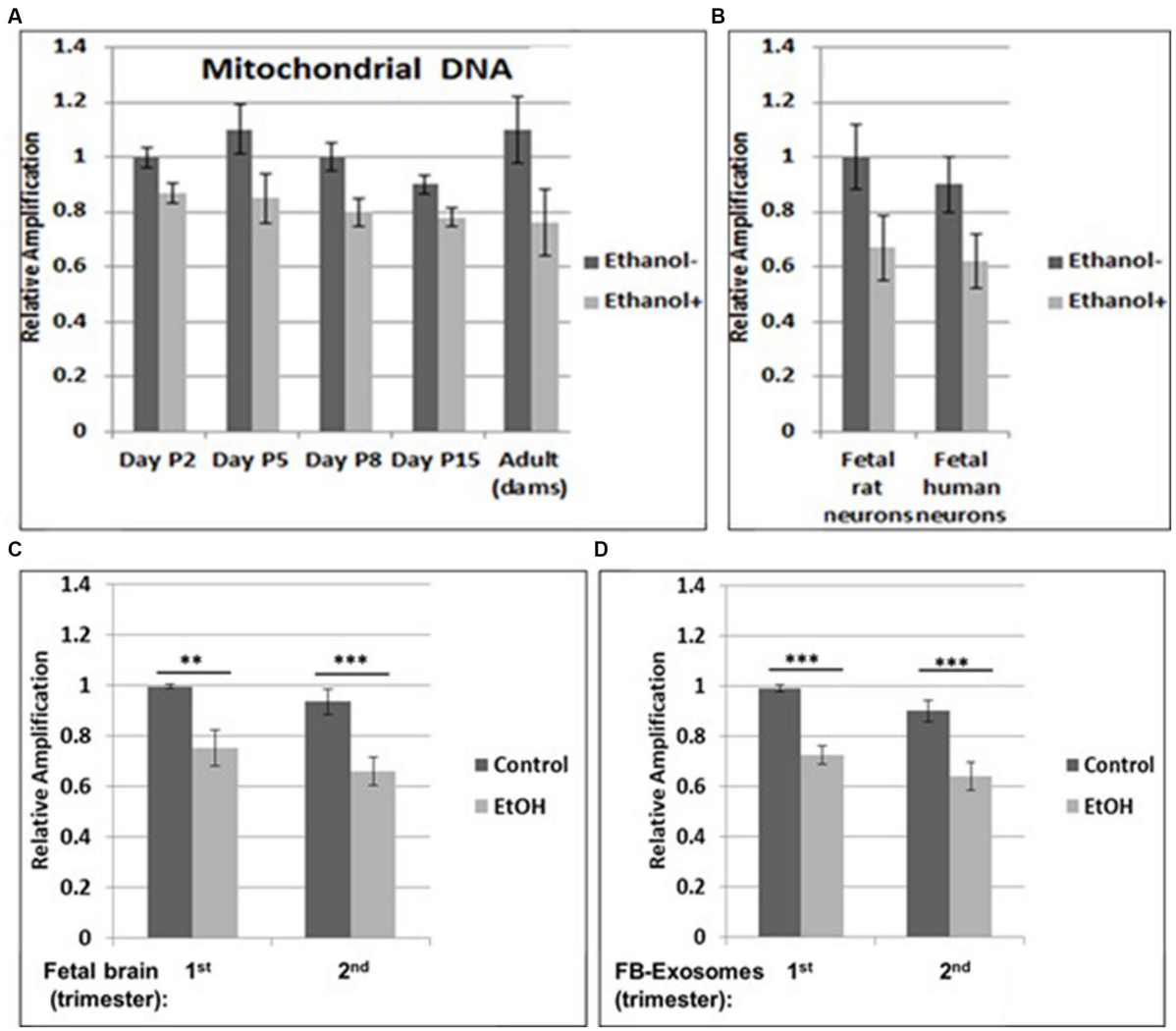


FIGURE 1
Increased mtDNA damage by EtOH. **(A)** Brain tissues from EtOH-fed rat pups ($n = 4$) were analyzed by qPCR with mitochondrial-specific primers, comparing long (16.5 kbp) and short (200) PCR products. **(B)** Fetal rat and human neuronal cells were incubated with EtOH (50 mM) or 48 h. **(C)** mtDNA damage in human fetal brains from two trimesters, and in fetal brain-derived exosomes **(D)**. mtDNA damage increased in human FB-Es from maternal blood from EtOH cases ($n = 10$/trimester). Relative amplification is shown for the mtDNA band intensities (treated/control [AD/AC] or damaged versus undamaged). The data are shown as the mean ± SD from three independent experiments. The decrease in relative amplification is shown by graphs. Assays were performed in triplicates and value of p was calculated using ANOVA and Student's t-test.

5′-TTTCATCATGCGGAGATGTTGGATGG-3′ (RH1066). *mtDNA quantification.* Fluorescence of each product was detected at a wavelength of 530 nm. Relative concentrations of mtDNA were calculated for each mitochondrial transcript as the ratio of its average signal in triplicate assays to that of the housekeeping gene globin (Hunter et al., 2010; Darbinian et al., 2020). The quantitative loss (damage) or gain (repair) in fluorescence was detected during the PicoGreen analysis of control and treated QPCR products. DNA damage was quantified by comparing the relative amplification of long fragments (approximately 16 kb) of DNA from EtOH exposed or treated samples to controls, then by normalizing this to the amplification of short (200 bp) DNA fragments. If A_t represents the amplification of EtOH-treated samples and A_o is the amplification of untreated controls, then the relative change in mtDNA = A_t/A_o.

2.9. Droplet digital PCR (ddPCR)

For absolute quantitation of mRNA copies, ddPCR was performed using the QX200 ddPCR system. Fifty ng of human fetal total RNA were used with the 1st Strand cDNA Synthesis Kit (Qiagen, Valencia, CA, United States). All procedures were performed according to Darbinian et al. (2021a, 2023). The ddPCR data were exported to Microsoft EXCEL for further statistical analysis.

2.10. Isolation of Fetal brain-derived exosomes (FB-Es) from maternal plasma, and ELISA quantification of Exosomal proteins

Human FB-Es were isolated as described previously (Goetzl et al., 2016, 2019a; Darbinian et al., 2023). Two hundred and fifty µL of

maternal plasma were used to precipitate with antihuman contactin-2/TAG1 antibody (clone 372,913, R&D Systems, Inc., Minneapolis, MN USA). Because our previous studies revealed that EtOH reduced the number of FB-Es, all exosomal assays were normalized against the exosomal marker CD81.

2.11. Superoxide dismutase activity assay

SOD activity was measured in primary neurons, incubated with EtOH for 48 h (Darbinian et al., 2020). Cells were analyzed by Superoxide Dismutase (SOD) assay by comparing SOD activity using the OxiSelect SOD Activity Assay kit. The activity of SOD is determined as the inhibition of chromogen reduction. In the presence of SOD, superoxide anion concentration is reduced, yielding less colorimetric signal. SOD activity is shown in % of control.

2.12. ATP assay

ATP level was measured using ATP Assay Kit (Darbinian et al., 2020). Human fetal neurons were incubated with EtOH or IGF-1. ATP was assayed using the ATP Determination Kit (Molecular Probes, Eugene, OR). Bioluminescence was measured using a Luminometer (Femtomaster FB 12 luminometer, Zylux).

2.13. Quantification of brain cell injury: caspase-GLO 3/7 activity assay

Apoptosis was assessed for activation of Caspase-3, using the Caspase-Glo™ 3/7 assay kit (Promega, Madison, WI, USA), according to the manufacturer's instructions. Approximately 1,000 of rat pup's brain cells, were analyzed in a final volume of 100 microliters culture medium per well. One hundred microliters of Glo reagent were added to the culture medium (1,1), then after cell lysis induction, the luminescence was recorded (RLU/s) on a Luminometer (Zylux Corporation). Data were analyzed using Excel software.

2.14. Microscopy

Human neurons were seeded in poly-L-Lysine coated glass slide chambers, and after 48 h incubation with 50 mM of EtOH, cells were analyzed by microscopy (Darbinian et al., 2021a). Phase-contrast images were captured using IPLAB software. Original magnification for phase images was 200x.

2.15. Statistical analysis

Statistical analysis was described previously (Darbinian et al., 2021a, 2023). In brief, analysis was performed using SPSS (IBM Corp., released 2017. IBM SPSS Statistics for Windows, Version 25.0. Armonk, NY). All data are represented as the mean ± standard error for all performed repetitions. Means were analyzed by a one-way ANOVA, with Bonferroni correction. Statistical significance was defined as $p < 0.05$. Sample numbers are indicated in the figure legends. More details are in Darbinian et al. (2021a, 2023).

2.16. Ethics statement

Human Subjects. Consenting mothers were enrolled between 11 - 21 weeks gestation, under a protocol approved by our Institutional Review Board (IRB). This protocol involved no invasive procedures other than routine care. Maternal EtOH exposure was determined with a face-to-face questionnaire that also included questions regarding many types of drugs/medications used (Goetzl et al., 2016, 2019a,b, Darbinian et al., 2021a, 2023). The questionnaire was adapted from that designed to identify and quantify maternal EtOH exposure in the NIH/NIAAA Prenatal Alcohol and SIDS and Stillbirth (PASS) study (Dukes et al., 2014).

All procedures for collection and processing of human brain tissues and blood were performed according to NIH Guidelines by a trained Study Coordinator. All investigators completed Citi Program - Human Subject training, Blood-Borne Pathogens Training, and Biohazard Waste Safety Training annually (see details in Darbinian et al., 2023).

Written informed consent has been obtained from the parents of patient(s) for studies, and deidentified samples were used for this publication. Informed Consent forms were maintained by the Study Coordinator. The de-identified log sheets contain an assigned accession number, and the age, sex, ethnicity, and race of the patient. Except for an assigned accession number, no identification was kept on the blood samples.

Vertebrate Animals. Experiments with rats were designed with the primary goal of minimizing the numbers of animals used. Toward this end, we have considered the minimal number of animals necessary for achieving statistical significance in all experiments (n = 4 for all time points). Animals were purchased and maintained in the medical school's animal facility in accordance with all federal and state regulations on the humane care and use of animals in research, including the provisions of the Animal Welfare Act and the Public Health Service Policy on Humane Care and use of animals in research (PHS Policy on Humane Care and Use of Laboratory Animals, 2015, https://olaw.nih.gov/policies-laws/phs-policy.htm).

For tissue harvesting for RNA and protein, and behavioral studies, we utilized male and female rats which were monitored by animal facility personnel for 2 days prior to exposure to EtOH diet and then pups were sacrificed at 2-, 5-, 8- and 15-days postnatally.

Adult rats were euthanized by inhalation of CO2 without other manipulation, according to the recommendations of the Panel on Euthanasia of the American Veterinary Medical Association. Female pregnant rats were maintained on an EtOH-containing (6.7% v/v) liquid diet for 6 days until delivery, based on a Temple University IACUC-approved protocol.

3. Results

3.1. Increased mtDNA damage by prenatal EtOH exposure

Brain tissues from EtOH-fed rat pups were studied by qPCR with mitochondrial-specific primers, for relative mtDNA levels, comparing PCR products between EtOH-exposed groups and unexposed controls at four postnatal days. Increased mtDNA damage (lower relative amplification) was found in all EtOH groups (Figure 1A). A similar pattern of decreased mtDNA amplification was found in fetal rat and

human cortical neurons (Figure 1B), and in human fetal brains (Figure 1C). Data from human fetal brains from 1st and 2nd trimesters (Table 1) were compared to results in fetal brain-derived exosomes isolated from matching maternal blood (Figure 1D). Relative mtDNA levels were lowest in EtOH groups.

Our previous data in primary OL cultures and fetal neural exosomes from EtOH-exposed maternal blood, demonstrate an association between EtOH injury and neuronal/OL markers. Molecular markers in FB-Es isolated during pregnancy can predict which at-risk fetus will develop FASD. Therefore, we isolated FB-Es from plasma to study the impact of EtOH exposure on mtDNA damage in the fetal brain, by measuring exosomal mtDNA damage, and a pattern of reduced mtDNA in FB-Es from EtOH-exposed plasma compared to control FB-Es. Interestingly, EtOH cases from both 1st and 2nd trimesters had more damaged mtDNA compared to non-exposed controls (Figures 1C,D). The similarity in the degree of EtOH-associated reduction in mtDNA levels between fetal brain and FB-Es shown in these graphs suggests that FB-Es from maternal blood might be useful as a surrogate marker for mtDNA in fetal brain.

3.2. Reduced cell viability and Sod activity By EtOH exposure

Neuronal cells with increased mtDNA damage by EtOH exposure (Figure 1B) were also studied for neuronal cell viability and SOD activity assays. EtOH treatment strongly affected cell survival, as only 72% of neuronal cells survived after 48 h of incubation with 50 mM EtOH (Figures 2A,B), probably in part, due to a reduced SOD activity (59%) in EtOH-treated cells (Figure 2C).

3.3. The neuroprotective growth factor, IGF-1, rescues mtDNA from damage caused By EtOH In neuronal cells

Previously, we demonstrated neuroprotective role of IGF-1 in neuronal cells (Wang et al., 2014) toxic effects of EtOH on neuroprotective IGF-1 in fetal brain during development (Darbinian et al., 2021a), and suggested that downregulation of IGF-1 by EtOH exposure could be a cause of neuronal loss. Here, by exogenously adding IGF-1 to human neuronal cells, we studied the role of IGF-1 in rescuing mtDNA damage from EtOH. Incubation of cells with IGF-1 reverses EtOH-mediated mtDNA damage (Figure 3A). Interestingly, IGF-1 improved the quality of mtDNA when added to cells as shown in Figures 3A,B by comparing bar 3 to bar 1 (1.5-fold increase in mtDNA amplification).

3.4. Etoh downregulates mtDNA repair protein, OGG1, and IGF-1 reverses toxic effects of EtOH On OGG1 expression, and on mitochondrial energy metabolism In human neuronal cells

Next, we assayed mtDNA damage repair protein, OGG1 mRNA expression, and studied whether neuroprotective IGF-1 can rescue mtDNA repair protein, and mitochondrial energy metabolism markers

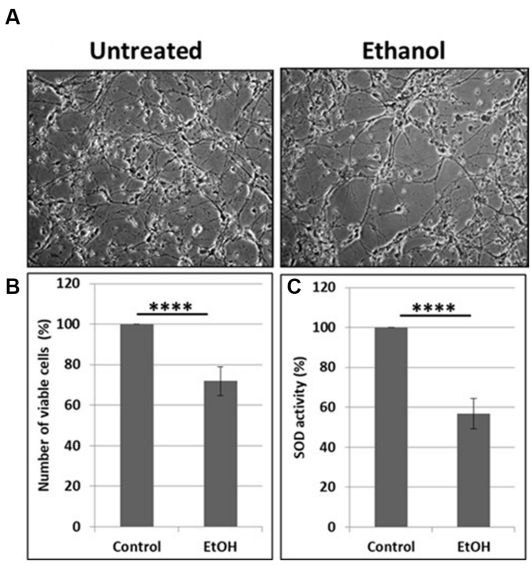


FIGURE 2
Reduction in cell viability and SOD activity. **(A)** Representative human neuronal cell images, incubated with EtOH (50 mM). **(B)** Cell viability assay in human neuronal cells. **(C)** SOD activity in neuronal cells presented as % control in human neuronal cells following exposure to EtOH (50 mM), with an OxiSelect SOD Activity Assay kit.

(catalase and ATPase activity) from EtOH caused toxic effects. As shown in Figures 4A,B, EtOH strongly downregulated OGG1 mRNA expression (compare bar 2 with bar 1), while IGF-1 reversed the toxic effects of EtOH on mtDNA repair protein (compare bar 4 with bar 2). Similar effects were seen for markers of mitochondrial energy metabolism, catalase (Figure 4C), and ATPase activity (Figure 4D).

3.5. Downregulation of the OGG1 mRNA expression by EtOH In fetal brain-derived exosomes

We developed non-invasive methods to study effects of prenatal EtOH exposure on fetal brain development by isolating fetal brain-derived exosomes from maternal blood. Downregulation of the OGG1 mRNA expression in EtOH-exposed fetal brain-derived exosomes was assayed by RealTime PCR (Figure 5A). Downregulation was greatest in the cases with EtOH exposure. The downregulation of OGG1 mRNA by EtOH was studied by ddPCR for both trimesters (Figure 5B). A 44% downregulation of OGG1 mRNA expression was found in the 2nd trimester cases (451 copies/μL in EtOH FB-Es vs. 682 copies/μL in control exosomes).

3.6. IGF-1 rescues mtDNA from damage caused by both EtOH and neurotoxic TNFα in neuronal cells

In our previous studies we demonstrated that prenatal EtOH exposure not only inhibits neuroprotective IGF-1, but also upregulates neurotoxic TNFα in fetal brains (Darbinian et al., 2021a). Here, we demonstrate the protective role of IGF-1 in the direct effect of

10.3389/fnins.2023.1214958

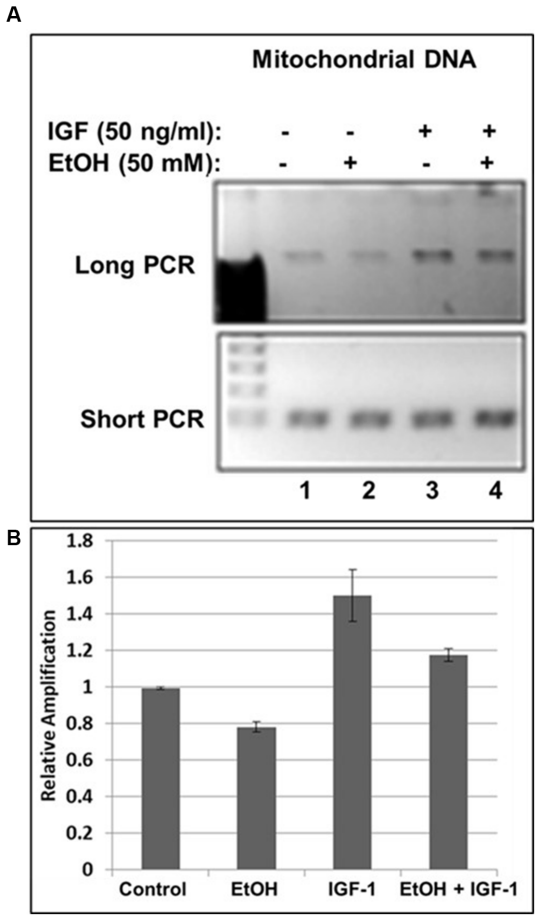


FIGURE 3
IGF-1 rescues mtDNA from the damage caused by EtOH. **(A)** Agarose gel images for long (16.2 kbp) or short (0.2 kbp) PCR products. Human neuronal cells were incubated with IGF-1 and EtOH. Total genomic DNA was isolated and long mtDNA qPCR was performed. **(B)** Relative amplification for mtDNA products.

EtOH on mtDNA damage, and on the EtOH-associated indirect effect, via TNFα, as revealed by qPCR assays in human cortical neuronal cells (Figure 6). IGF-1 efficiently reversed EtOH-caused mtDNA damage (compare lane 4 with lane 3 in Figure 6A, or bar 4 with bar 3 in Figure 6B). Similar protective effects were seen for IGF-1 in TNFα-treated cells (compare lane 6 with lane 5 in Figure 6A, or bar 6 with bar 5 in Figure 6B).

3.7. IGF-1 protects human neuronal cells from loss caused by EtOH and TNFα

To investigate the impact of IGF-1 on cell survival, human cortical neuronal cells were incubated with IGF-1, TNFα or EtOH (50 mM) alone or in combinations, for 48 h, and a cell viability assay was performed (Figure 6A). Reduction in number of neurons was seen in cases with EtOH treatment (68.3%), and TNFα incubation (72.3%), while IGF-1 reversed the toxic effects on cell survival from both EtOH- (89%) and TNFα- (92%) treated cells. Representative cell images of TNFα- and EtOH-treated cells used for the cell survival assay are also presented (Figure 6B).

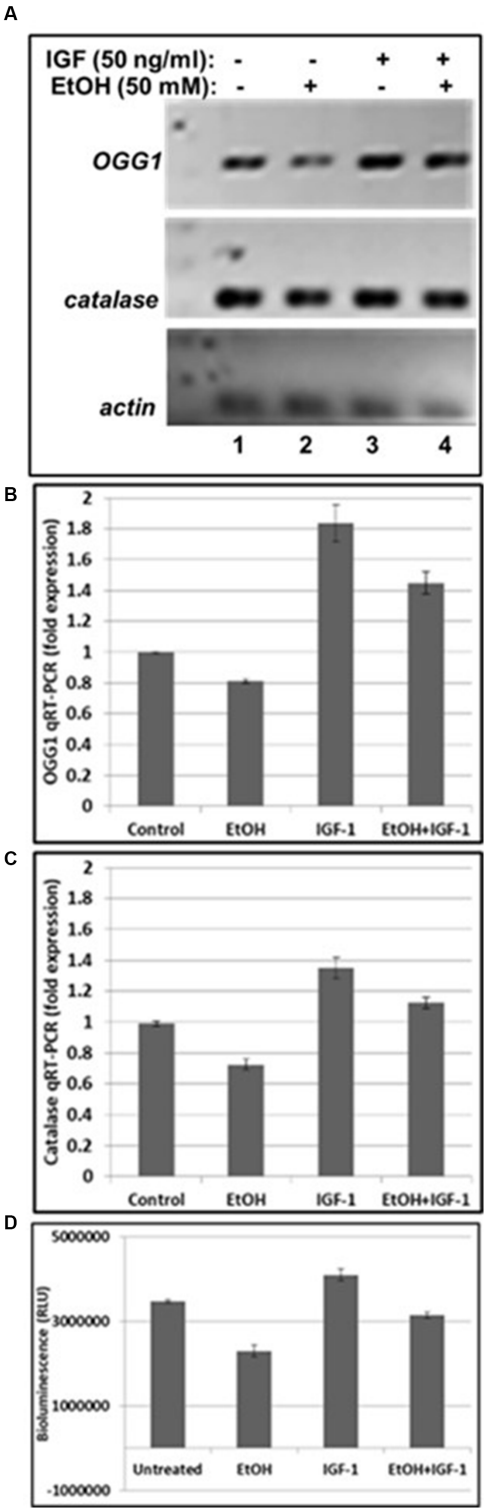


FIGURE 4
IGF-1 reverses toxic effects of EtOH on mtDNA repair protein in human cortical neurons. **(A)** qRT-PCR was performed using primers for mtDNA repair enzyme OGG1 and catalase. OGG1 is involved in the mtDNA damage repair mechanisms. Human neuronal cells were incubated either with EtOH, or IGF-1 alone or in combination, for 48 h. **(B)** Quantification of OGG1 qRT-PCR product. **(C)** Quantification of catalase qRT-PCR product. Results are presented in arbitrary units and shown as folds. **(D)** ATP activity. ATP assay was performed in neurons, incubated with EtOH, to demonstrate changes in ATPase activity.

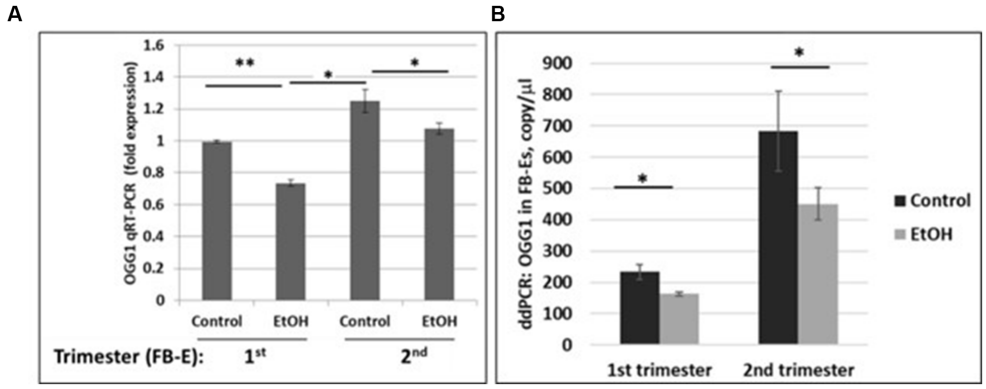


FIGURE 5
Downregulation of the OGG1 mRNA expression by EtOH in human fetal brain-derived exosomes (FB-Es). **(A)** Real-Time PCR for OGG1 mRNA in FB-Es. Downregulation was statistically significant ($p < 0.05$). Values are shown in fold expression (normalized to housekeeping *actin* gene). **(B)** ddPCR of OGG1 mRNA expression. Plasma from 20 patients with or without EtOH, were studied by ddPCR for OGG1 mRNA. Downregulation was greatest in the cases with EtOH exposure during 2nd trimester (graphs show means from triplicate assays +/− SD). Downregulation was statistically significant ($p < 0.05$). For absolute quantitation of OGG1 by ddPCR, values are shown in copies/µL.

3.8. Downregulation of IGF-1 mRNA and upregulation of TNFα mRNA by EtOH In FB-Es from patients with EtOH exposure

The effects of EtOH exposure on IGF-1 and TNFα expression seen in fetal brain tissues (Darbinian et al., 2021a) and human cortical neurons (Figure 7), were reproduced in FB-Es. qRT-PCR was performed for both markers during the 1st and 2nd trimesters. There was a significant downregulation of IGF-1 by EtOH (Figure 8A). TNFα was upregulated in FB-Es from the EtOH group in both trimesters (1.25-fold and 2.08-fold respectively).

Thus, we were able to reproduce data previously obtained in fetal brains (Darbinian et al., 2021a) in human cortical neurons (Figure 7), and in fetal brain-derived exosomes from maternal blood, indicating availability of a novel well-developed non-invasive tool to study events in fetal brain by using maternal plasma during pregnancy.

3.9. Correlations between rat pup Eye size and mtDNA damage. Prenatal alcohol exposure is associated with increased caspase-3 activity and morphological alterations in the rat

We investigated effects of alcohol on rat pup eye formation in the *in vivo* rat model of FAS. There was a negative correlation between prenatal EtOH intake by dams (6.7% liquid diet) and several parameters of the development of pups (Figure 9). The body weight of pups prenatally exposed to EtOH was lower than that of the control group at postnatal days 8 and 15 (P8 and P15; Figure 9A). At P2, the body weight of pups from the ethanol group was slightly higher than that of the control group. This difference was reversed at days P5 and P8. EtOH exposure also was associated with decreased weight and size (length and width) of the pups' brains and decreased face size. These effects were most pronounced at later GAs. We also examined the effect of prenatal EtOH exposure on apoptotic activity in the brain tissue. Lysates prepared from brains of pups, either untreated or treated with EtOH, were analyzed for cleaved active caspase-3/7 using the GLO caspase-3/7 apoptotic assay. Luminescence was recorded as RLU/s. The Glo assay results depicting caspase 3/7 cleavage in cells after EtOH diet are shown in Figure 9C. The values represent the readings from the Luminometer. Compared to controls, there was an increase in active caspase-3 levels in the brains of the EtOH groups at all developmental stages.

3.10. Prenatal EtOH exposure delays body and eye development in rat pups

A negative correlation was found between prenatal ethanol uptake by dams (6.7% liquid diet) and anatomical parameters of their pups (Table 2). Comparative measurements of the body length and eye size of EtOH diet and control diet rat pups, and other morphological changes, confirmed the toxic effects of EtOH on eye development. The body length of pups from the ethanol group was slightly less than that of the control group at day P2. This difference also was found on day P15. Thus, a consistent pattern of reduced eye size was observed with EtOH exposure in the rat pups.

Negative correlation was between prenatal EtOH intake by dams and the body weight of their pups (Figure 9A), pup face size (Figure 9B). Measurements (mm) were performed using a soft measuring tape, forceps and a ruler. EtOH diet increased brain caspase-3/7 activity at all developmental stages (Figure 9C). Tissue lysates prepared from brains of untreated pups, and pups treated with EtOH, were analyzed for cleaved (active) caspase-3, assessed with the substrate DEVD-aminoluciferin in the Caspase-Glo™ 3/7 assay kit. Delayed reduction in brain weight in EtOH-exposed pups from P2-P15 was measured (Figure 9D). EtOH also reduced brain length in pups from the EtOH group (Figure 9E) and brain width (Figure 9F). Correlations between pups' eye size and mtDNA damage in brain was significant (Figure 9G), while similar analysis of pups' brain width vs. mtDNA damage failed to show statistically significant differences.

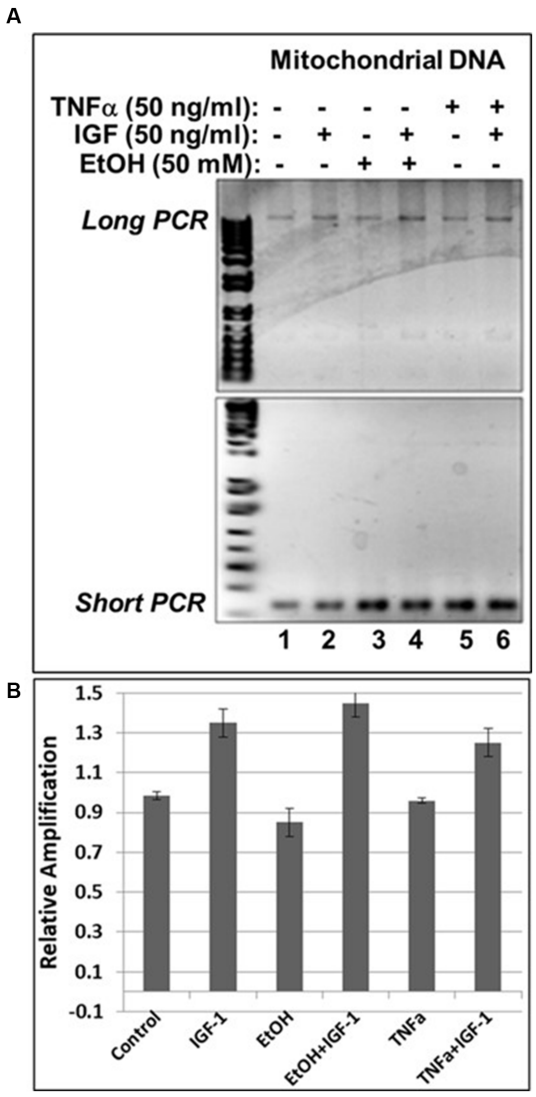


FIGURE 6
IGF-1 reverses mtDNA damage caused by EtOH or neurotoxic TNFα toxicity. **(A)** Agarose gel images for mtDNA amplification products. Human neuronal cells were incubated with EtOH, IGF-1 and TNFα alone or in combination and incubated for 48 h. **(B)** mtDNA damage was measured and presented as a relative amplification (graphs show means from triplicate assays +/− SD).

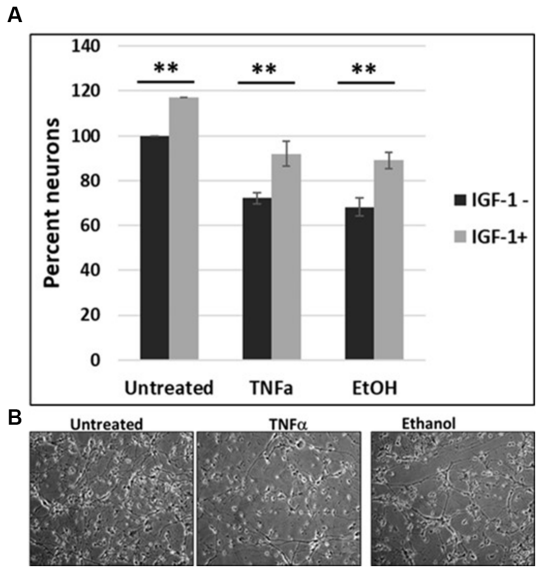


FIGURE 7
IGF-1 reverses neuronal loss caused by EtOH or TNFα toxicity. **(A)** Human cortical neurons were incubated with IGF-1, TNFα or EtOH (50 mM) alone or in combinations, for 48 h, and a cell survival assay was performed. Reduction in the number of neurons was assayed by a cell viability assay. Means and SD of the % of cells. Untreated = 100%. **(B)** Representative cell images.

3.11. Correlations between human fetal Eye size and fetal brain-derived exosomal mtDNA damage

Eye diameters were measured in histological sections (Darbinian et al., 2023). mtDNA levels were measured by qPCR (for relative amplification). Correlation between change in eye size (difference between EtOH-exposed fetus and its paired control) and reductions in exosomal mtDNA amplification for mtDNA damage levels was significant (Figure 10).

4. Discussion

Although FASD is diagnosed in only a small number of children exposed prenatally to EtOH, the frequency with which FASD is diagnosed has been increasing. Unfortunately, FASD remains underdiagnosed. The present study demonstrates that mtDNA and mitochondrial energy metabolism markers in FB-E can suggest the presence of FASD very early during fetal development. These exosomes can be isolated noninvasively from maternal blood samples.

The contents of FB-E isolated from the blood of pregnant women who consumed EtOH revealed an increase in mtDNA damage. Thus, future clinical studies could be aimed at using FB-Es from maternal blood to detect fetal mtDNA damage early in pregnancies and whether this can predict FASD in postnatal at-risk children.

We previously established primary cultures of neurons and OLs (Amini et al., 2009; Darbinyan et al., 2013a,b, 2021; Darbinian et al., 2021a,b), and showed that in these cultures, and in FB-E from EtOH-exposed maternal blood, there was an association between EtOH exposure and several brain cell markers (Goetzl et al., 2016, 2019a; Darbinian et al., 2021a, 2023). These studies have now been extended to demonstrate that FB-Es from EtOH-exposed fetuses can carry additional markers for abnormalities of mtDNA and mitochondrial function pathways (e.g., low levels of mtDNA, OGG1 mRNA, and low levels of IGF-1), and thus may be a source of additional molecular markers for FASD. As far as we know, these are the first EtOH-exposed cases that have been studied for mtDNA and mitochondrial markers, OGG1, and IGF-1 using FB-Es.

We showed the effects of EtOH exposure on mtDNA damage in primary cortical rat and human neurons, in fetal brain tissues, and in fetal brain-derived exosomes (FB-Es). Our FB-E noninvasive method can enable studies of mtDNA damage affected by EtOH and other neurotoxic agents with further translational impact. We determined whether molecules in these fetal-derived exosomes can predict which at-risk fetuses will be born with FASD, the most common cause of developmental intellectual disability in the US, affecting quality of life by causing early aging. Non-invasive *in utero* diagnosis could lead to

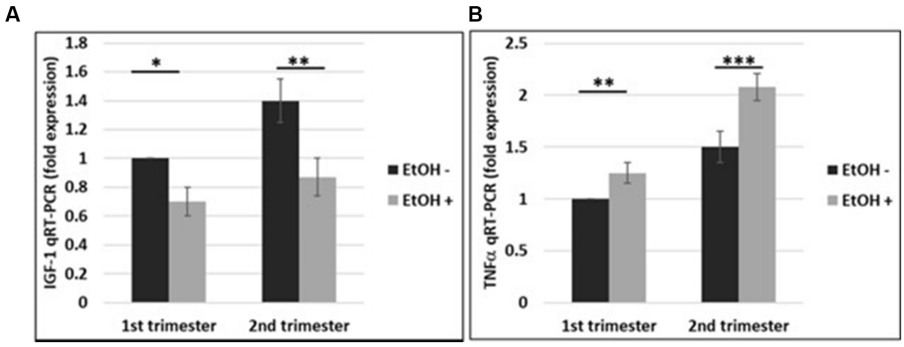


FIGURE 8
EtOH downregulates IGF-1 and upregulates TNFα in human fetal brain-derived exosomes. **(A)** Downregulation of the IGF-1 mRNA in FB-Es from EtOH-exposed cases. FB-Es from plasma were measured for IGF-1 mRNA by qRT-PCR, using specific primers for IGF-1. Downregulation was greatest in the cases with EtOH exposure (graphs show means from triplicate assays +/− SD). Downregulation was statistically significant ($p < 0.05$). **(B)** qRT-PCR was performed for TNFα in the same FB-Es. Plasma from 20 patients ($n = 10$ from 1st trimester, and $n = 10$ from 2nd trimester) with or without EtOH, were used for isolating FB-Es, and studied by Real-Time PCR. Upregulation was greatest in the cases with EtOH exposure (graphs show means from triplicate assays +/− SD). Upregulation was statistically significant ($p < 0.05$).

earlier detection and better research in therapies to prevent or ameliorate FASD.

Previously, we and others identified that IGF-1 in EtOH-exposed human subjects and *in vitro* studies regulate neuronal and OL injury and survival (Wang et al., 2014; Darbinian et al., 2021a; Darbinian and Selzer, 2022). IGF-1 improved mitochondrial function and reduced mitochondrial generation of reactive oxygen species (Ribeiro et al., 2014). IGF-1 protected OLs from TNFα-induced injury (Ye and D'Ercole, 1999; Lagarde et al., 2007), while OL progenitors of IGF-1-deficient mutant mice did not accumulate, proliferate, or survive. Thus, IGF-1 signaling plays an essential role in remyelination (Mason et al., 2003). IGF-1 also has been tested for treatment of neurological diseases. Five controlled clinical studies have evaluated human recombinant IGF-1 (rhIGF-1) as a treatment of ALS and Rett syndrome. These findings have been strengthened and expanded in the present study, in which we demonstrated: (i) Levels of the generally neuroprotective peptide IGF-1 were reduced in EtOH-exposed FB-Es, while levels of the generally neurotoxic peptide TNFα were increased; (ii) mtDNA damage was increased in fetal brain and neuronal cultures exposed to either EtOH or TNFα; (iii) IGF-1 protected neurons from EtOH-associated apoptosis; (iv) IGF-1 protected mtDNA from the effects of EtOH or TNFα.

We do not yet know which of the biomarkers, including those studied in our previous work (Goetzl et al., 2016, 2019a; Darbinian et al., 2023) and in the present investigation, will turn out to be the most accurate and sensitive predictors of FASD in at-risk infants. However, the present findings suggest that damage to mtDNA might be a promising biomarker because its measurements in FB-Es revealed a significant correlation between the increase in mtDNA damage and magnitude of one of the anatomical phenotypic hallmarks of FASD, i.e., reduced eye size (Hoyme et al., 2016). This was true for both rat pups (Figure 9) and human fetuses (Figure 10). A similar correlation had been found previously between MBP levels and reduced eye diameter (Darbinian et al., 2023). Large scale prospective studies in pregnancies brought to term, could test the diagnostic value of FB-E cargos, including those relating to mtDNA and mitochondrial repair, in predicting the emergence of FASD postnatally.

4.1. Limitations

Quantification of EtOH consumption was based on the subjects' information in face-to-face interviews, not on biochemical assays, e.g., blood alcohol levels or hair ethyl glucuronide (EtG) levels. This is because such tests remain positive only for a limited time after cessation of alcohol exposure (blood and urine EtG levels detect alcohol use only for the previous few days to weeks), although EtG can be detected in hair for up to 90 days (Berger et al., 2014). At best, these tests could verify recent alcohol use, but could not rule out early prenatal use, and certainly not quantify it, and it seems more likely that subjects might deny use than falsely report use of alcohol. A relative's opinion also was not always available for confirmation of alcohol use, particularly given the personal nature of the decision to terminate the pregnancy. We used another questionnaire to exclude exposure to SSRIs, opioids, marijuana and other medications and drugs. In general, we were confident about most of the subjects' information in this patient population, because in previous studies, regular use of other drugs was confirmed by biochemical assays.

We did not validate our animal model by performing behavioral studies. Initially, we focused our animal studies on molecular, not behavioral effects of EtOH exposure. Later we obtained grant support to perform human exosomal studies, which have led to the observations reported here. Future clinical studies are planned to determine whether the molecular markers suggested by the present and other studies from our laboratory can predict which at-risk infants will develop FASD.

5. Conclusion

The present findings on human and murine tissues suggest involvement of mtDNA damage in EtOH-exposed fetal brain. The results on FB-E and on neuronal cultures were similar, and thus have the potential to be extended to non-invasive diagnostic analyses of fetal development that could predict the emergence of FASD prenatally. As a corollary, the data on FB-E from the blood of 20 pregnant women who drank EtOH, and 20 non-drinking controls,

10.3389/fnins.2023.1214958

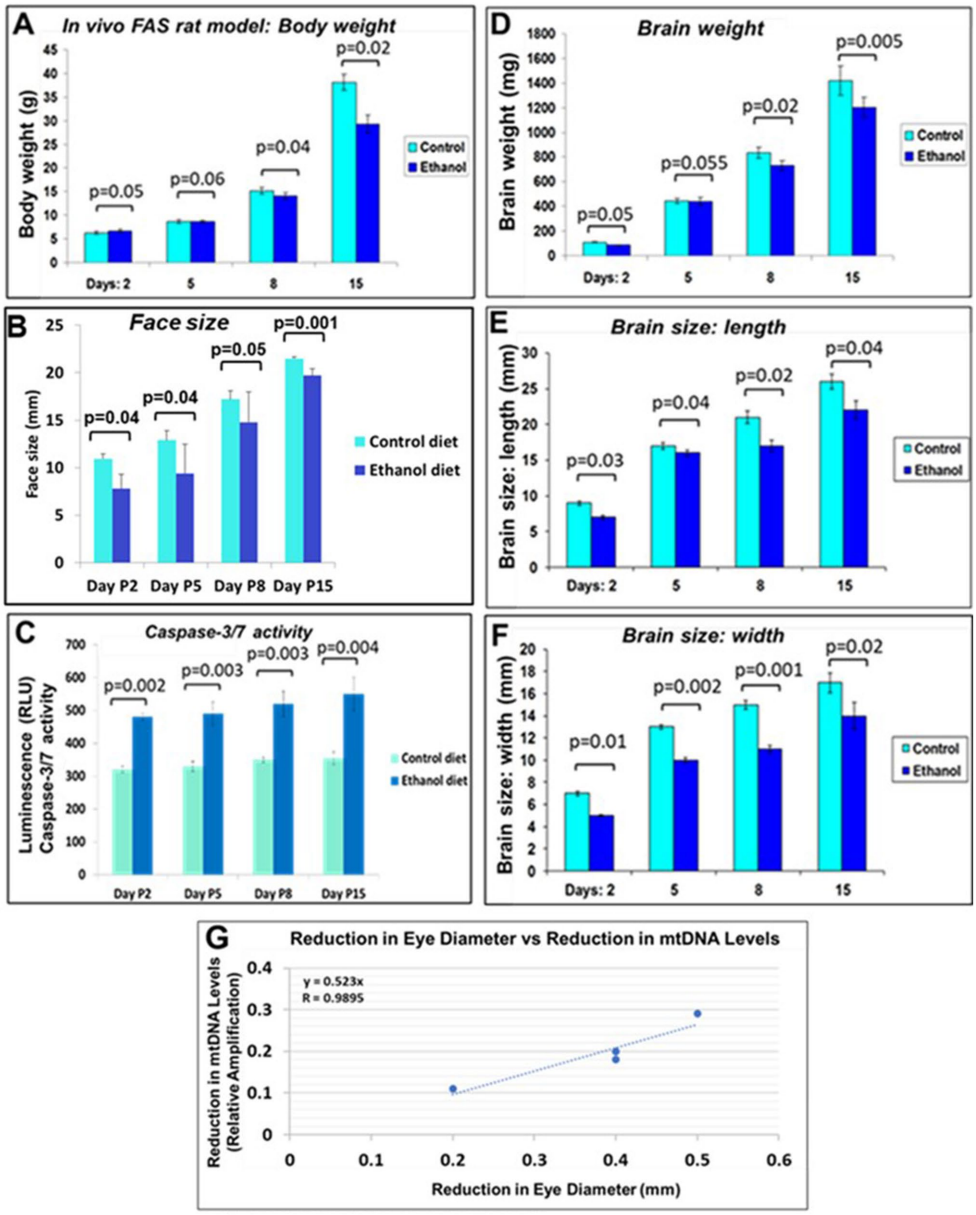


FIGURE 9
Correlations between rat pup eye size and mtDNA damage. Effect of prenatal EtOH exposure on morphological phenotype and caspase-3 activity in rat pups from age P2-P15. Rat dams were fed a liquid diet with or without 6.7% EtOH, and the effect on rat pup developmental parameters measured from postnatal days 2–15. **(A)** Negative effect of prenatal EtOH intake by dams on the body weight of their pups. **(B)** Effect of EtOH exposure and gestational age on pup face size increases during development. Measurements were performed using a soft measuring tape, forceps, and a ruler (mm). **(C)** EtOH diet increased brain caspase-3/7 activity at all developmental stages. Tissue lysates prepared from brains of untreated pups, and pups treated with EtOH, were analyzed for cleaved (active) caspase-3, assessed with the substrate DEVD amino luciferin in the Caspase-Glo™ 3/7 assay kit (Promega, Madison, WI, United States). Luminescence was recorded as RLU/s. The histogram shows caspase 3/7 activity, the error bars show the standard deviation from three independent readings. **(D)** Delayed reduction in brain weight in EtOH-exposed pups from P2-P15. **(E)** EtOH exposure reduced brain length in pups. **(F)** EtOH reduced brain width. **(G)** Correlations between pups' eye sizes and mtDNA levels in brain. Eye diameters were measured in histological sections. mtDNA levels were measured by qPCR. At each time point from postnatal days 2, 5, 8, and 15, eye tissues from four EtOH-exposed pups were paired with age-matched controls. Correlation between reduction in eye size (difference between EtOH-exposed pups and its paired control) and reduction in mtDNA levels presented as a scatter plot. Calculations in **(G)** are based on Spearman's correlation on exact Two-Tailed Probabilities critical *p* values for $N > 2 < = 18$, estimated using the Edgeworth approximation (Ramsey, 1989; Fowler et al., 2009).

showed that gene expression for the DNA repair protein OGG1 and for IGF-1 was lower in EtOH-exposed fetuses, while gene expression for TNFα was higher, and these results were reproduced in fetal cortical neuronal cultures. Neuronal viability *in vitro* was reduced by EtOH, as was SOD activity, ATPase activity and catalase mRNA expression. All these findings are consistent with the hypothesis that global mitochondrial pathways are significantly impaired in fetuses exposed to EtOH. The findings of reduced IGF-1 levels in

TABLE 2 Negative correlation between prenatal EtOH intake by rat dams (6.7% liquid diet) and the development of rat pups.

	Body length, cm (tail not included)	Eye diameter, mm
Control P2, $n=4$ (±SD)	3.5 ± 0.2	3.5 ± 0.1
FAS P2, $n=4$ (±SD)	3.0 ± 0.1	3.1 ± 0.2
Control P15, $n=4$ (±SD)	5.5 ± 0.2	4.0 ± 0.3
FAS P15, $n=4$ (±SD)	5.0 ± 0.3	3.8 ± 0.2
Male Fetal Sex (%)	50	50

Comparative measurements of the body length and eye size of the FAS (EtOH diet) and Control (control diet) rat pups. The n for each group represents the number of rat pups. For each pup, both eyes were measured, and the mean diameter was used for the calculations in the table.

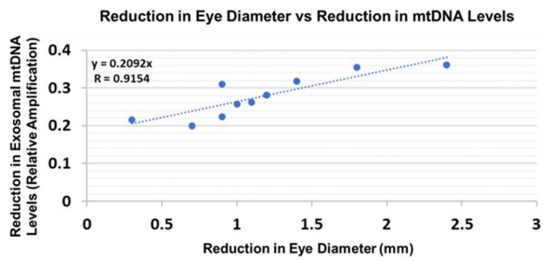


FIGURE 10
Correlations between human fetal eye size and fetal brain-derived exosomal mtDNA levels. Eye diameters were measured in histological sections. mtDNA levels were measured by qPCR (for relative amplification). Ten EtOH-exposed fetal eye tissues each were paired with an age- and sex-matched control, and with their matching maternal blood samples from 1st and 2nd trimester pregnancies (n = 20 total). Assays were performed in triplicate on contents of FB-Es isolated from the maternal blood. Correlation between reduction in eye size (difference between EtOHexposed fetus and its paired control) and reduction in mtDNA levels presented as a scatter plot. Calculations are based on Spearman's correlation on exact Two-Tailed Probabilities critical p values for $N > 2 < = 18$ (Ramsey, 1989; Fowler et al., 2009).

EtOH-exposed fetuses suggest the need for follow-up studies to determine whether IGF-1 administration might help protect fetuses exposed to EtOH, as previously suggested for EtOH-induced neuronal and OL injury (Darbinian et al., 2021a, 2023). The knowledge derived could lead to use of FB-E cargo assays as diagnostic and prognostic tools for the development of therapies to prevent or treat FASD and early aging. That this might be so is suggested by the close correlation found between the increase in mtDNA damage in FB-Es and an anatomical hallmark of FASD, i.e., the reduction in eye diameters demonstrated in both rat and human fetuses.

Data availability statement

The raw data supporting the conclusions of this article will be made available by the authors, without undue reservation.

Ethics statement

The studies involving human participants were reviewed and approved by Temple University Institutional Review Board (IRB). The patients/participants provided their written informed consent to participate in this study. The animal study was reviewed and approved by Temple University Institutional Animal Care and Use Committee (IACUC)-approved protocol.

Author contributions

ND: designing of the experiments, developing exosome studies, managing the project, supervising all experimental processes, writing of the first draft, participation in reviewing and editing the manuscript, and supporting the project financially. AD: conceptualization, idea, methodology, data analysis, writing, reviewing, and editing, and visualization. NM: flow cytometry analysis, supervising students, participated in exosome isolation, and editing of the manuscript. MK: discussion, editing, and carrying out data collection. GT: statistical support. SA: reviewing and editing the manuscript and supporting the project financially. LG: reviewing, and editing of the manuscript, developing exosome studies, and supporting the project financially. MS: designing of the study and interpretating the data, provided overall scientific expertise, participated in the writing of the first draft of the manuscript, reviewing and editing the final manuscript, and supporting the project financially. All authors have read and approved the last version of the manuscript.

Funding

This work was supported by NIH grant to SA; NIH grant R01HD069238, and Gates Foundation grant OPP1119489 to LG, by NIH grants R01NS97846, R01NS097846-02S1 and R01NS092876 awarded to MS; Shriners research grant SHC-85400 awarded to MS; and United States Pennsylvania State Health Department grant Project 10: 420491–04400-02 to ND.

Acknowledgments

We thank study coordinators, Gabrielle Rebillard and Tamara Tatevosian-Geller (MPH) for their assistance in the collecting of blood samples. We also wish to thank Anna-Mariya Kukuyan for important suggestions in the use of fluorometric quantification software for mtDNA quantification.

Conflict of interest

The authors declare that the research was conducted in the absence of any commercial or financial relationships that could be construed as a potential conflict of interest.

Publisher's note

All claims expressed in this article are solely those of the authors and do not necessarily represent those of their affiliated organizations, or those of the publisher, the editors and the reviewers. Any product that may be evaluated in this article, or claim that may be made by its manufacturer, is not guaranteed or endorsed by the publisher.

References

Abdullaev, S., Gubina, N., Bulanova, T., and Gaziev, A. (2020). Assessment of nuclear and mitochondrial DNA, expression of mitochondria-related genes in different brain regions in rats after whole-body X-ray irradiation. *Int. J. Mol. Sci.* 21:1196. doi: 10.3390/ijms21041196

Ahn, S. J. (1996). José Costa, Janet Rettig Emanuel, PicoGreen quantitation of DNA: effective evaluation of samples pre-or Psost-PCR. *Nucleic Acids Res.* 24, 2623–2625. doi: 10.1093/nar/24.13.2623

Amini, S., Merabova, N., Khalili, K., and Darbinian, N. (2009). p38SJ, a novel DINGG protein protects neuronal cells from alcohol induced injury and death. *J. Cell. Physiol.* 221, 499–504. doi: 10.1002/jcp.21903

Balaraman, S., Lunde, E. R., Sawant, O., Cudd, T. A., Washburn, S. E., and Miranda, R. C. (2014). Maternal and neonatal plasma microRNA biomarkers for fetal alcohol exposure in an ovine model. *Alcohol. Clin. Exp. Res.* 38, 1390–1400. doi: 10.1111/acer.12378. Epub 2014 Mar 3

Balaraman, S., Schafer, J. J., Tseng, A. M., Wertelecki, W., Yevtushok, L., Zymak-Zakutnya, N., et al. (2016). Plasma miRNA profiles in pregnant women predict infant outcomes following prenatal alcohol exposure. *PLoS One* 11:e0165081. doi: 10.1371/journal.pone.0165081

Bartho, L. A., Fisher, J. J., Cuffe, J. S. M., and Perkins, A. V. (2020). Mitochondrial transformations in the aging human placenta. *Am. J. Physiol. Endocrinol. Metab.* 319, E981–E994. doi: 10.1152/ajpendo.00354.2020

Batagov, A. O., and Kurochkin, I. V. (2013). Exosomes secreted by human cells transport largely mRNA fragments that are enriched in the 3′-untranslated regions. *Biol. Direct* 8:12. doi: 10.1186/1745-6150-8-12

Berger, L., Fendrich, M., Jones, J., Fuhrmann, D., Plate, C., and Lewis, D. (2014). Ethyl glucuronide in hair and fingernails as a long-term alcohol biomarker. *Addiction* 109, 425–431. doi: 10.1111/add.12402

Bijnens, E. M., Derom, C., Weyers, S., Janssen, B. G., Thiery, E., and Nawrot, T. S. (2019). Placental mitochondrial DNA content is associated with childhood intelligence. *J. Transl. Med.* 17:361. doi: 10.1186/s12967-019-2105-y

Boiteux, S., and Radicella, J. P. (1999). Base excision repair of 8-hydroxyguanine protects DNA from endogenous oxidative stress. *Biochimie* 81, 59–67. doi: 10.1016/s03009084(99)80039-x

Boiteux, S., and Radicella, J. P. (2000). The human OGG1 gene: structure, functions, and its implication in the process of carcinogenesis. *Arch. Biochem. Biophys.* 377, 1–8. doi: 10.1006/abbi.2000.1773

Bukiya, A. N. (2019). Fetal cerebral artery mitochondrion as target of prenatal alcohol exposure. *Int. J. Environ. Res. Public Health* 16:1586. doi: 10.3390/ijerph16091586

Carelli, V., and Chan, D. C. (2014). Mitochondrial DNA: impacting central and peripheral nervous systems. *Neuron* 84, 1126–1142. doi: 10.1016/j.neuron.2014.11.022

Cardozo-Pelaez, F., Brooks, P. J., Stedeford, T., Song, S., and Sanchez-Ramos, J. (2000). DNA damage, repair, and antioxidant systems in brain regions: a correlative study. *Free Radic. Biol. Med.* 28, 779–785. doi: 10.1016/s0891-5849(00)00172-6

Casula, M., Bosboom-Dobbelaer, I., Smolders, K., Otto, S., Bakker, M., De Baar, M. P., et al. (2005). Anthony de ronde, infection with HIV-1 induces a decrease in mtDNA. *J. Infect. Dis.* 191, 1468–1471. doi: 10.1086/429412

Cline, S. D. (2012). Mitochondrial DNA damage and its consequences for mitochondrial gene expression. *Biochim. Biophys. Acta* 1819, 979–991. doi: 10.1016/j.bbagrm.2012.06.002

Côté, H. C., Brumme, Z. L., Craib, K. J., Alexander, C. S., Wynhoven, B., Ting, L., et al. (2002). Changes in mitochondrial DNA as a marker of nucleoside toxicity in HIV-infected patients. *N. Engl. J. Med.* 346, 811–820. doi: 10.1056/NEJMoa012035

Cutler, R. G. (2005) Fall). Oxidative stress and aging: catalase is a longevity determinant enzyme. *Rejuvenation Res.* 8, 138–140. doi: 10.1089/rej.2005.8.138

Darbinian, N., Darbinyan, A., Merabova, N., Selzer, M. E., and Amini, S. (2020). HIV-1 and HIV-1-tat induce mitochondrial DNA damage in human neurons. J HIV. *AIDS* 6:176. doi: 10.16966/2380-5536.176

Darbinian, N., Darbinyan, A., Sinard, J., Tatevosian, G., Merabova, N., D'Amico, F., et al. (2023). Molecular markers in maternal blood exosomes allow early detection of Fetal alcohol Spectrum disorders. *Int. J. Mol. Sci.* 24:135. doi: 10.3390/ijms24010135

Darbinian, N., Darbinyan, A., Merabova, N., Bajwa, A., Tatevosian, G., Martirosyan, D., et al. (2021a). Ethanol-mediated alterations in oligodendrocyte differentiation in the developing brain. *Neurobiol. Dis.* 148:105181. doi: 10.1016/j.nbd.2020.105181

Darbinian, N., Darbinyan, A., Merabova, N., and Amini, A. (2021b). Fetal brain injury models of Fetal alcohol syndrome (FAS): examination of neuronal morphologic condition using Sholl assay. *Methods Mol Biol* 2311, 195–201. doi: 10.1007/978-1-0716-1437-2_16

Darbinian, N., Darbinyan, A., Merabova, N., and Amini, S. (2021c). Isolation of Primary Human and Rodent Brain Microvascular Endothelial Cells: Culturing, Characterization, and High-Efficiency Transfection. *Methods Mol. Biol.* 2311, 185–193. doi: 10.1007/978-1-0716-1437-2_15

Darbinian, N., Khalili, K., and Amini, S. (2014). Neuroprotective activity of pDING in response to HIV-1 Tat. *J. Cell Physiol.* 229, 153–161. doi: 10.1002/jcp.24392

Darbinian-Sarkissian, N., Darbinyan, A., Otte, J., Radhakrishnan, S., Sawaya, B. E., Arzumanyan, A., et al. (2006). p27(SJ), a novel protein in St John's Wort, that suppresses expression of HIV-1 genome. *Gene Ther.* 13, 288–295. doi: 10.1038/sj.gt.3302649

Darbinian, N., and Selzer, M. (2022). Oligodendrocyte pathology in the developing brain in Fetal alcohol syndrome. *Neural Regen. Res.* 17, 497–502. doi: 10.4103/1673-5374.314294

Darbinyan, A., Kaminski, R., White, M. K., Pozniak, P. D., Darbinian, N., and Khalili, K. (2021). Isolation and propagation of primary human and rodent embryonic neural progenitor cells and cortical neurons. *Methods Mol. Biol.* 2311, 51–61. doi: 10.1007/978-1-0716-1437-2_5

Darbinyan, A., Kaminski, R., White, M., Darbinian-Sarkissian, N., and Khalili, K. (2013a). Polyomavirus JC infection inhibits differentiation of oligodendrocyte progenitor cells. *J. Neurosci. Res.* 91, 116–127. doi: 10.1002/jnr.23135

Darbinyan, A., Pozniak, P., Darbinian, N., White, M. K., and Khalili, K.. Compartmentalized neuronal cultures: *Methods Mol. Biol.* (2013b); Chapter 12, 1078:147–152. doi: 10.1007/978-1-62703-640-5_13

De Simone, F. I., Darbinian, N., Amini, S., Muniswamy, M., White, M. K., Elrod, J. W., et al. (2016). HIV-1 tat and cocaine impair survival of cultured primary neuronal cells via a mitochondrial pathway. *J. Neuroimmune Pharmacol.* 11, 358–368. doi: 10.1007/s11481-016-9669-6

Dizdaroglu, M., Coskun, E., and Jaruga, P. (2017). Repair of oxidatively induced DNA damage by DNA glycosylases: mechanisms of action, substrate specificities and excision kinetics. *Mutat. Res. Rev. Mutat. Res.* 771, 99–127. doi: 10.1016/j.mrrev.2017.02.001

Dukes, K. A., Burd, L., Elliott, A. J., Fifer, W. P., Folkerth, R. D., Hankins, G. D. V., et al. (2014). The safe passage study: design, methods, recruitment, and follow-up approach. *Paediatr. Perinat. Epidemiol.* 28, 455–465. doi: 10.1111/ppe.12136

Ebrahimkhani, S., Vafaee, F., Young, P. E., Hur, S. S. J., Hawke, S., Devenney, E., et al. (2017). Exosomal microRNA signatures in multiple sclerosis reflect disease status. *Sci. Rep.* 7:14293. doi: 10.1038/s41598-017-14301-3

Fowler, J., Cohen, L., and Jarvis, P., (2009), *Practical statistics for field biology*, p. 132. John Wiley & Sons. New Jersey

Fruhbeis, C., Frohlich, D., and Kramer-Albers, E. M. (2012). Emerging roles of exosomes in neuronglia communication. *Front. Physiol.* 3:119. doi: 10.3389/fphys.2012.00119

Furda, A., Santos, J. H., Meyer, J. N., and Van Houten, B. (2014). Quantitative PCR-based measurement of nuclear and mitochondrial DNA damage and repair in mammalian cells. *Methods Mol. Biol.* 1105, 419–437. doi: 10.1007/978-1-62703-739-6_31

Goetzl, L., Darbinian, N., and Goetzl, E. J. (2016). Novel window on early human neurodevelopment via fetal exosomes in maternal blood. *Ann Clin Transl Neurol* 3, 381–385. doi: 10.1002/acn3.296

Goetzl, L., Darbinian, N., and Merabova, N. (2019a). Noninvasive assessment of Fetal central nervous system insult: potential application to prenatal diagnosis. *Prenat Diagn* 39, 609–615. doi: 10.1002/pd.5474

Goetzl, L., Thompson-Felix, T., Darbinian, N., Merabova, N., Merali, S., Merali, C., et al. (2019b). Novel biomarkers to assess in utero effects of maternal opioid use: First steps toward understanding short- and long-term neurodevelopmental sequelae. *Genes Brain Behav.* 18:e12583. doi: 10.1111/gbb.12583

Gureev, A. P., Shaforostova, E. A., Starkov, A. A., and Popov, V. N. (2017). Simplified qPCR method for detecting excessive mtDNA damage induced by exogenous factors. *Toxicology* 382, 67–74. doi: 10.1016/j.tox.2017.03.010

Gyllenhammer, L. E., Rasmussen, J. M., Bertele, N., Halbing, A., Entringer, S., Wadhwa, P. D., et al. (2022). Maternal inflammation during pregnancy and offspring brain development: the role of mitochondria. *Biol Psychiatry Cogn Neurosci Neuroimaging* 7, 498–509. doi: 10.1016/j.bpsc.2021.11.003

Hoek, J. B., Cahill, A., and Pastorino, J. G. (2002). Alcohol and mitochondria: a dysfunctional relationship. *Gastroenterology* 122, 2049–2063. doi: 10.1053/gast.2002.33613

Hoyme, H. E., Kalberg, W. O., Elliott, A. J., Blankenship, J., Buckley, D., Marais, A. S., et al. Updated clinical guidelines for diagnosing Fetal alcohol Spectrum disorders. Pediatrics (2016), 138, e20154256. Available at: https://pediatrics.aappublications.org/content/138/2/e20154256 (accessed on 1 August 2016).

Hunter, S. E., Jung, D., Di Giulio, R. T., and Meyer, J. N. (2010). The QPCR assay for analysis of mitochondrial DNA damage, repair, and relative copy number. *Methods* 51, 444–451. doi: 10.1016/j.ymeth.2010.01.033

Kaarniranta, K., Pawlowska, E., Szczepanska, J., Jablkowska, A., and Blasiak, J. (2019). Role of mitochondrial DNA damage in ROS-mediated pathogenesis of age-related macular degeneration (AMD). *Int. J. Mol. Sci.* 20:2374. doi: 10.3390/ijms20102374

Kovalenko, O. A., and Santos, J. H. (2009). Analysis of oxidative damage by gene-specific quantitative PCR. *Curr. Protoc. Hum. Genet.* 62, 19.1.1–19.1.13. doi: 10.1002/0471142905.hg1901s62

Kramer-Albers, E. M., Bretz, N., Tenzer, S., Winterstein, C., Mobius, W., Berger, H., et al. (2007). Oligodendrocytes secrete exosomes containing major myelin and stressprotective proteins: trophic support for axons? *Proteomics Clin. Appl.* 1, 1446–1461. doi: 10.1002/prca.200700522

Lagarde, W. H., Benjamin, R., Heerens, A. T., Ye, P., Cohen, R. I., Moats-Staats, B. M., et al. (2007). A nontransformed oligodendrocyte precursor cell line, OL-1, facilitates studies of insulin-like growth factor-I signaling during oligodendrocyte development. *Int. J. Dev. Neurosci.* 25, 95–105. doi: 10.1016/j.ijdevneu.2006.12.006

Mason, J. L., Xuan, S., Dragatsis, I., Efstratiadis, A., and Goldman, J. E. (2003). Insulin-like growth factor (IGF) signaling through type 1 IGF receptor plays an important role in remyelination. *J. Neurosci.* 23, 7710–7718. doi: 10.1523/JNEUROSCI.23-20-07710.2003

May, P. A., Gossage, J. P., Kalberg, W. O., Robinson, L. K., Buckley, D., Manning, M., et al. (2009). Prevalence and epidemiologic characteristics of FASD from various research methods with an emphasis on recent in-school studies. *Dev. Disabil. Res. Rev.* 15, 176–192. doi: 10.1002/ddrr.68

May, P. A., Baete, A., Russo, J., Elliott, A. J., Blankenship, J., Kalberg, W. O., et al. (2014). Prevalence and characteristics of fetal alcohol spectrum disorders. *Pediatrics* 134:855866, 855–866. doi: 10.1542/peds.2013-3319

May, P. A., Chambers, C. D., Kalberg, W. O., Zellner, J., Feldman, H., Buckley, D., et al. (2018). Prevalence of Fetal alcohol Spectrum disorders in 4 US communities. *JAMA* 319, 474–482. doi: 10.1001/jama.2017.21896

Meyer, J. N. (2010). QPCR: a tool for analysis of mitochondrial and nuclear DNA damage in ecotoxicology. *Ecotoxicology* 19, 804–811. doi: 10.1007/s10646-009-0457-4

Moore, E. M., and Riley, E. P. (2015). What happens when children with Fetal alcohol Spectrum disorders become adults? *Curr. Dev. Disord. Rep.* 2, 219–227. doi: 10.1007/s40474-015-0053-7

Nishioka, K., Ohtsubo, T., Oda, H., Fujiwara, T., Kang, D., Sugimachi, K., et al. (1999). Expression and differential intracellular localization of two major forms of human 8-oxoguanine DNA glycosylase encoded by alternatively spliced OGG1 mRNAs. *Mol. Biol. Cell* 10, 1637–1652. doi: 10.1091/mbc.10.5.1637

PHS Policy on Humane Care and Use of Laboratory Animals, (2015), Available at: https://olaw.nih.gov/policieslaws/phs-policy.htm

Pirini, F., Guida, E., Lawson, F., Mancinelli, A., and Guerrero-Preston, R. (2015). Nuclear and mitochondrial DNA alterations in newborns with prenatal exposure to cigarette smoke. *Int. J. Environ. Res. Public Health* 12, 1135–1155. doi: 10.3390/ijerph120201135

Prakash, A., and Doublié, S. (2015). Base excision repair in the mitochondria. *J. Cell. Biochem.* 116, 1490–1499. doi: 10.1002/jcb.25103

Ramsey, P. H. (1989). Critical values for Spearman's rank order correlation. *J. Educ. Statistics Fall* 14, 245–253. doi: 10.3102/10769986014003245

Ribeiro, M., Rosenstock, T. R., Oliveira, A. M., Oliveira, C. R., and Rego, A. C. (2014). Insulin and IGF-1 improve mitochondrial function in a PI-3K/Akt-dependent manner and reduce mitochondrial generation of reactive oxygen species in Huntington's disease knock-in striatal cells. *Free Radic. Biol. Med.* 74, 129–144. doi: 10.1016/j.freeradbiomed.2014.06.023

Pejznochová, M., Tesařová, M., Honzík, T., Hansíková, H., Magner, M., and Zeman, J. (2008). The developmental changes in mitochondrial DNA content per cell in human cord blood leukocytes during gestation. *Physiol. Res.* 57, 947–955. doi: 10.33549/physiolres.931246

Rice, A. C., Keeney, P. M., Algarzae, N. K., Ladd, A. C., Thomas, R. R., and Bennett, J. P. Jr. (2014). Mitochondrial DNA copy numbers in pyramidal neurons are decreased and mitochondrial biogenesis transcriptome signaling is disrupted in Alzheimer's disease hippocampi. *J. Alzheimers Dis.* 40, 319–330. doi: 10.3233/JAD-131715

Skog, J., Würdinger, T., van Rijn, S., Meijer, D. H., Gainche, L., Sena-Esteves, M., et al. (2008). Glioblastoma microvesicles transport RNA and proteins that promote tumour growth and provide diagnostic biomarkers. *Nat. Cell Biol.* 10, 1470–1476. doi: 10.1038/ncb1800

Skotland, T., Ekroos, K., Kauhanen, D., Simolin, H., Seierstad, T., Berge, V., et al. (2017). Molecular lipid species in urinary exosomes as potential prostate cancer biomarkers. *Eur. J. Cancer.* 70, 122–132. doi: 10.1016/j.ejca.2016.10.011

Spong, C. Y., Mercer, B. M., D'Alton, M., Kilpatrick, S., Blackwell, S., and Saade, G. (2011). Timing of indicated latepreterm and early-term birth. *Obstet. Gynecol.* 118, 323–333. doi: 10.1097/AOG.0b013e3182255999

Thakur, B. K., Zhang, H., Becker, A., Matei, I., Huang, Y., Costa-Silva, B., et al. (2014). Double-stranded DNA in exosomes: a novel biomarker in cancer detection. *Cell Res.* 24, 766–769. doi: 10.1038/cr.2014.44

Thangaraj, A., Periyasamy, P., Liao, K., Bendi, V. S., Callen, S., Pendyala, G., et al. (2018). HIV-1 TAT-mediated microglial activation: role of mitochondrial dysfunction and defective mitophagy. *Autophagy* 14, 1596–1619. doi: 10.1080/15548627.2018.1476810

Tseng, A. M., Chung, D. D., Pinson, M. R., Salem, N. A., Eaves, S. E., and Miranda, R. C. (2019). Ethanol exposure increases miR-140 in extracellular vesicles: implications for Fetal neural stem cell proliferation and maturation. *Alcohol. Clin. Exp. Res.* 43, 1414–1426. doi: 10.1111/acer.14066

Vaidya, M., Sreerama, S., Gaviria, M., and Sugaya, K. (2022). Exposure to a pathological condition May be required for the cells to secrete exosomes containing mtDNA aberration. *J Nucleic Acids.* 2022, 1–9. doi: 10.1155/2022/7960198

Valadi, H., Ekström, K., Bossios, A., Sjöstrand, M., Lee, J. J., and Lötvall, J. O. (2007). Exosome-mediated transfer of mRNAs and microRNAs is a novel mechanism of genetic exchange between cells. *Nat. Cell Biol.* 9, 654–659. doi: 10.1038/ncb1596

Valenzuela, C. F., Puglia, M. P., and Zucca, S. (2011). Focus on: neurotransmitter systems. *Alcohol Res. Health* 34, 106–120

Verjat, T., Dhénaut, A., Radicella, J. P., and Araneda, S. (2000). Detection of 8-oxoG DNA glycosylase activity and OGG1 transcripts in the rat CNS. *Mutat. Res.* 460, 127–138. doi: 10.1016/s09218777(00)00022-7

Wang, J. Y., Darbinyan, A., White, M. K., Darbinian, N., Reiss, K., and Amini, S. (2014). Involvement of IRS-1 interaction with ADAM10 in the regulation of neurite extension. *J. Cell. Physiol.* 229, 1039–1046. doi: 10.1002/jcp.24528

Westbrook, D. G., Anderson, P. G., Pinkerton, K. E., and Ballinger, S. W. (2010). Perinatal tobacco smoke exposure increases vascular oxidative stress and mitochondrial damage in non-human primates. *Cardiovasc. Toxicol.* 10, 216–226. doi: 10.1007/s12012-010-9085-8

Witwer, K. W., Soekmadji, C., Hill, A. F., Wauben, M. H., Buzás, E. I., di Vizio, D., et al. (2017). Updating the MISEV minimal requirements for extracellular vesicle studies: building bridges to reproducibility. *J Extracell Vesicles* 6:1396823. doi: 10.1080/20013078.2017.1396823

Wong, A. W., McCallum, G. P., Jeng, W., and Wells, P. G. (2008). Oxoguanine glycosylase 1 protects against methamphetamine-enhanced fetal brain oxidative DNA damage and neurodevelopmental deficits. *J. Neurosci.* 28, 9047–9054. doi: 10.1523/JNEUROSCI.2557-08.2008

Yakes, F. M., and Van Houten, B. (1997). Mitochondrial DNA damage is more extensive and persists longer than nuclear DNA damage in human cells following oxidative stress. *Proc. Natl. Acad. Sci. U. S. A.* 94, 514–519. doi: 10.1073/pnas.94.2.514

Yang, J. L., Weissman, L., Bohr, V. A., and Mattson, M. P. (2008). Mitochondrial DNA damage and repair in neurodegenerative disorders. *DNA Repair (Amst)* 7, 1110–1120. doi: 10.1016/j.dnarep.2008.03.012

Ye, P., and D'Ercole, A. J. (1999). Insulin-like growth factor I protects oligodendrocytes from tumor necrosis factor-alpha-induced injury. *Endocrinology* 140, 3063–3072. doi: 10.1210/endo.140.7.6754

Zhao, L., and Sumberaz, P. (2020). Mitochondrial DNA damage: prevalence, biological consequence, and emerging pathways. *Chem. Res. Toxicol.* 33, 2491–2502. doi: 10.1021/acs.chemrestox.0c00083

frontiers | Frontiers in Neuroscience

TYPE Original Research
PUBLISHED 09 August 2023
DOI 10.3389/fnins.2023.1152038

Check for updates

OPEN ACCESS

EDITED BY
Kirsten A. Donald,
University of Cape Town, South Africa

REVIEWED BY
Xiangyu Long,
University of Calgary, Canada
Srinivas Dannaram,
Banner - University Medical Center Phoenix, United States
Ahmet Özaslan,
Gazi University, Türkiye

*CORRESPONDENCE
Julia M. Stephen
✉ jstephen@mrn.org

RECEIVED 27 January 2023
ACCEPTED 24 July 2023
PUBLISHED 09 August 2023

CITATION
Boateng T, Beauchamp K, Torres F, Ruffaner-Hanson CD, Pinner JFL, Vakamudi K, Cerros C, Hill DE and Stephen JM (2023) Brain structural differences in children with fetal alcohol spectrum disorder and its subtypes. *Front. Neurosci.* 17:1152038. doi: 10.3389/fnins.2023.1152038

COPYRIGHT
© 2023 Boateng, Beauchamp, Torres, Ruffaner-Hanson, Pinner, Vakamudi, Cerros, Hill and Stephen. This is an open-access article distributed under the terms of the Creative Commons Attribution License (CC BY). The use, distribution or reproduction in other forums is permitted, provided the original author(s) and the copyright owner(s) are credited and that the original publication in this journal is cited, in accordance with accepted academic practice. No use, distribution or reproduction is permitted which does not comply with these terms.

Brain structural differences in children with fetal alcohol spectrum disorder and its subtypes

Theresah Boateng[1], Kathryn Beauchamp[2,3], Faerl Torres[3], Chaselyn D. Ruffaner-Hanson[4], John F. L. Pinner[3], Kishore Vakamudi[3], Cassandra Cerros[5], Dina E. Hill[6] and Julia M. Stephen[3]*

[1]Department of Special Education, The University of New Mexico, Albuquerque, NM, United States, [2]College of Pharmacy, University of New Mexico Health Sciences Center, Albuquerque, NM, United States, [3]The Mind Research Network, Division of the Lovelace Biomedical Research Institute, Albuquerque, NM, United States, [4]Department of Neurosciences, University of New Mexico Health Sciences Center, Albuquerque, NM, United States, [5]Department of Pediatrics, University of New Mexico Health Sciences Center, Albuquerque, NM, United States, [6]Department of Psychiatry and Behavioral Sciences, University of New Mexico Health Sciences Center, Albuquerque, NM, United States

Introduction: The teratogenic effects of prenatal alcohol exposure (PAE) have been examined in animal models and humans. The current study extends the prior literature by quantifying differences in brain structure for individuals with a fetal alcohol spectrum disorder (FASD) compared to typically developing controls, as well as examining FASD subtypes. We hypothesized the FASD group would reveal smaller brain volume, reduced cortical thickness, and reduced surface area compared to controls, with the partial fetal alcohol syndrome (pFAS)/fetal alcohol syndrome (FAS) subtypes showing the largest effects and the PAE/alcohol-related neurodevelopmental disorder (ARND) subtype revealing intermediate effects.

Methods: The sample consisted of 123 children and adolescents recruited from a single site including children with a diagnosis of FASD/PAE (26 males, 29 females) and controls (34 males, 34 females). Structural T1-weighted MRI scans were obtained on a 3T Trio TIM scanner and FreeSurfer v7.2 was used to quantify brain volume, cortical thickness, and surface area. Analyses examined effects by subgroup: pFAS/FAS (N = 32, M_{age} = 10.7 years, SE_{age} = 0.79), PAE/ARND (N = 23, M_{age} = 10.8, SE_{age} = 0.94), and controls (N = 68, M_{age} = 11.1, SE_{age} = 0.54).

Results: Total brain volume in children with an FASD was smaller relative to controls, but subtype analysis revealed only the pFAS/FAS group differed significantly from controls. Regional analyses similarly revealed reduced brain volume in frontal and temporal regions for children with pFAS/FAS, yet children diagnosed with PAE/ARND generally had similar volumes as controls. Notable differences to this pattern occurred in the cerebellum, caudate, and pallidum where children with pFAS/FAS and PAE/ARND revealed lower volume relative to controls. In the subset of participants who had neuropsychological testing, correlations between volume and IQ scores were observed. Goodness-of-Fit analysis by age revealed differences in developmental patterns (linear vs. quadratic) between groups in some cases.

Discussion: This study confirmed prior results indicating decreased brain volume in children with an FASD and extended the results by demonstrating

differential effects by structure for FASD subtypes. It provides further evidence for a complex role of PAE in structural brain development that is likely related to the cognitive and behavioral effects experienced by children with an FASD.

KEYWORDS

brain volume, fetal alcohol spectrum disorders, magnetic resonance imaging, prenatal alcohol exposure, children

1. Introduction

Fetal alcohol spectrum disorders (FASDs) constitute a range of conditions from mild to severe and can include deficits in cognition and behavior as well as neurological and physical abnormalities as a result of prenatal alcohol exposure (PAE). Fetal alcohol syndrome (FAS), partial fetal alcohol syndrome (pFAS), and alcohol-related neurodevelopmental disorder (ARND) constitute the component subtypes of FASD (Hoyme et al., 2016). Physical effects, cognitive deficits, and behavioral challenges, and concomitant social and adaptive functioning difficulties have been documented as sequelae of PAE (Franklin et al., 2008; Mattson et al., 2013; Williams and Smith, 2015). A significant percentage of children with an FASD, especially those with an ARND subtype, are not diagnosed, under-diagnosed, or misdiagnosed due to the focus on craniofacial anomalies, confusion with diagnostic terminologies, and attribution of symptoms to other disorders, such as attention deficit hyperactivity disorder (ADHD) (Aase, 1994; Astley, 2010; Chasnoff et al., 2015; Hoyme et al., 2016). The Center for Disease Control and Prevention (CDC) has estimated the prevalence of FASD in the United States to be in the range of 1–5 per 100 school children (Sharma, 2001; May et al., 2009, 2014, 2018), which indicates a need for further understanding of the effects of PAE on brain development.

Magnetic resonance imaging (MRI) studies of individuals with PAE have identified structural changes in brain size and shape (including microcephaly), gray and white matter volumes, cortical thickness (CT), and surface area (SA) in children, adolescents, and young adults (Sowell et al., 2002b; Riley et al., 2004; Lebel et al., 2011; Zhou et al., 2011; Roussotte et al., 2012; Yang et al., 2012a). While the severity of abnormalities is positively correlated with higher doses of PAE (Sowell et al., 2008; Zhou et al., 2011; Hoyme et al., 2016; Marshall et al., 2022), some studies found teratogenic effects due to PAE even in cases of minimal alcohol consumption in humans (Joseph et al., 2014; Williams and Smith, 2015; Marshall et al., 2022).

The corpus callosum, cerebellum, and subcortical regions, including the hippocampus and basal ganglia, have consistently emerged as significantly affected due to PAE in earlier autopsy and imaging studies (Jones et al., 1973; Riley et al., 2004). For example, Jacobson et al. (2017) reported significantly smaller corpus callosum in infants subsequently diagnosed with FAS (n = 43) relative to controls. Previous studies revealed total brain volume reductions in gray and white matter in individuals with PAE relative to controls (Archibald et al., 2001; Inkelis et al., 2020), with reports of total brain volume decreases in the pFAS/FAS groups (Archibald et al., 2001; Treit et al., 2016). In addition, Sowell et al. (2002b) showed regional increases in gray matter (GM) volumes in FASD participants. Similarly, Treit et al. (2014) reported less cortical thinning with age in children with FASD. In contrast, reports from Zhou et al. (2018) revealed volume reductions in all brain regions among the PAE group, where total GM in PAE showed a negative correlation with age. These inconsistent reports of the teratogenic effects of PAE on brain volume may be due to variability in dosage, duration, and timing of alcohol exposure, genetics, maternal nutrition, and maternal and fetal metabolism (Petrelli et al., 2018).

Regional volume analyses indicated that inferior parietal/perisylvian regions and the anterior and orbital frontal cortices were significantly reduced in individuals with PAE relative to the control groups (Archibald et al., 2001; Sowell et al., 2002a). However, parietal lobes showed greater reductions than the frontal and temporal lobes in human studies (Archibald et al., 2001; Sowell et al., 2002a; Fernández-Jaén et al., 2011).

While brain volume encompasses both SA and CT, these measures may differ independently, providing additional insight into the underlying mechanisms related to PAE-induced brain damage. PAE-related SA decreases were reported (Migliorini et al., 2015), even within ARND sub-types. However, right temporal lobe SA only approached significance in the ARND groups in Rajaprakash et al. (2014), and the SA analysis performed by Migliorini et al. (2015) was limited to the anterior cingulate cortex. Thus, there is limited knowledge regarding PAE effects on SA throughout the brain.

There are reports of decreased CT among individuals with PAE compared to controls in children (Robertson et al., 2016), children and adolescents (Zhou et al., 2018), and adolescents and adults (Zhou et al., 2011), including reduced CT in the PAE group relative to controls in bilateral regions of frontal, temporal, parietal, and occipital cortices; there was no evidence of increased CT in PAE. In contrast, other studies reported increased CT among the PAE groups relative to controls in children (Treit et al., 2014), children and adolescents (Fernández-Jaén et al., 2011), and in children, adolescents, and young adults (Sowell et al., 2008). Some of these differences may be related to differences in age across these studies.

The most prominent reductions in brain morphology were evident in pFAS/FAS groups (i.e., individuals with dysmorphic physical features) relative to the PAE/ARND and control groups (Roussotte et al., 2012; Yang et al., 2012b). Individuals diagnosed with FAS had the most severe agenesis and general malformations in the brain (Sowell et al., 2002a; Riley et al., 2004; Lebel et al., 2011; Yang et al., 2012a). However, few studies have directly compared

FASD subtypes with respect to volume, CT, and SA across age categories (infants, children, adolescents, young adults, and adults) or sex, although, to the best of our knowledge, all human studies examining brain structure in FASD included male and female participants.

Animal models have shown similar results (O'Leary-Moore et al., 2011; Coleman et al., 2012; Leigland et al., 2013; Zhang et al., 2019) providing additional evidence of the robustness and generalizability of PAE effects on brain structure. These similarities include overall decreases in brain volume (Coleman et al., 2012; Leigland et al., 2013) and dose effects with greater structural abnormalities associated with higher doses of alcohol (Leigland et al., 2013; Zhang et al., 2019). Similar to human studies, there are some conflicting reports of the effects of PAE on brain volume. Coleman et al. (2012) reported decreased brain volume in mice with PAE, while Zhang et al. (2019) revealed no effect of ethanol exposure on whole brain volume in mice. Regional analysis largely focused on frontal and hippocampal regions, with only recent explorations of the functional alterations in parietal lobe (O'Leary-Moore et al., 2011; Leigland et al., 2013; Wang and Kroenke, 2015). PAE-related SA decreases (Leigland et al., 2013) and CT decreases (O'Leary-Moore et al., 2011; Coleman et al., 2012; Leigland et al., 2013; Wang and Kroenke, 2015) were reported in mice. Animal models provide important information regarding metrics that are difficult to control in human studies including exposure amounts to prenatal alcohol. However, large differences in overall brain structure, alcohol metabolism rates and developmental trajectories lead to some challenges in direct translation between animal and human studies.

The purpose of the current study was to examine structural brain differences in children with an FASD; specifically, to investigate effects in FASD subtypes versus control children in a relatively large sample collected at a single site. Structural MRIs (sMRIs) were collected in conjunction with our ongoing MEG studies for source analysis (Stephen et al., 2012; Coffman et al., 2013). We hypothesized that children with an FASD would show smaller brain volume, reduced CT, and reduced SA compared to controls with regionally specific deficits and differential effects in those with and without dysmorphic features due to PAE resulting in the smallest volumes in the pFAS/FAS subtype, mid-level values in the PAE/ARND subtype, and the largest volume measurements in controls. The examination of structural brain metrics in this cohort allowed us to examine if brain structure differs between FASD subtypes potentially indicating differences between those with and without dysmorphic features.

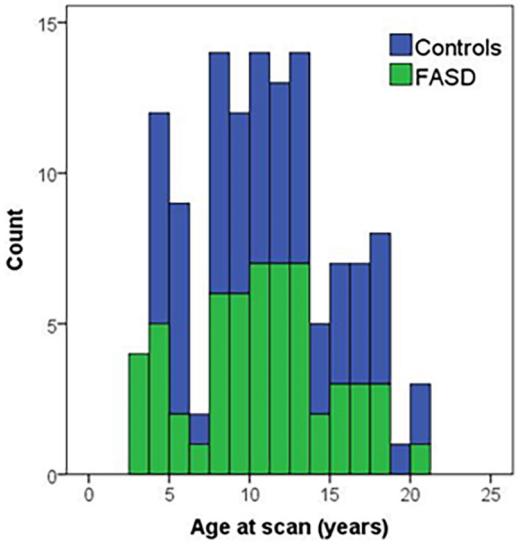


FIGURE 1
Histogram of age of participants at the time of the MRI scan by group. Controls are in blue and FASD is shown in green.

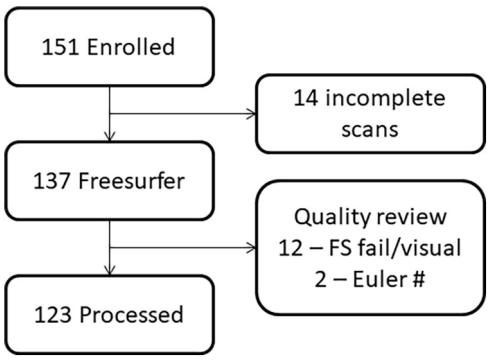


FIGURE 2
Flowchart demonstrating the loss of participants due to challenges in imaging young children versus data quality.

2. Materials and methods

2.1. Participants

The study procedures and human subjects' protocol were approved by the University of New Mexico Health Sciences Center Human Research Review Committee (UNMHSC HRRC). All parents were consented and children ≥7 years of age were assented prior to study participation. Participants were recruited under a single Internal Review Board protocol designed to understand the effects of PAE on brain development. Children from different age ranges (3–7, 8–12, and 12–21 years) were recruited across a 10-year period, representing different cohorts and different cognitive assessments appropriate for age. Sex was self-reported by the parent/participant. Data were collected between 2010 and 2019. Of 151 individuals (total number of children with FASD and neurotypical controls) initially enrolled in the MRI portion of the study, we successfully collected a T1 MRI sequence from 137 children. Of these, 123 sMRIs were of sufficient quality (after excluding $N = 14$ due to subject motion or other artifact) to undergo auto-analysis processing through the FreeSurfer pipeline to allow for volume quantification (see **Figures 1**, **2**).

Children with an FASD and PAE were recruited from the FASD clinic located within the Center for Development and Disability, a University Center for Excellence in Developmental Disabilities Education, Research, and Service housed within the Pediatrics Department of the University of New Mexico Health Sciences Center. Diagnosis on the FASD continuum was based on consensus from an interdisciplinary assessment team comprised of a clinical psychologist, neuropsychologist, and pediatrician using

the Institute of Medicine guidelines and the revised guidelines (Stratton et al., 1996; Hoyme et al., 2016). Children with a differential diagnosis due to a genetic disorder or exposure to other teratogens were excluded. Maternal alcohol consumption was confirmed through either maternal interview, eyewitness reports of maternal drinking during pregnancy, or legal records documenting alcohol consumption during pregnancy (e.g., birth records or recorded incident of driving while intoxicated). Information on maternal alcohol consumption during pregnancy was collected as part of the FASD clinical assessment; however, specific estimates of quantity of alcohol consumption during pregnancy were generally not available. PAE was defined to include documentation of ≥6 drinks per week for ≥2 weeks during pregnancy, ≥3 drinks per occasion on ≥2 occasions during pregnancy, intoxication or history of treatment of an alcohol-related condition, and an assessment using screening tools. Children diagnosed with FAS met the following criteria: at least two of three characteristic facial anomalies, growth restriction and/or deficient brain growth, and cognitive and/or behavioral impairments. Children diagnosed with pFAS with known PAE met the following criteria: at least two of three characteristic facial anomalies and cognitive and/or behavioral functioning impairments. Children diagnosed with pFAS without confirmed PAE met the following criteria: at least two of three characteristic facial anomalies, deficient brain growth, and cognitive and/or behavioral functioning impairments. Total number of participants with FAS (N = 25) and pFAS (N = 7) was 32. Lastly, children diagnosed with ARND (N = 15) met the following criteria: age 3 years or older, confirmation of PAE, and cognitive and/or behavioral functioning impairments. The PAE participants (N = 8) were recruited from the FASD clinic and met criteria for PAE without meeting all criteria demonstrating cognitive/behavioral effects. The control participants (N = 68) were recruited from the community on the basis of reported absence of PAE and other prenatal exposures including tobacco and illicit substances (including cannabis) based on parental interview, no known neurodevelopmental disorder, and, if tested, IQ scores > 70.

2.2. Neuropsychological/cognitive assessment

Depending on the study cohort, participants were provided neuropsychological testing using the Wechsler Abbreviated Scale of Intelligence second edition (WASI-II Full Scale) to assess IQ scores. The WASI-II was not collected for some children between 3 and 11 years of age (some data were collected as a part of pilot data collection that did not include neuropsychological testing), such that the number of participants with reported IQ scores was 86 (40 FASD and 46 controls). Similarly, a subset of children (N = 71; 25 FASD and 46 controls) was assessed using the Grooved Pegboard (GPB) test to measure fine motor function. Because the data were collected in age- and sex-matched cohorts the cognitive testing was applied equally across groups.

2.3. Structural MRI (sMRI) data acquisition

This analysis included participants who were recruited into three different studies across a 10-year period who underwent a sagittal T1-weighted anatomical MRI scan in a Siemens TIM Trio 3 Tesla MRI system with a five-echo 3D MPRAGE sequence [TR/TE/TI - 2530/1.64, 3.5, 5.36, 7.22, 9.08/1200 ms, flip angle - 7 deg, field of view (FOV) 256 × 256 mm, 1 mm thick slice, 192 slices, GRAPPA acceleration factor - 2]. Over the 10-year data collection period, a single change in the sMRI imaging protocol occurred with an upgrade from a 12-channel to a 32-channel head coil. Since children were recruited in age-matched cohorts, groups (FASD vs. controls) were well-matched for use of 12- or 32-channel head coils. FreeSurfer version 7.2 (Dale et al., 1999) was used to perform cortical reconstruction and volume segmentation.[1] The FreeSurfer pipeline included motion correction (Reuter et al., 2010), segmentation, and intensity normalization. All MRIs were visually checked for data quality. For MRIs that showed some motion artifact, cortical parcelation was verified visually following Freesurfer processing. Finally, the Euler number, which is a quantitative approach to evaluate motion (Rosen et al., 2018), was extracted following the Freesurfer processing for each MRI; two participants (1 PAE, 1 FAS) were excluded for being statistical outliers (outside the 3rd quartile ± 1.5 × interquartile range). The statistical analysis focused on total brain volume, CT, SA, region of interest analysis (cerebellum, thalamus, caudate, putamen, pallidum, hippocampus, and amygdala), and lobar analysis (frontal, temporal, parietal, occipital) defined by the Desikan-Killiany FreeSurfer atlas.

2.4. Statistical analyses

The final output from the FreeSurfer analysis was transferred to SPSS v.20 for statistical analysis. Given previous research identifying the cerebellum, thalamus, caudate, putamen, pallidum, hippocampus, and amygdala as regions most impacted by FASD, we conducted region of interest (ROI) analyses of these regions specifically. To compare with prior studies, we also examined FreeSurfer generated estimates of frontal, temporal, parietal, and occipital volumes. For all but the corpus callosum and subcortical structures, repeated measures analyses across hemispheres were performed to identify hemispheric differences and interactions between group and hemisphere. We also explored potential differences in CT and SA in the frontal, parietal, temporal, and occipital lobes.

One-way and repeated measures ANOVAs were used to assess two sets of group differences, FASD vs. control, and pFAS/FAS vs. PAE/ARND vs. control, for demographic, behavioral, and sMRI variables (volume, CT, SA). All variables were evaluated for outliers. There were four participants with outlier data representing nine data points identified from the Freesurfer variables (participant 1: left and right parietal SA, right occipital SA, right occipital gray matter (GM) volume; participant 2: left hippocampus, left and right amygdala; and participants 3&4: corpus callosum). Volumes of individual structures were evaluated with and without estimated total intracranial volume (eTIV) as a covariate to determine if the volume was affected similarly relative to the intracranial volume across groups. For regional volume analyses, only analyses with eTIV as a covariate were performed to determine if there were region-specific reductions. One-way ANCOVAs were used

1 http://surfer.nmr.mgh.harvard.edu/

TABLE 1 Mean (M) values and standard errors (SE) of volume, cortical thickness, and surface area.

	Control		FASD		PAE/ARND	pFAS/FAS
Volume (mm^3)	M (SE)	Age	M (SE)	Age	M (SE)	M (SE)
Total brain vol w/o ventricles	1153384 (15036)	Quad	1036993 (16345)	Quad	1127036 (23822)	960852 (20404)
eTIV	1508244 (21401)	Linear	1370717 (23406)	Linear	1494456 (32963)	1278524 (28233)
Cortical GM	271068 (3514)	Quad	246039 (3844)	Quad	267354 (5380)	230513 (4608)
Corpus callosum vol	3404 (70)	Linear	3013 (75)	Quad	3207 (112)	2860 (97)
Cerebellum cortex vol	54492 (639)	Quad	48071 (699)	Linear	50843 (1019)	45955 (872)
Thalamus vol	7814 (107)	Linear	6946 (117)	Linear	7614 (161)	6444 (138)
Caudate vol	3901 (61)	n/a	3201 (67)	n/a	3550 (95)	2942 (82)
Putamen vol	5229 (81)	Linear	4690 (88)	n/a	5058 (129)	4415 (111)
Pallidum vol	2042 (32)	Linear	1745 (35)	Quad	1921 (50)	1614 (43)
Hippocampus vol	4103 (58)	Linear	3668 (64)	Quad	3924 (94)	3473 (81)
Amygdala vol	1750 (25)	Linear	1583 (27)	Linear	1730 (38)	1471 (33)
Frontal vol	101105 (854)	Quad	97664 (936)	Quad	99033 (1382)	96600 (1330)
Parietal vol	70723 (916)	Linear	70079 (1003)	n/a	73236 (1460)	67230 (1405)
Temporal vol	57820 (535)	Quad	55499 (586)	Quad	56067 (872)	55088 (839)
Occipital vol	25845 (401)	Linear	24651 (444)	n/a	25256 (657)	24133 (624)
Cortical thickness (CT) (mm)						
Mean CT	2.673 (0.014)		2.651 (0.016)		2.653 (0.024)	2.650 (0.021)
Frontal CT	2.796 (0.015)		2.790 (0.017)		2.793 (0.026)	2.789 (0.022)
Parietal CT	2.560 (0.014)		2.558 (0.015)		2.568 (0.024)	2.551 (0.020)
Temporal CT	2.983 (0.017)		2.907 (0.018)		2.922 (0.029)	2.900 (0.025)
Occipital CT	2.050 (0.020)		2.024 (0.022)		2.017 (0.034)	2.031 (0.030)
Surface area (SA) (mm^2)						
Total SA	84867 (526)		84676 (576)		85596 (854)	83924 (822)
Frontal SA	30878 (242)		30264 (265)		30381 (394)	30212 (380)
Parietal SA	24148 (209)		24295 (231)		24984 (335)	23682 (318)
Temporal SA	16502 (125)		16293 (137)		16291 (205)	16319 (197)
Occipital SA	11144 (127)		11178 (141)		11266 (210)	11107 (199)

for the structures that were not examined by hemisphere (brain segmentation w/out ventricles, eTIV, corpus callosum) including group and sex as between-subjects factors and coil channel count as a covariate of no interest. Repeated measures ANCOVA analyses using the general linear model were used to conduct ROI analyses with hemisphere as a within-subjects factor, group and sex as between-subjects factors, coil channel count as a covariate of no interest, and eTIV as a covariate for volume and SA analyses for all regions. Partial correlations were used to conduct exploratory analyses investigating the association between volume and cognitive measures (IQ and GPB), controlling for age and examining the effects when eTIV was included as an additional covariate. GPB time to completion was used for the partial correlation to match with the un-corrected brain volume data. Only individuals > 9 years of age were included in the GPB correlations due to the change in testing instructions at 9 years of age. No children under 8 years of age received the GPB testing, so elimination of only 8-year-olds resulted in a loss of eight datapoints. For ANOVAs, we controlled for 25 comparisons (accounting for all variables included in Table 1) in the FDR correction and used a $q = 0.05$. For correlations, we only examined correlations with brain volume, limiting the number of comparisons to 13. Corrected p-values are reported based on the Benjamini-Hochberg correction (Benjamini and Hochberg, 1995).

Due to the broad age range of our participants (3–20 years), we conducted a Goodness-of-Fit analysis to determine if age was a possible contributing factor to the results. To accomplish this, we examined linear and quadratic associations with age for all variables. To assess associations with age, we conducted Goodness-of-Fit analyses on all variables both linearly and quadratically. Linear vs. quadratic fit was not assessed by subtypes due to the smaller sample size.

3. Results

We report results by structure (cortical GM volume, corpus callosum, cerebellum cortex, thalamus, caudate, putamen,

TABLE 2 Demographics.

Measure	Controls (*N* = 68)	FASD (*N* = 55)	PAE (*N* = 8)/ ARND (*N* = 15)	pFAS (*N* = 7)/ FAS (*N* = 25)
Age (years)	11.1 (0.54)	10.7 (0.61)	10.8 (0.94)	10.7 (0.80)
Head coil (%12/32)	51.5/48.5	50.9/49.1	56.5/43.5	46.9/53.1
Reported sex (M/F)	34/34	26/29	11/12	15/17
Race (%)*†				
American Indian	10.3	63.6	73.9	59.4
Asian	5.9	1.8	0	3.1
African American	1.5	1.8	0	3.1
Caucasian	79.4	27.3	21.7	31.3
Unreported	2.9	3.6	4.3	3.1
% Hispanic*†	42.7	20	17.4	21.9
IQ*†	107 (2)	80 (2)	82 (3.5)	78 (2.8)
Grooved Pegboard	73.4 (3.0)	83.18	78.7 (5.9)	87.3 (5.7)

*$p < 0.05$ controls different than FASD, †$p < 0.05$ controls different than FASD subtypes.

pallidum, hippocampus, and amygdala) and lobe (frontal, parietal, temporal, occipital). In these analyses, we compared FASD vs. controls and PAE/ARND vs. pFAS/FAS vs. controls.

The analysis included 123 participants (68 controls and 57 FASD) who ranged in age from 3 to 21 years of age. The sample was well matched on age across the age spectrum (see Figure 1; $p = 0.63$), use of 12- vs. 32-channel head coil ($p = 0.79$), and reported sex ($p = 0.76$). The control sample included a diverse representation of the local demographics with 42% Hispanic and 10% Native American. The FASD group represented the demographics of the FASD outreach clinics with 63% Native American and 20% Hispanic. Both race and ethnicity were significantly different by group ($p < 0.05$). As expected, IQ scores in the FASD group were lower than the control group ($p < 0.001$) and both FASD subtypes were significantly lower than controls ($p < 0.001$) but not different from each other ($p = 0.36$). There was no significant group or subtype difference in GPB time to completion ($p > 0.05$). More details on the study population are provided in Table 2.

3.1. Comparison of total brain volume, cortical thickness, and surface area between FASD and control participants. Covariates: head coil (12- vs. 32-ch)

As shown in Tables 1, 3, children with FASD had significantly reduced total brain volume and reduced volume in each of the individual structures assessed (corpus callous, cerebellum, thalamus, caudate, putamen, pallidum, and hippocampus). When controlling for eTIV, there was additional loss of volume beyond that expected based on the smaller head size in cerebellum, thalamus, caudate, pallidum, and hippocampus. There were no significant interactions between hemisphere and group. Similarly, there were main effects of sex, which in all cases revealed greater volume in males vs. females. However, there were no significant interactions between sex and group. For the lobar analyses, eTIV was included as a covariate. After correcting for multiple comparisons, significant group effects were seen in frontal and temporal GM volume and temporal lobe GM thickness with FASD less than controls in all cases.

3.2. Comparison of total brain volume, cortical thickness, and surface area between FASD and control participants: goodness-of-fit analyses by age, linear vs. quadratic

Potential group differences in associations with age suggest reported group differences may be influenced by different developmental patterns. Linear vs. quadratic fit are noted in Table 1. Only fits that revealed statistical significance are noted. Cases that did not fit either model are noted as n/a. There were seven structures (corpus callosum, cerebellum, putamen, pallidum, hippocampus, parietal volume, and occipital volume) that revealed different patterns between controls and FASD across age.

3.3. Comparison of total brain volume, cortical thickness, and surface area between PAE/ARND, pFAS/FAS, and control participants. Covariate: head coil (12- vs. 32-ch)

Subtype statistical analyses are presented in Table 4 and example data from different structures are presented in Figures 3, 4. There was a significant difference in overall brain volume when comparing controls vs. the two FASD subtypes with *post hoc* analysis demonstrating the pFAS/FAS group was significantly smaller than PAE/ARND and controls, with no significant difference between PAE/ARND vs. controls. Individual structures revealed significant differences between the three groups, similar

TABLE 3 Statistical results for volume comparing controls to FASD.

	Group $F(1,120)$ p-value	Sex $F(1,120)$ p-value	Group (eTIV) $F(1,119)$ p-value
Brain seg w/o ventricles	27.46 0.000025	37.97 0.000025	–
eTIV	18.88 0.000075	32.35 0.000012	–
Cortical GM	23.08 0.000018	24.57 0.000017	4.39 n.s.
Corpus callosum	14.63 0.00048	6.73 0.027	2.42 n.s.
Cerebellum cortex	45.93 0.000008	21.67 0.000033	23.37 0.000018
Thalamus	29.78 0.000006	21.74 0.00004	9.45 0.0067
Caudate	59.15 0.0000049	3.48 n.s.	35.8 0.000009
Putamen	20.35 0.000047	13.47 0.0011	n.s.
Pallidum	38.18 0.000012	17.02 0.00024	16.66 0.00024
Hippocampus	25.10 0.000008	12.54 0.0028	6.91 0.018
Amygdala	20.30 0.000044	23.15 0.000025	3.93 n.s.
Frontal GM	6.88 0.018	0.002 n.s.	
Parietal GM	0.21 n.s.	0.96 n.s.	
Temporal GM	7.97 0.011	0.3 n.s.	
Occipital GM	3.64 n.s.	1.24 n.s.	

n.s., not significant.

to the group analysis described above. In most cases, the pFAS/FAS group values were significantly smaller than the other two groups. However, there were some notable exceptions. For cerebellum, caudate, and pallidum, controls had significantly greater volume than both FASD subtypes, and the PAE/ARND subtype had greater volumes than the pFAS/FAS subtype. When eTIV was included as a covariate the following structures continued to reveal group differences above and beyond those expected based on the differences in overall brain volume: cortical GM volume, cerebellum, thalamus, caudate, pallidum, hippocampus, and amygdala. There were no significant interactions between hemisphere and group.

Regional analysis revealed significant group differences in frontal, parietal, and temporal lobe GM volume with controls generally revealing significantly greater volume than the pFAS/FAS group. Furthermore, there was a significant difference in temporal lobe GM thickness with controls having greater CT than the pFAS/FAS group. Finally, there was a significant difference in parietal lobe SA with differences only revealed between PAE/ARND vs. pFAS/FAS groups. In this case, the PAE/ARND group had greater SA than controls and pFAS/FAS, although the difference was only significant between the FASD subtypes.

3.4. Correlation between brain structure and IQ and GPB measures

Regions that revealed a significant group difference were evaluated for correlations with behavioral measures. Correlations were examined across the full sample. Age was included as a covariate in all analyses and left and right hemisphere values were summed to create total volume for structures that did not reveal a significant effect of hemisphere. IQ score was highly correlated with all brain structural measures assessed (see **Table 5**). When including eTIV as an additional covariate, a significant correlation with IQ score remained for cerebellum, left and right caudate, and left pallidum (see example correlations in **Figure 5**). There were no regions that revealed a significant correlation with GPB following correction for multiple comparisons.

4. Discussion

We hypothesized that the FASD group would show smaller brain volume, reduced CT, and reduced SA compared to controls and that PAE/ARND subtype would reveal intermediate values between controls and the pFAS/FAS subtype. Consistent with this hypothesis, the FASD participants presented with significantly smaller brain volume compared to the control participants. However, in many cases, individuals with the PAE/ARND subtype did not differ significantly from controls, revealing volumetric differences present only in the pFAS/FAS subtypes of FASD. However, participants with pFAS/FAS and PAE/ARND had similarly decreased volume compared to the control group in other regions, and the controls presented with significantly increased volume in the caudate, cerebellum, and pallidum structures compared to both FASD groups. Participants with FASD had significantly decreased total SA compared to the controls, specifically in the frontal region. Goodness-of-Fit analysis by age with linear and quadratic models indicated the fit between linear and quadratic models for both the FASD and control participants showed mixed results. This indicates differences in developmental patterns may partially explain the group differences in an otherwise well-matched sample.

The results of this large single-site study are consistent with studies that used sMRI to document reduced sizes of the corpus callosum, caudate, and eTIV in individuals with FAS relative to the other FASD subtypes (Archibald et al., 2001; Riley et al., 2004; Inkelis et al., 2020; Krueger et al., 2020) and provide partial replication of prior findings in an independent sample with a diverse representation.

The results reported here are consistent with prior findings when comparing FASD and control groups. Archibald et al. (2001) reported a significant decrease in caudate volumes in the FAS group compared to the control group. Consistent with Inkelis et al. (2020), in a study of adolescents and young adults (13–30 yrs), brain volume reductions were evident in adulthood in corpus callosum and caudate (reported volume decreases in adulthood).

TABLE 4 Statistical results for volume controls vs. PAE/ARND vs. pFAS/FAS.

	Group $F(2,118)$ (p-value)	Sex $F(1,118)$ (p-value)	Group (eTIV) $F(1,117)$ (p-value)	*Post hoc* comparisons†
Brain seg w/o ventricles	29.3 (0.000025)	37.85 (0.000025)	–	C,A>F
eTIV	23.7 (0.000012)	33.6 (0.000012)	–	C,A>F
Cortical GM	27.38 (0.000008)	27.09 (0.000008)	4.15 (0.03)	C,A>F (C,A>F)
Corpus callosum	10.57 (0.0001)	7.59 (0.017)	1.5 (n.s.)	C,A>F
Cerebellum cortex	32.59 (0.000005)	24.87 (0.000001)	12.21 (0.000075)	C>A>F (C>A,F)
Thalamus	34.07 (0.000004)	26.23 (0.000006)	8.29 (0.0011)	C,A>F (C,A>F)
Caudate	46.6 (0.0000035)	2.32 (n.s.)	20.18 (0.000009)	C>A>F (C>A>F)
Putamen	18.48 (0.000004)	12.41 (0.0019)	2.09 (n.s.)	C,A>F
Pallidum	33.0 (0.000003)	15.78 (0.00042)	9.59 (0.0047)	C>A>F (C>A,F)
Hippocampus	20.4 (0.000006)	12.02 (0.002)	3.38 (0.046)	C,A>F (C>F)
Amygdala	25.6 (0.000002)	22.38 (0.00002)	4.84 (0.02)	C,A>F (C,A>F)
Frontal GM	5.94 (0.031)	0.18 (n.s.)		C>F
Parietal GM	4.2 (0.03)	1.97 (n.s.)		C,A>F
Temporal GM	4.07 (0.033)	0.65 (n.s.)		C>F
Occipital GM	2.5 (n.s.)	1.96 (n.s.)		

C, controls, A-PAE/ARND group, F-pFAS/FAS group. n.s., not significant. †Significant *post hoc* comparisons for group without and with eTIV (in parentheses) included as a covariate after accounting for multiple comparisons.

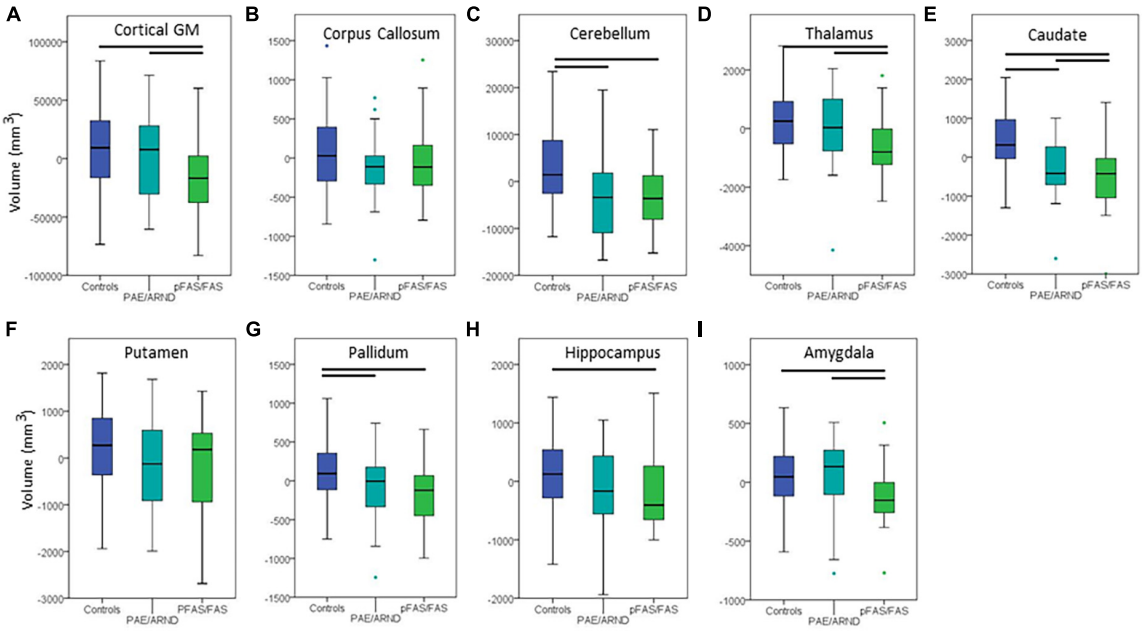


FIGURE 3
Differences in cortical volume between controls and FASD subtypes: **(A)** Cortical GM, **(B)** corpus callosum, **(C)** cerebellum, **(D)** thalamus, **(E)** caudate, **(F)** putamen, **(G)** pallidum, **(H)** hippocampus, and **(I)** amygdala. All data represent the residuals taking into account the covariates of coil channel number and eTIV. The most common pattern observed is consistent with panel **(A)**. Total cortical GM volume in which controls and the PAE/ARND subtype had greater volume than the pFAS/FAS subtype. However, a few structures revealed a significant reduction in volume in both subtypes, as in panel **(C)** cerebellum. In some cases, group differences were only significant between controls and pFAS/FAS subtype with no significant difference of PAE/ARND from either group, as in panel **(H)** hippocampus. A few of the examined structures revealed no group differences, such as **(F)** putamen after including eTIV as a covariate.

Jacobson et al. (2017) reported a significant decrease in corpus callosum volume in infants heavily exposed to prenatal alcohol among the FAS group relative to control groups irrespective of age and sex. Krueger et al. (2020) reported decreased caudate and intracranial volumes in a PAE group compared to controls with no significant differences in age and sex. These results underscore the teratogenic effects of prenatal alcohol irrespective of age of assessment or sex.

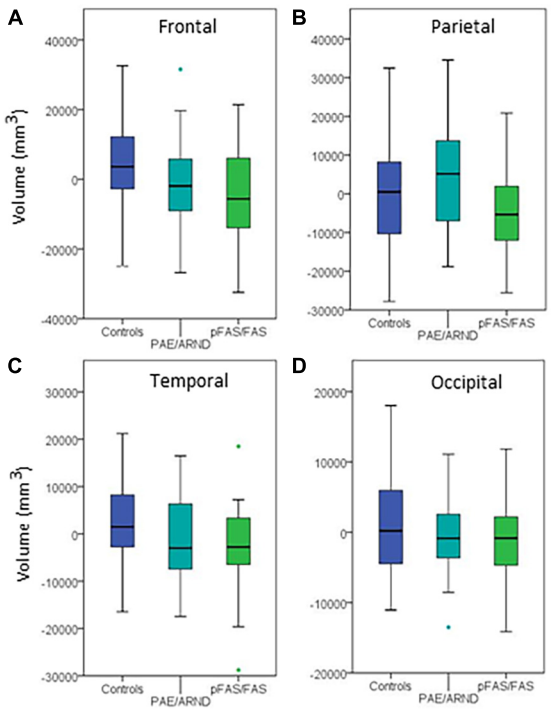


FIGURE 4
Regional differences in cortical volume between controls and FASD subtypes: **(A)** Frontal lobe, **(B)** parietal lobe, **(C)** temporal lobe, and **(D)** occipital lobe. Although three of the regions showed group differences before controlling for eTIV, none revealed significant differences when controlling eTIV after multiple comparisons correction.

TABLE 5 Correlations between IQ and brain volume adjusted for age, eTIV and channel number.

	IQ *r* (*N* = 86) (*p*-value)
Total GM volume	0.26 (n.s.)
Corpus callosum	0.057 (n.s.)
Cerebellum	0.259 (n.s.)
Thalamus	0.182 (n.s.)
Caudate	0.355 (0.003)
Putamen	0.194 (n.s.)
Pallidum	0.241 (n.s.)
Hippocampus	0.106 (n.s.)
Amygdala	0.048 (n.s.)
Frontal lobe	0.263 (n.s.)
Parietal	0.095 (n.s.)
Temporal	0.257 (0.042)
Occipital	0.176 (n.s.)

n.s., not significant.

Our lobar analysis results showed significant group differences in frontal, and temporal lobes with greater volumes in the controls compared to FASD group. Regional analyses indicated that inferior parietal/perisylvian regions and the anterior and orbital frontal cortex are significantly reduced in individuals with PAE relative to controls (Archibald et al., 2001; Sowell et al., 2002a). However, parietal lobes showed greater reductions than frontal and temporal lobes in other studies (Archibald et al., 2001; Riley et al., 2004; Fernández-Jaén et al., 2011). The current results are not consistent with the prior findings demonstrating the greatest effect in parietal lobe. This may be related to smaller sample size in prior studies and the current results indicating a regression to the mean with larger samples or differences in drinking patterns which may differ by site (May et al., 2018).

Limited differences in CT are consistent with the differences in temporal lobe volume with decreases in temporal GM thickness in the FASD group relative to controls. Prior results on CT are mixed with small clinical samples (Treit et al., 2014). A rat model of PAE (Leigland et al., 2013) revealed cortical thinning, whereas a sample of individuals with PAE were reported as having increased CT (Fernández-Jaén et al., 2011). More recent multi-site studies have demonstrated robust group differences with reduction in CT with PAE (Zhou et al., 2018). Other results reveal different developmental patterns in CT across childhood (Zhou et al., 2011). This variability in results in CT across studies could be attributed to small samples, differences in the amount or patterns of maternal alcohol consumption, synaptic development and myelination related to age effects, imaging protocols, statistical analysis, differences in demographics, and differences in the age of the cohorts across studies.

PAE-related SA decreases are reported in both human and animal models [(Leigland et al., 2013) - mice; (Migliorini et al., 2015) - PAE; (Rajaprakash et al., 2014) – ARND). Our current study revealed differences in the parietal lobe SA only with the PAE/ARND subtype having greater SA when controlling for eTIV relative to both the controls and the pFAS/FAS. Sowell et al. (2002b) reported a reduced SA in participants with an FASD in the orbital frontal cortex. The SA analysis performed by Migliorini et al. (2015) was limited to only the anterior cingulate cortex and found decreased SA in the sample of heavy PAE exposed individuals relative to controls. Since brain volume is a combination of CT and cortical SA and we found no differences in CT in parietal lobe, the current results indicate that volumetric differences in parietal lobe are more likely related to SA changes rather than CT.

An important consideration in comparing results across studies in childhood is that brain structure changes with development. That is, cortical thinning in adolescence is expected as a part of typical development. Inkelis et al. (2020) showed a quadratic relationship with age among the FASD group compared to controls. Though inconsistent across structures, the current results revealed different developmental patterns (linear vs. quadratic) between controls and FASD groups as a function of age. These group differences in brain volume indicate that results may differ as a function of age and must be considered when determining if results replicate across samples.

The primary contribution of the current analysis was the examination of the effect of FASD subtype on brain structure. The pattern of results differed by structure with some structures revealing that only the pFAS/FAS group differed from controls, whereas volume was smaller than controls in both subtypes in other structures. While FASD subtype does not necessarily equate to dose effects, finding consistent differences in both subtypes supports the idea that certain brain regions are more susceptible to PAE than other structures. This sensitivity may be related to different patterns of drinking instead of a direct link to amount of alcohol consumed. This result demonstrates the importance of examining volumetric differences by FASD subtype to fully understand the

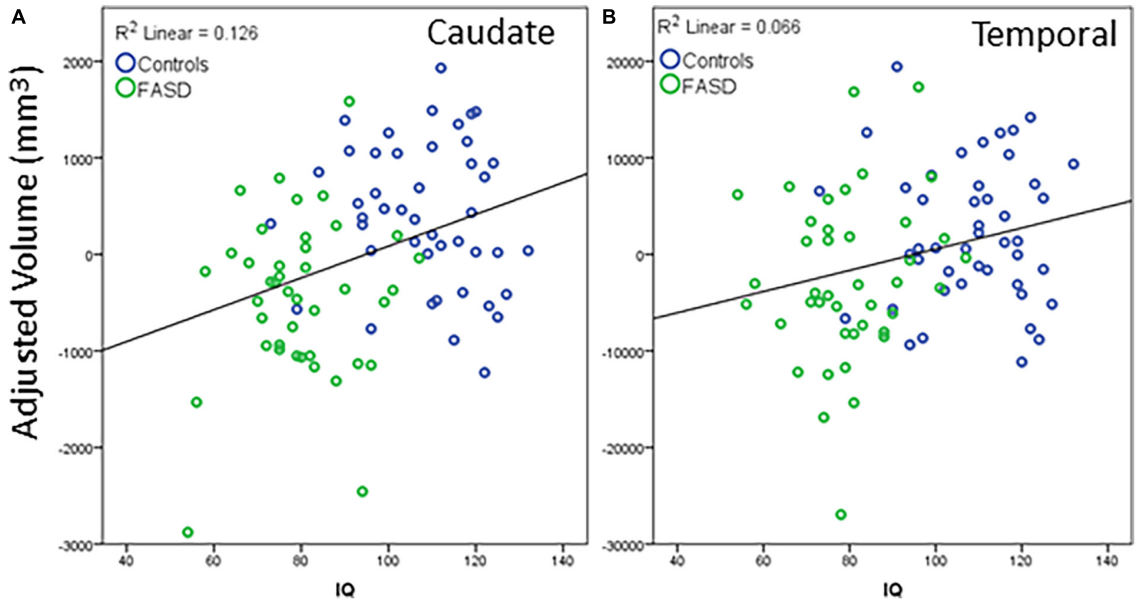


FIGURE 5
Example correlations of IQ scores with cortical volume: **(A)** Caudate and **(B)** temporal lobe. The data represent the residuals with covariates of age, eTIV, and channel number regressed out. All significant correlations revealed a similar positive correlation between structure volume and IQ scores. Blue dots are controls, green dots are FASD.

effects of PAE on brain growth parameters. Most of the prior results have not examined results relative to FASD subtype likely due to limited sample size.

Overall IQ scores were highly correlated with all the structures assessed (see **Table 4**) with cerebellum, left and right caudate, and left pallidum revealing significance when controlling for age and eTIV. The significance of the correlations without controlling for eTIV is expected given the group differences in IQ and the group differences in cortical volume. The structures, which remain significant when controlling for eTIV, reveal that subcortical structures are relevant to overall estimates of intelligence. These results are similar to those of Gautam et al. (2014), which revealed a positive correlation between IQ scores and white matter volume changes with increasing age in the FASD participants relative to controls. Hendrickson et al. (2018) and Zhou et al. (2018) reported no correlation between IQ and regional brain volume, which is consistent with the current results showing no relationship with parietal, frontal and occipital lobar volumes when controlling for eTIV.

A strength of the current study is the almost equal representation of males and females and the equal distribution of FASD subtypes and control groups across age. Additionally, the participants were recruited from one site, which likely reduced variability in diagnostic criteria and variability in scanner protocols relative to prior multi-site studies (Roussotte et al., 2012; Yang et al., 2012a; Treit et al., 2016; Zhou et al., 2018). Despite being relatively large, the FASD sample size remains a limitation of the current study due in part to the inherent variability in alcohol exposure that is present in human studies of FASD. Due to the limitations in alcohol biomarkers to independently assess drinking during pregnancy and a lack of consistent tracking of alcohol consumption during pregnancy and during prenatal care, the samples from different studies may represent different overall drinking patterns *in utero* which may lead to variation across studies. Zhou et al. (2011) cited comorbidities and additional exposure to drugs as factors that may contribute to discrepancies in cortical thinning among participants with an FASD. Additional co-exposures were not tracked in the reported sample and should be incorporated into future studies. An additional limitation of the current study is that it is cross-sectional rather than longitudinal. Therefore, the differences in developmental patterns across age cannot be easily interpreted. Instead, the primary analysis focused on group differences on this well-matched sample across the age spectrum. This study examined sex as a variable of interest in line with recommendations (De Castro et al., 2016; Heidari et al., 2016). However, biological sex was parent-/self-reported and we did not inquire separately about gender. Future studies should capture biological sex at birth as well as current gender. Furthermore, assessing hormone levels will facilitate our understanding of how PAE influences brain development in the presence of different hormone levels (Fung et al., 2020). Finally, all participants in the FASD group were recruited from the FASD clinic and do not represent a community sample of children with PAE. Future large-scale studies that include longitudinal assessments, additional pre- and post-natal exposure data, and a community sample of children with PAE may bring clarity to the variability in results.

The current study reinforces the teratogenic effects of PAE resulting in abnormalities in brain volume and SA in children and adolescents with PAE. The results of the study are consistent with previous findings with smaller sample sizes and studies with large sample sizes derived from multisite cohort samples. The current study uniquely captured data solely from one site with a comparatively large sample. Despite total brain volume indicating that children with PAE/ARND are statistically equivalent to controls, analysis of key brain structures reveal

patterns that indicate similar levels of brain damage in both FASD subtypes. Unlike past studies that have indicated that dysmorphology is related to greater structural abnormalities, the current results indicate that some structures are sensitive to PAE at an equivalent level in the absence of facial dysmorphology. The variation in results by FASD subtype may help explain why individuals with ARND perform similarly to children with FAS/pFAS on certain cognitive tasks. These results underline the importance of minimizing PAE to reduce the long-term effects on brain development.

Data availability statement

The raw data supporting the conclusions of this article will be made available by the authors, without undue reservation.

Ethics statement

The studies involving human participants were reviewed and approved by the University of New Mexico Health Sciences Center Human Research Review Committee. Written informed consent to participate in this study was provided by the participants' legal guardian/next of kin.

Author contributions

JS and DH contributed to the conception and design of the study. CC and DH oversaw participant assessment and reporting of neuropsychological testing results. KB, CR-H, JP, and JS extracted the data and performed the statistical analysis. TB created the first draft of the manuscript. TB, KB, FT, KV, and JS wrote the sections of the manuscript. All authors contributed to the manuscript revision and read and approved the submitted version.

Funding

The work was supported by the National Institutes of Health (P20 AA017068-03S1, P50AA022534, P30GM122734, and R01AA029605) and the National Science Foundation (1539067).

Acknowledgments

We thank the families and research participants for their time and willingness to engage in research. We also thank Daniel Savage and the New Mexico Alcohol Research Center for the overall support of the FASD research.

Conflict of interest

The authors declare that the research was conducted in the absence of any commercial or financial relationships that could be construed as a potential conflict of interest.

Publisher's note

All claims expressed in this article are solely those of the authors and do not necessarily represent those of their affiliated organizations, or those of the publisher, the editors and the reviewers. Any product that may be evaluated in this article, or claim that may be made by its manufacturer, is not guaranteed or endorsed by the publisher.

References

Aase, J. M. (1994). Clinical recognition of FAS: Difficulties of detection and diagnosis. *Alcohol. Health Res. World* 18, 5–9.

Archibald, S., Fennema-Notestine, C., Gamst, A., Riley, E., Mattson, S., and Jernigan, T. (2001). Brain dysmorphology in individuals with severe prenatal alcohol exposure. *Dev. Med. Child Neurol.* 43, 148–154.

Astley, S. J. (2010). Profile of the first 1,400 patients receiving diagnostic evaluations for fetal alcohol spectrum disorder at the Washington state fetal alcohol syndrome diagnostic and prevention network. *Can. J. Clin. Pharmacol.* 17, e132–e164.

Benjamini, Y., and Hochberg, Y. (1995). Controlling the false discovery rate – a practical and powerful approach to multiple testing. *J. R. Stat. Soc. Ser. B-Methodol.* 57, 289–300.

Chasnoff, I. J., Wells, A. M., and King, L. (2015). Misdiagnosis and missed diagnoses in foster and adopted children with prenatal alcohol exposure. *Pediatrics* 135, 264–270. doi: 10.1542/peds.2014-2171

Coffman, B., Kodituwakku, P., Kodituwakku, E., Romero, L., Sharadamma, N., Stone, D., et al. (2013). Primary visual response (M100) delays in adolescents with FASD as measured with MEG. *Hum. Brain Mapp.* 34, 2852–2862. doi: 10.1002/hbm.22110

Coleman, L., Oguz, I., Lee, J., Styner, M., and Crews, F. (2012). Postnatal day 7 ethanol treatment causes persistent reductions in adult mouse brain volume and cortical neurons with sex specific effects on neurogenesis. *Alcohol* 46, 603–612. doi: 10.1016/j.alcohol.2012.01.003

Dale, A., Fischl, B., and Sereno, M. (1999). Cortical surface-based analysis. I. Segmentation and surface reconstruction. *Neuroimage* 9, 179–194. doi: 10.1006/nimg.1998.0395

De Castro, P., Heidari, S., and Babor, T. (2016). Sex and Gender Equity in Research (SAGER): Reporting guidelines as a framework of innovation for an equitable approach to gender medicine commentary. *Ann. Ist. Super Sanita* 52, 154–157. doi: 10.4415/ANN_16_02_05

Fernández-Jaén, A., Fernández-Mayoralas, D., Quiñones Tapia, D., Calleja-Pérez, B., García-Segura, J., Arribas, S., et al. (2011). Cortical thickness in fetal alcohol syndrome and attention deficit disorder. *Pediatr. Neurol.* 45, 387–391. doi: 10.1016/j.pediatrneurol.2011.09.004

Franklin, L., Deitz, J., Jirikowic, T., and Astley, S. (2008). Children with fetal alcohol spectrum disorders: Problem behaviors and sensory processing. *Am. J. Occup. Ther.* 62, 265–273. doi: 10.5014/ajot.62.3.265

Fung, M., Taylor, B., Frenzel, M., Eastman, J., Wang, Y., Calhoun, V., et al. (2020). Pubertal testosterone tracks the developmental trajectory of neural oscillatory activity serving visuospatial processing. *Cereb. Cortex* 30, 5960–5971. doi: 10.1093/cercor/bhaa169

Gautam, P., Nuñez, S., Narr, K., Kan, E., and Sowell, E. (2014). Effects of prenatal alcohol exposure on the development of white matter volume and change in executive function. *Neuroimage Clin.* 5, 19–27. doi: 10.1016/j.nicl.2014.05.010

Heidari, S., Babor, T., De Castro, P., Tort, S., and Curno, M. (2016). Sex and gender equity in research: Rationale for the SAGER guidelines and recommended use. *Res. Integr. Peer. Rev.* 1:2. doi: 10.1186/s41073-016-0007-6

Hendrickson, T., Mueller, B., Sowell, E., Mattson, S., Coles, C., Kable, J., et al. (2018). Two-year cortical trajectories are abnormal in children and adolescents with prenatal alcohol exposure. *Dev. Cogn. Neurosci.* 30, 123–133. doi: 10.1016/j.dcn.2018.02.008

Hoyme, H. E., Kalberg, W. O., Elliott, A. J., Blankenship, J., Buckley, D., Marais, A. S., et al. (2016). Updated clinical guidelines for diagnosing fetal alcohol spectrum disorders. *Pediatrics* 138:e20154256. doi: 10.1542/peds.2015-4256

Inkelis, S., Moore, E., Bischoff-Grethe, A., and Riley, E. (2020). Neurodevelopment in adolescents and adults with fetal alcohol spectrum disorders (FASD): A magnetic resonance region of interest analysis. *Brain Res.* 1732:146654. doi: 10.1016/j.brainres.2020.146654

Jacobson, S., Jacobson, J., Molteno, C., Warton, C., Wintermark, P., Hoyme, H., et al. (2017). Heavy prenatal alcohol exposure is related to smaller corpus callosum in newborn MRI scans. *Alcohol. Clin. Exp. Res.* 41, 965–975. doi: 10.1111/acer.13363

Jones, K. L., Smith, D.W., Ulleland, C. N., and Streissguth, P. (1973). Pattern of malformation in offspring of chronic alcoholic mothers. *Lancet* 1, 1267–1271. doi: 10.1016/s0140-6736(73)91291-9

Joseph, J., Warton, C., Jacobson, S. W., Jacobson, J. L., Molteno, C. D., Eicher, A., et al. (2014). Three-dimensional surface deformation-based shape analysis of hippocampus and caudate nucleus in children with fetal alcohol spectrum disorders. *Hum. Brain Mapp.* 35, 659–672. doi: 10.1002/hbm.22209

Krueger, A. M., Roediger, D. J., Mueller, B. A., Boys, C. J., Hendrickson, T. J., Schumacher, M. J., et al. (2020). Para-limbic structural abnormalities are associated with internalizing symptoms in children with prenatal alcohol exposure. *Alcohol. Clin. Exp. Res.* 44, 1598–1608. doi: 10.1111/acer.14390

Lebel, C., Roussotte, F., and Sowell, E. R. (2011). Imaging the impact of prenatal alcohol exposure on the structure of the developing human brain. *Neuropsychol. Rev.* 21, 102–118. doi: 10.1007/s11065-011-9163-0

Leigland, L., Ford, M., Lerch, J., and Kroenke, C. (2013). The influence of fetal ethanol exposure on subsequent development of the cerebral cortex as revealed by magnetic resonance imaging. *Alcohol. Clin. Exp. Res.* 37, 924–932. doi: 10.1111/acer.12051

Marshall, A. T., Bodison, S. C., Uban, K. A., Adise, S., Jonker, D., Charles, W., et al. (2022). The impact of prenatal alcohol and/or tobacco exposure on brain structure in a large sample of children from a South African birth cohort. *Alcohol. Clin. Exp. Res.* 46, 1980–1992. doi: 10.1111/acer.14945

Mattson, S. N., Roesch, S. C., Glass, L., Deweese, B. N., Coles, C. D., Kable, J. A., et al. (2013). Further development of a neurobehavioral profile of fetal alcohol spectrum disorders. *Alcohol. Clin. Exp. Res.* 37, 517–528. doi: 10.1111/j.1530-0277.2012.01952.x

May, P. A., Baete, A., Russo, J., Elliott, A. J., Blankenship, J., Kalberg, W. O., et al. (2014). Prevalence and characteristics of fetal alcohol spectrum disorders. *Pediatrics* 134, 855–866. doi: 10.1542/peds.2013-3319

May, P. A., Chambers, C. D., Kalberg, W. O., Zellner, J., Feldman, H., Buckley, D., et al. (2018). Prevalence of fetal alcohol spectrum disorders in 4 US communities. *JAMA* 319, 474–482. doi: 10.1001/jama.2017.21896

May, P. A., Gossage, J. P., Kalberg, W. O., Robinson, L. K., Buckley, D., Manning, M., et al. (2009). Prevalence and epidemiologic characteristics of FASD from various research methods with an emphasis on recent in-school studies. *Dev. Disabil. Res. Rev.* 15, 176–192. doi: 10.1002/ddrr.68

Migliorini, R., Moore, E., Glass, L., Infante, M., Tapert, S., Jones, K., et al. (2015). Anterior cingulate cortex surface area relates to behavioral inhibition in adolescents with and without heavy prenatal alcohol exposure. *Behav. Brain Res.* 292, 26–35. doi: 10.1016/j.bbr.2015.05.037

O'Leary-Moore, S., Parnell, S., Lipinski, R., and Sulik, K. (2011). Magnetic resonance-based imaging in animal models of fetal alcohol spectrum disorder. *Neuropsychol. Rev.* 21, 167–185. doi: 10.1007/s11065-011-9164-z

Petrelli, B., Weinberg, J., and Hicks, G. (2018). Effects of prenatal alcohol exposure (PAE): Insights into FASD using mouse models of PAE. *Biochem. Cell Biol.* 96, 131–147. doi: 10.1139/bcb-2017-0280

Rajaprakash, M., Chakravarty, M., Lerch, J., and Rovet, J. (2014). Cortical morphology in children with alcohol-related neurodevelopmental disorder. *Brain Behav.* 4, 41–50. doi: 10.1002/brb3.191

Reuter, M., Rosas, H., and Fischl, B. (2010). Highly accurate inverse consistent registration: A robust approach. *Neuroimage* 53, 1181–1196. doi: 10.1016/j.neuroimage.2010.07.020

Riley, E. P., McGee, C. L., and Sowell, E. R. (2004). Teratogenic effects of alcohol: A decade of brain imaging. *Am. J. Med. Genet. C Semin. Med. Genet.* 127C, 35–41. doi: 10.1002/ajmg.c.30014

Robertson, F., Narr, K., Molteno, C., Jacobson, J., Jacobson, S., and Meintjes, E. (2016). Prenatal alcohol exposure is associated with regionally thinner cortex during the preadolescent period. *Cereb. Cortex* 26, 3083–3095. doi: 10.1093/cercor/bhv131

Rosen, A., Roalf, D., Ruparel, K., Blake, J., Seelaus, K., Villa, L., et al. (2018). Quantitative assessment of structural image quality. *Neuroimage* 169, 407–418. doi: 10.1016/j.neuroimage.2017.12.059

Roussotte, F. F., Sulik, K. K., Mattson, S. N., Riley, E. P., Jones, K. L., Adnams, C. M., et al. (2012). Regional brain volume reductions relate to facial dysmorphology and neurocognitive function in fetal alcohol spectrum disorders. *Hum. Brain Mapp.* 33, 920–937. doi: 10.1002/hbm.21260

Sharma, A. (2001). Letters to the editor. *Pediatrics* 107, 1227–1240.

Sowell, E. R., Mattson, S. N., Kan, E., Thompson, P. M., Riley, E. P., and Toga, A. W. (2008). Abnormal cortical thickness and brain-behavior correlation patterns in individuals with heavy prenatal alcohol exposure. *Cereb. Cortex* 18, 136–144. doi: 10.1093/cercor/bhm039

Sowell, E. R., Thompson, P. M., Peterson, B. S., Mattson, S. N., Welcome, S. E., Henkenius, A. L., et al. (2002b). Mapping cortical gray matter asymmetry patterns in adolescents with heavy prenatal alcohol exposure. *Neuroimage* 17, 1807–1819. doi: 10.1006/nimg.2002.1328

Sowell, E. R., Thompson, P. M., Mattson, S. N., Tessner, K. D., Jernigan, T. L., Riley, E. P., et al. (2002a). Regional brain shape abnormalities persist into adolescence after heavy prenatal alcohol exposure. *Cereb. Cortex* 12, 856–865. doi: 10.1093/cercor/12.8.856

Stephen, J., Kodituwakku, P., Kodituwakku, E., Romero, L., Peters, A., Sharadamma, N., et al. (2012). Delays in auditory processing identified in preschool children with FASD. *Alcohol. Clin. Exp. Res.* 36, 1720–1727. doi: 10.1111/j.1530-0277.2012.01769.x

Stratton, K., Howe, C., and Battaglia, F. P. (eds) (1996). *Institute of Medicine. Fetal alcohol syndrome: Diagnosis, epidemiology, prevention, and treatment*. Washington, DC: National Academy Press.

Treit, S., Zhou, D., Chudley, A., Andrew, G., Rasmussen, C., Nikkel, S., et al. (2016). Relationships between head circumference, brain volume and cognition in children with prenatal alcohol exposure. *PLoS One* 11:e0150370. doi: 10.1371/journal.pone.0150370

Treit, S., Zhou, D., Lebel, C., Rasmussen, C., Andrew, G., and Beaulieu, C. (2014). Longitudinal MRI reveals impaired cortical thinning in children and adolescents prenatally exposed to alcohol. *Hum. Brain Mapp.* 35, 4892–4903. doi: 10.1002/hbm.22520

Wang, X., and Kroenke, C. (2015). Utilization of magnetic resonance imaging in research involving animal models of fetal alcohol spectrum disorders. *Alcohol. Res.* 37, 39–51.

Williams, J. F., and Smith, V. (2015). Fetal alcohol spectrum disorders. *Pediatrics* 136, e1395–e1406. doi: 10.1542/peds.2015-3113

Yang, Y., Roussotte, F., Kan, E., Sulik, K. K., Mattson, S. N., Riley, E. P., et al. (2012a). Abnormal cortical thickness alterations in fetal alcohol spectrum disorders and their relationships with facial dysmorphology. *Cereb. Cortex* 22, 1170–1179. doi: 10.1093/cercor/bhr193

Yang, Y., Phillips, O., Kan, E., Sulik, K., Mattson, S., Riley, E., et al. (2012b). Callosal thickness reductions relate to facial dysmorphology in fetal alcohol spectrum disorders. *Alcohol. Clin. Exp. Res.* 36, 798–806. doi: 10.1111/j.1530-0277.2011.01679.x

Zhang, C., Kurniawan, N., Yamada, L., Fleming, W., Kaminen-Ahola, N., Ahola, A., et al. (2019). Early gestational ethanol exposure in mice: Effects on brain structure, energy metabolism and adiposity in adult offspring. *Alcohol* 75, 1–10. doi: 10.1016/j.alcohol.2018.04.008

Zhou, D., Lebel, C., Lepage, C., Rasmussen, C., Evans, A., Wyper, K., et al. (2011). Developmental cortical thinning in fetal alcohol spectrum disorders. *Neuroimage* 58, 16–25. doi: 10.1016/j.neuroimage.2011.06.026

Zhou, D., Rasmussen, C., Pei, J., Andrew, G., Reynolds, J., and Beaulieu, C. (2018). Preserved cortical asymmetry despite thinner cortex in children and adolescents with prenatal alcohol exposure and associated conditions. *Hum. Brain Mapp.* 39, 72–88. doi: 10.1002/hbm.23818

frontiers | Frontiers in Neuroscience

TYPE Original Research
PUBLISHED 18 September 2023
DOI 10.3389/fnins.2023.1203597

Check for updates

OPEN ACCESS

EDITED BY
Hermes H. Yeh,
Dartmouth College, United States

REVIEWED BY
Sandra Mooney,
University of North Carolina at Chapel Hill, United States
Kelly J. Huffman,
University of California, Riverside, United States
Rajesh Miranda,
Texas A&M University, United States

*CORRESPONDENCE
Kristin M. Hamre
✉ khamre@uthsc.edu

†These authors have contributed equally to this work and share senior authorship

RECEIVED 11 April 2023
ACCEPTED 25 August 2023
PUBLISHED 18 September 2023

CITATION
Xu F, Thomas JD, Goldowitz D and Hamre KM (2023) The ameliorative effects of choline on ethanol-induced cell death in the neural tube of susceptible BXD strains of mice. *Front. Neurosci.* 17:1203597. doi: 10.3389/fnins.2023.1203597

COPYRIGHT
© 2023 Xu, Thomas, Goldowitz and Hamre. This is an open-access article distributed under the terms of the Creative Commons Attribution License (CC BY). The use, distribution or reproduction in other forums is permitted, provided the original author(s) and the copyright owner(s) are credited and that the original publication in this journal is cited, in accordance with accepted academic practice. No use, distribution or reproduction is permitted which does not comply with these terms.

The ameliorative effects of choline on ethanol-induced cell death in the neural tube of susceptible BXD strains of mice

Fannia Xu[1], Jennifer D. Thomas[2], Dan Goldowitz[1†] and Kristin M. Hamre[3*†]

[1]University of British Columbia, Centre for Molecular Medicine and Therapeutics, Vancouver, BC, Canada, [2]Center for Behavioral Teratology, San Diego State University, San Diego, CA, United States, [3]Department Anatomy and Neurobiology, University Tennessee Health Science Center, Memphis, TN, United States

Introduction: Fetal alcohol spectrum disorders (FASD) are the leading preventable cause of intellectual disability, providing the impetus for evaluating various potential treatments to ameliorate ethanol's teratogenic effects, particularly in the nervous system. One treatment is the dietary supplement choline which has been shown to mitigate at least some of ethanol's teratogenic effects. The present study was designed to investigate the effects of genetics on choline's efficacy in ameliorating cell death in the developing neural tube. Previously, we examined BXD recombinant inbred mice, and their parental C57BL/6 J (B6) and DBA/2 J strains, and identified strains that were sensitive to ethanol's teratogenic actions. Thus, we used these strains to identify response to choline treatment.

Materials and methods: Timed pregnant mice from 4 strains (B6, BXD51, BXD73, BXD2) were given either ethanol or isocaloric maltose-dextrin (5.8 g/kg in two administrations separated by 2 h) with choline at one of 3 doses: 0, 100 or 250 mg/kg. Subjects were exposed via intragastric gavage on embryonic day 9 and embryos were collected 7 h after the initial ethanol administrations. Cell death was analyzed using TUNEL staining in the developing forebrain and brainstem.

Results: Choline ameliorated the ethanol-induced cell death across all 4 strains without causing enhanced cell death in control mice. Choline was effective in both the developing telencephalon and in the brainstem. Both doses diminished cell death, with some differences across strains and brain regions, although the 100 mg/kg dose was most consistent in mitigating ethanol-related cell death. Comparisons across strains showed that there was an effect of strain, particularly in the forebrain at the higher dose.

Discussion: These results show that choline is effective in ameliorating ethanol-induced cell death at this early stage of nervous system development. However, there were some strain differences in its efficacy, especially at the high dose, providing further evidence of the importance of genetics in influencing the ability of choline to protect against prenatal alcohol exposure.

KEYWORDS

recombinant inbred mice, fetal alcohol spectrum disorders, genetics, choline, apoptosis, forebrain, brainstem

Introduction

Fetal alcohol spectrum disorders constitute a constellation of phenotypes caused by exposure to ethanol during early development (e.g., Glass et al., 2023). Ethanol exposure has been shown to have teratogenic effects on the developing central nervous system (CNS), which can have life-long impacts for the exposed individual (Chokroborty-Hoque et al., 2014; Glass et al., 2023). Although the teratogenic effects of ethanol have been known for at least half a century and despite publicity campaigns, the incidence of FASD remains as high as 5 in every 100 live births (May et al., 2018, 2021). This has led to a focus on identifying treatments and therapeutics that can ameliorate ethanol's teratogenic effects.

One of the most effective treatments, to date, has been choline supplementation. Choline is an essential nutrient that has several functions within the cell, influencing synthesis of phospholipids in cell membranes, synthesis of the neurotransmitter acetylcholine, and acting as a methyl donor in a number of cellular processes (Wallace et al., 2020). In animal models, choline has been shown to mitigate many, but not all, of the effects of developmental ethanol exposure during development ranging from brain to behavioral changes (Thomas et al., 2000, 2009, 2010; Monk et al., 2012; Bottom et al., 2020; Baker et al., 2022; Ernst et al., 2022; Naik et al., 2022). Choline is effective whether administered during prenatal alcohol or after birth (Thomas et al., 2009, 2010). Initial clinical studies have provided promising results that choline may be an effective treatment for at least some of ethanol's teratogenic effects, particularly as they relate to the CNS (Jacobson et al., 2018; Wozniak et al., 2020; Warton et al., 2021; Ernst et al., 2022; Gimbel et al., 2022). In fact, choline deficiency has been shown to exacerbate ethanol's teratogenic effects (Idrus et al., 2017).

Although choline continues to show promise as an effective intervention, it is critical to understand factors that can influence choline's efficacy. One factor that has been proposed to be important is genetics. Two lines of evidence provide support for the role of genetics in choline's efficacy. First, a study by Fischer and colleagues examined the relationship between the level of choline and its metabolite betaine in breast milk, and the amount of choline consumed in women with differing genetic backgrounds. Their results showed that polymorphisms in two choline-related enzymes, phosphatidylethanolamine-N-methyltransferase (PEMT) and methylenetetrahydrofolate dehydrogenase 1 (MTHFR), had a significant effect on either the basal levels of choline or on changes in the levels in breast milk following choline supplementation (Fischer et al., 2010a,b; Corbin and Zeisel, 2012). Second, a recent study examined children with FASD that were given choline supplementation or placebo and tested for tasks that assessed learning and memory functions along with concomitant evaluation of single nucleotide polymorphisms (SNPs) in various choline-metabolizing genes. The results demonstrated a significant association between SNPs in the gene for the choline transporter gene solute carrier family 44 member 1 (SLC44A1) and the ability to perform the tasks (Smith et al., 2021). The current study is designed to further evaluate the role of genetics in choline's efficacy in ameliorating ethanol-induced cell death early in the development of the CNS.

Mouse models are frequently used to study the genetic pathways involved in FASD and possible candidates for the genetic variation. The BXD recombinant inbred (RI) panel is the largest mouse RI mapping panel, derived by crossing B6 and D2 mouse strains (Peirce et al., 2004). BXD recombinant inbred strains have often been used to study the genetics and epigenetics of alcoholism, since they show significant differences in their preference for ethanol (Cunningham, 1995; Philip et al., 2010). Additionally, a study by Downing et al. (2012) examined morphological phenotypes (such as abnormalities in the digits and kidney) across BXD strains following prenatal alcohol exposure and found differential sensitivity in these strains. Previous work in our lab identified strains of BXD mice that were more susceptible to ethanol's induction of cell death in the neural tube ("high cell death strains") and those that were less susceptible ("low cell death strains"). We examined three BXD strains that have been identified as high cell death strains in the present study: BXD2, BXD51, and BXD73 (although there was low cell death in the brainstem) (Theberge et al., 2019). Additionally, the parental B6 strain was also a high cell death strain and was thus also evaluated in the current study.

In the present study, we examined these 4 high cell death strains to address the following. (1) Previous work has shown that choline can ameliorate ethanol-induced cell death (Wang and Bieberich, 2010) and this study was undertaken to confirm the previous report *in vivo*. (2) Previous work in rats and sheep has suggested that, at certain doses and phenotypes examined, choline itself can be teratogenic (Goeke et al., 2018; Carugati et al., 2022) and this study was undertaken to determine if differing genetic backgrounds showed evidence of baseline teratogenicity due to choline. (3) Choline may improve performance on some, but not all, behavioral outcomes, so we examined two brain regions to assess choline's efficacy across brain regions. (4) We evaluated two doses of choline, a moderate dose (100 mg/kg body weight) and a high dose (250 mg/kg body weight) to determine if one dose was more or less effective. (5) We evaluated the effects of the genetic background by determining if the effects were equivalent across embryos of differing genetic backgrounds.

Materials and methods

Animals

All animal work was conducted under the auspices of the Institutional Animal Care and Use Committee at the University of Tennessee Health Science Center. Previously, we determined the levels of ethanol-induced cell death in over 25 recombinant inbred BXD strains, as well as the parental C57BL/6J (B6) and DBA/2J mouse strains (Theberge et al., 2019). From this analysis we identified strains that were highly vulnerable to ethanol's teratogenic insult and strains that were resistant to ethanol's effects. In the present study we focused on the analysis of 4 of the most vulnerable strains: BXD2, BXD51, BXD73 and B6.

Ethanol exposure, tissue collection and processing

The breeding and ethanol exposure paradigm was conducted as previously described (Theberge et al., 2019). Briefly, females were mated with males of the same genotype for 4 h beginning at 9 a.m. Vaginal plugs were checked and the presence of a plug denoted embryonic day zero (E0). On E9, each dam was weighed and given the appropriate solution via intragastric gavage. Because we previously showed little

difference between non-handled and gavaged controls, only the gavaged controls were used and therefore, all dams received solutions via gavage. Dams were given either 5.8 g/kg of ethanol in sterile saline divided into 2 doses separated by 2 h or the control isocaloric solution of maltose/dextrin also in saline. Specific groups were also given choline chloride (Balchem Corp., New Hampton, NY, United States) at a dose of either 100 or 250 mg/kg. The choline was included in the solutions given via gavage to minimize the handling of the mice. In this study, the following 6 groups were included in each strain: (1) Maltose/dextrin no choline control group, (2) Maltose/dextrin +100 mg/kg choline, (3) Maltose/dextrin +250 mg/kg choline, (4) Ethanol no choline group, (5) Ethanol +100 mg/kg choline, (6) Ethanol +250 mg/kg choline. Seven hours after the first injection, dams were euthanized, the individual embryos were dissected out of the uterus, and embryos with closed anterior neuropores were immersion fixed in 4% paraformaldehyde in 0.1 M phosphate buffered saline (PBS) for 1 h (embryos with open anterior neuropores were discarded). The somite number at this point of development was typically between 15 and 25. After 1 h, the embryos were removed from the fixative and placed in PBS at 4°C. Embryos were subsequently embedded in paraffin using standard techniques. Single embryos were embedded for sectioning in the horizontal plane. Embryos were serially sectioned at 8 um and mounted on glass slides (Fisher Scientific).

Detection of apoptotic cell death

Slides with sections of the developing telencephalon and brainstem were selected for staining to demonstrate dead and dying cells in the neuroepithelia. Terminal deoxynucleotidyl transferase dUTP nick end labeling (TUNEL) assays were used to label cells undergoing apoptotic DNA fragmentation (Nikolic et al., 2000). TUNEL-positive cells were labelled using the ApopTag *In Situ* Apoptosis Kit (Millipore Sigma) according to the manufacturer's protocol. Sections were deparaffinized and rehydrated with graded ethanols, incubated with 20 µg/mL of proteinase K, blocked with 2% hydrogen peroxide, and incubated with terminal deoxynucleotidyl transferase (TdT) followed by an anti-digoxigenin peroxidase conjugated antibody. 3,3′-diaminobenzidine (DAB) was used to visualize the digoxigenin-labelled DNA fragments. Sections were counterstained with 0.5% methyl green to provide contrast with the DAB staining. Labelled TUNEL-positive (apoptotic) cells are brown, and non-apoptotic cells are green. The sections were dehydrated and coverslipped with Permount (Fisher Scientific).

Quantification of cell death

TUNEL-positive cells were manually counted within the regions of interest using a brightfield microscope with a 40x objective (Standard Zeiss ICS Brightfield Microscope). Cells undergoing apoptosis were defined as cells with brown TUNEL staining within the confines of the cell, or tightly clustered brown TUNEL staining. Cells with only a faint brown stain that was not confined within the cell were not counted as TUNEL-positive.

The telencephalon and brainstem were the regions of interest for the determination of cell death. The telencephalon was demarcated as the neuroepithelium rostral to the optic vesicles; the brainstem was demarcated as the neuroepithelium at the level of the otic placodes (Supplementary Figure S1). For each region of interest, 2 sections per region were sampled per embryo, and 3 embryos were quantified per litter. The first sections analyzed in the forebrain and hindbrain were at the level of the optic and otic vesicles, respectively. The second sections for analysis were at least 32 um away to ensure that the same cell was not counted twice. For each section, the whole brainstem or forebrain was analyzed.

To quantify the area of the region of interest, a Zeiss 200 M Axiovert Inverted Microscope with AxioVision 4.6 software (Carl Zeiss Microscopy, Jena, Germany) was used to image the tissue. Images of brainstem and forebrain sections were taken using a 20x objective at preset dimensions of 1,300 × 1,030 pixels. Images taken from the Zeiss Inverted Microscope were uploaded into the software ImageJ version 1.53c (National Institutes of Health, Bethesda, MD), which was used to calculate the area of the regions of interest. The region of interest was selected using the freehand selection tool to measure the area. The image was scaled at 1,900 pixels per mm to convert the area measured in square pixels to equivalent dimensions in mm^2.

The average density of apoptotic cells in the brainstem and forebrain was calculated by dividing the number of TUNEL-positive cells in each region of interest by the area of the region (in mm^2) for each sampled section. For each embryo, the average TUNEL-positive cells per mm^2 for all sections sampled in a given region from that embryo yielded an apoptotic cell density for that region. Finally, an average value for TUNEL-positive cells per mm^2 for each embryo in a litter was used to calculate the average apoptotic cell density for that litter for each brain region. The litter means for cell death were used as the unit of analysis. For each strain, 5–8 litters were analyzed for each EtOH and choline dose, and 3–5 litters were analyzed for each MD and choline dose.

Data analysis

Three levels of analysis were applied to the data using linear regression models with significance set at $p < 0.05$ using IBM SPSS Statistics Version 29.0. The first level of analysis examined each brain region across all strains and doses to assess the efficacy of choline in ameliorating apoptotic cell death. The second level of analysis compared whether there were dose or regional differences within each strain. The third level of analysis was conducted to compare choline's ability to reduce cell death toward control values across the different strains. Because there were differences in baseline levels of ethanol-only induced cell death across strains, we calculated adjusted values to compare data between strains. The adjusted value was determined by subtracting the average cell death of the MD-treated controls that were not administered choline from each individual litter cell death average of the ethanol+choline treatment groups. Any adjusted cell death values that were negative were set at zero.

Results

Choline is effective in ameliorating ethanol-induced cell death

One of the aims of our study was to confirm previous reports that choline can ameliorate ethanol-induced cell death. To test this, we quantified the levels of apoptosis in E9.5 embryos that were exposed to EtOH and administered either a moderate (100 mg/kg) or high (250 mg/kg) dose of choline and compared the amount of cell death to control embryos that were not administered choline. Choline

was able to effectively reduce the amount of ethanol-induced cell death in the developing neural tube. In all 4 strains, there were fewer apoptotic cells and fewer clusters of apoptotic cells in the choline-treated embryos compared to controls that did not receive choline (Figure 1). Quantitative comparisons of apoptotic cell density showed that both the 100 mg/kg (χ^2 (1, N = 54) = 10.096, p = 0.001 for brainstem and χ^2 (1, N = 54) = 16.656, p < 0.001 for forebrain) and 250 mg/kg (χ^2 (1, N = 55) = 6.241, p = 0.012 for brainstem and χ^2 (1, N = 55) = 8.361, p = 0.004 for forebrain) doses of choline effectively reduced cell death in both regions of interest across all strains (Figures 2, 3; Supplementary Figure S2).

Choline does not increase cell death in the developing neural tube

We administered choline to control, M/D treated litters to determine whether there were increases in cell death in the 4 strains of mice used in this study. Previous work has suggested that choline itself, at higher doses, may in fact be teratogenic (Goeke et al., 2018; Carugati et al., 2022). We administered choline to control, M/D treated litters to determine whether there increases in cell death in the 4 strains of mice used in this study. Patterns of apoptosis in both the 100 mg/kg and 250 mg/kg doses were similar to controls that did not receive any choline (Figure 1). Comparisons were done within each strain for each brain region. Within each strain, neither dose caused an increase in cell death (p > 0.05 for all strains and regions), and both doses had comparable levels of cell death to controls that were not administered choline (Figures 2, 3). While there were moderate differences between doses, levels of apoptosis did not reach comparable levels to ethanol-induced cell death. This shows that there are no baseline differences in choline-induced cell death in any of the strains examined.

Choline was effective in reducing cell death at both dosages used

Neither dose was effective in the brainstem of BXD73 embryos (χ^2 (1, N = 12) = 3.176, p = 0.075 for 100 mg/kg and χ^2 (1, N = 12) = 0.209, p = 0.647 for 250 mg/kg). We also aimed to identify whether there are dose differences (100 vs. 250 mg/kg) in choline's efficacy to reduce ethanol-induced cell death by comparing levels of cell death across different choline doses within each strain using a linear regression model. Both doses effectively reduced alcohol-related apoptosis in the brainstem of the BXD51 (χ^2 (1, N = 14) = 9.461, p = 0.002 for 100 mg/kg and χ^2 (1, N = 14) = 14.024, p < 0.001 for 250 mg/kg) and BXD2 (χ^2 (1, N = 15) = 7.933, p = 0.005 for 100 mg/kg and χ^2 (1, N = 16) = 10.515, p = 0.001 for 250 mg/kg) strains (Figure 2). Only the 100 mg/kg dose was effective in reducing apoptosis in the brainstem for the B6 strain (χ^2 (1, N = 13) = 12.085, p < 0.001) while the 250 mg/kg dose failed to significantly reduce apoptosis (χ^2 (1, N = 13) = 3.341, p = 0.068). Neither dose was effective in the brainstem of BXD73 embryos (p = 0.075 for 100 mg/kg and p = 0.647 for 250 mg/kg), which was not surprising given that the baseline level of ethanol-induced cell death was lower for this strain in the brainstem region. In the forebrain, both doses were effective in B6 (χ^2 (1, N = 13) = 61.261, p < 0.001 for 100 mg/kg and χ^2 (1, N = 13) = 32.276, p < 0.001 for 250 mg/kg), BXD51 (χ^2 (1, N = 14) = 6.146, p = 0.013 for 100 mg/kg and χ^2 (1, N = 14) = 6.941, p = 0.008 for 250 mg/kg), and BXD2 (χ^2 (1,

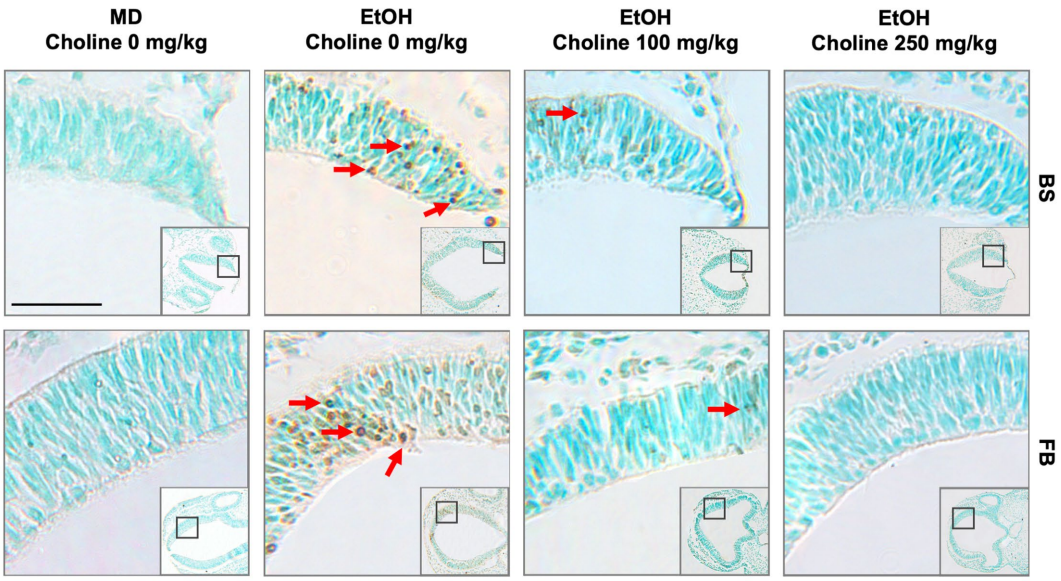


FIGURE 1
Choline is effective in ameliorating ethanol-induced cell death in the brainstem and forebrain as shown in the BXD51 mouse strain as illustrative of all 4 strains examined. Representative images of TUNEL-stained sections at E9.5 to illustrate apoptotic cells in each of the treatment conditions (top of panels) and brain regions (right of panels). TUNEL staining of apoptotic cells in brainstem (top, BS) and forebrain (bottom, FB) of BXD51 mice treated with MD or ethanol on embryonic day 9 (low magnification inset indicates the region of embryonic brainstem or forebrain shown at higher magnification). Treatment was supplemented by a choline dose of 0, 100, or 250 mg/kg. Dark deposits of DAB indicate cells undergoing apoptosis (examples highlighted by red arrows). Cells with lighter brown staining are associated with transit through the cell cycle and/or background and were not counted. Cells were counterstained with methyl green. MD = maltose-dextrin. Scale bars = 50 mm.

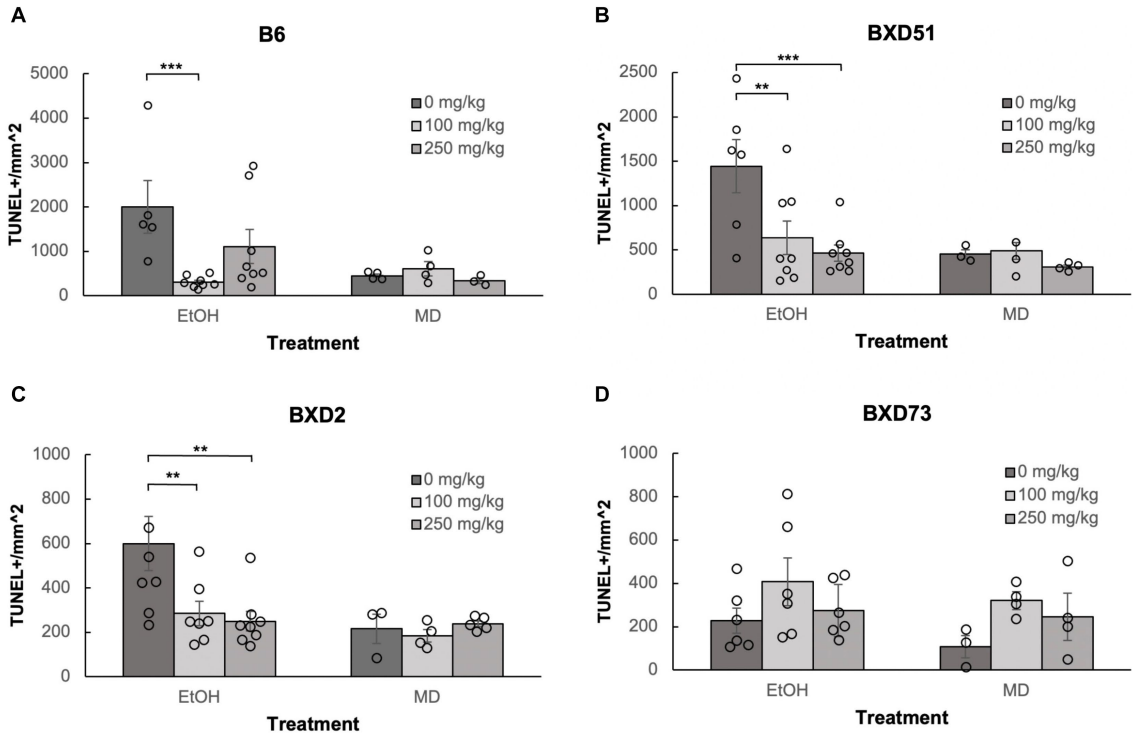


FIGURE 2
Choline is effective in ameliorating ethanol-induced cell death in the brainstem of B6, BXD51, and BXD2 embryos. Graphs represent the amount of cell death in the brainstem of ethanol-treated and maltose-dextrin (MD) control embryos that also received choline treatment with either 0 mg/kg, a moderate (100 mg/kg), or high (250 mg/kg) dose. Statistical comparisons among the three ethanol-treated groups are shown in the graphs. Choline+EtOH and choline+MD treated groups were compared at the same dose and there were no statistically significant differences. There were no statistically significant differences between the three MD-treated groups in any of the strains examined. **(A)** Significant difference in the level of cell death between embryos that do not receive choline and embryos that receive 100 mg/kg choline in the B6 strain. There is no significant effect of the 250 mg/kg dose on cell death. For EtOH-treated embryos, $N = 5$ for 0 mg/kg and $N = 8$ for 100 mg/kg and 250 mg/kg. For MD-treated embryos, $N = 4$ for 0 mg/kg and 100 mg/kg and $N = 3$ for 250 mg/kg. **(B)** Significant differences in levels of cell death between embryos that do not receive choline and embryos that receive 100 or 250 mg/kg choline in the BXD51 strain. For EtOH-treated embryos, $N = 6$ for 0 mg/kg and $N = 8$ for 100 mg/kg and 250 mg/kg. For MD-treated embryos, $N = 3$ for 0 mg/kg and 100 mg/kg and $N = 4$ for 250 mg/kg. **(C)** Significant differences in levels of cell death between embryos that do not receive choline and embryos that receive 100 or 250 mg/kg choline in the BXD2 strain. For EtOH-treated embryos, $N = 8$ for 0 mg/kg and 250 mg/kg and $N = 7$ for 100 mg/kg. For MD-treated embryos, $N = 3$ for 0 mg/kg, $N = 4$ for 100 mg/kg, and $N = 5$ for 250 mg/kg. **(D)** No significant differences are seen between embryos that do not receive choline treatment and embryos that receive either 100 or 250 mg/kg choline in the BXD73 strain. For EtOH-treated embryos, $N = 6$ for 0 mg/kg, 100 mg/kg and 250 mg/kg. For MD-treated embryos, $N = 3$ for 0 mg/kg and $N = 4$ for 100 mg/kg and 250 mg/kg. Error bars indicate standard error of the mean (SEM). $*p < 0.05$, $**p < 0.01$, $***p < 0.001$.

$N = 15) = 6.783$, $p = 0.009$ for 100 mg/kg and χ^2 (1, $N = 16) = 15.425$, $p < 0.001$ for 250 mg/kg) strains, but only the 100 mg/kg dose (χ^2 (1, $N = 14) = 4.823$, $p = 0.028$) effectively reduced cell death in the BXD73 strain (χ^2 (1, $N = 13) = 2.375$, $p = 0.123$ for 250 mg/kg) (Figure 3). There were no significant differences in efficacy between the 100 and 250 mg/kg doses in any strain or region except in the forebrain of the B6 strain (χ^2 (1, $N = 16) = 5.986$, $p = 0.014$) where the 100 mg/kg dose was more effective in ameliorating ethanol-induced cell death.

Another way to view these data is to calculate the percent reduction by choline in ethanol-induced cell death (Table 1). This was obtained by dividing [(choline + ethanol) – (MD)] by [(Ethanol) – (MD)]. In the brainstem, the 100 mg/kg dose reduced cell death by 100% in the B6 strain, 81.1% in the BXD51 strain, and 81.9% in the BXD2 strain. The 250 mg/kg dose reduced cell death by 57.6% in the B6 strain, 98.8% in the BXD51 strain, and 91.1% in the BXD2 strain. In the forebrain, the 100 mg/kg dose reduced cell death by 99.4% in the B6 strain, 86.3% in the BXD51 strain, 100% in the BXD2 strain, and 79.1% in the BXD73 strain. The 250 mg/kg dose reduced cell death by 72.2% in the B6 strain, 91.7% in the BXD51 strain, 100% in the BXD2 strain, and 57.7% in the BXD73 strain. There were no statistically significant differences between the ethanol+choline group and the MD control group that did not receive choline.

There were limited differences between forebrain and brainstem in the effectiveness of choline

We compared cell death in the developing brainstem and telencephalon to assess whether choline is similarly effective across different brain regions. Overall, choline was able to reduce cell death in both the brainstem and forebrain. There were no significant regional differences in choline efficacy in 3 of the 4 strains we examined. In the BXD73 strain, there was a significant regional difference in choline's ability to reduce cell death at the 250 mg/kg dose (χ^2 *(1, N = 12)* = 5.173, $p = 0.023$). Choline was effective in reducing apoptosis in the forebrain but not brainstem of BXD73 embryos.

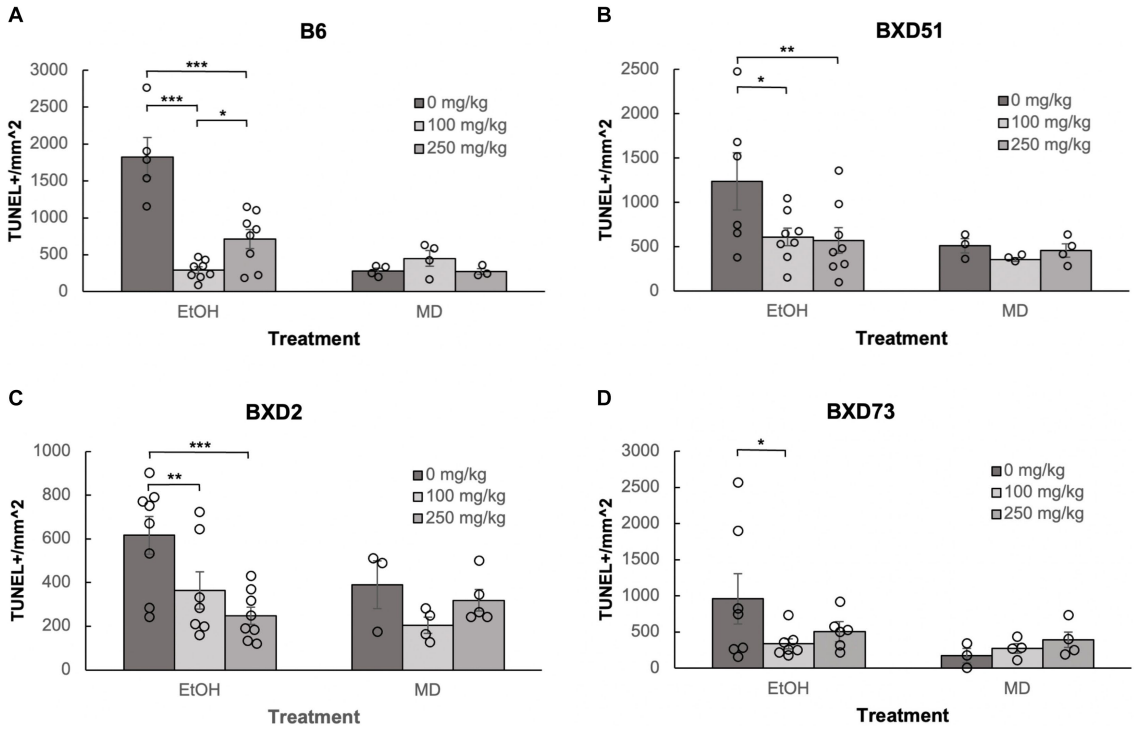


FIGURE 3
Choline is effective in ameliorating ethanol-induced cell death in the forebrain of B6, BXD51, BXD2, and BXD73 embryos. Graphs represent the amount of cell death in the forebrain of ethanol-treated and maltose-dextrin (MD) control embryos that also received choline treatment with either 0 mg/kg, a moderate (100 mg/kg) or high (250 mg/kg) dose of choline. Statistical comparisons among the three ethanol-treated groups are shown in the graphs. Choline+EtOH and choline+MD treated groups were compared at the same dose and there were no statistically significant differences. There were no statistically significant differences between the three MD-treated groups in any of the strains examined. **(A)** There are significant differences in levels of cell death between embryos that did not receive choline and embryos that received 100 or 250 mg/kg choline in the B6 strain. The 100 mg/kg dose was more effective in reducing cell death than the 250 mg/kg dose. For EtOH-treated embryos, $N = 5$ for 0 mg/kg, $N = 8$ for 100 mg/kg and 250 mg/kg. For MD-treated embryos, $N = 4$ for 0 mg/kg, 100 mg/kg and $N = 3$ for 250 mg/kg. **(B)** There are significant differences in levels of cell death between embryos that did not receive choline and embryos that received 100 or 250 mg/kg choline in the BXD51 strain. For EtOH-treated embryos, $N = 6$ for 0 mg/kg, $N = 8$ for 100 mg/kg and 250 mg/kg. For MD-treated embryos, $N = 3$ for 0 mg/kg, 100 mg/kg and $N = 4$ for 250 mg/kg. **(C)** There are significant differences in levels of cell death between embryos that did not receive choline and embryos that received 100 or 250 mg/kg choline in the BXD2 strain. For EtOH-treated embryos, $N = 8$ for 0 mg/kg, 250 mg/kg and $N = 7$ for 100 mg/kg. For MD-treated embryos, $N = 3$ for 0 mg/kg, $N = 4$ for 100 mg/kg, and $N = 5$ for 250 mg/kg. **(D)** There is a significant difference in the level of cell death between embryos that did not receive choline and embryos that received 100 mg/kg choline in the BXD73 strain. There was no significant effect of the 250 mg/kg dose on cell death. For EtOH-treated embryos, $N = 6$ for 0 mg/kg, $N = 7$ for 100 mg/kg and 250 mg/kg. For MD-treated embryos, $N = 3$ for 0 mg/kg, $N = 4$ for 100 mg/kg and 250 mg/kg. Error bars indicate standard error of the mean (SEM). $*p < 0.05$, $**p < 0.01$, $***p < 0.001$.

TABLE 1 Percentage reduction in ethanol-induced cell death following choline treatment in the brainstem and forebrain across strains. The values were calculated as described in the Results.

	BRAINSTEM		FOREBRAIN	
Choline Dose	100 mg/kg	250 mg/kg	100 mg/kg	250 mg/kg
B6	100%	57.6%	99.4%	72.2%
BXD51	81.1%	98.8%	86.3%	91.7%
BXD2	81.9%	91.1%	100%	100%
BXD73	0%*	0%*	79.1%	57.7%

*There was no percentage reduction in cell death in the brainstem of BXD73 embryos because ethanol causes little cell death in the brainstem of this strain (see Discussion).

There were choline dose-dependent strain differences in efficacy

One key aim of this study was to determine whether there are genetic differences in choline's efficacy in ameliorating ethanol-induced cell death. Previous research shows that there are genetic differences in susceptibility to ethanol's teratogenic effects (Theberge et al., 2019). Thus, we suspected that there may also be genetic differences in response to choline treatment. To test this, we compared the effectiveness of choline to reduce ethanol-induced cell death to levels seen in MD controls. We assessed levels of apoptosis in 4 different strains in mice that were either administered 100 mg/kg, 250 mg/kg, or no choline using the adjusted cell death values as defined in the Materials and Methods section. Overall, there are strain differences in choline's efficacy in reducing ethanol-induced cell death (Supplementary Figure S3). Qualitative assessment of treatment with a 250 mg/kg dose of choline shows differences in the patterns of cell death in the developing forebrain across different strains of mice (Figure 4). Quantitative assessment of cell death and statistical analysis show that there are strain differences (Figure 5). There were significant differences across all 4 strains in both the brainstem (χ^2 (3, $N = 30$) = 7.908, $p = 0.048$) and forebrain (χ^2 (3, $N = 30$) = 18.609, $p < 0.001$) of embryos administered the 250 mg/kg dose of choline. When comparing between individual strains, significant differences were found between the B6 strain and all 3 of the BXD strains in the

brainstem at the 250 mg/kg dose (χ^2 (1, $N = 16$) = 5.680, $p = 0.017$ for BXD51, χ^2 (1, $N = 16$) = 5.302, $p = 0.021$ for BXD2, and χ^2 (1, $N = 14$) = 4.373, $p = 0.037$ for BXD73). There were also significant differences between the B6 and both the BXD51 (χ^2 (1, $N = 16$) = 6.444, $p = 0.011$) and BXD2 (χ^2 (1, $N = 16$) = 15.513, $p < 0.001$) strains as well as between the BXD2 and BXD73 strains (χ^2 (1, $N = 14$) = 9.162, $p = 0.002$) in the forebrain at the 250 mg/kg dose. There was no significant effect of strain at the 100 mg/kg dose in either region of interest (χ^2 (3, $N = 29$) = 6.178, $p = 0.103$ for brainstem and χ^2 (1, $N = 30$) = 4.119, $p = 0.249$ for forebrain).

Discussion

The present study demonstrates that choline was effective in ameliorating ethanol-induced cell death in the early developing neural tube. This is consistent with the study by Wang and Bieberich (2010) that demonstrated that choline treatment prevented ethanol-induced cell death at the same age in neural crest derived cell cultures. The ability of choline to reduce apoptosis in the face of other insults, such as folate deficiency, has also been shown at older ages (Craciunescu et al., 2003), suggesting that choline may protect against cell death at multiple developmental periods. This study provides additional validation for the use of choline as a potential treatment for ethanol-induced teratogenesis and demonstrates that even in early prenatal development of the CNS, choline can mitigate ethanol-related neuropathology.

It is interesting to note that both doses of choline were shown to be effective in ameliorating the cell death induced by ethanol (see Figures 2, 3). In the present study, both 100 mg/kg and 250 mg/kg doses of choline were used, and both of these doses have been used in previous studies and have been shown to be effective in different paradigms in ameliorating a range of phenotypes that are both behavioral and morphological (Thomas et al., 2000, 2009, 2010; Monk et al., 2012; Baker et al., 2022; Ernst et al., 2022; Naik et al., 2022). However, it is interesting to note that the low dose of choline was more consistent than the high dose in ameliorating ethanol-induced cell death, providing a potential cautionary warning about high doses.

Equally as important, these results show little evidence for enhanced ethanol-induced cell death caused by choline treatment. This is shown both by the lack of effect of choline in the control animals and the lack of additional cell death in the ethanol-exposed embryos that also received choline. Our findings align with the majority of previous studies which have shown that choline is safe for the developing embryo (Thomas et al., 2009, 2010; Kwan et al., 2021; Baker et al., 2022) although there have been a few exceptions, particularly at high doses such as 100 mM (Goeke et al., 2018; Carugati et al., 2022).

One of the important findings of this study is that there are strain differences in choline's ability to ameliorate ethanol-induced cell death but only at the higher dose. This adds to the growing literature that suggests that genetics play an important role in choline's efficacy (e.g., Smith et al., 2021). This is consistent with previous studies showing that allelic differences in various enzymes in the choline metabolic pathway can impact its efficacy (Fischer et al., 2010a,b). Further research is needed to assess whether these allelic differences are present within these BXD RI strains. Moreover, these results suggest that, at low doses, the effect of genetics is less apparent which could have important implications for its use in human populations.

These studies show the efficacy of choline but do not provide clues as to the mechanism of choline's protection. Choline has numerous effects but three are most likely to act within the CNS. First, choline is part of the pathway for synthesis of the neurotransmitter acetylcholine (ACh). At older ages, it is likely that this is a relevant mechanism for choline's efficacy. However, at this early developmental stage, it is unclear how much ACh is present (Schambra et al., 1989; Abreu-Villaca et al., 2011) and therefore this mechanism is unlikely to be important at this age. Second, it is a component of phospholipid synthesis for cell membrane components. Ethanol can affect membrane composition (e.g., Naik and Ramadoss, 2023) and while it is unclear whether this is the mechanism of choline's efficacy, it is a strong potential mechanism. Third, it is a methyl donor that is essential for methylation which is an important epigenetic modification. Several studies have shown that ethanol exposure during development can alter DNA methylation and choline can modify ethanol's effects (Balaraman et al., 2017; Sarkar et al., 2019). Previously, we examined several epigenetic modifications across multiple brain regions in neonatal mice given ethanol 7 h prior to tissue collection (Schaffner et al., 2020). The results demonstrated that there were both altered DNA methylation and altered gene expression in this short timeframe, suggesting that altered methylation of either DNA or histones could be a significant mechanism for choline's protective actions with the early neural tube.

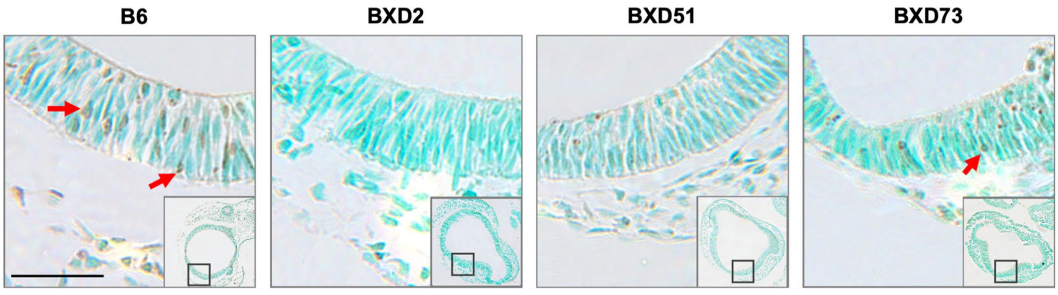


FIGURE 4
Strain differences in levels of TUNEL-positive cells in the forebrain across mouse strains exposed to ethanol and 250 mg/kg choline. Representative images of TUNEL-stained sections at E9.5 to illustrate apoptotic cells in B6, BXD2, BXD51, and BXD73 mouse forebrain (low magnification inset indicates the region of embryonic forebrain shown at higher magnification). Dark deposits of DAB indicate cells undergoing apoptosis (examples highlighted by red arrows). Cells were counterstained with methyl green. Scale bars = 50 mm.

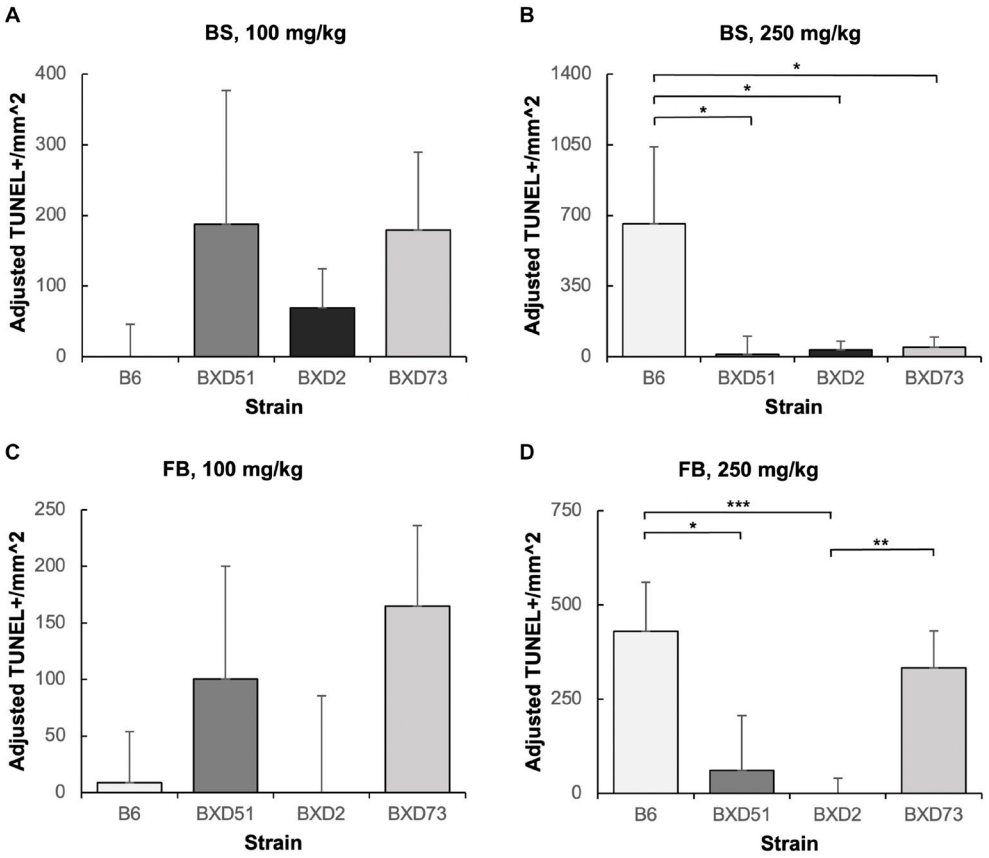


FIGURE 5
Strain differences in choline's ability to ameliorate ethanol-induced cell death. Graphs represent adjusted values for cell death in the developing brainstem (BS) and forebrain (FB) after administration of moderate (100 mg/kg) and high (250 mg/kg) doses of choline. Adjusted TUNEL+ cells/mm^2 values were calculated by subtracting the average cell death of the MD-treated controls that were not administered choline from each individual litter cell death average of the ethanol+choline treatment groups. Any adjusted cell death values that were negative were set at zero. It should be noted that there are substantial differences in the y-axis scales between panels as well as between the above graphs and those in Figures 2, 3. **(A)** No strain differences were seen in the brainstem (BS) region of ethanol-treated embryos administered a 100 mg/kg dose of choline. $N = 8$ for B6 and BXD51, $N = 7$ for BXD2, and $N = 6$ for BXD73. **(B)** There are significant differences between the B6 strain and all 3 of the BXD strains in the forebrain (FB) of ethanol-treated embryos administered a 250 mg/kg dose of choline. $N = 8$ for B6, BXD51, and BXD2, and $N = 6$ for BXD73. **(C)** No strain differences were seen in the forebrain (FB) region of ethanol-treated embryos administered a 100 mg/kg dose of choline. $N = 8$ for B6 and BXD51, and $N = 7$ for BXD2 and BXD73. **(D)** There are significant differences between the B6 strain and both the BXD51 and BXD2 strains as well as between the BXD2 and BXD73 strains in the forebrain (FB) of ethanol-treated embryos administered a 250 mg/kg dose of choline. $N = 8$ for B6, BXD51, and BXD2, and $N = 7$ for BXD73. Error bars indicate standard error of the mean (SEM). $^*p < 0.05$, $^{**}p < 0.01$, $^{***}p < 0.001$. Note the differences in the y-axis scales between panels.

Our results indicate that whatever the mechanism(s) of neural protection is/are, it needs to help explain the complex nature of the protective effects: the strain-, dose-, and region-specific differences seem amongst the four strains that were analyzed in this study. Data from human clinical trial work using choline has discovered allelic differences in key choline utilization genes, cellular choline transporter gene solute carrier family 44 member 1 (SLC44A1) (Smith et al., 2021), methylenetetrahydrofolate dehydrogenase 1 (MTHFR, also known as Mthfd1 in the mouse) (Fischer et al., 2010a) and phosphatidylethanolamine-N-methyltransferase (PEMT) (Fischer et al., 2010a,b) that alter choline related phenotypes. To speak to the polymorphisms found in humans using a mouse model, it would be interesting to examine SNPs in reference populations like the BXD RI lines to see if a gene of interest can have a phenotypic impact. For example, in the BXD population there are two alleles of the *mthfd1* gene that segregate the BXD51 and BXD2 lines as distinct from the BXD73 line. Therefore, the BXD population can be used to examine polymorphisms in other genes as they relate to choline's ability to reduce ethanol-induced cell death.

The dose of ethanol used in the present study was a relatively high one. The rationale for this is three-fold. First, as the purpose of the present study was to evaluate the efficacy of choline in reducing ethanol-induced cell death, this dose was chosen because it has been shown to more reliably cause cell death with similar dosages used by ourselves and others (Young et al., 2005; Young and Olney, 2006; Goldowitz et al., 2014; Theberge et al., 2019; Boschen et al., 2021). Second, the alcohol exposure used in the present study models binge ethanol consumption which is the most common drinking pattern in women of child-bearing age and is characterized as episodes of high ethanol consumption in a short time window (Kanny et al., 2018; Bohm et al., 2021). Finally, the high dose used in the present study is to achieve effectiveness as small animals, including mice, metabolize ethanol at a faster rate than humans (Cederbaum, 2012).

Importantly, there are several limitations to the present study. First, the sex of the embryos remains unknown and there could be differential effects based on sex (Kwan et al., 2017). This is an important consideration and will be done in the future. Second, this study examined the acute effects of choline on mitigating ethanol-induced cell death. It will be important to determine if the effects of choline translate into long-term amelioration of ethanol-related cell loss. Third, only two doses of choline were examined and it is possible that additional differences would be detected at either higher or lower doses of choline. The current data suggest that a threshold effect was achieved at 100 mg/kg in all strains, but it would critical to know if genetics influences the minimal choline level needed, given variation in choline intake and need among clinical populations. Fourth, there could be differences in bioavailability of choline to the embryos and whether or not alcohol impacts this bioavailability. Currently, this interesting phenomenon has not been examined, but will be evaluated in future studies.

Conclusion

In the present study, we confirm that choline is effective in ameliorating ethanol-induced cell death in the developing neural tube but further demonstrate that there are strain differences in these effects. Moreover, the differential strain effects are most pronounced at the high dose suggesting that the lowest effective dose would likely be the most beneficial and the least likely to have untoward other effects. Currently, the mechanism behind either choline's protective effects or the molecular pathways that underlie the genetic differences are unknown. However, because the liver is an essential organ in metabolizing choline and is the first organ to encounter choline after absorption, the potential for differences in liver metabolism of choline across strains exists and this may prove to be important for understanding genetic differences in humans (Smith et al., 2021). Future research will be needed to address this issue as well as to gain a better understanding of how choline protects against ethanol's teratogenic actions.

Data availability statement

The raw data supporting the conclusions of this article will be made available by the authors, without undue reservation.

Ethics statement

The animal study was approved by Institutional Animal Care and Use Committee at the University of Tennessee Health Science Centre. The study was conducted in accordance with the local legislation and institutional requirements.

Author contributions

KH, JT, and DG contributed to conception and design of the study. KH, DG, and FX contributed to the generation of all data in the manuscript and analyses of the data. KH, FX, and DG wrote the first draft of the manuscript. All authors contributed to the article and approved the submitted version.

Funding

This research was funded by National Institute on Alcohol Abuse and Alcoholism R01AA023508 (KH, DG), University of Tennessee Health Science Center CORNET Award (KH), and the BC Children's Hospital Research Institute (DG).

Acknowledgments

The authors wish to acknowledge Emma Norman, Leya Gouto, Jessica Baker and Jo Bright for assistance in animal husbandry and generation of animals. The authors would like to thank Constance de Schaetzen, Sam Mok, Elizabeth Nguyen and Justin Sidhu for help with the sectioning of the many blocks used in this analysis; Andrew Wilk and Pierre Collet for help with the staining of sections, Yasi Hariri for the analysis of material, and Cheryl Tan for help in passing on her knowledge of the handling of the tissue prepared for analysis and the counting of TUNEL+ cells. Yuliya Badayeva provided invaluable support in the imaging of embryos and figure construction. The authors are particularly indebted to Jeff Bone for his guidance for the statistical analysis of the data.

Conflict of interest

The authors declare that the research was conducted in the absence of any commercial or financial relationships that could be construed as a potential conflict of interest.

Publisher's note

All claims expressed in this article are solely those of the authors and do not necessarily represent those of their affiliated organizations, or those of the publisher, the editors and the reviewers. Any product that may be evaluated in this article, or claim that may be made by its manufacturer, is not guaranteed or endorsed by the publisher.

Supplementary material

The Supplementary material for this article can be found online at: https://www.frontiersin.org/articles/10.3389/fnins.2023.1203597/full#supplementary-material

SUPPLEMENTARY FIGURE S1
Illustration of the regions of interest for quantification of cell death in E9.5 embryos. To the left is shown a schematic of an E9.5 embryo depicting an idealized plane of section that passes through the two regions of the brain that were analyzed: the forebrain at the level of the optic vesicle (OpV) and the brainstem at the level of the otic vesicle (OtV). To the right is shown an actual TUNEL-stained, methyl green counterstained section from an E9.5 embryo to illustrate the anatomical regions that were analyzed for cell death

following the various treatments used in this study. The regions of interest analyzed are outlined in black dashed lines. The entirety of the outlined regions of interest were analyzed in appropriate sections. A = anterior, P = posterior, V = ventral, D = dorsal.

SUPPLEMENTARY FIGURE S2
Main effects of choline dose on ethanol-induced cell death irrespective of strain. Graphs represent the amount of cell death in ethanol-treated embryos that also received choline treatment with either 0 mg/kg, a moderate (100 mg/kg), or high (250 mg/kg) dose. At each dose, all the values across the 4 strains are shown in each bar. Statistical comparisons among the three ethanol-treated groups are shown in the graphs. **(A)** Main effects of choline dose in the brainstem. There is a significant effect of both the 100 mg/kg and 250 mg/kg doses on cell death compared to the 0 mg/kg dose. The two doses were equally effective at reducing cell death. **(B)** Main effects of choline dose in the forebrain. There is a significant effect of both the 100 mg/kg and 250 mg/kg dose on cell death compared to the 0 mg/kg dose. The two doses were equally effective at reducing cell death. Error bars indicate standard error of the mean (SEM). *$p < 0.05$, **$p < 0.01$, ***$p < 0.001$.

SUPPLEMENTARY FIGURE S3
Main effects of strain on ethanol-induced cell death irrespective of choline dose. Graphs represent the amount of cell death in ethanol-treated embryos that also received choline treatment with either 0 mg/kg, a moderate (100 mg/kg), or high (250 mg/kg) dose in each of the 4 strains: B6, BXD51, BXD2, and BXD73. For each strain, all the values across the 3 choline doses are shown in each bar. Statistical comparisons among the four strains are shown in the graphs. **(A)** Main effects of strain in the brainstem. There is a significant difference in ethanol-induced cell death between the B6 strain and BXD2 strain, between the B6 strain and BXD73 strain, between the BXD51 strain and BXD2 strain, and between the BXD51 strain and BXD73 strain. **(B)** Main effects of strain in the forebrain. There is a significant difference in ethanol-induced cell death between the B6 strain and BXD2 strain. Error bars indicate standard error of the mean (SEM). *$p < 0.05$, **$p < 0.01$, ***$p < 0.001$.

References

Abreu-Villaca, Y., Filgueiras, C. C., and Manhaes, A. C. (2011). Developmental aspects of the cholinergic system. *Behav. Brain Res.* 221, 367–378. doi: 10.1016/j.bbr.2009.12.049

Baker, J. A., Breit, K. R., Bodnar, T. S., Weinberg, J., and Thomas, J. D. (2022). Choline supplementation modifies the effects of developmental alcohol exposure on immune responses in adult rats. *Nutrients* 14:2868. doi: 10.3390/nu14142868

Balaraman, S., Idrus, N. M., Miranda, R. C., and Thomas, J. D. (2017). Postnatal choline supplementation selectively attenuates hippocampal microrna alterations associated with developmental alcohol exposure. *Alcohol* 60, 159–167. doi: 10.1016/j.alcohol.2016.12.006

Bohm, M. K., Liu, Y., Esser, M. B., Mesnick, J. B., Lu, H., Pan, Y., et al. (2021). Binge drinking among adults, by select characteristics and state - United States, 2018. *MMWR Morb. Mortal. Wkly Rep.* 70, 1441–1446. doi: 10.15585/mmwr.mm7041a2

Boschen, K. E., Fish, E. W., and Parnell, S. E. (2021). Prenatal alcohol exposure disrupts sonic hedgehog pathway and primary cilia genes in the mouse neural tube. *Reprod. Toxicol.* 105, 136–147. doi: 10.1016/j.reprotox.2021.09.002

Bottom, R. T., Abbott, C. W. 3rd, and Huffman, K. J. (2020). Rescue of ethanol-induced Fasd-like phenotypes via prenatal co-administration of choline. *Neuropharmacology* 168:107990. doi: 10.1016/j.neuropharm.2020.107990

Carugati, M., Goodlett, C. R., Cudd, T. A., and Washburn, S. E. (2022). The effects of gestational choline supplementation on cerebellar Purkinje cell number in the sheep model of binge alcohol exposure during the first trimester-equivalent. *Alcohol* 100, 11–21. doi: 10.1016/j.alcohol.2022.01.002

Cederbaum, A. I. (2012). Alcohol metabolism. *Clin. Liver Dis.* 16, 667–685. doi: 10.1016/j.cld.2012.08.002

Chokroborty-Hoque, A., Alberry, B., and Singh, S. M. (2014). Exploring the complexity of intellectual disability in fetal alcohol spectrum disorders. *Front. Pediatr.* 2:90. doi: 10.3389/fped.2014.00090

Corbin, K. D., and Zeisel, S. H. (2012). The nutrigenetics and nutrigenomics of the dietary requirement for choline. *Prog. Mol. Biol. Transl. Sci.* 108, 159–177. doi: 10.1016/B978-0-12-398397-8.00007-1

Craciunescu, C. N., Albright, C. D., Mar, M. H., Song, J., and Zeisel, S. H. (2003). Choline availability during embryonic development alters progenitor cell mitosis in developing mouse hippocampus. *J. Nutr.* 133, 3614–3618. doi: 10.1093/jn/133.11.3614

Cunningham, C. L. (1995). Localization of genes influencing ethanol-induced conditioned place preference and locomotor activity in Bxd recombinant inbred mice. *Psychopharmacology* 120, 28–41. doi: 10.1007/BF02246142

Downing, C., Balderrama-Durbin, C., Kimball, A., Biers, J., Wright, H., Gilliam, D., et al. (2012). Quantitative trait locus mapping for ethanol teratogenesis in Bxd recombinant inbred mice. *Alcohol. Clin. Exp. Res.* 36, 1340–1354. doi: 10.1111/j.1530-0277.2012.01754.x

Ernst, A. M., Gimbel, B. A., De Water, E., Eckerle, J. K., Radke, J. P., Georgieff, M. K., et al. (2022). Prenatal and postnatal choline supplementation in fetal alcohol Spectrum disorder. *Nutrients* 14:688. doi: 10.3390/nu14030688

Fischer, L. M., Da Costa, K. A., Galanko, J., Sha, W., Stephenson, B., Vick, J., et al. (2010a). Choline intake and genetic polymorphisms influence choline metabolite concentrations in human breast milk and plasma. *Am. J. Clin. Nutr.* 92, 336–346. doi: 10.3945/ajcn.2010.29459

Fischer, L. M., Da Costa, K. A., Kwock, L., Galanko, J., and Zeisel, S. H. (2010b). Dietary choline requirements of women: effects of estrogen and genetic variation. *Am. J. Clin. Nutr.* 92, 1113–1119. doi: 10.3945/ajcn.2010.30064

Gimbel, B. A., Anthony, M. E., Ernst, A. M., Roediger, D. J., De Water, E., Eckerle, J. K., et al. (2022). Long-term follow-up of a randomized controlled trial of choline for neurodevelopment in fetal alcohol spectrum disorder: corpus callosum white matter microstructure and neurocognitive outcomes. *J. Neurodev. Disord.* 14:59. doi: 10.1186/s11689-022-09470-w

Glass, L., Moore, E. M., and Mattson, S. N. (2023). Current considerations for fetal alcohol spectrum disorders: identification to intervention. *Curr. Opin. Psychiatry* 36, 249–256. doi: 10.1097/YCO.0000000000000862

Goeke, C. M., Roberts, M. L., Hashimoto, J. G., Finn, D. A., and Guizzetti, M. (2018). Neonatal ethanol and choline treatments Alter the morphology of developing rat hippocampal pyramidal neurons in opposite directions. *Neuroscience* 374, 13–24. doi: 10.1016/j.neuroscience.2018.01.031

Goldowitz, D., Lussier, A. A., Boyle, J. K., Wong, K., Lattimer, S. L., Dubose, C., et al. (2014). Molecular pathways underpinning ethanol-induced neurodegeneration. *Front. Genet.* 5:203. doi: 10.3389/fgene.2014.00203

Idrus, N. M., Breit, K. R., and Thomas, J. D. (2017). Dietary choline levels modify the effects of prenatal alcohol exposure in rats. *Neurotoxicol. Teratol.* 59, 43–52. doi: 10.1016/j.ntt.2016.11.007

Jacobson, S. W., Carter, R. C., Molteno, C. D., Stanton, M. E., Herbert, J. S., Lindinger, N. M., et al. (2018). Efficacy of maternal choline supplementation during pregnancy in mitigating adverse effects of prenatal alcohol exposure on growth and cognitive function: a randomized, double-blind, placebo-controlled clinical trial. *Alcohol. Clin. Exp. Res.* 42, 1327–1341. doi: 10.1111/acer.13769

Kanny, D., Naimi, T. S., Liu, Y., Lu, H., and Brewer, R. D. (2018). Annual Total binge drinks consumed by U.S. adults, 2015. *Am. J. Prev. Med.* 54, 486–496. doi: 10.1016/j.amepre.2017.12.021

Kwan, S. T. C., King, J. H., Yan, J., Jiang, X., Wei, E., Fomin, V. G., et al. (2017). Maternal choline supplementation during murine pregnancy modulates placental markers of inflammation, apoptosis and vascularization in a fetal sex-dependent manner. *Placenta* 53, 57–65. doi: 10.1016/j.placenta.2017.03.019

Kwan, S. T. C., Ricketts, D. K., Presswood, B. H., Smith, S. M., and Mooney, S. M. (2021). Prenatal choline supplementation during mouse pregnancy has differential effects in alcohol-exposed fetal organs. *Alcohol. Clin. Exp. Res.* 45, 2471–2484. doi: 10.1111/acer.14730

May, P. A., Chambers, C. D., Kalberg, W. O., Zellner, J., Feldman, H., Buckley, D., et al. (2018). Prevalence of fetal alcohol Spectrum disorders in 4 us communities. *JAMA* 319, 474–482. doi: 10.1001/jama.2017.21896

May, P. A., Hasken, J. M., Hooper, S. R., Hedrick, D. M., Jackson-Newsom, J., Mullis, C. E., et al. (2021). Estimating the community prevalence, child traits, and maternal risk factors of fetal alcohol spectrum disorders (Fasd) from a random sample of school children. *Drug Alcohol Depend.* 227:108918. doi: 10.1016/j.drugalcdep.2021.108918

Monk, B. R., Leslie, F. M., and Thomas, J. D. (2012). The effects of perinatal choline supplementation on hippocampal cholinergic development in rats exposed to alcohol during the brain growth spurt. *Hippocampus* 22, 1750–1757. doi: 10.1002/hipo.22009

Naik, V. D., Lee, J., Wu, G., Washburn, S., and Ramadoss, J. (2022). Effects of nutrition and gestational alcohol consumption on fetal growth and development. *Nutr. Rev.* 80, 1568–1579. doi: 10.1093/nutrit/nuab119

Naik, V. D., and Ramadoss, J. (2023). Untargeted and targeted blood Lipidomic signature profile of gestational alcohol exposure. *Nutrients* 15:1411. doi: 10.3390/nu15061411

Nikolic, P., Jarlebark, L. E., Billett, T. E., and Thorne, P. R. (2000). Apoptosis in the developing rat cochlea and its related structures. *Brain Res. Dev. Brain Res.* 119, 75–83. doi: 10.1016/S0165-3806(99)00161-3

Peirce, J. L., Lu, L., Gu, J., Silver, L. M., and Williams, R. W. (2004). A new set of Bxd recombinant inbred lines from advanced intercross populations in mice. *BMC Genet.* 5:7. doi: 10.1186/1471-2156-5-7

Philip, V. M., Duvvuru, S., Gomero, B., Ansah, T. A., Blaha, C. D., Cook, M. N., et al. (2010). High-throughput behavioral phenotyping in the expanded panel of Bxd recombinant inbred strains. *Genes Brain Behav.* 9, 129–159. doi: 10.1111/j.1601-183X.2009.00540.x

Sarkar, D. K., Gangisetty, O., Wozniak, J. R., Eckerle, J. K., Georgieff, M. K., Foroud, T. M., et al. (2019). Persistent changes in stress-regulatory genes in pregnant women or children exposed prenatally to alcohol. *Alcohol. Clin. Exp. Res.* 43, 1887–1897. doi: 10.1111/acer.14148

Schaffner, S. L., Lussier, A. A., Baker, J. A., Goldowitz, D., Hamre, K. M., and Kobor, M. S. (2020). Neonatal alcohol exposure in mice induces select differentiation- and apoptosis-related chromatin changes both independent of and dependent on sex. *Front. Genet.* 11:35. doi: 10.3389/fgene.2020.00035

Schambra, U. B., Sulik, K. K., Petrusz, P., and Lauder, J. M. (1989). Ontogeny of cholinergic neurons in the mouse forebrain. *J. Comp. Neurol.* 288, 101–122. doi: 10.1002/cne.902880109

Smith, S. M., Virdee, M. S., Eckerle, J. K., Sandness, K. E., Georgieff, M. K., Boys, C. J., et al. (2021). Polymorphisms in Slc44A1 are associated with cognitive improvement in children diagnosed with fetal alcohol spectrum disorder: an exploratory study of oral choline supplementation. *Am. J. Clin. Nutr.* 114, 617–627. doi: 10.1093/ajcn/nqab081

Theberge, E. T., Baker, J. A., Dubose, C., Boyle, J. K., Balce, K., Goldowitz, D., et al. (2019). Genetic influences on the amount of cell death in the neural tube of Bxd mice exposed to acute ethanol at Midgestation. *Alcohol. Clin. Exp. Res.* 43, 439–452. doi: 10.1111/acer.13947

Thomas, J. D., Abou, E. J., and Dominguez, H. D. (2009). Prenatal choline supplementation mitigates the adverse effects of prenatal alcohol exposure on development in rats. *Neurotoxicol. Teratol.* 31, 303–311. doi: 10.1016/j.ntt.2009.07.002

Thomas, J. D., Idrus, N. M., Monk, B. R., and Dominguez, H. D. (2010). Prenatal choline supplementation mitigates behavioral alterations associated with prenatal alcohol exposure in rats. *Birth Defects Res. A Clin. Mol. Teratol.* 88, 827–837. doi: 10.1002/bdra.20713

Thomas, J. D., La Fiette, M. H., Quinn, V. R., and Riley, E. P. (2000). Neonatal choline supplementation ameliorates the effects of prenatal alcohol exposure on a discrimination learning task in rats. *Neurotoxicol. Teratol.* 22, 703–711. doi: 10.1016/S0892-0362(00)00097-0

Wallace, T. C., Blusztajn, J. K., Caudill, M. A., Klatt, K. C., and Zeisel, S. H. (2020). Choline: the neurocognitive essential nutrient of interest to obstetricians and gynecologists. *J Diet. Suppl.* 17, 733–752. doi: 10.1080/19390211.2019.1639875

Wang, G., and Bieberich, E. (2010). Prenatal alcohol exposure triggers ceramide-induced apoptosis in neural crest-derived tissues concurrent with defective cranial development. *Cell Death Dis.* 1:e46. doi: 10.1038/cddis.2010.22

Warton, F. L., Molteno, C. D., Warton, C. M. R., Wintermark, P., Lindinger, N. M., Dodge, N. C., et al. (2021). Maternal choline supplementation mitigates alcohol exposure effects on neonatal brain volumes. *Alcohol. Clin. Exp. Res.* 45, 1762–1774. doi: 10.1111/acer.14672

Wozniak, J. R., Fink, B. A., Fuglestad, A. J., Eckerle, J. K., Boys, C. J., Sandness, K. E., et al. (2020). Four-year follow-up of a randomized controlled trial of choline for neurodevelopment in fetal alcohol spectrum disorder. *J. Neurodev. Disord.* 12:9. doi: 10.1186/s11689-020-09312-7

Young, C., and Olney, J. W. (2006). Neuroapoptosis in the infant mouse brain triggered by a transient small increase in blood alcohol concentration. *Neurobiol. Dis.* 22, 548–554. doi: 10.1016/j.nbd.2005.12.015

Young, C., Roth, K. A., Klocke, B. J., West, T., Holtzman, D. M., Labruyere, J., et al. (2005). Role of caspase-3 in ethanol-induced developmental neurodegeneration. *Neurobiol. Dis.* 20, 608–614. doi: 10.1016/j.nbd.2005.04.014

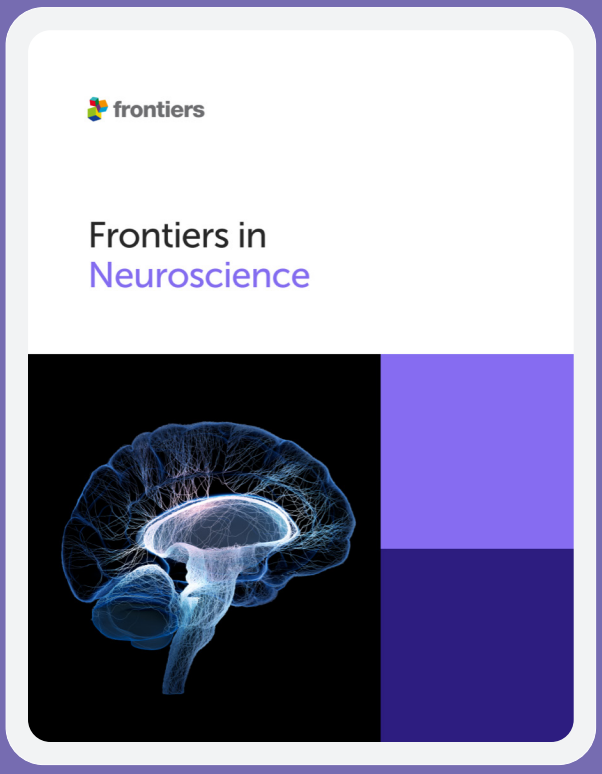
Frontiers in Neuroscience

Provides a holistic understanding of brain function from genes to behavior

Part of the most cited neuroscience journal series which explores the brain - from the new eras of causation and anatomical neurosciences to neuroeconomics and neuroenergetics.

Discover the latest Research Topics

See more →



Frontiers

Avenue du Tribunal-Fédéral 34
1005 Lausanne, Switzerland
frontiersin.org

Contact us

+41 (0)21 510 17 00
frontiersin.org/about/contact